TAILINGS AND MINE WASTE 2020

November 15-18, 2020

CIVIL AND ENVIRONMENTAL ENGINEERING
COLORADO STATE UNIVERSITY

TAILINGS AND MINE WASTE '20

PROCEEDINGS OF THE 24TH INTERNATIONAL CONFERENCE ON TAILINGS AND MINE WASTE

COLORADO STATE UNIVERSITY

Published by: UBC Studios
University of British Columbia
110 – 2329 West Mall
Vancouver BC, V6T 1Z4

Preface

This proceedings includes 72 state-of-the-art papers. These papers address the important issues faced by the mining industry today and will provide a record of the discussions at the conference that will remain of value for many years.

The organizing committee wishes to thank all who have contributed to this year's conference including authors, presenters, keynote speakers, sponsors, and exhibitors.

Organization

The Tailings and Mine Waste 2020 conference was organized by the Department of Civil and Environmental Engineering, Colorado State University, Fort Collins, Colorado in conjunction with the University of Alberta, Edmonton, Alberta and the University of British Columbia, Vancouver, British Columbia.

PATRON SPONSOR

Measurand & RST Instruments

GOLD SPONSORS AND ORGANIZING COMMITTEE

Colorado State University	Christopher Bareither, *Conference Chair*
AECOM, Denver, CO	Jason Hilgers
Barr Engineering Co., Minneapolis, MN	Kurt Schimpke
BGC Engineering, Montrose, CO	Michael Henderson
CETCO, Evergreen, CO	Andy Jung
ConeTec, Inc., Salt Lake City, UT	Shawn Steiner
Engineering Analytics, Fort Collins, CO	Daniel Overton
Gannett Fleming, Phoenix, AZ	Dean Durkee
Golder Associates, Inc., Lakewood, CO	Ryan Shedivy
INR	
Klohn Crippen Berger, Ltd., Vancouver, BC	Kate Patterson
Knight Piésold Consulting, Denver, CO	Zach Fox
MineBridge Software Inc., Calgary, AB	Carlo Cooper
NewFields, Denver, CO	Nicholas Rocco
Paterson & Cooke, Denver, CO	Matt Bachman
SRK Consulting, Inc., Fort Collins, CO	Larry Cope
Stantec, Denver, CO	Melanie Davis
TetraTech, Fort Collins, CO	Dary Longwell
Tierra Group International, Ltd., Lakewood, CO	Matt Fuller
Wood, Englewood, CO	Daniel Servigna

Conference Partners

University of Alberta, Edmonton, AB	Dave Sego
University of British Columbia, Vancouver, BC	Dirk Van Zyl

SILVER SPONSORS

Geosyntec Consultants, Columbia, MD
INTERA Incorporated, Fort Collins, CO
Parsons, Calgary, AB

Table of Contents

FILTERED TAILINGS

GEOCHEMISTRY

GEOSYNTHETICS AND LINERS

GEOTECHNICAL ENGINEERING

IMAGING AND SPATIAL ANALYSIS

NEW TECHNOLOGIES

RECLAMATION AND REMEDIATION

REGULATIONS

RISK INFORMED DESIGN

SITE CHARACTERIZATION AND MONITORING

WATER MANAGEMENT

The Conferences

The first conference in the series was on Uranium Mill Tailings Management and was held in 1978. It was organized by the Geotechnical Engineering Program of the Civil Engineering Department of Colorado State University, Fort Collins, Colorado. The organizing committee consisted of John Nelson, Thomas Shepherd, Steven Abt, Wayne Charlie, and John Welsh. The series of conferences on uranium mill tailings continued through 1985. The nine volumes of proceedings were published totaling some 3,700 pages. By 1984, the Uranium Mill Tailings Remedial Action (UMTRA) Project was well underway. The development of new uranium mines had declined and interest in uranium tailings was no longer wide-spread. Thus in 1984 and 1985, the conference title was expanded to Management of Uranium Mill Tailings, Low-level Waste and Hazardous Waste.

In 1986, the organizing committee, this time consisting of Steve Abt, John Nelson, Richard Wardwell, and Dirk van Zyl, changed the title and focus to Geotechnical and Geohydrological Aspects of Waste Management. They noted the following reasons for this change in the preface: "The first five annual symposia focused on the design, construction, and operation of uranium tailings impoundments. The sixth and seventh were of broader scope, and included low-level and hazardous waste management. This eighth symposium continues the process of technology transfer but focuses more precisely on the geotechnical and geohydrological aspects of waste management: the two engineering areas of prime importance in the design and operation of waste disposal facilities." This symposium attracted about fifty-five papers with the proceedings being 558 pages. This same focus was maintained for the 1987 conference.

By 1988 the uranium market had declined, uranium mills had closed, and support for a symposium on uranium mill tailings, hazardous waste, or most any topic associated with mine waste had declined. Thus the conference was not held from 1988 until 1994. In 1994, Colorado State University, the sponsor of the uranium mill tailings conferences, resuscitated the conference series as Tailings and Mine Waste, the title by which the series goes today. The proceedings of 1994 contain twenty-seven papers. The proceedings from 1995 contain a mere fourteen. By 2003, the paper count was up to sixty and the venue was Vail, Colorado. In 2004 the paper count and attendance reduced leading to a negative financial situation for the conference and reluctance on the part of the management of the Department of Civil Engineering at Colorado State University to support the conference series, thus the conference was not held from 2005 until 2008.

In late 2007 an organizational committee was established in Colorado and through the support of a number of consulting engineering companies, Engineering Analytics, Golder, Knight Piésold, MWH Global, Robertson GeoConsultants, Inc., SRK Consulting, Inc. Tetra Tech, Inc. and URS Corporation, a stable financial basis was established for the conferences in Colorado. It was also decided to rotate the conference series between Colorado State University and two Canadian Universities. The following sequence was established: even years, Colorado State University, odd years alternating between University of Alberta and University of British Columbia.

There now are specialty conferences on mine closure, paste tailings, and many other focus topics that were once part of this series. In spite of the specialty meetings, this series remains the best attended and provides the most overall focus of tailings and mine waste.

Table 1: Conference proceedings details, 1978 to 2017

Year	Title	Date and Location	Pages	Papers	Publisher
1978	Uranium Mill Tailings Management	Fort Collins, CO., November 20 - 21	172	11	Geotechnical Engineering Program, Colorado State University
1978	Uranium Mill Tailings Management, Volume II	Fort Collins, CO., November 20 - 21	126	9	Geotechnical Engineering Program, Colorado State University
1979	Uranium Mill Tailings Management	Fort Collins, CO., November 19 - 20	308	26	Geotechnical Engineering Program, Colorado State University
1980	Uranium Mill Tailings Management	Fort Collins, CO., November 24 - 25	573	30	Geotechnical Engineering Program, Colorado State University
1981	Uranium Mill Tailings Management	Fort Collins, CO., October 26 - 27	727	43	Geotechnical Engineering Program, Colorado State University
1982	Uranium Mill Tailings Management	Fort Collins, CO, December 9 - 10	556	38	Geotechnical Engineering Program, Colorado State University
1984	Management of Uranium Tailings, Low-Level Waste and Hazardous Waste	Fort Collins, CO, February 1 to 3	670	66	Geotechnical Engineering Program, Colorado State University
1985	Management of Uranium Tailings, Low-Level Waste and Hazardous Waste, Volume I	Fort Collins, CO, February 6 to 8	252	60	Geotechnical Engineering Program, Colorado State University
1985	Management of Uranium Tailings, Low-Level Waste and Hazardous Waste, Volume II	Fort Collins, CO, February 6 to 8	334	34	Geotechnical Engineering Program, Colorado State University
1986	Geotechnical and Geohydrological Aspects of Waste Management	Fort Collins, CO, February 5 to 7	558	55	A.A. Balkema, Rotterdam
1987	Geotechnical and Geohydrological Aspects of Waste Management	Fort Collins, CO, February 1 to 6	312	26	Lewis Publishers, Inc.
1994	Tailings and Mine Waste ‘94	Fort Collins, CO, January 19 to 21	259	27	A.A. Balkema, Rotterdam
1995	Tailings and Mine Waste ‘95	Fort Collins, CO, January 17 to 20	131	14	A.A. Balkema, Rotterdam
1996	Tailings and Mine Waste ‘96	Fort Collins, CO, January 16 to 19	664	69	A.A. Balkema, Rotterdam
1997	Tailings and Mine Waste ‘97	Fort Collins, CO, January 13 to 17	788	83	A.A. Balkema, Rotterdam
1998	Tailings and Mine Waste ‘98	Fort Collins, CO, January 26 to 28	968	99	A.A. Balkema, Rotterdam
1999	Tailings and Mine Waste ‘99	Fort Collins, CO, January 24 to 27	808	88	A.A. Balkema, Rotterdam
2000	Tailings and Mine Waste ‘00	Fort Collins, CO, January 23 to 26	566	61	A.A. Balkema, Rotterdam
2001	Tailings and Mine Waste ‘01	Fort Collins, CO, January 16 to 19	472	52	A.A. Balkema, Rotterdam
2002	Tailings and Mine Waste ‘02	Fort Collins, CO, January 27 to 30	520	64	A.A. Balkema, Rotterdam
2003	Tailings and Mine Waste ‘03	Vail, CO, October 12 to 15	526	63	A.A. Balkema, Lisse
2004	Tailings and Mine Waste ‘04	Vail, CO, October 10 to 13	428	48	A.A. Balkema, Leiden
2008	Tailings and Mine Waste ‘08	Vail, CO, October 19 to 22	449	41	Taylor and Francis Group, London

Year	Title	Date and Location	Pages	Papers	Publisher
2009	Tailings and Mine Waste '09	Banff, Alberta, November 1 to 4	901	79	University of Alberta Geotechnical Center, University of Alberta
2010	Tailings and Mine Waste '10	Vail, CO, October 17 to 20	471	46	Taylor and Francis Group, London
2011	Tailings and Mine Waste '11	Vancouver, British Columbia November 6 to 9	861	72	University of British Columbia Available on-line: https://circle.ubc.ca/
2012	Tailings and Mine Waste '12	Keystone, CO, October 14 to 17	666	58	University of British Columbia
2013	Tailings and Mine Waste '13	Banff, Alberta November 3 to 6	663	64	University of Alberta Geotechnical Center, University of Alberta
2014	Tailings and Mine Waste '14	Keystone, CO, October 5 to 8	566	51	University of British Columbia
2015	Tailings and Mine Waste '15	Vancouver, British Columbia October 25 to 28	699	61	University of British Columbia
2016	Tailings and Mine Waste '16	Keystone, CO October 2 to 4	939	86	University of British Columbia
2017	Tailings and Mine Waste '17	Banff, Alberta November 5 to 8	780	75	University of Alberta Geotechnical Center, University of Alberta
2018	Tailings and Mine Waste '18	Keystone, CO Sept. 30 – October 2	900	82	University of British Columbia
2019	Tailings and Mine Waste '19	Vancouver, BC November 17-20	1464	113	University of British Columbia

Tailings Dam Safety - Have We Resolved the Crisis?

Norbert R. Morgenstern, PhD, PEng, FCAE, NAE

Distinguished University Professor Emeritus
Civil and Environmental Engineering
University of Alberta

ABSTRACT: Recent high-profile failures of tailings dams have created a crisis associated with the lack of trust in the safety of these storage facilities on the part of multiple stakeholders. The Lecture will summarize the root causes associated with this crisis and recent measures taken to resolve it. The Lecture will note that notwithstanding considerable progress made in guiding mining companies to better practice in the design, construction, operation and closure of tailings facilities, more advances will be needed on the part of the design and regulatory communities before the crisis will be resolved.

Global Ramifications of the Brumadinho Tailings Dam I Failure

David J. Williams, PhD, CPEng

Professor of Geotechnical Engineering
School of Civil Engineering
The University of Queensland

ABSTRACT: There have been landmark tailings dam failures over time, the most fatal of which have brought change. These include the El Cobre tailings dam failure in Chile following the 1965 earthquake, and the Brumadinho Tailings Dam I failure in 2019. The El Cobre failure initially caused doubt that tailings dams could safely be designed, constructed, and operated in Chile's highly seismic setting. The industry responded by radically changing the approach to tailings storage, driven by the need to cater for high seismicity, which has served Chile and Peru reasonably well since. In the e-connected world we now live in, the Brumadinho failure led to a global response. Concern by the Church of England, as an investor in the mining industry, about the safety of tailings dams following the Brumadinho failure, led to the global tailings review. The review was co-convened by the International Council on Mining and Metals, the United Nations Environment Programme and the Principles for Responsible Investing. The review led to the production of the Global Industry Standard on Tailings Management. The new Standard promotes a multi-stakeholder approach to tailings management, with the aim of zero harm to people and the environment. It addresses accountability, expectations, a robust basis of design, emergency response and public disclosure. It presents a framework for safe tailings facility management while affording Operators flexibility as to how best to achieve this goal. The Standard defaults to an 'Extreme' Consequence Classification external loading criteria or the current Classification, with upgrade to 'Extreme' maintained throughout the tailings facility lifecycle. The Keynote Lecture will briefly describe the El Cobre and Brumadinho failures, and highlight the changes that they have brought and will bring to tailings management, respectively.

A Comparative Study of Methods Used to Determinate the Factor of Safety

Hugo A. Brandão
Pimenta de Ávila, Nova Lima, Minas Gerais, Brazil

Rodrigo R. V. de Oliveira
Pimenta de Ávila, Nova Lima, Minas Gerais, Brazil

Luiza F. Almeida
Pimenta de Ávila, Nova Lima, Minas Gerais, Brazil

Guilherme H. S. Pinto
Pimenta de Ávila, Nova Lima, Minas Gerais, Brazil

ABSTRACT: Stability analysis is a key element of dam safety evaluation. Many safety regulations established by institutions such as Australian Committee on Large Dams (ANCOLD) or Canadian Dam Association (CDA), state that a minimum factor of safety must be achieved based on specific conditions of the dam. Current practice employs different methods of analysis such as the Limit Equilibrium Method (LEM) and the Shear Strength Reduction method (SSR) in order to estimate the dam factor of safety. The objective of this article is to analyze the advantages and disadvantages of using LEM and SSR as methods to determine the factor of safety of a dam cross section. To do so, we simulated a tailings dam with a layer of a low strength soil (colluvium) in the foundation and estimated the factor of safety using both LEM, considering circular and non-circular surfaces, and SSR methods.

1 INTRODUCTION

One of the major issues in geotechnical engineering is the study of stability in slopes and various commercial software have been developed to evaluate the stability of dam structures. The most commonly used methods to determine the Factor of Safety (FS) are the Limit Equilibrium Method (LEM) and the Shear Strength Reduction Method (SSR).

In order to evaluate dam stability, it is essential to determine a value for what will be known as the minimum factor of safety. This parameter can be defined as the relationship between acting shear stress divided by the resistant shear stress (Duncan and Wright, 2005). This parameter must be defined based on the uncertainties of the structure in hand, such as soil parameters, pore pressure conditions and others. The federal regulations and recommendations for slope stability analysis establish a minimum value of factor of safety based on each stage of dam development (e.g. end of construction, operation and closure).

Many researchers have compared the results between LEM and SSR and found similar factors of safety for similar failure surfaces. Many of these studies were limited to homogeneous soil slopes, where the geometry is relatively regular with no special features (for example the presence of a thin layer of soft material or a special geometry). In addition, comparing the critical failure surface from LEM and SSR is usually depicted as a secondary study objective, and is not highlighted in most studies. In this paper, the two methods are compared taking into considerations the same initial conditions: pore pressure, geometry and soil parameters.

Another aspect that influences the FS value is the soil's resistance parameters. This becomes more relevant when the soil behavior, whether it is drained or undrained, determines the

parameters that will be used on the analysis and in order to establish the target FS value. It is important to understand that the behavior of the material is one of the most important aspects in the selection of the appropriate method to be used, whether it is an effective stress analysis (ESA) or undrained stress analysis (USA). Indiscriminate use of ESA may completely overlook the physical behavior of the materials under shear stress, causing the stability analysis to produce a FS that misrepresents the dam's safety conditions. Ladd (1991) defined ESA as one that assumes that the effective stress during shear is unchanged from the one immediately prior. This assumes that the shear is slow enough to dissipate the excess pore pressure and/or the excess pore pressure is low enough for the material to present an undrained behavior. This concept applies independent of the soil grain size and portrays the shear rate.

The USA is one way to consider the shear-induced pore water pressure generated by undrained shears and assumes that shearing occurs in undrained conditions. This type of analysis associates negative excess pore pressure for dilatant materials or positive excess pore pressure for contractive materials during the shear response. Thus, using the wrong analysis, ESA for contractive materials or USA for dilative materials, can lead to FS misrepresenting the structural conditions, giving a false impression of dam safety.

The Brazilian Association of Technical Standards ("Associação Brasileira de Normas Técnicas") recommends, in the guideline ABNT NBR 13.028/2017 for dam designs, that the minimum value for the FS in an operating dam is 1.50. This recommendation also states that the designer of the dam is responsible for defining whether the analysis considers drained or undrained parameters. After the Brumadinho upstream dam collapse in January 2019, the Brazilian National Mining Agency "Agência Nacional de Mineração"), released, on August 8th of 2019, a new resolution (nº 13), setting the minimum FS as 1.30 for undrained strength parameters dam analysis.

2 METHODOLOGY

The LEM is a traditional and well-established method to determine the FS. In most cases, this solution is statically indeterminate, and some assumptions must be made to further define the FS. Morgenstern (1992), and other authors pointed that, for simple models, the FS can be numerically close when applied different methods (Janbu, Bishop, Spencer, etc). The LEM does not consider the initial stress state.

To define the FS, the LEM considers equations of balance of forces and motion along a surface to calculate the ratio between resistance and acting stress. In this method, the FS is constant along the surface, and the critical surface is the one that presents the lowest ratio between those efforts. To apply the LEM, calculation premises and methods have been developed to transform the system into an isostatic one. Each method presents specific premises that allow for the analysis of the system, satisfying one or more equilibrium equations (Duncan and Wright, 2005). A LEM analysis has the following premises (Abramson *et al*. 2005):

- The failure surface is well defined (circular or non-circular);
- The FS is unique and constant over the potential failure surface; and
- The Mohr-Coulomb criteria are satisfied over the potential failure surface.

To define the FS a dam stability analysis considering the LEM was developed with Slide2 (from Rocscience) and Slope/W from the GeoStudio 2020 (from Geoslope). The LEM method was applied associated with the Morgenstern – Price / GLE associated with the function $f(x) = \sin(x)$ to determinate the forces between slices. Krahn (2001) and Abramson *et al.* (2005) have pointed out that the function ($f(x)$) may be critical for some special cases, but this is generally not the case unless the problem is highly complicated.

The analysis considered three types of surfaces: (a) circular; (b) non-circular; (c) non-circular optimized. The optimization process was made with the process of surface altering, using 0,0001 to FS tolerance, in both software, which is sufficiently accurate for the present study. In both software the standard search method was applied to define the failure surface.

Optimization in slope stability analysis is used to minimizing the FS of the minimum failure surface by a nonlinear, nonconvex and discontinuous problem (Mafi *et. Al* 2020). Before the optimization process begins, is necessary determinate the initial shape of the potential failure

surface. Then, the surface altering optimization process starts by dividing the critical slip surface into a number of straight-line segments. Next, the end points of each line segments are individually modified to evaluate the potential for a lower FS. Adjustments are then made to the next point along the slip surface until, again, the lowest factor of safety is found. This process is repeated for all the points along the slip surface until the global minimum FS is obtained (GEO-SLOPE 2015).

Another way to determine the FS is to use the SSR method. This mechanism assumes that the critical surface is associated with a shear strain zone. To evaluate the FS, this method reduces the soil parameters, cohesion and friction angle, using a reduction factor, until the failure happens due to the increase of shear stress (Matsui & San, 1992). As pointed by Cheng (2007), some advantages of this method include:

- The critical failure surface is found automatically from the shear strain arising from the application of gravity loads and the reduction of shear strength;
- It requires no assumption on the interslice shear force distribution; and
- It is applicable to many complex conditions and can give information such as stressors, movements, and pore pressures which are not possible with the LEM.

The SSR solution was applied using FLAC-Slope8.1 developed from Itasca.

3 GEOMETRY AND STRENGHT PARAMETERS

This paper presents the analysis of a theoretical dam with a height of 51m, as seen in Figure 1. The dam started with a 22m landfill (clay compacted) and was raised using compacted cyclone underflow tailings. This scenario represents a typical centerline designed dam. The dam was constructed above a 7m thick colluvium layer which is placed on residual soil. The model adopted a phreatic surface as shown in Figure 1. The materials and their properties are summarized and described in Table 1 and applied as depicted in Figure 1.

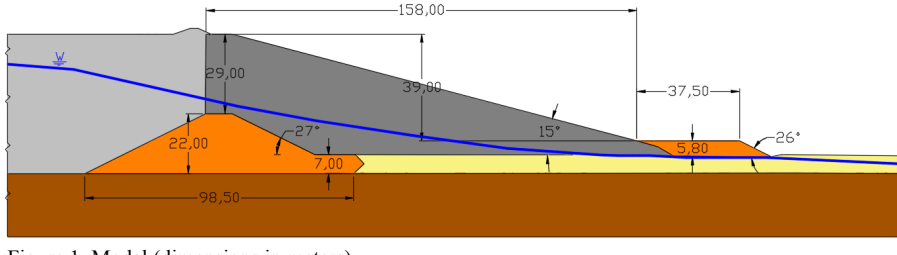

Figure 1. Model (dimensions in meters).

Table 1. Soil parameters

Material	Legend	Unit Weight (kN/m³)	Shear Strength			
			Drained		Undrained	
			c´(kPa)	f ' (°)	Su_{min} (kPa)	Su/s'_{v0} (yield)
Residual Soil		20.0	22.0	27.0	-	-
Colluvium		18.0	-	-	10.0	0.2
Landfill		19.5	30.0	27.0	-	-
Overflow		17.0	-	28.5	-	-
Underflow		18.0	1.0	34.0	-	-

As explained in the introduction, it is relevant to understand that the soil behavior is one of the most important issues in determining the most representative FS of the structure. In this way, the colluvium (a low resistance soil) and overflow were considered contractive under shearing and were simulated with total resistance parameters. The landfill and the underflow were compacted with quality control in order to induce a dilatant behavior during shearing and drained parameters were used for both materials. The residual soil has a dilatant behavior during shearing, so drained parameters were used for this material.

4 RESULTS

The FS calculated are shown in Table 2. There are significant differences between the FS values calculated by different methods and for different types of surfaces. The circular calculated values considering LEM method were equal to 1.50. The non-circular FS, in both LEM software, were higher than 1.30. The FS calculated with SSR and non-circular optimized LEM solutions, were lower than 1.30. The optimization process reduces the FS in 19.33% in both software.

Table 2. FS resume

Software	Surface	FS
Slide2 (Roscience)	Circular	1.50
	Non-circular	1.33
	Non-circular optimized	1.21
GeoStudio2020 (GEO-SLOPE)	Circular	1.50
	Non-circular	1.35
	Non-circular optimized	1.21
FLAC-Slope 8.1 (ITASCA)	SSR	1.26

As shown in Figures 2-4 the failure surface obtained from SSR method is geometrically similar to the non-circular optimized in both software and the circular surfaces are geometrically different from all the other surfaces. This behavior is expected due to the presence of ai thin layer of low resistance soil in the foundation where the use of a non-circular surface is more suitable to represent the failure surface. The SSR solution provides a shear strain zone where the maximum increment is associated with the failure surface, as shown in this study.

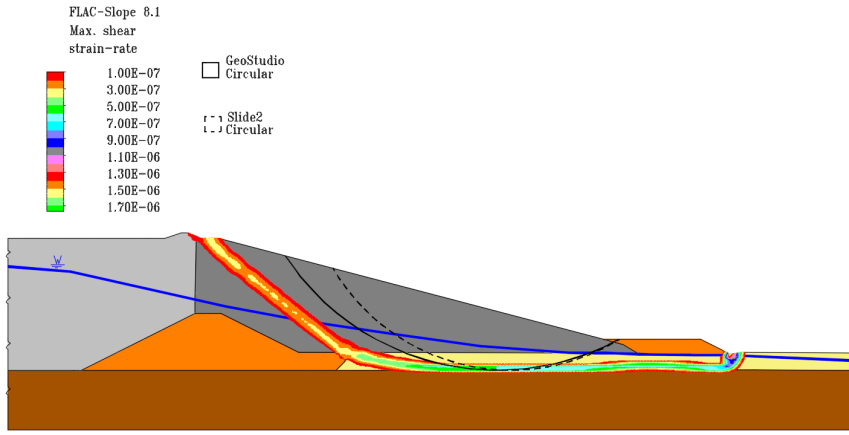

Figure 2. Comparison between circular probably failure surface and SSR max shear strain rate.

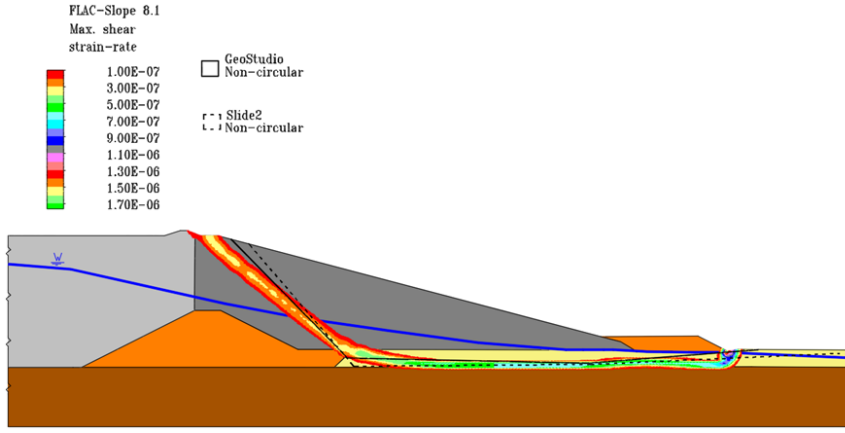

Figure 3. Comparison between non-circular probably failure surface and SSR max shear strain rate.

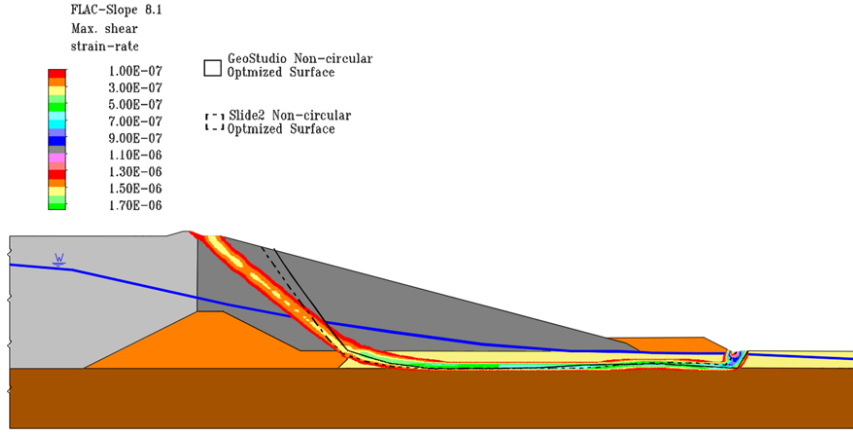

Figure 4. Comparison between non-circular optimized probably failure surface and SSR max shear strain rate.

During analysis of the SSR solution, shown in Figures 2-4, the shear strain can be seen increasing from the dam crest until it reaches the toe of the dam downstream from the crest. This behavior is expected in this scenario, once the low resistance in the foundation creates a preferential failure path. This analysis can be expanded to the non-circular optimized surfaces which are geometrically similar, even though they present with lower FS values. The circular surfaces, as mentioned by Duncan and Wright (2005), are recommended for homogeneous and isotropic structures. In the analyzed dam, the low resistance colluvium layer makes the application of this type of surface not indicated.

Based on current Brazilian regulations and recommendations, this structure would meet the minimum FS stablished on resolution n°13 by ANM and ABNT NBR 13.028 if considered the circular surface (FS ≥ 1.50). If the non-circular surface were considered, the analyzed structure would meet the minimum FS of resolution n° 13 by ANM (FS ≥ 1.30), but it would not meet the minimum FS defined by ABNT NBR 13.028 (FS ≥ 1.50). The structure would not meet the minimum FS set by both Brazilian regulations when analyzed by the SSR and LEM associated with optimized non-circular surfaces. The difference between the calculated values in FS may be as high as 20%.

5 CONCLUSION

As shown by the results, if the designer considered only the LEM method associated with circular surfaces to calculate the FS, the structure would meet the minimum FS according to ABNT recommendations and the ANM regulations (FS ≥ 1.50). When considering the LEM method associated with the non-circular surface, the dam would not meet the minimum FS according to the ANM resolution n° 13 (FS ≥ 1,30). If the same dam was analyzed considering the LEM method associated with optimized non-circular surfaces or the SSR method, the dam would not meet the minimum FS according to ABNT recommendation and ANM regulation (FS < 1.30).

When analyzing the geometry of the failure surfaces between both methods, the failure surface obtained using the LEM, associated with an optimized non-circular surface, has a geometry similar to the failure surface obtained with the SSR method. For the problem in question, these failure surfaces were able to adequately estimate the failure surface, resulting in a more realistic value for FS.

A comparison between the failure surfaces shows the importance of a proper selection of the selected failure surface type when calculating the dam FS. The colluvium layer under the dam creates a preferential path of the failure surface, changing the boundary conditions and, consequently, the necessary method to establish the FS value. For the evaluated scenario it would be recommended to use the SSR method or the LEM associated with the optimized non-circular surface to better estimate the FS.

It is extremely important to evaluate all possible failure surfaces when evaluating dam safety. As shown, the SSR method is an important tool to ensure the minimum FS, calculating the failure surface without any assumption of type of potential failure surface.

It is worth mentioning that, in Brazil, ABNT NBR 13.028/2017 recommendations and ANM resolution nº 13 both state that the designer is responsible for defining the minimum factor of safety for the structure. The authors strongly believe that the minimum or target factor of safety must be defined based on the variable aspects in each dam's formation.

6 ACKNOWLEDGMENT

The authors would like to thank Pimenta de Ávila for creating an environment that encourages technical development and a special thanks to Joaquim Pimenta de Ávila for his support in the development of this article.

REFERENCES

Abramson, L. W.; Sharma, S.; Boyce, G. M. (2º ed.) 2005 *Slope Stability and Stabilization Methods*. Hoboken: Wiley.

Agência Nacional de Mineração – Resolução nº 13, August 2019. Accessed in 07/11/2020. Available in: http://antigo.anm.gov.br/portal/assuntos/barragens/resolucao-anm-no-13-de-8-de-agosto-de-2019.pdf/view.

Associação Brasileira de Normas Técnicas – ABNT NBR 13028. Mining — Preparation and presentation of design of tailings, sediments and/or water dams — Requirements. November 2011, 3º ed, Rio de Janeiro - BR.

Cheng, Y. M., Lansivaara, T., & Wei, W. B. (2007). Two-dimensional slope stability analysis by limit equilibrium and strength reduction methods. *Computers and Geotechnics*, 34(3), 137–150.

Duncan, J. M.; Wright, S. G. (2º ed) 2005 Soil Strength and Slope Stability, Hoboken: Wiley.

GEO-SLOPE. 2015. *Stability Modeling with SLOPE/W An Engineering Methodology*. Calgary: Canada.

Herza J.; Ashley M.; Thorp J. 2017. Factor of Safety? – Do We Use It correctly? *ANCOLD Conference*.

Krahn J. The 2001 R.M. Hardy Lecture; the limits of limit equilibrium analysis. *Canadian Geotechnical Journal* 2003;40(3):643–60.

Ladd, C.C. 1991. Stability evaluation during staged construction. The 22nd Karl Terzaghi Lecture, Boston, 1986, *Journal of Geotechnics* Eng., ASCE, Vol. 117: pp. 537-615.

Mafra, José M. Q. 2016. Barragem construída com rejeito ciclonado: uma possível solução para disposição de rejeitos no Brasil? *XVIII Congresso Brasileiro de Mecânica dos Solos e Engenharia Geotécnica., COMBRAMSEG*. pp. 19-22.

Matsui, T.; San, K.C. 1992. Finite element slope stability analysis by shear strength reduction technique. Soils and Foundations, *Japanese Society of Soil Mechanics and Foundation Engineering*. Vol. 32, (1): pp. 59-70.

Morgenstern, N.R. 1992 The evaluation of slope stability – a 25 year perspective. Stability and performance of slopes and embankments – II, *Geotechnical Special Publication* No. 31, ASCE; 1992.

Ramin Mafi, Sina Javankhoshdel, Brigid Cami, Reza Jamshidi Chenari & Amir H. Gandomi (2020): Surface altering optimisation in slope stability analysis with non-circular failure for random limit equilibrium method, *Georisk: Assessment and Management of Risk for Engineered Systems and Geohazards*.

Stability Assessment of a Tailings Dam with Frozen Tailings

Paul M. Bedell
Golder Associates Ltd., Vancouver, BC, Canada

Maria "Mavi" Sanin
Golder Associates Ltd., Vancouver, BC, Canada

Chris Hiemstra
Centerra Gold Inc., Kemess Mine (formerly of Endako Mine), BC, Canada

ABSTRACT: This paper describes the approach and key considerations for the stability assessment of a tailings dam at the Endako Mine in north central British Columbia. An interesting component in the stability assessment was the presence of a zone of frozen tailings in the dam and the upstream tailings. The frozen tailings contained well-bonded ice in the dam and deposited tailings; no visible ice is present in the dams. This zone is "artificial permafrost", is relatively warm as it is just below 0ºC and is as a result of winter deposition operations.

The stability assessment of Tailings Pond 2 was recently updated as an input into the closure planning for the tailings facility. The stability assessment focused on the liquefaction susceptibility of the tailings both in the dam and upstream of it. Current industry-recognized seismic and liquefaction potential approaches were used as part of the stability assessment. A detailed geotechnical investigation, including boreholes, cone penetration testing, and sample recovery and laboratory testing, was carried out prior to the stability assessment. The methodology outlined in Thornley et al. (2017) was applied for the frozen tailings; the characterization and consideration of the zone of frozen tailings in the stability assessment will be discussed in this paper. The results of the stability assessment show that the minimum required factors of safety are provided for the dams.

1 INTRODUCTION

The Endako Mine is in north-central British Columbia, Canada, about 20 km from Fraser Lake, 155 km from Prince George, and 550 km from Vancouver as the crow flies. Operations at the mine began in 1965 to exploit molybdenum from open pits. Tailings were produced and transported as slurry to the three tailings facilities, Tailings Ponds 1, 2, and 3; Figure 1 shows the site layout.

The tailings were deposited amongst the three tailings facilities throughout operations to support water management and reclaim water clarity and to limit dam raising rates (the maximum rate of dam raising is estimated to be in the order of 5 m per year. Tailings Ponds 1 and 3 were eventually transitioned into a single facility. Tailings Pond 2 reached its storage capacity in 2012 and tailings were deposited solely into Tailings Ponds 1 and 3 thereafter.

Deposition activities required regular dam raising; the rockfill starter dams of the various perimeter dams were raised upstream using the sand fraction of the tailings; cycloned initially and segregated thereafter for each of the perimeter dams. Dam construction was typically carried out between March and November of each year to support deposition and water management activities. Underdrainage for the dams is provided by drainage blankets and finger drains. Minimum freeboard and beach length requirements were in-place during operations and continue to-date.

The processing rates of the process plant varied over time from 11,000 tonnes per day (tpd) during early operations to as high as 24,000 tpd to 28,000 tpd during the 1990s to 2012; the processing rate from 2012 to 2014 was 55,000 tpd with the new process plant. The processing rates varied throughout operations because of low commodity prices, including a suspension from 1982 to 1986, and the new process plant being brought online in 2012. Operations were ceased again at the end of 2014 because of low commodity prices and the site entered care and maintenance in mid-2015. Regular monitoring, inspections, and water management (for provide minimum freeboard and beach length requirements) continue to-date.

Figure 1. Site layout of tailings storage facilities.

As a result of the storage capacity of Tailings Pond 2 having been achieved in 2012, its closure design and planning is in-progress. A component of this work included a detailed geotechnical investigation, including geotechnical drilling and sampling, seismic cone penetration testing (SCPT) and laboratory testing, to characterize the tailings, and a stability assessment of the perimeter dams; this stability assessment is the focus of this paper. An interesting component in the stability assessment was the identification and characterization of zones of frozen tailings in both the dams and the upstream tailings; this zone is considered to be "artificial permafrost" and is the result of winter deposition operations and dam raising activities during freezing conditions.

2 SITE CHARACTERISTICS

2.1 *Site Location and Climate*

The site is located at 54º2'5"N and 125º6'6"W with the process plant sitting at about elevation 1,000 m above sea level (masl). The Endako Mine is located on the Nechako Plateau; the plateau ranges in elevation between about 850 masl, and 1,500 masl.

The Endako Mine is characterized by a continental climate having cold, snowy winters and cool to warm summers. Snowfall is typically experienced between late October and early May with averages up to 0.42 m for December and January; annual total average snowfall is in the order of 1.8 m. Average annual rainfall is about 0.35 m with rainfall experienced throughout the year. Maximum average daily rainfall is experienced from May to October, inclusive, with values between 0.04 m to 0.06 m.

The average daily temperate is about 4ºC. Average daily freezing temperatures are experienced between November and March; the coldest months are January, February, and December which

have average daily temperatures of about -8ºC, -10ºC, and -6ºC, respectively. The site experiences about 1,200 freezing degree days per year. The maximum average daily temperature, typically experienced in July and August, is 15ºC. There is no naturally occurring permafrost within the Endako Mine; areas of alpine permafrost are present at much higher elevations in the region.

2.2 *Seismicity*

A seismic hazard assessment was carried out for the Endako Mine. The site is "Class C" as defined by the National Building Code of Canada. The peak ground acceleration (PGA) and moment magnitude are 0.077g and 7.4, respectively. The return period, based on guidance from CDA (2019) is halfway between the 1-in-2,475 year and 1-in-10,000 year; namely, 1-in-6,238 year.

It is noted that a site-specific hazard assessment will be required for the full closure design.

3 TAILINGS POND 2

3.1 *Description*

Tailings Pond 2 comprises three perimeter dams: South Dam, East Dam, and Saddle Dam; refer to Figure 2. Each of these dams comprise a rockfill starter dam and drainage elements (finger and blanket drains). The starter dams were raised upstream throughout operations to support deposition and water reclaim operations. The initial dam raises were carried out by placing cycloned tailings; later raises were carried out by using the coarser tailings fraction obtained from the tailings segregated during deposition.

3.2 *Tailings Distribution and Deposition System*

Tailings deposition included the delivery of slurry to the crest in a 1.0 m diameter steel pipe header with spigots spaced about every 10 m along the length of the dam. The spigots were used during warmer months, typically from March to November, in support of dam construction. The coarser fraction of the tailings segregated from the flows from the spigots; this material was used for dam construction; the finer fraction was deposited upstream of the dams. Large diameter (1.0 m) overflows were spaced at select locations along the dams to enable deposition of the slurry during winter months; the use of the overflows enabled deposition during winter to make use of the dam raising operations carried out during the warmer months. Figure 3 shows the typical setup of a header, several spigots, and an overflow for deposition from the dam crest.

3.3 *Dam Raising Description*

Dam raising including bulldozing the coarse tailings from the beach back towards the dam crest to form a berm; this comprised a raising bench of the dam. Deposition and additional tailing segregation was carried out "up and over" the berm. After a defined height of berming had been achieved, a defined step-in towards the upstream was made and the tailings distribution and deposition pipelines were moved. This construction method and configuration resulted in an overall dam slope of about six horizontal to one vertical (6H:1V) or about 10 degrees. The South Dam, the highest structure of Tailings Pond 2, has a maximum height of 147 m; see Figure 4. The average maximum rate of dam raise construction is estimated to be in the order of 5 m per year.

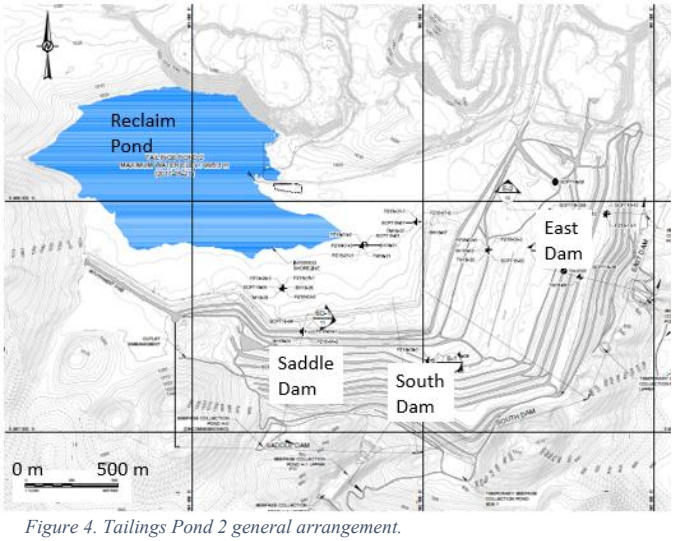

Figure 4. Tailings Pond 2 general arrangement.

Figure 3. Typical dam crest tailings distribution and deposition piping configuration.

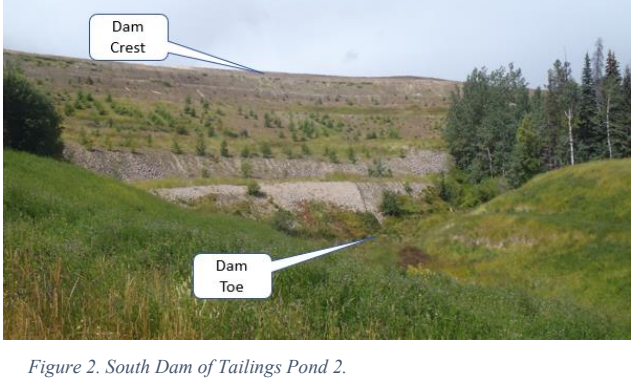

Figure 2. South Dam of Tailings Pond 2.

3.4 *Consequence Classification*

All dams in British Columbia are required by BCMEMPR to have their consequence classification determined using CDA (2019). The consequence classification is also used to obtain guidance for design and assessment loadings and conditions from CDA (2019). The dams of Tailings Pond 2 have a consequence classification of "high"; this determination is based on the results of a dam break and inundation study and discussions with various stakeholders.

3.5 *Proceeding to Facility Closure*

With the storage capacity of Tailings Pond 2 being achieved in 2012, the tailings facility could no longer receive tailings and closure design and planning was started. Water management, comprising the monitoring and control of the reclaim pond, has continued to-date such that the minimum required freeboard and beach length requirements are provided at all time.

With reference to CDA (2019), Tailings Pond 2 is in the "closure—active care" phase in the life of a tailings dam. In consideration of limited characterization of the tailings, both deposited and placed within the dam during raising, current loading conditions for stability assessments, and current state of practice for geotechnical characterization and stability modelling, a detailed geotechnical investigation and laboratory testing program was carried out. The results from the geotechnical investigation were then used for the stability assessment.

4 GEOTECHNICAL INVESTIGATION

Previous investigations carried out for the design and development of Tailings Pond 2 provided sufficient characterization of the foundation of the dams; however, a complete characterization of the tailings within the dams and deposited in the tailings facility was not possible with the existing information. To enable a complete characterization of theses tailings, a detailed geotechnical investigation, comprising boreholes, sampling, standard penetration testing (SPT) and SCPT, was carried out. Six boreholes and 11 SCPTs were advanced. Standard penetration testing and Shelby tube sampling was carried out. Vane shear tests were also carried out during drilling operations. Vibrating wire piezometers were installed at seven locations; several of these were nested to enable the evaluation of vertical gradients.

Nine thermistors were installed to measure the temperature profiles of the frozen tailings. These were installed such that thermistor strings could be installed and removed, as appropriate, to reduce the number of thermistor strings to be read at any time. Two thermistor strings were installed during the geotechnical investigation; ongoing monitoring will determine when it is appropriate to relocate the strings to different locations.

4.1 *Materials Encountered*

4.1.1 *Tailings*

The tailings were classified into two material types based on their respective grain sizes: coarse-grained and fine-grained. Typically, the dams comprise coarse-grained tailings and their associated properties.

4.1.2 *Frozen Tailings*

Frozen tailings were encountered during the geotechnical investigation. The presence of frozen tailings was expected based on investigations in Tailings Ponds 1 and 2 during 2001, 2003, and 2009; however, these were expected to be limited in extent. It is noted that no physical sampling of the frozen tailings was carried out in these earlier investigations.

Zones of frozen tailings were encountered during the 2018 geotechnical investigation. Samples were obtained and thermistors were installed at select locations. In general, the frozen tailings were encountered upstream of the dam crests (i.e., within the deposited tailings) or beneath the existing dam crests. The frozen tailings were encountered some 9.4 m to 16.5 m below existing ground surface and extended between 8.7 m to 31.8 m in thickness; these extents are greater than

those previously identified. The frozen tailings were well-bonded with no visible or excess ice. Some ice lenses were encountered within the deposited tailings well upstream of the dams. The average salinity of the pore water was within the range of fresh water, thereby indicating a freezing point of about 0ºC.

The frozen tailings are due to tailings deposition during winter and early spring dam raise construction. Dam raise construction in the early spring would have trapped frozen tailings and near-dam ice along the highly saturated downstream limit of the beach. The tailings placed over these frozen materials would serve to insulate them, thereby disabling their ability to thaw. The frozen tailings are, therefore, considered to be "artificial permafrost". Permafrost is defined as ground (rock, soil, or, in this case, tailings) at or below 0ºC for a continuous period of at least two

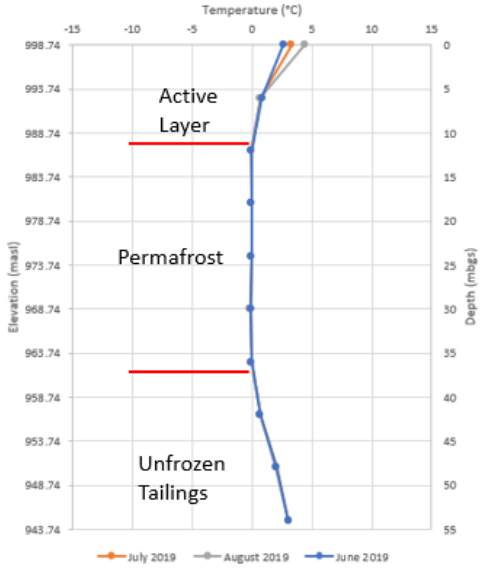

Figure 5. Typical thermistor profile through frozen tailings.

years. The frozen tailings in Tailings Pond 2 are estimated to have been frozen for some 10 to 16 years. The frozen tailings are "warm permafrost" as their temperature, below the active layer, is just below 0ºC; see Figure 5. The active layer is the near-surface zone in permafrost that seasonally freezes and thaws. A typical nodal temperature timeline for one of the thermistor installations is shown in Figure 6; the seasonal effects of air temperature are seen for the shallower nodes but the deeper nodes are insulated by the overlying tailings and their temperatures are constant throughout the year; these are typical results for permafrost conditions.

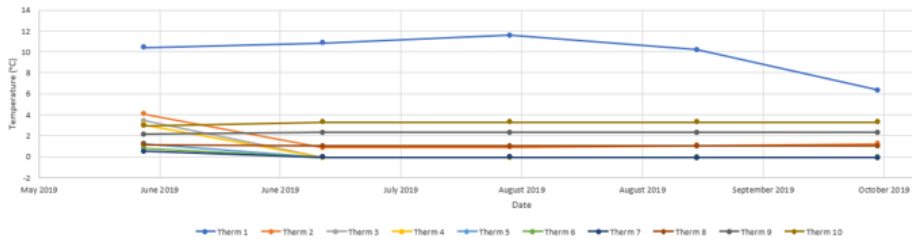

Figure 6. Typical thermistor nodal temperature timeline. Increasing node numbers correspond to increasing depths.

4.1.3 *Dam Foundation*

The foundation materials consist of soft silt to clay, having a thickness of about 2 m, of medium to high plasticity overlying dense till. No laboratory testing of these materials was carried out as part of the 2018 geotechnical investigation; all boreholes were terminated in these materials. The results from the previous investigations, as noted above, were used to characterize these materials.

4.2 *Laboratory Testing Program*

The samples obtained during the geotechnical investigation were sealed and shipped for laboratory testing. Typical index testing (water content, grain size, specific gravity, Atterberg limits, unit weight, and maximum and minimum densities) was carried out in general accordance with the relevant ASTM International (ASTM) standards.

Advanced geotechnical testing was also carried out to determine strength parameters and liquefaction potential assessment using critical state approaches. The advanced testing comprised cyclic simple shear, direct shear, and critical state determination (i.e, triaxial compression testing). The triaxial compression testing was carried out following the recommendations of Jefferies and Been (2016) and in general accordance with ASTM International standards ASTM D7181-11 and D4767-11.

4.3 *Characterization of Materials*

4.3.1 *Tailings*

The materials encountered in Tailings Pond 2 include mainly two types of tailings; namely, coarse-grained tailings and fine-grained tailings. While the distribution of the tailings is generally layered with interbedded layers of coarse- and fine-grained tailings, visual observations during borehole logging, interpretation of the CPTs, and results of the laboratory testing allowed to identify zones with predominantly coarse-grained or predominantly fine grained tailings. Figure 8 presents the range of grain size distribution of the tailings of Tailings Pond 2 for each of the coarse- and fine-grained tailings. Laboratory index testing was carried out to characterize the tailings according to the grain size and the mechanical behaviour. The tailings were then defined in the laboratory based on composite samples of the coarse- and fine-grained tailings.

4.3.1.1 Coarse-Grained Tailings

Coarse-grained tailings are predominantly composed of non- to low-plastic, compact to dense silty sand materials with fine content ranging from about 10% to 45% as shown in Figure 7. Predominantly compact to dense coarse-grained tailings were encountered in the shell of the East Dam, and upper 10 m to 20 m of the Saddle Dam.

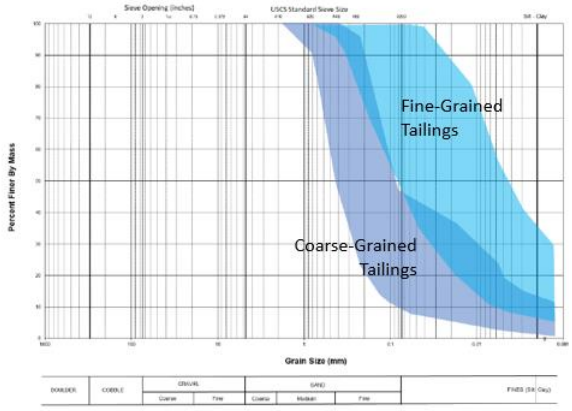

Figure 7. Grains size distributions of tailings.

The critical state locus (CSL) of the coarse-grained tailings was measured in the laboratory following the methodology presented in Jefferies and Been (2016).

The cyclic resistance ratio of the coarse-grained tailings was measured from cyclic simple shear (CSS) testing for two different densities representative of what was encountered in the field.

4.3.1.2 Fine-Grained Tailings

Fine-grained tailings are predominantly composed of low to high plasticity, silt to silt and clay, with ranging consistency from soft to stiff. Fines content range from about 50% to 100% as shown in Figure 7. Predominantly silty tailings with medium to high plasticity were encountered upstream of the Tailings Pond 2 Dams, close to the pond. Interbedded layers of fines were encountered in the shell of the Saddle Dam and the South Dam.

4.3.1.3 Frozen Tailings

Frozen tailings were encountered during the field investigation in all the boreholes except one. The frozen materials were identified during the geotechnical investigation for their extent and described. Identification of the presence of frozen layers was used to validate the interpretation of the SCPTs carried out in the vicinity of each borehole.

The water content of the frozen tailings was measured in situ to avoid loss of water during transportation.

4.3.1.4 Foundation Materials

The interpreted friction angles from the previous investigations for soft silt to clay (fine foundation materials) ranged between about 25 degrees and 30 degrees. The interpreted average friction angle for glacial till foundation materials is 35 degrees.

Bedrock was not encountered in the SCPT holes and boreholes, but it was encountered in test pits conducted at the Southwest Dike of the right abutment of Pond 2 Dams; a discussion of the test pits is not presented in this paper.

5 LIQUEFACTION SUSCEPTIBILITY ASSESSMENT

A key component to input into the stability assessment is the characterization of the materials, including strength parameters and liquefaction susceptibility assessment results. Loose saturated granular soils and tailings tend to contract when subjected to cyclic loading. Contraction of these materials causes an increase in excess pore water pressures and associated decrease in effective stresses. The result is loss of strength and stiffness that contributes to large deformations, or liquefaction. Liquefaction can lead to slope failure, potential dam overtopping, and internal erosion. The Health, Safety and Reclamation Code for Mines in British Columbia (HSRC) Guidance Document (BCMEMPR 2016) and Canadian Dam Association (CDA 2007, 2013, and 2019) recommend the evaluation of liquefaction potential of dams as a failure mode as part of the dam global stability.

The liquefaction susceptibility assessment of Tailings Pond 2 was carried out using the recommended procedure presented by Idriss and Boulanger (2008) and the approach presented by Jefferies and Been (2016). Both methods are stress-based approaches and are based on the results of the geotechnical investigation. The stress-based approach compares the earthquake induced cyclic stress with the cyclic strength of the tailings. The earthquake-induced stresses and the cyclic resistance are normalized with respect to the vertical effective consolidation stress to obtain the induced cyclic stress ratio (CSR) and the cyclic resistance ratio (CRR). The factor of safety against liquefaction (FS_{Liq}) is calculated as follows:

$$FS_{Liq} = \frac{CRR}{\mathrm{CSR}}$$

If FS_{Liq} is less than 1, the tailings are susceptible to liquefaction.

The cyclic resistance of the tailings was also measured in the laboratory with cyclic simple shear (CSS) testing and used to compare the results of the CRR estimated from the stress-based approach.

5.1.1 *Earthquake-Induced Cyclic Stress Ratio*

The earthquake-induced CSR was estimated using the Seed and Idriss simplified procedure as described in Idriss and Boulanger (2008). This approach is generally valid for depths that are less than about 20 m. The depth of the Tailings Pond 2 is greater than 20 m. However, for completeness, the analysis was carried out using the simplified method, and the results were compared and validated by other methods.

The tailing materials are assumed to be fully saturated below the phreatic surface interpolated from piezometric readings and SEEP/W analysis.

5.2 *Cyclic Resistance Ratio (CRR)*

5.2.1.1 CRR from Field Penetration Data (SCPT and SPT)

The CRR of non-plastic soils and tailings is generally obtained with semi-empirical relationships developed from in situ testing compiled from case histories where liquefaction has or has not been observed. The analysis for Tailings Pond 2 used the procedure presented in Idriss and Boulanger (2004 and 2008) to estimate the CRR of non-plastic soils using cone penetration test (CPT) and standard penetration test (SPT) data

The estimated CRR was corrected for fines content using average fines content measurements from laboratory testing of samples collected during field investigation; for earthquake magnitude and effective overburden stress.

5.3 *CRR Using the Critical State Approach*

The critical state parameters of coarse and fine tailings for Tailings Pond 2 were determined following the methodology presented in Jefferies and Been (2016). Triaxial specimens tested to determine the critical state locus (CSL) were reconstituted using the moist tamping method to different densities and consolidated isotropically to a range of confining stresses (100 kPa to 800 kPa). Once consolidated, the specimens were sheared under both drained and undrained conditions. The critical state of a soil is the state at which the soil continues to deform at constant stress and constant void ratio. After reaching the critical state, accurate moisture contents were determined by freezing the samples. The critical state locus was defined by the conventional (semi-log, linear) and improved (curved) idealization models presented by Jefferies and Been (2016). The models relate the void ratio at the critical state, to the mean effective stress.

The in situ state of a soil relative to the critical state is defined as the difference between the in situ void ratio, e, and the critical void ratio, e_c, at the in situ mean effective stress. This difference is referred to as the state parameter (ψ):

$$\psi = e - e_c$$

A positive state parameter indicates the soil has a contractive behaviour when sheared. A negative state parameter indicates the soil has a dilative behaviour when sheared. SCPT data was used to estimate profiles of state parameter (Jefferies and Been 2016) of materials using the Shuttle and Cunning (2007) method.

The CRR was then obtained from the state parameter as summarized in Jefferies and Been (2016) as:

$$CRR = 0.06\, e^{-9 \cdot \psi}$$

State parameters of tailings were also calculated using unit weights measurements on Shelby tube samples collected in the geotechnical investigation.

5.4 *CRR from Cyclic Simple Shear Testing*

The cyclic responses of the fine- and coarse-grained tailings were measured with constant volume cyclic simple shear (CSS) tests for two different densities representative of the density measured for the tailings from Shelby tubes and the corresponding confining stress levels where the materials were encountered.

The procedure for earthquake load characterization and laboratory-based liquefaction resistance (Idriss and Boulanger 2008) suggests that, depending on the magnitude of the earthquake, the CRR can be represented in the laboratory by a number of uniform loading cycles. For an earthquake with magnitude M7.4, the number of equivalent loading cycles is about 15 cycles for sand-like soils (Idriss and Boulanger 2008). Accordingly, cyclic stress ratios (CSR) were plotted against the number of cycles to trigger liquefaction (N_L) for each sample. The CRR is obtained as the CSR required to trigger liquefaction in 15 cycles. Figure 8 presents the estimated CRR from laboratory testing for coarse- and fine-grained tailings.

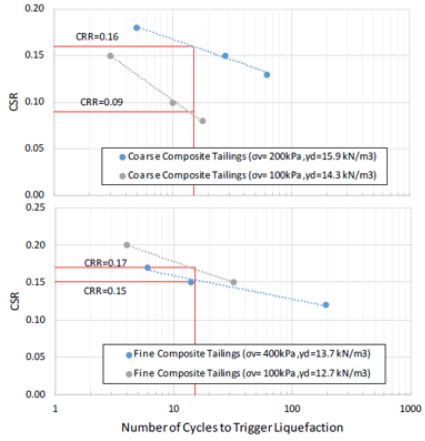

Figure 8. Cyclic resistance ratios of coarse-grained (upper) and fine-grained (lower) tailings.

5.5 *CRR of Frozen Tailings Using Thornley et al. (2017) Approach*

Tailings, when frozen, are not susceptible to liquefaction. However, thawed tailings might be susceptible to liquefaction during earthquake load.

SCPT tip resistances, SPT blow-counts, and shear wave velocity (Vs) readings can be elevated in frozen materials when compared to thawed materials; hence, the measured penetration resistance in frozen tailings may not be representative for tailings in thawed conditions.

Liquefaction assessment of frozen layers when thawed was conducted using the approach recommended by Thornley et al. (2017). This approach estimates the in situ density of thawed tailings from the in situ water content of frozen samples below the ground water level, and assumes the volume does not change as the material goes from frozen to thawed state. Below is summary of procedure recommended by Thornley et al. (2017):

- Calculate in situ void ratio, e for tailings located below phreatic surface from measured water content, W_c, and specific gravity, G_s, assume tailings are fully saturated:

$$e = W_c . G_s$$

- Calculate relative density, D_r, for tailings samples from calculated void ratio, maximum void ratio, e_{max}, and minimum void ratio, e_{min}:

$$D_r = \frac{e_{max} - e}{e_{max} - e}$$

Where e_{max} and e_{min} are determined in the laboratory.

- Calculate blow counts of thawed soils $(N_1)_{60}$ using Skempton (1986) relationship:

$$(N_1)_{60} = 46 * D_r{}^2$$

- Calculate CRR for frozen layers which will undergo thawing in the future using the calculated $(N1)_{60}$ and semi-empirical method.

5.6 *Results of Liquefaction Susceptibility Assessment*

The liquefaction susceptibility of the coarse- and fine-grained tailings materials from Tailings Pond 2 was evaluated.

The results of liquefaction assessment showed that saturated tailings materials of the dam shells have mostly negative state parameters. Furthermore, the calculated CRR of saturated tailings using various methods are greater than the estimated CSR. Hence, tailings in those SCPT locations are not likely to liquefy during an earthquake event with a return period of halfway between 1 in 2,475 and 1 in 10,000 years.

The results of the liquefaction assessment upstream of the dams, towards the tailings pond, show that layers of saturated tailings have positive state parameters which indicate the presence of contractive materials (loose). The calculated CRR from state parameter approach, for saturated tailing layers with $\Psi > 0$, is found to be lower than the CSR. However, the CRR calculated using semi-empirical method by Boulanger and Idriss (2004) approach show that the CRR is higher than the CSR. Given that the semi-empirical method by Boulanger and Idriss (2004) has not been validated for materials below 20 m depth, and that the state parameter approach intrinsically accounts for the mechanical behaviour of the material, the saturated contractive layers encountered were considered to be susceptible to liquefaction during an earthquake event with a return period of halfway between 1 in 2,475 and 1 in 10,000 years.

The cyclic resistance ratio calculated using Thornley et al. (2017) approach for frozen tailings showed generally lower values when compared to CRR calculated using field SPT data (Boulanger and Idriss 2004). The discrepancy may be a result of the assumption that there is no volume change, and therefore no densification, during thawing.

6 SLOPE STABILITY ASSESSMENT

6.1 *Minimum Requirements*

The design criteria for the slope stability are based on the HSRC Guidance Document (BCMEMPR 2016). The HSRC Guidance Document provides minimum static slope stability factor of safety and return periods for earthquake design ground motion for tailings dams based on the dam consequence classification. The HRSC Guidance Document refers to the CDA Dam Safety Guidelines for further context and guidance where design criteria are not included in the HSRC. The minimum factors of recommended for a dam under static and seismic conditions are presented in Table 1.

Table 1. Minimum Required Factors of Safety for Slope Stability Assessment.

Load Type	Loading Condition	Minimum Factor of Safety
Static	Long-term (steady seepage state)	1.5
Seismic	Psuedo-static	1.0
	Post-earthquake	1.2

The stability analyses were completed for select sections for static, pseudo-static, and post-liquefaction (where required) loading conditions using the slope stability modelling program Slope/W (GEOSLOPE International 2019). The Morgenstern-Price method of slices was employed with the Mohr-Coulomb failure criterion to find potential failure surfaces and their corresponding factor of safety.

6.2 *Stratigraphy and Material Strength Parameters*

Results from the geotechnical investigation were used to identify zones with predominately coarse-grained or fine-grained tailings within the dams' sections. Drained friction angles (ϕ') of the different materials were calculated using both SPT and SCPT data. Kulhawy and Mayne (1990) was used to calculate friction angle friction angle using cone tip resistance. Various methods were also used to calculate friction angles for tailings and foundation materials from SPT data, where available.

The geotechnical strength parameters used for the static, pseudo-static, and post-liquefaction stability analyses are summarized in Table 2. According to the degree of compactness, coarse tailings were separated into dense and compact.

Table 2. Material Strength Parameters use for Stability Modelling.

Material	Unit Weight (kN/m^3)	Shear Strength for Static	Shear Strength for Pseudo-static [(a)]	Shear Strength for Post-liquefaction
Dense Coarse Tailings	20	c' = 0 kPa ϕ'= 35°	c' = 0 kPa ϕ'= 29°	c' = 0 kPa ϕ'= 35°
Compact Coarse Tailings	20	c' = 0 kPa ϕ'= 32°	c' = 0 kPa ϕ'= 27°	c' = 0 kPa ϕ'= 32°
Fine Tailings	19	c' = 0 kPa ϕ'= 31°	c' = 0 kPa ϕ'= 26°	c' = 0 kPa ϕ'= 31°
Fine Foundation Materials	18	c' = 0 kPa ϕ'= 27°	c' = 0 kPa ϕ'= 22°	c' = 0 kPa ϕ'= 27°
Liquefied Tailings	18	N/A	N/A	S_r/σ'_v= 0.05
Glacial Till	22	c' = 19 kPa ϕ'= 35°	c' = 19 kPa ϕ'= 35°	c' = 19 kPa ϕ'= 35°

c' = effective cohesion.
Φ' = effective friction angle.
S_r/σ'_v = normalized residual shear strength.
N/A = not applicable.

For the pseudo-static analysis, the tailings and soft fine-grained foundation materials strengths were reduced to 80% of the peak strength (Hynes-Griffin and Franklin 1984) to account for potential strain softening due to pore pressure generation during cyclic loading. The reduction was only applied to materials that would potentially generate elevated pore pressures during cyclic loading.

The liquefaction of tailings can result in reduction of undrained shear strength due to an increase in excess pore water pressure in the liquefiable layer. The post-liquefaction normalized residual shear strength (S_r/σ'_v) of tailings was calculated using the method summarized by Idriss and Boulanger (2008) and Jefferies and Been (2016). The lower bound of calculated S_r/σ'_v, equal to 0.05, was used in the Slope/W limit equilibrium analysis for post-liquefaction stability scenarios.

6.3 *Stability Analysis Results*

The stability analysis results indicate that the static, pseudo-static, and post-liquefaction slope stability factors of safety for the downstream slopes of Tailings Pond 2 dams meet the requirements of CDA (2013 and 2019) and BCMEMPR (2016).

7 SUMMARY

The liquefaction potential of coarse- and fine-grained tailings encountered at Tailings Pond 2 of the Endako Mine were assessed based on results of a geotechnical investigation that included field and laboratory testing. The liquefaction susceptibility analyses were carried out using the critical state approach proposed by Jefferies and Been (2016) and the method proposed by Idriss and Boulanger (2008 and 2014). The Jefferies and Been approach was preferred for this study because it offers a mechanics-based approach that considers the soil intrinsic properties. This is of importance in soils with high fines content that are susceptible to liquefaction as the method does not depend on correction factors for fines content. Therefore, the conclusions and recommendations presented herein for the liquefaction susceptibility assessment of the low-plasticity silt are based on the results of the Jefferies and Been (2016) approach.

Limit equilibrium analyses to assess the stability of the dams at Tailings Pond 2 were carried out. Results of the liquefaction assessment were incorporated in the post-earthquake slope stability analyses. Results of the analyses are summarized below:

- Coarse- and fine-grained tailings located in the Tailings Pond 2 dam shells have a dilative behaviour, with negative state parameters. The estimated cyclic resistance ratio is greater than the seismically induced cyclic stress ratio, and therefore are not likely to liquefy under the design earthquake loading.
- Coarse and fine-grained tailings located upstream of the Tailings Pond 2 dams, towards the pond, have generally a contractive behaviour with layers of positive state parameters. The estimated cyclic resistance ratio at these locations is less than the seismically induced cyclic stress ratio, and therefore are susceptible to liquefaction under the design earthquake loading.
- Liquefaction susceptibility assessment carried out on layers of frozen tailings encountered in Tailings Pond 2 using Thornley et al (2017) approach indicate that the frozen tailings are not likely to liquefy, when thawed, under the design earthquake loading.
- The static limit equilibrium analysis carried out on four cross-sections of Tailings Pond 2 indicate that the three dams meet the CDA (2013 and 2019) and BCMEMPR (2016) minimum factor of safety recommended for long-term (steady state seepage) loading conditions.
- The pseudo-static and post-earthquake stability assessments carried out on four cross-sections of Tailings Pond 2, indicate that the three dams meet the CDA (2013 and 2014) and BCMEMPR (2016) minimum factor of safety recommended for a design earthquake loading with a return period of half between 2,475 and 10,000 years.

8 REFERENCES

ASTM (ASTM International). 2011a. D4767-11. Standard Test Method for Consolidated Undrained Triaxial Compression Test for Cohesive Soils.

ASTM. 2011b. D7181-11. Method for Consolidated Drained Triaxial Compression Test for Soils.

BCMEMPR (British Columbia Ministry of Energy, Mines & Petroleum Resources). 2016. Guidance Document: Health, Safety and Reclamation Code for Mines in British Columbia. Version 1.0. Updated

July 2016.
CDA (Canadian Dam Association). 2007. Technical Bulletin: Geotechnical Considerations for Dam Safety.
CDA. 2013. Dam Safety Guidelines. Revised 2013.
CDA. 2019. Technical Bulletin: Application of Dam Safety Guidelines to Mining Dams (2019 Edition).
GEOSLOPE (GEOSLOPE International Ltd.). 2019. Stability Modelling with GeoStudio. Calgary AB.
Hynes-Griffin, M.E. and Franklin, A.G. 1984. Rationalizing the Seismic Coefficient Method. U.S. Army Corps of Engineers. July 1984.
Idriss, I.M, and Boulanger, R.W. 2004. Semi-Empirical Procedures for Evaluating Liquefaction Potential During Earthquakes. Proceedings of 11th International Conference on Soil Dynamics and Earthquake Engineering and 3rd International Conference on Earthquake Geotechnical Engineering, (eds. D.Doolin, A.Kammerer, T.Nogami, R.B.Seed, and I.Towhata), Vol. 1, pp. 32-56. Stallion Press.
Idriss, I.M, and Boulanger, R.W. 2008. Soil Liquefaction During Earthquakes. Earthquake Engineering Research.
Jefferies, M. and Been, K. 2016. Soil Liquefaction—A Critical State Approach. Second Edition. Taylor & Francis Group, LLC.
Kulhawy, F.H. and Mayne, P.W. 1990. Manual on Estimating Soil Properties for Foundation Design. Report EPRI EL-6800. Electric Power Research Institute. Palo Alto. 360p.
Shuttle, D.A, and Cunning, J. (2007). Liquefaction Potential of Silts from CPTu. Canadian Geotechnical Journal, 44(1), 142-145.
Thornley, J.D, Moran, N., Daggett, A., and Krzewinski, T.G. 2017. Estimating Liquefaction Potential of Thawing Permafrost Soils, An Evaluation of Frozen and Recently Thawed Soils. 17th International Conference on Cold Regions Engineering. September 10-13, 2017. Duluth, Minnesota.

Deformation and Cracking of an Upstream Gold TSF Embankment Due to Yielding of Underlying Rock

Rynier Shields Pr Eng
Jones & Wagener Engineering & Environmental Consultants, Johannesburg, Gauteng, South Africa

Dr Martin Rust Pr Eng
Jones & Wagener Engineering & Environmental Consultants, Johannesburg, Gauteng, South Africa

Danie Brink Pr Eng
Jones & Wagener Engineering & Environmental Consultants, Johannesburg, Gauteng, South Africa

ABSTRACT: In 2017 signs of distress were noted along an embankment of an active, upstream gold tailings storage facility (TSF) in South Africa. Cracks extended diagonally up and parallel to the slope and increased with time. Bulging was observed at the toe. Deposition on the facility was halted immediately and detailed surveillance was implemented. An investigation ensued to determine the cause and understand the mechanism for the observed TSF behaviour. Possible mechanisms were identified and assessed. It was concluded that yielding of the underlying rock, in turn underlain by highly compressible strata, was the most plausible mechanism. The way forward included assessment of the available geological information to determine if similar conditions exist elsewhere along the TSF embankments. Mitigation and remedial measures were compiled and implemented to restore the TSF to an acceptable and safe condition and the facility was recommissioned in March 2019. Close monitoring of the TSF continues with no further signs of distress to date.

1 INTRODUCTION

The Mispah Tailings Storage Facility (TSF) forms part of Harmony Gold Mining Company Limited's (HGM) Moab Khotsong operations, approximately 4km south east of the Vaal River and 25km south of the town of Klerksdorp, South Africa. The TSF consists of two compartments, Dam 1 and Dam 2. Mispah Dam 1 was commissioned in 1995 and is currently approximately 40m high. The dam was constructed in an upstream ring-dyke manner by conventional day wall deposition methods commonly employed in South Africa. The day wall deposition methodology and its role in the limited extent of the observed deformation is discussed in the paper.

The western flank of Mispah Dam 1 displayed signs of distress in November 2017 in the form of a series of cracks. Note the approximately parallel cracks on

Figure 1-1 which formed and became wider within the first month following an initial crack on the outer wall. Some of these cracks were up to 400m in length and could be observed over the top of the entire facility and exciting at the toe. Bulging was noticed at the toe downstream of the cracked area.

The dam was active at the time of this observation and had been active since commissioning in 1995. Deposition on the facility subsequently stopped in December 2017.

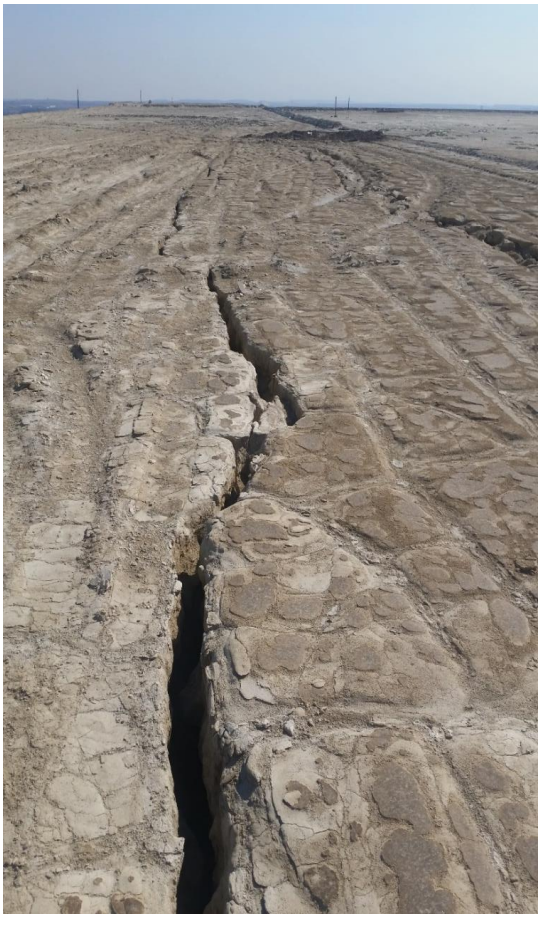

Figure 1-1 Crack formation on the western embankment (day wall)

2 SITE LOCALITY AND DAM DESCRITION

HGM's Moab Khotsong operations are located near the Vaal River, forming the border between the North West and Free State provinces of South Africa. Figure 2-1 shows the layout of the TSF complex with Dam 1 to the north, Dam 2 to the south and the dormant Kopanang Pay Dam (KPD) to the east. Topographically, the highest point of natural ground level is on the south eastern corner of the complex, falling gradually toward the north western corner where the storm- and return water facilities are situated.

The dams are operated using a method referred to as 'Day wall' deposition, commonly used in South Africa. This method entails the formation of a paddock around the outer edge of the tailings dam, approximately 30m wide and ideally approximately 1m higher than the adjacent basin. An example of a daywall is shown in Figure 2-2. Tailings is deposited into these paddocks during the day and into the internal basin at night. The rate of rise (rate of vertical growth) of these types of dams is limited to allow drying out of the day walls. Typically, the maximum allowable rate of rise of such a TSF would be 2m per annum. As an example Mispah 1 was approximately 40m high and had been in operation for 22 years at the time of this event.

The intent of this method of construction is to allow desiccation of tailings in the day wall and the formation of an unsaturated outer wall.

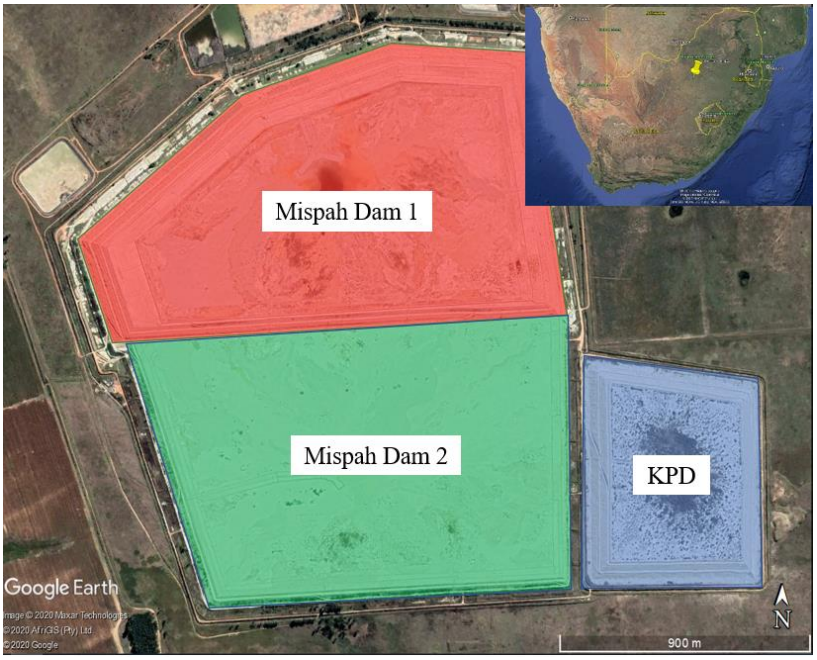

Figure 2-1 Mispah TSF locality plan

Figure 2-2 Day wall on Mispah Dam 2 (Mispah Dam 1 in the background)

3 INVESTIGATION

A site investigation was carried out to determine the cause of the observed cracks. The cracks are shown in Figure 3-1. The cracks extended over the entire western flank of the facility,

approximately 400m in length. Several cracks ran roughly parallel, however, the largest and most persistent of the cracks was found on the western outer wall of the dam.

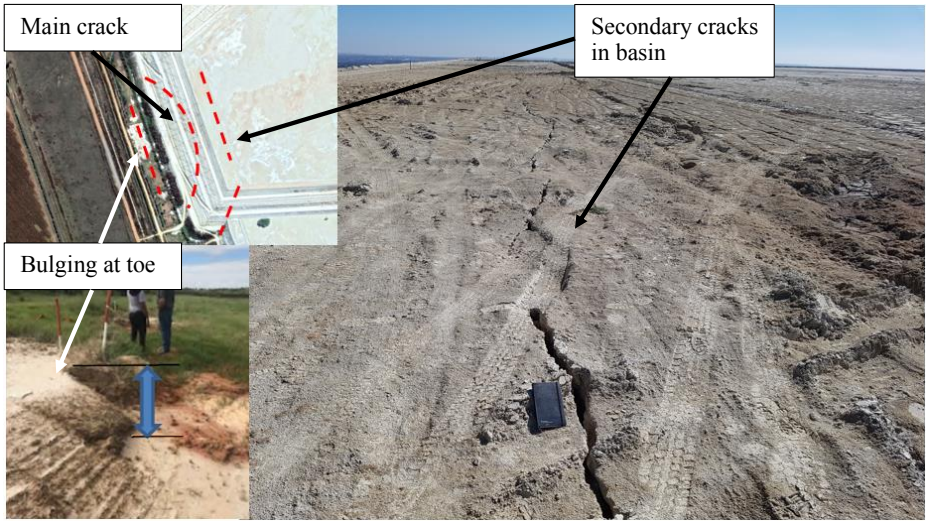

Figure 3-1 Western wall observed cracks

3.1 *Design report of the TSF*

In November 1992 J&W carried out a geotechnical investigation for the proposed Slimes Dam M Vaal Reefs, now known as Mispah Dam 1. The investigation comprised air photo interpretation, the excavation of 53 test pits and the drilling of 30 percussion boreholes. In addition, in situ permeability tests were undertaken and laboratory testing of representative samples took place.

The summary contained within the report indicates the following:

"*It was found that the site is covered by a relatively thick layer of windblown sand overlying residual Karoo rocks and Malmani dolomite of the Transvaal Sequence. The Karoo/dolomite contact roughly coincides with the northern boundary of the farm Mispah. The Karoo cover over the dolomite increases from this boundary in a southerly direction to over 20m thick. The Karoo rocks consist of sandstone and siltstone underlain by diamictite. A number of palaeo-sinkhole features were recognised during the investigation.*

One active sinkhole through Karoo rock was encountered where a palaeo-sinkhole was reactivated by water ingress. There will be a risk of sinkhole formation when a slimes dam is built on the site. By moving the slimes dam to the south, onto the thicker Karoo diamictite cover, the sinkhole risk would be reduced but not eliminated."

And further on:

"*Although there is a risk of sinkhole development on the site, it is the best area available at Vaal Reefs for the construction of a slimes dam.*"

3.2 *Site geology*

According to the published 1:250 000 geological map, sheet 2626 West Rand, much of the Mispah TSF No 1 is underlain by dolomite and chert (Vm) of the Malmani Subgroup, Chuniespoort Group of the Transvaal Supergroup. However, the geological map does indicate, albeit with a dashed line indicating uncertainty, that the south east of the dam is underlain by sandstone, shale and coal beds (Pv) of the Vryheid Formation, Ecca Group, Karoo Supergroup.

Significant diabase, alternatively termed dolerite, intrusions are present to the north east of the site. The regional geology is illustrated in a extract from the 1 : 1 000 000 geological map presented in Figure 3-2.

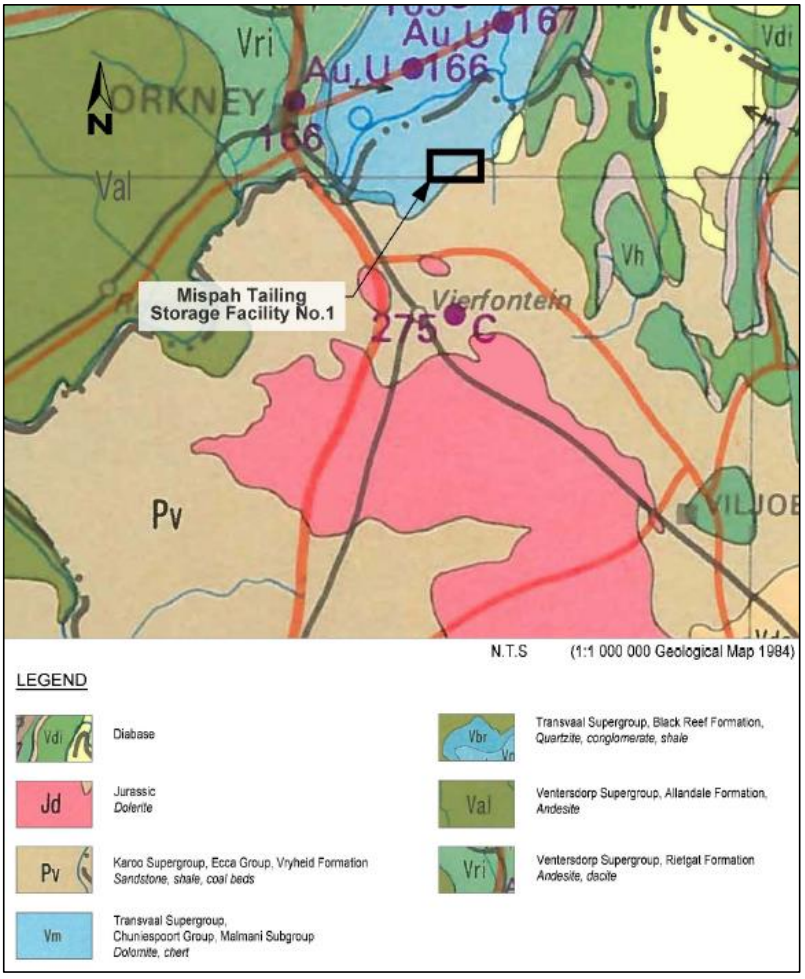

Figure 3-2 Mispah TSF regional geology (Sheet 2626, South African Council of Geoscience)

3.3 *LiDAR surveys*

The extent of the vertical wall movement as well as the period during which the majority of the movement occurred, was determined by comparing the available digital surveys, i.e. 2011, 2014, August 2017, February 2018 and May 2018.

Cross sections of the walls where significant vertical movement was measured for the 2014 to 2018 period were prepared to determine the extent and direction of movement. Figure 3-3 shows the location of the Cross Sections A to F. The maximum vertical and horizontal displacement was measured at Section B; approximately midway along the western wall. A section through the wall in this position is shown in Figure 3-4.

Figure 3-4 shows the change in geometry of the wall from 2011 to May 2018. The following observations can be made from the figure:

- No significant displacement was observed between 2011 and 2014, displacement only apparent in the May 2018 survey.
- The displacement of the slope between the first and second bench was insignificant.
- The displacement of the lower section of the wall was in an outwards and upwards direction.
- The maximum displacement was measured along the slope between the second and third bench. This section moved 2.06 meters towards the inside of the dam and 1.04 meters downwards.
- Bulging occurred in the paddock post the August 2017 survey.
- The wall displacement predominantly took place between 2014 and 2017.

In order to determine whether vertical displacement continued after the main cracking incident and stopping deposition in December 2017, the surveys of February 2018 and May 2018 were compared. Figure 3-5 shows the vertical displacement of Mispah Dam 1. It can be seen that the day-wall along the western flank as well as the northern section of the eastern wall settled between 100mm and 200mm during this period. The settlement of the pool area in the basin of the dam was expected as the area would have dried out and consolidated after deposition stopped.

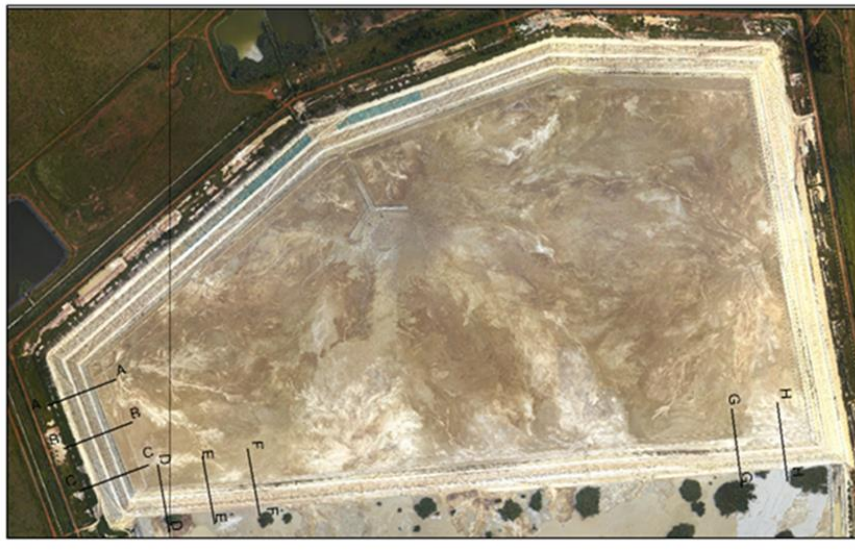

Figure 3-3 Location of cross-sections

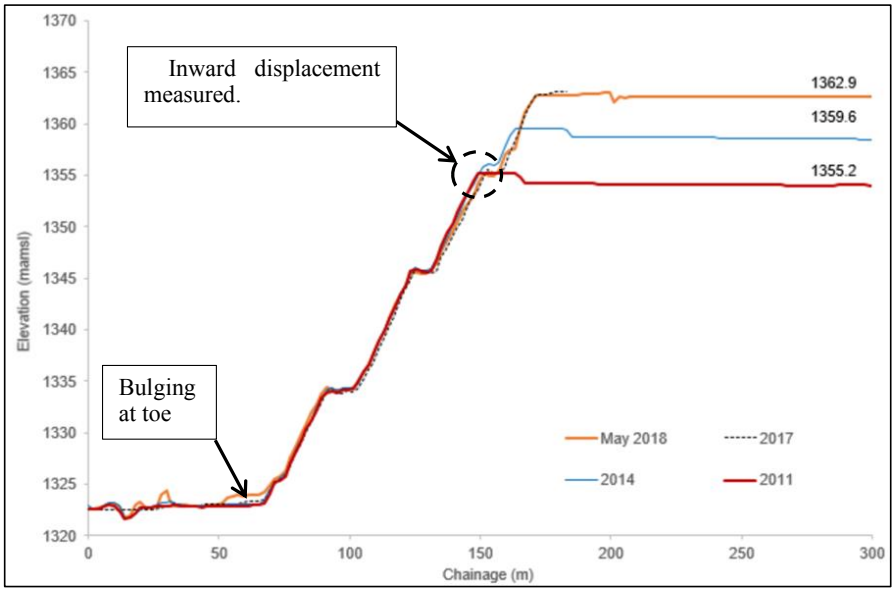

Figure 3-4 Western flank cross-section

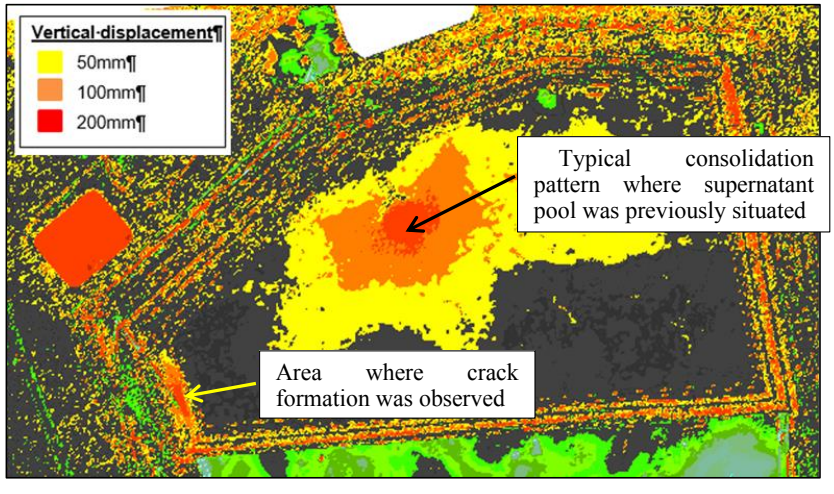

Figure 3-5 Mispah Dam 1 vertical displacement measured between February and May 2018

3.4 *Microgravity survey*

A microgravity survey was conducted around the perimeter of the TSF as anomalies in gravimetric readings are used to indicate changes in the Dolomitic substrate. Experts use the results to identify potential underground cavities or areas with low density. The microgravity survey results showed numerous low residual gravity anomalies which generally occurred along the toe of the western flank. These zones are generally associated with karst features such as preferential weathering of the dolomite bedrock, voids and increased depth to bedrock. Zones of

high gradient gravity variations may also be associated with karst features as it is indicative of strong density and depth variations within the subsurface. Steep gradients were noted in the southern portion of the site, with a zone of high residual gravity flanked by low gravity anomalies north and south of this zone noted.

The previous gravity survey, carried out for Mispah Dam 2, indicated a gravity high along the western boundary of the dam which corresponds to the high gradient encountered in the southern portion of the current survey area. Similarly, a distinct gravity low was noted along the western portion of Mispah Dam 2. This gravity low, coupled with the low gradients noted along the toe of the western flank of Mispah Dam 1, suggests that a low north-south trending gradient extends below the western portion of Mispah Dam 1.

3.5 *Drilling and CPTu testing*

The data gathered during the site investigation was used to prepare an idealised geological cross section (Figure 3-6) of the western flank. The profile consists of tailings, sandy and clayey soils, soft to medium hard Karoo rock, WAD with fragments of Chert and Dolomite followed by soft to medium hard rock Dolomite. The soils overlying the Karoo rock comprise three layers, namely a sandy layer of varying thickness, silty clay described as slicken-sided and a silty sand with Chert gravel layer.

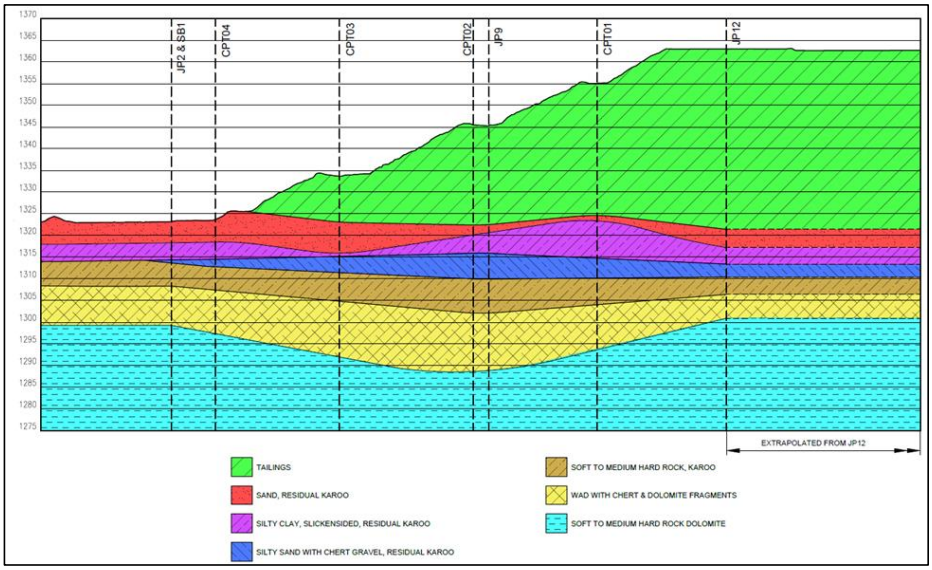

Figure 3-6 Idealised geological cross-section of Dam 1's western flank

Important observations from the idealised geological section, are:

- The thickness of the soft to medium hard Karoo rock layer within the subsided area is variable. The average thickness of this layer was approximately 4 meters based on the 15 boreholes drilled within this area.
- The WAD-rich layers (which is manganese rich dolomite residuum dolomite) generally vary between 1m and 6m thick within the failed zone. WAD is known to be a very weak, compressible and highly erodible material.
- No borehole data is available to define the geological profile to the right (east) of JP12. In the idealised geological profile in Figure 3-6, the JP12 profile was simply extrapolated.

Figure 3-7 shows the May 2018 wall geometry, CPTu test and borehole locations along the section as well as the CPTu test results. The cone resistance is denoted by the solid red line and the dynamic pore pressure response by the solid blue line. These were used to determine the stratigraphy of the facility. Based on this information as well as the relevant sonic logs, the current ground level denoted by the solid black line was determined. The original ground level presented by the broken black line was obtained from a topographical map prior to the construction of the TSF. The results indicate a significant downward displacement of the natural ground level in the order of 3 meters below the day wall compared to the ground elevation prior to construction.

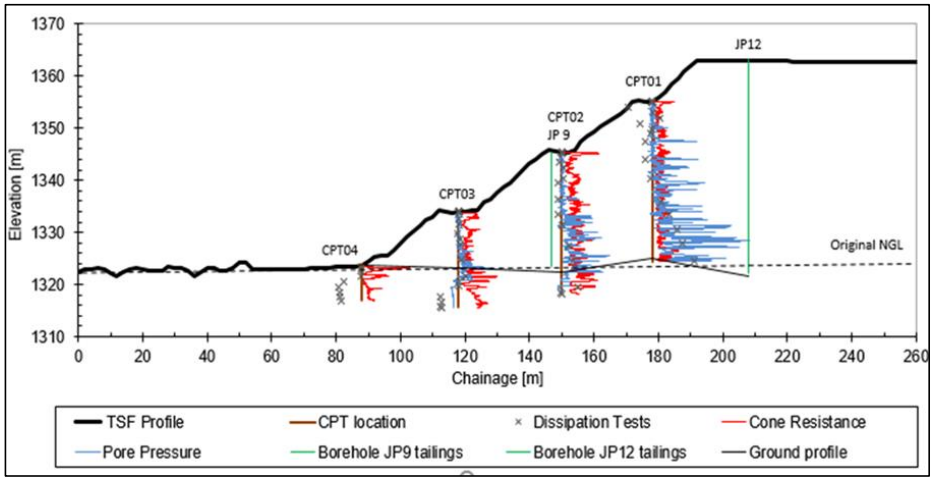

Figure 3-7 Interpretation of CPTu results on the western flank of Dam 1

The ambient pore pressure measured by the CPTu is presented by the grey crosses in the figure. These were used to determine the phreatic water level as well as the gradient of pore pressure build up. It was found that the phreatic level was relatively deep below the tailings surface and that the gradient of pore pressure build up was significantly less than hydrostatic; varying between 2.0 kPa/m for CPT03 and 6.7 kPa/m for CPT01. This could be attributed to the drains installed below the outer wall as well as the permeable sandy transported and residual Karoo layers below the dam. The dam is clearly well-drained and this is also supported with the observation that there are no signs of seepage on the western wall or the remainder of the perimeter.

An analysis of the CPTu results indicates that the tailings generally has a low potential for liquefaction based on the extent of the unsaturated zones in the profile and the state parameter as described by Jeffries and Been (2015). This means that should a trigger mechanism occur, such as the subsidence and lateral movement that occurred towards the end of 2017, that the tailings in the affected area is unlikely to liquify and flow.

Water levels measured in the percussion drilled boreholes indicated that the water table below the TSF is located at the contact between the Karoo rock and Wad.

4 ANALYSIS OF MECHANISMS

Four possible mechanisms were assessed by the technical team consisting of Engineers from three consulting companies and experts from AngloGold Ashanti and Harmony Gold. The team evaluated these mechanisms by comparing observed and measured behavior to the expected behavior should these mechanisms manifest. The mechanisms considered were:

- Consolidation of the underlying clay horizon.
- Slope failure of the TSF embankment.
- Sinkhole formation below the embankment.

- Yielding of the Karoo rock.

After careful consideration of the data collected the team concluded that the most plausible mechanism leading to the observed behavior was 'Yielding of the Karoo rock' (described in the remainder of this section).

The Karoo origin rock layer below the western flank consisting of sedimentary Sandstone and Siltstone layers is estimated to be about 4m thick on average. Based on the percussion drilling records it is relatively competent and could span across the underlying compressible WAD in its natural state. Subsequent loading due to the TSF exceeded this capacity, resulting in a brittle failure of the foundation.

Following the yielding of the rock, the load is progressively transferred to the compressible WAD. The conclusion that this is the correct mechanism is supported by the following:

- The survey information suggests that a trigger mechanism occurred during the last three years of deposition, suggesting that the Karoo rocks had the capacity to span over the WAD until this point.
- Interpretation of the CPTu test results and sonic drilling logs indicate that the current natural ground elevation is lower than the original ground elevation below the day-wall. Downward displacement of the substrata in this area has thus occurred.
- The average thickness of the Karoo rock is 4m which may not be sufficient to support the additional load of the 40m high tailings dam.
- Deposition on Mispah Dam 1 ceased in December 2017 (when significant cracking and displacement had already occurred). Despite this, continued vertical displacement varying between 100mm and 200mm were measured in the day-wall area between February and May 2018 (Figure 3-5). These displacements are relatively large for the short period of time and were not measured on the remainder of the facility outer wall. These settlements are attributed to continued compression of the WAD.
- The direction of movement of the outer wall was predominantly downward and inward. Of all the mechanisms considered, only this one could explain the observed displacement adequately.

This supports the hypothesis that the Karoo rock horizon fractured below the western wall of the TSF as the load exceeded the capacity of the competent rock to sustain the load. Once the overlying rock layer had fractured, load was transferred onto the compressible WAD, leading to the movements that were recorded.

5 REMEDIAL MEASURES

The risk of further subsidence along the Western flank and similar subsidence events along other parts of Dam 1 and 2 cannot be discounted. However, the potential for liquefaction of tailings in the affected zone leading to the catastrophic outflow of tailings, is regarded as low due to the largely unsaturated profile (and predominantly dilatant behavior of the saturated zone). This is provided that the dam remains largely unsaturated, and monitoring strategies to verify this have been implemented.

The mechanism identified is triggered by increased loading over time. As the foundation below the outer walls of the upstream facility is not subjected to increased loading, an increase in load is only be expected under the active part of the TSF where deposition is occurring. A 100m step-in of the day-wall on Dam 1 was implemented to ensure the unsaturated outer wall remains unsaturated and is not subjected to any further loading. The rate of tailings deposition on the facility was also significantly reduced (by approximately 50%) and the operational pool is kept as small as practically possible. Requirements for freeboard were increased significantly to ensure that, in the case of further settlement of any of the outer walls, legislated freeboard would be maintained.

Continued frequent monitoring of this facility by LiDAR survey will assist with early identification of similar patterns.

A subsequent detailed geophysical and drilling program was undertaken to assess whether similar geological conditions were prevalent over the remainder of the site. Where such geological features were found similar measures were applied.

6 CONCLUSIONS

It was found that yielding of the competent but reasonably thin underlying Karoo rock, underlain by highly compressible weathered Dolomite (WAD), was the most plausible mechanism leading to movement of the embankment and crack formation observed. It was concluded that the way forward entailed assessing the available geological information to determine if similar conditions existed elsewhere along the TSF embankments. Mitigation and remedial measures were compiled to restore the TSF to an acceptable and safe condition. These measures were implemented, and the facility was recommissioned in March 2019. Close monitoring of the TSF continues and no further signs of distress have been noted.

Of interest to the wider discussion on the stability of upstream tailings dams, this is an example of an upstream tailings dam entirely built out of tailings deposited hydraulically. The TSF was exposed to significant deformation (a trigger mechanism) resulting in displacements of up to 2m. However, due to the nature of the TSF (being largely unsaturated and non-liquefiable) no catastrophic failure followed. This is due to strict application of construction methods that have been designed to encourage desiccation and drying out of the tailings forming the outer wall of the facility as well as permeable foundation soils further assisting the drying out of the dam.

REFERENCES

Engelbrecht, J. (2018). *The monitoring of surface deformation at a tailings facility near Orkney (CSIR/M1/EOSIT/IR/2018/0002/CAA8/92/4353).* Pretoria: CSIR Meraka institute.

Fritz Wagener Consulting Geotechnical Engineer. (2005). *Geotechnical Report for Extensions to Mispah Tailings Dam – Vaal River Operations (FW03/05/108).* Johannesburg.

Jefferies, M., & Been, K. (2015). *Soil Liquefaction, A Critical State Approach.* Boca Raton: CRC Press.

Jones & Wagener. (1992). *Geotechnical investigation for Slimes Dam M - Vaal Reefs (AA8/92/4353).* Johannesburg.

Jones & Wagener. (2018). *Mispah Tailings Storage Facility No 1 - Western Flank Geotechnical Investigation Factual Report (JW103/18/G853-00-Rev0).* Johannesburg.

Jones & Wagener. (2018). *Mispah Tailings Storage Facility No 1 - Western Flank Plausible Mechanism and Remedial Measures Report (JW127-00/18/G853-Rev3).* Johannesburg.

Open Ground Resources. (2018). *Gravity investigation at the Mispah tailings Dam 1 East of Orkney in the North West Province to map dolomite karst topography (2560/2018).* Pretoria.

Rust, E. (2018). *Mispah Piezocone Probing Project. Site TSF.* Pretoria: Osimo CC.

Internal Erosion Assessment for Existing Mining Dams

Cori Creba
Tetra Tech Canada, Nanaimo, British Columbia, Canada

Fatemeh Yazdandoust
Tetra Tech Canada, Vancouver, British Columbia, Canada

Chris Johns
Tetra Tech Canada, Kelowna, British Columbia, Canada

ABSTRACT: The risks associated with embankment failure due to internal erosion are well documented; however, there is a wide range of methods available to assess internal erosion potential. To effectively manage internal erosion risk, it is proposed that the level of assessment and mitigation effort should be related to the consequence classification of the dam. Most protocols for internal erosion assessment recommend event tree analysis and no-erosion/continuing erosion classification. However, there can be significant variation in the level of effort undertaken to select soil properties and determine the hydraulic gradients that support internal erosion assessment. Two case studies of mining dams are presented that describe internal erosion assessments and mitigation efforts for two differently classified mining dams. The level of effort associated with the investigation, assessment, and mitigation of internal erosion risk is linked to the consequence classification for the dam, which was developed under protocols described in Canadian Dam Association (CDA) guidelines.

1 INTRODUCTION

Internal erosion occurs when soil particles within an embankment dam or dam foundation are carried downstream by seepage. In a statistical analysis of worldwide dam failures (excluding Japan pre-1930 and China), internal erosion was identified as the cause of 46% of known embankment dam failures; this is only 2% less than overtopping related failures (Foster et al. 2000), making it the second highest cause of embankment dam failures. In another analysis, it was determined that 22% of tailings dams had failed by internal erosion (also called piping), making it the number one cause of failure (Lyu et al. 2019). Many of these dams were not designed with adequate filter and drainage zones. Since the development of modern-day filter design, in the late 1970s and early 1980s, failures due to internal erosion have been reduced. There have been no cases of embankment dam failures where the dam had effective filters in place (Ripley 1982).

For existing dams without adequate filters, there is considerable uncertainty in identifying the presence of erodible soils and determining the adequate function of existing filters and drains. For large and/or relatively high-risk dams, event tree type statistical analysis can be a useful and warranted approach. However, detailed event tree methods can require large amounts of data obtained from costly investigations, sampling, and testing methods.

Internal erosion assessment is more challenging than other embankment dam evaluations because it cannot be analyzed using deterministic methods (USBR 2019). The lack of commonly applied assessment protocols makes design assessment quality and reliability uncertain. In addition, since internal erosion occurs out of sight, within the dam or foundation, the potential for early detection is limited, and erosion will often have progressed enough to be visible or confirmed by measurement trends before detection (Mattsson et al. 2008).

Remediation approaches can include “seepage control” (filters and drains) and “seepage reduction” (barriers) measures (ICOLD 2017). The selected approach depends on a range of factors, including risk reduction and cost. Seepage control methods can be preferable when they involve standard earthworks construction methods that permit a high standard of quality control. Remediation efforts can be costly and, in some cases, may be redundant if the dam is not at significant risk of internal erosion. The consequence classification of a dam, which was developed for these dams under protocols described in the Canadian Dam Association (CDA) guidelines, can provide a useful reference to determine the appropriate level of effort in assessment and remediation.

Two case studies are presented that describe internal erosion assessments and mitigation efforts completed for one mining dam with a High consequence classification and another type of mining dam with a Low consequence classification. The level of effort associated with the investigations, assessments, and mitigations of internal erosion risk was linked to the risk posed by the dam as defined by its consequence classification.

2 BACKGROUND

2.1 *Current guidelines and practice*

The CDA provides guidelines for determining the consequence classification for mining dams (Fig. 1). Their Dam Consequence Classification system is based on the incremental consequence of hypothetical failure for Population at Risk, Loss of Life, Economic and Social Losses, and Environmental and Cultural Losses (CDA 2013). The design criteria for earthquake and flood hazards are established based on the dam classification. The CDA recommends assessing mining dams for internal erosion; however, they do not provide standard methods for the assessment or correlate the level of effort to the dam consequence classification.

Dam Classification	Population at Risk [1]	Loss of Life	Economic and Social Losses	Environmental and Cultural Losses
Low	None	0	Low economic loss; area contains limited infrastructure or services.	Minimal short-term loss or No long-term loss.
Significant	Temporary Only	The appropriate level of safety required depends on the number of people, the exposure time, the nature of their activity, and other considerations.	Losses to recreational facilities, seasonal workplaces, and infrequently used transportation routes.	No significant loss or deterioration of habitat; or Loss of marginal habitat only. Restoration or compensation in kind highly possible.
High	Permanent	1-10	High economic losses, affecting infrastructure, public transportation, and commercial facilities.	Significant loss or deterioration of important habitat. Restoration or compensation in kind highly possible.
Very High	Permanent	10-100	Very high economic losses affecting important infrastructure or services (e.g., highway, industrial facility).	Significant loss or deterioration of critical habitat. Restoration or compensation in kind possible but impractical.
Extreme	Permanent	>100	Extreme losses affecting critical infrastructure or service (e.g., hospital, major industrial complex).	Major loss of critical habitat. Restoration or compensation in kind impossible.

[1] Definitions of Population at Risk:
None – No identifiable population at risk, so loss of life is not possible other than through unforeseeable misadventure.
Temporary – People are only temporarily in the dam breach inundation zone (e.g., using seasonal cottages, passing through on transportation routes, participating in recreational activities).
Permanent – The population at risk is ordinarily located in the dam breach inundation zone (e.g., as permanent residents); three consequence classes (high, very high, extreme) are proposed to allow for more detailed estimates of potential loss of life (to assist in decision making if the appropriate analysis is carried out).

Figure 1. Dam Classification (CDA 2013)

The Federal Energy Regulatory Commission (FERC), the International Commission on Large Dams (ICOLD), the United States Bureau of Reclamation (USBR), and the US Army Corps of Engineers (USACE) also describe protocols for internal erosion assessments using event tree methods.

2.2 *Internal erosion mechanism and failure process*

Internal erosion refers to any process that results in erosion of soil particles from within or beneath an embankment due to seepage flows (Bonelli et al. 2013) (ICOLD 2017). Internal erosion can be categorized into four distinct mechanisms:

(i) Concentrated Leak Erosion – occurs when water flows through an open pathway, such as a desiccation crack, leading to erosion of the embankment;

(ii) Contact Erosion – occurs when seepage through a coarse soil layer erodes an adjacent layer of finer soil;
(iii) Suffusion (internal instability) – occurs when a fine soil fraction is removed from a coarser soil matrix; and
(iv) Backward Erosion Piping (BEP) – occurs when soil erosion begins at an unfiltered seepage exit and progresses backward beneath an embankment.

Each of these failure modes can be broken down into four phases:

1) initiation of erosion (particle detachment);

2) continuation of erosion (inadequate particle retention);

3) progression of erosion (continuous particle transport and enlargement of erosion pathway); and

4) initiation of breach.

2.3 *Analysis Approach for Internal Erosion*

FERC, ICOLD, USBR, and USACE recommend assessing the likelihood of initiation, continuation, and progression of any internal erosion mechanism using event trees. An event tree is a risk analysis method that was developed based on a sequence of logical events (nodes). In the case of internal erosion, it describes the failure process for internal erosion mechanisms.

The initiation node is typically considered the critical event in the failure mode sequence and represents the probability that erosion will initiate. The key factors for erosion to be initiated are material susceptibility, critical hydraulic loads, critical stress conditions, defects, and existing penetrating structures.

If internal erosion is initiated, it must continue to become a threat to the dam. Filters may interrupt or stop the erosion in the soil downstream of where it is initiated. Evaluation of the continuation phase of internal erosion relies primarily on examining the filter compatibility with modern criteria and continuity of an unfiltered exit.

Erosion, if initiated and not arrested by filter action in the dam, will progress if:

- The soil being eroded can “hold a roof” over a pipe,
- “Crack filling” or clogging action will not stop the erosion process, and
- Flow in the developing pipe is not restricted by hydraulic losses (ICOLD 2017).

Based on the criteria developed by Fell et al. (2008), the most important factor in holding a roof over developing erosion pipes is the fines content, and the likelihood of internal erosion to progress in soils with more than 15% fines content (% passing 0.075 mm) is very high. For crack filling to occur, a granular zone upstream of the core must have particle sizes small enough to be transported by water into the crack and to fill it. Hydraulic losses may occur when there is a fine-grained granular material upstream or if there is a concrete face slab or core wall.

For concentrated leak erosion and BEP, progression is the process of developing and enlarging an erosion pathway through the embankment core or foundation. Currently, there is no uniform practice for evaluation of progression for other internal erosion processes.

Ultimately, if erosion progresses and there is no filter to prevent the erosion, the dam may breach. Figure 2 shows an event tree describing a breach caused by internal erosion through an embankment.

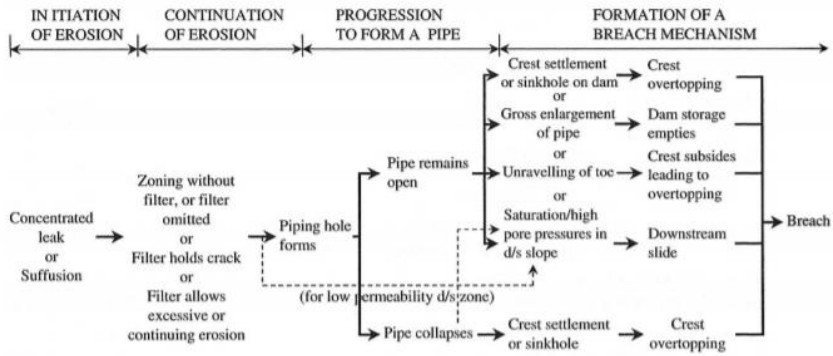

Figure 2. Failure path diagram for failure by piping through an embankment (Foster 1999)

3 APPROACH BASED ON CONSEQUENCE CLASSIFICATION

The internal erosion assessment methods recommended by FERC, ICOLD, USBR, and USACE do not consider the consequence of dam failure. However, engineers are well versed in linking the level of analysis to the amount of information and level of understanding of the site and to the consequence of failure. Examples include the Canadian Highway Bridge Code, CSA S6 (CHBSC) and the Federal Highway Administration (FHWA), which suggest varying factors of safety depending on the site degree of understanding. The consequence classification system laid out by CDA allows dam owners with lower consequences of failure to assess their dams using lower magnitude earthquake and flood events.

Using the same logic as the guidelines developed by FHWA and CDA, it may be useful to have a framework that matches the effort put into subsurface exploration, methods of assessment, and mitigation options to the consequence classification of a dam. The level of effort for subsurface exploration should also be based on the amount of background information available, including construction records, instrumentation records, and geotechnical data. The following two case studies highlight how the consequence classification of the dams was considered in the level of effort for subsurface investigation, methods of assessment, and mitigation options.

4 CASE STUDY 1 – HIGH CONSEQUENCE TAILINGS DAM

4.1 *Dam Characteristics*

The first case study is for a tailings dam at a gold mine in southern British Columbia, Canada. A zoned earthfill starter dam was constructed in 2003 and raised by 2.5 m using centreline construction methods in 2015. The dam is currently 11.5 m high and has a crest length of 300 m. The dam was constructed with a relatively low permeability core, a shallow compacted till cutoff below the core, and a silty sand and gravel shell. A nominal 0.3 m thick sand blanket drain was constructed below the downstream shell. The embankment was designed with upstream and downstream slopes of 2H:1V. The dam was constructed on glaciofluvial foundation soils of variable characteristics that were dominantly well-drained sands and sandy silts. The foundation soils also included softer sandy silt zones at the northern end of the dam. In 2016, a 90 m long, 8 m high, and 12 m wide buttress was constructed along the northern embankment to improve stability. Finger drains were installed below the buttress to convey seepage water from the original toe to a new downstream seepage collection ditch.

The facility is currently inactive, and slurry tailings were deposited from the embankment crest such that the tailings beach forms an integral part of the design. The facility contains approximately 32,000 tons of tailings, and approximately 126,000 cubic metres of storage is available in the current geometry for tailings and the operating water pond. The facility is unlined, and seepage flow and quality are monitored at three locations downstream of the dam.

4.2 *Dam consequence classification*

The dam was classified in 2014 to be in the High category under CDA guidelines (CDA 2013). No permanent population or infrastructure was at risk, and this classification was based on the potentially significant environmental impact of a release that could reach a downstream creek.

4.3 *Internal erosion assessment*

An internal erosion assessment was carried out based on the recommended event tree process, as described in guidelines. The geotechnical model of the dam and foundation was developed based on dam design and construction reports and drawings, geotechnical investigations results (including cone penetration tests, sonic drilling, and vibrating wire piezometer records), seepage monitoring, and laboratory testing results of the encountered soil.

4.3.1 *Initiation*

The potential initiation of internal erosion within and below the tailings facility structure was analyzed. The following soil units were identified for the analysis:

- Sandy silt to silty clay till core (SM, ML, CL)
- Clay foundation soils (CI)
- Glaciofluvial foundation soils (SM, ML, SW)

Gradations for these soil units were analyzed for factors that could measure the potential for internal instability, including uniformity of particle size, mass and size of particles, fine particles percentage, and the slope of the gradation curve (USBR 2011). The cohesionless soils within the core and foundation were considered erodible, whereas the clay foundation soils were considered non-erodible, due to their cohesive properties (PI > 7).

In addition, a seepage assessment was completed to assess whether the hydraulic conditions necessary to cause internal erosion could occur. The normal operating levels for the decant pond were adopted for the analysis. The records of the existing vibrating wire piezometers on the dam crest were reviewed to calibrate the seepage assessment. Based on the results for different seepage scenarios, the average hydraulic gradient at the tailings dam was assessed as High under protocols described by Rivard (1981).

It should be noted that the Hazard Potential described in Table 1 is not the same as the CDA Consequence Classification framework. The Rivard (1981) guideline, presented in Table 1, was developed based on information from Terzaghi & Peck (1967), Sherard et al. (1963), United States Department of the Interior, Bureau of Reclamation (1974), and Prairie Farm Rehabilitation Administration case studies for dams on pervious foundations.

Table 1: Conditions requiring foundation treatment based on soil type, hydraulic gradient, and hazard potential (Rivard 1981)

Soil type[1]	Resistance to piping	Average hydraulic gradient	Hazard potential[2]		
			High	Medium	Low
ML SM	Low to very low	>1/12.5 1/12.5 to 1/25 <1/25	T T,O NT,O	T O,T NT,O	T O NT
SP	Medium to low	>1/10 1/10 to 1/20 <1/20	T T,O NT,O	T O,T NT,O	T,O O NT
SW GM GP	Medium to high	>1/8.5 1/8.5 to 1/17 <1/17	T T,O NT,O	T,O O,T NT	O,T NT NT
SC GW	High	>1/5 1/5 to 1/10 <1/10	T, O O,T NT	O,T NT NT	O NT NT
GC Clay etc.	Very high	-	NT	NT	NT

1. Soil Types are based on Unified Soil Classification
2. NT – No foundation treatment required
   O – Observe and monitor
   T – Foundation treatment required

Based on Table 1, the silt and sand core material and glaciofluvial soils were considered susceptible to internal erosion. Moreover, the empirical approach introduced by the Lane

method (Das 2014) was used to estimate the weighted creep ratio based on the highest pressure head and shortest flow path. The results showed that the calculated ratio was less than the safe ratio for foundation silts and sands.

4.3.2 *Continuation*

The core and shell zones in the tailings dam were assessed using modern filter design methods. The core, clay foundation, and glaciofluvial foundation zones were considered as base soils in the zoning compatibility analysis. The filtering ability of the dam shell and buttress were assessed based on the filtering criteria outlined in USBR (2011).

The assessment result showed:

- The dam shell and buttress material will act as a filter for the core;
- The dam shell and buttress material will filter the glaciofluvial foundation soils where seepage exits through the shell or buttress; and
- The dam shell and buttress material will not act as a filter for the glaciofluvial soils where seepage exits the glaciofluvial foundation soils and could lead to the continuation of internal erosion.

4.3.3 *Progression*

The likelihood of soil units being able to support a roof to an erosion pipe was assessed based on the criteria developed by Fell et al. (2008). The glaciofluvial foundation soils consisted of silty sand and gravel (SM and GM) with more than 15% fines content, and sandy silt (ML) with more than 50% fines content. Both were likely to hold a roof and allow internal erosion to progress.

Seepage modelling showed that the hydraulic gradient where seepage exited the dam foundation into the downstream collection ditch was large enough for erosion to progress. There was no upstream fine-grained material or concrete face slab to limit the flow. Therefore, internal erosion could progress through the foundation glaciofluvial materials.

4.4 *Mitigation Strategy*

The assessment indicated that breach by internal erosion of foundation soil into the downstream collection ditch was a viable failure mode. To manage the risk associated with internal erosion, a filter zone was designed following the methods described in the USBR (2011) standard. The filter zone was constructed along the downstream toe to intercept foundation seepage and designed to prevent particle migration and allow seepage to drain. An erosion protection layer was incorporated into the filter design. The as-constructed alignment and features of the filter are shown in Figure 3 and Photographs 1a and 1b.

Other mitigation options considered included installation of a barrier system, such as a diaphragm wall or a grout curtain, or upstream impermeable blanket to reduce seepage through the foundation. The construction of an upstream impermeable blanket was not viable due to the tailings contained in the basin. The diaphragm wall and grout curtain options were considered more expensive and to have greater uncertainty in long-term performance. Filter construction was adopted because it involved standard construction methods and was economically viable.

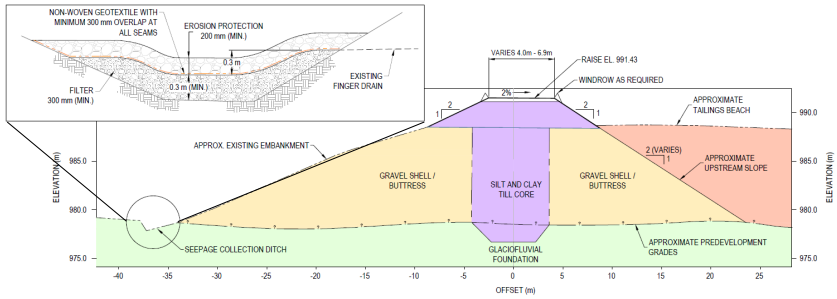

Figure 3. Tailings dam cross-section with constructed filter details

Photographs 1a (left) and 1b (right). Filter installation at northern and southern downstream toe

5 CASE STUDY 2 – LOW CONSEQUENCE SEDIMENT POND DAMS

5.1 *Dam Characteristics*

The second case study considers several sediment pond dams at a coal mine in a glaciated valley in southern British Columbia, Canada. The sediment ponds were constructed to capture runoff from upslope mining areas and allow for particle settlement before the water is released into the receiving environment. A typical section through a sediment pond, included in Figure 4, shows the geometry of an upstream mine waste rock dump, primary settling ponds, and main storage pond and dam.

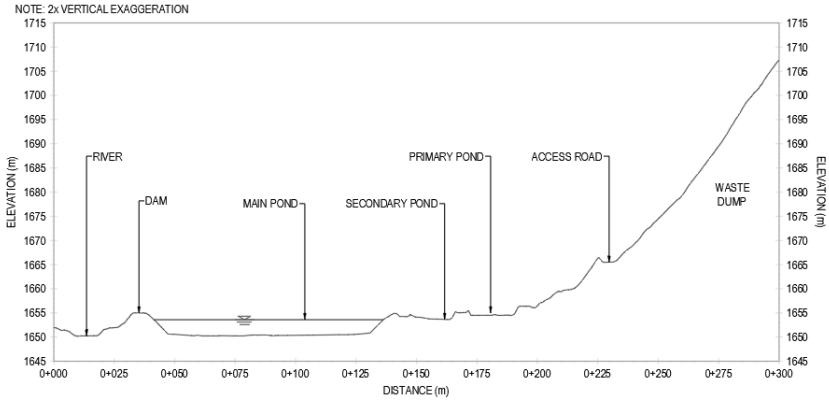

Figure 4. Typical sediment pond section

The dams are generally founded on high-level terraces that border the floodplain of a river or are within the floodplain itself. The terraces consist of gravel overlain by glaciolacustrine silt and clay, or successively by till followed by glaciolacustrine sediments. The sequence has locally been incised by glacial outwash and covered in some areas by fluvial soils and colluvium. The embankments were built using cut and fill methods and were generally less than 10 m high with nominal slopes of 2H:1V both upstream and downstream. These dams were built several decades ago as homogeneous earthfill dams without any zoning or filters included in the design.

Limited dam construction information was available, and no geotechnical investigations had been completed as part of design or construction. Drilling investigations were completed as part of this study to collect information on the dam structures and foundations to assess dam safety. The drilling investigation generally consisted of up to three sonic testholes per dam with limited in-situ testing. Laboratory testing included grain-size analysis, moisture contents, and Atterberg limits where fine-grained soils were encountered. Sonic drilling allowed for continuous cores to be recovered in soil and rock. Testholes were generally advanced from the crest of the dam through the dam fill and into the foundation soils. Vibrating wire and standpipe piezometers were installed in the embankment fill and foundation soils to record groundwater levels.

5.2 *Dam consequence classification*

The potential inundation zones for these dams do not include residential or industrial infrastructure. Therefore, they are classified as Low consequence dams under CDA and Ministry of Energy, Mines and Petroleum Resources (EMPR) criteria.

5.3 *Internal erosion assessment*

A simplified geotechnical model of the soil and groundwater conditions, in the dam and foundation, was developed based on site observations, historical facility performance, and the information gathered during the geotechnical investigation. Seepage assessments were completed that considered normal and upset operating conditions. The modelled phreatic surface was used to estimate the average hydraulic gradients, which were determined by dividing the head of water over the base of the structure. These values were used to determine the resistance to internal erosion (piping) and the potential need for mitigation based on the approach described by Rivard (1981). The sediment ponds dams were considered to have Low hazard potential based on the internal erosion risk criteria shown in Table 1.

For each dam, the risk associated with the four mechanisms of internal erosion was considered. The initiation of each mechanism was assessed separately:

- Concentrated leak erosion requires cohesive soils that can hold a crack and a mechanism to create a crack, for example, desiccation or cracking due to an earthquake.
- Contact erosion requires a coarse-grained material to be in contact with a fine-grained material and high enough seepage velocity to erode the fine-grained material.
- Backward piping erosion requires a high enough hydraulic gradient to initiate erosion, based on soil type.
- Suffusion can occur in gap graded or broadly graded soils, with a high enough hydraulic gradient to initiate erosion based on soil type.

For most of these dams, the risk of concentration leak erosion was low due to the granular nature of the soils. Contact erosion was not considered a significant risk because there were no embankment zones or filters and therefore no adjacent coarse and fine-grained layers. Backward piping erosion was a possibility where high average gradients exist, and this risk may be reduced by monitoring through regular inspection by qualified personnel. Due to the variability of the geologic materials used in construction, suffusion was a risk at some dams.

5.4 *Mitigation Strategy*

The mitigation strategies for these Low consequence dams are still under consideration. Targeted and strategically timed visual inspection of seepage areas as part of the monitoring program may be adequate risk mitigation for sediment ponds where recently measured and anticipated future gradients are relatively low. The installation of a filter at the downstream

toe may be required in some cases. For cases where slope instability was also a geotechnical risk, toe berms that incorporate a filter will be recommended to manage risk.

6 CONCLUSION

The different internal erosion assessment methods and mitigation strategies adopted in these case studies were developed using engineering judgement and risk assessment, which are linked to the dam consequence classification. The first case study involved a High consequence dam that stored tailings. A filter was designed and installed based on a detailed internal erosion assessment developed from an advanced geotechnical model of the dam and foundation. The second case study involved several Low consequence sediment ponds, and the internal erosion mitigation options were developed based on a simplified geotechnical model. For some of these sediment ponds, targeted and strategically timed monitoring was considered an acceptable mitigation strategy. A protocol for the level of effort associated with internal erosion assessment and mitigation at existing dams could be developed based on the dam consequence classification.

REFERENCES

Bonelli, S., Fell, R. & Benahmed, N. 2013. Concentrated Leak Erosion.

Canadian Dam Association. 2013. Dam Safety Guidelines 2007 (2013 Edition).

Das, B.M. 2014. *Advanced Soil Mechanics (4 ed.)*. Taylor & Francis Group.

Ministry of Energy, Mines and Petroleum Resources. 2016. Health, Safety and Reclamation Code for Mines in British Columbia Guidance Document. British Columbia: Ministry of Energy, Mines and Petroleum Resources.

Ministry of Energy, Mines and Petroleum Resources. 2017. Health, Safety and Reclamation Code for Mines in British Columbia.

Federal Energy Regulatory Commission. n.d. FERC Engineering Guidelines Risk-Informed Decision Making. Chapter R10 Internal Erosion and Piping DRAFT. Retrieved from https://www.ferc.gov/industries/hydropower/safety/guidelines/ridm.asp#guide

Federal Highway Administration. 2009. Design and Construction of Mechanically Stabilized Earth Wall and Reinforced Soil Slopes – Volume I and II.

Foster, M.A. 1999. The probability of failure of embankment dams by internal erosion and piping. School of Civil and Environmental Engineering. The University of New South Wales.

Foster, M., Fell, R. & Spannagle, M. 2000. The statistics of embankment dam failures and accidents. *Canadian Geotechnical Journal*, 1000-1024.

Garner, S.J. & Fannin, R.J. (2010). Understanding internal erosion: A decade of research following a sinkhole event. *International Journal on Hydropower Dams*, 93-98.

International Commission on Large Dams. 2017. Internal Erosion of Existing Dams, Levees and Dikes, and their Foundations. Bulletin 164. ICOLD.

Lyu, Z., Chai, J., Xu, Z., Qin, Y. & Cao, J. 2019. A Comprehensive Review on Reasons for Tailings Dam Failures Based on Case History. Retrieved from https://www.hindawi.com/journals/ace/2019/4159306/

Mattsson, H., Hellström, J.G. & Lundström, T. S. 2008. On Internal Erosion in Embankment Dams, A literature survey of the phenomenon and the prospect to model it numerically. Luleå University of Technology.

Ripley, R.F. 1982. Discussion. *ASCE Journal of Geotechnical Engineering*, 1194.

Rivard, P.J. 1981. Report on Seepage Control and Exit Gradients Beneath Dams. Department of Regional and Economic Expansion Prairie Farm Rehabilitation Administration Engineering Service.

Sherard, J.L., Woodward, R.J, Gizienski, SF., & Clevengar. W.A, 1963. Earth and Earth-Rock Dams. New York: John Wiley and Sons.

Terzaghi, K., & Peck, R.B, 1967. *Soil Mechanics in Engineering Practice, second edition*. New York: John Wiley and Sons.

United States Army Corps of Engineers. 2017. Internal Erosion Risks for Embankments and Foundations. Part D - Embankments and Foundations.

United States Department of the Interior. 2011. Design Standards No. 13: Embankment Dams, Chapter 5: Protective Filters (9 ed.).

United States Department of the Interior, Bureau of Reclamation. 1974. *Design of Small Dams*. Washington D.C.: United States Government Printing Office.

United States Department of the Interior, Bureau of Reclamation. 2019. Internal Erosion Risks for Embankments and Foundations, Chapter D-6.

Modeling Slope Instability Due to Undrained Creep

Ross W. Boulanger
University of California, Davis, CA, USA

Tyler J. Oathes
University of California, Davis, CA, USA

ABSTRACT: Undrained creep rupture in saturated silts and clays that are initially loose of critical state can lead to delayed slope instability after relatively minor changes in loading, and has been suspected as contributing to a number of static failures in tailings dams. This paper illustrates the numerical modeling of undrained creep rupture for a hypothetical tailings dam using the two-dimensional finite difference program FLAC with a new user-defined strain-rate dependent constitutive model PM4SiltR. The constitutive model is introduced briefly, followed by single element simulations to illustrate its stress-strain responses under a range of loading conditions and strain rates. Simulations are then presented for the tailings dam with different initial seepage conditions and modest wetting-induced increases in loading. The analysis results illustrate the process of undrained creep rupture leading to slope instability, including the potential for small changes in loading to cause delayed instability. The numerical modeling approach and constitutive model are shown to provide reasonable approximations of undrained creep behaviors that can be important for static slope stability evaluations.

1 INTRODUCTION

Undrained creep in saturated silts and clays that are initially loose of critical state (e.g., normally or lightly over-consolidated) has the potential to cause delayed slope instability after relatively minor changes in loading. Undrained creep rupture in hydraulically placed fine-grained tailings or weak sedimentary strata has been suspected as contributing to a number of static failures in tailings dams, including the recent failure of Feijão Dam I near Brumadinho (Robertson et al. 2019). Undrained creep is a potential triggering mechanism for materials that are initially loose of critical state but stable under drained conditions.

The strain-rate dependent behavior of clays and plastic silts has been extensively studied for a range of loading conditions, as reviewed by Mitchell and Soga (2005). Peak undrained shear strengths (s_u) have been observed to increase by an average of about 9-10% per logarithmic cycle of shear strain rate (e.g., Graham et al. 1983, Kulhawy and Mayne 1990, Sheahan et al. 1996), although some studies indicate this rate effect becomes smaller (approaching zero) at extremely low strain rates and greater at extremely high strain rates (e.g., Ladd and DeGroot 2004). Kulhawy and Mayne's (1990) compilation of test data for 26 clays show that s_u values at strain rates of 10^{-2} to 10^{-3} %/hr are as low as 70-80% of the s_u value at a reference strain rate of 1%/hr. Undrained creep rupture has been observed in tests with constant static shear stresses greater than about 70-80% of the s_u determined at standardized laboratory test strain rates (e.g., Campanella and Vaid 1974), with this lower limit on s_u often described as corresponding to a static or inviscid yield surface (e.g., Sheehan 1995). Secondary compression studies have shown that the change in preconsolidation stress per logarithmic cycle of strain rate is about 3-5% in the range of standardized laboratory strain rates, but decreases toward zero at extremely low strain rates, where

the preconsolidation stress has a lower limit of about 0.7 times the preconsolidation stress determined from standard 24-hr load increment laboratory tests (Watabe et al. 2012). Numerous constitutive models have been developed to approximate these strain-rate dependent behaviors for a range of applications, including elasto-viscoplastic models by Kutter and Sathialingam (1992), Wang et al. (1997), Leoni et al. (2008), Yuan and Whittle (2018), and Shi et al. (2019).

This paper illustrates the numerical modeling of undrained creep rupture for a hypothetical tailings dam with an upstream construction geometry using the two-dimensional finite difference program FLAC with a new user-defined strain-rate dependent constitutive model PM4SiltR. The constitutive model was developed with a focus on applications to undrained creep rupture and rate-dependent strengths, and structured to facilitate calibration to parameters commonly used in practice. The constitutive model is introduced briefly, followed by single element simulations to illustrate its stress-strain responses for a range of loading conditions and strain rates. Simulations are then presented for the tailings dam with different initial seepage conditions and modest wetting-induced increases in loading. The analysis results illustrate conditions under which undrained creep rupture can lead to slope instability, including the potential for small changes in loading to cause delayed instability. The numerical modeling approach and constitutive model are shown to provide reasonable approximations of undrained creep behaviors that can be important for static slope stability evaluations in practice.

2 NUMERICAL MODEL

2.1 *Numerical model*

A tailing dam with the upstream construction geometry shown in Figure 1 was modeled using the finite difference program FLAC (Itasca 2019). The tailings dam is 50 m tall, has a 4:1 (horizontal:vertical) face, and is underlain by a 20 m thick foundation layer. The finite difference mesh used 0.5 m tall by 1.0 m wide rectangular zones, except near the dikes and face where zone dimensions were adjusted to approximate the more complex geometry. The tailings were assumed to be a lightly over-consolidated, low-plasticity silt and were modeled using PM4SiltR (Boulanger et al. 2020, beta version). The foundation was assumed to be a stiffer clayey silt, and was also modeled using PM4SiltR. The dikes were assumed to be nonplastic silty sand and were modeled using PM4Sand (Boulanger and Ziotopoulou 2017, Ziotopoulou and Boulanger 2016).

The phreatic surface was set at a height z_w above the foundation layer at the left boundary and set at the ground surface beyond the toe on the right side. The hydraulic conductivity of the tailings and foundation layer are assumed equal, with the horizontal conductivity 10 times greater than the vertical conductivity. The hydraulic conductivity of the dikes is 100 times those of the tailings and foundation. Capillary rise was 6 m in the tailings and 1 m in the dikes.

The numerical analyses were performed in a sequence of steps. Steady seepage and initial static equilibrium were established using Mohr Coulomb material models and the results checked for reasonableness as discussed in Boulanger and Beaty (2016). The material models were then switched to PM4Sand and PM4SiltR (with its rate dependence suppressed), and static equilibrium solved for again. The rate dependent parameters for PM4SiltR were then assigned (see next section), and the analysis for creep initiated with the tailings and foundation modeled as fully undrained and the dikes modeled as fully drained. The creep analysis was stopped when the potential for further creep induced strength loss was negligible or the slope became unstable, as indicated by large and accelerating slope deformations.

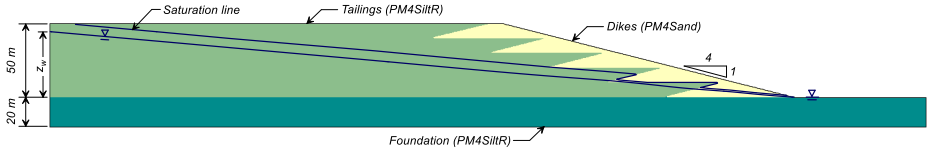

Figure 1. Tailings impoundment geometry with the phreatic surface and saturation surfaces from the steady seepage analysis case for z_w = 45 m.

2.2 *Tailings: Constitutive model, parameters, and responses*

The tailings were assumed to have the following uniform engineering characteristics to which the constitutive model was calibrated. The peak undrained shear strength ratio in direct simple shear (DSS) loading at standard strain rates ($s_{u,ref}/\sigma'_{vc}$) is 0.29, and the fully remolded or critical state undrained shear strength ratio ($s_{u,cs,ref}/\sigma'_{vc}$) is 0.10. The shear wave velocity at a vertical effective stress of 101 kPa (1 atm) is 145 m/s. The initial void ratio is 0.95 and the dry unit weight is 13.6 kN/m^3. Target stress-strain responses were based on typical responses for tailings having similar characteristics. The strain rate dependence is 8% per logarithmic cycle of strain rate.

The PM4SiltR model used to represent the tailings is a modified version of the stress-ratio and critical state based bounding surface plasticity model PM4Silt (Boulanger and Ziotopoulou 2018, 2019). Viscoplasticity was added to the PM4Silt model using a consistency approach wherein the bounding, dilatancy, and critical state surfaces were made rate-dependent (e.g., Wang et al. 1997, Martindale et al. 2012) and transient responses and stress relaxation were controlled through an internal strain rate and auto-decay process (e.g., Clarke and Hird 2012, Yuan and Whittle 2018). The critical state line and critical state stress ratio (M_{cv}) are dependent on the internal shear strain rate ($\bar{\dot{\gamma}}$) as,

$$p'_{cs} = p'_{cs,ref}\left(1+F_p \log\left(\frac{\bar{\dot{\gamma}}}{\dot{\gamma}_{ref}}+0.001\right)\right) \tag{1}$$

$$M_{cv} = M_{cv,ref}\left(1+F_M \log\left(\frac{\bar{\dot{\gamma}}}{\dot{\gamma}_{ref}}+0.001\right)\right) \tag{2}$$

where $\dot{\gamma}_{ref}$ = reference shear strain rate, p'_{cs} = mean effective stress at critical state for the current void ratio and internal strain rate, $p'_{cs,ref}$ = p'_{cs} at the reference strain rate, M_{cv} = stress ratio at critical state for the current internal strain rate, $M_{cv,ref}$ = M_{cv} at the reference strain rate, F_p = rate parameter for p'_{cs}, and F_M = rate parameter for M_{cv}. The numerical constant 0.001 in both expressions sets the critical state surface for static (zero strain rate) loading conditions at p'_{cs} and M_{cv} values equal to 1-3F_p and 1-3F_M times their respective values for the reference strain rate. The bounding and dilatancy surfaces are functions of M_{cv} and the state parameter, and thus are strain-rate dependent as well. For example, bounding surfaces for a fixed void ratio at different strain rates are shown in Figure 2 for the example calibration presented later. The strain rates are expressed in this figure as strain rate ratios (SRR), which are the logarithm of the internal shear strain rate normalized by the reference shear strain rate:

$$SRR = \log\left(\frac{\bar{\dot{\gamma}}}{\dot{\gamma}_{ref}}\right) \tag{3}$$

The bounding surface for SRR = 0 corresponds to the reference strain rate, and every integer change in SRR represents a factor of 10 change in strain rate. Bounding surfaces for SRR < -3 are almost equal to the static bounding surface, per Equations 1 and 2. The bounding surfaces at different SRR reflect changes in both p'_{cs} (note that $p'_{c,ref}$ is determined from the specified $s_{u,cs,ref}$) and M_{cv}. Stress relaxation and the rate of response to changing strain rates are controlled through the updating of the internal strain rate, which is controlled by the parameter θ_{ref} (default value 0.5), and an auto-decay process, which is controlled by the parameter β_{ref} (default value 0.999). The other input parameters and their calibration are identical to those for PM4Silt, for which the calibration process and example responses are provided in Boulanger et al. (2018) and Boulanger and Wijewickreme (2019).

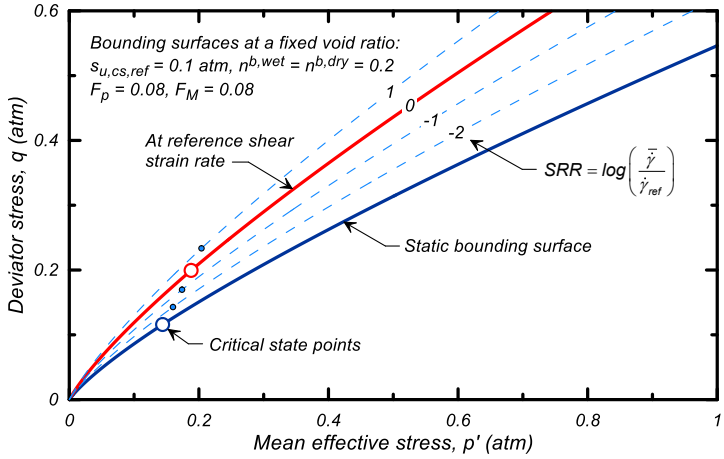

Figure 2. Rate-dependent bounding surfaces at a fixed void ratio using the example calibration presented later with $s_{u,cs,ref}$ = 0.1 atm and $M_{cv,ref}$ = 1.06 which together set $p'_{cs,ref}$.

The input parameters used herein for PM4SiltR were: shear modulus coefficient G_o = 500, $s_{u,cs,ref}/\sigma'_{vc}$ = 0.10, contraction rate parameter h_{po} = 100, rate parameters $F_p = F_M$ = 0.08, $\dot{\gamma}_{ref}$ = 5%/hr, bounding surface parameters $n^{b,wet} = n^{b,dry}$ = 0.2, and plastic modulus ratio h_o = 0.05. All other parameters retained their default values.

Single-element simulations of various loading conditions are presented to illustrate the range of responses obtained. The response to undrained DSS loading at the reference strain rate after consolidation to σ'_{vc} = 101 kPa with initial horizontal static shear stress ratios ($\alpha = \tau_{hv}/\sigma'_{vc}$) of 0.0, 0.1, 0.2, 0.3, and 0.35 are shown in Figure 3. The peak s_u/σ'_{vc} = 0.29 for α = 0.0, and progressively increases to about s_u/σ'_{vc} = 0.36 for α = 0.35, consistent with experimental trends for plastic, fine-grained soils. The responses to undrained plane-strain compression (PSC) and plane-strain extension (PSE) at the reference strain rate after anisotropic consolidation to σ'_{vc} = 101 kPa with $K_o = \sigma'_{hc}/\sigma'_{vc}$ values of 1.0, 0.8, 0.6, and 0.5 are shown in Figure 4. The peak s_u/σ'_{vc} in PSE and PSC are equal for isotropic consolidation (K_o = 1), as expected for the present model which does not include inherent anisotropy features. Anisotropic consolidation, while keeping σ'_{vc} constant, leads to slightly smaller s_u in PSC and significantly smaller s_u in PSE; this stress-induced s_u anisotropy is largely controlled by the plastic modulus parameter h_o (a greater h_o produces less s_u anisotropy). These simulated responses are consistent with general trends observed in experimental studies on similar soils, and illustrate that anisotropic consolidation leads to strain softening initiating at smaller strains in DSS or PSC loading.

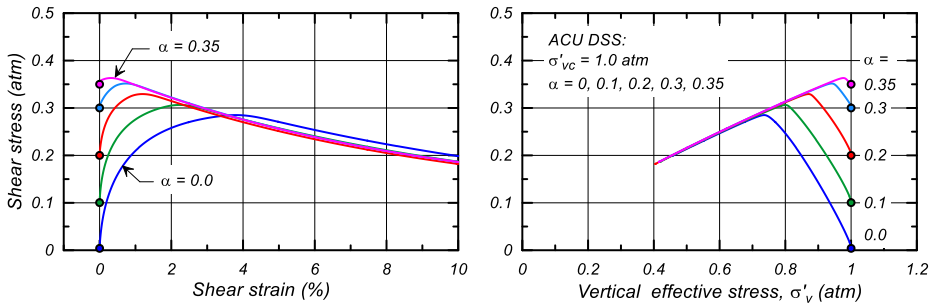

Figure 3. Single-element simulations of undrained direct simple shear loading with initial horizontal static shear stress ratios (α) of 0.0, 0.1, 0.2, 0.3, and 0.35 at the reference shear strain rate with PM4SiltR.

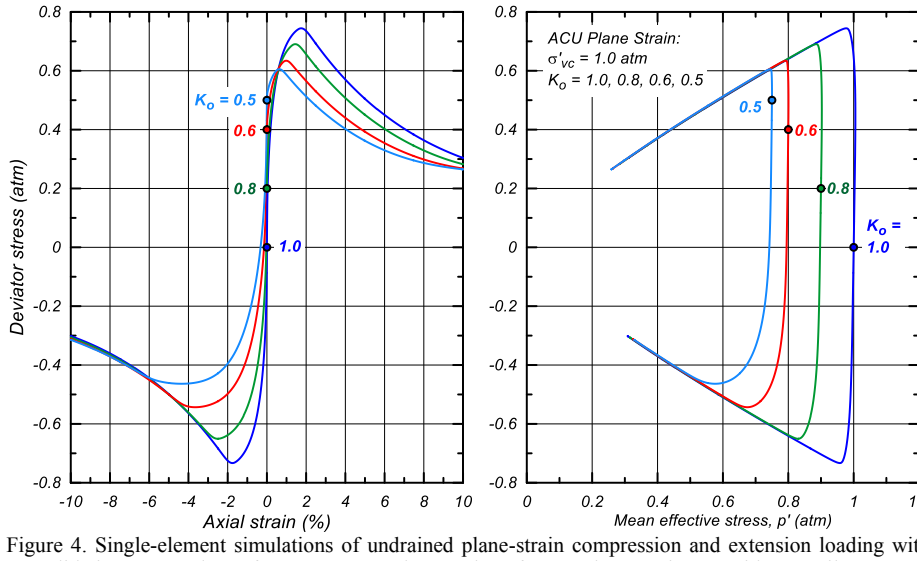

Figure 4. Single-element simulations of undrained plane-strain compression and extension loading with consolidation to K_o values of 1.0, 0.8, 0.6, and 0.5 at the reference shear strain rate with PM4SiltR.

The response to undrained DSS loading at shear strain rates of 10^{-4}, 10^{-2}, 1, 10^{2}, and 10^{4} times the reference strain rate are shown in Figure 5 for consolidation to σ'_{vc} = 101 kPa with α = 0.0. The peak s_u and the strain at peak s_u both increase with increasing strain rate.

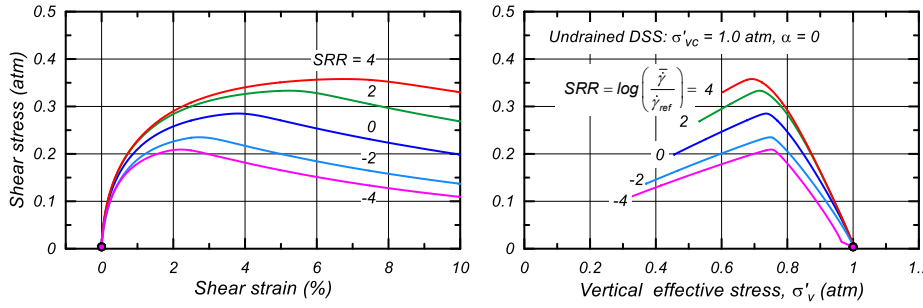

Figure 5. Single-element simulations of undrained direct simple shear loading with α = 0.0 at shear strain rates of 10^{-4}, 10^{-2}, 1, 10^{2}, and 10^{4} times the reference strain rate with PM4SiltR.

The variation of peak s_u with strain rate ratio is shown in Figure 6, with s_u normalized by its value at the reference strain rate. The peak s_u increases by about 8% per logarithmic cyclic of strain rate (as it was calibrated to do), with the static (lower limit) s_u being about 0.72 times $s_{u,ref}$.

The undrained creep response in DSS loading at different stress ratios is shown in Figure 7 for consolidation to σ'_{vc} = 101 kPa with α = 0.0. After initial consolidation, the shear stresses were applied at a standard strain rate under undrained conditions until they reached target percentages of $s_{u,ref}$, after which they were kept constant. Stable conditions developed for $\tau_h/s_{u,ref} \leq 0.70$, whereas undrained creep rupture developed for $\tau_h/s_{u,ref} \geq 0.75$ and the time for creep rupture decreased with increasing stress ratio.

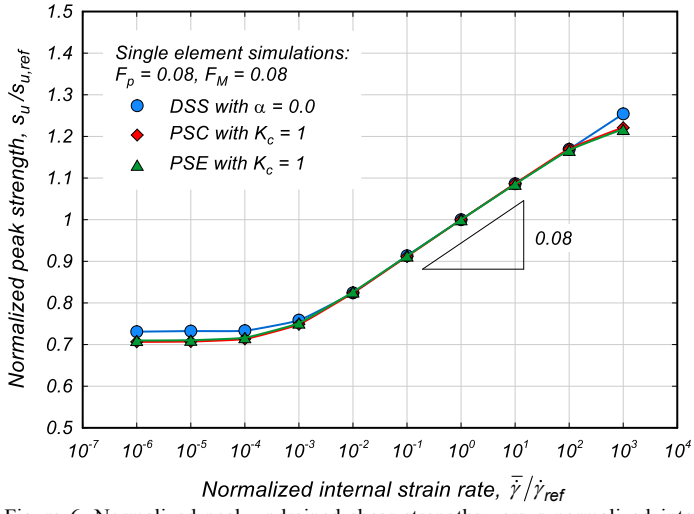

Figure 6. Normalized peak undrained shear strengths versus normalized internal shear strain rate from single-element simulations of DSS, PSC, and PSE loading with PM4SiltR.

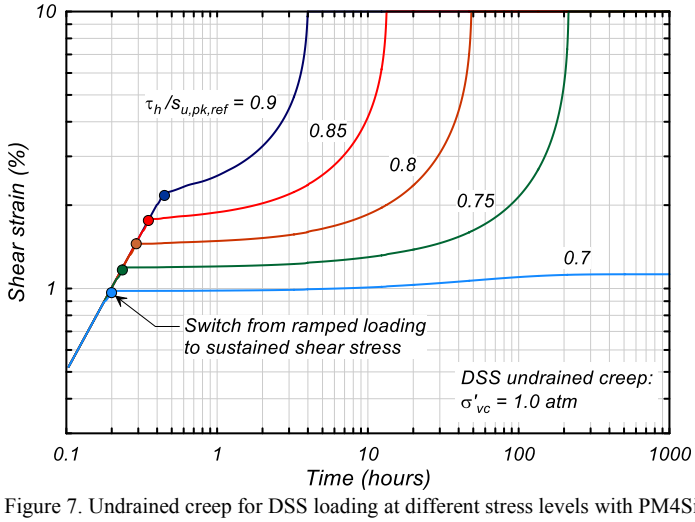

Figure 7. Undrained creep for DSS loading at different stress levels with PM4SiltR.

2.3 *Foundation: Constitutive model, parameters, and responses*

The foundation soils were assumed to be stronger and less sensitive than the tailings, but to have otherwise similar characteristics. For simplicity, the input parameters for PM4SiltR were all kept the same as for the tailings, except that the $s_{u,cs,ref}/\sigma'_{vc}$ was increased to 0.40. These parameters produce a non-strain-softening response in undrained DSS loading with the peak and critical state $s_{u,ref}/\sigma'_{vc}$ both equal to 0.40. This peak strength is about 30% greater than for the tailings, which in combination with a non-strain-softening response, resulted in deformations and instability being controlled by the tailings.

2.4 *Dikes: Constitutive model, parameters, and responses*

The dike materials, modeled with PM4Sand, were assumed to be medium-dense silty sands. The specified input parameters were a relative density D_r = 55%, G_o = 677, and h_{po} = 0.40. All other parameters retained their default values (Boulanger and Ziotopoulou 2017). The dike materials are modeled as drained. The mobilized peak effective friction angles varied with loading path and effective confining stress, but were generally about 33-38 degrees for the selected parameters and stress conditions in the dikes.

3 SIMULATION RESULTS

3.1 *Initial stress conditions*

The initial static stress conditions for an analysis case with the phreatic surface at the left boundary set to z_w = 45 m (Figure 1) are illustrated in Figure 8 showing contours of α and the anisotropic consolidation stress ratio ($K_c = \sigma'_{1c}/\sigma'_{3c}$). In addition, the phreatic and saturation lines from the steady seepage analysis for this case are shown on Figure 1, which shows that about half of the tailings are saturated beneath the dam face. The α values are between 0.1 and 0.2 in most of the tailings beneath the dam face, and as high as 0.25 in the foundation layer near the toe. The K_c values are between 1.5 and 2.5 in most of the tailings beneath the dam face, and as high as 3.0 at the bottom of the foundation layer near the toe.

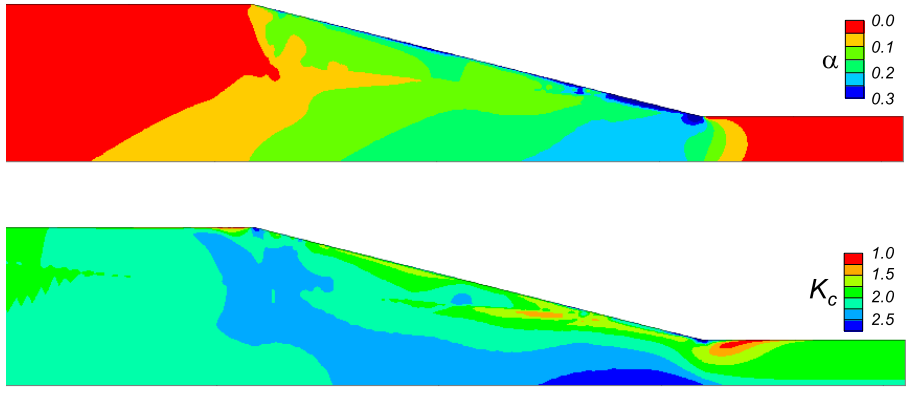

Figure 8. Contours of initial static horizontal shear stress ratio (top) and consolidation stress ratio (bottom) for the initial stress conditions for the tailings impoundment with z_w = 45 m.

3.2 *Creep-induced deformations for different water levels*

The analysis for creep was started after the initial stress conditions were established, by setting the parameters F_p and F_M to their calibrated values. The effects of different water levels on creep-induced deformations are illustrated in Figure 9 showing the horizontal displacement for a point at mid-slope on the dam face versus time for two different water levels, z_w, at the left boundary (Figure 1). The analysis with z_w = 45 m (i.e., phreatic surface 5 m below the tailings surface at the left boundary) resulted in about 35 mm of slope displacement over about 10 days, after which the slope stabilized and creep deformations became negligible. The potential for further creep deformation becomes negligible once the current stress state is within or on the static bounding surface for all points within the slope, as tracked in PM4SiltR through an internal creep index parameter. The analysis with z_w = 50 m (i.e., phreatic surface at the tailings surface at the left boundary) resulted in about 52 mm of slope displacement in the first 10 days and another 10 mm

of displacement over the following 50 days, after which displacements began to accelerate. The horizontal displacement increased to 100 mm at 95 days, after which creep rupture developed rapidly with instability occurring at 103 days. Thus, increasing z_w from 45 to 50 m was sufficient to transition from a stable to unstable condition, even though the elevation of the phreatic surface beneath the mid-face of the dam only differs by about 1.0 m for these two cases.

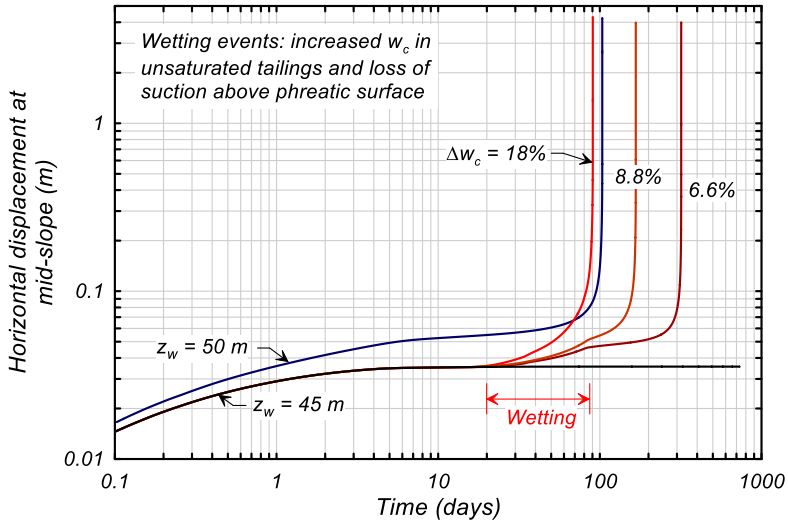

Figure 9. Horizontal displacement at mid-slope versus time after start of creep analysis for two different water levels and with three different wetting events.

3.3 *Effect of a wetting event*

The initiation of undrained creep rupture by a wetting event (e.g., rainfall, runoff, or rising pool) was evaluated for the otherwise stable creep analysis case with z_w = 45 m. The slope was first allowed to stabilize through 20 days of creep. Over the following 65 days, the water content in the unsaturated tailings (above the saturation line) was progressively increased to a final increment of 6.6%, 8.8%, or 18% and the suctions (negative pore pressures) in the capillary rise zone (between the phreatic surface and saturation line) were progressively reduced to zero. The change in water content increases the total unit weight by the same percentage. The driving shear stresses in the slope increase by only a fraction of this percentage though, because the unit weights of the dike and saturated tailings are unaffected. The horizontal displacements versus time in Figure 9 show that all three wetting events led to undrained creep rupture and slope instability, with instability developing at 90 days with Δw_c = 18%, at 167 days with Δw_c = 8.8%, and at 317 days with Δw_c = 6.6%. The slope remained stable in an analysis with Δw_c = 4.4%.

3.4 *Progressive failure*

The slope failures due to undrained creep in the above cases involved progressive failure in the strain-softening tailings. In all cases, undrained creep rupture or strain softening in the tailings initiated just above the foundation layer beneath about the mid-point on the dam face. This initiation of strain softening led to progressive failure. The progressive nature of failure is illustrated in Figure 10 showing contours of shear strain when the dam face has moved horizontally 75 mm, 100 mm, 200 mm, and 4000 mm in the analysis case with z_w = 45 m and the wetting event with Δw_c = 8.8%. The creep rupture initiated at the most strongly stressed location in the slope, as indicated by comparing the contours of initial stress ratios in Figure 8 with the location where shear strains first localized (Figure 10). Relatively small shear strains were

required to initiate strain softening at this location, consistent with the effects of anisotropic consolidation (Figures 3 and 4). The shear strain contours also show how failure surfaces at the toe began to form both above and below the lowest dike, but eventually fully developed in the tailings above the dike. Complementary shear bands formed in the slide mass above the primary failure surface, but the slide mass generally moved as a coherent block, as illustrated by the horizontal displacement contours shown in Figure 11.

The progressive nature of the slope failures explains why the time to instability (Figure 9) is several times greater than the time for undrained creep rupture at an elemental level (Figure 7). Once creep strains become large enough to initiate strain softening at one point, the shedding of shear stress leads to increasing shear stresses at other points, which in turn begin to develop creep-induced shear strains and subsequent strain softening. The extent of strain softening progressed with only modest slope deformations until the slope was close to being unstable, after which deformations accelerated. Thus, the sequential nature of undrained creep rupture along the final failure surface is why the time to instability was several times that required for undrained creep rupture at an element level.

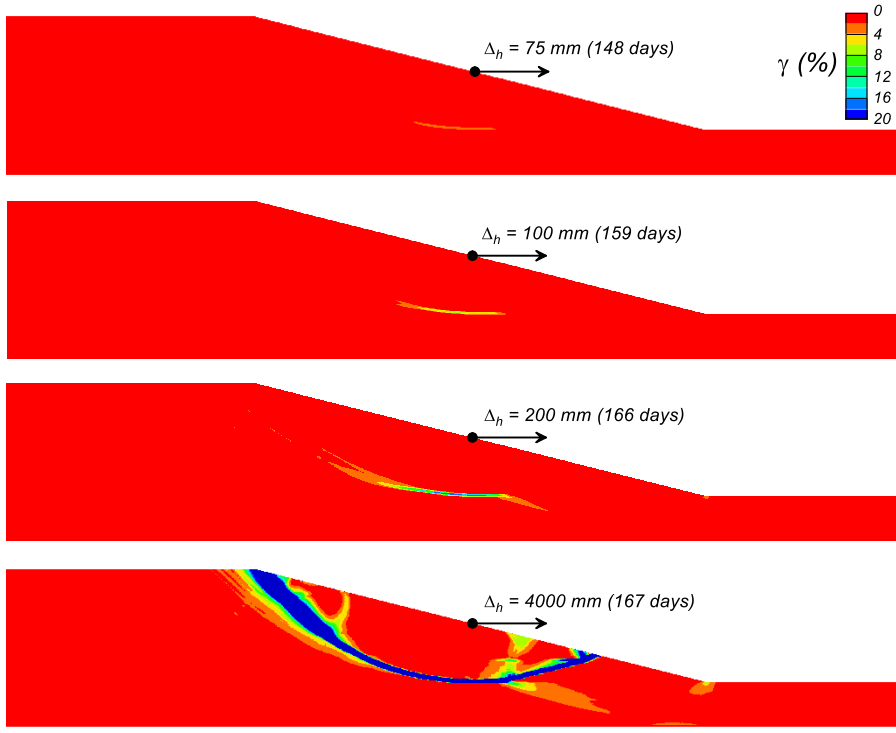

Figure 10. Contours of shear strain at different levels of horizontal displacement at mid-slope for the analysis case with z_w = 45 m and wetting-induced instability with Δw_c = 8.8%.

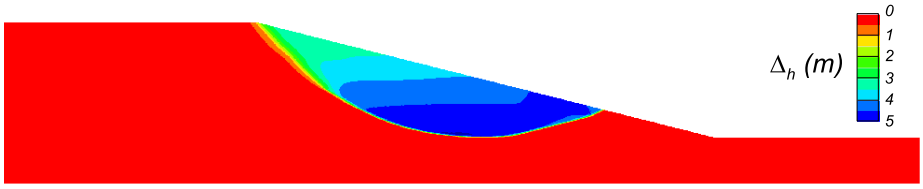

Figure 11. Contours of horizontal displacements for the analysis case with z_w = 45 m and wetting-induced instability with Δw_c = 8.8%, at the time when the peak displacement has reached 5 m.

3.5 *Limitations*

The present analyses assumed undrained conditions in the tailings, which mean that the beneficial effects of consolidation (pore pressure diffusion) during creep were not considered. If the time for undrained creep rupture to progress is significantly smaller than the time required for significant consolidation to occur, then the potential benefits of consolidation may be small. If the rate of consolidation is much quicker, perhaps due to high permeability lenses throughout the tailings, it is possible that consolidation could reduce the potential for creep and progressive failure to cause slope instability. Accurately modeling the rate of creep and creep relaxation would require more extensive testing for calibration than is commonly performed, and accurately modeling the rate of consolidation requires extensive characterization studies or field loading data upon which to calibrate the analyses. The development of procedures and guidance for the coupled modeling of creep and consolidation phenomena in practice requires further study.

The present analyses will exhibit a degree of mesh sensitivity because the materials are strain softening and the failure involved strain localizations. The inclusion of viscoplasticity has been shown to provide a measure of regularization (Needleman 1988, Niazi et al. 2013), at least for some initial range of shear strains (Oathes and Boulanger 2019, 2020). The development of procedures and practical guidance to account for mesh dependency and mesh regularization during undrained creep also requires further study.

4 DISCUSSION

There are several challenges to accurately quantifying the effects of creep and progressive failure on slope stability in tailings or other contractive materials, including aspects related to material characterization and numerical analyses. Estimates of rate-dependent material properties may be obtained from empirical correlations or site-specific laboratory testing. However, empirical correlations for creep behaviors in contractive soils are not well developed for a range of important soil types, including various tailings materials with intermediate characteristics (e.g., low-plasticity silty sands, sandy silts, or clayey sands). Site-specific testing to determine rate-dependent material properties involves more advanced testing equipment than is commonly available and can be obscured by sample disturbance effects. Numerical analyses of creep rupture are complicated by several issues, including: (1) limited availability of appropriate constitutive models, (2) mesh sensitivity when modeling strain softening and localization behaviors, (3) estimating time scales for consolidation relative to creep, and (4) performing analyses with coupling of the creep and consolidation processes. Despite these challenges, the potential effects of undrained creep need to be considered in design or analysis, either indirectly or directly. For example, recognizing creep and progressive failure effects can inform the selection of soil strengths, assumptions regarding the potential for static liquefaction triggering, and allowable factors of safety in limit equilibrium analyses. Alternatively, the direct simulation of creep and progressive failure in numerical analyses has the potential to provide valuable insights for specific projects and development of generalized guidance, despite these challenges and limitations.

5 CONCLUDING REMARKS

The numerical modeling of undrained creep in saturated silts and clays that are initially loose of critical state (e.g., normally or lightly over-consolidated) was illustrated for a hypothetical tailings dam using the two-dimensional finite difference program FLAC with a new user-defined strain-rate dependent constitutive model PM4SiltR. The constitutive model was introduced and its stress-strain responses for a range of loading conditions and strain rates were illustrated through single-element simulations. The numerical analyses of the tailings dam illustrated the process of undrained creep rupture leading to slope instability, including the potential for small changes in loading to cause a delayed slope failure.

The potential for undrained creep rupture and progressive failure in contractive soils needs to be recognized in analysis and design, despite the challenges with accurately quantifying these effects and either indirectly or directly accounting for them. The numerical and constitutive modeling approach described herein shows promise as a means for explicitly evaluating these effects in practice.

6 ACKNOWLEDGMENTS

The work described herein was funded in part by the California Department of Water Resources under Contract 4600009751. Any opinions, findings, or recommendations expressed herein are those of the authors and do not necessarily represent the views of this organization. The authors benefited from discussions regarding constitutive and numerical modeling with Professors Bruce Kutter and Katerina Ziotopoulou. The authors appreciate the above support.

7 REFERENCES

Boulanger, R. W., and Beaty, M. H. 2016. Seismic deformation analyses of embankment dams: A reviewer's checklist. Proceedings, Celebrating the Value of Dams and Levees – Yesterday, Today and Tomorrow, 36th USSD Annual Meeting and Conference, United States Society on Dams, Denver, CO, 535-546.

Boulanger, R. W., and Wijewickreme, D. 2019. Calibration of a constitutive model for the cyclic loading responses of Fraser River Delta Silt. Proc., VII International Conference on Earthquake Geotechnical Engineering, Rome, Italy, June 17-20.

Boulanger, R. W., and Ziotopoulou, K. 2017. PM4Sand (Version 3.1): A sand plasticity model for earthquake engineering applications. Report No. UCD/CGM-17/01, Center for Geotechnical Modeling, Department of Civil and Environmental Engineering, University of California, Davis, CA, 113 pp.

Boulanger, R. W., and Ziotopoulou, K. 2018. PM4Silt (Version 1): A silt plasticity model for earthquake engineering applications. Report No. UCD/CGM-18-01, Center for Geotechnical Modeling, Department of Civil and Environmental Engineering, University of California, Davis, CA, 108 pp.

Boulanger, R. W., and Ziotopoulou, K. 2019. A constitutive model for clays and plastic silts in plane-strain earthquake engineering applications. *Soil Dynamics and Earthquake Engineering*, 127(2019): 105832, 10.1016/j.soildyn.2019.105832.

Boulanger, R. W., Price, A. B., and Ziotopoulou, K. 2018. Constitutive modeling of the cyclic loading response of low plasticity fine-grained soils. GSIC 2018, Proc. GeoShanghai 2018 International Conference: Fundamentals of Soil Behaviours, A. Zhou et al. (Eds.), Springer Nature Singapore Pte Ltd., pp. 1–13, https://doi.org/10.1007/978-981-13-0125-4_1.

Boulanger, R. W., Ziotopoulou, K., and Oathes, T. J. 2020. PM4SiltR (Version 1): A silt plasticity model with rate effects for slope stability applications. Center for Geotechnical Modeling, University of California, Davis, CA (draft).

Campanella, R. G., and Vaid, Y. P. 1974. Triaxial and plane strain creep rupture of an undisturbed clay. *Canadian Geotechnical Journal*, 11(1), 1-10.

Clarke, S. D., and Hird, C. C. 2012. Modelling of viscous effects in natural clays. *Canadian Geotechnical Journal*, 49, 129-140, doi:10.1139/T11-08

Graham, J., Crooks, J. H. A., and Bell, A. L. 1983. Time effects on the stress-strain behaviour of natural soft clays. *Géotechnique*, 33(3), 327–340.

Itasca (2019). FLAC - Fast Lagrangian Analysis of Continua, Version 8.1, Itasca Consulting Group, Inc, Minneapolis, Minnesota.

Kulhawy, F. H., and Mayne, P. W. 1990. Manual on Estimating Soil Properties for Foundation Design, Report EPRI EL-6800, Electric Power Research Institute, Palo Alto, CA.

Kutter, B. L., and Sathialingam, N. 1992. Elastic-viscoplastic modelling of the rate-dependent behaviour of clays. *Géotechnique*, 42(3), 427-441.

Ladd, C. C., and DeGroot, D. J. 2004. Recommended practice for soft ground site characterization: Arthur Casagrande Lecture. Proc., 12th Panamerican Conference on Soil Mechanics and Geotechnical Engineering, Massachusetts Institute of Technology, Cambridge, MA USA, June 22 – 25, 2003.

Leoni, M., Karstunen, M., and Vermeer, P. A. 2008. Anisotropic creep model for soft soils. *Géotechnique*, 58(3), 215-226, 10.1680/geot.2008.58.3.215.

Martindale, H., Chakraborty, T., and Basu, D. 2012. A rate dependent constitutive model for clay. GeoCongress 2012: State of the Art and Practice in Geotechnical Engineering, Geotechnical Special Publication 225, ASCE, 859-868.

Mitchell, J. K., and Soga, K. 2005. *Fundamentals of Soil Behavior*. John Wiley & Sons, Inc.

Needleman, A. 1988. Material rate dependence and mesh sensitivity in localization problems. *Computer Methods in Applied Mechanics and Engineering*, 67, 69-85.

Niazi, M. S., Wisselink, H. H., and Meinders, T. 2013. Viscoplastic regularization of local damage models: Revisited. *Computational Mechanic*s, 51(2), 203–216.

Oathes, T. J., and Boulanger, R. W. 2019. Numerical Evaluation of Strain-Rate Effects on Strain-Softening and Localization in Saturated Clays. Proc., Second City - Second Chances: Stories of Rehabilitation, Modification, and Revitalization, 39th USSD Annual Meeting and Conference, United States Society of Dams, Chicago, IL, 1–15

Oathes, T. J., and Boulanger, R. W. 2020. Influence of strain-rate on localization and strain-softening in normally consolidated clays with varying strength profiles. Geo-Congress 2020: Modeling, Geomaterials, and Site Characterization. Geotechnical Special Publication 317, J. P. Hambleton, R. Makhnenko, and A. S. Budge (eds), ASCE, 247-255.

Robertson, P.K., de Melo, L., Williams, D.J., and Wilson, G.W. 2019. Report of the Expert Panel on the Technical Causes of the Failure of Feijão Dam I.

Sheahan, T. C. 1995. Interpretation of undrained creep tests in terms of effective stresses. *Canadian Geotechnical Journal*, 32: 373-379.

Sheahan, T. C., Ladd, C. C., and Germaine, J. T. 1996. Rate-Dependent Undrained Shear Behavior of Saturated Clay. *Journal of Geotechnical Engineering*, 122(2), 99–108.

Shi, Z., Hambleton, J. P., and Buscarnera, G. 2019. Bounding surface elasto-viscoplasticity: A general constitutive framework for rate-dependent geomaterials. *Journal of Engineering Mechanics*, 145(3): 04019002, 10.1061/(ASCE)EM.1943-7889.0001578.

Wang, W. M., Sluys, L. J., and De Bort, R. 1997. Viscoplasticity for instabilities due to strain softening and strain-rate softening. *International Journal for Numerical Methods in Engineering*, 40: 3839-3864.

Watabe, Y., Udaka, K., Nakatani, Y., and Leroueil, S. 2012. Long-term consolidation behavior interpreted with isotache concept for worldwide clays. *Soils and Foundations*, Japanese Geotechnical Society, 52(3): 449-464.

Yuan, Y., and Whittle, A. 2018. A novel elasto-viscoplastic formulation for compression behaviour of clays. *Géotechnique*, 68(12), 1044-1055, 10.1680/jgeot.16.P.276.

Ziotopoulou, K., and Boulanger, R. W. 2016. Plasticity modeling of liquefaction effects under sloping ground and irregular cyclic loading conditions. *Soil Dynamics and Earthquake Engineering*, 84 (2016), 269-283, 10.1016/j.soildyn.2016.02.013.

Dynamic Effective Stress Analysis of a Centerline Tailings Dam – Case Study

Paola Torres
Knight Piésold Consultores S.A., Lima, Lima, Peru

Jorge Macedo
Georgia Institute of Technology, Atlanta, Georgia, United States

Solange Paihua
Knight Piésold Consultores S.A., Lima, Lima, Peru

ABSTRACT: This study presents the results for the dynamic effective stress analysis performed to evaluate the seismic performance of a center-line tailings dam in the South American Andes. To characterize the seismic demand at the project site, a probabilistic seismic hazard analysis (PSHA) was performed, producing deterministic-based and probabilistic-based seismic design criteria. The PSHA study shows that the project site is affected by both subduction interface and subduction intraslab ground motions. In addition, the PSHA study produced spectrally matched ground motions for the subsequent dynamic analyses. This paper presents the 2D dynamic analysis of a tailings dam subjected to the maximum credible earthquake (MCE). The centerline tailings dam is planned to be raised up to 90-m high, and it will be composed by a starter dam and successive raisings. The dynamic analyses were performed with the software FLAC, using the UBCHYST constitutive model for materials that are not expected to produce large excess pore pressures, and the PM4Silt model for the materials that may generate excess pore pressures due to cyclic loading. The results suggest that there are no failure mechanisms by the end of the ground motions during the numerical simulations; however, there are considerable displacements. The results help to plan the overall operational management of the tailings facility.

1 INTRODUCTION

This paper presents the dynamic effective stress analysis of a centerline tailings dam, located in the South American Andes. The centerline construction method has been selected to build the dam that is part of the tailings storage facility (TSF) because it allows optimization of available storage while minimizing the volume of dam material. The dam will retain tailings during the operation, and also after closure. It will have a height of 90 m, and its crest length will be approximately 56 0m. The dam will be built in six stages, which consider a starter dam and five sequential center-lined raisings supported by an upstream rockfill platform. Downstream slopes are equal to 2H:1.0V and 2.3H:1.0V for the starter dam and raisings, respectively, whereas the upstream slopes are 1.7H:1.0V and 1.5H:1.0V.

The analyses performed in this study were conducted to evaluate the seismic performance of the dam, which is controlled by the earthquake-induced permanent deformations and the intactness of the seepage control system. There are a number of simplified procedures to perform initial evaluations of the overall seismic performance of a dam (e.g. Bray & Macedo, 2019; Bray et al., 2018). However, when liquefiable materials are present in the dam body or its foundation, more rigorous procedures should be employed, which was the strategy considered in this study.

This paper presents the results of fully coupled stress-flow dynamic analyses using design ground motions provided by a probabilistic seismic hazard study (PSHA) for the dam area. We have captured the tailings behavior observed in cyclic laboratory tests by using the constitutive

model PM4Silt (Boulanger & Ziotopoulou, 2018). The nonlinear behavior of non-liquefiable materials was accounted for by employing the model UBCHYST (Naesgaard, 2011). These user-defined constitutive models are incorporated into the commercially available computer code FLAC 8.0 (Itasca, 2016).

2 DESCRIPTION OF THE DAM, FOUNDATION, AND TAILINGS MATERIALS

The information collected from geotechnical site investigations was reviewed and interpreted to characterize the dam, foundation, and tailings materials. The dam considered in this study has not been built yet; hence, some material properties have been estimated based on laboratory tests performed on samples obtained from quarries and tailings samples obtained from a pilot process plant. Foundation properties were estimated based on field tests (e.g., permeability and geophysical tests) when this information was available.

2.1 *Dam*

The dam is mainly composed of structural fill, in addition to the core, filter/drain, and rockfill materials, which are also present. The structural fill and core consist of moraine material (gravelly clay, GC); the core materials have a plasticity index (PI) of 15. The filter/drain is composed of coarse and medium sand, while the rockfill platform material is mainly composed of cobbles and boulders. The starter dam also includes an upstream geomembrane to prevent contact water from getting into the dam body. The soil particle-size fraction distribution of these materials is shown in Table 1, and Figure 1 presents the maximum cross-section of the dam, which has been considered in this study.

Table 1. Soil particle-size fraction distribution of the dam construction materials

Classification of soils	Structural fill [%]	Core [%]	Filter/drain [%]	Rockfill platform [%]
Cobbles and boulders	0 – 20	0 – 5	0	10 – 75
Gravel	30 – 50	15 – 40	0 – 35	25 – 45
Sand	20 – 40	30 – 40	65 – 95	0 – 40
Fines content*	10 – 30	25 – 45	0 – 5	0 – 5
Max. Particle Size	6"	4"	1"	6"
Plasticity Index	8 – 15	> 15	Non-plastic	Non-plastic

*Fines content defined as percent passing 0.075 mm (N°.200 sieve)

2.2 *Foundation*

The foundation is composed of two groups of rocks that belong to the Ambo and Copacabana geological groups, respectively. The Ambo group is mainly composed of a large proportion of quartz sandstone with thin horizons of siltstone and bituminous shales. The rock is moderately weathered, has a low to medium strength, and is slight to moderately fractured. The Copacabana group is mainly composed by limestone rocks with intercalations of dolomite horizons, calcareous breccia, calcareous sandstone, and siltstone. The upper stratum of this group is moderate to highly weathered, has a low strength, and is moderate to very fractured, while the lower stratum is slight to moderately weathered, has a medium to high strength, and is slight to moderately fractured.

2.3 *Tailings*

In the first year of operation, the TSF will receive tailings from the new process plant; after the second year, it will store tailings from an additional process plant, increasing the volume of tailings that need to be stored. Therefore, two types of tailings, denominated as tailings R and C, were characterized as part of this study. Tailings R classifies as silty clays (CL), have low to medium plasticity (PI = 9), 98% fines content, and an average specific gravity of 2.8. Tailings C classify mainly as sandy silts (ML), with an average fines content of 65%. They have null to low plasticity (PI = 4) and an average specific gravity of 2.81.

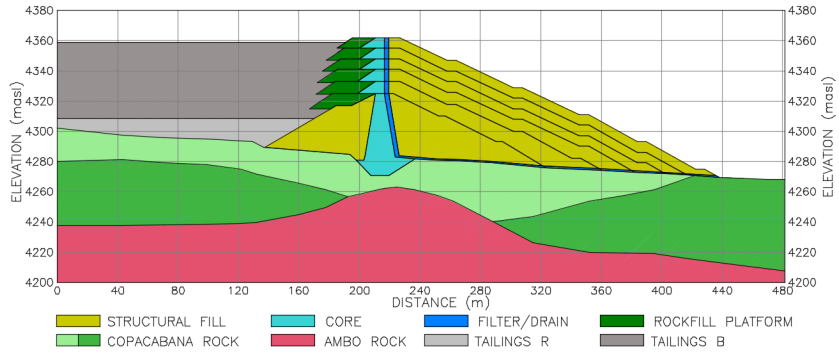

Figure 1. Maximum cross-section of the dam

3 SEISMIC DESIGN CRITERIA

Using the Canadian Dam Association (CDA) dam safety guidelines, the seismic risk associated with the dam was classified as "Extreme". For extreme hazard dams, CDA (2013) recommends the MCE or 10,000-year earthquake. The MCE was ultimately selected as the appropriate design earthquake for the dam. The resulting peak horizontal ground accelerations (PGA) for the MCE is 0.34g based on the 84th percentile of the deterministic acceleration spectrum, and it is associated with a Magnitude 8.0 Intraslab earthquake at a distance of 120 km from the project site.

Three acceleration design time-histories, provided by the PSHA study, have been used for the analyses. These time histories correspond to spectrally matched records that used recorded ground motions from the following earthquakes: (1) Lima, 1974; (2) Moquegua, 2001; and (3) Pisco, 2007. The ground motions used for the dynamic analyses are presented in Figure 2, and were applied to a quiet-boundary base of the numerical model as stresses.

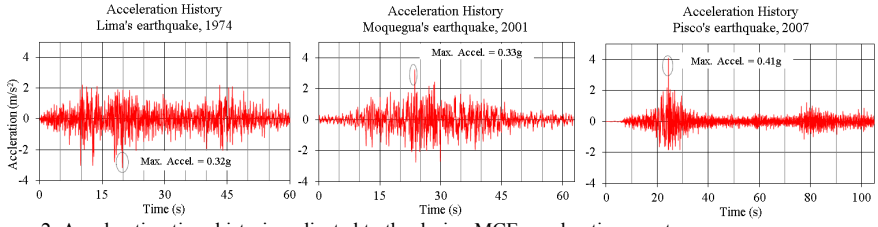

Figure 2. Acceleration time-histories adjusted to the design MCE acceleration spectrum

4 NUMERICAL MODEL

The dam was modeled using FLAC, which allows users to solve stress-strain geotechnical problems considering a fully explicit time-marching numerical formulation. The dimensions of the model and zones satisfy seismic wave transmission requirements according to Kuhlemeyer & Lysmer (1973) recommendations, which state that maximum zone dimension should be less than one-tenth of the maximum shear wavelength for a given material. The thickness of the zones in the FLAC model were 1 m. Figure 3 presents the FLAC dam model.

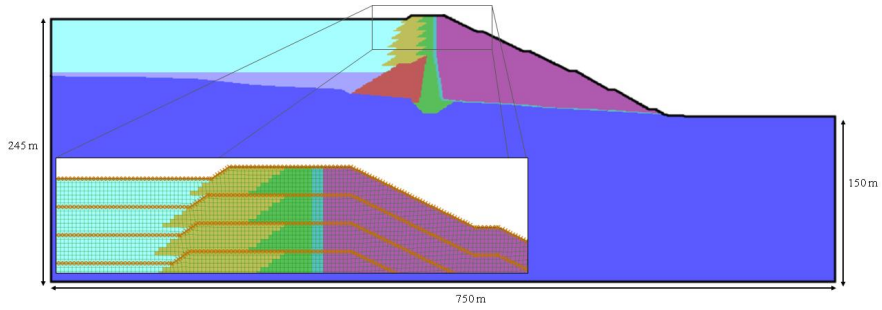

Figure 3. FLAC model for the dam evaluated in this study

5 STATIC ANALYSIS

Before performing the dynamic analyses, the dam body and its foundation have been analyzed under gravity loads with drained conditions to establish the pre-earthquake stress state. We used the Mohr-Coulomb model for tailings and dam materials, and an elastic model for the bedrock. Bedrock elastic parameters were obtained from the multichannel analyses of surface waves (MASW), while for the dam materials, the properties were estimated based on shear wave velocity (Vs) measured on similar materials in the dam area. Along with the static analysis, flow analyses were performed to establish the pre-earthquake pore pressure distribution, i.e., the steady-state flow condition. Groundwater boundary conditions were applied to the model to obtain a water table descending through the filter/drain chimney and to assure the saturated condition of tailings. This represents a critical stability condition for the TSF, which was considered appropriate for the analyses. Table 2 presents the properties considered for the static and flow analyses, and Figure 4 presents the model's initial stress state.

Table 2. Material properties for static and flow analysis

Material	**Dry unit weight** γ_{dry} **(kN/m³)**	**Friction angle** ϕ' **(°)**	**Cohesion** **c** **(kP)**	**Poisson ratio** **ν**	**Shear stiffness** **G*** **(MPa)**	**Bulk Modulus** **K**** **(MPa)**	**Porosity** **n**	**Hydraulic conductivity** **k** **(m/s)**
Structural fill	21.0	38	0	0.35	70	210	0.30	1E-07
Core	20.0	34	8	0.35	67	200	0.35	1E-07
Filter/drain	17.0	35	0	0.33	46	120	0.33	2E-03
Rockfill platform	20.5	40	0	0.30	78	169	0.26	1E-03
Tailings	14.5	30	0	0.35	3.5	10.5	0.48	1E-07
Bedrock	25.0	-	-	0.28	382	740	0.15	1E-06

*Static shear stiffness (G) was taken as $0.1G_{max}$. G_{max} is the small strain shear modulus estimated as $G_{max}=\rho V_s^2$, where ρ is the total density of the material.
**Bulk modulus (K) is calculated as K=G*2*(1+ ν)/(3*(1-2 ν)).

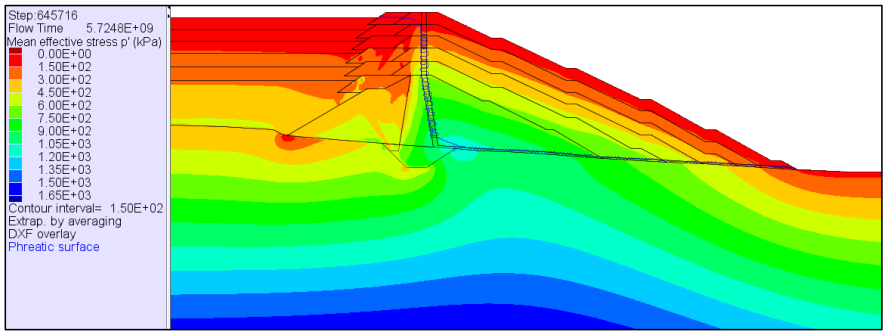

Figure 4. Pre-earthquake mean effective stress (p') and water table location

6 DYNAMIC ANALYSIS

6.1 *Constitutive models*

The UBCHYST constitutive model was selected for the structural fill, core, filter/drain, and rockfill platform materials. These materials have been considered non-liquefiable due to their high permeability, particle size, or compaction degree. The non-linear hysteretic UBCHYST model is a robust, relatively simple, total stress model. UBCHYST was developed at the University of British Columbia for dynamic analyses of soil subjected to earthquake loading. Typically, the model is used for fine-grained soils (silts and clays) with undrained strength parameters, for free-draining granular soil with drained strength parameters or in non-saturated granular soils. Its characteristics include the reduction of the shear secant modulus with strain, emulation of marching or ratcheting to occur when there is a static shear bias, and the option of allowing a permanent modulus reduction as a function of maximum past shear stress ratio (Naesgaard 2011).

The PM4Silt constitutive model was selected to represent the response of tailing materials because they are expected to be susceptible to liquefaction. Tailings have not been deposited at the TSF yet, so there is no field available data from the likes of cone penetration tests (CPTs). Nevertheless, due to tailings nature is inferred that tailings would develop excess pore water pressures and/or likely undergo liquefaction due to earthquake shaking. The PM4Silt plasticity model was developed and implemented by Boulanger & Ziotopoulou (2018) for representing low-plasticity silts and clays in geotechnical earthquake engineering applications. The model is focused on approximating a range of undrained monotonic and cyclic loading responses of saturated low-plasticity silts and clays that exhibit stress-history normalized behaviors, as opposed to the responses of purely nonplastic silts and sands (Boulanger & Ziotopoulou, 2018).

6.2 *Non-liquefiable materials input parameters*

That small strain (dynamic) shear stiffness, G_{max}, for bedrock was estimated from the shear wave velocity measurements. The Bedrock was modeled as an elastic material with a shear wave velocity of 1200 m/s. In the case of the filter/drain, structural fill, and rockfill platform, G_{max} was estimated using shear wave velocity measurements in similar material from existing dams. Furthermore, G_{max} of the core material was estimated based on resonant column test results. The G_{max} values for different materials were applied to the model with an effective confinement stress dependency according to Equation 1, proposed by Seed et al. (1970, 1984),

$$G_{max} = 21.7k_{2,max}Pa(\frac{\sigma'_m}{Pa})^{0.5} \quad (1)$$

where G_{max}, $k_{2,max}$, P_a and σ'_m are the small strain shear modulus, modulus coefficient, atmospheric pressure, and the mean confining pressure, respectively. Equation 1 makes G_{max} and bulk modulus values vary with depth across the height of the dam.

Table 3. Dam and foundation properties for dynamic analysis

Material	Model	Dry unit weight γ_{dry} (kN/m^3)	Modulus coefficient $k_{2,máx}$	Poisson ratio N	Small strain shear modulus G_{max} @1atm (MPa)	Bulk modulus K_{max} @1atm (MPa)
Structural fill	UBCHYST	21.0	160	0.35	350	1049
Core	UBCHYST	20.0	140	0.35	308	924
Filter/drain	UBCHYST	17.0	110	0.33	242	631
Rockfill platform	UBCHYST	20.5	180	0.30	396	858
Bedrock	Elastic	25.0	-	0.28	3817	7402

The summary of the dam and foundation dynamic properties is presented in Table 3 and it shows the $k_{2,máx}$ values selected for construction materials which are in the range expected for gravels according to Seed et al. (1984).

The shear modulus and damping ratio curves used in the dynamic analyses were calibrated using several references. The curves from Rollins et al. (1998) were considered for rockfill materials, the curves from Darendeli (2001) were considered for the structural fill and filter/drain material, and the Seed & Idriss (1970, 1986) curves for sands and gravels were also considered. Shear modulus reduction and damping ratio curves for the core material were obtained from resonant column (RC) tests and were also considered for the structural fill due to its similarity. All these experimental-based and laboratory curves were used to calibrate the UBCHYST model. Figure 5 presents the cyclic FLAC simulations obtained for the dam materials.

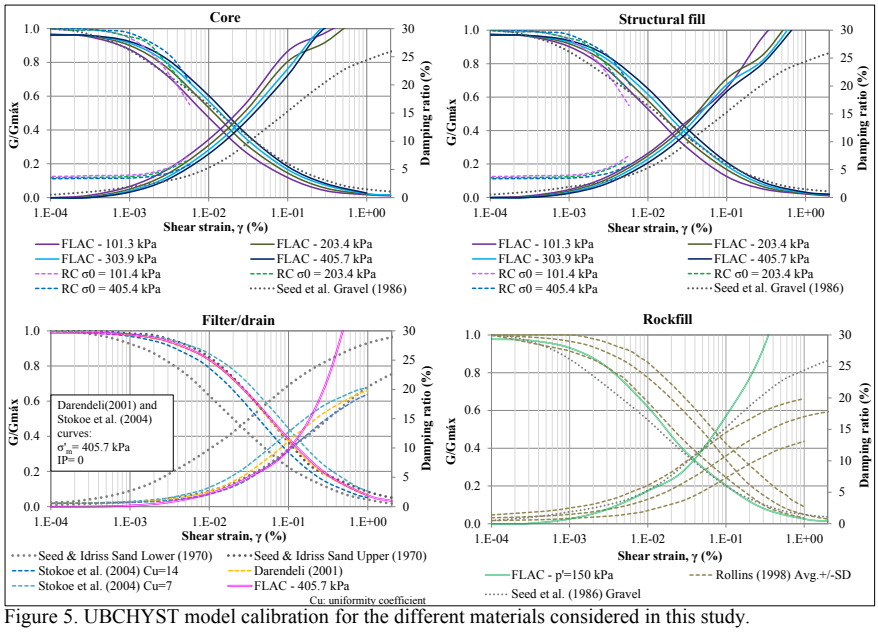

Figure 5. UBCHYST model calibration for the different materials considered in this study.

The strength parameters of the rockfill platform and structural fill were estimated based on data from Leps (1970). The parameters selected for the rockfill platform are between the lower-bound values and the average values for rockfill materials, whereas the parameters selected for the structural fill are comparable to the lower-bound values. The friction angle ϕ was estimated based on Barton & Kjaersnli (1981), using Equation 2:

$$\phi = \phi_1 - \Delta\phi log(\frac{\sigma'_3}{Pa}) \quad (2)$$

where, σ'_3, ϕ_1, and $\Delta\phi$ are minor principal effective stress, reference friction angle (at σ'_m = Pa), and friction angle reduction for every log cycle of stress level increase, respectively.

The summary of the strength parameters and UBCHYST calibration parameters for the dam materials are presented in Table 4. These are the final values used in FLAC simulations curves shown in Figure 5. Calibration parameters for core and structural fill were obtained for specific stress ranges by using results of resonant column test.

Table 4. Strength parameters and UBChyst calibration parameters

Material	Friction angle			Cohesion	Mean effective stress range	UBCHYST calibration parameters				
	ϕ (°)	ϕ_1 (°)	Δϕ (°)	c (kPa)	σ'_m (kPa)	Hn	Hrf	Hrm	Hdfac	Hdmofl
Structural fill	LEPS	40	6	0	0-150	2.0	0.98	1	0.7	1
					150-250	2.5				
					250-350	2.7				
					350-450	2.7				
					>450	2.7				
Core	34	-	-	8	0-150	3.0	0.98	1	0.7	1
					150-250	3.5				
					250-350	3.7				
					350-450	3.7				
					>450	3.7				
Filter/drain	35	-	-	0	0	1	0.98	1	0.6	1
Rockfill platform	LEPS	45	6	0	0	2	0.7	1	0.8	1

6.3 *Liquefiable materials (tailings) input parameters*

As previously discussed, the PM4Silt constitutive model was used to model the response of-tailings materials. To characterize the tailings cyclic behavior and to calibrate the PM4Silt constitutive model several laboratory tests were conducted: cyclic simple shear (CSS), consolidated undrained, and drained triaxial shear (CUTX and CDTX), monotonic simple shear (DSS) and bender element test.

As commonly observed for tailings, the slope of the liquefaction resistance curves (i.e. cyclic stress ration or CRS versus number of cycles for liquefaction) defined by multiple CSS tests for both types of tailings are quite flat. All cyclic resistance ratio (CSR) values are modest; they do not exceed a value of 0.2. It was also observed that raising the consolidation stress level from 100 kPa to 300 kPa or 400 kPa did not produce the expected reduction in normalized cyclic resistance, often characterized by a Kσ factor less than 1, but in fact, appeared to slightly raise the resistance. This resistance may be related to the compressible nature of the fine tailings, as there is a general trend for the densities to be higher for higher stress specimens.

The primary input parameters of the PM4Silt constitutive model are the undrained shear strength ratio ($S_{u,cs}/\sigma'_{vc}$) (or undrained shear strength $S_{u,cs}$), the shear modulus coefficient (G_o), the contraction rate parameter (h_{po}), and an optional post-strongshaking shear strength reduction factor. The secondary input parameters of the model have default values, but they can be set according to the available information for the material being evaluated.

$S_{u,cs/\sigma'vc}$ value was estimated from DSS tests, as well as the secondary parameter bounding surface parameter ($n_{b,wet}$). The parameter $n_{b,wet}$ was set to 1.0 because this limits the peak shear resistance to $S_{u,cs,eq}$ in the simulation, which matches the strain-hardening response observed in the DSS test. Moreover, G_o and shear modulus exponent (n_G) values were calculated from the bender element test results. Finally, secondary parameters φ_{cv} y λ were obtained from the critical state line (CLS). CLS for tailings R and B were generated from CU and CD triaxial data.

Based on previously defined parameters, undrained cyclic loading with uniform CSR was simulated on FLAC to find the value of h_{po} that would best adjust the fit to the experimentally observed liquefaction resistance curves. We also examined the stress-strain and stress-path responses in the experiments and the numerical simulations to modify secondary parameters in the model. The secondary parameters were modified to flatten the liquefaction resistance curve and to generate stress-strain and excess pore-pressure responses similar to those experimentally observed. The summary of the input parameters for the PM4Silt model are presented in Table 5. Figure 6 shows the experimental-based and numerical-based liquefaction resistance curves.

Table 5. Input parameters for PM4Silt calibrations for tailings

Input parameters		**Default value**	**Calibration parameters**	
			Tailings R	**Talings B**
Primary parameters				
Undrained shear strength ratio at critical state	$S_{u,cs}/\sigma'_{vc}$	-	0,2	0,16
Shear modulus coefficient	G_o	-	413	451
Contraction rate parameter	h_{po}	-	14	6.5
Secondary parameters				
Initial void ratio	e_o	0.9	0.82	0.98, 0.86*
Shear modulus exponent	n_G	0.75	0.712	0.657
Critical state friction angule	φ_{cv}	32	35	36
Compressibility in e-ln(p') space	λ	0.06	0.063	0.0454
Sets bounding p_{min}	$r_{u,max}$	$p_{min}=p_{cs}/8$	Default	Default
Bounding surface parameter	$n^{b,wet}$	0.8	1	1
Bounding surface parameter	$n^{b,dry}$	0.5	Default	Default
Dilation surface parameter	n^d	0.3	Default	Default
Dilatancy parameter	A_{do}	0.8	0,6	Default
Plastic modulus ratio	h_o	0.5	Default	Default
Fabric term	Z_{max}	$10\leq 40(S_u/\sigma'_{vc}) \leq 20$	80	65
Fabric growth parameter	c_z	100	75	Default
Strain accumulation rate factor	c_ξ	$0.5\leq(1.2S_u/\sigma'_{vc}+0.2)\leq 1.3$	0.9	Default
Modulus degradation factor	C_{GD}	3	Default	Default
Plastic modulus factor	$C_{k\alpha f}$	4	Default	Default

*0.98 value was used for the ten superficial meters of tailings, for deeper tailings, the value 0.86 was assigned.

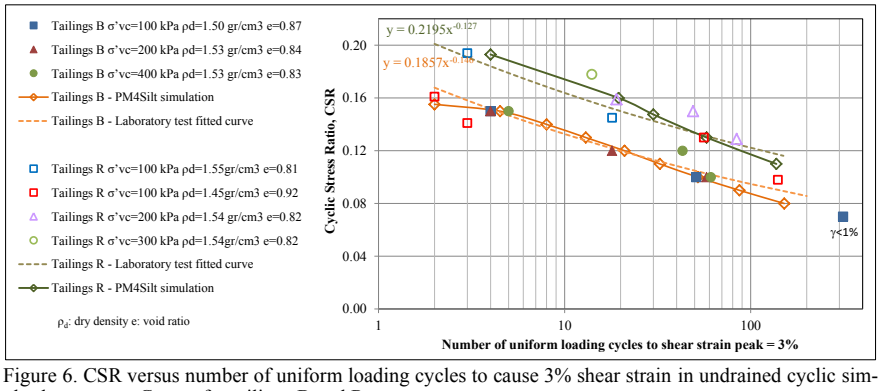

Figure 6. CSR versus number of uniform loading cycles to cause 3% shear strain in undrained cyclic simple shear tests – Curves for tailings B and R

7 RESULTS AND DISCUSSION

We discuss in this section the seismic response of the tailings-dam-foundation system, considering the design ground motion that led to the more conservative results. The FLAC model estimated maximum horizontal displacement at the dam crest of 2.75 m and 1 m towards the upstream and downstream direction, respectively, as shown in Figure 7. In addition, a maximum vertical deformation of 1.4 m was computed, as shown in Figure 8. The filter/drain and core experienced a range of horizontal displacements between 0.3 m to 1.0 m in the crest and up to 1.0 m of vertical displacement. These displacements are considered to be acceptable as it is not expected that they could affect the continuity of core materials, which have an original width of 3 m and 4 m, respectively.

Figures 7 77and 8 also show that the area with the highest displacements is the upstream part of the crest. Displacements at the dam crest are caused primarily by an upstream rotation of the top portion of the upstream rockfill platform into the liquefied tailings. It should be noted that the analyses considered that the pond in the tailings deposit is in contact with the upstream crest slope and that the tailings and core material are saturated. These conditions allowed the generation of pore pressures, which promoted the generation of shear strain deformations in specific areas inside the core. However, these shear strains did not extend towards the upstream or downstream direction during the analyses, so a failure mechanism was not apparent. An additional observation is that the horizontal and vertical displacements in the rockfill platforms caused by the design ground motions consistent with the MCE earthquake may temporarily damage the tailings pipeline system.

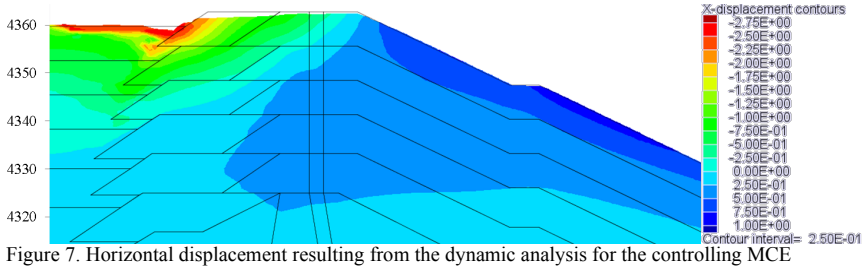

Figure 7. Horizontal displacement resulting from the dynamic analysis for the controlling MCE

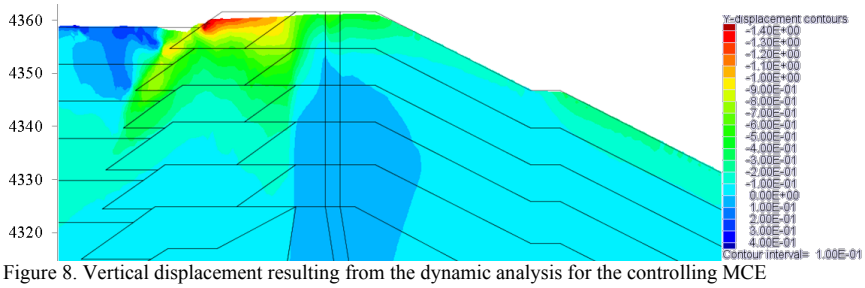

Figure 8. Vertical displacement resulting from the dynamic analysis for the controlling MCE

The seismic-induced excess pore water pressure ratio, Ru (u/σ'_{vo}), was monitored in all tailings zones of the model. During the analyses, zones where liquefaction has been triggered (pore pressure ratio Ru > 0.70 to 1.0) are tracked. These zones are shown in red color in Figure 9. It can be observed the almost 30 m to 40 m depth of tailings have liquefied.

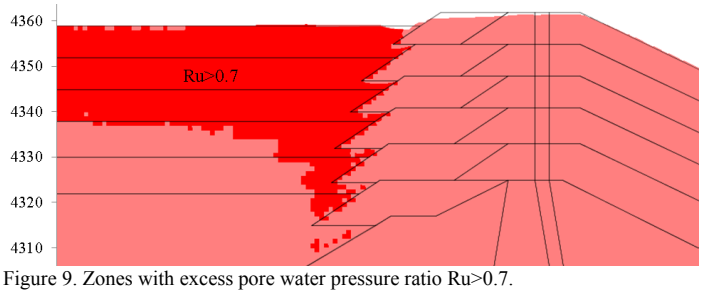

Figure 9. Zones with excess pore water pressure ratio Ru>0.7.

8 SUMMARY AND CONCLUSIONS

The results suggest that there are no clear failure mechanisms by the end of the numerical simulations considering the design ground motion used in this study. Furthermore, the numerical results suggest that the damage to the core and filter/drain would be minor to moderate and that the loss of freeboard may not compromise the dam function during the MCE. However, it is likely that reparations may be needed after an earthquake comparable with the MCE earthquake considered in this study.

The results also highlight the need to maintain a tailings beach in well-drained conditions - with the pond away from the crest dam - and also the importance of reinforcement with rockfill platforms. A tailings beach in well-drained conditions would limit the generation of pore pressures during a seismic event; likewise, the reinforcement with rockfill platforms is expected to contribute to the dam's seismic performance.

The results from this study are applicable only if the material properties during the dam rainings (e.g., dam properties and tailing properties) are consistent with the assumptions made in this study; hence, these properties should be evaluated during the operation. In addition, a larger set of dynamic analyses with a large set of ground motions should be performed to better characterize the dynamic response of the dam. Finally, the design ground motions considered in this study were based on ground-motion models (GMMs) that are expected to be updated in the near future (e.g, based on the. NGASub project outcomes). Hence, the design ground motions should be updated once updated GMMs are made available to the geotechnical earthquake engineering community.

9 REFERENCES

Barton, N. & Kjærnsli, B., 1981. Shear strength of rockfill. *J. of the Geotech. Eng. Div., Proc. of ASCE*, Volume 107:GT7: 873-891. Proc. Paper 16374, July.

Boulanger, R. W., & Ziotopoulou, K., 2018. PM4Silt (Version 1): a silt plasticity model for earthquake engineering applications. *Report No. UCD/CGM-18/01, Center for Geotechnical Modeling, Department of Civil and Environmental Engineering, University of California, Davis, CA, 108 pp.*

Bray, J. D., Macedo, J., & Travasarou, T., 2018. Simplified procedure for estimating seismic slope displacements for subduction zone earthquakes. *Journal of Geotechnical and Geoenvironmental Engineering*, *144*(3), 04017124.

Bray, J. D., & Macedo, J., 2019. Procedure for estimating shear-induced seismic slope displacement for Shallow Crustal Earthquakes. *Journal of Geotechnical and Geoenvironmental engineering*, *145*(12), 04019106.

Darendeli, M. B., 2001. Development of a new family of normalized modulus reduction and material damping curves [Ph. D. dissertation]. Austin: University of Texas.

Itasca 2016, FLAC 8.0 (Fast Lagrangian Analysis of Continua) User Manual, Itasca Consulting Group, Inc., Minneapolis

Kuhlemeyer, R. L., & Lysmer, J., 1973. Finite element method accuracy for wave propagation problems. *Journal of Soil Mechanics & Foundations Div*, *99*(Tech Rpt).

Leps, T.M. 1970. Review of Shearing Strength of Rockfill. American Society of Civil Engineers, *Journal of Soil Mechanics and Foundation Division*, Volume 96: 1159-1170.

Naesgaard, E. 2011. A hybrid effective stress-total stress procedure for analyzing embankments subjected to potential liquefaction and flow. Ph.D. thesis, Civil Engineering Department, The University of British Columbia, Vancouver, B.C.

Rollins, K. M., Evans, M. D., Diehl, N. B., & III, W. D. D., 1998. Shear modulus and damping relationships for gravels. *Journal of Geotechnical and Geoenvironmental Engineering*, *124*(5), 396-405.

Seed, H. B., Wong, R. T., Idriss, I. M., & Tokimatsu, K., 1984. Moduli and damping factors for dynamic analyses of cohesionless soils. Rep. No.EERC 84-14, Earthquake Engineering Research Center, Univ. of California, Berkeley, California.

Seed, H. B., Wong, R. T., Idriss, I. M., & Tokimatsu, K., 1986. Moduli and damping factors for dynamic analyses of cohesionless soils. *Journal of geotechnical engineering*, *112*(11), 1016-1032.

Stokoe, K. H., Darendeli, M. B., Gilbert, R. B., Menq, F. Y., & Choi, W. K., 2004. Development of a new family of normalized modulus reduction and material damping curves. In *International Workshop on Uncertainties in Nonlinear Soil Properties and their Impact on Modeling Dynamic Soil Response*.

Seismic Stability Assessment of Upstream Raised TSF on the African Rift Belt

Michelle Theron
Geotechnical Analyses Group, Johannesburg, Gauteng, South Africa

ABSTRACT: This paper presents a case study of a tailings storage facility where the design capacity was increased by additional upstream wall raises. The facility is in Tanzania on the African Rift belt. The feasibility to raise the facility was evaluated numerically and considered both static and dynamic loading conditions. It was found that the facility could safely be raised by an additional 30 m. Construction of the first wall raise commenced in 2010. The facility has subsequently been subjected to several large earthquakes, the most recent in 2017 and showed no signs of distress despite being raised with upstream construction.

Following the completion of the second upstream raise, the stability of the facility was assessed to confirm the predicted behavior during design. Both drained and undrained conditions were considered as the tailings were liquefiable. A dynamic finite element analysis was carried out to model the behavior of the facility in an earthquake.

1 INTRODUCTION

The design of tailings dam wall raises is often based on finite element analyses that incorporates the properties of the tailings and foundation material well as the forecasted construction sequence and tonnages. The accuracy of the predicted behavior is a function of the quality of the input soil parameters and actual construction sequence. Few case studies exist where the performance of the structure is confirmed.

This case study presents a tailings storage facility (TSF) where the performance of the upstream wall raise is confirmed. The facility is located in Tanzania on the African Rift belt. It was designed as a valley dam to be raised in phases. The first phase entailed a waste rock wall with a layer of compacted silty clay on the upstream face of the wall (Figure 1). The embankment crest width was 10 m with 1V:2H and 1V:3H upstream and downstream side slopes, respectively. The wall was raised via downstream construction with waste rock.

In 2009 the mine investigated the feasibility of increasing the capacity of the facility. Several wall building geometries and materials were considered. It was found that the facility could safely be raised by an additional 30 m. Construction of the first wall raise commenced in 2010.

The stability of the facility was assessed in 2019 following the completion of the second wall raise to confirm the predicted stability and performance of the raise.

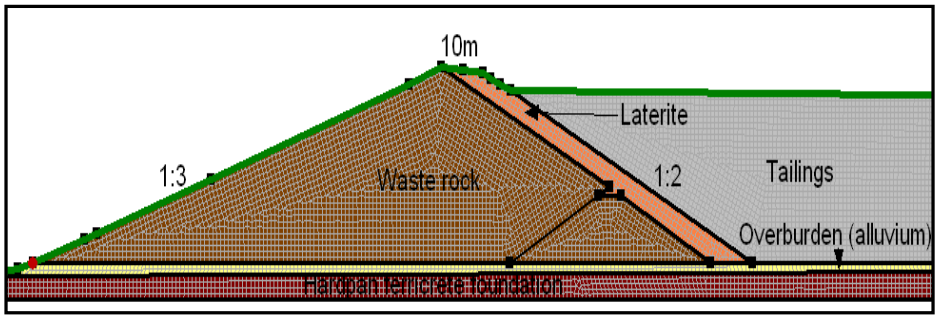

Figure 1. Schematic presentation of TSF embankment prior to the wall raise

2 WALL RAISE DESIGN

The design of the wall raises was carried out in two phases. A site investigation comprising of in-situ and laboratory testing followed with numerical modelling of proposed wall geometries.

2.1 *Seismicity in the vicinity of the site*

The central region of Tanzania is classified as a seismically active region. The earthquakes in this region are tectonic of origin with the majority of the epicenter points trending in a NE-SW direction. Table 1 summarizes the significant earthquakes that occurred in Tanzania and surrounding areas from 1910 to 2019. It can be seen that several moderate (i.e. magnitude of 5.0 to 5.9) to strong (i.e. magnitude 6.0 to 6.9) earthquakes occurred in Tanzania. According to the United States Geological Survey database (USGS), the mean peak ground acceleration corresponding to a 10% probability of exceedance in a 50-year period is 0.38 g.

Table 1. Summary of significant earthquakes in Tanzania and surrounding countries (after National Geophysical Data Centre)

Year	Location	Latitude (Degree)	Longitude (Degree)	Depth (km)	Magnitude
2018	Masumbwe, Tanzania	-3.434	32.384	10	4.6
2017	Mwanza, Tanzania	-3.050	32.890	10	4.4
2016	Nsunga, Tanzania	-1.036	31.618	40	5.9
2015	Cyangugu, Rwanda	-2.296	28.900	11	5.8
2015	Gitega, Burundi	-3.536	29.919	10	4.4
2014	Bukoba, Tanzania	-1.383	32.392	10	4.3
2010	Mwaro, Burundi	-3.424	29.764	10	3.8
2010	Kasulu, Tanzania	-4.609	30.424	10	4.2
2009	Cyangugu, Rwanda	-2.296	28.900	10	5.9
2008	Kalemie, Congo	-6.268	29.673	8	5.8
2008	Tanzania	-5.399	36.053	10	4.7
2007	Tanzania	-2.753	36.337	8	5.9
2005	Congo, Tanzania: Lake Tanganyika	-6.175	29.717	22	6.8
2005	Congo: Kalemie	-6.224	29.83	22	6.8
2004	Burundi: Ruyaga	-3.393	29.558	10	4.7
2002	Congo: Goma, Lwiro, Bukavu. Rwanda: Kigali	-1.884	29.004	11	6.2
2002	Rwanda: Gisenyi	-1.684	29.077	15	4.7
2002	Tanzania: Bunda	-2.907	33.733	10	5.5
2000	Tanzania: Nkansi	-7.977	30.709	34	6.5
1994	Uganda: Fort Portal, Kabarole, Bund Ibugyo, Kasese	0.593	30.037	14	6
1992	Congo: Kabalo	-6.087	26.651	11	7
1966	Uganda: Kichwamba, Bondigogyo	0.7	29.8	24	7

Year	Location	Latitude (Degree)	Longitude (Degree)	Depth (km)	Magnitude
1966	Uganda: Bwamba	1.4	31.5	-	7.5
1964	Tanzania	-4	34.9	33	6
1960	Congo: Lake Tanganyika	-3.6	29	28	6.6
1960	Congo,Uganda: Musaka	0	32	-	6
1945	Uganda: Masara	0	32	-	6
1910	Zambia	-8	31	-	7.5

2.2 *Site investigation*

A piezocone investigation was carried out to assess the pore pressure regime and stratigraphy of the tailings. Fourteen test locations were probed in the vicinity of the waste rock wall and along the tailings beach. Figure 2 shows the build-up of ambient pore pressure at the piezocone locations. It was found that hydrostatic conditions predominantly prevail in the beach. A marked decrease in ambient pore pressure were noted as the piezocone entered the waste rock wall. The water table remained at a constant elevation across the beach profile. This was attributed to the low permeability layer of one to three meters in thickness that was encountered before entering the underlying strata. The permeability of this layer was one to two orders of magnitude lower than the average permeability of the tailings. This layer prevented drainage into the underdrainage resulting in horizontal flow of water in the tailings. Inspection of the geotextile cover of the underdrains revealed that it was clogged.

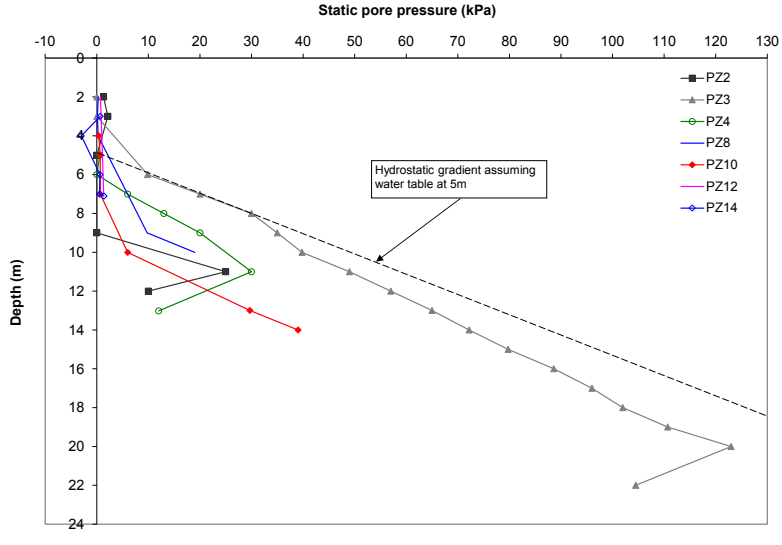

(a)

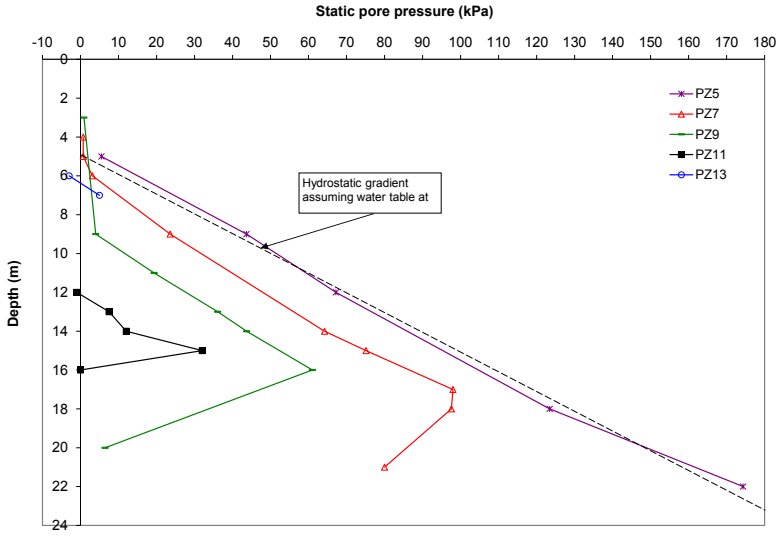

(b)

Figure 2. Change in static pore pressure with depth for the (a) wall and (b) pool area

The feasibility of depositing tailings by means of cycloning and using it for wall building material was included as one of the alternatives. A test run with a 300 mm diameter cyclone was conducted early in September 2007. It was found that the cyclone material has a yield of about 18 % of underflow (coarse tailings). Samples of the cyclone feed, underflow, and overflow were collected during the test run. These together with disturbed surface tailings samples were tested in geotechnical laboratories to determine their shear strength, permeability, compressibility, and composition. The latter was investigated by means of x-ray diffraction (XRD) and scanning electron micrographs (SEM).

The tailings was classified as a clayey silt with the clay sized particles varying between 10 % and 20 %. The results of the XRD tests revealed that the tailings consist mainly of quartz (45 % – 53 %) and mica (8 % -18 %). The presence of kaolinite, a non-active clay was also noted. Triaxial shear test results indicated that both the cyclone underflow and overflow display phase transfer. This implies that at strains below this point the material will contract but beyond it will dilate to increased shear strength. The phase transfer friction angle was used in the stability analysis.

Ten disturbed tailings samples were collected in the beginning of 2009 by the mine at 50 m to 80 m from the waste rock wall. The samples were sent to two laboratories in the UK for dynamic testing where it was combined into a single sample. This was done to ensure that the material tested was representative of the in-situ material. Cyclic triaxial and oedometer tests were carried out to determine the Martin, Finn, and Seed (MFS) pore pressure parameters (Figures 3 and 4) while resonant column tests results were used to determine the damping ratio (Table 2) and variation of small strain shear stiffness with effective stress (Figure 5).

Table 2. Summary of damping ratios use the dynamic finite element analyses

	Damping ratio	Maximum damping ratio
Waste rock	0.20	0.21
Laterite	0.10	0.12
Overburden	0.10	0.12
Tailings	0.45	0.47
Foundation	0.20	0.21

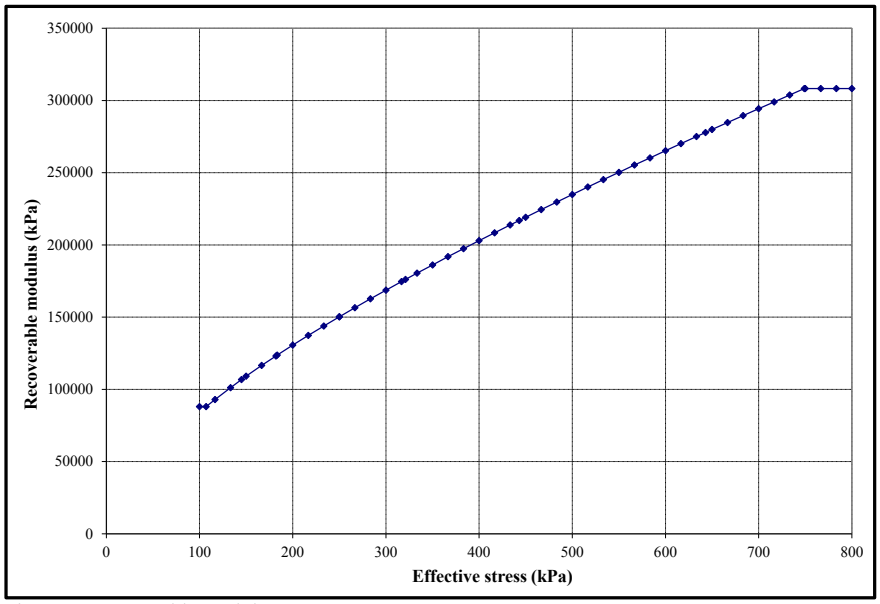

Figure 3. Recoverable modulus

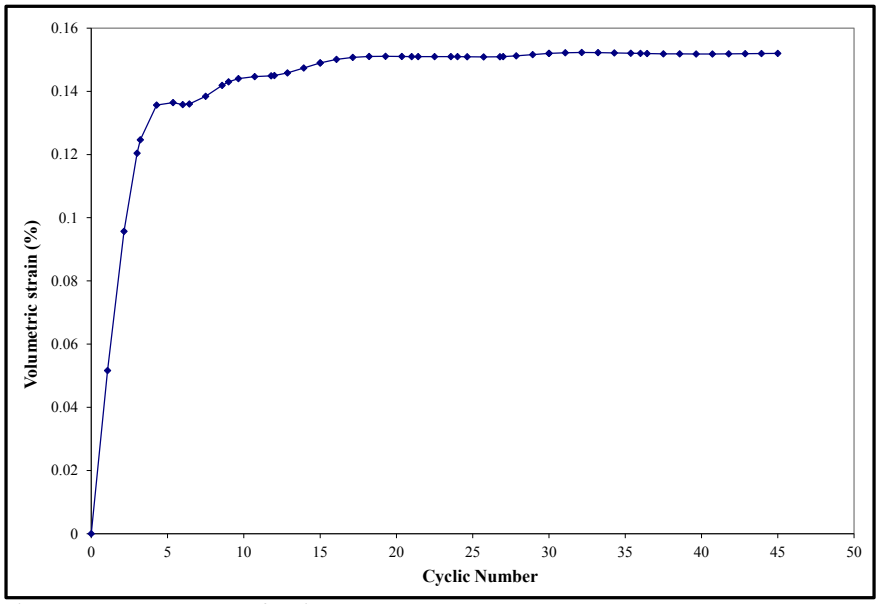

Figure 4. MFS pore pressure function

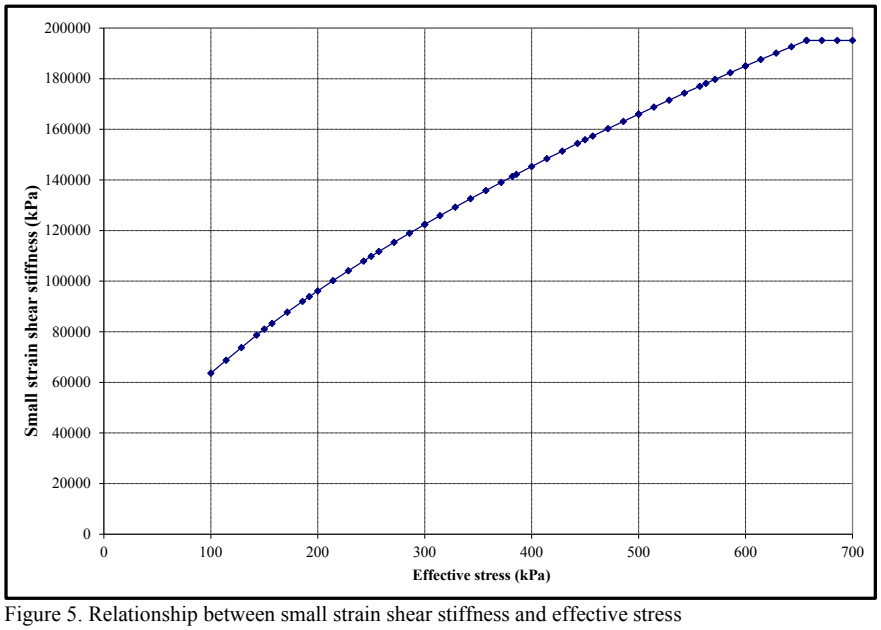

Figure 5. Relationship between small strain shear stiffness and effective stress

2.3 *Wall geometries considered*

Various wall geometries and materials were considered during the feasibility design phase. These were evaluated in terms of their stability under static and dynamic loading conditions as well as the practicality at this remote site.

Waste rock is being produced by the mining operation and the use of this material for wall building proved to be cost effective. Geometric modeling indicated that the downstream raise required a large amount of waste rock (approximately four times more than the upstream hybrid raise). A large volume of waste rock needs to be placed downstream of the original wall before any gain in elevation is obtained. This proved to be a problematic as this volume of waste rock could not be placed before the facility reaches its previous design capacity. In addition, the downstream wall raises required a larger footprint, thereby extending the toe line of the TSF into the downstream river. Downstream construction was therefore not further developed.

Figure 6 is a schematic presentation of the raised wall geometry that proved to be the most feasible. The philosophy of the upstream outer wall was to create a wide unsaturated zone to act as a containment wall and reduce the size of the liquefiable zone. A pioneer layer was introduced at the base of each raise to drain the adjacent tailings. The pioneer layer was to be constructed of waste rock, 75 m in length, 2 m in thickness, and extend 10 m beyond the base of the corresponding raise. The crest width of each raise was 40 m and outer slope of 1V:3H. A substantial drain at the interface between the existing and raised embankments was included in the design to mitigate the blocked underdrainage system.

The consolidation behavior of the tailings due to the wall raise was modelled by means of coupled consolidation analysis followed by limit state equilibrium analyses under static, pseudo static, and dynamic loading conditions. Data gathered during the field and laboratory testing program were used in the models. Figure 7 shows the potentially liquefiable zone under dynamic loading conditions. It can be seen that the pioneer layer at the base of each raise is effective in draining the adjacent tailings, thereby reducing the size of the liquefiable zone (yellow shading). Table 3 summarizes the predicted factors of safety (FoS) under static and dynamic loading conditions for the original downstream wall and end of construction geometries at the highest wall location. The FoS of the original wall (i.e. lower slope) remained at 2.38 during the wall raises.

The high FoS achieved for the upper slope for the pseudo static and dynamic loading conditions could be attributed to the reduced pore pressures in the vicinity of the wall and corresponding reduced liquefiable zone.

Table 3. Computed factors of safety at the highest wall location

Description	Static analysis	Pseudo static analysis	Dynamic finite element analysis
Original wall geometry (Downstream)	2.38	1.42	1.44
Upper slope - Waste rock raise 1	3.67		
Upper slope - Waste rock raise 2	3.39		
Upper slope - Waste rock raise 3	3.38		
Upper slope - Waste rock raise 4	3.32		
Upper slope - Waste rock raise 5	3.06	1.56	2.31

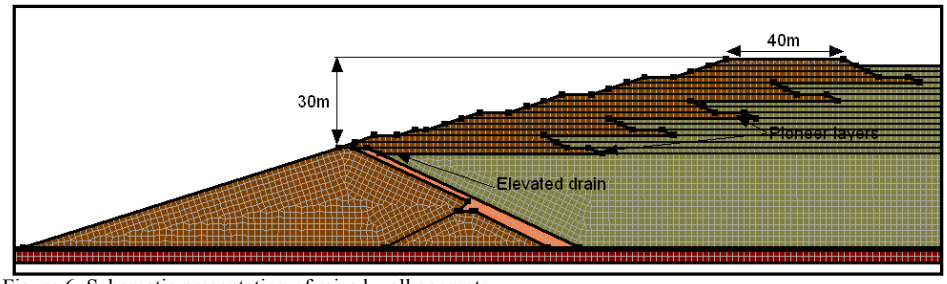

Figure 6. Schematic presentation of raised wall geometry

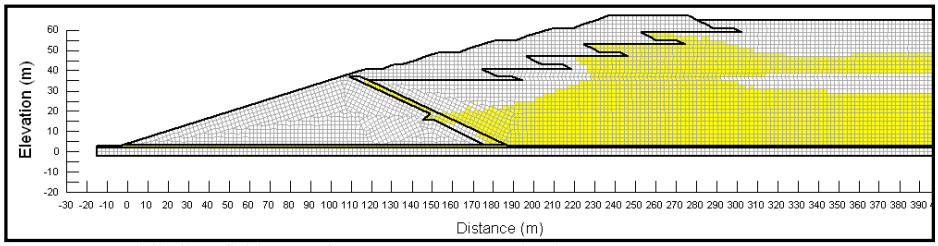

Figure 7. Potentially liquefiable zone for upstream waste rock raise

3 ASSESSMENT OF CONSTRUCTED WALL RAISES

The mine requested in 2019 that the predicted stability of the wall raises be confirmed following the completion of the second wall raise. A study that entailed piezocone testing followed by numerical modelling was carried out during 2019.

3.1 *Piezocone investigation*

Four piezocone lines consisting of three tests were carried out on the beach. Where possible, the piezocone tests were carried out in the vicinity of previous test locations. Representative cross sections of the piezocone test lines were based on aerial and as-built survey information, field observations made during the geotechnical investigation and piezocone test results. Figure 6 is a cross section of the constructed wall at the design cross section location. The cone resistance is denoted by the red line whilst the blue line presents the ambient pore pressure. The presence of the hardpan ferricrete is marked by the sharp increase in cone resistance. The stratigraphy of the cross sections was determined using the piezocone measurements.

Figure 9 shows the variation in ambient pore pressure with depth for the various piezocone tests. It can be seen that the ambient pore pressure increase is approximately hydrostatic. Figure 10 shows the ambient pore pressure response of the piezocone tests carried out in the vicinity of the wall. It can be seen that the ambient pore pressure remains zero for the height of the previous wall raises confirming the effectiveness of the pioneer layer to drain the tailings near the wall.

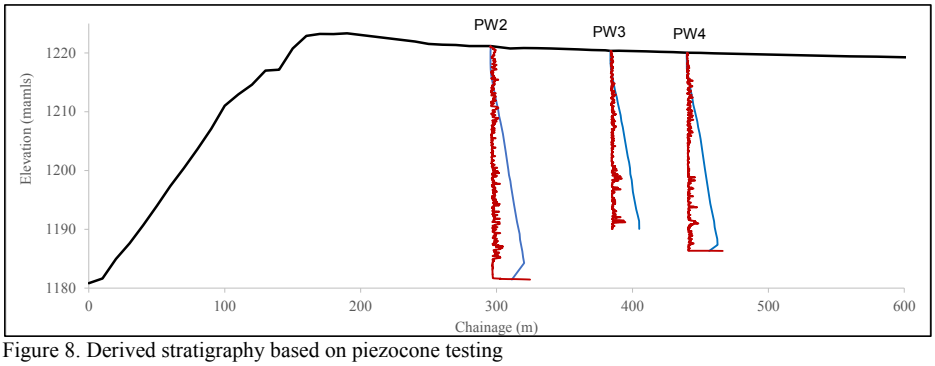

Figure 8. Derived stratigraphy based on piezocone testing

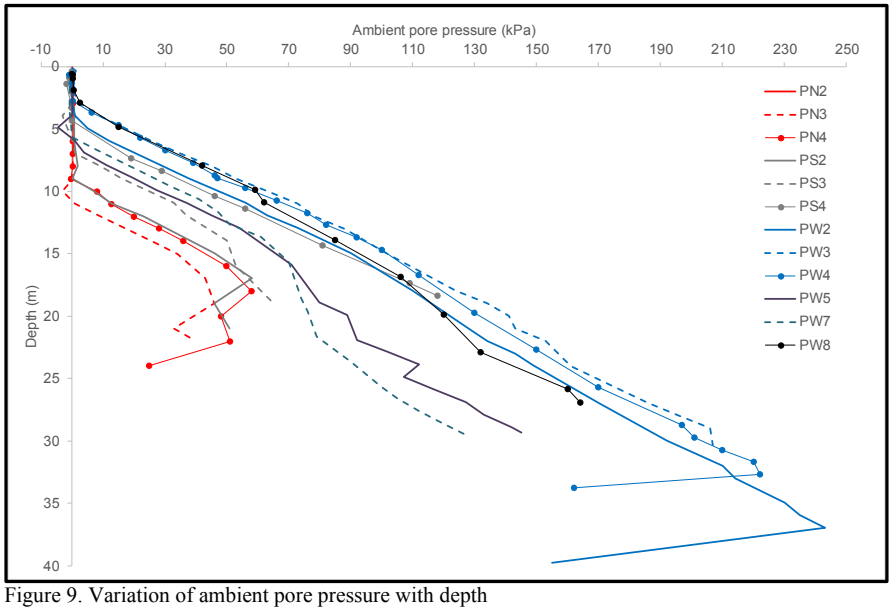

Figure 9. Variation of ambient pore pressure with depth

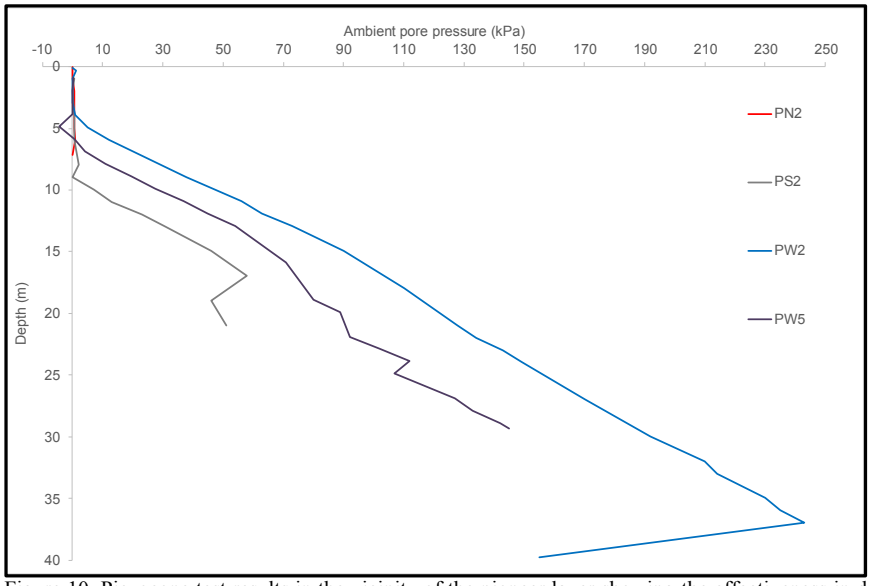

Figure 10. Piezocone test results in the vicinity of the pioneer layer showing the effectiveness in draining the tailings

3.2 *Numerical analyses*

Numerical analyses of four representative cross sections were carried out to confirm the stability of the 2019 geometry following the completion of the second waste rock raise. This paper compares the predicted performance of the raises with the actual performance following the construction of the second wall raise. For this reason, only the results of the comparative cross section is considered.

3.2.1 Static liquefaction potential analysis

Static liquefaction potential analyses were carried out to determine whether the tailings had a potential to liquefy. The analyses were based the Shuttle and Jefferies (1998) approach which is a refinement of the Been and Jefferies (1985) method. The method assesses the static liquefaction potential in terms of its state (i.e. void ratio and stress) using the state parameter (ψ). The state parameter defined as the difference in void ratio between the initial soil state and steady state conditions at the same effective stress. Depending on the polarity of the state parameter, the material will dilate or contract during shear as follows:

Less than -0.05 = dilatant (Been, 2008)
High positive = contractive (liquefiable)

The liquefaction potential of the tailings was assessed using the 2019 piezocone tests as well as the 2008 and 2012 laboratory tests carried out on the fine tailings. The derived parameters for the analysis were as follows:

- Small strain shear modulus (G_0) at a reference vertical effective stress of 100 kPa. The G_0 measured by the resonant column test at 100 kPa confining pressure was 63.8 MPa. A value of 64 MPa was used in the analysis.
- M_{tc} is the gradient of the critical state line in stress space and is related to the internal friction angle (ϕ') as shown in Equation 1:

$$M_{tc} = \frac{6\sin\phi'}{3-\sin\phi'} \quad (1)$$

The internal angle of friction at critical state is 30° which is equivalent to a M_{tc} of 1.2.

- λ is the gradient of the normal consolidation line. Oedometer tests carried out on the beach material was used to determine the gradient of the normal consolidation line. The gradient of the normal consolidation line at the applicable effective vertical stress was applied to each piezocone test.
- H is the plastic hardening modulus of the material and generally ranges in value from 50 to 500. In the absence of pressure meter test results Been and Jefferies suggested that H can be approximated by 4/λ.
- Poisson's ratio (υ) for the material was assumed to be 0.3. Been and Jefferies suggest a range of values of 0.1 to 0.3 for sands. It is expected that tailings will fall in the higher end of this range.

It was found that the tailings are liquefiable below the water table. Both drained and undrained stability analyses were therefore required.

3.2.2 *Stability assessment under static loading conditions*

The stability analyses were based on the 2019 piezocone results, 2016 LIDAR survey, as-built survey of the second waste rock raise, field observations, calibrated seepage analyses and historic laboratory test results. The software package GeoStudio 2019 R2, SlopeW limit equilibrium module was used to perform the stability analysis.

The results of the static liquefaction potential analyses indicated that both drained and undrained stability analyses under static loading conditions are required. The drained analyses assumed that Mohr-Coulomb failure criteria applied to all materials. Mohr-Coulomb failure criteria only applied to the drained material in the undrained analysis. An undrained shear strength and minimum undrained shear strength was applied to the liquefiable material.

The variation of undrained shear strength of the tailings with effective stress was specified as a function in SlopeW. The undrained shear strength ratio of the tailings at yielding point and minimum undrained shear strength was calculated from the piezocone cone resistance using two independent methods namely:

Olsen and Stark (2003):

$$\left({}^{c_u}/_{\sigma_v'}\right) yield = 0.205 + 0.0143 q_c \pm 0.04 \qquad (2)$$

for $q_c \leq 6.5$MPa

where:

q_c Cone resistance

σ_v' Vertical effective stress

Terzaghi (1943)[1]:

$$\left({}^{c_u}/_{\sigma_v'}\right) yield = \left[\frac{q_c - \sigma_v}{N_{kt}}\right] \Big/ \sigma_v' \qquad (3)$$

where:

q_c cone resistance

σ_v vertical total stress

N_{kt} A constant. The average value for tailings is 15 with a range of 10 to 20 (Lunne and Kleven, 1982, Jamiolkowski et al., 1982 and Teh, 1987). A value of 15 was used in the analyses.

Table 4 summarizes the soil parameters employed in the limit equilibrium analysis. The drained parameters were obtained from the laboratory test carried out in 2007 and 2009 whilst the undrained shear strength was derived as described above. Table 5 summarizes the factors of safety against failure of the upper, lower and overall slopes of the various walls. It can be seen that the factors of safety of the facility is above 1.5 and compares well with the corresponding predicted FoS.

[1] Note that this method is not applicable to sand, i.e. where $q_c > 6.5$ MPa.

Table 4: Summary of soil parameters employed in the limit equilibrium analyses

	Bulk unit weight	Drained Analysis Cohesion	Effective friction angle	$(c_u/\sigma_v')_{yield}$	Undrained Analysis Min. c_u	Cohesion	Effective friction angle
	kN/m³	kPa	Degrees		kPa	kPa	Degrees
Waste rock	24.0	0	40			0	40
Laterite	20.7	0	32			0	32
Overburden	20.7	0	32			0	32
Tailings	22.0	0	30	0.11	5		
Foundation (hardpan)	24.0	0	40			0	40

3.2.3 *Dynamic liquefaction potential*

Dynamic finite element analysis consisted of a static finite element analysis where the initial conditions were specified, dynamic finite element analysis and finite element slope stability analysis based on the pore pressures generated during the dynamic analysis. The QuakeW module of Geostudio 2019 R2 was used to model the dynamic response of the TSF.

The local seismographs were not functional the during the recent earthquakes that took place in the vicinity of the site. Consequently, it was decided to use the ground acceleration record used in the 2010 numerical modelling and the peak ground acceleration of the area of 0.38 g in the analyses.

The following parameters were included in the model.

- Ground acceleration record (Figure 11).
- Damping ratio and maximum damping ratio (Table 2).
- MFS pore water pressure function (Figure 4).
- Recoverable modulus function (Figure 3).
- Shear modulus. (Figure 5).
- Steady state strength and slope of the collapse surface. The steady state strength of the tailings was derived from the piezocone cone resistance using the Olsen and Stark (2002) correlation to determine the liquefied undrained shear strength ratio (Equation 4).

$$\left({}^{c_u}/_{\sigma_v'}\right) liquified = 0.03 + 0.0143 q_c \pm 0.03 \qquad (4)$$

for $q_c \leq 6.5$MPa

where:

q_c, Cone resistance

σ_v' Vertical effective stress

The steady state strength was found to be 15 kPa. Kramer (1996) suggested that in the absence of data, the slope of the collapse surface can be estimates as two thirds of the internal friction angle. A value of 20° was thus adopted.

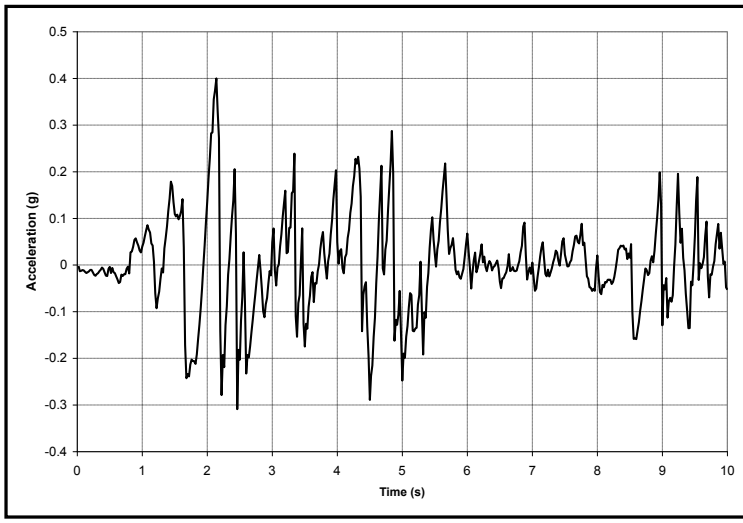

Figure 11. Strong ground motion used in the dynamic finite element analyses

Table 5 summarizes the factors of safety obtained from the dynamic finite element analysis. The facility has adequate factors of safety against instability under earthquake loading conditions. This could be attributed to the pioneer layers that ensures that the tailings of the upstream raises in the vicinity of the wall remains unsaturated and non-liquefiable as shown in Figure 12. The liquefiable zone is indicated in yellow while the non-liquefiable zone in white. It was found that liquefaction occurs in all the material apart from the waste rock, founding material, and unsaturated tailings.

Table 5: Summary of factors of safety

Description	**Static loading conditions (Actual)**	**Static loading conditions (Predicted)**	**Dynamic loading conditions (Actual)**
Drained analysis			
Upper slope	3.75	3.39	1.49
Lower slope	2.59	2.38	2.59
Overall slope	2.96		2.94
Undrained analysis			
Upper slope	1.77		
Lower slope	2.59		
Overall slope	2.87		

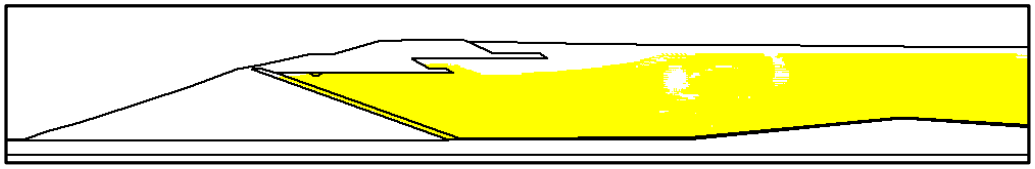

Figure 12. Zone of potential dynamic liquefaction following completion of second wall raise

4 CONCLUSIONS

Numerical modelling based on piezocone and advanced laboratory tests indicated that the capacity of the TSF could be increased by five 6 m high upstream waste rock wall raises. The numerical modelling showed that the stability of the upstream raises was governed by the waste rock pioneer

layer and large wall that drains the material in the vicinity of the wall. The tailings thus remains unsaturated and can therefore not liquefy.

The stability of the TSF was assessed following the completion of the second wall raise to confirm the predicted behavior. The four piezocone test measurements in the vicinity of the waste rock wall confirmed that the ambient pore pressures remained around zero up for the height of the two waste rock raises. It therefore confirms that the pioneer layer and wall drain the tailings as predicted.

Although the stability was assessed at four locations, only the cross section that corresponded to the original design was considered in this paper. The factors of safety under dynamic loading conditions was only assessed for the original and final geometries and the results could therefore not be compared. The factors of safety for static loading conditions compared well with each other.

5 REFERENCES

Been, K. and Jefferies, M. G. 1985. A state parameter for sands. *Geotechnique 35(2): 365 - 381.*

Jefferies, M and Been, K. 2006. Soil liquefaction, a critical approach. *2nd Ed*.

Kramer, S.L. 1996. Geotechnical Earthquake Engineering. *1st Ed*.

Lunne, T., Kleven, A. 1981. Role of CPT in North Sea Foundation Engineering. *International Symposium on Cone Penetration Engineering Division, ASCE, 49–75.*

Macheyeki, A.S., Delvaux, D., De Batist, M. and Mruma, A. 2008. Fault kinematics and tectonic stress in the seismically active Manyara-Dodoma Rift segment in Central Tanzania – Implications for the East African Rift. *Journal of African Sciences, Vol 51, 163-188*.

Martin G. R., Finn W. D. L. and Seed H. B. 1975. Fundamentals of liquefaction under cyclic loading. *Journal of the Geotechnical Engineering Division, ASCE, GT 5, 423 -438.*

Mmari, A. G. 1996. Source characterisation and attenuation of seismic waves along Rukwa Rift zone and seismic hazard assessment of Tanzania. *MSc Thesis, University of Bregen, Norway.*

Olsen, S. M. and Stark, T. 2002. Liquefied strength ratio from liquefaction flow failure case histories. *Canadian Geotechnical Journal, Vol. 39, 629-647.*

Olsen, S. M. and Stark, T. 2003. Yield Strength Ratio and Liquefaction Analysis of Slopes and Embankments. *Journal of Geotechnical and Geoenvironmental Engineering, Vol. 129, Issue 8.*

Shuttle, D. A. and Jefferies, M. G. 1998. Dimensionless and unbiased CPT interpretation in sand. *International Journal of numerical and analytical methods in Geomechancis, Vol. 22, 351-391.*

Teh C. 1987. An analytical study of the cone penetration test. *PhD thesis, Oxford University*.

Terzaghi, K. 1943. Theoretical soil mechanics. *John Wiley and Sons. Inc., New York*

Numerical Modelling of a Mine Waste Dump-heap Leach Pad with Different Constitutive Models

Myzael Valdivia, Roberto Quispe, Jesus Negrón, Renzo Ayala & Denys Parra
Anddes, Lima, Peru

ABSTRACT: A review of different constitutive models was carried out for the comprehensive numerical modeling of a heap leach pad facility founded on a mine waste dump. A key issue is the consideration of an appropriate constitutive model that allows the future leach pad settlement estimation to define alert levels for the geotechnical monitoring instrumentation. This instrumentation involves settlement cells installed below the heap leach liner system, inclinometers, and survey control points located in the waste dump slope. The thoroughness of the selected model should be strict so it can determine any liner deformation that compromises its integrity and any mine waste dump failure.

The first challenge of this project involved a calibration process in determining the most suitable constitutive model based on the current behavior of both facilities obtained from geotechnical monitoring records. The calibration analysis and process used Plaxis 2D program and the constitutive models used to assess its suitability were: Hardening Soil, Soft Soil, Soft Soil Creep, and SCLAY1S-Creep. Besides, the calibration considered the formation sequence of waste dump and leach pad, and different laboratory tests performed.

According to the analyzes and comparisons made with the above models, the Soft Soil Creep and SCLAY1S-Creep models identified the creep phenomenon observed in the geotechnical monitoring data. Subsequently, anisotropic behavior of waste material was best modeled by SCLAY1S-Creep according to the calibration results. By completing the calibration and determining the most suitable constitutive model, the settlement of the mine waste dump affected by the subsequent stages of ore stacking in the heap leach pad was explored, obtaining its corresponding alert levels to provide performance operation parameters.

1 INTRODUCTION

The selection of a constitutive model to evaluate an earth structure geotechnical behavior is an essential process during the design phase since it involves the response of a structure in the face of changing conditions and initial parameters. With these models, the geotechnical engineer can predict maximum settlements, factors of safety, or other performance indicators of the structure. Nevertheless, by using a geotechnical model integrated with a soil constitutive model, different configurations may be explored to determine the most suitable configuration that meets minimum requirements from regulators, reduce operational risk, and generates economic value also in operation.

The geotechnical design also involves a geotechnical instrumentation plan that allows control and performance measurement of the structure during the operation period. Some necessary instruments are survey control points, inclinometers, radar measurements, and satellite

measurements. The results of such measures are compared to threshold values that assure a proper safety performance level of the structure, but also are used to validate the results of the numerical modeling and the corresponding constitutive model. These threshold values or alert levels are implemented in a site-specific operation, maintenance, and surveillance (OMS) manual of the mining facility.

The amount of instrumentation in a structure is such that we can know the structure behavior by measuring its displacements and understand and predict its impact on physical stability. In this study, the authors identified the occurrence of creep as another critical feature to consider as a part of the performance indicators in geotechnical design, even for coarse materials such as ore or waste rock. Creep can vary from low to high values, for instance, in Brumadihno tailings dam, using InSAR measurements, a millimeter magnitude of creep influenced the dam failure (Robertson et al., 2019). Likewise, Giacomo et al. (2019) have described the virtues of InSAR satellite measurements in tailings dams and mine waste dumps, as well as the early detection of a landslide failure that occurred in an open-pit due to creep effects and that were detected by this type of measurement system (Carla et al., 2018). In the case of high creep values, conventional measurements such as measurements with survey control points and inclinometers have allowed the identification of creep (Kermani et al., 2018.). Therefore, understanding creep effects on satellite measurement systems such as InSAR, leads to new challenges to reduce the risk of mining facility physical instability.

Alert levels estimation is carried out by different methods. One of these methods involves reviewing a case study of a similar structure. Another method consists in performing a numerical analysis that predicts the structure behavior (direct method), so it will be necessary to use the appropriate constitutive model. If a rigorous material characterization has been executed, the model will present reliable results. The direct method would be the most recommended since it allows for more robust control of the structure, not only knowing its value of safety factor, but also its future response. For example, one of the lessons of Mount Polley (Morgenstern et al., 2015) indicated a lack of alert levels determination in the area where the failure occurred. Therefore, adequate performance could not be determined and even prevent an undesirable condition.

As noted above, both the geotechnical instrumentation and the alert levels are two essential components in geotechnical monitoring that must be linked through numerical analysis. Therefore, by involving the Engineer of Records (EoR), the instrumentation measurements of a structure should be compared with the geotechnical model defined during the design as a way to retrofit the model and determine whether it is meeting the alert levels set in the OMS.

These concepts were considered for the monitoring of a heap leach pad located in the Andes of Peru. Due to the ore continued exploitation and lack of space, a part of the new pad expansion was built on top of an existing mine waste dump. The issue in question is the consideration of an appropriate constitutive model that allows the adequate future estimation of the heap leach pad settlements associated with the mine waste dump as a foundation. Alert levels for the instrumentation of the geotechnical monitoring will be defined through this analysis. The instrumentation installed in the structure involves settlement cells installed bellow the leach pad liner, that is, at the crest of the mine waste dump; on the slope of the mine waste dump, inclinometers and survey control points were installed. The thoroughness of the selected model must allow the calibration with the current instrumentation record and confirm any change in the grade of collection system of the leach pad.

2 THEORETICAL BACKGROUND

The selection of a constitutive model for the present work focused on a mine waste material behavior, which depends mainly on the type of plastic deformations expected. Most of these models are based on plasticity theory, some of the most common and used in the industry correspond to the Hardening Soil (Schanz et al., 1999) and Soft Soil models (Brinkgreve et al., 2019), both being isotropic. However, in some specific projects, it is necessary to consider other characteristics of the material behavior, such as anisotropy and creep effects. In this case, the models used are based on the theory of visco-plasticity. In the present work, two additional constitutive models were used: the Soft Soil Creep (Vermeer & Neher, 1999) and Creep-

SCLAYS1 (Sivasithamparam et al., 2015) models, both of them allow the effects of creep; however, additionally the second model considers anisotropy behavior. In summary, three conditions govern the models mentioned above: they have a yield surface, a potential plastic surface or flow rule, and a hardening rule.

The Hardening Soil (HS) is an isotropic-constitutive-model formulated within the framework of plasticity. The yield surface allows the compatibility of stress vs. strain relationship with greater control of deviatoric strains than volumetric strains, the sum of both being plastic strains. Plastic volumetric strains are not null in this model, but they are small compared to deviator strains, which leads them to be considered negligible. This flow rule of this model is not associated, which means that it has a potential plastic surface different from the yield surface, which allows controlling the direction of the strains since this direction is perpendicular to the potential plastic surface and a dilation angle controls it.

The Soft Soil (SS) is also an isotropic-constitutive-model within plasticity theory. Both the HS model and the SS model allow separating elastic and plastic strains with the yield surface. However, unlike the HS model, the SS model enables the compatibility of stress vs. volumetric strains relationship. The flow rule of this model is associated, and therefore it is not possible to control the direction of the plastic strains, being necessarily perpendicular to the yield surface. The hardening rule or expansion of the yield surface on this model occurs with increased plastic volumetric strains. Two main parameters of this model correspond to the modified compression index (λ^*) and the modified expansion index (κ^*), which are a function of the total and elastic volumetric strains, respectively.

Visco-plastic models allow the introduction of time effects in plastic models, such as the creep phenomenon. The Soft Soil Creep (SSC) model is an isotropic-constitutive-model within the theory of visco-plasticity. This model also uses the λ^* and κ^* parameters of the SS model. However, the SSC model allows modeling creep phenomenon as parameter μ^*, defined as the modified creep index. In this type of model (visco-plastic) the separation of elastic and plastic strains with the yield surface is not possible, since the creep phenomenon occurs all the time, with its hardening rule similar to the SS model. However, creep value decreases due to the constant expansion of the yield surface due to the continuous increase in the preconsolidation stress, which has an indirect relationship with the creep parameter. Other similar features with the SS model is that SSC is an associated model, therefore, control of the direction of plastic deformations is not allowed.

The Creep-SCLAYS1 model is a visco-plastic model that also includes anisotropy. This model has similar characteristics to the SSC model with input parameters λ^*, κ^*, and μ^*. Additionally, the model incorporates parameters to consider soil anisotropy. Figure 1 presents the constitutive Creep-SCLAYS1 model. The value α shown in the figure is a scalar value used to describe the initial orientation or rotation (initial anisotropy) of the principal stress surface (CSS) and the normally consolidated surface (NCS). This model has up to three hardening rules, the first due to volumetric strains creep surface expansion, which is similar to the SS and SSC model. The second flow rule is related to anisotropy evolution that considers changes due to deviator and volumetric strains. The model assumes an associated flow rule; however, controlling the creep surface rotation allows greater control in the direction of volumetric and deviator strains. The third flow rule is related to reducing the bonding of the material; however, it was not considered in the modeling of mine waste material.

All the models described above are developed in the Plaxis finite element program, making it ideal for practical use in the mining industry.

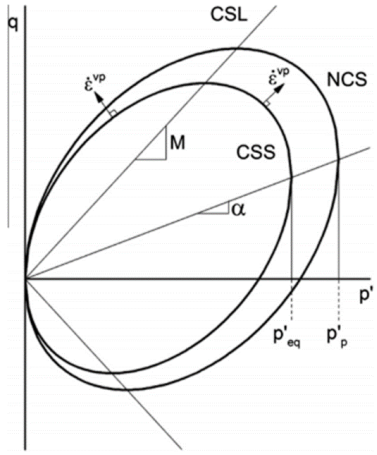

Figure 1. Current State Surface (CSS) and Normal Consolidation Surface (NCS) of the Creep-SCLAY1S model and the direction of viscoplastic strains (Sivasithamparam *et al.*, 2015)

3 CASE STUDY GEOTECHNICAL OVERVIEW

The case study is located in southern Peru and corresponds to a heap leach pad currently in operation. Due to space limitation for the leach pad expansion (Phase C), the top surface of a mine waste dump was occupied. Figure 2 presents the volumetrics of both components. The final design of the heap leach pad is approximately 100 m, but in the expansion area where the foundation is mine waste material, the heap is up to 40 m high. On the other hand, the mine waste dump has a height of 100 m, reaching up to 250 m from toe to crest, as shown in the section of Figure 3.

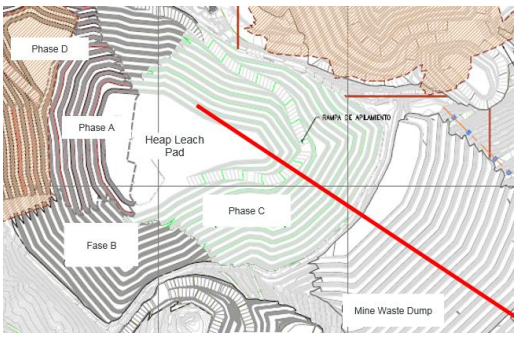

Figure 2. Plan view of the heap leach pad and mine waste dump.

The geotechnical instrumentation control in the mine waste dump-heap leach pad is such that it is possible to monitor the direction of movements and thus estimate the leach pad future settlements, which will allow verifying the integrity of the pad collection system. Different geotechnical investigation campaigns have been carried out to determine the geological-geotechnical profile of the waste dump. Figure 3 shows a layout of the test pits and borehole in a cross-section. Geotechnical instrumentation equipment consisting of survey control points, inclinometers, and settlement cells have been installed to determine the mine waste dump-heap leach pad performance. Finally, a finite element numerical model calibration was carried out with Plaxis to verify the liner system geometry and estimate settlements of the waste dump produced

by the ore stacking loads of the heap leach pad. In Figure 4 a section of the geotechnical model is presented, control points A through L represent the instrumentation used for model calibration.

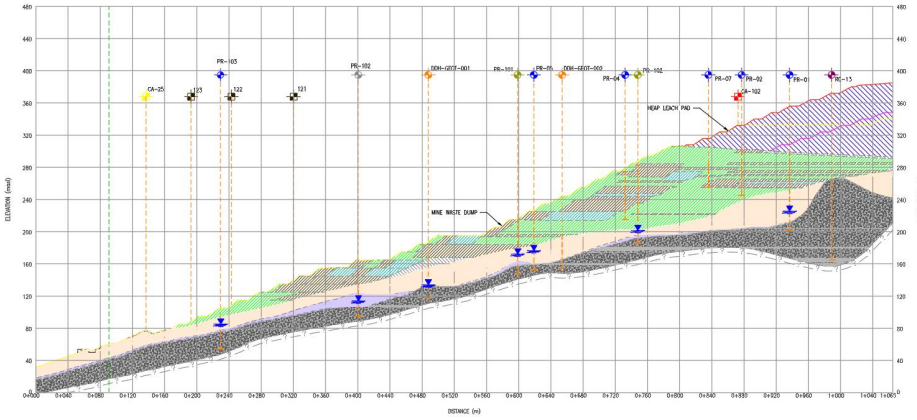

Figure 3. Geological-geotechnical profile of the mine waste dump-heap leach pad.

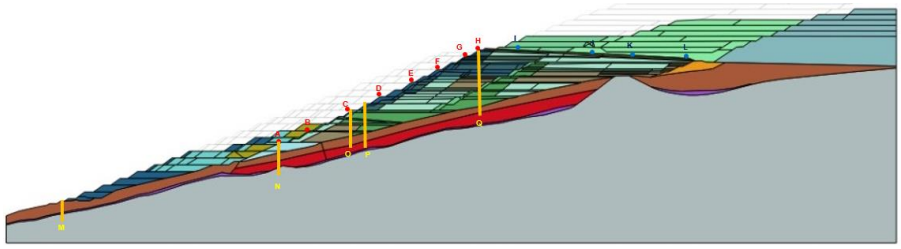

Figure 4. Geotechnical model generated in Plaxis and location of selected instrumentation - red points, blue points, and yellow lines correspond to survey control points, settlement cells, and inclinometers, respectively.

4 GEOTECHNICAL PROPERTIES

Field investigations and laboratory tests carried out through all levels of engineering and operation were reviewed to characterize the materials. At the same time, the information collected was complemented with different tests to understand the material behavior. The interpretation of the investigations and laboratory results allow discretizing the section of analysis based on the different properties of each layer. Besides the field tests carried out, laboratory testing such as CU triaxial, CD triaxial, edometric tests, etc. were performed. The waste material was classified based on its fines content: type A, mine waste with fines content below 15%, type B, mine waste with fines content between 15% a 30%, and type C with fines content between 30% to 45%.

Subsequent operation in the mine waste dump required stacking quality control (QC) and quality assurance (QA) by the EoR for rigorous monitoring of the waste material, thus, easing identification of the type of mine waste deposited for calculations in determining the stability for future expansions of the heap leach pad. The QC and QA range from different activities such as controlling mine waste material obtained in the pit, reviewing fines content of the mine waste by soil classification tests in the laboratory, verifying the rock alteration at the mined pit, controlling the number of trucks carrying different kinds of material to the waste dump, excavating test pits for verification, performing field tests such as density determination by the water replacement method and global grain size, and also performing additional laboratory tests such as specific gravity, maximum and minimum density. To provide a constant source of the mechanical behavior

of the waste material, triaxial and edometric tests were performed. Finally, the mine operation continued installing geotechnical instrumentation such as inclinometers and survey control points based on the EoR recommendations.

Based on the field, laboratory, and geotechnical instrumentation monitoring, different models were used to calibrate mainly the waste material as explained in chapter 5; other materials were also calibrated by using conventional models of the industry (Mohr-Coulomb and HS). Tables 1, 2, and 3 present the final parameters of each material involved with the prediction model of chapter 7.

The parameters of the Creep-SCLAY1S model were not only obtained by a typical calibration process but also estimated from a preliminary calibration with the Hardening Soil constitutive model. These preliminary parameters were subsequently interpreted to obtain specific initial parameters of the Creep-SCLAY1S model and then validated with edometric laboratory tests of the mine waste. This test comprehends a device that allowed to test a maximum particle size of 2", thus using a representative sample of the material stacked in the waste dump.

Table 1. Final shear strength Parameters used in the analysis

Materials	Total unit weight (kn/m^3)	Saturated unit weight (kn/m^3)	Shear strength parameters	
			Cohesion (kpa)	Friction angle (°)
Basement rock	23	24	*	
Residual soil	20	21	0	30
Low permeability soil and geomembrane interface	18	19	**	
Low permeability soil	18	19	1	33
Structural fill 1	18	19	1	35
Structural fill 2 (platform)	19	20	7,5	33
Till deposit 1	18	19	20	38
Till deposit 2	18	19	25	42
Ore	17	18	0	36,5
Mine waste - Type A1 and A2	19	20	7,5***	35
Mine waste - Type B	18	19	7,5***	33
Mine waste - Type C	16,5	17,5	7,5***	28

*It is defined using the elastic model.
** It is determined in a nonlinear normal stress and shear strength relationship.
*** Cohesion was used in the calculation of the safety factor.

Table 2. Final elastoplastic parameters used - Hardening Soil and Mohr - Coulomb constitutive models

Materials	Constitutive model	E (MPa)	υ	E_{50}^{ref} (MPa)	E_{edo}^{ref} (MPa)	E_{ur}^{ref} (MPa)	p^{ref} (kPa)	m
Basement rock	Lineal elastic	2500	0,2	-	-	-	-	-
Residual rock	Mohr-Coulomb	100	0,3	-	-	-	-	-
Low permeability soil	Lineal elastic	30	0,2	-	-	-	-	-
Structural fill 1	Mohr-Coulomb	30	0,3	-	-	-	-	-
Structural fill 2 (platform)	Hardening soil	-	-	15	15	45	150	0,8
Till deposit 1	Hardening soil	-	-	80	80	240	150	0,8
Till deposit 2	Hardening soil	-	-	200	200	600	150	0,8
Ore	Hardening soil	-	-	25	25	75	100	0,5

Table 3. Final elastoplastic parameters used - Creep-SCLAY1S constitutive model

Material	K*	λ*	ν'_{ur}	Mc	Me	w	w_d	α_0	μ*	K_0^{nc}
Mine waste - Type A1	0,00676	0,15	0,0169	1,418	0,963	8000	0,0001	0,001	0,0026	04264
Mine waste - type A2	0,008	0,15	0,02	1,418	0,963	7000	0,0001	0,001	0,0026	0,4260
Mine waste - Type B	0,012	0,15	0,03	1,331	0,922	4500	0,0001	0,001	0,0026	0,4553
Mine waste - Type C	0,014	0,15	0,035	1,113	0,812	4000	0,0001	0,001	0,0026	0,5300

k*: Modified swelling index
λ*: Modified intrinsic compression index
v'_{ur}: Drained Poisson's ratio
Mc: Slope in critical state line in compression
Me: Slope in critical state line in extension
w, w_d y α_0: Anisotropy parameters
μ*: Modified intrinsic creep index
K_0^{nc}: Coefficient of lateral stress in normal consolidation

5 GEOTECHNICAL ANALYSIS - CALIBRATION ANALYSIS

Figure 4 shows the geotechnical instrumentation data considered for model calibration in Plaxis. Since the analysis was performed in a two-dimensional (2D) section, the data considered belonged to the nearest instrumentation. Instrumentation located on the mine waste dump slope consisted of eight topographic control points and five vertical inclinometers, on the mine waste dump crest or at the base of the heap leach pad, comprised of four settlement cells. To represent the construction sequence, the model considered different topography surveys.

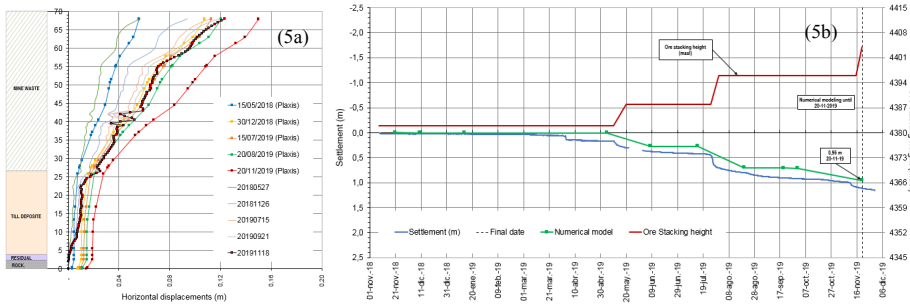

Figure 5a. Displacements described in the field by inclinometer INC-22 (P in Figure 4) and 5b. Settlement cell SA-404 (I in Figure 4) vs. displacements described in the model with Hardening Soil.

The calibration began by analyzing the general behavior of the mine waste dump with different constitutive models. Initially, the mine waste was modeled by HS, although it was able to approximate the behavior of the inclinometers and settlement cells in specified locations, it was still challenging to represent the displacements described by survey control points, as observed in Figures 5 and 6. Figure 6 shows that the model cannot reach the level of displacements obtained by the field data of survey control points, mainly in vertical displacements. Moreover, in the HS model, the horizontal displacements are more significant than the vertical displacements, in contrast, the survey data shows larger vertical displacements than horizontal displacements. These effect means a greater control of the volumetric strains in the model.

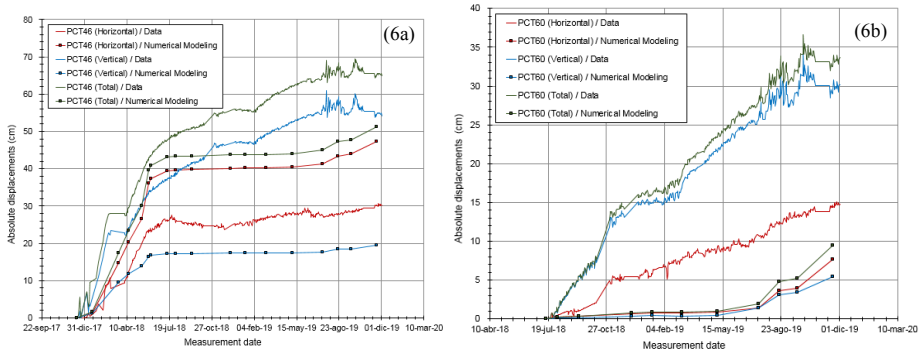

Figure 6a. Displacements described in the field by the survey control point PCT46 (E in Figure 4) and 6b. Survey control point PCT60 (H in Figure 4) vs. displacements described in the model with Hardening Soil.

Then, the SS model was used for a better calibration of the vertical displacements. Although there is a better fit of the vertical displacements (and therefore of the volumetric strains), the horizontal displacements could not be adjusted based on survey control points and inclinometer data as shown in Figures 7a and 8a.

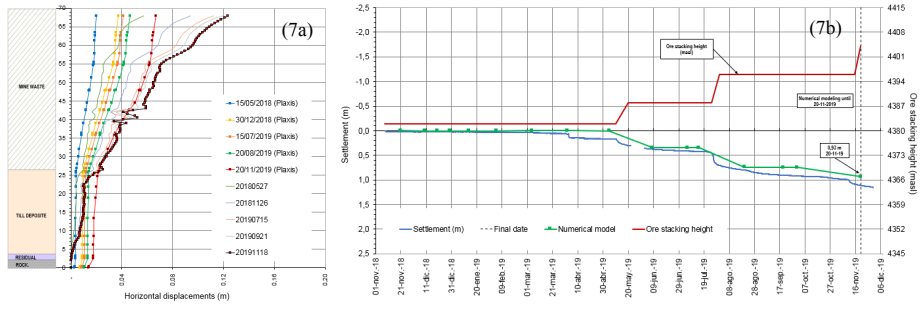

Figure 7a. Displacements described in the field by inclinometer INC-22 (P in Figure 4) and 7b. Settlement cell SA-404 (I in Figure 4) vs. displacements described in the model with Soft Soil.

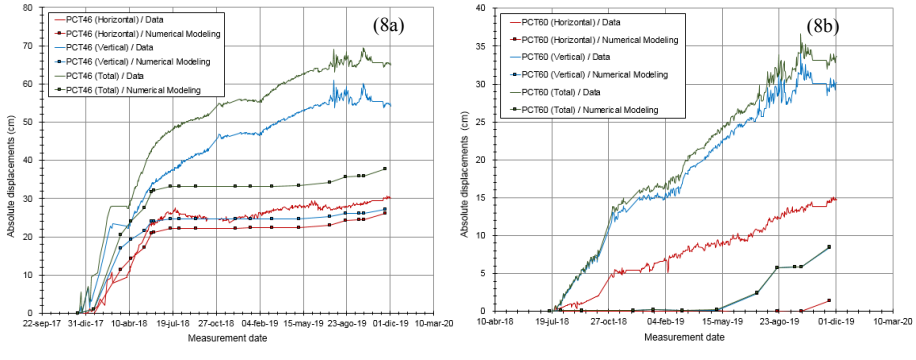

Figure 8a. Displacements described in the field by the survey control point PCT46 (E in Figure 4) and 8b. Survey control point PCT60 (H in Figure 4) vs. displacements described in the model with Soft Soil.

It is worth noticing that when comparing survey control point PCT46 (see Figures 6a and 8b), both the HS and SS models profoundly differ in the performance of volumetric strains, being the

vertical displacements more significant than the horizontal displacements in the SS model. However, when looking at survey control point PCT-60 (see Figures 6b and 8b) and settlement cell SA-404 (see figures 5a and 5b), neither model predict the creep behavior as is observed in the instrumentation data, while the settlement and the survey control points show zero displacements values before May 2019.

Based on the results of the calibration using HS and SS models, a new model was explored to represent the creep effect observed in the instrumentation data; it was also necessary that the model considers control of volumetric strains. Given this need, the authors opted to use the Soft SSC model (see Figures 9 and 10). Similarities of the model and the instrumentation data show a significant improvement, with a better match to vertical displacements, especially in the settlement cell SA-404 (see Figure 9b) and the survey control point PCT60 (see Figure 10b) that is to say, creep effects are matched. However, in the case of horizontal displacements, both inclinometer INC-22 (see Figure 9a) and survey control point PCT46 (see Figure 10a) show continuous increments beyond the observed in the instrumentation. Therefore, uncontrollable increments of horizontal displacements will continue developing when modeling future projections of ore and mine waste stacking. This uncontrollable increase in horizontal displacement was also observed at other survey control points located on the mine waste dump slope.

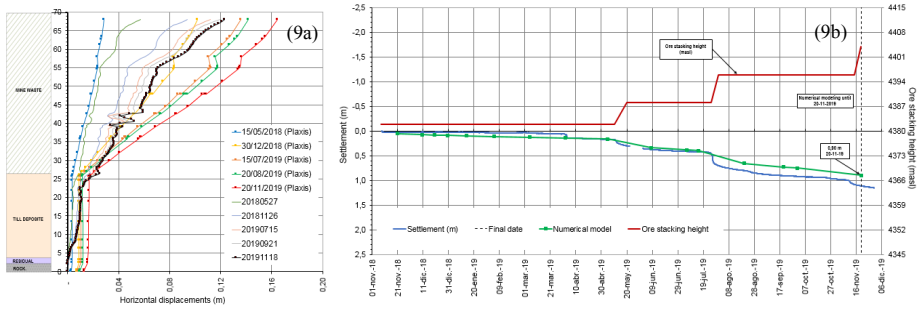

Figure 9a. Displacements described in the field by inclinometer INC-22 (P in Figure 4) and 9b. Settlement cell SA-404 (I in Figure 4) vs. displacements described in the model with Soft Soil Creep.

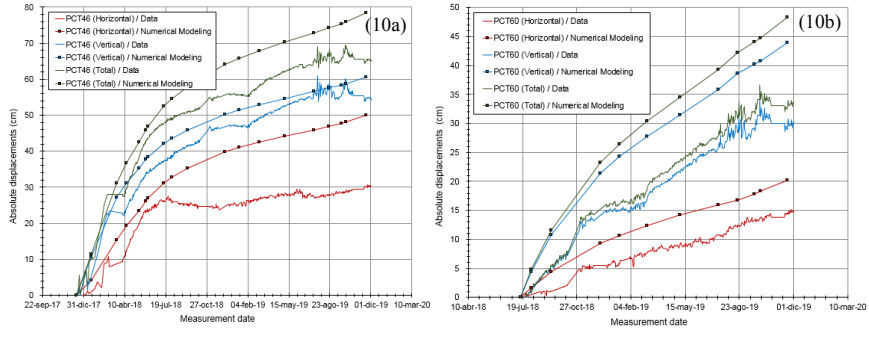

Figure 10a. Displacements described in the field by the survey control point PCT46 (E in Figure 4) and 10b. Survey control point PCT60 (H in Figure 4) vs. displacements described in the model with Soft Soil Creep.

6 VERIFICATION OF THE MODEL WITH CREEP-SCLAY1S

Finally, the Creep-SCLAY1S model was used to predict the horizontal displacements caused by creep and anisotropy, which was considered to be controlled by deviatoric creep strains. Table 3 presents the Creep-SCLAY1S model parameters. The value of α_0 is almost zero and represents the best fit value, which means that this model would be similar to the SSC model in that it does not have anisotropy behavior. However, controlling displacement direction due to deviatoric and volumetric creep strains suggest an anisotropy behavior in the model. According to Sivasithamparam et al. (2015), a null value of w_d allows control of volumetric creep strains than deviatoric creep strains, and for an infinite value of w_d the reverse control is given. In this case study, an effect of greater control of volumetric creep strains was considered, thus reducing the impact of deviator creep strains. This control using Creep-SCLAY1S shows the difference with the SSC model. Therefore, the model will begin without an unnoticed anisotropy until the creep phenomenon occurs due to volumetric creep strains ending in a rotation approaching a target value of $3\eta/4$ (η is the stress ratio) as stated by Sivasithamparam et al. (2015).

Figures 11 and 12 present the results using Creep-SCLAY1S constitutive model, in which an adequate representation of the model is obtained by matching the geotechnical instrumentation data of the facility. The results also show improvements of horizontal displacements in the inclinometer INC-22 and survey control point PCT46.

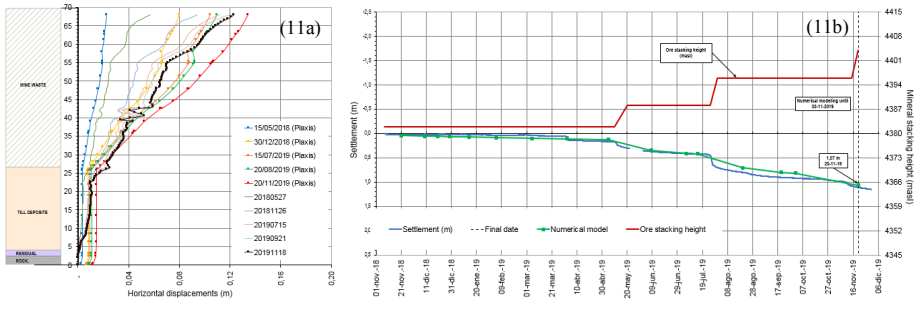

Figure 11a. Displacements described in the field by inclinometer INC-22 (P in Figure 4) and 11b. Settlement cell SA-404 (I in Figure 4) vs. displacements described in the model with Creep-SCLAY1S.

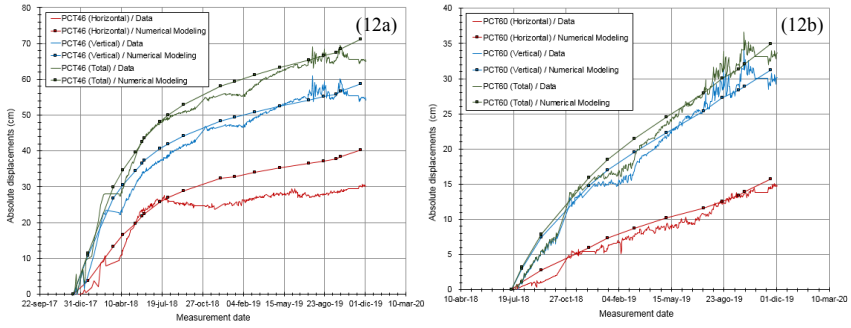

Figure 12a. Displacements described in the field by the survey control point PCT46 (E in Figure 4) and 12b. Survey control point PCT60 (H in Figure 4) vs. displacements described in the model with Creep-SCLAY1S.

7 ALERT LEVELS AND FACTOR OF SAFETY ESTIMATION

The use of the constitutive model Creep-SCLAY1S allows the estimation of updated alert levels of the installed instrumentation in the mine waste dump. For example, a better estimation of the values to control and verify as settlements in the mine waste dump as part of the leach pad expansion, and it will allow to intrinsically check the slope change of the heap leach pad collection system. A profile of the heap leach pad collection system can be obtained by reviewing a cross-section through the line that connects all the settlements cells installed, that is, the blue points in Figure 4. Figure 13 shows the change of the collection system slope at the end of the operation, with values starting from 7% ending at 2%, this value at the end of the operation will ensure a proper performance of the collection system.

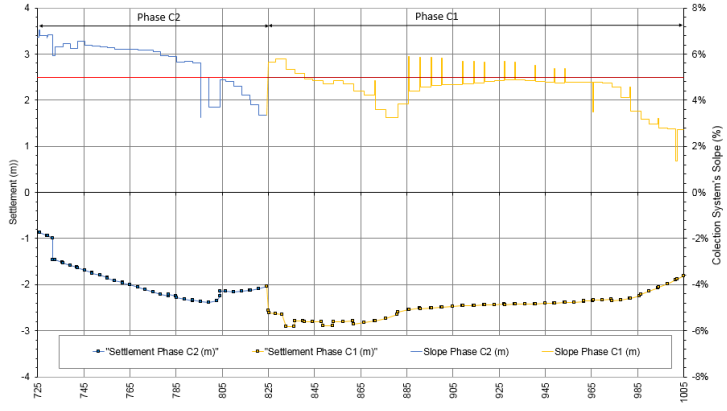

Figure 13. Future settlements and verification of the heap leach pad collection system slope in Phase C1 and C2 (May 2022).

Finally, the factors of safety (FOS) at different stages of ore stacking have been calculated by numerical and analytical methods for comparison. While in conventional condition FOS by numerical analysis is practically the same than FOS by limit equilibrium method (LEM), the results of this study suggest a lower FOS in numerical analysis than LEM, from 1.52 to 1.48 in the current condition represented by the section in Figure 14, and 1.68 to 1.60 for the final condition of the heap leach pad and mine waste dump. This behavior follows the different stress stages influenced by the creep phenomenon in the waste material. Additionally, the observed increase of FOS from 1.48 to 1.60 by LEM, is due to the final mine waste dump configuration with a more extended slope that increases the FOS.

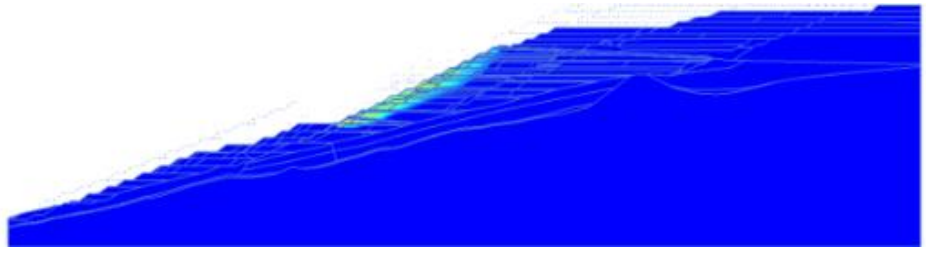

Figure 14. Failure surface for the current condition of the mine waste dump by numerical analysis with strength reduction method

8 CONCLUSIONS

This paper presents the practice carried out to adequately control and monitor a critical facility over a foundation with significant variability of materials. It involved a rigorous material control by the EoR, QC and QA, laboratory testing, abundant geotechnical instrumentation with most of the instruments deployed as real-time systems, identifying the critical controls and possible failure modes involved in the facility (liner system, slope failure) and a numerical model with rigorous calibration of the materials involved. This study focused on the challenge of the selection of an appropriate constitutive model for an atypical and quiet variable material to current sources of literature such as mine waste. Within most of the models used, based on plasticity and visco-plasticity theory, SCLAY1S-Creep constitutive model proved to give the best matching results to the instrumentation data. This model considers anisotropy and creep effects that also allowed to estimate future settlements in the waste dump, providing information to update the alert levels and verify the liner system behavior of the heap leach pad by the end of operation. This work, in turn, allows linkage of the geotechnical instrumentation and alert levels that are mainly involved in the control of the operator and EoR, and provides parameters for the adequate performance of the facility. Finally, the numerical model also influences the calculation of FOS of the slope stability when comparing to limit equilibrium method, being this due to creep, which highlights the importance of such phenomenon in the geotechnical design.

REFERENCES

Brinkgreve R., Zampich L. & Manoj N. 2019. PLAXIS CONNECT Edition V20. Plaxis bv, Bentley Systems, incorporated. Printed in the Netherlands.

Carlà, T., P. Farina, E. Intrieri, H. Ketizmen & N. Casagli. 2018. Integration of ground-based radar and satellite InSAR data for the analysis of an unexpected slope failure in an open-pit mine. Engineering Geology 235:39-52.

Giacomo F., Sara Del Conte, Nora T. & Alain B. 2019. InSAR as a Complementary Technology for Monitoring Programs of Tailings Storage Facilities and Waste Piles. Proceedings of Tailings and Mine Waste 2019 (Vancouver-Canada). 529-542.

Kermani M., Konrad J. & Smith M. 2018. In Situ Short-Term and Long-Term Rockfill Compressibility as a Function of Void Ratio and Strength of Parent Rock. J. Geotech. Geoenviron. Eng. 144(4):04018009.

Morgenstern, N.R., Vick, S. and van Zyl, D. 2015. Report on Mount Polley Tailings Storage Facility Breach, Independent Expert Engineering Investigation and Review Panel, Province of British Columbia.

Robertson P., de Melo L., Williams D. & Wilson G. 2019. Report of the Expert Panel on the Technical Causes of the Failure of Feijao Dam I.

Schanz. T., Vermeer P. & Bonnier P. 1999. The hardening-soil model: Formulation and Verification. In R.B.J. Brinkgreve, Beyond 2000 in Computational Geotechnics, Balkema, Rotterdam. 281-290.

Vermeer P.A. & Neher H.P. 1999. A soft soil model that accounts for creep. In: Proccedings of the international symposium on 'Beyond 2000 in Computational Geotechnics'. Amsterdam. p. 249-61.

Field Water Release and Consolidation Performance of XUR Treated Fluid Fine Tailings

S. Jeeravipoolvarn, E.J. Wu & S.A. Proskin
Thurber Engineering Ltd., Calgary, AB, Canada

A. Junaid & G. Freeman
Canadian Natural Resources Limited., Calgary, AB, Canada

ABSTRACT: A field trial to evaluate field water release and consolidation performance of the XUR polymer-treated fluid fine tailings (FFT) was conducted between 2018 and 2019 by Canadian Natural Resources Limited (Canadian Natural). The test was conducted at the field pilot scale with the in-line polymer injection at 400-440 g/tonne of solids, and the total deposited volume of treated FFT of about 2600 m^3. The material was monitored for its water release and consolidation performance for 267 days. Geotechnical laboratory tests were conducted using remoulded samples from the field to characterize the tailings and measure dewatering, consolidation, and strength properties. A finite strain consolidation back-analysis was performed using the field data to determine the water release and consolidation properties representative of the field performance. The field data indicated that the material demonstrated enhanced dewatering performance showing a 43% volume reduction within the monitoring period. The laboratory and analysis results also indicated that the material had a similar compressibility to typical oil sands FFT while the hydraulic conductivity was on the upper bound for typical oil sands FFT. The compressibility and hydraulic conductivity results are substantially different from the past geo-column studies on XUR-treated materials, which is believed due to a combination of lower dosage used in the current study, material variability and substantial pipeline shearing during transport. Vane shear strength testing was also conducted on the field samples indicating the strength sensitivity between 2 to 7, a typical range of polymer treated FFT.

1 INTRODUCTION

Chemical amendment by polymeric flocculant is a promising technique for oil sands tailings treatment (Matthews et al. 2013). However, typical hydrolyzed polyacrylamide (HPAM) polymers alone do not seem to be adequate to treat oil sands FFT to reach rapid dewatering, solids concentration, and material strength suitable for reclamation. Canadian Natural has been investigating the potential of an alternative polyethylene oxide (PEO)-based XUR polymer manufactured by Dow Chemical Company to accelerate dewatering and reclamation of tailings. Past laboratory-scale study using large strain consolidation and 3 m high geo-column test of the XUR treated FFT with 1900 g/tonne showed promising results with the higher hydraulic conductivity compared to the conventional HPAM treated FFT (Poindexter et al. 2015, Stianson et al. 2016a). A field pilot-scale 10 m deep casing experiment on a similar XUR treated FFT (dosage of 1500 g/tonne and the fill rate of 2.27 m^3/h) also demonstrated favorable performance compared to other treatments (Stianson et al. 2016b). Subsequently, a study with lower dosages was conducted to further optimize the dewatering performance and chemical use using a laboratory scale settling test (Poindexter et al. 2016, Rostro et al. 2018). The results indicated that

the dewatering performance can be maintained with lower treatment dosage of between 350-1000 g/tonne, and the performance was not significantly affected by the shearing during mixing.

This field trial was conducted in 2018 by Canadian Natural to evaluate the water release and consolidation performance of the XUR treated FFT with a lower dosage in a field scale test cell. The pilot scale test was executed under field operational conditions with the solids flow rate of approximately 1.2 tonne/minute (volume flow rate of 245 m^3/h) and total deposited volume of about 2,600 m^3. The XUR dosage was between 400-440 g/tonne. The material was monitored under the field conditions for 267 days (from August 2018 to May 2019). This paper analyzes performance of this material through laboratory and field measurements.

2 CELL CONFIGURATION AND POUR

The test cell for the XUR treated FFT is referred to as Test Cell 5. The cell was located at the Modified Atmospheric Fines Drying (MAFD) test site at Jack Pine Mine (JPM). The cell had as-built dimensions of approximately 35 m × 10 m × 4.5 m (base length × base width × depth). Plan view for the test cell is shown in Figure 1. The cell was built using sand without a geomembrane liner. Underdrainage and ground water interaction with surrounding conditions were expected. The cell was instrumented with vibrating wire piezometer (VWP) to track excess pore water pressure dissipation; total pressure cell (TPC) for tracking total stress change due to filling and water cap level; staff gauge for monitoring tailings and supernatant water levels; thermistor strings for temperature profiling during the monitoring period; and a mud-plate with a piezometer for top tailings level. Two instrumentation poles, namely P3 and P4, were installed in this regard on the centerline of the cell along the length as shown. The instrumentation work was completed by O'Kane Consultants Inc. (OKC).

The cell was filled on August 15, 2018 over a period of ~11.5 hours. The XUR-treated tailings (dosage: 400-440 g/tonne) was generated by injecting the polymer into a continuously flowing untreated FFT stream and subjecting the mixture through an in-line static mixture. The treated FFT stream was then deposited into Cell 5 approximately 1.0-1.5 km (pipeline distance) away from the injection point through a single 10" (25.4 cm) pipe discharge at an average volume flow rate of 245 m^3/h. The solids flow rate was approximately 1.2 tonne/min and the total deposited volume was ~2,600 m^3. A photograph of the cell on October 25, 2018 (71 days after deposition) is shown in Figure 2. Two floating docks were constructed to be aligned with the instrumentation poles P3 and P4 following the deposition.

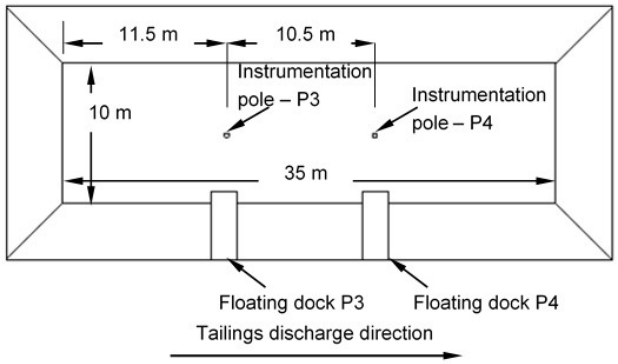

Figure 1. Test Cell 5 Plan View and Instrument Locations

Figure 2 Photograph of Cell 5 Filled with the XUR-treated FFT (taken on October 25, 2018)

3 LABORATORY TEST RESULTS

Tailings samples were obtained from the deposit at the P3 and P4 instrumentation locations using a piston sampling technique (Cyre sampler). The samples were subjected to laboratory material characterization, vane shear strength testing, and consolidation testing.

The material characterization test results are provided in Table 1. Particle size distribution and plasticity chart are provided in Figure 3 and Figure 4.

The material is classified as clay of high plasticity (CH) with average fines and clay contents of 98% and 47%, respectively, typical of the oil sands FFT materials. Atterberg limits are also typical of FFT with the Activity value between 0.89 to 1.05 classified as "normal". The plasticity from this study was also compared with the previous geo-column study on XUR treated FFT in Table 1 and Figure 4 showing elevated liquid limit and plasticity index compared to the previous studies. As well Methylene Blue Index (MBI) of the Test Cell 5 material were also greater than the geo-column study.

Table 1 Material characterization

Material	Test Cell 5 at P3	Test Cell 5 at P4	GC2	GC3 (pour 1)	GC3 (pour 2)
UCSC	CH	CH	-	-	-
UOSTCS	F-1	F-1	-	-	-
Initial solids content, %	24.9	24.9	31.0	28.3	28.8
Specific gravity	2.48	2.53	2.24	2.28	2.24
Fines content (≤ 44 um), %	96.9	98.3	89.5	89.6	88.9
Clay content (≤ 2 um), %	47.7	45.9	-	-	-
SFR	0.03	0.02	0.12	0.12	0.12
Liquid limit, %	67	65	48	48	47
Plastic limit, %	24	24	23	28	26
Plasticity index, %	43	41	25	20	21
Activity	1.05	0.89	-	-	-
MBI	11.1	10.4	7.0	6.8	6.6

Note: GC data from previous study by Stianson et al. 2016a.

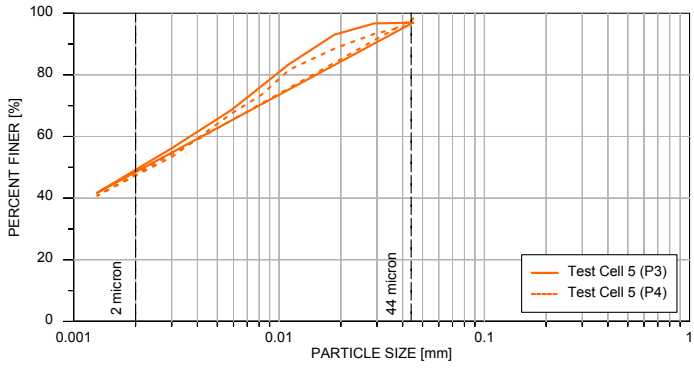

Figure 3 Particle size distribution

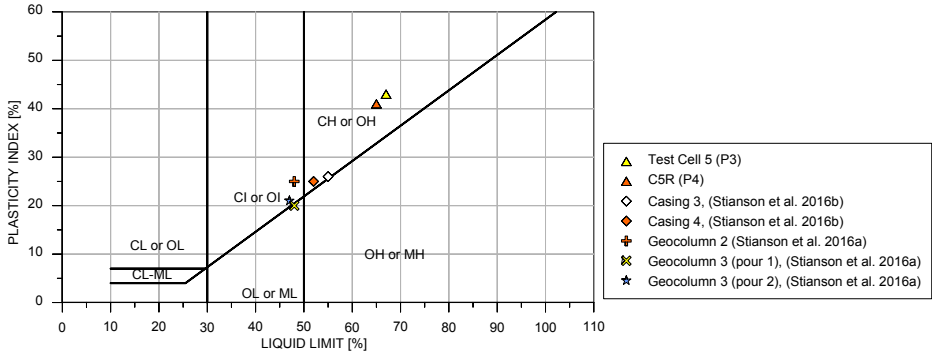

Figure 4 Plasticity chart

The samples obtained from the test cell were homogenized and remoulded to prepare specimens for consolidation testing with manual hand mixing to reduce shearing. Regrettably, end-of-pipe samples (with minimal disturbance) were not available for testing. Two types of consolidation tests were conducted – the step loading large strain consolidation test (LSC, Thurber 2019a based on Monte and Krizek, 1976) and the rapid centrifuge consolidation test (RCC, Thurber 2019b based on Weiland et al. 1994, Eckert et al. 1996, and McDermott and King 1998) with two test results (Duplicated Runs 1 and 2).

The LSC testing was conducted using a sealed piston cell with back pressure for saturation control. The load was applied incrementally, and at the end of consolidation for each loading step, hydraulic conductivity testing (ASTM D5856) was conducted. The RCC testing was conducted by incrementally applying centrifuge gravitational acceleration and monitoring material response with time. The RCC test results were then analyzed in a centrifuge finite strain consolidation numerical model to extract the material parameters.

The results from the consolidation tests of the remoulded sample are given in Figure 5 and Figure 6. The LSC and RCC results provide a similar trend of the material having a compressibility similar to untreated FFT and with the hydraulic conductivity towards the upper bound of the untreated FFT.

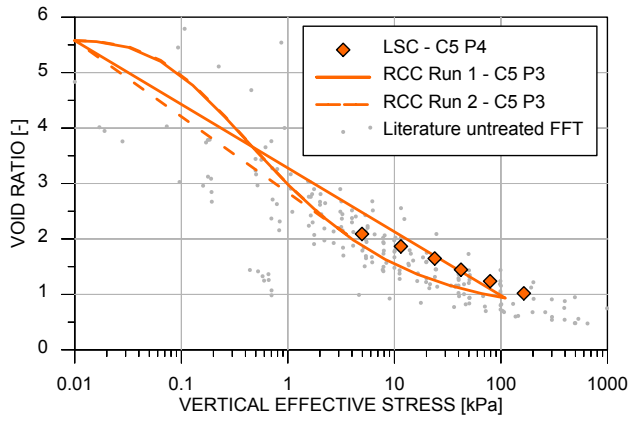

Figure 5 Compressibility of XUR treated tailings – remoulded sample

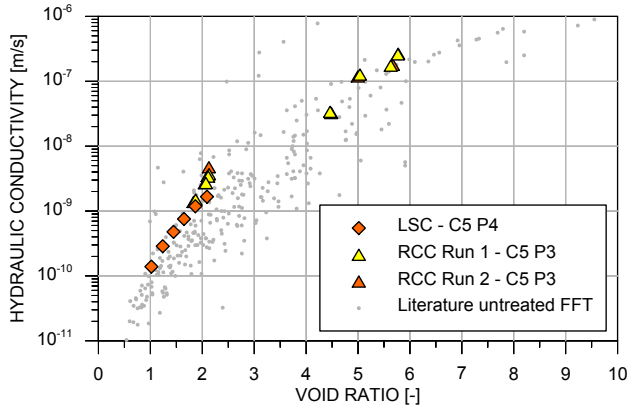

Figure 6 Hydraulic conductivity of XUR treated tailings – remoulded sample

The vane shear strength test results are shown with the liquidity index in Figure 7. The peak and residual strength measurements and the strength sensitivity of the material for liquidity index above 1 are similar to values for flocculated oil sands FFT reported by Beier et al. (2013). Previous studies on strength sensitivity on oil sands flocculated FFT (Jeeravipoolvarn 2010, Beier et al. 2013) suggested that the sensitivity decreases with the liquidity index/void ratio. In other words, as the material is dewatered, the flocculant influence on strength decreases.

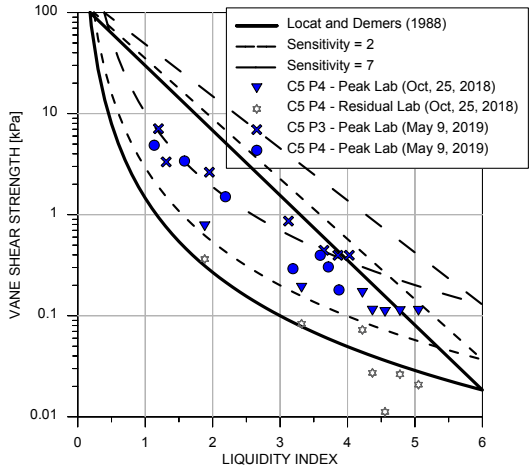

Figure 7 Liquidity index vs vane shear strength

4 FIELD TEST RESULTS AND CONSOLIDATION BACK ANALYSIS

The back-analysis is referred to calibration of the material constitutive parameters using the finite strain consolidation theory to obtain a match between the field observation and the theoretical analysis. The resulting parameters from the analysis signify the global response of the material under the theoretical framework and the assumptions. The results are considered a representative working hypothesis. The back-analysis method is often used when there are limited number of high-quality laboratory data available, or when the material quantity is large, and when material variability is expected. The back-analysis parameters can be used for consolidation projections for different operational scenarios for design and analysis, under the observation approach (Peck, 1969).

The was conducted by using field parameters (initial solids content, fines content, material height, fill rate, cell boundary pore water pressure and cell geometry) to construct initial and boundary conditions. The material constitutive parameters were then calibrated in a finite strain consolidation model to replicate tailings water interface, solids content and pore water pressure evolutions with time. Key assumptions utilized for the analysis are as follows (in addition to the finite strain consolidation theory assumptions (Gibson et al. 1967)):

1) Seasonal temperature effects were neglected.
2) Quiescent condition was assumed (no dry mass gain/loss).
3) Hydrogeologic boundary condition (Schiffman et al. 1994) was assumed (without water table fluctuation).

FSCA Version 2.1.2, the finite strain consolidation analysis software, was employed for the back analysis.

The comparisons between the measured and simulated tailings-water interface, solids content profile and pore water pressure profiles results are showed in Figure 8 and Figure 9, respectively.

Figure 8 shows that at the end of the monitoring period of 267 days, the tailings settled from about 4.2 m to 2.4 m (approximately 1.8 m settlement or 43% volume reduction) and that the material was still undergoing compression at the end of the field trial.

Solids content profiles in Figure 9 show that the material consolidated from bottom upward with the solids content increasing with depth; and as time progressed these values increased toward the top (as expected from typical consolidation behaviour under the hydrogeological boundary condition).

Pore water pressure profiles in Figure 9 shows that the base pore water pressures were lower than the hydrostatic pressure indicating that the cell was under-drained. In this condition, water dissipates through both top and bottom boundaries. As the bottom boundary pressure was lowered than the hydrostatic pressure, the effective stress was higher than self-weight effective stress.

The back-analysis results showed (in Figure 8 and 9) that the analysis can replicate the field results within reasonable bounds of the constitutive relationships. The back-analysis relationships are taken as representative constitutive relationships for the materials.

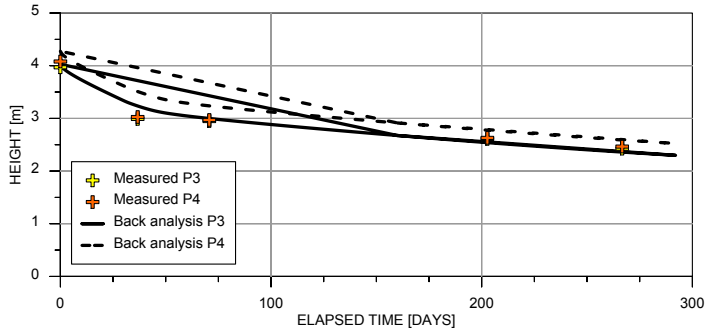

Figure 8 Tailings-water interface measurement vs. back analysis

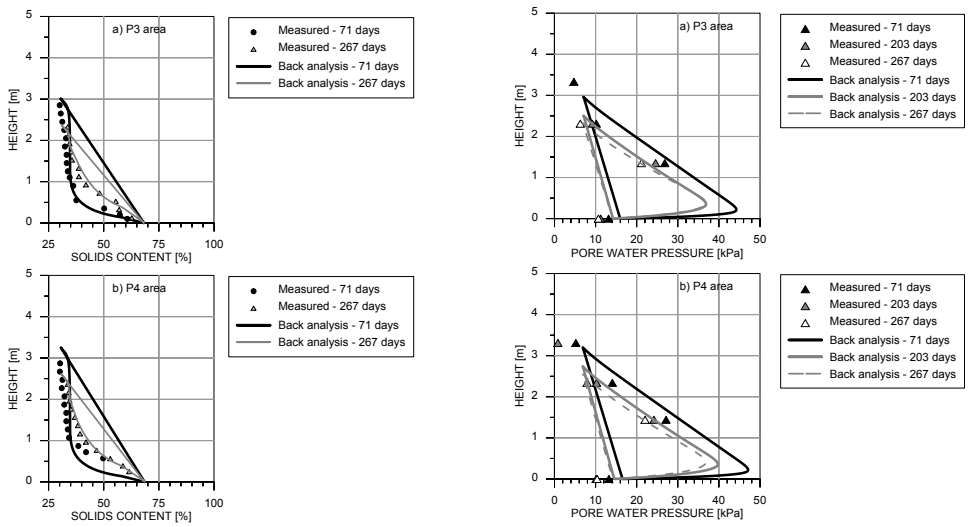

Figure 9 Solids content and pore water pressure profiles measurement vs. back-analysis

The field constitutive relationships for the XUR treated FFT in Test Cell 5 are compared with following data sets in Figure 10 and Figure 11:

- The LSC and RCC data for the XUR treated FFT in this study;
- Untreated FFT literature data;
- Syncrude's in-line thickened tailings; and
- XUR treated FFT with higher dosage (GC2 Model).

The XUR treated FFT in the Test Cell 5 had compressibility similar to untreated FFT and with the hydraulic conductivity towards the upper bound of the typical untreated FFT. Compared to

the material from the higher dosage smaller-scale study (GC2 Model), the material in the Test Cell 5 was less compressible, and has a lower hydraulic conductivity. The comparison also shows that the Test Cell 5 material behaves similarly to Syncrude's ILTT.

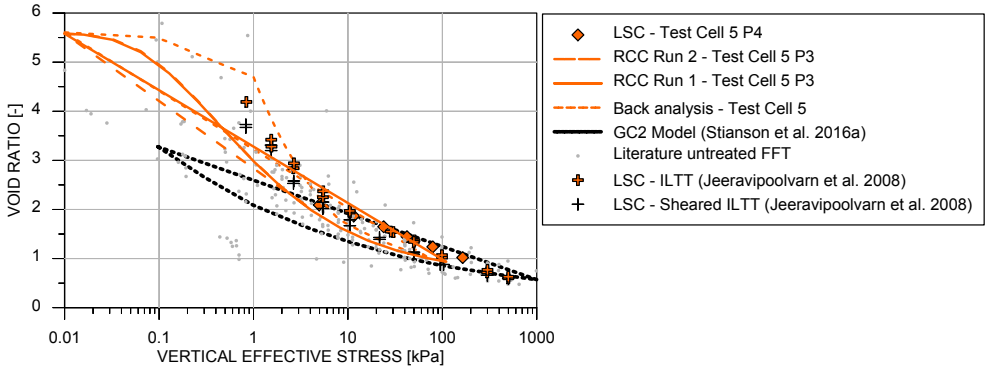

Figure 10 Comparison between field and laboratory compressibility

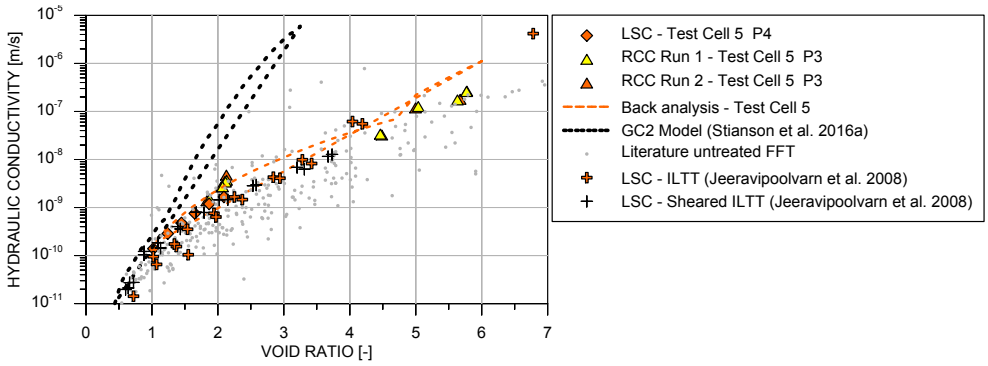

Figure 11 Comparison between field and laboratory hydraulic conductivity

5 DISCUSSION

The XUR treated FFT in this trial had a compressibility similar to untreated FFT and with its hydraulic conductivity towards the upper bound of the typical untreated FFT. When compared to the XUR treated FFT from a higher dosage (1900 g/tonne) smaller-scale (3 m geo-column) past study (GC2 Model), the material in this study was less compressible, and the hydraulic conductivity was substantially lower at void ratio above 1.

The characterization results indicated that the material in the Test Cell 5 had liquid limit and plasticity index greater than the previous smaller-scale trial. Similarly, the MBI was also slightly higher than the previous studies. These results imply that the material in the Test Cell 5 has different fundamental properties compared to the previous studies and could impact chemical and physical treatments of the material.

Other factors might have also contributed to the reduced performance in the larger scale trial – shearing during pipe-line transportation, and inefficient flocculation under the pilot-scale operational conditions (e.g. feed variability, injection and mixing).

Future research and development activities should target better understanding the impacts of shear, dosage and clay content on the efficacy of flocculation with the XUR polymer. Also, going

forward, fast screening techniques such as rapid centrifuge consolidation (RCC), Net Water Release (NWR), MBI, Zeta potential and alike can be used with proper analysis and quality control for field use.

6 SUMMARY

The Cell 5 trial test was conducted to evaluate the dewatering and consolidation performance of low dosage (400-440 g/tonne) XUR treated FFT material as an alternative to conventional HPAM treated analogues. The material demonstrated enhanced water release in a relatively short period of time (43% volume reduction in 267 days). The field and laboratory data indicated further settling beyond the test period.

Laboratory testing, field investigation, and numerical analysis were successfully conducted to interpret the field water release and consolidation performance of the material. Compressibility and hydraulic conductivity representing the material under the field trial operational conditions and assumptions were obtained.

Compared to the previous studies with smaller scale and higher dosages, the compressibility and hydraulic conductivity results are substantially different. It is believed that a combination of lower dosage, material variability and substantial pipeline shearing during transport contributed to the changes in the overall performance in the current study. Future research is required to improve the understanding of these impacts on the dewatering and consolidation performance of XUR treated FFT.

7 ACKNOWLEDGEMENT

O'Kane Consultants Inc., GeoForte Services Limited, and ConeTec Investigations Limited for their field instrumentation and testing support.

8 REFERENCE

ASTM D5856-15, Standard Test Method for Measurement of Hydraulic Conductivity of Porous Material Using a Rigid-Wall, Compaction-Mold Permeameter, ASTM International, West Conshohocken, PA, 2015, www.astm.org

Beier, N., Wilson, W., and Sego, D. 2013. Impact of flocculation-based dewatering on the shear strength of oil sands fine tailings. Canadian Geotechnical Journal, 50: 1001–1007.

Eckert, W. F., Masliyah, J. H., Gray, M. R., & Fedorak, P. M. (1996). Prediction of sedimentation and consolidation of fine tails. AICHE Journal, 42(4), 960–972.

FSCA, 2018. User manual, Finite strain consolidation analysis software by Bright Beacon Co.Ltd.

Gibson, R.E., England, G.L. and Hussey M.J.L. 1967. The Theory of One-dimensional Consolidation of Saturated Clays. I. Finite Non-linear Consolidation of Thin Homogeneous Layers. Géotechnique, 17(3): 261–273.

Matthews J, Masliyah J, Czernecki I, Xu Z, eds. Tailings management. Handbook on Theory and Practice of Bitumen Recovery from Athabasca Oil Sands, Vol. II: Industrial Practice. Edmonton: Kingsley Knowledge Publishing; 2013:291-319.

McDermott IR and King AD (1998) Use of a bench-top centrifuge to assess consolidation parameters. Proceedings of the Fifth International Conference on Tailings and Mine Waste '98, Fort Collins, Colorado, USA, pp. 281-288.

Monte J.L. and Krizek, R.J. (1976). One dimensional mathematical model for large-strain consolidation. Geotechnique, 26(3), 495-510.

Peck, R.B., 1969. Advantages and limitations of the observational method in applied soil mechanics, Geotechnique, 19(2):171-187.

Jeeravipoolvarn, S., Scott, J.D., Chalaturnyk, R.J., Shaw, W., and Wang, N., 2008. "Sedimentation and Consolidation of In-Line Thickened Fine Tailings", Proceedings of International Oil Sands Tailings Conference, December 7-10, Edmonton, AB, pp. 209-223.

Jeeravipoolvarn, S., 2010. Geotechnical behaviour of in-line flocculated oil sands tailings. PhD thesis, University of Alberta, Edmonton, AB, 431p.

Poindexter, M.K., Gilles, P.A., Moore, J.S., Tubbs, J. Mahood, R., and Freeman, G. 2015. Geotechnical

column evaluation of new flocculant technology for dewatering oil sands mature fine tailings, TWM 2015.

Rostro, L.R., Gilles, P.A., Chen, W., Poindexter, M.K. and Tubbs, J. 2018. Robust low dosage treatment across multiple oil sands fluid fine tailings samples using a new amendment. IOSTC 2018, Edmonton, AB, December 9-12, 2018: 8-13.

Schiffman, R. L., McArthur, J. M. & Gibson, R. E., 1994. Consolidation of clay layers: Hydrogeologic boundary conditions. Journal of Geotechnical Engineering, Volume 120(6), pp. 1089-1093.

Stianson, J., Mahood, R., Fredlund, D.G., and Sun J. 2016a. Large strain consolidation modeling to determine representative tailings consolidation properties from two meso-scale column test. IOSTC 2016, Lake Louise, AB, December 4-7, 2016: 40-50.

Stianson, J., Mahood, R., Thomas, D., Song, J., and Li, L. 2016b. A Shell Tailings Consolidation Casing Experimental Pilot Project (TCCEPP). IOSTC 2016, Lake Louise, AB, December 4-7, 2016: 40-50.

Thurber Engineering Ltd. 2019a. Large strain consolidation (LSC) test - standard operating procedure.

Thurber Engineering Ltd. 2019b. Rapid centrifuge consolidation (RCC) test - standard operating procedure.

Weiland, R.H., Bunnaul, P. and Hogg, R. 1994. Centrifuge dewatering of flocculated clays. Minerals and Metallurgical Processing, 11:37-40.

Consolidation Modeling for Design of Complex In-pit Tailings Storage Facility

Sudhir Tripathi; MS, EI
Knight Piésold and Co., Denver, Colorado, USA

Jordan Scheremeta; MS, PE
Knight Piésold and Co., Denver, Colorado, USA

Jeff Coffin; PhD, PE
Knight Piésold and Co., Denver Colorado, USA

Jason Reiva, PE
Knight Piésold and Co., Denver, Colorado, USA

ABSTRACT: Suitable locations for safe and economic disposal of mine tailings that pose low long-term liability are limited at many mine sites. In recent years, backfilling of existing mine pits with tailings has garnered attention as one viable alternative. The case presented herein, despite having some fundamental resemblance to typical in-pit filling practices, is unique due to the hydrogeology of the area and envisioned complexities of the tailings deposit development within the open pit over the life cycle of the facility. Consolidation modeling was conducted to assess the life-cycle of the facility and the anticipated performance of a proposed intermediate separation layer and overlying geomembrane liner system constructed over soft tailings that are needed to mitigate local groundwater contamination.

Owing to the mine's plan to develop the in-pit Tailings Storage Facility (TSF) as two separate deposits – 1) Lower Deposit, and 2) Upper Deposit – separated by a free-draining separation layer, the consolidation modeling approach consisted of several three-dimensional (3D) and one-dimensional (1D) models using the finite-difference CONDES consolidation software developed at the University of Colorado at Boulder. The first step included development of a 3D consolidation model to assess the anticipated void ratio distribution of the unlined Lower Deposit at the end of deposition within that portion of the TSF. The Lower Deposit is planned to be unlined because the hydrogeology of the area provides a hydraulic sink toward the pit and the groundwater is maintained below a certain level by continuous pumping, which mitigates the potential for groundwater contamination. The Upper Deposit is located above the hydraulic sink elevation and will require a geomembrane liner system to prevent contamination of groundwater sink. This required the design of a rockfill Separation Layer on the surface of the Lower Deposit to account for continued consolidation-settlement of the Lower Deposit and the Separation Layer due to self-weight and filling of the Upper Deposit.

To model this deformation and design the necessary camber on the Separation Layer, a 3D consolidation model was completed on the TSF Upper Deposit to assess the void ratio profile and average dry density of the material driving the consolidation of the Lower Deposit. The predicted average dry density was used to estimate the combined uniform surcharge pressure exerted on the Lower Deposit by the overlying rockfill Separation Layer and the Upper Deposit. Next, several 1D consolidation models were completed under the anticipated combined uniform surcharge pressure to predict differential settlements of the geomembrane liner system due to the compressibility of the unlined Lower Deposit. These analyses were used to design the necessary camber on the Separation Layer to mitigate damage to the geomembrane liner system of the Upper Deposit and to maintain gravity flow across the Separation Layer (below the hydraulic sink elevation) to perimeter collection sumps. Finally, the modeling results were combined to estimate the anticipated dry density of the tailings at the end of filling of the overall TSF.

1 INTRODUCTION

Large volumes of tailings are generated worldwide as a result of mining. Conventionally, these mine tailings are stored by constructing cross-valley embankments or perimeter dikes with the help of waste rock and/or naturally occurring fill material readily available nearby. However, as mine sites age, a shortage of suitable locations for safe and economic disposal of mine tailings often presents itself, with mine operators looking for new and innovative alternatives. In recent years, in-pit Tailings Storage Facilities (TSFs) have garnered attention as one viable alternative. As the name suggests, these are storage facilities where an historic open pit is backfilled with mine tailings. This method is attractive to mine operators as open pits can often be filled at a fraction of the costs associated with designing, constructing, and operating a conventional TSF. In addition, pit walls eliminate the need for perimeter dikes, and thus the risk associated with embankment instability is greatly reduced or eliminated (EPA, 1994). However, there are also many potential risks associated with in-pit TSFs such as potential for groundwater contamination near the pit, poor consolidation characteristics of the tailings deposited within the pit and potential hazards associated with it, and reduced rework potential of the backfilled pit.

As with design of any TSF, estimating storage capacity of the TSF is essential part of the process, which is dependent on the consolidation behavior of material under self-weight and the rate of rise of the tailings during deposition. As a result of advancements in the understanding of large-strain consolidation characteristics of tailings slurries, this can be accomplished to a relatively high degree of accuracy by combination of laboratory Seepage Induced Consolidation (SIC) tests and computer-based consolidation models. Specialized applications of consolidation modeling can also be used in other steps of the design process in addition to estimating tailings storage capacity. The planned in-pit TSF discussed herein is unique because it utilizes a combination of three-dimensional (3D) and one-dimensional (1D) consolidation models during design of an open pit TSF due to the hydrogeology of the area and envisioned complexities of the tailings deposit development within the open pit.

The planned development of this in-pit TSF is envisioned to consist of a layered system, which includes: 1) the Lower Deposit, 2) the Separation Layer, and 3) The Upper Deposit. The Lower Deposit is planned to be unlined because the hydrogeology of the area provides a hydraulic sink toward the pit and the groundwater is maintained below a certain level by continuous pumping, which mitigates the potential for groundwater contamination. The Upper Deposit is located above the hydraulic sink elevation and will require a geomembrane liner system to prevent contamination of groundwater sink. The Lower Deposit is designed to be below approximately elevation 3340 meters above sea level (masl). Subaqueous tailings deposition will be used for the Lower Deposit and a water cover will be maintained to keep the tailings submerged. A separation layer is envisioned to be constructed between the Lower Deposit and Upper Deposit to provide a drain layer and buffer/monitoring zone such that local groundwater levels are maintained below the 3350 masl hydraulic sink level. For this, a Separation Layer Pumping System is planned to be installed. In addition, the Separation layer will provide the foundation for the Upper Deposit.

The Upper Deposit will be constructed as a fully lined basin with the geomembrane liner system installed atop the separation layer and along a ring embankment constructed in approximately three, 30 meter lifts. The ring embankment will be supported at its base by the Separation Layer. The tailings deposited within the Upper Deposit are envisioned to span from approximately 3350 to 3438 masl (3440 masl ultimate crest elevation) for a maximum thickness of 88m. Figure 1 shows a conceptual schematic of the planned development of the tailing deposits and rockfill separation layer within the pit.

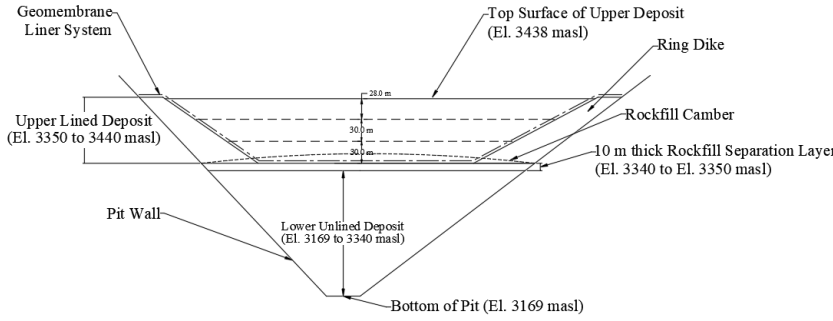

Figure 1. Planned Development of Tailing Deposits and Rockfill Separation Layer within Pit

The main objective of this paper is to illustrate the use of consolidation modeling to: 1) design the necessary camber for the Separation Layer to mitigate damage to the Upper Deposit geomembrane liner system and to maintain gravity flow across the Separation Layer (below the hydraulic sink elevation) to perimeter collection sumps, and 2) estimate anticipated dry density of the tailings within the TSF at the end of filling for the purpose of providing an estimate of the total storage capacity of the TSF.

2 TAILINGS MATERIAL PROPERTIES AND DEPOSITION RATE

The tailings material to be deposited into the proposed in-pit TSF will be mix of Flotation and Cyanide Leach Tailings denoted as "Mixed Tailings". The laboratory testing performed on the Mixed Tailings material included index property tests such as particle size analysis with hydrometer, specific gravity testing, and Atterberg's limit test. Based on results of these laboratory tests, the Mixed Tailings classify as non-plastic Silt with Sand (ML) according to USCS classification. Additionally, relationships between void ratio and effective stress, and between void ratio and saturated hydraulic conductivity, were evaluated using Seepage Induced Consolidation (SIC) testing. Figures 2 and 3 provide graphical representations of these relationships for the Mixed Tailings.

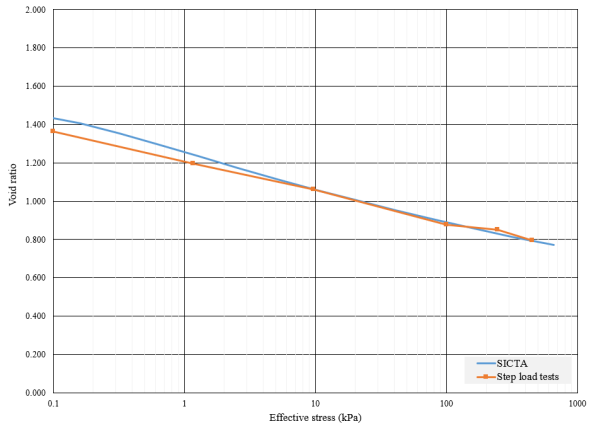

Figure 2. Variation of Void Ratio with Effective Stress from SICTA for the Mixed Tailings

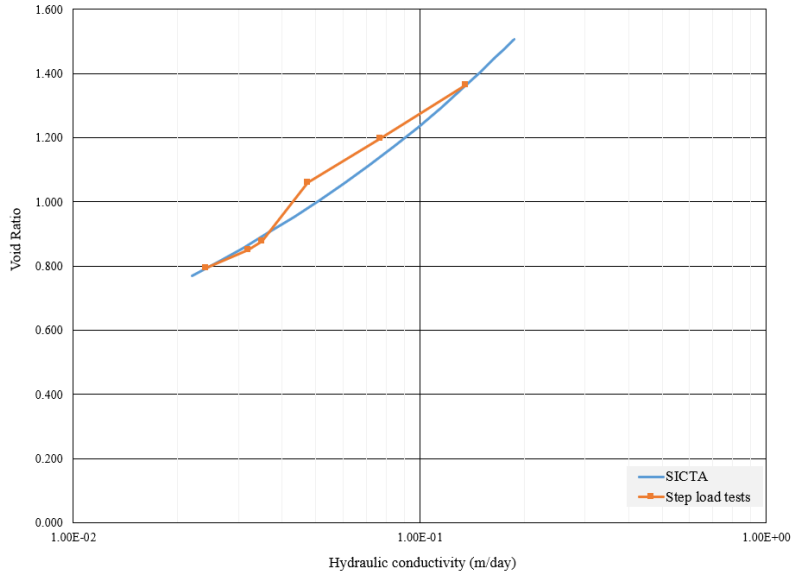

Figure 3. Variation of Void Ratio with Hydraulic Conductivity (m/day) for the Mixed Tailings

The above graphical relationships are represented by the following functions:

Compressibility: $e = A(\sigma' + Z)^B$ (1)
Hydraulic Conductivity: $k = C\ e^D$ (2)

Where: e= void ratio
k=hydraulic conductivity
σ'=vertical effective stress
A, B, C, D, and Z =curve-fit parameters (A, Z, and C depend on the system of units, and are provided herein for SI units)

The compressibility function (1) was formulated by Liu and Znidarcic (1991); whereas the permeability function was developed by Somogyi (1979). Table 1 presents the SIC testing curve-fit parameters for the tested Mixed Tailings. Table 2 presents the summary of relevant index and geotechnical engineering properties associated with the Mixed Tailings.

Table 1. Testing Results – SIC Testing Curve-Fit Parameters

Curve-Fit Parameter	Mixed Tailings
A	1.26
B	-0.076
Z (kPa)	0.09
C (m/d)	5.06×10^{-2}
D	3.19

Table 2. Testing Results – Mixed Tailings Material Properties

Material Property	Mixed Tailings
USCS Classification	Silt with sand (ML)
Gravel (%)	0.0
Sand (%)	28.7
Fines (%)	71.3
Liquid Limit (LL)	Non-Plastic
Plastic Limit (PL)	Non-Plastic
Specific Gravity	2.742
Void Ratio at Zero Effective Stress (e_0)	1.519
SIC Dry Density	1.16 – 1.46 t/m^3 over an effective over stress range of 0-100 kPa
Saturated Hydraulic Conductivity	1.56 x 10^{-4} – 4.06 x 10^{-5} cm/sec over the stress range of 0-100 kPa

The mine plans to deposit Mixed Tailings into the TSF at a deposition rate of approximately 7.37 million tons per year (Mt/y) starting from year 2027 through approximately 2039. Figures 4 and 5 show the volumetric filling curves for the Lower Deposit and Upper Deposit, respectively.

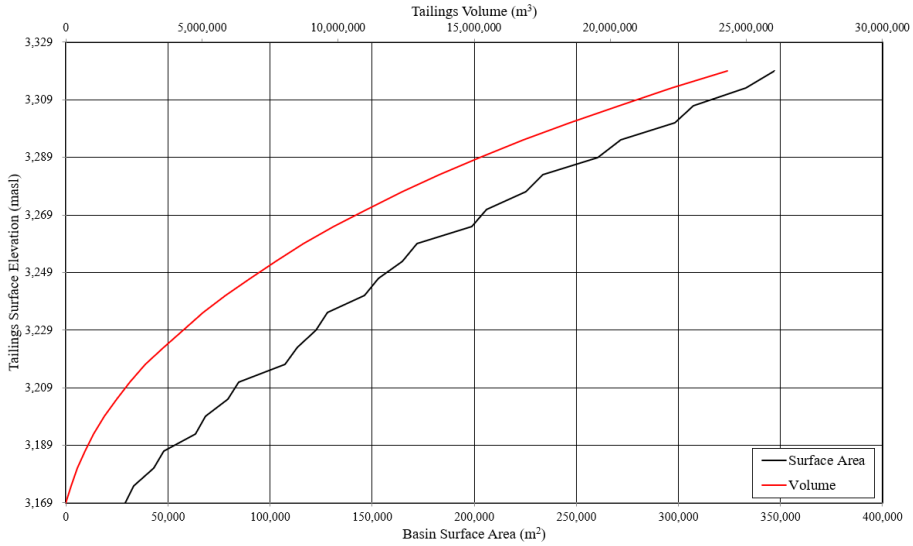

Figure 4. TSF Filling Curve – Lower Deposit

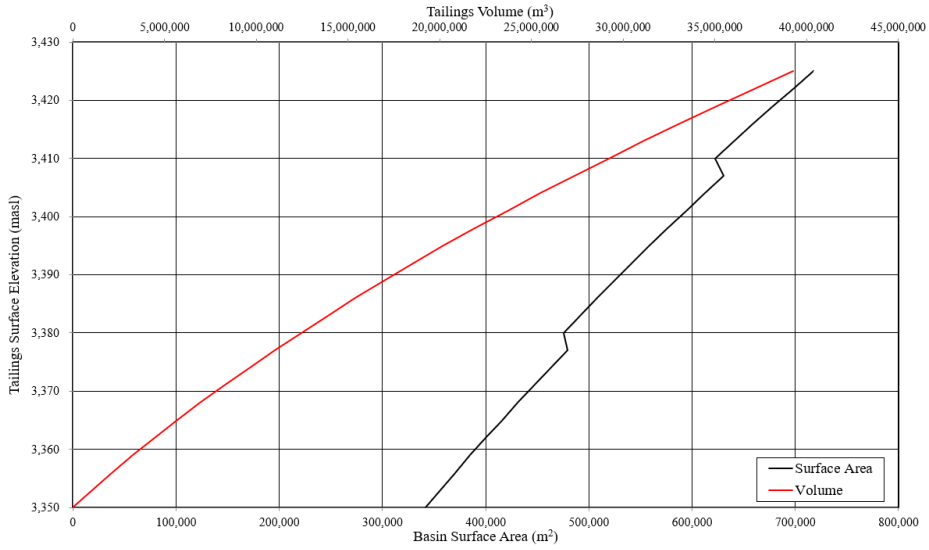

Figure 5. TSF Filling Curve – Upper Deposit

3 CONSOLIDATION MODELING

3.1 *Consolidation modeling software*

Consolidation modeling was performed using the results from the laboratory testing described above and the modeling algorithm described by Gjerapic and Znidarcic (2007), which was implemented into the CONDES consolidation software developed at the University of Colorado Boulder. CONDES is a finite-difference program which solves the non-linear, partial differential equation proposed by Gibson et al (1967) as shown below, which describes 1D consolidation.

$$\pm\left(\frac{\rho_s}{\rho_f}-1\right)\frac{d}{de}\left[\frac{k(e)}{1+e}\right]\frac{\partial e}{\partial z}+\frac{\partial}{\partial z}\left[\frac{k(e)}{\rho_f(1+e)}\frac{d\sigma'}{de}\frac{\partial e}{\partial z}\right]+\frac{\partial e}{\partial t}=0 \tag{3}$$

Where ρ_s is the unit weight of solids, ρ_f is the unit weight of fluid, $k(e)$ is the coefficient of hydraulic conductivity as a function of the void ratio e, and z is the height of solids from a specified datum. The Gibson equation (Gibson et al, 1967) allows for non-linear, stress-dependent representations of the void ratio-effective stress and void ratio-hydraulic conductivity relationships without restriction on the shape of these functions. The CONDES software provides a numerical solution to the consolidation equation. This solution is combined with the planned tailings production and the geometry of the impounding TSF such that concurrent deposition and consolidation can be modelled; similar to the process expected by depositing slurry tailings into the TSF. The filling scheme is such that the model accounts for the three-dimensionality of the impoundment for a more accurate estimate of the average dry density developed within the TSF. Both 1D and 3D versions of the CONDES software are available, and both were used for different aspects of this project. The 3D version was used to model consolidation during filling, while the 1D version was used in various locations to understand the potential for differential settlement of the separation layer.

3.2 *Modeling Assumptions and Simplifications*

The following assumptions were made in developing the consolidation modeling presented herein.

1. The in-pit TSF will be developed as two separate deposits (Lower Deposit and Upper Deposit). Beach slopes will be developed during the filling of both the Upper and Lower Deposits to their respective maximum average tailings elevation. It is assumed these developed beach slopes will not significantly impact the results of the consolidation modeling.
2. The Upper and Lower Deposits will attain two different average dry densities at the end of consolidation due to the presence of the Separation Layer, the Upper Deposit being geomembrane lined, and differing effective stress regimes acting upon each deposit; therefore, separate consolidation models were performed for the Lower Deposit and the Upper Deposit.
3. Additional differential consolidation settlement is expected to occur within the Lower Deposit due to the surcharge load developed by the Separation Layer and the development of the Upper Deposit above the separation layer. This was accounted for in the overall assessment through the completion of several 1D consolidation models using the 1D version of CONDES. The surcharge pressure applied to each of the 1D models was estimated and uniformly distributed over the top surface of the Lower Deposit. The immediate embedment of the Separation Layer into the Lower Deposit that will develop due undrained shearing during construction of the Separation Layer over the soft tailings in the Lower Deposit was not incorporated as a part of consolidation modeling exercise, and is not expected to significantly impact the results estimated herein.
4. An average production rate of 20,180 tons per day (tpd) was assumed based on the average of the planned deposition rates for years 2027 through 2039 (~7.37 Mt/y).
5. Segregation of the material is anticipated to be limited and the tailings will be sufficiently homogeneous such that a single set of material properties is representative of the new Mixed Tailings to be deposited into the TSF.
6. The planned Mixed Tailings will contain high concentrations of gypsum. It is anticipated the gypsum will create a binding effect along the unlined pit wall boundary within the Lower Deposit to promote minimal bottom drainage, thus a no-flow bottom boundary was assumed for consolidation modeling of the Lower Deposit. The Upper Deposit is planned to be a geomembrane lined; therefore, a no-flow bottom boundary was also adopted for consolidation modeling on the Upper Deposit.
7. The supernatant fluid was assumed to be water.

3.3 *Consolidation Modeling Approach*

Since the lifecycle of this In-pit TSF involves recurring periods of construction and deposition, and continuous monitoring of groundwater, it is necessary for the modeling approach to consider the major consolidation processes during the time period. The approach discussed herein effectively captures the following processes:

- Concurrent deposition and self-weight consolidation of the Lower Deposit.
- Simultaneous consolidation of the Lower Deposit due to development of the overlying Separation Layer and Upper Deposit.
- Concurrent deposition and self-weight consolidation of the Upper Deposit.

The modeling does not account for embedment of the rockfill Separation Layer due to undrained shearing that would occur during its placement onto the deposited tailings at the surface of the Lower Deposit. This process has been handled separately outside of the scope of this paper.

During tailings deposition within the Lower Deposit (from elevation 3169 to 3340 masl), concurrent self-weight consolidation of the tailings will occur. To assess the anticipated void ratio distribution within this portion of the deposit at the end of the deposition, a 3D consolidation model was completed. During filling, surface (surcharge) loading and evaporation were assumed to be zero due to the sub-aqueous deposition plan. The results of this modeling were used to estimate the average dry density of the tailings over time and to estimate the expected time needed to fill the unlined lower portion of the pit to an average tailings elevation 3340 masl.

The role of Separation Layer overtop the Lower Deposit is to maintain the ground water level below the elevation of the hydraulic sink. An additional function of the separation layer is to mitigate potential groundwater contamination above the hydraulic sink level by providing a competent foundation for the Upper Deposit geomembrane liner system and opportunity for seepage collection from both the Upper (downward seepage) and Lower Deposits (upward drainage during consolidation). As such, the separation layer needs to be carefully designed such that there will be no damage to the geomembrane liner system overtime due to continued consolidation-settlement of the Lower Deposit and the Separation Layer due to self-weight and filling of the Upper Deposit.

To model this deformation and design the necessary camber on the Separation Layer to prevent damage to the geomembrane liner system, a 3D consolidation model was completed on the Upper Deposit (from elevation 3350 to 3438 masl) to assess the void ratio profile and average dry density of the surcharge material driving additional consolidation of the Lower Deposit. As before, surface loading and evaporation were assumed to be zero. The predicted average dry density of the Upper Deposit was used to estimate the combined uniform surcharge pressure exerted on the Lower Deposit tailings by the overlying rockfill Separation Layer and the Upper Deposit. Next, several 1D consolidation models were completed under the anticipated combined surcharged pressure to predict differential settlements of the geomembrane liner system due to the compressibility of the unlined Lower Deposit (i.e., settlement of the top surface of the Lower Deposit).

After completion of the 3D and 1D consolidation models, the maximum time rate of consolidation from 1D consolidation models was compared against the total time required for simultaneous filling and self-weight consolidation of Upper Deposit to confirm that the consolidation-settlement under surcharge is generally completed before the end of Upper Deposit deposition (limited long-term additional consolidation of the Lower Deposit post-operations). Meeting this criterion was a crucial part of modeling for closure design consideration of the TSF. The results of these analyses were used to design the necessary camber on the Separation Layer to mitigate damage to the geomembrane liner system of the Upper Deposit and to maintain gravity flow across the Separation Layer (below the hydraulic sink elevation) to perimeter collection sumps.

3.4 *Consolidation Modeling Results*

Figures 6 and 7 provide a variation of tailings surface elevation and average dry density over time for filling and self-weight consolidation within the Lower Deposit and Upper Deposit, respectively. The key findings from the modeling such as average dry density, approximate time to filling, and estimated total storage tonnages are presented in Table 3.

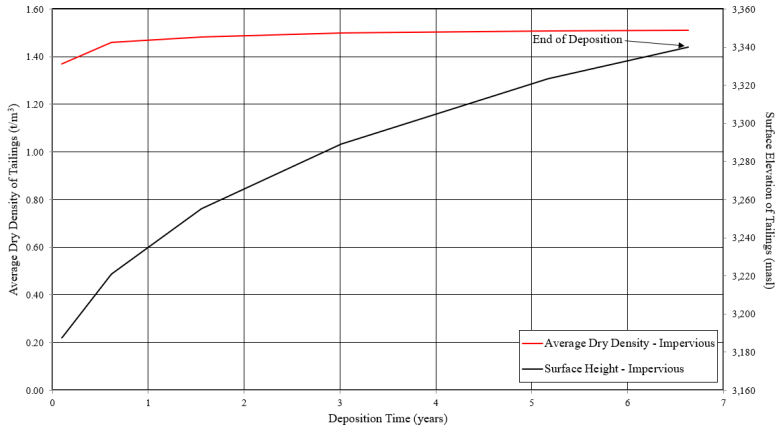

Figure 6. Lower Deposit - Tailings Surface Elevation & Average Dry Density over Time

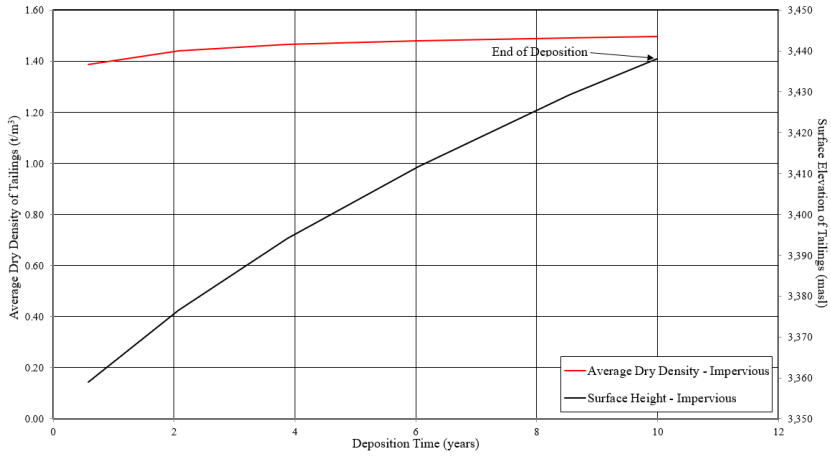

Figure 7. Upper Deposit-Tailings Surface Elevation & Average Dry Density over Time

Table 3. Summary – Self-Weight Consolidation Modeling Results

In-Pit TSF Deposit	Bottom Boundary Condition	Average Dry Density (t/m^3)	Approximate Time to Fill (years)	Estimated Total Storage (Mt)
Lower Deposit (unlined)	Impervious	1.51	6.6	48.5
Upper Deposit (lined)	Impervious	1.50	9.9	72.7

Figures 8 and 9 provide dry density profiles for the in-situ tailings at the thickest points for the Lower Deposit and Upper Deposit, respectively. As seen on Figures 8 and 9, the density profiles are relatively parallel throughout the TSF development. Thus, it can be qualitatively assessed that the materials will be approximately normally consolidated under self-weight loading during filling. This means that minimal excess (i.e. above hydrostatic) pore pressure is expected within the tailings and limited long-term settlement is expected to occur due to self-weight loading. Therefore, for the Upper Deposit, significant additional consolidation is not expected without additional applied loading or reduction in phreatic surface after deposition is completed within the TSF. However, since the Lower Deposit will experience surcharge loading due the overlying Separation Layer and development of the Upper Deposit, the tailings within the Lower Deposit will undergo further settlement after filling of that portion of the deposit. This was accounted for by completing six 1D consolidation models. These six models represent six concentric annuli of varying height which collectively form the simplified 3D geometry of Lower Deposit impoundment used in the 3D consolidation modeling. The central annulus was the tallest, and the height of each annuli decreased moving outward with the pit walls. As a result, six height vs void ratio profiles were developed. These models were run with an estimated surcharge pressure of 1875 kPa uniformly distributed over the top surface of the Lower Deposit which was calculated considering the average saturated unit weight of Upper Deposit Mixed Tailings (19 kN/m^3) over a depth of 98m (10 m thickness of rockfill plus 88 m depth of tailings within the Upper Deposit from 3350 to 3438 masl). The dry unit weight of the Separation Layer rockfill was assumed to be the same as the saturated unit weight of the Upper Deposit Mixed Tailings to simplify the modeling approach. Table 4 presents the results of 1D consolidation models completed.

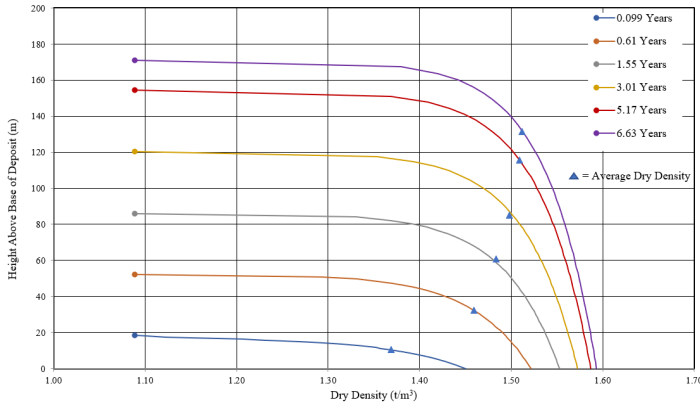

Figure 8. Lower Deposit – Tailings Dry Density Profile – Mixed Tailings

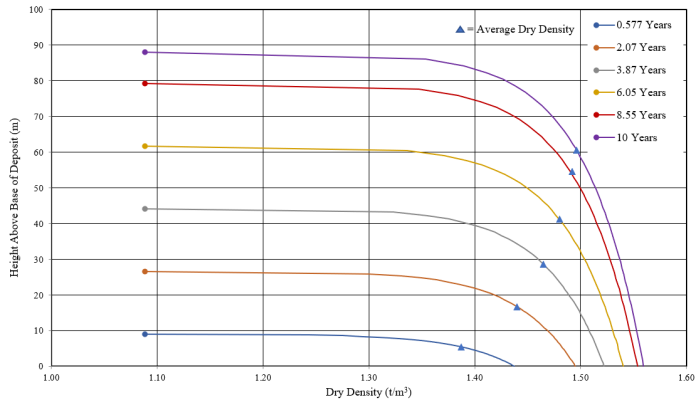

Figure 9. Upper Deposit – Tailings Dry Density Profile – Mixed Tailings

Table 4. Summary – Surcharge Consolidation Modeling Results

Annulus ID	Annulus Surface Area (m^2)	Annulus Height after Self-Weight Consolidation (m)	Annulus Final Height (m)	Total Settlement (m)	Approximate Time for Consolidation (days)
1	120,352	16.7	14.7	2.0	19
2	97,611	50.8	46.5	4.3	139
3	72,569	84.9	79.0	5.9	334
4	59,385	118.9	111.7	7.2	579
5	46,926	152.6	144.2	8.5	858
6	29,160	171.0	162.1	8.9	1022

The Annuli (numbered 1 through 6) represent the top surface area of the Lower Deposit, with Annulus 1 being the outermost shell and shallowest portion of the deposit, and Annulus 6 being the central "column" and deepest portion of the deposit. Annuli 2 through 5 represent the

intermediate portions of the deposit between Annuli 1 and 6. As shown in the table, the outermost annulus (Annulus 1) experiences the least settlement due to the lower thickness of the Lower Deposit along the edge of the TSF. The annulus settlements increase moving inward toward the deeper/thicker portions of the deposit. The central annulus (Annulus 6) experiences the maximum settlement of roughly 8.9 m over 1,022 days (~2.8 years). As seen in Table 3 above, it is estimated that the Upper Deposit will be filled and consolidated under its own weight in approximately 9.9 years. Therefore, the Lower Deposit surcharge load consolidation will be achieved concurrently with the filling and self-weight consolidation of the Upper Deposit, and long-term settlement of the Lower Deposit due to the surcharge load is not anticipated after deposition within the Upper Deposit ceases.

The Separation Layer was designed with camber to accommodate the differential settlements shown in Table 4 with appropriate factors of safety implemented to account for variability from modeled settlement values. As the Upper Deposit is developed, the Lower Deposit tailings will continue to experience the consolidation settlement which will be balanced by the proposed camber based on the settlement values provided in Table 4 such that when consolidation is completed, the floor of Upper Deposit (at the location of the geomembrane liner system) remains slightly cambered such that the settlement beyond a level configuration will not impart excessive strain on the Upper Deposit geomembrane liner system.

4 CONCLUSION

The tailings deposited into the in-pit TSF described in this paper was modeled using a combination of 1D and 3D large-strain consolidation models to estimate the anticipated dry density of the tailings in the Upper and Lower deposits at the end of filling and to design necessary camber on the proposed rockfill Separation Layer between the two deposits to prevent excessive strains in the proposed geomembrane liner system which will be constructed between the two deposits. This work was completed using the consolidation modeling software, CONDES, developed at the University of Colorado at Boulder. The input parameters were developed with the use of seepage induced consolidation testing (SICT) performed on the proposed Mixed Tailings which will be deposited into the facility. While estimating storage capacity using large-strain consolidation models is common during design and management of tailings storage facilities, additional applications of these types of models can further aid in the understanding of and help to provide solutions to additional challenges identified during design and development of these facilities as illustrated by the work completed and presented herein.

REFERENCES

EPA (1994). Technical Report – Design and Evaluation of Tailings Dams, U.S. Environmental Protection Agency, Office of Solid Waste, Washington:.63

Gibson, R.E., England, G.L. & Hussey, M.J.L. (1967). *The Theory of One-Dimensional Consolidation of Saturated Clays*. Geotechnique, 17, 261-273.

Gjerapic, G & Znidarčić, D. (2007). A Mass-Conservative Numerical Solution for Finite-Strain Consolidation during Continuous Soil Deposition. *In:* Siegel, T.C., Luna, R., Hueckel, T. & Laloui. L., eds. *Geo-Denver 2007: Computer Applications in Geotechnical Engineering: New Peaks in Geotechnics (GSP 157) conference proceedings*. Denver, CO, CD-ROM.

Liu, J. C., & Znidarčić, D. (1991). Modeling one-dimensional compression characteristics of soils. *Journal of Geotechnical Engineering*, *117*(1), 162-169.

Somogyi, F. (1979). Analysis and prediction of phosphatic clay consolidation: implementation package. *Lakeland: Florida Phosphatic Clay Research Project (Technical Report)*.

BIBLIOGRAPHY

Coffin, J. G. (2006). *A Three-Dimensional Model for Slurry Storage Facilities (*Unpublished doctoral dissertation). University of Colorado, Boulder, Colorado, USA.

In-pit tailings storage. (n.d.). Retrieved from https://www.tailings.info/storage/inpit.htm

Calibration of Tailing Consolidation Parameters using Field Measurements

Nicholas Brink & Zygi Zurakowski
Stantec Consulting Inc., Denver, CO, United States

ABSTRACT: Segregation and layering is common in tailings impoundments, leading to challenges when extrapolating small-scale laboratory testing to the actual behavior of tailing within a TSF. Large-strain consolidation testing is traditionally used to characterize consolidation behavior of tailings. These impose an idealized homogeneous/isotropic state which may be unrepresentative of field conditions, particularly where horizontal tailing segregation occurs and where complex drainage conditions exist. Use of lab data alone can easily result in tailing consolidation estimates being mis-characterized a priori. Once in operation, data from the TSF can be used to refine and improve consolidation forecasts following a similar theoretical approach to interpreting and extrapolating laboratory data. A simple method is presented for calibrating "apparent" consolidation properties using field data to account for actual behavior of impounded tailing, allowing for more representative forecasts of impoundment density. Case histories are presented to show how this method has improved density forecasts at operating facilities.

1 INTRODUCTION

Impounded tailings can undergo large volumetric strains during operations and post-closure which may significantly impact estimated future impoundment storage capacity and rate of rise (ROR). Accurately forecasting the consolidation behavior of impounded tailing enables owners/operators to better plan for sustaining capital items such as embankment raises or timing for relocation and construction of peripheral facilities. In addition, accurate forecasts of consolidation and release of water can improve accuracy of water management plans. Consolidation forecasts are also commonly required for closure and post-closure planning of final impoundment slopes.

Large-strain consolidation laboratory tests are traditionally conducted to characterize the consolidation behavior of tailings. Test methods include Seepage-Induced Consolidation Tests (SICTs) and Trautwein cells. These tests are conducted in an idealized small-scale condition leading to characterization of the tailing in an isotropic state and with one-dimensional (vertical) drainage. Laboratory test data are fitted to theoretical curves (mathematical relationships of compressibility and hydraulic conductivity versus confining stress) by adjusting the parameters of each relationship. The fitted relationships are then applied within a numerical filling model to forecast consolidation during and after impoundment filling. This is reasonable where impoundment characteristics generally match laboratory test conditions (i.e. homogeneous and isotropic material, with predominantly one-dimensional loading and drainage). For new facilities or proposed facilities in design stages, these test data represent a reasonable starting point and are often relied upon for design of the facility. Where segregation and/or anisotropic drainage occur and play a significant role in overall consolidation behavior, more representative properties must be developed to accurately forecast consolidation behavior. A number of tests can be conducted

on coarse and fine-grained tailing to represent proximal and distal segregation; however, this still does not effectively characterize the horizontal layering within an impoundment which can significantly differentiate actual field consolidation (with both vertical and horizontal drainage) from laboratory consolidation data (vertical drainage only) and numerical calculations. Because of these differences, it is important to regularly update the tailing density forecast and embankment material balance during operations.

Operating facilities should be documenting deposited tonnages as well as surveyed impoundment volumes which can be used to back-calculated the average density of the impoundment. Those data may be used to calibrate numerical filling models based on observed behavior of the impoundment. Calibration implicitly accounts for the complexities introduced by tailing segregation and/or anisotropic drainage through layers of coarser tailing, along with other phenomena occurring in the TSF which are not simulated in laboratory tests. Calibrated, or "apparent," consolidation properties may then be applied to forecasting simulations to improve estimates of key parameters such as tailing elevation, ROR, and average impoundment dry density. This paper outlines a simple method to estimate apparent impoundment properties by iteratively adjusting consolidation parameters in a large-strain consolidation numerical model. The method presented herein may be applied using any numerical consolidation model or code which is capable of simulating continuous filling and simultaneous consolidation. Case histories are then presented showing example applications of this method exemplifying the improved simulation accuracy when using calibrated consolidation parameters.

2 DATA REQUIRED FOR CALIBRATION

Several pieces of data are required to calibrate a numerical filling analysis. These data include an impoundment stage-area curve, actual/historical tailing deposition rates, tailing specific gravity of solids, back-calculated impoundment dry density, and measured tailing surface elevations or topographic surveys of the impoundment surface. Back-calculated dry densities represent the chief measure used to evaluate accuracy of calibration, followed by measured tailing surface elevation.

Some numerical codes assume a perfectly horizontal tailing surface, whereas the tailing surface in an actual impoundment usually shows some topographic variability. Where topographic variability is significant, the stage-area curve should be developed using the average tailing surface elevation as opposed to reporting the tailing elevation at a designated location.

Filling and consolidation analyses are also sensitive to the specific gravity of tailing solids (ratio of tailing solids density to water density, herein referred to simply as "specific gravity", or G_s). Most numerical codes require a single representative specific gravity value. Care must be taken to input a G_s value representative of the full volume of impounded tailing.

3 METHOD FOR CALIBRATING CONSOLIDATION PARAMETERS

The calibration method uses an iterative process whereby initial consolidation parameters are assumed (based on laboratory testing or literature values) and then iteratively adjusted until the simulated impoundment elevation and simulated tailing dry density approximately matches measured and/or back-calculated values. A detailed summary of the proposed method is presented here along with lessons learned from application of this method across several facilities.

The one-dimensional computer code CONDES (Yao & Znidarcic, 1997) is used in this paper. CONDES is applied in a pseudo-three-dimensional algorithm to simulate actual impoundment geometries (Coffin, 2010). It is presumed that the reader is at least generally familiar with these types of filling and consolidation analyses. The method is equally applicable to other codes, though different codes may use different input parameters and therefore some of the recommendations relating to specific parameters may differ. CONDES requires five input values: compressibility parameters A, Z, and B; and permeability parameters C and D. The relationships defined by these parameters are shown in Equations 1 and 2 respectively. In these equations 'e' represents the tailing void ratio (ratio of void volume to volume of tailing solid particles), σ_v' is

vertical effective stress, and k is the tailing hydraulic conductivity. Note that parameters B, C, and Z are dependent on the system of units being used.

$$e = A(\sigma'_v + Z)^B \quad (1)$$
$$k = Ce^D \quad (2)$$

3.1 *Summary of the Calibration Method*

Calibrating apparent consolidation properties is accomplished through a simple procedure which is shown diagrammatically on Figure 1. The steps involve selecting an initial set of consolidation properties, comparing model results with these initial properties to the actual tailing dry density, then iteratively adjusting the properties to achieve an approximate match between actual and simulated density and elevation. Finally, the calibrated properties may be applied in a forecasting model to simulate future tailing density and elevation. Each of these steps is described in detail in the following sub-sections.

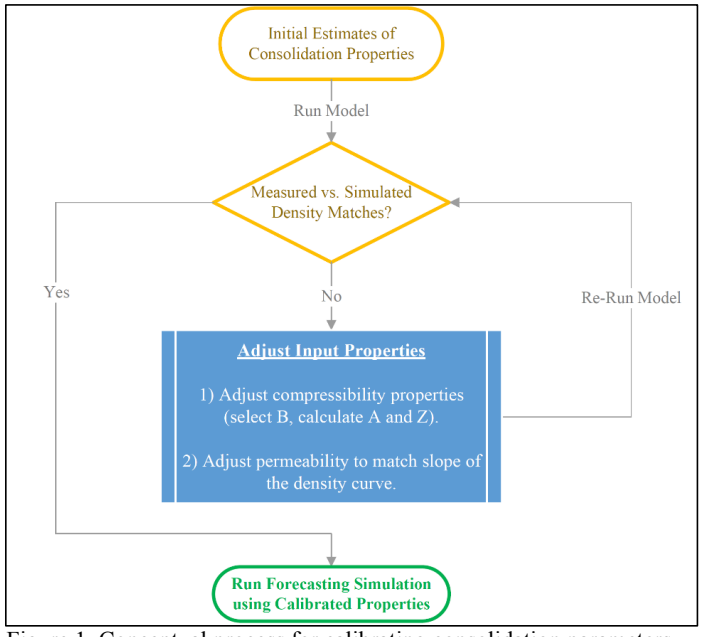

Figure 1. Conceptual process for calibrating consolidation parameters

3.1.1 *Initial Estimates of Consolidation Properties*

Thoughtful selection of initial 'seed' consolidation properties (parameters A, B, Z, C, and D in CONDES) can significantly reduce the time and effort required to achieve reasonable calibration. These seed inputs should be selected based on material-specific laboratory testing, where possible. Large-strain consolidation test data are representative of the tailing and are the preferred starting point for calibration, even if they do not fully capture the complex behavior of the impounded tailing. These test data will typically only require minor to moderate changes during calibration to accurately represent the behavior of the active impoundment. Other laboratory data may also be used to inform selection of seed parameters where large-strain consolidation data are unavailable. Useful data may be obtained, for example, from oedometric consolidation tests (ASTM D2435; ASTM, 2020a), the consolidation phase of consolidated-undrained (ASTM D4767; ASTM, 2020b) or consolidated-drained (ASTM D7181; ASTM, 2020c) triaxial tests, permeameter tests (ASTM D5084; ASTM, 2016), or others.

Where no test data are available, a literature search for characteristic values can be conducted or initial parameters can be selected based on similar operating facilities. However, calibrations will rely heavily upon experience and engineering judgement (for both selection of seed values, and during the calibration process). The calibration effort may be significant in this case, and there will likely be several sets of calibrated parameters which appear to appropriately simulate the actual tailing density and elevation. The modeler must exercise good engineering judgement to understand which sets of properties are reasonable and which are not.

3.1.2 *Comparing Model Results to Actual Density and Elevation Curves*

A filling/consolidation analysis is first performed by applying the selected seed parameters. The results are judged by comparing the simulated versus actual tailing density (and if desired, the measured and simulated tailing elevation). More than likely the initial fit will be poor, and some adjustments to the input parameters will be required.

3.1.3 *Iterative Adjustment of Consolidation Properties*

In the procedures below, the primary criterion used to judge calibration quality is comparison of measured versus simulated impoundment dry density. This is done to simplify the explanations – in practice it may help to compare measured and simulated tailing elevation as well.

Efficiency of the overall calibration process is greatly improved when the modeler begins with reasonable estimates of the apparent initial void ratio (directly related to the apparent initial dry density) at very low effective stresses, and the ultimate void ratio (ultimate dry density) corresponding to the maximum anticipated vertical effective stress at the bottom of the ultimate impoundment. The apparent initial void ratio should be selected to coincide with actual dry density values early in the impoundment's operation. An ultimate void ratio is most easily estimated from an oedometer compression curve or other laboratory consolidation data, however literature values have been successfully applied when other data are unavailable.

The calibration process begins by iteratively adjusting the compressibility relationship while holding the seed permeability parameters constant. First a trial value of parameter B is selected, often using the SICT value (if available). If no other data are available, a starting value of -0.15 usually represents a reasonable starting point. Parameter A is then calculated so that the compressibility curve passes through the data point representing the ultimate void ratio and the maximum anticipated vertical effective stress in the impoundment. Parameter Z is then adjusted so the compressibility curve begins at the apparent initial void ratio (usually this is evaluated at a vertical effective stress of 0.1 kPa or 0.01 kPa). The filling/consolidation model is then run using these new parameters. Comparing the measured versus simulated average impoundment dry density curves indicates how parameter B should be adjusted (lower, or more negative, values of B result in overall lower simulated dry density, see Figure 2). The parameter B should continue to be adjusted to find the closest reasonable match between the measured and simulated dry density curves. Each time B is adjusted, parameters A and Z should be re-calculated so the compressibility curve continues to pass through the apparent initial void ratio and the ultimate void ratio.

Next, new values for the permeability coefficients are selected, while leaving compressibility parameters constant. Increasing the value of C increases the overall tailing permeability and leads to faster simulated consolidation (i.e. pushes the simulated dry density curve left, see Figure 3). Parameter D is usually left constant in the early stages of calibration and may only be needed to "fine-tune" the calibration. Parameter D controls the slope of the permeability curve, where higher values of D lead to a flatter slope in the permeability function which causes slower consolidation at lower void ratios.

Additional refinements may be made, if required, by adjusting B (with parameters A and Z recalculated for each now value of B), then again by adjusting permeability parameters C and D. This back-and-forth between adjusting compressibility and permeability may be required several times before an adequate calibration is achieved. If calibration is overly difficult or even elusive, the selected values of apparent initial void ratio and/or ultimate void ratio may need to be adjusted.

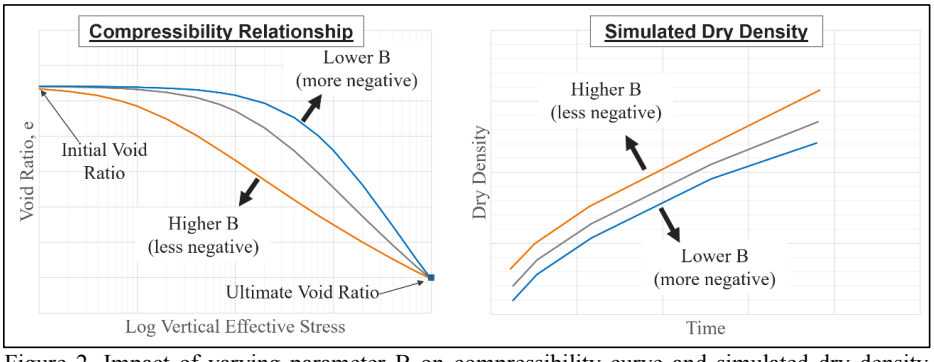

Figure 2. Impact of varying parameter B on compressibility curve and simulated dry density (permeability parameters held constant, and parameters A and Z recalculated for each value of B)

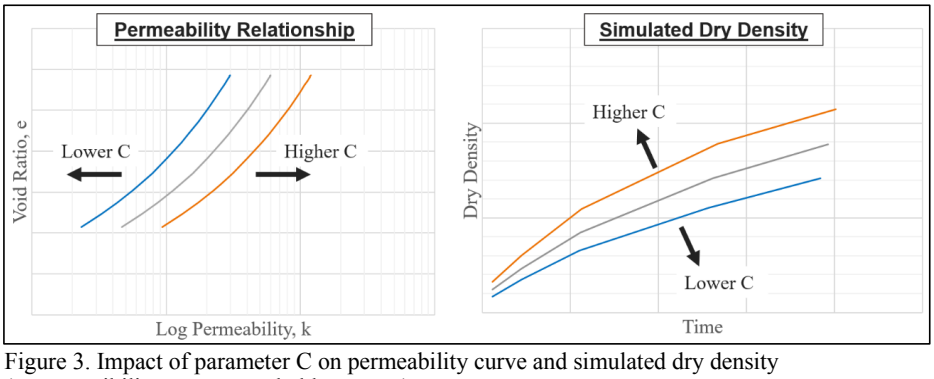

Figure 3. Impact of parameter C on permeability curve and simulated dry density (compressibility parameters held constant)

3.1.4 *Apply Calibrated Parameters in Forecasting Simulations*

Once the model is calibrated, the "apparent" calibrated parameters may be applied to forecasting simulations. It is recommended that after forecasting simulations are completed, the results be checked against actual impoundment conditions to corroborate the model calibration. This applies to TSFs in both operating and closure or post-closure conditions.

3.2 *Limitations of the Proposed Method*

The most accurate calibrations are made when there is a longer operational history. Relatively new facilities with limited operational data may result in greater error, which should be understood and taken into consideration when using the results. In general, the average impoundment dry density vs. time curve (density curve) tends to start at a steeper slope during early operations. The slope tends to flatten with time, and many facilities show a "break point" at which the slope of the density curve changes notably. The proposed calibration procedure is more accurate for facilities where this "break point" has already been observed and where the slope of the curve after the "break point" is well defined.

Facilities which have not started operation or which are in design phases are clearly not candidates for this method. In those situations, traditional methods involving laboratory testing of pilot mill/concentrator plant tailing samples should continue to be applied.

The use of this method is predicated upon the assumption that the impoundment conditions (especially drainage conditions) and the overall operating conditions (ore type and grind, deposition system, etc.) in the future will remain similar to those during the calibration period. Significant changes in these and other conditions would need to be accounted for separately when forecasting impoundment filling and consolidation. For example, if the tailing body begins to cover a zone of significantly higher foundation permeability, the calibrated (or apparent) permeability may no longer be representative. Similarly, if deposition practices change or if segregation potential of the tailing is significantly altered, the calibration may be invalidated. In these situations especially, the forecasted impoundment densities and tailing elevations should be regularly checked against actual back-calculated dry densities and measured elevations to decide whether the model calibration should be updated.

Finally, the compressibility relationship applied within the CONDES model is limited in its ability to represent a true minimum void ratio. The mathematical relationship in Equation 1 is an inverse exponential function (since B is a negative value) which approaches a void ratio of zero at very large effective stresses. The slope of this function at relatively high stresses is much steeper than the actual material compressibility curve would dictate. If calibration occurs over a range of stresses where the compressibility curve slope is unrealistically steep, the forecasted ultimate impoundment dry density could be over-estimated as a result. Manually imposing an ultimate void ratio corresponding to the anticipated maximum effective stress in the impoundment helps to reduce the likelihood of such calibration errors. The actual impact of this error has not been thoroughly studied by the authors, and it is recommended that modelers consider this error and apply caution when simulating tailing with steeply sloping compression curve near the ultimate/maximum effective stress.

4 EXAMPLE APPLICATIONS OF THE CALIBRATION METHOD

Three example case histories are presented where the calibration method described above was applied. Table 1 contains a general summary of these case histories, and each site is described in greater detail below. CONDES calibration runs were carried out using both the "Pervious" and "Impervious" bottom boundary conditions with the calibration goal being to cause these two simulated dry density curves to straddle the back-calculated dry density values, assuming the actual foundation drainage conditions to be somewhere between these two simulated conditions.

4.1 *Case History No. 1*

Case History No. 1 represents a TSF operated as part of an open pit copper mine where ore is crushed and concentrated in flotation cells. Concentrator throughput is significant at more than 100,000 tonnes per day. Tailing is partially dewatered via large-diameter thickeners. Underflow from the thickeners exits at approximately 55% solids by mass. A portion of the thickened tailing stream is processed through hydro-cyclones where underflow sand is recovered and used to construct embankment raises. Overflow from the cyclones are deposited from the embankment crest into a broad, dendritic impoundment. Whole tailing is deposited from both the embankment and from around the perimeter of the impoundment. All tailings are deposited sub-aerially. The impoundment foundation is generally competent rock with relatively thin alluvium in the valley-floor.

SICTs were performed on pilot plant tailing samples prior to construction of this TSF. After startup, samples of actual whole tailing and the cyclone overflow were tested. One sample was created by blending overflow and whole tailing to approximately the proportions in which they are deposited in the impoundment. Calibration of the filling/consolidation model was desired to check and improve accuracy of the forecasts, which are regularly relied upon for material and water balance updates. SICT seed properties listed in Table 1 represent the blended whole tailing and overflow sample.

Table 1. Summary of Example Case Histories

Case history ID	Primary recovered mineral	Average tailing deposition rate	Average tailing D_{50} (1)	Average tailing plasticity index (2)	G_s (3)	Seed consolidation parameters (4)	Calibrated consolidation parameters (5)
-	-	t/d	mm	-	-	-	-
1	Copper	> 100,000	0.05	NP	2.78	A = 1.96 B = -0.225 Z = 0.274 kPa C = 4.81E-3 m/d D = 2.55	A = 1.71 B = -0.150 Z = 12.5 kPa C = 9.43E-3 m/d D = 2.55
2	Copper	18,000	0.1	NP	2.83	A = 2.15 B = -0.171 Z = 0.019 kPa C = 1.56E-3 m/d D = 3.80	A = 2.15 B = -0.171 Z = 0.150 kPa C = 5.29E-3 m/d D = 2.50
3	Coal	1,800	0.05	NP to 10	1.82	A = 1.41 B = -0.150 Z = 0.038 kPa C = 3.92E-4 m/d D = 5.95	A = 0.79 B = -0.100 Z = 0.0001 kPa C = 7.00E-4 m/d D = 5.95

(1) "D_{50}" = particle diameter at which approximately 50% of the material (by mass) is finer, based on dry sieving analysis per ASTM D6913 (ASTM, 2017a).
(2) "NP" = non-plastic. Plasticity index is determined per ASTM D4318 (ASTM, 2017b).
(3) "G_s" = specific gravity of tailing solids.
(4) "Seed parameters" represent the initial values applied at the start of the iterative calibration process (these represent SICT data for Case Histories 1 and 2, and a synthesis of several sets of other laboratory test data for Case History 3).
(5) "Calibrated parameters" are the final values selected during calibration, leading to a reasonable match between the measured and simulated impoundment dry density and tailing elevations.

Calibration of Case History No. 1 led to the apparent permeability being slightly higher than the seed permeability values, which is attributed to the anisotropic flow conditions caused by layering of coarser and finer tailing. The compressibility curve slope was reduced during calibration resulting in stiffer modeled tailing behavior relative to the seed SICT values. The stiffer apparent behavior is attributed to depositional segregation leading to higher initial density. Note that at the time this calibration was carried out, the back-calculated densities had not yet exhibited a clear "break point" in the slope of the density curve. The calibrated model forecasts a lower ultimate impoundment density which leads to a reduced operating lifespan relative to the SICT properties (Figure 4). In this case the SICT properties would over-estimate the TSF capacity and operating life, which could lead to operational challenges toward the end of TSF operations.

4.2 *Case History No. 2*

Case History No. 2 represents another TSF operated as part of an open pit copper mine. Ore is crushed and milled prior to entering flotation cells where copper is recovered. A small portion of the tailing stream is routed through scavenger recovery circuits where additional milling and flotation occur. The whole tailing stream (combined tailing from the primary flotation and the scavenger flotation circuits) is partially dewatered by large-diameter mechanical thickener cells which increases the tailing solids content to approximately 60% solids by mass. Tailings are deposited into a TSF comprising a rockfill embankment which impounds a relatively narrow and tall impoundment. Deposition occurs along the crest and around the perimeter of the impoundment. The tailing beach is managed through cycling of discharge points to maintain a relatively large free water pond which covers the majority of the tailing surface. Tailings are deposited in some areas sub-aqueously, and in some areas sub-aerially. Some segregation is observed during tailing deposition. Some layering of coarser and finer tailing was also observed,

likely due to cycling of the deposition points. The impoundment foundation can be characterized as competent rock or as having a low-permeability blanket to limit seepage.

SICTs were carried out on three samples of the impounded tailing (collected over a period of four years) prior to undertaking the calibration. As in the previous case history, the SICT parameters could not fully match the back-calculated dry densities. Detailed closure planning for this TSF was about to begin, and accurate estimates of post-closure consolidation settlement were desired to decide between various closure and cover options. Given the relatively large amount of available back-calculated density information, model calibration was an ideal method to improve these post-closure settlement estimates. Note that the early densities in about the first nine months of operation were estimated and not truly back-calculated (Figure 5).

Similar to Case History No. 1, calibration resulted in an increase in apparent tailing permeability and reduction of the initial void ratio relative to the SICT values. These trends are linked to apparent effects of horizontal tailing segregation. In this case the compressibility characteristics produced by the SICT data were mostly representative of observed conditions, and compressibility parameters A and B remained unchanged.

4.3 *Case History No. 3*

Case History No. 3 represents a small tailing storage cell operated as part of a surface coal mine. Run-of-mine ore is processed using basic washing techniques in a coal handling and preparation plant (CHPP). Tailing waste material from the CHPP primarily comprises residual overburden soils with significant ash content (hence the low G_s of the tailing, see Table 1). Residuals from the coal crushing and sorting processes comprise a relatively small fraction of the CHPP tailing. The combined tailing stream exits the CHPP at varying moisture contents (the percent solids varies substantially based on the degree of contamination of the ore and the amount of washing required) and is deposited into a storage cell impounded by an unlined homogeneous earthfill perimeter dike several meters in height. Tailing is deposited from around the perimeter of the dike, and deposition usually occurs from one or sometimes two adjacent discharge points which are regularly rotated. Some potential for segregation exists based on the well-graded nature of the tailing, however field observations were unable to confirm whether segregation actually occurs during deposition. Outward seepage from the impoundment is minimal as indicated by a lack of observed seeps in surrounding topographic low-points downstream of the tailing cell and dry readings in standpipe piezometers located within the earthfill dike.

Calibration of the consolidation model was requested to improve tailing density estimates which will be used to calibrate the site water balance, as well as for operational planning purposes. SICT data were not available for these tailings. However, the mine owner recently performed a suite of laboratory tests on samples of CHPP tailing including settlement column tests, single-stage oedometer tests (at low confining pressures), specific gravity, and permeameter tests. These data were used in conjunction with sparsely available historical data (including consolidated-undrained triaxial test data) to estimate seed values for the consolidation parameters. Filling/consolidation simulations using these seed values are shown on Figure 6. The mine owner has not performed bathymetric surveys at this site and therefore no back-calculated tailing density information was available. Data from recent LIDAR surveys were used to estimate the tailing volume to back-calculate approximate impoundment dry densities. Dry density data from soon after startup could not be calculated since LIDAR data were not available, therefore an initial void ratio was estimated based solely on settlement column test data. The LIDAR data resolution was relatively low and it is believed that the back-calculated densities may be associated with some level of error (the error margin has not been explicitly defined).

The initial calibration produced an inadequate match between simulated and back-calculated dry densities. Several iterations were required surrounding both the initial void ratio and the ultimate void ratio values to achieve reasonable calibration results. A relatively high value of C was selected near the beginning of the calibration to impose a condition where excess pore pressures disperse faster than tailing is deposited, based on the relatively low impoundment ROR. This allowed for calibration to focus only on compressibility parameters. Case History No. 3 highlights the applicability of the calibration method to cases where data may be sparse; the effort required to calibrate the model is substantially more, though a reasonable calibration is still possible.

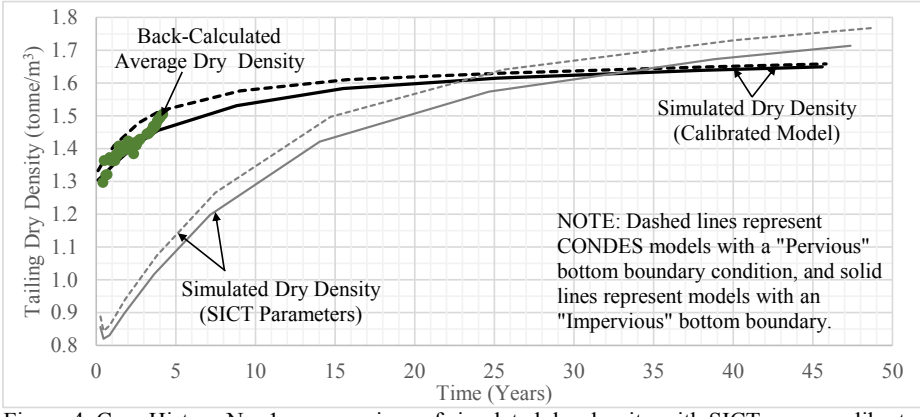

Figure 4. Case History No. 1 – comparison of simulated dry density with SICT versus calibrated parameters

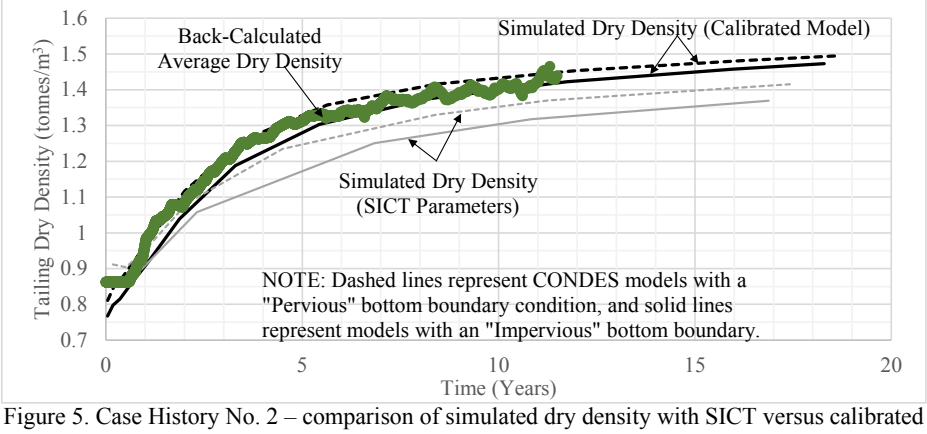

Figure 5. Case History No. 2 – comparison of simulated dry density with SICT versus calibrated parameters

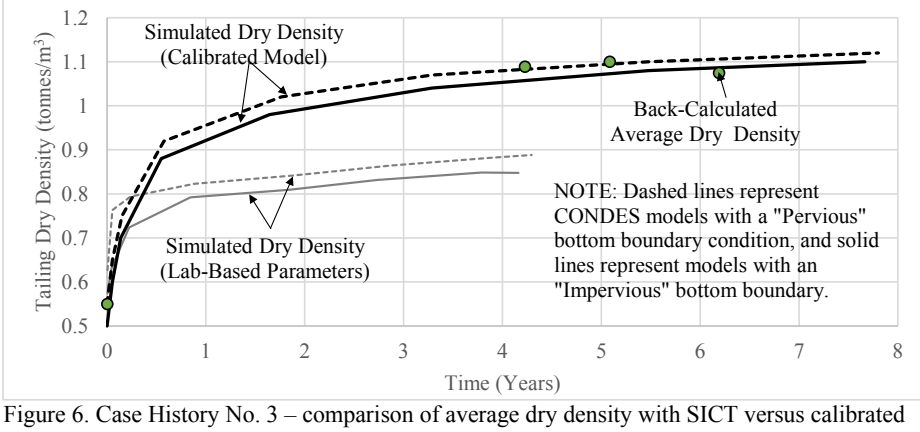

Figure 6. Case History No. 3 – comparison of average dry density with SICT versus calibrated parameters

5 SUMMARY AND CONCLUSIONS

A simple method is presented in this paper for calibrating large-strain consolidation parameters for tailing deposited into an active TSF. The method involves iteratively updating the parameters in a methodical process to approximately match simulated and observed impoundment parameters, especially the impoundment average dry density. Recommendations are given for selecting initial (seed) parameters, and a systematic approach to the iterations is presented which increases efficiency of the calibration process. Three example case histories are presented in which this method was applied to calibrate consolidation properties for active facilities. Calibrated parameters for these facilities are presented for reference.

Calibrated parameters developed using this method represent the apparent behavior of the facility as a whole, which may differ (in some cases substantially) from conditions imposed in typical laboratory testing. Deviations from laboratory conditions are generally related to tailing segregation within the impoundment, or lateral drainage features in the impoundment foundation. The case histories presented in this paper show that calibrated parameters, which account for actual tailing segregation and layering behaviors, result in higher apparent tailing permeability and lower initial void ratio relative to available laboratory test data. To date the forecasted impoundment densities using these calibrated parameters have matched well with observed back-calculated dry densities. Actual dry densities will continue to be tracked with the goal of presenting updated comparisons in a future publication.

REFERENCES

American Society of Testing and Materials (ASTM). 2016. ASTM D5084-16a, Standard Test Methods for Measurement of Hydraulic Conductivity of Saturated Porous Materials Using a Flexible Wall Permeameter, ASTM International, West Conshohocken, PA, 2016.

American Society of Testing and Materials (ASTM). 2017a. ASTM D6913 / D6913M-17, Standard Test Methods for Particle-Size Distribution (Gradation) of Soils Using Sieve Analysis, ASTM International, West Conshohocken, PA.

American Society of Testing and Materials (ASTM). 2017b. ASTM D4318-17e1, Standard Test Methods for Liquid Limit, Plastic Limit, and Plasticity Index of Soils, ASTM International, West Conshohocken, PA.

American Society of Testing and Materials (ASTM). 2020a. ASTM D2435 / D2435M-11(2020), Standard Test Methods for One-Dimensional Consolidation Properties of Soils Using Incremental Loading, ASTM International, West Conshohocken, PA.

American Society of Testing and Materials (ASTM). 2020b. ASTM D4767-11(2020), Standard Test Method for Consolidated Undrained Triaxial Compression Test for Cohesive Soils, ASTM International, West Conshohocken, PA, 2020.

American Society of Testing and Materials (ASTM). 2020c. ASTM D7181-20, Standard Test Method for Consolidated Drained Triaxial Compression Test for Soils, ASTM International, West Conshohocken, PA, 2020.

Brink, N.R. 2014. Numerical Modeling of Consolidation Processes in Hydraulically Deposited Soils. Masters Thesis, University of Colorado Boulder. July.

Coffin, J. 2010. A Three-Dimensional Model for Slurry Storage Facilities. Doctoral Dissertation, University of Colorado Boulder. April.

Gjerapic, G. Johnson, J. Coffin, J. & Znidarcic, D. 2008. Determination of Tailings Impoundment Capacity via Finite-Strain Consolidation Models. *GeoCongress 2008*. March 9-12, 2008. New Orleans, Louisiana, United States of America. DOI 10.1061/40972(311)99.

Yao, D. & Znidarcic, D. 1997. Crust Formation and Desiccation Characteristics for Phosphatic Clays – Users Manual for Computer Program CONDES0. Prepared for Florida Institute of Phosphate Research. October, 1997. Publication No. 04-055-134.

Sand Capping Trial on Frozen Centrifuged Tailings Deposit

E.J. Wu, S. Jeeravipoolvarn & S.A. Proskin
Thurber Engineering Ltd., Calgary, AB, Canada

A. Junaid & G. Freeman
Canadian Natural Resources Limited., Calgary, AB, Canada

ABSTRACT: Canadian Natural Resources Limited (Canadian Natural) conducted a sand capping trial on a frozen centrifuged fluid fine tailings (FFT) deposit. The objectives of the trial were to assess the efficacy, practicality, and failure potential of a sand capping technique on a frozen treated-tailings deposit, and measure the material responses to the cap. Specifically, the target was to evaluate consolidation of the underlying material due to the cap load, study the impact of sand cap thickness on thawing time of the frozen layer and evaluate mixing/impregnation of sand cap material into the tailings deposit. The trial consisted of bearing capacity assessment, sand capping activities, and subsequent field geotechnical observations on a 50.0 m × 10.0 m × 3.7 m (length × width × average tailings layer thickness) deposit cell filled with polymer treated centrifuged FFT (3,260 m^3 volume) of an average 55 wt.% solids concentration. Approximately 1,200 m^3 of sand was placed onto a tailings deposit in three days using a combination of excavator and dozer. Significant surface deformation was observed during capping. The tailings and sand near the interface tended to form a thin (0.2 m) mixed layer. The distinct soil interface comprising a mixture of the sand cap and underlying centrifuged FFT indicated that a cap can be placed onto a frozen tailings deposit without losing the benefits of capping. However, the effect of the sand cap thickness on the thawing time of the frozen tailings surface was inconclusive due to inadequate data.

1 INTRODUCTION

Sand capping is a proven technique to assist in the consolidation and strengthening of deposits (COSIA, 2012). However, the efficacy of the capping is dependent on the type, condition, and characteristics of the deposited material. For chemically amended oil sands tailings, sand capping had been considered for increase in consolidation and strength post-deposition, potentially leading to faster land reclamation (Sawatsky et al. 2018). However, the success of this technique is not yet established for oil sands tailings treated under different conditions and with various mechanical and chemical processing methods. Especially, there is no prior study on either its efficacy or conditions for potential failure on frozen treated-tailings deposits. Given the prevailing winter conditions in Alberta, this is an important study for considering commercial application of sand capping for oil sands tailings.

In 2018, Canadian Natural Resources Limited (Canadian Natural) undertook a field trial to evaluate the consolidation performance and investigate potential failure conditions for sand capping on the frozen surface of a chemically amended centrifuged fluid fines tailings (FFT) deposit. A geotechnical program, consisting of deposit sampling, bearing capacity assessment, sand capping activities, and subsequent field investigations, commenced following pouring of the test cell and continued post-capping. This paper summarizes the findings of this field trial.

2 TEST PROGRAM OVERVIEW

2.1 *Deposition and monitoring*

The centrifuged FFT deposit test cell, referred to as Test Cell 1 or Cell 1, was located at the Modified Atmospheric Fines Drying (MAFD) test site at Canadian Natural's Albian Jack Pine Mine (JPM). The plan view for the test cell is shown in Figure 1. The as-built dimensions of the cell was 50.0 m x 10.0 m x 3.7 m (length x width x average tailings layer thickness at pour). The test cell was instrumented with vibrating wire piezometers (VWP), total pressure cell (TPC), and thermistor strings.

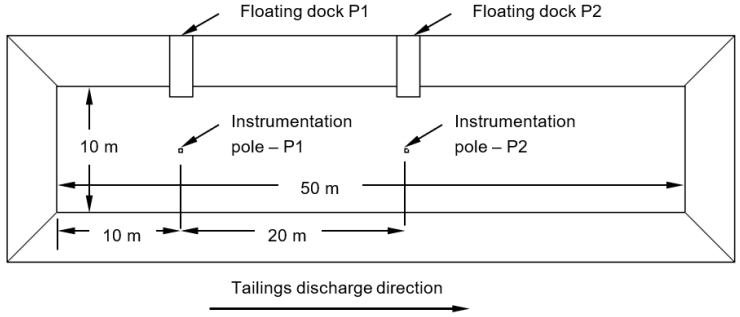

Figure 1. Test Cell 1 Plan View and Instrument Locations

In July-August 2018, Cell 1 was filled with FFT treated with a hydrolyzed polyacrylamide (HPAM) polymeric flocculant (Kemira 4993, dosage: 1000 g/t) and then centrifuged at the JPM centrifuge plant facility. The approximate volume of the centrifuged FFT was 4,500 m^3 at deposition into the test cell which was monitored for 267 days under quiescent conditions to simplify the consolidation analysis. Over this period the material lost some of the free water at the surface due to evaporation and a partial breach of the containment dam.

Subsequently, in the early spring of 2019, the sand capping trial was executed on the frozen surface of the deposit to assess the practicality and potential failure conditions for this capping technique on centrifuged FFT and evaluate the material responses due to the cap. At this time, the deposit had an average solids content of approximately 55% and a volume of 3,260 m^3 with the immediate surface in a frozen and partially thawed state. A photograph of the completed test cell after deposition is shown in Figure 2.

Figure 2 Photograph of Complete Test Cell 1

2.2 *Frozen surface bearing capacity guideline*

Prior to the capping trial, a frozen surface investigation was conducted to estimate the bearing capacity for the frozen surface of the test cell. This estimate was made by measuring the frozen surface thickness and calculating the bearing capacity following Shoop's trafficability of frozen ground over soft ground method (Shoop, 1995). Shoop's formula is expressed in Equation 1 below:

$$P = C \times z^2 \tag{1}$$

Where P is the allowable load in meganewtons, C is a parameter that depends on the strength of the frozen material, and z is the frost depth in meters.

Shoop proposed that for wet conditions (saturated material with water content in the order of 500% to 800%), the C value is 0.86; and for dry conditions (less than saturated), the C value is 0.35. Although Shoop's method was developed for peat and natural soils, it should be a conservative estimate for frozen tailings as encountered in Test Cell 1.

The z parameter was measured by drilling holes through the frozen surface and taking direct measurement of the its thickness (Government of Alberta 2013). Twenty-two test hole (TH) locations with their identifications are shown in Figure 3.

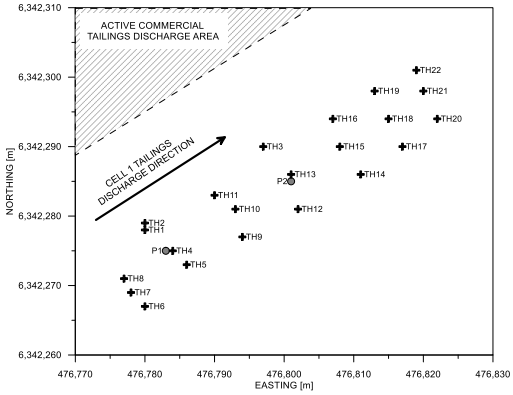

Figure 3 Frozen surface investigation test hole locations

2.3 *Sand capping campaign*

The planned sand capping configuration for Cell 1 is illustrated in Figure 4 (plan view) and Figure 5 (cross-section view). The capping was planned by virtually dividing the deposit into the following three test areas:

1) Area 1: 3 m sand cap.
2) Area 2: 1 m sand cap.
3) Area 3: No sand cap.

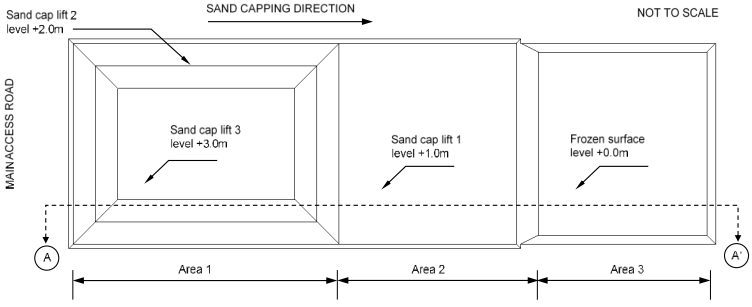

Figure 4 Capping configuration plan on Test Cell 1 - plan view

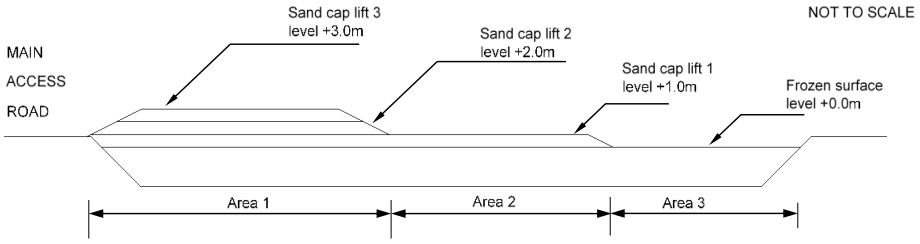

Figure 5 Capping configuration plan – cross-section view A-A'

The sand cap was to be placed in three lifts (1 m per lift) to the desired geometry. The placement direction was to proceed from the main access road toward the toe of the deposit and the tailings pond. The capping campaign started on March 26, 2019 and was completed on March 28, 2019. A combination of a Deere 870G excavator and Caterpillar D8T dozer (with a standard operating weight of 39.75 metric tons) were selected by the Canadian Natural operator for capping.

2.4 *Geotechnical investigation after sand capping*

The geotechnical investigation was conducted after capping and involved the following tasks:

1) Gamma Cone Penetration Testing (GCPT).
2) Electronic Vane Shear Testing (EVST).
3) Sampling using a piston sampler.
4) Surface topographical surveying.

The geotechnical investigation plan showing the GCPT, sampling and EVST locations is presented in Figure 6. Cross-sections A-A', B-B', C-C' and D-D' were selected to illustrate the as-built geometry of the sand and tailings layers within Test Cell 1, as shown in Figure 6.

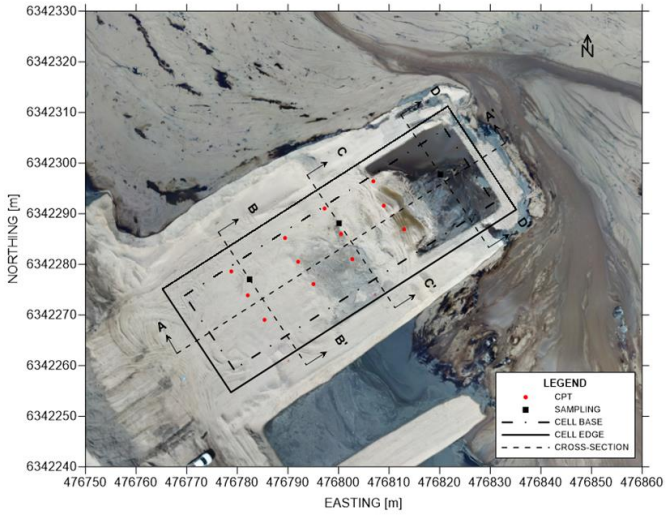

Figure 6 Test Cell 1 plan view - geotechnical investigation plan

3 RESULTS

3.1 *Frozen surface bearing capacity estimation*

Frozen surface thickness of Test Cell 1 was measured to calculate the bearing capacity of the frozen surface and evaluate the trafficability. The frozen surface thickness varied approximately between 27 cm to more than 50 cm.

A summary of key bearing capacity values for both dry and wet (frozen) conditions estimated by the Shoop method is given in Table 1. The bearing capacity values across the surface of Test Cell 1 at dry and wet conditions are shown in Figure 7 and Figure 8 respectively. Based on this assessment, the average bearing capacity of the frozen surface varied between 8 and 19 metric tons.

Table 1 Bearing Capacity Estimation Summary Results from Frozen Surface Investigation

Bearing capacity value (metric ton)	Shoop's C=0.35 (dry condition)	Shoop's C=0.35 (wet condition)
Minimum	2.6	6.4
Maximum	8.9	21.9
Average	7.7	18.8

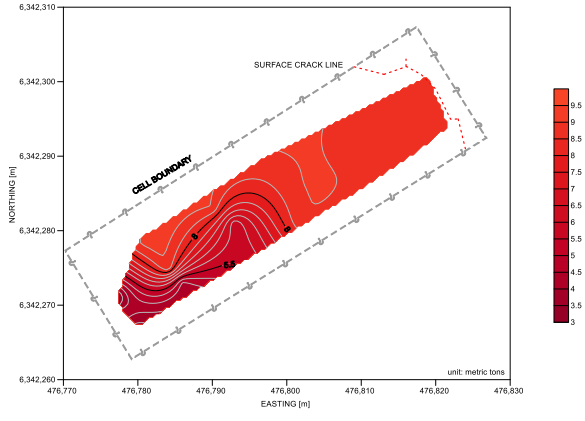

Figure 7 Bearing Capacity across Test Cell 1 Surface Estimated by Shoop's Formula - Dry Condition

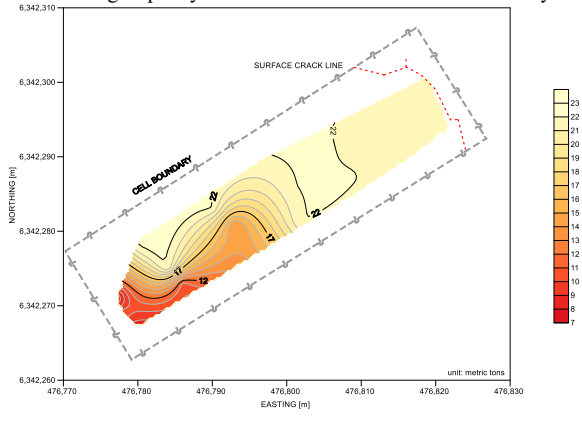

Figure 8 Bearing Capacity across Test Cell 1 Surface Estimated by Shoop's Formula - Wet Condition

3.2 *Weather records*

The weather data was recorded using a nearby weather station. Figure 9 shows the air temperature during the period of the field trial. The frozen surface investigation was conducted while the average daily temperature was -13.7 °C. Following the investigation, the average daily temperature rose above 0 °C on March 11, 2019 and remained above 0 °C for 14 days before sand capping started. After sand capping was completed, the average temperature remained above 0 °C for 38 days until geotechnical field investigation started. The average temperature during the geotechnical field investigation reached around 11°C.

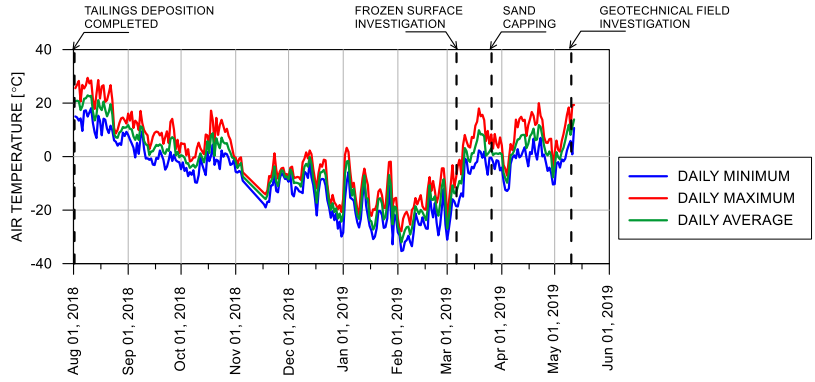

Figure 9. Weather Data – Air temperature

3.3 *Sand Gap Geometry and Profiles*

Two capping methods were used: deposition by excavator and by dozer. The first 1 m lift was successfully capped using the excavator. The second and third 1 m lifts were placed together using a D8T dozer working from the main access road area of Test Cell 1 (discharge area). The capping process took approximately 3 days to complete.

Figure 10 shows an aerial photograph of Test Cell 1 after the sand capping campaign was completed. The detailed cross-sections A-A', B-B', C-C' and D-D' before capping are shown in Figure 11, including the cell base and initial tailings surface prior to capping. The sand-tailings interface and deposit surface after capping at these cross-sections are shown in Figure 12. The sand-tailings interface profile is based on the CPT data and test results on recovered samples. Due to the limited number of CPT and sampling locations, the interface boundary between the sand and fine tailings is approximate only. The initial and final surface profiles were obtained by LiDAR and drone surveying.

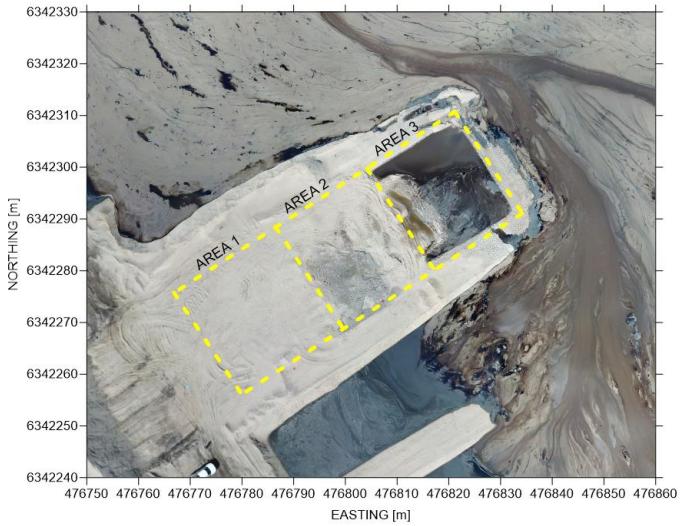

Figure 10 Aerial photo of Test Cell 1 after capping: May 14, 2019

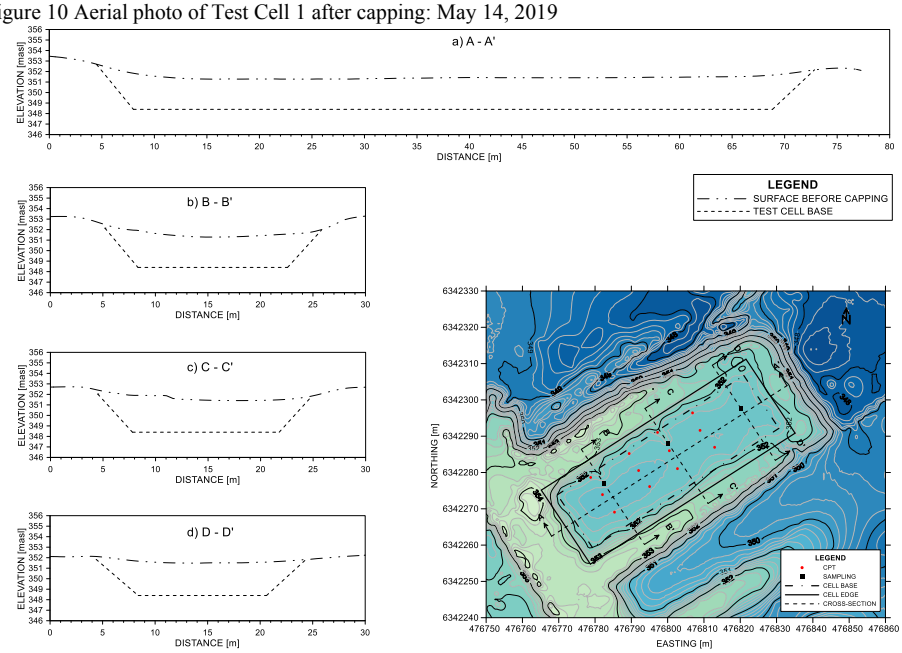

Figure 11 Profiles of cross-section a) A-A', b) B-B', c) C-C' and d) D-D' before capping

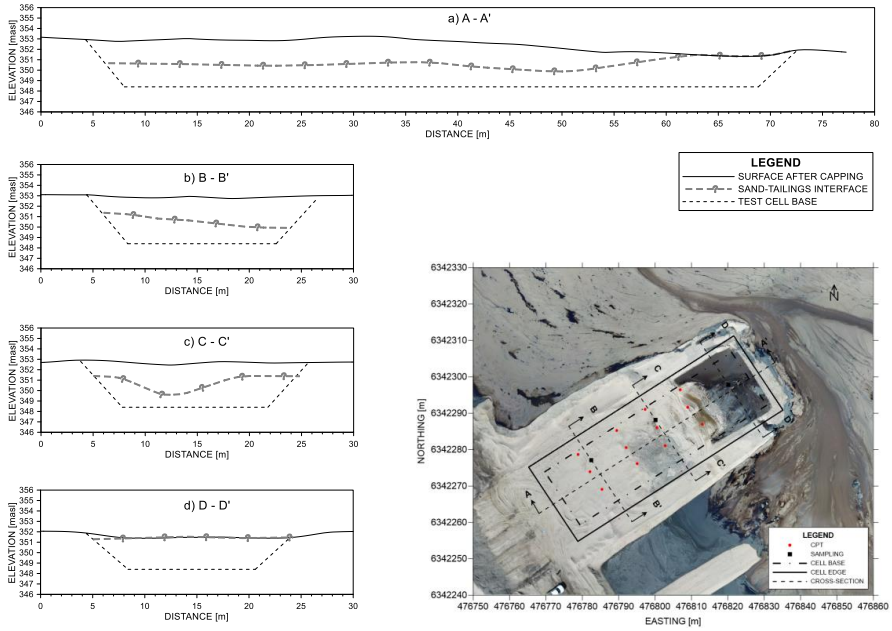

Figure 12 Profiles of cross-section a) A-A', b) B-B', c) C-C' and d) D-D' after capping

The volumes of deposited tailings and sand were estimated with the surface geometrical survey data before and after the capping campaign, as well as the assumed geometry of the cell base of Test Cell 1 and sand-tailings interface inferred from CPT and sampling data. Table 2 summarizes the estimated material volumes before and after sand capping. Approximately 1,200 m^3 of sand was used to capped the tailings deposit of 3,260 m^3 contained in Test Cell 1.

Table 2. Volume of deposited tailings and sand before and after capping in Test Cell 1

	Before capping (October 19, 2018)	After capping (May 14, 2019)
Tailings volume (m^3)	3260	3260(1)
Sand volume (2) (m^3)	-	1200
Total volume (m^3)	3260	4460

Notes: (1) Tailings volume change during capping was assumed to be zero.

(2) Sand volume was estimated based on the assumed zero volume change of the tailings.

3.4 *Temperature Profiles*

The temperature profiles of the tailings before and after capping are shown in Figure 13 at each of the three locations. The March 2019 measurements are from thermistor strings while May 2019 data are measurements made on samples retrieved. The temperature of the samples was all above 0 °C and most of the samples were above 5 °C.

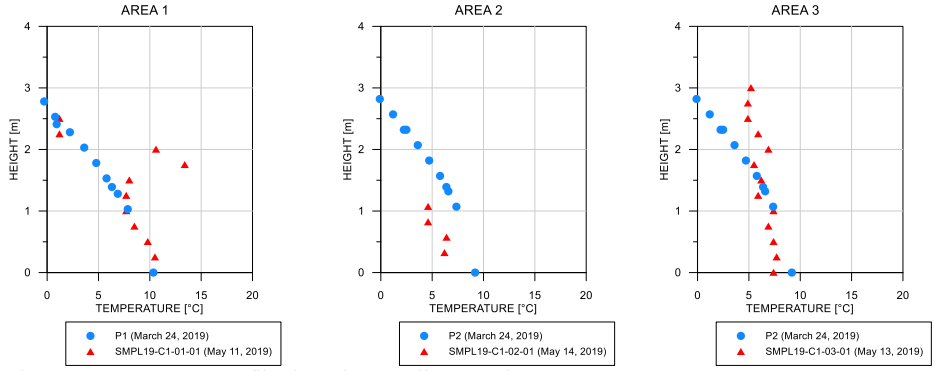

Figure 13. Temperature Profile along the Sampling Locations

4 OBSERVATIONS AND DISCUSSION

Surface deformation and buckling of the frozen surface layer were observed in Area 1 during the second and third lifts, as shown in Figure 15. More deformation was observed in Area 3 as capping continued (Figure 16).

The excavator method caused low disturbance/deformation to the tailings deposit. However, it may not be practical for large-scale field operations. The D8T dozer was heavier than the bearing capacity estimate, and introduced considerable deformation during capping. Lighter equipment with operating weights below the bearing guideline would likely have reduced the surface and tailings deformation observed in the field trial.

At the commencement of the capping, the maximum air temperature on March 26, 2019 reached 8.3 °C. These warm temperatures likely facilitated partial thawing of the frozen surface and consequently lowered the bearing capacity of the ground surface. Earlier capping activity would be beneficial when the surface is still frozen and average daily temperatures remain below 0 °C.

Figure 14 First one-meter lift deposited by excavator

Figure 15 Placing cap mechanically with a dozer, and observed surface deformation in Area 1

Figure 16 Surface deformation at the end of one-meter lift

The tailings and sand near the interface tended to mix and form a thin layer approximately 0.2 m thick. This sand cap and fine tailings interface was observed both in the samples and in many of the test holes CPT. It indicates that the sand cap can be placed on a tailings deposit without complete loss of sand into the tailings deposit. Multiple fines and mixed soil layers were also found within the sand cap deposit. These intermittent layers of tailings within the sand cap were likely due to the surface deformation during capping.

The temperature profiles in Area 3 (Figure 13) suggest the temperature changes with time within the tailing deposit with no apparent effect of the sand cap. The temperature profiles suggest the increasing temperature near the surface of tailings in Area 1, while the temperature near the base remained the same as before capping. The temperature of samples collected in Area 2 near the base were found to be lower. The results are inconclusive on the effects of the sand cap thickness on the thawing of the frozen tailings surface and more research will be required.

5 SUMMARY

During the sand capping trial, a total of approximately 1,200 m^3 of sand was placed on top of a 3,260 m^3 tailings deposit (Test Cell 1) using a combination of excavator and dozer. At the time of capping, the average air temperature was above 0 °C, and the deposit had an average solids content around 50% with the frozen/partially frozen deposit surface. Considerable surface deformation was observed during capping, particularly when a D8T dozer was used (heavier than the bearing capacity guideline). Ideally, to reduce the surface deformation during capping, smaller equipment can be utilized, and the capping be conducted earlier in the late winter when the average daily temperature is below zero. The tailings and sand near the interface tended to be mixed and formed a thin layer of approximately 0.2 m. The distinct cap-tailings interface indicates that the sand cap can be placed onto a frozen tailings deposit without losing the benefits of the sand cap. Multiple fines and mixed layers were also found within the deposited sand cap, likely due to the surface deformation observed during placement.

6 ACKNOWLEDGEMENT

We'd like to gratefully acknowledge O'Kane Consultants Inc., GeoForte Services Limited, and ConeTec Investigations Limited for their field instrumentation and testing support.

7 REFERENCE

COSIA. 2012. Technical Guide for Fluid Fine Tailings Management. Available at: https://www.cosia.ca/uploads/documents/id7/TechGuideFluidTailingsMgmt_Aug2012.pdf

Government of Alberta. 2013. Best Practice for Building and Working Safely on Ice Covers in Alberta. In 2013th edition. Government of Alberta, Edmonton, Alberta. Available from www.worksafe.alberta.ca.

Sawatsky, L., Hyndman, A., McKenna, G. and Vandenberg, J. (2018). Fluid Fine Tailings Processes: Disposal, Capping, and Closure Alternatives. In the Proceedings of the International Oil Sands Tailings Conference, Edmonton, AB, Canada. December 9-12, 2018.

Shoop, S.A. 1995. Vehicle bearing capacity of frozen ground over a soft substrate. *Canadian Geotechnical Journal*, 32: 552-556.

Thurber Engineering Ltd. 2019. Cell 1 sand capping experiment estimate of frozen surface bearing capacity, May 3, 2019, 14p.

Thurber Engineering Ltd. 2019. Test Cell 1 and 5 Geotechnical Characterization and Consolidation Investigation, draft submitted to Canadian Natural.

Thurber Engineering Ltd. 2019. Test Cell 1 Sand Capping Study Results Summary, draft submitted to Canadian Natural.

Hydrographs for Tailings Dam Breach Analysis – A Review of Common Estimation Methodologies

Mark G. Walden
NewFields Mining Design and Technical Services, LLC, Lone Tree, CO

Nicholas T. Rocco
NewFields Mining Design and Technical Services, LLC, Lone Tree, CO

ABSTRACT: Loss of life and environmental and economic damage can result from earthen tailings dam breaches. As such, preemptive and accurate modelling of the potential tailings breach scenarios is common in the industry and becoming a regulatory requirement in many jurisdictions. The results of the modeling are of great significance for the development of appropriate hazard classification, monitoring, mitigation procedures, and emergency preparedness and response plans. Tailings dam breach simulations typically require a hydrograph in order to establish the fluidized tailings outflow from the assumed breach in relation to time. Tailings flows are fundamentally different from water flows and typically classify as non-Newtonian due to high solids contents. The flow characteristics of non-Newtonian flows, and thus the outflow hydrograph from the corresponding dam breach, can vary greatly as a function of the sediment concentration, breach size and formation time, and the tailings rheology. The method selected for determining the outflow hydrograph should be appropriately tailored to the expected conditions of the tailings dam breach. This article presents a summary of two common methodologies used to estimate tailings breach hydrographs. The methodologies investigated include the Tailings Dam Failure Volume Estimate Tool and the U.S. Army Corps of Engineers Hydrologic Engineering Center Hydrologic Modeling System (HEC-HMS). The procedures utilized by each methodology are described and discussed. The advantages and disadvantages of each method are summarized, along with general recommendations to help guide practitioners in development and selection of breach hydrographs for use in tailings breach simulations.

1 INTRODUCTION

The process of dam breach analyses involve estimation of the volume released during an embankment failure, and routing of the flow, or flood, downstream of the site. The flood event is modeled with a hydrograph that captures the volume of materials released from the embankment at the breach location versus time. This paper reviews two common methods used to develop the flood hydrograph including the Tailings Dam Failure Estimate Tool (TDFET) and the U.S. Army Corps of Engineers Hydrologic Engineering Center Hydrologic Modeling System (HEC-HMS).

Most methods used to predict the hydrograph resulting from a dam breach require the breach dimensions to be input into the model. The breach dimensions are typically estimated using empirical equations developed from analysis of dam breaches through earthen embankments. Typical methods used for determination of dam breach parameters are discussed briefly in the section below.

2 DAM BREACH PARAMETERS

The determination of dam breach parameters, including peak discharge flow, failure duration, and breach geometry, involves a high degree of uncertainty and requires significant engineering judgment (Wahl, 2004). Generally, dam breach parameters are determined using empirically

derived equations and a variety of dam breach parameter determination methods are considered. After careful consideration, the most appropriate parameters are selected based on engineering judgement and other site specific design criteria. A modest parametric study of the breach parameters is recommended to assess the impacts of changing variables on the resulting hydrograph. Table 1 presents some of the common methods used to determine dam breach parameters.

Table 1. Common Dam Breach Parameter Determination Methodologies

Methodology	Peak Discharge	Failure Duration	Breach Width	Side Slope Ratio
Johnson and Illes, 1976	-	-	✓	-
Singh and Snorrason, 1982, 1984	-	✓	✓	-
Macdonald, 1984	✓	✓	✓	✓
USBR, 1988	-	✓	✓	-
Von Thun and Gillette, 1990	-	✓	✓	✓
FERC Guidelines, 1987	-	✓	✓	✓
Froehlich, 1995	✓	✓	✓	✓
Rico et. al., 2007 and Costa, 1985	✓	-	-	-
Froehlich, 2008	-	✓	✓	✓
Pierce, 2010	✓	-	-	-

The majority of these methods, with the exception of Rico et al. (2007) and Costa (1985), were developed for water retaining dam breaches, which requires consideration when assessing and simulating flows for tailings embankment failures as tailings flows are typically non-Newtonian and fundamentally different than clear water flows.

The volume released during the duration the dam breach is also required to determine the hydrograph. The volume released is typically determined using empirical equations such as those outlined by Rico et. al., (2007), Larrauri and Lall (2018), and Rourke and Luppnow (2015).

Using the release volume and geometric and temporal breach parameters, the flood hydrograph can be estimated.

3 HYDROGRAPH DETERMINATION

3.1 *Tailings dam failure estimate tool*

3.1.1 *Overview*

The TDFET was developed by Engineering Analytics Inc. in association with FLO-2D and is used within the FLO-2D flood routing model. The TDFET breach volume screening tool estimates the breach geometry and employs empirical correlations of documented failures to define a worst case scenario. The tool uses risk analysis methods developed by the US Bureau of Reclamation for water storage dams, and user inputs to predict the potential of tailings embankment failure and calculate the subsequent release volume of stored tailings as a flood hydrograph (Tocher et. al., 2014).

Determination of the hydrograph is dependent on the predicted failure mode and volume released, which can be estimated by the TDFET. The breach volumes predicted by the tool are typically disregarded and replaced with an estimated release volume based on empirical correlations.

Prior to generating the hydrograph, the volume of water released during the breach, the failure duration, the maximum sediment concentration by volume (C_v), and the porosity of the tailings are defined. A short description of the primary inputs necessary for the development of the breach hydrograph follow.

3.1.2 *Water Released During the Breach*

The TDFET provides four options for volume of water released during the breach including the minimum, maximum, average, or a user defined volume. The TDFET will define the minimum, maximum and average release volumes if the tailings dam parameters have been defined.

The user defined option allows the user to forgo input of the tailings dam parameters and input a specific pre-determined failure release volume. This option can be useful in back-analysis type evaluations. The user defined release volume only includes the volume of water released in the breach does not include the volume of solids, which is taken into account through the sediment concentration parameter.

3.1.3 *Failure Duration*

The failure duration is the amount of time in hours that the tailings will flow from the breach. The failure duration is typically estimated using any number of empirical correlations presented in Table 1. As previously stated, a modest sensitivity evaluation around this parameter is prudent.

3.1.4 *Maximum Sediment Concentration*

The maximum sediment concentration represents the maximum ratio of solids volume to water volume released during the breach. The maximum sediment concentration is estimated from the total volume released, the supernatant pond volume, and the volume of water entrained in the tailings.

3.1.5 *Hydrograph Distribution Selection*

The predicted volume of the breach can be distributed over one of six typical unit hydrograph shapes with variable time of peak discharge. Engineering judgment and experience are required to select the most appropriate hydrograph for the breach scenario. The six typical unit hydrographs are presented on Figure 1.

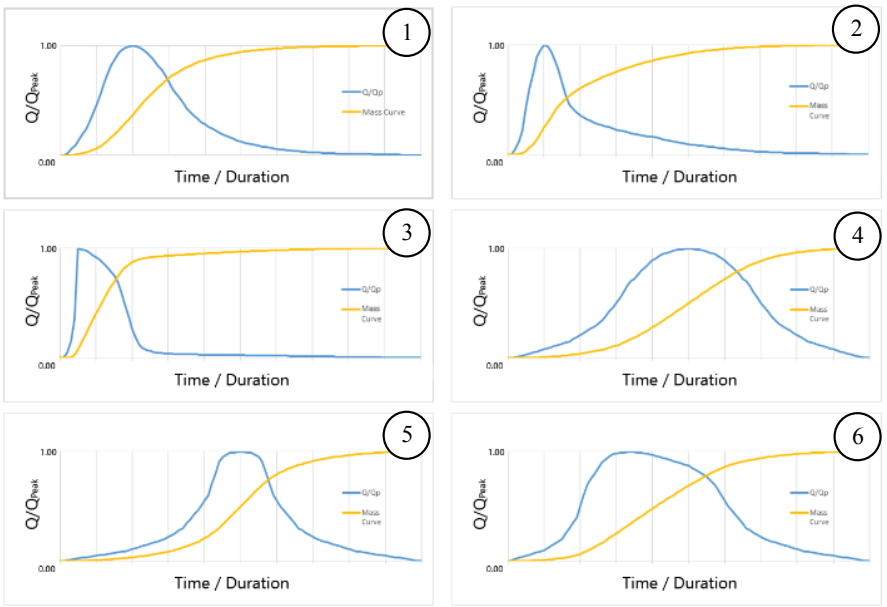

Figure 1. TDFET Hydrograph Distribution Curves.

Each of the six hydrographs display a hydrograph curve and a mass curve. The hydrograph curve demonstrations the flow rate from the breach over time and the mass curve demonstrates the total mass released from the breach over time. The general applicability of each hydrograph option (numbered 1 through 6) is discussed below.

Hydrograph 1, 2, and 3 may be applicable to breach scenarios where the breach opening is expected to develop quickly, as may occur during a seismic event or during widespread liquefaction that rapidly impacts tailings containment. Each of these three hydrographs show the flow rate rapidly increase to a maximum value, and the majority of the tailings mass is released prior to 50% of the development time. Hydrographs 1, 2, and 3 transition from a more gradual release of tailings to a more sudden release, respectively.

Hydrographs 4 and 5 curves present the maximum flow rate occurring towards the middle of the breach development time. These hydrographs may be applicable to scenarios where the breach opening is expected to develop more slowly, or in a scenario where the supernatant pond is separated from the breach opening and does not immediately influence the flow. The two hydrographs vary slightly as hydrograph 4 demonstrates a slightly more gradual development and release than hydrograph 5.

Hydrograph 6 curve shows the flow rate reaching its maximum towards the beginning of the breach development time and remaining high until approximately 60% of the breach development time has passed. This hydrograph may be applicable to scenarios where the maximum flows out of the breach are expected to remain at a constant high flow rate for an extended duration, such as failure of a secondary embankment that is much smaller than the primary embankment. In this type of scenario, the hydraulic loading at the breach location might not attenuate quickly and thus maximum flows are maintained for a longer duration.

3.1.6 *Sediment Concentration Distribution Selection*

The sediment concentration during a dam breach will vary with time. The TDFET allows the user to select the concentration by volume and distribute it over the duration of the hydrograph. There are six typical sediment concentration distributions available, as presented on Figure 2. The tool internally adjusts the total volume to account for the sediment concentration by volume and the porosity. The volume of sediment is calculated by adjusting the maximum concentration by volume to populate a table of sediment concentration by volume versus breach time. The general applicability of the sediment concentration distribution curves (numbered 1 through 6) are discussed below.

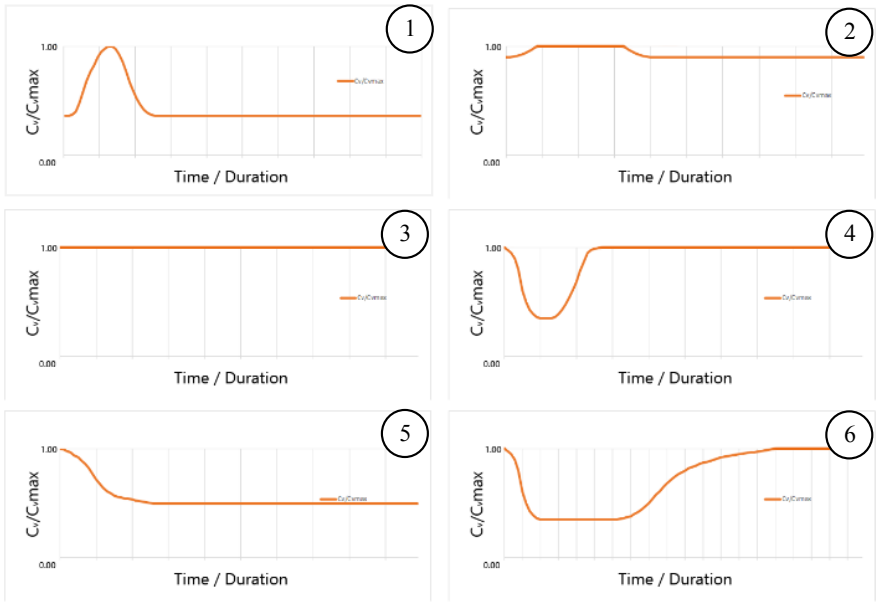

Figure 2. TDFET Sediment Concentration Distribution Curves.

Curve 1 portrays a breach scenario where the sediment concentration spikes at the start of the breach duration and then drops back down and remains constant for the remaining duration of the breach. This sediment concentration may be applicable in a breach scenario where the flow and erosion rates are highest at the beginning of the breach (i.e. significant erosion of the embankment and immediately downstream of the embankment after which sedimentation controls).

Curve 2 portrays a breach scenario where the sediment concentration spikes slightly at the start of the breach duration and then remains at the elevated concentration for a short while before dropping back down and remaining constant for the remainder of the breach. This sediment concentration may be applicable in a breach scenario where the flow and erosion rates slightly elevated at the beginning of the breach.

Curve 3 is often used in dam breach analyses and is a simplified approach. This simplified method assumes a sediment concentration of the fluidized tailings where the free water mixes instantaneously with the tailings deposit, creating a homogenous slurry at a specified solids content, which remains constant for the duration of the breach.

Curves 4, 5 and 6 present variation of a decreasing sediment concentration at the start of the breach duration. Curves 4 and 6 may be representative of breach scenarios where the initial breach of the embankment material releases water from the supernatant pond, which over time leads to further release of the stored tailings mass. Curve 5 may be representative of a scenario where the initial breach of the embankment material leads to release of a less concentrated homogenous tailings mass.

3.1.7 *Summary*

The TDFET generates unit hydrographs for the predicted release volumes so that the user can evaluate the potential tailings dam flood hazard for existing or greenfield projects. The tool provides a variety of common simplified hydrograph and sediment concentration distributions that must be selected based on engineering judgement, a clear understanding of the facility design, and topographic and geologic conditions immediately downstream of the facility. The tool was designed to be incorporated with the FLO-2D flood routing model to allow the resulting breach hydrograph to be easily input into the program and routed downstream, but the tool can also be used to generate hydrographs for other software or applications.

3.2 *U.S. Army Corps of Engineers Hydrologic Engineering Center Hydrologic Modeling System (HEC-HMS)*

3.2.1 *Overview*

HEC-HMS is public-domain software that is designed to simulate the precipitation-runoff process of dendritic watershed systems. The software has a wide range of capabilities and is designed for a range of possible hydraulic problems including modeling large river basin water supplies, flood hydrology, and watershed runoff. The HEC-HMS dam breach feature was developed for water retaining dams and clear water flows. The hydrographs produced by HEC-HMS can be combined with other software such as those utilized for dam breach analysis.

In order to generate a dam breach hydrograph using HEC-HMS a “reservoir” must first be defined and assigned a meteorologic model. For a breach evaluation, the reservoir is the tailings facility and the materials contained therein. The meteorologic model will define the meteorologic inflows over the duration of the dam breach simulation. Once the reservoir and reservoir volume have been defined, the HEC-HMS dam break method is utilized for selection of one of two breach types: a breach generated by overtopping or via internal erosion and piping. In both scenarios, dam breach parameters including elevation of the breach (top and base), bottom width, side slopes, and development time are defined in order to compute the outflow hydrograph. The breach parameters are generally determined using the relationships presented in Table 1. HEC-HMS also requires definition of a trigger method and a progression method in order to determine when the breach will be triggered and how the breach will grow over the time the breach develops. The model allows inflows into the tailings facility during the breach to be defined, which can be used for rainy day simulations occurring during design storm events or cascading type failures of adjacent facilities.

The inputs necessary to develop a breach hydrograph using HEC-HMS are discussed in the following sections.

3.2.2 *Reservoir*

A reservoir, as defined in HEC-HMS, is an element that has one or more inflow elements and one computed outflow element. The reservoir must be paired with a storage curve that defines the reservoir volume by area or elevation. Three methods are available for computing inflow in HEC-HMS including none, discharge gauge, and constant flow. If none is selected the source will have zero discharge into the flow network during the simulation. The discharge gage method requires a time series discharge gauge, which defines the discharge to use during each time interval during the simulation. The constant flow method requires that a constant flow rate be selected. The reservoir model in HEC-HMS also allows for embankment seepage, additional release volumes, spillway discharge, and evaporation to be accounted for when generating the dam breach hydrograph, if these types of hydraulic fluxes are expected during an embankment breach.

3.2.3 *Breach Type*

The overtopping dam break feature is designed to represent a failure that has been generated through overtopping of the reservoir. During overtopping, the flow will begin to erode the face of the embankment. This method assumes that the failure will begin at a point on the crest of the embankment and expand in a trapezoidal shape until it reaches the maximum defined size. Flow through the expanding breach is modelled as trapezoidal weir flow.

The piping dam break feature is intended to represent internal erosion failures through the embankment. Piping can occur anywhere that water seepage through the embankment can cause erosion and carry soil particles away from the embankment. HEC-HMS initiates piping failures on the face of the embankment and erodes backwards and radially, although in reality, piping failures can also begin internally within the embankment. Piping can occur within embankment fill or within filters, drains, foundation, or abutments of the embankment. A piping elevation must be specified in the model, and engineering judgement is required to identify a reasonable, worst case scenario of the location piping could occur. HEC-HMS models flow through the circular opening as orifice flow and when the opening reaches the crest of the embankment, the continued expansion is trapezoidal in shape and the outflows are modelled as weir flow.

A piping coefficient must also be defined and represents the energy losses as the water moves through the opening. This coefficient directly effects the magnitude of the peak outflow hydrograph for any given breach. Recommended values for the piping coefficient in an earthen embankment typically range from 0.5 to 0.6, since piping failures are not a hydraulically designed openings and it is usually assumed that the flow entrance is hydraulically inefficient.

3.2.4 *Trigger Methods*

There are three available trigger methods to initiate the failure. These trigger methods include elevation, duration at elevation, and specific time. The parameters required vary depending on the trigger method selected by the user.

The elevation method allows for specification of the initial failure elevation. The breach will begin to form when the reservoir pond elevation reaches the specified elevation. This method is often used for both overtopping and piping failures, although it is likely most appropriate for an overtopping failure since the breach can be set to begin when the pond elevation reaches the crest of the embankment.

The duration at elevation method allows for specification of the elevation and duration to define when the breach will begin to form. The reservoir pond elevation must remain at or above the specified elevation for a specified duration of time in order to initiate the failure. This method can be utilized for initiating piping failures and is how a piping failure would be expected to occur as the water would take time to transition through the embankment and initiate the erosion process.

The specified time method allows for specification of the time that the breach will begin to form, regardless of the reservoir pond elevation. This method is not typically used for dam breach analyses.

3.2.5 *Progression Methods*

A progression method is selected to define how the breach geometry will grow from initiation to the maximum size over the specified development time.

The linear method allows the breach to grow quickly in equal increments of depth and width. The sine wave method allows the breach to grow quickly in the early stages of breach development and growth rate decreases as the breach approaches the specified maximum size. The user defined option allows the breach to grow according to any specified pattern. The linear and sine wave methods are both common for tailings breach simulations and provide reasonable estimates for the growth of the breach geometry.

3.2.6 *Summary*

The dam breach hydrograph created by HEC HMS can be defined through either an overtopping failure or a piping failure. HEC-HMS allows for definition of a dam breach hydrograph based on user defined breach parameters, and specification of the breach type, trigger method (overtopping or piping), and rate at which an initially small breach grows over the development time. The software uses weir and orifice hydraulic flow calculations along with the breach parameters to define the breach hydrograph. HEC-HMS can model inflows into the tailings facility during the failure, which is advantageous for rainy day simulations and cascading type failures. The software can also account for additional outflows from spillways, embankment seepage, and evaporation, but generally additional outflows are disregarded as the failure time is rather brief.

4 COMPARATIVE STUDY

A comparison of the hydrographs resulting from the two software programs was completed using the dam breach parameters from a recently completed dam breach analysis. In this comparative study it was assumed that the volume of tailings and water stored in the facility at the time of the breach was 9.5 million cubic meters (Mm^3). The tailings were assumed to be liquefiable and have a porosity of 0.51. The embankment was assumed to have breached through piping during the sunny day event and the volume of mobilized tailings released during the breach includes both the volume of tailings, as estimated assuming a 3.5-degree cone of depression from the base of the breach, and the supernatant volume pond at the time of failure. The piping failure was assumed to occur along the drain at the base of the embankment and the piping coefficient was estimated to be 0.5. For simplification, the fluidized tailings were characterized as a homogenous mixture of the materials released from the impoundment (tailings and water). The dam breach parameters are presented on Table 2 and a side by side comparison of the resulting hydrographs is presented on Figure 3.

Table 2. Dam Breach Parameters

Parameter	Value	Program Input	
		HEC-HMS	TDFET
Peak Discharge (m^3/s)	13,823	-	-
Failure Duration (hr)	0.64	✓	✓
Breach Width (m)	180	✓	-
Side Slope Ratio (H:1V)	0.7	✓	-
Volume Stored Prior to Breach (Mm^3)	9.5	✓	-
Volume Released (Mm^3)	5.8	-	✓

The dam breach parameters required for HEC-HMS include the failure duration, breach width, side slope ratio and volume stored in the facility. In addition to the dam breach parameters HEC-HMS requires a filling curve for the facility, the top and bottom elevation of the embankment, the elevation that piping was expected to occur, the piping coefficient, and the trigger elevation of the pond level. A linear progression method was used for the HEC-HMS hydrograph.

The dam breach parameters required for the TDFET include the failure duration, and volume released during the breach. In addition to the dam breach parameters, the TDFET requires the volume of water released, the sediment concentration, and the tailings porosity.

The resulting hydrographs from the TDFET and HEC-HMS are presented in Figure 3.

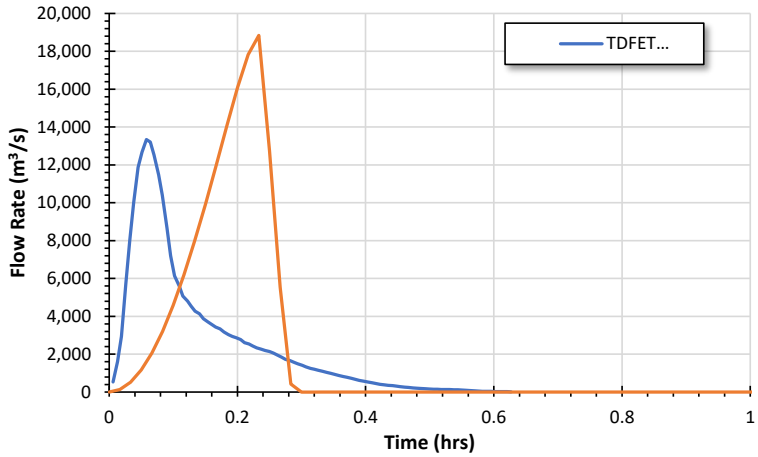

Figure 3. TDFET and HEC-HMS Hydrograph Comparison

The TDFET hydrograph predicts a peak discharge of 13,339 m^3/s, which is 4 percent lower than the breach parameter estimated peak discharge, shown in Table 2. The breach is expected to develop quickly and therefore a front loaded hydrograph distribution was selected. The total release volume indicated by the hydrograph is equivalent to the calculated release volume in Table 2. Overall, the TDFET produces a hydrograph with a peak discharge that is close to the value that was estimated from the dam breach parameters, and has a reasonable distribution of flows given the failure mode.

The hydrograph produced by HEC-HMS has a peak discharge of 18,840 m^3/s, which is 36 percent higher than the breach parameter estimated peak discharge. The HEC-HMS hydrograph indicates that the entire volume stored in the reservoir was released (9.5 Mm^3). Overall, the HEC-HMS hydrograph has a higher peak flow than estimated from the breach parameters and released a much greater volume.

The breach distribution produced by HEC-HMS is similar to that of the TDFET in that it is front loaded, however it does have a slightly more gradual increase in flow rate, and a much sharper decline.

It is clear that the HEC-HMS hydrograph determination method is designed specifically for clear water flows and does not take into account the fact that some tailings will remain in the facility after the breach. HEC-HMS calculates the volume released and flow rates based off of the breach parameters and hydraulic flow calculations making it difficult for the user to define a specific breach release volume. The TDFET relies more on the user's discretion to select an appropriate release volume and hydrograph distribution, but can be tuned to produce a hydrograph that fits well with the estimated volume released and estimated peak discharge. In this specific case, it is the author's opinion that the TDFET produces a more realistic hydrograph for the modeled dam breach scenario.

5 DISCUSSION

Two different analytical tools, or models, have been presented that can be utilized to develop breach hydrographs for tailings failure simulations. The inputs necessary for each model are slightly different, and simplifying assumptions are inherent in their utilization. Both models are

widely used in the industry, and are appropriate tools for determining dam breach hydrographs provided that the limitations are understood and appropriately considered.

In general, HEC-HMS is more simplified and easier to use, since the model can run a simulation to determine the dam breach hydrograph distribution with only appropriate facility volumetrics and breach parameters specified. The TDFET requires fewer breach parameters and volumetric inputs, but requires additional understanding and engineering judgement in the selection of the flow and sediment distributions over time. Selection of the appropriate distributions is simple within the model, but the underlying impacts on the results are larger and warrant careful consideration. Each of the hydrograph and sediment concentration distributions should be considered, and the distributions that represents the most critical of the credible scenarios selected. The TDFET is a more applicable tool to use when a specific hydrograph and sediment concentration are expected.

HEC-HMS is designed specifically for Newtonian (clear water) flows and the program determines the hydrograph and release volume based on the breach parameters and user inputs. As demonstrated in comparative study, the hydrograph and release volume determined by HEC-HMS may not be appropriate for every dam breach scenario, especially when dealing with non-Newtonian flows from tailings breaches.

One advantage of the HEC-HMS model is that ability to account for meteorological data and consider inflows and outflows to the tailings facility while the breach is forming. The meteorological feature may not be relevant for fair weather (sunny day) breach scenarios; however, it could be relevant for flood induced (rainy day) breach events that occur while the design precipitation event is ongoing. This allows for better simulation of rainy day events (i.e. addition inflows adding to the tailings storage volume and additional outflows, such as an activated spillway removing storage), as well as cascading type failures of adjacent tailings facilities. The TDFET tool is limited in the fact that the hydrograph computation cannot account for influence of additional inflow and outflow from meteorological factors, or features such as spillways.

Overall HEC-HMS incorporates a wider range of inputs that can influence the resulting hydrograph and it may be a more applicable tool when analyzing a breach with an active spillway, or where meteorological inputs are expected to have a significant impact on the model. However, HEC-HMS only generates one hydrograph distribution curve, from the user defined data, which can be limiting if that curve does not fit the expected distribution, while the TDFET provides a variety of options for the distribution of both the hydrograph and sediment concentration. The TDFET also has the added benefit of being able to directly account for sediment concentration, whereas HEC-HMS does not.

In general, a complete understanding of the tailings facility design, meteorological events, subsurface conditions, and tailings rheology are required in order to determine an appropriate breach hydrograph for tailings flood simulations. Development of accurate hydrographs initiates with reasonable estimates of the materials contained within the facility and identification of breach parameters utilizing empirically derived relationships. The majority of breach parameter relationships were developed for water retaining facilities, which should be taken into account as tailings flows are typically non-Newtonian and are fundamentally different than water flows. Oftentimes it is assumed that simulations using clear water flows are more conservative than non-Newtonian tailings flows as the run-out lengths are longer, but in our experience the impacts of modeling Newtonian versus non-Newtonian flows is not that simple. It is prudent to consider a modest parametric study of the breach parameters to assess the sensitivity of the results to variations in individual parameters.

6 REFERENCES

Costa, J.E. 1985. Floods from Dam Failures. in: V.R. Baker, et al. (Eds.), Flood Geomorphology, Wiley, New York, 1988, pp. 439–463.

Federal Energy Regulatory Commission (FERC). 1987. Engineering Guidelines for the Evaluation of Hydropower Projects. July. Engineering Guidelines for the Evaluation of Hydropower Projects, Chapter 3.

Froehlich, D.C. 1995. Embankment Dam Breach Parameters Revisited. January. First International

Conference, Water Resources Engineering, Environmental and Water Resources Institute (EWRI), 14 – 18 August 1995. ASCE, water Resources Engineering Proceedings, pages 887-891.

Froehlich, D.C. 2008. Embankment Dam Breach Parameters and Their Uncertainties. ASCE, Journal of Hydraulic Engineering, Vol. 134, No. 12 December 2008

Hydrologic Modelling Systen (HEC-HMS), 2018. Version: 4.3. Us. Army Corps of Engineers Institute for Water Resources Hydrologic Engineering Center, 609 Second Street, Davis CA 95616-4620

Laurrauri, P.C., and Lall, U., 2018. Tailings Dams Failures: Updated Statistical Model for Discharge Volume and Runout. Environments 2018, 5(2), 28.

Macdonald, T.C. and Langridge-Monopolis, J., 1984. Breaching Characteristics of Dam Failures. ASCE Journal of Hydraulic Engineering, Vol 110, No. 5, May 1984

Tocher, R.J., O'Brien, J, Chao, K.C., Overton, D.D. 2014. Predicting Tailings Dam Failure and Release Volumes, Proceedings of the 18th International Conference on Tailings and Mine Waste, Keystone, Colorado, October 6 - 8.

Pierce, M.W., Thornton, C. I. Abt, S. R. 2010. Predicting Peak Outflows from Breached Embankment Dams. June. Colorado State University, Daryl B. Simons Building at the Engineering Research Center, Fort Collins, CO. Prepared for: National Dam Safety Review Board Steering Committee on Dam Breach Equations

Singh, K.P., and Snorrason, A. 1982, 1984. Sensitivity of Outflow Peaks and Flood Stages to the Selection of Dam Breach Parameters and Simulation Models. August. Journal of Hydrology, Vol. 68, Issues 1-4, February 1984, pages 295-310. Global Water: Science and Engineering the Ven Te Chow Memorial Volume.

Rico, M. Benito, G. Diéz-Herrero, A. 2007. Floods from Tailings Dam Failures. October. Journal of Hazardous Materials 154 (2008), pages 79–87.

Rourke, H., and Luppnow D., 2015. The Risks of Excess Water on Tailings Facilities and Its Application to Dam-break Studies. Tailings and Mine Waste Management for the 21st Century, Sydney, NSW, 27–28 July 2015

Tailings Dam Failure Volume Estimate Tool (TDFET), 2019. Engineering Analytics Inc.

U.S. Army Corps of Engineers. 2016. Hydrologic Modelling System HEC-HMS. Version 4.2. August. Approved for public release. US Army Corps of Engineers, Institute of Water Resources, Hydrologic Engineering Center, 609 Second Street, Davis CA 95616.

U.S. Bureau of Reclamation. 1988. Downstream hazard classification guidelines. ACER Technical Memorandum No. 11, U.S. Bureau of Reclamation, Denver, Colorado. Retrieved March 20, 2017, from https:// www.arcc.osmre.gov

von Thun, L.J., and Gillette, D.R. 1990. Guidance on Breach Parameters. March. Unpublished internal document, U.S. Bureau of Reclamation, Denver, Co.

An Overview on Methodologies for Tailings Dam Breach Study

Shielan Liu
BGC Engineering Inc, Vancouver, British Columbia, Canada

Michael Henderson
BGC Engineering Inc., Denver, Colorado, USA

ABSTRACT: A tailings dam breach study (TDBS) is a key component that defines dam hazard classification, provides input to emergency action plans, and identifies risk reduction solutions for the dam safety program. During the life cycle of tailings dams which spans hundreds of years, the site conditions of the tailings storage facility, the floodplain, and downstream infrastructure can change significantly. Tailings dam breach studies are required to be updated periodically to reflect these changes. This paper provides a high-level overview of simplified to comprehensive methodologies for TDBS in practice. The level of detail for a TDBS should balance the trade-off between the available data, the consequences of the failure, the required resolution, the certainty of the analysis, and the cost of the study.

1 INTRODUCTION

Tailings dams form structures to store mine waste and contaminated water from mineral extraction. Tailings dams are not designed and built to fail. However, catastrophic tailings dam failures in recent years, such as Mount Polley failure in 2014, Mariana dam failure disaster in 2015, and the Brumadinho dam failure disaster in 2019, have pressed the mining industry to commit to safer tailings dam management and operation (https://globaltailingsreview.org/). Tailings Dam Breach Studies (TDBSs) play a significant role in a dam safety program through the life cycle of a tailings dam, from planning and design, to construction and operation, to closure and post closure (MAC, 2019).

TDBSs assume a hypothetical dam failure with a plausible failure mechanism, analyze the potential tailings flow characteristics and assess potential impacts to downstream areas. The purposes and objectives of a TDBS can vary through the various life stages. For instance, a TDBS can assist in site selection, define dam design criteria and guide tailings deposition planning at the initial planning and design stage. From dam construction and onwards, a TDBS can provide input to the emergency preparedness plan (EPP) or emergency action plan (EAP), while study results can be used to facilitate communication with people at risk. The outputs from a TDBS, and hence dam hazard classification, can also impact dam monitoring programs and the frequency of dam safety inspections. Where risk mitigation measures are required, a TDBS is a useful tool for evaluating the effect of mitigation solutions.

In practice, the TDBS framework is primarily inherited from those developed for Water Dam Breach Studies (WDBSs) (ANCOLD, 2012; FEMA, 2013), including the components of the tailings dam breach, runout, and deposition analyses, with optional hydrological analysis and failure impact assessment such as population at risk (PAR) or potential loss of life (PLL) assessments. However, the site conditions of tailings storage facilities (TSFs) are more complex than that of water reservoirs. Tailings dam type can be defined by construction method: Upstream, Centerline,

Downstream or Water retention. TSFs can also be configured as single or multiple Cross-Valley, Side-Hill, Valley-Bottom impoundments, or single and segmented Ring-Dike impoundments (Vick, 1990). Not only do TSFs store a mixture of solids and water, but also the presence of supernatant water and/or fluid tailings near the dam crest varies through the life stage of tailings dams (Small et al., 2017) and under varying climatic conditions. Indeed, tailings dam can fail even in the absence of a supernatant pond, as demonstrated by the Brumadinho dam failure.

The stakeholders of tailings dams, including dam owners, regulators and dam engineers, have a growing desire to standardize TDBS methodologies and improve the dam safety program systematically. The Canadian Dam Association (CDA) is currently developing a technical bulletin to guide engineering practitioners on what a TDBS should consider step by step (Martin et al., 2019; CDA, 2020). As a complementary discussion to the CDA efforts, this paper is intended to capture a snapshot of current methodologies for tailings dam breach, runout and deposition simulations that are uniquely applicable for TDBSs. Further, this paper discusses the level of detail required for a TDBS through its life cycle and the rationale of model selection and data needs. Finally, this article discusses the research and development needs with respect to TDBSs.

2 TAILINGS DAM FAILURE MODE AND BREACH ANALYSIS

2.1 Failure mode

All failure modes are related to gravity and the presence of water. Tailings dams can fail due to a hydraulic condition such as: overtopping, seepage or internal erosion (piping) failure; or collapse due to foundation failure or sliding that is trigged by static liquefaction or earthquakes. The complex configuration of TSFs can also result in a cascade failure of multiple dams (USCOLD, 1994; UNEP, 1996; ICOLD, 2001; Azama &Li, 2010; Lyu et al., 2019).

The discussion on what failure mode should be considered as the worst credible scenario for a TDBS is beyond the scope of this paper. Table 1 lists the preliminary failure modes and the number of casualties for several high-profile tailings failure incidents in recent years. The descriptions of these incidents can be found in the research papers and incident reports in the reference column.

Table 1. Tailings dam breach cases (https://www.wise-uranium.org/).

Incident	Year	Failure Mode	Casualty	Reference
Stava	1985	Cascade collapse of two dams	268	Takahashi et al (2014)
Merriespruit	1997	Overtopping and slope failure	17	Wagener et al. (1998)
Kolontár	2010	Piping failure	10	Grenerczy (2011)
Mount Polley	2014	Foundation and overtopping failure	0	IEEIRP (2015)
Mariana	2015	Earthquake triggered static liquefaction	19	FTDRP (2016)
Cadia	2018	Foundation failure	0	ITRB (2019)
Brumadinho	2019	Collapse due to static liquefaction	270	Roberston P.K et al (2019)

For TSFs with a supernatant pond or under an extreme storm event, the preliminary failure modes are similar to those for water dams (FEMA, 2013): overtopping, seepage or piping failure. In contrast, a slope or foundation failure is typically preliminary failure mode for sites without a pond or a pond far away from the crest, such as closed and inactive sites or dry stacks.

Different from the current CDA effort that focuses on dam breach analysis methodologies based on a matrix of presence/absence of a pond and liquefiable tailings (Small et al., 2017; Martin et al, 2019), this paper focuses on the modelling methodologies applied to different failure processes in practice.

2.2 Breach analysis methods

2.2.1. Overtopping and piping failure

For tailings dam overtopping and piping failures, practitioners have traditionally followed the roots of hydraulic modelling and applied one-dimensional (1D) breach modelling packages

developed for water dams. The modelling methods, summarized in inundation mapping guidelines by FEMA (2013), include: empirical equations (Wahl, 1997, 2010; Costa, 1988); physically-based model such as NWS-BREACH (Fread, 1998) WinDAM series (Visser et al., 2012); and, hybrid models such as HEC-HMS (USACE, 2016) and HEC-RAS (USACE, 2016). The governing equations and strengths of each of the methods are summarized in Table 2.

Table 2. Overtopping and piping failure hydrograph estimate methods (after FEMA, 2013).

Method	Governing Equations	Strengths
Empirical Equations	Empirical relationships derived based on analysis of historical dam failures	• Fast and simple to use • Minimal input data (dam height and release volume)
Physically-based models (e.g. NWS BREACH, WinDAM B, WinDaM C)	• Sediment transport • Broad weir equation (Overtopping) • Orifice flow equation (Piping) • Stress-based, energy-based head cutting equations available as analysis options. • The outflow hydrograph is obtained through a time- stepped solution.	• Physically-based model using erosion and sediment transport principals; • Estimate dam saturation degree and hydraulic pressure for sudden collapse estimate, integrated with side slope stability analysis • Model head cutting and downstream tailwater effects
Hybrid analytical models (e.g. USACE HEC-HMS, HEC-HAS)	• Continuity equation and an analytical or empirical relationship between TSF/reach storage and discharge • Level pool routing	• Ease use • Inherently stable • Monte Carlo simulation for uncertainty analysis

When applied to a tailings dam breach, these methods have limitations in that the following should be considered:

- Estimating input breach dimensions based on characteristics of tailings dams;
- Defining the failure surface by considering the residual shear stress of the remaining tailings;
- Taking account of physical processes involved with the dam collapse due to the hydraulic pressure of tailings mass;
- Simulating the erosion of tailings;
- Assessing the sediment concentration change by time during the failure process; and
- Calculating breach flow rate by considering the rheological properties of the tailings.

These limitations either come from lack of knowledge or lack of experimental or monitoring data for model development. Practitioners usually make some simplified assumptions to accommodate these limitations; for example, estimating the released tailings volume based on empirical analysis (Lucia, 1981; Rico et al., 2008; Larruai & Lall, 2018), or running breach models first, then averaging the sediment concentration in the breach hydrograph by using the porosity of tailings and estimated total released tailings volume.

2.2.2. Slope failure

Slope failure analysis belongs in the domain of geology or geotechnical engineering and tightly connects with landslide runout modelling. Theoretically, practitioners could use geomechanical modelling for slope instability, such as two-dimensional (2D) or three-dimensional (3D) limit equilibrium analyses to estimate the failure plane and the volume of slumped material. However, the data requirements are complex for these analyses. For instance, soil stratigraphy, strength, pore pressures and loading conditions usually are the mandatory input to the modelling packages. Therefore, the modelling cost is relatively high for this type of analysis. As the TDBS doesn't focus on the trigger mechanism analysis, practitioners often use simplified assumptions that are based on historical case studies (Lucia et al., 1981; Blight & Fourie, 2003) to estimate the failure

plane and slumped volume. Engineering judgement always plays an essential role in these assumptions.

Many landslide runout modelling packages could seamlessly model the slope failure and tailings runout by pre-defining a post-failure surface (McDougall & Hungr, 2006,2016; Chen & Lee, 2012, 2014; Ghahramani et al., 2019).

In contrast, a slope failure hydrograph is required for other hydrodynamic models (FLO-2D, 2018). Estimating the hydrograph of a slope failure is possible, as demonstrated by Takahashi et al. (2014), McPhail (2015) and Liu (2019). Takahashi estimated a triangle shape hydrograph by calculating the failure volume and duration time with a simple but practical approach for Stava failure. McPhail developed a model to estimate the cone formation and tailings mass release processes with three slope failure modes. Liu back calibrated the tailings release hydrograph for the Brumadinho failure with a simplified mass balance model using dynamic mass release rates.

2.2.3. Foundation failure and others

A foundation failure usually triggers secondary failure modes such as overtopping, piping or slope instability. As a result, practitioners often simplify the analysis or modelling process as either overtopping by assuming the dam crest settlement reaches the pond water level or a slope failure to mimic the sudden release of tailings mass.

In case of a cascade failure, the combination of overtopping, piping and slope failure analysis methods could be integrated for the specific site conditions.

2.3 Summary

With any of these failure modes analyses, the objective is to develop a tailings breach hydrograph or identify the initial slope failure surface and the total release volume, which is then the primary input for tailings flow runout and deposition analysis, with the ultimate objective of delineating the tailings flow impact and deposition zone.

3 TAILINGS FLOW RUNOUT AND DEPOSITION MODELLING METHODS

3.1 Flow type of tailings flow

The spatial scale for tailings flow runout can range from hundreds of meters to hundreds of kilometers, while the temporal scale can range from minutes to a few days.

In essence, tailings are the mining waste materials separated from the ore by mechanical and chemical processes. The particle sizes of tailings distribute from sand to a few micrometres (US EPA, 1994). The mixture of the tailings solids and water exhibits diverse flow characteristics under different site and downstream conditions. Under hydraulic failure conditions, the released flow can vary from water flood to mud flood (hyperconcentrated flow) to mudflow. In contrast, for a slope failure, the tailings could runout as a slump and deposit a short distance downstream or travel a long distance, and transition from a landslide to mudflow to mud flood to streamflow while being diluted by the flows in the receiving watercourse.

There were no well-defined terms for tailings flow in early research (Lucia, 1981; Jeyapalan et al.,1983a, b; Vicky 1991) other than “flow slide” or “slurry flow,” which was incapable of communicating the attributes of different types of tailings flow. Based on reviews on flow types (O’Brien, 1986; Coussot & Meunier; 1995; Hungr et al., 2001), Liu (2014) introduced a single volumetric sediment concentration (C_v) curve, that was developed by O’Brien (1986) for mudflows, to provide a conceptual view of flow and mass movement. CDA is adopting this flow type classification in the current technical bulletin (CDA,2020), as illustrated in Figure 1.

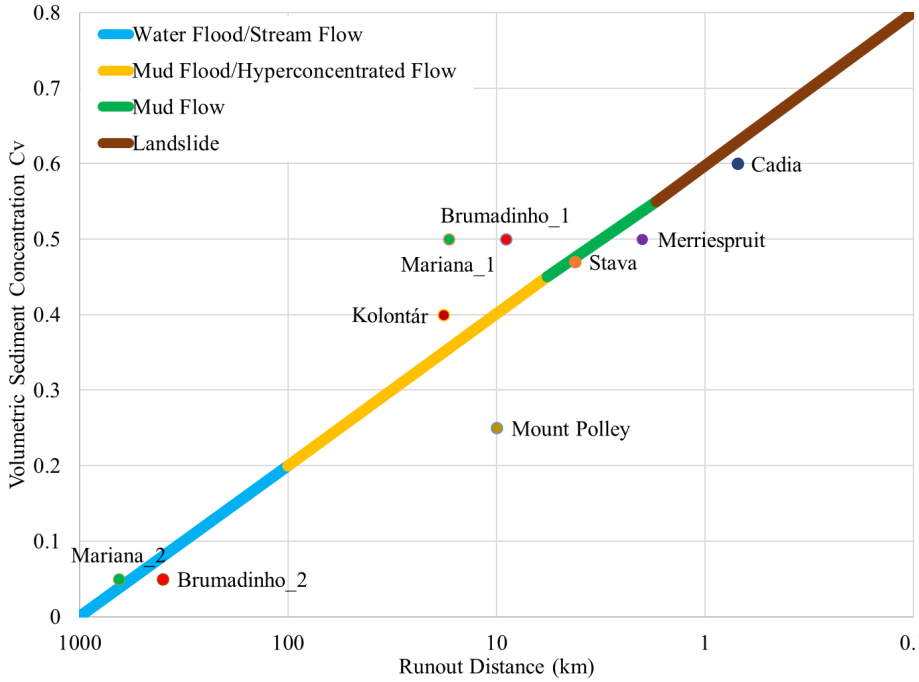

Figure 1. The relation between the runout distance and volumetric sediment concentration C_v.

It has been recognized that the C_v globally decreases when the tailings flow varies from landslide, to mudflow, to mud flood, and then to streamflow. Notably, the physical material properties of tailings, such as specific gravity, dry density or the plasticity indices, can be similar or very different from natural clay, sand, and gravel. Therefore, the limits of C_v for the different flow types are only conceptual and qualitative. In practice, the flow types should be investigated with the specific material properties and site conditions. Other attributes, for instance, the pH values, fine contents or temperature, may be required for defining the tailings flow type when the knowledge becomes available.

The flow mechanics are different for each of the flow types, as briefly summarized in Table 3.

Table 3 Tailings flow type, transport and deposition mechanics.

Volumetric Sediment Concentration C_v	Flow Type	Tailings Transport Mechanics	Preliminary Tailings Deposition Mechanics
C_v < ~20%	Streamflow	Bed load, Suspension	Settling
~20% < C_v< ~45%	Mud flood	Newtonian or non-Newtonian flow	Settling or Yield Stress
~45% < C_v < ~55%	Mud flow	non-Newtonian flow	Yield Stress and Friction
55% <C_v	Landslide, Debris avalanche	Slump	Conservation of momentum and friction

When C_v is greater than about 55%, such as a “dry” waste dump failure (for example, the Cadia dam failure), the tailings would not behave like liquified flow. Rather, the tailings would slump and stop by cause of the conservation of momentum and friction (Golder, 1992).

When C_v is between 45% to 55%, liquefied tailings behave like a single-phase non-Newtonian flow, and are capable of travelling a long distance with high speed before eventually depositing

due to the yield stress and friction (for instance, Stava, Samarco and Brumadinho dam failures). This kind of tailings flow may be the most catastrophic flow type from a tailings dam safety perspective. All three failure cases mentioned above occurred in the daytime on sunny days, which gave very little warning time to the inhabitants in downstream areas. Particularly, the failed dam at Brumadinho had been closed for three years prior to its collapse, which imposes significant challenges on long term tailings dam management.

Tailings flow can be Newtonian or non-Newtonian when C_v is between 20% to 45%, which is defined as the mud flood regime. Depending on the tailings properties and ground slope conditions, the flow could propagate along the flow path with significant capacity for channel erosion (for instance, Mount Polley failure). For these flows, the tailings can deposit along the flow path by gravitational settling or yield stress, as observed from the Kolontár failure.

When C_v is less than 20%, tailings are diluted by water or the TSF is essentially functioning as a contact water storage facility, the tailings would be transported by bedload and suspension with gravitational settling.

Intuitively, the fluid and deposition mechanics of different flow types will influence the tailings runout distances and inundation areas. Figure 1 also plots the inverse correlated relations between C_v and tailings travel distance for the case histories listed in Table 1. Both C_v and the tailings travel distances are extracted from the literature or estimated by personal experience. Note that the run out distance for Mount Polley is relatively short due to the downstream presence of Quesnel Lake. Multiple case histories, such as the Mariana and Brumadinho failures, indicate that the flow type can transit from one to another during the runout and deposition processes and result in extremely long travel distance of tailings.

3.2 Tailings rheological models and properties

Given the aforementioned fluid mechanics of tailings flow, it is crucial to understand the rheology and properties of the tailings.

Rheological research has been carried out in the minerals industries for a few decades. This research has focused on slurry pumping and thickened disposal strategies for tailings management (Shook et al.,2002; Boger,2009). According to the investigation of red mud (bauxite residue) slurry transport, the material exhibits Newtonian fluid behaviour at low concentrations. However, non-Newtonian characteristics are generally observed at higher concentrations, which matches O'Brien's (1986) conceptualization of flow types.

The difference between Newtonian and non-Newtonian flow behaviour lies in the function of the shear stress and shear rate. A Newtonian flow presents a direct proportionality between shear stress and shear rate, while non-Newtonian flows behave more diversely. Flow deformation starts when the shear stress exceeds a critical yield stress. A few mathematical explanations to the non-Newtonian models (FLO-2D, 2018; Chen & Lee, 2002; Yavari-Ramshe et al, 2015) have been found to be useful in describing tailings flow, including Bingham, Quadratic, Herschel-Bulkley, Voellmy and Coloumb-viscous models (Shook et al.,2002, Liu, 2018; Ghahramani et al, 2019).

Many lab testing results show that the yield stress has an exponential relation with the solids mass fraction (O'Brien & Julien, 1985). However, this relation is very different while comparing the yield stress concentration behaviours for tailings from different minerals (e.g., aluminum bauxite, gold, coal, nickel, and copper) (Boger, 2009). It is worth noting that the true yield stresses required to initiate flow may be distinct from the apparent yield stress that is obtained by back analysis flow data via modelling.

For large shear rates such as might occur on the steep slopes, turbulent and dispersive stresses may suppress the viscous stress and dominate the flow behavior. Therefore, the viscosity of a slurry can only be measured if the shear rate is low or the particles settle slowly. In general, the viscous stress increases when the fine contents increase (O'Brien & Julien, 1985; Shook et al., 2002). However, viscous stresses are still negligible for some types of tailings, for instance, oil sands tailings (Shook et al., 2002).

3.3 Modelling methods

Once the fluid and deposition mechanics have been conceptualized, analytic and numerical models can be reasonably developed or selected. The research on the tailings flow runout analysis methods keeps evolving, particularly in the last decade with increased computational power.

Similar to breach analyses, both empirical analysis and numerical modelling approaches are taken in practice.

Lucia (1980), Rico et al. (2008) and Larrauri & Lall (2018) analyzed a few case histories and developed empirical relations to estimate the tailings release volume and runout distance. At a screening level, these methods can be used for dam hazard classifications for efficiency.

Jeyapalan et al. (1983a, 1983b) developed a 1D non-Newtonian Bingham model to represent tailings flow behaviour mathematically. The National Weather Service (NWS) of the United States developed FLDWAV, a generalized 1D flood or mud/debris flow routing program that includes the Herschel-Bulkley model for tailings flow runout modelling. However, these models did not get popular in practice, either because of the deficiency in the outdated solvers or lack of technical support to the old computer operating system where these models were based. With the development of user interface applications, automation on data processing and open data strategy, a 1D model may not necessarily save much cost than building a 2D model.

To date, many computational fluid dynamic (CFD) models initially developed for inundation or runout analysis of stream flows, mud flood, mudflows, and landslides are sufficiently advanced to simulate tailings runout and deposition processes. These CFD modelling packages are based on the shallow-water St-Venant equations, governed by the continuity equation and momentum equation. With the function of sediment concentration or density, some modelling packages could predict fluid motion transition between the viscous flow and turbulence flow as well as the flow cessation due to the yield stress. However, modelling the transition between sediment transport and non-Newtonian flow remains a challenge for many modelling packages.

It is not possible to compile an exhausted list of the available models in this paper. Table 4 lists a few selected modelling packages that have been used in the industry, along with the rheological models and main features that are related to TDBS of those packages.

Table 4. Selected CFD modelling packages for TDBS.

Modelling Package	Rheological model	Main Feature
FLO-2D (https://flo-2d.com/)	Quadratic	• Flow initiation from a hydrograph • Sediment transport in water flood/stream flow • Non-Newtonian flow range from mud flood to mud flow • Temporal variation of sediment concentration, yield stress and viscosity based on O'Brien & Julien (1985) • Finite volume method/structured mesh
HEC-RAS (https://www.hec.usace.army.mil/software/hec-ras/)	*Quadratic* *Bingham* *Coulomb* *Herschel-Bulkley*	• Flow initiation from a hydrograph • Sediment transport and water quality modelling (1D) • *Sediment transport (2D) and non-Newtonian flow modules are under development* • Finite volume method/Flexible mesh
Riverflow2D (http://www.hydronia.com/riverflow2d)	Quadratic Bingham Coulomb Granular	• Flow initiation from a failure surface or a hydrograph • Sediment transport in water flood/stream flow • Multiple rheological models for Non-Newtonian flow range from mud flood to mud flow, granular flow • Temporal variation of flow density, yield stress and viscosity • Multiple tailings size fractions • Finite volume method / Flexible mesh
DHI MIKE 21/3 (https://www.mikepoweredbydhi.com/products/mike-21)	Bingham	• Flow initiation from a hydrograph • 2D and quasi 3D Sand/mud transport • Non-Newtonian flow range from mud flood to mud flow • Temporal variation of sediment concentration, yield stress and viscosity • Finite-volume method/Flexible mesh

Modelling Package	Rheological model	Main Feature
FLOW3D (https://www.flow3d.com/)	Herschel-Bulkley	• Flow initiation from a hydrograph • Sediment transport (2D) • Non-Newtonian flow (2D) range from mud flood to mud flow, granular flow • Two-phase flows • Structured finite difference/control volume meshes • High quality data visualization
DAN3D (Not commercialized) (McDougall & Hungr, 2006, 2016)	Bingham Voellmy Frictional Plastic	• Flow initiation from a failure surface • Multiple rheological models for non-Newtonian flow range from mud flow to landslide • Depth-averaged (quasi-3D), Lagrangian, meshless model based on Smoothed Particle Hydrodynamics (SPH) • Change rheological parameters while model runs • Include an automatic parameter calibration module
MADflow (Not commercialized) (Chen & Lee, 2002, 2006; Chen & Becker 2014; Chen et al., 2019)	Bingham Voellmy Frictional Quadratic Coulomb Herschel-Bulkley	• Flow initiation from a failure surface or a hydrograph • Multiple rheological models for non-Newtonian flow range from mud flow to landslide • Temporal variation of flow density, yield stress and viscosity • Zonation of rheological parameters • Finite element method/Structure mesh

The computing/cost effort for these modeling packages ranges from medium to relatively high when considering the license price, the required input data, the level of effort for data pre and post-processing, and the time required for modeling.

All these models could provide the maps required for an EPP or EAP, which show the maximum flow depths, flow velocities, inundation zone and deposition zone. However, all the models have simplified the physical tailings flow runout processes to some degree. Further, sediment transport modelling is often skipped in practice from an inundation mapping perspective, despite its importance for evaluating the environmental consequences from the spilled tailings composed with toxic heavy metals (Palu & Julien, 2019). Considerable work remains to develop and validate the models for tailings flow runout and deposition processes. Benchmarking modelling with different models would be a useful future endeavor.

4 SELECTION OF LEVEL OF DETAIL

Given that mining is an essential ongoing economic activity, the number of tailings ponds worldwide is expected to increase over time. As a result, the cost of dam management will also keep increasing steadily. Dam owners are particularly interested in a systematic approach that balances the cost and level of the detail of the study while providing an adequate level of information for planning and dam safety. Dam breach study practitioners also need to select the level of detail that meets the intended objective and correlate the sophistication and accuracy of the analyses with the scale and complexity of the dam and downstream area under investigation within the context of available information, time, and budget.

In general, when the level of detail increases, the system error or uncertainties of the study decreases; however, costs increase along with the increased effort (Overton & Meadows, 1976). Logically, for the different dam hazard classifications and life stages, the acceptable error tolerance for the TDBS varies. The uncertainty tolerance should be decreased as the dam hazard consequence categories go from low to extreme.

Table 5 illustrates a conceptual and subjective uncertainty tolerance matrix for TDBSs by looking at the life stage of tailings dams and hazard classification that is adopted from the Global Tailings Standard (ICMM, UNEP & PRI, 2020).

Table 5. Uncertainty tolerance of TDBS.

TSF Life Stage	Consequence Categories				
	Low	Significant	High	Very high	Extreme
Planning	45%	45%	45%	45%	45%
Design	45%	45%	45%	35%	25%
Construction	45%	35%	25%	15%	10%
Operation/ ongoing construction	45%	35%	25%	15%	10%
Closure/Post Closure	45%	35%	25%	15%	10%

These trade-off relations between system complexity and cost have been considered in guidelines for WDBSs by ANCOLD (2012) and FEMA (2013). However, the current CDA draft only briefly mentioned desktop level and detailed level of study for TDBSs. The authors consider the following tiered approach that uses three levels of assessment as appropriate for TDBSs in practice:

- An initial assessment may suffice when a dam hazard classification rating is evident from existing knowledge. The empirical estimate methodologies mentioned in this paper can be used given an uncertainty tolerance of around 45% for the TDBS (i.e., Table 5).
- An intermediate assessment can apply to a TDBS that has an uncertainty tolerance range of 25-35%. This level of assessment requires a more quantitative assessment of the consequences of a dam break. For this level of assessment, scenarios under different weather conditions are typically considered. Modeling methods with medium effort can be selected for this level of assessment.
- A comprehensive assessment would be needed for a TDBS with an uncertainty tolerance range from 10% to 15% (Table 5). The comprehensive assessment usually requires quantified (i.e., modeled) information about failure modes, inundation areas, velocity and depth of the flood flows, travel times, together with estimates of the extent. Other information includes the type of damage and loss, as well as estimates of the PAR or PLL. The analysis should consider a range of dam failure scenarios and breach locations. Sensitivity analyses are generally required to evaluate the impact of parameters with high uncertainties. 2D models are employed at a minimum.

Taking a proposed dam as an example, the potential dam hazard classification would impact the dam design criteria and tailings deposition plan. However, little information is available at a conceptual design stage, and a simplified method can then be used to assess the potential impact zone and population at risk initially.

Similarly, simplified analysis may suffice for low-hazard potential dams situated upstream of sparsely populated areas. For example, if a TDBS was to be carried out for the Cadia dam, practitioners may perform an initial assessment to estimate the potential impact zone while an intermediate assessment would be required for Mount Polley to quantify the environmental impact to the downstream lakes.

By contrast, for the analysis of high-hazard potential dams located upstream of populated areas or complex floodplains, such as the rest of the sites listed in Table 1, more sophisticated modeling and additional sensitivity studies should be utilized to properly assess the consequences of a dam failure and prepare an EPP or EAP.

The demand for data accuracy and details increases along with the level of detail required for the TDBS. Critical information includes the resolution of the DEM, the detail of land covers, the accuracy of the bathymetry of rivers or lakes, and the representative rheological properties of the tailings.

However, one has to be aware that despite the level of effort expended in a comprehensive assessment, inherent uncertainties remain that would not be eliminated in a TDBS. These uncertainties are attributed to lack of knowledge, lack of survey data for calibration, no detailed information of the site, and the lack of appropriate models that can simulate the interaction of water

and tailings during dam breach and runout processes. Dam owners need to be aware of these uncertainties while preparing the EPP or EAP and evaluate mitigation measures.

5 SUMMARY

TDBSs play a vital role in a dam safety program. Benchmark modeling with different modeling packages would help practitioners understand the capabilities and limitations of each modeling package and assist in choosing the right tools. Selecting the appropriate level of detail for a TDBS would help meet dam owners needs for prioritizing dam safety management systematically.

With the recent focus on TDBSs from the industry, data collection techniques, methods, and modeling packages are expected to be advanced for TDBSs in the near future. Some future research directions identified include:

- The published investigation reports are mainly focused on the cause of the dam failure and answering the questions of why the failure occurred. There is very little data on the downstream impact in the literature. As the post-failure impact information is invaluable for TDBSs, innovative remote sensing technology may be advanced to analyze topographic differences pre and post of a tailings dam failure event on a large scale. These data would support the development of tailings runout and deposition modelling significantly.
- To better characterize the tailings dam breach dimensions, more experimental research on these topics is required. For example, comprehensive research on the relation between the water volume, tailings residual shear stress and original ground slope would provide insight on the tailings released volume and peak flow estimate.
- Despite recent advances, tailings flow types remain loosely defined. There is no existing database for tailings rheological properties available for TDBS's yet. It is possible to fit the rheological parameters by back analyzing case histories. However, the experimental validation of the apparent rheological parameters are needed. A systematic industry coordination and sharing of knowledge would benefit TDBS's in general.

REFERENCES

ANCOLD. (2012). Guidelines on the consequence categories for dams, October 2012, Australian National Committee on Large Dams, https://www.ancold.org.au.

Blight, G.E. & Fourie, A.B. (2003). A review of catastrophic flow failures of deposits of mine waste and municipal refuse. *International Workshop on Occurrence and Mechanisms of Flow in Natural Slopes and Earthfills*, Sorrento, Italy.

Boger, D.V. (2009) Rheology and the resource industries, Chemical Engineering Science, 64 (2009) 4525 – 4536.

CDA (Canadian Dam Association). (2007). Technical Bulletins. Published as a set to supplemental Dam Safety Guidelines. Complete listing available on CDA website at www.cda.ca.

CDA (2013). Dam Safety Guidelines 2007 (2013 Edition).

CDA (2020, in progress). Technical Bulletin: Tailings Dam Breach Analyses (Draft), Prepared by Tailings Dam Breach Working Group, August 2020.

Chen, H. & Lee C.F. (2002). Numerical simulation of debris flows. Journal of Geotechnical and Environmental Engineering, Vol. 128, No. 12, December 1, 2012, 1032-1042.

Chen, H. & Becker, D. (2014). Dam Breach Tailings Runout Analysis. Proceedings of Canadian Dam Association, 2014 Annual Conference, Banff, Alberta, Oct. 4-9, 2014.

Chen, H., Chin, B. & Friedel, R., (2019). Dam Breach Tailings Runout Modelling for Inactive/Closed Tailings Storage Facility. *Proceedings of Canadian Dam Association, 2019 Annual Conference, Calgary, Alberta, Oct. 6-9, 2019*

Costa, J.E. (1988). Floods from dam failures. In V.R. Baker, R.C. Kochel, & P.C. Patton (Eds.), Flood Geomorphology (pp. 439-469). John Wiley and Sons, New York.

FEMA (Federal Emergency Management Agency). (2013). Federal Guidelines for Inundation Mapping of Flood Risks Associated with Dam Incidents and Failures. First Editions. FEMA P-946, July 2013.

FLO-2D. (2018). FLO-2D Reference Manual. Nutrioso, AZ: FLO-2D.

Fread, D.L. & J. M. Lewis. (1998). NWS FLDWAV Model: Theoretical Description and User Documentation. Hydrologic Research Laboratory, Office of Hydrology, National Weather Service.

FTDRP (Fundão Tailings Dam Review Panel: Norbert R. Morgenstern, Steven G. Vick, Cássio B. Viotti, Bryan D. Watts) (2016), Report on the Immediate Causes of the Failure of the Fundão Dam, August 25, 2016.

Ghahramani, N., Rana, N. M., Liu, S., Chen, H., Clohan, D., McDougall, S., Evans, S. G. and Take, A. 2020. A Preliminary Benchmarking Numerical Modelling Exercise for Tailings-Flow Runout Analysis. Mine Waste and Tailings Conference. 2020 (accepted).

Golder Associates Ltd. (1992) Interim report to department of Supply and Services Contact No. 23440-9198/01 – X8G, Re Runout Characteristics of Debris From Dump Failures in Mountainous Terrain, Stage 1 Data Collection, Volume I Text and Tables. 912-1413.

Grenerczy, G.& Wegmüller, U. (2011) Persistent scatterer interferometry analysis of the embankment failure of a red mud reservoir using ENVISAT ASAR data. Nat Hazards 59,1047. https://doi.org/10.1007/s11069-011-9816-6.

ICMM (International Council on Mining & Metals), UNEP (United Nation Environment Programme) & PRI (Principles for Responsible Investment) (2020). Global Industry Standard on Tailings Management, August 2020.

Hungr O, Evans SG, Bovis MJ, Hutchinson JN (2001) A review of the classification of landslides of the flow type. Environmental & Engineering Geoscience VII(3):221-238. doi:10.2113/gseegeosci.7.3.221

ICOLD (International Commission on Large Dams). 2001. Tailings Dams – Risk of Dangerous Occurrences: Lessons learnt from practical experience. Bulletin 121.

IEEIRP (Independent Expert Engineering Investigation and Review Panel), (2015), Report on Mount Polley Tailings Storage Facility Breach, January 30, 2015

ITRB (Independent Technical Review Board, Michael Jefferies, Nobert R. Morgenstern, Dirk Van Zyl, John Wates), (2019), Report on NTSF Embankment Failure Cadia Valley Operations for Ashurst Australia, April 17, 2019.

Jeyapalan, J.K., Duncan, J.M., & Seed H.B. (1983a). Analyses of flow failures of mine tailings dams. ASCE, Journal of Geotechnical Engineering, 109(2), 150-171.

Jeyapalan J.K., Duncan J.M., & Seed H. B. (1983b). Investigation of flow failures of tailings dams. ASCE, Journal of Geotechnical Engineering, 109(2), 172-189.

Larrauri, P.C. & Lall, U. (2018). Tailings Dams Failures: Updated Statistical Model for Discharge Volume and Runout. Environments, 5, 28. https://doi.org/10.3390/environments5020028.

Liu, H. (2018). An experimental and numerical study of runout from a tailings dam failure. (Doctoral dissertation), School of Civil, Environmental and Mining Engineering, The university of Western Australia.

Liu,S. (2014). Dam Breaks with/without Free Water - Numerical Models and Limitations. Presented in Workshop A: Tailings Dam Breach Analysis: Beyond the State of Practice. CDA Annual Conference October 4-9, 2014, Banff, Alberta.

Liu, S. (2019). Back Analysis of Feijao Failure. Presented in Short Course 3: Tailings Dam Breach Analysis – addressing the challenges from Owner, Regulator, Practitioners and Researchers Perspective. Tailings and Mine Waste Conference 2019.

Lucia P.C., Duncan, J.M., & Seed H. B. (1981). Summary of research on case histories of flow failures of mine tailings impoundments. Mine Waste Disposal Technology, Proceedings of the Bureau of Mines Technology Transfer Workshop, Denver, Colorado, p. 46-53.

Lyu, Z.; Chai, J.; Xu, Z.; Qin, Y. & Cao, J.(2019) A Comprehensive Review on Reasons for Tailings Dam Failures Based on Case History, Advances in Civil Engineering . 6/20/2019, p1-18. 18p.

Martin, V., Al-Mamun, M., & Small, A. (2019) CDA technical bulletin on tailings dam breach analyses. Proceedings of the ICOLD 2019 Symposium, June 9-14, 2019, Ottawa, Canada.

McDougall, S. & Hungr, O. (2004). A model for the analysis of rapid landslide motion across three-dimensional terrain. Canadian Geotechnical Journal, 41, 1084-1097.

McDougall, S. (2006). A new continuum dynamic model for the analysis of extremely rapid landslide motion across complex 3D terrain. Ph.D. Thesis. The University of British Columbia.

McDougall, S. (2016). 2014 Canadian Geotechnical Colloquium: Landslide runout analysis – current practice and challenges. Canadian Geotechnical Journal. 00: 1-16.

McPhail, G. (2015). Probabilistic dam break assessment and flow slide analysis for tailings storage facilities. Tailings 2015, 3rd International Seminar on Tailings Management.

Ming, J. & D.L. Fread. (1997). One-Dimensional Routing of Mud/Debris Flows Using NWS FLDWAV Model. Proceedings of the First International Conference on Debris-Flow Hazards Mitigation. San Francisco, CA: USGS.

National Weather Service (2009). Transition from FLDWAV to HEC-RAS; Forecast Implications and Transition Tools. National Oceanic and Atmospheric Administration, National Weather Service, Office of Hydrologic Development. Retrieved January 7, 2011, from http://www.nws.noaa.gov/oh/hrl/hsmb/hydraulics/FLDWAV2HEC-RAS.html.

O'Brien J.S., & Julien, P.Y. (1985). "Physical properties and mechanics of hyper-concentrated sediment

flows". In Proceedings ASCE Specialty Conference on Delineation of Landslides, Flash Flood and Debris-Flow Hazards, Bowles, D. (Editor), Utah Water Research Laboratory, Utah State University, Logan, Utah, 260-279.

O'Brien, J.S. (1986). Physical Processes, Rheology, and Modeling of Mud Flows. Ph.D. Dissertation, Colorado State University, Fort Collins, Colorado.

Overton, D. C., & Meadows, M. E. (1976), Storm water modeling, Academic, New York.

Palu M.C. & Julien P.Y. (2019) Modeling the Sediment Load of the Doce River after the Fundao Tailings Dam Collapse, Brazil, Journal of Hydraulic Engineering, 2019, 145(5): 05019002.

Perry, R.H., Green D. & Maloney, J.O.(1984), Perry's Chemical Engineers' Handbook, McGraw-Hill, New York, 6th Edition.

Rico, M., Benito, G., & Diez-Herrero, A. (2008). Floods from Tailings Dam Failures. Journal of Hazardous Materials, 154(1-3), 79-87. https://doi.org/10.1016/j.jhazmat.2007.09.110.

Roberston P.K, De Melo L., Williams D. J., Wilson G. W., (2019) Report of the Expert Panel on the Technical Causes of the Failure of Feijão Dam I, December 12, 2019.

Shook C.A, Gillies R.G., Sanders R.S. (2012) Pipeline hydrotransport with applications in the oil sand industry, SRC Publication No. 11508 – 1 E02.

Small, A., James, M., & Al-Mamun, M. (2017). Advancing the State of Practice for Tailings Assessment Using Empirical Correlations. Proceedings of the Canadian Dam Association 2017 Annual Conference, Kelowna, BC, Oct. 16-18, 2017.

Takahashi, T., & Das, D. K. (2014). Debris flow: mechanics, prediction and countermeasures. *CRC press*.

USArmy Corps of Engineers (USACE), (2016), HEC-RAS River Analysis System User's Manual Version 5.0, February 2016.

US Army Corps of Engineers (USACE) (2016, August). Hydrologic Modeling System HEC-HMS User's Manual. Version 4.2

US EPA. (1994). Technical Report: Design and Evaluation of Tailings Dam, EPA 530-R-94-038, NTIS PB94-201845.

Visser, K., Tejral, R.D.& Neilsen, M.L. (2015). WinDAM C earthen embankment internal erosion analysis software. In Proc. of the Joint Federal Interagency Sedimentation and Hydrologic Modeling Conference, Apr. 19-23, 2015, Reno, Nevada. 10 p. http://acwi.gov/sos/pubs/3rdJFIC/index.html.

Vick, S. G.(1990).Planning, design, and analysis of tailings dams.Vancouver:BiTech.

Vick SG (1991). Inundation risk from tailings dam flow failures. Proc. 9th Panamerican Conf. SM&FE, Viña del Mar, vol 3, pp 1137-1158.

Wagener, F, Craig, H J, Blight, G E, McPhail, G, Williams, A B, & Strydom, J H, (1998). The Merriespruit tailings dam failure — a review. In Proceedings of the Conference on Tailings and Mine Waste '98, Colorado State University, Fort Collins, January 1998, pp. 925–952.

Wahl, T. L. (1997). Predicting Embankment Dam breach Parameters – A Needs Assessment. Proceedings of the U.S. Bureau of Reclamation, XXVIIth IAHR Congress. San Francisco, CA

Wahl, T. (2010). Dam Breach Modeling- An Overview of Analysis Methods. Published in the Joint Federal Interagency Conference on Sedimentation and Hydrologic Modeling, June 27 – July 1, 2010, Las Vegas, NV.

Yavari-Ramshe, S. & Ataie-Ashtiani, B. (2015). A rigorous finite volume model to simulate subaerial and submarine landslide-generated waves. Landslides. doi:10.1007/s10346-015-0662-6.

Effect of Different Tailings Dam Environments and Conditions on Phreatic Conditions

Luke Clarkson
The University of Queensland, Brisbane, Queensland, Australia

Todd Armstrong
AECOM Australia Pty Ltd, Brisbane, Queensland, Australia

David J Williams
The University of Queensland, Brisbane, Queensland, Australia

ABSTRACT: This paper explores the influence of common external factors in the tailings dam environment on phreatic conditions. The phreatic condition in tailings dams and deposited tailings responds differently as a result of material permeability and changes in external conditions. It is important for operators and designers to understand the influence of external conditions on the phreatic condition, and how/when these changes might reflect at discrete piezometer locations. Pore water pressure changes induced at one location in the tailings dam can take a significant amount of time to propagate to a given piezometer location and hence a delayed effect could be expected. The paper describes a numerically modelled, observational approach. Calibration of onsite piezometer measurements with pore water pressures modelled in SEEP/W allowed consideration of the effect of pond level rise, lateral variation of hydraulic conductivity, and the introduction of an external load on tailings dam pore water pressure conditions.

1 INTRODUCTION

The demand for tailings storage is increasing exponentially with time, along with the associated risks. It is estimated that the potential risk of tailings dams increases by 20-fold approximately every 30 years (Robertson 2012). Chambers (2016) tailings dam failure database describes an average annual rate of failure of 1 in 700 to 1 in 1,750, or two to five annual failures for the roughly 3,500 tailings dams worldwide (LePoudre 2015 & Davies, Martin & Lighthall 2002). By comparison, the estimated probability of failure for a conventional water dam is 1 in 10,000 (Davies, Martin & Lighthall 2002). Tailings dam failures, and the potential to forecast these failures ahead of time based on a better understanding of existing conditions and performance is the focus of the first author's research. Understanding the capabilities of the installed instruments and recorded data is clearly a critical necessity; however, the environmental conditions and an understanding of the piezometer data are equally important.

One of the most common instruments installed in tailings dams is the piezometer, used for the purpose of measuring phreatic surface (level where water is in equilibrium with atmospheric pressure) and pore water pressures (void fluid pressure acting on the tailings particles) to characterise the pore water pressure profile and select appropriate parameters and methods for stability analyses. Typically, piezometers are installed in locations that will provide key information to compare against design assumptions and the findings of seepage and stability analyses, in particular comparison against allowable and safe limits. Naeini & Akhtarpour (2018) describe the purpose of seepage analyses aligning with one of three objectives:

1. "Locating the phreatic surface, managing the water resources or providing inputs for stability analyses";
2. "Determining the safety factor under static and/or pseudo-static conditions"; or
3. "Hydro-mechanical analyses to address the complex behaviour of tailings dams during staged construction".

This research focuses on seepage analysis for the intent of objective #1 above: understanding the potential impact of external conditions on broad pore water pressure conditions, combined with appropriate interrogation of the piezometer readings to better understand the performance of any particular tailings dam. This not only enhances the ability to proactively respond to unfavourable changes in the dam, but also informs practitioners as technology progresses to "real-time". Understanding that the measurement may be in real-time, but that the condition being measured could be a delayed response to pore water pressure changes elsewhere, is important when considering a true understanding of dam performance.

There are a multitude of parameters that might influence the flow of water in a tailings dam environment, including those characteristic of the tailings deposit, as well as external conditions that are a function of the climate, location, and operation of the tailings dam (among others). Understanding the phreatic surface fluctuation and overall level in the tailings dam is pertinent to guide operational responses to maintain the pore water levels within acceptable performance limits and to take appropriate action against established trigger levels.

To further understand the effect of different tailings dam environments and external conditions on piezometer response and reliability in terms of understanding tailings dam phreatic conditions, this research undertakes sensitivity tests on influential parameters to better understand their effects. This paper focuses on their effects on upstream construction. The influential parameters assessed align with Vick's (1990) description of the factors that have the most significant effect on the phreatic surface location, as (in order of prevalence, for upstream construction):

- Beach width, describing the location of ponded water with respect to the embankment crest;
- Lateral permeability variation, as produced by grain-size segregation of the tailings deposit during hydraulic placement; and
- Boundary flow conditions, described by starter dam permeability and foundation permeability.

For this paper, the two most influential factors on the upstream embankment phreatic surface are suggested to be the beach width and lateral permeability variation. These are modelled together with the introduction of an external load, which is introduced in an attempt to simulate objective #3 above in understanding the effect of staged construction on phreatic conditions.

2 MATERIALS AND METHOD

The numerical modelling scenarios simulated hydrodynamic time lag and change in total elevation head as a result of the time taken for pore water pressure changes to transmit through the tailings. Different external conditions were assessed using numerical simulations to explore their influence on seepage through the tailings and subsequent influence on pore water pressure conditions at discrete locations, including:

- Pond level rise and beach width change. "The location of the ponded water with respect to the embankment crest, or the width of the exposed tailings beach, is often the most important factor influencing phreatic surface location" (Vick 1990);
- Lateral variation of hydraulic conductivity. "The variation in permeability is characterised by the ratio of tailings permeability at the spigot point (k_0) to the permeability at the edge of the ponded water at the slimes zone (k_L)" (Vick 1990); and
- External loading. While a potential function of many different influences, the excess pore water pressure generated as a result of a theoretical load increase was checked.

2.1 *Model Theory*

The numerical model was generated using proprietary software, SEEP/W (GEO-SLOPE 2019). SEEP/W adopts a number of assumptions and approaches whereby expressing understanding of some basic definitions in terms of the hydraulic conductivity aids understanding of this research (US EPA 2010):

- "Homogeneous means that hydraulic conductivity (K) (or the coefficient of permeability) in the material (natural soil or the embankment) is independent of position";
- "Isotropic means that hydraulic conductivity is independent of direction at the point of measurement";

- "If hydraulic conductivity is dependent on position then the media is heterogenous"; and
- "If hydraulic conductivity of a media is dependent on direction at the point of measurement then the media is anisotropic".

This research assumes homogeneous materials; however, a balance between isotropic and anisotropic materials is used, as described further in Section 2.2.3.

2.2 *Model Setup*

2.2.1 *Model Geometry*

The numerical model was developed based on existing conditions and dam arrangements at an unnamed mine site in Australia. The tailings dam is constructed using the upstream method and has been modelled in stages describing construction and deposition of the progressive lifts. The progression of dam construction and deposition analysed is presented conceptually in Table 1.

The initial pore water pressure conditions were defined by a steady-state condition and dependent on the initial water table, which was modelled based on an understanding of groundwater and tailings water level characteristics at this particular site. This initial regime was used as the 'parent' analysis in the modelling approach. Each of the following stages represent a 'child' analysis to the stage prior, modelled as transient seepage cases, but dependent on the 'parent' analysis for initial pore water pressure conditions. The main reasoning behind the selection of a transient seepage condition (while the authors are aware of the limitations and sensitivity of material model parameters in this analysis type), was to allow a time-stepped development of the phreatic surface, which in turn could be compared against measured piezometric readings from site operations (see Section 2.2.2).

Table 1. Start and end stages of Staged construction and deposition of modelled tailings dam.

Stage	**Modelled Scenario**
Start Stage 3 Construction (January 2011 to March 2012)	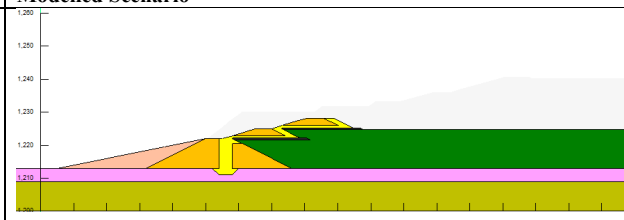
End Stage 6 Deposition (September 2019 to May 2020)	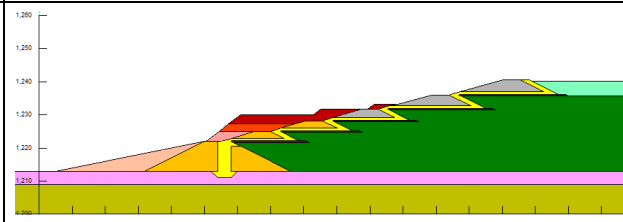

2.2.2 *Model Calibration*

"It is common for the rate of seepage through a tailings embankment to be estimated on the basis of a conventional flow net analysis assuming steady seepage conditions" (Mittal and Morgenstern 2011). However, as Stark et al. (2015) state, "there is interest in performing transient unsaturated seepage analyses to calibrate transient seepage models with piezometric data and investigate the level of conservatism with a design based on steady-state conditions." In the case of this research, the primary reason for utilising transient seepage analysis was to leverage nearly 10 years' worth of piezometric data and understanding. This was further supplemented by observations during the same period, to develop a model more reflective of actual conditions. This research focuses on transient seepage conditions as a result of boundary conditions, as opposed to a comparison between transient seepage and steady-state seepage behaviour.

The steps taken to calibrate the SEEP/W model against actual piezometer data were:

1. The push-in vibrating wire piezometer readings collected from site were embedded as a "Water Total Head" Boundary Condition. This represented the baseline 'target' for actual conditions:
   a. Readings have been collected approximately monthly since 2011;
   b. Individual 'Water Total Head' boundary condition functions were created for each piezometer to model the piezometer readings over time;
   c. This was then applied at the different stages of the tailings dam construction and deposition (when the piezometers were brought online), aligning well with the time-based transient seepage approach; and
   d. The piezometer locations are identified in Figure 1.
2. The model was cloned, and the 'Water Total Head' boundary conditions were removed. The material parameters were altered (hydraulic conductivity and anisotropy ratio, using a saturated material model) to simulate the baseline model. As the transient, saturated/unsaturated material models present a relatively complex visualisation of phreatic behaviour, taking an initial assumption of full saturation allowed a single phreatic surface to be the focus. This step is predominantly to ensure that the phreatic surface is appropriately trending through different materials, in terms of relative hydraulic conductivity and anisotropy ratios between the different material types. To test the sensitivity of the model simulating actual conditions and response to changing environments, the forced boundary conditions at the discrete piezometer locations would need to be removed or they would bias the phreatic surface.
3. Once the phreatic surface behaved as closely as possible to that generated from actual piezometer data, the material models were converted to saturated/unsaturated (suited to transient seepage analysis):
   a. In this research, the SEEP/W model adopted the software's built-in estimation methods as described in Section 2.2.3, using the same hydraulic conductivity as derived for the different materials during Step 2; and
   b. Modified boundary condition assumptions so that water total head outputs match piezometer readings.
4. The sensitivity of the model was tested through application of different External Condition Scenarios (Section 2.3).

By relying on the observational approach, this methodology presented a higher degree of confidence in the model and allowed the opportunity to then apply the external condition scenarios and simulate differences in response.

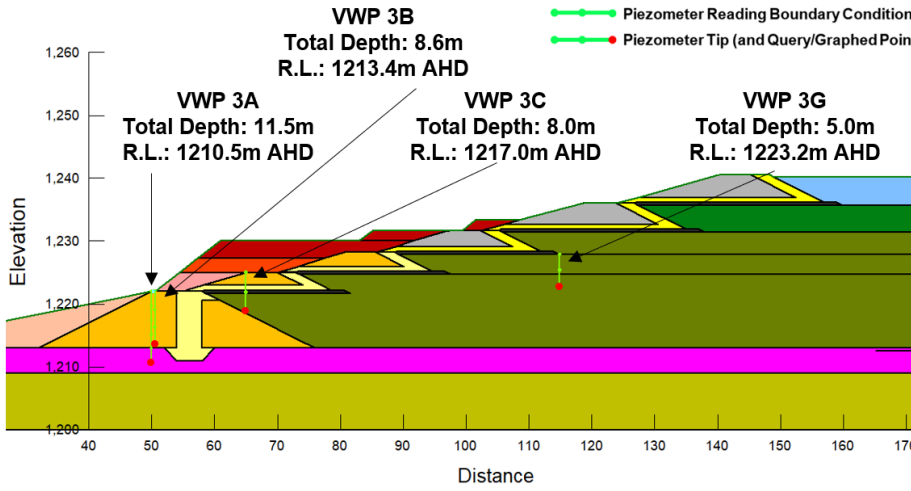

Figure 1. Location of push-in piezometer installations

2.2.3 *Material Parameters*

The material and associated parameters applied to the different regions within the model are given in Table 2. The material parameters shown are the end result of the model calibration exercise described (Section 2.2.2). All materials adopted the Fredlund-Xing-Huang estimation method for the hydraulic conductivity function.

Table 2. Material parameters adopted in SEEP/W model

Colour	Name	Saturated Kx (m/s)	Ky'/Kx Ratio	Material Model	Coefficient of Volume Compressibility /kPa	Sample Function	Saturated Water Content (%)
	1A	1×10^{-10}	1	Sat/Unsat	1×10^{-5}	Clay	12
	1A1	1×10^{-8}	1	Sat/Unsat	1×10^{-5}	Clay	12
	1C	1×10^{-6}	1	Sat/Unsat	1×10^{-5}	Clay	12
	3B	1×10^{-5}	1	Sat Only			
	3C Rock Fill	1×10^{-3}	1	Sat Only			
	Drain	1×10^{-6}	0.1	Sat Only			
	Foundation 1	1×10^{-8}	0.1	Sat Only			
	Foundation 2	1×10^{-11}	0.1	Sat/Unsat	3×10^{-5}	Clay	15
	Fresh Tailings	1×10^{-5}	0.5	Sat/Unsat	0.00012	Silty Sand	5
	Recently Placed Tailings	5×10^{-7}	0.75	Sat/Unsat	6×10^{-5}	Silty Sand	5
	Old Tailings	1×10^{-9}	1	Sat/Unsat	6×10^{-5}	Silty Sand	5
	Stage 4 Buttress	1×10^{-5}	1	Sat/Unsat	0	Silty Sand	3
	Stage 5 Buttress	1×10^{-5}	1	Sat/Unsat	0	Silty Sand	3
	Stage 6 Buttress	1×10^{-5}	1	Sat/Unsat	0	Silty Sand	3

The legitimacy of the material parameters was also compared against years' of experience and testing of the borrow materials onsite (for embankment construction), tailings behaviour, and observations from successive Cone Penetration Test (CPT) campaigns, as well as a comparison between modelled and actual conditions (see Section 2.2.2 for calibration exercise).

2.3 *External Condition Scenarios*

Three external condition scenarios were modelled to assess their influence on phreatic surface behaviour. These are described in Table **3**.

Table 3. External condition scenarios

External Condition	Reasoning	Approach	Cross-Section (shown at Stage 5 – Construction)
Calibrated Model	For comparison between cross-sections		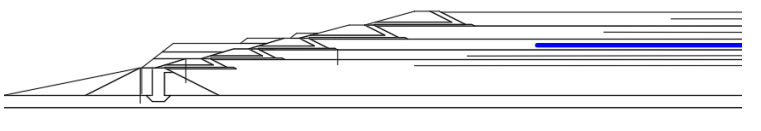
Pond level rise and beach width change.	"The location of the ponded water with respect to the embankment crest, or the width of the exposed tailings beach, is often the most important factor influencing phreatic surface location" (Vick 1990).	The "water total head" boundary condition line that modelled the decant water level in the dam was changed from being located 75 m from the embankment upstream toe, to being located 37.5 m from the beach-embankment intercept. The decant level was raised by 2 m to simulate pond level rise.	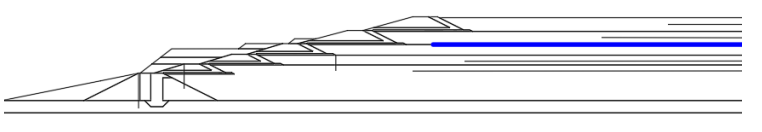 - Decant water level boundary condition (to right hand side of model) elevated from Calibrated Model. - Beach width reduced by 50% compared to Calibrated Model. - Material parameters equal to Calibrated Model.

Lateral variation of hydraulic conductivity.	"The variation in permeability is characterised by the ratio of tailings permeability at the spigot point (k0) to the permeability at the edge of the ponded water at the slimes zone (kL)" (Vick 1990).	Material changes were made to the different tailings Ky'/Kx' ratio (also known as the anisotropic ratio). The sensitivity of this was checked by changing the anisotropic ratio to 0.1 for all tailings materials.	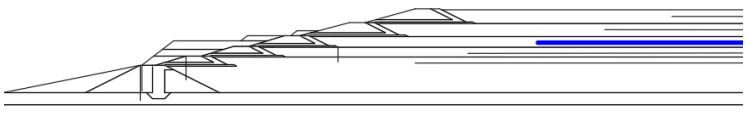 - Decant water level boundary condition (to right hand side of model) equal to Calibrated Model. - Beach width equal to Calibrated Model. - Material parameters changed to decrease anisotropic ratio.
External loading.	While potentially a function of many different influences, the excess pore water pressure generated as a result of a theoretical load increase was checked.	A conservative approach was taken to simulating external loading in order to represent the scenarios entirely in SEEP/W (as opposed to adopting a coupled stress/PWP analysis in SIGMA/W, for example). It was assumed that application of a 20 kPa load could be simulated by raising the "water total head" line by 2 m, representing a short-term scenario where the pore water pressure also increased by 20 kPa at this location and not considering the dissipation of pore water pressures in the long term. This was applied to the measured decant level during Stage 3 construction for Piezometer 3C and during Stage 5 construction for Piezometer 3G, to simulate a temporary increase coincident with the piezometer location.	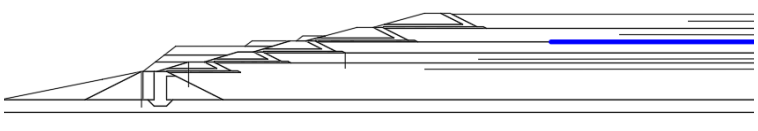 - Decant water level boundary condition (to right hand side of model) elevated from Calibrated Model during Stage 5 Construction. Decant water level boundary condition equal to Calibrated Model during all other stages. - Beach width equal to Calibrated Model. - Material parameters equal to Calibrated Model.

2.4 *Assumptions*

Several key assumptions were adopted due to the limitations of a numerical model to simulate reality or in order to be able to model the scenarios in the most practical way possible. These included, but were not limited to:

- Instrumentation remained fully intact and operable, despite changes in external conditions;
- The piezometers modelled assume perfect installation, with no anomalies as a result of installation methodology;
- Materials incorporated were considered homogeneous;
- Two-dimensional behaviour was adopted. No consideration was given to any three-dimensional influence, including the likelihood for induced conditions to dissipate laterally or take a different path of least resistance;
- The materials and phreatic conditions were developed based on the deposition and construction phases; however, this development did not allow for modelling of progressive filling of tailings material aside from that captured by the decant pond level rise. This may have some influence on the magnitude of change that is observed at the transition between deposition and construction phases, however considering the phreatic surface being strongly influenced by the decant pond level (which was modelled as a hydraulic boundary, water total head against time), the results are considered representative for the purpose of this research; and
- Transient flow conditions were adopted in the numerical models, based on typical flow conditions at tailings dam facilities. Steady state conditions are still considered relevant (albeit conservative when determining pore water pressure) and are applicable in line with Darcy's equation.

3 RESULTS

The quantitative change as a result of the External Condition Scenarios was measured at the locations of the piezometers, as described in Figure 1. These represented:

- 3A: Pore water pressure in the foundation below the initial dam;
- 3B: Pore water pressure at the base of the initial dam embankment;
- 3C: Pore water pressure within the tailings beneath the first raise; and
- 3G: Pore water pressure in the tailings below the third raise.

Within the transient analysis, particularly when considering the saturated/unsaturated material model, the phreatic surface is much more variable than that presented in a steady-state seepage model. Hence, the calibration focused on reaching as near as practicable the total head elevation at different piezometer points. The results of the calibration, showing total head elevation against time, are shown for Piezometer 3C and Piezometer 3G in Figure 2 and Figure 3, respectively. These piezometers were selected as representative based on the quality of their installation and the reliability of the data from onsite observations.

The 'actual piezometer data' plot is generated by the piezometer readings onsite, 'calibrated' shows the modelled seepage profile without the piezometer-enforced boundary conditions, while the 'pond level rise', 'lateral variation' and 'external load' reflect the different external condition scenarios.

It is important to recognise the limitations of the 'calibrated' model in reflecting the measured conditions onsite. Evidently, the fluctuations in onsite data would be near-impossible to model perfectly in a theoretical scenario, which assumes consistent conditions as described in Section 2.4. Hence, the difference between the 'actual piezometer data' and 'calibrated' conditions is suggested to be due to actual external conditions that could not be appropriately considered/accounted for in the calibrated model.

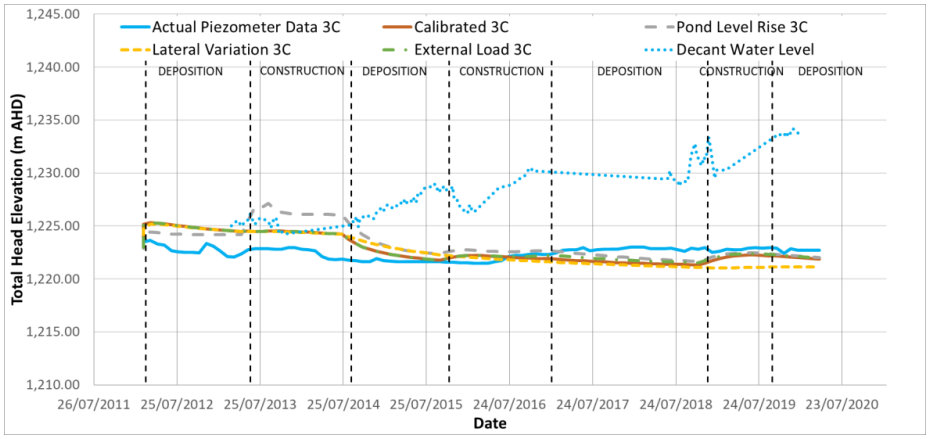

Figure 2. Total Head Elevation against time for Piezometer 3C

Piezometer 3C (Fig. 2) showed a generally decreasing trend over time. This is largely attributed to a drain that was installed between the Stage 1 and Stage 2 embankments (1222 m Australian Height Datum (AHD)). This drain acted as a "sink" and was modelled to simulate discrete drainpipes installed through the clay liner for control of seepage water by lowering the phreatic surface. As the total head elevation increases, it is expected that the pore water pressures recharging from the decant pond would dissipate through this drain more readily (due to the total head difference), in turn seeing the total head elevation readings converge over time toward the approximate elevation of the drain and with relatively less influence from external conditions. Piezometer 3C did not exhibit a similar, distinct response to changes in decant water level, nor changes between construction (despite buttress placement above 3C in late 2014 and again in late 2015) and three deposition phases when compared against Piezometer 3G (Fig. 3).

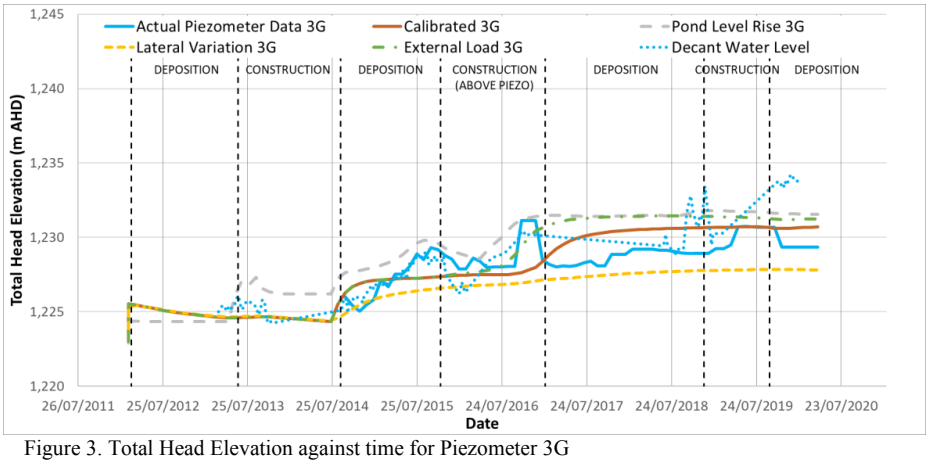

Figure 3. Total Head Elevation against time for Piezometer 3G

Piezometer 3G (Fig. 3), showed the greatest effect from introduction of external condition scenarios, anticipated due to the proximity to the decant pond, greatest influence of construction loading and subsequent porewater pressure increase, and also the reliability of the installation method and condition of this piezometer to represent actual conditions. The data presented some observable trends:

- The magnitude of variance between the actual piezometer readings and the calibrated model observed:
  - 'Lateral hydraulic variation' indicated a maximum total head difference of 2.9 m (06/03/2018);
  - 'Introduction of an external load' presented a maximum total head difference of 2.5 m (15/12/2016); and
  - 'Pond level rise' presented a maximum total head difference of 3.5 m (16/10/2017).
- A distinct inflexion point could be observed between a deposition period and a construction period. This is related to the assumption (Section 2.4) within the model that does not allow for progressive filling of tailings. In reality, it would be expected that this change would still occur in the phases that it does, however it would be expected gradually over time as related to the gradual increase in pore water pressure, with a peak at time of construction of the embankment construction in this local area (for Piezometer 3G, this could be suggested to be around 16/09/2016);
- At the earlier and lower elevation stages of the tailings dam construction and deposition, both the actual piezometer data and modelled trends were observed to reflect the changes in decant water level as tailings deposition typically occurred directly above the piezometers and hence the closer proximity was anticipated to facilitate connectivity between the decant pond and piezometer locations. However, in later deposition stages upstream, the data did not reflect changes as readily and it could be suggested that the piezometer level was a function of the naturally descending phreatic surface due to lateral separation of the decant pond (recharging point) and piezometer location (discussed further in Section 4);
- The behaviour described in the previous point was exacerbated by the boundary conditions modelled for 'pond level rise' (reduced beach width and hence increased connectivity between decant recharge and piezometer response);
- The 'introduction of external load' and 'pond level rise' external conditions increased the total head elevation and shortened the response time;
- Comparing the pore water pressure values at different piezometer locations for the 'introduction of an external load' at Stage 5 construction, it was observed that the pore water pressure divergence from the 'calibrated' condition was observed early in the stage for Piezometer 3G (23/10/2015), but was delayed from this for Piezometer 3C (20/01/2016): a three month difference; and
- The change in 'lateral hydraulic variation' external condition reduced the total head elevation and showed a less significant response to changes in deposition/construction cycles.

The overall magnitude of the change in total head elevation was generally achieved, and the modelled response was within 3.7 m (inclusive of data spikes) or 2.2 m (not inclusive of data spikes), when comparing onsite piezometer readings against elevation levels generated within the calibrated model.

4 DISCUSSION

The numerical modelling calibrated total head elevations against push-in vibrating wire piezometers readings, then applied external conditions to assess the effect on piezometer response and reliability. In summary, the findings showed that:

- While pore water pressures in Piezometer 3C were influenced by the drain between Stage 1 and Stage 2 embankments, Piezometer 3G was observed to present the readings most influenced by the decant water level. This influence was more prevalent in the earlier stages of the life cycle (when the piezometer was closer to the decant pond) compared to the later stages of the life cycle. This is suggested to indicate a few key points:
  - For large dams, piezometers that are installed at the earlier stages of construction are more readily influenced by the decant pond level and the column of saturated tailings that was recently placed above their location;
  - As the dam raises, and the decant pond (or recharge point) and tailings placement become further from the piezometer tip location, the time taken for the piezometer to respond to a

change in phreatic condition as well as the resulting behaviour are less representative of the change itself; and
  - This suggests that variables such as material parameters, boundary conditions, anisotropy ratios, and transient flow conditions should be considered in order the understand the overall phreatic condition of the dam as these factors complicate the phreatic behaviour and the resultant pore water pressures when compared against simplified steady-state modelling.
- While the tailings dam and water balance were generally managed well at the case mine site, the hypothetical pond level rise and introduction of an external load increased the total head elevations. Piezometer 3G's response suggested that pond level rise caused the largest rise in total head elevation. This result aligns with Vick's (1990) theory, which stated that pond level rise "is often the most important factor influencing phreatic surface location". The hypothetical 'lateral variation in hydraulic conductivity', which reduced the anisotropic ratio, reflected a reduction in pore water pressure values;
- The different external conditions reflect different total head elevation behaviours;
- Observing the Stage 5 embankment construction as an individual event, a difference in response time between piezometer locations was observed. Stage 5 construction phase was modelled to simulate a 2m rise in pore water pressures. The pore water pressure divergence from 'calibrated' conditions occurred 3 months earlier for the piezometer it was constructed directly on top of (Piezometer 3G), than for a piezometer 50m downstream and with its tip installed at an elevation lower by 4m (Piezometer 3C). This suggests that a change in phreatic conditions upstream is not immediately reflected downstream, and should be considered in terms of a delayed and prolonged response as the effect transitions through the dam;
- In addition, while both trends started to re-converge with the 'calibrated' conditions following the event, neither piezometer suggested that excess pore water pressures had yet dissipated from the event at the end of available readings (4.5 years later). This is considered to be the result of excess pore water pressures generated during Stage 5, which trended towards the calibrated condition in later stages. If the modelling were continued, it is anticipated that the trends would re-converge; and
- The fluctuations in total head elevation measured by the piezometers during the early stages of dam deposition/construction (start of measurements to 25/01/2017) were best simulated by the pond level rise external condition. Between 25/01/2017 and end of measurements, the calibrated pore water pressure appeared to best simulate the total head elevation measured from the piezometers. This was suggested to be because, after 2017, the external condition changes occurring upstream of the piezometers to be largely influenced by the naturally descending phreatic surface and the installed drains, in this particular dam.

Depending on the amount and duration of data available, which can be obtained from existing and new tailings dams, the ability to iteratively update the seepage (and in turn stability) models to assess tailings dam performance is fundamentally achievable. It is anticipated that designers and operators could gain value in developing seepage models that are forced to match the piezometer readings (by utilising boundary conditions), and by comparing the phreatic surface profile with that assumed in the initial and staged designs.

It is not anticipated that this approach would be feasible without having accurate monitoring data to rely on. Hence, the authors recommend the use of steady-state seepage as an appropriate approach during tailings dam design phases. The risk associated with variable tailings dam environments, the inability to predict this prior to the dam being built and hence the assumptions made in modelling that contradict this variability (such as assuming homogeneous units), and the implications that this may have for the true seepage behaviour, is not considered to be a safe nor appropriate approach.

It is suggested that future modelling could be improved through better understanding of the initial conditions. Ideally, the dam site should be modelled over its entire lifecycle (considering historical land use and pre-mining state), to create a holistic model of the dam's lifecycle. For this research; however, the objective was mainly to observe relative change and hence this was not explored.

5 CONCLUSION

This research demonstrates a valid approach to utilising the observational approach, in combination with a calibrated numerical model, to improve understanding of unique tailings dam responses to external conditions. The phreatic behaviour of a tailings dam in Australia was numerically modelled based on the measurements recorded from a cross-section instrumented with push-in vibrating wire piezometers. By calibrating the model against the behaviour observed from the piezometer readings, the research allowed the sensitivity of external conditions on the tailings dam to be assessed. It was observed that external conditions more readily influenced later stage construction and deposition. For the case study undertaken, this was suggested to be as a result of the installation of embankment toe drains between the Stage 1 and Stage 2 embankments (at the end of Stage 4 construction), as well as the proximity of piezometer locations to the decant pond and recently placed, saturated tailings columns. The hypothetical pond level rise and introduction of an external load increased the total head elevations from measured and calibrated values, with pond level rise causing the largest magnitude of change. Decreasing the anisotropy ratio (lateral variation of hydraulic conductivity) reduced the pore water pressures. Different external conditions were observed to influence the way that the total head elevation trended over time, and the response time when alternating between construction and depositional phases differed between the different external conditions.

When comparing a discrete event that influenced the phreatic condition nearby an upstream piezometer, the downstream piezometer was also observed to respond to the same change, but with a 3-month delay. Based on this, the author reiterates that a progression to real-time monitoring may not necessarily reflect full understanding of the phreatic condition due to limitations of the piezometer or the conditions that it is subject to. Significant changes to the phreatic condition could occur upstream within the dam before they are identified by the downstream piezometer. An interpolation between the pore water pressures read on any two piezometers in the hope to understand the phreatic condition through the dam would be a coarse assumption when considering the complexity of transient phreatic response to external conditions, as demonstrated in this research.

The methodology is able to add value to an observational approach. The case for adopting steady-state seepage during the design phase is reiterated, where this method relies on accurate monitoring data trends that would not exist until some time after the dam is established and operating.

6 REFERENCES

Chambers, D (2016). *Tailings Dam Failures 1915-2016.* <http://www.csp2.org/tsf-failures-1915-2017> (May 11, 2018).

Davies, M, Martin, D & Lighthall, P 2002. *Mine Tailings Dams - When Things go Wrong.*

GEO-SLOPE International Ltd. (GEO-SLOPE) (2012). "Seepage Modelling with SEEP/W", viewed 08 June 2020, <http://downloads.geo-slope.com/geostudioresources/8/0/6/books/seep%20modeling.pdf?v=8.0.7.6129>

LePoudre, D.C. 2015. *Examples, Statistics and Failure modes of tailings dams and consequences of failure.* PowerPoint slides, REMTECH.

Mittal, H.K. and N.R. Morgenstern. 1976. "Seepage Control in Tailings Dams." *Canadian Geotechnical Journal*, Vol. 12, pp. 235-261.

Naeini, M, & Akhtarpour, A 2018, "A numerical investigation on hydro-mechanical behaviour of a high centreline tailings dam", *Journal of the South African Institution of Civil Engineering*, Vol. 60, No. 3, pp. 49-60

Robertson, A.M. (2012). "FMEA Risk Analysis: Failure Modes and Effects Analysis." PowerPoint slides.

Stark, T.D., Jafari, N.H., Leopold, A.L., & Brandon, T.L. 2015. Soil Compressibility in Transient Unsaturated Seepage Analyses. *International Foundations Congress and Equipment Expo, Proc. intern. symp., San Antonio,* 17-21 March 2015: Texas: American Society of Civil Engineers

U.S. Environmental Protection Agency (US EPA) 2010, Technical Report – Design and Evaluation of Tailings Dams, EPA 530-R-94-038, NTIS PB94-201845, viewed 08 June 2020, <https://nepis.epa.gov/Exe/ZyPURL.cgi?Dockey=2000EF89.TXT>.

Vick, S.G. 1990. Planning, design, and analysis of tailings dams. Vancouver: BiTech.

Lupin Mine – A Case Study in Adaptive Tailings Management

Alvin Tong
Stantec, Calgary, Alberta, Canada

James McKinley
Stantec, Calgary, Alberta, Canada

Karyn Lewis
Lupin Mines Incorporated, BC, Canada

ABSTRACT: The Lupin Gold Mine (Lupin) is located approximately 285 km southeast of Kugluktuk, Nunavut and is owned by Lupin Mines Incorporated (LMI). The original tailings closure and management plan at Lupin was to isolate the tailings within a tailings containment area and then cover the tailings with 1 m of esker. Data indicated that the active layer was extending deeper than 1m and that it would require thicker cover to encapsulate the tailings completely within permafrost. To mitigate the risks with potentially doubling the cover thickness, Lupin evaluated the use of a partially saturated cover. To confirm performance of the partially saturated cover, LMI conducted a variety of field investigations and climate modeling. Results demonstrated that saturation is being maintained in the cover, there is no visible oxidation of tailings, and the water quality has remained largely unchanged since the installation of the standpipes nearly 20 years ago.

1 INTRODUCTION

The Lupin Gold Mine (Lupin) is located approximately 285 km southeast of Kugluktuk, Nunavut and is owned by Lupin Mines Incorporated (LMI), a wholly owned indirect subsidiary of Mandalay Resources Corporation. Lupin is a remote high-arctic site that is situated in an area of continuous permafrost and is only accessible year-round by air.

The original (late 1980s to mid-2000s) tailings closure and management plan at Lupin, as with a number of other mines in the north, was to isolate the potentially acid generating (PAG) tailings within permafrost-core dams in a tailings containment area (TCA) and then cover the tailings with 1 m of esker for encapsulation by permafrost (Figure 1). As part of the long-term performance monitoring of the TCA, thermistors were installed to monitor the ground temperature profile and dam frozen core conditions. After decades of monitoring, ground temperature data indicated that the annual thaw zone (active layer) was extending deeper than 1m and that it would require thicker cover to encapsulate the tailings completely within permafrost if the temperature trend continued.

To mitigate the risks to the mine plan, schedule, and costs associated with potentially doubling the esker cover thickness in order to meet the permafrost encapsulation goal, Lupin evaluated the use of a partially saturated (store and release) esker cover to maintain a high degree of saturation in cover material and tailings and to limit acid generation. The partially saturated cover concept does not rely on permafrost encapsulation, is significantly less sensitive to annual temperature changes or global warming, and offers better support for vegetation, making it ideal for a site such as Lupin. This change in closure concept was approved in 2006 as part of the interim abandonment and reclamation plan (IARP). As part of the closure concept change, standpipes were installed in one of the tailings cells to observe water quality in the cover. In 2017, LMI decided to end their Care and Maintenance period and submitted a Final Closure and Reclamation Plan (FCRP) for Lupin to the Nunavut Water Board (NWB) in 2018. Stakeholder parties submitted various requirements for acceptance of the plan, which included:

- One-time geophysical survey conducted along two selected dams to confirm the condition of frozen cores
- Analysis of a range of emission scenarios (low to high future forcing) from multiple climate models and considering multiple parameters (precipitation, permafrost thaw, etc.), which will be determined following consultation with climate change experts, for consideration in the Final Reclamation and Closure Plan
- One-time visual inspection (test pits) to ground truth the status of the cover nearby one of the installed standpipes (note: water quality data will be collected from all standpipes and presented in the context of historical water quality data from the standpipe information)

In addition to the work requested by stakeholder parties, LMI also collected data from thermistors, moisture meters, and standpipes installed throughout the TCA to monitor permafrost conditions within the dams and cover, and the degree of saturation within the cover. This article presents the findings from the various field tasks and climate modeling in the context of long-term TCA closure design and performance monitoring related to predicted climate change in the north.

2 METHODOLOGY

In order to confirm performance of the partially saturated cover, establish a baseline for climate modeling, and generally improve the confidence of the stakeholder parties on the closure design, a number of tasks were completed.

2.1 Instrumentation

Thermistors were installed in the TCA between 1995 and 2004 to monitor the performance of the dams and tailings covers (Figure 1). Of the seven functioning thermistors, five are in the perimeter dams and two are in the internal dams. The thermistors were read monthly during operation up until 2006, and then only the dam thermistors were read semi-annually during Care and Maintenance. The most recent readings were collected in 2019. The thermistor data trends were used to established current conditions and the site-specific baseline for thermal modeling.

Standpipes were also installed in the oldest tailings cell (Cell 1) in the early 2000s to monitor the water quality and water levels within the cover. These standpipes were retrofitted in 2019 for long-term continuous data collection. Standpipes were sampled in 2019 to compare the water quality in the esker cover with historical data from 2002 to evaluate if the cover was indeed limiting oxygen ingress into the tailings and associated acid production. A minimum of three wellbore volumes were purged from the standpipes prior to sample collection. Samples were analyzed for general and inorganic parameters, and total metals.

To provide insight into the performance of the partially saturated cover, volumetric moisture sensors were installed in the Cell 1 and Cell 3 covers in 2018. The TEROS-12 VWC sensors measure volumetric water content, temperature and electrical conductivity every 12 hours and record the readings to dataloggers. Both cells each have one string of five sensors installed within the cover (C2VWC and C3VWC). The sensor spacings and background material are provided in **Error! Reference source not found.**. The most recent readings were downloaded in 2019.

Table 1 – VWC Installation Details

VWC ID	Cell 1-1		Cell 3-1	
	Depth (m)	Material	Depth (m)	Material
Port 5	1.0	Fine Sand (Cover)	0.35	Sand and Gravel (Cover)
Port 4	1.2	Fine Sand (Cover)	0.5	Sand and Gravel (Cover)
Port 3	1.4	Fine Sand (Cover)	0.6	Sand and Gravel (Cover)
Port 2	1.6	Fine Sand (Cover)	0.7	Sand and Gravel (Cover)
Port 1	1.8	Tailings	1.0	Sand and Gravel (Cover)

The intent of the sensors is to define the degree of saturation throughout the year at various depths within the cover. It should be noted that sensors register ice as a dry void. Thus, as the pore water freezes and ice forms, the moisture content readings in the sensors drop sharply. In order to calculate the volumetric water content, an assumed void ratio is assigned to each sensor string based on the cover material type. The assumed void ratio for Cell 1 cover is 0.42 which corresponds to a fine sand and Cell 3 cover is 0.33 which corresponds to a gravelly sand.

2.2 Geophysical Survey

One internal (Dam 3D) and one perimeter dam (Dam 4) were selected by for geophysical surveys. These dams were specifically selected because they both have thermistors installed for calibration. Aurora Geosciences Ltd. completed the surveys and the methods in 2019. Ground penetration radar (GPR) and Electrical Resistivity Tomography (ERT) surveys were selected as the best combination to characterize the presence and configuration of the frozen cores within the dams. The results were used to confirm the assumption of a continuous frozen core as requested by the stakeholder parties.

2.3 Field Investigation

In 2019, two test pits were excavated in Cell 1 and Cell 2, the oldest covered cells, to visually confirm the cover performance (Figure 1). Test pits were advanced by an excavator until frozen material was encountered. Mr. Alvin Tong, P.Eng., a senior Geotechnical Engineer with Stantec, oversaw the excavation of the test pits. The test pit in Cell 1 was dug nearby a standpipe to confirm the cover thickness and the tailings contact for water level confirmation. The goal was to confirm the depth of cover, saturation zone, and the status of the tailings beneath as requested by the stakeholder parties.

2.4 Thermal Modeling

Information from the Environment Canada and Climate Change (ECCC) report titled "Changing Climate Report" (CCCR, 2019) was used for the thermal modeling, most specifically Chapter 8 Section 8.4.1: Changes in northern Canada. This section references two northern Canada emission scenarios and the ECCC climate change expert noted that: "the range of projected changes provided for various global emission scenarios (i.e., Representative Concentration Pathways or RCPs) in Canada's Changing Climate Report are derived from an ensemble of 29 climate models". The projected increase in mean annual air temperature (MAAT) from the ECCC was based on a distribution of outcomes from the 29 CMIP5 (Coupled Model Intercomparison Project) climate models. The increase in MAAT ranges anywhere from 2°C to 9°C over the next 100 years.

The projections from ECCC were used to simulate three emission scenarios (low: +2°C, medium: +4°C, and high-emissions scenarios: +8°C). Using the baseline data established by the thermistors, LMI performed thermal modelling to assess the potential for long-term permafrost thaw of frozen tailings containment structures (dams) under the three climate warming scenarios to evaluate the potential impact of the climate change to the frozen core dams.

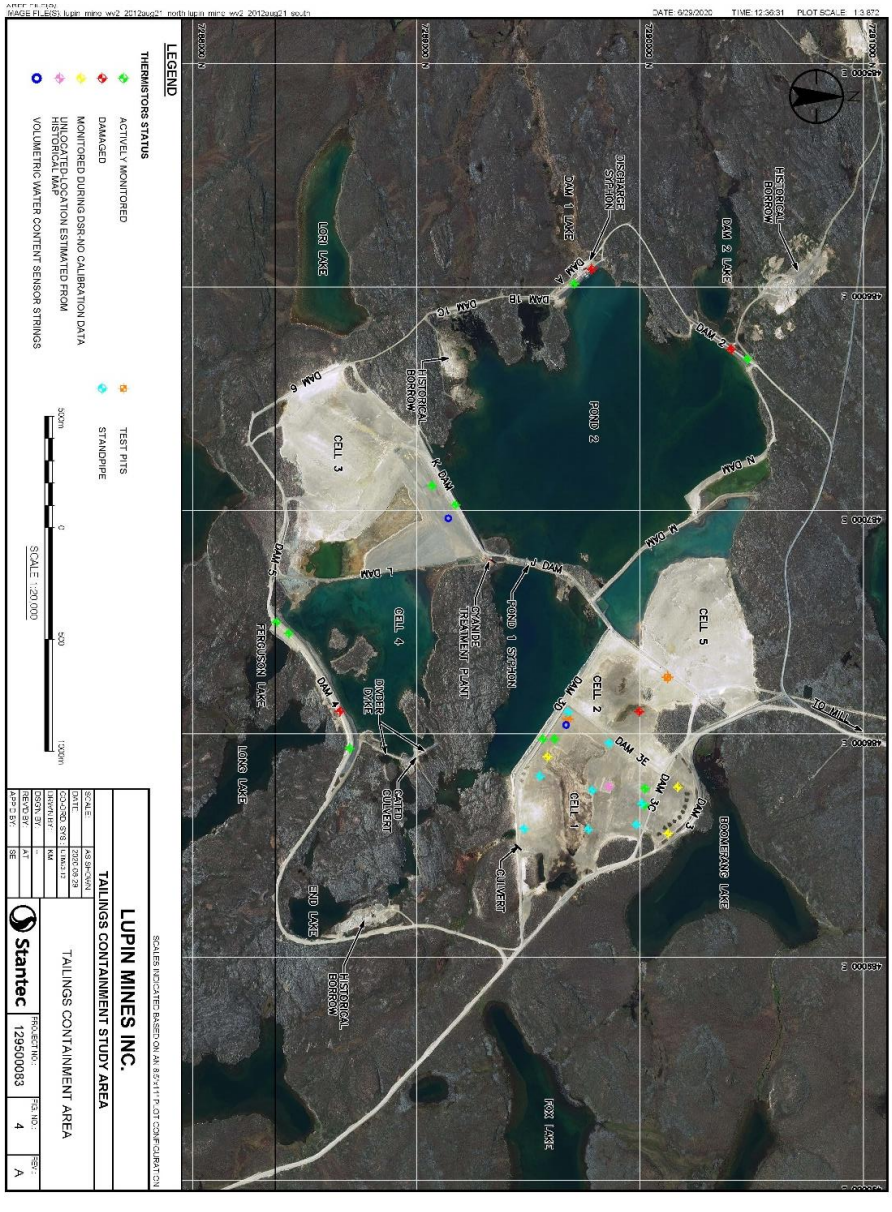

Figure 1 – Site Map with Associated Instrumentation

3 RESULTS

3.1 Thermistors

To provide a point of reference for this article, selected data series between August and September, from 2010 to 2019, are shown for comparison, while maximum values are calculated from the entire series from the first available records to 2014. For the perimeter dams, the five functioning thermistors are less than 20m deep. Representative thermistor readings from Dam 1A are shown in Figure 2 below. The data suggests the 2019 readings are within the historical variations, taking into account annual climatic variations and the time of reading. Generally, the active layer (thaw zone) ranges from 2m to 3m depth, as interpolated by the 0°C gradient line. This active zone is deeper than the thickness of esker covering the tailings (≈1m).

Figure 2 – Representative Thermistor Readings (Dam 1A)

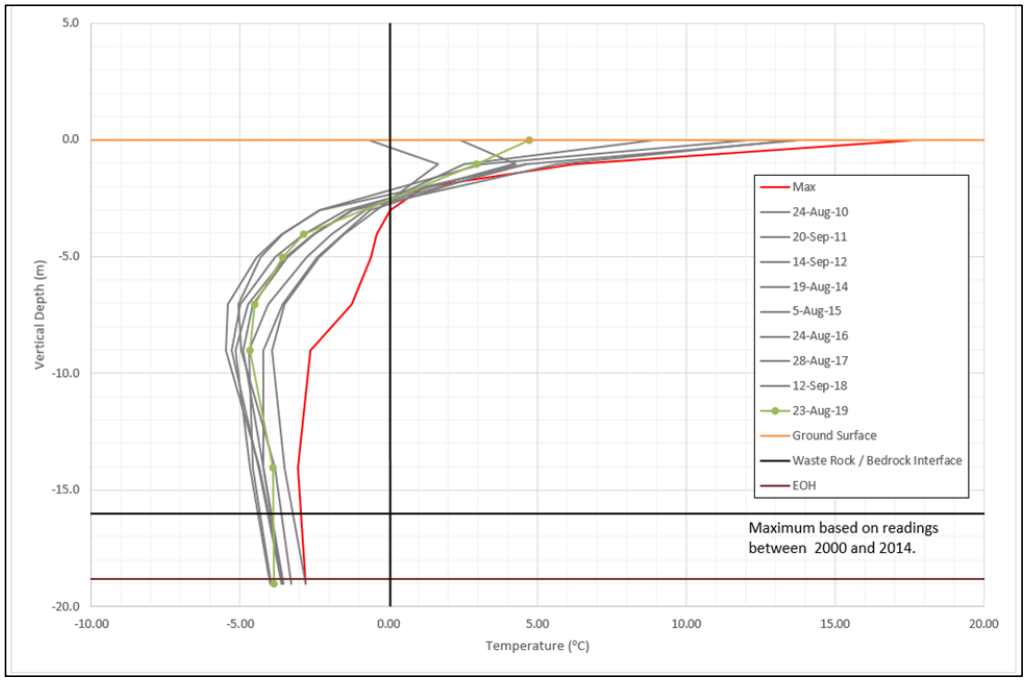

3.2 Standpipe Data

Cover saturated thickness, estimated based on the depth of water in the wells, and water quality results are presented in Table 2 and Table 3, respectively, with historical data from Holubec (2005). The water levels further support the conclusion that the cover is partially saturated. The water quality comparison splits each parameter into two columns in the tables; the first column represents historical data collected in 2002 and the second column represents data collected in 2019. Field results indicate that water quality has remained largely unchanged since the installation of the standpipes nearly 20 years ago.

Table 2 – TCA Cell 1 Cover Saturated Thickness

Standpipe ID	Cover Saturated Thickness - (m)	
	2002	2019
P-2	0.32	0.44
P-3	0.22	0.17
P-4	0.49	0.58
P-5	0.94	0.74
P-6	0.62	0.61
P-7	0.21	0.37
P-8	0.42	0.59
P-9	0.20	0.28

Table 3 – TCA Cell 1 Standpipe Water Quality Results

Standpipe ID	pH		Arsenic-Total (mg/L)		Copper-Total (mg/L)		Cyanide-Total (mg/L)		Lead-Total (mg/L)		Nickel-Total (mg/L)		Zinc-Total (mg/L)	
	2002	2019	2002	2019	2002	2019	2002	2019	2002	2019	2002	2019	2002	2019
P-2	3.96	4.80	0.005	0.008	0.310	0.177	0.002	<0.0050	0.025	0.001	1.320	0.319	0.620	0.191
P-4	5.70	5.10	0.004	0.013	0.190	0.079	0.060	<0.0050	0.010	0.001	0.850	0.318	0.320	0.120
P-5	5.00	5.10	0.020	0.676	0.250	0.023	0.004	<0.0050	0.020	0.003	3.510	0.550	0.910	0.152
P-6	5.90	5.10	0.004	0.078	0.006	0.013	0.002	<0.0050	0.002	0.001	0.015	0.125	0.035	0.049
P-8	4.90	4.90	0.019	0.058	0.042	0.288	0.002	<0.0050	0.003	0.004	1.110	0.661	0.300	0.342

3.3 Moisture Meters

The data from 2019 indicates at both sensor strings (Cell 1 and Cell 3) there is a zone of saturated material above the tailings. The majority of the sensors show frozen conditions between October/ November and June/July. There is a spike in saturation percentage in the top sensors in June/July signaling overall thawing. The 2019 data indicates that the deeper sensors on the strings were above 85% saturation once thawed. Representative moisture sensor readings are shown in Figure 3 below. An 85% saturation at the tailings contact would curtail the ARD potential according to MEND (2009). Due to the constant void ratio used for the calculation, the Port 5 (near surface) reports an above 100% saturation,

and Port 3 (middle of cluster) report a <85% saturation despite the ports above and below recording greater degrees of saturation.

Figure 3 – Representative Moisture Sensor Readings

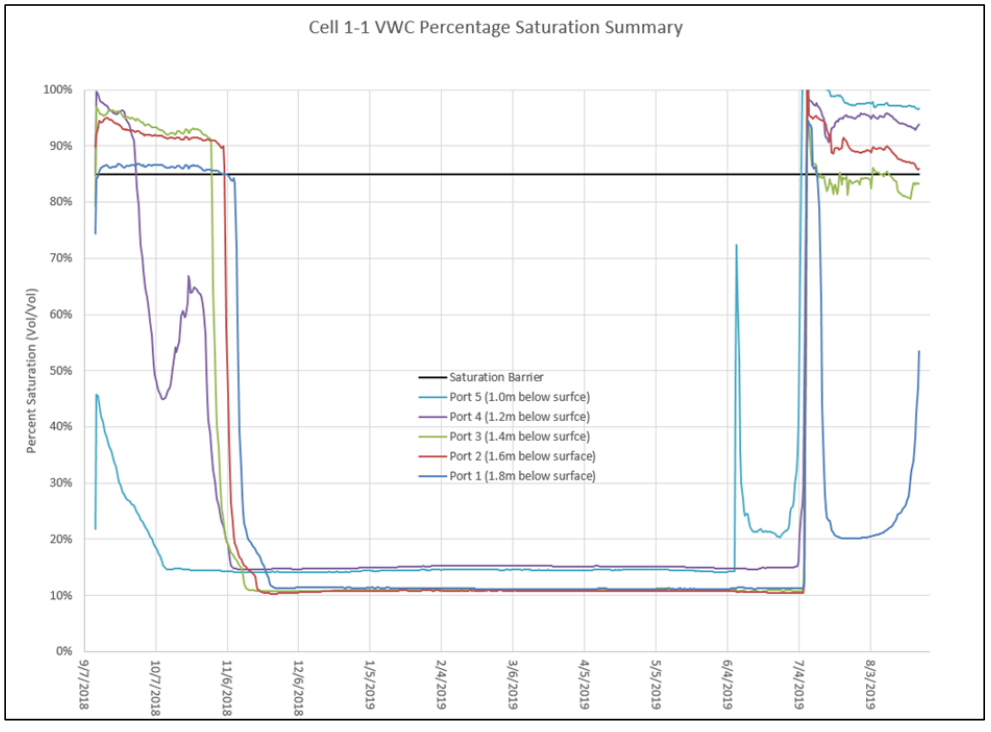

3.4 Geophysical Survey

Both the ERT and GPR results shows a mostly continuous reflective surface, indicating no break or absence in the ice core of Dam 3D or Dam 4. The surveys indicated that frozen material was encountered at a depth of approximately 2.5m within the dams, which corresponds to sub-zero temperature readings from the existing thermistors on both dams. The combination of the surveys and the thermistor readings indicate that the TCA dams contain a continuous frozen core. Figure 4 below show a clip of the ERT results along Dam 3D.

Figure 4 – Clip of ERT result for Dam 3D

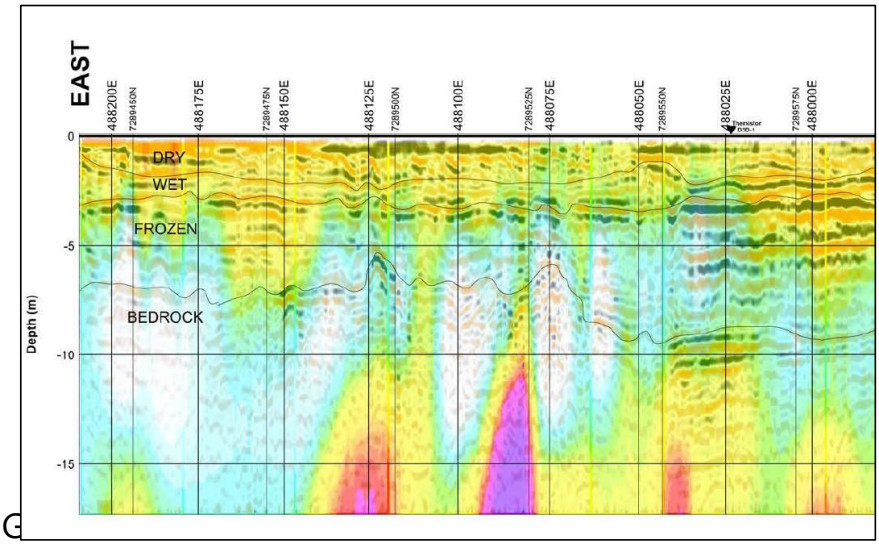

FIG

3.5 Test Pit Observations

The weather during the test pit excavation work was clear and warm. The general condition of the cover was dry without any nearby ponded water. Test Pit 1 was excavated within Cell 2, which was covered in 2004. The cover material was observed to be a well graded sand with some gravel. Wet material was encountered approximately 0.6 m below ground surface (bgs). A thin layer of cold, wet tailings was encountered approximately 1.2 m bgs and frozen tailings was encountered approximately 1.3 m bgs. No oxidized tailings were observed in the test pit. Furthermore, a zone of 0.6m of wet to saturated cover was found above tailings. A photograph of the test pit is provided in Figure 5 below.

Figure 5 - Test Pit 1 Photograph and Descriptions

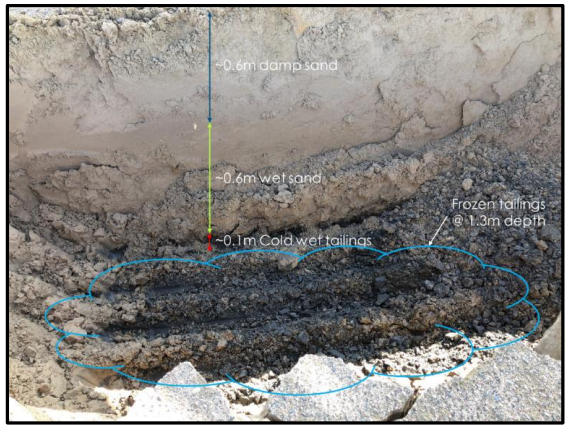

3.6 Thermal Modeling

Two emission scenarios are presented in this paper, low and high, as they represent the extremes of the design criteria. In the low-emissions scenario (LES), which involves a MAAT increase of approximately 2°C, the maximum annual thaw depth (termed the active layer depth) in 1995 is 2.3 m, which deepens to 2.8 m by year 2100, indicating an active layer thickness increase of 0.5 m (Figure 6). The LES does not result in long-term progressive permafrost thaw.

Figure 6 – Low-Emissions Scenario Results

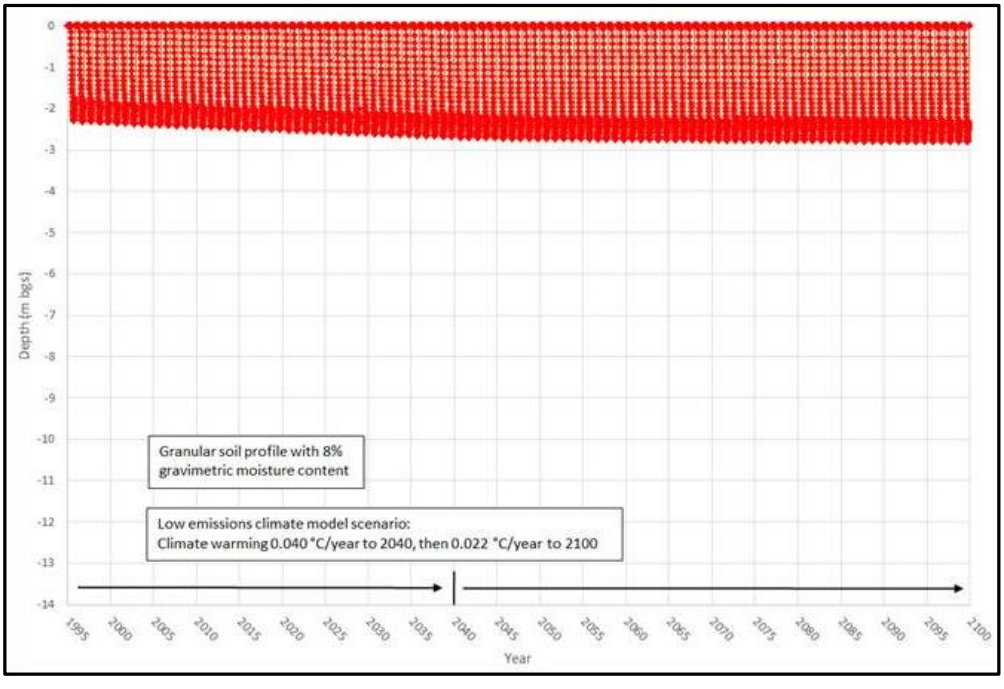

In the high-emissions scenario (HES), which involves a MAAT increase of approximately 9°C, the maximum annual thaw depth (termed the active layer depth) in 1995 is 2.3 m. Climate warming causes small incremental increases in the depth of the active layer each year until about 2075. After 2075, the annual winter frost depth does not penetrate to the base of the active layer (top of permafrost), and long-term progressive permafrost thaw deepening begins after that point in time. By the year 2100, the top of the permafrost is predicted to located 14 m below ground surface (Figure 7) under the HES. This means that a closure design could not rely on permafrost encapsulation as a control measure under the HES.

Figure 7 – High-Emissions Scenario Results

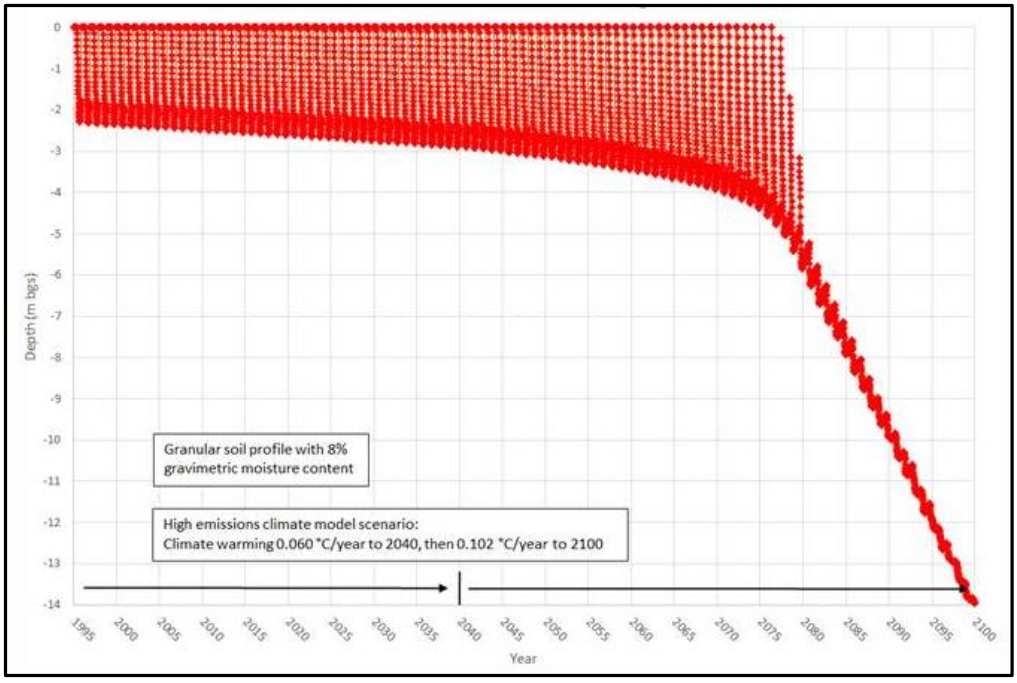

CONCLUSIONS

Thermistor readings demonstrated that the active zone (2-3 m) within the Lupin TCA extends lower than the contact between stored tailings and esker cover (~1 m). Given the depth of the active zone, a TCA closure plan that relied on permafrost encapsulation would not be appropriate for the site. Further to the current conditions, thermal modeling indicates that the active zone will deepen significantly, using site specific conditions, given the ECCC high-emissions scenario and the associated temperature increase of approximately 9°C. It is becoming increasing important for projects in the north to not only demonstrate that their closure technologies are appropriate given the current climatic environment, but that they will continue to be appropriate under potential climate change scenarios.

Field confirmation investigations (test pits and standpipe measurements) and instrument readings demonstrated that partial saturation is being maintained in the esker cover, there is no visible oxidation of tailings beneath the cover, and the water quality has remained largely unchanged since the installation of the standpipes nearly 20 years ago. Although the TCA closure would not have functioned adequately with permafrost encapsulation, the closure has functioned and continues to function adequately with the partially saturated cover. Although there is significant uncertainty regarding the extent to which climate change and temperature increases in the north will occur, the TCA closure cover at Lupin Mine should continue to function as designed, regardless of the extent of temperature increases. Any increases in the frequency and intensity of rainfall as a consequence of climate change will only serve to increase the moisture stored in the TCA cover material.

As part of the TCA closure plan (Holubec, 2005), seepage out of the TCA under a fully melted scenario (no ice cores in the TCA dams) was modeled. The results of the modeling indicated that when the esker cover was successful in minimizing oxidation of placed tailings, seepage from the TCA, due to the very low permeability of the tailings and the overall low gradient of the structures, should not have deleterious effects on the surrounding environment. Once the active phase of closure activities are completed, LMI proposes a two-year TCA monitoring plan, developed in consultation with stakeholder parties, to insure that water quality is not being impacted by the tailings cells before the TCA is opened for passive environmental discharge.

Developing closure plans in the context of climate change is quickly becoming the rule rather than the exception. Historically, closure plans were required to look ahead years if not decades. However, given the timeframe over which climate change is potentially projected to occur, closure plans must now look ahead in terms of centuries. The ability to successfully retrofit the Lupin TCA cover design while accounting for climate change uncertainty, supported by sound engineering and sufficient site evidence, illustrates an important lesson that can hopefully be used by other mines in the world.

REFERENCES

I. Holubec Consulting Inc. 2005. Closure Plan for Tailings Containment Area. Prepared for Kinross Gold Corporation – Lupin Operation.

II. MEND Report 1.20.1 (MEND) 2009. Prediction Manual for Drainage Chemistry from Sulphidic Geologic Material, December 2009.

The Impact of Thickening on Fast Filtration of Tailings

Kenneth Rahal & Todd Wisdom
FLSmidth, Midvale, Utah, USA

ABSTRACT: More mining companies are investigating filtered tailings as part of their long-term sustainability plans and to reduce risks associated with tailings storage. FLSmidth (FLS) recommends that miners conduct tailings solutions technology trade-off studies which includes analyzing different tailings solutions options, including different flowsheets and equipment. This analysis includes determining the most economic approach for each solution. One of the options for filtered tailings is the use of pressure filters, perhaps due to high tonnages or difficult to filter material. The primary factors that affect filtration are the settling rate of the solids, feed density to the filters, particle size distribution (PSD), particle shape, and target moisture. The impact of feed density on filtration will be the main focus of this paper.

For shorter cycle time material, FLS will include the evaluation of fast filtration to achieve the most economic dewatering of the tailings. Fast filtration aims to achieve cycle times less than 10 minutes by using high pressure feed, fast opening and closing of the filter press, no use of membranes and minimal cake air flow. This reduction in cycle time has the potential to reduce the number of filters required and subsequently the cost of filtration.

This paper presents two case studies that included fast filtration in the tailings study. The first case study compares the cost of filtration with and without a thickener prior to filters. This case study was for a mine that did not currently thicken the tailings and wanted to understand the significance of thickening on filtration. The second case study investigated filtration as a function of feed density. This was included to determine if it was more economic to use the customer's existing high rate thickener or replace it with a high-density thickener. The comparisons presented from the case studies include CAPEX and OPEX.

1 INTRODUCTION

More mining companies are investigating filtered tailings as part of their long-term sustainability plans and to reduce risks associated with tailings storage. FLSmidth (FLS) recommends that miners conduct tailings solutions technology trade-off studies which includes analyzing different tailings solution options, including different flowsheets and equipment. This analysis includes determining the most economic approach for each solution. Filtered tailings is often included to determine if the increased recycling of process water can be part of the mine's sustainability plan. FLSmidth's own program in support of sustainability, MissionZero, has the goal of offering solutions that support zero water waste by 2030. We already have technology that enables our

customers to recover up to 95% of their process water. This dry-stack tailing solution also solves problems associated with waste water management and is economically competitive with alternative water management options such as desalination, even for high tonnages

However, it can be difficult to justify the extra capital expense associated with filtered tailings during studies due to unquantified or underestimated costs. As discussed by Carneiro and Fourie (2019), studies often underestimate closure costs and less tangible costs are not included. Even if as many costs are known/estimated as possible, the difference in risks and consequence of failure for different tailings solutions are often ignored. Pyle et al (2019) have shown that if past tailings failures are used to assign a value to the risk and cost of failure of a traditional wet impoundment then filtered tailings can become economically competitive for some projects. As each mine site is different, it is important to understand the factors that can help guide the process to determine which solution is best. These factors include:

- Water cost and availability
- Space requirements for waste (tailings and waste rock)
- Regulatory requirements

If the above factors lead to the decision to use a high-performance dewatering unit operation on the tailings, there are multiple types of equipment (see Schoenbrunn et al (2016) for more details) that can be used to achieve low moisture contents, including:

- Dewatering Screens
- Vacuum filters
- Centrifuges
- Pressure filters

These different technologies have different capacities, dewatering capabilities, capital costs, and operational costs. Below are criteria that impact the rate at which the slurry will dewater and its impact on the cycle time or filtration area required to meet the specified conditions.

- Settling Rate – In substitution of basic filtration test work, a general rule for expectation of a slurries ability to dewater is relative to its ability to settle. Filtration rates trend with settling rates. When filtration rates are higher, the filter selection will be geared toward equipment with fast cycle times and low mechanical times.
- Feed Solids – The feed solids percentage by weight determines the hydraulic loading the filtration or dewatering equipment will process. As the feed solids increases, the amount of liquid to be removed decreases. Filtration cycle times will be reduced, and terminal cake solids are increased as feeds solids is increased.
- PSD – The particle size distribution or PSD will provide insight into how the slurry will react to pressure filtration. A narrow band can impact cake formation by packing tightly, limiting flow. Having a disproportionate number of fine particles smaller than 10 microns can cause poor cake formation, with the fines limiting the flow through the cake.
- Particle Shape – The shape of the particle plays a role in the expected filtration. When the aspect ratio of the face to edge increases, the particles are more platelet in nature (Clays, Mica, etc.). This type of particle creates bridging and blinding, drastically reducing filtration rates and limiting the effectiveness of the air blow step.
- Target Moisture – The target moisture for the product discharged from the filter determines the total amount of energy required by the equipment. As the target moisture, liquid remaining in the cake, decreases it typically requires a greater amount of energy and time. Low target moisture rates often result in the need for more filtration surface area.
- Minerology – The mineralogy of the material can impact the filtration process. Swelling clays are known to have some of the largest impact on filtration rates due to their absorption of moisture, small particle size and potential blinding of filter media. FLS uses its proprietary CEC clay analysis to determine presence of swelling clays during the characterisation of samples.
- Solids SG – The specific gravity of the solids affects the filtration throughput as lower density particles lead to less mass in a given filter cake volume.

Once the basics of the slurry are understood and tested, the selection of the proper equipment becomes an easier exercise. The case studies in this paper focus on the impact of feed solids on the filtration process. If test work results in the recommendation to use pressure filters, perhaps due to high tonnages or difficult to filter material, then FLSmidth recommends the evaluation of

fast filtering for the application. Fast filtering is designed to achieve quick pressure filter cycle times of less than 10 minutes. This is achieved through:

- High pressure feeding up to 15 Bar terminal pressure that
    - Is possible due to feed ports in the lower part of the plate;
    - Does not require membrane squeeze;
    - Reduces cake formation time;
- Fast Opening and Closing; and
- Reduced/eliminated Cake Blow.

The low plate feed ports, as seen below in Figure 1a, are necessary to achieve high terminal pressure without membranes as uniform filling in the chambers. Turbulence in the feed eye and chamber is maintained which allows for the cake to form in layers throughout the entire chamber (Figure 1b). This results in uniform pressure throughout the filter. The formation of the cake in layers against the media results in a homogenous cake (Figure 1c).

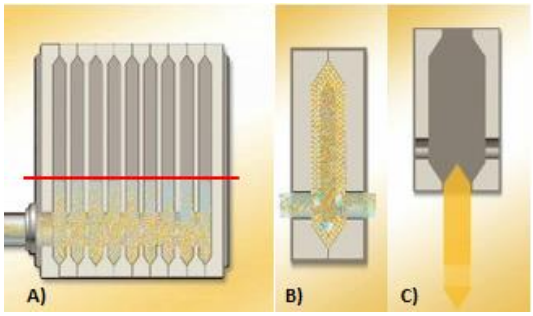

Figure 1: Lower Feed Eye allow a) uniform filling, b) layered cake formation and c) homogenous cakes.

If an upper feed port is used, as seen below in Figure 2a, gravity causes the non-uniform filling of the chambers. As the chambers are not evenly filled, a pressure gradient forms, which at high feed pressure can cause damage to the plates.

Another side effect of an upper feed port is that turbulence is not maintained so the particles settle in the chamber at different rates as seen in Figure 2b, due to particle size, and can form a non-homogenous cake (Figure 2c).

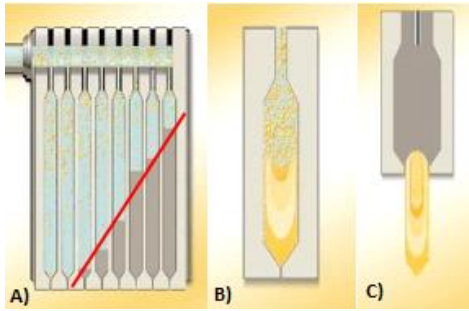

Figure 2: Upper Feed Eye result in a) non-uniform filling, b) stacked cake formation and c) non-homogenous cakes..

Fast filtering can achieve higher density cakes than low pressure feed filters, without the use of membranes, therefore the moisture content of the cake is reduced. This allows for the reduction

of air blowing of the cake. This in turn decreases the filtration cycle time and increases throughput. This reduction in air blow also reduces CAPEX and OPEX by reducing the number of compressors needed to achieve the target moisture. If waste rock is available for blending with the filtered tailings, then the cake blow can potentially be eliminated. Figure 3 shows an example of the impact of eliminating the cake blow on the filtration rate. If the target moisture for the filtered tailings alone is 15 %, by total weight, and the target moisture is increased to 20% for the EcoTails™ (comingled) solution then the filtration rate increases from 125 kg/m2/hr to 250 kg/m2/hr for the blend (design basis). This is a 100% increase in the filtration rate.

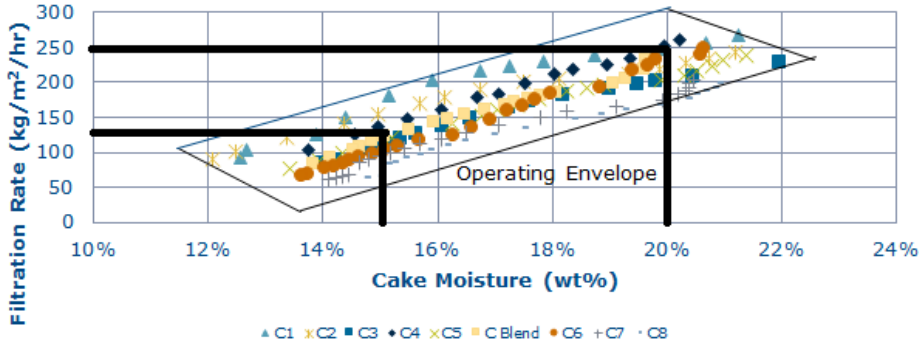

Figure 3: Cake Target Moisture vs Filtration Rate.

The purpose of fast filtering is to achieve the lowest possible cycle time that can achieve the moisture target. Lower cycle times lead to higher filtration rates and fewer filters to achieve the required throughput. Lower geotechnical strengths can be mitigated by using EcoTails® and Geowaste™ technology as shown by Wisdom et al (2018).

2 CASE STUDIES

These case studies are based on lab testing and are conceptual in nature with an accuracy of ±30%. Throughputs have been rounded to respect customer confidentiality. These case studies are based on obtaining a single moisture requirement for a fixed tailings storage facility design. Due to this requirement, no consideration is taken for cost impacts of alternate storage facility designs that could alter the moisture requirements and hence the cost of dewatering. It should be noted that the FLS sizing methodology requires a minimum of 15% excess capacity on filters to allow for maintenance.

2.1 *Medium Tonnage Copper/Gold Mine*

The first case study compares the cost of filtration with and without a thickener prior to filters. This case study was for a mine that did not currently thicken the tailings and wanted to understand the significance of thickening on filtration. This operation produces 1250 mtph of tailings at 45 wt% solids. The target density of the filter cake was 85 wt% solids. The particle size distribution, PSD, of the tailings is described in Table **1**.

Table 1: Medium Tonnage Tailings PSD

Property	Value
P80 (µm)	125
% Passing 10 microns	25

The pressure filter testing was conducted using 10 bar feed pressure at 45 wt%, and 70 wt% solids in the filter feed. The costs used for determination of OPEX are shown in Table **2**.

Table 2: Medium Tonnage OPEX Assumptions

Cost	Value
Normalized Labor Cost ($/hr)	$50.00
Normalized Power Rate ($/kWhr)	$0.10
Flocculant Consumption (g/ton)	25
Flocculant Cost ($/kg)	$2.00

All CAPEX is for equipment and does not include installation.

2.1.1 *45 wt% Solids*

The customer's current process produces tailings at 45 wt% solids. The lab testing resulted in the following dewatering equipment list to achieve 85 wt% solids in the filter cake:

- Eight (8) pressure filters with 2m by 2m plates, 50 mm chambers and greater than 19 m^3 of total filtration volume

The installed power including tanks, pumps, air compressors & receivers, filter discharge feeders, and instrumentation is 5.6 mW. The consumed power is 46% lower due to the batch operation of the pressure filters. The reduction in power does not include pumping efficiencies or the base loading of auxiliary equipment when not in use. Consumed power can also be impacted by shared resources in a batch operation, which can be evaluated during more detailed engineering studies.

2.1.2 *70 wt% Solids*

The lab testing revealed that the tailings could be thickened to 70 wt% solids and resulted in the following dewatering equipment list to achieve 85 wt% solids in the filter cake:

- 40 meter diameter Thickener
- Five (5) pressure filters with 2m by 2 m plates, 50 mm chambers and greater than 19 m^3 of total filtration volume

The installed power including thickener, underflow pumps, tanks, pumps, air compressors & receivers, filter discharge feeders, and instrumentation is 3.9 mW. The consumed power is 46% lower due to the batch operation of the pressure filters. The reduction in power does not include pumping efficiencies or the base loading of auxiliary equipment when not in use. Consumed power can also be impacted by shared resources in a batch operation, which can be evaluated during more detailed engineering studies.

The increase in feed density from 45 wt% to 70 wt% solids to the pressure filters by installing a high rate thickener reduced the number of filters by 3 and the overall CAPEX by 31.2%. The increase in feed density led to a reduction in OPEX of 14.3%, in terms of $/year. This OPEX includes labor, power, filter media, flocculant, and spares/consumables. The reduction in CAPEX and OPEX is shown in Figure 4, below. The costs are normalized to the 45% solids scenario to highlight the reduction in cost.

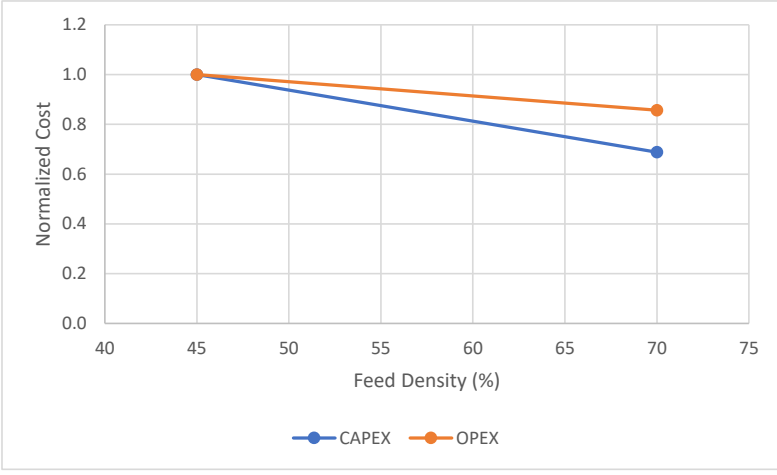

Figure 4: Cost Comparison for MT Gold Mine.

2.2 *High Tonnage Copper/Gold Mine*

The second case study investigated filtration as a function of feed density. This was included to determine if it was more economic to use the customer's existing high rate thickener or replace it with a high-density thickener. This operation produces 3750 mtph of tailings at 35 wt% solids. The target density of the filter cake was 85 wt% solids. The PSD of the tailings is described in Table 3.

Table 3: High Tonnage Tailings PSD

Property	Value
P80 (µm)	125
% Passing 10 microns	23

The pressure filter testing was conducted using 15 bar feed pressure at 56 wt%, 60 wt%, and 63 wt% solids in the filter feed. The costs used for determination of OPEX are shown in Table **4**.

Table 4: High Tonnage OPEX Assumptions

Cost	Value
Normalized Labor Cost ($/hr)	$50.00
Normalized Power Rate ($/kWhr)	$0.10

All CAPEX is for equipment only and does not include installation.

2.2.1 *56 wt% Solids*

The customer's exiting high rate thickening technology was able to achieve an underflow density of 56 wt% solids. The lab testing resulted in the following dewatering equipment list to achieve 85 wt% solids in the filter cake:

- Nineteen (19) pressure filters with 2m by 4m plates, 50 mm chambers and greater than 38 m^3 of total filtration volume

The installed power including tanks, pumps, air compressors & receivers, filter discharge feeders, and instrumentation is 28 mW. The consumed power is 42% lower due to the batch operation of the pressure filters. The reduction in power does not include pumping efficiencies or the base

loading of auxiliary equipment when not in use. Consumed power can also be impacted by shared resources in a batch operation, which can be evaluated during more detailed engineering studies.

2.2.2 *60 wt% Solids*

The lab testing resulted in the following dewatering equipment list to achieve 85 wt% solids in the filter cake:

- 70 meter diameter High Density Thickener
- Seventeen (17) pressure filters with 2m by 4m plates, 50 mm chambers and greater than 38 m^3 of total filtration volume

The installed power including tanks, pumps, air compressors & receivers, filter discharge feeders, and instrumentation is 25 mW, not including new thickener or underflow pumps as these are close to the existing thickener. The consumed power is 46% lower due to the batch operation of the pressure filters. The reduction in power does not include pumping efficiencies or the base loading of auxiliary equipment when not in use. Consumed power can also be impacted by shared resources in a batch operation, which can be evaluated during more detailed engineering studies.

2.2.3 *63 wt% Solids*

The lab testing resulted in the following dewatering equipment list to achieve 85 wt% solids in the filter cake:

- 70 meter diameter High Density Thickener
- Eleven (11) pressure filters with 2m by 4m plates, 50 mm chambers and greater than 38 m^3 of total filtration volume

The installed power including tanks, pumps, air compressors & receivers, filter discharge feeders, and instrumentation is 17 mW, not including new thickener or underflow pumps as these are close to the existing thickener. The consumed power is 5% lower due to the batch operation of the pressure filters. The reduction in power does not include pumping efficiencies or the base loading of auxiliary equipment when not in use. Consumed power can also be impacted by shared resources in a batch operation, which can be evaluated during more detailed engineering studies.

The increase in feed density from 56 wt% to 60 wt% solids to the pressure filters by installing a high-density thickener reduced the number of filters by 2 and the overall CAPEX by 7.5%. The increase in feed density from 56 wt% to 63 wt% to the pressure filters by installing a high-density thickener reduced the number of filters by 8 and the overall CAPEX by 38.8%. New thickener is included in the CAPEX but not in the following OPEX as it is assumed to be comparable to existing thickener for this paper. The increase in feed density from 56 wt% to 60 wt% and 63 wt% led to reductions in OPEX of 9.3% and 38.1%, respectively, in terms of $/year. This OPEX includes labor, power, filter media, and spares/consumables. The costs are normalized to the 56wt% solids scenario to highlight the reduction in cost.

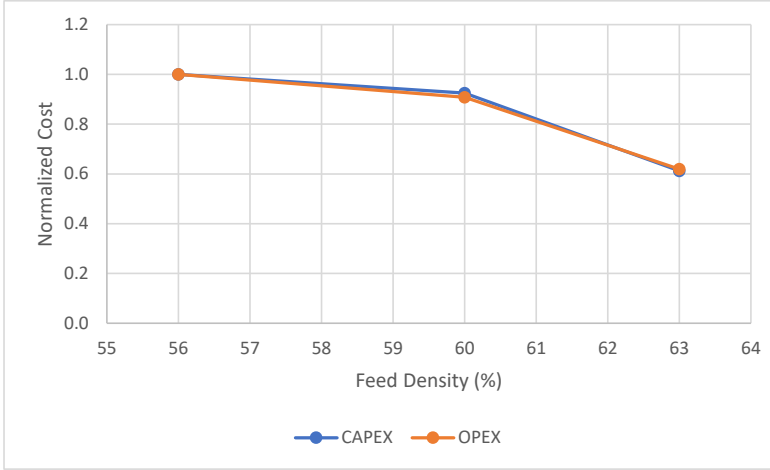

Figure 5: Cost Comparison for HT Gold Mine.

3 CONCLUSIONS

FLSmidth is conducting an increased number of tailings dewatering studies as interest in the industry increase for methods of tailings storage that reduce companies' risks and improve sustainability. Two of these studies included investigations of the impact of filter feed density on the CAPEX and OPEX of a filtered tailings solution. The results of these studies indicated:

- The additional cost of the thickener to achieve higher feed density was less than the reduction in CAPEX related to the pressure filters.
  - This included replacing an existing HRT with an HDT to achieve higher densities.
- The reduction in the number of filters due to increased feed density resulted in lower OPEX.
  - The additional cost of flocculant when investigating on whether to include thickening or not was less than the saving realized from fewer filters.

4 REFERENCES

Carneiro A and Fourie AB. 2019. An integrated approach to cost comparisons of different tailings management options. In: *Proceedings of the 22nd International Conference on Paste, Thickened and Filtered Tailings*; Perth, WA Australia.

Pyle M, Whittering R and Lane G. 2019. Economic Drivers for High-Capacity Tailings Pressure Filtration. In: *Proceedings of the 6th International Seminar on Tailings Management*; Santiago, Chile.

Schoenbrunn F, Wisdom T, Neumann R, and Chaponnel J. 2016. Tailings Filtration Demonstration Plant. In: *Proceedings of the 19th International Seminar on Paste and Thickened Tailings*; Santiago, Chile.

Wisdom T, Jacobs M and Chaponnel J. 2018. GeoWaste™ – continuous comingled tailings for large-scale mines. In: Proceedings of the 21st International Seminar on Paste and Thickened Tailings; Perth, WA Australia.

Filtered Tailings Facilities and Upset Conditions

Nicholas Kent
Klohn Crippen Berger, Brisbane, Queensland, Australia

Mary-Jane Piggott
Klohn Crippen Berger, Vancouver, British Columbia, Canada

ABSTRACT: Filtered tailings disposal is seen by many as one of the best available solutions for tailings stewardship and is increasingly being evaluated as the industry seeks to improve the management of tailings. However, there are operational challenges, specific to filtered tailings facilities that can increase the complexity of operations, that require consideration during the planning and design phases of a project. Additionally, experience has shown that successful operation of a filtered tailings facility requires a robust strategy for dealing with a range of upset conditions that can generally be categorized as: process, mechanical or weather-related upsets. This paper outlines strategies that can be adopted to deal with upset conditions and presents a simplified climate analysis procedure that can be used during design to quantify how often weather-related upsets can be expected to occur on new filtered tailings projects.

1 INTRODUCTION

Filtered tailings technology is increasingly being evaluated for implementation on both new and existing mining projects. Filtered tailings facilities are generally more complex to operate than conventional tailings facilities. Consequently, there is increased potential for "upset conditions" to occur (where the routine placement of tailings is disrupted). Upset conditions can be categorized as:

- Mechanical upsets: total or partial loss of capacity to filter tailings resulting from, equipment failures, scheduled or unscheduled maintenance.
- Process upsets: inability of the filter plant to dewater tailings to the required specification.
- Weather/placement upsets: rainfall, on-stack trafficability or marginally over-wet filter cake prohibits routine placement and compaction of filtered residue to the required specification.

Identifying the type and frequency of upset conditions that are likely to impact a site is a key component of the design and planning process for a new filtered tailings facility. Experience from sites where tailings filtration is employed indicates that a robust strategy for managing upset conditions is required to maintain operational continuity. This paper outlines strategies that have been implemented on sites to deal with upset conditions. Quantification of the expected frequency of weather-related upsets for new filtered tailings projects is also considered through a simplified climate analysis procedure, which has been successfully applied during the planning phase of new filtered tailings projects. The proposed procedure can also be used to determine the required size of temporary storage areas.

2 UPSET MANAGEMENT STRATEGIES

Strategies for managing upset conditions can be grouped into the following categories:

- alternate placement areas;
- temporary stockpiles; and
- on-stack management options.

Experience from operating filtered tailings facilities shows that sites typically implement a combination of these strategies to mitigate against the occurrence of upset conditions. While many of the strategies outlined below have the effect of reducing the occurrence of upset conditions, the rationale behind their implementation is often not centered solely on the management of upset conditions.

2.1 *Alternate Placement Areas*

Hydraulic placement of tailings as slurry within a conventional tailings facility is a management strategy that is an effective contingency against any form of upset conditions related to tailings filtration. While such a strategy is a robust form of contingency, the cost associated with its implementation is likely to be prohibitive in most situations as it requires construction and maintenance of an additional tailings disposal facility. Using a conventional tailings facility as an alternate placement area during upset conditions may be a viable form of contingency on sites where there is a suitable pre-existing facility or in situations where long duration upsets occur. Consideration of this option is recommended for sites that currently operate a conventional tailings storage facility and are considering converting to filtration.

The Karara Mine in Western Australia, is an example of a site that has used a conventional slurry tailings facility to mitigate against process and mechanical upsets within the filter plant. It is understood that during initial operations the filter plant was unable to produce filtered tailings to the required moisture content, resulting in the need to transport and place tailings as slurry (Hore & Luppnow, 2014). While the slurry was initially placed within the footprint of the filtered tailings stack, ongoing issues within the dewatering system resulted in the mine constructing a dedicated slurry tailings facility to allow the plant to operate at its design capacity (Klohn Crippen Berger, 2017).

The placement of tailings as backfill within an underground mine or an open pit is a further alternate placement option that is available to some sites. The efficacy of this option as an upset contingency is dependent on the availability of the alternate placement area and level of dewatering that is required to facilitate placement. Tailings that are placed as underground backfill are typically dewatered to either a paste or filter cake consistency and mixed with cement to form a paste (Klohn Crippen Berger, 2017). Consequently, placement of tailings as underground backfill will generally only provide contingency for weather-related upset conditions. There are several sites that operate a filtered tailings stack and place a portion of their tailings as underground backfill. Examples include: Greens Creek Mine, in Alaska (Erikson et al., 2017); Pogo Mine, in Alaska (Klohn Crippen Berger, 2017) and Escobal Mine, in Guatemala (Klohn Crippen Berger, 2017).

2.2 *Temporary Stockpiles*

Temporary stockpiles are a common contingency for weather-related upsets and can be either covered or uncovered. Covered stockpiles are often used by sites that have low throughputs and experience high annual rainfall to temporarily store filtered tailings during wet weather. While the size of the covered storage area required to enable continuous production of filtered tailings depends on a site's climate and other available contingencies, covered stockpiles that allow for storage of 2-5 days of production are typical. Examples of sites that use covered stockpiles include: Greens Creek Mine, in Alaska (Klohn Crippen Berger, 2017) and Marlin Mine, in Guatemala (Klohn Crippen Berger, 2017).

Uncovered temporary stockpiles are another option for dealing with on-stack trafficability issues that are a consequence of wet weather conditions. To minimize the adverse effects of placing filtered tailings during wet weather, tailings can be stockpiled in mounds immediately adjacent to the filter stack or placement area. Once weather conditions improve the stockpiles can be cut and ideally dozed down to the placement area and compacted. Once the material is

relocated to the filter stack it is likely that the tailings will require additional re-working or farming to remove excess moisture (Erikson et al., 2017).

While some form of temporary stockpiling of material can be readily implemented at most sites at low capital cost, temporary stockpiling does result in material rehandling, which adds to operational costs. When undertaking planning for a filter stack where temporary stockpiling is to be used, it is important to assess if the operation can place material on the stack at a rate that is higher than the average rate of placement in periods of good weather to make up for placement time that is lost during wet weather.

2.3 *On-stack Management Options*

There are several placement or on-stack management strategies that can be deployed to mitigate against the effects of upset conditions. Zonation of material within the filtered residue stack is an example of an on-stack management option that can be used as an upset management strategy. Process or weather-related upsets can occasionally make placement and compaction of filter cake to the target density specified by the construction specification difficult to consistently achieve. Material that meets the specification and can be placed in good weather, is placed within an outer structural "shell" zone. Slightly off-spec material or material, which is placed during poor weather conditions, is placed within an internal zone that is encapsulated by the outer shell. While the placement of off-spec material can affect the stability of the stack, placing this material in the interior of the stack minimizes its impact. Davies et al. (2011) notes that implementation of zonation is almost always operationally beneficial and is normally implemented at most sites (Davies, 2011).

The prevalence of wet weather upsets can be reduced through the implementation of measures that aid on-stack trafficability. Construction of on-stack access roads and the use of low ground pressure equipment to transport and place tailings can reduce the prevalence of weather-related upsets. Access roads can be constructed from crushed rock, tailings and geosynthetics or a combination of these materials. The additional cost that construction of on-stack access roads add to the operation of a filter stack depends on the availability of suitable road building materials and can vary widely across operations. When evaluating the use of on-stack access roads, it is important to consider the impact that abandoned roads will have on the long-term physical stability of the stack. Erikson et al. (2017) notes that abandoned roads constructed from crushed rock within the Greens Creek filter stack became "perched aquifers" which wicked water into the surrounding tailings and created soft spots that inhibited placement (Erikson et al., 2017).

On-stack "farming" of filtered tailings can assist in managing process and weather-related upsets, which result in over-wet tailings. Once placed, over-wet tailings can be farmed by a dozer towing a rotovator, harrow or disc plough to accelerate the air-drying process. When the target moisture content is reached, the filtered tailings can be compacted to the target dry density. Farming is most effective in warm climates with high evaporation. It is understood that on-stack farming of tailings is used at the Escobal Site in Guatemala (Klohn Crippen Berger, 2017).

2.4 *Case Studies*

Table 1 summarizes upset-management strategies that are employed by sites where filtered tailings have been implemented. The information contained in Table 1 is part of the public domain.

Table 1. Upset Management Strategies Implemented at Sites

Site	Ore	Net Precipitation (mm)	Tailings Throughput (tpd)	Known Upset Contingencies	Reference
Greens Creek, Alaska	Polymetallic	1,080	2,200	- Underground backfill - Covered temporary stockpile - Uncovered temporary stockpile - Tailings/geosynthetic on-stack access roads	Erikson et al., 2017, Klohn Crippen Berger, 2017
Raglan, Quebec	Nickel, Copper	420	3,520	- Crushed rock access roads - Emergency tailings storage pad (1 to 2 days storage)	Klohn Crippen Berger, 2017
Marlin, Guatemala	Gold, Silver	25	6,000	- Lime and cement added to improve strength and trafficability - Covered shed (2 days storage)	Klohn Crippen Berger, 2017
Escobal, Guatemala	Silver	840	1,530	- Uncovered temporary stockpile - Farming to aid drying	Klohn Crippen Berger, 2017
Karara, Western Australia	Iron ore	-2,250	35,000	- Conventional slurry tailings facility	Klohn Crippen Berger, 2017

3 QUANTIFICATION OF WEATHER UPSETS

3.1 *Methodology*

For new facilities, the identification and selection of appropriate contingencies requires a level of insight into the frequency at which upset conditions can be expected to occur. Wet weather conditions disrupt filtered tailings placement when the moisture content of surficial tailings becomes excessively high. During wet weather conditions, tailings with excessively high moisture contents can rut as they are worked, and this can lead to poor compaction as well as long-term "soft spots" that inhibit future placement. In addition, high moisture content can:

- limit access to work fronts as placed filtered tailings become not trafficable to construction equipment; and
- prohibit achievement of the specified compaction and density.

While it is generally not possible to generate an analytical estimate of how often upset conditions will occur at a given site with a high level of accuracy, it is possible to get some indication of how often weather-related upsets occur by analyzing historical climate data recorded at or near a site. A site-specific estimate of weather-related upsets can be coupled with data from dewatering equipment manufactures to generate a comprehensive estimate of the expected frequency of upset conditions.

Application of the proposed procedure requires a rainfall record of suitable length to capture annual and inter annual climate variations. It is preferable that the rainfall record used have a timestep that is at least sub-daily (6 hourly or 1 hourly). While it is possible to modify the procedure to allow for the use of daily data its accuracy will be diminished.

The procedure works by defining the duration of weather-related upsets associated with various amounts of rainfall within a given time period. While it is assumed that placement occurs daily during the morning and afternoon across a 12-hour shift, the procedure could be adapted to account for 24-hour placement. The duration of a weather-related upset depends on both the amount of rainfall recorded, the intensity of the rainfall, and the timing of the rainfall within the day. Rainfall recorded in the afternoon of a 12-hour day shift will result in a smaller amount of downtime than a comparable amount of rainfall in the morning. A series of "if then" type rules that determine the length of a weather-related upset for a given amount of rainfall within a given period during the day are defined (El-Rayes & Moselhi, 2001). It is assumed that rainfall amounts of less than 2 mm will not result in a weather-related upset. Adopted weather-upset rules are outlined in Table 2.

Determining the amount of rainfall that results in a weather-related upset and the delay associated with certain amounts of rainfall, is generally a subjective judgement-based determination made during the planning and design phases of a project. Wetting and drying cycles are complex processes that depend on meteorological factors (rainfall and evaporation), surface grading, surface conditions (loose or compacted, smooth or rough), residue material plasticity (shrink-swell) and permeability (infiltration). It is recommended that adopted rainfall thresholds are continuously re-evaluated as a project progresses from design to operations.

Table 2. Weather Upset Rules

Rule	Rainfall (mm)	Period	Upset Duration – Current Day (days)	Upset Duration – Following Days (days)	Total Upset Duration (days)
1	2 to 15	Night	0.5	0	0.5
2	2 to 15	Morning	1	0	1
3	2 to 15	Afternoon	0.5	0	0.5
4	2 to 15	Night + Morning	0.5	0	0.5
5	2 to 15	Morning + Afternoon	0.5	0	0.5
6	15 to 40	Night	1	0.5	1.5
7	15 to 40	Morning	1	1	2
8	15 to 40	Afternoon	0.5	1	1.5
9	15 to 40	Night + Morning	1	0.5	1.5
10	15 to 40	Morning + Afternoon	0.5	1	1.5
11	≥40	Night	1	1.5	2.5
12	≥40	Morning	1	2	3
13	≥40	Afternoon	0.5	2	2.5
14	≥40	Night + Morning	1	1.5	2.5
15	≥40	Morning + Afternoon	0.5	2	2.5

Once the rules are applied to a rainfall dataset, summary statistics for the estimated proportion of time that weather-related upsets occur, the duration of weather-related upsets and the estimated maximum stockpile size (if relevant) can be calculated.

3.2 *Example Rainfall Dataset*

The efficacy of the previously described analysis procedure to quantify weather-related upsets, is demonstrated by applying it to a rainfall data record from Central Queensland, Australia. There are several mineral processing facilities with significant tailing storage facilities located in the area and some operations are considering implementing tailings filtration. The average annual rainfall and pan evaporation at the site is 922 mm and 1844 mm respectively. The rainfall record

used has been recorded by a pluviograph and runs from 1996 to 2019 (24 years of data). The data has been processed to convert it to an hourly timestep.

3.3 *Results*

Table 3 presents summary statistics for the proportion of time that weather-related upsets occur in each year of the 24-year data set. The results show that most years are tightly concentrated around the mean value of 11.6%. It is notable though, that there is some significant inter year variability, the minimum and maximum proportion of time that weather-related upsets occur is 5.6% and 21.5% respectively across the years.

Table 3. Calculated Weather Upsets

Parameter	Weather Upset % of time
Mean	11.6%
Median	11.6%
25th Percentile	10.1%
75th Percentile	12.7%
Minimum	5.6%
Maximum	21.5%

Figure 1 shows the distribution of weather upset durations calculated across the data set. It is notable that approximately 85% of weather-related upsets are predicted to be equal to or less than 2 days in duration.

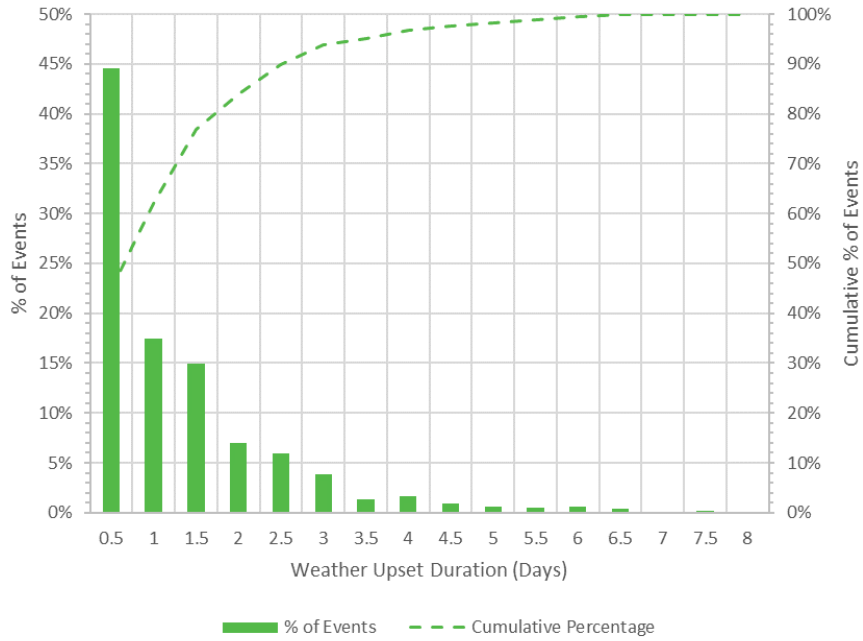

Figure 1. Predicted Weather Upset Duration

If filtered tailings are temporarily stockpiled during weather-related upsets, depletion of the stockpile once weather conditions improve requires that the rate of tailings placement be increased above the average placement rate. Consecutive weather-related upsets during a wet season can result in a stockpile not being fully depleted in the time between each weather-related upset. The extra capacity likely to be available within the earthworks fleet to place stockpiled tailings needs to be considered when sizing temporary stockpiles. Extra capacity can be gained by either extending placement hours or by increasing the size of the earthworks fleet. Figure 2 shows the distribution of expected stockpile size across the 24-year data set as a proportion of time, when it is assumed that the rate of placement can be increased by 25%.

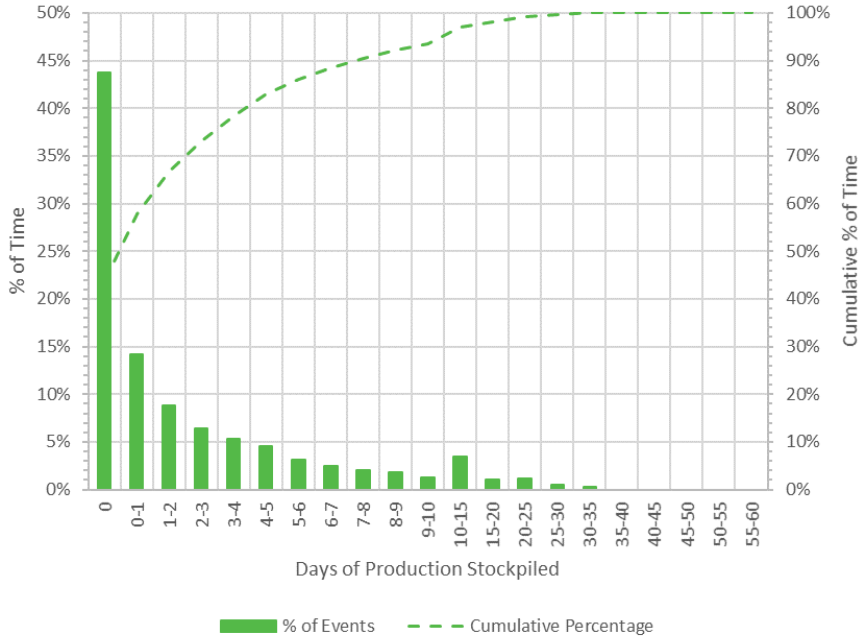

Figure 2. Predicted Stockpile Volume

Review of Figure 2 shows that a temporary stockpile would be expected to be not in use approximately 44% of the time. The stockpile size is predicted to contain less than 7 to 8 days of production approximately 90% of the time and the maximum stockpile size is between 30- and 35-days production.

3.4 *Sensitivity Analysis*

As noted previously, selection of the rainfall thresholds is not straightforward and requires a degree of subjective judgement. A sensitivity analysis has been conducted on the rainfall thresholds defined in Table 2. Two alternate scenarios were considered: higher rainfall thresholds; and lower rainfall thresholds (see Table 4).

Table 4. Calculated Weather Upsets

Rules	Base Case Threshold (mm)	Higher Rainfall Threshold (mm)	Lower Rainfall Threshold (mm)
1-5	2 to 15	4 to 20	1 to 10
6-10	15 to 40	20 to 50	10 to 30
11-15	≥40	≥50	≥30

Summary statistics for the sensitivity analysis are presented in Table 5. The distribution of weather-related upset durations for the sensitivity analysis is shown in Figure 3. It is notable that changes to the rainfall thresholds do not significantly affect estimates of the proportion of time subject to weather-related upsets or the duration of weather-related upsets.

Table 5. Calculated Weather Upsets

Parameter	Base Case - Weather Upset % of time	Higher Rainfall - Weather Upset % of time	Lower Rainfall - Weather Upset % of time
Mean	11.6%	8.3%	15.5%
Median	11.6%	8.4%	15.3%
25th Percentile	10.1%	7.1%	13.7%
75th Percentile	12.7%	9.3%	16.5%
Minimum	5.6%	3.8%	8.4%
Maximum	21.5%	15.9%	26.7%

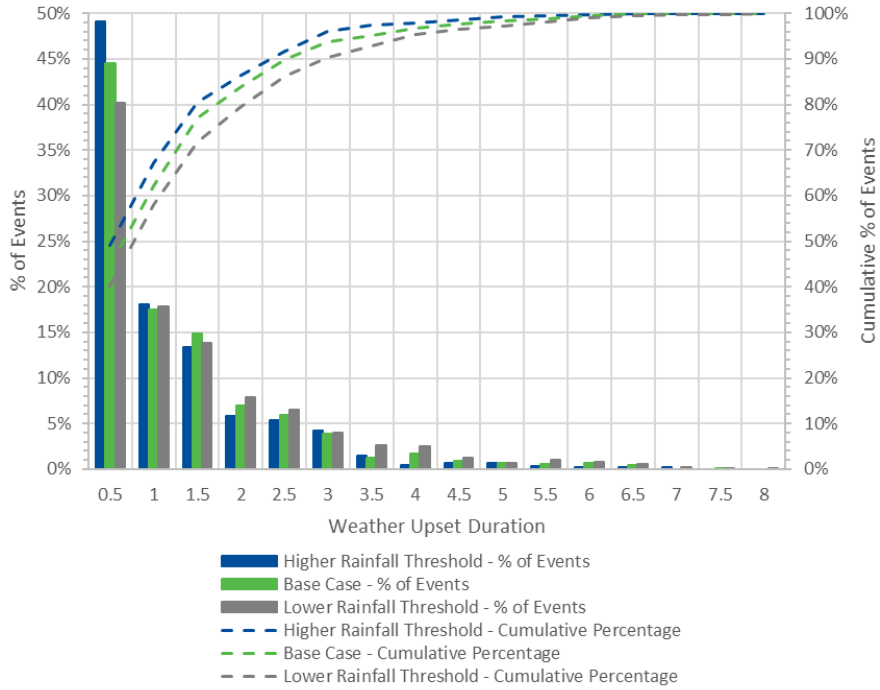

Figure 3. Predicted Weather Upset Duration – Sensitivity Analysis

Figure 4 illustrates the impact of changes in the rainfall thresholds on the volume of material that accumulates within a temporary stockpile. Review of Figure 4 shows that changes in the rainfall thresholds can have a notable impact on the amount of material that accumulates in a stockpile, particularly during wet periods where significant amounts of material accumulate within a stockpile. For the higher and lower rainfall thresholds, the 90th percentile is 3 to 4 days and 20 to 25 days respectively, compared to 7 to 8 days for the base case. The results suggest that if there were no alternate placement areas available and limited capacity to increase the rate of placement following wet periods, a temporary stockpile that could contain around 2 months production may be required to provide for continuous operations.

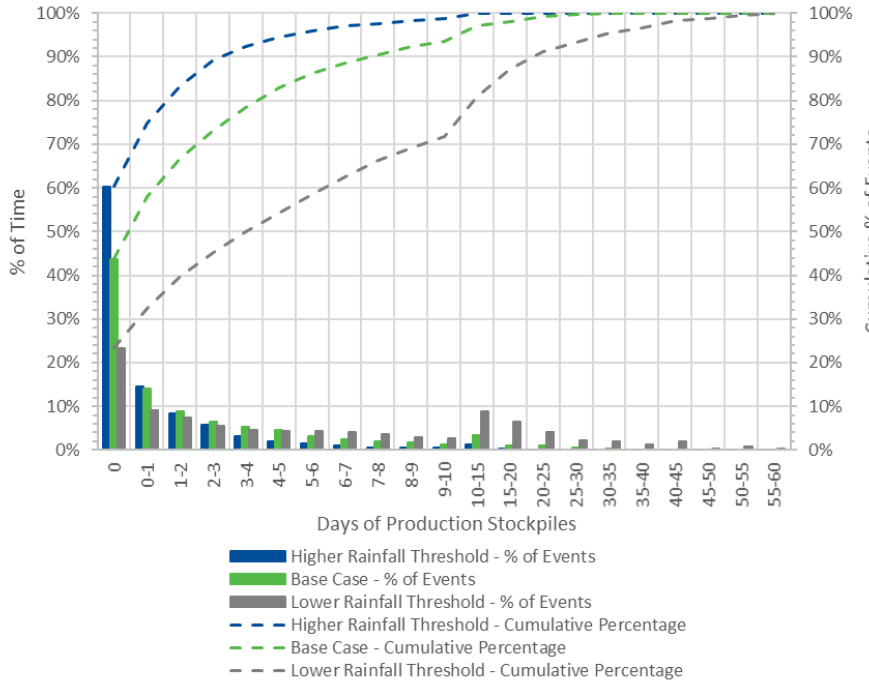

Figure 4. Predicted Stockpile Volume – Sensitivity Analysis

4 CONCLUSION

Adoption of filtered tailings disposal is increasingly being evaluated for new and existing mines as the mining industry looks to improve tailings stewardship. When undertaking the planning and design of new filtered tailings facilities, it is important to consider the potential for upset conditions to impact the placement of filtered tailings, along with upset management strategies. Upset conditions can generally be categorized as: process, mechanical or weather-related upsets. Experience from operating filtered tailings facilities shows that sites typically implement a combination of different upset management strategies outlined in this paper to ensure continuity of operations.

The climate analysis procedure presented in this paper offers a simple means to gain an order of magnitude estimate on the frequency and duration of weather-related upsets that can be expected for new facilities. While there is a level of subjectivity involved in the definition of rainfall thresholds and the delay associated with various amounts of rainfall, a rudimentary sensitivity analysis shows that the example site is not particularly sensitive to changes in the thresholds. Application of the analysis procedure to the sizing of temporary stockpiles demonstrates that in situations where there are no alternate placement areas available and limited capacity to increase the rate of placement, a significant temporary stockpile may be required to ensure operational continuity.

REFERENCES

Davies, M. 2011. Filtered Dry Stack Tailings – The Fundamentals. *In proceedings, Tailings and Mine Waste 2011*. Vancouver, British Columbia, Canada, 6-9 November, 2011.

El-Rayes, K. Moselhi, O. 2001. Impact of Rainfall on the Productivity of Highway Construction. *In Journal of Construction Engineering and Management*. Vol 127, No. 2, March/April, 2001.

Erikson, B. Butikofer, D. Marsh, A. Friedel, R. Murray L. Piggott, MJ. 2017. Filtered Tailings Disposal Case History Operation and Design Considerations Part I. *In proceedings, International Conference on Tailings and Mine Waste*. Banff, Alberta, Canada, 5-8 November, 2017.

Hore, C. & Luppnow, D. 2014. Karara Iron Ore TSF – design considerations for a unique large dry stack facility. *In proceedings of Tailings and Mine Waste 2014*. Keystone, Colorado, USA, 5-8 October 2014.

Klohn Crippen Berger. 2017. Study of Tailings Management Technologies. *Mine Environment Neutral Drainage Project. MEND Report 2.50.1.*

Enhancing Vacuum Belt Filter Dewatering to Adapt to Finer Tailings Grind – A Case Study

O. Whatnall & K. Barber
Jord International, Shortland, NSW, Australia

P. Robinson
The University of Newcastle, Callaghan, NSW, Australia

ABSTRACT: Investigation and uptake of filtered tailings continues to grow throughout the globe. This is driven by a wide range of site-specific considerations, which include such factors as tailings characteristics (e.g., amenability to filtration), production rates, climate, water availability, cost drivers, environmental requirements and social factors. Despite the aforementioned technological growth, the currently-available filtration technology is not able to meet the needs of many operations and projects that would otherwise adopt the technology. The 2017 report commissioned by the Mine Environment Neutral Drainage (MEND) Project Secretariat Study of Tailings Management Technologies identified "*cost and scalability of filtered tailings is one of the deterrents for mining companies*."

1 INTRODUCTION

Experience with large-scale industrial filtration shows that vacuum belt filter systems meet the needs of many modern users, exceptions being the inability to effectively dewater tailings at altitude and/or with a fine particle size distribution: a potential fatal flaw. This paper presents a case study on the utilization of the patented Viper Filtration technology on gold tailings to overcome this challenge and shares the resultant full-scale plant design, highlighting the features designed to overcome cost and scalability deterrents. This technology is a novel mechanical process which complements the vacuum pressure in dewatering the filter cake as it travels along the belt filter.

1.1 *Filtered tailings*

Investigation and uptake of filtered tailings continues to grow throughout the globe. This is driven by a wide range of site-specific considerations, which include such factors as tailings characteristics (e.g., amenability to filtration), production rates, climate, water availability, cost drivers, environmental requirements and social factors. Despite the aforementioned technological growth, the currently-available filtration technology is not able to meet the needs of many operations and projects that would otherwise adopt the technology. The 2017 Study of Tailings Management Technologies report commissioned by the Mine Environment Neutral Drainage (MEND) Program Secretariat identified "*cost and scalability of filtered tailings is one of the deterrents for mining companies*."

1.2 *Viper Filtration technology*

A recently commercialized, patented technology, utilizes a series of vibration roller assemblies which are coupled to the top side of a vacuum belt filter which complements the vacuum pressure in dewatering the filter cake as it travels along the belt filter. This technology overcomes the cost and scalability deterrents.

1.3 *Gold Mine and Processing Plant*

The case study is an underground gold mine. The mine produces 500,000 ounce (oz) gold per annum via a conventional carbon-in-pulp (CIP) processing plant. This processing plant produces slurry tailings of which, approximately 100 tph is filtered to a low moisture content and then trucked to the mine to re-pulp as paste backfill.

In 2017, a conventional vacuum belt filter with a filtration area of 158 square meters (m^2) was installed to wash (i.e., remove cyanide) and dewater the tailings for paste backfill. Since that time, the specification for paste backfill has been for a finer particle size distribution (PSD) of solids, which could not be effectively dewatered at the required rate from the existing vacuum belt filter.

1.4 *Pilot plant testing*

This project commenced with a pilot testing program, which successfully met the objective to rigorously test, measure and record any performance improvements achieved when engaging the Viper technology compared to the conventional vacuum belt filter. This pilot testing facilitated measurement of operating and design data, which forms the basis of the full-scale system design and resultant equipment supply of three vibration roller assemblies for retro-fitting on the existing vacuum belt filter.

2 PROCESS SUMMARY

2.1 *Original design basis*

A portion of the slurry tailings from the process plant for paste backfill are deslimed and thickened to meet the required specification, particularly the PSD. The tailings are washed for residual cyanide removal and dewatered on the vacuum belt filter prior to being stockpiled as filter cake. To facilitate the design and supply of the 158m^2 vacuum belt filter, the original specification for paste backfill was 131 tph of solids with a P80 ranging from 150-190µm, with 15-20% <20µm and 7-10% <10µm.

2.2 *Project justification*

The tailings deslime and filtration circuit was commissioned in late 2017, meeting design expectations for feed to the underground paste fill plant. Since 2017, the specification for paste backfill has been revised to a finer PSD, of the order of 40% <20um which cannot be effectively dewatered at the required rate from the existing vacuum belt filter. Modifying the filter plant in order to achieve this paste specification at existing design throughput rates is the objective of the project.

3 PILOT PLANT TESTING

3.1 *Objective*

The objective of the pilot program was to rigorously test, measure and record any process performance improvements achievable using the Viper Filtration technology compared to the pilot scale conventional vacuum belt filter. The pilot scale testing begins with the control to obtain the baseline before the technology is engaged.

Additionally, the pilot testing allows for measurement of operating and design data, which will form the basis of the full-scale Viper modules and retrofit design. The testing program considered two sample types, namely CIP tails (P_{80} ~40µm) and tailings thickener underflow (TUF), a combination of CIP tails and slimes from the existing tailings deslime circuit (P_{80} ~30µm), both of which are deemed acceptable for feeding into the paste backfill plant. PSD information is shown in Figure 1.

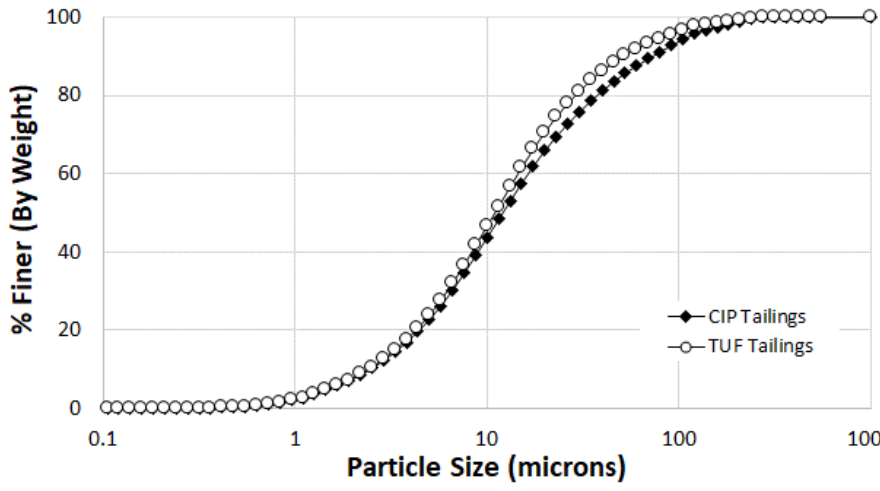

Figure 1. PSD chart comparing CIP and TUF tailings.

Specifically, the target process performance is consistent with achieving <20% moisture content by weight (%w/w) of the tailings filter cake whilst maximizing the throughput rate.

3.2 *Equipment*

The pilot plant is installed and operated at The University of Newcastle in New South Wales, Australia. The base filter is a vacuum belt filter with 1.6m^2 of filtration area (0.4m width x 4.0m length). Installed in series on the top side of the machine are three vibration roller assemblies, each bolted to the filter frame as shown in Figure 2. The filtration plant also includes the filter ancillaries - filtrate receiver vessel, filtrate pump and liquid ring vacuum pump.

Figure 2. Pilot vibration roller assemblies.

3.3 *Process description*

The slurry tailings are pumped onto the filter via the feedbox. The filter feed is continuously presented at the feed end of the machine and begins travelling along the length of the filter via the moving filter cloth and carrier belt (see Figure 3).

Figure 3. Filter feedbox and overflowing weir distribution system.

The pilot filter has distinct zones/areas:

i. Feed – the feed slurry is spread evenly across the width of the belt, by the overflowing weir (see Figure 3) and is immediately exposed to the vacuum. For the given feed slurry, the cake thickness is set by the speed of the belt and the flowrate of the feed pump. The cake thickness was a maximum of 12 millimeters (mm) and was consistently operating between 9mm to 12mm.
ii. Form – The prepared slurry continues to be subjected to vacuum and results in filtrate being drawn from the slurry. The slurry is formed into a wet 'cake', with or without surface water prior to the vibration roller assemblies.
iii. Mechanical dewatering – the cake travels under a series of three vibration rollers which provide consolidation, compaction and vibration energy into the cake while under constant vacuum pressure. Each vibration roller assembly can be optimized by changing the roller weight, diameter, surface profile, vibrator type and vibration intensity as well as flexibility to reposition the roller along the length of the filter. Post the third and final vibration roller, vacuum continues to be applied to the cake to allow further drying. This is the final stage of the filtration process.
iv. Cake discharge – following filtration, the filter cloth follows an alternate path and separates from the carrier belt. The filter cloth travels over the cracking roller and discharges the cake continuously (see Figure 4).

Figure 4. Filter cake discharge.

v. Filtrate & vacuum system – all filtrate drawn from the slurry via the vacuum box is captured in the filtrate receiver vessels, and is continuously pumped from the vessels by the filtrate pumps. Vacuum is provided by the liquid ring vacuum pump, which connects via the filtrate receivers through the vacuum hoses and vacuum box. The design vacuum suction pressure was -70 kilopascals (kPa).
vi. Filter cloth wash – following cake discharge, the cloth is cleaned with water by spray bars to ensure process and cloth tracking performance.
vii. Filter cloth and belt return – both the filter cloth and carrier belt travel independently along the underside of the machine. Upon return to the feed end, both travel under the dam roller, which creates a seal prior to the feed preparation zone

3.4 *Results*

Results from the pilot program were tested, measured and recorded through the course of processing CIP tailings and TUF tailings. Visual inspection recorded cleaner, more efficient cake discharge when operating the pilot plant with the vibration roller assemblies engaged compared to the conventional vacuum belt filter. Figure 5 shows the snapshot of the results for both sample types, with and without the vibration roller assemblies.

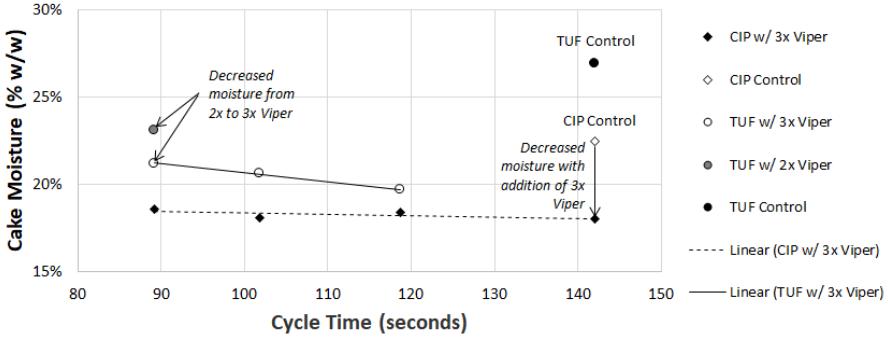

Figure 5. Cake moisture versus cycle time with addition of vibration roller assemblies.

Across both tailings types tested, cake moistures >20%w/w were recorded when operating the pilot plant as a conventional vacuum belt filter. When operating the pilot plant with three vibration roller assemblies engaged, cake moisture contents <20%w/w were measured for the CIP tailings for the range of cycle times between 142 and 119 seconds, and for the TUF tailings with a cycle time of 119 seconds.

When processing CIP tailings, on average, a 4.2%w/w moisture content reduction was recorded when operating the pilot plant with the Viper Filtration system engaged compared to the conventional vacuum belt filter. When processing TUF tailings, on average, a 5.7%w/w moisture content reduction was recorded when operating the pilot plant with the Viper Filtration system engaged compared to the conventional vacuum belt filter.

As demonstrated, the cake moisture content increased with increased belt speed; however, the gradient of the moisture increase versus belt speed trend is relatively flat, particularly for the CIP tailings. This indicates the lack of time dependence for dewatering via the vibration roller assemblies, which is not the case for reducing cake moisture via conventional 'drying'. This is further evidenced by the data point in Figure 5 taken when operating with only two vibration roller assemblies (rather than three), which had a significantly higher moisture content despite all else being equivalent.

This outcome indicates that increased throughput can be achieved by using the vibration roller assemblies to reduce the overall filter cycle time. This increased throughput is quantified in Figure 6.

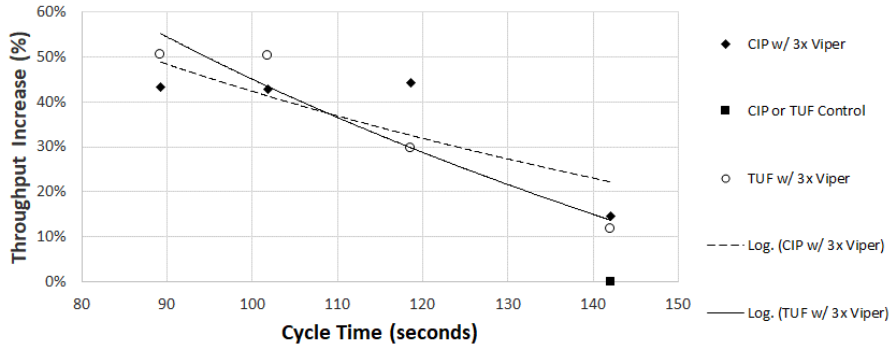

Figure 6. Throughput increase versus cycle time with addition of vibration roller assemblies.

Throughput increases in the order of 10-50% compared to the control were measured. For the CIP tailings sample, these throughput increases were achieved in combination with a cake moisture content <20%w/w. For the TUF sample, throughput increase at the top end of the range resulted in cake moisture >20%w/w (20-22%w/w for increases of ~50%).
A summary of raw results is provided below in Table 1.

Table 1. Summary of raw test data.

Material	Cycle Time (seconds)	Cake Moisture (%w/w)	Equipment Configuration	As Tested Throughput Increase vs. Control (%)	Washing Allowance Throughput Increase vs. Control (%)	Moisture Reduction vs. Control (%w/w)
CIP	142	22.5	Control	0	0	0
	142	18.0	3x Viper	15	15	4.5
	119	18.4	3x Viper	63	44	4.1
	102	18.1	3x Viper	59	43	4.4
	89	18.6	3x Viper	62	43	3.9
TUF	142	26.9	Control	0	0	0
	142	23.4	3x Viper	12	12	3.5
	119	19.7	3x Viper	33	30	7.2
	102	20.6	3x Viper	68	50	6.3
	89	21.2	3x Viper	70	50	5.7
	89	23.1	2x Viper	61	43	3.8

4 FULL-SCALE DESIGN

The pilot testing program facilitated measurement of operating and design data, which forms the basis of a full-scale system design and resultant equipment supply for three vibration roller assemblies to be retro-fitted on the existing vacuum belt filter. The 3D model screenshot in Figure 7 illustrates the three green Viper Filtration modules near the discharge end of the vacuum belt filter. Figure 8 shows the 3D model of a single Viper Filtration module.

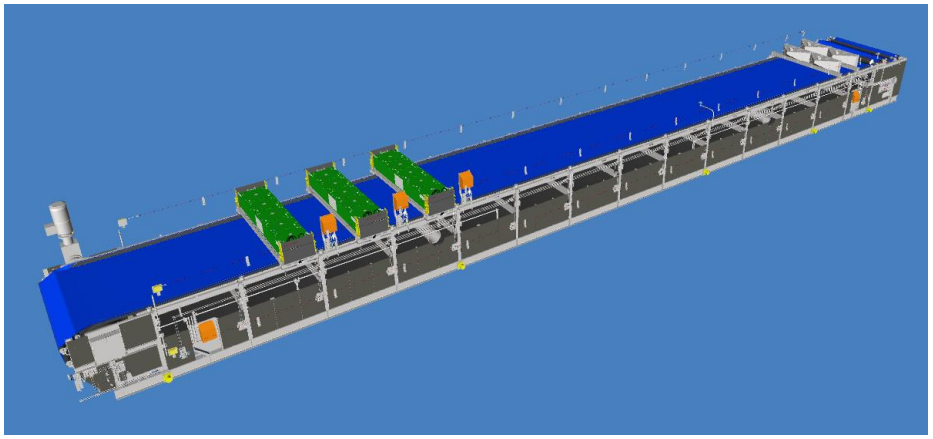

Figure 7. 3D model of the Viper Filtration modules installed on the vacuum belt filter.

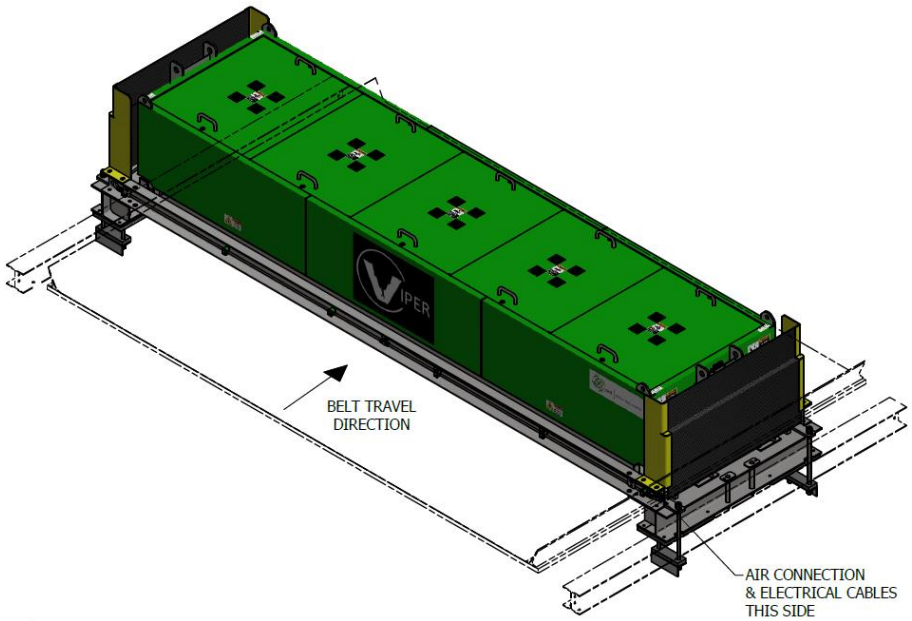

Figure 8. 3D model of a Viper Filtration module.

The vibrating action of these rollers improves not only the moisture content, but also the production rate and the discharge performance of the cake, particularly for thin cakes. The Viper Filtration technology is also resilient to variance in the feed characteristics. The control system

will adapt the settings of the system in response to changes in the process to maintain a consistent output. Elements of Viper Filtration that deliver these positive outcomes include:

i. Substitute the 'drying' zone of the filter with more efficient mechanical dewatering using the vibration roller assemblies. Less filter area is required to 'dry' the filter cake, making more filter available for 'forming'.
ii. Operating with thinner cake optimizes the 'form' time - the thinner the cake the more efficient the 'forming' - the Viper can operate with thin cake as the cake discharge performance is optimized by the boundary layer formed at the cake/cloth interface.
iii. Maximizing the available vacuum pressure further optimizes the 'form': a) with more of the filter area used for forming; and b) mechanical 'drying' of the cake removing the porosity of the cake - the vacuum pressure loss via high airflow are minimized.
iv. The performance of the mechanical dewatering is superior to conventional 'drying' delivering the reduced cake moisture.

The technology can be easily scaled up to achieve increased throughput. For instance, considering dewatering of the CIP tailings, multiplying the above system by eight (i.e., 8 belt filters, each with 3 vibration units) is capable of achieving a throughput of 50,000 tpd at ~18%w/w moisture content. Using data from a recent similar project which includes eight belt filters with vibration units (see Figure 9), the operating cost of the equipment for consumables including filter cloths is approximately $0.10(AUD)/tonne and the installed power requirement was 4 MegaWatts (MW).

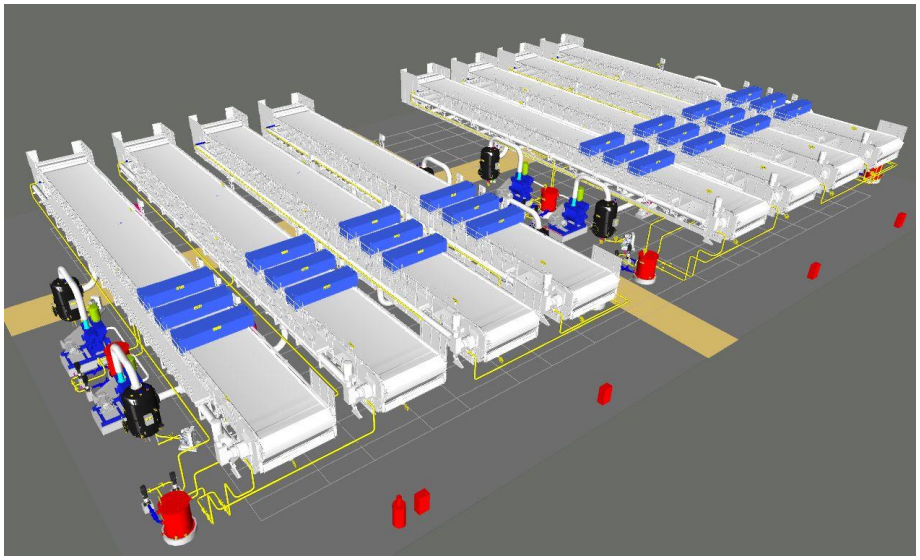

Figure 9. Layout of 8 off 158m^2 vacuum belt filters equipped with vibratory Viper technology.

5 CONCLUSIONS

The testing program in this case study provided the justification to proceed to full scale site implementation. The three Viper Filtration modules have been delivered and await retrofit to the existing conventional vacuum belt filter. More broadly, this technology has beneficial industry implications, the most significant being the opportunity to utilize Viper Filtration technology to effectively dewater fine-grained mineral processing tailings at an increased scale. This technology is one of many to answer the call from the MEND (2017) Program for the industry to improve technology in support of improved and safer tailings management. The project identified herein is for improved dewatering of tailings for use in paste backfill; however, the technology is also

directly translatable for use in dewatering tailings for surface disposal or concentrate filtration applications.

Large, multiple vacuum belt filter installations are not uncommon in the minerals processing industry as they meet the needs of the modern user, including:

i. Simple, scalable technology with more than 25 years of operational history in the industry
ii. Continuous processing machine with high availability (>90%)
iii. Operates with a single filter cloth (typical lifetime 6-12 months)
iv. Low supporting infrastructure costs and complexity
v. Cake discharge from multiple machines can be directed to an overland conveyor

The technology discussed in this paper delivers these features that can be used to dewater large-scale mineral tailings suitable for surface disposal ('dry stack'), co-disposal or paste backfill as well as concentrate applications.

REFERENCES

Mine Environment Neutral Drainage (MEND) Program. 2017. "Study of Tailings Management Technologies." MEND Report 2.50.1. October 2017. http://mend-nedem.org/wp-content/uploads/2.50.1Tailings_Management_TechnologiesL.pdf

Decoupling the Effects of Ultrafine Solids and Residual Bitumen on the Filterability of Oil Sands Tailings

Dong Wang, Hongbiao Tao, Kaipeng Wang, Xiaoli Tan, Qi Liu
University of Alberta, Edmonton, Alberta, Canada

ABSTRACT: Mine tailings can typically be dewatered by filter press to stackable filter cakes that contains >=85 wt% solids, ready for reclamation. However, under the same conditions, Alberta fluid fine tailings can only be dewatered to about 60 wt% solids. The two most likely contributing factors, ultrafine solids and residual bitumen in the oil sands tailings, were investigated in this research and their possible synergy, or lack thereof, was studied. It was found that while removing the ultrafine solids and residual bitumen by strong centrifugal forces indeed improved the filtration performance of the oil sands tailings substantially, pinpointing the detrimental effect to either the ultrafine solids or the residual bitumen was no easy matter. This paper reports the findings of a study that was aimed at decoupling these effects.

1 INTRODUCTION

The oil sands resource in northern Alberta is important for the energy requirement of Canada, and almost 96% of oil reserves of Canada are from the oil sands. The Clark hot water extraction method has been commercially used since 1967 to extract the value hydrocarbon, bitumen, from the ore. This process entails adding warm water (~50ºC) and caustic to the oil sands ores with mechanical conditioning followed by bitumen flotation. In this process, a large volume of slow-settling tailings are produced and are discharged to tailings ponds. In the first several months, the tailings separate into 3 distinct layers. The water released forms the top layer, and the coarse sands settle quickly to the bottom. The middle layer of the tailings contains about 20 wt% fine solids, known as fluid fine tailings (FFT), which consists of clay, fine silt, coarse silt, and fine sand particles suspended in water. After several years, this middle layer settles to form a stable and viscous suspension commonly called mature fine tailings (MFT) (Zhang et al. 2017, Loerke et al., 2017). On average, approximately 2 barrels MFT and 13 barrels of coarse tailings (Hande 2014) are generated to produce one barrel of bitumen. By 2016 the accumulated MFT had reached about 5 billion barrels (800 million m^3) in the tailings ponds, imposing a major challenge on the tailings management in the oil sands industry (Beier and Sego 2008).

Many dewatering technologies have been devised by the oil sands industry over the last several decades to accelerate the solid-liquid separation and consolidate the oil sands tailings. The composite tailings (CT) technology began to be used commercially in 2000 by Syncrude to treat the increasing challenge of fine tailings management (Matthews et al. 2002, Islam 2014). Also, other technologies such as the thickened tailings technology (paste technology) as well as the new emerging technologies (in-line thickening with thin lift, centrifugation, filtration, etc.) have been developed or proposed (Sobkowicz 2012). Most of those technologies involve the use of polymer flocculants to accelerate solid-liquid separation to dispose of these voluminous oil sands mining wastes. The addition of polymers in the FFT enhances the permeability and settling rate of FFT and promotes the recovery of water. However, the results of treatment are generally not satisfactory as high dosages of expensive high molecular weight polymers are required to achieve

a reasonable water release rate, and large disposal areas (called Dedicated Deposition Areas, or DDA) and high capital expenditures are needed. Even with the polymer amendment, the MFT still retains a considerable amount of water after gravity settling or centrifugation and remains in a viscous fluid state, containing only 50-55 wt% solids. Using pressure filtration, the solids content can reach about 60 wt% (Zhu et al. 2017).The oil sands tailings need to be dewatered to about 75 wt% solids for reclamation (Revington et al. 2018).

Therefore, the key requirement is to separate the liquid water from the fine solids to achieve the required solid contents. The solids are composed of fine minerals/clays, and the liquid phase is composed of water, residual bitumen, and dissolved species. The majority of the research so far has focused on the fine solids in the MFT, but the role of bitumen has not received much attention. The bitumen, which is insoluble in water and only partially soluble in most organic solvents, may create challenging problems for solid-liquid separation. Only a few studies mentioned that bitumen in the MFT could decrease hydraulic conductivity, block pores, impede water release and hinder consolidation (e.g., Suthaker & Scott 1996), while the effect of bitumen on the flocculation and settling behavior of fine solids is not clear (Klein et al. 2013). The presence of the bitumen may exert an extra effect on the suspension of MFT so that the conventional methods for the two-phase solid-liquid separation may not necessarily work well (Efal 1969).

Herein, the filtration of MFT and a model kaolinite slurry were conducted using a lab filter press. The filterability of different components of MFT was also examined and compared to that of the model solids (i.e. kaolinite, montmorillonite, and titanium dioxide) using a modified vacuum filtration device. Finally, the effects of residual bitumen and ultrafine solids on the filterability of MFT were evaluated.

2 EXPERIMENT MATERIALS AND METHODS

2. 1 Materials

The MFT sample collected from an oil sands operator in northern Alberta in 2016 was used in this study. It contained 31.8 wt% solids, 3.1 wt% bitumen, and the remainder was water, as determined by the Dean-Stark procedure. After centrifuging the MFT at 9,900 rpm (17,340 RCF, relative centrifugation force) for 3 h, three distinct layers were formed: supernatant, middle layer (ML), and bottom layer (BL), as shown in Figure 1(a). The thin top layer of the ML was designated as the Top ML with the rest of the ML as the Low ML (Figure 1(a)). According to previous work on a MFT of similar composition and under the same centrifugation conditions, the ML and BL accounted for 20 wt% and 29.9 wt% of the whole MFT, respectively (Loerke 2016), and the ML was composed of 40.2 wt% water, 17.9 wt% bitumen, and 41.9 wt% fine solids that had an average size of 450 nm. The BL comprised mainly sands and fine solids (69.2 wt%) with the remainder being water and traces of bitumen.

In order to further fractionate the ML, the ML was removed and dispersed in deionized (DI) water and centrifuged at 14,000 rpm (27,000 RCF) for 2 h. After centrifugation, a blackish "ML_top" and a greyish "ML_bottom" fraction were obtained, as shown in Figure 1(b). The solids contents of the ML_top and ML_bottom were 48.9 wt% and 64.7 wt%, respectively, determined by drying the sample in a vacuum oven at 70°C for 12 h.

To prepare the bitumen-free ML top and ML bottom samples, the ML was repeatedly washed with toluene until the toluene phase was colorless. The toluene-washed ML was then re-suspended with water and toluene at 1:1 volume ratio followed by centrifugation at 14,000 rpm (27,000 RCF) for 2 h. This yielded bitumen-free ML_top and ML_bottom with the solids content of 43.9 wt% and 63.6 wt%, respectively, as shown in Figure 1(c). In this process, some bi-wetted solids at the water and toluene interface were also formed and were not collected because the amount was very small. Since the ML needed to be re-suspended by water before centrifugation, the weight percentages of the ML_top and ML_bottom in the ML were not measured at present.

Kaolinite (BASF ASP 600), montmorillonite (Ward's Sciences), and titanium dioxide (TiO_2, US Research Nanomaterials) were used as representative clay, swelling clay, and non-clay solid samples, and were used as received. Chemical analyses of these samples were conducted using a

Bruker CTX Countertop XRF Analyzer, and particle size distribution (PSD) of these samples was measured by a Malvern Mastersizer 3000, and the results were listed in Table 1.

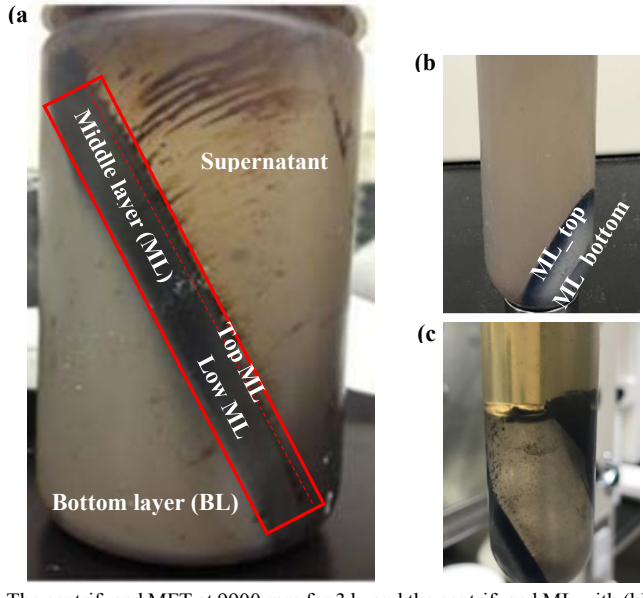

Figure 1. (a) The centrifuged MFT at 9900 rpm for 3 h, and the centrifuged ML with (b) water and (c) water and toluene at 14,000 rpm for 2 h.

In some tests, bitumen-coated model solid samples were prepared using a bitumen-toluene mixture containing 24 wt% bitumen which was from a Dean-Stark test of a bitumen froth sample. Specifically, 20 g of the model solids were treated in 100 mL of the bitumen-toluene mixture for 7 days followed by toluene washing and centrifugation with toluene at 14,000 rpm for 2 h.

An anionic polyacrylamide (A3335) from SNF and a cationic polyDADMAC polymer (Alcomer 7115) from BASF were used as polymer flocculants. According to the vendors, A3335 had a molecular weight of 17×10^6 g/mol and an anionic charge density of 30%, and the Alcomer 7115 had a molecular weight between 2×10^5 and 4×10^5 g/mol and a high cationic charge density. Stock solutions of 0.4 wt% A3335 and 2.0 wt% of Alcomer 7115 were prepared with DI water and used within one day of preparation. The polymer dosages (g/t) were based on grams of dry polymer per tonne of MFT solids or kaolinite.

Table 1. Chemical analyses of kaolinite, montmorillonite, and titanium dioxide samples.

Elements, wt%		Kaolinite	Montmorillonite	Titanium dioxide
Al_2O_3		34.52	15.62	0.68
SiO_2		48.12	54.54	0.10
MgO		0.77	2.85	1.28
K_2O		0.13	0.41	0.05
Ti		0.91	0.08	51.12
Fe		0.50	3.25	0.02
Ca		0.04	1.01	0.07
PSD, µm	d_{10}	0.88	0.98	0.34
	d_{50}	3.92	2.86	0.67
	d_{90}	11.90	15.50	1.32

2.2 Filter press filtration

A SERFILCO 0.02-7PPHM Lab Press was used to filter the MFT and kaolinite slurry, and the filterability of the sample was evaluated by the solids content of the filter cake. The chamber volume of the filter press was 280 cm^3 and a cake with a thickness of 2.5 cm could be formed. The filter pressure was set as 6.2 bar, and polypropylene filter cloth with a pore size of 15 µm was used as the filter medium. The total filter area was 220 cm^2, and the filtration test was run for 1 h.

An unbaffled vessel with a diameter of 130 mm and a 4-blade 45° PBT axial-flow impeller (D/T = 0.77) with a diameter of 100 mm were used to prepare samples for filtration. A Heidolph RZR 2052 electric stirrer was used to control the impeller speed which also recorded the torque acting on the impeller. Typically, the sample was prepared in 500 g batches by homogenizing at 300 rpm for 10 mins. In some cases, MFT and kaolinite slurry were treated with polymer flocculants (A3335 and Alcomer 7115) at certain dosages before filtration. After homogenizing the sample, the A3335 was injected to the impeller tips by a syringe while the mixing speed was maintained. The Alcomer 7115 was added in the same manner 5 seconds after the torque reached a peak. The stirring was then stopped 5 seconds after the torque reached a second peak. The prepared sample was directly pumped or preloaded into the filter chamber for filtration. Finally, the solids content of the filter cake was obtained by drying the cake in a vacuum oven at 70°C and 0.8 bar for 24 hours. More detailed information on the dual-polymer treatment and the filter press operations can be found from previous publications (Zhu 2015, Loerke 2016).

2.3 Vacuum filtration

A vacuum filtration device equipped with a customized graduated tube (2–12.4 mL) was assembled (Figure 2). This device required 20 mL feed slurry for filtration, and the tube allowed for timing the volume of the filtrate. Each filtration test was run for 30 mins. The initial negative pressure was set as 1 mbar, but the effective working pressure varied from 30 to 50 mbar depending on the sample, as displayed on the monitor of the device. The P2 grade paper (Fisher Scientific) with a pore size of 1–5 µm was used as the filter paper.

Typically, 40 mL slurry of the filtration feed sample at a certain solids content was prepared with DI water with the use of a 200 mL beaker. The slurry was stirred by a magnetic stirring bar at 800 rpm for 2 mins, treated in an ultrasound bath for 3 mins, and then stirred for another 5 mins. Finally, 20 mL of the prepared slurry was quickly transferred to the feed funnel using a 20 mL syringe for filtration, and the filtrate volume was recorded as a function of time at an interval of 1 minute.

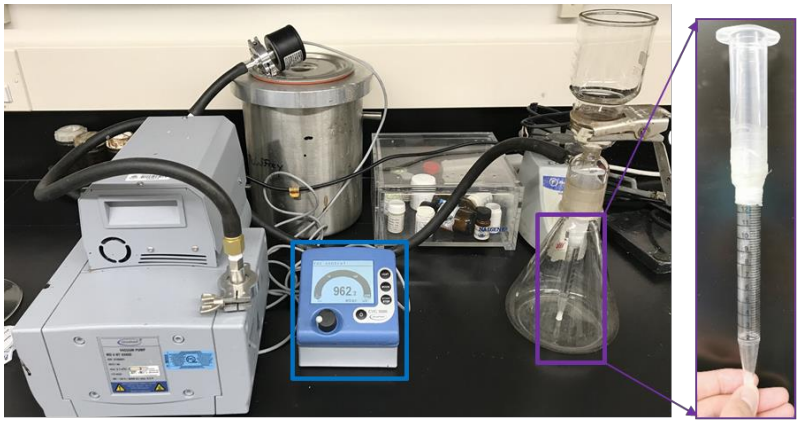

Figure 2. The vacuum filtration device and the graduated tube for filtrate collection.

3 RESULTS AND DISCUSSION

3.1 Filter press filtration of MFT and model kaolinite slurry

The lab filter press was used to filter the MFT and the model kaolinite slurry samples following the previously developed flocculation–filtration scheme (Loerke 2016). The filtration performance of the samples was assessed by measuring the solids content of the final filter cake, and the results are shown in Figure 3. As can be seen, the solids content of the filter cake was 67.6 wt% for MFT after treatment with 1000 g/t A3335 and 3000 g/t Alcomer 7115. In contrast, the model kaolinite slurry at 37 wt% solids showed a better filterability, forming a cake of 69 wt% solids without the need of the polymer flocculants.

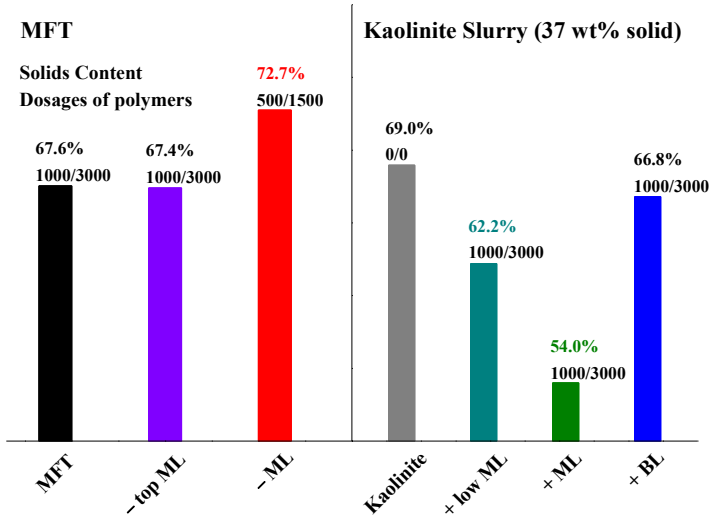

Figure 3. Comparison of the final solids content of the filter cakes of MFT and model kaolinite.

To explore the effect of residual bitumen on the filterability of MFT and kaolinite, filter press tests were conducted after specific treatment of MFT and kaolinite slurries. As shown in Figure 3, skimming off the top thin layer of ML (Top ML) from the MFT only resulted in a cake with similar solids content (67.4 wt%) to that of the filtered raw MFT (67.6 wt%) under the same filtration conditions. But when the entire ML was removed from the MFT, the solid content increased to 72.5 wt% and required only half of the polymer dosages (i.e. 500 g/t A3335 + 1500 g/t Alcomer 7115).

For the model kaolinite slurry, the addition of the lower portion of the ML (Low ML) to match a bitumen content of 3 wt% caused a dramatic drop on the filterability of the kaolinite. Without polymer treatment, the slurry was unfilterable and could not form a solid filter cake. After treating this slurry with 1000 g/t A3335 and 3000 g/t Alcomer 7115, a cake of 62.2 wt% solids was generated, much lower than the original kaolinite slurry which achieved 69 wt% solids in the cake without the need of any polymer. When the entire ML was added to the kaolinite slurry, it became unfilterable without polymer treatment, and even with high dosages of polymers treatment the solids content of the cake was only 54 wt%. Not surprisingly, the addition of the BL at the same amount as the whole ML only slightly affected the filterability of the kaolinite slurry, and the solids content of the cake (66.8 wt%) thus obtained after 1000 g/t A3335 and 3000 g/t Alcomer 7115 treatment was close to that of the filtered raw kaolinite (69 wt% solids) without any polymers.

The highly improved filterability of MFT without the ML, and the significantly decreased filterability of kaolinite slurry with the ML addition, indicate that ML played a critical role in dictating the filterability of both MFT and kaolinite slurry. Considering that most of the residual bitumen in MFT was concentrated in the ML, the residual bitumen was likely responsible to the

low filterability of MFT. This argument seemed logical because, compared with mine tailings, residual bitumen was a unique component of oil sands tailings and may have contributed to its uniquely lower filterability than typical mine tailings.

Remarkably, the results showed that the different MFT sub-fractions (i.e. Top ML, Low ML, ML, and BL) affected filtration very differently. Therefore, their effects were investigated separately using a vacuum filtration setup that ran faster and required less sample than the filter press.

3.2 Vacuum filtration of MFT components and model solids

To pinpoint the components dictating the filterability of MFT, the filterability of each component of the centrifuge fractionated MFT, and their effects on the filtration of kaolinite slurry were studied via the vacuum filtration setup. Figure 4 presents the filtration results of the top ML, low ML, ML, and BL (Figure 1(a)) at different dilution ratios with DI water.

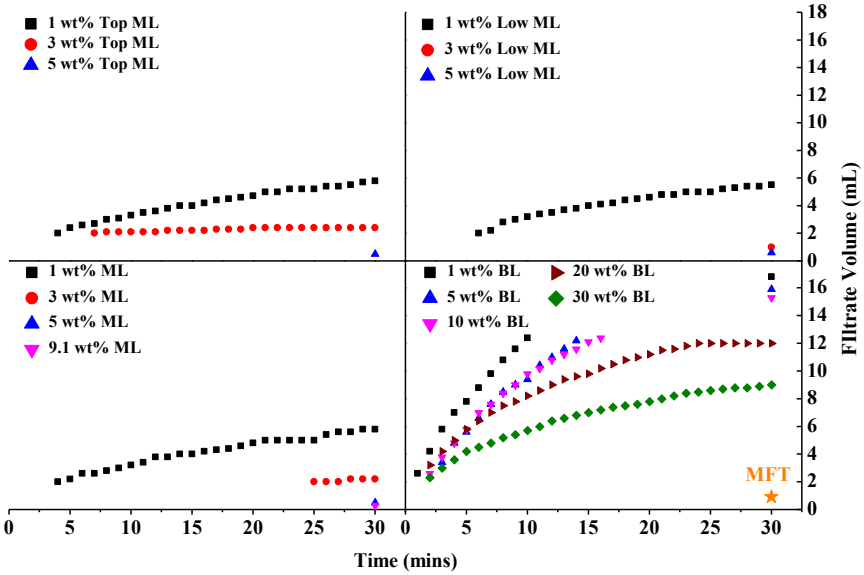

Figure 4. Vacuum filtration curves of the Top ML, Low ML, ML, and BL from the centrifuged MFT.

As expected, the vacuum filtration curves of the samples showed similar trends of variation, i.e. the filterability of the sample decreased as the solids/bitumen content of the sample increased. Surprisingly, the vacuum filtrate rate of the Top ML, Low ML, and ML was very low even when the samples were diluted by around 50 times to 1 wt% solids. When diluted to 3 wt% solids they were unfilterable and behaved just like the raw MFT. On the other hand, the BL remained filterable even after dilution by only 2 times to 30 wt%.

Figure 5 shows the filtration curves of kaolinite slurry at 37 wt% solids with/without the addition of MFT components. The kaolinite slurry alone showed reasonable filterability in the vacuum filtration, which was consistent with its high filterability in the filter press tests. But the filterability of the kaolinite slurry was severely reduced by introducing the Top ML or Low ML to a concentration of only 1 wt%, and after adding 3 wt% the slurry was almost unfilterable. On the other hand, the addition of BL even up to 10 wt% exerted negligible effects on the filtration rate of the kaolinite slurry. The observations were consistent with the filter press results.

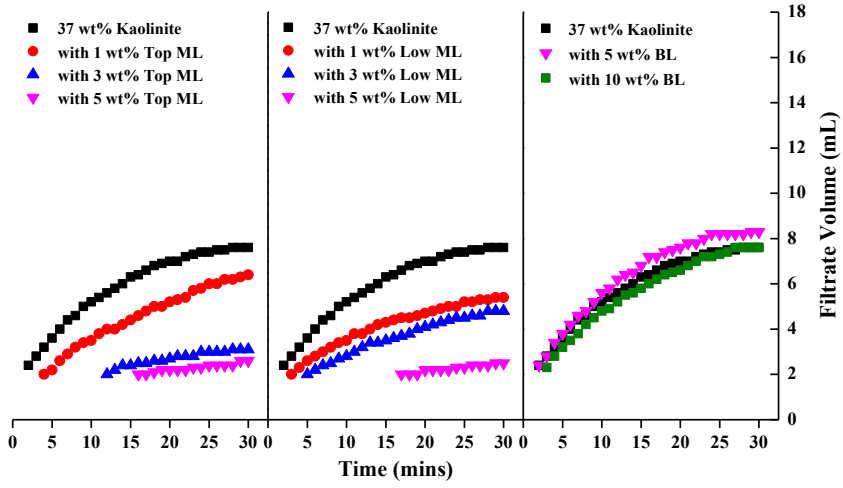

Figure 5. The effect of the top ML, low ML, and BL on the filtration curve of kaolinite slurry.

Given the vital role of the ML in the filtration of MFT and kaolinite, and the un-sophisticated and un-repeatable ways of separating the "Top ML" and "Low ML", the ML was further studied by separating the ML into the ML_top and the ML_bottom fractions using higher centrifugation speed (14,000 rpm, or 27,000 RCF) after dilution with water (see Figure 1(b)).

Figure 6 compares the filtration rates of the ML_top, ML_bottom, and kaolinite slurry with/without adding the ML_top and the ML_bottom material. The ML_top caused lower filterability of the kaolinite slurry than the ML_bottom. In fact, the ML_bottom did not seem to affect kaolinite filtration when added at 3 wt%. Therefore, it seemed that the ML_top fraction was the culprit which caused the poor filterability of MFT.

As mentioned earlier, the residual bitumen and fine/ultrafine solids have been considered as the two most likely factors responsible for the low filterability of MFT. To understand the underlying reasons making the ML_top material as a dominant deleterious material for filtration, the filterability of MFT and its components (i.e. ML, ML_top and the ML_bottom) and model solids (i.e. kaolinite, montmorillonite, and titanium dioxide) samples were studied.

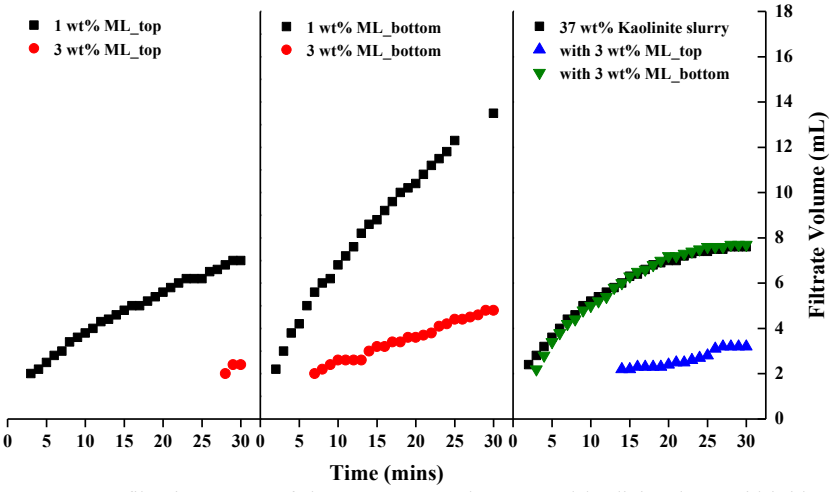

Figure 6. Vacuum filtration curves of the ML_top, ML_bottom, and kaolinite slurry with/without the addition of the ML_top and ML_bottom.

3.3 The effect of residue bitumen on filtration

The components of MFT, i.e., ML, ML_top and ML_bottom, were washed with toluene repeatedly to remove bitumen emulsion and/or bitumen coating on the surface of fine solids. The cleaned samples were then used in the vacuum filtration tests and the results are shown in Figure 7. As can be seen, the filterability of the ML, ML_top, and ML_bottom before and after the toluene-washing remained almost the same.

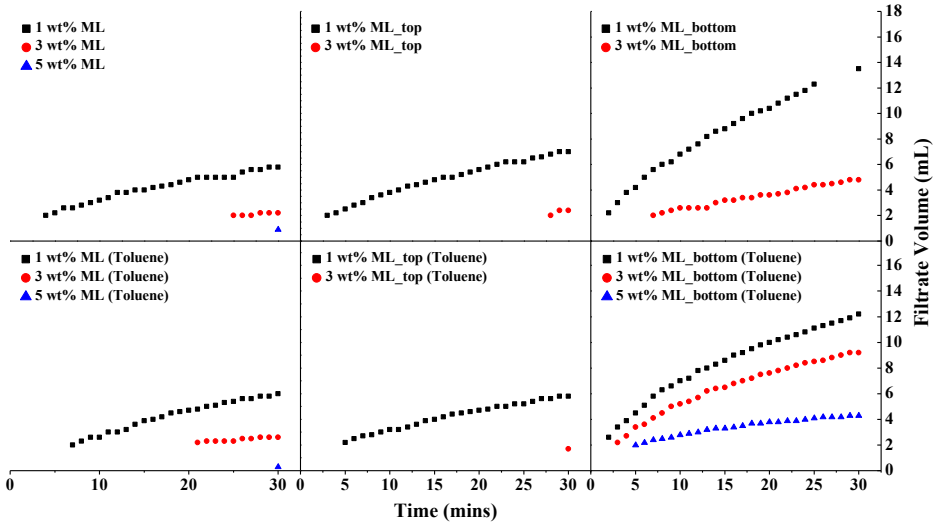

Figure 7. Vacuum filtration curves of the ML, ML_top, and ML_bottom before and after being washed with toluene. Top panel: without toluene wash. Bottom panel: after toluene wash.

Figure 8 shows the filtration of 37 wt% kaolinite slurry with/without the addition of 3 wt% ML_top or ML_bottom samples. The ML_top and ML_bottom samples were either washed or not washed with toluene. As can be seen, removing the bitumen by toluene wash did not change the effect of the ML_top and ML_bottom on the filterability of the kaolinite slurry.

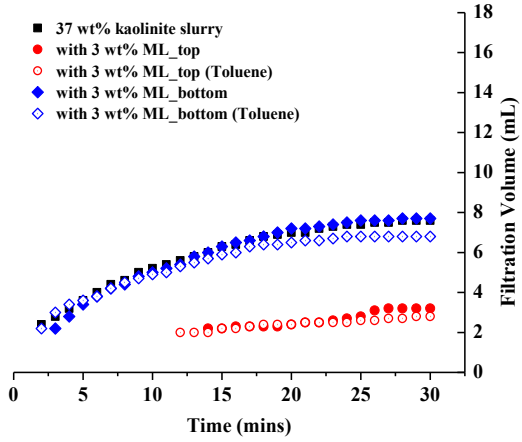

Figure 8. The effect of the raw/toluene-washed ML_top and ML_bottom on the filtration rate of kaolinite slurry.

If the detrimental effect was not caused by residual bitumen, then was it due to the fine and ultrafine solids? We have tested the vacuum filtration of fine and ultrafine model samples of

montmorillonite (median size 2.9 µm) and titanium dioxide (median size 0.7 µm). In some tests these fine and ultrafine solids were also treated with a bitumen-toluene solution to generate a bitumen coating on the fine solids surface. The filtration results are shown in Figures 9 and 10 for montmorillonite and titanium dioxide, respectively. As can be seen, the bitumen coating on the montmorillonite and titanium dioxide surface did not seem to make any difference in their vacuum filtration behavior. In fact, if anything, the coating seemed to make the filtration rate slightly faster.

Therefore, it is likely that removing residual bitumen from the MFT or coating the inorganic solids with bitumen would not significantly affect the filterability of the resulting samples in vacuum filtration. However, it should be noted that the residual bitumen in MFT is a complex mixture, existing as free bitumen, emulsified bitumen, and organics coated on mineral solids surface. The free bitumen can be removed by the combined toluene-washing and centrifugation, but certain bitumen components adsorb irreversibly on the surface and cannot be removed by toluene (Chen and Liu 2019). Therefore, the role of residual bitumen in the process of vacuum filtration is not conclusive and needs to be further investigated.

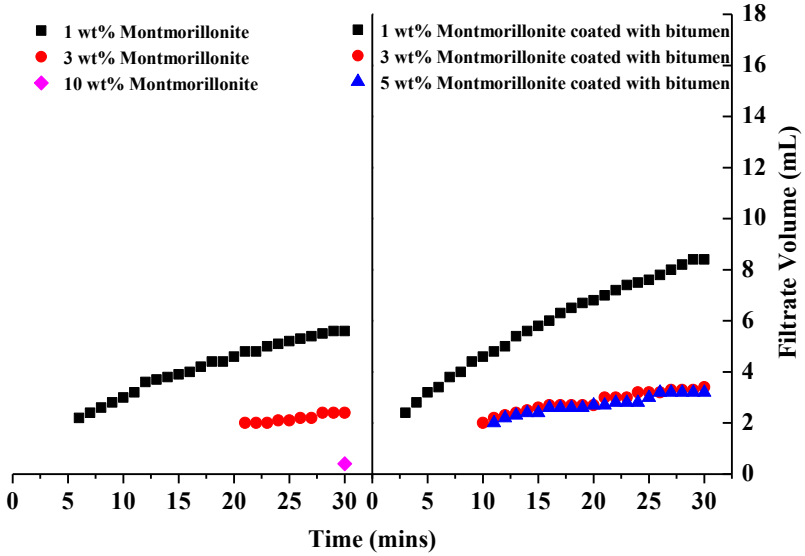

Figure 9. Vacuum filtration curves of montmorillonite before and after treatment with a bitumen-toluene solution for one week.

3.3 The effect of fine/ultrafine solids on filtration

Figures 9 and 10 show an interesting observation, i.e., that the ultrafine sub-micron titanium dioxide filtered fairly fast in the vacuum filtration test, while the coarser montmorillonite filtered very slowly even at the much lower slurry concentration. Therefore, it appeared that particle size may not be the dominant factor controlling filtration, while the type of the fine solids also matters.

To further confirm this observation, Figure 11 shows the filtration rate of the three tested model solids, titanium dioxide, montmorillonite, kaolinite, and the MFT components ML_top and ML_bottom. The particle sizes were also shown in Figure 11 in brackets ($d_{10}/d_{50}/d_{90}$).

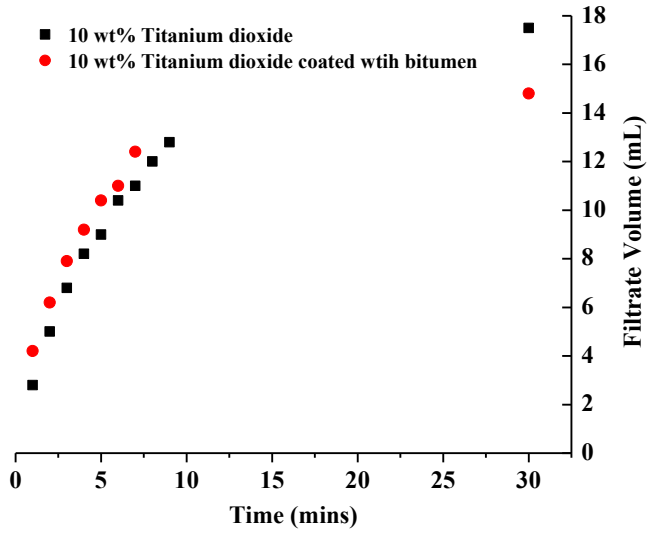

Figure 10. Vacuum filtration curves of titanium dioxide before and after being treated in a bitumen-toluene solution for one week.

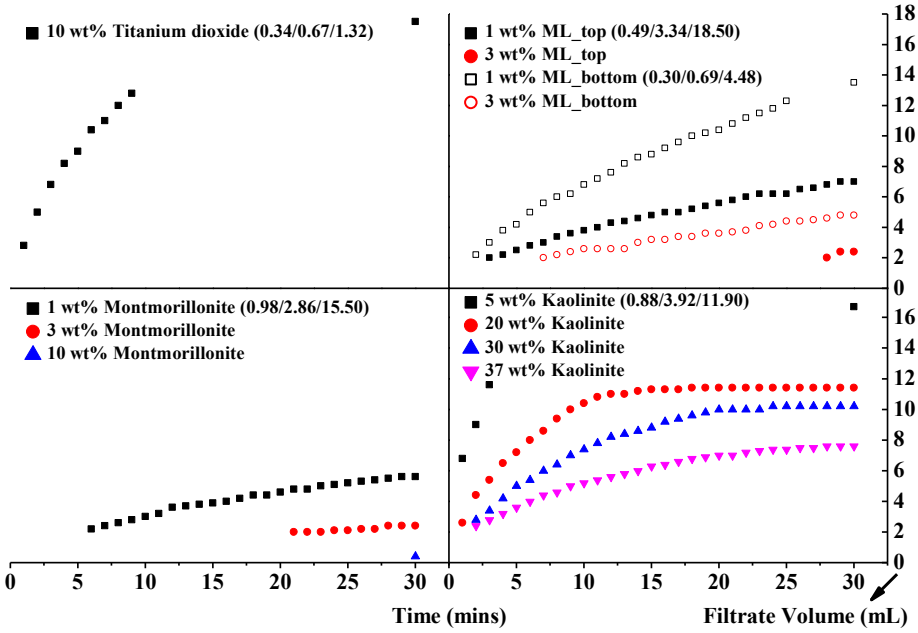

Figure 11. Vacuum filtration curves and particle size distribution ($d_{10}/d_{50}/d_{90}$, µm) of titanium dioxide, ML_top, ML_bottom, montmorillonite, and kaolinite at different solids contents.

Of the samples shown in Figure 11, titanium dioxide had the smallest particle size which was predominantly less than 1.3 µm but its filtration rate was the highest even at 10 wt% solids. Kaolinite and montmorillonite had similar particle sizes, with median sizes at 3.9 and 2.9 µm, respectively, but the filtration rate of kaolinite, even at 37 wt% solids, was faster than montmorillonite at 1 wt% solids. Collectively, these phenomena indicated that particle size played

a much lesser role than the type of solids, and it seems that clays, especially the swelling clays, possess extremely poor filterability.

The ML_top was on top of the ML_bottom after centrifugation, so one would expect the measured particle size of ML_top to be smaller than the ML_bottom. However, the PSD measurements by the Malvern Mastersizer 3000 showed that ML_top had a larger particle size (median size 3.3 μm) than the ML_bottom (median size 0.7 μm). This could be attributed to the light and loose organic aggregates in the ML_top fraction, such as the humic matter which has been reported as polar and toluene-insoluble organics in oil sands (Kotlyar et al. 1987, Darcovich et al. 1989). In addition, it is speculated that the blackish color of the solid particles in the ML_top fraction was originated from the organic coatings on fine solids surface. But to what extent would the surface modification of fine clays by the organic matter change the inter-particle interactions to such a degree so that it starts to significantly affect filtration? The answer is far from clear at present. Moreover, the ML_top fraction showed comparable filterability to montmorillonite (Figure 11), and incidentally, their particle sizes were similar, too, with median sizes at 3.3 and 2.9 μm, respectively. Could it be that montmorillonite-like clay minerals, i.e., swelling clays, were present in the ML_top component of MFT? Montmorillonite is a well-recognized swelling clay mineral in the smectite group with an appreciable water-holding capacity. According to Yong & Sethi, the water-holding ability of the sample closely relates to its easiness of water release during filtration (Yong & Sethi 1978). Therefore, we hypothesize that the constituent swelling clay minerals together with associated bitumen may be responsible for the extremely low filterability of the ML_top, which in turn results in the extremely low filterability of MFT when the material in the ML_top was inoculated to the MFT. We are currently investigating the mineralogical compositions of the subfractions of the centrifuged MFT as well as the identity of the coated organics on mineral solids surface in order to understand their effects on oil sands tailings filtration and design processing methods to mitigate their detrimental effects.

4 CONCLUSIONS

Based on the observations from both pressure filtration and vacuum filtration tests, it can be concluded that:

(1) Different components of MFT affected the filterability of MFT differently. A fine fraction with a median size of 3.3 μm obtained after double centrifugation (called ML_top fraction in this paper) was found to be responsible to the poor filterability of MFT.
(2) The filterability of the ML_top itself was extremely low, and the addition of a small amount of it (3 wt%) to model solid samples such as kaolinite immediately turned the sample unfilterable.
(3) Removing bitumen from MFT with toluene wash, or coating model inorganic solid samples with bitumen seemed to have little effect on the filterability of the resulting sample.
(4) The particle size of solids was not found to be a primary factor contributing to the poor filterability of all the samples tested in this work.
(5) The type of solids was found to significantly impact filterability. We observed that swelling clay such as montmorillonite was the worst to filter, and it was unfilterable even at 3 wt% solids with a median size of 2.9 μm; On the other hand, a non-clay solid, titanium dioxide, with a median size of 0.7 μm, filtered readily even at 10 wt% solids.
(6) The filterability of the ML_top fraction was found to be similar to montmorillonite. We are currently investigating (i) the mineralogical composition of the ML_top, (ii) the identity of organic coatings on the constituent minerals and (iii) the microstructures of these minerals/organic matter on their filtration behavior in order to find mitigation measures to promote oil sands tailings dewatering by filtration.

5 REFERENCES

Baillie, Robert A., and Earl W. Malmberg. 1969. Removal of clay from the water streams of the hotwater process by flocculation. U.S. Patent No. 3,487,003.

Beier, Nicholas, and David Sego. 2008. The oil sands tailings research facility. *Geotechnical News* 26 (2): 72–77.

Chen, Qiang, and Qi Liu. 2019. Bitumen coating on oil sands clay minerals: a review. Review-article. *Energy and Fuels* 33 (7): 5933–43.

Darcovich, K., L. S. Kotlyar, W. C. Tse, J. A. Ripmeester, C. E. Capes, and B. D. Sparks. 1989. Wettability Study of Organic-Rich Solids Separated from Athabasca Oil Sands. *Energy and Fuels* 3 (3): 386–91.

Hande, Aharnish Bhojaraj. 2014. Accelerated dewatering and drying treatment of oil sands tailings by electrical resonant auto-transformer. *The University of Alberta*.

Islam, Shriful. 2014. Thickening of mature fine oil sands tailings. *The University of Western Ontario*.

Klein, Colin, David Harbottle, Lana Alagha, and Zhenghe Xu. 2013. Impact of fugitive bitumen on polymer-based flocculation of mature fine tailings. *Canadian Journal of Chemical Engineering* 91 (8): 1427–32.

Kotlyar, L. S., H. Kodama, B. D. Sparks, and P. E. Grattan-Bellew. 1987. Non-Crystalline Inorganic Matter-Humic Complexes in Athabasca Oil Sand and Their Relationship to Bitumen Recovery. *Applied Clay Science* 2 (3): 253–71.

Loerke, Rosalynn S. 2016. Pressure filtration of mature fine tailings. *The University of Alberta.*

Loerke, Rosalynn S, Xiaoli Tan, and Qi Liu. 2017. Dewatering of oil sands mature fine tailings by dual polymer flocculation and pressure plate filtration. *Energy and Fuels* 31 (7): 6986–95.

Matthews, J.G., W.H. Shaw, M.D. MacKinnon, and R.G. Cuddy. 2002. Development of composite tailings technology at syncrude. *International Journal of Surface Mining, Reclamation and Environment* 16 (1): 24–39.

Revington, Adrian Peter, et al. 2018. Process for flocculating and dewatering oil sands mature fine tailings. U.S. Patent No. 9,909,070

Sobkowicz, John. 2012. Oil sands tailings technology deployment roadmap. Vol. 2.

Suthaker, Nagula N., and J. Don Scott. 1996. Measurement of hydraulic conductivity in petroleum sand tailings slurries. *Canadian Geotechnical Journal* 33 (4): 642–53.

Yong, Raymond N., and Amar J. Sethi. 1978. Mineral particle interaction control of tar sand sludge stability. *Journal of Canadian Petroleum Technology* 17 (4): 76–83.

Zhang, Dan, Thomas Thundat, and Ravin Narain. 2017. Flocculation and dewatering of mature fine tailings using temperature-responsive cationic polymers. *Langmuir* 33 (23): 5900–5909.

Zhu, Ying. 2015. Cationic and anionic dual polymer pairs for mature fine tailings flocculation and dewatering. *The University of Alberta.*

Zhu, Ying, Xiaoli Tan, and Qi Liu. 2017. Dual polymer flocculants for mature fine tailings dewatering. *Canadian Journal of Chemical Engineering* 95 (1): 3–10.

Geochemical Characterization of Sulfurized Tailings and Waste Rock of a Graphite Mine

Veronik Lord, Benoît Plante & Isabelle Demers
Université du Québec en Abitibi-Témiscamingue, Rouyn-Noranda, Québec, Canada

Martine Paradis
Nouveau Monde Graphite, Québec, Québec, Canada

ABSTRACT: Nouveau Monde Graphite owns the Matawinie property located 6 km south-west of Saint-Michel-des-Saints in the province of Quebec (Canada). The waste (tailings and waste rocks) expected to be generated by the future mine is potentially acid generating. Two types of tailings will be produced: sulfide tailings and desulfurized tailings.

This project aims to study the geochemistry of waste rocks and tailings using laboratory column tests. Post-dismantling characterizations were performed using optical microscopy and scanning electron microscopy to assess the sulfide oxidation progress and identify secondary minerals. The column tests are part of the environmental characterization campaign aimed to guide the mine waste management of the Matawinie project. The wastes will be managed using the co-disposition of waste rocks and tailings to avoid the oxidation of sulfide minerals. The hydrogeochemical behavior of the future Matawinie wastes are also studied using numerical modeling and in-situ experimental cells based on the column test results.

1 INTRODUCTION

Graphite is a mineral composed of carbon layers bounded with electrostatic strength (USGS 2017). This atomic configuration results in a great electric conductivity and a great potential to accumulate electrical charges (USGS 2017, Yuan et al. 2011). Those properties are used in modern applications such as lithium ion batteries (Wihelm & L'Heureux 2006, Yuan et al. 2011), which are currently used in automobile industry to manufacture electric vehicles (Wihelm & L'Heureux 2006). The recent infatuation for electric vehicles increased the global request for graphite (Fragasso 2015).

Natural graphite has a great potential to manufacture lithium ion batteries (USGS 2017). Historically, the province of Quebec counted one (1) major graphite exploitation that is active since 1989 and other graphite exploration projects in the Quebec province have emerged in recent years, such as the Matawinie project of Nouveau Monde Graphite (NMG) (Fragasso 2015). As all mine projects in Quebec, NMG has to plan the closure of the site before starting the operations.

The environmental behavior of graphite mine wastes is sparsely documented. Graphite is generally formed in metamorphic geological environments that promote the formation of sulfide minerals (Simandl et al. 2015, Stamatelopoulou-seymourmour & Maclean 1984). Indeed, most of the graphite mine projects in Quebec are associated with sulfide minerals (DRA-Metchem 2018, GoldMinds Géoservices Inc. et al. 2015, Hatch 2015, Hinterland Geoscience and Geomatics 2017, Roche Ltd. 2012, Tetra Tech 2016). Therefore, it is relevant to assess the potential for acid mine drainage (AMD) of future graphite wastes.

AMD is formed upon sulfide oxidation with the lack of sufficiently efficient neutralization. Indeed, sulfide oxidation occurs when mine wastes (waste rocks and tailings) are exposed to an oxidant, such as atmospheric oxygen (Blowes et al. 2014). For example, when one (1) mole of pyrite (FeS_2) is exposed to atmospheric oxygen, it produces two (2) moles of H^+, as shown in Equation 1 (Nordstrom 1982).

$$FeS_2(s) + \frac{7}{2}O_2 + H_2O \rightarrow Fe^{2+} + 2SO_4^{2-} + 2H^+ \quad (1)$$

The released Fe^{2+} can also react with O_2 to be oxidized to Fe^{3+}. The produced Fe^{3+} can thereafter react with water and generate H^+, as shown in Equation 2 (Blowes et al. 2014).

$$Fe^{3+} + 3H_2O \rightarrow Fe(OH)_3 + 3H^+ \quad (2)$$

In acidic conditions (pH < 4), the major oxidant of pyrite is Fe^{3+} which leads to the generation of even more H^+. Thus, the oxidation of pyrite and other sulfide minerals decreases the mine drainage pH. The precipitation of secondary minerals, such as gypsum, goethite, and ferrihydrite, can also be associated with the oxidation of sulfide minerals (Blowes et al. 2014).

Those chain reactions can be influenced by several parameters such as bacterial activities that catalyze the oxidation of sulfide minerals (Blowes et al. 2014). Pyrrhotite ($Fe_{1-x}S$) can also oxidize following similar patterns as pyrite. The kinetics of pyrrhotite oxidation is 20 to 100 times faster than that of pyrite oxidation (Blowes et al. 2014). Moreover, the oxidation of pyrrhotite can be partially completed and can lead to the accumulation of partially oxidized sulfur species such as native sulfur (S^0) (Blowes et al. 2014, Gunsinger et al. 2006, Janzen et al. 2000).

In order to limit risks associated with AMD, mine waste management is frequently aimed to minimize sulfide minerals oxidation. This can be achieved by avoiding water or oxygen infiltration or by removing sulfide minerals of mine waste. The desulfurization of tailings can significantly reduce the volume of acid generating materials (Bussière 2007). Moreover, the desulfurized tailings can be used to manage problematic tailings. Those desulfurized tailings can be used to limit the oxygen infiltration by consuming the oxygen with its residual sulfide minerals and by keeping the acid generating tailings saturated (Demers et al. 2008, 2009).

This research aims to study the geochemical behavior of the Matawinie materials (ore, waste rocks and tailings) without mitigation measures. Laboratory column tests were used to assess the geochemistry of each individual materials under oxidizing conditions. Results from this study are part of a broader environmental characterization campaign. Thus, results from this study have also been used in hydrogeochemical modeling that has guided the design of the co-disposal management concept and closure plan of the waste rock and tailings of the Matawinie mine. In addition, field scale experimental cells were installed on the Matawinie property in order to assess the performance of the co-disposal concept to avoid sulfide oxidation and mine water contamination.

2 MATERIAL AND METHODS

2.1 *Study site and materials*

The study site corresponds to the Matawinie property owned by the mining company NMG. NMG plans to extract this graphite deposit with an entirely electrically operated open pit. The Matawinie property is composed of 220 claims and covers a total surface area of 11,945 ha. The property contains many exploration blocks. The exploration work focused on the Tony block due to its greater graphite mineralization potential, which contains 145 claims that cover a total surface area of 7544 ha (DRA-Metchem 2018).

The Matawinie property is located approximately 150 km North of Montreal in the Lanaudière administrative region. More precisely, the mining project is located 6 km to the southwest of the Saint-Michel-des-Saints municipality (Fig. 1) (DRA-Metchem 2018, SNC-Lavalin 2019b). The topography on the property varies from elongated hills to slightly steep valleys. The climate at the property is considered to be soft subpolar and subhumid; winters are cold and summers are hot. The climate allows a long period for vegetation growth and there is no dry season in the area. The mean annual temperature and precipitation are respectively 3.1°C and 929.6 mm (SNC-Lavalin 2019b).

The mining wastes (tailings and waste rocks) expected to be generated by the future mine has a sulfur content (S_{total}) of maximum 3 %, mainly present as pyrrhotite, and are potentially acid generating. In order to manage those materials, NMG plans to incorporate a desulfurization circuit to its extraction mill in order to reduce the total volume of acid generating tailings (DRA-Metchem 2018; SNC-Lavalin 2019b) and to use the non-acid generating tailings in a co-disposal design (SNC-Lavalin 2019b). Thus, two (2) types of tailings are generated: the PAG and NAG tailings.

The NAG tailings are desulfurized tailings that are non-acid generating. NAG tailings represent 78 % of the total tailings. PAG tailings correspond to a sulfide concentrate and are considered to be potentially acid generating. PAG tailings represent 22 % of the total tailings (DRA-Metchem 2018).

Moreover, NMG will use a co-disposal method to store waste rocks, the NAG and the PAG tailings, to ensure that reactions leading to AMD will be limited (SNC-Lavalin 2019b). The preliminary co-disposal concept is to encapsulate the filtered PAG tailings and potentially acid generating waste rocks within filtered NAG tailings. The co-disposal will take advantage of the hydrogeological properties of the different materials to keep a high degree of saturation in the PAG tailings (SNC-Lavalin 2019a). Moreover, the remaining fraction of sulfides in the NAG tailings will consume oxygen and limit oxygen flow in potentially acid generating waste rocks and PAG tailings (SNC-Lavalin 2019a). The Figure 2 shows the preliminary configuration of the co-disposal concept. The detailed engineering (layers thickness and geometry) of the co-disposal concept will be precise using the results of National Research Council Canada (NRCC) modeling and of upcoming experimental field cells results and interpretations (Conseil national de recherches Canada 2020).

The waste rocks lithologies are the following: Mixed Paragneiss (80 %), Charnockite (12 %), Biotite Paragneiss (6 %), Meta-Gabbro (1 %), and Graphitic Paragneiss (1 %). The Graphitic Paragneiss is the graphitic ore, with a cutoff value of 2.32 % of carbon; only residual amounts are expected in the waste rocks (DRA-Metchem 2018). The samples that were used to perform this study correspond to composites of each lithology. The composites include an assembly of selected subsamples of each lithology that represent the main geology of the site.

2.2 *Initial characterization*

Initial characterizations were performed on the materials studied in column tests. The initial characterizations included acid base accounting test (ABA). Total carbon and sulfur concentrations were determined using an induction furnace. The neutralization potential (NP) were determined using the modified Sobek procedure (Lawrence & Wang 1997). The chemical composition of the materials was determined using a four acids digestion ($HCl/HNO_3/HF/HClO_4$) on pulverized solid samples followed by Inductively coupled plasma atomic emission spectrometry (ICP-AES) analysis. The quantitative mineralogical composition of the materials was determined using Quantitative Evaluation of Minerals by Scanning Electron Microscopy (QEMSCAN).

2.3 *Colum tests*

Column tests were used in order to assess the AMD generation and metal leaching potentials of the lithologies and tailings (NAG and PAG), in order to optimize the design of the co-disposal technique to be used. They are used to accelerate the sulfide oxidation and acid neutralization reactions (Benzaazoua et al. 2004; MEND 2009) in order to assess the long-term potential to generate AMD. The geochemistry of the leachates can also be used to qualitatively identify potential contaminants. A total of seven (7) column tests were performed as part of this study: one for each type of materials (2 columns of tailings and 5 columns of ore and waste rocks).

The methodology used for the column tests is inspired by the works of Marchant and Lawrence (1991). Plexiglass columns with a 14 cm diameter were used in this study. For the waste rocks, the materials were sieved to < 2 cm. The target thickness of waste rocks in the columns was 70 cm, which represents ± 20 kg of materials. For the Meta-Gabbro lithology, only 4 kg of materials were used in the column test due to the reduced availability of this material. Flushes were performed every 2 weeks with 2 L of deionized water (400 mL for Meta-Gabbro to have the same liquid/solid ratio as the other columns). The columns were left to air-dry between flushes. For the Biotite Paragneiss, Graphitic Paragneiss and Mixed Paragneiss lithologies, a total of 19 leaching cycles were performed. For the Charnockite and the Meta-Gabbro lithologies, a total of 12 leaching cycles were performed.

For the tailings, the target thickness of materials in the columns was 30 cm, which represents ± 8 kg of materials. Flushes were performed on a monthly basis with 2 L of deionized water. For the PAG Tailings, a total of 17 leaching cycles were performed. The NAG Tailings column is still active.

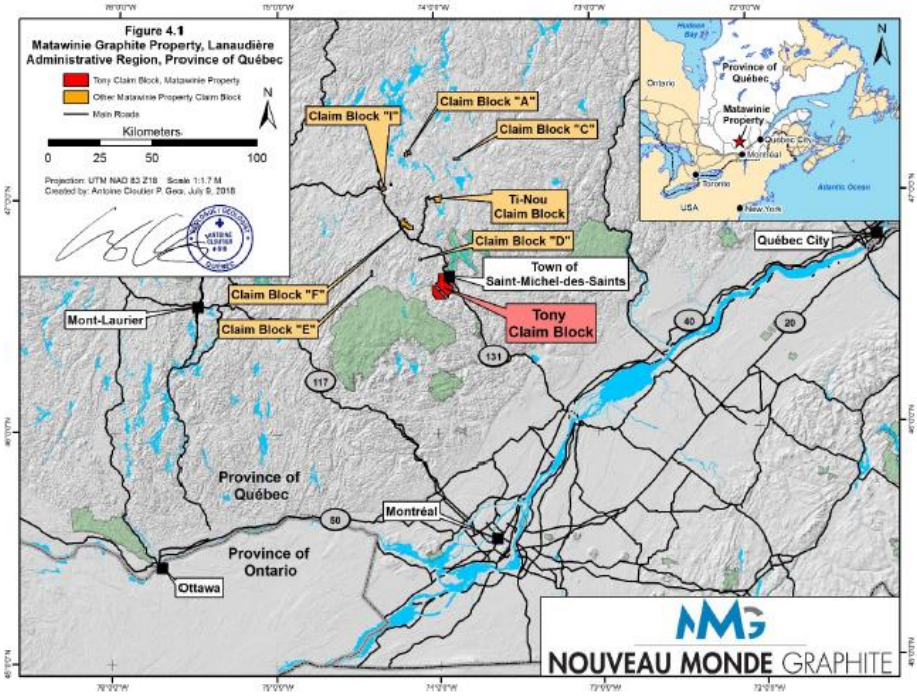

Figure 1. Location of the Matawinie property, taken from DRA-Metchem (2018)

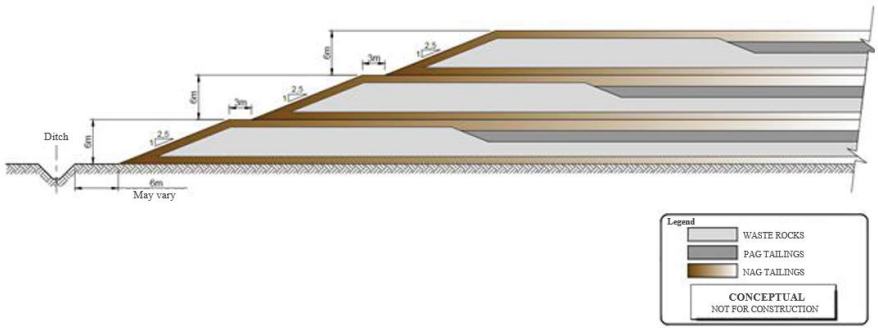

Figure 2. Preliminary configuration of the co-disposal concept, adapted from SNC-Lavalin (2019a).

2.4 *Leachate chemistry*

Leachates were analyzed for pH, oxidation-reduction potential (Eh), electrical conductivity (EC), acidity, alkalinity, metal concentrations, and sulfur speciation. Acidity and alkalinity were measured using Metrolm 848 Titrino Plus. Samples were filtered (0.45 µm nylon membrane filter) and titrated using 0.02N NaOH and 0.02N H_2SO_4. Metal concentrations were measured using

coupled plasma mass spectrometry (ICP-MS) and atomic emission spectrometry (ICP-AES). Sulfur species concentrations were determined using ion chromatography (IC). All samples were filtered (0.45 µm nylon membrane filter). For the metal concentrations measurements, samples were acidified with 2 % HNO_3 and treated with 37 % H_2O_2 in order to prevent metal precipitation prior to the analysis.

2.5 *Post-dismantling analyses*

Post-dismantling analyses were performed in order to identify secondary minerals formed as a product of sulfide oxidation and to describe the hard pan that developed within some of the column tests. Polished sections were used to perform these analyses and were manufactured with materials collected from completed column tests.

As a preliminary step, the software Visual MINTEQ was used to perform thermodynamic equilibrium calculations. Using the physico-chemical parameters of each leachate and an integrated database, this software calculates the different chemical species that should be dissolved or precipitated for a balanced system. This preliminary step had allowed targeting mineralogical analyses of secondary precipitates.

The post-dismantling analyses included observations under a polarized optical microscope. The optical mineralogy was used in order to identify and to describe alteration textures and structures resulting of sulfide oxidation (MEND 2009). Also, specific areas on the polished sections were identified in order to perform scanning electron microscopy (SEM). Finally, SEM was performed on the polished sections in order to estimate the chemical composition of the different mineralogical phases targeted under the optical microscope.

3 RESULTS

3.1 *Initial characterization*

Table 1 presents the results of the following initial characterizations: ABA, 4 acid digestion and QEMSCAN. The results show that the sulfur content is highest in the PAG tailings, mainly associated to pyrrhotite. The NAG tailings contain a residual sulfur content of 0.16 %. The Graphitic Paragneiss contains the highest sulfur content, mainly as pyrrhotite. It is also important to note that the metal content seems to be positively correlated to the sulfide content since metal content is higher in the PAG tailings and Graphitic Paragneiss samples. Traces of calcite were detected within most of the materials.

3.2 *Leachate chemistry*

The main components observed in the column leachates are presented in Figure 3. The majority of the materials produced leachates with neutral pH. In the case of waste rocks, the pH values of the following materials stayed at near-neutral values throughout the test: Mixed Paragneiss, Biotite Paragneiss, Meta-Gabbro, Charnockite. In the case of Graphitic Paragneiss, the pH values decreased throughout the column test. Indeed, before the 14th flush, the pH values were above 6. After the 14th flush, the pH values decreased and reached a minimum value of 4.74. In the case of tailings, the pH values of the PAG tailings stayed between 2.95 and 4.36 throughout the column test. The pH values of NAG tailings generally stayed at near-neutral values except during the 10th and the 11th flushes, where the pH values reached a minimum value of 3.54 before going back to near-neutral values for the subsequent flushes. The release of the different sulfur species also seems to be positively correlated to low pH values in the leachates. Indeed, the concentration of sulfate was higher in the PAG column (mean value of 4866 mg/L) and slightly higher in Graphitic Paragneiss column (mean value of 896 mg/L) than in other columns. It is also interesting to note that thiosulfate was observed at concentrations between 0.5 and 3072 mg/L in the PAG column and at concentrations around 15 mg/L in Graphitic Paragneiss column. The concentration of this sulfur species in other columns was under the detection limit (1 mg/L).

The main metals detected in the leachates are Fe, Ni and Zn and their concentrations were generally higher in materials that generated acidity. The concentration of Fe in the PAG column was between 276 and 4950 mg/L. Also, the concentration of Fe in Graphitic Paragneiss was <

10 mg/L before the 11th flush inclusively and increased up to 122 mg/L after the 11th flush. Ni concentrations in PAG column were near 30 mg/L in the three (3) first flushes of the column test. On the 4th flush, the Ni concentrations decreased to 0.3 mg/L and then increased up to 22 mg/L in the subsequent flushes. Ni concentration in Graphitic Paragneiss was maximal in the first flush (4.22 mg/L). Ni concentrations seemed to increase between the 2nd and the 12th flushes and then stabilized at values near 3 mg/L in subsequent flushes. The PAG column showed mean Zn concentrations of 22.5 mg/L. The NAG column generated mean Zn concentrations of 1.6 mg/L throughout the test. Moreover, Fe and Ni concentrations showed a peak on the 10th flush but were near detection limit on other flushes of the NAG tailings. Metal concentrations in other columns (Mixed Paragneiss, Biotite Paragneiss, Meta-Gabbro, Charnockite) were generally near or under the respective detection limits.

The Ca and Mg release is associated with the dissolution of neutralising minerals (mainly feldspars, biotite, and traces of calcite in the materials) in response to sulfide oxidation and acid generation. The mean concentrations of Ca and Mg were 537 mg/L and 247 mg/L and of 156 mg/L and 64 mg/L respectively in the PAG and Graphitic Paragneiss columns, respectively. The Ca and Mg releases observed suggest that neutralising minerals are dissolving throughout the tests, and enable to buffer the pH to near-neutral values for all materials except the PAG tailings and the Graphitic paragneiss. Since the Graphitic paragneiss lithology corresponds to the ore and only represents 1 % of the expected waste rocks, it is possible that a representative composite of the expected waste rock composition (containing 1 % of graphitic paragneiss) would not be acid generating. This hypothesis will be verified using subsequent tests.

Table 1. Initial characterizations results

Analysis	Waste Rocks					Tailings	
	Graphitic Paragneiss	Mixed Paragneiss	Biotite Paragneiss	Charnockite	Meta-Gabbro	PAG	NAG
ABA							
S (weight %)	2.99	0.81	0.04	0.11	1.05	17.0	0.16
PA (t $CaCO_3$/1000 t)	52.2	20.3	0.75	2.56	17.8	485	3.12
PN (t $CaCO_3$/1000 t)	18.2	16.5	10.6	15.8	21.5	6.20	12.0
PNN (t $CaCO_3$/1000 t)	-34.1	-3.85	9.98	13.2	3.63	-479	9.38
PN/PA	0.43	1.76	16.1	9.96	4.70	0.01	4.00
4 acid digestion (µg/g)							
Ca	10,000	18,000	22,000	14,000	46,000	7200	14,000
Cu	110	66	13	18	79	450	13
Fe	47,000	47,000	34,000	24,000	93,000	23,000	8900
Mg	8500	12,000	10,000	3900	58,000	5100	7600
Ni	170	56	15	4.1	110	1100	17
Zn	200	90	87	88	270	950	75
QEMSCAN (weight %)							
Pyrrhotite	6.40	1.72	0.07	0.02	2.31	39.5	0.20
Pyrite	1.04	0.08	0.01	0.20	0.01	4.90	0.04
Quartz	55.1	46.4	22.7	26.8	2.97	28.8	56.0
Feldspar	19,6	24,1	56,2	59.3	28.4	12.8	25.0
Pyroxene	0.12	2.10	8.79	0.28	39.0	0.20	0.63
Biotite	5,58	4,66	5.12	5.89	6.09	3.61	5.30
Grenat	1,96	14,5	1.94	0.64	5.76	2.40	2.80
Calcite	0.12	0.32	0.40	0.65	0.19	0.11	0.15

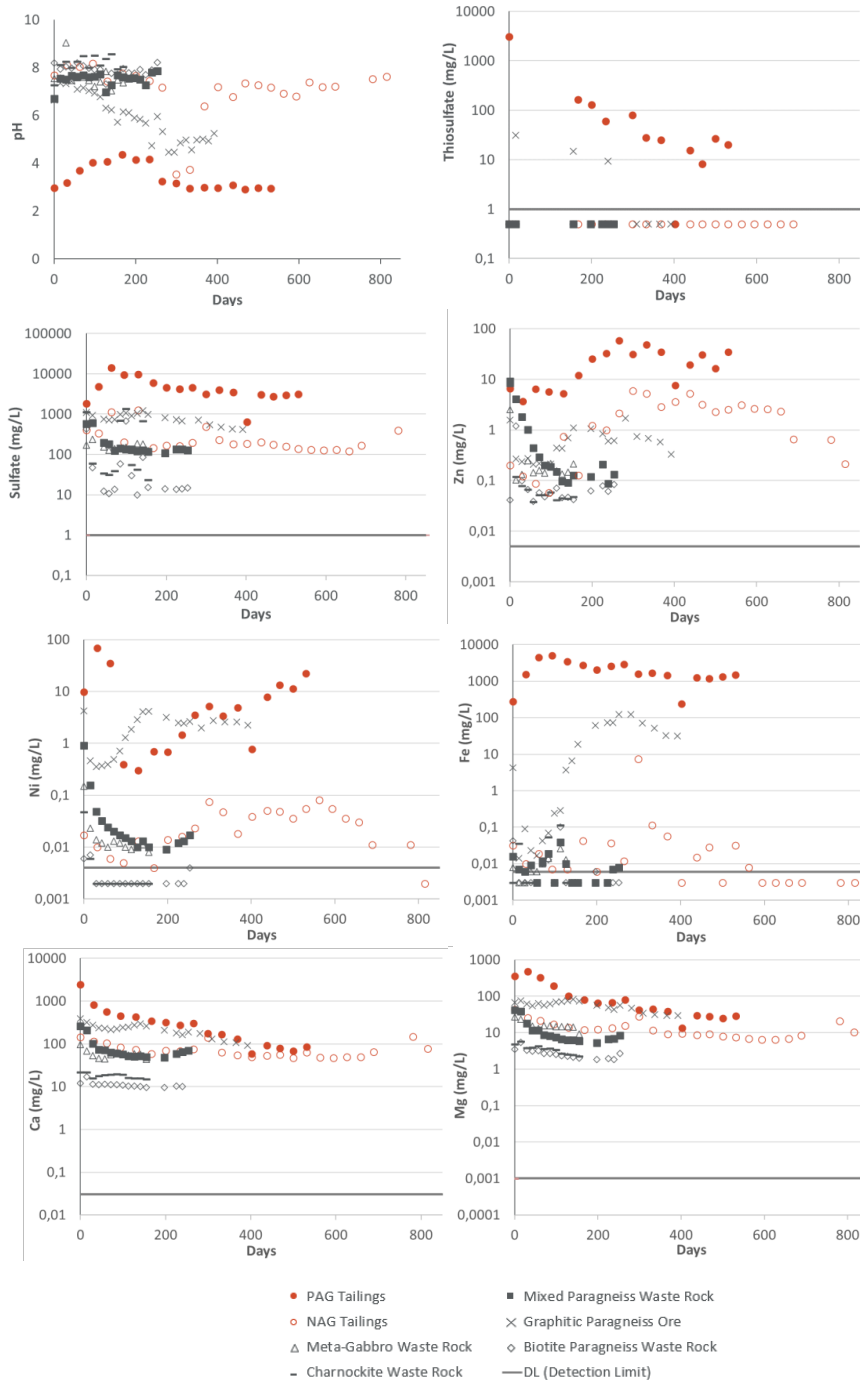

Figure 3. Chemical composition of column leachates

3.3 *Post-dismantling*

Post-dismantling analyses were performed on PAG tailings and Graphitic Paragneiss materials. Post-dismantling analyses are also planned to be performed on the NAG material when the column test will be completed. Macroscopic observations of the NAG column showed no evidence of oxidation (Fig. 4A). The PAG column was dismantled in four (4) layers: TOP (≈0.1 cm), 0-10 cm, 10-20 cm and 20-30 cm. The Graphitic Paragneiss column was dismantled in three (3) layers: 0-20 cm, 20-40 cm and 40-70 cm. The PAG column was highly cemented and ocher. It presented whitish deposits on top and contained greyish non-oxidized PAG inclusions (Fig. 4B). The Graphitic Paragneiss column was partially cemented all over the column, the top section of the column being more oxidized than the bottom (Fig. 4C).

A total of four (4) polished sections were prepared to observe the post-dismantling PAG layers:

1. Fine grains < 125 µm (10-20 cm layer);
2. Coarse grains > 125 µm (10-20 cm layer);
3. Fine grains < 125 µm (TOP layer);
4. Fragments with non-oxidized PAG inclusions.

Optical microscope observations identified alteration structures around pyrrhotite. Alteration structures correspond to a greyish and streaked halo (Fig. 5A, 5C). Bluish hardpan was also observed around altered pyrrhotite. Oxidation structures seem more important in the coarse grains. Non-oxidized PAG inclusions seem to be associated with fine-grained PAG materials. SEM analysis included semi-quantitative chemical composition characterization. Greyish halos were frequently composed of iron oxyhydroxides containing Ni. Alterations around pyrrhotite also showed what seem to be native sulfur. Hardpans are usually composed of iron oxyhydroxides.

A total of two (2) polished sections were made from post-dismantling Graphitic Paragneiss :

1. Fine grains < 2 mm (0-20 cm layer);
2. Coarse grains > 2 mm (0-20 cm layer).

Bluish hardpan and greyish and streaky alteration halos were also observed under the optical microscope for the graphitic paragneiss (Fig. 5B, 5D). The semi-quantitative chemical composition of the hardpan and the alteration halos obtained with the SEM were similar to that of the PAG. Alteration structures were frequently observed at the outer borders of the grains. SEM and optical microscope analyses also identified residual graphite and disseminated rutile, chalcopyrite, and sphalerite.

Thermodynamic equilibrium calculations were used to deduce the saturation indices of possible secondary phases within the columns; these results are shown in Figure 6 for gypsum and goethite. The saturation indices are coherent with the post-dismantling observations. Indeed, as shown on Figure 6A, the precipitation of gypsum was not favored in the columns. However, oxyhydroxides seem to be precipitating in the PAG and Graphitic Paragneiss columns. The thermodynamic equilibrium calculations suggest that many oxyhydroxides are oversaturated in the other columns (as illustrated using goethite in Figure 6B), because of the near-neutral pH of their leachates, which reduces the solubility of most iron oxyhydroxides.

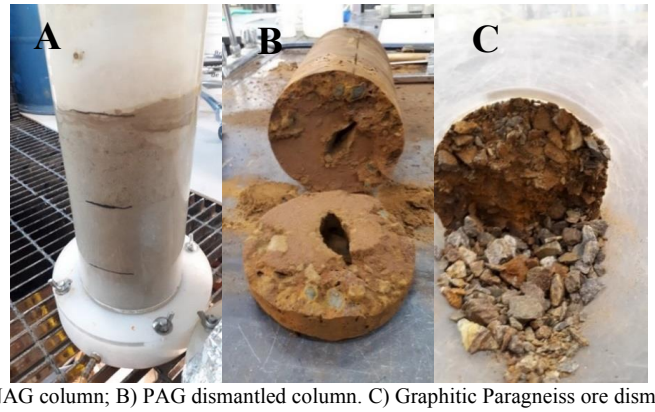

Figure 4. A) NAG column; B) PAG dismantled column. C) Graphitic Paragneiss ore dismantled column.

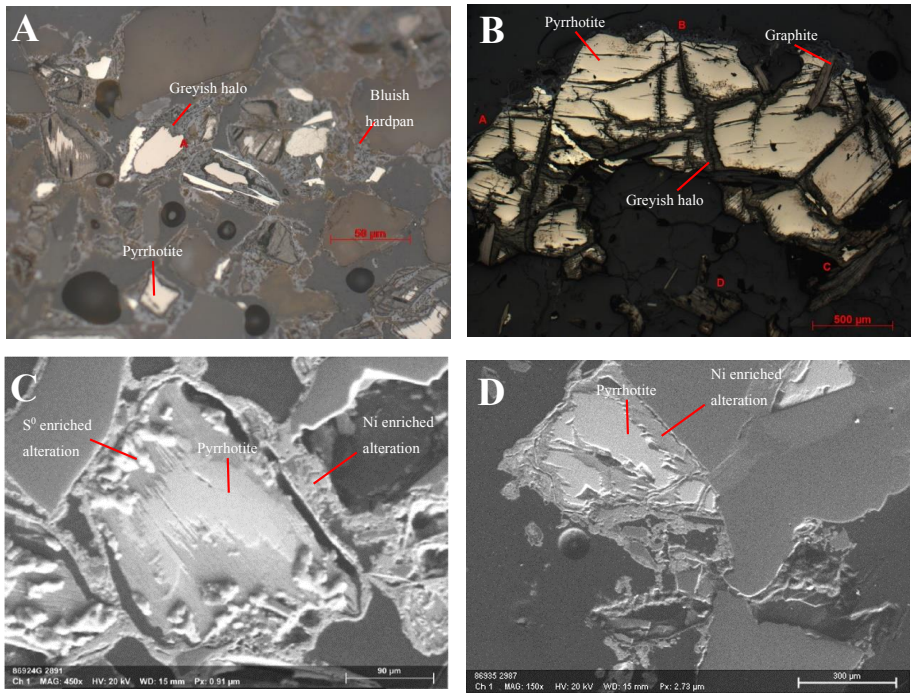

Figure 5. A) Post-dismantled PAG observed with optical microscope. B) Post-dismantled Graphitic Paragneiss ore observed under optical microscope. C) Post-dismantled PAG observed with SEM. D) Post-dismantled Graphitic Paragneiss ore observed with SEM

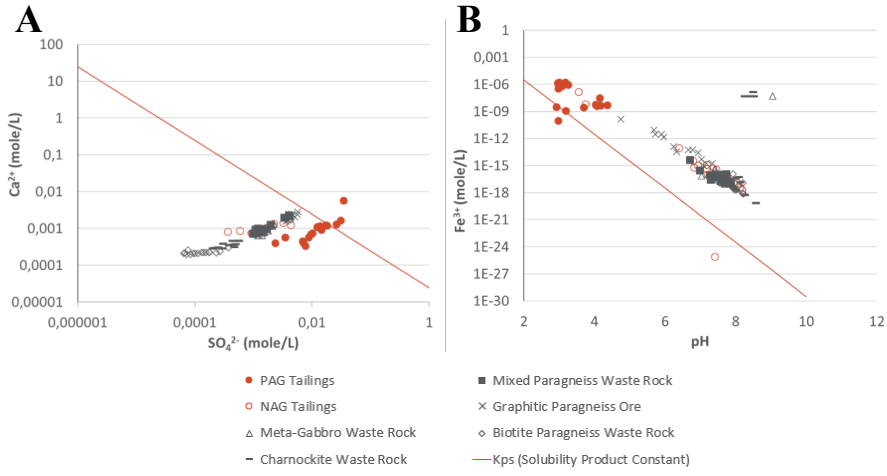

Figure 6. A) Gypsum equilibrium calculations; B) Goethite equilibrium calculations

4 CONCLUSIONS AND FUTURE WORK

In conclusion, geochemical analyses were performed on the five (5) different lithologies (Graphitic Paragneiss ore, Mixed Paragneiss, Biotite Paragneiss, Charnockite and Meta-Gabbro) encountered on the Matawinie property owned by NMG and on the two (2) types of tailings (PAG and NAG) that will be generated by the mine.

Initial characterizations suggested that the Graphitic Paragneiss ore and the PAG have the highest sulfur content, mostly as pyrrhotite. Column test results confirmed that Graphitic Paragneiss ore and PAG are potentially acid generating. In the oxidizing conditions of the columns, the pH in PAG leachates remained between 2.95 and 4.36 throughout the column test. In the case of the Graphitic Paragneiss ore, the pH values seemed to decrease throughout the column test and reached a minimum value of 4.74. The highest metal concentrations were associated with acidic leachates. The main metals encountered in column test leachates are Fe, Ni and Zn. The pH in NAG column leachates stabilized at near neutral values. Zn was the main metal leached from the NAG, while significantly less Ni and Fe were leached from the NAG than from the PAG tailings.

Post-dismantling analyses were performed with an optical microscope and SEM. They allowed to observe alteration structures such as streaked halos around pyrrhotite and the accumulation of secondary iron oxyhydroxides. Alteration structures were mainly composed of iron oxyhydroxides occasionally enriched in Ni and of S^0 enriched products.

Results from this study are part of the NMG environmental characterization campaign that includes hydrogeochemical modeling and experimental field cells to assess the performance of the co-disposal strategy designed to avoid sulfide oxidation and metal leaching. Ongoing engineering includes further interpretations of experimental field cells and will enable to assess scale differences between the laboratory column tests and more representative in situ conditions.

5 ACKNOWLEDGEMENTS

Funding of this research was provided by NMG and the Ministère des Ressources Naturelles du Québec. The authors thank the staff of Unité de recherche et de service en technologie minérale (URSTM) and more particularly Alain Perreault, Yvan Poirier, Emmanuelle Cecchi, Jean-Christophe Turcotte and Bini Mangane for assistance in the laboratory and field. The authors also thank the NMG staff for their cooperation and involvement.

6 BIBLIOGRAPHY

Benzaazoua, M., Bussière, B., Dagenais, A.-M., & Archambault, M. 2004. Kinetic tests comparison and interpretation for prediction of the Joutel tailings acid generation potential. *Environmental Geology*, 46(8): 1086–1101.

Blowes, D. W., Ptacek, C. J., Jambor, J. L., Weisener, C. G., Paktunc, D., Gould, W. D., & Johnson, D. B. 2014. The Geochemistry of Acid Mine Drainage. In *Treatise on Geochemistry*:131–190.

Bussière, B. 2007. Colloquium 2004: Hydrogeotechnical properties of hard rock tailings from metal mines and emerging geoenvironmental disposal approaches. *Canadian Geotechnical Journal*, 44(9): 1019–1052.

Conseil national de recherches Canada. 2020. Modeling of Co-disposal Concepts for Design Criteria. *Mid-term Technical Note.* NRC-EME-56096.

Demers, I., Bussière, B., Benzaazoua, M., Mbonimpa, M., & Blier, A. 2008. Column test investigation on the performance of monolayer covers made of desulphurized tailings to prevent acid mine drainage. *Minerals Engineering*, 21(4): 317–329.

Demers, I., Bussière, B., Mbonimpa, M., & Benzaazoua, M. 2009. Oxygen diffusion and consumption in low-sulphide tailings covers. *Canadian Geotechnical Journal*. 46(4): 454–469.

DRA-Metchem. 2018. Updated Technical Pre-Feasibility Study Report for the Matawinie Graphite Project. Prepared for Nouveau Monde Graphite. [NI 43-101]: pp. 367

Fragasso, D. 2015. Le graphite. Ministère de l'énergie et Des Ressources Naurelles Du Québec. Consulted on 2019-11-12. https://mern.gouv.qc.ca/mines/quebec-mines/2015-11/Graphite.asp.

GoldMinds Géoservices Inc., Tekhne Research Inc., Met-Chem, Soutex Inc., & Gesmine Inc. 2015. NI 43-101 Technical report: Resources update and feasibility study, Lac Guéret graphite project, Québec, Canada. Mason Graphite: pp. 334.

Gunsinger, M. R., Ptacek, C. J., Blowes, D. W., & Jambor, J. L. 2006. Evaluation of long-term sulfide oxidation processes within pyrrhotite-rich tailings, Lynn Lake, Manitoba. *Journal of Contaminant Hydrology*, 83(3–4): 149–170.

Hatch. 2015. Mason Graphite Inc. Exploitation du gisement de graphite du Lac Guéret. Étude d'impact sur l'environnement. No. H348328-0000-07-236–0001: pp. 645.

Hinterland Geoscience and Geomatics. 2017. NI 43-101 Lac aux Bouleaux Graphite Property Graphite Energy Corp: pp. 69.

Janzen, M. P., Nicholson, R. V., & Scharer, J. M. 2000. Pyrrhotite reaction kinetics: Reaction rates for oxidation by oxygen, ferric iron, and for nonoxidative dissolution. *Geochimica et Cosmochimica Acta*, 64(9): 1511–1522.

Lawrence, R. W., & Wang, Y. 1997. Determination of Neutralization Potential for Acid Rock Drainage Prediction. *Proc, 4th International Conf on Acid Rock Drainage (ICARD). Vancouver, Canada*: 451–464.

Marchant, B., & Lawrence, R. W. 1991. *Acid Rock Drainage Prediction Manual.* (CANMET under MEND , Mines and Resources Canada, Canada).

MEND. 2009. *Prediction Manual for Drainage Chemistry from Sulfidic Geology*. (1.20.1; By Price, W.A. CANMET, Natural Resources Canada, Canada.).

Nordstrom, D. 1982. Aqueous pyrite oxidation and the consequent formation of secondary iron minerals. In: Hossner LR, Kittrick JA, and Fanning DF (eds.). Acid Sulfate Weathering. *Soil Science Society of American Press.*

Roche Ltd. 2012. NI-43-101 Technical Report on the Lac Knife Graphite Project. Submitted to Focus Metal Inc. Focus Metals. 061975.001-200: pp. 87.

Simandl, G. J., Paradis, S., & Akam, C. 2015. Graphite deposit types, their origin, and economic significance. *British Columbia Geological Survey Paper* 2015–3: 163–171.

SNC-Lavalin. 2019a. Projet Matawinie—Étude d'impact environnemental et social. Volume 3. Étude d'impact sur l'environnement déposée au ministre de l'Environnement et de la Lutte contre les changements climatiques. Saint-Michel-des-Saint, Québec, Canada. No. 3211-16–019: pp. 774.

SNC-Lavalin. 2019b. Projet Matawinie—Étude d'impact environnementale et social. Volume 1. Étude d'impact sur l'environnement déposée au ministre de l'Environnement et de la Lutte contre les changements climatiques. Saint-Michel-des-Saint, Québec, Canada. No. 3211-16–19: pp. 905.

Stamatelopoulou-seymourmour, K., & Maclean, W. H. 1984. Metamorphosed Volcanogenic Ores at Montauban, Grenville Province, Quebec. *Canadian mineralogist* 22: 595–604.

Tetra Tech. 2016. NI 43-101 Technical report and preliminary economic assessment for the miller graphite and marble property, Grenville township, Quebec, Canada. Report to Canada Carbon Inc. No. 735-1500690100-REP-R0001-03: pp. 275

USGS. 2017. Graphite. Professional Paper Chapitre J; Critical Mineral Resources of the United States—Economic and Environmental Geology and Prospects for Future Supply: pp. 36.

Wihelm, H.-A., & L'Heureux, J. 2006. Graphite naturels et synthétiques pulvrulents. Production et principales utilisation industrielles. *L'actualité Chimique*. No. 295–296: pp. 4

Yuan, X., Liu, H., & Zhang, J. 2011. *Lithium-Ion Batteries: Advanced Materials and Technologies*. — Google Livres. CRC Press. https://books.google.ca/books?hl=fr&lr=&id=uruKWWpWYewC&oi=fnd&pg=PP1&dq=battery+lithium+ion+graphite+principles&ots=TkrvbkB5S4&sig=sqY0Q0dDPWuMT07gIRLD8jpqyKw&redir_esc=y#v=onepage&q=battery%20lithium%20ion%20graphite%20principles&f=false

Innovative Leachate Treatment using Passive Biochemical Reactors

Jamie Robinson and Jason Dodd
SLR Consulting Limited, Bradford On Avon, Wiltshire, UK

Ian Andrews
SLR Consulting Limited, Sheffield, Yorkshire, UK

James Gusek and L Josslyn
Linkan Engineering, Denver, Colorado, US

Eric Clarke
Saint-Gobain Construction Products Limited (trading as British Gypsum), Robertsbridge, E Sussex, UK

ABSTRACT: A passive biochemical reactor with iron scrubbers was identified as the most viable option and bench scale trials were established in 2019 at the site. This included the use of Biochemical Reactor (BCR) with different proportions of wood chips, straw, manure, limestone and biochar to culture sulfate reducing bacteria. In addition the concept of 'bugs on booze' was trialled, using Fix Bed Anaerobic Bioreactor (FBAR), where alcohol added to enhance the sulfate reducer activity. In total three BCRs and two FBARs were set up for this stage of the assessment. The resulting treated leachate was then passed through different iron media types (haematite, magnetite and iron filings) to remove hydrogen sulfide generated by the bacteria, with an aerobic wetland used to polish the effluent. The success of the project led to a pilot scale system being constructed in Spring 2020, the initial results of which confirm the success of the bench scale testing

1 INTRODUCTION

SLR Consulting was appointed by British Gypsum (Saint-Gobain Construction Products UK Ltd trading as British Gypsum) to investigate options for the treatment of leachate emanating from an old landfill disposal site at their property in East Sussex. The options analysis undertaken by SLR highlighted a passive treatment option for the removal of the sulfate, to below discharge standards, was a potential option but that it required treatability/feasibility testing. The concept involved the use of naturally occurring material containing sulfate reducing bacteria to remove the sulfate with the resulting dissolved sulfide in the water being 'scrubbed' by an iron oxide filter. An aerobic wetland would then be used to polish any final effluent before it is discharged. The design of the system was undertaken with Linkan Engineering who also supervised the construction and commissioning of the system with support from SLR.

2 THE TREATMENT PROCESS

When the design of a treatment system is necessary, its design would be based on the results of a "staged process" of bench and pilot-scale testing. Typically flow rates of c.5 to 10 ml/min or less are termed "bench-scale" with "pilot scale" test as one that would treat about 4 litres/min or more.

Bench scale testing is an effective way to advance a project toward to full scale implementation while gaining useful knowledge about appropriate media, reaction rates, and functionality that increase confidence and overall effectiveness. The overall footprint may be reduced from outline design stage, which leads to lower capital costs and maintenance. The typical passive biological treatment process for sulfate reduction utilizes an anaerobic Biochemical Reactor or BCR. While BCRs receiving Mining Impacted Minewater (MIW) may be configured as "up-flow" or "down- flow", experience has shown that up-flow BCRs are better than down-flow BCR in treating sulfate rich and metal poor leachates. The system is required for such a water which is being generated by a closed landfill. A schematic view of a pilot and full BCR is shown in Figure 1.

Figure 1. Biochemical Reactor Schematic Cross Section

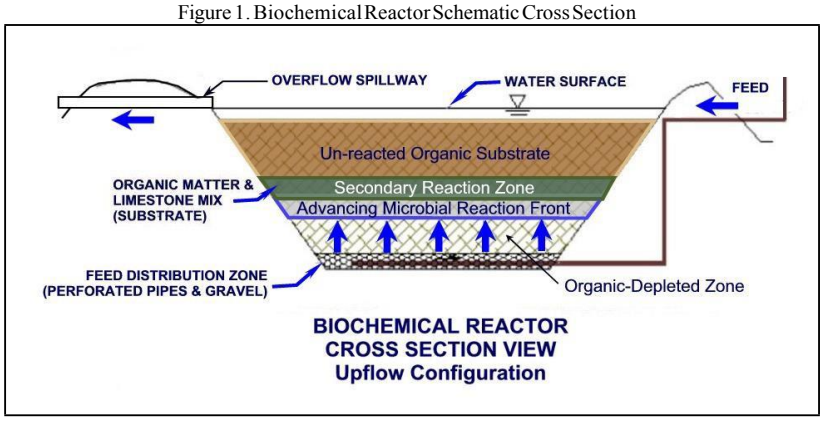

The organic substrate comprises hard wood chips, limestone, straw and biochar in varying proportions. 0.1% animal manure is added to provide the naturally occurring sulfate reducing bacteria. The sulfate in the influent leachate is then consumed by the bacteria and produces sulfide:

$$SO_4^{2-} + 2\ CH_2O = H_2S + 2\ HCO_3^-$$

Usually when such systems are used the dissolved metal ions in the mine water react with the sulfide to precipitate insoluble metal sulfides in the wetland/BCR substrate.

The lack of suitable metals in the British Gypsum discharge requires a metal ion will need to be added passively to sequester the sulfide generated through the sulphate reduction process. The dissolved sulphide will precipitate as an insoluble metal sulphide or potentially as free sulfur. For example, at the British Gypsum site, iron was added at bench scale via a treatment substrate such that the following reaction (through precipitation of dissolved iron or on metal iron surfaces), in the substrate will occur, shown simplistically below:

$$Fe^{2+} + S^{2-} \rightarrow FeS$$

Sulfur sequestration is the primary problem with a sulfate-only BCR. While minor amounts of native sulfur will accumulate on the surface of an up-flow BCR, experience has shown that the BCR effluent, bearing dissolved sulfide ion (HS^-), needs to be scrubbed with an inexpensive sacrificial metal. This metal can be either in the zero-valent state such as scrap iron, or as an oxide. However, care in media selection is warranted. An Aerobic Polishing Wetland (APW) is also a lined shallow pond filled with soil and locally-harvested or cultivated vegetation (if available). The purpose of this process feature is to re-aerate the anoxic effluent from the BCR. The terms “aerobic polishing wetland” and “reed bed” are interchangeable in this regard. This will also remove iron as an oxy-hydroxide. In some cases, it has been shown that oxidation of the BOD and any dissolved iron from the scrubber, can be optimized by including areas of open, un-vegetated water used for settling of organic matter.

3.1 BENCH SCALE SET UP

To test the theory of a passive wetland treatment solution, a bench scale system was set up at the site to run for 20 weeks. The bench scale system comprised:

- A single source Intermediate Bulk Container (IBC) of raw leachate;
- 3 No. Biochemical Reactors (BCRs) – pump fed, each filled with a different test mixture comprising different proportions of manure, wood chips, hay, limestone and biochar;
- 3 No. Sulfide Scrubbers (SCs), each filled with a different test mixture comprising magnetite, hematite and iron filings;
- 3 No. Aerobic Polishing Wetland (APW) cells planted with wetland plants from the site; and
- 2 No. Fixed Bed Anaerobic Bioreactors (FBAR) with 2 No. Sulfide Scrubbers, Aeration Tub and Settlement Tub;

A conceptual layout of the process units used in the bench scale test layout is provided in Figure 2. As part of the treatability, it was also decided to consider the use of a hybrid-passive approach which involves the additional of a soluble form of hydrocarbon such that the bacteria would react more quickly that the less soluble forms held in natural organic matter such as sawdust/manure. In this Fixed Bed Anaerobic Reactor (FBAR) small quantities of ethanol is added to a small system to provide a food source for the bacteria. The reasoning being that with a more soluble food source the bacteria will consume more of the sulfate and hence less area will be needed for the treatment at pilot and full-scale. This also has an active aeration and settling tank in replacement of the aerobic wetland system to act as a comparison.

Figure 2 – Bench Scale Test Flow Diagram

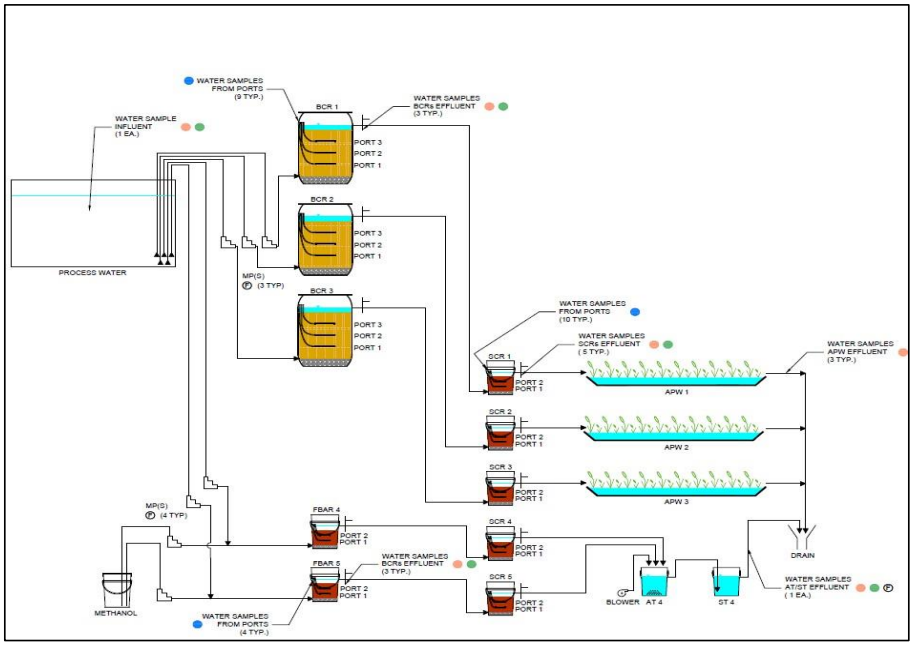

Figure 3. Bench Scale Test Set Up

4 MONITORING AND RESULTS

The system was monitored for a variety of analytes along with the flows throughout the system, Weekly field-based monitoring of pH, redox and conductivity was undertaken along with the following analytical suite: Sulfate, sulfide, nitrate, calcium and magnesium. At monthly intervals the following was also included in the analysis: phosphate, alkalinity, hardness, iron, nickel, zinc and TOC.

The flows through the reactor were typically 6l/d for the BCRs and 25l/d for the FBARs. The latter was also reduced at the end of the treatment to be closer to the BCR flow rate to act as a comparison. The process flow diagram for the system is shown above in Figure 2 and this shows not only the flow process for each of the treatability tests – but also the location and frequency of the sampling of the various parts of the system to assess the treatment progress over time. The monitoring of the system was undertaken at weekly intervals where the redox and pH of the various components coupled with the flow rates were taken. The sulfate and other components were tested at an offsite UKAS accredited laboratory. The results of the treatability study are shown in figures below:

Figure 4. Sulfate Concentrations

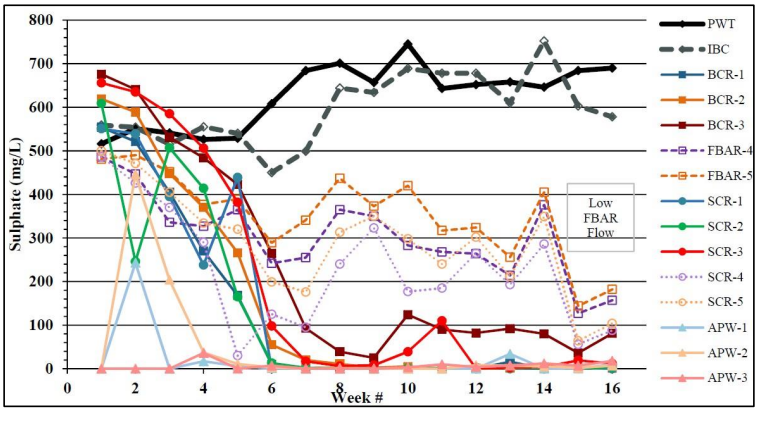

Figure 5. BCR Sulfate Reduction Rate

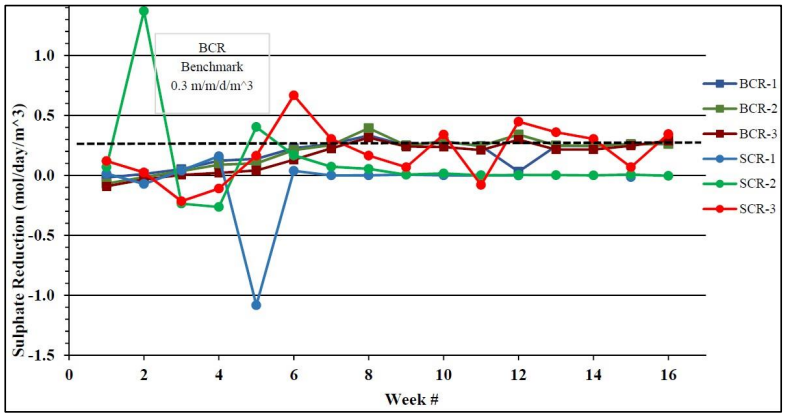

Figure 6. FBAR and BCRSulfate Reduction Rate

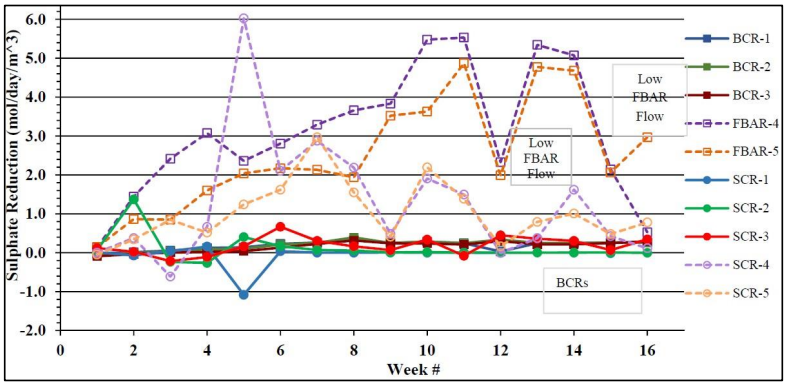

Figure 7. Sulfide Concentrations

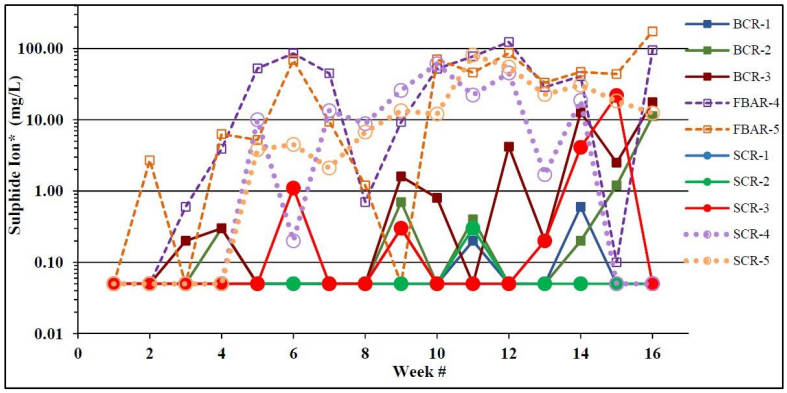

The bench scale test results indicated that both BCRs and FBAR treatment will produce an effluent that would meet a 250 mg/L sulphate limit. In mine water treatment systems sulfate reduction rates typically range form 0.1 – 0.3 moles/m^3 substrate/ day. The rates for this study are shown to be at the upper end of this range. In addition, the FBAR rate of sulfate reduction was c.15 times that of the BCR reduction rate. Consequently, the media volume required to accomplish this with a BCR will be c.15 times greater than for the media volume for an FBAR

with an identical treatment capacity. The land area footprint required for an FBAR treatment unit would therefore also be 15 times smaller than that required for a BCR. However, the FBAR process will require the delivery of a steady and reliable supply of alcohol as a microbial nutrient.

The BCR process does not require addition of nutrient, as alcohol, and therefore is seen as more passive aside from pumps to move the leachate to the treatment system.

The scrubbers sequestered sulfide ion present in the BCR and FBAR effluents. However, the bench scrubbers that received the FBAR effluents, proved to be undersized. The aerobic wetland system was effective in removing the iron leached from the scrubbers and did have a positive impact on the organic carbon which came through the system. In future studies the Biochemical Oxygen Demand (BOD) will be measured.

The results of the bench scale testing were very encouraging. This has led to the design and development of a pilot scale system at the site.

5 PILOT SCALE TESTING

The success of the bench scale trials led to the design and installation of a pilot scale system in Spring 2020 on the site. The purpose of the system was to confirm the success of the bench scale study by using the sulfate removal coefficients and preferred media option. The latter comprised mixing of wood chips, biochar, limestone, wheat straw, bench scale organic material and goat manure. The latter was the sulfate reducing bacteria inoculum. The desired flow being introduced into the system was 0.5-l/min and above and there was no additional of alcohol as nutrient.

The bench scale testing showed that free sulfur was generate din the BCRs and FBRs and hence the scrubbers were not required. However the pilot scale system allowed for them to be added if the system required additional sulfide removal.

Conceptually the pilot scale system had the original orientation of sequential treatment, although three biochemical reactors were established such that variety in flow rate and other parameters can be used to test the system.

Figure 8. Pilot Plant Concept

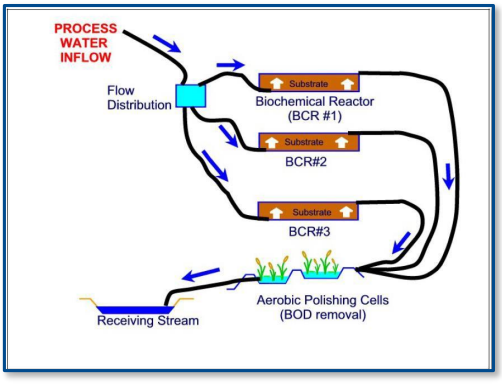

To construct the pilot plant, available infrastructure was used. Cargo containers were used for the three BCRs. These were waterproofed and lined with insulation on the base and sides and reinforced such that they could hold the substrate and the water. Sampling ports were established such that different horizons in the units could be analyzed if required.

The aerobic polishing reed beds was designed with baffles to lengthen the flow in the wetland and was designed for the removal of BOD/TOC. Facility was also made to add on the iron

sequestering unit should monitoring indicate that sulfide is leaving the system at concentrations which were unsustainable from an environmental perspective.

Figure 9. Pilot Plant Layoutand Monitoring

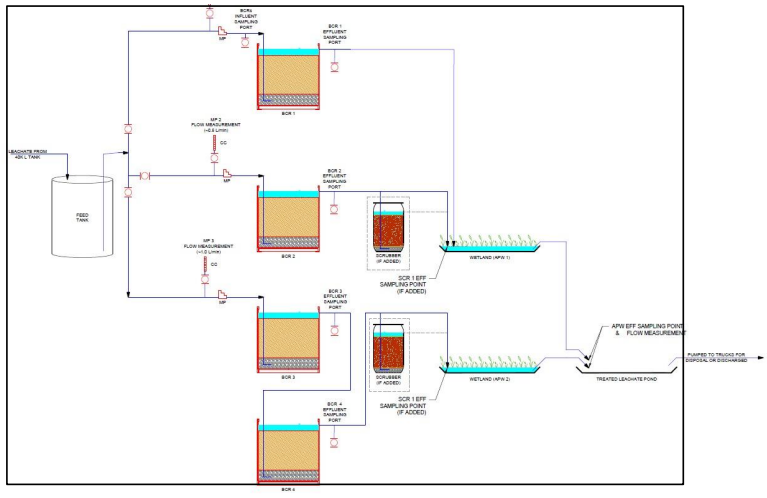

Figure 10. Pilot Plant Installation

		
Mixing BCR contents	Placing substrate in BCR	Materialbefore spreading
		
Aerobic reed bed installed	Process /leachate water pumped into feed tank image. Pumps suction from here to BCRs	System installed

The pilot system became live through a commissioning phase in Spring 2020 before the COVID emergency, and monitoring was undertaken by a skeleton staff on site since. A number of sampling points were included in the system such that depth of redox in the anaerobic material could be monitored along with the input concentrations at various locations along the system.

The results of the first quarter monitoring are available, and these have indicated an excellent sulfate removal with no sulfide detectable in the effluent. Thus far the pilot cell is confirming the results of the bench scale testing with influence sulfate of 819mg/l being reduced to 10mg/l in the effluent, thus providing robust design data for the full-scale system. The pilot system is still in operation (August 2020) and the intention is to operate the system through the summer and winter of 2020 with final results reported by the end of 2020. Notwithstanding additional data will be produced for the presentation as the COVID emergency and lock down is lifted.

ACKNOWLEDGEMENTS

SLR Consulting Limited would like to thank St Gobain for giving permission to prepare this paper and embracing an innovative technology for sulfate treatment. Lee Josselyn and Jim Gusek at Linkan Engineering are thanked for their continued support on the project, along with the dedicated project team from St Gobain and SLR.

Innovative Field Characterization Method for Self-heating Potential of Sulphidic Paste Backfill

Bret Timmis
Golder Associates Ltd., St. John's, NL, Canada

Valerie Bertrand
Golder Associates Ltd., Ottawa, ON, Canada

David Brown
Golder Associates Ltd., Toronto, ON, Canada

Chris Lee
Golder Associates Ltd., Sudbury, ON, Canada

Matthew Stewart
Vale Newfoundland and Labrador Inc., St. John's, NL, Canada

ABSTRACT: Tailings produced through processing of sulphide mineral bearing ores have occasionally been observed to develop self heating behaviour due to exothermic sulphide oxidation. In some instances, self-heating of high sulphide pastefill underground has been documented to result in dangerous temperatures, fires, SO_2 gas production, interrupted production, and sterilized ore. The potential for self-heating is commonly evaluated using a laboratory test where crushed material is exposed to air and temperature conditions which promote oxidation. The laboratory conditions differ from cemented paste backfill which occurs as large blocks (>10 m^3) with very low permeability to oxygen and moisture. This paper discusses a recently implemented field scale test methodology to assess the self-heating potential of cemented paste backfill at near full-scale under various exposure scenarios. The underground mine environment was simulated via deposition of cemented paste backfill inside shipping containers. Field testing indicated a much lower self-heating potential as compared to laboratory tests.

1 INTRODUCTION

Mine tailings, ore, waste rock, and cemented paste backfill (CPB) have exhibited self-heating behaviour largely due to the exothermic oxidation of sulphide minerals, most notably pyrrhotite, with oxygen and water. The by-products of this reaction include heat and SO_2 gas. The potential for self-heating in paste backfill has also been documented in several mines (Bernier and Li, 2003; Good, 1977; Fong et al., 2009; Nantel and Lecuyer, 1983; Patton, 1952) and has been seen to result in dangerous temperatures and SO_2 gas concentrations which have affected production. Therefore, characterization of self-heating potential is an important component of mine planning with respect to health & safety as well as identification of risks to continuity of mine operations.

Presently, the potential for self-heating is typically evaluated using a laboratory scale test initially developed by Noranda (now Glencore), and then further refined at McGill University by Dr. Jan Nesset, referred to in this paper as the Noranda Test. It uses a modified calorimeter apparatus and relies on the use of heated air which is forced through crushed tailings that are at the worst-case moisture content for self-heating potential to assess the potential for self-heating. However, due to the monolithic nature of the paste backfill which includes a very low permeability to both oxygen and moisture, and lower surface area to mass ratios than crushed material, it is intuitively expected that the Noranda test may not be representative of field conditions. This paper presents an evaluation of a new field-scale methodology for evaluation of self-heating potential of paste backfill (as monoliths) alone or in conjunction with ore in order to provide a greater degree of certainty than the Noranda laboratory test alone. Field-scale testing was conducted at Voisey's Bay Mine, Newfoundland and Labrador, Canada.

2 SELF-HEATING OF SULPHIDE BEARING MINE WASTES

Sulphide mineral oxidation is an exothermic reaction. Pyrrhotite ($Fe_{1-x}S$) is of particular concern for self-heating due to its fast oxidation reaction rate upon exposure to air (oxygen) and moisture (20-100 times faster than pyrite) and the ability of pyrrhotite to self-heat on its own whereas other self-heating cases require a mix of sulphide minerals (i.e. pyrite and chalcopyrite, Wang, 2007). When pyrrhotite content is elevated or when pyrrhotite occurs with other sulphide minerals where galvanic interaction increases the oxidation rates, the heat generated by oxidation may not dissipate quickly enough and can result in self-heating (Wang 2007, Payant et al, 2012). Heat generation at a rate insufficient to overcome cooling by ambient air is not classified as self-heating. Pyrrhotite oxidation can generate elemental sulphur (S^0) that will oxidize into sulphur dioxide gas (SO_2) through direct oxidation reaction involving proton acidity (H^+):

$$Fe_{1-x}S + (1-x)/2O_2 + 2(1-x)H^+ = (1-x)Fe^{2+} + S^0 + (1-x)H_2O \text{ (with x=0.1)} \quad (1)$$

$$S^0 + O_2 = SO_2 \quad (2)$$

Alternatively, hydrogen sulfide gas (H_2S) can be generated through an oxidation reaction involving H^+:

$$Fe_{1-x}S + H^+ = (1-3x)Fe^{2+} + 2xFe^{3+} + H_2S \text{ (with x=0.1)} \quad (3)$$

Several papers have reported self-heating events leading to SO_2 emissions in underground mines, either from backfill (Bernier and Li, 2003; Nantel and Lecuyer, 1983; Patton, 1952) or ore (Good, 1977; Fong et al., 2009). Previous studies suggest that CPB has reduced self-heating potential as compared to the source ore, tailings, or waste rock. The addition of cement and binder supports the formation of a low-permeability monolith with added neutralisation capacity to prevent mobilisation of acidity generated through sulphide oxidation.

3 SITE CHARACTERISTICS

The Voisey's Bay Underground Mine project is expected to contain a very high level of pyrrhotite content in the ore (66 to 72% in high-grade ore). As part of development of underground operations, Vale proposes to use milled tailings from the processing of underground ore to generate CPB to place in mined out stopes for underground structural support and improved ore recovery. This approach will also serve to minimise the surface disposal of the potentially acid-generating tailings.

Milled tailings contain high pyrrhotite contents (32-75%). Cement and slag binder (10% normal Portland cement and 90% ground granulated blast furnace slag, respectively) is to be added to CPB to provide strength and to help control self-heating reactions. The addition of cement adds neutralisation capacity to the reactive tailings while the hydration products of the binder that partially coat the tailings can reduce the effective permeability to water and air contact and increase the water retention capacity of the CPB both limiting oxidation and self-heating.

Laboratory tests were completed to assess the self-heating capacity of CPB with 2% to 4% binder content. The samples were prepared by crushing, drying, and re-crushing and grinding the cured paste cylinders; determination of self-heating capacity was conducted as described in Nessetech (2018). These test results indicated that CPB with 2% binder had a propensity for self-heating and therefore were not recommended for backfill, while CPB samples with 4% binder were not anticipated to self-heat. However, an increase in binder content from 2% to 4% represented a significant economic impact. Thus, the self-heating potential of CPB with 2% binder was evaluated at field-scale in order to evaluate the effect of the monolithic character of the backfill and more closely represent actual mineral reaction rates.

4 METHODOLOGY

4.1 Design Overview

The test cells were designed to simulate a monolithic mass of CPB that would more closely resemble a backfilled underground stope but in a controlled, above ground setting. CPB and ore were placed in shipping containers ("test cells"); a test size that would allow the installation of required instrumentation and equipment to control the temperature and moisture conditions. The test cells concept was to create conditions favourable to the development of self-heating by accelerating the self-heating reaction pathway and evaluating self-heating potential over a practical period of time.

Each test cell was instrumented with sensors to monitor oxygen, sulphur dioxide, temperature, and humidity. Humidity was controlled by a mister system which sprayed water (as mist) into the cell at multiple locations controlled by an automatic timer to activate it at pre-set intervals, with user intervention as needed to increase or decrease activation frequency based on monitoring data. Temperature was controlled by a heating and ventilation system with a user-adjustable thermostat adjusted as necessary to align with planned heating cycles as described in Section 4.3. Sulphur dioxide and oxygen were monitored to identify geochemical reactions potentially indicative of self-heating. Sensor data from all test cells were recorded and stored in data loggers in an adjacent shipping container used as a field office for the test. The SO_2 sensors used have a sensitivity of 0.6 ppm. Bernier and Li (2003) reported an odour threshold of 3-5 ppm for SO_2. Newfoundland & Labrador prescribes short-term occupational exposure limits (OEL-STEL) of 0.25 ppm. O_2 sensors used have a sensitivity of 5000 ppm.

The following characteristics could not be fully represented:

1) An underground stope is larger than the test cells. However, the spatial dimensions of the test CPB is considered to be adequate to represent surface interactions.

2) Variability in cement content of the CPB and variability in sulphide content of tailings and ore.

3) Explosives can be an ignition source of self-heating (Fong et al., 2009). This aspect was not part of the testing program.

4.2 Test Cell Preparation

Paste was prepared in the mill by pumping fresh tailings into a concrete ready-mix truck, removing supernatant after settling, and adding cement binder after adequate thickening was achieved. Some variability in paste composition is a potential result of the time between collection of tailings for each test cell. The required binder mass was calculated and added to the drum . The drum was rotated for a minimum of one hour to fully mix binder and tailings to produce paste. The paste was then poured into lined formwork in the test cell, the cell was closed, and the curing period initiated. Paste was cured in a closed environment for the period of time defined in Table 1, with variations between Cells 2 and 3 to evaluate if curing time affected the development of self-heating.

Following completion of the curing period, the test cells were exposed and ore was placed beside and in direct contact with the paste (Cells 2 and 3 only). Cell 1 consisted of a "control" cell, to evaluate the potential for self-heating conditions in the paste alone. Ore material particle size distribution was from zero to approximately 200 mm. The volume of ore added to Cell 2 and Cell 3 was similar (+/- 15%) to the volume of paste. At the time of placing the ore in the test cells, visible ore oxidation was minimal to absent. The test cells are shown in Figure 1.

Figure 1: External Photograph of Test Cells.

4.3 Test Operation

The test was conducted as per the dates presented in Table 1. Sensor data was logged continuously and evaluated for indications of self-heating throughout each day.

Table 1. Testing Phases

Event	Cell 1	Cell 2	Cell 3
CPB poured	June 11, 2018	June 14, 2018	June 22, 2018
Ore placement	N/A	July 12, 2018	July 12, 2018
Start of test (no heat)	July 12, 2018		
Initiation of heating cycles	July 18, 2018		
End of heating cycles	August 8, 2018		
End of test	August 28, 2018		

The objective of these temperature increase time periods was to generate favourable conditions for self-heating (high temperature, high humidity, and presence of ore in contact with the paste). Each cell was submitted to nine heating periods of 24 hours. During heating cycles, the heater unit was activated to reach the target temperature and it was maintained for 24 hours after which the heater unit was turned off for 24 hours. For the first three heating cycles, the target temperature was 40 °C. The remaining 6 heating cycles were operated to reach the maximum temperature possible out of the heater (45 to 55 ºC inside air temperature); this temperature limit was influenced by external climate.

The heating cycle from July 25th through 29th was extended to determine if running the heater for an extended period would reach higher air temperatures: it did not. The maximum temperatures tested are beyond maximum safe temperatures for an underground mine work environment; however, the higher temperatures were used to promote reactions which may lead to self-heating. Relative humidity inside the test cells was targeted to be in a range 80-90% using automatic sprayers to represent the underground mine environment.

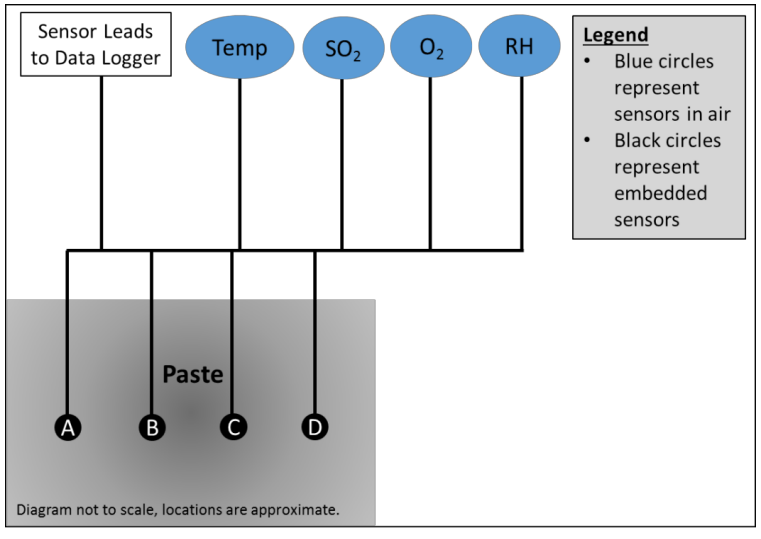

Figure 2: Schematic of Sensor Locations in Cell 1.

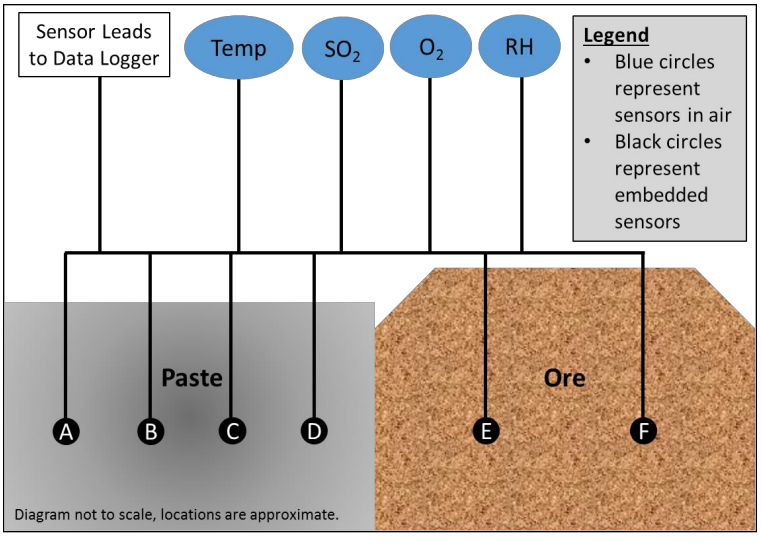

Figure 3: Schematic of Sensor Locations in Cells 2 and 3.

5 RESULTS

5.1 Test Cell Instrumentation Results

Sulphur dioxide measurements were within the standard error of the sensor at all times during the test. Accordingly, these values are not discussed further and are inferred to indicate that no appreciable generation of sulphur dioxide occurred. At the initiation of the test period following removal of formwork (all cells) and placement of ore (Cell 2 and Cell 3), negligible changes in instrumentation data were observed until heating was initiated.

5.1.1 Temperature

Figure 4 illustrates the changes in air temperatures inside each cell and in outside air. Outside air temperatures influence internal (inside cell) air temperatures, particularly when heating is not activated, and also as a control on the upper limit of inside air temperatures during heating. Figure 5 presents internal paste and ore temperature results for each temperature sensor, showing differences with respect to sensor location and differences between each cell.

Table 2. Range of Measured Air Temperatures Over the Test Period (°C) After Initiation of Heating

	Outside Air	Cell #1	Cell #2	Cell #3
Minimum	3.4	9.1	12.7	12.6
Average	12.5	23.9	28.0	27.6
Maximum	31.6	47.8	54.1	52.9

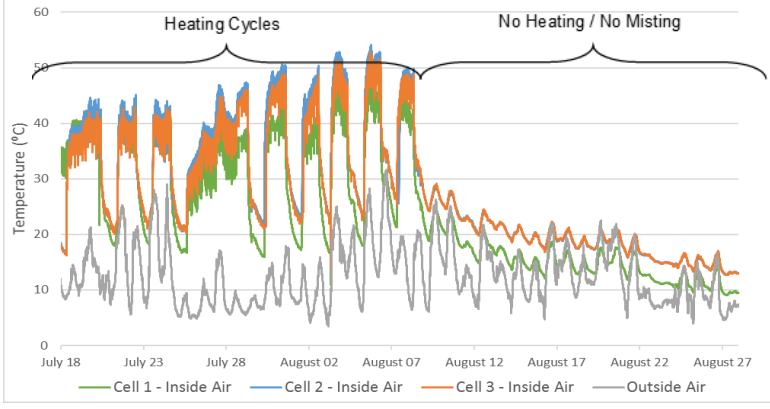

Figure 4: Temperature of Air Inside Test Cells and Outside Air Temperature

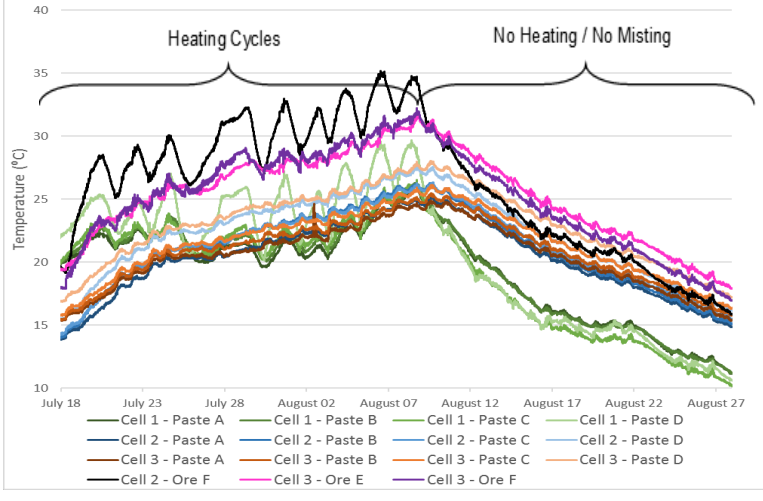

Figure 5: Temperatures Reported by Sensors Embedded in Paste and Ore (locations described in Figure 3). A to F refer to sensor location.

Results show that activation of the heater is the primary control upon internal air, paste, and ore temperatures. The secondary control is external air temperatures in the natural environment. At the end of the heating cycles through to the end of the test, a steady decrease in temperatures is observed (Figure 4). During periods when the heater is not active, changes in internal cell temperatures are directly relatable to external air temperatures and sunlight on test cells. Temperatures in Cell 1 generally exhibited greater variability and lower values than in the other cells; this is interpreted to be primarily due to the lack of insulating effect from ore. Because the sidewall of the paste in Cell 1 is in direct contact with air, the paste temperature at that location changes more rapidly.

No evidence exists for sustained increases in temperature other than as a direct result of heating applied in the test procedure. If any heat was generated from sulphide oxidation, it occurred at an insufficient rate to overcome cooling towards ambient conditions during no-heat periods.

5.1.2 Oxygen

Relative humidity and oxygen inside the test cells were influenced by operation of the heating and ventilation unit which introduced outside air to each cell when active. Evaluation of results from the three test cells (Figure 6) indicates that relative humidity decreases when internal temperature increases (ventilation blows out humidity) while O_2 increases (ventilation brings fresh air). Analysis of recorded oxygen concentrations do not show evidence of sustained consumption of oxygen from oxidation of sulphides (and potential self-heating) during any phase of the test. The test cells are not airtight and ingress of oxygen over time is expected. The cause of increased variability in Cell 2 results is unclear and potentially related to inconsistency in the sensor given the lack of correlating changes in any other parameters. Cell 3 results are interpreted to be lower due to a calibration error but appear to be consistent with Cell 1 over time.

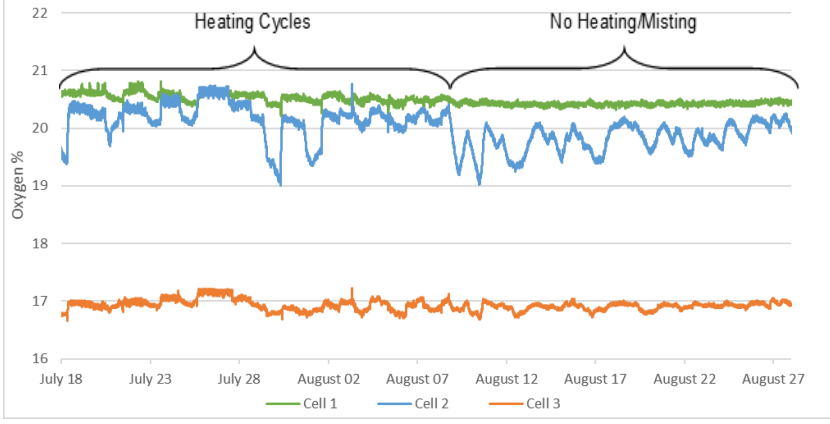

Figure 6: Oxygen Content over Evaluation Period

5.1.3 Relative Humidity

From the complete dataset recorded, relative humidity data ranged between 19.2% and 99.9% (Figure 7). The relative humidity inside the test cells was targeted to be in the range of 80-90% over the testing period using automatic sprayers to represent the underground mine environment; however, when the heating and ventilation unit was active, added humidity was quickly lost and the high humidity was not maintained, while excess humidity was present when the heating and ventilation was not active. Actual moisture content of paste was assumed to be at a higher level

than heated air due to ingress of water during high humidity periods which would not be withdrawn from paste during the 24-hour heating cycles. This assumption was confirmed during the post-test visual inspection which determined that the first 1 cm of paste was unsaturated, while all paste beyond 1 cm depth was water saturated.

Cell 1 generally was observed to have the highest humidity values, which may be due to quicker settling of the mist in the space next to the paste, whereas in the other cells, airborne water could only circulate in the limited headspace above both paste and ore resulting in increased loss through ventilation. Cell 2 generally has higher humidity values than Cell 3; paste and ore placement is the same in both cells and there is no clear driver for this variation.

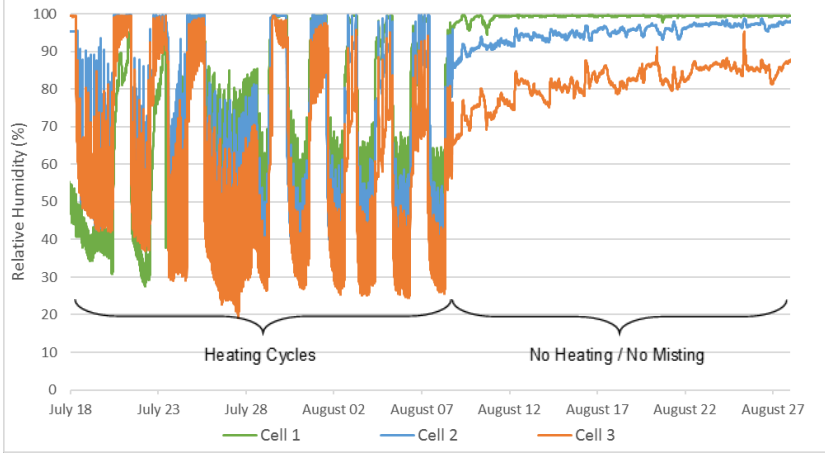

Figure 7: Relative Humidity over Evaluation Period

5.2 Mineralogical and Geochemical Results

Prior to the initiation of testing, samples of ore and wet paste were collected for geochemical and mineralogical analysis. Samples collected following completion of the field test were submitted for the same analyses. Pre-test results are used to confirm the test materials are consistent with expected characteristics for paste backfill underground at Voisey's Bay, and as a baseline reference for post-test samples. Post-test paste samples were collected at surface (<1 cm depth) to 75 cm depth from the closest edge of the paste block to evaluate changes in geochemical and mineralogical composition resulting from the field test. Results for selected parameters of interest are summarized in Table 3.

Cell 1 samples have lower abundance of sulphide minerals and greater abundance of silicate minerals than Cell 2 and Cell 3; this difference is attributed to heterogeneity in the tailings feed. Surface shavings samples (VB2-2, VB3-1) which were anticipated to potentially demonstrate stronger effects from testing due to directly exposed surface area, did not yield any notable differences compared to samples collected at greater depth.

Table 3. Comparison of Average Paste Properties Prior to and After Test (Mineralogy as Reported by XRD)

Property	Prior to Test		After Test																	
Test Cell	2		1						2						3					
Sample ID	2A	2B	1-1	1-2	1-3	1-4	1-5	1-6	2-1	2-2	2-3	2-4	2-5	2-6	3-1	3-2	3-3	3-4	3-5	3-6
Sulphide %	20	22	14	14	15	15	15	15	23	24	25	25	24	24	25	27	25	27	25	26
Sulphate %	10	7	11	11	10	11	11	10	19	19	17	15	19	18	9	11	9	9	11	10
Neutralizing Potential (t $CaCO_3$ /1000 t)	25	26	58	48	51	49	49	50	36	46	29	31	30	30	35	24	26	22	23	24
Acid Potential (t $CaCO_3$ /1000 t)	613	672	428	444	456	459	453	456	731	763	769	766	747	759	794	828	788	841	794	813
Pyrrhotite/ Troilite %	77	73	35	34	39	Not analysed			67	63	72	Not analysed			74	76	74	Not analysed		
Other Sulphides %	0.6	0.6	1.5	1.3	-				-	-	-				-	-	1.2			
Sulphates %	-	-	1.2	0.5	-				-	-	-				-	-	0.5			
Silicates %	16	21	53	58	56				27	27	21				15	16	17			
Oxides %	6	6	6	7	4				5	7	6				9	9	8			
Carbonates %	-	-	2.6	-	1.3				1.4	3.0	0.9				2.7	-	-			

5.3 Visual Inspection of Test Cells After Termination

Following the completion of the field test, a visual inspection of the test materials was undertaken to identify any evidence of test related effects. In both Cell 2 and Cell 3, ore was observed to have taken a reddish tarnish, indicating that surficial oxidation of the sulphides had occurred. In contrast, paste showed no evidence of evolution over the testing period and no oxidation products were evident. Paste was water saturated at shallow depth (less than 1 cm from surfaces), and no defined crust was present. The paste appearance was uniform across horizontal and vertical position.

Figure 8: Cell 2 Paste with Partially Excavated Ore

6.0 DISCUSSION

Key findings of the test cell monitoring results can be summarized as follows:

- Paste and ore temperatures rose during heating periods, and fell during all periods when heating was not active;
- Sulphur dioxide values were not detected above minimum sensor sensitivity at any time;
- Oxygen was not consumed at a rate to indicate rapid oxidation reactions and self-heating; and
- If heat was generated from sulphide oxidation, it occurred at an insufficient rate to overcome cooling towards ambient conditions during no-heat periods.

The test results indicate that sulphide oxidation over the test period was primarily limited to ore, with no evidence of oxidation in CPB. Self-heating conditions (generation of heat at a rate sufficient to overcome cooling with ambient air during no-heat periods) were not observed through any of the measurements made during and after the test. Visual inspection of the CPB determined that it was water saturated, which is an important characteristic for the prevention of sulphide oxidation and therefore self-heating.

The test results indicate that CPB with 2% binder did not develop significant self-heating conditions in the field test cells, given that paste and ore temperatures fell during all periods where the external heat source was no longer applied. All instances of increasing paste and ore

temperatures can be directly related to elevated ambient air temperatures, either due to activation of the heating unit or due to external (natural) temperature increase. The tailings and the addition of the binder are favourable for maintaining high water saturation in paste pore space that in turn limit oxygen diffusion. The test was designed as an analogue to underground paste backfill; however, the test cells are not a perfect representation of the underground environment due to factors including, but not limited to the following:

- Duration of testing (shorter than underground exposure);
- Differences in ventilation and ambient humidity and temperature;
- Presence of ore likely to occur on multiple sides of the paste in underground development rather than only one side in the test cells;
- Blasting (heat generated by blasting) conducted adjacent to paste in underground development;
- Minor differences in mineralogy and geochemistry of paste derived from underground ore compared to ore derived from the open pit used in the test cell; and
- Differences in paste preparation procedure (batches produced in a mix truck for test cells vs. continual production in a paste plant for underground use).

7.0 CONCLUSIONS

Field study results indicate that the potential for self-heating of the CPB under evaluation in this study was low under the study test conditions. This finding is in conflict with previous laboratory scale testing completed (i.e. The Noranda Test), which indicated high potential for the development of self-heating conditions in the materials tested. Therefore, evidence from the present study supports the hypothesis that laboratory scale testing of pulverised material may be overly conservative relative to actual conditions. Long-term monitoring of full-scale paste backfill deposition is required to validate this hypothesis.

The unique composition of minerals present at any given site may result in different outcomes than those described herein. Regardless of further refinement and validation of the procedures described in the current study, laboratory scale testing methods are anticipated to remain as important preliminary screening tools to determine whether additional study is required. However, the current findings suggest that laboratory scale test results of self-heating should not be relied upon in isolation to determine that an increased binder content is required to prevent the development of self-heating. Rather, the proponent should review the potential for field-scale testing to identify a lower binder content relative to long-term costs of increased binder content. If field-scale testing is deemed a desirable approach to evaluate whether binder content can be reduced, the proponent should engage with qualified experts in mine backfill technology and sulphide geochemistry.

8.0 ACKNOWLEDGMENTS

Golder Associates Ltd. appreciates the support of Vale Newfoundland and Labrador in sharing the results of this innovative field trial with the scientific community and advancing the body of knowledge in the field of self-heating.

REFERENCES

1. Bernier, L. R., and Li, M. 2003. High temperature oxidation (heating) of sulfide paste backfill: a mineralogical and chemical perspective. [In:] *Proceedings of Sudbury Mining and the Environment Conference*.

2. Fong et. al. 2009 - Fong, G., Isagon, I., Lebonté, G., and Wheeler, R. 2009. *Self-Heating Issues due to Oxidation of High-Sulphide Content in Ore, Waste and Paste Backfill, Notes from the Site Visit Conducted at Brunswick Mine and Smelting, Bathurst, NB, on Dec. 17-18, 2008*.

3. Good, B.H. 1977. Sulphide Fires - The "Hot Muck" Problem, The Oxidation of Sulphide Minerals in the Sullivan Mine, CIM Bulletin, June 1977.

4. Nantel, J. and N. Lecuyer. 1983. Assessment of slag backfill properties for the Noranda Chadbourne Project Noranda, Quebec, *CIM Bulletin*, V. 76, No. 849.

5. Nessetech, 2018. *Self-Heating Tests – Vale Voisey's Bay Samples*. Report prepared for Golder Associates Ltd.

6. Patton, F. E. 1952. Backfilling at Noranda. *Canadian Institute of Mining & Metallurgy Transactions*, V. 55, pp. 137-143.

7. Payant, R., F. Rosenblum, J.E. Nesset, J.A. Finch. 2012. The self-heating of sulphides: galvanic effects. In Minerals Engineering. Volume 12, p 57-63.

8. Wang, X. August 2007. Exploring Conditions Leading to Self-Heating of Pyrrhotite-Rich Materials. A thesis submitted to McGill University in partial fulfilment of the requirements of the degree of Master of Engineering.

Large-scale instrumented column test to assess oxidation and leachate

Chenming Zhang, David J. Williams, Ximing Lei, Sebastian Quintero
The University of Queensland, Brisbane, Queensland, Australia

Tony Ferguson
Grange Resources, Burnie, Tasmania, Australia

ABSTRACT: Placing a cover over a surface dump containing potentially acid generating (PAG) waste rock is the key to minimizing oxygen ingress and the net percolation of rainfall that could lead to acid rock drainage (ARD). To optimize cover design using materials available on site, six large columns, of 1 m in diameter and 4 m height, were constructed on site at the Savage River Iron Ore Mine in north-western Tasmania. The first three columns were constructed as controls, filled with loosely-placed, coarse-grained, non-acid generating (NAG) A-Type and B-Type wastes, and PAG D-Type waste. The fourth column was filled with compacted A-Type waste overlying loosely-placed D-Type waste. The fifth column was filled with compacted B-Type waste overlying loosely-placed D-Type waste, and the sixth column was filled with evenly-mixed, loosely-placed D-Type, B-Type and A-Type wastes. The surface of the filled columns was open to local weather conditions, which were monitored by a weather station. A camera was installed on the top of the columns to monitor the settlement of the wastes. Drainage was allowed at the column base through a U-bend, with a reservoir for water sample collection. All of the columns were instrumented with sensors designed and manufactured at The University of Queensland, to monitor continuously and in real-time moisture, suction, temperature and oxygen profiles with depth in the columns. This paper reports on the instrumented column set-up and the two years of monitoring results obtained to date.

1 INTRODUCTION

Acid rock drainage from surface dumps containing PAG waste rock poses serious risks to the receiving environment. The generation of ARD is predominantly due to the oxidation of pyrite within the waste rock, on its exposure to atmospheric oxygen and rainfall infiltration through the dump, leading to the transport of the oxidation products. The generation of ARD from surface waste rock dumps can be minimized by the placement of cover material to reduce the ingress of oxygen and/or the net percolation of rainfall into the dump.

Compacted clay covers are considered to be the most appropriate, due their low hydraulic and air conductivities. However, at many mine sites, suitable clay is not available, and the clay cover can only be constructed at the end of the dumping activities, before which acid generation cannot be prevented. In the absence of suitable clay, NAG and/or acid neutralizing wastes may provide an acceptable cover material. To address this at the Savage River Iron Ore Mine, six large columns were constructed on site to investigate the effectiveness of various covers comprising NAG and acid neutralizing wastes in inhibiting acid generation in PAG wastes.

2 METHODOLOGY

2.1 *The columns*

The schematic design of the columns, the different combinations of wastes in the columns, and a photograph of the site set-up are shown in Figures 1 to 3, respectively. The columns are constructed on a concrete base, and comprize 1 m diameter by 1 m high concrete pipe sections raised to a height of approximately 4 m. They were filled with wastes as the sections were added. During construction, the base and joints between the concrete sections were sealed to minimize air entry, and the insides of the pipe sections are also painted to seal the concrete. Outlets from each column are located at the base, and include a U-bend to prevent venting from the atmosphere. The outlets are piped to a tipping bucket to record continuously the flow rate, and the leachate is collected in a tank that is sampled monthly for water quality testing by the site.

The six columns are unsupported since their stability is ensured once they are filled with wastes. The columns are located next to two installed weather stations, recording rainfall, temperature and humidity, wind direction and intensity, and solar intensity, from which potential evaporation is calculated.

As shown in Figure 1, the six columns are filled with:

Column 1: Loosely-placed, coarse-grained, NAF A-Type waste.

Column 2: Loosely-placed, coarse-grained, NAF B-Type waste.

Column 3: Loosely-placed, coarse-grained, PAG D-Type waste.

Column 4: 3 m of loosely-placed, coarse-grained D-Type waste covered by 1 m of compacted, coarse-grained A-Type waste.

Column 5: 3 m of loosely-placed, coarse-grained D-Type waste covered by 1 m of compacted, coarse-grained B-Type waste.

Column 6: Loosely-placed, well-mixed A, B and D Type wastes in the same proportion.

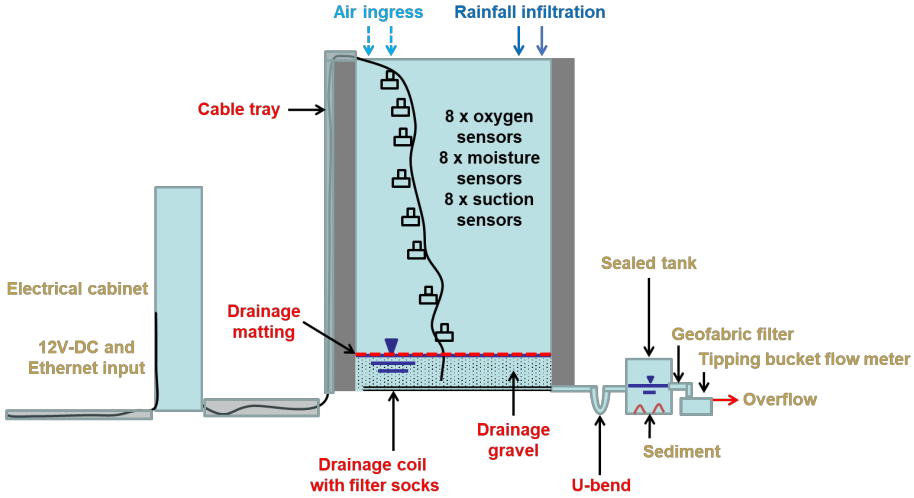

Figure 1. Schematic design of columns.

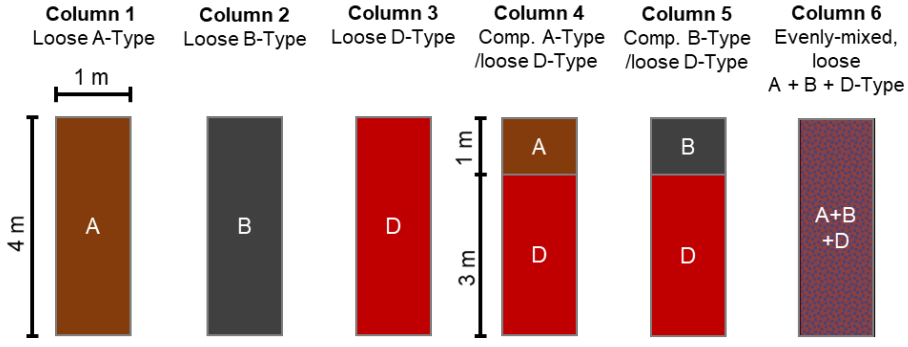

Figure 2. Combinations of A-Type, B-Type and D-Type wastes in Columns 1 to 6.

Figure 3. Site set-up.

2.2 *Instrumentation*

The column instrumentation included moisture, suction, oxygen and temperature sensors to monitor profiles with depth down the center of each column and radially at a few locations, plus the continuous monitoring of leachate flow rate by tipping bucket and monthly sampling and testing of water quality by the site (Figure 4). The surface of the filled columns was subjected to local weather conditions monitored by two weather stations. A camera was installed on the top of the columns to monitor settlement of the wastes. The sensors and two dataloggers were developed and manufactured in-house by the Geotechnical Engineering Center at The University of Queensland. The monitoring data are collected continuously and are accessible via a web address.

2.3 *Characterization of wastes*

Figure 5 to 7 shows photographs of the wastes, their soil-water characteristic curves, and their mineralogy before and after being subjected to wetting and drying cycles, respectively. The particle size of the wastes ranged from fine sand-size (nominal 0.5 mm) to cobble-size (nominal 100 mm). The soil-water characteristic curves, obtained using a Fredlund cell performed on loosely-placed samples, show the sandy nature of the wastes, with air entry values of about

10 kPa, and a rapid decrease in volumetric water content with increase in suction beyond 10 kPa. The residual volumetric water content is achieved at a suction of about 500 kPa. The wastes were initially relatively dry on placement in the columns.

The mineralogy of the wastes, obtained using X-ray diffraction analysis before and after wetting and drying cycles, showed differences in the main minerals in each of the waste types. The mineralogy of each before and after wetting and drying cycles are similar, indicating that they are not soluble and are chemically stable. A-Type waste is rich in chlorite (31%), albite (18%) and quartz (16%), B-Type waste is dominated by mica (42%) and quartz (33%), and D-Type waste is dominated by chlorite (17%), albite (16%), talc (16%) and amphibole (13%). Pyrite is found in A-Type waste (2%) and D-Type waste (4%). This is consistent with the field observation that D-Type waste is in general PAG, although A-Type waste is found to be NAG. No pyrite was found in the B-Type waste.

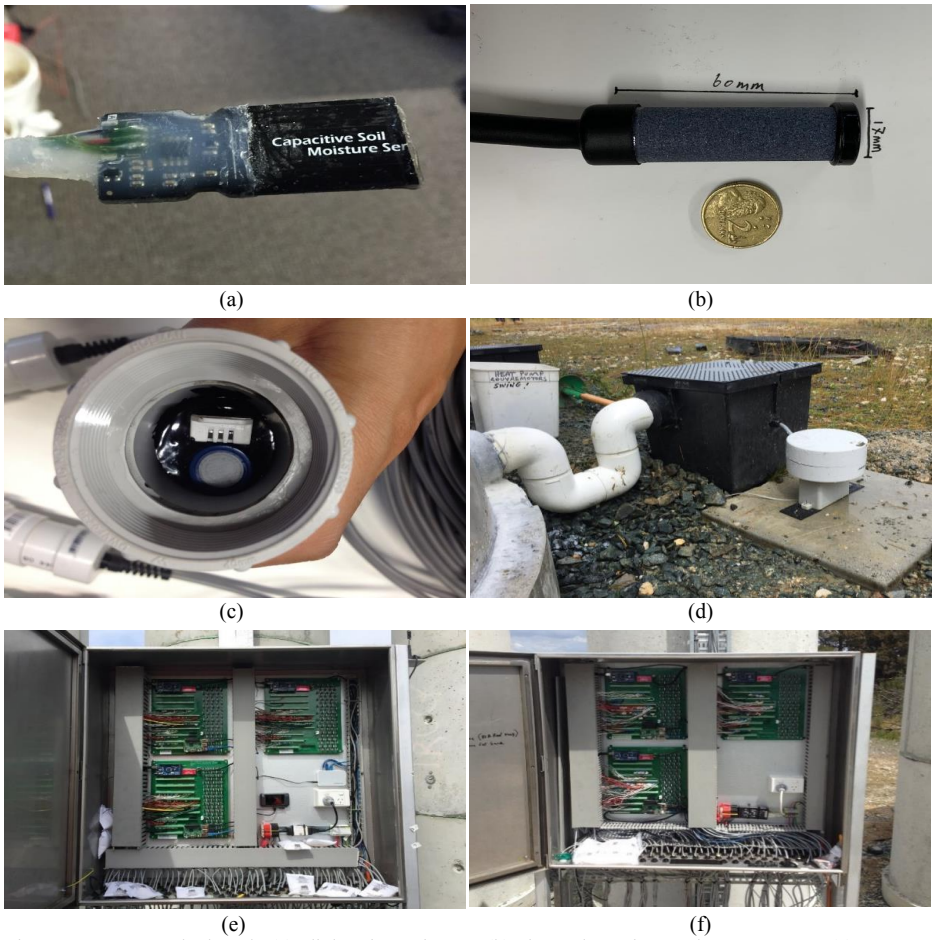

(a) (b) (c) (d) (e) (f)

Figure 4. Sensors deployed: (a) dielectric moisture, (b) thermal suction and temperature, (c) oxygen concentration, (d) collection tank and tipping bucket, (e) datalogger 1, and (f) datalogger 2.

(a) (b) (c)

Figure 5. Photographs of: (a) A-Type, (b) B-Type, and (c) D-Type wastes.

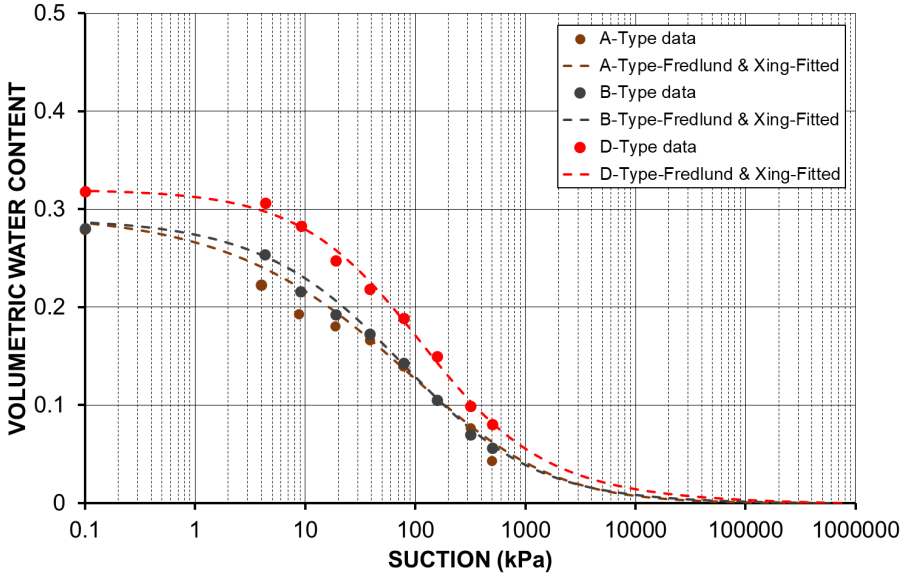

Figure 6. Soil-water characteristic curves of loosely-placed wastes.

3 MONITORING RESULTS

3.1 *Temperature*

Figure 8 shows the monitored temperature in the columns over 2 years. During the winter months (June to September), the average temperature is about 5°C, with daily fluctuation of about ±5°C. During the summer months (December to February), the average temperature is about 15°C, with a daily fluctuation of about ±8°C. Due to direct exposure to the atmosphere, the daily variations in temperature are more pronounced towards the tops of the columns. All the columns showed consistent temperature profiles over 2 years, with no apparent temperature spikes induced by oxidization.

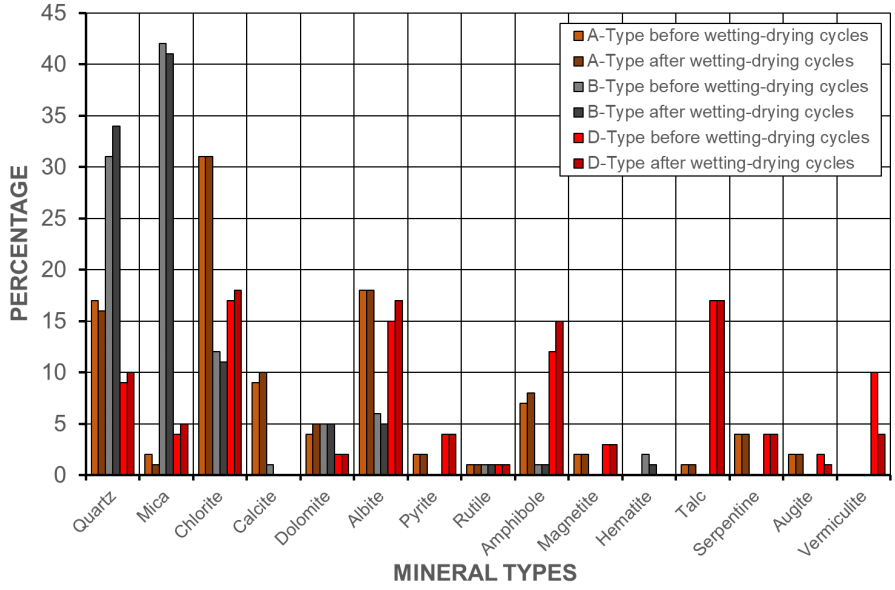

Figure 7. Mineralogy of A-Type, B-Type and D-Type wastes before and after wetting and drying cycles.

3.2 *Moisture*

Figure 9 shows the profiles of moisture with depth in the columns over 2 years. Moisture is affected by the amount of rainfall, infiltration and evaporation over time. The wastes were initially relatively dry, with a volumetric moisture content in the range from 0 to 0.04 (equivalent to a gravimetric moisture content of 0 to 1.5%). With rainfall infiltration and gravity drainage through the columns, the wetting front expanded from the surface. However, the distribution of moisture down the columns was non-uniform, with some depths holding water. Moisture was held-up in the upper sections of Column 3 (in loose D-Type waste), of Column 5 (in compacted B-Type waste), and of Column 6 (in loose, mixed A, B and D-Type wastes), while not in compacted A-Type, or loose A-Type or B-Type wastes. Further, some deeper sensors in all columns, apart from Column 6, recorded moisture before shallower sensors, indicating preferred pathway flow. Only Column 6 showed flow incrementing with depth.

Once infiltration reached the base of the columns (by mid-2019), the moisture profiles with depth became relatively stable in all six columns. In general, hydrostatic pore water pressures developed in the lower sections of the columns. No apparent delay was observed between rainfall events and moisture rises within the columns, suggesting that the wastes have relatively high hydraulic conductivities, although there was a substantial lag before the onset of outflow from the base of the columns.

The hold-up of moisture in the upper 1 m depth of Columns 3, 5 and 6 would limit oxygen ingress into the wastes below. However, the moisture content within this upper 1 m depth varied significantly, probably due to the cycles of rainfall and evaporation. Higher evaporation from the upper moist layer may also reverse the gravity drainage of any ARD.

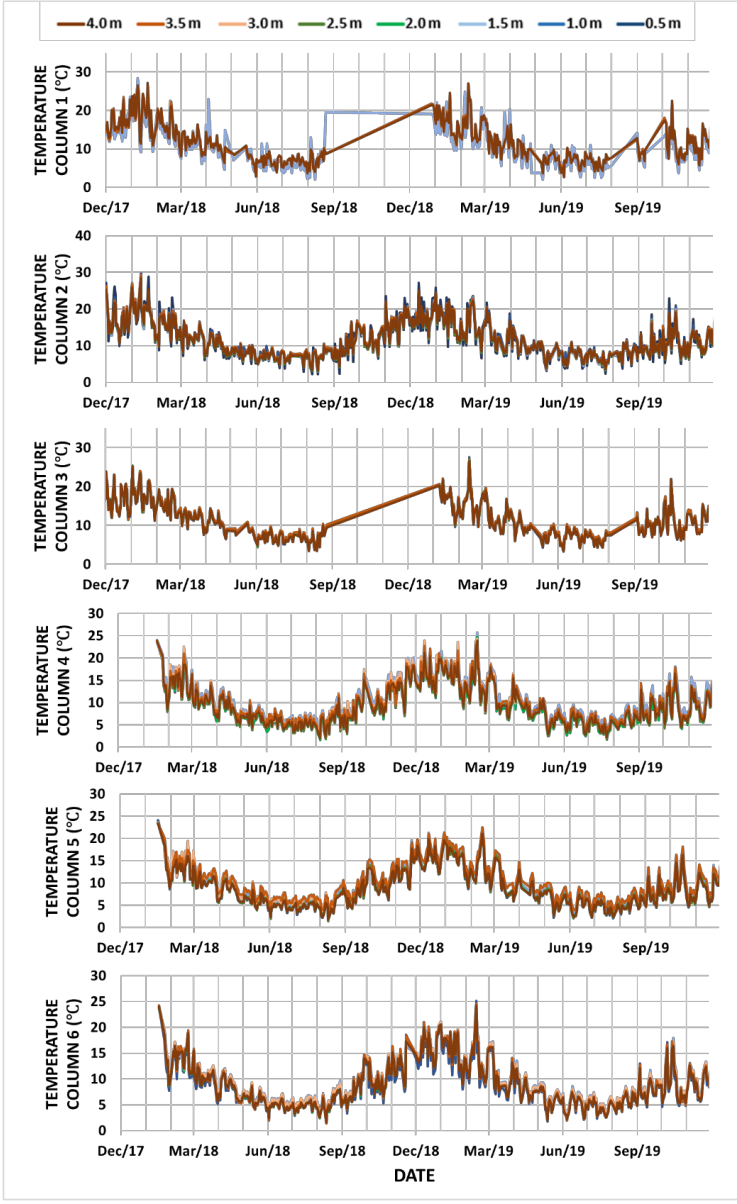

Figure 8. Monitored temperature over time in Columns 1 to 6.

3.3 *Leachate outflow*

Figure 10 shows the outflow of leachate from the base of the columns. The cumulative rainfall from May to December 2019 was about 1,200 mm, while the cumulative outflow for the same period was far less due to further rainfall infiltration being stored in the columns and evaporative losses. The cumulative outflow was highest for Column 3, promoting ARD, then Column 2, Column 4 and Column 5, apparently decreasing due to decreasing rainfall infiltration. The low

recorded outflow from Columns 1 and 6 was due to leakage at the U-bends. A slight delay occurs between rainfall and outflow.

3.4 *Oxygen level in wastes*

Figure 11 shows the monitored weather conditions (rainfall and potential evaporation) and oxygen levels in the wastes with depth over time. Six extreme rainfall events were selected to illustrate the effect of rainfall on oxygen concentration in the wastes. A decline in oxygen concentration occurred immediately after significant rainfall events, likely due to saturation of the upper sections of the columns. Oxygen levels appear to bounce back slightly during the drier season from November to February, due to evaporation from the upper sections of the columns allowing oxygen ingress. Compaction of the upper wastes is seen to be effective in reducing oxygen ingress (Columns 4 and 5), as is mixing the wastes (Column 6), which is likely related to the holding-up of rainfall infiltration in the upper section of the columns.

3.5 *pH and electrical conductivity in wastes*

Figure 12 shows a slight decline in the pH of the leachate from the columns over time, from alkaline to near neutral. Despite the X-ray diffraction analysis showing little change in the mineralogy of the wastes after wetting and drying cycles (Figure 7), naturally occurring carbonic acid in rainwater apparently caused the dissolution of the aluminosilicate minerals in the wastes (Jurjovec et.al. 2002; Jambor et.al. 2003).

Figure 13 shows low electrical conductivity for the A-Type and B-Type wastes in Columns 1 and 2, and the relatively high initial electrical conductivity for the four columns (3 to 6) containing at least some D-Type waste, which roughly halves over the 2-year monitoring period, indicating improving water quality on wetting-up of the columns over time.

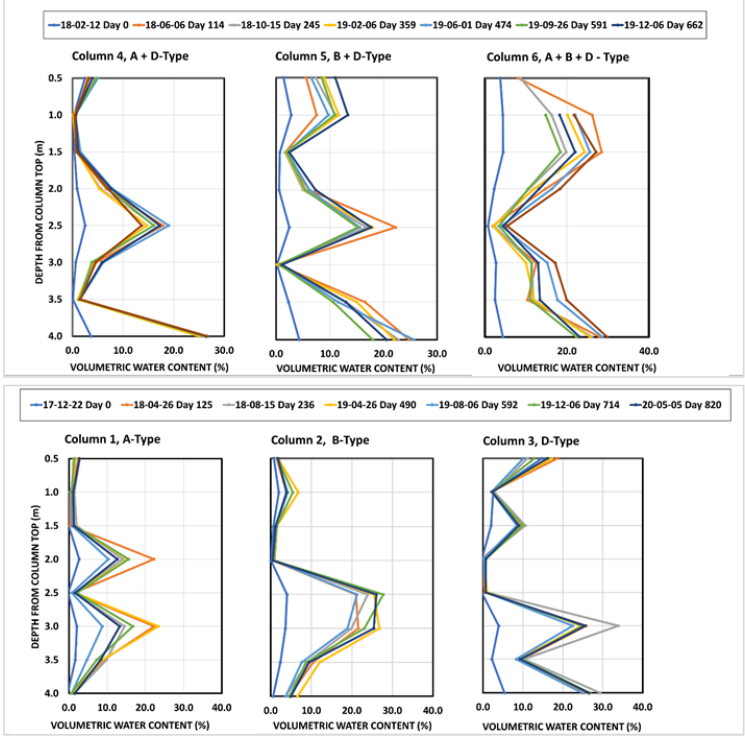

Figure 9. Volumetric moisture content profiles in Columns 1 to 6 over time.

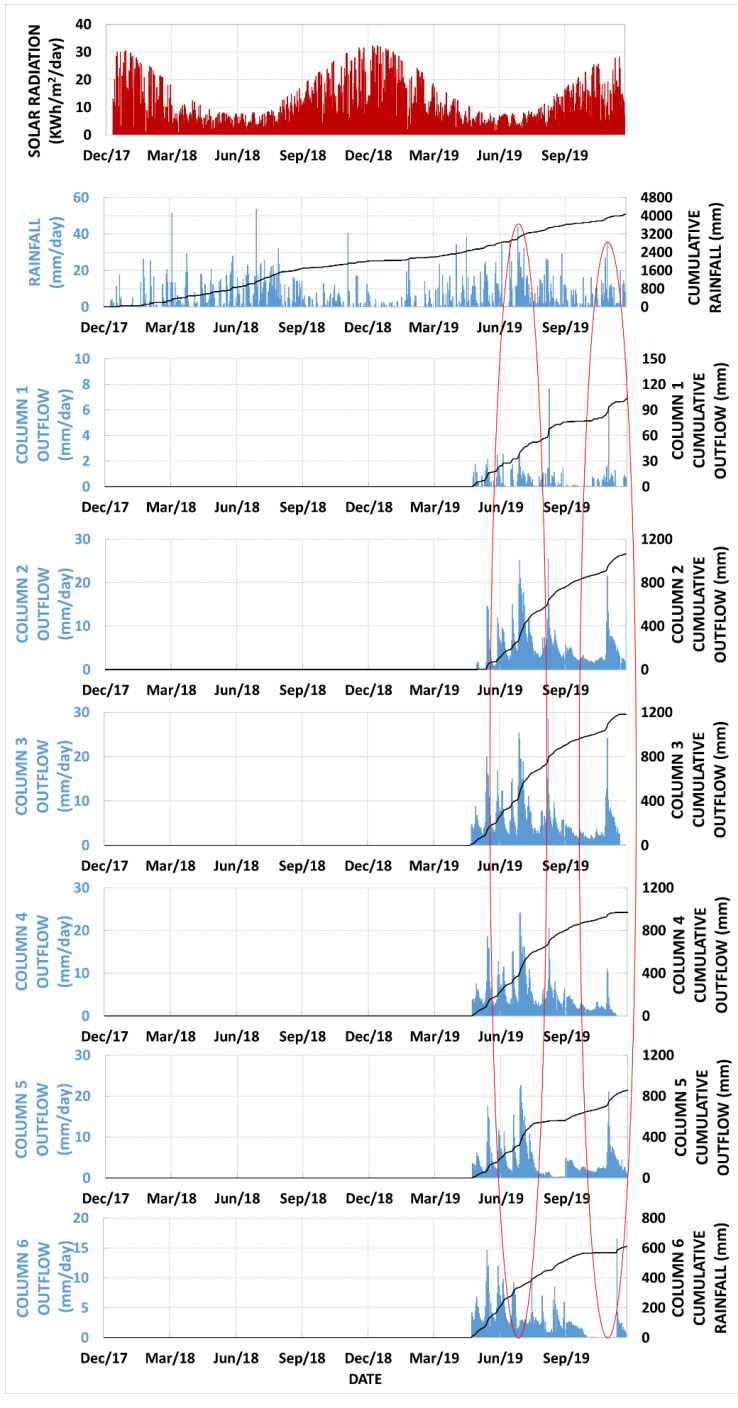

Figure 10. Recorded drainage from tipping bucket flow meters for Columns 1 to 6, with red circles highlighting two major rainfall events and induced drainage with slightly delayed occurrence.

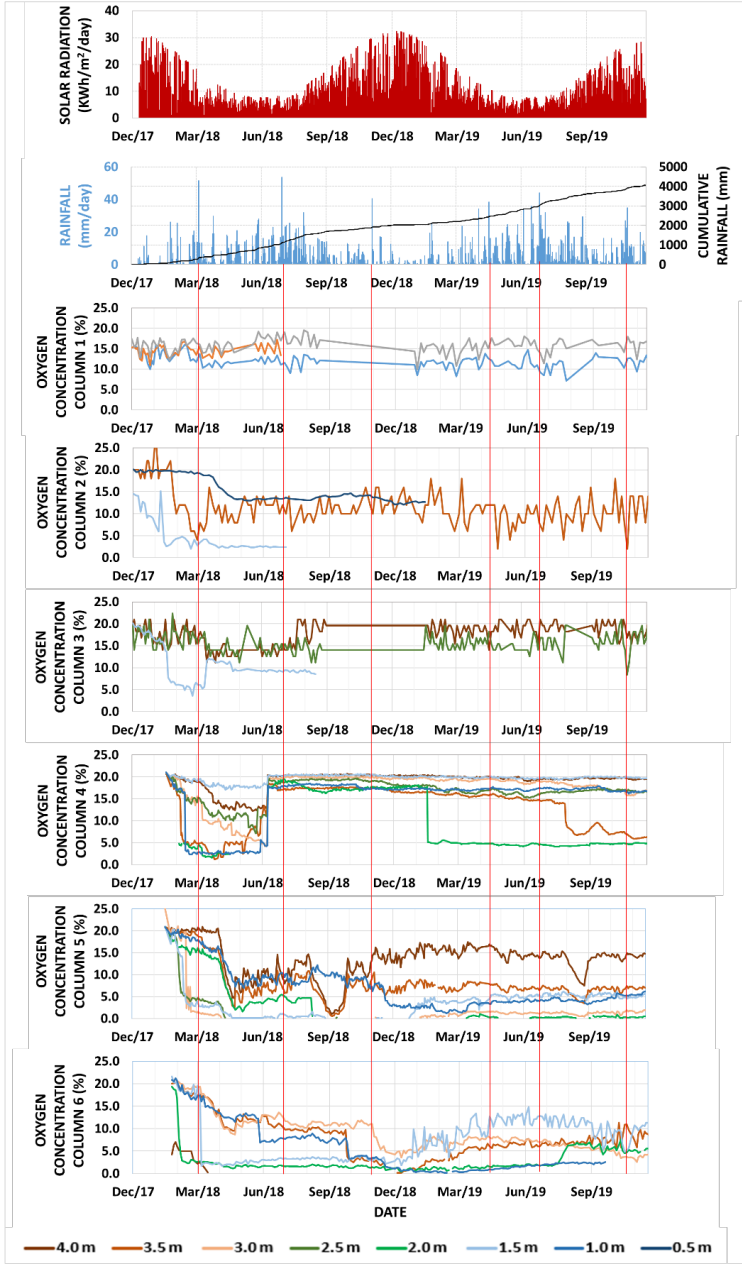

Figure 11. Monitored weather conditions (potential evaporation and rainfall) and oxygen levels in Column 1 to 6 over time, with red vertical lines highlighting six major rainfall events.

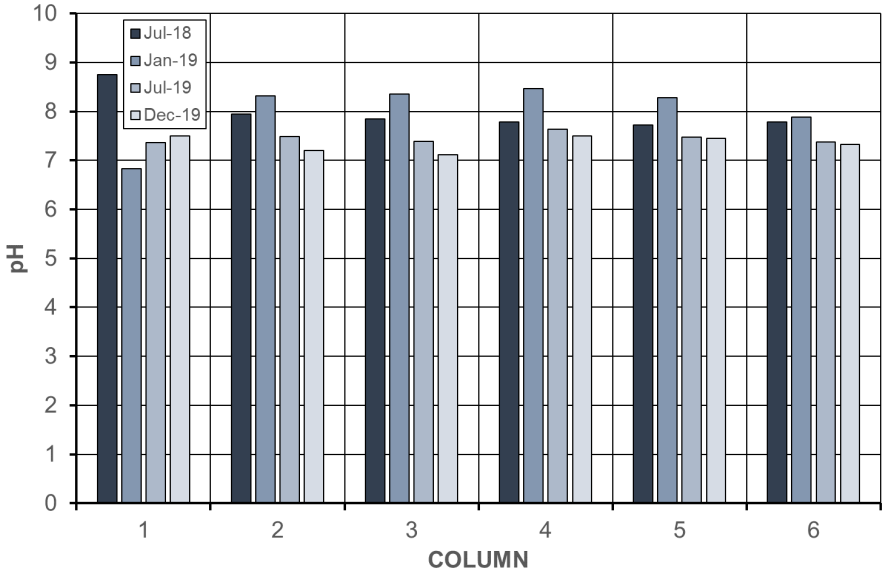

Figure 12. pH of leachate collected at different times from outlets of Columns 1 t 6.

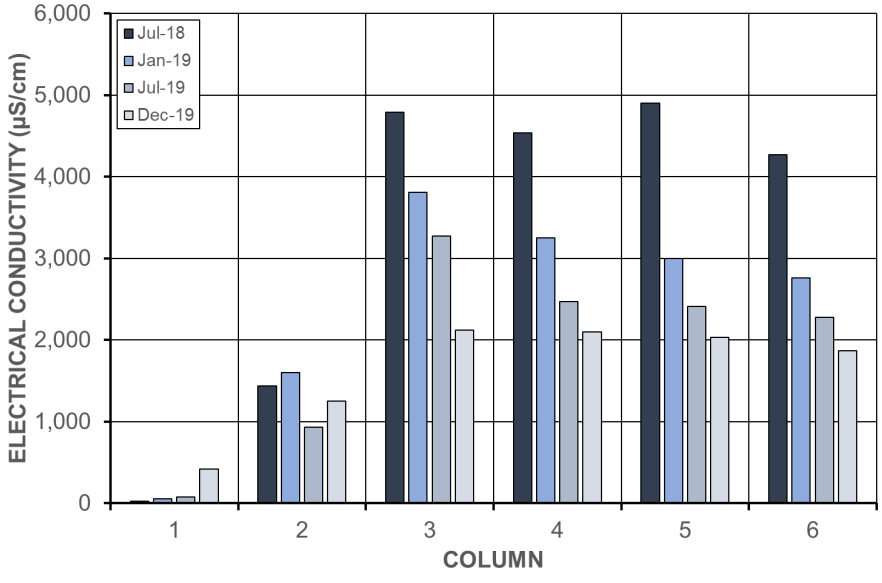

Figure 13. Electrical conductivity of leachate collected at different times from outlets of Columns 1 to 6.

4 CONCLUSIONS

Based on the monitoring data from December 2017 to December 2019, Column 5 containing compacted B-Type waste over loose D-Type waste and Column 6 containing loose, mixed A, B and D-Type wastes, performed best in terms of minimising oxygen ingress and leachate outflow, which has remained neutral over the 2-year monitoring period.

The compaction of B-Type waste in the upper section of Column 5 reduced the hydraulic conductivity of this layer, holding-up rainfall infiltration and hence reducing the rate of outflow of leachate. However, the compaction of A-Type waste in Column 4 did not show this favorable result. The hold-up of rainfall in the upper part of Column 6, which comprised loose, mixed A, B and D-Type wastes, helped to minimize oxygen ingress, and the hold-up of rainfall near the surface also increased evaporation and reduced the outflow of leachate.

The analysis of the leachate showed that the pH of the wastes in the columns dropped slightly over the 2-year monitoring period from slightly alkaline to near-neutral, while the electrical conductivity remained relatively low for Column 1 with only A-Type waste and Column 2 with only B-Type waste. The relatively high initial electrical conductivity for the four columns (3 to 6) containing at least some D-Type waste, roughly halved over the 2-year monitoring period, indicating improving water quality on wetting-up of the columns over time.

5 REFERENCES

Jambor, J.L., Blowes, D.W., Ptacek, C.J. and Weisener, C.G. 2003. *The geochemistry of acid mine drainage*. National Water Research Institute. Burlington, Ontario, Canada.

Karem, W.A., and Lee, C.S. 2008. Settlement evaluation of end dumped coal mine spoil fill. *Journal American Society of Mining and Reclamation*, 2008(1), 488-509.

Hydraulic Conductivity of Geosynthetic Clay Liners to Synthetic Mine Waste Leachates

Anna Norris & Neelufar Aghazamani
Department of Civil & Environmental Engineering, Colorado State University, Fort Collins, CO

Joel Conzelmann
Geosyntec Consultants, Chicago, IL

Joseph Scalia
Department of Civil & Environmental Engineering, Colorado State University, Fort Collins, CO

Charles Shackelford
Department of Civil & Environmental Engineering, Colorado State University, Fort Collins, CO

ABSTRACT: The use of geosynthetic clay liners (GCLs) in mining applications can result in GCL exposure to concentrated inorganic solutions potentially with extreme pH (pH < 3 and pH > 12). Site-specific hydraulic compatibility tests are necessary to identify specific combinations of permeant solution, bentonite (and bentonite enhancements), and effective stress that may result in hydraulic incompatibility (i.e., high hydraulic conductivity). The results of hydraulic conductivity tests on two fiber-reinforced GCLs containing (1) natural sodium bentonite with high manufacturer reported peel strength, MRPS, of 3500 N/m (HPS GCL) and (2) a polymer enhanced bentonite (EB) with a MRPS of 2900 N/m are reported for tests performed with three synthetic mining solutions simulating gold (Au-PS; pH = 6), copper (Cu-PS; pH = 1), and bauxite (BX-PS; pH = 12) process solutions at low and high effective stresses (27 and 500 kPa). At low effective stress, the HPS GCL exhibited a high hydraulic conductivity (> 10^{-10} m/s) to each leachate. At high effective stress, the HPS GCL exhibited high hydraulic conductivity (> 10^{-8} m/s) to Cu-PS but low hydraulic conductivity (< 10^{-12} m/s) to BX-PS, illustrating the importance of testing at stress levels representative of field conditions, particularly for GCLs with high peel strength intended for high stress applications. The EB-GCL has exhibited (test still ongoing) a low hydraulic conductivity (< 10^{-11} m/s) with BX-PS at low and high effective stresses, but high hydraulic conductivity (> 10^{-8} m/s) with Cu-PS at both stress levels. For BX-PS, high viscosity effluent continued to be eluted after one year of permeation indicating elution of at least a portion of the polymer enhancement which may cause the hydraulic conductivity to rise with continued permeation. These results illustrate that high stress and polymer enhancement may be insufficient to ensure a low hydraulic conductivity. For BX-PS, the EB-GCL exhibited a similar low hydraulic conductivity at low effective stress relative to the HPS GCL at high effective stress (3.3×10^{-13} m/s vs. 8.6×10^{-13} m/s), demonstrating the importance of both increased stress and enhancements to achieve target barrier performance. This study illustrates the importance of site-specific hydraulic compatibility tests on candidate GCLs, and the importance of using representative effective stresses during testing.

1 INTRODUCTION

The use of geosynthetic clay liners (GCLs) in mining applications, such as liners for uranium mill tailings, brine evaporation ponds, waste rock dumps, and secondary liners for heap leach pads (Bouazza 2010), can result in GCL exposure to aggressive solutions, including concentrated inorganic leachates and/or solutions with extreme pH, i.e., 3 > pH > 12 (Ruhl and Daniel 1997; Benson et al. 2010a; Bouazza 2010; Lange et al. 2010; Shackelford et al. 2010). When containment of aggressive solutions is required, traditional GCLs comprising natural sodium-bentonite have been shown to be potentially ineffective hydraulic barriers under low confining stresses, e.g., < 50 kPa (Benson et al. 2010a, Bouazza and Gates 2014, Chen et al. 2018). Thus,

site-specific hydraulic compatibility tests are often necessary to identify if the combination of permeant liquid, bentonite, GCL fiber reinforcing, and effective stress result in high hydraulic conductivity. Often, these tests are conducted at low effective stress (~ 27 kPa) due to the difficulty of running high effective stress tests with aggressive solutions, and the typical increased duration of tests on low hydraulic conductivity GCLs at high stress. If the anticipated site conditions result in an unacceptably high hydraulic conductivity, then the GCL is deemed incompatible with the permeant liquid, often necessitating the use of an alternative technology.

Enhanced bentonites (EBs) have emerged as an alternative technology in applications where the traditional GCL proves incompatible. Enhanced bentonites are produced with various proprietary types of amendments and by various amendment methods (e.g. Donovan et al. 2016a,b). Enhanced bentonite GCLs like bentonite-polyacrylic-acid composite (e.g. Benson et al. 2014) and dense-prehydrated GCLs (e.g. Kolstad et al. 2004b) have shown potential to produce a low hydraulic conductivity at both pH extremes, whereas other EB GCLs produce a low hydraulic conductivity ($< 10^{-10}$ m/s) to hyper-alkaline (pH > 12) solutions but not to hyper-acidic (pH < 2) solutions (e.g. Benson et al. 2010a). Limited data exist on the hydraulic conductivity of EB GCLs to real-world, extreme pH leachates, which can contain multiple species of multivalent cations and have high ionic strengths (> 100 mM) (e.g. Chen et al. 2018).

Recent studies have begun to evaluate the impact of higher effective stress on the hydraulic conductivity of GCLs with aggressive solutions. A three order-of-magnitude decrease in hydraulic conductivity of a sodium bentonite GCL permeated with four coal combustion product leachates (electrical conductivity, EC = 2-41 mS/cm, pH = 8.5-11, ionic strength = 39.5-755 mM) by increasing the effective stress from 20 kPa to 450 kPa. However, only one GCL exhibited a hydraulic conductivity less than 10^{-10} m/s at 450 kPa effective stress (Chen et al. 2018). A commercial EB GCL also was tested with the most aggressive coal combustion product leachate but increasing the effective stress from 20 kPa to 450 kPa resulted in only an order-of-magnitude reduction in hydraulic conductivity (Benson et al. 2014). Wang et al. (2019) also reported that increasing the effectives stress from 10 kPa to 200 kPa resulted in a 6.6 times reduction in the hydraulic conductivity of a sodium bentonite GCL permeated with acid mine drainage (EC 3.25-5 mS/cm, pH = 2.5). Limited studies of the effects of increase in the effective stress on the hydraulic conductivity of fiber-reinforced sodium bentonite and EB GCLs permeated with extreme pH solutions have been reported.

The purpose of this study is to evaluate the ability of a commercially available, high internal shear strength GCL to contain three synthetic, mining process solutions representative of a broad range of permeant chemistries, viz., a neutral pH, gold solution (Au-PS), a high pH, bauxite solution (BX-PS), and a low pH, copper solution (Cu-PS). For GCLs that exhibit hydraulic incompatibility at low effective stress (27 kPa), the effect of increased effective stress (500 kPa vs. 27 kPa), and/or selecting a commercially available EB GCL are evaluated. The results of this study inform selection of GCL products for site-specific hydraulic compatibility testing in mining applications.

2 MATERIALS

A commercially available, high peel strength, fiber-reinforced GCL (HPS GCL) and a commercially available enhanced bentonite GCL (EB GCL) were used. The HPS GCL has a manufacturer reported peel strength (MRPS) of 3500 N/m, representing GCLs with higher degrees of fiber reinforcing that are designed for potential use in higher-stress mining applications. The EB GCL is a commercially available GCL designed for enhanced hydraulic compatibility to coal combustion residuals with an MRPS of 2900 N/m containing bentonite amended with proprietary polymer additives. Properties of the two commercial GCLs are summarized in Table 1.

Four permeant solutions were used in this study: a synthetic, conservative soil pore water (CW), Au-PS, BX-PS, and Cu-PS (see Ghazi Zadeh et al. 2018). The CW (EC = 0.51 mS/cm, pH 6.0) provides a baseline, low concentration solution (ionic strength, I = 6 mM), but with a low ratio of monovalent-to-divalent cations, RMD (= 0.19 $mM^{1/2}$), defined as the ratio of the concentrations (mM) of all monovalent cation to the square root of the concentrations (mM) of all divalent cations. The Au-PS (EC = 3.4 mS/cm, pH = 5.1, I = 49 mM, RMD = 10 $mM^{1/2}$) represents an average leachate encountered in gold heap leap mining operations. The BX-PS (EC = 12.6 mS/cm,

pH = 12.0, I = 67 mM, RMD = 26 $mM^{1/2}$) represents an average leachate encountered in bauxite mining operations and the Cu-PS (EC = 67.7 mS/cm, pH = 1.2, I = 2200 mM, RMD = 32 $mM^{1/2}$) represents a possible worst-case scenario leachate encountered in copper heap leach mining operations. These solutions were selected to assess how a broad range of mining leachates affect the hydraulic conductivity of GCLs. The Au-PS, BX-LS, and Cu-PS provide near neutral, alkaline (pH = 12.0), and acidic (pH = 1.2) mining leachates, respectively. Preparation of solutions was completed following Ghazi Zadeh et al. (2018).

Table 1. Properties of Geosynthetic Clay Liners (GCLs)

	HPS GCL	EB GCL
Bentonite type	Coarse Granular	
Average dry bentonite mass/area (kg/m^2) (ASTM D5993)	3.6	4.4
Geotextile MUA (g/m^2) (ASTM D5261)	600[(a)]	550[(b)]
Carrier geotextile	Nonwoven	
Cover geotextile	Nonwoven	
MRPS (N/m) [(c)]	3500	2900
Initial thickness (mm)	8.54	6.48
Initial gravimetric water content (%)	5.7-10	9.6-10.7
Bundle size (mm) [(d,e)]	1.05 (SD = 0.25, n = 20)	0.90 (SD = 0.27, n = 80)
No. of bundles/area (bundles/m^2) [(d)]	105000 (SD = 13000, n = 10)	73000 (SD = 9400, n = 4)
No. of fibers/bundle [(d,e)]	41 (SD = 14, n = 20)	27 (SD = 5, n = 80)
% area covered by bundles [(d,f)]	9.0	4.6

[(a)] Manufacturer reported
[(b)] Measured as part of this study
[(c)] Manufacturer reported peel strength
[(d)] Values given are average with SD = standard deviation and n = number of samples when multiple tests were performed
[(e)] Based on manual measurement using stereoscopic microscope
[(f)] Assuming average values for fiber bundle size and assuming cylindrical fiber bundles

3 METHODS

The methods and equipment described in Conzelmann et al. (2016) were used for the hydraulic compatibility testing of GCLs under low effective stress (27 kPa) or high effective stress (500 kPa) at an average hydraulic gradient of 200. All tests were permeated until the hydraulic equilibrium termination criteria of ASTM 5084-16a, and for select tests the chemical equilibrium termination criteria of ASTM D6766-18, were achieved. ASTM 6766-18 termination criteria were not met in tests where either (1) preferential flow appeared to be controlling the hydraulic conductivity or (2) the hydraulic conductivity was steady over multiple pore volumes of flow, PVF. Note that PVF was defined with respect to the inflow. After the specified termination criteria were achieved, GCLs exhibiting high hydraulic conductivity (> 10^{-10} m/s) were tested for possible preferential flow paths by adding a rhodamine WT dye (5 mg/L) to the influent.

4 RESULTS AND DISCUSSION

4.1 *High Peel Strength GCL*

Results of the hydraulic conductivity tests for the HPS GCL measured at low effective stress (27 kPa) are summarized in Table 2 and shown in Fig. 1. The HPS GCL hydraulic conductivity tests permeated with CW under low effective stress resulted in a low hydraulic conductivity (2.6×10^{-11} m/s). The hydraulic conductivity tests permeated with the Au-PS, BX-PS, and Cu-PS produced higher hydraulic conductivities of 1.1×10^{-8} m/s, 5.7×10^{-10} m/s, and 6.3×10^{-7} m/s, respectively. Rhodamine-WT dye was added to the influent liquid and permeated through specimens that exhibited high hydraulic conductivity. The dyed specimens revealed preferential flow along some, but not all, reinforcing fiber bundles for tests with the Au-PS and BX-PS as shown in Figs. 2a,c and 2b,d, respectively. The hydraulic conductivities measured for the HPS GCL permeated with CW, Au-PS, and BX-PS were initially of the same order of magnitude, as shown in Fig. 1, but divergent behavior is observed after 4 PVF at which point the fiber bundles are hypothesized to have been sealed shut by bentonite swelling in the CW test. The high hydraulic conductivity measured for the GCL permeated with Cu-PS (6.3×10^{-7} m/s) was attributed to limited swelling of the bentonite granules due to the aggressive nature of the solution (high EC/low pH). The bentonite aggregation due to the Cu-PS solution during permeation is illustrated in Fig. 2e. Preferential flow was not specifically observed along fiber bundles.

Table 2. Hydraulic conductivity testing summary

Material	Permeant	Effective Stress (kPa)	Permeation Time (days)	Pore Volumes of Flow (PVF)	Final Measured Hydraulic Conductivity, *k* (m/s)
HPS GCL	CW	27	17	8.0	2.6×10^{-11}
	Au-PS		0.4	6.1	1.1×10^{-8}
	BX-PS		2.3	9.0	5.7×10^{-10}
	Cu-PS		< 1	13	6.3×10^{-7}
	BX-PS	500	362	1.5	8.6×10^{-13}
	Cu-PS		< 1	28	7.0×10^{-8}
EB GCL	BX-PS*	27	293+	4.5+	8.3×10^{-12}
	Cu-PS		< 1	12.6	7.6×10^{-7}
	BX-PS*	500	365+	0.26+	3.3×10^{-13}
	Cu-PS		<1	27.9	2.5×10^{-8}

*Ongoing Tests

These results indicate that GCLs with traditional sodium bentonite and higher degrees of fiber reinforcement, like the HPS GCL, may produce a high hydraulic conductivity when permeated with aggressive mining leachates under low effective stress due to preferential flow conducted along some fiber bundles (e.g., Scalia & Benson 2010b). However, HPS are not intended for low effective stress applications where high strength is not needed. Therefore, hydraulic compatibility tests at low effective stress (< 30 kPa) may not be relevant for HPS GCLs intended for higher stress applications. The origin of preferential flow along the fiber bundles is hypothesized in Scalia and Benson (2010b) and is likely exacerbated by the number of fibers within in a bundle (bundle size) in the HPS GCL.

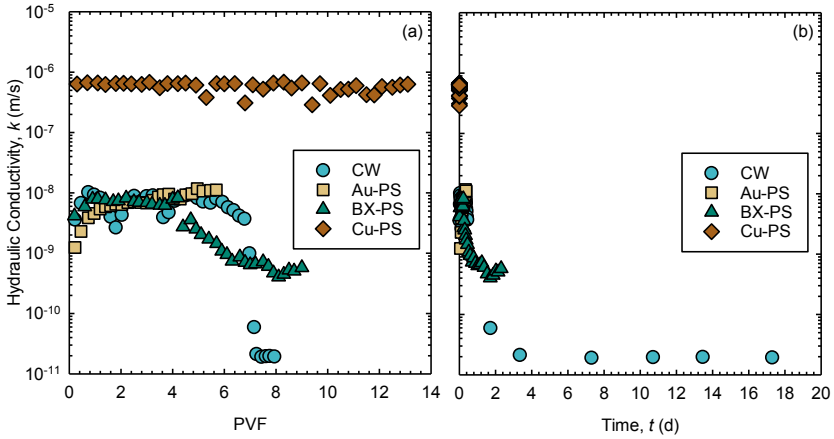

Figure 1. Hydraulic conductivity of high peel strength (HPS) geosynthetic clay liner (GCL) as a function of (a) pore volumes of flow (PVF) and (b) permeation time for tests with conservative water (CW), gold synthetic mining process solution (Au-PS), bauxite synthetic mining process solution (BX-PS), and copper synthetic mining process solution (Cu-PS), at low effective stress (27 kPa).

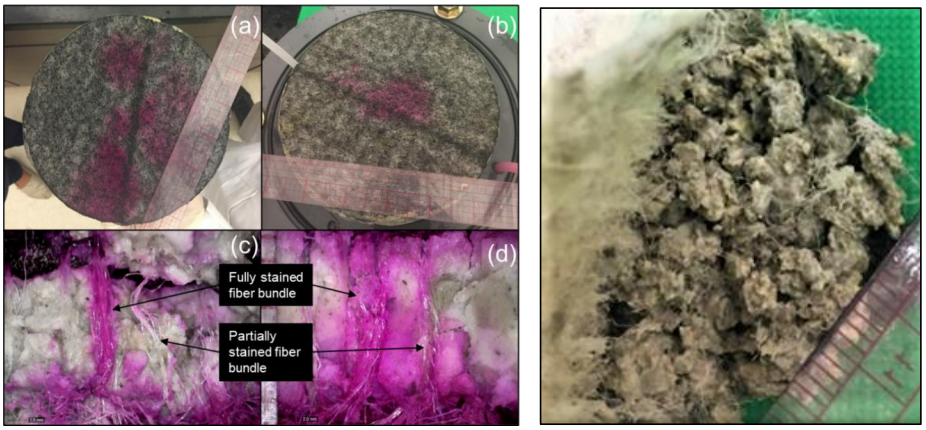

Figure 2. Images of HPS GCL under low effective stress (27kPa) specimens permeated with Rhodamine-WT dye to exhibit preferential flow along fiber bundles in tests producing high hydraulic conductivity, using permeant solutions (a,c) synthetic gold mining process solution (Au-PS) and (b,d) synthetic bauxite mining process solution (BX-PS) for outflow site (a,b) and in cross section (c,d), and (e) bentonite granules removed from the GCL post-permeation from the HPS GCL permeated with the synthetic copper mining process solution (Cu-PS) solution.

4.2 *Effects of increasing effective stress*

The results of the hydraulic conductivity tests of the HPS GCL conducted at high effective stress (500 kPa) with BX-PS and Cu-PS are summarized in Table 2 and shown in Fig. 3. The increase in effective stress had a favorable effect in reducing preferential flow along the fiber bundles in the HPS GCL permeated with BX-PS, and reducing the hydraulic conductivity at low effective stress (27 kPa) from 5.7×10^{-10} m/s to 8.6×10^{-13} m/s. The favorable effects of increasing effective stress were not observed in the hydraulic conductivity test of the HPS GCL permeated with the Cu-PS. An increase in effectives stress from 27 kPa to 500 kPa reduced the hydraulic conductivity

by approximately one order of magnitude from 6.3×10^{-7} m/s to 7.0×10^{-8} m/s. However, the hydraulic conductivity is still greater than 10^{-10} m/s (high). Preferential flow along the fiber bundles was confirmed to be the cause of the high hydraulic conductivity, as shown in Fig. 4. The pattern of the dyed area in Fig. 4a and the select dark purple fiber bundles in Fig. 4b-d indicate that preferential flow occurred through select bundles.

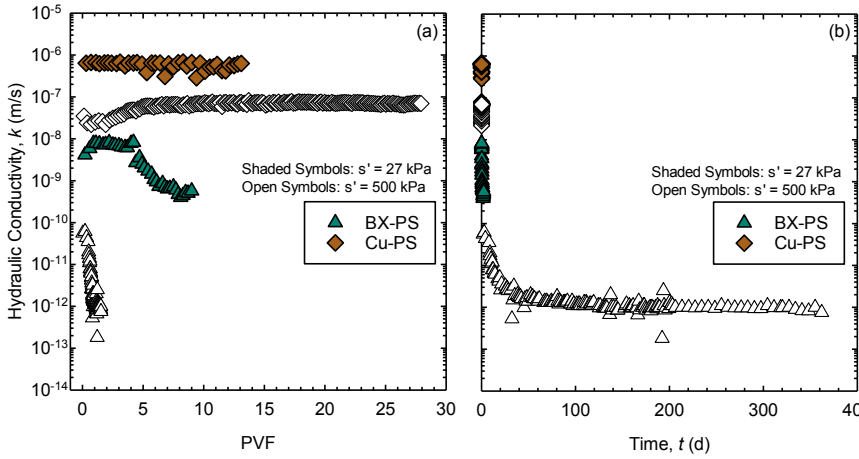

Figure 3. Hydraulic conductivity of high peel strength (HPS) geosynthetic clay liner (GCL) as a function of (a) pore volumes of flow (PVF) and (b) time, measured in two permeant solutions, bauxite synthetic mining process solution (BX-PS) and copper synthetic mining process solution (Cu-PS) at low (27 kPa) and high (500 kPa) effective stress.

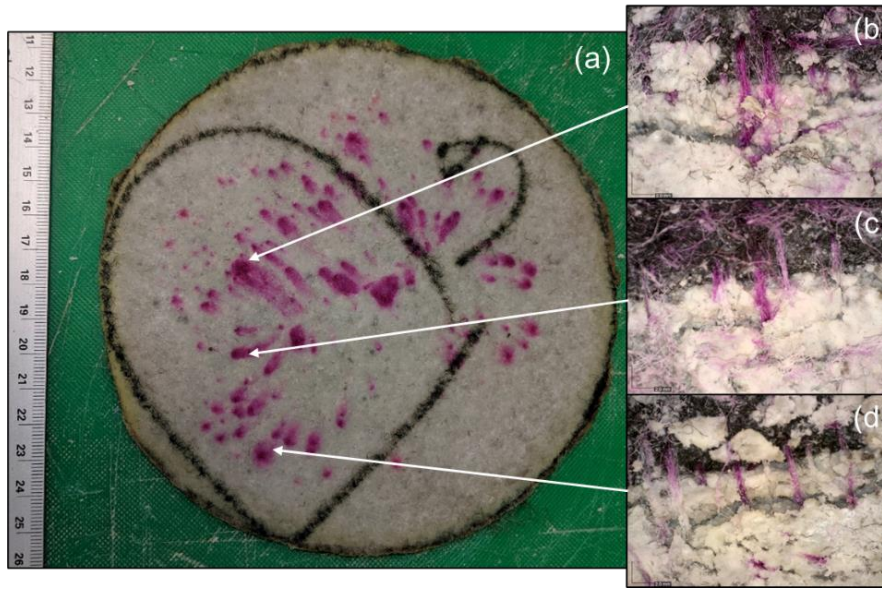

Figure 4: Images of HPS GCL specimen (a) outflow side permeated with Rhodamine-WT dye to exhibit preferential flow along fiber bundles (b, c, d) under high effective stress (500kPa), using synthetic copper process solution (Cu-PS).

4.3 *Effect of enhanced bentonite*

The results of the hydraulic conductivity tests with the EB GCL performed at both low and high effective stresses are summarized in Table 2 and shown in Fig. 5. Hydraulic conductivity tests on EB GCL permeated with the BX-PS at low and high effective stress are still ongoing and the data herein reflect the behavior to date. At low effectives stress, the hydraulic conductivity of the EB GCL is stable and low at 8.3×10^{-12} m/s, indicating that the EB GCL offers an initial resilience to the BX-PS and does not (over 293 days) exhibit the preferential flow exhibited by the HPS GCL to BX-PS at low effective stress. However, the test continues to produce a viscous effluent, suggesting elution of the polymer enhancement. The test will continue to be permeated until the viscosity of the effluent reduces to ensure that loss of enhancement does not cause an increase in hydraulic conductivity.

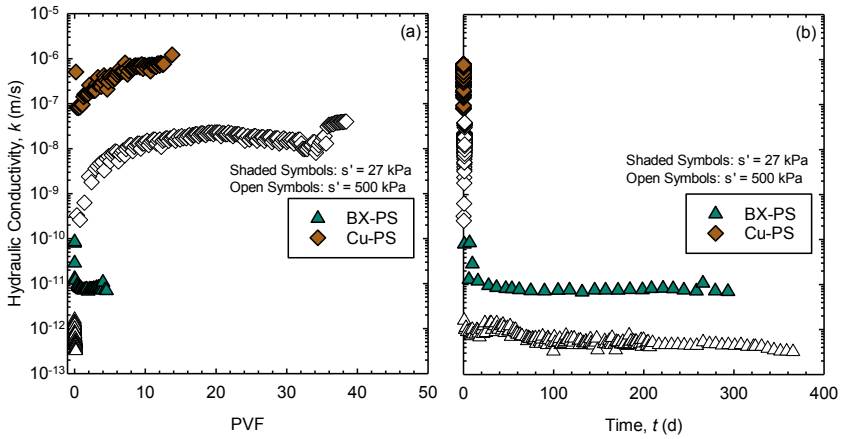

Figure 5. Hydraulic conductivity of enhanced bentonite geosynthetic clay liner (EB GCL) as a function of (a) pore volumes of flow (PVF) and (b) time for tests conducted with bauxite synthetic mining process solution (BX-PS) and copper synthetic mining process solution (Cu-PS) at low effective stress (27 kPa) and high effective stress (500 kPa).

The hydraulic conductivity of the EB GCL permeated with the Cu-PS at low effective stress was high (7.6×10^{-7} m/s) and within the same order of magnitude as that for the HPS GCL permeated with the Cu-PS under the same effective stress. The similar hydraulic conductivity values can be explained by the similar preferential flow behavior along the fiber bundles, as shown in Fig. 6(a,c). Upon examination post-permeation, the EB GCL had visible polymer hydrogel on the inflow (Fig. 6b) and outflow (Fig. 6a) side geotextiles and within the bentonite pores (Fig. 6d). Unfortunately, the pore clogging mechanism hypothesized to produce low hydraulic conductivity when hydrogel forms in EB GCLs (Scalia et al. 2014, Scalia et al. 2018) did not prevent flow along the fiber bundles in this product.

At high effective stress, the EB GCL produced similar, but lower, hydraulic conductivities relative to those for the low stress tests in the same solution. The EB GCL permeated with BX-PS at high effective stress has maintained a low hydraulic conductivity (3.3×10^{-13} m/s), but has produced very little viscous outflow (~0.3 PVF) after 365 days of permeation. The EB GCL permeated with Cu-PS at high effective stress exhibited the same behavior as observed at low effective stress, producing a high hydraulic conductivity (4.0×10^{-8} m/s) and preferential flow along the fiber bundles (Fig. 7a-c) although hydrogel formed within the bentonite pores (Fig. 7d). The viscous effluent and hydrogel formation exhibited by the EB GCLs permeated with BX-PS at low and high effective stress with hydraulic conductivities of 8.3×10^{-12} m/s, 3.3×10^{-13} m/s, respectively, is in stark contrast to the behavior of the EB GCL permeated with the Cu-PS at low and high effective stress with hydraulic conductivities of 7.6×10^{-7} m/s, 4.0×10^{-8} m/s, respectively, which did not exhibit an elevated effluent viscosity and produced results similar to the HPS GCL.

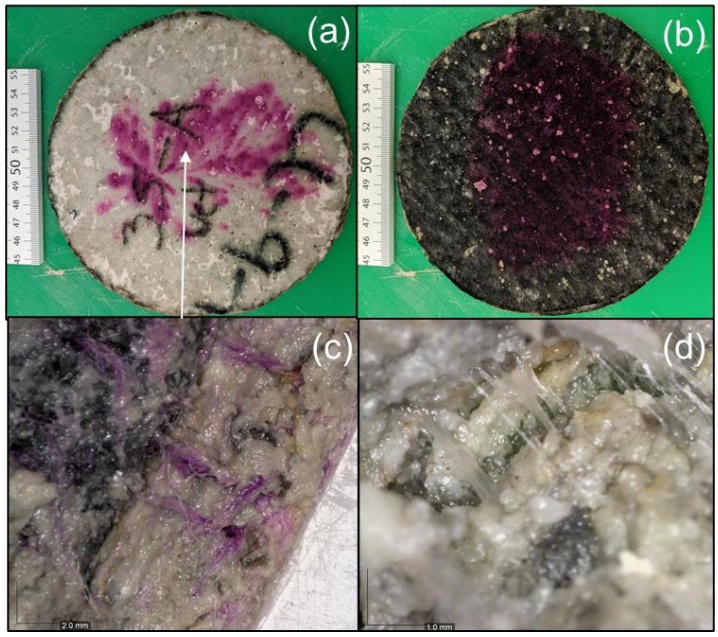

Figure 6. Images of EB GCL specimen (a) outflow side, and inflow side (b) permeated under low effective stress (27kPa), using synthetic copper process solution (Cu-PS) permeant solution and Rhodamine-WT dye to exhibit (c) preferential flow along fiber bundles and of visible polymer hydrogel (d) between the bentonite granules.

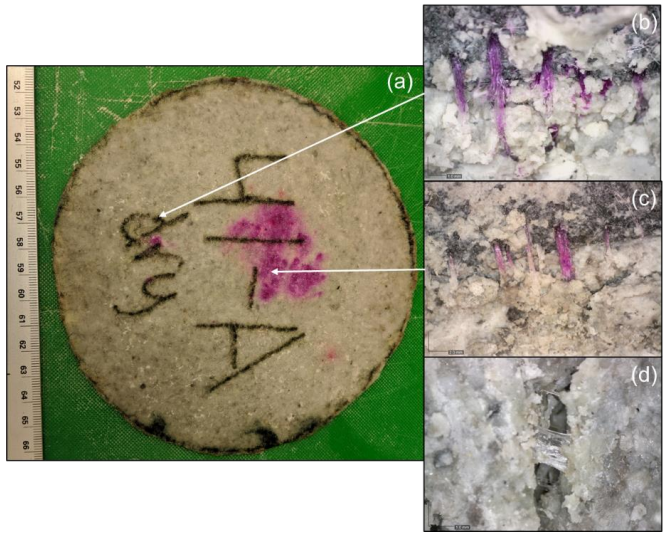

Figure 7. Images of EB GCL specimen (a) outflow side permeated with Rhodamine-WT dye to exhibit preferential flow along fiber bundles (b, c) under high effective stress (500kPa), using synthetic copper process solution (Cu-PS) and of visible hydrogel (d) between bentonite granules.

As illustrated in Fig.8, increasing the effective stress from 27 kPa to 500 kPa consistently reduced the hydraulic conductivity by at least an order of magnitude, with the largest reduction of almost three orders of magnitude for the HPS GCL permeated with the BX-PS. The increase in effective stress to 500 kPa was not successful in closing the preferential flow paths created in both the HPS GCL and the EB GCL with Cu-PS. The creation of the preferential flow paths, even at high effective stress, may occur due to the degree of the fiber reinforcement or the severe detrimental effects of the low pH Cu-PS on the bentonite swelling behavior.

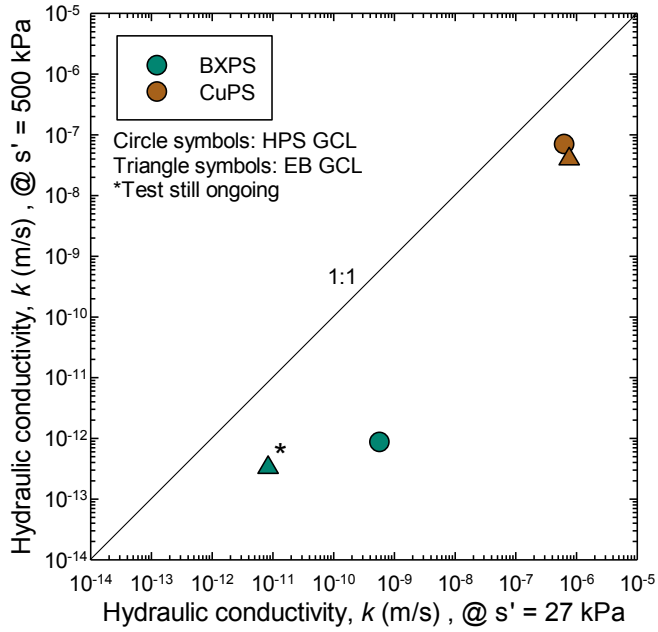

Figure 8. Final measured hydraulic conductivity of high peel strength geosynthetic clay liner (HPS GCL) and enhanced bentonite (EB GCL) measured at low effective stress (27 kPa) as a function of the final measured hydraulic conductivity of the same GCL at high effectives stress (500 kPa) in bauxite synthetic mining process solution (BX-PS) and copper synthetic mining process solution (Cu-PS).

5 CONCLUSIONS

The hydraulic conductivities of two fiber-reinforced GCLs (1) HPS GCL and (2) EB GCL were tested with three synthetic mining process solutions, viz., a gold solution (Au-PS), a bauxite solution (BX-PS), and a copper solution (Cu-PS), at low and high effective stresses (35 kPa and 500 kPa). At low effective stress, the HPS GCL exhibited a high hydraulic conductivity (> 10^{-10} m/s) to both Au-PS, BX-PS, and Cu-PS. At high effective stress, the HPS GCL exhibited high hydraulic conductivity (> 10^{-8} m/s) to Cu-PS, but low hydraulic conductivity (< 10^{-12} m/s) to BX-PS, illustrating the importance of testing at stress levels representative of field conditions, particularly for GCLs with high peel strength intended for high stress applications.

The EB-GCL exhibited a low hydraulic conductivity (< 10^{-11} m/s) with BX-PS at low and high effective stresses (test ongoing), but high hydraulic conductivity (> 10^{-8} m/s) with Cu-PS at both stress levels. For BX-PS, high viscosity effluent continued to be eluted after one year of permeation, indicating elution of at least a portion of the enhancement which may cause the hydraulic conductivity to rise with continued permeation (in progress). These results illustrate that

high stress and polymer enhancement may be insufficient to ensure a low hydraulic conductivity. For BX-PS, the EB-GCL exhibited a similar (low) hydraulic conductivity at low stress relative to the HPS GCL at high effective stress (8.3×10^{-12} m/s vs. 8.6×10^{-13} m/s), demonstrating the importance of both increased stress and leachate-specific enhancements to achieve target barrier performance. This study illustrates the importance of site-specific hydraulic compatibility tests on candidate GCLs, and the significance of using representative effective stresses during testing.

REFERENCES

Benson, C., Chen, J. & Edil, T. (2014). Engineering properties of geosynthetic clay liners permeated with coal combustion product leachates, Report No. 3002003770. Electric Power Research Institute (EPRI), Palo Alto, CA, USA.

Benson, C., Oren, A. & Gates,W. (2010a). Hydraulic conductivity of two geosynthetic clay liners permeated with a hyperalkaline solution. Geotextiles and Geomembranes, 28(2), 206–218.

Bouazza, A. (2010). Geosynthetics lining in mining applications. Proceedings of Sixth International Conference on Environmental Geotechnics, New Delhi, India, International Society for Soil Mechanics and Geotechnical Engineers, 221–259.

Bouazza, A. & Gates, W. (2014). Overview of performance compatibility issues of GCLs with respect to leachates of extreme chemistry. Geosynthetics International, 21(2), 151–167.

Chen, J., Benson, C., Edil, T. & Likos,W. (2018). Hydraulic conductivity of geosynthetic clay liners with sodium bentonite to coal combustion product leachates. Journal of Geotechnical and Geoenvironmental Engineering, 144(3), 04018008.

Conzelmann, J., Scalia, J., & Shackelford, C. (2017). Effect of backpressure saturation on the hydraulic conductivity of GCLs. Geotechnical Frontiers, Orlando, FL, ASCE, Reston, VA (CD-ROM).

Donovan, M., Valorio, R., & Gebka, B. (2016a) Polymer enhanced geosynthetic clay liners for extreme leachate chemistries. Proc., EuroGeo6 Conf., International Geosynthetics Society, Jupiter, FL, USA.

Donovan, M., Valorio, R., & Gebka, B. (2016b). Chemical compatibility of polymer modified GCLs in coal combustion residual leachates. Proc., Geoamericas 2016 Conf., International Geosynthetics Society, Jupiter, FL, USA.

Ghazi Zadeh, S., Bareither, C., Scalia, J., & Shackelford, C. (2018). Synthetic solutions for evaluating GCLs in mining applications, Journal of Geotechnical and Geoenvironmental Engineering, 144(10), 06018011.

Lange, K., Rowe, R.K., & Jamieson, H., (2007). Metal retention in geosynthetic clay liners following permeation by different mining solutions. Geosynthetics International, 14(3), 178–187.

Ruhl, J., & Daniel, D. (1997). Geosynthetic clay liners permeated with chemical solutions and leachates. Journal of Geotechnical and Geoenvironmental Engineering, 123(4), 369–381.

Scalia, J., & Benson, C. (2010b). Preferential flow in geosynthetic clay liners exhumed from final covers with composite barriers. Canadian Geotechnical Journal, 47(10), 1101–1111.

Scalia, J., Benson, C., Bohnhoff, G., Edil, T. & Shackelford, C. (2014). Long-term hydraulic conductivity of a bentonite-polymer composite permeated with aggressive inorganic solutions. Journal of Geotechnical and Geoenvironmental Engineering, 140(3), 1–13.

Scalia, J., Bohnhoff, G., Shackelford, C., Benson, C., Sample-Lord, K., Malusis, M., & Likos, W. (2018). Enhanced bentonites for containment of inorganic waste leachates by GCLs. Geosynthetics International, 25(4), 392–411.

Shackelford, C., Sevick, G., & Eykholt, G. (2010). Hydraulic conductivity of geosynthetic clay liners to tailings impoundment solutions. Geotextiles and Geomembranes, 28(2), 149–162.

Wang, B., Dong, X., & Chen, B. (2019). Hydraulic conductivity of geosynthetic clay liners permeated with acid mine drainage. Mine Water Environment 38, 658–666.

Successful Tailings Dewatering Design Using Multi-Linear Drainage Geocomposites

Pascal Saunier
AFITEX-Texel inc., Vancouver, BC, Canada

Jacek Mlynarek
JM-TEX Alliance, previously Groupe CTT Group, Ste Hyacinthe, QC, Canada

Rob Stafford
Western GeoSystems, Reno, NV, USA

Andy Jung
Western GeoSystems, Denver, CO, USA

ABSTRACT: Tailings Storage Facilities (TSFs) are used for the long-term disposal of mining tailings. This storage method can cause large scale casualties and environmental devastation in the case of a dam failure. Tailings Dewatering has emerged as a method to naturally thicken and stabilize slurry tailings in order to make it both less likely for a dam failure to occur and easier to reclaim in the future. Reducing the water content of those tailings also has a major economic impact on projects because of the reduced volume of tailings to be stored. Each pond will therefore see its lifetime expand by a factor of 1.5 to 2. Tailings Dewatering process is done by enabling the drainage of liquid from the tailings and into a water management facility. However, the physical and chemical nature of many TSFs can cause tremendous stress on dewatering designs. High compressive loads and concentrations of fines can lead to reductions in drainage. Additionally, high acidity can lead to accelerated degradation of the drainage components. Multi-Linear Drainage Geocomposites (MLdG) have been successfully used in several low pH dewatering designs with high compressive loads and high contents of fines. Unlike drainage geocomposites with a net core, MLdGs are not sensitive to geotextile intrusion nor are they as susceptible to creep under extremely high compressive loads. In high fines applications, a filter geotextile component is designed and tested before being used to reduce mineral clogging. It is therefore advised that, with site specifics in mind to specify the correct product, laboratory gradient ratio tests need to be performed to determine which filter is suitable. Project examples will share the proper lab techniques to be followed to evaluate product and technology selection. Case studies will also be shared.

1 INTRODUCTION

1.1 *Type area*

The safe and economical storage of tailings generated by modern day mining operations is possibly the single largest challenge faced by miners today. By nature, tailings are a waste product that have little to no economic value. Yet, their physical and chemical contents can pose incredible environmental hazards if not stored correctly. The variety of factors that are met when designing Tailing Storage Facilities (TSFs), means that in most cases, a low-cost solution is sought to accomplish storage, meet environmental regulations, and adhere to industry best practices. TSF can be large Dam face structures or smaller structures like retention/evaporation lined ponds.

Water management is potentially the single largest factor that miners and designers must contend with when constructing a TSF. Water is a necessary component in the process of extracting ore but can be difficult and expensive to remove once it is mixed with solid tailings particles. As a result, the most common disposal of these water containing tailings, called a slurry, is to simply discharge into an embanked TSF (Vick, 1990). These structures, just like any other

water retaining dam, can breach releasing contents downstream. Despite modern advancements in TSF design, there have been numerous dam failures that have resulted in tragic loss of life and ecological devastation. Most notably in the last decade, the Brumadinho and Mariana Dam disasters in Brazil killed 278 people in downstream communities when TSF dams failed in 2019 and 2015, respectively (Rotta at el., 2020). Similarly, in 2014, the Mount Polley tailings spill in British Columbia was the second largest tailings spill on record and caused extensive damage to adjacent watershed ecosystems when the TSF embankment was breached (Byrne at el., 2018). While there were indeed numerous unique and underlying factors present in each of these structural failures, a shared element in the devastation was the large-scale release of unstable liquefied tailings.

The aftermath of the disaster in Brumadinho after the TSF dam collapsed. Photo by Felipe Werneck/Ibama, Wikimedia Commons

View of the Mount Polley Mine Tailings pond Breach – Photo by Jonathan Hayward/Canadian Press

Environmental and stability concerns aside, slurry requires a much greater volume in a TSF than solid tailings alone (Saunier, 2018). TSF Expansions are costly and many times accomplished through vertical "lifts" of the embankments as to not extend the footprint. Better utilization of the existing TSF volume creates an economic advantage for mining operations. Various methods have been used to dewater tailings for both stabilization and to minimize the overall volume they occupy. Moisture can be removed from the solids using an extensive filtration process prior to the tailings being placed in their final location. This technique, known as Dry Stacking, provides the most stable tailings product, but requires an immense filtration facility and increased operating costs. Natural and polymer-based thickeners can be added to slurry tailings to stabilize its structure. However, this method does not provide a solution to the issue of volume.

Gravity-based dewatering using drainage geocomposite may be the most cost-effective solution for many mining operations. This process utilizes a geosynthetic product, known as a geocomposite, consisting of two layers of geotextile encapsulating a drainage media on the upslope side of a TSF embankment. This method effectively relies on the natural settlement of solid particles withing the slurry. Subsequent smaller particles work to build up a natural filter while the drainage component removes the liquid from the tailings. However, the physical and chemical nature of many TSFs can cause tremendous stress on traditional geocomposites. As TSFs grow larger in size, high compressive loads can cause compression of the drainage core and intrusion of the geotextile component. These phenomena, known as creep and intrusion respectively, can cause large reductions in dewatering capability. Further, high concentrations of fines can lead to clogging of the geotextile filter. High acidity can further accelerate degradation of the drainage components.

2 DESCRIPTION OF MULTI-LINEAR DRAINAGE GEOCOMPOSITE

2.1 *Technology*

The use of geomembranes in mining applications has been widely documented. However, geocomposite compatibility studies with mined material are scarce and very limited information is available. A study by Smith and Zhao (2004) clearly shows that drainage geocomposites lead to improved service and cost reduction in heap leaching. Gulec et al. (2005) indicated there were no major changes in the hydraulic and mechanical properties of polypropylene geotextiles after immersion in acid mine drainage for 22 months.
The MLdG used in this study is developed by AFITEX-TEXEL and called DRAINTUBE®. It is composed of (Figure 1):

- a nonwoven polyethylene geotextile acting as a filter,
- a series of corrugated polypropylene tubes spaced at regular intervals (1 to 4 m width). These perforated tubes provide most of the drainage capability of the product; and
- a nonwoven thick polypropylene geotextile acting as the drainage medium and as a cushion to protect the underlying geomembrane.

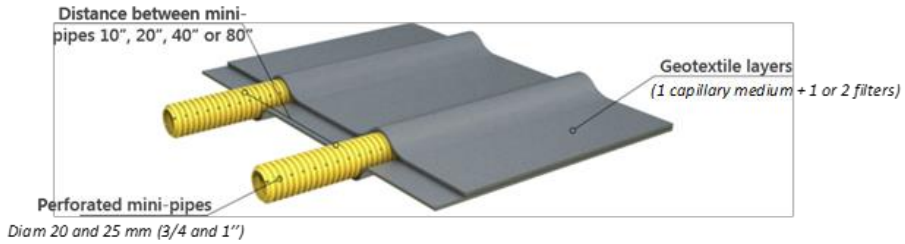

Figure 1: Drain Tubes Multi-Linear Planar Geocomposites

Filtration applications with mine residues may be among the most challenging filtration applications. First, the high seepage forces and suspended particles that must be filtered can lead to clogging. Second, leachate is typically a highly loaded solution and mineralization can lead to chemical clogging (Faure, 2004; Fourie et al., 2010; Legge et al., 2009). Although it is likely that a clogging problem would also occur with mineral drainage systems (such as gravels, see Giroud, 1996). In order to check if DTPG are able to fulfil the function of a drainage and dewatering layers, long-term hydraulic properties, soil retention, and chemical resistance must be evaluated. Results of experimental studies aiming at checking these points are presented in the following sections.

2.2 *Behavior under High Compressive Load*

With an ore density between 1.5 and 1.8, the compressive load on the drainage layer can reach 2 MPa (Thiel and Smith, 2004; Castillo, 2005). For traditional planar geocomposites involving a planar drainage core (such as biplanar or triplanar geonet), it has been shown by several authors that the hydraulic properties of these geosynthetics are adversely affected by such high compression stresses. However, Saunier et al. (2010) have shown that the particular structure of drain tube planar geocomposites is favorable to the development of an arching effect around the pipe. As a consequence, the transmissivity is not affected by the compression stress, nor by time, as no creep can develop in the pipe. Their results are reported in Figure 2.

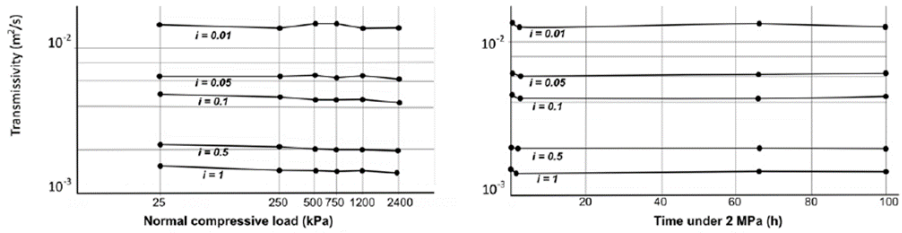

Figure 2: Transmissivity under Different Loads up to 2 Mpa and 100 h (i = Hydraulic Gradient) (after Saunier et al, 2010)

Based on these observations, it can be concluded that circulation of sulfuric acid through the ore/geocomposite system is not likely to create any clogging problem on the surface nor in the drainage media, with the particular DTPG tested involving a 25 mm diameter perforated pipe and a geotextile having a 120µm filtration opening size. Although the experiment was conducted under a normal load of 100 kPa, the lack of sensitivity of the product to compression loads up to 2,400 kPa suggests that these observations are likely to be applicable to the high normal loads which are typically experienced in heap leach pads.

3 FILTRATION COMPATIBILITY WITH TAILINGS AND GRADIENT RATIO

3.1 *Methodology*

The tailings are conveyed to their storage facility in a slurry form. Slurries are highly challenging materials for geotextile filtration because the presence of a high concentration of fines separated from the soil can create a cake on the surface of the geotextile and reduce its permeability, thus endangering the efficiency of the system and the stability of geotechnical structure.

To evaluate the filtration behavior of the geotextile used as a filter in the MLdG, a modified gradient ratio test was developed to model the mechanisms prevailing that the slurry is deposited on the geotextile filter. The following hypotheses were considered to develop the experiment:

- First, the slurry reaches the geotextile with a solid / water ratio of 70% water / 30% solid.
- In the early stage of the slurry/geotextile interaction, the water head will be similar to the height of the slurry, and the system will settle,
- Eventually, more material will reach the deposit, and will increase the water head, and eventually hydraulic gradient prevailing in the vicinity of the interface;

Considering these hypotheses, a testing strategy was developed, using a testing apparatus conforming to ASTM D5101, modified in order to model the above described scenario.

A slurry was prepared to the prescribed solid / water ratio, using the tailing which particle size distribution is presented on Figure 3-a. To initiate the test, this slurry was deposited in a liquid from (Figure 3-b) on the surface of the geotextile filter, selected for its filtration opening size of 60-70 µm (per CGSB 148.1 n°10). This led to a total head of about 300 mm above the geotextile.

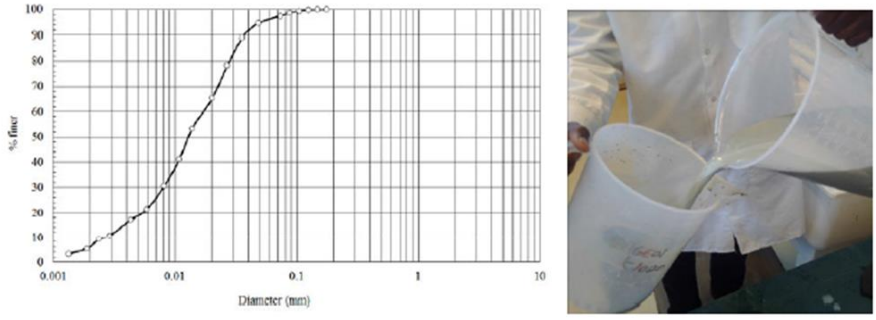

(a) Gradation *(b) consistency for deposition*

Figure 3: Gradation of the tailing

3.2 *Testings*

A valve located downstream of the geotextile was opened immediately to initiate the test, connecting the downstream section of the test cell to a container with a free surface maintained at a height of 150 mm above the geotextile. Taking this into account, the initial conditions prevailed were a water (slurry) head of about 300 mm upstream the geotextile, and 150 mm downstream. A 'slurry head' of 150 mm was thus applied on the geotextile filter, initiating a flow through the geotextile at the same time the slurry was settling. The hydraulic head was monitored under the geotextile, at distances of 25 and 75mm above the slurry. The flow rate was also measured. These conditions, combining a falling head and sedimentation of the tailing, were maintained until stabilization of the upstream head to 150 mm = identical to the downstream head. During that stage, the soil / geotextile interface has developed its structure in a manner similar to what is likely to be taking place on-site.

After stabilization, the upper portion of the test cell was closed, and the standard gradient ratio test was initiated using the standard apparatus (Figure 4), applying a hydraulic gradient of 1.0. During the test, the same hydraulic head was monitored, under the geotextile, at distances of 25 and 75mm and above the soil/slurry, as well as the flow rate.

As there is no precise limit differentiating a 'soil' from a 'slurry' during the deposition phase, it was not possible to determine a flow length in the porous media, therefore to calculate a permeability of a soil, geotextile, or slurry of course. It was thus decided to determine a 'permittivity' of the entire system, by dividing the flow rate by the total water head. This value was considered to be an indicator, sufficient to observe a trend, i.e. an increase or a reduction of

permeability over time. It is also a practical way to normalize the flow rate to the water head, to analyze the geotextile interface behavior during the slurry deposition stage of the test.

Results and observations are presented in Figures 5 to 8.

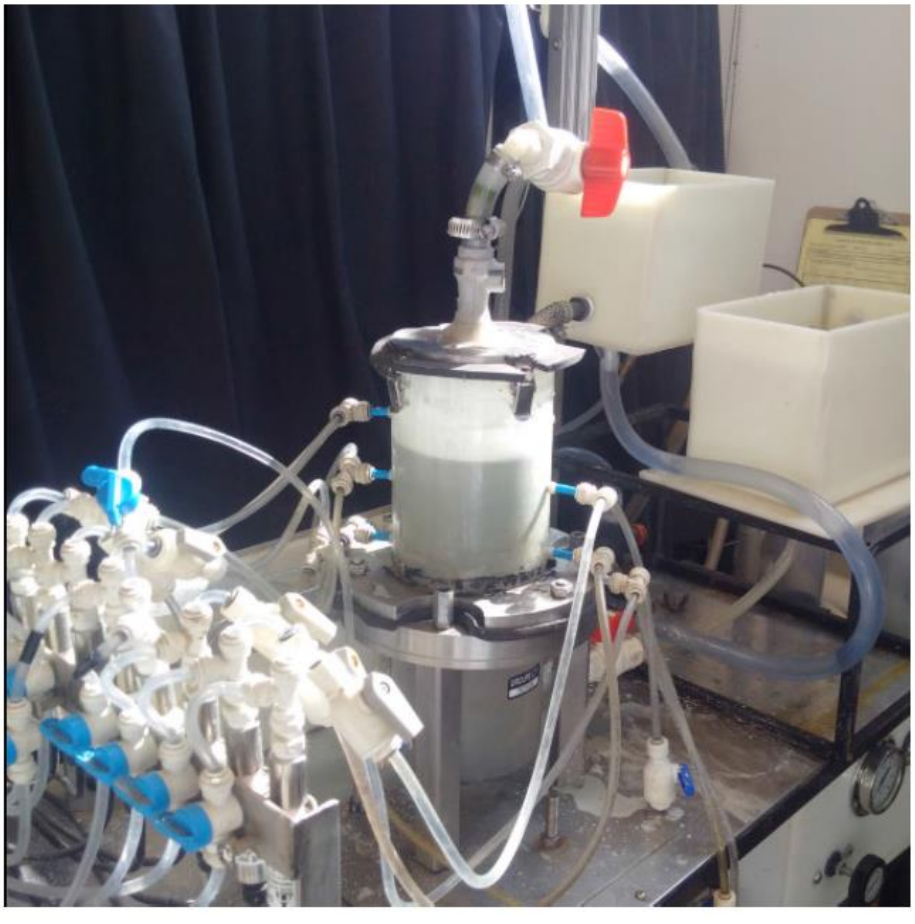

Figure 4: Set-up of the filtration test (Gradient Ratio, ASTM D5101)

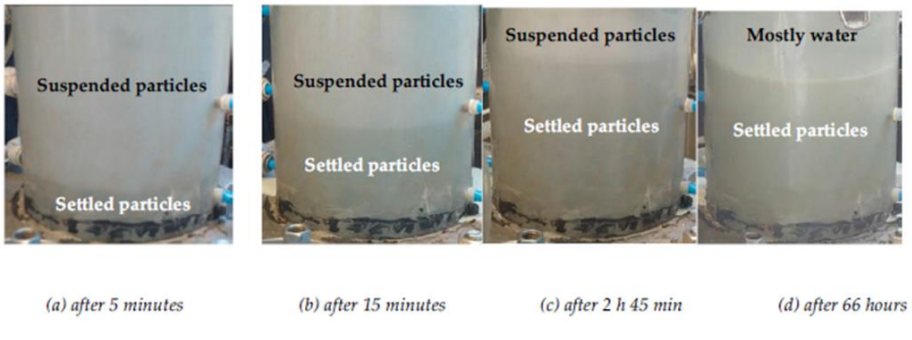

Figure 5: Settlement of the slurry during the first stage of the test

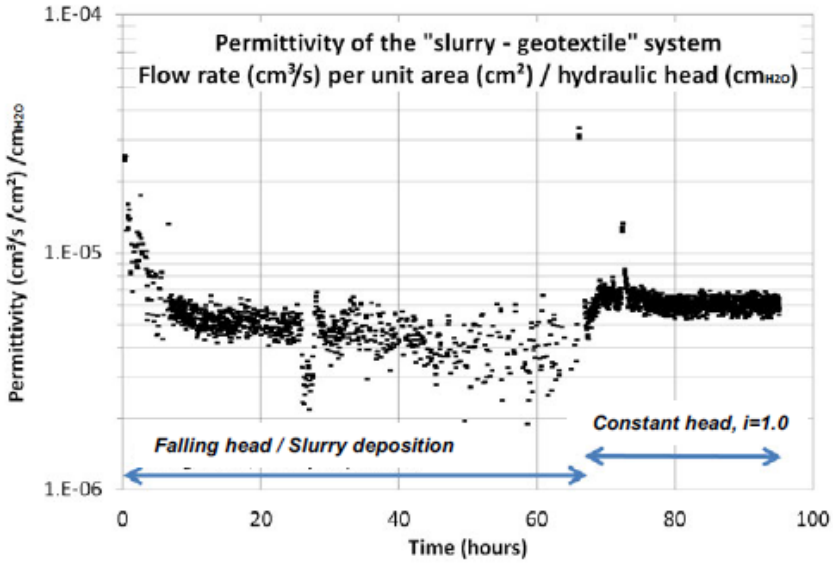

Figure 6: Permitivity versus time

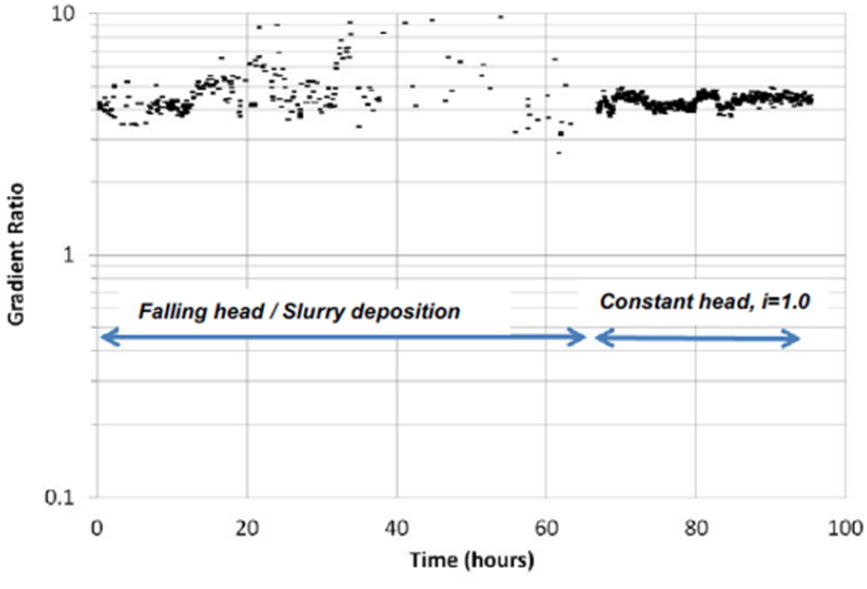

Figure 7: Gradient ratio versus time

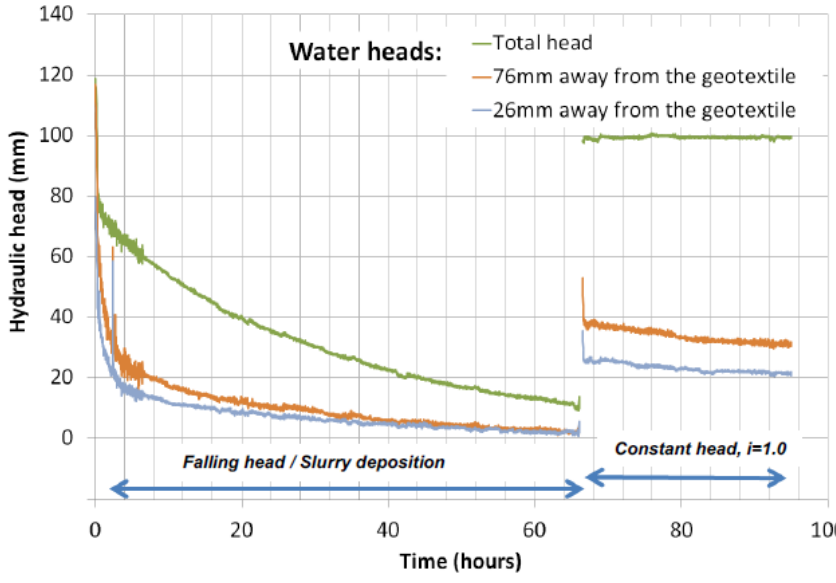

Figure 8: Water head versus time

3.3 *Observations*

The following observations could be made:

- The permittivity of the system, calculated by dividing the flow rate per unit area at a given time by the total hydraulic head, first decreased to reflect the accumulation of soil particles at the surface of the geotextile (Figure 5). It eventually stabilized to remain stable until the end of the first part of the test (sedimentation). After the complete settlement / deposition of the soil particles, the second phase of the test was initiated with the constant head test, and the permittivity remained at the same level as what had been measured before. It was therefore concluded that the permittivity of the system was stable over time, so that no clogging mechanism developed as the water flows through the system. In order to estimate the permeability of the tailing / geotextile system, the permittivity can be multiplied by the height of soil after deposition (measured from the outside of the cell, as shown on Figure 5-d). A value of 6E10-5 cm/s was determined, which was reported to be similar to the permeability of the tailing as documented by the owner. With a permeability of the system similar to the permeability of the native material and no decrease of permeability over time, the system was considered to be stable.

- Gradient ratio values of approximately 3 were observed and remained stable through the duration of the test (Figure 7). Although 3 is at the upper limit of what is generally considered acceptable, it must be analyzed taking into account two factors:
  - First, the soil was not compacted but installed in a slurry form. As a consequence, the arrangement of sedimented particles is likely to be more compact in the vicinity of the filter, where the water has the greatest potential for being evacuated and to generate a soil-like structure rather than sludge.
  - Second, it does not evolve over time, indicating that the permeability of the tailing / geotextile interface does not decrease more rapidly than the permeability of the tailings, measured at a distance from the interface.

- It is concluded from the gradient ratio test that the geotextile filter is not blocked/clogged because the gradient ratio values remained stable through the duration of the test.

- The analysis of the evolution of the water heads (Figure 8) shows that more than half of the head loss occurs between the top of the soil and the piezometer located at a distance of 76mm from the geotextile, i.e. on the very top of the sedimented slurry. This observation can be explained by the sedimentation process, which favors segregation of the particles with the coarser particles settling first. As a result, the gradation of the soil progresses, with a decreasing concentration of coarser particles, as the distance to the geotextile increases. This mechanism favors creation of a very fine grained layer on the top of the soil surface, which exhibits a lower permeability, thus a higher head loss on the upper layer, as observed on Figure 8.

4 CONCLUSION

The results of gradient ratio test indicate that the geotextile filter is not blocked/clogged and the gradient ratio values remained stable through the duration of the test.

It was observed that the permittivity of the system is stable over time, so that no clogging mechanism developed as the water flows through the system. Even more, a permeability of the geotextile/tailing system was similar to the permeability of the native material and no decrease of permeability over time was observed and the system is considered to be stable.

Overall, it is concluded that the tested geotextile, with a FOS of 70µm (as measured per CGSB 148.1 n°10) offers a good filtration performance of the tailing with the given particle size distribution, prepared as a 28 % solid / 72 % water slurry, during both sedimentation and filtration under a hydraulic gradient of 1.0.

Based on these observations, and the fact that MLdG components offer both filtration and maintained transmissivity under high normal loads as demonstrated by Saunier et al., Multi-Linear Drainage Geocomposites should be considered as solutions in environments such as tailings dewatering and heap leach applications that involve potentially harsh chemical conditions and fine grained material.

References

Arab, R., Cherifi, F. and Loudjani, F. 2009. Landfill drainage with geocomposites, *Colloque International Sols Non Saturés et Environnement*, Tlemcen, Algeria.

ASTM D 3895. Standard Test Method for Oxidative-Induction Time of Polyolefins by Differential Scanning Calorimetry, American Society for Testing and Materials, West Conshohocken, Pennsylvania, USA.

ASTM D5101, Standard Test Method for Measuring the Filtration Compatibility of Soil-Geotextile Systems, American Society for Testing and Materials, West Conshohocken, Pennsylvania, USA.

Blond, E., Bouthot, M., Vermeersch, O.G. and Mlynarek, J. 2003. Selection of protective cushions for geomembrane puncture protection, *56th Annual Canadian Geotechnical Conference*, Winnipeg, Manitoba, Canada.

Blond, Fourmont, Saunier 2013. Biological clogging resistance of tubular drainage geocomposites in leachate collection layers, *proceedings of Geosynthetics'2013*, Long Beach, California

Saunier, P., Ragen, W. and Blond, E. 2009. Assessment of the Resistance of DTPG to high compressive loads, *Proceedings of 9th International Conference on Geosynthetics*, 2010, Brazil, 3: 1131.

Bickert, G. 2004. Tailings Dewatering Technologies for Australian Coal Processing Plants. *Australian Coal Industry's Research Program*, Brisbane, Australia.

Caldwell, J., Revington, A., McPhail, G., Charlebois, L. 2014. "Optimised seasonal deposition for successful management of treated mature fine tailings." In *Proceedings of 17th International Seminar on Paste and Thickened Tailings - Paste2014*, Vancouver, Canada, 371-381

New Lighter, Longer GCLs for Mining Applications

Michael S. Donovan Ph.D.
CETCO®, Hoffman Estates, IL, USA

Barbara Gebka
CETCO®, Hoffman Estates, IL, USA

Dennis Wind
CETCO®, Hoffman Estates, IL, USA

ABSTRACT: Geosynthetic clay liners (GCLs) have been used for more than a quarter century as a substitute for the compacted clay component of composite liners in various industrial applications. For waste storage, the primary use of GCLs has been as a component in the composite liner system of tailings dams or as liners for heap leach pads. One limitation for traditional GCLs can be simply the length of the product rolls, which can limit the project design of sloped walls to accommodate a particular product roll length. Another limitation is the product mechanical properties. The internal and interfacial shear performance can be limited by choice of geotextiles or the strength of the fiber-bundles developed during the manufacturing process. Research into new blends of clay with tailored polymer systems has shown the hydraulic conductivity can be significantly reduced compared to sodium bentonite GCLs. This innovation has allowed for the reduction in mass per unit area of the active components of the product while delivering improved hydraulic conductivity compared to traditional GCLs. The development of these lighter weight products has allowed for improvements in the geotechnical properties such as interfacial shear performance. This paper describes the performance limits of a new lighter weight polymer modified GCL in terms of chemical compatibility and internal/interfacial shear performance. The new GCL should allow for more flexible engineering of the liner system to improve the economics of cell design.

1 INTRODUCTION

1.1 *Background*

Geosynthetic clay liners (GCLs) are gaining interest for use in industrial waste disposal and ore processing applications. GCLs can be an economical choice as a component of a composite liner system. The use of GCLs can allow for a more environmentally responsible design which will minimize the risk of leakage into the environment. Additionally, GCLs can provide manufactured quality assurance and ease of installation. One disadvantage of traditional geosynthetic clay liners is that typically contain mass per unit areas of around 3.7 – 5.0 kg/m^2, which has been written in to local regulations. The mass per unit area can often increase transportation costs to deliver materials to a jobsite (typically in remote areas). In addition, the mass per unit area can also influence the dimensions of the GCL roll itself, which can limit the waste cell design flexibility (for example the spacing between benches).

Enhanced ore extraction techniques, such as heap leaching, have become popular in recent years due to the steep increases in the prices of precious metals. Heap leaching is an ore processing technique where run-of-mine or crushed and/or agglomerated ores are stacked over an engineered low permeability leaching pad and exposed to a lixiviant solution which is collected after percolation through the ore (Zanbak, 2012). Additionally, the processed ore can be stored in stacks, disposed of in tailings impoundments or the heap can be decommissioned in place. These waste cells can represent a challenge for long-term management due to the chemical composition

of the ore, potential radioactivity and other factors that could impact the physical stability of the pad.

Extraction conditions can generate leachates with high ionic strength and in particular high concentrations of di- and trivalent ions such as aluminum, magnesium and calcium. These extreme conditions represent a compatibility challenge for traditional bentonite based GCLs, since the swelling/gelling capacity of bentonite is reduced in aggressive leachates. New GCL products that offer improved chemical compatibility with mining and coal ash leachates have recently been developed, which are referred to as polymer-modified GCLs (PMG). The polymer-clay technology can be tailored to provide low hydraulic conductivity against a wide range of aggressive leachates, as demonstrated for coal ash and red mud storage applications (Donovan et al., 2016; Benson and Athanassopoulos, 2015).

1.2 *Approach*

The purpose of this study is to evaluate a new lightweight polymer-modified GCL for use in applications with high concentrations of divalent ions, such as calcium. The intent of the study is to determine how the design factors of the PMG influences both the chemical compatibility and geotechnical properties. The PMG design factors studied in this work include the mass per unit area of the polymer/clay blend and the polymer content of the polymer clay blend. The mass per unit area of the active material in the PMG ranged from 2.5 kg/m^2 to 5.0 kg/m^2. The polymer loading (expressed as a weight % in the bentonite) from 2% to 12%. The hydraulic conductivity of the PMG samples were tested against calcium chloride solutions with electrical conductivities ranging from 1200 to 18700 µS/cm. This work demonstrates that the new lighter-weight polymer modified GCLs can deliver low hydraulic conductivity when exposed to moderate strength leachates. In addition, the polymer modified GCLs demonstrate relatively high peak interfacial friction angles. These combined properties should allow geotechnical engineers more design flexibility and lower installation costs for ore processing.

2 METHODOLOGY

2.1 *Leachate Characterization*

The PMG samples were tested for hydraulic conductivity using a variety of calcium chloride solutions of increasing ionic strength. For example, the solution with an ionic strength of 0.01 M $CaCl_2$ was prepared by dissolving 1.11 grams of $CaCl_2$ in 1 liter of deionized water. Information regarding the leachates tested against the standard bentonite GCL, which are available on request, are from a historical database.

2.2 *Electrical Conductivity*

Electrical conductivity (EC) was measured using a Mettler Toledo SevenGo Pro conductivity meter ("METTLER TOLEDO®" and "SEVEN2GO®" are the registered trademarks of Mettler-Toledo, GMBH, Switzerland". The EC was expressed as microSiemens per centimeter (µS/cm). The pH of the leachates were measured using an Oakton Ion 700 pH meter equipped with an Oakton Acorn model 35811-98 probe ("OAKTON®" and "ACORN®" are the registered trademarks of Cole-Parmer Instrument Company LLC, Vernon Hills, Illinois). Chloride content was estimated by QuanTab® Test Strips ("QuanTab®" is a registered trademark of the Hach Company, Loveland, CO). The sulfate/bisulfate content was estimated by ICP.

2.3 *Inductively Coupled Plasma (ICP) and Loss on Ignition (LOI)*

The ICP and LOI testing procedures used are described elsewhere (Donovan 2016).

2.4 *Ionic Strength Calculation*

The ionic strength, I, of a solution is a function of the concentration of all ions present in that solution, where c_i is the molar concentration of ion i (mol·dm^{-3}), z_i is the charge number of that ion, and the sum is taken over all ions in the solution. Relative abundance of monovalent and multivalent cations was characterized by the ratio of monovalent to divalent ions RMD of each test solution. The RMD is defined as the ratio of the total molarity of monovalent cations to the

square root of the total molarity of multivalent cations at a given ionic strength. ICP data were used to compute the RMD of the leachate.

2.5 *Polymer Modified Geosynthetic Clay Liner Construction and Testing*
Prototype needle punched PMGs were produced with nonwoven cap and base geotextiles. The cap and base geotextiles were both 200 grams per square meter nonwovens. The clays used were granular western sodium bentonite type clays with a maximum 10% retained on 18 mesh (850 microns) and maximum 15% passing 200 mesh (75 microns). The polymer type is proprietary. The polymer content in the bentonite mixture ranged from 2% to 12%. The PMG samples were produced at total active mass per unit area of either 2.5 or 5.0 kg/m^2.

2.6 *Hydraulic Conductivity Testing*
Hydraulic conductivity tests on GCL specimens in calcium chloride solutions were conducted in a flexible wall permeameter using the falling headwater / rising tail water method described in ASTM D6766. The GCLs were hydrated with permeant liquid in the permeameter for 48 hr at an effective confining stress of 35 kPa. During the tests, the hydraulic gradient was set at approximately 150. Influent for the specimen was injected using a bladder accumulator.

2.7 Direct Shear Tests
Shear testing was done according to ASTM method D6243. Tests were performed using PMG samples with dimensions of 30 cm x 30 cm against a textured HDPE membrane with spike texturing (information on the membrane available on request). Samples were prehydrated and consolidated with two different methods. In the first method, the sample was hydrated in tap water directly in the shear box under a 1 psi surcharge load for a minimum of 24 hours. In a second method, the samples were hydrated in a similar fashion in a plastic tub using metal weights to apply the surcharge. In both cases, the samples were consolidated at a rate of at 2.5 pounds per square inch per hour. Normal pressures of 4500, 8500 and 12,500 pounds per square foot were applied to the samples. The weights were removed, and the sample was transferred to the shear box for consolidation and testing. A shear rate of 0.04 inches per min was used to measure the peak interfacial friction angle, the cohesion intercept and post-peak strength.

2.8 *Internal Peel Strength Test*

Internal peel strength values for the PMGs were measured according to ASTM method D6243.

3 RESULTS AND DISCUSSION

3.1 Hydraulic Conductivity Results
Shown in Table 1 is the leachate chemistry information. The leachates had a pH range of 6.5-6.9 for the calcium chloride leachates to as high as 11 for the coal ash leachate. The electrical conductivities range from 1200 µS/cm to as high as 46800 µS/cm. Ionic strength ranged from 0.02 to 1.05 mol/L. For the coal ash and mining leachates the RMD ranges from 0.05 to 4.76 M$^{1/2}$, where lower RMD values denote higher relative divalent ion concentrations.

Shown in Tables 2 and 3 are the hydraulic conductivity results for the samples produced at 2.5 and 5.0 kg/m^2 active material, respectively. For estimating the hydraulic conductivity of polymer modified GCLs, it is recommended to test the samples to much greater than 2 pore volumes of flow (PVF), since the polymer added to the bentonite can add extra exchangeable ions. Prior studies from our laboratory has shown that a minimum of 15 PVF be used to test the PMGs to ensure chemical equilibrium between the leachate and the permeate (Donovan, 2016).

Prior studies on bentonite GCLs have shown that there are several leachate-chemistry factors that can influence the hydraulic conductivity. As the ionic strength of the leachate increases, the hydraulic conductivity can concomitantly increase. Also, leachates with higher divalent cation concentrations (such as calcium) can have a greater effect than corresponding monovalent cation leachates of the same ionic strength. The influence of the electrical conductivity on the hydraulic conductivity of sodium bentonite based GCLs is shown below in Figure 1 and 2. As the electrical conductivity of the leachates reaches approximately 1000 µS/cm the hydraulic conductivity is observed to increase above 1x10^{-8} cm/sec. Figure 1 shows the response of the PMG samples

produced at 2.5 kg/m^2. Samples produced with 2 wt% polymer show hydraulic conductivities below 1x10^{-9} cm/sec against leachates with an electrical conductivity of 1200 µS/cm. Increasing the polymer loading to 4 wt% in the blend allows for hydraulic conductivities of < 2x10^{-9} cm/sec for electrical conductivities as high as 3000 µS/cm. Higher polymer loadings of 8% and higher do not appear to provide improved performance with the higher ionic strength leachates (>12000 µS/cm). Further development on improved polymer systems is needed for better hydraulic performance against high ionic strength leachates at an MPU of 2.5 kg/m^2.

Table 1. Leachate chemistry testing results.

Permeant Type	Permeant pH	Permeant EC (µS/cm)	Permeant Ionic Strength by ICP (M)	Permeant RMD by ICP (M^0.5)
0.005 M $CaCl_2$	6.5	1200		-
0.01 M $CaCl_2$	6.5	2330		-
0.03 M $CaCl_2$	6.3	6150	0.09	-
0.07M $CaCl_2$	6.7	12920	0.21	-
0.1 M $CaCl_2$	6.9	18700	0.30	-
Coal Ash Leachate #1	8.5	2884	0.02	0.18
Coal Ash Leachate #2	10.9	2492	0.06	0.05
Coal Ash Leachate #3	11.0	46800	1.05	4.76
Mining Leachate #1	6.8	15800	0.21	0.704

Table 2. Hydraulic conductivity testing results for PMG samples with a 2.5 kg/m^2 MPU.

Additive	Target Loading (kg/m^2)	% Polymer	Permeant Type	Hydraulic Conductivity (cm/sec)	Running Time (hrs)	Pore Volume Flow (PVF)
PMG-2.5-2	2.5	2	0.005 M $CaCl_2$	8.6E-10	2049	16
PMG-2.5-2	2.5	2	Coal Ash Leachate #1	6.5E-10	310	3.1
PMG-2.5-2	2.5	2	Coal Ash Leachate #2	4.7E-10	310	1.1
PMG-2.5-2	2.5	2	Mining Leachate #1	7.0E-08	17	7
PMG-2.5-4	2.5	4	0.01 M $CaCl_2$	8.0E-10	2031	16
PMG-2.5-4	2.5	4	Coal Ash Leachate #2	8.6E-10	1673	4
PMG-2.5-4	2.5	4	Coal Ash Leachate #2	1.5E-09	264	9
PMG-2.5-4	2.5	4	Coal Ash Leachate #1	1.2E-09	1294	11
PMG-2.5-4	2.5	4	0.03 M $CaCl_2$	2.8E-08	49	13
PMG-2.5-4	2.5	4	0.03 M $CaCl_2$	3.7E-07	16	39
PMG-2.5-4	2.5	4	Mining Leachate #1	7.0E-08	5	29
PMG-2.5-8	2.5	8	0.03 M $CaCl_2$	7.4E-10	2030	30
PMG-2.5-8	2.5	8	Coal Ash Leachate #3	1.5E-07	10	12
PMG-2.5-8	2.5	8	Coal Ash Leachate #3	4.9E-06	1	14
PMG-2.5-12	2.5	12	0.07M $CaCl_2$	2.8E-07	15	19

Table 3. Hydraulic conductivity testing results for PMG samples with a 5.0 kg/m^2 MPU.

PMG	Target Loading (kg/m^2)	% Polymer	Permeant Type	Hydraulic Conductivity (cm/sec)	Running Time (hrs)	PVF
PMG-5.0-2	5.0	2	0.01 M $CaCl_2$	3.6E-10	3902	6
PMG-5.0-4	5.0	4	0.03 M $CaCl_2$	5.6E-10	4112	6
PMG-5.0-4	5.0	4	0.03 M $CaCl_2$	2.4E-09	2013	18
PMG-5.0-4	5.0	4	Mining Leachate #1	3.6E-10	2315	3
PMG-5.0-4	5.0	4	Coal Ash Leachate #3	5.9E-10	3980	9
PMG-5.0-4	5.0	4	Coal Ash Leachate #3	7.0E-10	3605	6
PMG-5.0-4	5.0	4	Coal Ash Leachate #3	9.5E-10	1839	6
PMG-5.0-4	5.0	4	Coal Ash Leachate #3	2.0E-09	2321	14
PMG-5.0-4	5.0	4	Coal Ash Leachate #3	1.8E-09	1939	26
PMG-5.0-8	5.0	8	0.07M $CaCl_2$	3.1E-10	4111	5
PMG-5.0-8	5.0	8	0.07M $CaCl_2$	7.7E-10	3970	9
PMG-5.0-8	5.0	8	0.1 M $CaCl_2$	1.7E-10	1505	47
PMG-5.0-12	5.0	12	0.1 M $CaCl_2$	5.9E-10	4020	4

The chemical resistance of PMGs can be improved by increasing the mass per unit area. Figure 2 shows the hydraulic conductivity performance of PMG samples produced with 5.0 kg/m^2 MPU. For the 2 wt% polymer sample, the hydraulic conductivity was measured to be 3.6x10^{-10} cm/sec with a 0.01M $CaCl_2$ solution. Increasing the polymer loading further to 4 wt% can deliver hydraulic conductivities of 2x10^{-9} cm/sec (or lower) against leachates with electrical conductivities as high as 46,800 µS/cm. In this range of leachate chemistries, increasing the polymer content to as high as 12 wt% does not appreciably decrease the hydraulic conductivity.

3.2 Interfacial Shear Testing Results

When using GCLs in composite lining systems for mine waste storage facilities, an important design aspect is slope stability. For situations such as canyon fills, there can be a high normal stress placed on the composite liner system by the waste deposited above it. The system must be engineered to deliver a robust interfacial friction angle between the geomembrane and the overlying GCL. The use of polymers to enhance the hydraulic performance of a GCL may impact the peak interfacial friction angle due to a lubrication effect of the polymer.

Shown in Table 4 are the results from the direct shear tests of the PMG samples placed over a spike-textured geomembrane. The testing was done at nominal normal stress values ranging from 216 to 599 kPa. Four PMG samples were tested with polymer contents of either 4 or 8 wt% and MPU values of either 2.5 or 5.0 kg/m^2. Internal peel strength values measured for the GCLs ranged from 21.2-26.6 N/cm. The peak interfacial friction angle was calculated from relationship between the nominal peak shear stress and the nominal normal stress (See Figure 3) (Bareither, 2018). The cohesion intercept value was estimated in a similar manner from calculating intercept of the nominal peak shear stress and the nominal normal stress. One aspect of testing that must be considered is sample preparation. Some laboratories will hydrate/consolidate the specimen outside of the shear box to allow for faster sample testing. We evaluated the difference in peak interfacial friction angle results using both "in-box" and "out of box" method. The results shown in Figure 4 demonstrate that "in-box" hydration and consolidation results in much higher peak interfacial friction angles. We suspect that hydration

of the samples "out of the box" can result in polymer escape or a reduction in internal peel strength after the removal of the weights placed on the specimen.

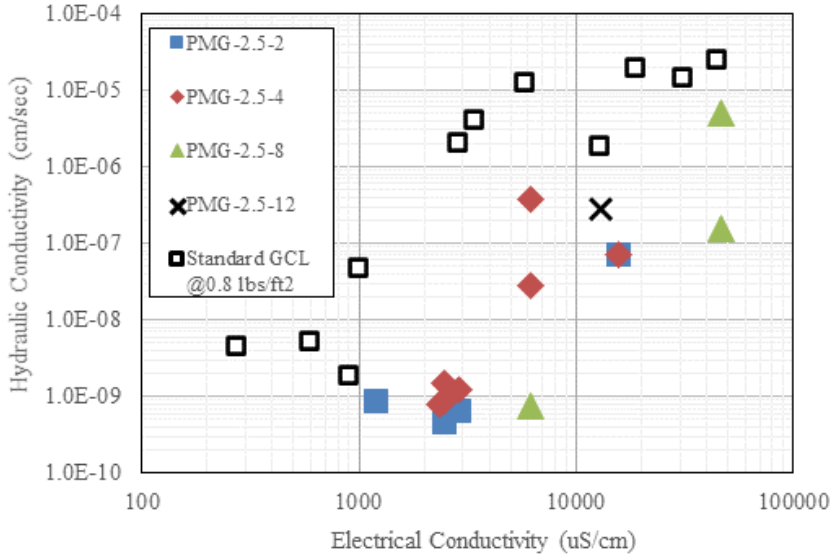

Figure 1. Hydraulic conductivity test results for PMG samples with 2.5 kg/m^2 MPU.

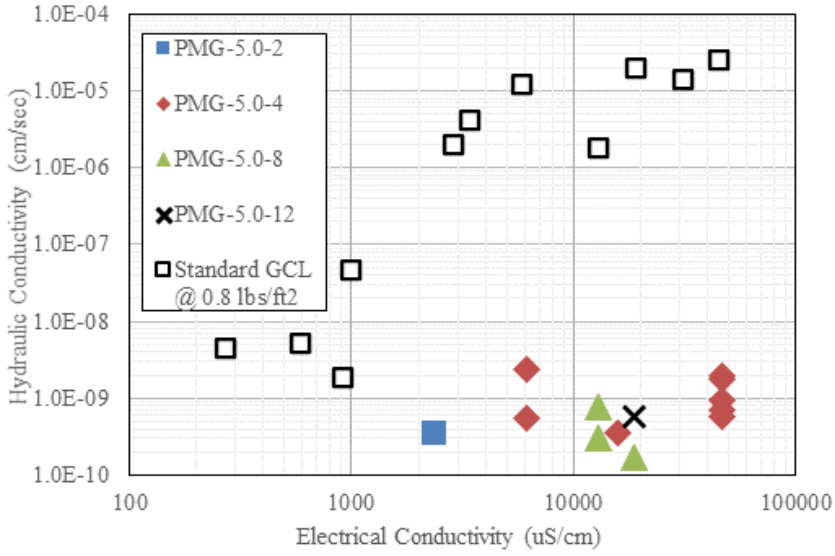

Figure 2. Hydraulic conductivity test results for PMG samples with 5.0 kg/m^2 MPU.

Table 4. Interfacial friction angle testing results for PMG samples with 4 and 8wt% polymer content.

PMG	Normal Stress	Peak Shear Stress	Post-Peak Shear stress (In Box Hydration)	Peak Friction Angle (In Box Hydration)	Cohesion Intercept (In Box Hydration)	Avg Peel Strength
	(kPa)	(kPa)	(kPa)	(Degrees)	(kPa)	N/cm
PMG-2.5-4	215.5	85.6	68.0			
PMG-2.5-4	407.0	154.9	46.3	22.5	-6.9	26.6
PMG-2.5-4	598.5	244.1	151.8			
PMG-5.0-4	215.5	83.0	50.7			
PMG-5.0-4	407.0	185.6	110.1	20.8	11.3	21.4
PMG-5.0-4	598.5	228.4	86.0			
PMG-2.5-8	215.5	86.6	52.4			
PMG-2.5-8	407.0	146.9	90.9	18.0	16.0	21.9
PMG-2.5-8	598.5	211.0	111.5			
PMG-5.0-8	215.5	90.7	58.7			
PMG-5.0-8	407.0	149.3	84.9	15.9	30.5	21.2
PMG-5.0-8	598.5	200.0	108.4			

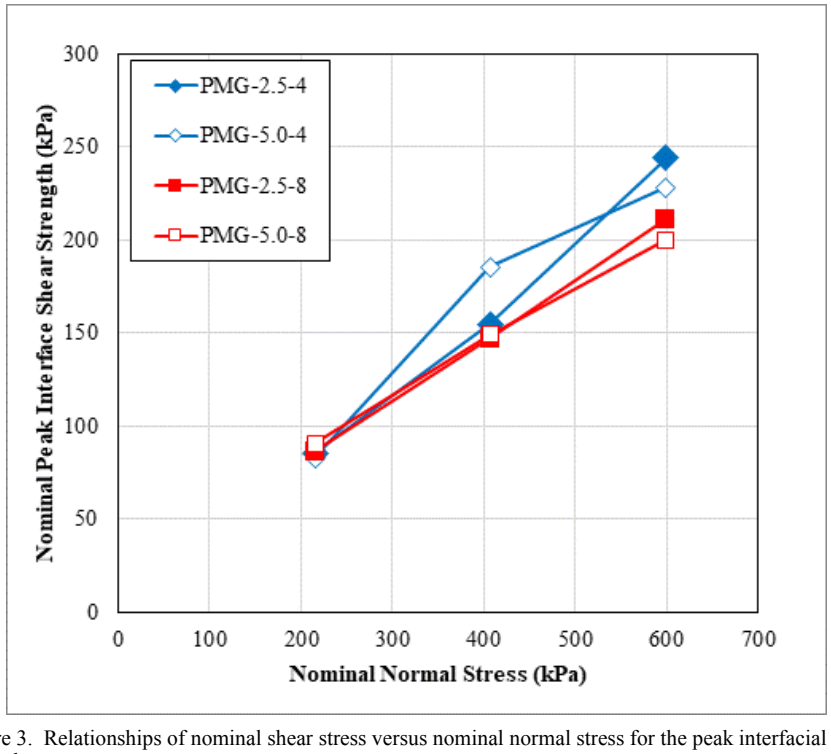

Figure 3. Relationships of nominal shear stress versus nominal normal stress for the peak interfacial shear strength.

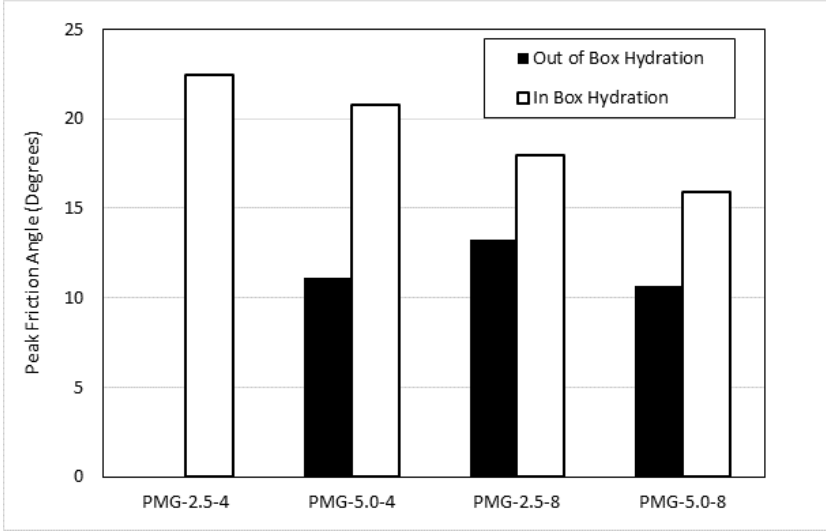

Figure 4. Comparison of "in-box" vs "out of box" hydration/consolidation.

4 CONCLUSION

New lightweight polymer modified GCLS were developed to deliver low hydraulic conductivity against moderate ionic strength coal ash and mining leachates. For aggressive leachates, the mass per unit area can be increased to deliver low hydraulic conductivity against higher ionic strength leachates. The GCLs samples had high peak interfacial friction angles ranging from 16 to 22 degrees, which is similar to traditional high strength bentonite based GCLs. For PMGs, it is important that direct shear experiments be done according to the ASTM guidelines with in-box hydration and consolidation. These new lightweight GCLs rolls can be made longer than traditional bentonite GCLs at 5.0 kg/m^2 which will allow for faster installation and economical waste storage designs.

5 REFERENCES

Benson, C.; Athanassopoulos, C. 2015. Hydraulic Conductivity of a Polymer-Modified GCL Permeated with High-pH Solutions. *Geosynthetics 2015*, Portland, USA.

Bareither, C. A. Soleimanian, M. and Ghazizadeh, S. 2018. Direct shear testing of GCLs at elevated temperature and in a non-standard solution. *Geosynthetics International*. 25(3): 350-368.

Donovan, M., Valorio, R., Gebka, B. 2016. Chemical Compatibility of Polymer Modified GCLs in Coal Combustion Residual Leachates. *GeoAmericas 2016*, Miami, USA.

Donovan M. S., Valorio R. S. and Gebka B. 2016. Polymer enhanced geosynthetic clay liners for extreme leachate chemistries. *Proceedings of EuroGeo6*, Ljubljana, Slovenia.

Zanbak, C. 2012. Heap Leaching Technique in Mining. *Euromines*, Turkey.

ASTM D6243 / D6243M-20, Standard Test Method for Determining the Internal and Interface Shear Strength of Geosynthetic Clay Liner by the Direct Shear Method, *ASTM International*, West Conshohocken, PA, 2020, www.astm.org

ASTM D6496 / D6496M-20, Standard Test Method for Determining Average Bonding Peel Strength Between Top and Bottom Layers of Needle-Punched Geosynthetic Clay Liners, *ASTM International*, West Conshohocken, PA, 2020, www.astm.org

ASTM D6766-20a, Standard Test Method for Evaluation of Hydraulic Properties of Geosynthetic Clay Liners Permeated with Potentially Incompatible Aqueous Solutions, *ASTM International*, West Conshohocken, PA, 2020, www.astm.org

Variability in Sand Characteristics – A Case Study at LKAB Mine Tailings Facility in Sweden

Karin Engström
LKAB, Kiruna, Sweden
Sara Töyrä
LKAB, Kiruna, Sweden
Sophie Danilov
LKAB, Kiruna, Sweden
Roger Knutsson
Tailings Consultants Scandinavia, Helsingborg, Sweden

ABSTRACT: In recent years, tailings instability has led to a series of catastrophic tailings dam failures around the world. In order to avoid these kind of events, assessment of tailings properties and stability of mine tailings dams and tailings facilities are essential. In-situ analysis as well as sampling and various laboratory analyses are commonly used for this purpose. There have been numerous publications related to procedures and methods used for evaluation of liquefaction potential in mine tailings. However, the problems related to sampling protocols, sampling frequency and variability within tailings facilities are scarcely identified or discussed in current research. This paper presents results from a recent study, aiming to understand and quantify the variability of important stability characteristics of mine tailings within a tailings facility of LKAB in Sweden. A comprehensive characterization of the tailings beach was made, where grain size distributions, void ratio and water content were determined. Results indicate high variabilities within very limited distances in the tailings facility. Repeated sampling campaigns in various parts of the facility all show similar results. The variabilities cause uncertainties both in developing reliable sampling protocols for tailings beach control and generalizing representative values for assessing strength and stability of the complete volume of mine tailings. The methods used in the case study describe promising tools for beach control at LKAB tailings facilities. The results from this study has also led to several improvements, both in spigot management and continuous quality control methods at the tailings facilities within LKAB.

1 INTRODUCTION

In recent years, tailings instability has led to a series of catastrophic tailings dam failures around the world. In order to avoid these kind of events, assessment of tailings properties is essential. In-situ analysis as well as sampling and various laboratory analyses are commonly used for this purpose. The results from such investigations are used for estimating tailings strength and corresponding stability of tailings facilities. Example of procedures and test methods associated to tailings instability and liquefaction are given by Robertson (2010), Reid (2019) and Dillon & Wardlaw (2010).

Representative sampling and measurement systems are essential in process industries. Measurements are used to evaluate raw material, control processes, assess final products, define environmental impact of waste material and for many other purposes. All sampling processes generate measurement uncertainty, but also sampling errors that only can be eliminated or minimized through understanding of how and why they originate. No matter if the measurement includes

physical sample extraction, or some form of in-situ measurement such as CPT or similar, sampling is being conducted in the sense that only a small part of the material is addressed. I.e. only a very limited portion of the total lot is being used in laboratory testing or analysed by the in-situ measurement device. The sampling errors arise from the fact that not all material in the lot is analysed and can therefore not be fully eliminated. However, by applying adequate and correct sampling protocols, the sampling errors can be controlled. (Esbensen & Paasch-Mortensen 2010, Gy 1998, Pitard 1993).

Scientific research and publications related to sampling problems in mineral processing is common and the Theory of Sampling (TOS), first developed related to the mineral industry, covers all aspects of sampling particulate material (Pitard 1993). For example, TOS provides a complete set of theoretical definitions of material heterogeneity and sampling variability and provides empirical methods for evaluation of sampling variability (Gy 1998, Minnitt and Esbensen 2017). However, the problems related to sampling protocols, sampling frequency and variability within mine tailings facilities are scarcely identified or discussed in current research, and there seem to be few examples where TOS is applied to the sampling in tailings facilities. Also, there are no established or published sampling protocols specifically for tailings facilities (Demers et al. 2017). Sampling procedures, number of samples etc. for tailings facilities are not specified, and development of correct sampling protocols are difficult if sand heterogeneity of the tailings is not known. Previous studies describe how sand in mine tailings facilities may be highly heterogeneous and have extreme variabilities in sand characteristics (Robertson et al 2000, Demers et al. 2017), which complicates the development of representative sampling procedures.

Experience show that current practices related to stability evaluations of mine tailings facilities (using drilling or physical sampling) rarely take the tailings heterogeneity into account when developing sampling protocols. Results from a sampling campaign in the LKAB tailings facility in Kiruna, planned and performed by an external consultant, indicated that the tailings in one area of the facility were not suitable for the planned upstream raise. These results initiated a review of the sampling protocol used in the campaign and it was concluded that the number of samples were very limited, and that the sampling protocol was considered likely to be non-representative as it resulted in uncontrolled sampling errors. One reason for this was that the level of material heterogeneity across the tailings facility was not known and therefore, the sampling protocol could not be adapted to the variability in the deposited tailings.

To enable development of a representative tailings beach sampling protocol, the knowledge about the tailings properties, distribution and heterogeneity was needed. This understanding was the first incentive for the current case study, where variabilities in the top layer the Kiruna mine tailings facility were evaluated. LKAB is currently developing a continuous tailings beach control program, to be used parallel to Cone Penetration Testing (CPT), in order to identify potentially unfavourable conditions at a stage where remedial measures are still possible to conduct. If loose conditions (i.e. larger void ratio than critical void ratio) are found at an early stage, densification via surface compaction is possible.

2 LUOSSAVAARA KIIRUNAVAARA AB

Luossavaara Kiirunavaara AB (LKAB) is a stateowned iron ore mining company and pellets producer with underground mines in Kiruna and Malmberget and open pit mines in Svappavaara. LKAB produces iron ore pellets in three steps; sorting, concentrating and pelletizing, at all three mine sites. The pellets are transported by railway to the harbors in Narvik (Norway) or Luleå (Sweden) and then shipped to customers around the world. Due local conditions, the tailings are managed differently at the three mine sites. The current case study focuses on the tailings facility at the Kiruna mine site.

Kiruna is located in the northernmost part of Sweden, 145 km north of the Arctic Circle. The climate is subarctic with short summers and long winters. The average annual temperature is -1°C (30.2 °F) and Kiruna has approximately 200 days/year of snow cover.

2.1 *LKAB tailings and water management facility*

Tailings management in Sweden has been, and in some cases still is, going through a transition. Moving from an older approach with impermeable dams with excess water circulating the system, to more optimized tailings depositions schemes with less water in the facility (Töyrä et al. 2017). This is the case for the mine tailings facility in Kiruna, Figure 1, that consists of one tailings pond with an adjacent clarification pond for clarification and water storage. The facility was first built in 1977, with impermeable dams that created an artificial lake and tailings were deposited by gravity flow in trenches. In 2012, the original tailings facility in Kiruna was full and upstream raises, with permeable dam constructions, were completed to increase the capacity of the facility. In 2014, the method of deposition was also changed from chutes to spigots to accommodate for the upstream dam raises. The dam between O and O2, hereon called dam O-O2 and the dam between C and C2, called dam C-C2, was raised upstream while the other dams are raised either downstream or centerline. Dam raises are performed regularly in order to increase the capacity of the facility, while the methods varies due to local conditions as well as national traditions and regulations (Töyrä et al. 2019).

The water in the tailings facility comes from precipitation directly on the surface of the tailings facility and from groundwater pumped from the underground mine. The latter is transported via the processing plants and added to the facility together with the slurry. Most of the seepage water from the facility is collected and lead back into the tailings facility. The major part of the water is recirculated back to the processing plants from the clarification pond, while excess water is discharged to the recipient.

2.2 *Tailings deposition at LKAB Kiruna*

In 2011 the natural trenches for tailings deposition were replaced with concrete chutes, both utilizing gravity flow. Up until 2014 the slurry had a solids content of 4 % by weight. However, since the change of depositing method in 2014, parts of the slurry is dewatered to 20-30 % by weight, pumped to the northern dams and deposited between point O and C2 by spigots. Excess water from the processing plants are still deposited in the tailings facility by the concrete chutes, Figure 1.

The surface of the tailings facility is measured by UVA scanning once or twice a year. The deposition scheme is then planned from the result of scanning, upcoming dam raises and seasonal changes. I.e. short pumping lines are used during winters, while areas far away from the plants are used during summers in order to avoid freezing in long slurry pipes during the cold winters.

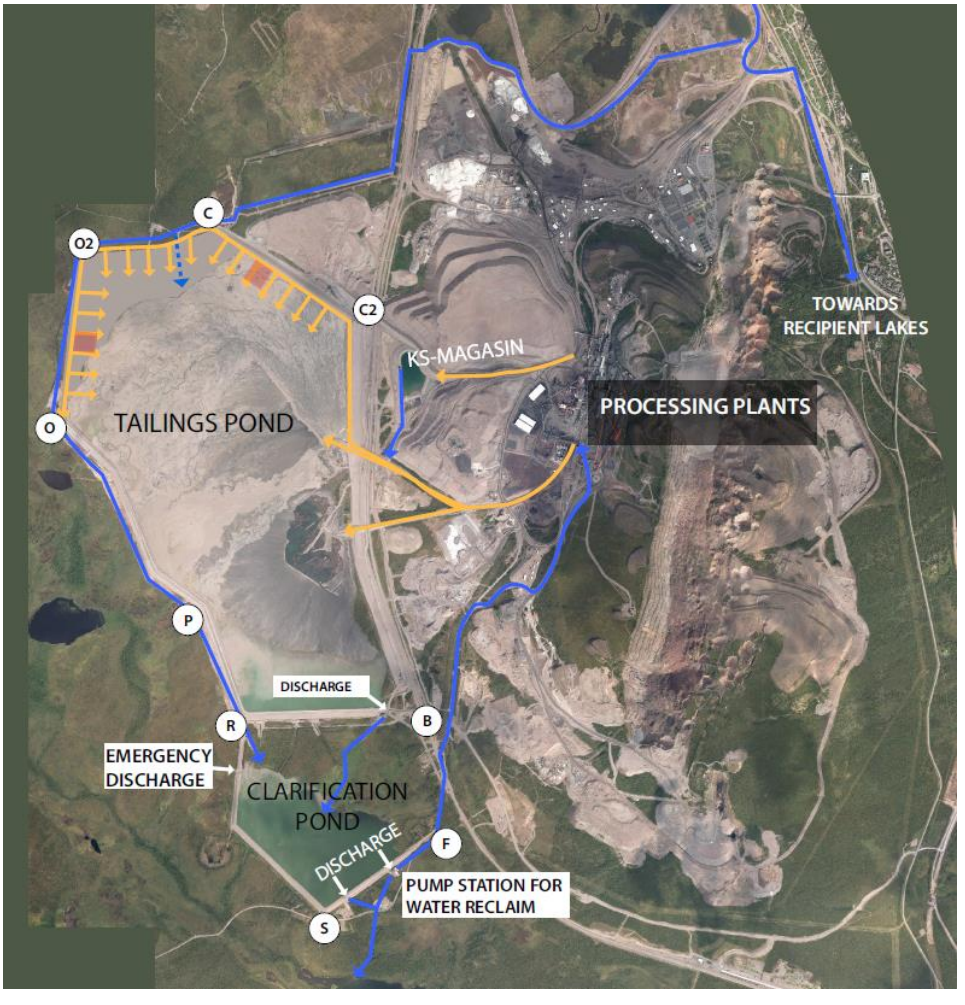

Figure 1. The tailings and water management facility at the Kiruna mine site. Yellow arrows show tailings flow and blue arrows show pumped water ways or seepage collection trenches. Red sections in the tailings facility indicate areas for the sampling campaigns in the current case study.

3 CASE STUDY

The current case study was performed on the beach of the LKAB mine tailings facility in Kiruna during 2018 and 2019. In 2018, the variability in grain size distribution was evaluated along the C-C2 dam and in 2019, the variability in grain size distribution and void ratio was evaluated along both C-C2 and O-O2 dams.

3.1 *Study objectives*

The main objective of the study was to enable development of a representative sampling protocol through a better understanding of the heterogeneity of the material to be sampled. A second objective of the sampling campaign in 2019 was to evaluate if either Balloon density equipment or Nuclear density gauge could be applicable for regular quality control of the void ratio on the beach of the tailings facility.

3.2 Material and methods

The two sampling campaigns in 2018 and 2019 used the same sample grid setup, Figure 2. The sampling campaign in 2018 was performed at dam C-C2 and in 2019, sampling grids were developed for both C-C2 and O-O2, Figure 1. Samples were located 2.5m apart along four sampling lines, two parallel to the dam crest (1P & 2P) and two perpendicular to the dam crest (1T & 2T). In the campaign in 2018, a third parallel line (3P) was positioned approximately 100m from the dam crest and all lines were 100m instead of 80m.

One of the perpendicular sampling lines was placed by a spigot (1T) and the other in between two spigots (2T). The purpose for the two perpendicular sampling lines was to evaluate if the size segregation and/or the variability is different by the spigots and in between spigots. The purpose of the two parallel sampling lines was to evaluate if the variability is different close to the dam crest and further out on the tailings beach.

The sampling campaign in 2018 was performed at dam C-C2 in late October, during early winter, and there was ground frost on the beach in Kiruna tailings pond. To enable extraction of samples, a concrete drill was used. The methods used in both campaigns include wet sieving for determination of % <63µm ("fines content" in Sweden) and Accupyc for determination of particle density. Balloon density equipment and Nuclear density gauge was also used in the 2019 sampling campaign in order to determine the void ratio in the beach.

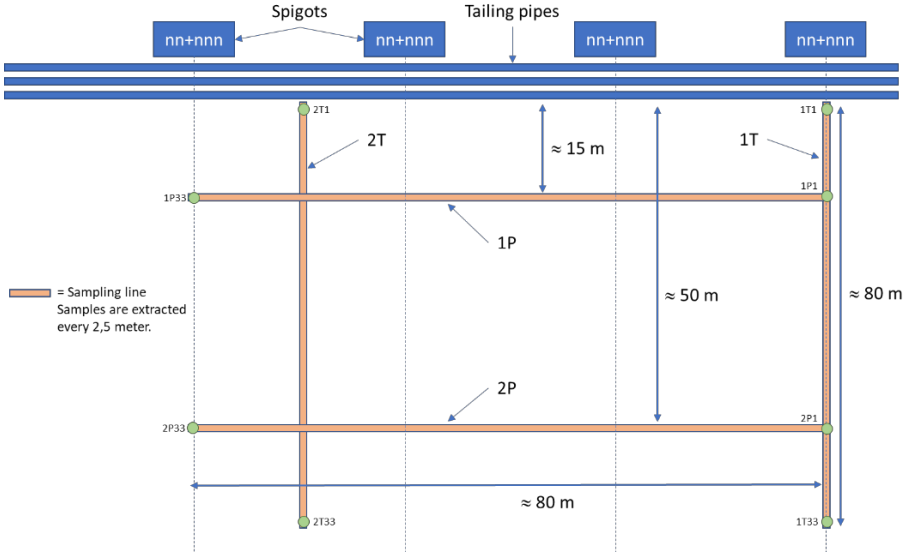

Figure 2. The sampling grid for all sampling campaigns were designed with two sampling lines parallel to the dam (1P & 2P) and two lines perpendicular to the dam (1T & 2T).

3.2.1 *Sampling campaign in 2019*

The sampling campaign in 2019 was performed at both dam C-C2 and O-O2, Figure 1. Due to wet and muddy conditions along the O-O2 dam, the sampling grid had to be modified as the sampling staff was not able to walk 50m out on the beach. The 2P sample line was deleted and the perpendicular sample lines (1T & 2T) had to be shortened. As a complement, a third vertical line (3T) was added at a spigot, Figure 3.

All sampling points were analysed with the Balloon density apparatus and all extracted samples were also analyzed for size distribution and particle density, Figure 4. The majority of the sample points was also analysed with a Nuclear density gauge. Both methods were used in accordance to applicable standard (SS 027110). One practical difference with the two methods was that the Nuclear density gauge is applied to the undisturbed tailings surface, whereas the Balloon density apparatus requires the top ten centimetres of the deposited tailings to be removed in order to reach a smooth surface, Figure 5.

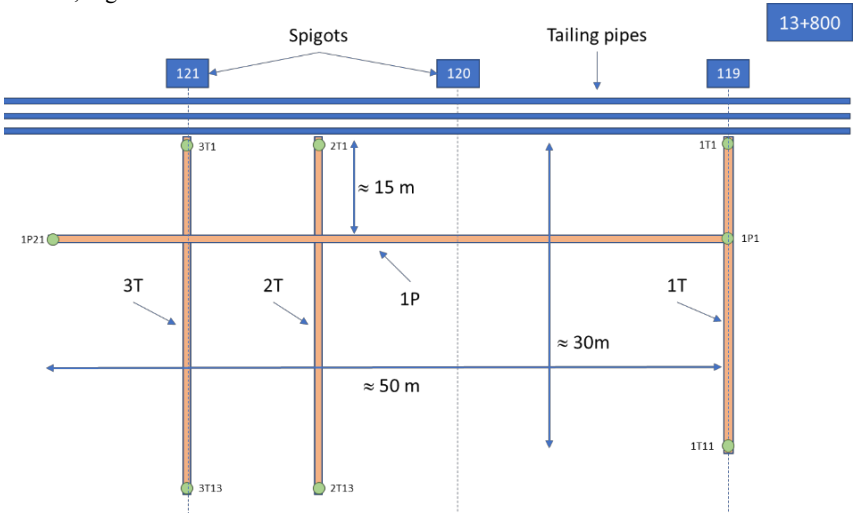

Figure 3. Modified sampling grid at dam O-O2 in 2019 due to wet and muddy conditions.

Figure 4. Sampling campaign in 2019, using the Balloon density apparatus.

Figure 5. Sampling campaign in 2019, using the Balloon density. The top layer, approximately 10cm of tailings, is removed before applying the apparatus.

3.3 *Results*

With the vast amount of data produced by the two sampling campaigns and three sampling grid locations, all results will not be presented here. Therefore, only a selection of the results is presented in the following sections.

Table 1. Observed variabilities for mass fraction <63µm for all analyzed sampling lines in 2018 and 2019.

% <63 µm	2018: C-C2/1T	2018: C-C2/2T	2019: O-O2/1T	2019: O-O2/2T	2019: O-O2/3T	2019: C-C2/1T	2019: C-C2/2T
Length of line	100m	100m	30m	30m	30m	80m	80m
Number of samples	20	20	11	12	12	30	32
Description	By a pigot	Inbetween spigots	By a pigot	Inbetween spigots	By a pigot	By a pigot	Inbetween spigots
Average	37.6	65.0	32.5	48.6	37.5	17.3	29.4
Std. Deviation	24.8	11.1	18.7	24.4	18.7	7.9	16.8
COV	65.9%	17.1%	57.7%	50.3%	49.9%	45.7%	57.3%

% <63 µm	2018: C-C2/1P	2018: C-C2/2P	2018: C-C2/3P	2019: O-O2/1P	2019: C-C2/1P	2019: C-C2/2P
Length of line	100m	100m	100m	50m	50m	50m
Number of samples	20	41	19	21	21	21
Description	20m from dam	60m from dam	100m from dam	15m from dam	15m from dam	50m from dam
Average	34.3	63.8	80.0	28.2	19.4	29.0
Std. Deviation	18.1	17.3	12.6	15.0	11.0	21.2
COV	52.9%	27.2%	15.7%	53.1%	56.7%	73.2%

3.3.1 *Grain size*

For simplicity, the tailings grain size presented only includes the fines content (i.e. the mass fraction <63µm). It is evident that in 2018 the variability in the perpendicular sampling lines is much higher for the line starting by a spigot (1T & 3T) than for the line in the middle of two spigots (2T), Table 1. This is likely due to that the spigots are creating the intended segregation close to the deposition point, while less segregation is created further away from the spigots. This means that the coarser particles settle close to the dam crest, while finer particles settle further away from the dam crest. See Figure 2 and 3 for sample grid setup and relation between dam crest, sample lines and spigots.

For the sample line in-between two spigots (2T), samples show that fine particles settle closer to the dam crest, Figure 6. There is a clear difference between the perpendicular sampling lines in the 2018 years campaign, where 1T (located at a spigot) show a clear trend with increasing amount of <63µm further away from the dam crest. For 2T (in-between spigots), the level of the mass fraction <63µm basically constant, even though the sample to sample variability can be very high in some instances, Figure 6.

From the parallel sample lines (1P, 2P & 3P), it can be seen that the average amount of fines is increasing further out in the deposit. This is shown by that the average of % <63µm is higher for 2P (50-60m from the dam crest) and 3P (100m from the dam crest) than for 1P (15-20m from the dam crest) for all sampling campaigns, Table 1. For the 2018 sampling campaign, the variability between samples is clearly lower further out in the deposit (see coefficient of variance (COV) for 1-3P for 2018). However, this is not the case in the 2019 years sampling campaign, Table 1.

In the 2019 sampling campaign, there is basically no difference in variability between the perpendicular sample lines. Especially for O-O2, the segregation between coarse and fine particles is similar for both perpendicular sampling lines, the one by a spigot (1T) and the one between two spigots (2T), Figure 6.

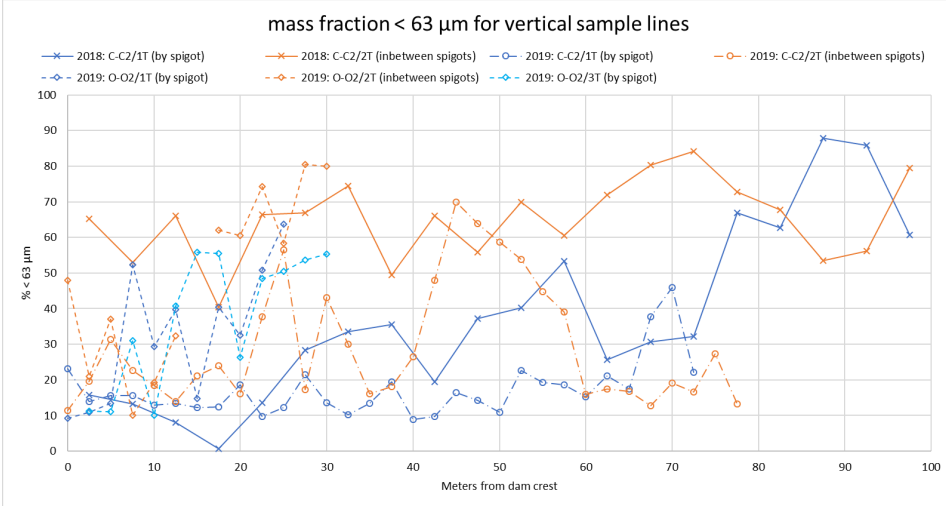

Figure 6. Mass fraction <63µm for all perpendicular lines in both sampling campaigns. Blue trends indicate sampling lines placed by spigots (1T & 3T). Orange trends indicate sampling lines placed in-between spigots (2T), Figure 2.

3.3.2 *In-situ density and Void ratio*

During the 2019 sampling campaign, the in situ dry density was determined by both a Balloon density apparatus and a Nuclear density gauge, Figure 7. The dry density, together with the particle density, was used to calculate the void ratio. For the beaches in Kiruna, the compaction criterion is expressed in terms of maximum void ratio.

The results show that there is a correlation between the results from the Balloon density apparatus and the nuclear density gauge. However, the low R^2-value indicate that the correlation is quite weak, especially if looking at the results from dam O-O2 separately. Paired t-tests for in-situ density show no statistically significant difference between the two methods.

The results show that the void ratio generally increases further out on the tailings beach, Figure 8. It is noticeable that the sampling lines in-between spigots (2T) show higher values (looser conditions) close to the dam crest, compared to the sampling lines by spigots (1T & 3T). As for the fines content, the variability for void ratio, between two samples spaced only 2.5m apart, can in some instances be very high. Relative changes of up to 40% between two consecutive sample points, indicating very high local variability in the sand, have been observed, Figures 8 and 9.

The calculated void ratios will be compared with the critical void ratio determined in the laboratory (not shown in these plots). If the calculated void ratio is larger than the critical void ratio, compaction will be required. The critical state line is known to vary with different grain size distributions. Due to the variability in the beach, the calculated void ratio should be compared to the critical void ratio for its corresponding grain size distributions. Result from the present case study indicate that there is some correlation between grain size and void ratio, where larger void ratio is related to finer material with higher mass fraction <63µm, Figure 10.

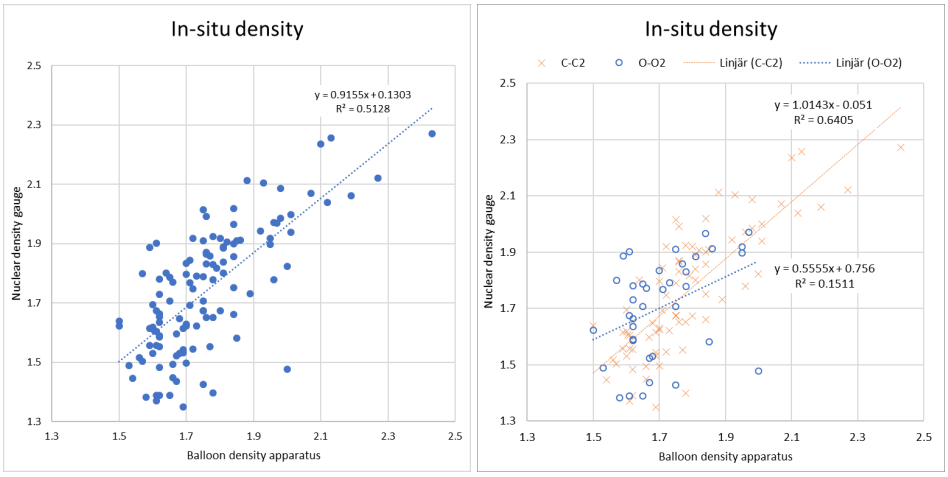

Figure 7. Correlation between nuclear density gauge and balloon density apparatus, left: all samples, right: divided into samples from C-C2 and O-O2 respectively.

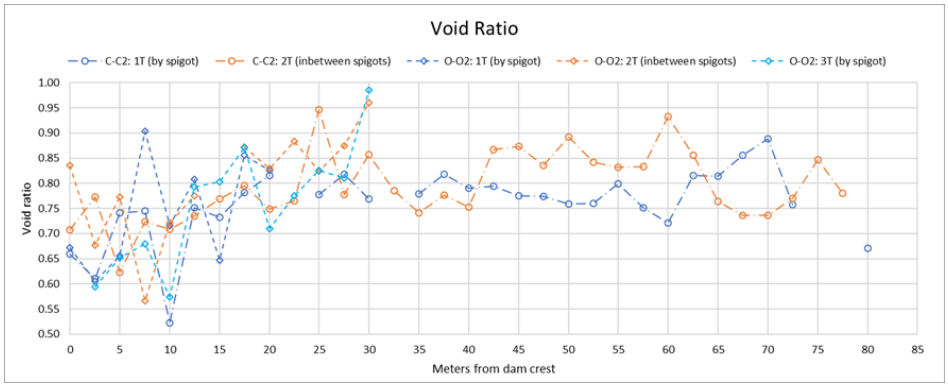

Figure 8. Void ratio for all perpendicular sample lines in the 2019 sampling campaign. Blue trends indicate sampling lines by spigots (1T, 3T) and orange trends indicate sampling lines in-between spigots (2T), Figure 2.

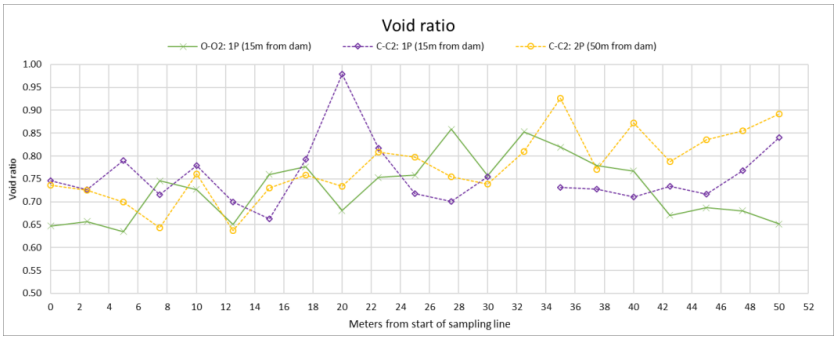

Figure 9. Void ratio for all parallel sample lines in the 2019 sampling campaign, see Figure 2.

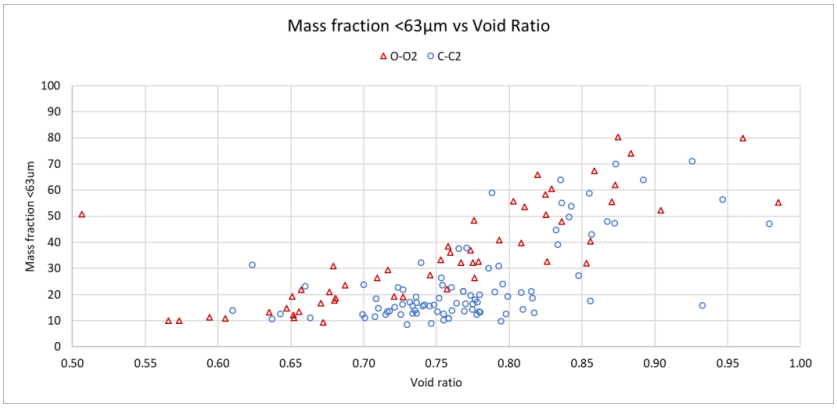

Figure 10. Mass fraction <63µm vs Void ratio for both sampling grids in the sampling campaign in 2019.

4 DISCUSSION

4.1 *Grain size*

The reason for the lower variability of % <63µm (i.e. less segregation of tailings, for the perpendicular sampling line in-between spigots in 2018) could be due to backwater from the spigots getting trapped close to the dam crest. This means that the water is moving slow or even standing still close to the dam crest, letting fine particles settle. On the contrary, the purpose of spigoting sand is to achieve a segregation of material, where coarser particles settle close to the dam crest, while finer particles settle further away from the dam crest. A change that followed upon the result of the 2018 sampling campaign, was that the distance between spigots was reduced from 24m to 18m. This was done to reduce the risk of backwater between spigots that had shown to trap finer particles close to the dam crest. As a result of this, the segregation along the 2T sampling lines (in-between spigots) in 2019 was improved.

The increased variability in the 2T sampling line (between spigots) indicate that the problem with backwater was reduced as there is not as much fine material close to the dam crest in 2019 as was evident in 2018. Another indication that the amount of fines has decreased close to the dam crests is that the % <63µm is lower for the 1P sampling lines (15m from the dam) and that the absolute standard deviation for the % <63µm also has decreased for the 1P sampling lines.

4.2 *In-situ density and Void ratio*

The reason for the weak correlation for In-situ density between the Balloon density apparatus and a nuclear density gauge could be explained by that the range of densities is quite small. As there is no statistically significant difference between the methods, the combination of sampling and measurement uncertainty could also explain the low R^2 result for the correlation. To further evaluate the correlation between the two methods, a more comprehensive comparison could be conducted over a wider range of densities. This might enable a more comprehensive understanding of the correlation between the methods. However, that has not currently not been deemed necessary within LKAB.

The results show that the void ratio is increasing further out on the tailings beach. However, for the perpendicular sampling lines in-between spigots, higher values for void ratio can be seen close to the dam crest in the 2019 sampling campaign. This means that the problem with backwater may still be present, even though it was reduced by decreasing the distance between spigots to 18m after the 2018 sampling campaign. There is also some correlation between the void ratio and amount of fines, which needs to be taken into account as the critical state line is dependent on the grain size of the tailings.

The local variability in void ratio was determined to be up to 40% relative between two consecutive sampling points, 2.5m apart. This high material heterogeneity poses great challenges related to sampling and how to reach representative conclusions regarding the sand properties in the tailings facility. Traditional sampling methods in tailings management generally imply collecting one sample at each location and the sampling locations are normally spaced far apart on the tailings beach. Random and/or composite sampling is seldom applied in the quality control of mine tailings facilities, even though it is one of the cornerstones of the representative sampling according to TOS (DS 3077).

With the sampling methods traditionally applied for characterization of mine tailings facilities, the large material heterogeneity at small distances, will lead to large sampling variabilities and reduce the possibility to draw accurate conclusions regarding the tailings properties. Some examples that may be applied to accommodate for large material heterogeneity and allow for representative sampling include increased sample mass or increased number of increments per primary sample. The latter is generally described as the most effective as it lowers both the fundamental sampling error as well as the grouping and segregation error (Pitard 1993).

5 CONCLUSIONS AND IMPLEMENTED IMPROVEMENTS

The results from this case study show that spigots may introduce a situation where backwater traps finer material close to the dam crest. It is important to pay attention to this problem in order to plan the spacing, flow, etc. of the spigots so that the tailings are distributed as intended. The distance between the spigots was reduced in the Kiruna mine tailings facility as a result from the 2018 sampling campaign, which also resulted in a better segregation of coarse and fine material on the beach and also reduced the problem with fine material being trapped in backwater close to the dam crest. Further testing, with changes in flow pattern and closed end pipes, is currently being done in order to further improve the sand distribution in the tailings facility.

The case study shows that there is no statistically significant difference between the Balloon density apparatus and the nuclear density gauge, but the correlation between them is quite weak in the evaluated density range. As the nuclear density gauge is both faster and less operator dependent, this method is recommended for continuous quality control of the in-situ density of deposited sand in the LKAB mine tailings facilities. The speed of the method is favourable since this generally increases the number of possible sampling points. This is an important aspect of the method selection as the large material heterogeneity implicate that a large number of increments or in situ analyses are necessary in order to reduce the sampling variability and reach representative sampling processes.

The results from the case study has also led to changes in the sampling methods for continuous quality control of the tailings characteristics on the beach of the Kiruna mine tailings facility. Composite sampling has been implemented, where a minimum of five increments are collected at each sampling location, to form a composite sample sent for analysis. The method of extracting samples has also been changed from shovelling to the use of a cylindrical sampling probe. This enables collection of a uniform cylindrical increment of a specified height. The sampling method entails that each increment is representative in regard to the layer of tailings being sampled. This means that the sample height can be adapted to represent a certain time frame of deposited tailings, by correlating the sample depth to the amount of deposited tailings in the specified time frame.

Since the Nuclear density gauge entails specific safety training and special permits, this device has not been implemented for routine quality control of the LKAB mine tailings facilities at this time. However, a similar case study, using a Nuclear density gauge coupled with density and size analysis, is currently being completed in another LKAB tailings facility in Malmberget.

6 ACKNOWLEDGEMENTS

The authors wish to acknowledge the support from LKAB in the execution of the case study and for the permission to publish the results. Furthermore, a special thanks to all sampling staff for their hard work in scorching sun as well as freezing cold and hailstorms to extract samples from the mine tailings facilities. Finally, thanks to the LKAB laboratory staff for finalizing the vast amount of analyses of all collected samples.

7 REFERENCES

Chronology of major dam failures. 2020. www.wise-uranium.org, accessed 2020-06-25.

Demers, I., Amara, H.S., Gasnier, M., Bernard, J-P. 2017. Development of a sampling strategy for mine waste characterization. *Proceedings of Tailings and Mine Waste '17, Banff,* Alberta, Canada, 5-9 November.

Dillon M.J. & Wardlaw H.J. 2010. Strength and liquefaction assessment of tailings. *First International Seminar on the Reduction of Risk in the Management of Tailings and Mine Waste*

DS 3077. 2013. *Representative sampling – Horizontal standard,* Danish standards.

Esbensen, K.H. & Paasch-Mortensen, P. 2010. Process Sampling: Theory of Sampling – the Missing Link in Process Analytical Technologies (PAT). *In Process Analytical Technology: Spectroscopic Tools and Implementation Strategies for the Chemical and Pharmaceutical Industries, 2nd ed*.; Bakeev, K., Ed.; 2nd ed.; John Wiley & Sons: Chichester, UK, pp. 37-80, ISBN: 978-0-470-72207-7.

Gy, P. 1998. Sampling for analytical purposes; John Wiley & Sons Ltd: West Sussex, UK, ISBN: 978-0-471-97956-2

Minnitt R.C.A. & Esbensen K.H. 2017. *Pierre Gy's development of the Theory of Sampling: a retrospective summary with a didactic tutorial on quantitative sampling of one-dimensional lots*. TOS Forum 7:7-19, DOI: 10.1255/tosf.96

Pitard, F.F. 1993. Pierre Gy's sampling theory and sampling practice: Heterogeneity, Sampling Correctness, and Statistical Process Control, 2nd ed.; CRC Press LLC, Boca Raton, USA, ISBN: 0-8493-8917-8.

Reid D. 2019. Estimating the in situ state of a thickened tailings deposit. *Paste 2019*, Cape Town, South Africa.

Robertson P.K. et al. 2000. The CANLEX project: summary and conclusions. *Canadian Geotechnical Journal 37(3):563-591.*

Robertson, P.K. 2010. Evaluation of Flow Liquefaction and Liquefied Strength Using the Cone Penetration Test. *Journal of Geotechnical and Geoenvironmental Engineering.*

SS 027110, 1994. Swedish standard, Geotechnical tests – Compaction properties – Field determination of density, edition 4.

Töyrä, S., Lundell, D. & Bjelkevik, A. 2017. Tailings management at the Kiirunavaara iron ore mine. *Proceedings of Tailings and Mine Waste '17, Banff, Alberta, Canada, 5-9 November.*

Töyrä, S., Bjelkevik, A., Lindahl, L., Sutton, R., Jonsson, J., 2019. Tailings Management –Current Practice in Sweden. *ICOLD-CIGB 2019 Symposium, Ottawa, Ontario, Canada, 9-14 june.*

TAILENG Mine Tailings Database

Jorge Macedo
Georgia Institute of Technology, Atlanta, GA, United States

Jonathan Bray
University of California Berkeley, Berkeley, CA, United States

Scott Olson
University of Illinois at Urbana Champaign, Champaign, IL, United States

Christopher Bareither
Colorado State University, Fort Collins, CO, United States

Cody Arnold
Georgia Institute of Technology, Atlanta, GA, United States

ABSTRACT: Georgia Tech, UC Berkeley, the University of Illinois at Urbana-Champaign, and Colorado State University under the umbrella of the TAILENG Center are undertaking a research project on the mechanical-based characterization of mine tailings. The project includes the collection of available experimental data (i.e., laboratory and field tests) as well as the generation of new experimental data (i.e., performing laboratory tests and field tests) to gain insights on the mechanical response of mine tailings. The current TAILENG database contains information on the static and cyclic response of mine tailings, considering both laboratory and field scales. This paper describes the characterization database, presents illustrative test results, and shares preliminary insights on evaluating the mechanical response of one of the mine tailings within the TAILENG database. Illustrative comparisons of interpretations from laboratory tests and stress-strain constitutive models are made.

1 INTRODUCTION

In moderate to high-risk tailings storage facility (TSF) projects, characterizing the mechanical response of the deposited tailings is required. For example, Figure 1 shows a case that corresponds to a centerline TSF where the response of the deposited tailings is key in the evaluation of the overall TSF stability. In this case, stiffness and compressibility of the tailings are crucial in evaluating potential static settlements and static liquefaction in the upstream area, whereas cyclic resistance of the tailings is crucial in evaluating seismic performance of the TSF.

Characterization of the mechanical response of mine tailings is also critical for the calibration of constitutive models that often are used by geotechnical engineers to evaluate static and seismic response of a TSF. This process is illustrated in Figure 2, which shows the use of triaxial tests to calibrate a stress-strain constitutive model as part of the forensic studies that followed the well-known 2015 Fundao dam failure in Brazil. This failure has been described as the worst environmental disaster in Brazil's history. Approximately 60 million cubic meters of iron ore tailings and waste flowed into the Doce River, causing toxic brown mudflows to pollute the river and beaches near the mouth when they reached the Atlantic Ocean 17 days later (https://en.wikipedia.org/wiki/Mariana_dam_disaster). The disaster created a humanitarian crisis as hundreds of people were displaced and cities along the Doce River suffered water shortages. Characterizing the mechanical response of the tailings materials was critical in understanding the likely causes of the Fundao dam failure. The responses of the different tailings retained in the TSF were key to understanding the lateral extrusion mechanism, which later led to static liquefaction and the catastrophic failure (Morgensten et al., 2016). This is a stark reminder of the importance

of tailings characterization and the subsequent conceptualization of this response through adequate design protocols in TSF projects.

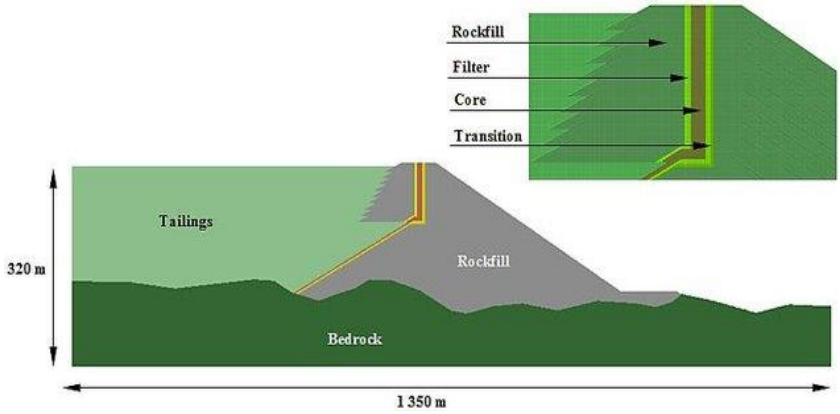

Figure 1. Example of a centerline TSF in which the mechanical response of the deposited tailings is critical in the evaluation of its overall performance (after Pretell-Ductram and Dismuke, 2016).

The processes that follow the deposition of mine tailings in a TSF are complex. For example, when tailings are deposited, coupled phenomena that include sedimentation, self-weight consolidation, and desiccation, can be crucial in understanding the mechanical response of mine tailings. These processes influence the static and cyclic strength of mine tailings, as well as their hydraulic parameters and chemical interactions. Adequate characterization of mine tailings is key to evaluating coupled processes within a TSF; for example, compressibility and permeability stress dependence are important to evaluate the water balance as well as physical stability of a TSF.

Mine tailings are generally intermediate materials classified as sandy silt to clayey silt. This presents a fundamental challenge in assessing their mechanical response because most existing approaches in geotechnical engineering have been developed for medium-to-high plasticity clay and quarzitic clean sand. Whereas there are a large number of studies on the behavior of clay and sand, there are comparatively few studies on intermediate (silty) soil. The database being developed by the Tailings and Industrial Waste Engineering (TAILENG) Center seeks to improve our understanding of intermediate soil and mine tailings. The TAILENG Center is comprised of researchers at Georgia Tech, Colorado State University, UC Berkeley, and the University of Illinois at Urbana-Champaign (http://taileng.ce.gatech.edu/).

2 DATABASE

The development of the TAILENG mine tailings database is an ongoing activity. The current TAILENG database contains information on the static and cyclic response of mine tailings at varying scale (i.e., laboratory and field scales). The laboratory and field tests typically included are: (1) soil index tests; (2) drained and undrained, monotonic and cyclic triaxial compression tests; (3) drained and constant volume, monotonic and cyclic direct simple shear tests; (4) consolidation and bender element tests; (5) in-situ penetration and field vane shear tests; and (6) field geophysical tests.

The collected tailings data sets are classified according to their quality and completeness to enable a comprehensive characterization of either the static or cyclic mechanical response of the material. There are four classes of data sets: A, B, C, and D, with D being substandard and, therefore, not utilized in future development of theoretical and empirical studies. The types of data typically required for each class of data are described below.

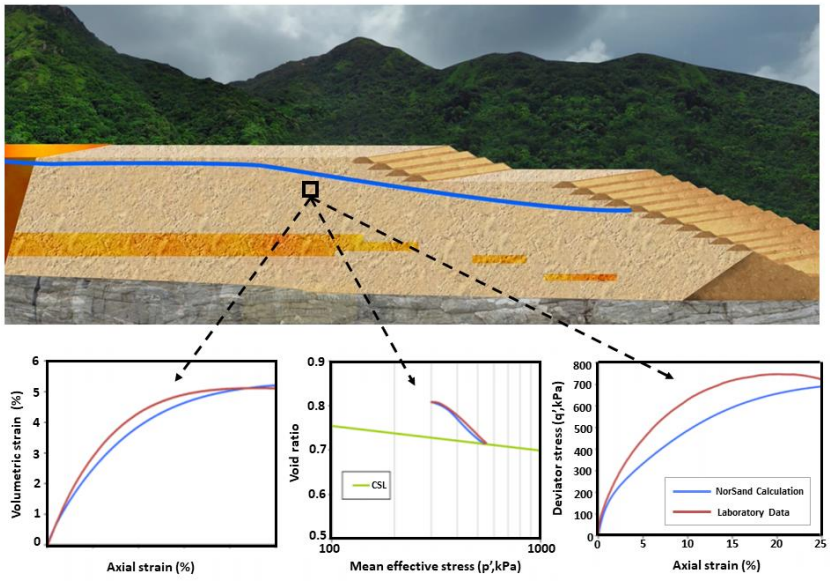

Figure 2. Illustration of the use of triaxial tests to calibrate a constitutive model in the forensic analyses of the Fundao dam failure (Morgensten et al., 2016).

Class A

- Electronic raw data files
- Index tests: water content (w_c), plasticity index (PI), particle size distribution, X-ray diffraction, and minimum and maximum void ratios (e_{min} and e_{max})
- Compressibility tests: constant rate of strain (CRS) or incremental loading (IL) consolidation tests
- Monotonic consolidated-drained (CD) and consolidated-undrained (CU) triaxial compression (TC) or triaxial extension (TE) tests using lubricated, enlarged end platens and with reliable pore water pressures (if applicable) as well as drained and constant-volume direct simple shear (DSS) tests. Tests should be sufficient to define critical state line (CSL) parameters.
- Cyclic DSS or cyclic TC tests
- Piezocone penetration test (CPTu) results, preferably with dissipation tests
- Vs measurements using bender element tests or field geophysical tests
- Small-scale (laboratory) and large-scale (field) vane shear tests
- Seepage-induced consolidation tests
- Soil water characteristic curves (SWCC)

Class B

- Electronic raw data files or high-resolution digitized data files
- Index tests: w_c, PI, and particle size distribution
- Compressibility tests: CRS or IL consolidation tests
- Monotonic TC, TE, or DSS tests sufficient to define CSL parameters
- Cyclic DSS or cyclic TC tests
- CPTu results
- Vs measurements using bender element tests or field geophysical tests

Class C (Focused on static liquefaction)

- High-resolution digitized data files
- Index tests: w_c, PI, and particle size distribution
- Compressibility tests: CRS or IL consolidation tests
- Monotonic TC, TE, or DSS tests sufficient to define CSL parameters
- CPTu results
- Field vane shear tests (FVST)

Class D

- Only low-resolution data plots available
- Index tests: w_c and PI
- Monotonic TC, TE, or DSS tests insufficient to define CSL parameters

Select trends for a subset of materials in the current TAILENG mine tailings database are shown in Figure 3. The critical state lines (CSLs) in Figure 3a were evaluated from CD and CU triaxial tests, considering 35 different materials. There is significant variation among the CSLs in Figure 3a [e.g., the CSL intercept varies from about 0.6 to 1.2 in void ratio (e) space] with some materials having a linear CSL in e vs. log mean effective stress (p) space and other materials a curved shaped CSL in e vs. log p space.

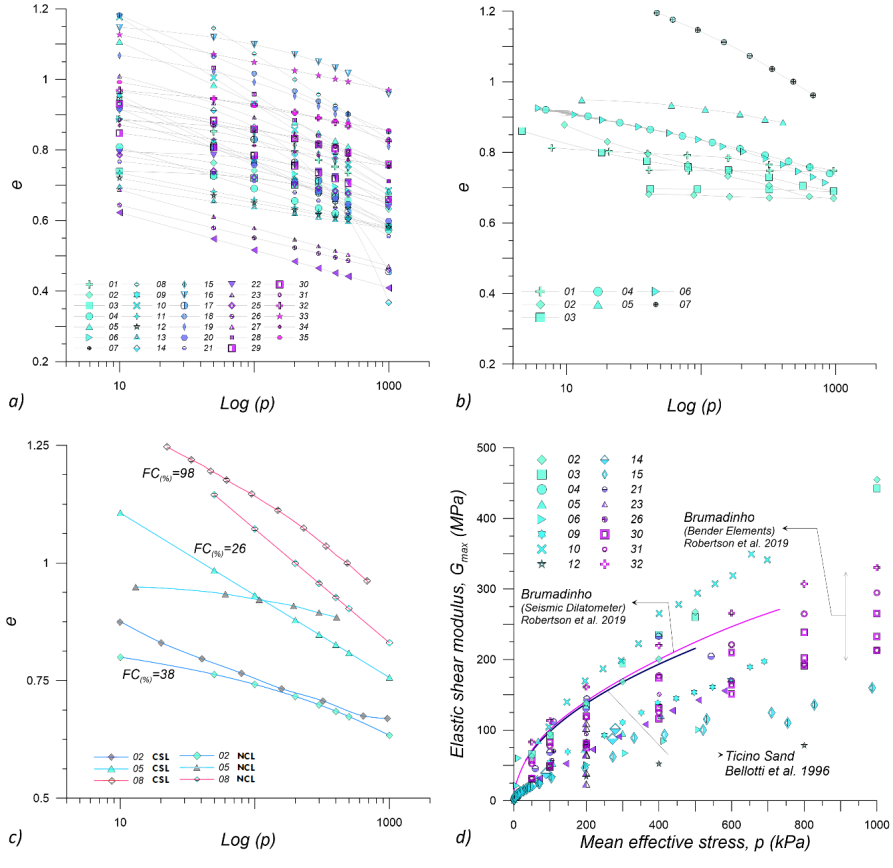

Figure 3. a) CSLs for a subset of the tailings materials in the TAILENG database, b) distribution of normally consolidation lines (NCL), c) comparison of CSL and NCL for a subset of materials, and d) distribution of shear modulus (G_{max}) versus mean effective stress (p) curves.

Consolidation curves for selected materials evaluated from constant rate of strain consolidation tests are shown in Figure 3b, and comparisons between CSLs and consolidation curves for three of the materials are shown in Figure 3c. Interestingly, as the fine contents ($FC_{\%}$) identified in Figure 3c increased, the curves become more parallel, which suggests a transition from "sand-like" to "clay-like" behavior using the Boulanger and Idriss (2006) terminology. Lastly, the trends of how the small-strain shear stiffness (i.e., G_{max}) varies as a function of effective stress from bender elements tests on select materials are shown in Figure 3d. These data illustrate the G_{max} of mine tailings increases nonlinearly as the applied mean effective stress increases, and mine tailings can exhibit G_{max} values comparable to those of sand materials.

3 EXAMPLE OF TAILENG DATABASE USE

The particle size distribution for a one of the tailings materials in the TAILENG database is shown in Figure 4. This mine tailings has a plasticity index of 3 and a limit liquid of 22. The Atterberg limits locate the material just above the "A-line" in the Unified Soil Classification System (USCS) plasticity chart, leading to classifying the material as ML. The database for this material includes four (4) CD triaxial tests, two (2) CU triaxial tests, six (6) bender elements, and six (6) cyclic DSS tests. Post-processing of the triaxial tests to establish the critical state line and stress-dilatancy relationships is shown in Figure. 5. The relationships in Figures 5a, 5b, and 5c illustrate calculation of the critical state stress ratio (M_{tc}), volumetric coupling (N), and state-dilatancy parameter (χ). Results from bender element tests to estimate the dependence of the maximum shear modulus on the mean effective stress are shown in Figure 5d. Results of two cyclic shear tests illustrating the dependence of the cyclic response to the applied cyclic stress ratio (CSR) are shown in Figures 6a and 6b. The cyclic tests exhibited liquefaction (defined as 3% of single amplitude shear strains) in 15 and 6 cycles, respectively, and could be used to establish the liquefaction resistance curve for this material after considering sample disturbance and test stress-path effects.

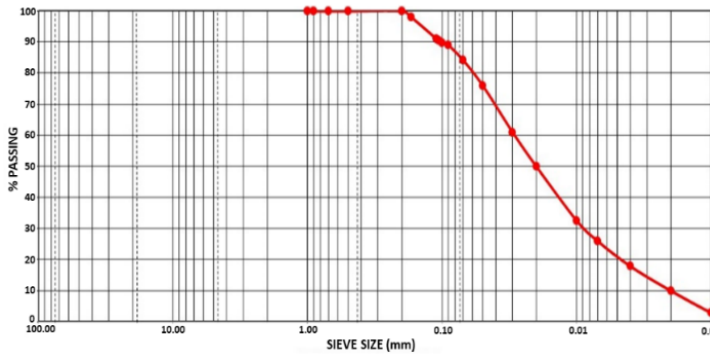

Figure 4. Particle size distribution of one of the tailings materials in the TAILENG database.

Two constitutive models (i.e., the NorSand model and the SANISAND model with its DM04 version) were calibrated using the results of the TX compression tests to illustrate the use of the laboratory test data on tailings materials in the TAILENG database. NorSand (Jefferies and Been, 2015) is a plasticity-based model formulated in the critical state framework, which states that any particulate material, upon sufficient shearing, will ultimately reach a unique state called the critical state at which the particulate material undergoes continuous deformation without further volume change. NorSand captures the effect of density and pressure dependence on the mechanical response of particulate materials and can be conceptualized as a generalization of the original Cam Clay model (Jefferies and Been, 2015), which means that Cam Clay is a particular case of NorSand. SANISAND is the name used for a family of Simple ANIsotropic SAND constitutive models (the name resulting from the foregoing uppercase letters) developed over the

past decade by Manzari and Dafalias and their colleagues (e.g. Manzari and Dafalias, 1997; Li and Dafalias, 2000; Dafalias and Manzari, 2004; Dafalias et al., 2004). The SANISAND model was developed within the framework of critical state soil mechanics and bounding surface plasticity. In this study, SANISAND 2004 was used is denoted as DM04 (Dafalias and Manzari 2004).

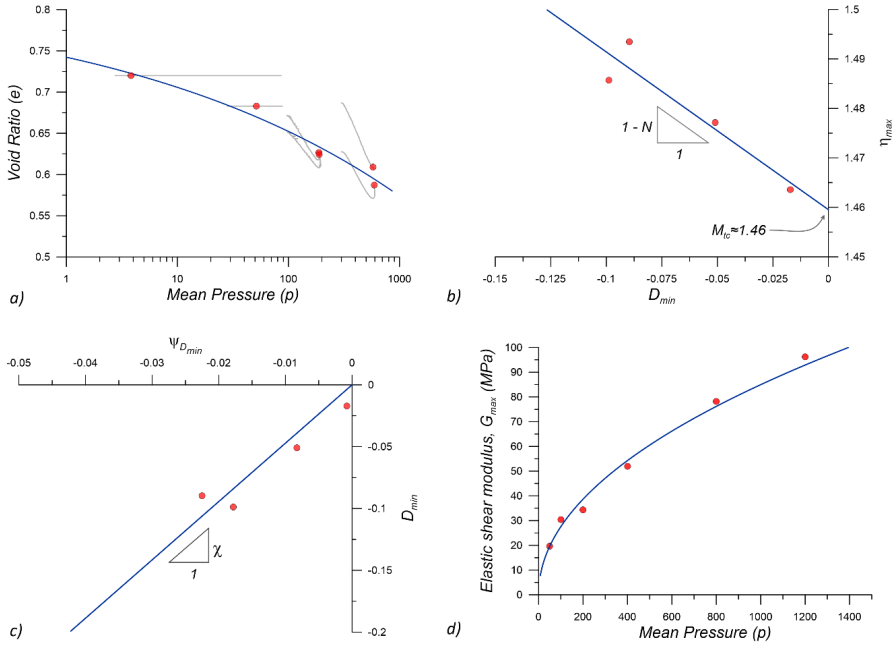

Figure 5. Illustration of the estimation of mechanical-based parameters for a selected tailings material: a) CSL estimation, b) stress ratio versus maximum dilatancy plot to estimate M_{tc} and N, c) state-dilatancy relationship to estimate χ, and d) G_{max} versus p plot to estimate the stress-dependency of the small shear modulus.

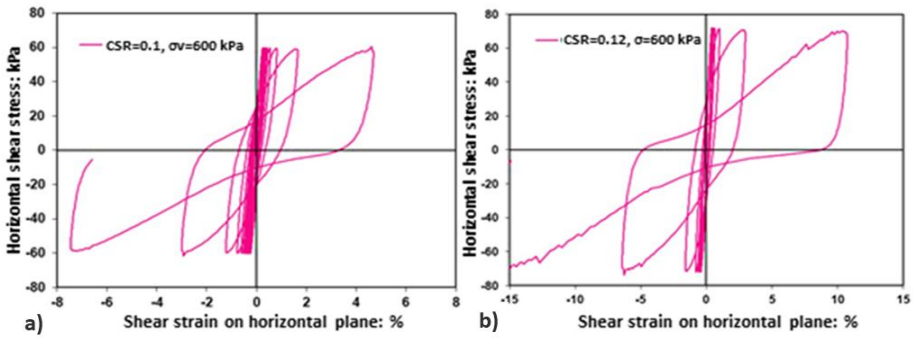

Figure 6. Results for selected stress-controlled cyclic direct simple shear tests.

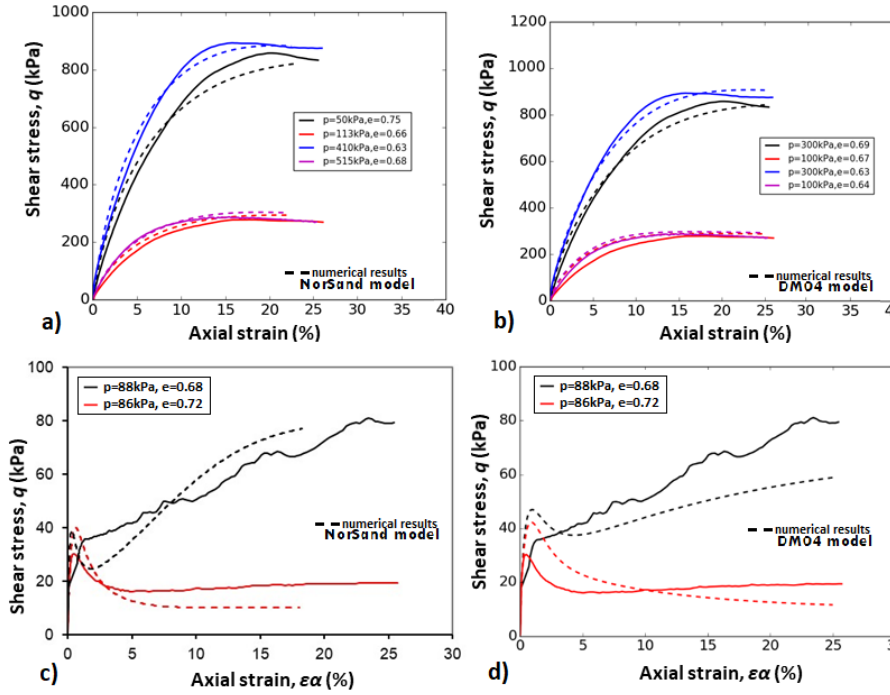

Figure 7. Calibration of soil constitutive models to capture material response in the triaxial static test: (a) CD triaxial tests with the NorSand model, (b) CD triaxial tests with the DM04 model, (c) CU triaxial tests with the NorSand model, and (d) CU triaxial tests with the DM04 model.

The DM04 model builds upon previous work by Manzari and Dafalias (1997), introducing three new aspects. The first aspect is a fabric-dilatancy related quantity, scalar-valued in the triaxial and tensor-valued in generalized stress space, which is instrumental in modeling macroscopically the effect of fabric changes during the dilatant phase of deformation on the subsequent contractive response upon load increment reversals and the ensuing realistic simulation of the sand behavior under undrained cyclic loading. The second aspect is the dependence of the plastic strain rate direction on a modified Lode angle in the multiaxial generalization, a feature necessary to produce realistic stress-strain simulations in non-triaxial conditions. The third aspect is a systematic connection between the simple triaxial and the general multiaxial formulation to use the model parameters of the former in the implementation of the latter.

Comparisons of static experimental and numerical-based responses obtained from the NorSand and DM04 models are shown in Figure 7. Consolidated drained triaxial test data are shown in Figures 7a and 7b and CU triaxial test data are shown in Figures 7c and 7d. The NorSand and DM04 models were used to simulation both drained and undrained experimental data. The models were calibrated using the experimental data provided in Figure 5 and the experimental stress-strain curves shown in Figure 7. Details on the calibration protocols for these models can be found in Jefferies and Been (2015) and Dafalias and Manzari (2004), which is beyond the scope of this paper. Both the NorSand and DM04 models capture key aspects of the undrained response of the selected tailings material (i.e., the CU TX compression test results) after being calibrated to reproduce the CD triaxial compression test results. Thus, one type of test in the mine tailings database can be used to calibrate a soil constitutive model to evaluate the ability of a model to capture the response of the same material in a different type of test in the database.

4 SUMMARY

Researchers at the TAILENG Center are developing a mine tailings database to enhance characterization of the mechanical response of mine tailings materials. The TAILENG mine tailings database includes the collection of experimental data (i.e., laboratory and field tests) as well as the generation of experimental data (i.e., performing laboratory tests and field tests) to gain insights on the mechanical response of mine tailings. The characterization of mine tailings presents a fundamental challenge because most existing approaches in geotechnical engineering have been developed for clay and sand. There is not an accepted framework to characterize the mechanical response of intermediate mine tailings. The TAILENG mine tailings database seeks to contribute to improving the understanding of silty soil and mine tailings through bringing together data from high-quality field and laboratory tests.

In this paper, key aspects of the TAILENG mine tailings database are described and potential uses for providing insights are illustrated. The mine tailings database includes four different classes of data depending on the data quality and completeness. Benefits of the TAILENG database are illustrated through examination of the trends in select test results on materials currently in the mine tailings database. One of the potential uses is the evaluation of the ability of constitutive models to capture key aspects of soil response.

REFERENCES

Boulanger, R.W., Idriss, I.M. (2006). "Liquefaction susceptibility criteria for silts and clays." *Journal of Geotechnical and Geoenvironmental Engineering*; 132(11): 1413-1426.

Dafalias, Y.F., Manzari, M.T. (2004). "Simple plasticity sand model accounting for fabric change effects." *Journal of Engineering Mechanics*; 130(6): 622–634.

Dafalias, Y.F., Papadimitriou, A.G., Li, X.S. (2004). "Sand plasticity model accounting for inherent fabric anisotropy." *Journal of Engineering Mechanics*; 130(11): 1319–1333.

Jefferies, M.G., Been, K. (2015). "Soil Liquefaction: A critical state approach." 2nd Edition, CRC Press Published September 21, 2015. 690 Pages - 386 B/W Illustrations. ISBN 9781482213683 - CAT# K21726.

Li, X.S., Dafalias, Y.F. (2000). "Dilatancy for cohesionless soils." *G´eotechnique*; 54(4): 449–460.

Manzari, M.T., Dafalias, Y.F. (1997). "A critical state two-surface plasticity model for sands." *G´eotechnique*; 47(2): 255–272.

Morgenstern, N.R., Vick, S.G., Viotti, C.B., Watts, B.D. (2016). "Fundão Tailings Dam Review Panel: 541." Report in the immediate causes of the failure of the Fundão Dam.

Pretell-Ductram, R., Dismuke, J. (2016). "Comparison of simplified and detailed analyses for assessment of dynamic displacement of a centerline tailings dam." *4th Itasca Symposium.* March 2016.

Use of High Performance Fibres to Enhance Tailings

Sebastian Quintero Olaya, Chenming Zhang, David J. Williams, Ximing Lei, Zicheng Zhao
The University of Queensland, Australia
Marcelo Llano-Serna
Klohn Crippen Berger Ltd., Brisbane, Queensland and The University of Queensland, Australia

ABSTRACT: Tailings are commonly deposited as a thickened slurry of low shear strength, which relies on consolidation and desiccation for densification and strength gain. However, in practice tailings sufficient consolidation and desiccation may not occur as the tailings layers are deposited, and the tailings may remain saturated and under-consolidated. Fibres have been used effectively in concrete as an additive that aids strength. They have also been used as a reinforcement in cemented tailings backfill, in pavements and in foundations. This paper demonstrates that plastic fibres can be introduced to improve the geotechnical parameters and behavior of thickened tailings after deposition. Characterization tests were carried out on red mud with two types of plastic fibres at different percentages. Further, a series of long-term drying tests was carried out in 10 liter basins instrumented with moisture and suction sensors. These tests show that fibres can improve tailings geotechnical parameters, and more importantly open pathways for water to flow freely, allowing the tailings to consolidate and dry more rapidly.

1 INTRODUCTION

Tailings are commonly deposited as a thickened slurry into a tailings storage facilities (TSF) where they consolidate and desiccate on exposure to the atmosphere (ICOLD, 2001). The degree of consolidation and desiccation depend on the rate of rise of the tailings and their permeability, and the extent and duration of exposure to desiccation, which in turn is a function of the weather conditions. Insufficient consolidation and desiccation leads to the tailings remaining wet and soft (Williams, 2015). Wet and soft tailings occupy a large storage volume due to their high moisture content, cannot support upstream raises, and are difficult to rehabilitate.

1.1 *Tailings parameters*

Similar to soil, the physical and chemical characteristics of tailings can be determined by laboratory testing (Williams and Zhang, 2017). Tailings undergo on deposition in a TSF the physical processes of beaching and hydraulic sorting, settling, consolidation and desiccation on exposure (Williams, 2016).

The important aspects of settling are the solids concentration achieved and the time required for settling (Zhang et al. 2019), which can result in very large strain and little strength gain since effective stresses are yet to develop. Self-weight consolidation can result in large strain and large strength gain as effective stresses develop. Desiccation on exposure to sun and wind is shallow, and results in minor strain and very large strength gain, but dropping off exponentially with depth due to the reduced permeability of the unsaturated surficial tailings.

1.2 *Tailings dewatering and reinforcement*

Tailings dam failures only started to be reported after 1915, and the International Commission on Large dams was only founded in 1928 (Bowker, 2015; ICOLD, 2001). The mechanical dewatering and thickening of tailings started to be accepted only during the mid-1970s, and its implementation has been slow and difficult due to many factors, including cost issues (Sofrà and Boger, 2011). Thickening of tailings using flocculants has expanded as flocculant costs have slowly decreased, and thickening technologies have improved. Cemented tailing s are also increasingly being used as underground backfill (Yilmaz and Fall, 2017).

Fibres are widely used and recognized as effective additives to enhance the tensile strength and other characteristics of concrete (Li and Shi, 2014). Fibres have also been used to reinforce cemented tailings backfill. The application of fibres to tailings has mainly been at a research level. Previous research found that fibres increase the UCS of cemented tailings backfill up to 4-fold (Consoli et al. 1999), suggesting that fibres may enhance the geotechnical parameters and behavior of thickened tailings.

2 METHODOLOGY

2.1 *Materials tested*

2.1.1 *Tailings*

The tailings used in this study is red mud from Queensland Alumina Limited in Gladstone, Australia. This silt-sized residue is the by-product of bauxite refining to alumina, which is neutralized with sea water to reduce its pH and deposited as a thickened slurry in a surface TSF (Quintero et al. 2017).

2.1.2 *Plastic fibres*

Two types of fibre manufactured by TEXO ReoCo were used in the study (as shown in Figure 1), comprising different percentages of polypropylene (PP) and polyethylene (PE) by mass:

- Red fibre: PP = 85%, PE = 10%, additives = 5%. Stiff, with a rough surface, and a specific gravity of 0.88.
- Black fibre: PP = 82%, PE = 10%, additives = 3%. Soft, with a smooth surface, and a specific gravity of 0.91.

2.2 *Red mud characterization tests*

The particle size distribution of the red mud, based on wet sieving of the fraction coarser than 75 µm and hydrometer analysis of the fine-grained fraction is shown in Figure 2 to be clayey silt-sized. The Liquid limit (using Casagrande method) and Plastic limit of the red mud were 47.9% and 33.5%, respectively, giving a Plasticity Index of 14.4%. Hence, the red mud has a Unified Soil Classification of ML, a silt-sized material of low plasticity.

2.3 *Settling tests*

Settling tests on the red mud, without and with each of the fibres, were carried out in graduated 1,000 cc measuring cylinders (as shown in Figure 3). The red mud was tested at 25% solids by mass to replicate the state on discharge to the TSF. For the tests with fibres added, the mass of fibres was 1%, 2% and 3% of the red mud dry mass.

The red mud was mechanically stirred at a speed of 1,500 rpm for about 30 min prior to being introduced into the measuring cylinders. For the settling tests with fibres, the fibres were added just prior to pouring into the measuring cylinders to replicate fibre addition as red mud was discharged to the TSF. As the red mud settled, readings of the level of the sediment were taken after 0.5 min, 1 min, 2 min, 4 min, 8 min, 15 min, 30 min and 60 min, after 1 hr, 2 hr, 4 hr, 8 hr, 12 hr, 24 hr, 48 hr, and daily until the settling ceased.

Figure 1. red (left) and black (right) fibres.

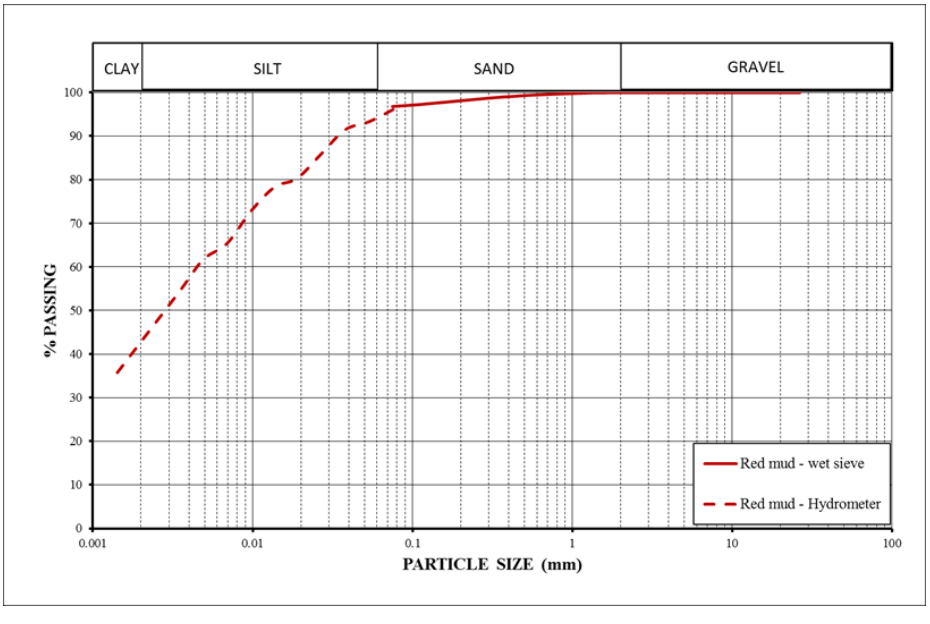

Figure 2. Red mud Particle Size Distribution.

Figure 3. Settling tests on red mud, without and with fibres.

2.4 *Vane shear tests*

Laboratory vane shear tests were carried out on the settled red mud samples, without and with fibres, using a vane with a length of 25 mm and diameter of 12.5 mm. The vane was rotated at a rate of 0.01 deg/min. Vane shear testing was carried out in the top and bottom sections of the settled samples.

2.5 *Instrumented basin desiccation tests*

Desiccation tests were carried out on red mud samples at 25% solids poured into a basin in three layers of 30 mm each and allowed to settle for 2 hrs prior to the next layer being poured (as shown in Figure 4). Three different basins were prepared: two basins were filled with red mud and 1% of red or black fibres added, and the third basin was filled with red mud only. The fibres were added to the tops of each layer prior to settling, and supernatant water was removed after the settling of each layer. Each basin was instrumented with three soil moisture sensors and three suction sensors located at the bottom, middle and top of the settled sample (15 mm 30 mm and 45 mm above the base of the basin). The basins were placed on separated scales to record the water loss due to drying over a month.

The moisture sensors measure volumetric water content indirectly through the dielectric permittivity of the sample. The thermal suction sensors measure the matric suction of the sample indirectly through the temperature rise on heating, which also provides the temperature of the sample. Desiccation of the final settled sample was achieved using a fan to minimize temperature changes. At the end of desiccation, the samples were re-wet using 5 L of process water.

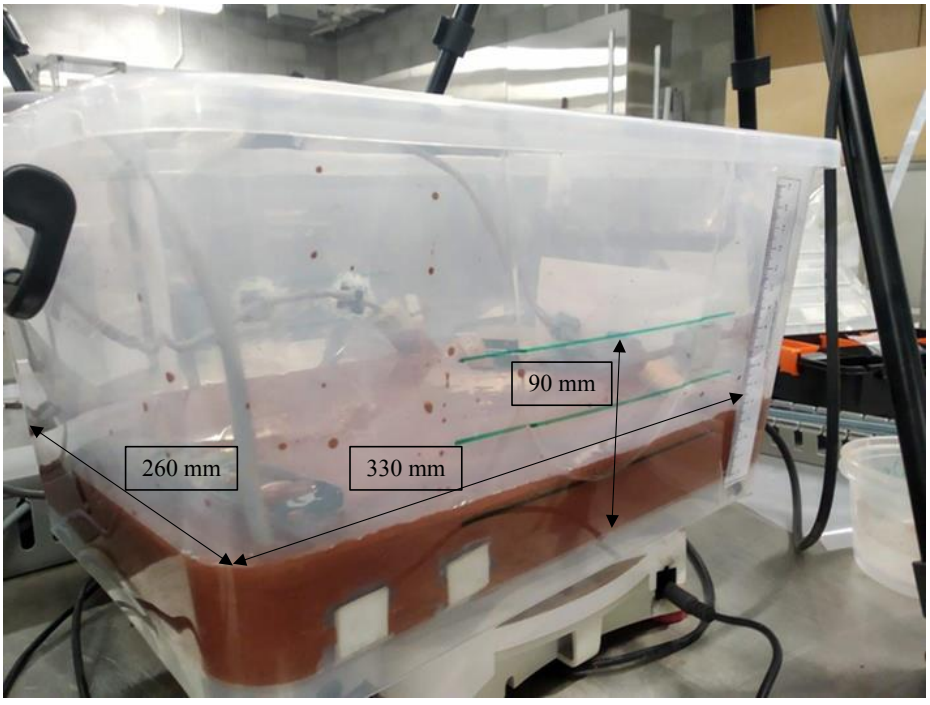

Figure 4 Desiccation basin test.

3 TEST RESULTS

3.1 *Settling tests*

Figures 5 and 6 compare the settling test results for the red mud without and with black fibres or red fibres. The red mud with black fibres showed faster settling than that of red mud only, whereas the red mud with red fibres settled progressively less than the red mud only.

A comparison of the settled dry densities of the samples is presented in Figure 7. The addition of black fibres increased the settled dry density of the red mud, achieving a highest value of 740 kg/m^3 with 2% black fibre addition. On the contrary, the settled dry density was reduced with the addition of red fibres.

Figure 8 shows the effect of fibre addition on the settling of the red mud in terms of solids concentration. The solids concentration of red mud alone was about 46%, which was increased to about 49% by adding 2% black fibres. Adding red fibres on the other hand decreased the solids concentration to as low as 42%.

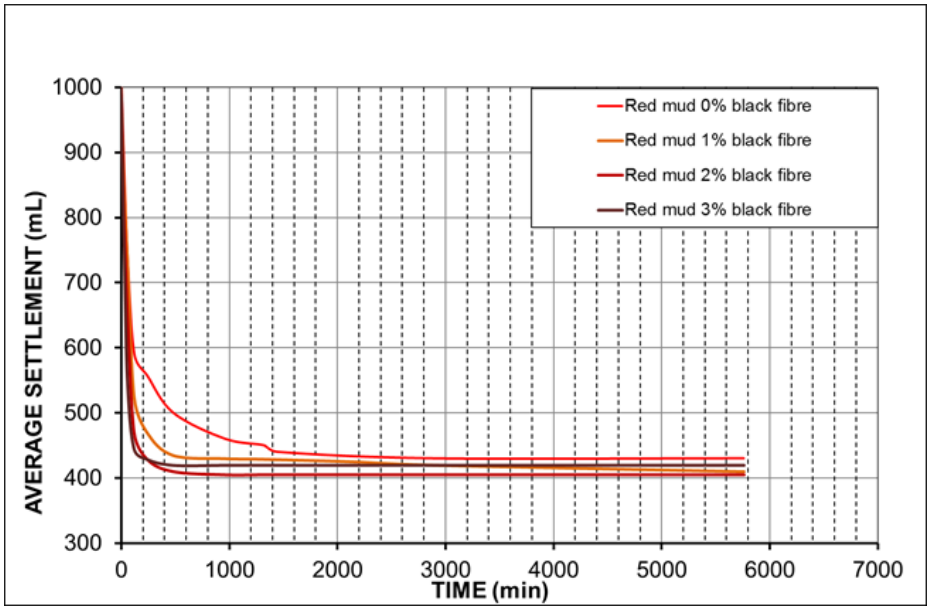

Figure 5. Settling of red mud without and with black fibres.

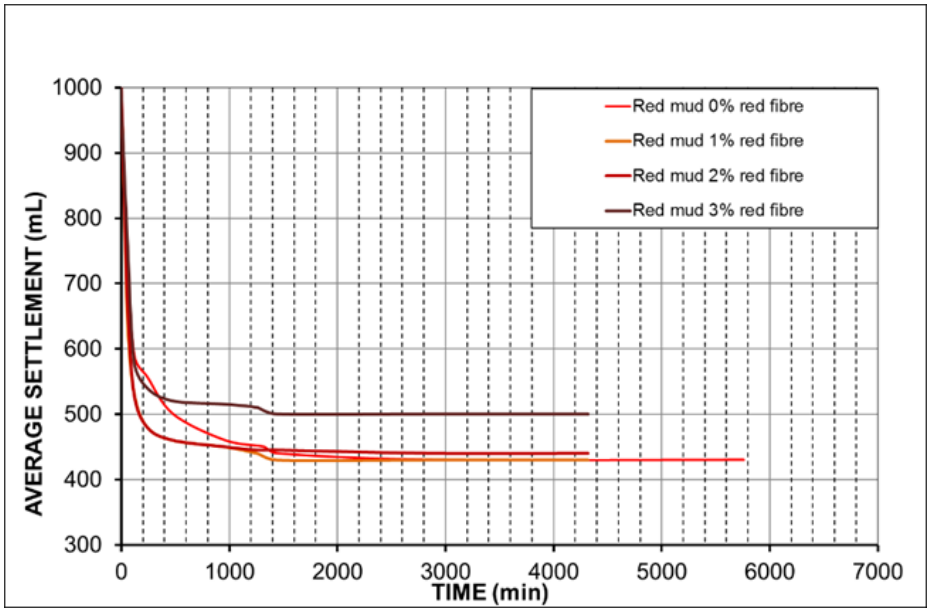

Figure 6. Settling of red mud without and with red fibres.

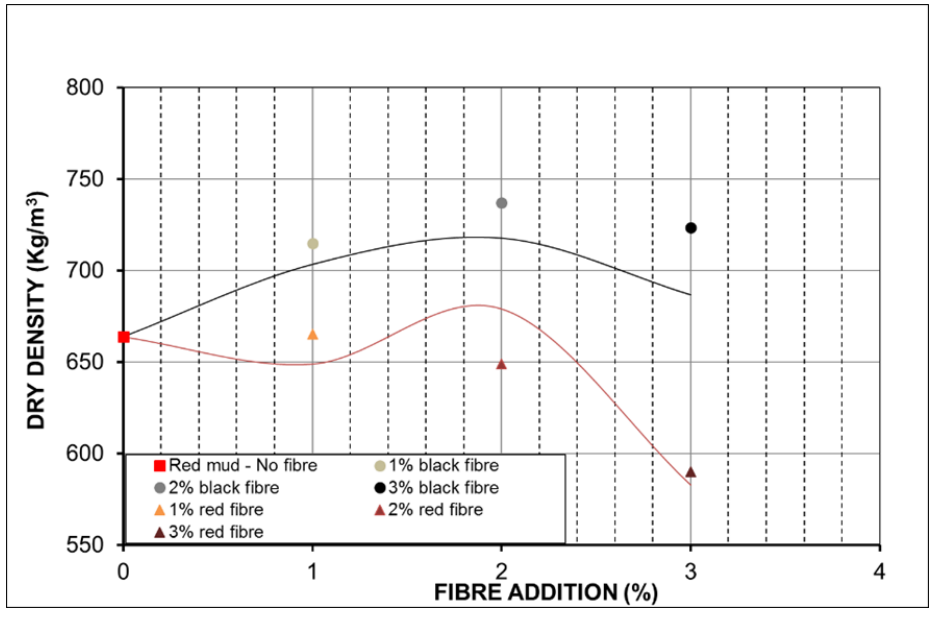

Figure 7. Settled dry densities of red mud without and with black and red fibres.

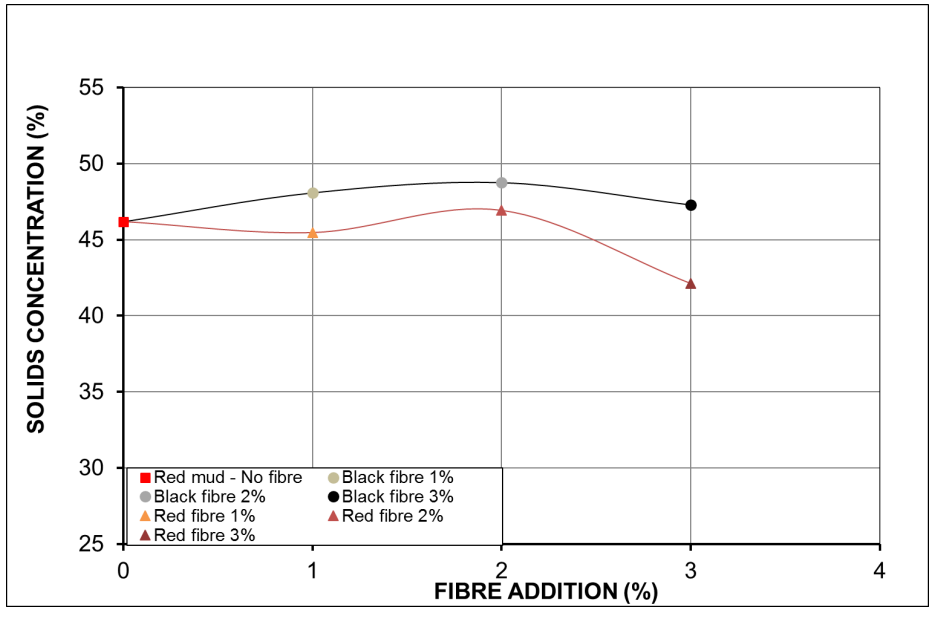

Figure 8. Settled solids concentration of red mud without and with black and red fibres.

3.2 *Vane shear tests*

Figures 9 and 10 show the increase of the peak vane shear stress of the settled red mud samples in the top and bottom sections of the settled samples, respectively. In the top section of the settled samples, only red fibres gave a measurable increase in vane shear strength (see Figure 9), while in the bottom section of the settled samples both fibres gave a measurable increase in vane shear strength, with the red fibres being most effective (see Figure 10). The increase in peak vane shear strength increases with increasing fibre content.

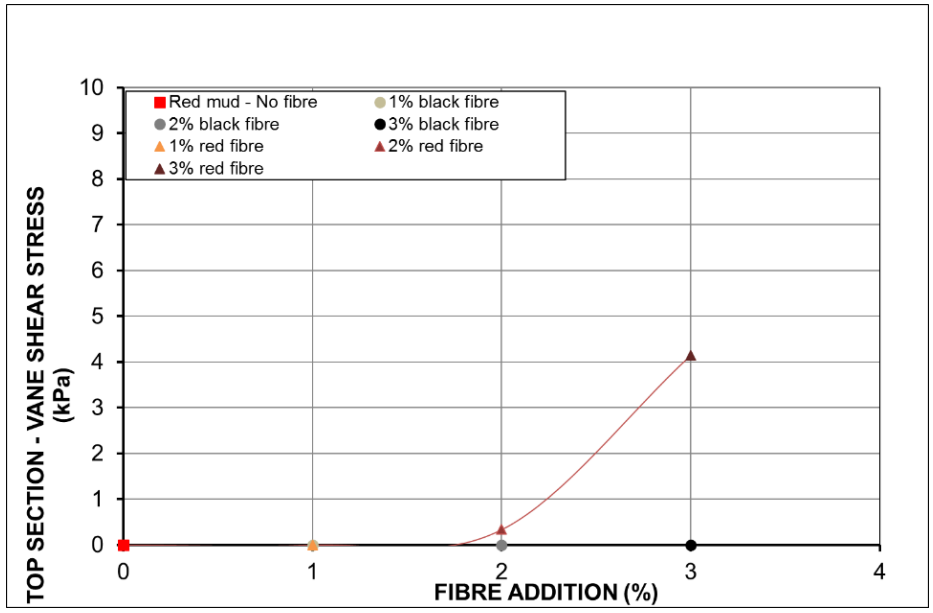

Figure 9. Peak vane shear strength in top section of settled red mud without and with fibres.

3.3 *Desiccation tests*

Figure 11 and 12 show, respectively, the desiccation behavior over 1 month of the red mud without and with 1% black fibre addition, in terms of cumulative evaporation, evaporation rate, degree of saturation and matric suction. For both tests, the initial evaporation rate from the wet samples was high. As evaporation continues, the moisture content (degree of saturation) decreases and the matric suction increases. This leads to the decrease of evaporation rate as the permeability drops, with the evaporation rate dropping to almost zero at the end of the tests. The cumulative evaporation after 1 month was about 45 mm.

Although the desiccation behaviors of the samples without and with 1% black fibre addition appear to be similar, a slight increase of evaporation rate is observed without fibres between 10 days and 15 days, which is likely induced by cracking of the surface, enlarging the area exposed to desiccation. This slight increase in evaporation rate is not observed for the sample with the black fibres added, since the fibres inhibit cracking.

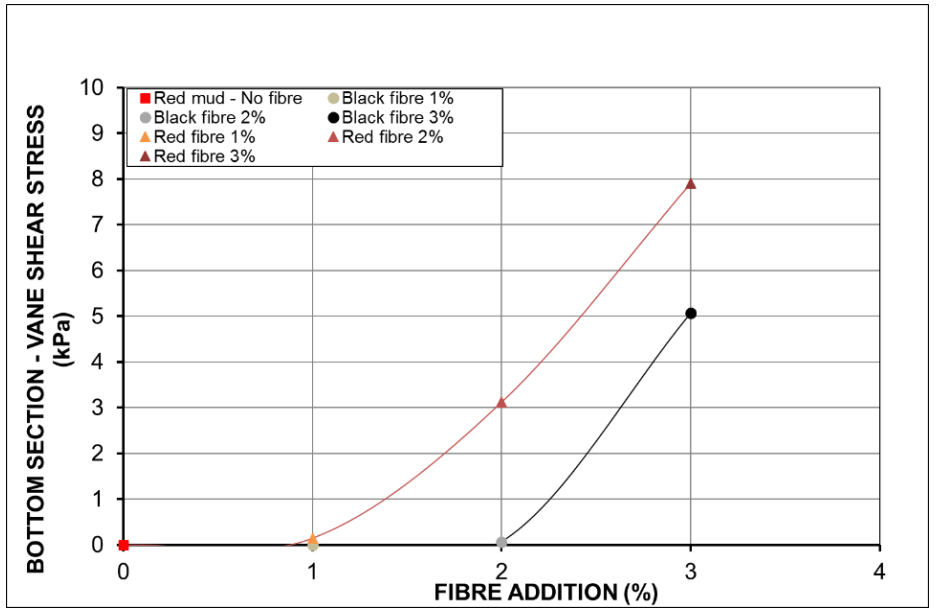

Figure 10. Peak vane shear strength in bottom section of settled red mud without and with fibres.

4 DISCUSSION AND CONCLUSIONS

The addition of plastic fibres can enhance tailings by increasing their shear strength and increasing their permeability. The results of settling tests indicated that the addition of black fibres enhanced the settling of red mud, reducing the required settling time and increasing the settled dry density, while the addition of red fibres had a negative effect on settling of the red mud. The vane shear tests indicated that fibre addition increases the shear strength of the red mud, which is otherwise negligible. The red fibres were more effective than the black fibres in increasing the shear strength of the red mud. The addition of 1% black fibres to red mud inhibits cracking, and slows the rate of desiccation and loss of permeability of the red mud, leading to a more uniform and uncracked mass.

The results of this study suggest the need for further research. The length, shape, specific gravity, stiffness and strength of the fibres may affect their potential to enhance the geotechnical parameters and behavior of red mud and other tailings. It is also necessary to investigate feasible means of introducing plastic fibres into tailings in the field, given that their low specific gravity will likely cause them to float, and progress down the tailings beach to the decant pond. As a result, fibres could not simply be added to the tailings discharge, and would need to be introduced mechanically, possibly from an amphirol, to settled tailings as they start to desiccate.

5 ACKNOWLEDGEMENT

Queensland Alumina Limited is acknowledged for allowing this research study to be done on red mud samples found on their premises. TEXO ReoCo is gratefully acknowledged for providing the two types of fibres used in this study.

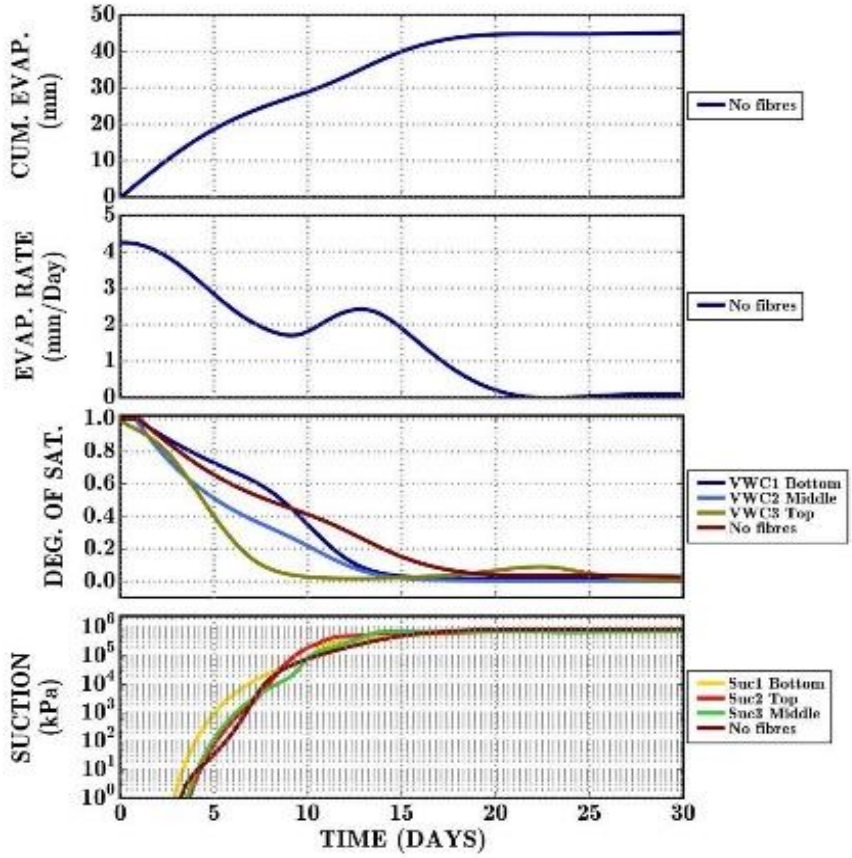

Figure 11. Desiccation of red mud with no fibres.

6 REFERENCES

Bowker, L.N.C. and David, M. 2015. The risk, public liability, and economics of tailings storage facility failures. Retrieved from *http://www.csp2.org/technical-reports;www.csp2.org/technical-reports*.

Consoli, N.C., Prietto, P.D.M. and Ulbrich, L.A. 1999. The behaviour of a fibre-reinforced cemented soil. *Ground Improvement*, 3(1), 21-30.

ICOLD. 2011. *Bulletin 139: Improving Tailings Dam Safety – Critical Aspects of Management, Design, Operation and Closure*. International Committee on Large Dams.

Li, Z. and Shi, Z. 2014. Comparative experiment on concrete performance of different kinds of polypropylene fibre. *Engineering Science and Technology*, 14 (31), 292-296.

Sofrà, F. and Boger, D. V. 2011. Rheology for thickened tailings and paste — history, state-of-the-art and future directions. *Proceedings of the 14th International Seminar on Paste and Thickened Tailings, Perth, Australia, 5-7 April 2011*, 121-133.

Quintero Olaya S., W.D.J., Durante Ingunza M.P. and Serati, M. 2017. Geotechnical characterisation of neutralised red mud for use in civil engineering construction and manufacturing. *Proceedings of the 32nd International Conference on Solid Waste Technology and Management, Philadelphia, USA, 19-22 March 2017*, 9 pp.

Williams, D.J. 2015. *Chapter 2 Placing Soil Covers on Soft Mine Tailings*. Elsevier.
Williams, D.J. 2016. *Gold Ore Processing, Chapter 37 Tailings Storage Facilities.*
Williams, D.J. and Zhang, C. 2017. A suite of tests for designing slurried tailings deposition. *Proceedings of the 4th International Seminar on Tailings Management, Santiago, Chile, 12-14 July 2017*, 9 pp.
Yilmaz, E. and Fall, M. 2017. *Paste Tailings Management*. Springer.
Zhang, C., Lei, X., Quintero Olaya, S. and Williams, D.J. 2019. Instrumented column testing of settling, consolidation and desiccation of coal tailings slurry under ambient weather conditions. *Proceedings of the 2019 ANZ Geomechanics Conference, Perth, Australia, 1-3 April 2019*, 5 pp.

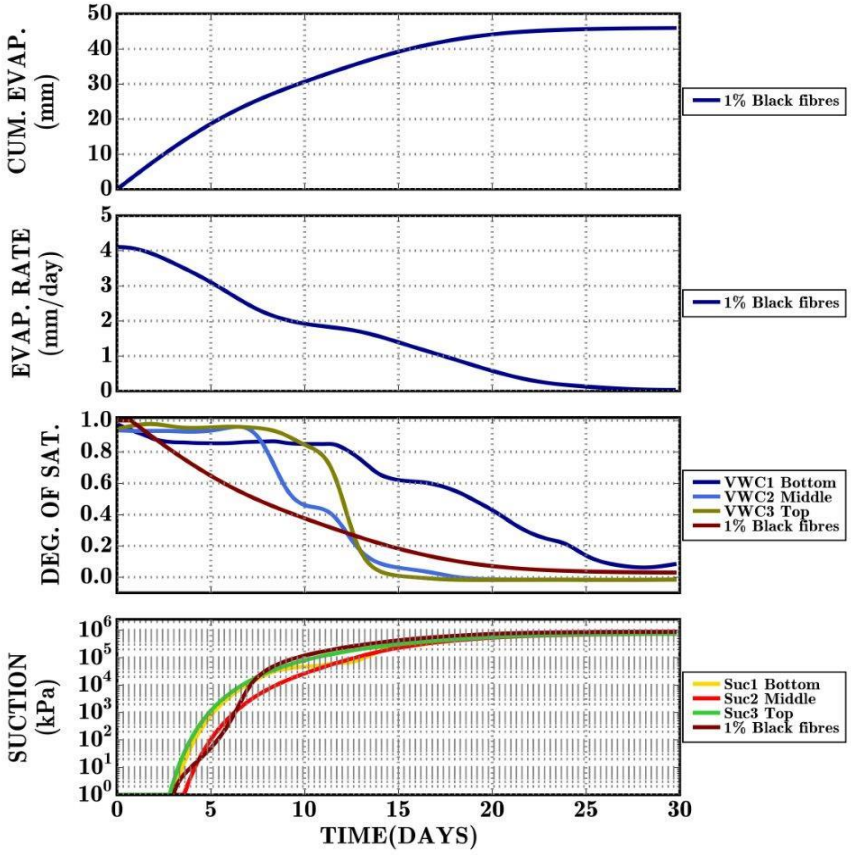

Figure 12. Desiccation of red mud with 1% black fibres.

Specimens Size Effect on the Compressive Strength of Geopolymerized Mine Tailings

Nan Zhang
Colorado School of Mines, Golden, CO, USA
Ahmadreza Hedayat
Colorado School of Mines, Golden, CO, USA
Linda Figueroa
Colorado School of Mines, Golden, CO, USA
Héctor Gelber Bolaños Sosa
Universidad Nacional de San Agustín de Arequipa, Arequipa, Arequipa, Peru
Juan José González Cárdenas
Universidad Nacional de San Agustín de Arequipa, Arequipa, Arequipa, Peru
Guido Edgard Salas Álvarez
Universidad Nacional de San Agustín de Arequipa, Arequipa, Arequipa, Peru
Victor Benigno Ascuña Rivera
Universidad Nacional de San Agustín de Arequipa, Arequipa, Arequipa, Peru

ABSTRACT: Mine tailing (MT) with rich aluminosilicates can be successfully used for production of geopolymer via an alkaline activation process. As an alternative approach to the deposition of the mine waste, geopolymerization can be used to reuse the MTs for preparation of construction materials such as pavements, concrete, and bricks. Besides factors that influence the compressive strength of the geopolymer, such as Si: Al ratio, Si/Al: NaOH ratio, and solid/liquid ratio, the specimen size effect can also play a major role. However, the effects of the specimen size on the compressive strength, damage process, and failure mechanisms of geopolymerized tailings under unconfined compression have largely been unexplored. In this study, the influence of the specimen size on the compressive strength was investigated. Cubical specimens of geopolymerized tailings with dimensions of 80, 60, 50, 40, 30 mm were systematically tested. Three specimens were tested for each specimen size using the same preparation with equal compaction effort and water/mine tailing (W/MTs) ratio. A series of unconfined compression tests (UCT) of cubic specimens with different sizes was performed after 28 days. In addition to the compressive strength, the fracture and damage mechanisms of the geopolymer specimens were also analyzed. The compressive strength of the geopolymer was found to decrease monotonically with the increase in the specimen size for the selected W/MTs ratio by analyzing the stress-strain curves.

INTRODUCTION

Mining operations produce abundant amount of mine tailing (MTs) after extracting valuable elements during the ore beneficiation process. A significant amount of MTs is generated with the continuous mining operation. However, the disposal of MTs can result in significant environmental issues. Therefore, the handling of the MTs is critically important. Several approaches have been used to mitigate potential environmental consequences such as storing or reusing of the MTs . Typically, the MTs are stored in accordance with the phases, for instance waste slurries are deposited into impounding lakes and solid wastes are simply packed as waste piles (e.g., Kiventera et al., 2018). However, with the further processing of lower grade ores, there is an increased need for additional storage, resulting in more economic, social and environmental issues. Therefore, reuse of MTs is an option that can be environmentally sound and economically viable.

Some alternative approaches for the reuse of the MTs include the re-extraction of the metals, use as fertilizer, use for backfilling, use as road pavements and construction materials (e.g., Golik et al., 2015; Priyono 2005; Chen et al., 2016; Chu et al., 2018; Gayana and Chandar 2018; Zhang

et al., 2020). However, re-exacting metals from the MTs is costly and depends on the quantities of the chemical components. The reuse as fertilizer depends on the specific components and chemical ingredients. The use of MTs directly as backfilling and pavement materials may result in metal leaching to the environment. Sintering the MTs to make bricks is energy intensive because of high temperature requirements (e.g., 800°C) which is costly. Therefore, reusing MTs as the construction and building materials is a potentially cost-effective beneficiation approach. There are two different applications reported in the literature: biopolymerization (e.g., Chen et al. 2015; 2016) and geopolymerization (e.g., Kiventera et al., 2018; Tho-In et al., 2018). Biopolymerization is an eco-friendly technique; however, the product may not be strong enough to meet the mechanical requirements for construction (e.g., Chen et al., 2016). Geopolymerization is applicable when the MTs are rich in aluminosilicates. Geopolymerization is a chemical process that activates the aluminosilicates by alkaline solutions with various OH- molarities (e.g., Davidovits 1991; Singh et al., 2015; Tho-In et al., 2018). Common wastes, such as glass wastes, slag, and mine tailings (e.g., Singh et al., 2015) that are rich in Al_2O_3 and SiO_2 can be geopolymerized, forming the chemical bonds to connect silicates (SiO_4-) and aluminates (AlO_4-) with connecting bonds (-Si-O-Al-) that cement the granular or powder-like MTs.

MTs based geopolymers, which is the product of geopolymerization, have been successfully developed and evaluated by several researchers (e.g., Ahmari and Zhang 2012; Kuranchie et al., 2016; Kiventera et al., 2018). Geopolymer bricks and concrete are the two common types of geopolymerized products for building and construction materials. Geopolymer bricks are usually created with a high temperature (~800ºC) for a shorter time compared to sintering bricks (Zhao and Sanjayan 2011). Geopolymer concrete only needs a slightly elevated temperature to accelerate the chemical reaction. The unconfined compressive strength (UCS) of geopolymerized MTs is an important property for construction applications. The UCS is influenced by the molar concentration of NaOH used for geopolymerization. The NaOH molar concentration typical ranges from 2M to 15M, and the UCS values can be as high as 30MPa (e.g., Zhang et al., 2020). Geopolymers with UCS larger than 8.6MPa can be used as bricks for buildings subjected to negligible weathering conditions, and geopolymers with the UCS values greater than 17.2MPa can be used as the construction materials in low weathering condition (ASTM C62).

Geopolymerized tailings are typically needed for construction purposes in a variety of sizes, similar to cementitious materials. The compressive strength values typically decrease with the increase of the specimen size (e.g., Bazant 1984; del Viso 2008; Rangari et al., 2018). In this study, the effect of specimen size on the compressive strength of geopolymers was investigated. Cubic geopolymer specimens with five different sizes,80, 60, 50, 40, 30 mm in height/width/length, were produced with a constant NaOH molarity. In addition, the influence of specimen size on the crack pattern and failure behavior was examined in this study.

1 MATERIALS

The MTs used in the study are gold MTs sampled from Mollehuaca, Arequipa, Peru. The geotechnical, mineralogical, and chemical properties of the MTs needed prior to geopolymerization are summarized in the following sections.

1.1 *Geotechnical Characterization*

The geotechnical properties of the MTs were obtained by performing a series of laboratory tests. Sieve analysis, hydrometer analysis, Atterberg limits, and compaction tests were conducted following ASTM standards D6913, D7928, D4318, and D698, respectively. Figure 1 shows the grain size distribution obtained from sieve and hydrometer analyses. The median particle size was characterized as 0.076mm with 49.9% of the particles smaller than sieve #200. The coefficient of uniformity, $C_u = D_{60}/D_{10}$, of the MTs was obtained from the GSD curve as 32.33. The liquid limit is 23, the plasticity index is 10, and the soil activity is 0.196. The optimum moisture content is 15.4% by conducting compaction tests by using Harvard Miniature Compaction (HMC) apparatus. The HMC mold has the dimension of 33.4mm in diameter and 71.6mm in height The

MTs with various moisture contents were compacted by using a 90-Newton tamper to compact 5 layers with 25 times each layer using HMC mold (e.g., Scavuzzo 1984). Table 1 lists all the characterized geotechnical properties of the MTs.

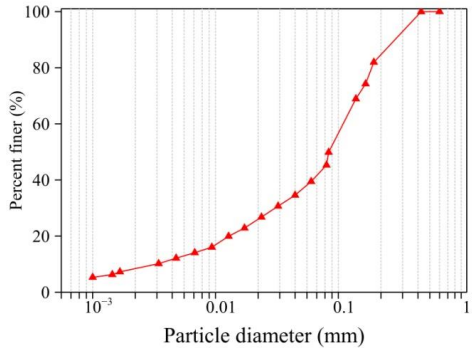

Figure 1. Grain size distribution of the MTs

Table 1. Geotechnical properties of the MTs

Properties	Value	Properties	Value
Specific gravity, G_s	2.750	D_{50}(mm)	0.076
Liquid Limit, *LL*	23	D_{60}(mm)	0.097
Plastic limit, *PL*	13	Pass #200 sieves, *F*(%)	49.9
Plasticity index, *PI*	10	Coefficient of uniformity, C_u	32.33
Soil activity, *A*	0.196	Coefficient of curvature, C_c	2.89
D_{10} (mm)	0.003	Optimum moisture content (%)	15.4
D_{30}(mm)	0.029	Maximum unit weight, γ_{max}(kN/m^3)	18.6

1.2 *Mineral and Chemical Characterization*

The mineral compositions were characterized by performing X-ray powder diffraction (XRD) analysis. For XRD analysis, the finer the powder, the more accurate the XRD pattern. Therefore, the dried MTs with particle size smaller than #30 sieves (0.595mm) were selected and scanned to avoid the aggregates within the MTs. The XRD pattern is shown in Figure 2. Different minerals had different crystalline/amorphous characteristics and thus different reflection patterns. The crystalline/amorphous phases were then identified and quantified by matching the crystalline phases to the database. Three major minerals identified were: Quartz (SiO_2), Muscovite ($(KF)_2(Al_2O_3)_3(SiO_2)_6$), and Calcite ($CaCO_3$), which had the mass percentage of 77.70%, 14.30%, and 4.20%, respectively. Among these minerals, the quartz and muscovites were identified as the dominant minerals, and the MTs were characterized as rich in aluminosilicate.

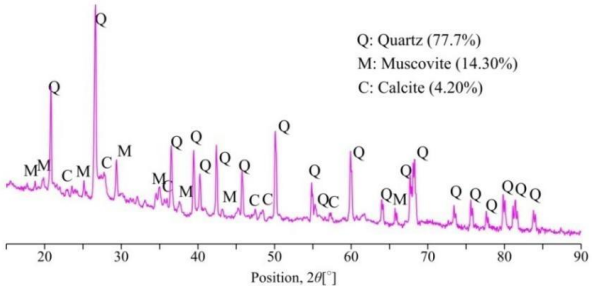

Figure 2. XRD pattern of the MTs

The chemical compositions of the MTs were characterized by using a Hitachi TM1000 Scanning Electron Microscopy Dispersive X-Ray Spectroscopy (SEM/EDS). The electron microscopy images were taken by SEM, and the chemical elements were obtained through use of EDS analysis of the same field of view as the images. Si, Al, and Fe were identified as the three major elements within the MTs. The Si to Al ratio was identified as 2.55, which falls in the range of 1 and 5, as suggested by Ahmari and Zhang (2013) for the successful geopolymerization.

2 GEOPOLYMERIZATION AND LABORATORY TESTING

2.1 *Geopolymer preparation procedure*

The MTs used in this study were reported to be successfully geopolymerized via alkaline activation (e.g., Zhang et al., 2020). In the study, NaOH solution was selected as the alkaline to activate the MTs. The steps to make geopolymer were as follows:

1. The NaOH solutions were made by mixing the NaOH pellets (purity 98%, Fisher Chemical) with water with regard to the different NaOH molarities.
2. The solutions were then stayed in the room for 15 minutes for cooling.
3. The MTs and NaOH solution were well mixed in a pan and stayed for 30 minutes to ensure the homogeneity of the geopolymer paste.
4. The geopolymer pastes were made by using the steel cubic molds following ASTM standard (ASTM C106) with the cubic dimensions of 80, 60, 50, 40, and 30 mm. During the casting, a 90-Newton tamper was used to compact the geopolymer specimen in 3 layers. The tamping number of each layer was calculated such that the tampering number per unit cross-section area was constant, such that the compacting times for each layer were 183, 103, 71, 46, and 26 times, respectively. The W/MTs ratio was kept at approximately 13%.
5. The geopolymer cast in the steel mold was then covered with a plastic wrap to stop the water from evaporation, and then placed into the oven with an elevated temperature of 75ºC for 24 hours. Then, the geopolymer specimens were demolded and placed in the ambient temperature (~22ºC) for 28 days. The elevated temperature was used to accelerate the geopolymerization. After 28 days curing, the geopolymer specimens were placed in the oven with the temperature of 75ºC without the plastic wrap for drying for 24 hours prior to testing. The geopolymer MT specimens are shown in Figure 4.

The experimental program was designed to study the specimen size effect on the mechanical behavior of the geopolymerized MTs. The geopolymer specimens were prepared in cubical shape, as shown in Figure 3, with the dimensions of 80, 60, 50, 40, and 30mm, respectively. The cubic molds used for casting were printed using 3D printer by using polylactic acid (PLA) biodegradable

filament with the thickness of 6-10mm except for C3.the molds were stiff enough to avoid the surface deflections during compaction. Three cubic specimens were made for each size following ASTM C106 standard. The W/MT ratio selected in the study were determined as approximately equal to 13%.

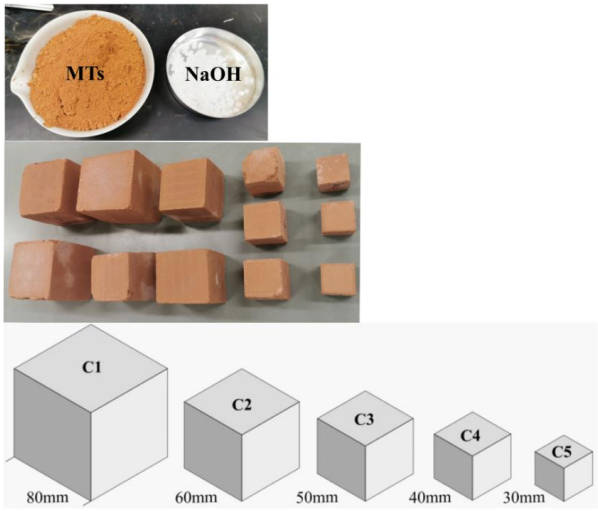

Figure 3. Geopolymer specimens

2.2 *Uniaxial compression tests*

The influence of the specimen size effects on the compressive strength behavior of the geopolymer was investigated by performing the UCT following ASTM C109 standard. All the geopolymer specimens were tested after 28 days. During the testing, the geopolymer cubes were placed between two aluminum plates. The displacement control was used in the UCT for all the specimens with the same strain rate, $\dot{\epsilon} = \dot{\delta}/L$, as shown in Table 2.

Table 2. Loading rate of the specimens

Specimen	Size, L (mm)	Loading rate (mm/min)
C1	80	0.36
C2	60	0.27
C3	50	0.22
C4	40	0.18
C5	30	0.13

3 RESULTS AND DISCUSSIONS

3.1 *Uniaxial compression test results*

The axial (compressive) stress as a function of the axial strain for different specimen sizes are shown in Figure 4. The x-axis represents the axial strain, which is the axial displacement divided by the undeformed height of the specimen. The vertical axis is the axial stress, which is defined as the axial force divided by the cross-section area of the geopolymer specimen. For the same

W/MTs ratio and NaOH molarity, the maximum stress was found to decrease with the increase in the specimen size (e.g., Bazant 1984; Yi et al., 2006; del Viso et al. 2008; Nikbin et al., 2014). The stress-strain curve showed a linear increase in stress as a function of strain after the initial seating deformation of the specimen followed by the strain softening. The geopolymer specimen with the largest size was found to have the lowest compressive strength value. That is because during the uniaxial compression of the geopolymer, the axial loading leads to the damage in the form of splitting microcracks that engenders from pores. The damage results in bands that can propagate either axially or laterally. The linear portion has a similar initial slope for different specimen sizes. However, there were slope losses prior to reaching the peak stress value (e.g., del Viso et al. 2008). The post-peak responses did not show a steep softening, which was potentially due to the volumetric energy dissipation as reported by del Viso et al., (2008), that the energies started to release due to the spalling. In addition, further energy was dissipated as a result of the ongoing deformation of the cube cores.

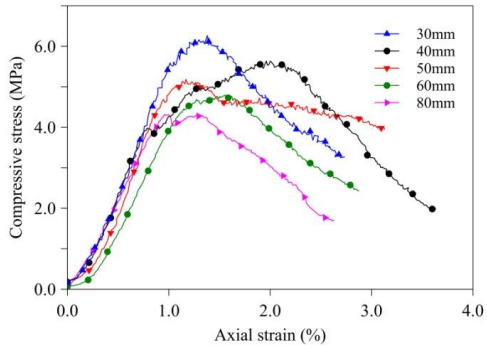

Figure 4. Stress-strain relationships of the geopolymer specimen for different sizes

Table 2 lists the mean UCS value along with the standard deviation for the different specimen sizes. σ_c and ε_c represent the UCS and failure strain, respectively. The compressive strength of the geopolymer decreased noticeably with the increases of specimen sizes. Table 2 shows that the stress and strain values at failure generally increased with an increase in the specimen size.

Table 2. Compressive strength and the corresponding failure strain

Specimen		σ_c(MPa)	ε_c (%)	Numbers.
C1	Mean	4.13	1.22	3
	Std.dev	0.30	0.03	
C2	Mean	5.80	1.60	3
	Std.dev	0.57	0.26	
C3	Mean	4.97	3.81	3
	Std.dev	0.93	3.18	
C4	Mean	6.01	1.95	3
	Std.dev	0.4	0.22	
C5	Mean	6.36	1.93	3
	Std.dev	0.29	1.06	

Figure 5 compares the normalized compressive stress as a function of the normalized axial strain for geopolymer specimens with different sizes when the peak point was considered as the

reference point for each specimen, that the stresses were normalized by the corresponded peak value and the axial strains were normalized by the corresponding axial strain value at failure. The results show great similarities in terms of the relation of the stiffness at pre-peak stage for all specimen sizes, indicating that the stress and strain values at the peak point were the main variables with the different specimen sizes.

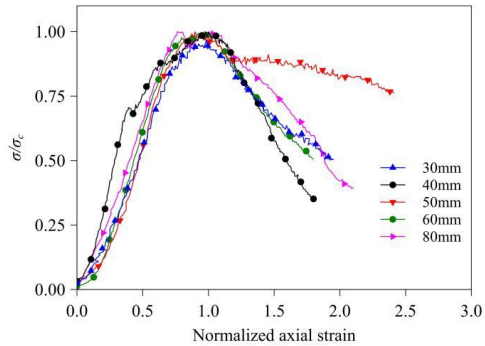

Figure 5. Relative stress versus axial strain for different sizes

Figure 6 shows the specimen size effect on the compression strength. The compressive strength for different sizes decreased noticeably with the increase of size. The error bars of each point indicate the standard deviations of the compressive strength for each set. The compressive strength of the geopolymer specimens C5 (L = 30mm) was almost twice that of the C1 (L=80 mm) specimen.

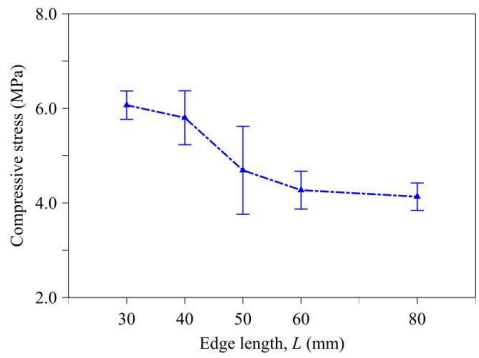

Figure 6. Size effects on the compressive strength

The failure pattern observed in Figure 7 was not found to be sensitive to the size of the specimens. Under uniaxial compression, most of the cubic geopolymer specimens were found to split with penetrating cracks from upper to lower surface at first. following that the specimen sides experienced spalling. The remaining cube cores were fragmented with respect to the compression and crushing. With the ongoing compression, the stress state inside the cubic cores may end-up forming column-like cracking and shear bands (C5 shown in Figure 7). The shear band observed from C5 resulted from the further axial displacing of the cube cores after spalling.

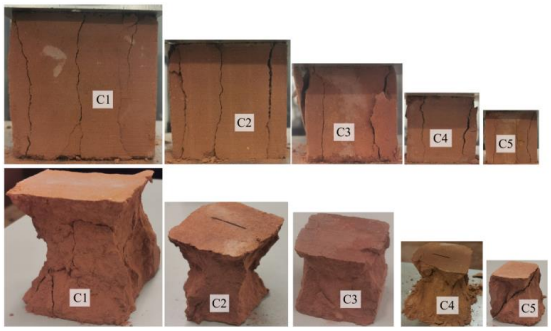

Figure 7. Crack pattern of the geopolymer specimens for different sizes

4 CONCLUSIONS

The influence of the specimen size on the compressive behavior of the MTs-based geopolymer was investigated in this study. Geopolymer specimens with five different sizes were considered. Results show that the stress-strain relationships for all specimen sizes were found to start with a linear ramp up for all the specimen sizes with a similar slope, indicating that the influence of specimen size on the tangential stiffness of the geopolymerized MTs is negligible. The compressive strength of the geopolymer was found to decrease with the increase in the specimen size. The compressive strength for the smallest specimen size was almost twice that of the largest specimen. The strain at failure generally increased with the increase in the specimen size.

The failure pattern of the cubic specimens initially consisted of splitting cracks followed by spalling of the specimen with the further compression. The further compression of the geopolymer specimens might end up with the crushed failure of cubic cores or even the emergence of shear band.

ACKNOWLEDGEMENT

The financial support provided by the Universidad Nacional de San Agustín (UNSA) through the joint Center for Mining Sustainability with the Colorado School of Mines is highly acknowledged.

REFERENCE

Ahmari, S., and Zhang, L. 2012. Production of eco-friendly bricks from copper mine tailings through geopolymerization. Construction and building materials, 29: 323-331.

Ahmari, S., and Zhang, L. 2013. Durability and leaching behavior of mine tailings-based geopolymer bricks.Construction and building materials,44: 743-750.

Bažant, Z. P. 1984. Size effect in blunt fracture: concrete, rock, metal. Journal of engineering mechanics, 110(4), 518-535.

Chen, R., Ding, X., Ramey, D., Lee, I., and Zhang, L. 2016. Experimental and numerical investigation into surface strength of mine tailings after biopolymer stabilization. Acta Geotechnica, 11(5), 1075-1085.

Chen, R., Lee, I., and Zhang, L. 2015. Biopolymer stabilization of mine tailings for dust control. Journal of Geotechnical and Geoenvironmental Engineering, 141(2), 04014100.

Chu, C., Deng, Y., Zhou, A., Feng, Q., Ye, H., and Zha, F. 2018. Backfilling performance of mixtures of dredged river sediment and iron tailing slag stabilized by calcium carbide slag in mine goaf. Construction and Building Materials, 189, 849-856.

Davidovits, J. 1991. Geopolymers: inorganic polymeric new materials. Journal of Thermal Analysis and calorimetry, 37(8), 1633-1656.

Del Viso, J. R., Carmona, J. R., and Ruiz, G. 2008. Shape and size effects on the compressive strength of high-strength concrete. Cement and Concrete Research, 38(3), 386-395.

Gayana, B. C., and Chandar, K. R. 2018. Sustainable use of mine waste and tailings with suitable admixture as aggregates in concrete pavements-A review. Advances in concrete construction, 6(3), 221.

Golik, V., Komashchenko, V., and Morkun, V. 2015. Innovative technologies of metal extraction from the ore processing mill tailings and their integrated use. Metallurgical and Mining Industry, 3, 49-52.

Guo, B., Liu, B., Volinsky, A. A., Fincan, M., Du, J., and Zhang, S. 2017. Immobilization mechanism of Pb in fly ash-based geopolymer. Construction and Building Materials, 134: 123-130.

Kiventerä, J., Lancellotti, I., Catauro, M., Dal Poggetto, F., Leonelli, C., and Illikainen, M. 2018. Alkali activation as new option for gold mine tailings inertization. Journal of cleaner production, 187: 76-84.

Kuranchie, F. A., Shukla, S. K., and Habibi, D. 2016. Utilisation of iron ore mine tailings for the production of geopolymer bricks. International Journal of Mining, Reclamation and Environment, 30(2), 92-114.

Nikbin, I. M., Dehestani, M., Beygi, M. H. A., and Rezvani, M. 2014. Effects of cube size and placement direction on compressive strength of self-consolidating concrete. Construction and Building Materials, 59, 144-150.

Rangari, S., Murali, K., and Deb, A. 2018. Effect of meso-structure on strength and size effect in concrete under compression. Engineering Fracture Mechanics, 195, 162-185.

Scavuzzo, R. 1984. *Use of the Harvard Miniature Apparatus for obtaining moisture-unit weight relationships of soils*. Geotechnical Branch, Division of Research and Laboratory Services, Engineering and Research Center.

Singh, B., Ishwarya, G., Gupta, M., and Bhattacharyya, S. K. 2015. Geopolymer concrete: A review of some recent developments. Construction and building materials, 85: 78-90.

Tho-In, T., Sata, V., Boonserm, K., and Chindaprasirt, P. 2018. Compressive strength and microstructure analysis of geopolymer paste using waste glass powder and fly ash. Journal of Cleaner Production, 172: 2892-2898.

Yi, S. T., Yang, E. I., and Choi, J. C. 2006. Effect of specimen sizes, specimen shapes, and placement directions on compressive strength of concrete. Nuclear Engineering and Design, 236(2), 115-127.

Zhang, N., Hedayat, A., Bolaños Sosa, H.G., González Cárdenas, J.J., Salas Álvarez, G.E., Ascuña Rivera, V., and González, J. 2020. Fracture and Failure Processes of Geopolymerized Mine Tailings under Uniaxial Compression. 54th US Rock Mechanics/Geomechanics Symposium, Golden, CO, USA

Zhang, Z., Provis, J. L., Reid, A., and Wang, H. 2014. Geopolymer foam concrete: An emerging material for sustainable construction. Construction and Building Materials, 56: 113-127.

Zhao, R., and Sanjayan, J. G. 2011. Geopolymer and Portland cement concretes in simulated fire. Magazine of Concrete research, 63(3), 163-173.

A Rapid Measurement Method to Determine Hydraulic Conductivity of Tailings Under Self-Weight Consolidation

Yagmur Babaoglu
Carleton University, Ottawa, ON, Canada

Paul H. Simms
Carleton University, Ottawa, ON, Canada

ABSTRACT: The hydraulic conductivity-void ratio relationship dominates the long-term behaviour of tailing impoundments and reclamation plans of mineral slurries. A new laboratory test column is introduced to evaluate the k-e relationship using the Instantaneous Profiling method (IPM). The theory evaluates the "instantaneous depth profiles" of pore water pressures and water content in a column setup to directly determine the k-e values with space and time. The column is equipped with multiple pore-water pressure sensors and capacitance-based volumetric water content sensors. The large strain consolidation behaviour of two tailings, a gold tailings and a flocculated fluid fine tailings was investigated, and the application of the IPM method is explored. Accuracy of the technique is confirmed by comparison with hydraulic conductivity values obtained by conventional measurement techniques. However, the relatively rich data set illustrates other phenomena in the two tailings not detectable by coarser measurements of *k-e*.

1 INTRODUCTION

The consolidation characteristics of tailings, particularly the hydraulic conductivity – void ratio function (*k-e*), governs the rate of settlement and densification in any tailings impoundment. Well-established methods exist to determine *k-e*, such as the large strain consolidation test or the seepage induced consolidation test, which involve a direct measurement of *k* at fixed void ratio and stresses, or column tests which are analyzed through back-calculation methods to arrive at a *k-e* function. The two first tests may take considerable time, months in the case of clayey tailings, while the latter are subject to various assumptions, such as the form of the *k-e* function, and assumptions as to the uniqueness of the compressibility function, for example. There are well-known procedures to back-calculate *k-e* from column tests (Abu-Hejleh and Znidarcic 1996, Pane and Schiffman 1997), which take advantage of special characteristics, such as the initial slope of the height versus time curve and the hydraulic conductivity at the surface (Been and Sills 1981). Recent proposed techniques for estimating *k-e* use special characteristics of the full settlement curve (Qi and Simms 2019, Qi et al. 2020), though they still presume certain forms for the *k-e* and compressibility functions. The power equation describes many if not most measured data sets of *k-e* (Babaoglu and Simms 2020), however, some data sets do suggest or more complex behaviour at high void ratios. Therefore, there is a need for more rapid and accurate measurements of k-e especially at high void ratio.

This study describes calculating the *k-e* relationship using the "Instantaneous Profiling Method" or IPM (Watson 1966), in a specially fabricated column. IPM requires high resolution of water content in space and time to calculate fluxes, and then calculates hydraulic conductivity directly from Darcy's law using measured head profiles. For the case of soft soils, the resolution of the measurements in time and space must be sufficient to ensure small-strain conditions. Similar researches have been conducted using the IPM method such as Leung et al. (2016), Askarinejad et al. (2012), Dikinya (2005), Fisher et al. (2008), while similar approaches have been used in slurry consolidation tests (Bartholomeeusen et al. 2002), though at relatively low

resolution. An advantage of this technique is that the computed hydraulic conductivity is independent of the compressibility curve, which may shift during consolidation at low stresses (Howlader et al. 2008). This paper presents a specialized column test designed to allow for nondestructive measurements of volumetric water content profiles and an automation system to allow for detailed profiling using capacitance-based sensors. Here we present data on tests on two different types of tailings, a gold tailings and a polymer flocculated oil sands fluid fine tailings (fFFT). *K-e* measurements obtained by IPM are compared with independent measurements, and the column data is also analyzed using a large strain consolidation software using the measured *k-e* and compressibility curves.

1.1 *Instantaneous Profiling Method (IPM)*

Originally proposed by Watson (1966), IPM uses the instantaneous profiles of macroscopic flow velocity and pore water pressure measurements to determine the permeability of the soil. The theory is based on Darcy's law and the derived relationships demonstrates proportionality between the instantaneous flow velocity and the corresponding potential gradient as shown in Equation 1.

$$\frac{\partial \theta}{\partial t} = K \frac{\partial^2 h}{\partial z^2} \tag{1}$$

Where θ is the volumetric water content, K is the hydraulic conductivity, h is the total potential (can be calculated by adding the total pore water pressure and hydraulic head) and z is the height above datum. Equation 1 allows for a fast, simultaneous, and non-destructive determination of permeability equation for soils, where the k values can be calculated at any time and depth. However, Eq. 1 is also based on a flow through a constant volume of soil. For slurry tailings, where the density changes in saturated conditions, reformulation of the equation into constant volume of solids would be more appropriate (Fox and Baxter 1997). A reformulated version of Equation 1 using the central scheme is presented in Equation 2.

$$\frac{\left(\frac{e_{t1}}{1+e_{t1}}\right) - \left(\frac{e_{t3}}{1+e_{t3}}\right)}{t_3 - t_1} = K \frac{h_1 - 2h_2 + h_3}{\Delta z^2} \tag{2}$$

The component z in Equation 2 should ideally be the height or thickness of solids under large strain conditions, and can be determined from the distribution of void ratio with depth over time. However, this can be ignored if the local strain is small over the time step. or in other words, if the resolution of the data is sufficient, then Equation 2 can be calculated as per small strain theory.

The method is independent of any assumptions with respect to dewatering mechanisms, i.e. sedimentation, consolidation, creep or thixotropy, which is one of the biggest advantages of the method compared to inverse modelling of column tests. However, for the successful implementation of the IPM method, the water content and pore water pressure profiles within the column need to be monitored comprehensively. High resolution density or water content measurements are essential for the application and the determination of this detailed profiles became the major challenge in the design process of the apparatus. The pore water pressure distributions are generally better constrained and can be interpolated based on experience of previous tests (e.g. Bartholomeeusen et al. 2002) using an adequate number of pore-water pressure sensors.

1.2 *Self-weight Consolidation Column Design*

The column is presented in Figure 1. It is 0.60 m high and has an inner diameter of 0.305 m (fabricated to 12 inches). There is a small column located (diameter 0.058 m or 2 inches) which accommodates the water content sensors. The column has 10 inlets at various locations to accommodate miniature pore-water pressure sensors (T5 from UMS), which are used to measure pore water pressures during the experiments. It might be necessary to point out that depending on

the thickness of the sample, the number of available inlets change; hence not all ten inlets are available for the tests.

For the high-resolution measurement profiles of water contents, capacitance-based sensors were selected after consideration of a range of ultrasonic and electromagnetic based techniques. These sensors are designed for long term continuous measurements and can measure the volumetric water contents non-intrusively, as contact of the sensors with the soil or tailings is not required. These sensing mechanisms can be targeted to water, as opposed to salinity or other possible interferences, by tuning of the excitation frequency. The sensors move up and down in the inner column in Figure 1. This inner column is connected to the bottom of the large column using a metal connection plate with multiple O-rings to eliminate possible water leakage in the pipe. The diameter and height of the column was selected based on a series of experiments investigating the potential for sidewall effects.

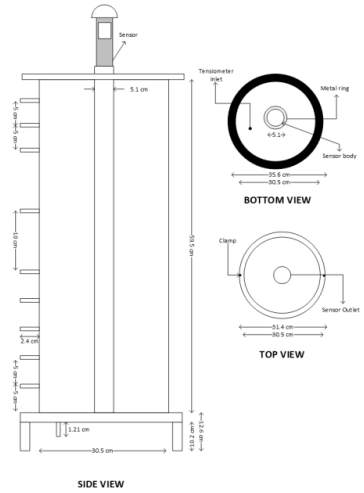

Figure 1: The schematics of the self-weight consolidation column

The VWC sensors (made by ENVIROSCAN, customized for the size of the inner column) are designed to obtain measurements along a ten-centimeter length; therefore, for more detailed profiling, a vertical motion of the sensor body is required. The first author designed an automation system for the movement which consists of a motor (12 V DC linear actuator is selected), Arduino board and multiple parts for the electronics design (such as relay modules to control the retraction of the actuator, connectivity relays for voltage compatibility). Arduino open-source software (Arduino 2015) controlled the whole system in this application. The water cotent sensor suite was programmed to take measurements at every 2 cm for the thickened gold tailings test and at every centimeter for the fFFT experiment.

Each sensor requires its own calibration, and is sensitive to small changes in the geometry of the inner tube. Therefore, the sensors are calibrated at each depth by collecting samples (and determined the water content by oven-drying) at the beginning and at the end of the experiment. As the sensors cannot directly measure the soil at the mudline directly, water contents close to the mudline are found algorithmically, through knowledge of how the readings progressively change as the sensor moves from the surface water into the tailings. The settlements during the experiments are observed using high-resolution cameras.

1.3 *The Properties of Tailings and Initial Conditions*

The geotechnical properties of the tailings, the initial and the final conditions of the two experiments are presented in Table 1. The solids content of conventional gold tailings is around 50% whereas this number can go up to 70% with the thickening technologies whereas for slurry

fluid fine tailings the initial solids content varies from 30-35% (Beier et al. 2013; Thomas 2015). The specifc gravity was determined according to the ASTM standard.

Table 1. Geotechnical Properties of Tailings and Initial conditions of the experiment

	Thickened Gold Tailings Test	**fFFT**
Initial VWC (%)	61	84
Initial GWC (%)	48	248
Initial Solids Content (%)	68	29
Initial e	1.55	5.25
Initial height (cm)	28	46
Final height (cm)	22.3	33.7
Specific Gravity	3.2	2.12
Miniature pressure sensor positions in the column (from bottom to top)	5-15-20	5-15-20-25-35
Test Duration (days)	1 day	25 days

The tailings wre shipped to Carleton University at a solids content of 68% for thickened gold tailings and 31% for untreated FFT sample. An anionic flocculant is utilized to prepare flocculated FFT at a specific dose.

2 RESULTS & DISCUSSION

The data collected by the PWP and water content sensors are shown in Figure 2, while the height data is shown in Figure 3. Final profiles of gravimetric water content with depth are extracted at the end of the test, which are used in the calibration exercise for the VWC sensors. The depth profile data is only shown for certain times. The volumetric water contents are measured at every 2 cm for the thickened gold tailings and at every 1 cm for the fFFT in the column.

The compressibility equation both experiments are calculated using two different methods; (I) from the final condition and (ii) by using the volumetric water content and pore water pressure measurements throughout the experiment, which are presented in Figure 4. Interestingly, the compressibility of the gold tailings seems relatively constant throughout the experiment, while it changes considerably for the fFFT. Particularly, while the compressibility seems to stabilize from Day 3 to 19, there is thereafter a substantial change in behaviour, which corresponds to additional dewatering occurring in the top half of the tailings (Figure 2).

The hydraulic conductivity value calculated by Equation (2), are shown in Figure 5. For comparison, previous studies (Qi et al. 2017) for the same gold tailings have reported $5 \times 10^{-6}\ e^{4}$, which is quite close to the best overall fit to the measured k values ($3.6 \times 10^{-6}\ e^{4}$). For the fFFT, independent measurements using a large strain consolidometer (Amoako et al. 2020) are shown. Additionally, Pane and Schiffman's equation is used to estimate hydraulic conductivity at the initial void ratio, which is shown on both figures. Finally, for the gold tailings, the hydraulic conductivity at the sedimentation-consolidation transition is estimated at this transition void ratio (~1.3), using the average gradient at and total flux through the tailings water interface. All this data suggests that the measured *k-e* values conform to the other estimates of hydraulic conductivity.

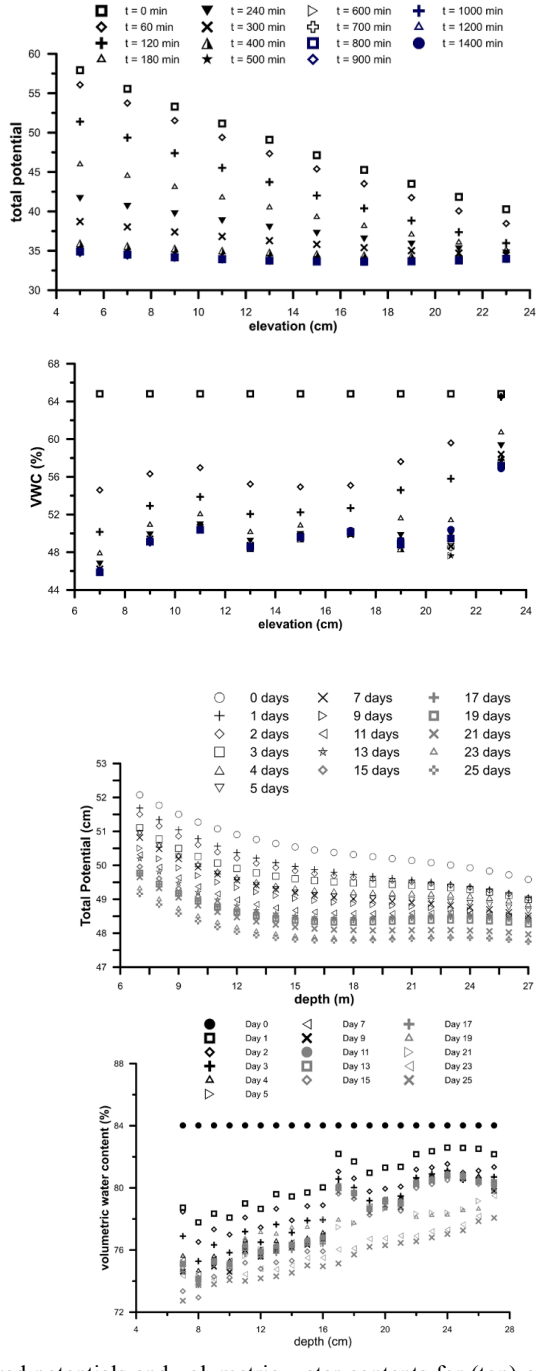

Figure 2: Measured potentials and volumetric water contents for (top) gold tailings (bottom) fFFT tailings

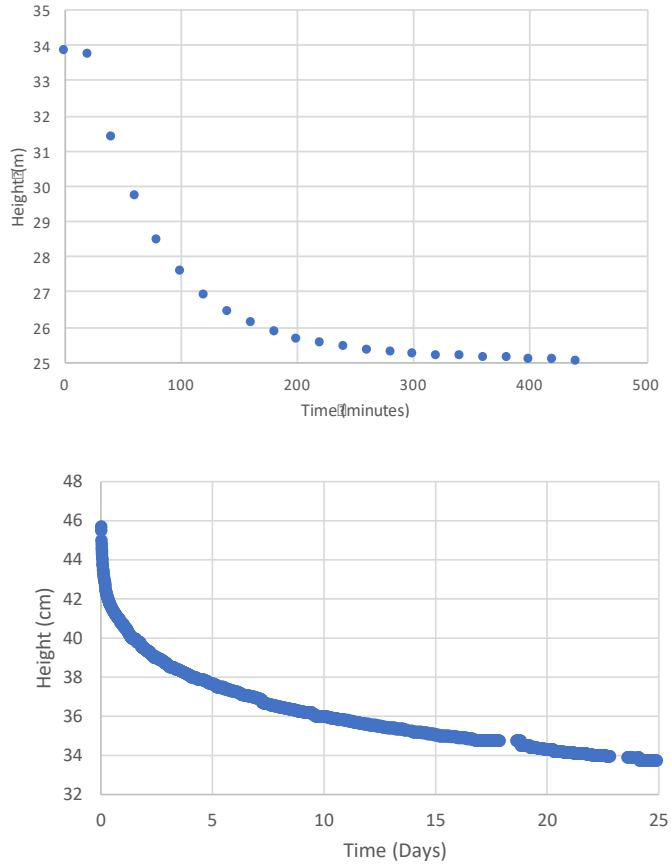

Figure 3: Settlement in the (top) thickened gold tailings (bottom) fFFT experiments

The compressibility equation for both experiments is calculated using two different methods; (i) from the final condition and (ii) by using the volumetric water content and pore water pressure measurements throughout the experiment, which is presented in Figure 4. Interestingly, the compressibility of the gold tailings seems relatively constant throughout the experiment, while it changes considerably for the fFFT. Particularly, while the compressibility seems to stabilize from Day 3 to 19, there is thereafter a substantial change in behaviour, which corresponds to additional dewatering occurring in the top half of the tailings (Figure 2).

The hydraulic conductivity value calculated by Equation (2), are shown in Figure 5. For comparison, previous studies (Qi et al. 2017) for the same gold tailings have reported 5 x 10^{-6} e^4, which is quite close to the best overall fit to the measured k values (3.6 x 10^{-6} e^4). For the fFFT, independent measurements using a large strain consolidometer (Amoako et al. 2020) are shown. Additionally, Pane and Schiffman's equation is used to estimate hydraulic conductivity at the initial void ratio, which is shown on both figures. Finally, for the gold tailings, the hydraulic conductivity at the sedimentation-consolidation transition is estimated at this transition void ratio (~1.3), using the average gradient at and total flux through the tailings water interface. All this data suggests that the measured *k-e* values conform to the other estimates of hydraulic conductivity.

Other interesting behaviours are apparent. In the gold tailings, there is an apparent delay during the first 20 minutes, where the settlement is much slower. This could be due to some dynamic effect due to deposition into the column, which was done quickly (within a minute), but also could be due to a real flocculation stage, where an increase in effective particle size would increase the rate of sedimentation. Also for the gold tailings, there is a divergence between the *k-e* values above and below the sedimentation threshold void ratio – the values at high void ratio are all calculated during the first 60 minutes, are so affected by the initial "slow settling" stage.

In the fFFT, the data generally lies somewhat above the trend through the LSC values. There, are, however, much data in tailings and other soft soils to suggest that hydraulic conductivity in the sedimentation phase can be different than during the consolidation phase – in fact, this is shown definitively for some other polymer-FFT mixtures (Amaoko et al. 2020). Finally, when modelling the height using a large strain consolidation software (UNSATCON, Qi et al. 2019, 2017), good agreement could only be achieved using two distinct power functions below and above the sedimentation- consolidation transition (Figure 6). This modelling is done using the compressibility curve fitted to the data between Day's 3 and 19.

As remarked earlier, there is also interesting behaviour at around Day 17. There is also a distinct plateau in the height behaviour between days 17 and 19, which is followed by a sharp decrease. This is reflected in the VWC data in the upper part of the tailings (Figure 2), which shows a sudden decrease after remaining mostly stable for 2 weeks. This is also present in the raw PWP data as shown in Figure 7 along with a blow up of the height data at that time. This second stage of dewatering is associated with the change in compressibility (Figure 3) at that time. Similar findings are reported in experiments in fFFT and centrifuge cake, looking at creep and ageing (Salam 2020).

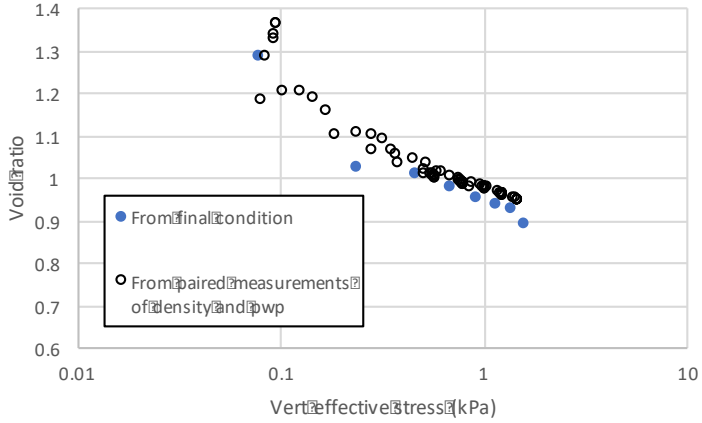

(i)

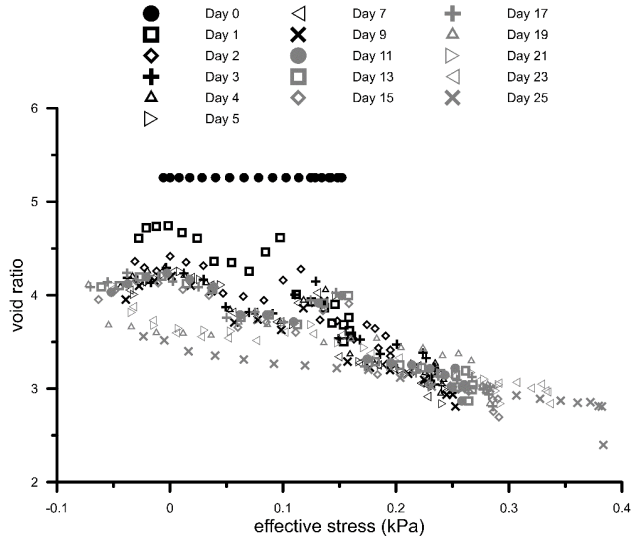

(ii)

Figure 4: The compressibility equation for (i) Gold Tailings, (ii) fFFT

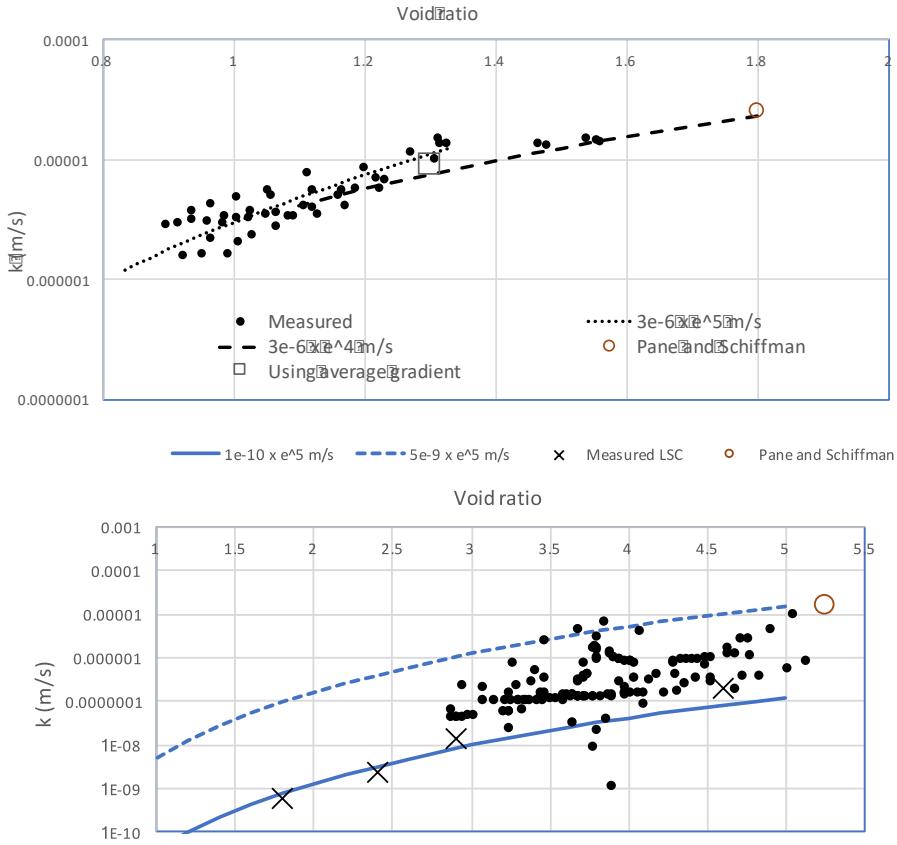

Figure 5: The *k-e* relationship for (top) Gold Tailings, (bottom) amended FFT tailings

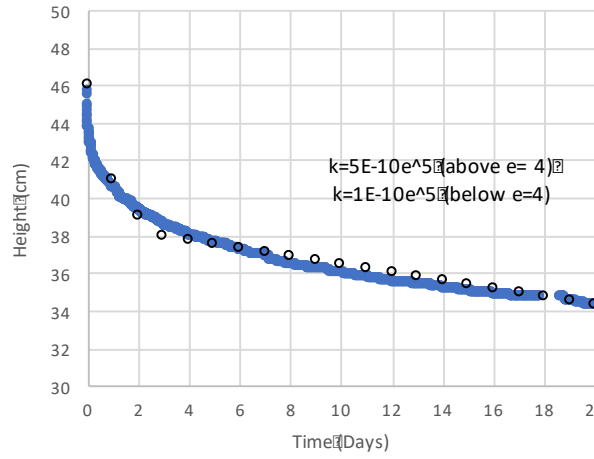

Figure 6. Modelling of the height data from the fFFT experiment, circles are model predictions.

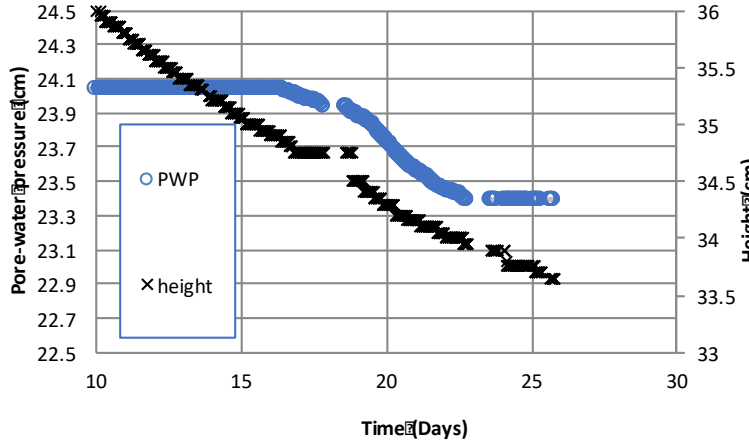

Figure 7. Pore-water pressure sensor at 25 cm elevation and tailings elevation in the fFFT experiment

3 LIMITATIONS

In terms of accuracy, there is still considerable scatter in the *k-e* data, especially for the fFFT. This is attributed to two reasons. In the fFFT, the choice of averaging time is important, especially at later stages in the experiment, when too small of an averaging time will mean the magnitude of fluxes approaches the resolution of the water content sensors, therefore the averaging times should be increased when fluxes become low. Second, aside from the resolution issue, the fluxes and PWP values seems robust, but the void ratio's themselves have some error associated with calibration. For example, calibration to the final gravimetric water content profile, or an ideal profile fitted using a compressibility curve function best fit to the final gravimetric water content profile, will change the calibration and produce some variation in the results. Using the presented data sets and other experimental results using the apparatus, the authors are developing a

procedure to minimize such errors. Even so, the accuracy of the results presented in this paper compares very well to *k-e* measured by other methods.

4 CONCLUSIONS

Column tests designed to calculate *k-e* for soft soils or tailings using the IPM method are presented. The IPM method provides estimate of *k-e* independent of the compressibility curve and from the assumed type of dewatering mechanism, or proscribed type of *k-e* function. The method requires high resolution of water content measurements. The employment of IPM in the particular column test described in this paper, yields measurements of *k-e* consistent with independent measurements in a gold tailings and in a flocculated fluid fine tailings. Additionally, the fineness of the data enables investigation of phenomena that are thought to affect consolidation at high void rations, such as the sedimentation-consolidation transition, creep, and ageing.

ACKNOWLEDGEMENTS

This work is supported by a Collaborative Research and Development Grant supported by the Natural Sciences and Engineering Research Council of Canada (NSERC) and Canada's Oil Sands Innovation Alliance (COSIA), awarded to the second author.

REFERENCES

Abu-Hejleh, A. N. and Znidarcic, D., 1996, Consolidation Characteristics of Phosphatic Clays, *ASCE Journal of Geotechnical Engineering,*122(4): 295-301.

Amoako, K., A. Abdulnabi, N. Beier, J. Soares, P. Simms 2020. Long-term Consolidation of Two New Polymer Treatments of Oil Sands Fluid Fine Tailings. GeoVirtual 2020 Canadian Geotechnical Conference, Calgary, Alberta, September 2020.

Arduino, S. A. 2015. Arduino. *Arduino LLC*.

Askarinejad, A., A. Beck, F. Casini, and S. M. Springman. 2012. Unsaturated hydraulic conductivity of a silty sand with the instantaneous profile method. In *Unsaturated Soils: Research and Applications*: Springer, 215-220.

Babaoglu, Y., and Simms, P. 2020. Improving Hydraulic Conductivity Estimation for Soft Clayey Soils, Sediments, or Tailings Using Predictors Measured at High-Void Ratio. *ASCE Journal of Geotechnical and Geoenvironmental Engineering,* Forthcoming article

Bartholomeeusen G, Sills GC, Znidarčić D, Van Kesteren W, Merckelbach LM, Pyke R, et al. 2002. Sidere: numerical prediction of large-strain consolidation. Géotechnique 52(9): 639-648 .

Been, K. & Sills, G. C. (1981). Self-weight consolidation of soft soils: an experimental and theoretical study. *Geotechnique* 31(4): 519-535.

Beier, N., W. Wilson, A. Dunmola, and D. Sego. 2013. Impact of flocculation-based dewatering on the shear strength of oil sands fine tailings. *Canadian Geotechnical Journal* 50 (9):1001-1007.

Dikinya, O. 2005. Comparison of the Instantaneous Profile Method and inverse modelling for the prediction of effective soil hydraulic properties. *Soil Research* 43 (5):599-606.

Fisher, R. A., M. Williams, M. de Lourdes Ruivo, A. L. de Costa, and P. Meir. 2008. Evaluating climatic and soil water controls on evapotranspiration at two Amazonian rainforest sites. *agricultural and forest meteorology* 148 (6-7):850-861.

Fox, P. J., and C. D. Baxter. 1997. Consolidation properties of soil slurries from hydraulic consolidation test. *Journal of geotechnical and geoenvironmental engineering* 123 (8):770-776.

Leung, A. K., J. L. Coo, C. W. W. Ng, and R. Chen. 2016. New transient method for determining soil hydraulic conductivity function. *Canadian Geotechnical Journal* 53 (8):1332-1345.

Qi, S, X. Chen, P. Simms, J. Zhou, X. Yang. 2020. Method for determining the permeability function parameters of soft soils considering synchronous sedimentation and consolidation. *Computers and Geotechnics*, In-Press.

Qi, S., P. Simms, F. Daliri, and S. Vanapalli. 2020. Coupling elasto-plastic behaviour of unsaturated soils with piecewise linear large-strain consolidation. *Géotechnique* 70 (6): 518–537.

Qi, S., & Simms, P. (2019). Robust methods to estimate large strain consolidation parameters from column experiments. *Canadian Geotechnical Journal.* Published online ahead of print. https://doi.org/10.1139/cgj-2018-0870.

Qi, S., P. Simms, and S. Vanapalli. 2017. Piecewise-linear formulation of coupled large-strain consolidation and unsaturated flow. I: Model development and implementation. *Journal of geotechnical and geoenvironmental engineering* 143 (7):04017018.

Qi, S**.,** Simms, P., Thomas, Wm, Hmidi, N. 2017. Hydro-geotechnical analysis of a thickened tailings deposit in Northern Canada via UNSATCON. *Proc. Tailings and Mine Waste*, Banff, Alberta, Nov 2017, University of Alberta Geotechnical Group, Edm., Alberta.

Salam, M. 2020. Effects of Polymers on short-and long-term dewatering of oil sands tailings. Ph.D. Thesis, Carleton Univrsity, publically available at: https://curve.carleton.ca/ad563655-a15c-4c1f-97f2-835582df17eb

Watson, K. 1966. An instantaneous profile method for determining the hydraulic conductivity of unsaturated porous materials. *Water resources research* 2 (4):709-715.

Exploring the Effects of Side Wall Friction in a Slurry Consolidometer Test

H.F.T. Barnard
Golder Associates Africa Pty Ltd, Waterfall City, Gauteng, South Africa

V. Venter
Golder Associates Africa Pty Ltd, Waterfall City, Gauteng, South Africa

ABSTRACT: The slurry consolidometer device is used to determine the compressibility and permeability of tailings samples. A slurry sample is typically prepared at a specified solids concentration and consolidated in stages at various confining pressures followed by permeability readings measured at each stage. As the slurry are being consolidated the plunger inside the stainless-steel chamber moves down due to the dissipation of excess pore pressure. The aim of this paper is to explore the effects of side wall friction between the hydraulic seals, connected to the plunger, and the chamber. Furthermore, the friction profile of the chamber was established by determine the minimum pressure required to move the plunger all the way down. The results from this study provides a pressure correction for the full ranges of applied pressure, to account for the friction losses during consolidation tests.

1 INTRODUCTION AND BACKGROUND

The slurry consolidometer device is used to determine the compressibility and permeability of tailings samples. A slurry sample is typically prepared at a specified solids concentration and consolidated in stages at various confining pressures followed by permeability readings measured at each stage. As the slurry are being consolidated the plunger inside the stainless-steel chamber moves down due to the dissipation of excess pore pressure. To quantify the side wall friction, the difference between the applied cell pressure and measure base pressure was determined by using only de-aired water inside the chamber. Both the applied cell pressure and base pressure was measured by means of 2,0 MPa pressure pumps. To understand the friction profile of the chamber, a series of tests at different cell pressures were conducted to establish the minimum required pressure to move the plunger to the bottom of the chamber. Figure 1 shows the slurry consolidometer set-up in the Golder advanced testing laboratory in Johannesburg, South Africa.

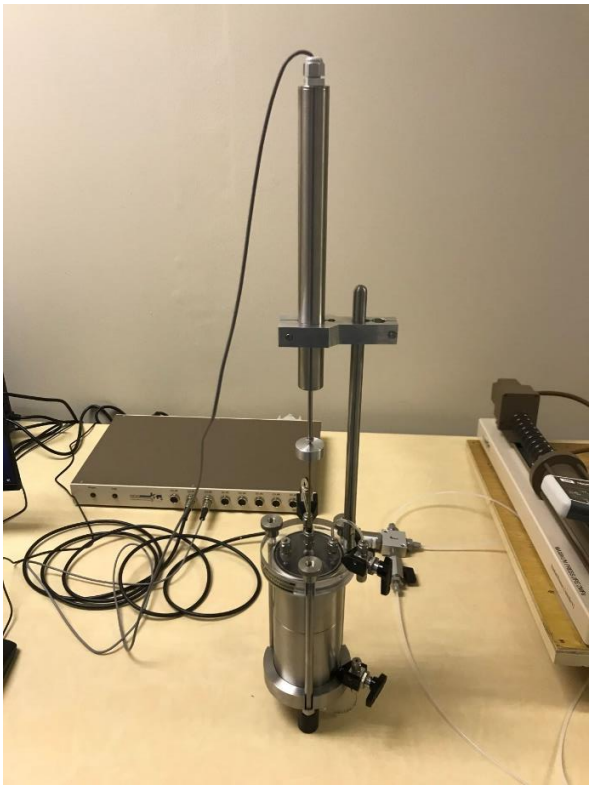

Figure 1. Slurry Consolidometer testing set-up

2 FACTORS AFFECTING SLURRY CONSOLIDOMETER RESULTS

The results of slurry consolidometer tests are affected by many factors, including but not limited to, the following list below:

- Different loading sequences for example constant rate of loading vs incrementally increasing loading (Shokouhi & Williams, 2015).
- Different duration of tests and consolidation stages (Estepho, 2011).
- Consolidation effects during the permeability stages (Estepho, 2011).
- Slurry added in layers to allow settling and consolidation under its self-weight (Shokouhi & Williams, 2015).
- Effectiveness of sample heights. It is suggested by Islam et al. (2019), that the sample height to be kept at maximum 100 mm, as greater heights take longer to consolidate due to low permeability.
- Test equipment's ability to apply low loads at early stages of test (Gan et al, 2011).
- Test equipment's ability to minimise the negative impact of seepage-induced consolidation (Gan et al, 2011).
- Piston (or plunger) and wall friction losses (Shokouhi & Williams, 2015).

3 SLURRY CONSOLIDOMETER EQUIPMENT SETUP

3.1 *Equipment description and function*

The slurry consolidometer split mold used in this study, is made up of two (2) stain-less steel chambers A (upper) and B (lower) with heights of 68.2 mm and 88.9 mm, respectively. Combined having an average height of 157.1 mm and an overall diameter of 71 mm (see Figure 2). The mold is secured by a bottom and top cap that is tightened with three stain-less steel rods as shown in Figure 1. The displacement transducer (LVDT) connects to the top cap and accurately records the vertical displacement during testing. De-aired water is used in the upper chamber to avoid compression of air in natural tap water. The plunger has an average height of 35.1 mm and an overall diameter of 71 mm including the 2 rubber hydraulic seals to tightly fit inside the chamber and ensure that there are no leaks.

The applied pressure is provided by three (3 No.) 2,0 MPa hydraulic pumps, that have an accuracy of ±1 kPa, connected to the slurry consolidometer in the following fashion:

- Cell-pressure pump (Above plunger): Connects through the top cap and is typically used to apply the vertical axial pressure above the plunger acting on the sample.
- Back-pressure pump (Below plunger): Connects directly to the plunger to apply back pressures below the plunger to the sample and to control a certain effective pressure during testing, which is defined as the difference between the cell and back pressure.
- Base pressure pump (Bottom of sample): Connects to the bottom of the slurry consolidometer and is used to measure pore pressure during consolidation. After each consolidation stage, the base and back pressure pumps are used together to create a constant flow through the sample to estimate permeability.

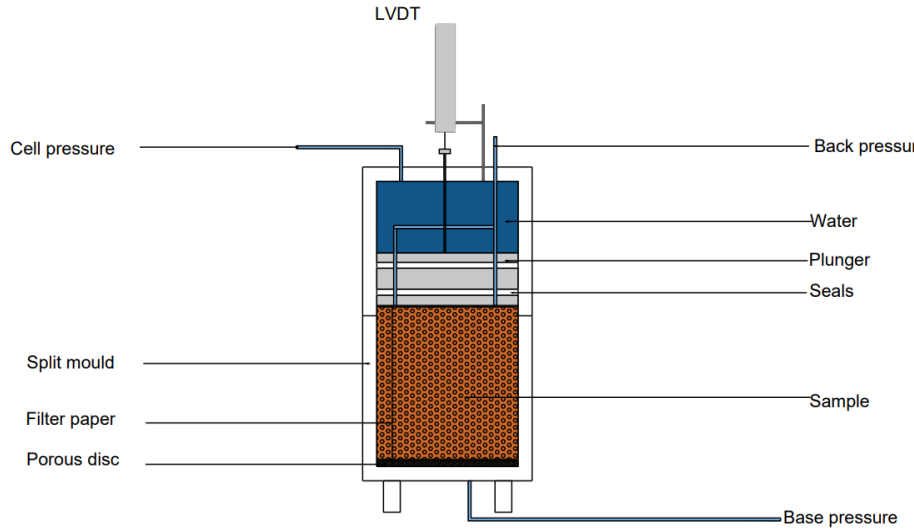

Figure 2. Schematic Diagram of Slurry Consolidometer test set-up

4 METHODOLOGY

4.1 *Quantifying the pressure transfer at three initial positions*

The slurry consolidometer was set up using only de-aired water in both upper and lower chambers. Silicon paste was used as an extra sealant between the top cap, split mold, and bottom cap. The inside of the cambers is sprayed lightly with a silicon-free multi-purpose lubricant as well as the hydraulic seals attached to the plunger. Initially three sample heights (F1, F2 & F3) were selected to estimate the load transfer between the applied cell pressure and the base pressure measured at the bottom of the chamber. Figure 3 shows a schematic diagram of the chamber and the positions of F1, F2 & F3 taken at 92.2 mm, 66.9 mm & 22.8 mm, respectively. At each height, the slurry consolidometer was setup from the start and the plunger pushed in by hand to the estimated heights. The cell and back pressure were set to 100kPa to stabilize the position height inside the chamber. After the 100kPa pressures were reached the back- and base pressure pumps were set to 'read-only' mode and given time to stabilize. The cell pressure was then incrementally increased, while the pressure responses in the back and base pumps were recorded. Section 5.1 below discuss the results obtain from this initial pressure transfer step.

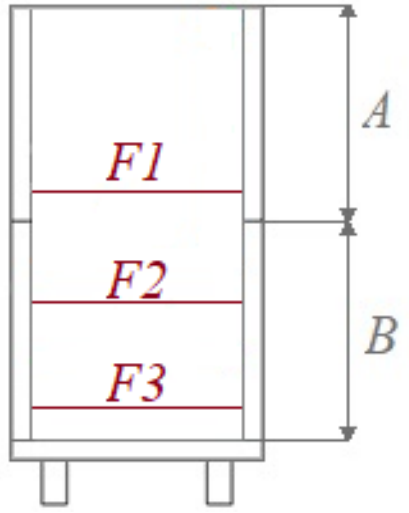

Figure 3. F1, F2, and F3 heights

4.2 *Exploring the side wall friction*

After the initial pressure transfer tests, there was a significant difference between the different heights on the chamber. This raised the question whether the chamber has a unique friction profile along the side walls. In order to explore the side wall friction, a movement test was conducted by setting up the slurry consolidometer with the plunger as high as possible, and applying different effective pressures to allow the plunger to slide all the way down the side walls. The cell & back-pressure pumps were again set to hold each 100kPa, thereafter the cell pressure was increased to various effective pressure. The aim for this step was to determine the minimum effective pressure required for the plunger to move from the top to the bottom without stopping. The initial effective pressure was selected as 25 kPa, and in the case where the plunger stopped moving, the pressure was increased until the plunger started moving down again. Once the minimum effective pressure was established, two larger pressures were run as well to understand the expected friction profile along the chamber.

4.3 *Quantifying the pressure transfer at most likely positions*

Once the friction profile was better understood, the two most critical positions (H1 & H2) were selected, representing the average initial and final sample heights based on prior experience. The plunger was placed as accurately as possible to the H1 position (57.4 mm) using a Vernier to confirm. Then a load transfer test was conducted as described in Section 4.1 above. After the H1 test, using the pumps the plunger was moved down to the H2 position (46.4 mm). When at the desired H2 height, a load transfer test was completed, and values recorded. Figure 4 shows a schematic diagram of the chamber and the positions of H1 & H2.

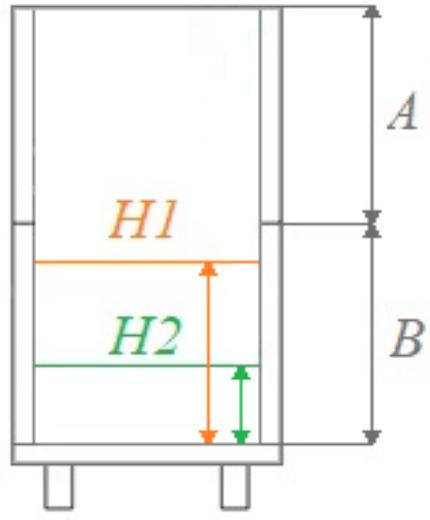

Figure 4. H1 and H2 heights

4.4 *Applying the pressure transfer correction to results*

The last step was to correct previous slurry consolidometer readings in terms of void ratio vs effective pressure plots by decreasing the vertical pressure recorded during testing to reflect the true pressure transfer applied to the slurry sample during loading.

5 DISCUSSION OF RESULTS

5.1 *Pressure transfer at initial F1, F2 & F3 positions*

Figure 5 shows the data obtained from the initial pressure transfer experiments. At each of the positions, the pressure transfer percentage was calculated for each pressure increment. The graph also indicates the pressure error observed for each pressure increment. The effective pressure at which the error percentage was less than 10%, ranged between 60 kPa (At position F2), and 400 kPa at position F3. This was an interesting phenomenon because it indicated that somewhere in the center of the chamber, the friction was to a certain degree less compared to the upper and lower portions of the chamber. Although the pressure transfer error for position F1 and F3 was similar, it did not correspond well with the pressure transfer at position F2. To better understand the friction profile of the chamber, the minimum required pressure to move the plunger all the way down had to be estimated.

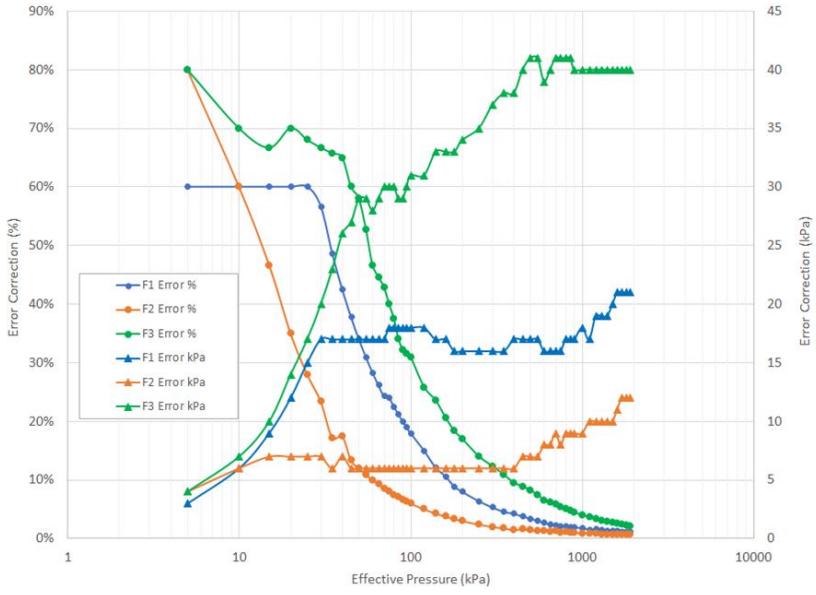

Figure 5. F1, F2, F3 pressure transfer error corrections

5.2 *Estimate the minimum required pressure*

The first attempt to estimate the minimum required pressure was an effective pressure of 25kPa. Figure 6 shows the change in sample height as the plunger was pushed down with the 25 kPa pressure. At around 70 mm sample height the sidewall friction became too much for the plunger to move further and therefore the pressure had to be increased to 30 kPa in order to move the plunger all the way down.

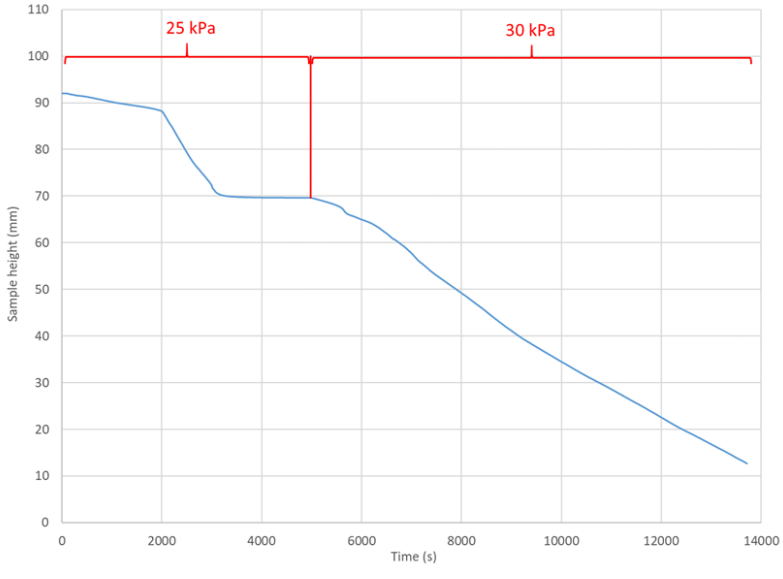

Figure 6. Effective pressure applied from 25kPa to 30kPa

The second attempt to estimate the minimum required pressure was conducted with a 30 kPa pressure as shown in Figure 7. The plunger again only reached a sample height of about 66 mm and the pressure had to be increased to 31 kPa to move the plunger all the way down the chamber.

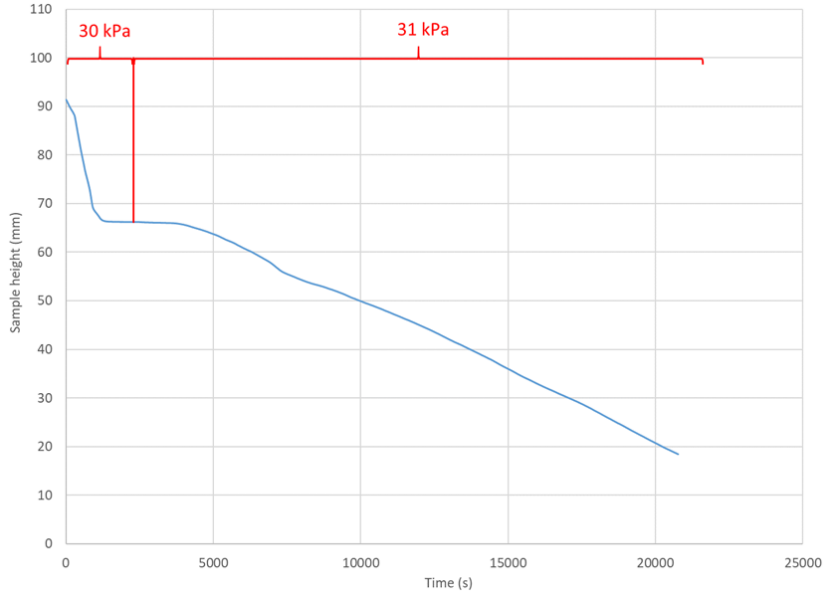

Figure 7. Effective pressure applied from 30kPa to 31kPa

The last attempt was conducted with a 35 kPa pressure and as shown in Figure 8, the plunger moved completely down the chamber without stopping in between due to sidewall friction.

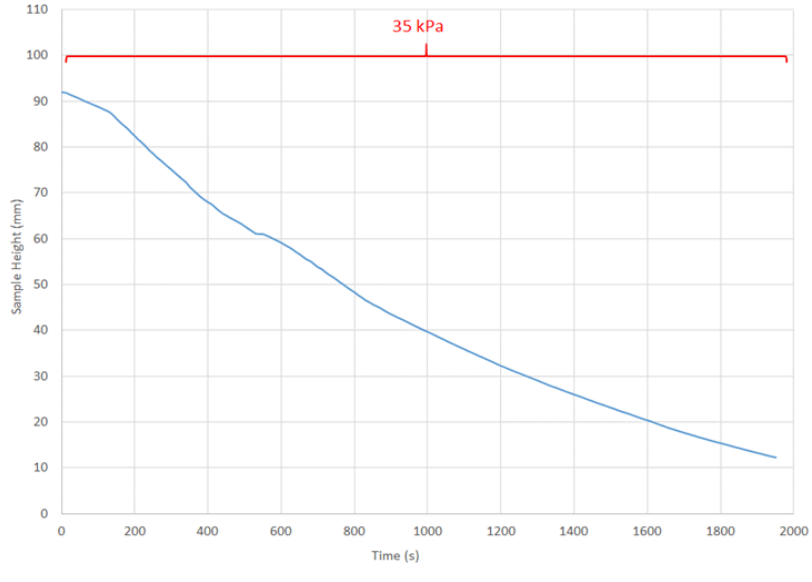

Figure 8. Minimum required pressure of 35 kPa

5.3 *Establish friction profile along sidewalls*

Once the minimum required pressure of 35 kPa to move the plunger completely down was established, a further two runs were conducted with a 40 kPa and 50 kPa effective pressure, respectively. The graph in Figure 9, indicate the change in movement rate as the sample height decrease. For all three pressures the movement rate increased up to about 80 mm sample height. Thereafter, there was between 10 to 20 mm of length where the movement rate slowed down and started to gradually decrease for sample heights less than 60 mm, indicating a low friction zone. These results showed a clear pattern of the friction profile of the stain-less steel chamber used in the South African Golder lab. Based on this observation two more positions were selected to evaluate the pressure transfer as explained above in section 4.3.

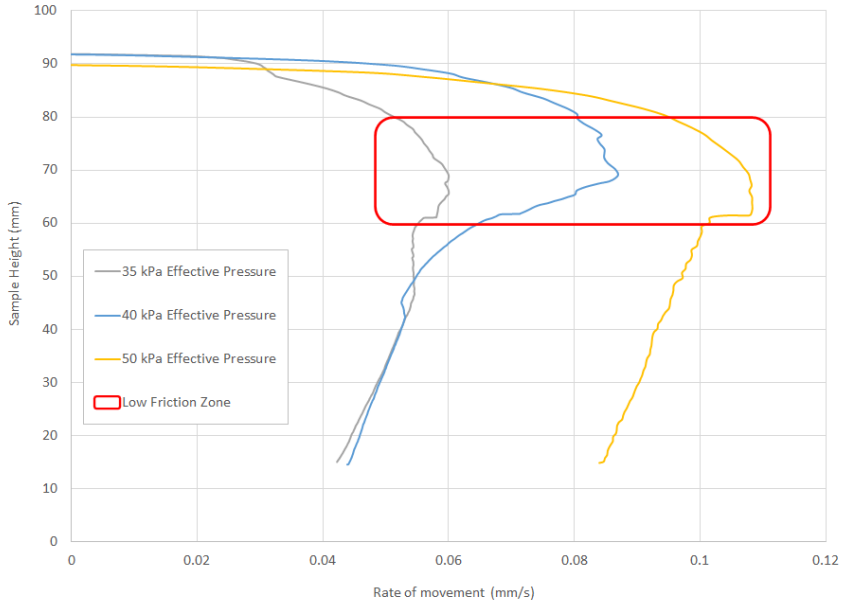

Figure 9. Rate of movement (mm/s) for three different effective pressures

5.4 *Pressure transfer for H1 and H2*

The average initial (H1) and final (H2) sample heights were calculated as H1: 57.38mm & H2: 46.38mm and corresponded well with the friction profile with sample heights less than 60 mm. As observed in Figure 10, the pressure transfer percentage and kPa errors were similar at position H1 and H2.

Figure 11 shows the average error correction in kPa that was used to correct the measured readings. The error correction between 10 kPa and 1200 kPa applied pressure ranged between 6 kPa (60%) and 35 kPa (3%), respectively. The error correction also shows a very small difference of only 2 kPa between the 300 kPa and 1200 kPa effective pressure.

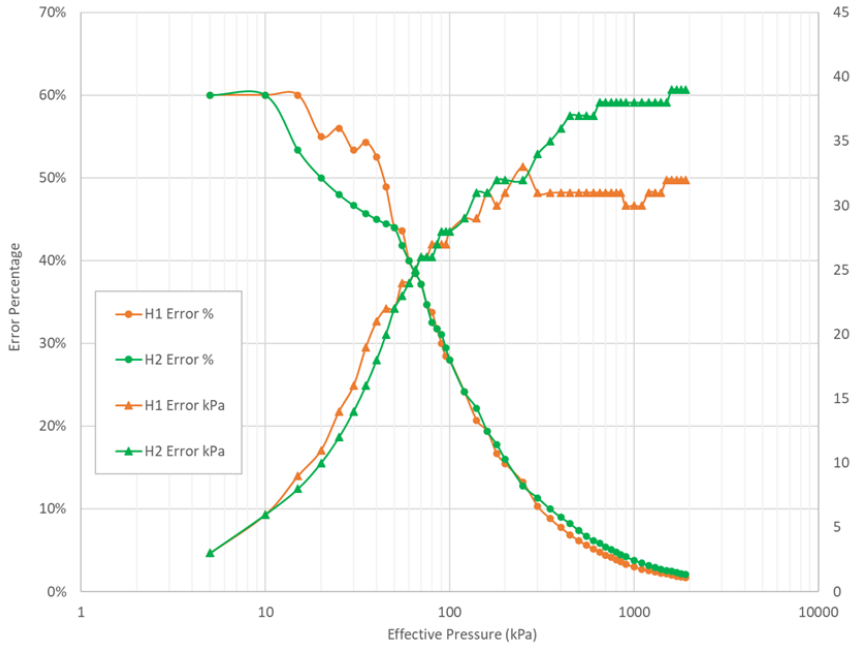

Figure 10. H1 & H2 Error % vs Error kPa

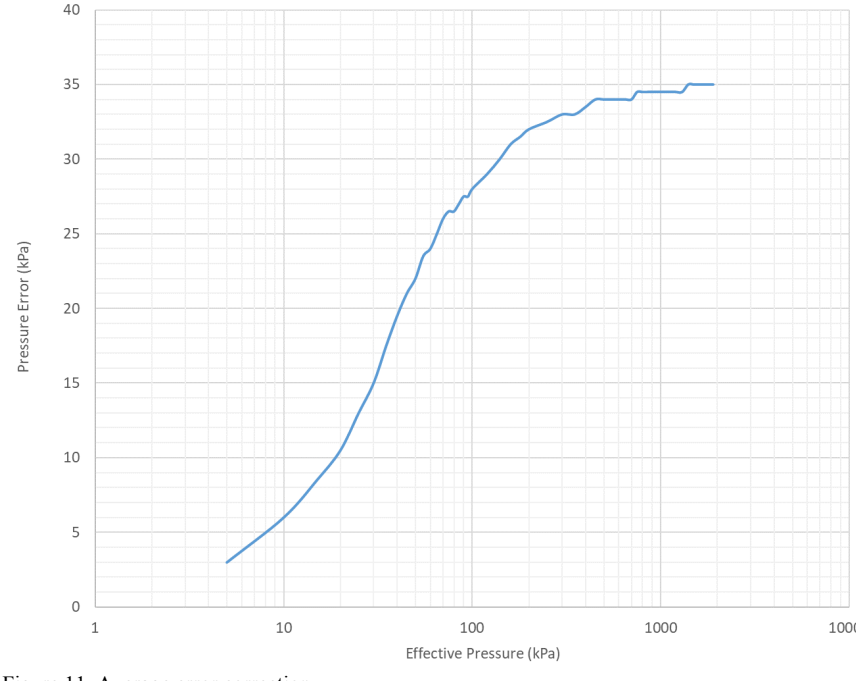

Figure 11. Average error correction

5.5 *Effect on slurry consolidometer results*

The error correction is calculated as the average between H1 and H2's error value and applied for each specific effective pressure. Figure 12 show the measured reading and the corrected readings of a typical slurry consolidometer result. The error becomes less than 10% for pressures larger than 300 kPa and has a minimal effect on the results. The error percentage correction between 10 kPa and 400 kPa ranged between 60% and 8.5%, respectively.

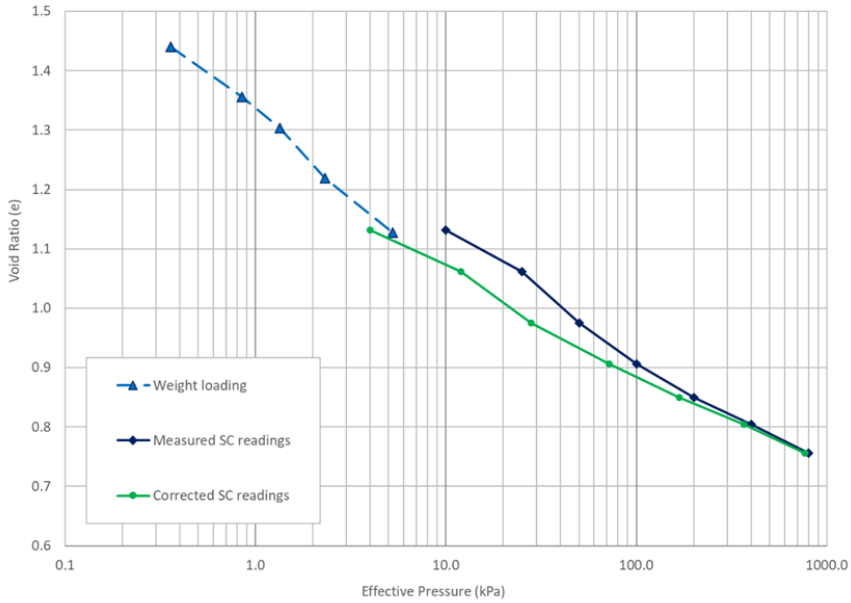

Figure 12. Effect on Void Ratio vs Effective Pressure

6 CONCLUSIONS

Based on the results obtain by this experimental testing the following conclusions were made:

- The results are specific to the apparatus used and that device specific curves could be developed for other devices using the framework laid out in this paper.
- The initial pressure transfer experiments showed a large variation in error percentage and indicated a center portion of the chamber with a lower friction compared to the upper and lower portions.
- It was estimated that a minimum of 35 kPa pressure would be required to move the plunger all the way down the chamber, when the chamber was only filled with de-aired water.
- The test results indicated a low friction zone for sample heights between 80 mm and 60 mm and the sidewall friction gradually increase for sample heights less than 60 mm.
- The pressure transfer errors for positions H1 and H2 with sample heights less than 60 mm, were similar and the average error was applied to real results.
- Results indicate that the error correction becomes less than 10% for pressures more than 300 kPa.

7 REFERENCES

Estepho, 2014. Seepage Induced Consolidation test: Characterization of Mature Fine Tailings. *PhD Thesis, The University of British Columbia.*

Gan et al, 2011. Consolidation and Hydraulic Conductivity Testing of Slurries. *Tailings and Mine Waste, Vancouver, BC, November 2011.*

Islam et al., 2019. Settling, consolidation and shear strength behaviour of coal tailings slurry. *International Journal of Mining Science and Technology.*

Shokouhi & Williams, 2015. Settling and consolidation behaviour of coal tailings slurry under continuous loading. *Tailings and Mine Waste, Vancouver, BC, October 2015.*

Evolution of Shear Strength and Consolidation Behavior of Mine Tailings from a Slurry to a Soil State

Kathy Tehrani, David J. Williams and Alexander Scheuermann
The University of Queensland, Brisbane, Queensland, Australia

ABSTRACT: In order to be able to predict the potential for tailings dam failure, it is necessary to understand and study their shear strength behavior from their initial slurry-like state on deposition to their eventual soil-like state. Also, the ongoing consolidation of mine tailings can be a major issue during operation and post-closure. The paper investigates and describes the evolution of the shear strength and consolidation behavior of red mud from the processing of bauxite to produce alumina, as it transitions from a slurry-like state on deposition to a soil-like state. For this purpose, rheometer, vane shear and direct shear tests were performed to assess the shear strength behavior of the red mud as it transitioned. Suction-induced consolidation testing (from 0.01 to 5 kPa applied stress) and conventional oedometer testing (from 5 to 1,280 kPa applied stress) were performed to assess the consolidation behavior of the red mud as it transitioned from slurry-like to soil-like states.

1 INTRODUCTION

Increasing amounts of mine tailings are being produced due to the increase in demand for minerals and metals (Hudson-Edwards et al. 2011) and reducing ore grades. Tailings are generally fine-grained and are produced in the form of a slurry, which is conventionally deposited hydraulically in surface tailings storage facilities. The high water content and low permeability characteristics of the tailings cause stability issues due to their low shear strength and large strain consolidation (Vick, 1990). The stability of tailing dams during the disposal and storage of tailings has become a major issue for the mining industry (Rout et al., 2013). Therefore, a comprehensive understanding of the shear strength and consolidation behaviors of tailings is critical to further improve the efficiency of disposal and the design of tailings storage facilities (Dimitrova & Yanful, 2011). Many studies have been conducted to investigate the mechanical characteristics of mine tailings, which vary for different kinds of tailings (Chang et al. 2011; Hu et al. 2017; James et al. 2011; Qiu and Sego, 2001; Wang et al. 2017).

In this study, a series of laboratory experiments was conducted to investigate the shear strength and consolidation behavior of red mud or bauxite residue, a major by-product from the refining of bauxite to alumina using the Bayer process (Abbasi et al., 2016; Autef et al., 2012; Gu et al., 2012; Rashad, 2013; Rout et al., 2013; Santini & Fey, 2018) at Queensland Alumina Limited. Queensland Alumina Limited is one of the largest alumina refineries by alumina production capacity in the world, and is located in Gladstone, Queensland, Australia. The red mud is disposed of as a slurry, thickened to a nominal 26% solids by mass, and neutralized with seawater. On disposal in the tailings storage facility the red mud settles and consolidates, and part of the deposit is "farmed" using scrollers and D6 Swamp Dozers to aid drainage and desiccation. The test material was sampled from the upper part of the beach, which had been scrolled and compacted

by D6 Swamp Dozer (Quintero and Williams, 2017). Most laboratory tests were carried out using ASTM standard test procedures, apart from some special testing techniques used to carry out sedimentation-consolidation tests.

2 CHARACTERIZATION OF RED MUD

The as-received gravimetric moisture content of the red mud sample was 87.5% (ASTM-D-2216-98, 1998), the specific gravity was 2.96 (ASTM D854, 2000), the Liquid limit was 49.0%, and the Plastic limit of 30.7% (ASTM D4318, 2005), which classifies the red mud according to the Unified Soil Classification System as "CL", a silty clay of low plasticity.

3 STRENGTH OF RED MUD

In soil mechanics, the term "strength" normally refers to the shear strength of the soil, which is defined as the soil resistance to shearing stress and depends on pore water pressure, cohesion and the friction angle between soil particles. The shear strength of tailings is normally measured under undrained conditions due to their low permeability. The undrained shear strength of a soil (Su) refers to the achievable shear strength when the soil is loaded at a rate faster than the rate at which it can drain. During the undrained application of stress, the incompressible pore water takes the stress, preventing effective stress from developing. Since water has no shear strength, effective stress is directly proportional to shear strength (Craig, 2004; Das, 2013). There are several methods to measure the shear strength of soils in the laboratory, including the rheometer, vane shear and direct shear tests, as described in the following sections.

3.1 *Rheometer testing of red mud*

Yield stress is an important concept in rheology, which refers to the stress level that causes plastic deformation (Raffer, 2003). In this study, the yield stress of the red mud samples tested at different moisture contents was measured using an Anton Paar MCR102 Rheometer, which applies a very low shear rate of 0.0010/sec over the 0.01 Pa to 10 kPa shear stress range, under controlled temperature. Figure 1 presents the results of the rheometer testing of red mud, which shows that reducing the gravimetric moisture content below 75% (about 1.5 times the Liquid limit) causes a dramatic increase in the yield stress of the red mud.

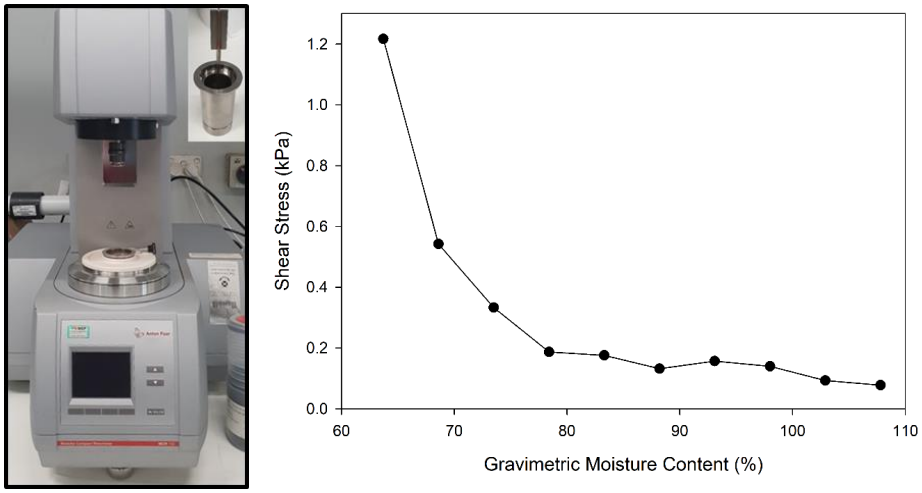

Figure 1. Anton Paar MCR102 Rheometer and test results for red mud.

3.2 *Vane shear testing of red mud*

The vane shear device is a common test method for measure the undrained shear strength of a soft soil in the field and the laboratory. The vane is fully inserted vertically in the sample to the test depth and torque (T) is applied at a constant rate until a maximum is recorded (ASTM D4648/D4648M-16, 2016). In this study, an automated Wille laboratory vane shear device has been used to test the shear strength of red mud at a range of different gravimetric moisture contents. Figure 2 presents the results of vane shear testing of red mud, which shows that red mud starts gaining shear strength from a gravimetric moisture constant of about 65% and continues to gain shear strength linearly with decreasing gravimetric moisture content to the Plastic limit of about 35%. These results are consistent with those from the Rheometer test, indicating that 1.2 to 1.5 times the Liquid limit represents the onset of a soil-like state.

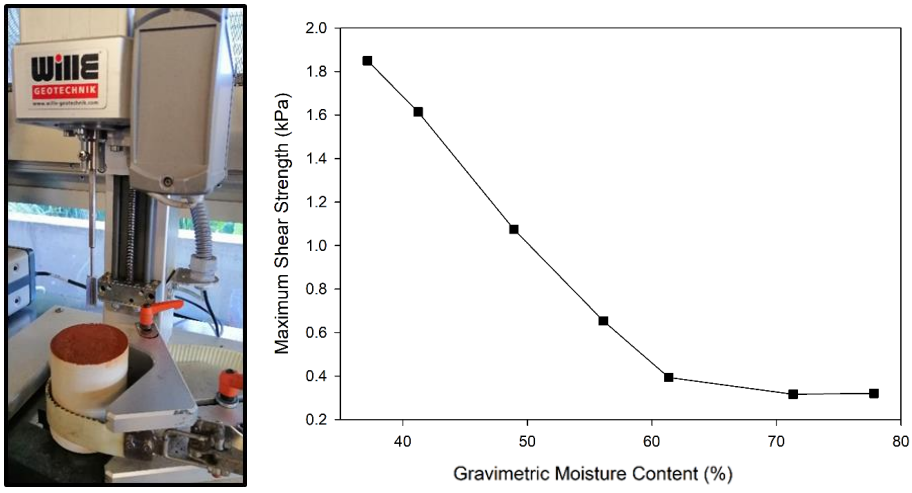

Figure 2. Wille laboratory vane shear and test results for red mud.

3.3 *Direct shear testing of red mud*

The direct shear test was carried out on remolded specimens of red mud at a settled gravimetric moisture content of about 42% according to ASTM D6528 (2017), in a 60 x 60 mm direct shear box with a nominal specimen height of 25 mm. The three specimens were left in a bath for 48 hours to wet-up, prior to the application of normal stresses of 100 kPa, 200 kPa and 400 kPa, and shearing at a rapid rate of 1 mm/min. Figure 3 presents the results of the direct shear testing of red mud, which shows a small friction angle of about 1° and an average apparent cohesion of 34 kPa.

4 CONSOLIDATION OF RED MUD

Consolidation is the time-dependent settlement of soils by the expulsion of water from the soil pores, which is conventionally measured using an oedometer (Craig, 2004; Das, 2013). The early stages of consolidation of slurry-like red mud can be tested in a suction-induced consolidation test, while the consolidation of soil-like red mud can be tested in an oedometer, as described in the following sections.

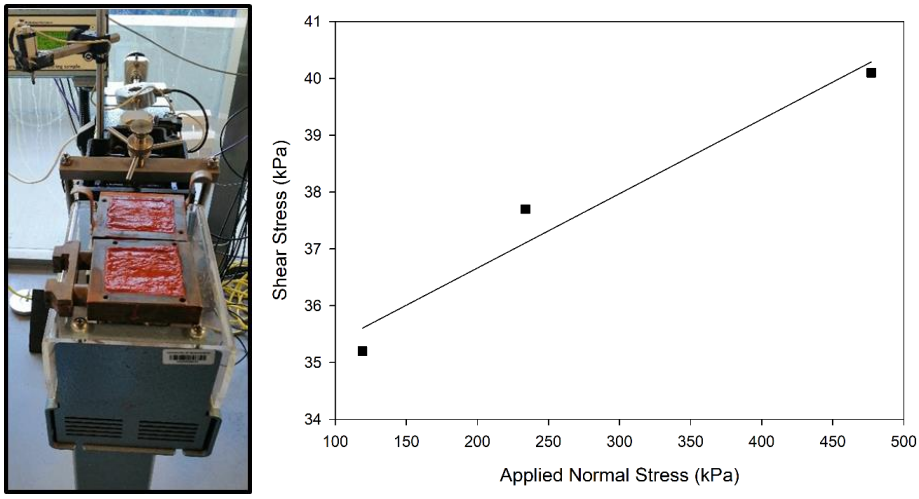

Figure 3. Direct shear and test results for red mud.

4.1 *Suction-induced consolidation of red mud*

Conventionally, sedimentation and consolidation are considered as two separate processes; however, practically they are interconnected and need to be analyzed together. A suction-induced consolidometer allows the combined sedimentation and consolidation of red mud from a slurry to be studied over the low stress range. The suction-induced consolidation test set-up is shown in Figure 4 which includes a cylindrical acrylic column of 70 mm internal diameter and 150 mm height with an outlet at the base, where a high air-entry ceramic disk is placed. The column is connected via a flexible tube to a water column to produce a suction at the base and also to keep the ceramic disk fully saturated. The ceramic disk is saturated in deionized water for 48 hours in a desiccator under vacuum pressure prior to the start of the test.

Red mud specimens were prepared at an initial gravimetric moisture contents of 209%, 151% and 93%, poured into three identical columns and left for 48 hours to settle and undergo self-weight consolidation. As presented in Figure 4, the higher the initial gravimetric moisture content the higher the sedimentation and self-weight consolidation (from 0 to 0.02 kPa pressure).

The three specimens were then subjected to suction-induced consolidation by maintaining the water column at different elevations. As presented in Figure 4, between 0.02 kPa and 1.0 kPa suction pressure all three specimens showed a similar declining trend in void ratio, but from different starting points due to their different initial gravimetric moisture contents. Beyond 1.0 kPa suction pressure, the three results came together, and remined so to the final suction pressure of 7 kPa.

4.2 *Oedometer testing of red mud*

Conventional oedometer testing was conducted on a red mud specimen extruded from the completed suction-induced consolidometer test. The specimen was tested under 24-hour applied stress increments from 5.0 to 1,280 kPa according to ASTM D2435 (2010). Figures 5 illustrates the resulting change of void ratio versus effective applied stress on the red mud specimen.

The oedometer test results are summarized in Table 1, which gives the calculated values obtained for the coefficient of consolidation c_v, the coefficient of volume decrease m_v, and the saturated hydraulic conductivity k, for each stress increment, together with the average values.

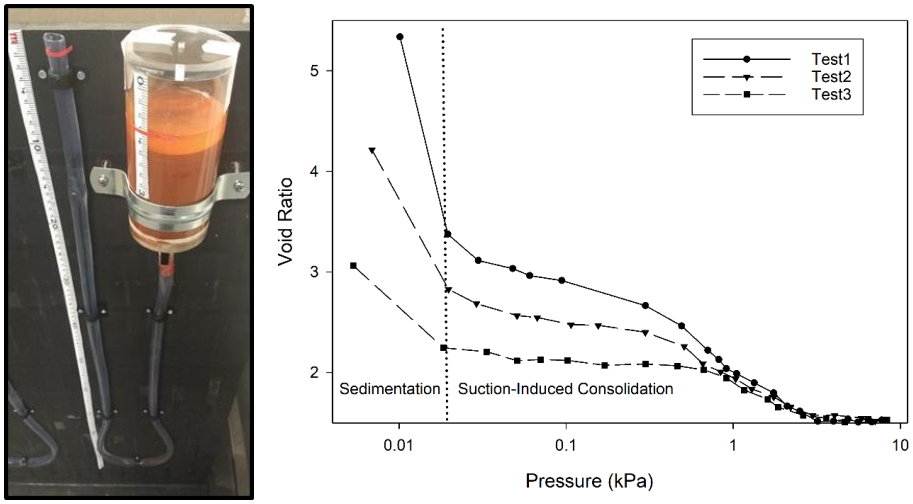

Figure 4. Suction-induced consolidometer and test results for red mud.

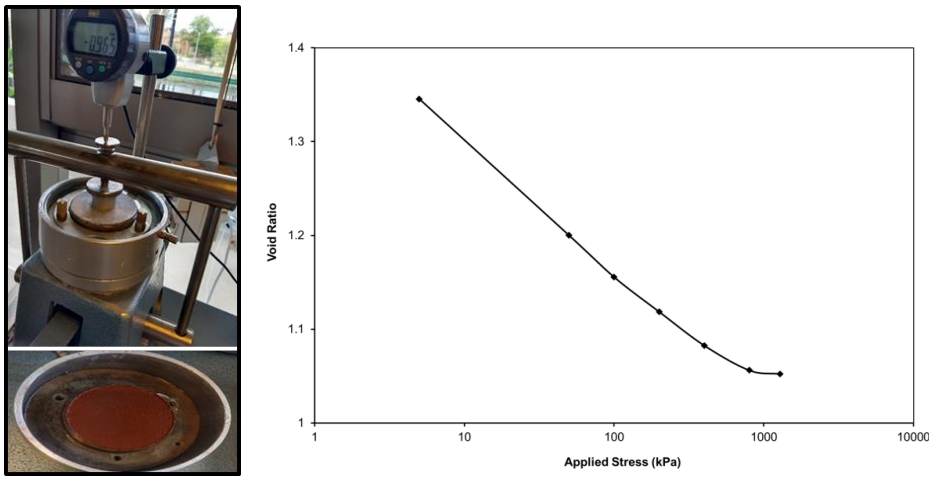

Figure 5. Oedometer test and test results for red mud.

Table 1. Results of oedometer testing of red mud.

σ_v (kPa)	e -	ρ_{dry} (t/m^3)	c_v (cm^2/s)	m_v (kPa^{-1})	k (m/s)
5	1.35	1.28	2.0E-04	2.0E-02	3.9E-09
50	1.20	1.36	1.7E-04	1.5E-03	2.5E-10
100	1.16	1.39	1.6E-04	4.1E-04	6.4E-11
200	1.12	1.42	1.5E-04	1.7E-04	2.6E-11
400	1.08	1.43	1.5E-04	9.3E-05	1.4E-11
800	1.06	1.44	1.5E-04	2.4E-05	3.4E-12
1,280	1.05	1.46	2.4E-04	7.8E-06	1.8E-12
Average values	1.15	1.39	1.7E-04	3.1E-03	6.0E-10

5 CONCLUSION

A series of laboratory experiments, including rheometer, vane shear, direct shear, suction-induced consolidation and oedometer testing, was carried out on red mud from Queensland Alumina Limited in Gladstone, Queensland, Australia. The red mud was tested from slurry-like to soil-like states. The red mud was classified as "CL", a silty clay of low plasticity.

The shear strength of the red mud ranged from the yield stress of about 0.2 kPa at 1.5 times the Liquid limit (gravimetric moisture content of 75%), through about 2 kPa at the Plastic limit (gravimetric moisture content of 31%) to 34 kPa at a gravimetric moisture content of 42%.

The red mud settled and consolidated under a suction pressure of 7 kPa to a void ratio of 1.35 (gravimetric moisture content of 46%), and consolidated further to a void ratio of 1.05 (gravimetric moisture content of 36%) in an oedometer, under an applied stress of 1,280 kPa.

6 REFERENCES

Abbasi, S.M., Rashidi, A., Ghorbani, A. and Khalaj, G. 2016. Synthesis, processing, characterization, and applications of red mud/carbon nanotube composites. *Ceramics International*, 42(15), 16738-16743.

ASTM-D-2216-98. 1998. *Standard Test Method for Laboratory Determination of Water (Moisture) Content of Soil and Rock by Mass*.

ASTM-D854. 2000. *Standard Test Methods for Specific Gravity of Soil Solids by Water Pycnometer*.

ASTM-D2435. 2010. *Standard Test Methods for One-Dimensional Consolidation Properties of Soils Using Incremental Loading*.

ASTM-D6528. 2017. *Standard Test Method for Direct Shear Test of Soils Under Consolidated undrained Conditions*.

ASTM-D4318, ASTM D 4318-10, and D4318-05. 2005. *Standard Test Methods for Liquid Limit, Plastic Limit, and Plasticity Index of Soils*.

ASTM D4648/D4648M-16. 2016. *Standard Test Methods for Laboratory Miniature Vane Shear Test for Saturated Fine-Grained Clayey Soil*.

Autef, A., Joussein, E., Gasgnier, G. and Rossignol, S. 2012. Role of the silica source on the geopolymerization rate. *Journal of Non-Crystalline Solids*, 358(21), 2886-2893.

Chang, N., Heymann, G. and Clayton, C. 2011. The effect of fabric on the behaviour of gold tailings. *Géotechnique*, 61(3), 187-197.

Craig, R.F. 2004. *Soil mechanics*. CRC press.

Das, B.M. 2013. Principles of Geotechnical Engineering. *Journal of Chemical Information and Modeling*, 53(9).

Dimitrova, R.S. and Yanful, E.K. 2011. Undrained strength of deposited mine tailings beds: effect of water content, effective stress and time of consolidation. *Geotechnical and Geological Engineering*, 29(5), 935-951.

Gu, H., Wang, N. and Liu, S. 2012. Characterization of Bayer red mud from Guizhou, China. *Mining, Metallurgy & Exploration*, 29(3), 169-171.

Hu, L., Wu, H., Zhang, L., Zhang, P. and Wen, Q. 2017. Geotechnical properties of mine tailings. *Journal of Materials in Civil Engineering*, 29(2), 4016220.

Hudson-Edwards, K.A., Jamieson, H.E. and Lottermoser, B.G. 2011. Mine wastes: past, present, future. *Elements*, 7(6), 375-380.

James, M., Aubertin, M., Wijewickreme, D. and Wilson, G.W. 2011. A laboratory investigation of the dynamic properties of tailings. *Canadian Geotechnical Journal*, 48(11), 1587-1600.

Qunitero, S. and Williams, D.J. 2017. Geotechnical characterisation of neutralised red mud for use in civil engineering construction and manufacturing. *Proceedings of 32nd International Conference on Solid Waste Technology and Management, Philadelphia, PA, USA, 19-22 March 2017*, 613-623.

Qiu, Y. and Sego, D.C. 2001. Laboratory properties of mine tailings. *Canadian Geotechnical Journal*, 38(1), 183-190.

Raffer, G. 2003. *Rotary Rheometer*. In: US 6,571,610 B1 (p. 15). Google Patents.

Rashad, A.M. 2013. Alkali-activated metakaolin: A short guide for civil Engineer – An overview. *Construction and Building Materials*, 41, 751-765.

Rout, S.K., Sahoo, T. and Das, S.K. 2013. Design of tailing dam using red mud. *Central European Journal of Engineering*, 3(2), 316-328.

Santini, T.C., and Fey, M.V. 2018. From tailings to soil: long-term effects of amendments on progress and trajectory of soil formation and in situ remediation in bauxite residue. *Journal of Soils and Sediments*, 18(5), 1935-1949.

Vick, S.G. 1990. *Planning, design, and analysis of tailings dams*. BiTech.
Wang, L., Ji, B., Hu, Y., Liu, R. and Sun, W. 2017. A review on in situ phytoremediation of mine tailings. *Chemosphere*, 184, 594-600.

On the Performance of Two Advanced Constitutive Models in Capturing the Element Response of Tailings

Renmin Pretell, Francisco Humire & Katerina Ziotopoulou
University of California, Davis, CA, USA

ABSTRACT: The potential for static and earthquake-induced liquefaction of tailings dams is increasingly assessed using advanced numerical simulations. The accuracy of these assessments mainly depends on the extent to which the employed constitutive models are able to capture key behaviors relevant to the problem at hand, the availability and quality of field data, and the calibration protocols followed. Here, the PM4Sand and PM4Silt constitutive models are introduced, and their ability to capture features of the behavior of tailings materials is evaluated. The evaluation is performed by comparing results from single-element simulations to undrained monotonic and cyclic direct simple shear tests conducted on tailings from the Cadia Valley Operations. Results suggest that both constitutive models can satisfactorily capture specific features of the tailings' behavior, and alternative sets of parameters can be used depending on the behaviors of interest.

1 INTRODUCTION

The evaluation of static and earthquake-induced liquefaction of tailings dams is increasingly assessed using nonlinear deformation analyses (NDAs). The accuracy of NDAs in estimating the performance of these structures, partly depends on the ability of the constitutive models to simulate and capture the response of tailings materials at the element level (e.g., Ziotopoulou et al. 2014). Limitations of the constitutive models to simulate the soil's response at the element level could propagate to the system level (Ziotopoulou & Boulanger 2015) and eventually lead to misestimations, and thus inappropriate designs or mitigation measures.

The PM4Sand (Boulanger & Ziotopoulou 2017), and PM4Silt (Boulanger & Ziotopoulou 2018b) constitutive models are evaluated in their ability to capture key features of the tailings' behavior to undrained monotonic and cyclic direct simple shear (DSS) loading. These features include the undrained shear strength, the stress-strain and stress path responses to loading, and the secant shear modulus reduction. The PM4Sand model is a stress-ratio controlled, critical state compatible, bounding surface plasticity model, developed to simulate the behavior of sands, primarily for geotechnical earthquake engineering applications. The PM4Silt model builds on the framework of the PM4Sand model, but is modified to capture features of monotonic and cyclic responses specific to low-plasticity silts and clays.

Data used for the evaluation presented herein consist of results from undrained monotonic and cyclic DSS tests conducted on remolded tailings samples from the Cadia Northern Tailings Storage Facility (NTSF), and subjected to different effective vertical and static shear bias stresses that cover a range of in-situ conditions (Jefferies et al. 2019). The availability of laboratory data from the Cadia NTSF study, provides the opportunity to investigate the ability of constitutive models to capture key behaviors under monotonic and cyclic loading, which are conditions of

interest for the assessment of static and earthquake-induced liquefaction of tailings dams, respectively. Results provide insights into the ability of the selected constitutive models to capture tailings' response to monotonic and cyclic loading.

2 CADIA NTSF AND EXPERIMENTAL DATA

2.1 *Background*

Cadia Operations, a mining and processing complex, is located in New South Wales (Australia). On March 9th, 2018, a 300-m long failure occurred at the southern wall of the Cadia NTSF leading to the release of tailings. No major damage was caused by this failure as the tailings were contained by the Southern TSF. A detailed investigation of the event was undertaken by an Independent Technical Review Board (ITRB), and findings were summarized by Jefferies et al. (2019). Three failure mechanisms were investigated as potentially leading to the instability of tailings at the Cadia NTSF: 1) progressive failure of foundation materials; 2) excessive yielding due to water table rising and the associated increased porewater pressure; and 3) porewater pressure buildup due to two M3.0 earthquake events that occurred the day before the failure. Monotonic and cyclic laboratory tests were conducted on the tailings and foundation materials to investigate the mechanisms leading to failure. The ITRB determined that the event was caused by static liquefaction of the tailings triggered by progressive failure of the foundation.

2.2 *Data considered and observed behaviors*

The tailings considered for the present work consisted of clayey silts, classified as CL-ML, with plasticity index (PI) from 4 to 6, fines content between 55 and 65%, and angular to subangular grains with concentrations of albite and quartz of 45% and 20%, respectively. Undrained monotonic and cyclic stress-controlled DSS tests were conducted on tailings samples remolded to a loose state. Samples considered herein were consolidated under vertical effective stresses (σ'_{vc}) of 50 and 300 kPa, representative of shallow and deep locations respectively, and subjected to an initial static shear bias ($\alpha = \tau/\sigma'_{vc}$) of 0 and 0.05, representative of level ground conditions away from the embankment, and $\alpha = 0.3$, representative of conditions close to or under the upstream raises of the embankment. The cyclic stress ratios (CSRs) used for cyclic tests ranged from 0.045 to 0.13 and were applied at a frequency of 1 Hz. Oedometer consolidation tests resulted in compressibility indices (C_c) ranging from 0.1 to 0.113. Shear wave velocity (V_s) was measured using bender elements on remolded specimens. Based on these measurements, relation (1) was developed for the small-strain shear modulus (Jefferies et al. 2019):

$$G_{\max} = 1.04\,(p')^{0.787} \tag{1}$$

In this expression, the mean effective stress is defined as: $p' = (\sigma'_{\mathrm{v}} + 2\sigma'_{\mathrm{h}})/3$, expressed in kPa.

Tailings specimens exhibited a contractive behavior during shearing, behavior characterized by strain softening, and a decrease in vertical effective stress (Fig. 1). The response of tailings during monotonic loading with $\alpha = 0.0$ showed a peak shear strength slightly higher than the post-peak strengths (Fig. 1a), and a rapid decrease in the vertical effective stress to 60% of the initial value (Fig. 1b). The post-peak undrained shear strength ratio, s_u/σ'_{vc}, measured in this test was 0.13, whereas a significantly higher s_u/σ'_{vc} was estimated for the sample subjected to $\alpha = 0.3$ prior to shearing, $s_u/\sigma'_{vc} = 0.23$. This difference was recognized by the ITRB and attributed to slight differences in sample preparation. Regarding the response to undrained cyclic DSS loading, the number of cycles required to yield 2.5% shear strain varied from 3.5 to 20.3, and approximately 3 more cycles to reach an excess porewater pressure ratio (r_u) of 0.9. The sample subjected to $\alpha = 0.3$ reached 2.5% shear strain and a maximum r_u of 0.55 at approximately 12 cycles.

3 BACKGROUND OF THE CONSTITUTIVE MODELS

3.1 *PM4Sand v3.1 (Boulanger & Ziotopoulou 2017)*

The PM4Sand model is a critical state compatible, stress-ratio controlled, bounding surface plasticity model that follows the framework presented by Dafalias & Manzari (2004), with modifications to improve the model's ability to approximate engineering relationships important to geotechnical earthquake engineering applications. This model is able to simulate the response of sand-like soils subjected to monotonic and cyclic loading. The model has three primary input parameters, 21 secondary parameters, the atmospheric pressure (P_a) which sets the units, and two flags. The model was developed such that it can be used given the three primary parameters, while all secondary parameters have been calibrated by the developers to reasonably approximate the range of behaviors exhibited by the broader body of data on clean sands. The secondary parameters can always be modified to better capture observed behaviors when laboratory test or any other data are available. The primary and most of the secondary parameters of the model are listed in Table 1. The PM4sand model is implemented for plane-strain applications as a user-defined dynamic link library (DLL) in FLAC (Itasca 2020).

The primary input parameters are the apparent relative density (D_R), the shear modulus coefficient (G_o), and the contraction rate parameter (h_{po}). D_R controls the dilatancy and stress-strain response of the soil. The coefficient G_o controls the small-strain shear stiffness (G_{max}) and can be calibrated to fit V_s measurements. The h_{po} parameter controls the contractiveness and thus the cyclic strength of the soil, and can be calibrated to obtain a target cyclic resistance ratio (CRR) obtained from experimental data or empirical correlations (e.g., Boulanger & Idriss 2015). Some secondary parameters of the model are: the critical state friction angle (ϕ'_{cv}) which determines the critical state ratio (M); the n^b and n^d parameters which are dials in the equations for the bounding and dilatancy surfaces, respectively; the plastic modulus ratio (h_o) that controls the plastic modulus and thus both the small-strain stiffness in monotonic loading and the softening of the model in cyclic loading (e.g., observed through the secant shear modulus reduction, G/G_{max}, curves); Q and R parameters presented by Bolton (1986) that determine the position of the critical state line; and z_{max} and C_z that control fabric evolution and, through it, the progressive accumulation of shear strains. Further details of the model formulation can be found in Ziotopoulou & Boulanger (2016), and Boulanger & Ziotopoulou (2017).

The philosophy for calibrating PM4Sand consists of estimating soil parameters, prioritizing behaviors of importance for the system at hand, and then calibrating the constitutive model to honor these properties and behaviors (Boulanger & Ziotopoulou 2018a). Soil parameters (e.g., CRR) can be estimated from common correlations used in practice (e.g., Boulanger & Idriss 2015), combined with or in addition to field and laboratory tests, or any other available pertinent information. Features of the soil behavior (e.g., stress-strain response, shear strain accumulation, soil softening in cyclic loading) can be based on results from laboratory tests, such as DSS. Several studies have shown the ability of PM4Sand to accurately capture features of the soil behavior at the element level (e.g., Kamai & Boulanger 2012, Ziotopoulou & Boulanger 2013), and the system level (e.g., Kamai & Boulanger 2013, Armstrong & Boulanger 2015, Montgomery et al. 2017, Tasiopoulou et al. 2019, Boulanger et al. 2019).

3.2 *PM4Silt v1.0 (Boulanger & Ziotopoulou 2018b)*

The PM4Silt model builds on the framework of the PM4Sand constitutive model with modifications to better approximate the cyclic response of low-plasticity silts and clays. The model has four primary input parameters, a secondary set of 20 parameters, and two flags. Similar to PM4Sand, PM4Silt can be used provided that values for the primary input parameters have been assigned, and considering default values for all secondary parameters to capture the typical behavior of clay-like soils. Parameters of the model are listed in Table 2. The PM4silt model is implemented for plane-strain applications as a user-defined dynamic link library (DLL) in FLAC (Itasca 2020).

The primary input parameters are the undrained strength at critical state ($s_{u,cs}$) or undrained strength ratio at critical state ($s_{u,cs}/\sigma'_{vo}$), the shear modulus coefficient (G_o), the contraction rate parameter (h_{po}), and the undrained shear strength reduction factor (F_{su}). The $s_{u,cs}$ is used to estimate the mean effective stress at critical state (p'_{cs}) using M and the critical state line (CSL) on the

e-ln(p') plane. The F_{su} parameter works as a scaling factor at the end of strong shaking to reduce $s_{u,cs}$, for instance to evaluate the post-seismic stability of earthen structures. Some secondary parameters and their function in the model include: the initial void ratio (e_o) which is used to estimate the state parameter (ξ, as defined by Been & Jefferies1985) given variations in volumetric strains; the n_G parameter that controls how the small-strain shear modulus varies with confinement; the soil compressibility (λ) that influences how ξ varies with changes in p'; the $n^{b,wet}$ and $n^{b,dry}$ parameters determine the bounding surface in loose and dense of critical conditions, respectively; and $r_{u,max}$ which determines the minimum achievable p' (p'_{min}). Further details of the model formulation can be found in Boulanger & Ziotopoulou (2018b, 2019).

The PM4Silt constitutive model has a similar calibration philosophy as PM4Sand. A recommended calibration process for the PM4Silt model has been described by Boulanger et al. (2018) and Boulanger & Wijewickreme (2019). Several studies have shown the ability of the PM4Silt constitutive model to accurately capture features of the soil behavior at the element level (e.g., Boulanger et al. 2018, Boulanger & Wijewickreme 2019), and the system level (e.g., Boulanger 2019, Pretell et al. 2020).

4 ELEMENT LEVEL RESPONSE OF CADIA NTSF TAILINGS

The PM4Sand, and PM4Silt constitutive models were calibrated to capture the key behavior of tailings samples from the Cadia NTSF (Jefferies et al. 2019) at the element level. Calibrations of the models were performed to reasonably capture the response of tailings to both monotonic and cyclic loading, as intended for the system-level assessment of static and earthquake-induced liquefaction. The model calibrations were performed using single-element simulations implemented in the finite difference software FLAC 8.1 (Itasca 2020), and accessible through the models' websites.

Two monotonic and three cyclic undrained DSS tests conducted on tailings materials were selected with the objective of examining the models' performance under different loading conditions, including two σ'_{vc} and three α values. The measured responses from the tests are presented overlaid by the simulated responses in Figure 1, and in the top portions of Figures 2-5. Target behaviors of the soils intended to be captured by the single-element simulations were selected based on what was considered relevant for a system-level evaluation of static and earthquake-induced liquefaction. The target behaviors under undrained monotonic loading were: 1) the small-strain shear stiffness; 2) peak shear strength; 3) the post-peak s_u; and 4) the maximum positive porewater pressure. Similarly, the target behaviors under undrained cyclic loading were: 1) the number of cycles to reach 2.5% of shear strain, considered as the liquefaction triggering criterion by the ITRB (Jefferies et al. 2019); 2) the maximum porewater pressure; 3) the cyclic degradation, i.e. secant shear modulus reduction curves; and 4) the shear strain accumulation.

To capture the target behaviors, two different calibrations were required for the tailings, corresponding to different α conditions: Calibration 1 captures the tailings' response to scenarios with $\alpha = 0.0$ to 0.05; and Calibration 2 captures the tailings' response to scenarios with $\alpha = 0.3$. Different parameters were also considered for monotonic and cyclic loading conditions when significant improvements for a specific behavior were obtained.

4.1 *Calibration of the PM4Sand model*

The PM4sand model was calibrated following a procedure similar to the one presented by Boulanger et al. (2018) and Boulanger & Wijewickreme (2019) for the PM4Silt model, but adapted for PM4Sand model and the context of this work. The procedures for Calibrations 1 and 2 were largely similar, thus a general description is presented with clarifications, when needed. The calibrated parameters are presented in Table 1.

4.1.1 *Step 1: Selection of D_R and G_o*

D_R and G_o were first selected. D_R is a parameter better related to granular soils (e.g., Bolton 1986, Kulhawy & Mayne 1990), and thus a $D_R = 30\%$ was considered appropriate and selected for the tailings samples as they were remolded to a loose state. The G_o parameter was estimated from relation (1), developed from V_s measurements using bender elements (Jefferies et al. 2019), but

modified to obtain the G_{max} functional form that relates G_o (Boulanger & Ziotopoulou 2017), yielding relations (2) and (3). G_o values of 290 and 480 were estimated for σ'_{vc} = 50 and 300 kPa, respectively.

$$G_{\max} = G_{\mathrm{o}}\, P_{\mathrm{a}} \left(\frac{\sigma'_{\mathrm{vc}}\left(\frac{1+K_0}{2}\right)}{P_a} \right)^{0.5} \tag{2}$$

$$G_{\mathrm{o}} = 93.5\, \sigma'^{0.287}_{\mathrm{vc}} \tag{3}$$

K_0: lateral pressure coefficient (assumed as 0.5 for DSS), and σ'_{vc}: vertical effective stress (kPa).

4.1.2 *Step 2: Selection of ϕ'_{cv}*

Data from monotonic DSS tests were used to estimate ϕ'_{cv}, assuming that the horizontal plane is also the plane of maximum obliquity, and considering the limitations described in Parra Bastidas (2016). This approach yielded a mobilized friction angle, ϕ'_{mob} = 31°, which was considered an appropriate approximation of ϕ'_{cv}.

4.1.3 *Step 3: Selection of n^b and n^d*

A lower value than the default one was used for n^b, to reduce the difference between the peak and post-peak shear strengths to the extent possible. Similarly, n^d was reduced from its default value to yield a contractive behavior at large strains, i.e. to suppress the dilation. Different values were selected for Calibrations 1 and 2, as needed to simulate the measured responses (Figs 1a and 1c).

4.1.4 *Step 4: Selection of h_o*

The h_o was reduced from its default value to capture the tailings' small-strain stiffness at shear strains lower than 1.5% measured during monotonic loading. Different values were selected for Calibrations 1 and 2. This parameter was then increased during the calibrations to capture the tailings' response to cyclic loading, such that the secant shear modulus at very low strains followed trends observed in commonly used G/G_{max} relationships, e.g., those proposed by Seed and Idriss for sands (1970), or by Vucetic & Dobry for clays as a function of PI (1991).

4.1.5 *Step 5: Selection of R*

The parameter R was slightly increased from 1.5 (default value) to 1.56 to improve the agreement of s_u at critical state measured during undrained monotonic DSS loading. The selection of a slightly higher value was informed by estimations done following the calibration procedure for R described by Boulanger & Ziotopoulou (2018a).

4.1.6 *Step 6: Other secondary parameters*

Some of the secondary parameters were calibrated to better honor the tailings response to cyclic loading. The parameters z_{max} and C_z were set as 10 and 50 to modify the dilative response at near-zero vertical effective stresses, and consequently improved the agreement between the measured and simulated shear strain accumulation and stress path patterns.

The procedure followed was iterative. Steps 1 and 2 consisted of the selection of parameters estimated from laboratory data and thus remained unchanged throughout the process. The parameter R (Step 5) is related to the material mineralogy (Bolton 1986), and thus was also considered to be consistent in all tailings samples and the same value was used for all calibrations. After Step 2, a trial h_{po} value was selected to simulate single-element undrained DSS tests to proceed with Steps 3 to 6. To some extent, Steps 3 to 5 were independent of Step 6, especially within the context of this work as the responses to undrained monotonic and cyclic DSS loading are both important and considered flexible to have different values for the same parameters. The h_{po} was also calibrated to capture the number of cycles to yield 2.5% of single amplitude shear strain estimated in laboratory tests (Fig. 4a), the liquefaction triggering criterion used for the Cadia NTSF study (Jefferies et al. 2019). Revisions were done between the calibration to the DSS tests performed with to α = 0.0 to 0.05 (one monotonic, two cyclic), and the DSS tests with α = 0.3 (one monotonic, one cyclic), such that the parameters were as consistent as possible. The simulated responses are presented in Figures 1-5.

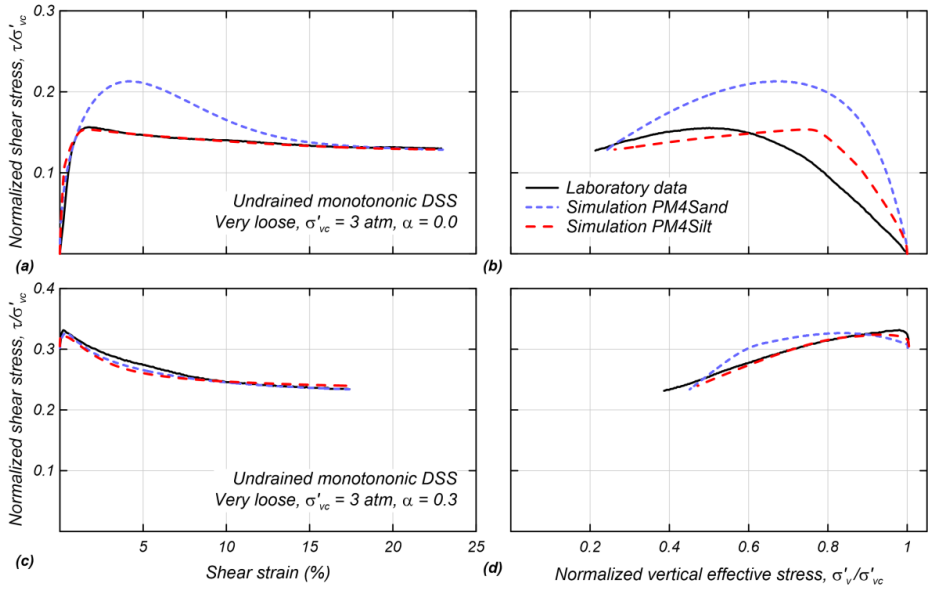

Figure 1: Measured and simulated responses to undrained monotonic DSS loading: (a) (b) stress-strain and stress path responses for $\alpha = 0.0$; (c) (d) stress-strain and stress path responses for $\alpha = 0.3$. *Laboratory data digitalized from the publicly available reports for the Cadia NTSF study (Jefferies et al. 2019).*

4.2 *Calibration of the PM4Silt model*

The PM4Silt model was calibrated following the procedures described by Boulanger et al. (2018) and Boulanger & Wijewickreme (2019). Similar to the PM4Sand model, the procedures for Calibrations 1 and 2 were largely similar, thus a general description is presented with clarifications when needed. The calibrated parameters are presented in Table 2.

4.2.1 *Step 1: Selection of $s_{u,cs}/\sigma'_{vc}$*

The $s_{u,cs}/\sigma'_{vc}$ was estimated as the post-peak s_u/σ'_{vc} from undrained monotonic DSS tests, considered appropriate for the present work. For cyclic conditions, the $s_{u,cs}/\sigma'_{vc}$ was increased such that 1) the demands imposed by α and the applied cyclic stress used during testing could be sustained; and 2) an approximate decrease in 10% of cyclic $s_{u,cs}/\sigma'_{vc}$ is obtained at 10 cycles, consistent with observations by Boulanger & Idriss (2007) for normally consolidated (NC) clays subjected to $\alpha = 0.05$. A similar approach was used for the test with $\alpha = 0.3$, with the difference that a higher $s_{u,cs}/\sigma'_{vc}$ was used according to laboratory test results (Fig. 1c) as described in Section 2.2, and no specific decrease at 10 cycles due to the effect of α. In all cases, strain-rate effects and multi-directional shaking were considered as having a compensating effect and canceling each other out.

4.2.2 *Step 2: Selection of ϕ'_{cv}, e_o, and λ*

A similar approach as the calibration of the PM4Sand model was used for ϕ'_{cv}. The reported void ratio for remolded samples prior to consolidation of each specific test were used for e_o. The e_o values ranged from 0.57 to 0.62 (Jefferies et al. 2019). The averaged $\lambda = C_c/2.3$ (C_c: compression index) was estimated based on oedometer consolidation data from tests performed on the same tailings studied herein (Jefferies et al. 2019).

4.2.3 *Step 3: Selection of G_o and n_G*

The G_o parameter was estimated by modifying relation (1) to obtain the target functional form for G_{max} (Boulanger & Ziotopoulou 2018b) while honoring the measured V_s. Following this approach, relation (4) was obtained, where $n_G = 0.787$. Differently from calibration of the PM4Sand model,

Table 1. PM4Sand calibrated model parameters

Parameter	Default value	Calibration 1 (α = 0 to 0.05)		Calibration 2 (α = 0.3)	
		Monotonic	Cyclic	Monotonic	Cyclic
D_R: apparent relative density	[b]	30%		30%	
G_o: shear modulus coefficient	[b]	Relation (3) [c]		Relation (3) [c]	
h_{po}: contraction rate parameter	[b]	4.3	2.0	1.05	4.2
h_o: plastic modulus ratio	$0.3 \leq (0.25+D_R)/2$	0.025	0.25	0.29	
e_{min}: minimum void ratio	0.5	-		-	
e_{max}: maximum void ratio	0.8	-		-	
ϕ'_{cv}: critical state friction angle	33°	31°		31°	
n^b: bounding surface parameter	0.5	0.05	-	0.19	
n^d: dilation surface parameter	0.1	0.01	-	-	
A_{do}: dilatancy parameter	1.26 to 1.45	-		-	
z_{max}: fabric term	$0.7 \exp(-6.1\xi_R) \leq 20$	10		10	
C_z: fabric growth parameter	250	50		50	
C_ε: strain accumulation rate factor	1.0 to 5.0	-		-	
C_{GD}: modulus degradation factor	2.0	-		-	
$C_{k\alpha f}$: plastic modulus factor	$4 \leq 5+220(D_R - 0.26)^3 \leq 35$	-		-	
C_{DR}: plastic modulus factor	$5+25(D_R - 0.35) \leq 10$	-		-	
Q: Bolton's parameter	10	-		-	
R: Bolton's parameter	1.5	1.56		1.56	
ν_o: Poisson ratio	0.3	-		-	

[a] List of parameters excluding post-shaking analysis parameters, and flag variables.
[b] Required input parameter, no default value.
[c] G_o = 290 and 480 for σ'_{vc} = 0.5 and 3 atm, respectively.

Table 2. PM4Silt calibrated model parameters

Parameter	Default value	Calibration 1 (α = 0 to 0.05)		Calibration 2 (α = 0.3)	
		Mo	Cy	Mo	Cy
$s_{u,cs}/\sigma'_v$: s_u ratio at critical state	[b]	0.13	0.15	0.23	0.30
G_o: shear modulus coefficient	[b]	350		350	
h_{po}: contraction rate parameter	[b]	10.0		30.0	12.0
n_G: shear modulus exponent	0.75	0.787		0.787	
h_o: plastic modulus ratio	0.5	0.07	0.15	-	0.25
e_o: initial void ratio	0.9	0.6		0.6	
λ: compressibility, in e-ln(p') space	0.06	0.05		0.05	
ϕ'_{cv}: critical state friction angle	32°	31°		31°	
$n^{b,wet}$: bounding surface parameter	0.8	-		0.38	
$n^{b,dry}$: bounding surface parameter	0.5	-		-	
n^d: dilation surface parameter	0.3	-		-	
A_{do}: dilatancy parameter	0.8	-		-	
$r_{u,max}$: sets bounding p'_{min}	$p'_{min} = p'_{cs}/8$	0.95		0.95	
z_{max}: fabric term	$10 \leq 40\ s_u/\sigma'_v \leq 20$	-		-	
C_z: fabric growth parameter	100	-		-	
C_ε: strain accumulation rate factor	$0.5 \leq (1.2 s_u/\sigma'_v+0.2) \leq 1.3$	-		-	
C_{GD}: modulus degradation factor	3.0	-		-	
$C_{k\alpha f}$: plastic modulus factor	4.0	-		-	
ν_o: Poisson ratio	0.3	-		-	

[a] List of parameters excluding post-shaking analysis parameters.
[b] Required input parameter, no default value.

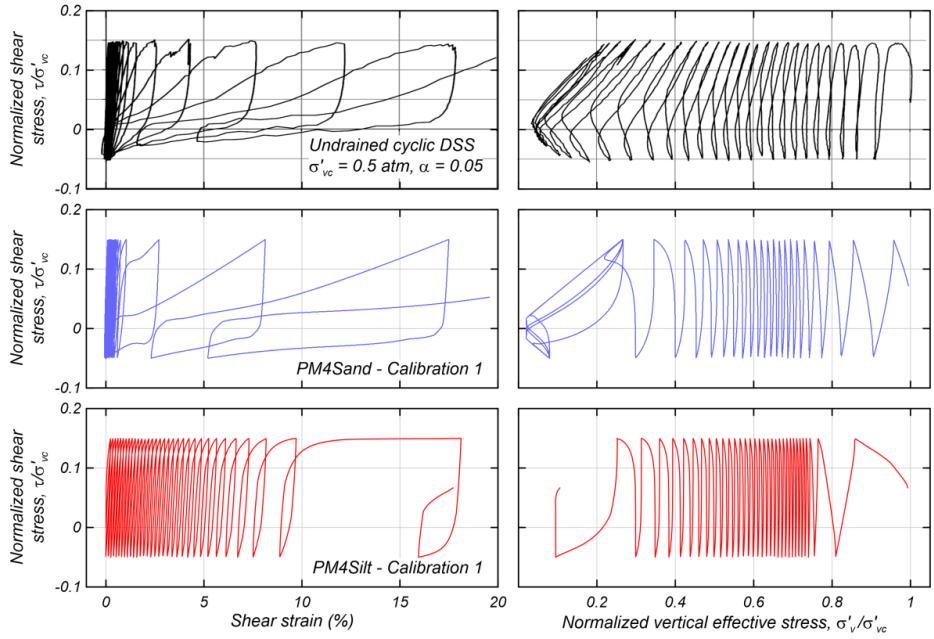

Figure 2: Measured and simulated responses to undrained cyclic DSS loading. Stress-strain loops and stress path responses, on the left and right sides, respectively. *Laboratory data from Jefferies et al. (2019).*

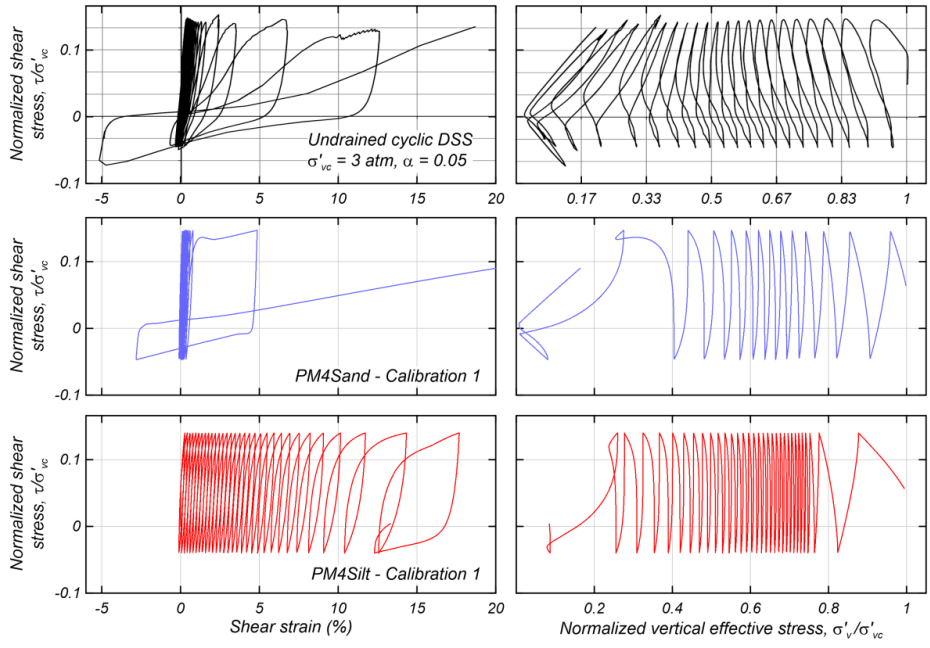

Figure 3: Measured and simulated responses to undrained cyclic DSS loading. Stress-strain loops and stress path responses, on the left and right sides, respectively. *Laboratory data from Jefferies et al. (2019).*

herein the use of n_G allows for the use of a G_o independent of the confinement stress $G_o = 350$.

$$G_{\max} = 350\, P_a \left(\frac{\sigma'_{vc}\left(\frac{1+K_0}{2}\right)}{P_a} \right)^{0.787} \tag{4}$$

4.2.4 *Step 4: Selection of $n^{b,wet}$*

The $n^{b,wet}$ parameter was reduced from its default value for Calibration 2. This increased the difference between the peak and the post-peak shear strengths and thus better captured the measured response (Figs 1c and 1d).

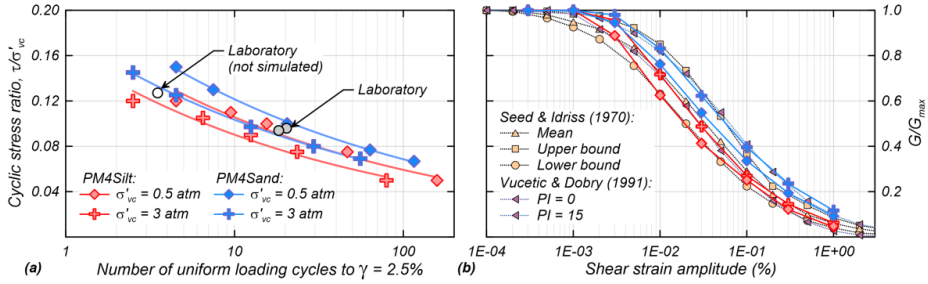

Figure 4: Measured and simulated responses for Calibrations 1: (a) cyclic stress ratio vs. number of uniform loading cycles to a shear strain of 2.5%; and (b) secant shear modulus reduction (G/G_{max}) curves simulated and from common relationships. *Laboratory data from Jefferies et al. (2019).*

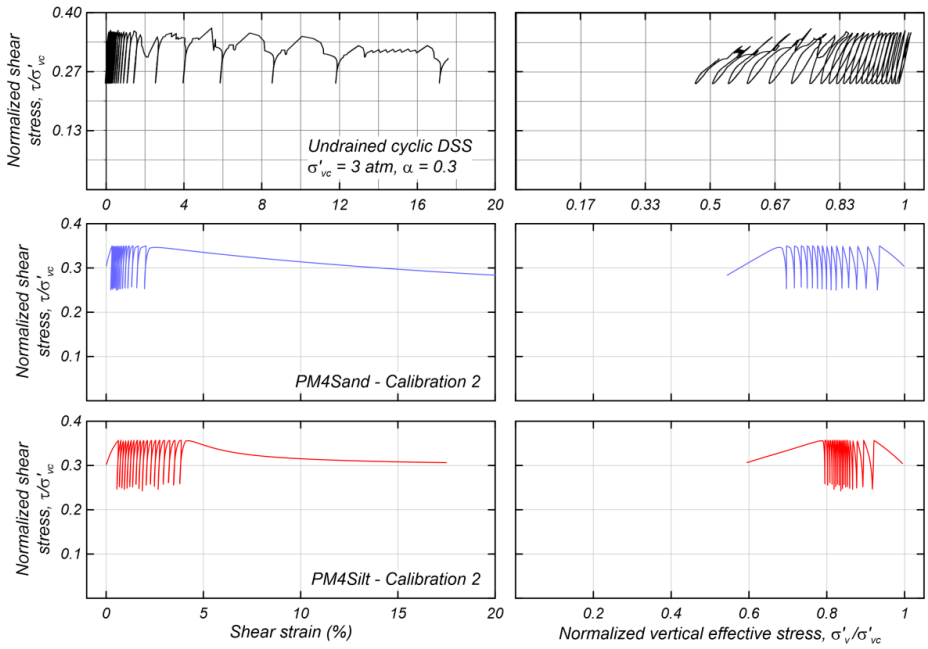

Figure 5: Measured and simulated responses to undrained cyclic DSS loading. Stress-strain loops and stress path responses, on the left and right sides, respectively. *Laboratory data from Jefferies et al. (2019).*

4.2.5 *Step 5: Selection of h_o*

Similar to Step 4 in the calibration of the PM4Sand constitutive model.

4.2.6 *Step 6: Selection of $r_{u,max}$*

The $r_{u,max}$ was set as 0.95 to let the cyclic-induced excess porewater pressure buildup without constraints. This parameter does not have an effect on the response to undrained monotonic DSS loading but was considered as 0.95 in all calibrations for consistency.

Similar to the PM4Sand calibration, the procedure followed was iterative. Steps 1 and 2 yielded more fundamental parameters that were unchanged throughout the process. After Step 2, a trial h_{po} value was selected to simulate single-element undrained DSS tests to proceed with Steps 3 to 6. Herein, Step 6 was independent, and used only once as it showed a slight improvement of the simulated response of tailings to cyclic loading. Steps 4 and 5, and the calibration of h_{po} required iterations to approximately capture the number of cycles to achieve 2.5% of single amplitude shear strain estimated in the laboratory tests (Fig. 4a) reported by Jefferies et al. (2019). Revisions were done between the calibration to all DSS tests such that the parameters were as consistent as possible. The simulated responses are presented in Figures 1-5.

5 DISCUSSION OF RESULTS

Single-element DSS simulations using both the PM4Sand and PM4Silt constitutive models were able to satisfactorily capture features of the tailings' response for specific loading conditions. The tailings' response to undrained monotonic DSS loading was well captured by the PM4Silt Calibrations 1 and 2 (Fig. 1), e.g. agreement between small-strain shear stiffness, and peak and residual shear strengths. Results from simulations using the PM4Sand Calibration 2 ($\alpha = 0.3$) captured well the response to monotonic DSS loading (Figs 1c and 1d). However, discrepancies were observed when the Calibration 1 ($\alpha = 0.0$ to 0.05) parameters were used (Figs 1a and 1b). The peak shear strength measured in this test (described in Section 2.2) was not captured after reasonable calibration efforts, thus only the measured initial stiffness and post-peak shear strengths were honored, while the peak shear strength reduced as possible. Differences between the measured and simulated stress paths (Figs 1b and 1d) were considered acceptable, especially given the agreement between the measured and simulated ultimate vertical effective stresses, suggestive of the maximum porewater pressure generated during undrained loading, critical in the assessment of static liquefaction.

The tailings' response to undrained cyclic DSS loading was well captured by the PM4Sand constitutive model Calibrations 1 (Figs 2-5), e.g. simulations yielded 15.5 to 20.5 cycles to reach 2.5% shear strain, while 18 to 20.5 were measured (Fig. 4a), and Calibration 2, e.g. 11 cycles yielded by the simulations, while 12 were measured. Some differences were observed at shear strains larger than 2.5%, but they were considered to be less relevant in the calibration process, given the little impact expected on an eventual system-level evaluation of earthquake-induced liquefaction. All calibrations led to secant shear modulus reduction (G/G_{max}) curves consistent with commonly used relations (Fig. 4b). Discrepancies in terms of porewater pressure buildup and stress-strain and stress path patterns (Fig. 3), were observed when PM4Silt was calibrated to simulate the tailings' response to undrained cyclic DSS loading, even when the target behaviors (e.g., number of cycles to 2.5% shear strain, and secant shear modulus reduction, G/G_{max}) were reasonably captured. These differences between the measured and simulated responses to cyclic loading were not surprising as the PM4Silt model was developed to capture the features specific to the clay-like soils' response to cyclic loading, i.e. slow strain accumulation and limited porewater pressure buildup.

6 FINAL REMARKS

The PM4Sand and PM4Silt constitutive models were briefly introduced and evaluated on their ability to capture features of the behavior of tailings materials from the Cadia NTSF embankment (Jefferies et al. 2019). This evaluation was performed by comparing results from single-element

direct simple shear (DSS) simulations implemented in FLAC against undrained monotonic and cyclic DSS tests performed under different loading conditions. Results suggest that both the PM4Sand and PM4Silt models were able to satisfactorily capture features of the tailings' response for specific loading conditions.

Results from the calibrations presented herein for tailings of the Cadia NTSF project, indicated that PM4Silt was able to capture the tailings' response to undrained monotonic DSS loading, whereas the PM4Sand model captured better the tailings' response to undrained cyclic DSS loading. Tailings of the Cadia NTSF exhibited a significantly different behavior when subjected to low and high sustained static bias prior to DSS shearing, conditions representative of tailings at distant and nearby to or under the embankment, respectively. The tailings' response to these conditions was appropriately captured by the PM4Sand and PM4Silt models, however adjustment of the h_{po} and the secondary parameters h_o, n^b, and n^d, was required. Based on these results, the PM4Silt model is recommended for the assessment of static liquefaction of the Cadia NTSF at the system level using NDAs, while the PM4Sand model is recommended for the assessment of earthquake-induced liquefaction. Also, different sets of parameters for different zones within the TSF are recommended depending on the initial loading conditions (e.g. static shear stress). Alternatively, a single model and set of parameters can be selected if a single failure mechanism and zone of interest are prioritized.

The proper simulation of the tailings response at the element level builds confidence on the forward predictions obtained from numerical simulations at the system level. The calibration of constitutive models, particularly when project-specific laboratory data are available, requires close examination of features of the soil's behavior and an understanding of the failure mechanism expected at the system level. In cases with more than one failure mechanism of interest or high variability of soil parameters, then it is recommended to explore the use of multiple sets of parameters together with sensitivity analyses.

7 REFERENCES

Armstrong, R.J., & Boulanger, R.W. 2015. Numerical simulations of liquefaction effects on piled bridge abutments. *Proc. in 6th Int. Conf. on Earthquake Geotech. Eng.*, 1 to 4 Nov. Christchurch, New Zealand.

Been, K., & Jefferies, M.G. 1985. A state parameter for sands. *Géotechnique* 35(2), 99–112.

Bolton, M.D. 1986. The strength and dilatancy of sands, Geotechnique 36(1), 65–78.

Boulanger, R.W. 2019. Nonlinear dynamic analyses of Austrian Dam in the 1989 Loma Prieta Earthquake. *Journal of Geotechnical and Geoenvironmental Engineering*, 145(11): 05019011.

Boulanger, R.W., & Idriss, I.M. 2007. Evaluation of cyclic softening in silts and clays. *Journal of Geotech. and Geoenviron. Eng.*, 133:6(641).

Boulanger, R.W., & Idriss, I.M. 2015. CPT-based liquefaction triggering procedure. *Journal of Geotech. and Geoenviron. Eng.*, 142(2): 04015065.

Boulanger, R.W., Munter, S.K., Krage, C.P., & DeJong, J.T. 2019. Liquefaction evaluation of interbedded soil deposit: Çark Canal in 1999 M7.5 Kocaeli Earthquake. *Journal of Geotechnical and Geoenvironmental Eng.*, 145(9): 05019007.

Boulanger, R.W., Price, A.B., & Ziotopoulou, K. 2018. Constitutive modeling of the cyclic loading response of low plasticity fine-grained soils. *Proc. GeoShangai 2018 In. Conf. Fund. Soil Behaviours*, 27 to 30 May. Shangai, China.

Boulanger, R.W., & Wijewickreme, D. 2019. Calibration of a constitutive model for the cyclic loading responses of Fraser River Delta silt. *Proc. in 7th Int. Conf. on Earthquake Geotech. Eng.*, 17 to 20 June. Rome, Italy.

Boulanger, R.W., & Ziotopoulou, K. 2017. PM4Sand (v3.1): A sand plasticity model for earthquake engineering applications. *Report No. UCD/CGM-17/01*, Davis, CA: University of California, Davis. https://pm4sand.engr.ucdavis.edu/

Boulanger, R.W., & Ziotopoulou, K. 2018a. On NDA practices for evaluating liquefaction effects. *Proc. in Geotechnical Earthquake Engineering and Soil Dynamics V*. Austin, TX.

Boulanger, R.W., & Ziotopoulou, K. 2018b. PM4Silt (v1.0): A silt plasticity model for earthquake engineering applications. *Report No. UCD/CGM-18/01*, Davis, CA: University of California, Davis. https://pm4silt.engr.ucdavis.edu/

Boulanger, R.W., & Ziotopoulou, K. 2019. A constitutive model for clays and plastic silts in plane-strain earthquake engineering applications. *Journal of Soil Dynamics and Earthquake Engineering*, 127(2019), 105832.

Dafalias, Y.F., & Manzari, M.T. 2004. Simple plasticity sand model accounting for fabric change effects. *Journal of Engineering Mechanics*, 130(6), 622-634.

Itasca 2020. FLAC, Fast Lagrangian Analysis of Continua, User's Guide, Version 8.1. Itasca Consulting Group, Inc., Minneapolis, MN.

Jefferies, M.G., Morgenstern, N.R., & Van Zyl, D. 2019. *Report on NTSF embankment failure Cadia Valley Operations for Ashurst Australia.* Independent Technical Review Board (ITRB).

Kamai, R., & Boulanger, R.W. 2012. Single-element simulations of partial-drainage effects under monotonic and cyclic loading. *Journal of Soil Dynamics and Earthquake Engineering*, 35, 29-40.

Kamai, R., & Boulanger, R.W. 2013. Simulations of a centrifuge test with lateral spreading and void redistribution effects. *Journal of Geotechnical and Geoenvironmental Eng., 139(8): 1250-1261.*

Kulhawy, F.H., & Mayne, P.W. 1990. Manual on Estimating Soil Properties for Foundation Design, Report EPRI EL-6800, Electric Power Research Institute, Palo Alto, CA.

Montgomery, J., Boulanger, R.W., & Ziotopoulou, K. 2017. Effects of spatial variability on the seismic response of the Wildlife Liquefaction Array. *Proc. in PDE Geotech. Eng., PBD-III.* Vancouver, Canada.

Parra Bastidas, A.M. 2016. Ottawa F-65 sand characterization. Ph.D. dissertation, *Dept. of Civil and Environmental Engineering*, University of California, Davis.

Pretell, R., Ziotopoulou, K., & Davis, C.A. 2020. Liquefaction and cyclic softening at Balboa Blvd. during the 1994 Northridge Earthquake. *Journal of Geotechnical and Geoenvironmental Eng. (accepted).*

Seed, H.B., & Idriss, I.M. 1970. Soil moduli and damping factors for dynamic response analyses. *Report No. EERC-70-10*, Earthquake Eng. Research Center. Berkeley, CA: University of California, Berkeley.

Tasiopoulou, P., Ziotopoulou, K., Humire, F., Giannakou, A., Chacko, J., & Travasarou, T. 2019. Development and implementation of semiempirical framework for modeling postliquefaction shear deformation accumulation in sands. *J. of Geotech. and Geoenviron. Eng.*, ASCE, 146(1): 04019120.

Vucetic, M., & Dobry, R. 1991. Effect of soil plasticity on cyclic response. *Journal of Geotechnical Engineering*, 117(1),89–107.

Ziotopoulou, K., & Boulanger, R.W. 2013. Calibration and implementation of a sand plasticity plane-strain model for earthquake engineering applications. *Journal of Soil Dynamics and Earthquake Engineering*, 53, 268-280.

Ziotopoulou, K., & Boulanger, R.W. 2015. Validation protocols for constitutive modeling of liquefaction. *Proc. in 6th Int. Conf. on Earthquake Geotech. Eng.*, 1 to 4 November. Christchurch, New Zealand.

Ziotopoulou, K., & Boulanger, R.W. 2016. Plasticity modeling of liquefaction effects under sloping ground and irregular cyclic loading conditions. *Journal of Soil Dynamics and Earthquake Engineering*, 84, 269-283.

Ziotopoulou, K., Maharjan, M., Boulanger, R.W., Beaty, M.H., Armstrong, R.J., & Takahashi, A. 2014. Constitutive modeling of liquefaction effects in sloping ground. *Proc. in 10th U.S. National Conference on Earthquake Engineering Frontiers of Earthquake Engineering.* Anchorage, AK.

Managing the Liquefaction Potential of Compacted Tailings Sand at Suncor

Ying Zhang, Ayman H. Abusaid & Gordon W. Pollock
Wood Environment & Infrastructure, Edmonton, Alberta, Canada

Jason Rhee & Ryan Moore
Suncor Energy Inc., Calgary, Alberta, Canada

ABSTRACT: Tailings sand placed hydraulically in a beach above water (BAW) setting can be potentially liquefiable when the structure is raised at a high rate. Dozers are commonly used during tailings placement to form a non-liquefiable shell for upstream tailings dams. Field testing, mainly SPT and CPT, are widely used to assess the liquefaction susceptibility of tailings sand.

Sand Dump 8 is an upstream tailings sand structure at Suncor, which has been constructed with 5 m lifts at a rate between 10 m and 20 m per year since 2012. CPT testing is regularly conducted to evaluate the liquefaction susceptibility of the compacted tailings sand. This paper presents the method in selecting CPT locations, liquefaction susceptibility analysis methods, the findings of the CPT testing, and the protocol adopted by Suncor in addressing potentially liquefiable zones encountered in the compacted sand. This approach reflects Suncor's use of best available technology (CPT) and best available practices (dozer compaction of hydraulically placed sand and liquefaction potential assessment methods) to manage liquefaction potential.

1 INTRODUCTION

Sand Dump 8 is a tailings sand structure at Suncor designed and constructed with a minimal pond size that results in a landform that is easier to reclaim at the end of construction compared to a conventional tailings pond. It is located at Suncor's Millennium mine site, north of Fort McMurray, Alberta, Canada, as shown in Figure 1.

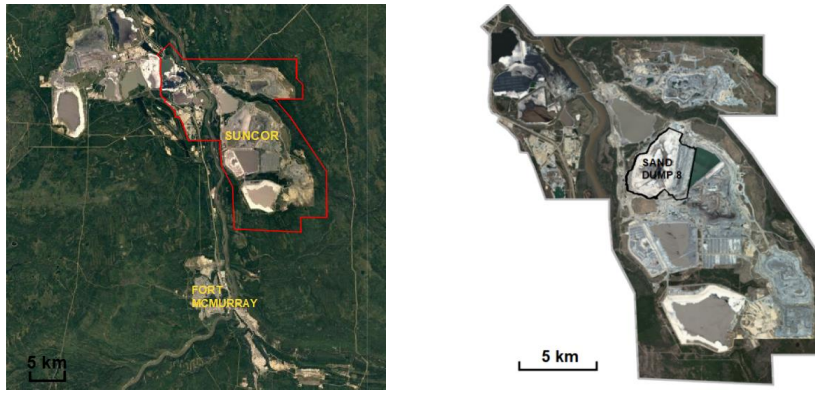

Figure 1 Location and plan view of Suncor Sand Dump 8

Figure 2 presents a recent site view of the key components of the structure. The final height of the sand structure is approximately 130 m and is expected to be completed by 2025. It has been constructed with 5 m lifts at a rate between 10 m and 20 m per year since 2012. A total height of 85 m tailings sand has been constructed to date. The design and construction with the project background information were discussed in Pollock et al (2014) and Mettananda et al (2014), respectively.

Figure 2 Plan view of Sand Dump 8 in May 2020

Although sand deposited in a beach above water (BAW) setting is often considered to be non-liquefiable, when deposited at high rates it can be potentially liquefiable. Two design elements have been incorporated to establish a minimum width of non-liquefiable sand for this upstream constructed tailings structure:

- dozer compaction that takes place continuously during placement of sand in the required compaction zone,
- and a basal drainage system to draw down the phreatic surface to facilitate downward drainage.

The compacted zone is constructed by spigotting tailings into a cell that is subdivided by several dry dykes, with one end of the cell left open to facilitate drainage of water and fine tailings towards the pond. In some cases, the end of the cell will have a dry dyke with a spill pipe installed to facilitate drainage out of the cell.

Figure 3 shows a typical profile of the east containment dyke. The effectiveness of the above two elements in providing a non-liquefiable sand zone and in drawing down the phreatic surface within the compacted sand zone is assessed by regularly conducting cone penetration testing (CPT) on the beaches. This approach reflects Suncor's use of best available technology (CPT) and best available practices (dozer compaction of hydraulically placed sand and employing liquefaction potential assessment methods) to manage liquefaction potential for a tailings structure.

This paper presents the criteria used in selecting CPT locations, liquefaction susceptibility analysis methods, the findings of CPT testing on liquefaction susceptibility, and the protocol adopted by Suncor in addressing potentially liquefiable zones encountered in the compacted sand at Sand Dump 8.

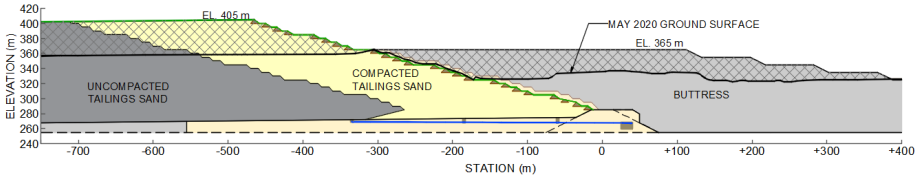

Figure 3 Typical profile of the east bound dyke of Sand Dump 8

2 SELECTION OF CPT LOCATIONS

CPT programs are conducted at least twice a year such that each newly placed sand lift is tested at the surface. In total, nearly thirty separate CPT programs with about 1200 CPTs in total have been conducted at Sand Dump 8 since 2012. The test locations are typically selected based on the following criteria:

- Provide a good distribution across areas within newly placed sand lifts. CPTs are pushed to refusal (up to 40 m deep at Sand Dump 8) or 1 m into the foundation to test the previously placed sand lifts.
- Target locations where potentially liquefiable zones were identified in previous programs to evaluate whether these zones continue to be potentially liquefiable.
- Target locations with low numbers of dozer passes. The GPS mounted on the dozers collects the location data at 3 m by 3 m grid points while dozers track-pack the tailings cell during hydraulic tailings placement. The number of dozer passes were colour coded to give an indication on the amount of compaction effort at the grid points. Where the dozer effort is suspected to be lower than average, a CPT is located in that area.
- Target wet/low locations suggested by satellite photos and field notes. The monthly georeferenced high-resolution satellite photos acquired by Suncor provide a direct view of the site condition. The field notes provided by the CPT contractor summarize the wet and soft spots encountered in previous programs, if any.
- Avoid the active construction areas. Tailings sand is continually being placed at several areas of Sand Dump 8 therefore test locations are limited to the areas safely accessible to the CPT rigs.

3 LIQUEFACTION SUSCEPTABILITY ANALYSIS METHODS

The definitions and fundamentals of liquefaction have been well described in many papers, such as Robertson & Wride (1998), Olson & Stark (2003), Robertson (2010), Jefferies & Been (2016),

Robertson (2016 & 2017), and Robertson et al. (2017). Figure 4 presents the methods used for screening liquefaction susceptibility of the compacted tailings sand at Sand Dump 8.

a) CPT1910-SD8-D11NC06-0275

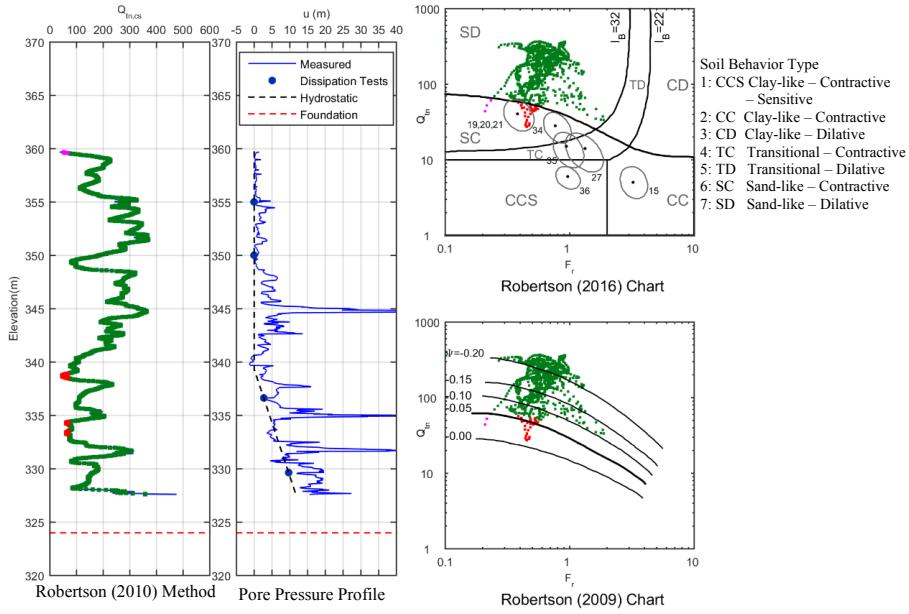

b) CPT1910-SD8-D11SC26-0600

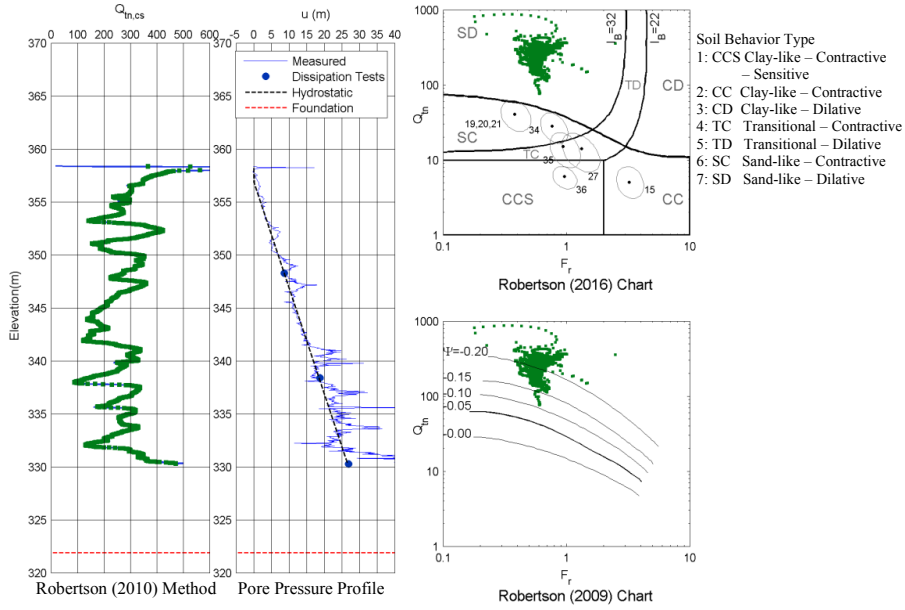

Figure 4 Methods for liquefaction susceptibility analysis

The data points were colour coded based on the liquefaction susceptibility analysis, with red dots indicating sand zones which are potentially liquefiable and green dots indicating non-liquefiable. The purple dots indicate that the potentially liquefiable sand is less than 0.3 m deep from the ground surface, where the interpretation is not reliable given the negligible confining stress and potential disturbance at ground surface. The methods for evaluating liquefaction susceptibility are discussed below. Note that evaluation of potential cyclic liquefaction induced by seismic events is not covered in this paper.

3.1 *$Q_{tn,cs}$ Method by Robertson (2010 & 2016)*

The $Q_{tn,cs}$ method by Robertson (2010) was used as the primary approach to assess the susceptibility to liquefaction at Sand Dump 8. $Q_{tn,cs}$ is the cone penetration resistance normalized to overburden stress and to an equivalent clean sand. This is an empirical criterion mainly based on six liquefaction failure case histories with complete CPT data including sleeve friction values, labeled Class A. Robertson (2010) proposed the contractant-dilatant (C/D) boundary at $Q_{tn,cs} = 70$, which represents the upper bound of the mean plus one standard deviation value of $Q_{tn,cs}$ within the zone that was considered to have experienced strength loss and involved in the slide in the six Class A case histories. The proposed contractant-dilatant (C/D) boundary of $Q_{tn,cs} = 70$ also represents the upper bound of the mean value of $Q_{tn,cs}$ within the zone that was considered to have experienced strength loss and involved in the slide in all the thirty six case histories, Classes A, B, C, D, & E. Individual CPT $Q_{tn,cs}$ data collected at an interval of 2.5 cm was compared to $Q_{tn,cs}$ of 70. The soil at a specific depth is considered to be susceptible to liquefaction if $Q_{tn,cs} \leq 70$.

It should be noted that there are some sources of uncertainties in the back analysis of the case histories (e.g. using CPT data outside the slide mass) and the difference between actual failure mechanism and failure mechanism assumed in the analysis (one slide mass vs retrogressive failure). Robertson (2016) also indicated that using $Q_{tn,cs} = 70$ is slightly conservative but it is considered as an appropriate screening tool for tailings structures with very high consequence.

Robertson (2016) incorporated the $Q_{tn,cs} = 70$ contour on the updated soil behavior type (SBT) chart. The SBT chart classifies soils based on the behavior (Q_{tn} and F_r) into seven groups: clay-like-contractive-sensitive, clay-like-contractive, clay-like-dilative, transitional-contractive, transitional-dilative, sand-like-contractive, and sand-like-dilative. The $Q_{tn,cs} = 70$ contour is the contractive/ dilative boundary. When $Q_{tn,cs} \leq 70$, the soils are expected to be contractive and therefore susceptible to liquefaction. The updated SBT chart in the upper right hand graph in Figures 4a and 4b was used to present the behavior categories of potentially liquefiable sand.

3.2 *Measured Pore Water Pressure*

Liquefaction can only occur in saturated or nearly saturated loose soils. Soils are likely not susceptible to liquefaction above the water table. The water table determined using CPT pore pressure dissipation (PPD) tests gives an indication of the saturation status at the time of testing, although re-saturation may occur with subsequent tailings placement.

The excess pore pressure (u_e) generated during cone penetration is the difference between the dynamic pore pressure (u_2) and equilibrium pore pressure (interpreted from PPD tests). It gives an indication of how the sand around the cone tip responds to the penetration/disturbance. Theoretically, positive u_e implies that sand particles tend to contract (loose sand) upon shearing and generate elevated pore pressure. Negative u_e implies that sand particles tend to dilate (dense sand) upon shearing and a reduction in pore pressure occurs. However, it has been noted that positive excess pore pressure response was observed at Sand Dump 8 in dense sand. The dynamic pore pressure is presented and discussed in a companion paper (Abusaid et al. 2020).

3.3 *State Parameter*

Under the critical state soil mechanics framework, Jefferies and Been (2016) applied the state parameter concept to soil liquefaction analysis. The state parameter (ψ) is defined as the difference between the in-situ void ratio, e_0, and the void ratio at critical state, e_{cs}, at the same mean effective stress. Jefferies and Been (2016) recommended the use of $\psi = -0.05$ as the boundary between liquefiable and non-liquefiable sand. Sand is considered liquefiable when $\psi > -0.05$.

Robertson (2009) plotted a set of state parameter contours on the SBT chart for comparison. The lower right hand graph in Figures 4a and 4b shows that the potentially liquefiable sand based on $Q_{tn,cs}$ method in general matches the state parameter approach ($\psi > -0.05$).

4 DATA INTERPRETATION AND ACTIONS

4.1 *Identifying Potentially Liquefiable Sand and Actions*

The potentially liquefiable zones within the newly placed sand lifts and previously placed sand lifts above the termination depths were identified using the charts plotted for individual CPTs using MATLAB – a computer programming language developed by MathWorks, as shown in Figure 4.

CPTs with potentially liquefiable zones in the top 0.3 m below the ground surface (i.e. purple dots in Figure 4) were not of concern for two reasons: these areas are expected to receive additional dozer compaction during the placement of the subsequent lift; the quality of near surface CPT data in interpreting liquefaction susceptibility is questionable due to the very low confining stress.

If the potentially liquefiable sand is in the upper 2 m, dozer compaction would be implemented prior to or at the beginning of the next lift placement. If it is at depths between 2 m and 5 m, immediate dozer compaction is requested, since the construction at Sand Dump 8 is year-round and the effectiveness of dozer compaction is limited to the upper few meters. For potentially liquefiable sand zones below 2m, recompaction with dozers at surface may result in limited improvement and therefore it is important to reassess the zone with CPT in subsequent testing programs to evaluate the lateral extent and potential improvement with subsequent construction loading. In addition, the CPT program may be adjusted (e.g., add more CPTs in areas of concern) during the field program as draft results are reviewed by the design team.

If potentially liquefiable zones are identified at depths greater than 5 m, the protocol described in the following sections is implemented. It has been observed that problem zones at depths are typically at lift contacts and therefore it is important to address these areas early on as described above.

4.2 *Assessment of Sand Improvement*

Tailings sand could potentially experience state improvement (i.e. increase in $Q_{tn,cs}$) for the following reasons:

- Tailings sand receives additional overburden load due to the subsequent sand lift placement.
- Tailings sand near the ground surface receives dozer compaction (i.e. load with vibration) during the subsequent sand lift placement.
- Downward seepage force may densify the tailings sand, and
- Tailings sand may further consolidate due to the suction created by desaturation of the newly placed lift.

Figure 5 presents a few examples of the comparison between the new CPT data and the CPT data at the same location from previous programs where potentially liquefiable sand was identified. Several of the looser sand (e.g. $Q_{tn,cs} < 100$) layers, which are of concern, experienced improvement as construction progressed. The denser sand (e.g. $Q_{tn,cs} > 100$) did not have a definitive trend in improvement of the sand state.

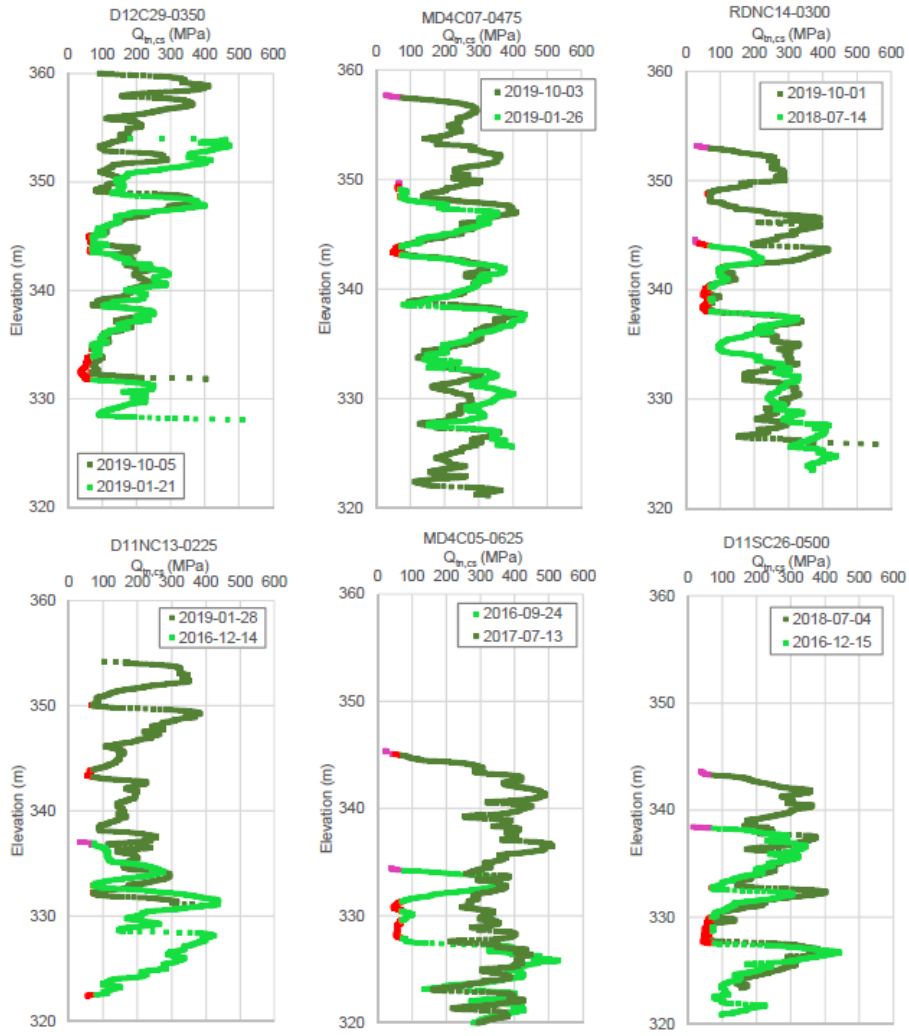

Figure 5 Comparison of CPT data at the same location from different CPT programs

4.3 *Assessment of Continuity of Potentially Liquefiable Zones*

Isolated areas of potentially liquefiable sand are not expected to pose stability risk to the Sand Dump 8 structure. Therefore, it is necessary to examine the continuity and extent of all potentially liquefiable zones that were not shown to be improved to non-liquefiable sand. Given the size of the structure, isolated pockets were considered to be less than 200 m diameter areas. All CPT data within the 100 m radius of the CPTs of concern were reviewed to assess lateral continuity of the potentially liquefiable zone, as shown in Figures 6 and 7. More than 99% of all the zones of concern are in the top 30 m from ground surface, as shown in Figure 7. To date, potentially liquefiable zones from previous CPT programs were shown to be either improved to be dilative as construction proceeded or isolated using subsequent CPT testing.

According to laboratory data and liquefaction case histories referenced in Robertson (2017), very loose sand near ground surface has high brittleness and is susceptible to liquefaction. Loose sand with an effective overburden stress higher than 2 atm to 3 atm loses brittleness and behaves

ductile during shearing. Regardless of the potential benefit of high overburden stress, Suncor monitors all potentially liquefiable zones at depth which have not yet been assessed to be isolated or that have densified such that they are non-liquefiable sand, whenever possible. This monitoring consists of completing additional CPT holes in the area of interest to evaluate whether an improvement in the state of the sand may have occurred with additional construction loading and/or to further assess lateral continuity of the potentially liquefiable zone.

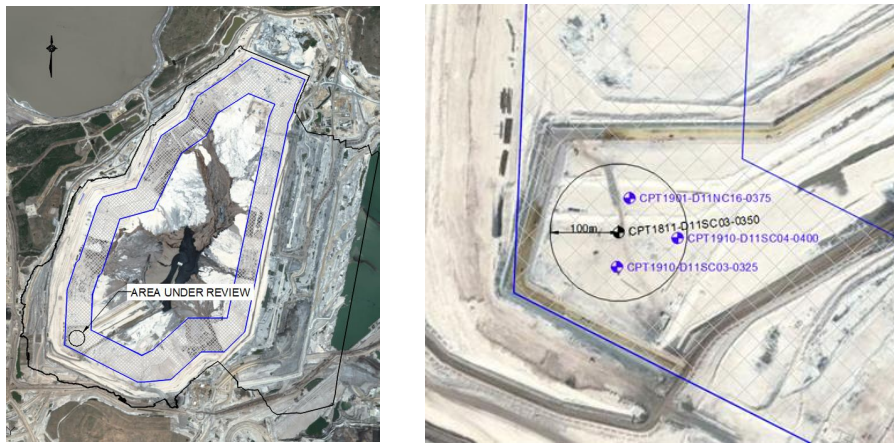

a) Overall site plan b) Local site plan with CPT locations

Figure 6 Site plan showing the locations of the CPTs under review

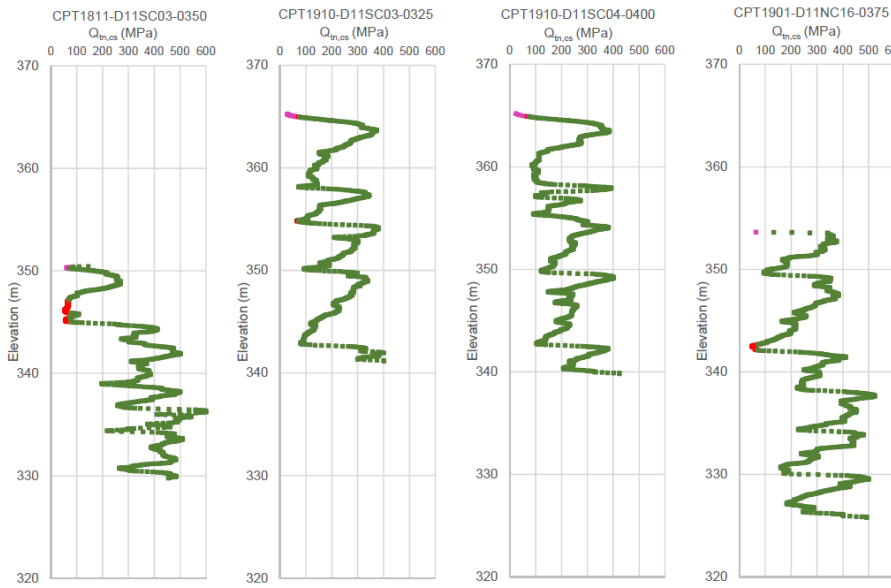

Figure 7 Examination of continuity of potentially liquefiable zone in compacted sand

5 REMEDIATION OPTIONS FOR CONTINUOUS LIQUEFIABLE LAYER

Areas where potentially liquefiable zones are identified can be divided into two main categories: ones that are accessible from the surface (shallow zones), and ones that are at a depth of greater than about 5 m below the surface (deep zones).

5.1 *Shallow Zones*

Potentially liquefiable zones close to the surface are recompacted by dozers either from the existing ground surface or after excavation to a certain depth (< 2m deep). These have been implemented at Sand Dump 8 along with the CPT programs.

5.2 *Deep Zones*

It is more challenging if potentially liquefiable zones were well below the surface (e.g. at depths greater than 5 m), and if these zones were shown to be continuous (not laterally isolated) in later CPT programs. Surficial compaction measures described above are not expected to be successful at resolving such problematic zones. Although such zones have not yet been encountered at Suncor Sand Dump 8, the following measures are available to potentially resolve these issues:

- Slope stability analysis would be carried out using liquefied strength for the zones of concern to evaluate the existing factors of safety of that area of the structure.
- Compaction of the area of potentially liquefiable zone using heavy hauler at ground surface.
- Installation of drainage system (e.g. lateral pipes and vertical pipes) to lower the water table.
- Construction of a toe berm for the slopes.
- Blast densification to densify the loose sand.
- Soil mixing to improve the density and strength.

New CPT testing locations are added over time and the number of CPT tests in a 5 m sand lift at a given elevation naturally increases as Suncor continues sand placement. It is likely that more potentially liquefiable zones will be found with additional testing in subsequent CPT programs. Although a deep continuous potentially liquefiable zone has not been seen yet at Sand Dump 8, Suncor continues monitoring and evaluating the areas with potentially liquefiable sand. Consideration has been given to the depths of the potentially liquefiable zones, the distance between the potentially liquefiable zones at the same depths, the height of the structure, and the depth of the water table. As mentioned, no continuous potentially liquefiable layer has been identified yet at Sand Dump 8.

6 CONCLUSIONS

Dozer compaction during active tailings placement, though challenging, has been successfully used at Suncor Sand Dump 8 to achieve dilative tailings sand. CPT testing has been regularly conducted to monitor the state of the compacted tailings sand. State of the art methodologies are used for the liquefaction susceptibility screening assessment. Suncor's protocol reflects the use of best available technology and best available practices to manage liquefaction potential for an upstream constructed tailings structure.

Potentially liquefiable zones from previous CPT programs were shown to be either improved to be dilative or isolated using subsequent CPT testing. It has been observed that problem zones at depths are typically at lift contacts and therefore it is important to address these areas early on while easily accessible. The findings indicated that the state of sand at Sand Dump 8 is generally non-liquefiable within the compacted zone.

The use of CPT in identifying potentially liquefiable zones is an evolving science. The methodology used in this paper is based on relatively recent studies presented in the literature.

However, it is anticipated that ongoing research in the industry will confirm, refine or challenge the criteria presented in those studies.

7 ACKNOWLEDGEMENTS

The authors would like to recognize E.C. McRoberts of Wood for his technical guidance throughout the project. The authors would also like to recognize Tanys MacGowan of Suncor for her stewardship of the Sand Dump 8 structure.

REFERENCES

Abusaid, A.H., Zhang, Y., Pollock, G.W., Moore, R. & Rhee, J. 2020. CPT Dynamic pore water pressure and liquefaction potential in tailings sand at Suncor, *Tailings and Mine Waste 2020*.

Jefferies, M.G., & Been, K. 2016. Soil Liquefaction: a critical state approach, 2nd edition. CRC Press.

Mettananda, D.C.A., Pollock, G.W. & MacGowan, T. 2014. Construction of Suncor's first tailings sand structure under Tailings Reduction Operation – Sand Dump, *Tailings and Mine Waste 2014*. Keystone, CO, USA. 463-475.

Olson, S. M., and Stark, T. D. 2003. Yield strength ratio and liquefaction analysis of slopes and embankments. *Journal of Geotechnical and Geoenvironmental Engineering*, 129(8): 727-737.

Pollock, G.W., Mettananda, D.C.A. & MacGowan, T. 2014. Design of Suncor's first tailings sand structure under Tailings Reduction Operations – Sand Dump 8, *Tailings and Mine Waste 2014*., Keystone, CO, USA. 449-462.

Robertson, P.K. & Wride (Fear), C.E. 1998. Evaluating cyclic liquefaction potential using the Cone Penetration Test, *Canadian Geotechnical Journal*, 35:442-459.

Robertson, P.K. 2009. Interpretation of cone penetration tests – a unified approach. *Canadian Geotechnical Journal*, 46(11): 1337–1355.

Robertson, P.K. 2010. Evaluation of flow liquefaction and liquefied strength using the cone penetration test. *Journal of Geotechnical and Geoenvironmental Engineering*, 136(6): 842–853.

Robertson, P.K. 2016. Cone penetration test (CPT)-based soil behaviour type (SBT) classification system — an update. *Canadian Geotechnical Journal*, 53(12):1910–1927.

Robertson, P.K. 2017. Evaluation of flow liquefaction: influence of high stresses. Earthquake Geotechnical Engineering PBD III, Vancouver, BC, Canada.

Robertson, P.K., Viana da Fonseca, A., Ulrich, B., & Coffin, J. 2017. Characterization of unsaturated mine waste: a case history. *Canadian Geotechnical Journal*, 54(12): 1752-1761.

Effect of Shear Strain Rate on Undrained Shearing Resistance of a Clean Silica Sand Measured in Direct Simple Shear Tests

Jiarui Chen
University of Illinois at Urbana-Champaign, Urbana, IL, USA

Scott M. Olson
University of Illinois at Urbana-Champaign, Urbana, IL, USA

Soham Banerjee
University of Vermont, Burlington, VT, USA

Mandar M. Dewoolkar
University of Vermont, Burlington, VT, USA

ABSTRACT: A number of studies examining the effect of shear strain rate on undrained shearing resistance of clean sands using conventional laboratory tests have been reported. Constant-volume direct simple shear laboratory tests were performed to model flow displacements at various shearing rates after triggering flow liquefaction. Tests on clean sand (Ottawa F-65 sand) at shear strain rates of 0.1%/min and 10%/min illustrated that the undrained yield (peak) shear strength at a shear strain rate of 10%/min was about 14% greater than that measured at a shear strain rate of 0.1%/min, while the undrained critical-state shear strength is relatively independent of shear strain rate for the shear strain rates (0.1%/min and 10 %/min), sand type, and initial state considered in this study.

1 INTRODUCTION

Whether the undrained shearing resistance of a cohesionless soil is affected by the shear strain rate is a subject of significant engineering importance. A significant number of conventional laboratory tests have been reported in the literature that explored this topic. Among laboratory tests, results from triaxial compression tests generally suggest that the strain rate has an effect on the undrained shearing resistance, especially undrained peak shear strength, of non-plastic, coarse-grained soils (Casagrande and Shannon 1948, Seed and Lundgren 1954, Nash and Dixon 1961, Whitman and Healy 1962, Reeves et al. 1967, Lee et al. 1969, Yamamuro and Lade 1993, Yamamuro et al. 2011, Suescun-Florez 2016). Table 1 summarizes undrained triaxial compression test results found in the literature, which cover shear strain rates ranging from 0.004%/min to 60,000%/min. Although the effect of shear strain rate on undrained peak shear strength varies greatly (Table 1), the overall trend appears to be that the undrained peak shear strength for a cohesionless soil increases with increasing shear strain rate. The increase is generally on the order of around +5% to +20% for each tenfold increase in shear strain rate (Seed and Lundgren 1954, Yamamuro and Lade 1993, Whitman and Healy 1962), but may reach of about 40% especially when the shear strain rate is very large, over 10^3 %/min (Reeves et al. 1967). Differences in drainage conditions, initial void ratio, and consolidation stress also result in variations in the increase in peak shear strength. However, because the tests compiled in Table 1 are triaxial compression tests, the observations related to increases in shearing resistance with shear strain rate are limited to relatively small shear (or axial) strains.

Table 1. Summary of the literature on the strain rate effect investigated using triaxial compression tests at small strains

Reference	Soil type	Saturation condition	Drainage condition	Loose or dense	Relative density or void ratio	Strain rate (%/min)	Consolidation stress (kPa)	Shear strain rate effect on peak shear strength[1]
Seed and Lundgren (1954)	Sacramento river sand	Saturated	Undrained	Dense and loose	0.59 to 0.83	0.7 to 60,000	200	Up to +10% to +15%
Nash and Dixon (1961)	Leighton Buzzard sand	Saturated	Undrained	-	-	2 to 8,000	700	-20%
Whitman and Healy (1962)	20-30 Ottawa sand	Saturated	Undrained	Dense	0.49	18 to 27,000[2]	275	No effect
		Saturated	Undrained	Loose	0.65	120 to 27,000[2]	70 to 350	+40%
Reeves et al. (1967)	20-30 Ottawa sand	Saturated	Undrained	Dense	0.5 and 0.6	2,900 to 12,750	200	Up to +38%
	Victoria sand	Saturated	Undrained	Dense	0.56	3,300 to 8,500	100	Up to +54%
	Arkansas sand	Saturated	Undrained	Dense	0.55	3,300 to 8,400	100	Up to +32%
Yamamuro and Lade (1993)	Uniform Cambria sand	Saturated	Undrained	Dense	89.5%	0.004 to 0.74	34000	+7%

Note: [1]With the increase of strain rate, + for increase and - for decrease; [2]Calculated using a specimen height of 4 inches according to the original investigators.

Because of the capability of imposing large shear displacement, extensive research using the ring shear device have been conducted on evaluating the shear strain rate effect on the critical state shear strength or the shear strength at large strains of non-plastic, coarse-grained soils. For example, based on the results from constant-volume ring shear tests on Ottawa 20/40 sand, Sadrekarimi (2009) concluded that the imposed strain rate (4.7 to 111.6 cm/min, which corresponds to approximate shear strain rates from 180%/min to 4,300%/min considering that the sample was 2.6 cm in height) did not influence the shearing resistance and effective normal stress at the critical state. Other constant-volume ring shear tests (e.g, Novosad 1964; Scarlett and Todd 1969; Savage 1982; Sassa 1984, 1985; Hungr and Morgenstern 1984; Lemos 1986; Fukuoka 1991; Tika et al. 1996; Infante-Sedano 1998) reported similar observations.

In this paper, the authors explore the effect of shear strain rate on the undrained shearing resistance of a loose, clean sand (Ottawa F-65 sand) at relatively large shear strain while the sand is liquefied using constant volume direct simple shear (DSS) test. Unlike conventional laboratory tests, the constant-volume DSS tests reported here were performed in two stages. First, the specimens were loaded cyclically until they liquefied. Following initial liquefaction, the second stage involved undrained monotonic loading at either 0.1%/min or 10%/min shear strain rate. Companion monotonic tests also were performed on specimens prepared to the same initial state (density and consolidation stress) and sheared at the same shear strain rates. To limit any differences caused by other test variables, all tests described here were performed on Ottawa F-65 sand at 10% relative density after Ko-consolidation, D_{rc}, to an effective vertical stress, σ'_{vc}, of 200 kPa in constant-volume condition.

2 TESTING MATERIAL AND SAMPLE PREPARATION METHOD

Ottawa F-65 sand is commercially available from U.S. Silica. It is a white, inert, uniformly graded, silica sand with rounded to subrounded particles. Silica content is 99.7% (U.S. Silica 2016) and fines content (weight of particles passing No. 200 sieve) is typically very small (around 0.05%). Sand gradations from batch to batch. Figure 1 illustrates one representative grain size distribution. The specific gravity of the sand was 2.65 (ASTM D854-14). The maximum and minimum void ratio were determined to be 0.839 and 0.538 using the method proposed by Lade et al. (1998). Table 2 summarizes the sand index properties, which closely match those reported by Parra Bastidas (2016). Test specimen in this study were prepared by moist tamping because of its capability of forming very loose to loose reconstituted sand specimens (Ishihara 1993).

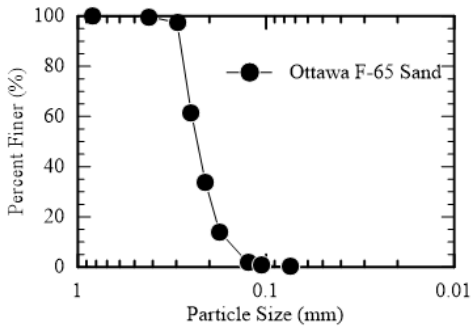

Figure 1. Grain size distribution of Ottawa F-65 Sand

Table 2. Index properties of the Ottawa F-65 sand

USCS	D_{50} (mm)	C_U	C_C	FC (%)	G_s	e_{max}	e_{min}
SP	0.23	1.56	1.0	< 1	2.65	0.839	0.538

Notes: USCS – Unified Soil Classification System; D_{50} – median particle size; C_U – coefficient of uniformity; C_C – coefficient of curvature; FC – fines content; G_s – specific gravity; e_{max} – maximum void ratio; e_{min} – minimum void ratio.

3 TESTING EQUIPMENT

Tests were carried out using the University of Illinois multidirectional direct simple shear (I-mcDSS) device (Bhaumik et al. 2017). This device allows load application in three independent axes, the vertical direction (z) and the two mutually orthogonal directions (x and y) in the horizontal plane (Figure 2). The control system allows both stress- and strain-controlled testing. Multi-stage tests also can be performed by setting various stress- or strain-controlled testing stages in the desired order.

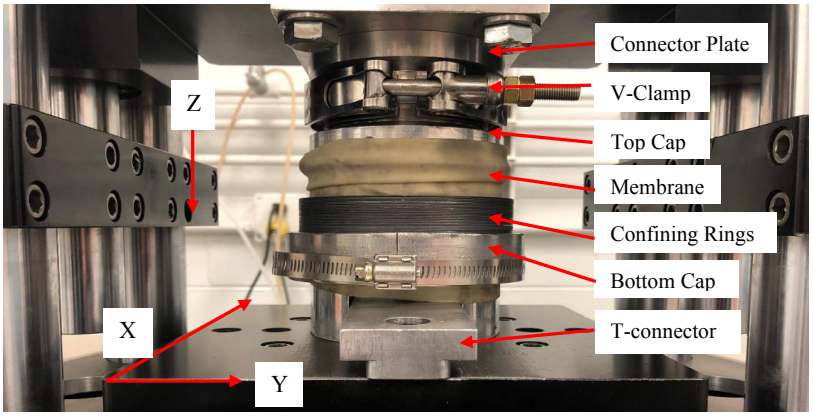

Figure 2. Specimen assembly on the University of Illinois multidirectional cyclic direct simple shear (I-mcDSS) device

4 DIRECT SIMPLE SHEAR TESTS

4.1 Initial condition

Two sets of DSS tests were completed in this study and test parameters are summarized in Table 3. As mentioned in the previous section, each set of DSS tests consisted of a two-stage test, a cyclic stage followed by a monotonic stage. A companion monotonic test was performed for each two-stage test. All two-stage and monotonic tests were performed under strain-controlled conditions and at identical shear strain rates. For Ottawa F-65 sand, a relative density of around 10% with an effective vertical stress of 200 kPa (Ko-consolidation) exhibited contractive behavior throughout constant volume monotonic DSS tests. Critical state conditions were defined when the shearing resistance and the inferred excess porewater pressure (interpreted using the change in the normal stress from constant volume DSS tests performed on dry specimens) became constant. These conditions suggest that the tendency for volume change was exhausted and a critical state was achieved.

Table 3. Summary of DSS tests performed in this study

Test No.	Test type	Monotonic shearing rate (%/min)	Drainage condition	Relative density after consolidation (%)	Consolidation stress (kPa)
1	Cyclic+Monotonic	10	Constant Volume	10.90	200
2	Monotonic			12.12	
3	Cyclic+Monotonic	0.1		13.75	
4	Monotonic			10.65	

4.2 Constant volume testing

In the current study, constant volume conditions were applied to mimic undrained conditions. Saturation is not needed in a constant volume test, and therefore, this protocol can greatly accelerate the testing process. In constant volume DSS testing, it is assumed that changes in applied vertical stress, as the specimen height is maintained constant during shearing, equals the excess pore pressure that would have been measured in an undrained test on saturated specimen with constant total vertical stress (Bjerrum and Landva 1966). The shear stress and the inferred porewater pressure response of the specimen during a constant volume DSS test were the same as those in the undrained saturated DSS tests (Iversen 1977, Dyvik et al. 1987). During the test, the vertical actuator was set to be fixed to maintain a constant specimen height. As the specimen was confined by the stacked rings, constant volume condition was achieved.

4.3 Cyclic and monotonic phases

The two-stage test started with a cyclic shearing stage and followed by a monotonic shearing stage. The cyclic stage was intended to liquefy the specimen and the following monotonic stage was aimed to evaluate the effect of strain rate on shearing resistance of the specimen when it was liquefied. In this study, the liquefaction caused by cyclic loading is defined as the condition that the inferred excess porewater pressure exceeds 95% of the initial effective vertical stress (σ'_{vc} in this case). For cyclic stages, trials proved that six sinusoidal cycles with a peak amplitude of 2% horizontal shear strain and a frequency of 0.1 Hz were sufficient to trigger liquefaction.

5 TEST RESULTS AND INTERPRETATION

Shear stress-shear strain and inferred porewater pressure responses for tests with different shear strain rates during the monotonic loading stages are illustrated in Figures 3 and 4. Stress paths for these tests are presented in Figure 5. In general, the Ottawa F-65 sand, Ko-consolidated to a relative density of around 10% under an effective vertical stress of 200 kPa, exhibits contractive behavior through the entire monotonic test. With that initial condition, the critical state was achieved within the displacement limit of the I-mcDSS device. The excess porewater pressures all become a constant value of around 167.3 kPa at large horizontal shear strains, confirming that there is no tendency for volume change. In addition, assuming the horizontal plane to be the plane of maximum stress obliquity at large shear strains (Wijewickreme et al. 2013), the mobilized friction angles at the end of the tests are all calculated to be around 32° (indicated in Figure 5), which is a typical value for the constant volume friction angle, ϕ'_{cv}, (friction angle mobilized at critical state, ϕ'_{cs}) for silica sand. This further confirms that a critical state was achieved in all tests.

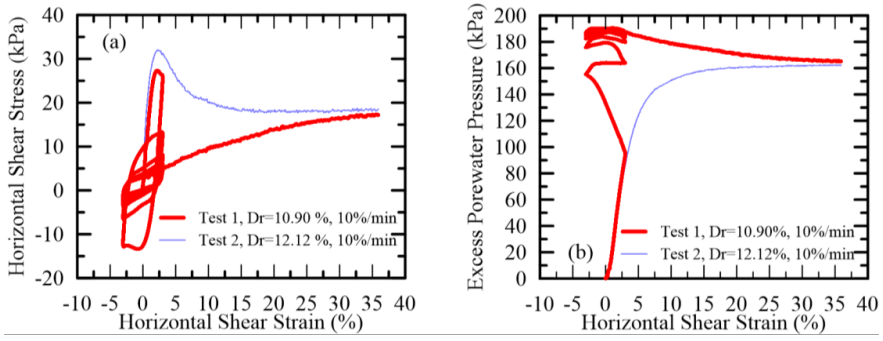

Figure 3. (a) Stress-strain response and (b) excess porewater pressure response for tests with 10%/min shearing rate.

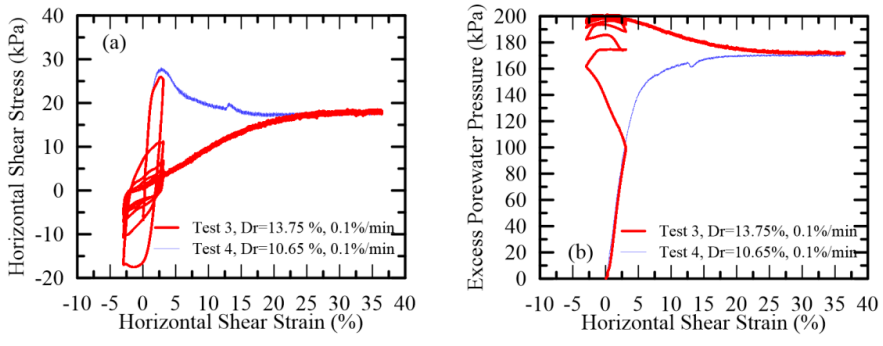

Figure 4. (a) Stress-strain response and (b) excess porewater pressure response for tests with 0.1%/min shearing rate.

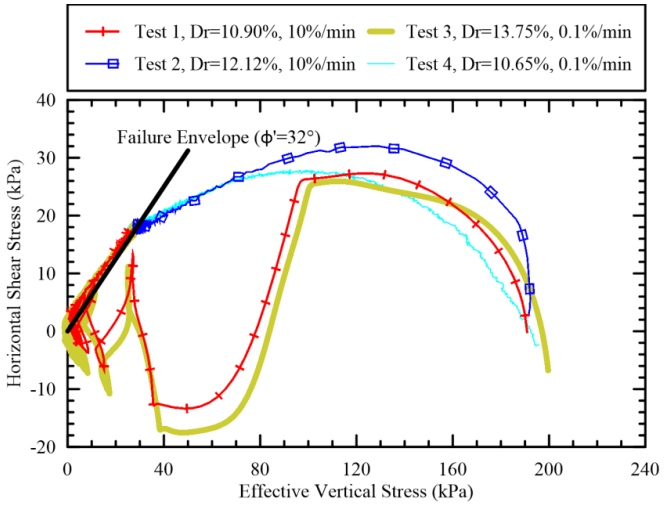

Figure 5. Stress paths for the DSS tests sheared at different strain rates

In the current study, differences in the shear strain rate indeed exhibited differences in yield shear strength (peak deviatoric stress), s_u(yield), under the initial state (density and consolidation stress) in constant volume DSS tests. Within the shear strain rates of 0.1%/min (Test 4) to 10%/min (Test 2), s_u(yield) increased by 14% from 28.1 kPa to 32.0 kPa. This increase agrees with results reported by Seed and Lundgren (1954) and Yamamuro and Lade (1993) for clean sands tested under undrained conditions.

Under a certain shear strain rate in a two-stage test, the monotonic stage (which followed the cyclic stage that liquefied the soil) exhibited the same critical state shear strength, s_u(critical), as that measured in the companion monotonic test (see Figures 3a and 4a). Similarly, the excess porewater pressures coincided in these tests (see Figures 3b and 4b). During the cyclic loading stage, as the cyclic loading proceeded, the effective stress path moved rapidly to the left as excess porewater pressure increased. After four cycles, the effective stress path started to oscillate along the effective stress failure envelope (ϕ'_{cs}), during which the effective stress path would pass through the origin. At the origin, the specimen is in an instantaneous state of zero effective stress, referred to as initial liquefaction by Seed and Lee (1966). If monotonic loading is applied at this condition, the specimen would dilate to its critical state shear strength, as indicated in Figures 3(a) and 4(a). This observation agrees well with tests reported by Ishihara et al. (1991).

In addition, the shearing resistance in all tests leveled off at about 18.3 kPa (Figures 3a and 4a). For practical purposes, the shearing resistance at the critical state for all tests (Tests 1, 2, 3, and 4) was the same. This value is quite consistent with DSS or Rotational Shear (RS) tests data reported by Olson and Mattson (2008) for contractive soils with σ'_{vc} of 200 kPa. The critical state (liquefied) shear strength ratio [s_u(critical)/σ'_{vc}] for these tests is computed to be 0.09. This value is within the range of 0.01 to 0.16 reported by Olson and Mattson (2008) for DSS or RS tests. The results of these tests suggest that s_u(critical) of Ko-consolidated clean Ottawa F-65 sand (D_{rc} ~ 10%, σ'_{vc} = 200 kPa) is independent of shear strain rate for shear strain rates of 0.1%/min and 10%/min in constant volume DSS tests. This corroborates the work of Novosad (1964); Scarlett and Todd (1969); Savage (1982); Sassa (1984, 1985); Hungr and Morgenstern (1984); Lemos (1986); Been et al. (1991), Fukuoka (1991); Tika et al. (1996); Infante-Sedano (1998) and Sadrekarimi (2009) who reported that shear strain rate does not influence the shearing resistance at the critical state.

As pointed out by Whitman and Healy (1962), sources of shear strain-rate effects consist of two candidate mechanisms under undrained conditions: (1) the friction angle is shear strain rate-dependent; or (2) the tendency to create excess porewater pressures is shear strain rate-dependent. The critical state of soil is defined as a state during which the mass of soil undergoes continued distortion at constant shear stress and constant volume (Schofield and Wroth 1968). This condition implies that there would be no tendency to create excess porewater pressure. And therefore, the tendency to create excess porewater pressure at the critical state would be rate independent. In addition, the friction angle at the critical state, ϕ'_{cs}, also would remain the same at different strain rates. The friction angle, ϕ', consists of two components: (1) inter-particle sliding friction, ϕ'_{μ}; and (2) geometrical interference, ϕ'_g. The geometrical interference can be expressed as the sum of ϕ'_d, which is produced by dilation or particle climbing, and ϕ'_p, caused by particle pushing and rearrangement (Rowe 1962, Rowe et al. 1964, Lee and Seed 1966, and Terzaghi et al. 1996). As the volumetric strain levels off at the critical state, the friction angle at the critical state, ϕ'_{cs}, depends only on ϕ'_{μ} and ϕ'_p because net dilation has ceased. The value of ϕ'_{μ} depends exclusively on surface micro-roughness and ϕ'_p typically is about 5° to 6° (Terzaghi et al. 1996). Therefore, for a certain material, ϕ'_{cs} is a constant, even the critical state was reached by shearing at different rates. As a conclusion, it is reasonable to expect that the s_u(critical) is independent of shear strain rate under controlled laboratory testing using specimens with the same initial states.

6 CONCLUSIONS

This paper describes laboratory tests conducted to evaluate the effect of shear strain rate on the shearing resistance of a liquefied clean sand. Results from two sets of constant volume DSS tests performed on loose Ottawa F-65 sand, each consisting of one two-stage test (a cyclic stage to trigger liquefaction followed by a monotonic stage) and one companion monotonic test are presented. The shear strain rate during the monotonic stages was varied to evaluate its influence on the critical state shear strength. These tests were designed to mimic flow displacements at

various shearing rates after triggering flow liquefaction. For clean sands with a relative density of about 10% after Ko-consolidation to an effective vertical stress of 200 kPa, the following conclusions can be drawn.

(1) The specimens exhibited contractive behavior during all monotonic tests despite the difference in shear strain rates (0.1%/min and 10%/min).
(2) The yield (peak) shear strength at the shear strain rate of 10%/min was about 14% greater than that at the shear strain rate of 0.1%/min.
(3) Specimens reached critical state in both the two-stage tests and the monotonic tests.
(4) Critical state shear strength given by the monotonic stage performed after liquefaction in a two-stage test was essentially identical to that measured on specimens at the same initial state tested in monotonic loading.
(5) The critical state shear strength appears independent of shear strain rate for the shear strain rates (0.1%/min and 10 %/min), sand type, and initial state considered in this study.

It is acknowledged that the observations reported here that the critical state shear strength is independent of the shear strain rate for liquefied specimens applies only to the gradation used in this study (Ottawa F-65 sand) Ko-consolidated to a single effective vertical stress (200 kPa) in constant volume DSS tests sheared at two strain rates (0.1%/min and 10 %/min). Further evidence, especially with more gradations and more strain rates, is needed to confirm these findings.

7 ACKNOWLEDGEMENTS

The authors are grateful to the National Science Foundation (award number 1728199) for supporting this work.

REFERENCES

ASTM (American Society for Testing and Materials) (2014). Standard test methods for specific gravity of soil solids by water pycnometer, D854 - 14, pp. 1-8.

ASTM (American Society for Testing and Materials). (2011). *Standard Practice for Classification of Soils for Engineering Purposes (Unified Soil Classification System)*, Standard D2487, West Conshohocken, PA.

Been, K., Jefferies, M. G. and Hachey, J. (1991). The critical state of sands. *Géotechnique*, 41(3), 365–381.

Bhaumik, L., Rutherford, C. J., Cerna-Diaz, A., Olson, S. M., Numanoglu, O. A., Hashash, Y. M., and Weaver, T. (2017). "Volumetric Strain in Non-Plastic Silty Sand Subject to Multidirectional Cyclic Loading." *Proc. Geotech. Frontiers*, ASCE, Orlando, FL, 150–159

Bjerrum, L. and Landva, A. (1966). "Direct simple shear test on a Norwegian quick clay." *Géotechnique*, 16(1), 1–20.

Casagrande, A., and Shannon, W. L. (1948). "Strength of soils under dynamic loads." *Proc. ASCE*, 74(4), 591–608.

Dyvik, R., Berre, T., Lacasse, S., and Raadim, B. (1987). "Comparison of truly undrained andconstant volume direct simple shear tests." *Géotechnique*, 37(1), 3–10.

Hazen, A. (1892). "Physical properties of sands and gravels with reference to their use in filtration." *Rept. Mass. State Board of Health*, p. 539.

Hungr, O. and Morgenstern, N. R. (1984). "High velocity ring shear tests on sand." *Géotechnique*, 34(3), 414-421.

Infate-Sedano (1998). "Constant volume ring shar test for sand." *PhD Dissertation*, University of Ottawa.

Iversen, K. (1977). "Avsluttende forsook I forbindelse med automatisk hoydekontroll ved statiske CCV-forso". *Internal Rep*, 56204-6.

Ishihara, K. (1993). "Liquefaction and flow failure during earthquake", *Géotechnique*, 43, 351-415.

Ishihara, K., Verdugo, R. & Acacia, A. A. (1991). "Characterization of cyclic behaviour of sand and postseismic stability analyses". *Proc. 9th Asian Reg. Conf: Soil Mech.* 2,45-67.

Lade P. V. (2016). *Triaxial testing of soils*, John Wiley & Sons.

Lade, P. V., Liggio, C. D. and Yamamuro, J. A. (1998) "Effects of Non-Plastic Fines on Minimum and Maximum Void Ratios of Sand". *Geotech. Test. J.* 21(4), 336–347.

Lee, K. L., Seed, H. B., and Dunlop, P. (1969). "Effect of transient loading on the strength of sand." Proc., 7th Int. Conf. Soil Mechanics and Foundation Engineering, Vol. 1, Sociedad Mexicana de Mecanica de Suelos, Mexico City, 239–247.

Lemos, L. J. L. (1986). "The effect of rate on the residual strength of soil." *PhD Dissertation*, University of London.

Nash, K. L., and Dixon, R. K. (1961). "The measurement of pore pressure in sand under rapid triaxial tests". *Proceedings, Conference on the Pore Pressure and Suction Soils* (pp. 21-25). London: Butterworths.

Novosad, J. (1964). "Studies on granular materials II." *Colln Czech. Chem. Commun*., 29, 2697.

Olson, S. M. and Mattson, B. B. (2008). "Mode of shear effects on yield and liquefied strength ratios". *Can. Geotech. J.*, 45(4), 574-587.

Parra Bastidas, A. M. (2016). "Ottawa F-65 Sand Characterization", *PhD Dissertation*, University of California, Davis.

Reeves, G. N., Coyle, H. M., and Hirsch, T. J. (1967). "Investigation of Sands Subjected to Dynamic Loading". *Texas A&M University.* College Statin: Texas Transportation Institute.

Rowe, P. W. (1962). "Stress dilatancy relation for static equilibrium of an assembly of particles in contact: In *Proceedings of the Royal Society*, Sr. A, Vol. 269.

Rowe, P. W., Barden. L., and Lee. I. K. (1964). "Energy Components During the Triaxial Cell and Direct Shear Tests." *Géotechnique* 14 (3): 247–61.

Sadrekarimi (2009). "Development of a new ring shear apparatus for investigating the critical state of sands" *PhD Dissertation*, University of Illinois at Urbana-Champaign.

Sassa, K. (1984). "The mechanism starting landslides and debris flows." *Proc. 4th Symp. Landslides, Toronto* 2, 349-354.

Sassa, K. (1985). "The mechanism of debris flow." *Proc. 11th Int. Conf. Soil Mech., San Francisco* 3, 1173-1176.

Savage, S. B. (1982). "Granular flows at high shear rates. In Theory of dispersed multiphase flow." In *Theory of dispersed multiphase flow* (ed. R. E. Meyer), pp. 339-358. Mathematical Research Center, University of Wisconsin.

Scarlett, B. and Todd, A. C. (1969). "The critical porosity of free flowing solids." *J. Soil Mech. Fdn Engng Am. Soc. Civ. Engrs.* A91, part 1, 478-488.

Schofield, A. and Wroth, P. (1968). *Critical State Soil Mechanics*. McGraw-Hill.

Seed, H. B. and Lee, K. L. (1966). "Liquefaction of saturated sand during cyclic loading". *Journal of the Soil Mechanics and Foundation Division*, 2(6), 105-134.

Seed, H. B., and Lundgren, R. (1954). "Investigation of the effect of transient loadings on the strength and deformation characteristics of saturated sands." *Proc. ASTM*, 54, 1288–1306.

Suescun-Florez (2016). "A study of strain rate effects on the mechanical behavior of sand." *PhD Dissertation*, New York University.

Terzaghi, K., Peck, R. B., and Mesri, G. (1996). *Soil mechanics in engineering practice*. John Wiley and Sons.

Tika, T. E., Vaughan, P. R. and Lemos., L. J. L. J. (1996). "Fast shearing of pre-existing shear zones in soil." *Géotechnique*, 46(2), 197-233.

Whitman, R. V., and Healy, K. A. (1962). "Shear strength of sands during rapid loading." *J. Soil Mech. Found. Div.*, 88(SM2), 99–132.

Wijewickreme, D., Dabeet, A. and Byrne, P. (2013). "Some observations on the state of stress in the direct simple shear test using 3D discrete element analysis." *Geotechnical Testing Journal*, 36 (2), 292–299.

Yamamuro, J. A., and Lade, P. V. (1993). "Effects of strain rate on instability of granular soils." *Geotech. Test. J.*, 16(3), 304–313.

Yamamuro, J. A., Abrantes, A. E., and Lade, P. V. (2011). "Effect of strain rate on the stress-strain behavior of sand". *J. Geotech. Geoenviron. Engr*, 137(12), 1169-1178.

Assessment of Liquefaction Triggering for Upstream Tailings Dams Using Limiting Equilibrium Methods

Gordan Gjerapic
University of Colorado, Boulder, Colorado, USA

Dobroslav Znidarcic
University of Colorado, Boulder, Colorado, USA

ABSTRACT: The upstream method to construct tailings embankment raises is considered the most economical approach for the tailings storage facility (TSF) development because it requires minimal amount of fill material for both the initial construction and the subsequent embankment raises. The TSF fill material typically consists of a course fraction of tailings from the cycloning process, native foundation soils or mine waste rock. While the embankment fill materials (placed along the TSF perimeter) may require compaction efforts, the tailings are typically hydraulically discharged from the TSF perimeter resulting in a relatively loose contractive soil deposit contained within the outside perimeter shell. Consequently, the TSF embankments constructed using the upstream method are susceptible to flow liquefaction failures due to either static or seismic triggering mechanisms.

This paper presents a comparison between two methods (Olson and Stark 2003, and Sadrekarimi 2016) to evaluate the stability of the upstream-raise TSF against flow failures considering both static and seismic liquefaction triggering mechanisms. The liquefaction triggering assessment is demonstrated using the approach that allows for the presence of multiple tailing types along the failure surface. Earthquake loads are determined using the simplified stress-based approach while considering limitations of the stress reduction coefficient estimates at large depths. The static liquefaction assessment is conducted for two scenarios considering potential bias in interpretations of seepage conditions and by considering effects of an elevated water table. The methodologies and the results presented in this study emphasize the need for a rational determination of the stress reduction coefficient when evaluating seismic loads and the importance of applying accurate seepage conditions to both static and seismic liquefaction triggering assessments.

Liquefaction assessments were conducted for a 50-meter high upstream-rise embankment containing tailings with the normalized tip resistance, q_{c1}, of 3.1 and 6.3 MPa. A comparison between Olson and Stark (2003) and Sadrekarimi (2016) methods resulted in a relative error of approximately 1 to 5 percent in the calculated post-seismic factor of safety for which the failure mode within the zone of liquefaction is dominated by simple shear. For cases where a significant part of liquefiable tailings is subjected to plane strain compression, the relative difference between the two methods increased to 23 and 32 percent. The paper proposes an alternative approach to initialize static shear stresses along the failure surface to improve consistency (reduce relative errors) between the two methods. Results in this study indicate that the liquefaction triggering assessment using limiting equilibrium methods requires increased scrutiny when applied to a scenario where re-distribution of stresses during the liquefaction triggering event is significant. Regardless of the adopted calculation methodology, the relative difference in the calculated factors of safety may exceed 20 percent for scenarios with erroneous representation of seepage forces, which includes models using linear interpolation of the phreatic surface between adjacent piezometers – the approach commonly used in today's engineering practice.

1 INTRODUCTION

The TSF failures in recent years have resulted in an increased scrutiny of the mining industry by the institutional investors and the general public. The reports on Samarco (Fundão) and Brumandinho (Feijão) disasters identified different triggering mechanisms to either instigate or increase the likelihood of flow liquefaction failures. In both cases, seismic activity and changes in the phreatic levels were considered as potential triggering mechanisms and may have contributed to the observed failures. At Fundão (Morgenstern et al. 2016), three small seismic shocks occurred approximately 90 minutes prior to failure accelerating horizontal displacements in the slimes at the left abutment. Inadequate drainage conditions due to the presence of tailings slimes at Fundão (Morgenstern et al. 2016), and fine tailings at Feijão (Robertson et al. 2019) resulted in elevated phreatic conditions directly contributing to failures. This paper presents the approach to evaluate the liquefaction triggering based on Olson and Stark (2003) and Sadrekarimi (2016) methods. Both Olson and Stark (2003) and Sadrekarimi (2016) assessments are based on the limiting equilibrium method (LEM) commonly used in today's engineering practice. While the Olson and Stark (2003) approach is typically used to assess the potential for liquefaction due to seismic triggering and the Sadrekarimi (2016) method was originally developed to assess the static liquefaction potential, both methods can be utilized to conduct a liquefaction assessment for a variety of triggering mechanisms. Considering that the liquefaction assessment for tailings dams often involves different types of contractive tailings materials (e.g. sands and slimes at Fundão and fine and coarse tailings at Feijão), it is useful to compare both of these methods using a case scenario involving non-homogeneous tailings.

A comparison between Olson and Stark (2003) and Sadrekarimi (2016) methods was conducted to evaluate stability of an upstream-raise embankment subjected to seismic activity and changes in seepage conditions. For simplicity, seismic triggering analysis was conducted by assuming a constant maximum acceleration at the surface of the TSF. Potentially liquefiable tailings were assumed to consist of two layers: 1) a weaker deposit at the base of the impoundment (e.g. a layer of subaqueous tailings, fine tailings and/or tailings slimes) and 2) a relatively stronger layer of tailings on top of the weaker bottom tailings (e.g., tailings sands deposited subaerially and/or tailings with somewhat higher strength due to changes in the milling process, different deposition practice, lower rate or rise or a different mineral origin).

2 APPROACH AND INPUT PARAMETERS

2.1 *Olson and Stark (2003) Method*

To determine whether the combined static, seismic and other shear stresses exceed the yield shear strength of the contractive tailings and to evaluate post-seismic stability, Olson and Stark (2003) proposed a procedure in which the initial state of in situ stresses is evaluated from a limiting equilibrium method analysis for a potential failure surface using the effective normal and shear stresses at the bottom of each slice in the analysis at the moment when the factor of safety is unity. The seismic induced shear stresses along the potential failure surface are evaluated from a site response analysis or from other simplified methods. By comparing the undrained shear strength in each slice to the sum of static and seismic shear stresses for the slice a decision is made for which slices the liquefaction is triggered and the residual shear strength should be assigned for the slice. Finally, the post liquefaction overall factor of safety is calculated. The steps of the Olson and Stark (2003) procedure can be summarized as follows:

1) Determine static shear stresses for the selected pre-failure geometry. Typically, a set of failure surfaces from the static limit equilibrium analyses are selected to investigate liquefaction triggering. Use fully mobilized shear strengths for nonliquefiable soils and iterate for the value of the driving static shear stress, $\tau_{driving}$, assigned to liquefiable soils that results in the factor of safety of unity ($FS_{pre\text{-}failure}$=1). For the purpose of triggering

analyses, Olson and Stark (2003) assume that static shear stresses for the non-liquefiable material are equal to their fully mobilized shear strengths. However, all compressible materials below the groundwater surface (potentially liquefiable materials) are assumed to mobilize only a fraction of their fully mobilized yield strength corresponding to the overall $FS_{pre\text{-}failure} = 1.0$.

2) Divide failure surface in the number of segments. For the purpose of this paper, each segment corresponds to an individual slice in the limiting equilibrium analysis.
3) Determine average effective stress, average total stress and average depth within the potential zone of liquefaction.
4) Estimate seismic shear stress based on site response analysis or apply a simplified liquefaction procedure (Seed and Idriss 1971) using average parameters determined in the previous step. Olson and Stark (2003) suggest finding average seismic shear stress along the failure surface considering all liquefiable materials.
5) Estimate "other" shear stresses, τ_{other}, responsible for liquefaction triggering (if applicable). In this paper, "other" shear stresses leading to static liquefaction due to increasing pore water pressures are considered.
6) Calculate s_u/σ'_{v0} (yield-strength ratio) using CPT data based on the desired level of conservatism (e.g. using percentile of tip resistance or different bounds for the s_u/σ'_{v0} values using correlations with CPT data proposed by Olson at Stark (2003)).
7) Calculate yield strength, driving shear stress for each segment by multiplying (s_u/σ'_{v0})_segment and $(\tau_{driving}/\sigma'_{v0,avg})$ with σ'_{v0} for this segment.
8) Calculate factor of safety against the triggering of liquefaction ($FS_{trigger}$) for each segment. Assign liquefied strength to segments with $FS_{trigger} < 1.0$. Segments within the zone comprising of potentially liquefiable material with $FS_{trigger} > 1.0$ are assigned their peak (yield) strengths.
9) Determine factor of safety against the liquefaction flow failures (FS_{flow}) using updated strengths within the zone of liquefaction. If $FS_{flow} \leq 1.1$, repeat the analyses by assigning the liquefied strength to all segments with the $FS_{trigger} \leq 1.1$. Compare FS_{flow} with the worst case scenario where all segments within the potentially liquefiable zone are assigned their post-liquefaction strengths. It is recommended to consider the worst case scenario to aid judgement regarding the need for redesign or remediation.

2.2 *Sadrekarimi (2016) Method*

To account for the plane strain boundary conditions, anisotropic consolidation ($K_c = \sigma'_3/\sigma'_1$) and mode of shear (plane strain compression, simple shear and plane strain extension), Sadrekarimi (2016) proposed to conduct stability analyses using the following procedure:

1) Determine critical failure surface and determine failure mode for each slice based on its base angle with the horizontal, θ.
2) Determine effective stress ratio at the base of each slice:

$$K_c = \frac{\sigma'_{3c}}{\sigma'_{1c}} = \frac{\sigma'_{nc} - (\tau_c/\cos\theta) + \tau_c \tan\theta}{\sigma'_{nc} + (\tau_c/\cos\theta) + \tau_c \tan\theta} \quad (1)$$

where σ'_{nc} and τ_c are normal effective stress and shear stress calculated at the base of each slice.

3) Calculate liquefied shear strength ratio, s_r/σ'_{v0} at the base of each slice based on the measured CPT data for the simple shear mode of failure. Use correlations based on estimated sensitivity to determine s_r/σ'_{v0} for the compression and extension modes of shear (see Sadrekarimi 2016).
4) Estimate pore pressure parameters (r_u, r_u*) and sensitivity parameters (IB* and IB) using

appropriate correlations (see Sadrekarimi 2016) based on the mode of failure.

5) Calculate yield strength ratio, s_u/σ'_{v0}, based on liquefied shear strength ratio, s_r/σ'_{v0}, and sensitivity parameter, IB.

$$\frac{s_u}{\sigma'_{v0}} = \frac{1}{1-I_B} \cdot \frac{s_r}{\sigma'_{v0}} \quad (2)$$

6) Calculate average vertical stress for each slice and determine if total driving shear at the base of the slice is larger than the yield strength. Liquefaction is triggered in a slice for which the yield strength, s_u, is smaller than the total driving shear, τ_c.
7) Repeat limit equilibrium analyses using liquefied strength for liquefied slices and non-liquefied shear strengths for non-liquefied slices below the water level. Assign drained strengths for slices above the water table.

2.3 *Proposed method for liquefaction triggering in non-homogeneous materials*

Olson and Stark (2003) method can be modified to account for the anisotropic consolidation and for the mode of failure by incorporating Sadrekarimi (2016) approach (Steps 1 to 5) into Olson and Stark (2003) methodology (Step 6). To account for multiple tailings material along the failure surface, one can also modify the initial step used to determine driving shear stresses as follows:

1) Determine effective vertical stresses, mode of failure and material type at the base of each slice defining the failure surface for a limiting equilibrium analysis.
2) Calculate strength ratios along the failure surface at the base of each slice (use either yield or liquefied strengths). Alternatively, assign stiffness ratios (shear modulus divided by vertical effective stress) for each slice or modify strength ratios by considering strain compatibilities of different materials along the failure surface.
3) Calculate relative strength ratio for each slice as $c_i=(s_u/\sigma'_{v0,i}) / (s_u/\sigma'_{v0,max})$
4) Assign strength ratios along the failure surface such that $s_u/\sigma'_{v0,i} = \alpha \times c_i \times (s_u/\sigma'_{v0,max})$
5) Calculate factor of safety by varying parameter α until reaching the factor of safety of unity.

2.4 *Model configuration*

The above methods were evaluated using the TSF configuration depicted in Figure 1

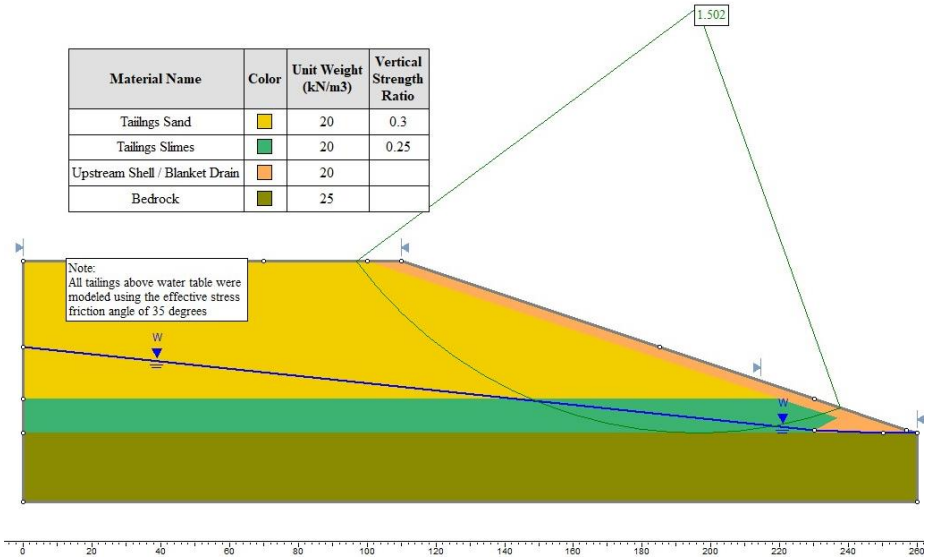

Figure 1. Baseline scenario using linear interpolation of phreatic levels between piezometers

The TSF cross-section in Figure 1 features a 50-meter high embankment with the side slopes of 3H:1V. Assuming the rate of rise of 2 meters per year, the TSF's starter dam was constructed with an initial height of 5 meters. The subsequent upstream raises were constructed with a relatively narrow shell using a nominal compacted width of 10 meters. The piezometer installed 110 meters upstream from the crest of the TSF embankment indicates the groundwater at 25 meters below the ground surface. The phreatic surface at the upstream toe of the starter dam is approximately 1 meter above bedrock. The water level used for the baseline stability analyses is linearly interpolated between these two points. The water level at the downstream toe is assumed to coincide with the bedrock surface, i.e. all downstream seepage is directed towards the toe collection trenches at the embankment perimeter.

2.5 *Input Parameters*

Input parameters used to conduct limiting equilibrium and seepage analyses for Olson and Stark (2003) assessment scenarios are summarized in Table 1.

Table 1. Model parameters.

Material	Unit weight (kN/m3)	Undrained Shear Strength Ratio at Yield Lower Bound - Mean	Hydraulic conductivity (m/sec)
Tailings Sand	20	s_u/σ'_{v0} = 0.26 - 0.30	1e-6
Tailings Slimes	20	s_u/σ'_{v0} = 0.21 - 0.25	5e-7
Tailings above water table	20	ϕ'_{cv} = 35°	<1e-7 (unsaturated)
Upstream Shell	20	ϕ'_{cv} = 40°	1e-4
Bedrock	25	Infinite strength	1e-10

The range of undrained yield strengths for tailings sands and tailings slimes in Table 1 were determined based on the lower bound and the mean correlations (Olson and Stark 2003) for the normalized tip resistance, q_{c1}, values of 6.3 and 3.1 MPa. The corresponding residual shear strengths were determined using the lower bound and the mean correlations from Olson and Stark (2003) and Sadrekarimi (2016) for the simple shear mode of failure. These residual strength estimates are summarized in Table 2.

Table 2. Residual strength.

Material	Residual Strength, s_r/σ'_{v0}	
	Olson and Stark (2003)	Sadrekarimi (2016)
Tailings Sand	0.090 – 0.120	0.108 – 0.129
Tailings Slimes	0.044 – 0.074	0.054 - 0.075

Liquefaction triggering assessments using the Sadrekarimi (2016) approach utilized the sensitivity parameter, I_B = 0.75, to account for scaling between the simple shear (SS) and the plane strain compression (PSC) failure modes, see Step 3 in Section 2.2 above.

Seismic shear stresses were determined using the simplified Seed method for the maximum acceleration of 0.3g and by modifying the stress reduction coefficient determined from Idriss (1999) for tailings locations with depths larger than approximately 20 meters. The approach by Idriss (1999) is mathematically applicable for depths smaller than 34 meters, however, Idriss and Boulanger (2008) recommend it for depths of less than 20 meters. Hence, the approach proposed by Ishihara (1977) was adopted in this study for larger depths. Ishihara (1977) proposed scaling of the stress reduction coefficient by considering the natural frequency (height and stiffness) of the soil column resulting in the following equation for the stress reduction coefficient:

$$r_d = \frac{v_s}{\omega z} \cdot sin\left(\frac{\omega z}{v_s}\right) \tag{3}$$

where z denotes the depth below ground surface, v_s is the shear wave velocity and ω is the natural

frequency of excitation of the soil column. For the soil column with the depth *H*, and the natural period of T=4H/vs, Equation (3) reduces to:

$$r_d = \frac{2H}{\pi z} \cdot sin\left(\frac{\pi z}{2H}\right) \quad (4)$$

as noted by Golesorkhi (1989). While Equation (4) does not account for soil stratigraphy, soil properties and the characteristics of the input motion, it is expected to provide a more realistic upper bound estimate of r_d at larger depths based on results reported by Iwasaki (1978) and Golesorkhi (1989). The variability of the stress reduction coefficient based on Ishihara's (1977) approach is compared with the estimates based on the simplified Seed approach used by Jefferies and Been (2016) and with the maximum average acceleration ratio for the depth of sliding mass reported by Makdisi and Seed (1978) in Figure 2.

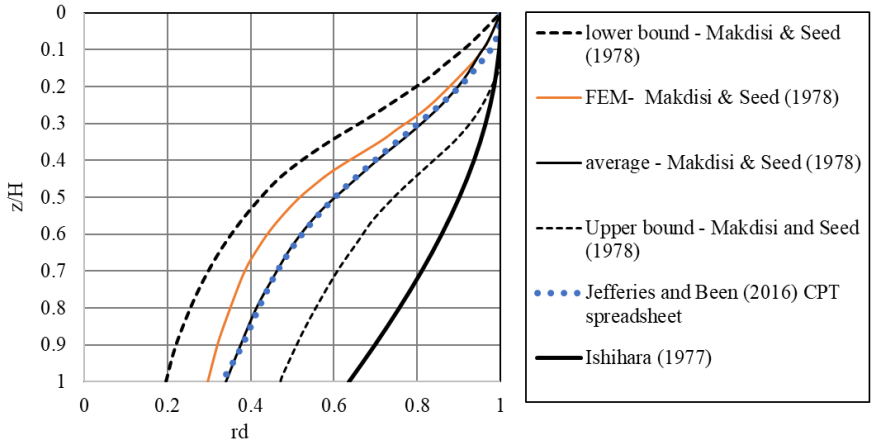

Figure 2. Stress reduction coefficient

3 RESULTS

The liquefaction triggering assessment in this study is conducted for two scenarios based on the piezometers installed at two locations. The first piezometer is located 110 meters upstream from the crest of the dam and reports the water level 25 meters above the bedrock surface. The second piezometer measures the water level at the upstream toe of the starter embankment and indicates the water level of approximately 1 meter above bedrock. Consequently, the liquefaction assessment is conducted for

- Case 1 – Baseline scenario using the piezometric surface based on the linear interpolation of phreatic levels recorded at the installed piezometer locations.
- Case 2 – Baseline scenario using the piezometric surface based on the finite element calculation where recorded piezometric levels are used as a boundary condition. For conservatism, the calculated phreatic surface from the finite element seepage analysis was input as a piezometric surface to conduct the liquefaction assessment calculations.

While the linear interpolation of recorded water levels between different piezometers is often employed in practice due to its simplicity, one has to make sure that such an assumption doesn't violate fundamental principles of water flow. When considering the Case 1 scenario depicted in Figure 1, a constant hydraulic gradient assumption (implied by linear change in the water levels along the flow path) is adopted and consequently the seepage velocity is constant along the flow path assuming no changes in hydraulic properties. Figure 1 shows that, from Station +150, the seepage is confined to the layer of tailings slimes with the cross-sectional area contributing to flow continuously decreasing until reaching the drainage layer at the upstream toe of the starter dam. From the principles of mass conservations, the product between the velocity and the cross-

sectional area should remain constant along the flow path. As the seepage velocity is constant along the flow path (neither the hydraulic gradient nor the hydraulic conductivity change), the continuously reducing flow area depicted in Figure 1 violates the principle of mass conservation and is therefore physically inadmissible. However, as the linear interpolation of phreatic surface is commonly employed in practice, Case 1 is used to explore potential implications of erroneous interpretations of seepage conditions on the TSF embankment stability assessment. In contrast, Case 2 scenario is evaluated by rationally accounting for seepage conditions, i.e. employing the phreatic surface determined from steady-state seepage analysis (a mass conservation problem is solved while rationally accounting for the geometry, material properties and boundary conditions). The direct consequence of such analysis is the gradual increase in hydraulic gradients towards the toe of the dam and the associated increase in piezometric line in the zone most critical for the stability.

Case 2 scenario is shown in Figure 3.

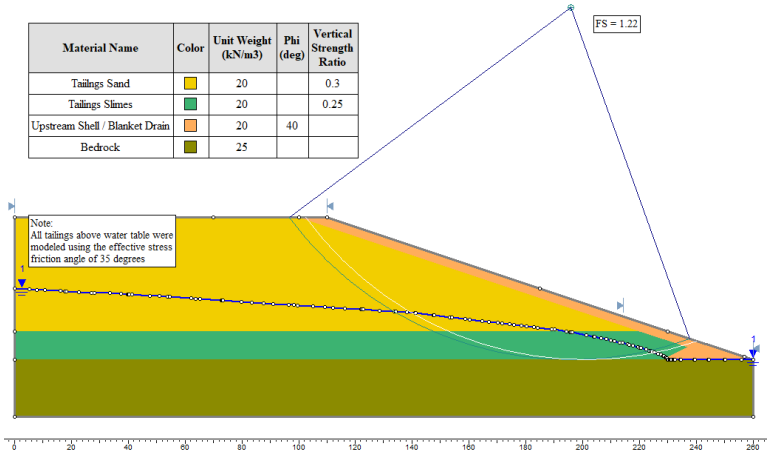

Figure 3. Baseline scenario using seepage analysis to determine phreatic surface

The static stability assessment using the mean strength paraments from Table 1 indicates a significant reduction in the factor of safety (19%) from the condition based on the linear interpolation of the piezometric surface and the condition using the piezometric surface adopted from the seepage analysis. The seismic liquefaction assessment was conducted for both case scenarios using the lower bound and the mean strength estimates (see Table 1 and Table 2). Results of these analyses are summarized in Table 3.

Table 3. Factors of safety – seismic trigger.

Scenario	Static Stability	Post-Seismic Conditions		
		Olson and Stark (2003)	Sadrekarimi (2016)	Proposed approach
Case 1	1.50	1.35 – 1.48	1.42 – 1.49	1.42 – 1.49
Case 2	1.22	0.61 – 0.70	0.81 – 0.86	0.62 – 0.67

Factors of safety against the seismic liquefaction triggering, $FS_{trigger}$, for individual slices using the lower bound and the mean strength estimates are shown in Figures 4 and 5. Results in these figures indicate relatively small changes in $FS_{trigger}$ between lower bound and mean strength parameters. In addition, results for Case 1 (solid markers in Figures 4 and 5) indicate that a relatively small number of segments, for stations larger than approximately +200, exhibit the $FS_{trigger}$ <1.0. Consequently, the post-seismic factors of safety, FS_{flow}, for Case 1 scenarios are not significantly smaller than the Case 1 static factor of safety of 1.5. E.g, in Figure 5, only 2 segments (slices) are assigned liquefied strengths based on $FS_{trigger}$ <1.0 when using Olson and Stark (2003) method and only about 4 when using Sadrekarimi (2016) method. Since the Case 1 slices with $FS_{trigger}$

<1.0 are located at the toe of the embankment, i.e. within the cross-section characterized by relatively low effective stresses, the strength contribution of these slices to global post-liquefaction stability is relatively small. Consequently, all Case 1 scenarios exhibit factors of safety FS_{flow} ranging from 1.35 to 1.49, i.e. there are no significant changes with respect to the factor of safety for static conditions of 1.5 (see Table 3). In contrast, results for Case 2 scenarios (hollow markers in Figures 4 and 5) indicate that most slices (below the water table) are liquefiable indicating relatively high likelihood of the flow liquefaction failure if the structure experiences the design seismic event. Results in Figures 4 and 5 demonstrate the importance of rigorously evaluating seepage conditions and pore pressures before and (if possible) during and after the liquefaction triggering effect. The importance of rigorous evaluation of seepage conditions is often overlooked in the geotechnical practice, i.e. the same set of in-situ observations may lead to different interpretations by practitioners. In particular, the linearization of collected records and other simplifications of the recorded data (including omission or disregarding of data when not fitting the numerical model) should be evaluated in terms of the potential consequences and the overall risk to the project.

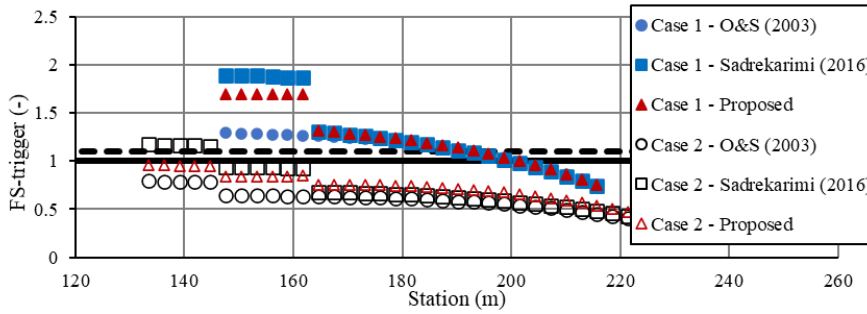

Figure 4. Factors of safety against seismic liquefaction triggering – lower bound strength

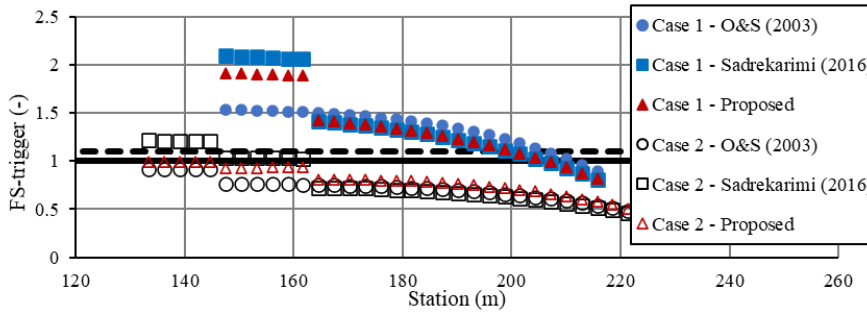

Figure 5. Factors of safety against seismic liquefaction triggering – mean strength

The sensitivity of the factor of safety to seepage conditions may be evaluated by considering static liquefaction mechanisms. The approach proposed by Olson and Stark (2003) can be applied for the assessment of static liquefaction. Olson and Stark (2003) define the liquefaction triggering for the condition where the static (driving), seismic and other shear stresses exceed the yield shear strength of the contractive soil:

$$FS_{trigger} = \frac{s_u}{\tau_{driving}+\tau_{seismic}+\tau_{other}} \quad (5)$$

For the triggering of static liquefaction, the seismic shear in Equation (5) can be set to zero and "other" shear stresses need to be defined based on the considered triggering mechanism. In this study, the liquefaction triggering assessment due to raising groundwater levels is considered. To

perform the liquefaction triggering assessment, "other" shear stresses in Equation (5) need to be expressed as a function of the increasing pore water pressure. Noting that the yield shear strength is primarily a function of the soil state, one should consider the stress path that best resembles the expected loading mechanism. For the known initial effective stresses (σ'_{v0}, σ'_{h0}, τ), one can define the corresponding mean effective and deviator stresses (p'_0, q_0):

$$p'_0 = \frac{\sigma'_{v0} + 2\sigma'_{h0}}{3} \tag{6}$$

and

$$q_0 = [(\sigma'_{v0} - \sigma'_{h0})^2 + 3\tau^2]^{1/2} \tag{7}$$

Equations (6) and (7) define the position of point A in Figure 6. While the critical state line (CSL) is defined by the effective friction angle, the onset of liquefaction for contractive soils is defined by the instability line (IL). Based on Jefferies and Been (2016), a notion that the mobilized stress ratio (i.e., the ratio between deviator stress and mean effective stress) at the onset of flow failure is much smaller than the critical friction was first suggested by Bishop (1971, 1973). Sladen et al. (1985) reported that different contractive samples prepared at the same initial void ratio, but tested from different initial stress conditions, form a locus of peak strengths in p'-q space which they termed the collapse surface. Another term synonymous with the collapse surface (instability line) is the flow liquefaction surface (see e.g. Kramer 1996).

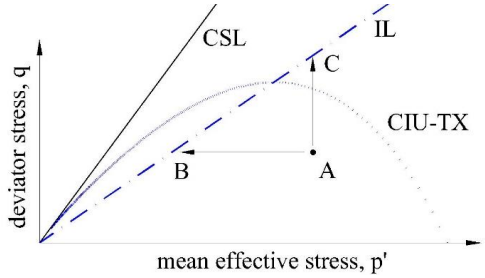

Figure 6. Baseline scenario using seepage analysis to determine phreatic surface

The slope of the instability line, η_L, may be significantly smaller than the slope of the critical state line, M. As both slopes are often determined using undrained triaxial tests on isotropically consolidated samples (CIU-TX), the impact of field conditions due to anisotropic consolidation is typically determined theoretically or using correlations with other laboratory tests (see e.g. Sadrekarimi 2016). For a given initial effective stress, σ'_{v0}, the undrained strength is often determined using CPT data, e.g. using correlations between the CPT tip resistance and the undrained strength ratio $k_{yield} = s_u/\sigma'_{v0}$. If one considers the stress path from Point A to Point B in Figure 4, representing reduction in the mean effective stress while the deviator stress remains constant, the change in the relative distance from Point A to the instability line can be accounted for by modifying Equation (5) as follows:

$$FS_{trigger} = \frac{s_u}{\tau_{driving} + \tau_{seismic} + k_{yield}\Delta u} \tag{8}$$

where the factor $k_{yield}\Delta u$ denotes the loss of shear strength due to the increased pore water pressure. One should note that the path A-C corresponds to the condition for which the deviator stress increases while the mean effective stress remains constant. E.g., this stress path may be representative of the slope steepening by erosion at the toe (Jefferies and Been 2016). Also, the path A-C is implied in Olson and Stark (2003) approach when evaluating the factor of safety against liquefaction triggering which should be taken into account when evaluating specific design scenarios.

In this study, the triggering of static liquefaction was evaluated by considering Case 1 and Case 2 scenarios (see Figures 1 and 3) with the initial groundwater elevation of 25 meters above the bedrock surface. Results of the liquefaction assessment considering the raising water table in the piezometer located 110 meters upstream from the crest of the TSF embankment by approximately 10 meters, i.e. by assuming that the water table raises to 35 meters above bedrock, are summarized in Table 4.

Table 4. Factors of safety – static trigger.

Scenario	Static Stability w/ GWT @25 m	Max. GWT level = 35 m above bedrock		
		Olson and Stark (2003)	Sadrekarimi (2016)	Proposed approach
Case 1	1.50	0.90 - 1.02	1.12 - 1.17	1.12 - 1.17
Case 2	1.22	0.55 - 1.02	0.86 – 1.15	1.10 – 1.15

Results in Table 4 demonstrate relatively good agreement between different methods for the scenarios calculated with mean strength parameters. For these scenarios, however, no liquefaction triggering was identified using Equation (8). I.e., $FS_{trigger} \geq 1.1$ was calculated for all analyzed segments (all slices) in the limiting equilibrium models using the mean strength parameters. The scenarios with the lower bound strength parameters, however, predicted a relatively significant extent of liquefied tailings, $FS_{trigger} \leq 1.1$, for the range of slices within tailings slimes when using Olson and Stark (2003) and Sadrekarimi (2016) methods. The zone of liquefaction identified by the Sadrekarimi (2016) method was approximately 26 percent smaller than the zone of liquefaction using the Olson and Stark (2003) approach as demonstrated graphically in Figures 6 and 7.

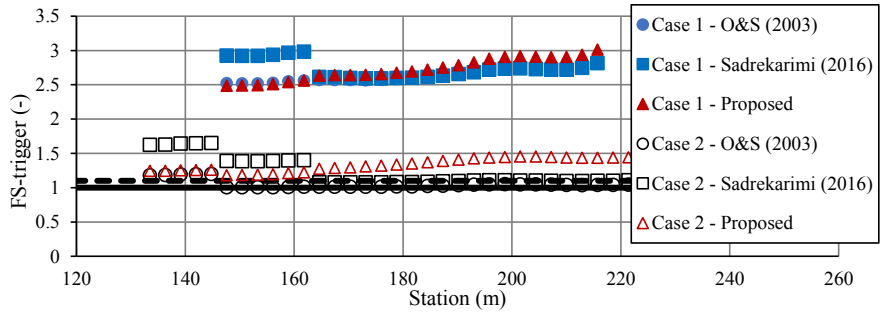

Figure 6. Factors of safety against static liquefaction triggering – lower bound strength

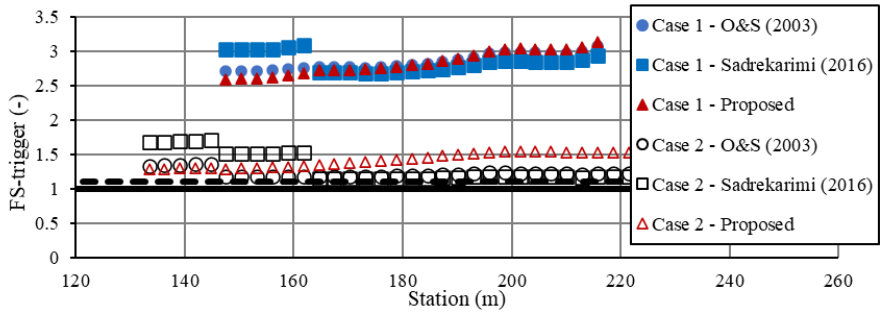

Figure 7. Factors of safety against static liquefaction triggering – mean strength

Therefore, results in Table 4 demonstrate the difficulty in selecting the appropriate analytical approach when predicting the triggering of flow liquefaction. Specifically, one should note that

no liquefaction triggering was predicted for the Case 1 scenario conducted with the lower bound strength parameters using Olson and Stark (2003) approach (solid circles in Figure 6), despite the fact that the limiting equilibrium analyses with the elevated ground water table resulted in the factor of safety smaller than unity (FS_{flow}=0.9 in Table 4). Hence, the investigated triggering methods seem to be applicable for scenarios with stress conditions relatively close to the flow liquefaction surface (i.e. for embankments exhibiting static stresses relatively close to the instability line). The ability of these methods to predict the on-set of liquefaction diminishes as the initial stress state moves further away from the instability line. Therefore, these methods should be used with caution when considering events with the potential for significant stress redistribution, e.g. earthquakes with very strong shaking or of long duration, or events resulting in significant changes in seepage conditions. For these conditions, the TSF design should provide sufficient redundancy and conservatism to minimize the likelihood of brittle failure, independent of the trigger mechanism as currently proposed in the draft version of the Global Tailings Standard (UNEP et al., 2019). Consequently, it is recommended that TSF stability is evaluated using residual strengths for all contractive tailings for which either static or seismic liquefaction triggering is physically feasible. For cases where this approach is not technically or economically feasible, the use of yield strengths should be restricted to tailings for which the designer can demonstrate that the stress path remains below the flow liquefaction surface (with the sufficient degree of conservatism) throughout the life of the facility. For these cases, it is strongly recommended that the risk assessment includes the estimated likelihood of failure based on the potential triggering mechanisms, e.g., seismic, changes in the phreatic surface, incremental loading, foundation subsidence and differential settlements. TSF designers are responsible for evaluating the risk against failure during construction, operation, closure and post-closure periods by taking into account the variability of material and seismic parameters, changes in tailings geometry and stratification, hydrological and hydrogeological conditions, potential for scour and piping, effects of ageing, creep, strain compatibility and strain localization, tensile cracking and other physical and chemical mechanisms with the potential to affect both the short and the long-term TSF stability. There are too many factors that must be considered simultaneously in the design for any predefined set of analyses or procedures to be considered a definitive answer when evaluating stability of a general TSF design configuration. While the "cookbook" approach may serve as a welcome aid when addressing regulatory and basic technical requirements, it should be viewed only as a necessary first step in the process of a comprehensive stability evaluation. Due to inherent complexities when evaluating the triggering of liquefaction, the TSF stability assessment using residual strengths for contractive tailings should be always considered as a benchmark case and as a point of comparison. See, e.g., Carrier (1991) discussion on the use of residual strengths (steady-state undrained strengths) to conduct TSF stability analyses.

4 CONCLUSIONS

This paper presents a comparison between two methods for the liquefaction triggering assessment. Presented results indicate the sensitivity of both methods to input parameters that are often chosen by using simplifying assumptions or by using interpolation of available data. The approach proposed in this paper accounts for the reduction in seismic shear stresses due to the embankment height, the mode of shear and stress anisotropy along the failure surface, and the presence of heterogeneous materials.

Presented methods are based on the limiting equilibrium approach. Therefore, they are expected to require significantly less effort than the stress-deformation analyses. Results in this study, however, indicate that the presented methods are suitable only for the initial/preliminary liquefaction triggering assessment, for the assessment of TSF designs where liquefaction failure does not represent a significant risk, and for designs with a relatively small magnitude of stresses caused by the liquefaction trigger (relative to stresses prior to the liquefaction triggering event). For the TSF designs where a significant stress redistribution is expected to occur during the liquefaction triggering event, the triggering analysis proposed by Olson and Stark (2003) may lead to un-conservative stability estimates.

The results in this study support the use of residual strengths when evaluating post-seismic stability of tailings embankments if relying on contractive tailings as a structural component in

the design. Furthermore, the TSF designer should consider the use of residual strengths when evaluating other triggering mechanisms for which the stress path may reach the collapse surface or for which the stress path evolution during the triggering event is uncertain.

Triggering calculations using peak strengths should be confined to materials that are not likely to exhibit significant loss of strength when subjected to the design triggering events. As noted by Jefferies and Been (2016): "Soil that is sufficiently loose to fail in undrained monotonic shear poses such a risk of catastrophic failure that engineers will always specify ground treatment of some form to improve its density. It is simply not worth the risk to do otherwise."

5 REFERENCES

Bishop, A.W. 1971. Shear strength parameters for undisturbed and remolded soil specimens. In Stress-Strain Behavior of Soils: Proceedings of the Roscoe Memorial Symposium, Cambridge (ed. R.H.G. Parry), pp. 3-58.

Bishop, A.W. 1973. The stability of tips and spoil heaps. Quaterly Journal of Engineering Geology, Vol 6, pp. 335-376.

Carrier, W.D. 1991. Stability of tailings dams. XV Ciclo di Conferenze di Geotecnica di Torino, University of Torino, Italy.

Idriss, I., M. 1999. An update to the Seed-Idriss simplified procedure for evaluating liquefaction potential in Proceedings, TRB Worskhop on New Approaches to Liquefaction, Publication No. FHWA-RD-99-165, Federal Highway Administration, January.

Idriss, I., M., Boulanger, R., W. 2008. Soil liquefaction during earthquakes. Monograph MNO-12, Earthquake Engineering Research Institute, Oakland, CA, 261 pp.

Ishihara K. 1977. Simple method of analysis for liquefaction of sand deposits during earthquakes. Soils and Foundations, Vol. 17, No. 3, pp. 1–17.

Jefferies, M., Been K. 2016. "Soil Liquefaction - A Critical State Approach", 2nd edition, CRC Press

Kramer, S.L. 1996. Geotechnical Earthquake Engineering, Pearson Education, ISBN-13: 978-0133749434, ISBN-10: 013374943. pp. 653.

Morgenstern, N.R., Vick, S.G., Viotti, C.B and Watts, B.D. 2016. Fundão Tailings Dam Review Panel – Report on the Immediate Causes of the Failure of the Fundão Dam. August 25, 2016 (http://fundaoinvestigation.com/the-report/)

UNEP, PRI and ICMM. 2019. Global Tailings Standard – Draft for Public Consultation. Standard for management of mine tailings facilities prepared by Global Tailings Review (Expert Panel consisting of seven members and Advisory Group chaired by Dr. Bruno Oberle) formed by United Nations Environment Program (UNEP), Principles for Responsible Investment (PRI) and International Council of Mining and Metals (ICMM), November 2019. (https://globaltailingsreview.org/wp-content/uploads/2019/11/EN-Global-Tailings-Standard_CONSULTATION-DRAFT.pdf)

Olson, S.M. and Stark, T.D. 2003. Yield Strength Ratio and Liquefaction Analysis of Slopes and Embankments, Journal of Geotechnical and Geoenvironmental Engineering, Vol. 129, No. 8, August 1, 2003, pp. 727-737

Robertson, P.K., de Melo, L., Williams, D.J and Wilson, G.W. 2019. Report of the Expert Panel on the Technical Causes of the Failure of the Feijão Dam I, December 12, 2019 (http://www.b1technicalinvestigation.com/report.html)

Sadrekarimi, A. 2016. Static liquefaction analysis considering principal stress directions and anisotropy. Geotechnical and Geological Engineering, 34(4), 1135 – 1154.

Seed, H.B. and Idriss, I.M. 1971. Simplified procedure for evaluating soil liquefaction potential. Journal of Soil Mechanics and Foundation Division of American Society of Civil Engineers, Vol 97, No. 9, pp. 1249-1273.

Sladen, J.A., D'Hollander, R.D and Krahn, J. 1985. The liquefaction of sands, a collapse surface approach, Canadian Geotechnical Journal, Vol. 22, No. 4, pp. 564-578.

3D DEM Undrained Tests to Elucidate Liquefaction Onset in Granular Media

Eduardo Martin
Universidad Nacional de San Juan, San Juan, Argentina

Colin Thornton
University of Birmingham, Birmingham, England, UK

Stefano Utili
Newcastle University, Newcastle upon Tyne, England, UK

ABSTRACT: in this paper the use of 3D Discrete Element Method (DEM) analyses is showcased to elucidate the physical mechanisms taking place at the grain level leading to the liquefaction of granular soils when subjected to seismic action. Cyclic undrained strain controlled triaxial tests were performed in a periodic cell under constant volume conditions. The influence of variables characterizing the granular assembly such as inertial number, geometrical coordination number, mechanical coordination number, redundancy index and Reynolds stresses on liquefaction is investigated. To elucidate the transition from solid-like to liquid-like behavior, an analysis of how particles cluster together is also presented. It emerges that, as the mean effective stress decreases, contacts are lost, with the maximum cluster size reducing at an increasing rate. The loss of contacts is uniformly distributed throughout the sample and no breakup of the largest cluster into smaller clusters is observed.

1 INTRODUCTION

A major cause of failure of sand tailing dams located in seismic countries is the occurrence of earthquakes (ICOLD 1995; ICOLD, 2001). As of today, several sand tailing dams are subject to a significant risk of earthquake induced failure. For instance in Chile the survey performed in 2010 by the National Service of Geology and Mining (Villavicencio et al., 2014) recorded the existence of 449 deposits of tailings, 9% of which were considered to be in unacceptable conditions and 50% were classified as marginal primarily due to the potential for mechanical instability, e.g. liquefaction, slope instability, overtopping, etc. During seismic events tailing sand dams have been shown to be very susceptible to seismic liquefaction. Such failures usually result from the generation of excess pore water pressures which cannot be dissipated quickly enough to prevent undrained loading conditions from prevailing. The effective confining pressure may be reduced to zero or near zero and the shear strength of the cohensionless tailings thus approaches zero. In this paper the use of the Discrete Element Method is advocated to elucidate the mechanisms occurring at the micromechanical scale, i.e. grain scale, leading to the liquefaction of granular soils (i.e. sands and gravels) subjected to seismic action.

Despite much research has been carried out to investigate the physical conditions leading to liquefaction using laboratory experiments, model testing and analytical/numerical methods. Regarding numerical methods, the analysis of the undrained response is traditionally based on a continuum approach. This approach however is unable to provide information on the physics occurring at the grain scale. On the contrary the discrete element method (DEM) Cundall and Strack (1979) provides detailed information of the micromechanical behavior at the grain scale. Research on undrained conditions (especially for loose sand) has been performed since the works of Bishop (1966, 1971) and Castro (1969). However, significant knowledge gaps remain for the liquefaction of granular materials induced by cyclic loadings.

As well summarized in Carrera et. al. (2011), in the geotechnical community there are two definitions of liquefaction: for some it simply indicates strain softening and compressive

undrained behavior, so that a sample under stress control would fail uncontrollably at the peak deviator stress, e.g. (Sladen et al., 1985); for others it occurs only when the granular material is subject to zero effective stress and zero strength, e.g. (Yamamuro & Covert, 2001). The first definition stems from the practical necessity of geotechnical engineers to design mitigation measures to prevent the occurrence of liquefaction: a criterion in terms of state of stresses for the onset of liquefaction is useful for the design of such measures. But from a phenomenological point of view, reaching a stress state that leads the sample to experience uncontrollable failure cannot be considered liquefaction since it can be argued that the sample is still in a solid-like state whereas the word liquefaction suggests the sample having experienced a state change: from solid-like to liquid-like. With regard to the second definition, we note that even in the liquefied state there are interparticle collisions, which, together with the stress contribution because of the fluctuating kinetic energy density, so-called Reynolds stresses, leads to a state of stress that is never actually zero but simply a rather small value in the context of traditional soil mechanics (Gong et al., 2012). In the granular physics community more attention is paid to the phenomena occurring at the microscale so liquefaction (the word unjamming tends to be used instead) indicates the transition from a solid-like behavior to a liquid-like behavior. A solid-like behavior is identified with persistent load bearing contact force chains while liquid like behavior is identified with the absence of such persistent load bearing force chains (Campbell, 2002; Chialvo et al., 2013). In this paper the phrase 'onset of liquefaction' is employed to indicate the mean effective stress becoming transiently equal to zero, which occurs with the medium still exhibiting a solid-like behavior, *i.e.* persistent load bearing contact force chains are present as will be shown later on, and full liquefaction to indicate the completion of the transition process from solid-like to liquid-like behavior that requires some significant extra straining to be imposed (see section RESULTS AND ANALYSIS).

In the paper a summary of the micromechanical investigation of liquefaction performed via 3D DEM simulations of cyclic undrained strain controlled triaxial tests in a periodic prismatic cell illustrated in (Martin et al., 2019) is reported. The purpose of the investigation is to shed light on the micromechanical signatures of the onset of liquefaction and the establishment of full liquefaction for granular media subject to seismic conditions.

The undrained behaviour of loose samples was first investigated via the DEM by Thornton and Barnes (1986), Ng and Dobry (1994), Sitharam et al. (2002), and Zhang (2003), who all employed dry samples loaded under constant volume, i.e. isochoric tests. Bonilla (2004) made a comparison between DEM isochoric simulations without pore fluid and DEM undrained simulations with fluid coupling, using two dimensional assemblies of elliptical particles, reaching the conclusion that "both methods provide similar results". More recently Gong et al., (2012) performed monotonic 3D DEM axisymmetric undrained compression triaxial tests in a prismatic periodic cell maintained at constant volume measuring effective stress paths that were qualitatively similar to published physical experimental results. Also, several recent works (Xu et al. 2015; Soroush and Ferdowsi, 2011; Sitharam et al. 2009; Sitharam and Govinda Raju, 2007; Sitharam and Dinesh, 2003) have successfully simulated undrained conditions by 3D DEM analyses without including the fluid in the model. The tests presented in (Martin et al., 2019) are of this type.

2 DISCRETE ELEMENT SIMULATIONS

To perform the simulations here described, the open source software YADE (Šmilauer et al., 2010) was employed. Several arrangements of particles of different grain size distributions were considered and, for each one of them, cyclic undrained triaxial test simulations were performed at different porosities. The DEM simulations were performed on dry granular assemblies, *i.e.* the fluid phase was ignored and all stresses were calculated from the orientational distributions of forces at the contacts between particles. Consequently, the effective stresses were calculated directly. This contrasts with laboratory experiments in which the total stresses and the pore water pressure are measured, and the effective stresses are obtained indirectly using Terzaghi's effective stress equation. This paper focuses on one such arrangement.

The work presented in this paper stemmed from the need to assess the liquefaction potential of a real gravelly deposit to be employed as the foundation of a concrete faced rockfill dam, called Punta Negra, located in the province of San Juan, Argentina. DEM simulations were initially

performed for four different grain size distributions (GSD) to study the influence of the sand content on the liquefaction resistance when subjected to cyclic loading under undrained conditions. Since the qualitative trends exhibited by these samples did not differ, here only the simulations run for one GSD are reported. The sample consists of 10,000 elastic spheres with an initial porosity of 0.416 and mean stress of 250 kPa, the grain size distribution is shown in Fig. 1.

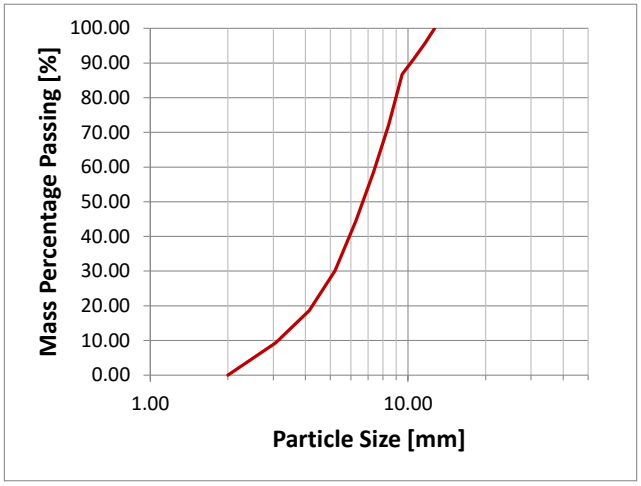

Figure 1: Grain size distribution employed in the DEM tests.

2.1 *Contact laws*

The contact law used in the tests here presented is the Hertz-Mindlin (HM) no micro-slip solution (Mindlin, 1949) which was implemented in YADE by (Modenese et al., 2012). The model considers nonlinear compression, linear rotational resistance, nonlinear tangential shearing with a Mohr Coulomb slip criterion, and nonlinear viscous damping in both the normal and tangential directions. The normal force is computed at each time step from the current overlap between two grains in contact. The tangential force, on the other hand, is updated incrementally.

To account for the effect of particle shape, rolling resistance is applied for both rolling and twisting moments incrementally, as for the tangential force:

$$M_{ROLL} = M_{ROLL} + K_R \cdot \Delta\theta_R \tag{1}$$

$$M_{TWIST} = M_{TWIST} + K_{TWIST} \cdot \Delta\theta_{TWIST} \tag{2}$$

where M_{ROLL} and M_{TWIST} are the rolling and twisting moments, K_R and K_{TWIST} are the linear rolling and twisting coefficients of the interaction, Θ_R and Θ_{TWIST} are the relative rolling and twisting rotations between particles in contact. Relative rotation - moments relationships were first proposed by (Iwashita & Oda 1998). Here they are employed to account for the fact that the directions of the normal forces exchanged between real gravel (non spherical) particles do not intersect the particle centers, thus generating torques that do not occur in the case of spherical particles (Ai et al., 2011). The rolling moment between two contacting particles is limited to a maximum value given by $\eta_R * R_{mean}$, whereas no limit is applied to the twisting moment.

2.2 *Quasi-static conditions*

The triaxial simulations were run under quasi-static conditions. To check the presence of quasi-static conditions, the so-called inertial number, I (Da Cruz et al., 2005), was employed:

$$I = \dot{\varepsilon} d \sqrt{\frac{\rho}{p'}} \tag{3}$$

with $\dot{\varepsilon}$ is the shear strain rate applied to the periodic cell, d is the average particle diameter, ρ is the particle density, and p' is the effective pressure applied to the arrangement. The density of all the grains is set to a value of 2600 kg/m^3 and no gravity is applied.

According to Radjai and Dubois (2011), the inertial number must be lower than 10^{-3} to guarantee that simulations are in the quasi-static regime. Consequently, the maximum deviator strain rate initially applied in the tests was 0.1 sec^{-1}. However, Radjai and Dubois (2011) employed an almost uniform particle size distribution in their tests, so the I value to be considered as threshold for quasi-static regime needs to be ascertained afresh for our specific PSD. Hence monotonic undrained (isochoric) triaxial tests were performed on four different samples, with the deviator strain rate varied from 0.016 sec^{-1} to 8.192 sec^{-1}. From our tests it emerged that a strain rate lower than 0.1 sec^{-1} is enough to avoid the influence of inertial effects on the stress-strain behavior during monotonic loading. The same is expected for cyclic deformation.

2.3 *Stress tensor*

The total stress tensor of a soil volume can be decomposed into the sum of the effective stress tensor due to the forces at the contacts between the particles and the pressure tensor of the fluid within the soil voids. The effective stresses can be calculated from the summation of the contact forces and the fluctuating part of the particle velocities (Thornton, 2000):

$$\sigma'_{ij} = \frac{1}{V} \sum l_i F_j + \frac{1}{2V} \sum m\, \tilde{u}_i \tilde{u}_j = \sigma'^{C}_{ij} + \sigma'^{R}_{ij} \tag{4}$$

where m is the mass of each particle, $\tilde{u}_i$ and $\tilde{u}_j$ are the fluctuating velocities of each particle, V is the volume of the sample, l is the distance between the centers of the two contacting spheres, and F is the contact force. The first term in Eq. 4 represents the Cauchy stress tensor, σ'^{C}_{ij} while the second term corresponds to the Reynolds stress tensor, σ'^{R}_{ij}. Under quasi-static conditions, Reynolds stresses are negligible but they have been calculated in order to check whether they remain negligible following the onset of liquefaction.

2.4 *Description of DEM simulations*

Following Salot et al (2009) and Modenese (2013), samples were prepared according to a three steps procedure: i) generation of non-overlapping particles randomly in space with an intergranular friction angle of 40°; ii) compression of the particles up to the development of a cell pressure of 250 kPa; iii) gradual decrease of the friction angle at constant pressure until the target porosity of 0.416 was reached. The intergranular friction angle is then returned to the value assigned at particle generation. To ensure quasi-static conditions throughout the preparation phase, the ratio of the average out-of-balance force of all the particles to the average force at all the contacts was maintained lower than 0.01.

Then, the assemblies were subjected to different values of cyclic deviator strain, ranging from ±0.2% to ±1%. The volume was kept constant by maintaining a constant value of the axial strain rate of 0.1 sec^{-1}, and half that value (0.05 sec^{-1}) in the two other orthogonal directions. Since it is not possible to measure total stresses during an isochoric (constant volume) DEM test, the total stress path during cyclic shearing is unknown and therefore the pore pressure too. The assembly was considered to be liquefied when the ratio of the mean effective stress of the assembly, p', to the initial confining pressure applied, p_0 = 250 kPa, fell below 0.01.

The main parameters used for all the DEM simulations are: Poisson's ratio $\nu = 0.1$; Young's modulus $E = 1 \cdot 10^9\ N/m$; friction coefficient $\mu = \tan(\varphi)$, with φ = 40°; coefficient of rolling stiffness $K_R = 7500\ J/rad$; coefficient of twisting stiffness $K_{TWIST} = 5000\ J/rad$; coefficient of rolling friction $\eta_R = 0.8$; normal coefficient of restitution $e_N = 0.9$; and tangential coefficient of restitution $e_T = 0.9$. Given that the value of Poisson's ratio and Young's modulus is the same

for all the particles within the arrangement, the ratio between the tangential and normal contact stiffness is 0.947 ($K_T = 0.947 \cdot K_N$).

3 RESULTS AND ANALYSES

Fig. 2 shows the observed macroscopic behavior of the tested sample under cyclic shear strain. The figure shows, in Fig. 2(a), that the amplitude of the Cauchy stress component oscillations gradually reduces to zero when the normalized effective pressure, shown in Fig. 2(b), becomes null. Figure 2(c) shows the deviator stress plotted against the deviator strain. It can be seen that the inclination of the hysteresis loops decreases as the simulation progresses as a consequence of the decrease in p', as shown in Fig. 2(d).

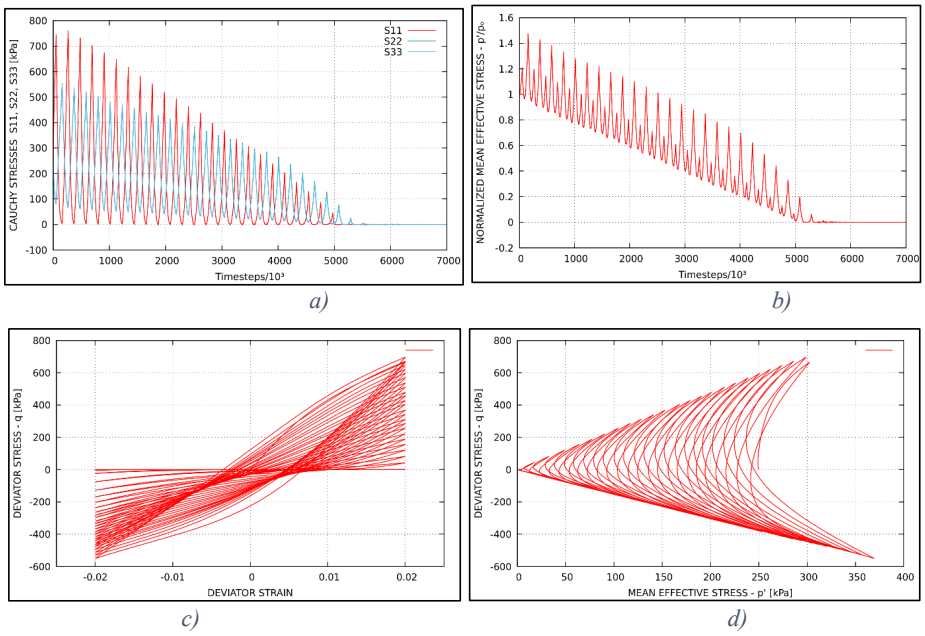

Figure 2. a) Cauchy stresses evolution during cyclic triaxial undrained simulation b) Normalized mean effective stress c) Deviator stress as a function of axial deviator strain d) p'- q diagram (after Martin et al., 2019).

3.1 *Micromechanical analyses*

The variables analyzed are the mechanical coordination number, the geometrical coordination number, the redundancy index, number of contacts, size and number of clusters, Reynolds stresses and inertial number.

The coordination number is defined as the average number of contacts per particle. Thornton (2000) introduced the so called mechanical coordination number Z_m to exclude particles that do not contribute to load bearing, i.e. floaters and rattlers, as:

$$Z_m = \frac{2C - N_1}{N - N_1 - N_0} \tag{5}$$

where C is the total number of contacts within the particle arrangement, N is the total number of particles, N_1 is the number of particles with only one contact, N_0 is the number of particles with

no contacts.When the mechanical coordination number was introduced by Thornton (2000) it was thought that, since the particles with only one contact were transient collisions, they did not significantly contribute to the stress tensor and therefore should be ignored. However, when considering isostaticity at any moment in time these contacts cannot be ignored. Consequently, it is more relevant to consider the geometrical coordination number Z_g (Thornton, 2015) which is defined as:

$$Z_g = \frac{2C}{N-N_0} \tag{6}$$

If the total number of constraints is equal to the total number of degrees of freedom, then the system is said to be isostatic on average. In 3D, the number of degrees of freedom per particle is 6 (3 translations and 3 rotations). In the simulations reported by Thornton (2000) the number of constraints per contact was 3 (the normal force and the two components of the tangential force). In the current simulations, three additional constraints are present due to the two components of the rolling resistance and the twisting resistance, therefore, the system is isostatic on average if $6C = 6(N-N_0)$ and substituting into Eq. (19) the threshold coordination number becomes $Z_{g\text{-iso}} = 2$.

An alternative, and perhaps a more reliable, parameter that can be used to assess the stability of the system is the redundancy index (Gong et al, 2012) or redundancy ratio (Zhou et al, 2017), redundancy factor (Kruyt and Rothenburg, 2009), constraint ratio (Cundall and Strack, 1983) which takes into account the number of contacts that are sliding and/or rolling at any moment in time. The redundancy index is defined as the ratio of the total number of constraints to the total number of degrees of freedom of the active particles. In the current simulations no limit was specified for the twisting moment therefore the redundancy index is here defined as:

$$I_R = \frac{6C_{NSR}+4C_S+4C_R+2C_{SR}}{6(N-N_0)} \tag{7}$$

where C_{NSR} is the number of contacts that are neither sliding nor rolling (6 constraints given by 3 forces and 3 moments); C_S is the number of contacts that are sliding (4 constraints given by the normal force and 3 moments); C_R is the number of contacts that are rolling (4 constraints given by the 3 force components and 1 twisting moment); C_{SR} is the number of contacts that are sliding and rolling simultaneously (2 constraints given by the normal force and the twisting moment); N is the total number of particles and N_0 is the number of particles with no contacts. The condition $I_R = 1$ identifies isostatic conditions on average for the granular system. Figure 3(a) shows that the onset of liquefaction from a stress state point of view, *i.e.* the occurrence of $p'/p_0=0$, coincides with the redundancy index reaching unity which also confirms the correctness of the definition of I_R.

3.2 *Micromechanical insight in the onset of liquefaction*

The calculation of stresses is based on contact forces and particle velocities (see Eq. (4)). It is important to note that the number of particles employed in the simulations is limited in comparison with nature, 10,000 rather than billions. This implies that the stresses measured in the periodic cell exhibit some small oscillations, stemming from the limited number of particles of the cell, that would not be seen in a much larger sample. Therefore, the stress threshold for the onset of liquefaction $p'/p_0=0$ is considered to be reached when $p'/p_0 < 0.01$. Using this criterion, the onset of liquefaction is identified to take place at about $5*10^6$ timesteps (see the blue vertical line in Figures 3 and 4). After this point the effective pressure increases due to the cyclic nature of the loading, until after a few more cycles p'/p_0 remains stable (null). From Fig. 3 it emerges that at the identified onset of liquefaction the geometric coordination number is very close to 2 indicating the sample to be isostatic on average. This is a rather remarkable finding since it indicates that the onset of liquefaction from a stress state point of view, *i.e.* the occurrence of $p'/p_0=0$ is associated with the geometrical coordination number approaching the value of the threshold geometrical coordination number expressing the isostatic condition for the granular system which has not previously been shown for assemblies of granular particles with rolling resistance.

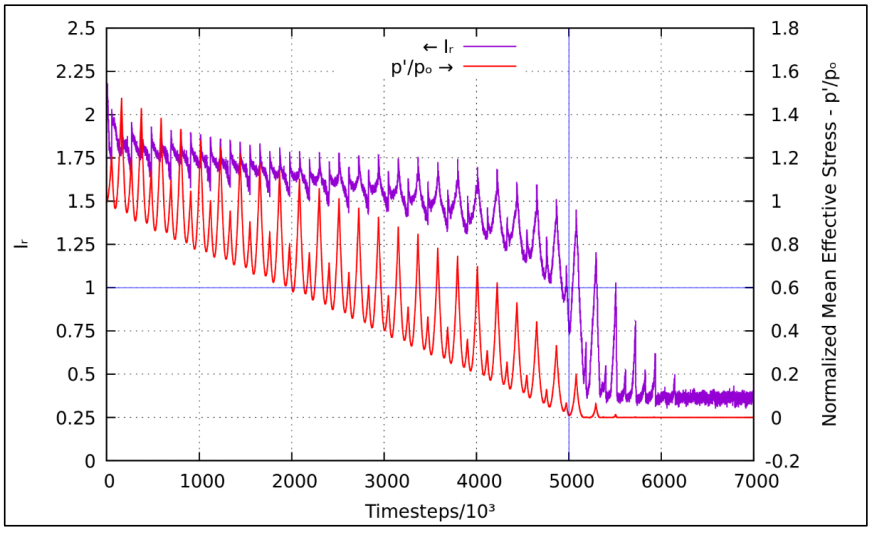

Figure 3: Evolution of the mean effective pressure and redundancy index (after Martin et al., 2019)

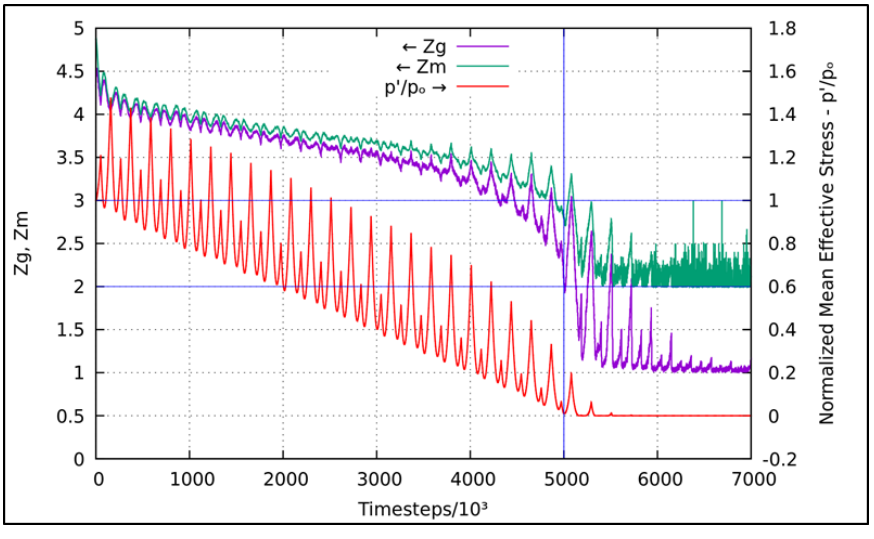

Figure 4: Evolution of the mean effective pressure and the mechanical and geometrical coordination numbers (after Martin et al., 2019).

Due to cyclic straining, fluctuations of p'/p_0 continue to occur for a while as reported already by (Ng & Dobry, 1994). Also from both Figure 3 and 4 it is clear that not only p'/p_0 but also the geometrical coordination number and redundancy index keep varying after the onset of liquefaction for some significant further shearing. This indicates liquefaction does not occur instantaneously but as a process whereby the granular medium behavior transitions from solid-like to liquid-like. The key question left open is: when the transitions ends or in other words when full liquefaction is established?

Looking at Figure 3 and 4 we can conclude that once full liquefied is established Z_m, Z_g and I_R remain constant at approximately 2, 1 and 0.35 respectively, which occurs at some point after $6*10^6$ time-steps. However, it is not straightforward to establish when they reach their steady value due to the strong oscillations exhibited. In the quest to clarify the solid-like to liquid-like transition, it is useful to analyze the clustering of the particles.

So far observations on the redundancy index suggest full liquefaction is established after $6*10^6$ time-steps. To elucidate further the transition from solid-like to liquid-like behavior, an analysis of how particles cluster together was undertaken.

A cluster is a group of particles in contact at any given timestep throughout the simulation. The cluster size is defined by the number of particles in the cluster and the number of clusters includes singlets. Figure 5 shows the evolution of the number of clusters and the size of the largest cluster. Initially, the largest cluster consists of 5000 particles and there are 5001 clusters. This means that all the particles that are not in the largest cluster are singlets, *i.e.* floaters and rattlers. As the mean effective stress decreases, the magnitude of the normal contact forces reduces. With continued decrease in the mean effective stress an increasing number of contact normal forces reduce to zero and contacts are lost and the maximum cluster size gradually reduces at an increasing rate.

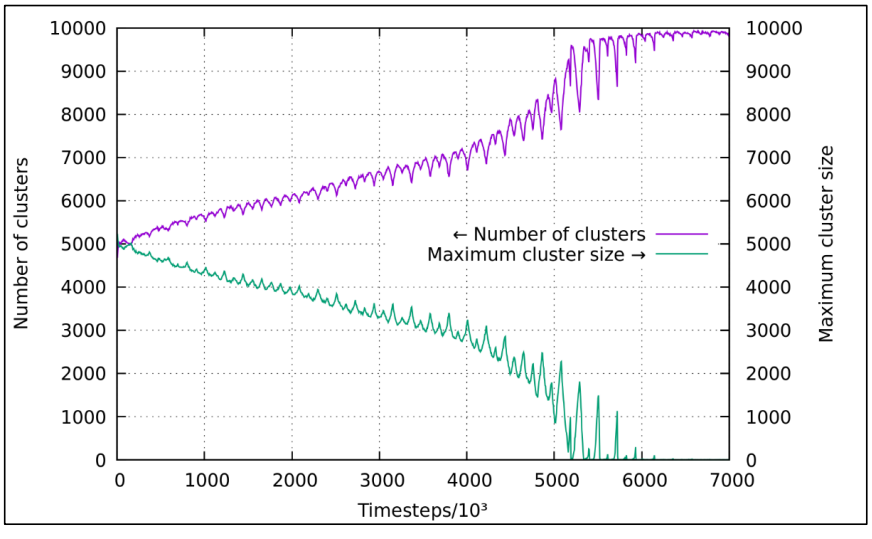

Figure 5: Clustering evolution during the cyclic simulations (after Martin et al., 2019).

To identify the establishment of full liquefaction, in figure 6 the evolution of the maximum cluster size, the number of particles per cluster, is plotted rescaled after the onset of liquefaction, *i.e.* after 5 million time-steps. Looking at this figure and its inset it can be concluded that full liquefaction is established after $6.6 \cdot 10^6$ timesteps with the maximum cluster size then oscillating between 3 and 20 particles (see Fig. 6 inset). This shows that after full liquefaction takes place, only a few particles are in contact with the geometrical coordination number and redundancy index oscillating around stable averages of 1 and 0.35 respectively (Fig. 3 and 4 respectively).

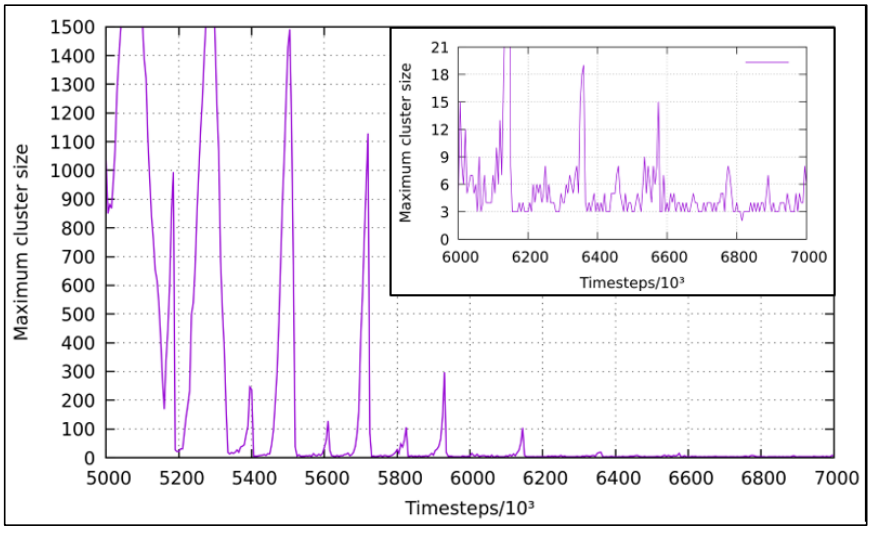

Figure 6: Evolution of the maximum cluster size after the onset of liquefaction (after Martin et al., 2019).

Figure 7 shows the force chain network within the largest cluster. Interestingly, the figure suggests that the loss of contacts is uniformly distributed throughout the assembly and that there is no breakup of the large cluster into smaller clusters. In addition, this appears to be a good example of diffuse failure (Darve, 1996). It emerges that, during degradation of the initial large cluster, only singlets are created increasing the number of 'rattlers'.

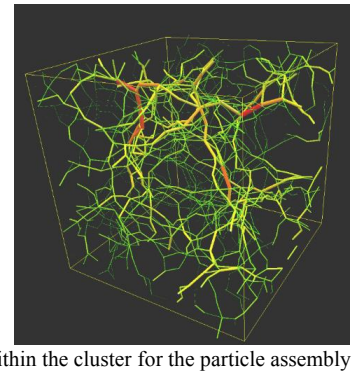

Figure 7: force chain network within the cluster for the particle assembly after 5 million timesteps (after Martin et al., 2019).

4 CONCLUSIONS

A comprehensive analysis at the micromechanical level of the phenomena leading to the onset of liquefaction in a granular soil subjected to seismic action has been carried out by performing 3D Discrete Element Method (DEM) simulations of undrained strain controlled triaxial tests on a standard desktop computer. The DEM is unique in its ability to elucidate the physical causes of the transition from solid-like to liquid-like behavior of the granular assembly.

From our findings emerges that as the mean effective stress decreases, the magnitude of the contact normal forces reduces and an increasing number of contacts are lost with the maximum cluster size gradually reducing at an increasing rate. The loss of contacts is uniformly distributed throughout the sample and there is no breakup of the large cluster into smaller clusters. This is

different from monotonic undrained tests on loose specimens in which the isostatic state is reached soon after the deviator stress reaches a maximum value (Gong et al., 2012).

From the presented investigation it turns out that the transition from solid-like to liquid-like behavior or, in other words, from the onset of liquefaction to full liquefaction can be ascertained rather well by analyzing the evolution of the geometrical coordination number, redundancy index, particle contacts and clusters. Full liquefaction is associated with the point in time when all these variables start to oscillate steadily around constant values. Further details of the investigation are available in (Martin et al., 2019).

REFERENCES

Ai, J., Chen, J., Rotter, J., Ooi J. 2011. Assessment of rolling resistance models in discrete element simulations. *Powder Technology* 206(3): 269–282.

Bishop, A.W. 1966. Strength of soils as engineering materials. 6th Rankine lecture. *Géotechnique* 16: 89-130.

Bishop, A.W. 1971. Shear strength parameters for undisturbed and remoulded soil specimens. *Proceedings of the Roscoe Memorial Symposium*: 3-58. Cambridge, USA.

Bonilla, R.R.O. 2004. Numerical simulations of undrained granular media. *Ph.D. thesis*, Univ. of Waterloo, Canada.

Campbell, C.S. 2002. A problem related to the stability of force chains. *Granular Matter* 5, 129-134. [DOI 10.1007/s10035-003-0138-6].

Carrera, A., Coop M. & Lancellotta L. 2011. Influence of Grading on the Mechanical Behaviour of Stava Tailings. *Géotechnique* 61(11): 935–946.

Castro, G. 1969. Liquefaction of sands. *Soil Mechanics Series* No. 81, Harvard University, Cambridge.

Chialvo S. & Sundaresan S. 2013. A modified kinetic theory for frictional granular flows in dense and dilute regimes. *Physics of Fluids* 25, 070603 [DOI: 10.1063/1.4812804].

Cundall, PA. & Strack, ODL. 1979. A discrete numerical model for granular assemblies. *Géotechnique* 29(1): 47-65.

Cundall, PA. & Strack, ODL. 1983. Modelling of microscopic mechanisms in granular material. In *Mechanics of Granular Materials: New Models and Constitutive Relations*, J.T. Jenkins, M. Satake eds., 137-149. Amsterdam: Elsevier.

Da Cruz, F., Emam, S., Prochnow, M., Roux, J.N., Chevoir F. 2005. Rheophysics of dense granular materials: Discrete simulation of plane shear flows. *Physical Review E*, 72.

Darve, F. 1996. Liquefaction phenomenon of granular materials and constitutive stability. *Engineering Computations*. 13(7): 5-28.

Gong, G., Thornton, C. & Chan, A. 2012. Simulations of Undrained Triaxial Behavior of Granular Material. *Journal of Engineering Mechanics*. 138(6): 560-566.

ICOLD 1995. INTERNATIONAL COMMISSION ON LARGE DAMS. *Tailings Dams and seismicity – Review and recommendations.* Bulletin 98.

ICOLD 2001. INTERNATIONAL COMMISSION ON LARGE DAMS. *Tailings Dams Risk of Dangerous Occurrences - Lessons Learnt From Practical Experiences.* Bulletin 121.

Iwashita, K. & Oda, M. 1998. Rolling resistance at contacts in simulation of shear band development by DEM. *J. Eng. Mech. ASCE*, 124: 285 -292.

Johnson, K.L. 1985. Contact mechanics, *Cambridge University Press*.

Kokusho, T. 2007. Liquefaction Strengths of poorly-graded and well graded granular soils investigated by lab tests. *Earthquake Géotechnical Engineering*, 159 – 184.

Kruyt, N.P. & Rothenburg, L. 2009. Plasticity of granular materials: a structural-mechanics view. In *Powders and Grains 2009* (M. Nakagawa and S. Luding, Eds.) American Institute of Physics, 1073-1076.

Martin E., Thornton C., Utili S., 2019 Micromechanical investigation of the liquefaction of a gravel by cyclic 3D DEM tests. *Geotechnique*, Doi:10.1680/jgeot.18.P.267.

Mindlin, R.D. (1949). Compliance of elastic bodies in contact. *Journal of Applied Mechanics* 16(1): 259-344.

Modenese C., Utili S., Houlsby GT (2012). DEM Modelling of Elastic Adhesive Particles with Application to Lunar Soil. *Earth and Space 2012*, *Proc. of the 13th Aerospace Division Conference on Engineering, Science, Construction, and Operations in Challenging Environments*: 45-54. Pasadena, USA.

Ng T-T & Dobry R. (1994). Numerical Simulations of Monotonic and Cyclic Loading of Granular Soil. *Journal of Geotechnical Engineering* 120, No. 2.

Radjai, F. & Dubois, F. 2011. Chapter 8 – Dimensional Analysis and Control Parameters. *Discrete Element Modeling for Granular Materials*. ISTE Ltd and John Wiley & Sons Inc. ISBN 1-84821-260-7.

Salot, P., Gotteland & Villard P. 2009. Influence of relative density on granular materials behavior: DEM simulations of triaxial tests. *Granular Matter* 11(4): 221-236.

Sitharam, T. G., Dinesh, S. V., & Shimizu, N. (2002). "Micromechanical modelling of monotonic drained and undrained shear behaviour of granular media using three-dimensional DEM." *Int. J. Numer. Anal. Methods Geomech*., 26(12): 1167–1189.

Sitharam, T.G. & Dinesh, S.V. 2003. Numerical simulation of liquefaction behaviour of granular materials using Discrete Element Method. *Proc. Indian Acad. Sci. (Earth Planet. Sci.)* 112(3): 479 – 484.

Sitharam, T.G. & Govinda Raju, L. 2007. Pore pressure generation in silty sands during cyclic loading. *Geomechanics and Geoengineering* 37(3): 210–226.

Sitharam, T.G., Vinod J.S. & Ravishankar B.V. 2009. Post-liquefaction undrained monotonic behaviour of sands: experiments and DEM simulations. *Géotechnique* 59(9): 739–749.

Sladen, J. A., D'Hollander, R.D. & Krahn J. 1985. The liquefaction of sands, a collapse surface approach. *Canadian Geotechnical Journal*, 22(4): 564-578.

Šmilauer V., Catalano E., Chareyre B., Dorofeenko S., Duriez J., Gladky A., Kozicki J., Modenese C., Scholtès L., Sibille L., Stránský J., & Thoeni K., *Yade Documentation, The Yade Project*, 1st ed., 2010.

Soroush, A. & Ferdowsi, B. (2011). Three dimensional discrete element modeling of granular media under cyclic constant volume loading: a micromechanical perspective. *Powder Technology* 212: 1–16.

Thornton, C. & Barnes, D.J. 1986. Computer simulated deformation of compact granular assemblies. *Acta Mechanica* 64, 45.

Thornton, C. 2000. Numerical Simulations of Deviatoric Shear Deformation of Granular Media. *Géotechnique* 50(1): 43-53.

Thornton, C. 2015. Granular Dynamics, Contact Mechanics and Particle System Simulations – A DEM Study. Particle Technology Series, vol. 24. New York, USA: Springer.

Villavicencio, G., Espinace, R., Palma, J. & Valenzuela P. 2014. Failures of sand tailings dams in a highly seismic country. *Canadian Geotechnical Journal*, 51: 449-464.

Xu, X. M., Ling, D.S., Cheng, Y.P. & Chen Y.M. 2015. Correlation between liquefaction resistance and shear wave velocity of granular soils: a micromechanical perspective. *Géotechnique* 65(5): 337–348.

Yamamuro, J.A., & Covert, K. M. 2001. Monotonic and cyclic liquefaction of very loose sands with high silt content. *Journal of Geotechnical and Geoenvironmental Engineering*, ASCE 127(4): 314-324.

Zhang, L. 2003. The behaviour of granular material in pure shear, direct shear and simple shear. *Ph.D. thesis*, Aston Univ., UK.

Zhou, W., Liu, J., Ma, G. & Chang, X. 2017. Three dimensional DEM investigation of critical state and dilatancy behaviors of granular materials. *Acta Geotechnica*, 12: 527–540.

EO4RM: Earth Observation Best Practices for the Mining of Raw Materials

Ton Peters
Deltares, Delft, the Netherlands

Stephen Wheston
LTMS, Naas, Ireland

Margreet van Marle
Deltares, Delft, the Netherlands

Brendan Morris
LTMS, Naas, Ireland

Zoltan Bartalis
ESA, Frascati, Italy

ABSTRACT: The objective of the EO4RM project is to unlock the potential of Earth Observation (EO) for the Raw Materials (RM) mining sector. EO products are identified that have the highest potential to be exploited for mining purposes. This has been done by a gap analyses between the current geoinformation needs of the mining sector and the strengths, limitations and opportunities of different EO products.

A mock-up environment was used to demonstrate the following products in real life cases:

- Stockpile measurements, where satellite technology is used to measure stockpiles on a regular basis and calculate ore volumes.
- Ground Stability monitoring, which covers the areas of land subsidence, tailings dam stability and pit slope stability.

Already valuable applications of EO technology are of use to the mining industry but to realize its full potential the EO industry needs to engage more with the mining sector.

1 INTRODUCTION

1.1 *Objective EO4RM project*

The objective of the EO4RM project is to fully unlock the potential of Earth Observation for the mining of Raw Materials and find new ways of exploiting the vast growing volume of EO data available today. The project is initiated and funded by the European Space Agency (ESA) in order to bridge the gap between the mining and EO sector.

The geoinformation needs, EO products available, and level of uptake for EO vary across the stages of the mining life cycle. Mining companies, consultants and other stakeholders were consulted by the project team during surveys, various expert interviews, a workshop and two webinars in order to study and validate:

- The geoinformation needs of the raw materials mining sector.
- The current utilization of EO technology in the sector.
- Subsequently, for every geoinformation need the corresponding mature EO products were identified and validated in a gap analysis.
- The sentiment (opportunities and challenges) towards further uptake of EO technology.

Finally, two products with high potential were demonstrated as a show-case in a mock-up environment and feedback was collected from different types of users.

1.2 *Utilization of EO in the mining sector*

Earth Observation Remote sensing is the gathering of information about the physical, chemical, and biological systems of the planet without making physical contact. Remote sensing can be satellite-based or based on nearer ground techniques including terrestrial scanners or observations

making use of Unmanned Aerial Vehicles (UAVs). In this study we are focusing solely on the satellite remote sensing part, often referred to as Earth Observation (EO).

The advantage of EO is that it has capabilities of continuous observations in time and often in space. For mining activities specifically, this provides the potential of monitoring continuously, often in remote areas, albeit at often a coarser spatial resolution than ground-based or UAV-based measurements. Over the past years, several EO solutions have been tested, especially in larger operations. However, it is believed that there is still a gap between the potential of EO and the uptake of EO by the mining sector to assist in mining operations. This is especially the case for middle and even smaller mining operations, and governments and regulating agencies that work with smaller resources.

The mining life cycle starts with Exploration and subject to feasibility moves on to Permitting, Design, Construction, Operation and finally Closure & Aftercare. Each of these phases require specific geoinformation data to progress and EO can be used to supply some of these data. In the exploration phase the technology is particularly useful for gathering data over expansive, remote areas. EO applications currently used by exploration companies include mapping of topography and geological mapping [Gomez 2005]. The technology is more typically used by the major exploration companies rather than the juniors.

The uptake of EO technology for the permitting stage of the mine cycle is limited. EO is used at this stage of mining to map existing mining activities [Lobo 2018], infrastructure, identify population densities, to characterize habitat and also to identify protected areas, which may include cultural heritage sites or biodiversity rich sites.

EO has use in the design and construction phase, but it is during operations that the technology offers significant value to mining companies. EO is providing a solution to replace traditional methods used such as aerial photography and ground-based data surveys. EO is starting to be used in the mining industry for measuring ground movement (subsidence or heave) and also movement of structures and is a very useful resource for assessing risk associated with ground collapse and stability of structures such as pits, tailings dams and waste rock dumps [Karam 2016, Du 2020].

In the closure and aftercare phase, EO technology is being used for various applications including the validation of the rehabilitation of mine sites and demonstration that agreed infrastructure has been removed. It also has potential for post closure ground stability monitoring and the mapping of vegetation health [Bao 2014].

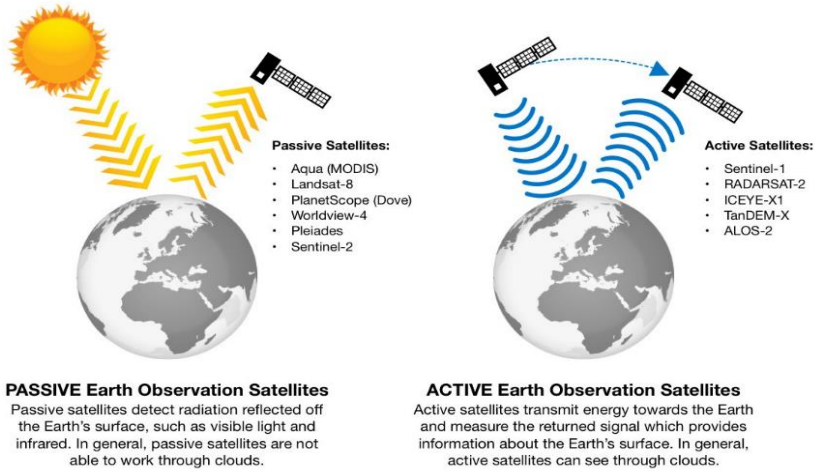

Figure 1. Passive and active EO Satellites (Source: Radiant.Earth)

1.3 *Potential EO technology for the mining sector*

EO technology is a relatively fast developing technology, while satellites have been fitted with sensors to monitor the earth for decades. In recent years there has been a proliferation in the

number of satellites that have been placed into orbit and the number of satellites that are proposed and planned. For example, November 2020 is the proposed launch date for the next in the Sentinel series of satellites (Sentinel-6A). There has also been a major advancement in the sensor technology, meaning that sensors are smaller, more powerful and measuring parameters that up until recently were not possible[1]. As such the potential for use of the technology has increased in recent times and is continuing to increase.

EO data is acquired by sensors mounted on satellites. The sensors can be active or passive, as depicted in Figure 1. An active sensor emits a signal or an energy in the direction of the target to be investigated, for example this might be a radar signal. It then collects the data that is reflected from the target area and interprets this data. A passive sensor, on the other hand, detects natural energy, such as radiation or light that is emitted or reflected by the target being observed. The most common source of radiation measured by passive sensors is reflected sunlight. When we focus on visible light, we call this Optical satellite imagery. Another type of passive sensor bases its source on the earth's Gravity field. The other products described in this study belong to the following types of instruments:

- Interferometric Synthetic Aperture Radar (InSAR) is an active system that is capable of mapping subsidence of the earth's surface at millimeter scale.
- Multispectral, passive instruments (M-Spectral) are sensitive to specific wavelengths beyond the visible light range (i.e. infrared and ultra-violet) and are used to collect information on, for instance, water, soil and vegetation.
- Hyperspectral imaging techniques (H-spectral) collect and process information from a set of images across the electromagnetic spectrum. [Meer, van der 2012].

When discussing the application of EO, the resolution of the available EO data is an important factor to evaluate the potential of the EO solution. Resolution can be divided into temporal, spatial and spectral resolutions. Temporal refers to the refresh rate of data – or in other words how often are measurements taken, for example real time, hourly, daily, or weekly etc. Spatial resolution refers to the size of the area that the measurement is taken over – in other words is the resolution per m^2, per km^2 or per 100 km^2, etc. Finally, the spectral resolution is the accuracy of the measurement – for example it may be to how many mm movement can be measured or parts per million, parts per billion or parts per trillion of an atmospheric parameter e.g. carbon dioxide, ammonia or particulate. The challenges associated with resolution can be an actual gap in the technology and sometimes a misconception that some people within the mining industry have about the technology.

The EO4RM project learned that there is a lack of knowledge within the mining industry of the cost of EO for use in the mining operations, with an opinion amongst some that the cost of the technology is prohibitively expensive. There are different types of raw data sources available. Sometimes data are publicly available via service providers such as ESA and NASA, but other data must be paid for. This differs per service provider. Often this is related with either: 1 - data gathered by commercially operated satellites, which has the advantage that the (spatial or temporal) resolution may be better; or 2 - data needs further processing requiring specific expertise and algorithms. So, although the raw data can sometimes be based on freely available data, the use of data processing algorithms and the presentation of the product in a tailored service need to be paid for.

2 GEOINFORMATION NEEDS

2.1 *Raw Materials Sector geoinformation needs*

Each of the mining phases as referred to in section 1 requires geoinformation. The EO4RM project identified sixty-seven items of geoinformation that are required over the life of a mining project, it described how they are currently achieved and the associated measurement specifications that are required by the mining industry and regulating agencies. This list was developed by mining experts that were part of the EO4RM team. Table 1 provides a summary of the requirements for a selection of the identified geoinformation needs.

[1] https://www.itc.nl/research/research-facilities/labs-resources/satellite-sensor-database/

Table 1. Selection of geoinformation needs per mining cycle phase

Cycle	Information type	Current technology used	Area assessed	Min. measurement requirements	
				Resolution (various)	Refresh rate
Exploration	E1. Topographic mapping of surface expressions	Digital Terrain Modeling / Optical Satellite imagery / Drones (LiDAR) / Field mapping surveys	Variable. Can be <1 km^2 to >1,000 km^2	1 m^2	Annual or greater
	E2. Geological mapping of sub-surface expressions	Maps / Previous exploration data / Geophysics	10 km^2 to 1,000 km^2	Minimum depth 30 m and up to 1000 m	Annual or greater
	E3. Geochemical signatures / anomalies	Maps / Walk-over portable XRF / Airborne / Sampling & assaying of soils and rocks / Drilling & Trenching / Vegetation assessment	1 km^2 to 1,000 km^2	Various measurement resolutions are required.	Annual or greater
Permitting	P1. Water catchment	Desktop study and field work	Various, can be >100 km^2	1 in 50,000 (1 cm on the map equals 0.5 km)	Annual or greater
	P2. Population centres / social impact	National Databases / Site assessment / fly over / drive through	Regional - 50 km^2 Local – 1 km^2	1 in 10,000 (1cm on the map equals 0.1 km)	Annual or minimum of every 10 years.
	P3. Characterization of flora and fauna	Published data / Biological Surveys	1 km^2 to 10 km^2	1 to 10 m^2	Monthly
Construction / Operation	O1. Site design and layout of infrastructure	Drones / LiDAR / Surveys	10 km^2	1:1000 (1cm on the map equals 0.01 km)	Weekly
	O2. Ground / Structural / Infrastructure / Stability	Surveys / Drones / LiDAR /	10 km^2	0.001 to 0.5 m	Continuous to annual
	O3. Stockpile measurement	Drones / Surveys	10 km^2	0.005 - 0.5 m	Daily to monthly
	O4. Groundwater monitoring	Published data / borehole monitoring	10 km^2 to 100 km^2	1 m^2	Monthly
Closure / Aftercare	C1. Demonstration of rehabilitation / revegetation	Fly over / Aerial photography / walk-over / Optical satellite imagery	1 km^2 to 10 km^2	1 m^2	Quarterly
	C2. Demonstration of infrastructure removal	Fly over / Aerial photography / walk-over / Optical satellite imagery	10 km^2 to 100 km^2	1 m^2	Monthly
	C3. Demonstrate long term structural stability of key infrastructure - Water Retaining Dams / Tailing Storage Facilities / Pits	Surveys / Water level monitoring	10 km^2 to 100 km^2	0.005 to 0.01 m	Continuous to annual

2.2 *Geoinformation users*

Geoinformation within the mining sector is acquired and used by many different organizations such as mining companies, regulatory authorities, consultants, academic institutions, community groups and other stakeholders. The techniques and methodologies used by different organizations will not vary significantly, although academic organizations and consultancies will often lead the way in terms of the development of new techniques to attain geoinformation. During the interaction with actors in the raw materials sector the following barriers in relation to advancements in geoinformation acquisition were identified:

- General unawareness of the potential of EO services and its related business rationales.
- Lack of knowledge of availability and capability of EO products by smaller companies.
- Lack of procurement procedures with commonly accepted terms of references.
- Availability of services and products that provide tailored information for the mining sector.
- Costs of product and services usage.
- Skilled personnel in EO technology at mining companies.
- Lack of well communicated, proven success stories on application of the EO products.

3 GAP ANALYSES

The next step is to identify potential opportunities for EO services and products for fulfilling the geoinformation needs by means of a gap analyses between geoinformation need of the sector on the one hand (Table 1) and the EO-based information products and services, as presented in section 3.1.

3.1 *EO product portfolio*

In total a portfolio of thirty EO products were identified and a product description is made available in the portal[2] of the European Association of Remote Sensing Companies (EARSC). Based on the findings of the GAP analysis a selection of the products with potential interest for the sector are presented in Figure 2, including to what geoinformation need the EO product is contributing. For example, EO1 fulfills information need E3, as presented in Table 1.

From each product some possible sources of data are presented. Some satellites are in the public domain (pub), others are only commercially (com) available. Of each satellite an indication is given of the spatial resolution (R) that can be achieved. Note that different EO products can use the same data source. In such cases the processing of the data, methodology of analyses and the presentation of the outcome leads to a product tailored to the information need. In some cases, multiple sources of data are combined (e.g. Hyperspectral analyses or different optical satellites).

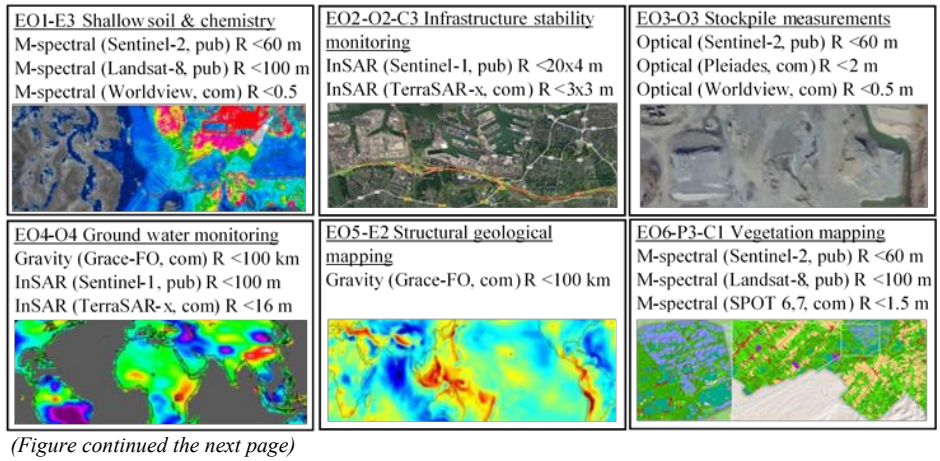

(Figure continued the next page)

[2] https://earsc-portal.eu/display/EO4RawMaterials/EO4RawMaterials

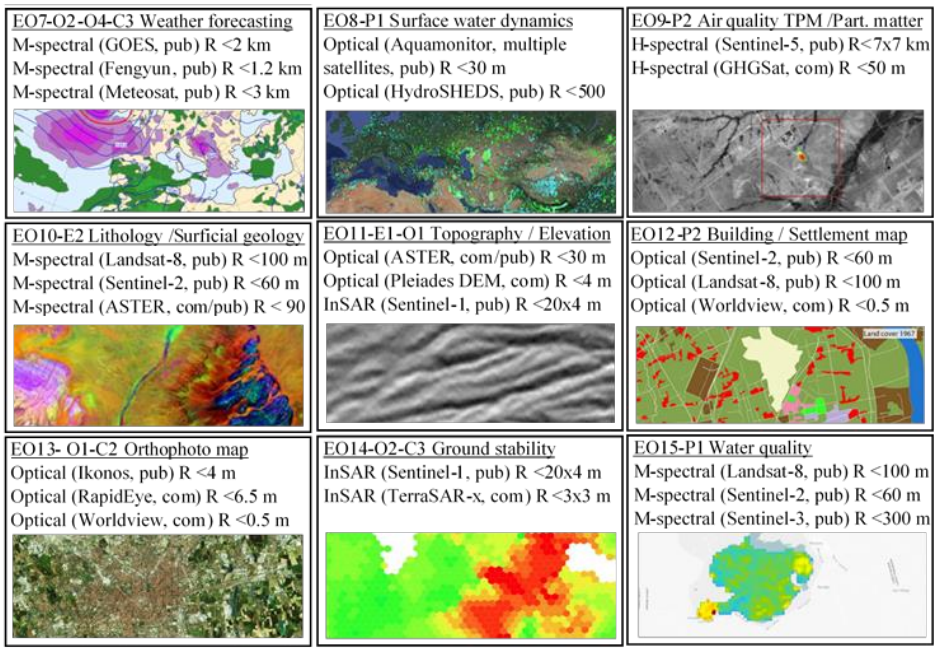

Figure 2. Overview key EO products beneficial to the raw materials mining sector
R represents the spatial resolution of the measurement.
Pub: satellite data is in the public domain; com: data is commercially available.

3.2 *Capability and utilization of Earth Observation products*

The EO capability evaluation has been focused on mature EO technologies with standardized processing of the satellite data into a tailored outcome presentation. An expert panel, made up of remote sensing specialists, evaluated the capability of the mature EO products in relation to the geoinformation needs of the mining sector. This evaluation was reviewed by the International Industry Board (IIB). The IIB is a group of experts from mining and remote sensing industry, part of the EO4RM project, that offers support and feedback to the project. Next to the ability to fulfill the geoinformation need, spatial resolution, the temporal resolution (refresh rate) and costs were taken into account during this evaluation. The following classification of EO capability was used:
1 – Low capability. The EO product can address the needs in a limited way. Long-term development of new sensors will be needed to fulfill the need.
2 – Medium capability. The EO product can often fulfil the demand, but there are some thematic content, accuracy, or delivery limitations to address the needs.
3 – High capability. The EO product meets the current and anticipated needs of the mining sector. Initiatives such as standards, training, and integrations tools can still benefit the industry.

Likewise, the utilization of EO was evaluated using the following classification:
1 – Low utilization. The mining sector is using only freely available satellite information sources.
2 – Medium utilization. Using commercial services and products, but better specification products are available, or they could utilize more of the product if better integration tools were available.
3 – High utilization. The mining sector uses the best available, mature products.

In Figure 3 the result of the evaluation of EO capability and utilization is presented. When a product is low on the vertical axis, then we consider this a R&D gap, because the product needs further tailoring towards the geoinformation needs or even the development of new instruments or new data processing tools. When a project is low on the horizontal axis, then we consider this

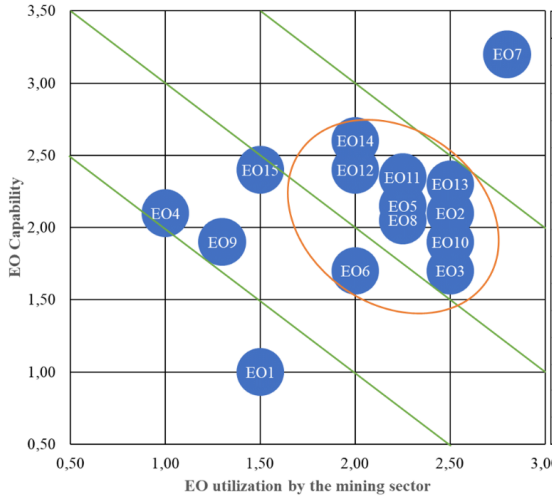

#	EO product
EO1	Shallow soil structure & Chemistry
EO2	Infrastructure stability monitoring
EO3	Stockpile measurements
EO4	Ground water monitoring
EO5	Structural geological mapping
EO6	Vegetation mapping
EO7	Weather forecasting
EO8	Surface water dynamics
EO9	Air quality TPM / Particulate matter
EO10	Lithology / Surficial geology
EO11	Topography / Elevation
EO12	Building / Settlement map
EO13	Orthophoto mapping
EO14	Ground stability monitoring
EO15	Water quality

Figure 3. Capability vs. utilization of EO within the raw materials mining sector

a utilization gap, the product may have good capabilities but barriers such as unawareness, lack of knowledge and cost may hinder full scale deployment. An example is Water quality (EO15).

The product with the highest score both in capability and utilization is Weather forecasting (EO7). This product is widely recognized and used at full scale with many companies offering tailored services. The product with the lowest score is Shallow soil and chemistry (EO1), mostly because of physical limitations of the sensors currently in use to fulfil the specific geoinformation needs by the mining sector. We have identified ten EO products (marked with the orange oval) that are already used by the mining sector at a certain level and show at least medium capabilities. These products are classified as high potential for wider uptake by the mining sector. Next to that, three products (EO4, EO9 and EO15) show a utilization gap.

4 PRODUCT CASES

For two of the high-potential products (section 3) mock-ups were developed. These can be used as an example to showcase to the raw materials mining sector the potential benefits and limitations. This provides insight and opens up the discussion on the barriers and challenges to application of the technology.

A selection process was completed by the project team to decide on which products to showcase. The selection process was facilitated by means of a questionnaire sent out to members of the raw materials sector and validated by the IIB. The selection prioritized services that:

- Address the identified critical challenges.
- Rank high in the multi-criteria evaluation screening performed as part of the project.
- Are relevant for several mining cycles.

The outcome was that stockpile measurement (EO3) and ground stability monitoring (EO14) were the two products that were most suitable to showcase. With respect to ground stability monitoring, this was broken down into two separate applications, namely tailings dam stability and pit slope stability. Stockpile measurements is a good example of a R&D gap; ground stability monitoring shows a utilization gap.

These showcases were presented in two webinars broadcasted in June 2020. One webinar targeted the European sector, and another targeted those on different time zones (e.g. the Americas). In total approximately 200 people attended the webinars and provided feedback, with a good cross-section across the sector including mine operators, consultants, regulators and researchers.

4.1 *Stockpile measurement*

Stockpiles are an important element of the mining business from an operational and financial perspective. Mining operations normally work on a dynamic basis. Ore and waste rock will be removed from the blasted face as soon as possible after blasting. Crushing and processing plants normally operate on a steady state basis. Continuous feed to the plant is managed by using stockpiles. Stockpiles also allow a mining operation to store ore of different grades and impurity content to be stockpiled separately and blended together at an appropriate ratio to provide an optimum feed to the processing plant, which ensures the ore is at the correct grade and impurities are below the threshold that customers set.

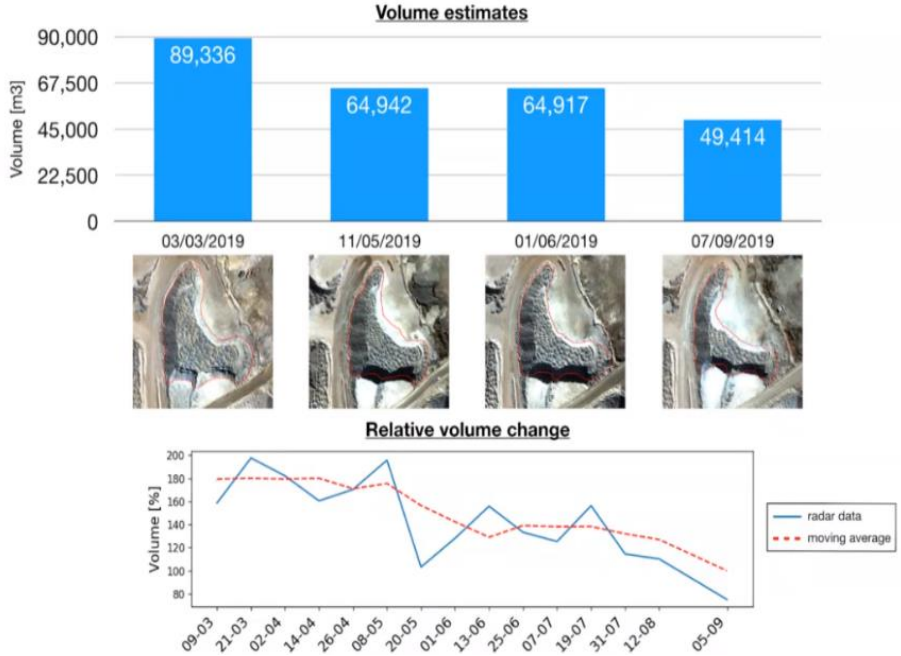

Figure 4 Stockpile showcase Skorpion zinc mine in Namibia
Stockpile measurements using the Pleiades satellite.

The EO4RM project chose to showcase the Skorpion Zinc Mine in Namibia. Satellite optical data from the Pleiades satellite was acquired and used to calculate the volume of selected stockpiles on the site for different time periods. The volume estimation is based on a machine learning algorithm that identifies the outline and general geometry of a stockpile in an optical image. Both these quantities are then used together with basic geometric relations to estimate the volume. Figure 4 shows an example of the outcome of the volume estimation for a single stockpile in the Skorpion mine over time using four optical images. Furthermore, a graph is included where the relative volume change was computed using SAR images based on the area and the amplitude of the radar signal. The trend of the decreasing volume in the optical images is also predicted by both the volume estimates techniques of the optical and SAR images. The SAR prediction can currently only be used to compute the relative volume change; hence the machine learning prediction is used for the quantitative assessment of the volumes.

The calculated volumes were compared against ground-based measurements to assess accuracy and precision. The stockpile measurement case studies that were completed by the EO4RM project team indicated that accuracy may be an issue. The webinar attendees indicated a minimum of 5% accuracy is required and this was not achieved on all occasions in the case studies. It was concluded that additional work is required by the service providers to better refine machine learning algorithms to ensure their product can provide more accurate results.

4.2 *Dam stability monitoring*

Tailings dams are used to store the residue or waste material after ore is processed. Given the relatively low proportion of minerals in ore and the high proportion of non-mineralized material, there is significant amounts of waste to be stored and tailings dams can be very large storage areas. Tailings dams must be monitored while the mine is operational and must also be monitored following the closure of a mine for a significant period thereafter. Various parameters are used to measure dam stability, EO offers the ability to be a technique to measure one of the key

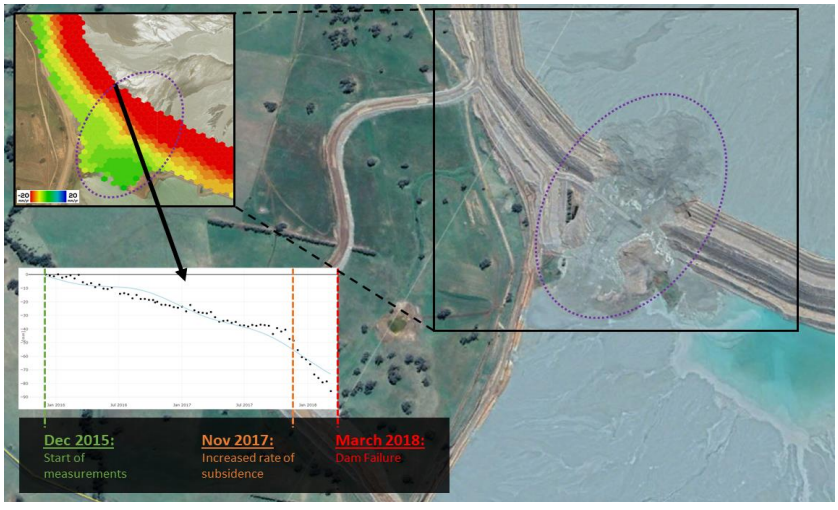

Figure 5 Cadia mine tailings dam failure showcase in Australia.
Ground stability monitoring using SAR from the Sentinel-1 satellite.

parameters, which is settlement or ground movement. The EO4RM project chose the 2018 tailings dam collapse in the Cadia gold mine in Australia as a test case. SAR data from Sentinel-1, with an acquisition interval of 12 days, was acquired and processed into settlement maps.

The results of this case study are presented in Figure 5 with data obtained covering the period December 2015 to March 2018. The dam wall was divided into polygons, with the movement of these polygons assessed over the time period. Data was presented with different colors being used to indicate the rate of movement. In the case of red, the dam is subsiding with more than 2 cm/yr, in the case of green the location is on average stable over time. To better understand these data, it can be inspected more closely from the underlying time series. Each polygon can be interrogated by the user to assess movement at each location on the dam wall. The picture in Figure 6 demonstrates how this section of the dam wall has subsided with more than 8 cm in 2 years.

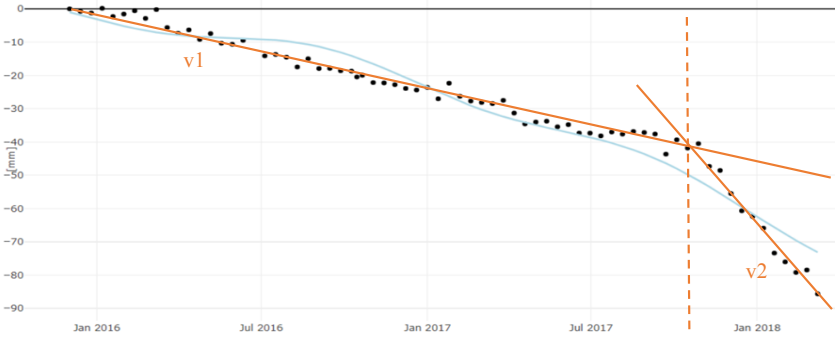

Figure 6 Cadia mine tailings failure showcase in Australia.
Subsidence rate increase in November 2017.

Depending on local conditions this can be a normal pattern for such a structure. However, when inspecting closely the area of the collapse in the InSAR time series data a dramatic increase in subsidence rate from v1 to v2 was seen around November 2017. This was nearly 4 months before the collapse and was potentially a significant leading indicator that could have alerted the operator of an imminent failure.

The embankment failure was investigated in 2019 and the two small earthquakes that occurred the day before the event were ruled out as a root cause (Jefferies 2019). The investigation team divided the event into two phases. Phase 1 was a slow movement event, and this was followed by phase 2 which consisted of accelerated movements. The report concluded that Phase 1 terminated without triggering phase 2. However, the mechanics of phase 1 were a necessary condition for the occurrence of phase 2. SAR data was used by the team to help investigate the incident. These data indicated surface deformation prior to the collapse and in the months preceding the event were accelerating, the report states that this was particularly evident in the InSAR data that was discovered subsequent to the event.

The conclusions in the final report highlight the value that satellite based SAR data can provide. Having these data available on a continuous basis may allow an operator identify changes in movement prior to a failure taking place, which allows the operator to possibly intervene to prevent the failure or where this is not possible take steps to minimize the impact and loss associated with the failure.

4.3 *Pit slope stability*

Pit slope stability is a major issue in open pit mines and while mining design can provide optimum mining methods, pit slope failure prediction is an integral part of good mining practice. Pit slope monitoring is normally carried out using traditional survey techniques and in-situ monitoring instrumentation. Pit slope failures can be gradual or dynamic and high-quality monitoring is essential to the safety of the operation. The ability to repetitively measure pit slopes to a high degree of accuracy is key to ensuring good practice. The Skorpion mine in Namibia had two localized pit collapses in 2019. Onsite controls were in place and there were no injuries, but production was significantly impacted. SAR data from Sentinel-1 was acquired and processed to monitor deformation of the slopes of the pit. The image shows ground movement using a color scale ranging from generally stable (green) to more than 2 cm/yr (red). It is clear from Figure 7 that there was an issue on the western slope of the pit, which shows strong deformation compared to the other sides of the pit.

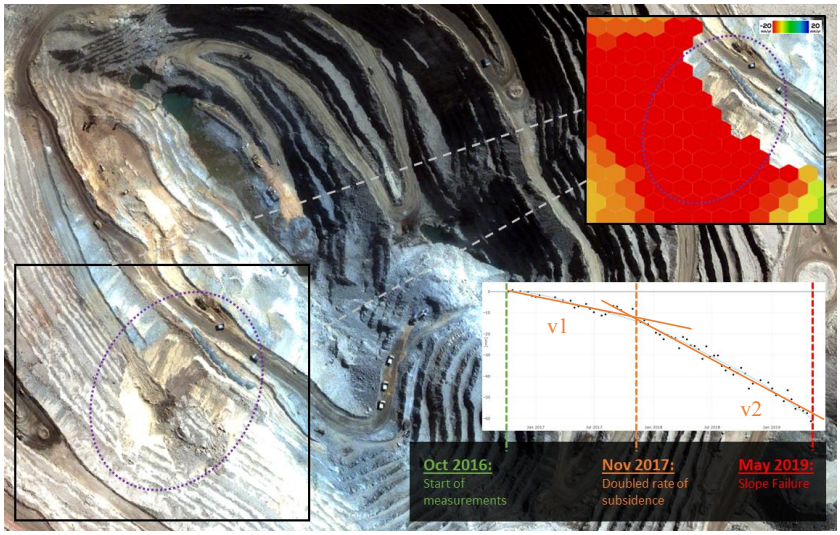

Figure 7 Skorpion mine pit collapse showcase in Namibia
Ground stability monitoring using SAR from the Sentinel-1 satellite.

When inspecting the data around this location, we see a relatively stable surface at first, but then from the beginning of 2018 onwards, a gradual increase in deformation rate from v1 to v2. It is considered most likely by the authors that this observed movement of the rock has led to the slope collapse more than 1 year later. Where a pit operator becomes aware of such trend changes there may be sufficient time to take local measures to prevent the collapse such as dewatering or cable bolting. This will reduce the likelihood of a collapse occurring. This indication of a movement and possible collapse will also allow an operator to take actions to minimize consequences in the event of a failure, for example implement 'no go zones' where people and equipment are not allowed as they are in the line of fire of a possible failure.

5 DISCUSSION

5.1 *Lessons learned from the stockpile and ground stability cases*

The application of EO for stockpile measurement is something that can be of benefit to the mining sector, however further refinement of the product is necessary to improve accuracy and precision. This may be an improvement in the technique, or it may be the need for users to work with the satellite data provider to calibrate their algorithms to the application, which will take into account the characteristics of the materials being measured (stable angles of repose etc.).

The application for stockpile measurement by EO does have advantages over conventional techniques in that it can be deployed anywhere across the world without the need to mobilize people or equipment. It will also be possible to acquire data more frequently. However, this is dependent on issues with accuracy and precision being resolved.

Using EO for ground stability is potentially a valuable application in the mining industry. The potential use of ground stability is applicable to different stages of the mining cycle (e.g. operations, closure and aftercare) and is also of use to many professionals working in the mining industry. For example this technology is expected to be beneficial to mine operators to allow them to monitor their own site, consultants can gain expertise in the application and sell their services to the industry. Lastly, regulatory authorities will have the ability to carry out independent checks on mining operations and may have a requirement themselves to carry out checks on abandoned mine sites that may have fallen into the stewardship of the State.

5.2 *The potential of EO for mine tailing dams*

The case on monitoring of tailings dam stability at the Cadia mine demonstrated that satellite data was able to provide information that indicated an acceleration in ground movement. This showed that satellite data could be used as an early warning to the mine operators of an impending failure well in advance so that they could have taken remedial actions. The issue of dam stability has always been one of high priority for the mining industry. Significant dam failures in recent years with major loss of life and property has elevated this issue to an even higher priority.

One limitation for application in tailings dams is the temporal resolution that is available. Satellite data may only refresh roughly every 6 days (free data from Sentinel-1). For dam stability applications, the closer to real-time the monitoring is, the better. However, it must be noted that this is not a fatal flaw of the application as the ground movement trends were identified months before the failure occurred, which means that a 6-day refresh rate is more than enough. Depending on coverage, a higher refresh rate can also be achieved by combining Sentinel-1 with commercial satellites such as TerraSAR-x and Cosmo-SkyMED.

In comparison with traditional monitoring techniques of tailing dams, there are two advantages of EO-based dam stability monitoring:

- When performing field surveys or installing instruments to monitor dam stability, the mine operator must select a number of locations for the measurements. This is based on technical requirements and limited by its cost. The advantage of the EO product is the capability to produce a map over a large area containing information from many more locations.
- The ability to access historic data is a significant advantage that EO has over other techniques. To understand a trend with respect to ground movement it is necessary to carry out a number of monitoring events and it could take significant time to understand if there is a trend. The

ability to look at a number of years' worth of historic data in one fell swoop is invaluable in allowing an organization to gain significant information in relation to ground stability.

6 CONCLUSIONS

The EO4RM project resulted in a clear insight into the geoinformation needs during the lifecycle of a mine and the understanding of the common practice of utilization of EO in the mining industry. A selection of the geoinformation needs were studied in detail and connected to EO solutions that can fulfil the need. By plotting the EO product in a capability-utilization chart, the utilization gaps and R&D gaps could be delineated next to products with a high potential.

EO technology is being used by the mining industry. Although some EO products need further development to become of added value to the mining sector, many products show significant potential for increased usage given the need that this sector has for geoinformation. Several barriers for the wider uptake of EO have been encountered during interaction with the sector. For example, while many people within the mining sector are aware of EO, there are a significant number of people and companies that are not aware of the EO potential and its business rationale for their operations.

It has been demonstrated that there are already valuable applications where EO technology is of use to the industry. The EO technology will continue to evolve with improvements in resolution and coverage, which will open up more applications within the mining industry or provide additional assurance to branches of the mining industry who have yet to be convinced.

To realize the full potential of the technology within the mining industry the EO industry needs to engage more with the mining sector to educate the sector on just what is available. What is a resolution gap for one application may not be for another application. This engagement will need to be ongoing and the resolution gaps that currently exist will become less with time. Importantly, not only is it necessary to educate the users within the mining sector, it is also necessary to ensure that others who use and review information from mining companies, such as government regulatory agencies, recognize the validity of EO based information.

7 REFERENCES

Bao, N. et al. 2014 SPOTing long-term changes in vegetation over short-term variability. *International Journal of Mining, Reclamation and Environment, volume 28 – issue 1.*

Du, Z. et al. 2020 Risk assessment for tailings dams in Brumadinho of Brazil using InSAR time series approach. *Science of The Total Environment, Volume 717*

Gomez, C et al. 2005. Using ASTER remote sensing data set for geological mapping, in Namibia. *Physics and Chemistry of the Earth, Parts A/B/C, Volume 30, Issues 1–3, Pages 97-108*

Jefferies, M. et al. 2019 Report on NTSF Embankment Failure, Cadia Valley Operations.

Karam, K.S. et al. 2016 Slope stability risk management in open pit mines. *International Geoinformatics Research and Development Journal, Vol 7, Issue 4.*

Lobo, F.L. et al. 2018. Mapping Mining Areas in the Brazilian Amazon Using MSI/Sentinel-2 Imagery (2017). *Remote Sens. 2018, 10, 1178*

Meer, van der F. et al. 2012. Multi- and hyperspectral geologic remote sensing: A review. *International Journal of Applied Earth Observation and Geoinformation, Volume 14, issue 1 pages 112-128*

8 ACKNOWLEDGEMENTS

The authors would like to thank the European Space Agency (ESA) for funding of the EO4RM project and the European Commission DG Grow and the European Institute of Innovation and Technology (EIT) Raw Materials for their continuing support. We acknowledge the crucial input of various actors among the mining industry, EO industry, regulating agencies, academia, the International Industry Board (IIB) and our partners in this project: GeoVille Austria and S[&]T (Sensar) in the Netherlands and Norway.

Creating TSF Histories using Modern Commercial and Declassified Cold War Satellite Photos

Gerry Mitchell, Jim Turner, & Sam Rivett
PhotoSat, Vancouver, BC, Canada

ABSTRACT: Recent dam failures have brought the world's mine tailing facilities under intense scrutiny by governments, investors, and insurers. Published investigations into the causes of dam failures and experience at other mining operations worldwide shows that many mines lack comprehensive, reliable, as-built survey records even for recent operations.

In 2010 PhotoSat developed a geophysical process that is used to produce monthly time stamped engineering grade surveys of entire mines using modern satellites. This process has now been adapted to include declassified cold war spy satellite photos going back to the early 1960's.

This paper will present a demonstration case study using Glencore's Mufulira TSF in Zambia as an example. At this site 315 satellite photos including declassified US spy satellite photos from 1967 were used to create a tailings dam history.

Satellite derived deposition and construction histories enable an independent third-party view of tailings dam construction and operation over decades.

1 INTRODUCTION

Recent catastrophic dam failures have driven the need for independent, verifiable information about not only how the dam is being operated today but also a history showing how the dam was constructed.

Many mines lack comprehensive, reliable, as-built survey records even for recent operations. For mines where TSF construction began decades ago there is often a complete lack of records. Even when survey data exists it is often uncertain and incomplete – a situation which is exacerbated by staff turn-over or changes of mine ownership.

PhotoSat is producing independent, satellite photo based, historical records of the construction, operation, and volumes of tailings dams. PhotoSat has provided satellite data to assist with several recent dam failure investigations and has recognized that there is a need for independent, verifiable histories of the construction, maintenance, and depositional history of mine tailings dams.

Glencore's Mufulira TSF in Zambia makes an excellent case study. At this site, 315 satellite photos including declassified US spy satellite photos from 1967 were used to create a tailings dam history. A series of as-built topographic surveys of the entire TSF were produced. These provide a 3D view of the successive embankment wall lifts, pond boundaries, the probable distribution of coarse sands and fine tailings and the construction in the surrounding areas. The stratigraphic cross sections show the construction of the dam over a period of over 30 years. The volumes and locations of successive deposits of tailings can be tracked over time from the dam's commissioning in 1987 to the present day. This includes the measurement of the total current volume of tailings and water in the dam at 10:31 AM on March 20th, 2020.

2 THE NEED FOR INDEPENDENT TAILINGS DAM INFORMATION

Following the Brumadinho dam failure in Brazil in January 2019 that killed over 250 people, tailings dam safety is the subject of intense international scrutiny. For many of the world's tailings dams, "as-built" historical survey records are either inadequate or don't exist.

An Independent Investigation Report to the Vale Board of Directors on the Brumadinho dam failure was released on February 20, 2020. This report describes how government safety permits were obtained for the Brumadinho Dam when the dam had a Factor of Safety of only 1.09. This was far below the minimum industry standard, and Vale's own minimum standard, of a Factor of Safety of 1.3 for tailings dams.

The Vale Director of Iron Ore Operations and the independent engineering auditors did not inform the Vale CEO and Senior Executive Team nor the Vale Board of Directors of the very low Factor of Safety of the Brumadinho dam. Investors and insurers reading the February 2020 Vale report are recognizing the importance of developing independent, verifiable, sources of information for tailings dam safety. Mine owners should benefit by being able to provide their potential investors and insurers with independent, verifiable, satellite survey reports on the construction and depositional history of their tailings dams.

3 MUFULIRA MINE TAILINGS DAM IN THE ZAMBIA-DRC COPPER BELT

The Mufulira Copper mine in Zambia has been in operation since 1933. The mine is currently owned 73.1% by Glencore, 16.9 % by First Quantum and 10% by ZCCM-IH. Mine tailings have been deposited in the current active Mufulira tailings dam since approximately 1987.

3.1 *Satellite Photo record of the Mufulira tailings dam*

The record of archive cloud free satellite photos over the Mufulira mine site begins with a September 22, 1967 stereo pair of US Keyhole spy satellite photos (see Figure 1, which shows four of the mine tailings deposits used up until 1967, and the large tailings embankment and water dam to the north that appears to be new in 1967). The satellite record ends, as of the date of this report, with a March 23, 2020 stereo pair of 30 cm ground resolution Maxar WorldView-3 satellite photos.

Between September 22, 1967 and March 23, 2020 there are 315 cloud free satellite photos over the Mufulira mine site.

3.2 *PhotoSat Mufulira mine site surveys*

PhotoSat routinely surveys mine sites in all the world's major mining districts. Using stereo photos from the Maxar WorldView satellites, PhotoSat surveys mine sites to an accuracy of 15 cm in elevation. The PhotoSat team has completed over 1,200 survey projects globally, with over 600 since 2012.

PhotoSat produced 1 m survey grids accurate to 15 cm in elevation from stereo WorldView satellite photos for the Mufulira mine site for the following dates: March 23, 2020, July 13, 2017, and September 6, 2010.

The March 23, 2020 PhotoSat survey is shown in Figures 2-4 below.

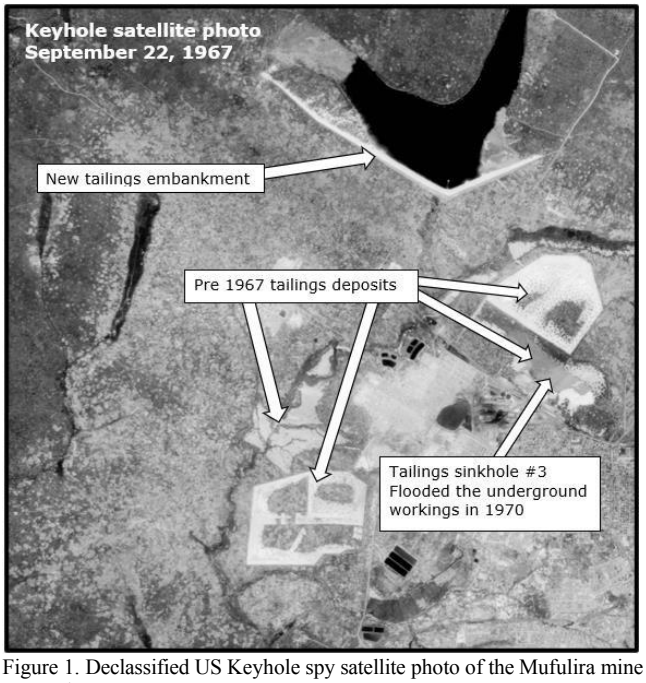

Figure 1. Declassified US Keyhole spy satellite photo of the Mufulira mine site and tailings dams taken on September 22, 1967.

Figure 2. WorldView-3 satellite photo of the Mufulira mine site and tailings dam taken on March 23, 2020.

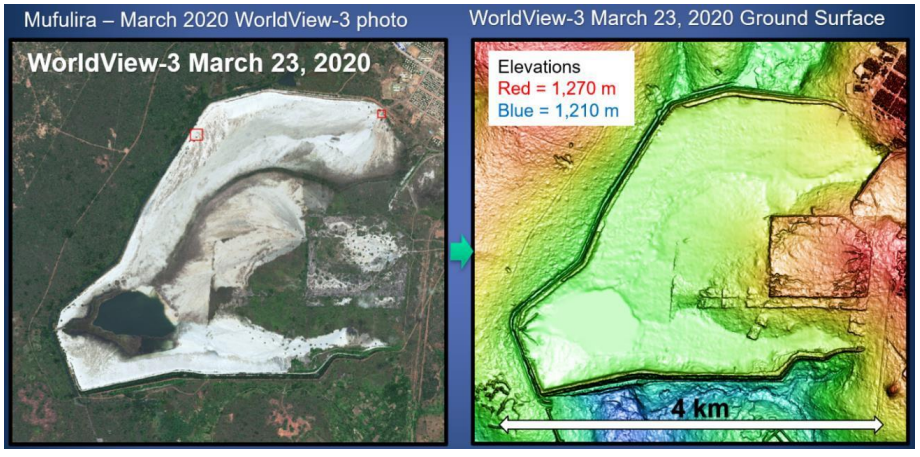

Figure 3. Elevation surface of the surface of the Mufulira tailings dam March 23, 2020 derived from WorldView-3 stereo satellite photos.

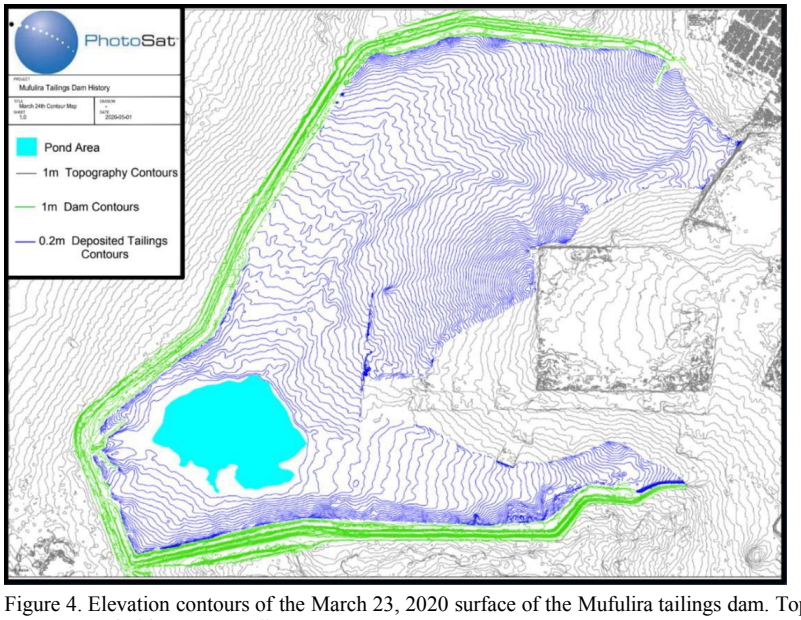

Figure 4. Elevation contours of the March 23, 2020 surface of the Mufulira tailings dam. Top of tailings 20 cm contours in blue. Surrounding area 1 m contours.

4 1967 STEREO KEYHOLE DECLASSIFIED US SPY SATELLITE PHOTOS OF THE MUFULIRA MINE SITE

In 1995 the US declassified archives of US spy satellite photos taken during the Cold War. This satellite photo program was designed to monitor the Soviet fleets of intercontinental nuclear bombers, the construction and launch sites for Soviet intercontinental nuclear missiles and Soviet and Chinese nuclear test sites.

4.1 *Topographic surface of the base of the Mufulira tailings dam produced from the 1967 Keyhole stereo satellite photos*

To measure the volumes and distribution of different fractions of the mine tailings in the Mufulira tailings dam over time, it is necessary to start with the topographic surface of the base of the tailings deposit. Fortunately, there are stereo US Keyhole spy satellite photos covering all the mines in the Zambia-DRC Copper Belt.

PhotoSat has developed a process and workflow to generate a topographic surface of the base of the tailings dam using the stereo Keyhole satellite photos. This is an extension to the proprietary stereo satellite elevation surveying system that PhotoSat first developed in 2008.

This 1967 topographic surface derived from the stereo Keyhole satellite photos has an estimated accuracy of one to two meters in elevation. The elevation grid of the base of the Mufulira tailings dam derived from the 1967 stereo Keyhole satellite photos is show in Figure 5.

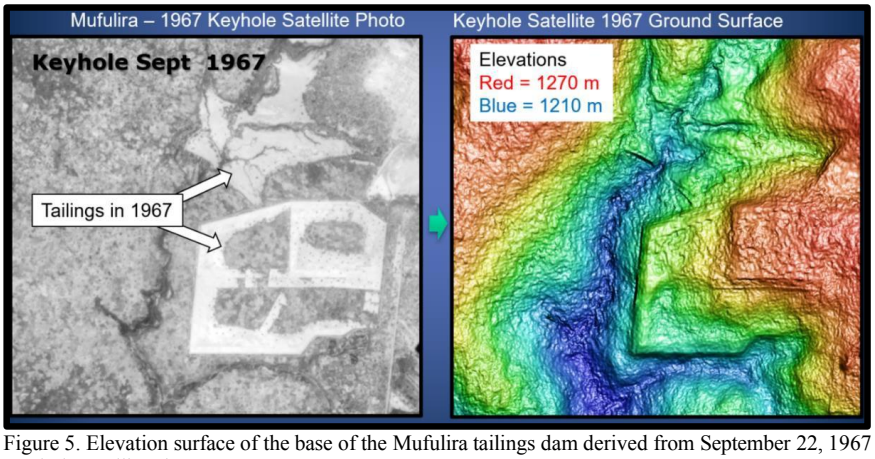

Figure 5. Elevation surface of the base of the Mufulira tailings dam derived from September 22, 1967 stereo Keyhole satellite photos.

4.2 *Measurement of the current thickness and volume of tailings in the Mufulira tailings dam derived from the satellite surveys*

PhotoSat has measured the current thickness and volume of mine tailings and water in the Mufulira dam. The current volume of tailings and water in the dam is 50,000 m3. This measurement is made by comparing the 1967 topographic surface, of what is now the base of the Mufulira tailings dam, with the present topographic surface created from the March 23, 2020 WorldView-3 stereo satellite.

The March 23, 2020 topographic surface of the Mufulira tailings dam is shown in Figure 6.

4.3 *Stratigraphic cross section of the Mufulira tailings dam*

The stratigraphic cross section of the Mufulira tailings dam shown in Figure 7 was created using the PhotoSat WorldView 2010, 2017 and 2020 surveys and the nearly 300 satellite photos taken between 1987 and 2020. The probable distribution of coarse sands, fine sands and tailings deposited beneath the pond is shown in the cross section.

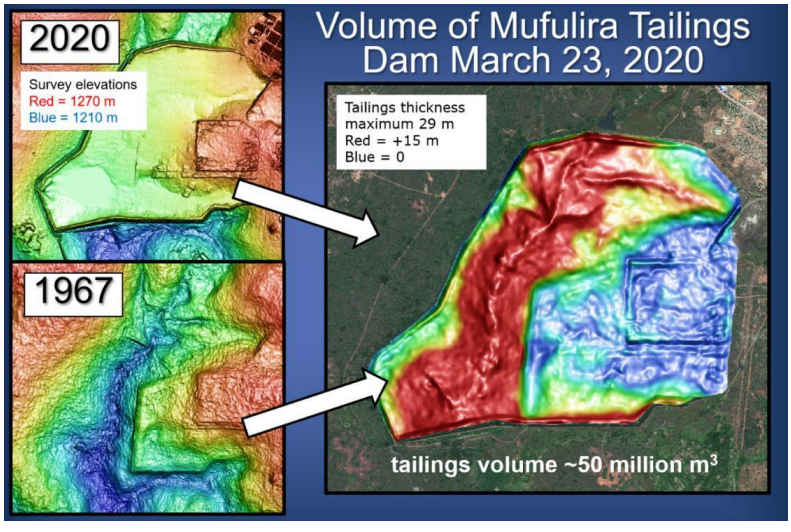

Figure 6. The tailings thickness and the volume of tailings and water in the Mufulira Tailings Dam on March 23, 2020. Maximum tailings thickness 29m.

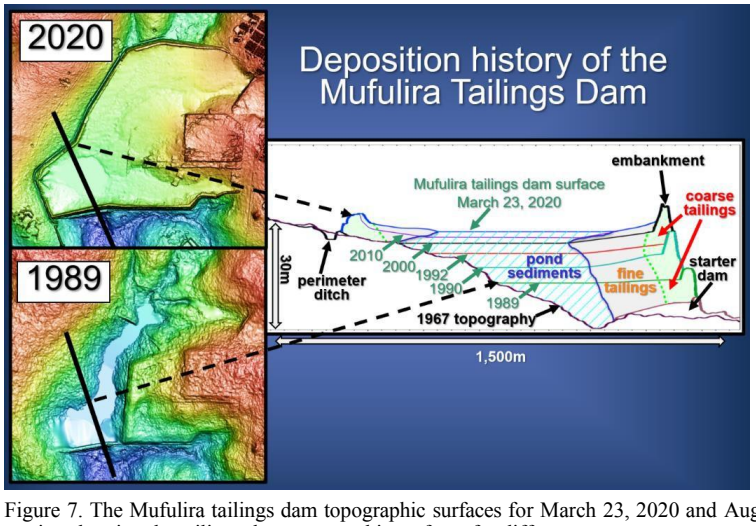

Figure 7. The Mufulira tailings dam topographic surfaces for March 23, 2020 and August 21, 1989. Cross section showing the tailings dam topographic surfaces for different years.

5 CONCLUSION

There is an urgent need for independent, verifiable information on tailings dams, and recent failures have brought the world's mine tailings dams under intense scrutiny by governments, investors, and insurers.

PhotoSat's independent satellite-based measurements show a current volume of 50 million m3 of mine tailings in the Mufulira tailings dam with an error of approximately 10%. In comparison, the Glencore response to the Church of England reports 79 million m3 of tailings for this tailings dam.

PhotoSat's 3D historical reconstruction of the Mufulira tailings dam shows the most probable current 3D distribution of coarse tailings, fine tailings and tailings deposited within the tailings pond.

From the total record of 315 satellite photos, it appears that the Mufulira tailings dam was probably well designed, carefully constructed, and well maintained over its history. More than 290 satellite photos taken between 1989 and 2020 show that the tailings pond was never allowed to come closer than 200 m to the Mufulira tailings dam embankment. This indicates that this upstream tailing dam embankment most probably consists entirely of coarse sands. This would give the dam a lower risk of failure than if the embankment was built on top of fine tailings and pond sediments, as was the case for Vale's Fundeo and Feijão failed tailings dams in Brazil.

This study does not determine the probable location of the current phreatic surface within the dam. Therefor this study cannot indicate whether the tailings dam embankment actually consists of unsaturated or water saturated sands.

The satellite survey history is only one component of the determination of a tailings dam Factor of Safety. An engineering determination of the Factor of Safety of a tailings dam requires on site investigations, probably including drilling, cone penetration testing, and measurements of the current phreatic surface, supervised and interpreted by qualified tailings dam engineers. However, satellite derived deposition and construction histories enable an independent third-party view of tailings dam construction and operation over decades.

REFERENCES

Feb 20, 2020. Executive Summary of the Independent Investigation Report – Failure of Dam 1 of the Corrego de Feijao Mine – Brumadinho – To the Board of Directors Vale. Available at: http://www.vale.com/PT/investors/documents/20.02.20_ciaea_report_i.pdf.

Dec 12, 2019. Report of the Expert Panel on the Technical Causes of the Failure of Feijão Dam I (Brumadinho). Available at: https://bdrb1investigationstacc.z15.web.core.windows.net/assets/Feijao-Dam-I-Expert-Panel-Report-ENG.pdf.

Robertson, P. K., de Melo, L, Williams, D. J., & Ward Wilson, G. December 12, 2019. Report of the Expert Panel on the Technical Causes of the Failure of Feijão Dam I. Available at: https://bdrb1investigationstacc.z15.web.core.windows.net/assets/Feijao-Dam-I-Expert-Panel-Report-ENG.pdf.

Oberle, B. November 15, 2019. GLOBAL TAILINGS STANDARD Draft for Public Consultation. Available at: https://globaltailingsreview.org/wp-content/uploads/2019/11/EN-Global-Tailings-Standard_CONSULTATION-DRAFT.pdf.

Independent Technical Review Board, Jefferies, M, Morgenstern, N. R., Van Zyl, D, & Wates, J. April 17, 2019. Report on NTSF Embankment Failure Cadia Valley Operations for Ashurst Australia. Available at:https://www.newcrest.com/sites/default/files/2019-10/190430_NTSF%20Embankment%20Slump%20Report%20-%20Market%20Release.pdf.

Improving Behavior of Gold Mine Tailings using Microbes Compared with Adding Cement, for Closure of In-pit Tailings

Hernan Cifuentes
The University of Queensland, Brisbane, Australia

David J. Williams
The University of Queensland, Brisbane, Australia

ABSTRACT: The closure of an in-pit tailings facility requires physical and chemical stability of the tailings, involving sufficient strength of the tailings to support capping, and minimising the generation and release of acid drainage. Due to the soft and wet nature of in-pit tailings, a solution could be the addition of 2% Portland cement to the tailings, however the cost would be prohibitive and the cement addition may risk the contamination of any groundwater resource due to increased alkalinity of the tailings. This warrants the evaluation of other alternatives to increase the physical strength of tailings, without adversely increasing the associated chemical risks. The feasibility of improving the physical and chemical behavior of the tailings using bacterially mediated calcite precipitation is investigated. This process involves the action of urease degrading microbes within the pores of the tailings to precipitate calcium carbonate crystals to form a natural cement, and raise the pH to ameliorate any acidity. The result of the cementing reactions is an increase in strength and reduced permeability. The paper examines the effects of microbial-induced calcium carbonate precipitation on gold mine tailings, and the results are compared against the same tailings treated with 2% Portland cement. Interpretation and analysis of the results achieved are presented, and their potential application under mine site conditions are discussed.

1 INTRODUCTION

The ability to manage mine wastes sustainably, with reduced environmental impacts, risks and long-term liabilities, will govern the prosperity and future of the mining industry. Despite the acknowledged importance of tailings management and their reclamation, the approaches adopted remain predominantly physical and/or chemical treatments, which are proving unable to meet these challenges. The development of biological treatments, paired with physical and chemical improvements, presents a significant opportunity, with the potential to utilize natural biological processes. Bacteria have been widely used worldwide in different areas of engineering, including the mining industry. For geotechnical applications, the use of microbial-induced calcium carbonate precipitation has become an interesting alternative for the improvement of poor soils (DeJong et al. 2010), which have similar characteristics to tailings.

Microbial-induced calcium carbonate precipitation takes place when microbes trigger the hydrolysis of urea, and create super-saturation by carbonates and ammonia, which increase the pH, making the surface of the bacteria an attractive place to attach calcium ions, if they are made available. Calcium carbonate precipitation then occurs, allowing the formation of the carbonate crystals, frequently occurring by successive stratification and binding together with other soil particles, resulting in a cementitious material with modified physical behavior (Castanier et al. 2000; Dhami et al. 2013).

Tailings management goals at the operational stage are not integrated with reclamation requirements and, in the majority of cases, actions are only taken at the end of the operational stage and mainly focus on capping the tailings in an attempt to minimize acid and metalliferous drainage (AMD) (Edraki et al., 2014). However, applying solutions from the operational stage(s) onwards is more cost-effective.

The integration of the main physical processes involved with tailings from operation to closure is described in the tailings continuum presented in Figure 1. The tailings continuum defines the change in the strength of the tailings from a slurry to a semi-solid soil-like state. Initial settling of the tailings is accompanied by a rapid volume reduction prior to the development of effective stress as the particles come into contact. The tailings then consolidate as the self-weight-induced excess pore water pressures dissipate, accompanied by far less volume reduction than settling, but considerable particle interaction resulting in the development of substantial effective stresses and strength. On exposure to the sun and wind, the tailings surface desiccates, accompanied by limited volume reduction, but a dramatic increase in strength due to suction (Williams, 2012). However, desiccation effects are shallow and diminish with depth below the surface, often necessitating additional actions to enable the tailings to be capped. This paper applies an integrative approach to compare the performance of tailings with microbial-induced calcium carbonate precipitation against Portland cement treatment.

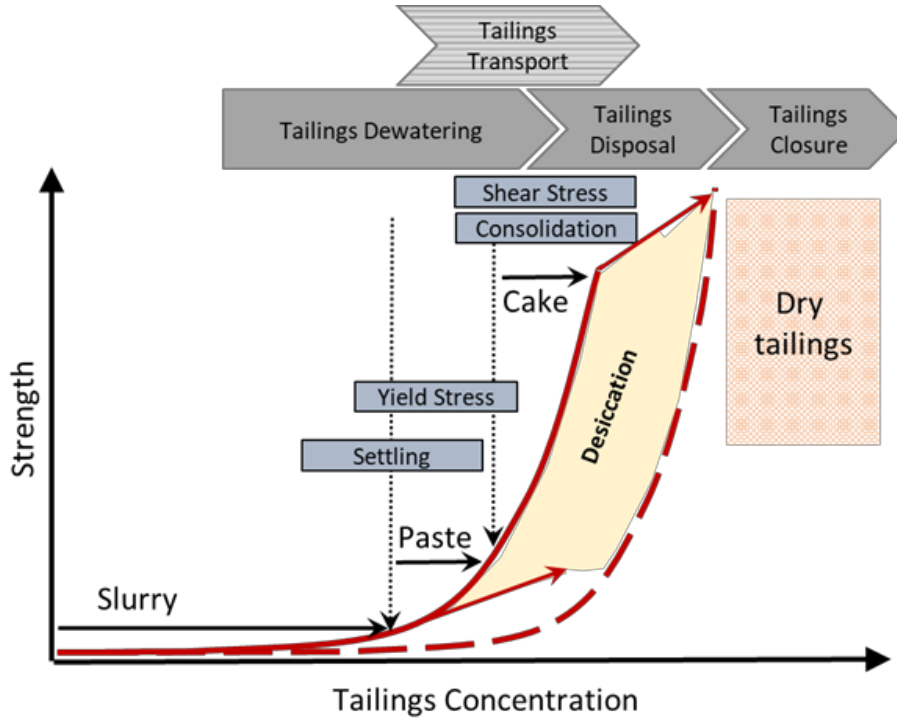

Figure 1. Tailings continuum describing main physical processes in tailings from operation to closure.

2 TAILINGS CHARACTERIZATION

Tailings and process waters were collected from a gold mine located in North Queensland, Australia. The results of geotechnical characterisation testing of the tailings are summarized in Table 1.

Table 1. Summary of gold tailings geotechnical characterisation test results.

Parameter	Value
% clay-sized (<2 μm) by mass	10
% silt-sized (2 to 60 μm) by mass	85
% sand-sized (>60 μm) by mass	5
Specific gravity	2.70
Liquid limit (%)	39
Plasticity Index (%)	6
Unified Soil Classification	ML
Soil description	Non-plastic silt-sized

3 TEST MATERIALS

3.1 *Urease micro-organism preparation*

A pure culture of urease degrading bacteria Sporosarcina Pasteurii (DSM-33; DSMZ-German Collection of Microorganisms and Cell Culture GmbH) was obtained and rehydrated under aseptic conditions using the recommended Medium 220 (OXOID CM131) to 2% urea, following the DSMZ instructions. Urea was sterilized separately by filtration using Millipore 0.22 μm filter paper and then added to the sterile Medium 220. Finally, the pH of the stock culture was adjusted to 7.3.

The pure culture of S. Pasteurii was sub-cultured into new fresh media monthly to ensure a viable stock of cells available, and stored in a refrigerator at 4°C. These sub-cultures were used as a source of inoculum for the experiments.

3.2 *Bacterial solution preparation*

The bacterial solution is adapted to the chemical conditions of the tailings process water through a series of sub-culturing processes. The adaptation of the bacteria to gold tailings process water required three sub-culturing processes, producing a fresh media after approximately 15 days. During that period, the changes in pH, conductivity and optical density (OD600) were monitored.

Once the bacteria showed some presence of urease activity, which can be related to the similar performance of the same bacteria grown within the same medium but prepared with distilled water, the cells were harvested by centrifugation, resuspended in fresh enrichment media, and tested for calcium carbonate precipitation performance. The bacterial solution was prepared with 10 g/L yeast extract, 20 g/L urea and 1 g/L glucose in non-sterilized process water.

3.3 *Cementation solution preparation*

The ability to induce calcium carbonate precipitation was triggered by the application of the cementation solution. The cementation solution is composed by 1M of urea and 1M of calcium chloride concentration in non-sterilized process water. For the cement treatment, standard Portland cement was chosen.

4 TESTING METHODOLOGY

4.1 *Tailings continuum approach*

The testing methodology started with settling column tests, after which the supernatant water was collected and subjected to chemical analysis. The sediment was carefully transferred to containers for rheological testing, and again carefully transferred to other containers for vane shear testing, which was carried out as the sediment progressively desiccated naturally at room temperature. The aim was to develop a relationship for shear strength from slurry-like to soil-like conditions.

Finally, the dry sediment was subjected to further chemical analysis of its potential for acid generation.

4.2 *Sample preparation*

The settling column tests were performed in graduated 1,000 ml measuring cylinders. The specimens were homogenized using a mechanical stirrer operated at 1,200 rpm for 25 min. Once the tailings were well mixed, 900 ml of tailings at 33% solids by mass was added to four measuring cylinders, and 900 ml of tailings at 36% solids by mass was added to four additional measuring cylinders.

All measuring cylinders were then made up to 1,000 mL in two stages, firstly by the addition of the bacterial solution, which was left to incubate for 24 hours at room temperature to allow the bacteria to grow. Secondly, after the incubation period, the cementation solution containing urea and calcium chloride was added to all specimens.

Two different dosages of bacterial solution and cementation solutions were prepared. Cement-treated specimens were prepared by adding 2% Portland cement to their respective dry masses. Finally, control specimens were prepared without the inoculation of bacteria, with the volume of bacterial solution replaced by adding process water. A summary of the volumes of solution added to the settling columns is presented in Table 2. The dosages for each specimen is summarized Table 3.

Table 2. Summary of solution volumes added to settling columns.

Specimen ID	Tailings (mL)	Bacterial solution (mL)	Process water (mL)	Cementation solution (mL)	Final volume (mL)
Control	900	0	25	75	1,000
Dosage 1	900	25	0	75	1,000
Dosage 2	900	50	0	50	1,000
2% cement	900	0	25	75	1,000

Table 3. Summary of dosages added to settling columns.

	Bacterial solution			Cementation solution		
Specimen ID	Yeast Extract (g)	Urea 2% (g)	Glucose 0.1% (g)	Urea (g)	Calcium chloride (g)	Portland cement 2% (g)
Control	0.00	0.00	0.00	4.50	8.32	0.00
Dosage 1	0.25	0.50	0.03	4.50	8.32	0.00
Dosage 2	0.50	1.00	0.05	3.00	5.55	0.00
2% cement	0.00	0.00	0.00	0.00	0.00	8.50

The filled measuring cylinders were shaken manually for 2 min to ensure good mixing of the additives with the tailings before the columns were allowed to settle, and the measurement of settling commenced.

After each settling test, the supernatant water was collected for chemical analysis. The tailings sediment was collected for rheological testing using an Anton Paar MCR 102 modular compact rheometer. Prior to rheometer testing, the specimen was tapped on the laboratory bench to remove entrained air bubbles. Rheometer testing was under stress-control, increasing the shear stress linearly 1 to 1,000 Pa, to simulate moving the tailings from a resting condition.

Subsequent vane shear testing was carried out using an automated Wille vane 14 mm in diameter and 35 mm in length, in a measuring cup 28.9 mm in diameter. Prior to rheometer and vane shear testing, the specimen was tapped on the laboratory bench to remove entrained air bubbles. Prior to vane shear testing, the specimen was tapped on the laboratory bench to remove entrained air bubbles. Sequential vane shear testing was carried out as the specimens progressively desiccated naturally at room temperature.

5 TEST RESULTS

5.1 *Settling and rheology*

Figure 2 shows similar settling behaviour for all tailings specimens treated with bacterial solution, which was slightly better than that of the control specimens that were treated with calcium chloride and urea only. The red dashed line in Figure 2 at 52% solids indicates the maximum % solids achieved by these tailings samples without any treatment, after more than 1 month of settling. Samples treated with bacterial solution at two different dosages surpassed the 52% solids limit, reaching in the best case 55% solids for the specimen treated with Dosage 2. A completely different performance was observed for the samples prepared with 2% cement, for which no change in settling behavior was observed.

The rheological behaviour of the settled tailings is presented in Figure 3, which shows typical shear-thinning behavior, as expected, for both the control and bacterially-treated specimens. As the tailings start to yield, no significant change can be seen in shear stress. In contrast, specimens treated with 2% Portland cement gave very high yield stresses, outside the range of the rheometer.

Both untreated and bacterially-treated specimens showed consistent yield stress values ranging from 50 and 120 Pa, making them well-suited for hydraulic transport using centrifugal pumps. On the other hand, specimens treated with 2% Portland cement are unsuitable for transport using centrifugal pumps, which would restrict the addition of Portland cement to just before disposal.

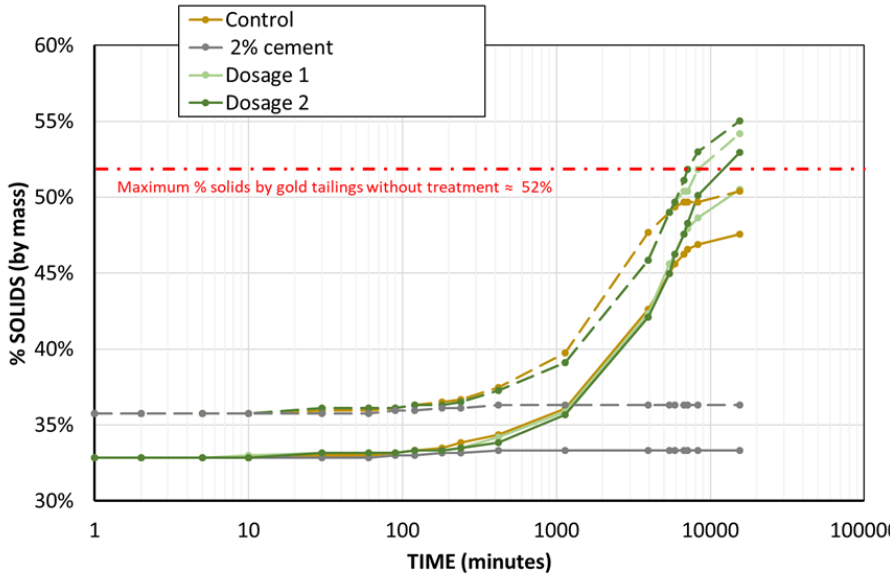

Figure 2. Behavior of specimens during settling columns test.

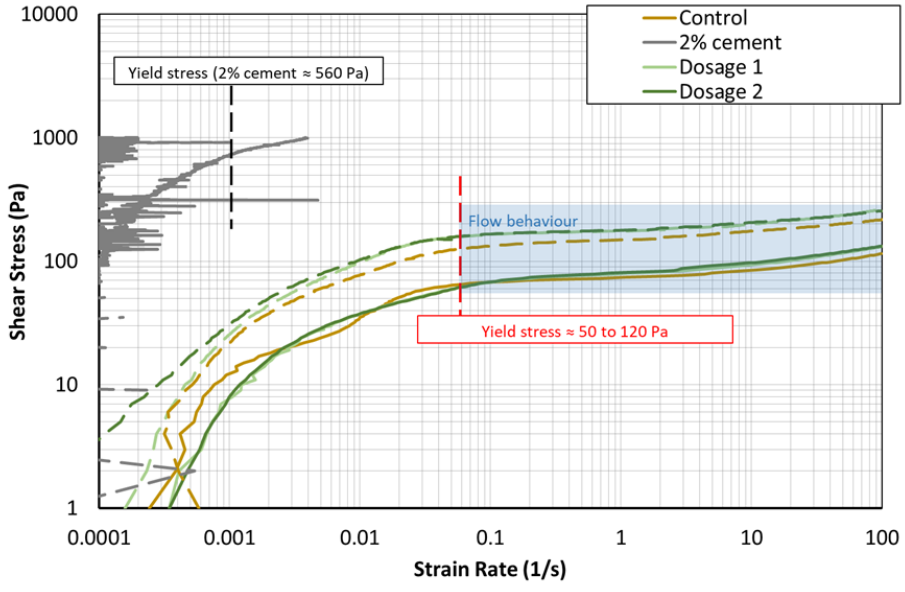

Figure 3. Rheological behaviour of specimens measured after settling.

A high yield stress may be considered preferable at the point of tailings deposition because a steeper beach angle could be achieved. However, pumping tailings with a high yield stress leads to high rake torques and pipeline pressure losses, which can adversely affect processing and lead to a significant increase in overall operational costs. Therefore, bacterial treatment is an attractive alternative to the use of cement.

5.2 *Shear strength*

A wide range of shear strengths was covered by vane shear testing of specimens as they desiccated from 94 to 7% gravimetric moisture content. This wide range covered the behavior of the tailings from slurry-like to a soil-like state, as shown in Figures 4 and 5 for the peak and remolded vane shear strengths, respectively.

Figure 4 shows the expected increase of the peak shear strength with decreasing gravimetric moisture content. However, the increase is substantially higher for those specimens treated with Portland cement, with the strength escalating rapidly within the slurry-like zone, reaching values of 20 kPa. The control specimens and the bacterially-treated specimens show considerable strength gain within the soil-like zone. For the bacterially-treated specimens, better performance is observed for Dosage 2, being also better than that of the control specimens.

The highest peak shear strength for the control specimens was 26.3 kPa and 22.3 kPa at 7% and 18% gravimetric moisture content, respectively. However, the tailings are still soft and unlikely to support the mechanical placement of capping. The highest peak shear strength achieved by specimens treated with Portland cement was 43.3 kPa at 41% gravimetric moisture content, but most of the Portland cement-treated specimens failed due to brittle cracking below a gravimetric moisture content of 60%. The highest peak shear strength value of 55.4 kPa was obtained for Dosage 2 at 13% gravimetric moisture content, almost twice the peak shear strength achieved for the untreated control specimens.

Comparing the peak shear strengths obtained for specimens treated with bacterial solution and cement, both can achieve firm to stiff tailings capable of supporting a D6 Swamp Dozer (with a bearing pressure of about 35 kPa) placing a capping.

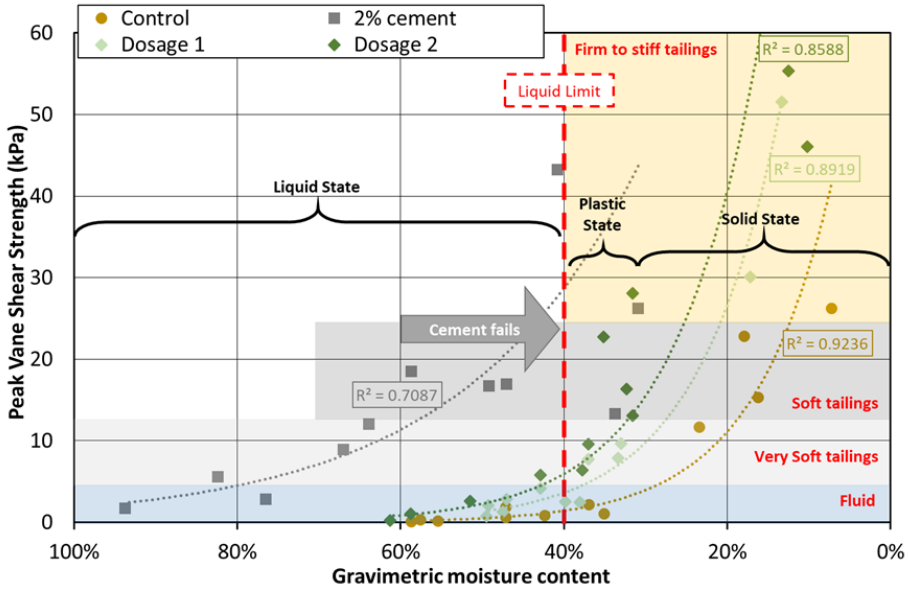

Figure 4. Peak vane shear strengths on desiccation.

The strength loss on remolding is presented in Figure 5, which shows that the untreated control specimens are the most ductile at below 20% gravimetric moisture content. The bacterially-treated specimens are more brittle on remolding due to the light bonding of particles, making them more sensitive to remolding than the untreated specimens. The Portland cement-treated specimens showed very high sensitivity and brittleness, with almost total loss of strength on remolding due to the loss of the strong bonding between particles.

5.3 *Process water quality*

Chemical changes arise due to changes in process water quality, which interacts with microbial-induced calcium precipitation and Portland cement treatments as presented in Table 4. There are substantial differences between the raw process water compared with the supernatant water from the settling column tests. The largest changes occurred in the pH of the specimens treated with urea and calcium chloride, and both dosages of bacterial treatment, which reduced on average by 1.4, likely due to calcium chloride and urea acting as a pH buffer. The supernatant water samples collected from Portland cement-treated specimens became more alkaline, with the pH increasing from an initial value of 9.9 to a final value of 11.7.

An increase in electrical conductivity was observed for the control and bacterially-treated specimens. The greatest increase was in the bacterially-treated specimens, due to the production of ionic species from non-ionic substrates caused by bacterial activity. In addition, the solute concentration increased in the bacterially-treated specimens, due to the addition of calcium. As expected, there was no observed change in overall electrical conductivity of the specimens treated with Portland cement.

The calcium carbonate precipitation potential (CCPP) is a reliable index to determine the expected mass of calcium carbonate ($CaCO_3$) available to dissolve or precipitate, which can be helpful to predict the deposition or dissolution capacity of the water. Since bacteria can induce the precipitation of calcium carbonate using the available calcium in the water, the additional calcium carbonate within the supernatant water after microbial action is therefore indicative of the efficiency of bacterially-induced calcium carbonate precipitation.

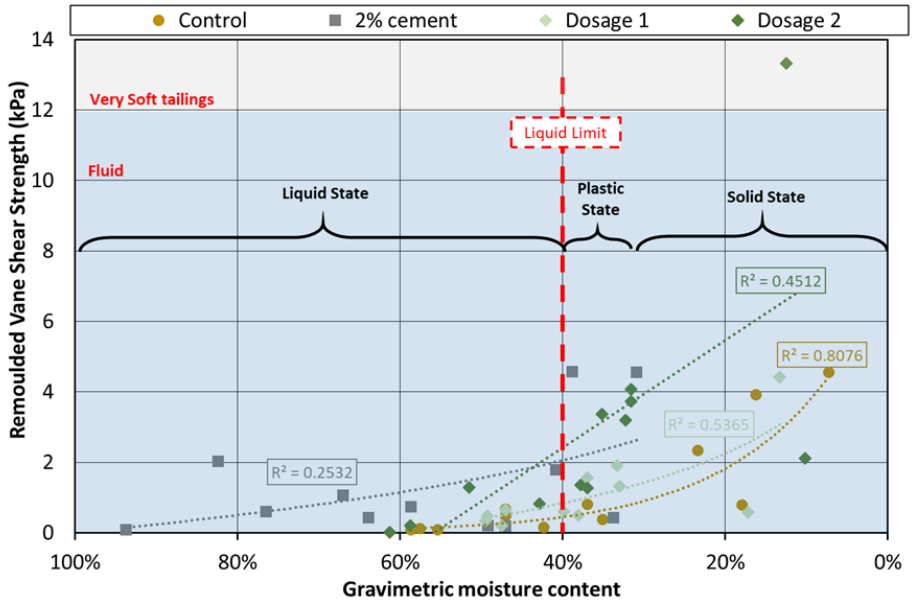

Figure 5. Remolded vane shear strengths on desiccation.

Table 4. Chemistry of supernatant water collected from settling columns.

Parameter	Process water	Control	Dosage 1	Dosage 2	2% cement
pH	9.9	8.1	8.4	8.7	11.7
Electrical conductivity (mS/cm)	3.3	14.5	19.4	15.4	2.6
CCPP	164	38.6	7.8	5.1	49.6
Total alkalinity as $CaCO_3$ (mg/L)	330	99	1,400	2,050	720
Sulfate as SO_4^{2-} (mg/L)	900	849	766	760	119
Ammonia as N (mg/L)	171	140	0.11	0.07	0.03
Total major cations:					
Calcium (mg/L)	170	2,190	14	7	50
Magnesium (mg/L)	<1	11	11	6	<1
Sodium (mg/L)	550	739	618	664	468
Potassium (mg/L)	80	104	115	121	50
Total metals:					
Aluminum (mg/L)	0.6	2.80	0.80	0.42	1.95
Barium (mg/L)	0.04	0.345	0.089	0.062	0.092
Cadmium (mg/L)	0.003	0.0003	0.0001	<0.0001	0.0001
Chromium (mg/L)	<0.001	0.021	0.006	0.004	0.008
Cobalt (mg/L)	0.36	0.428	0.361	0.352	0.198
Copper (mg/L)	13.2	6.87	4.68	6.98	3.51
Iron (mg/L)	3.6	19.8	4.85	4.58	6.96
Lead (mg/L)	<0.001	0.012	0.004	0.001	0.004
Nickel (mg/L)	0.28	0.187	0.052	0.131	0.052
Zinc (mg/L)	1.2	0.039	0.010	0.006	0.010

From the results, the raw process water is over-saturated with calcium carbonate, with a CCPP of 163.6 mg/L, which is the calcium available to precipitate. The untreated control specimens and specimens treated with Portland cement demonstrate a slight precipitation of calcium carbonate, reducing the CCPP to approximately 40. In contrast, for the bacterially-treated specimens, the

CCPP is reduced significantly, close to zero. This suggests that the bacteria solution has the ability to precipitate most of the calcium available.

Bacterially-treated specimens showed an increase in total alkalinity of four to seven-fold, mainly as a result of bicarbonate production due to the hydrolysis of urea. Alkalinity also increased for specimens treated with Portland cement approximately two to three-fold, however the increase was primarily due to hydroxide alkalinity as expected for Portland cement treatment.

Sulfate concentration did not change much for most of the specimens, apart from those treated with Portland cement, for which sulfate reduction was about four-fold, from 900 to between 104 mg/L and 119 mg/L.

Among the major cations, as expected, calcium is reduced substantially in bacterially-treated specimens, but is more reduced in specimens treated with Portland cement. Magnesium and potassium showed a slight increase in the bacterially-treated specimens, and sodium was approximately the same for all specimens.

Total metals Al, Ba, Cd, Cr, Co, Cu, Pb, Ni, Zn, Fe were analyzed by ICP-MS. Comparing the results of the treatments with raw process water, a considerable reduction of toxic metals Ba, Cd, Cu, Ni and Z was observed, which would be expected to be precipitated in the tailings sediment in the settling columns. Nonetheless, that performance is similar for specimens treated biologically and with Portland cement. The rest of the metals analyzed remained almost constant.

5.4 *Net acid generating potential*

The acid generation potential of the untreated and treated specimens is summarized in Table 5. Overall, net acid production potential (NAPP) and net acid generation (NAG) values indicate that all of the specimens are non-acid generating, likely due to the mineralogical characteristics of tailings, but all the treated specimens had forms of calcium added, which is an effective acid consumer buffering the effluents at neutral pH. Besides, all samples have less than 1% total sulfur, which is a useful indicator, confirming the low risk of acid generation.

The pH of the untreated and bacterially-treated specimens of 8.0 to 8.7 was markedly lower than the specimen treat with 2% Portland cement at 10.8. Sulfates are also two to four-fold lower in bacterially-treated specimens compared to those treated with Portland cement.

The chloride concentration of the untreated and bacterially-treated specimens is higher than in the specimen treated with 2% Portland cement, probably due to the calcium chloride added in the bacterial cementation solution.

Table 5. Potential acid generation for untreated and treated tailings.

Parameter	Control	Dosage 1	Dosage 2	2% cement
NAPP (kg H_2SO_4/t)	-17.9	-22	-21.9	-36
NAG (pH 4.5) (kg H_2SO_4/t)	<0.1	<0.1	<0.1	<0.1
NAG (pH 7.0) (kg H_2SO_4/t)	<0.1	<0.1	<0.1	<0.1
Total Sulfur (%)	0.67	0.71	0.66	0.69
pH	8.2	8.0	8.7	10.8
Sulfate as SO_4^{2-} (mg/kg)	1,320	2,260	1,030	5,790
pH (OX) (pH Unit)	9.9	10.0	9.9	10.4
ANC as H_2SO_4 (kg H_2SO_4/t)	38.4	43.7	42.1	57.1
ANC as $CaCO_3$ (%)	3.9	4.5	4.3	5.8
Fizz Rating (Fizz Unit)	2	2	2	2
pH KCl (pH Unit)	8.9	8.9	8.9	10.4
Titratable Actual Acidity (mole H^+/t)	<2	<2	<2	<2
Electrical conductivity (mS/cm)	3.45	5.30	2.74	1.06
Gravimetric moisture content (%)	6.3	10	34	37
Chloride (mg/kg)	5,570	8,300	4,890	740

6 DISCUSSION

Applying a continuum approach to improving the behavior of tailings from operation to closure shows the potential of bacterial treatment, which could be deployed using essentially the facilities available for tailings and water management, since managing bacterial treatment is similar to managing chemical treatment.

The increase in the final settled density of bacterially-treated tailings has significant benefits in terms of water recovery and reducing the final volume of stored tailings. Further, bacterial treatment does not affect the rheology of the tailings, so that bacterially-treated tailings can readily be pumped using centrifugal pumps.

Bacterial treatment produced a better average undrained shear strength than untreated tailings, indicating that microbially-induced calcite precipitation is a means of facilitating capping by mechanical means, and may even replace capping for benign tailings.

The pH reduction in the tailings due to bacterial treatment reduces the chemical risk in case of mine effluents being released. Furthermore, the calcium carbonate created by the bacteria serves as a buffer for the system, thereby reducing the acid generating potential of the tailings.

7 CONCLUSIONS

The results obtained demonstrate that an integrative approach to improve the behavior of tailings using microbial-induced calcium carbonate precipitation has potential. Bacterial treatment of the gold tailings studied was found to improve their settling behaviour, without changing their yield stress, unlike Portland cement addition, which restricts the use of centrifugal pumps. Further, bacterial treatment of the tailings produced a substantial shear strength increase, without the brittle behavior exhibited by tailings treated with Portland cement.

For both biological and Portland cement treatment, the ability to reduce the availability of heavy metals in the supernatant water by encapsulation within the settled tailings is promising. The pH is also lowered using bacterial treatment, making alkaline tailings more neutral, while treatment with Portland cement raises the pH, risking alkalinity. All samples tested showed no acid generation potential.

8 ACKNOWLEDGEMENTS

This paper is based on the PhD research of the first author, which is being funded by Minera Escondida-BHP, Chile. The authors acknowledge the suppliers of the tailings sample for testing. The authors are also very grateful to Dr Emma Gagen, Research Fellow in the School of Earth and Environmental Sciences at The University of Queensland, for her assistance and guidance on the microbiology activities performed.

9 REFERENCES

Castanier, S., Métayer-Levrel, G.L. and Perthuisot, J.-P. 2000. Bacterial Roles in the Precipitation of Carbonate Minerals. *Microbial Sediments*, 32-39.

DeJong, J.T., Mortensen, B.M., Martinez, B.C. and Nelson, D.C. 2010. Bio-mediated soil improvement. *Ecological Engineering*, 36(2), 197-210.

Dhami, N.K., Reddy, M.S. and Mukherjee, A. 2013. Biomineralisation of calcium carbonates and their engineered applications: a review. *Frontiers in Microbiology*, 4, 314.

Edraki, M., Baumgartl, T., Manlapig, E., Bradshaw, D., Franks, D.M. and Moran, C.J. 2014. Designing mine tailings for better environmental, social and economic outcomes: a review of alternative approaches. *Journal of Cleaner Production*, 84, 411-420.

Williams, D.J. 2012. Some mining applications of unsaturated soil mechanics. *Geotechnical Engineering*, 43, 83-98.

Glass from Tailings

Priscilla P. Nelson, Katharina Pfaff, Seetharaman Sridhar, and D. Erik Spiller
Colorado School of Mines, Golden, Colorado, USA

ABSTRACT: The "Glass from Tailings" team at the Colorado School of Mines is investigating the use of earth resources (including waste rock and process tailings) to produce a silicate-rich melt that can be pulled into fibers that in turn can be fabricated into fabric, building materials, rebar, ballistic cloth, and other chemically inert products that have advantageous properties.

Our approach is to determine the chemical and mineralogical characteristics of mine and process (mill) tailings, which will allow determination of melt composition and variability possible to achieve desired melt and glass-formation temperatures and viscosities. We report here on: (a) development of a tailings characterization protocol; (b) development of a data base of tailings mineralogy and geochemistry for bulk rock/tailings, splits (by particle size), assessment of chemical and mineralogical variability, and physical properties including density; and, (c) thermodynamic prediction of melting and glass formation temperatures and thermo-physical considerations for viscosity, etc.

1 INTRODUCTION

Naturally formed geologic melts abound and we see their cooled form as igneous rocks, and typically exhibit microcrystalline and/or glassy structure. Their typical chemical composition is 45–55 wt % SiO_2, 2–6 wt % total alkalis (K_2O, Na_2O, etc.), 0.5–2.0 wt % TiO_2, 5–14 wt % FeO, and 14 wt % or more Al_2O_3. CaO and MgO contents are commonly near 10 wt %, and in the range 5 to 12 wt %, respectively. While re-melting of tailings and subsequent controlled cooling for forming a solid with desired properties is a relatively recent concept (i.e., Deng et al. 2019; Karhu et al. 2019), a multitude of research projects and applications can be found in the literature, detailing the composition, properties and applications of basalt fiber and its composites (i.e., Wei et al. 2011; Farsani et al. 2014; Vasil'eva et al. 2014; Tirillo et al. 2017; Gao et al. 2018; Li et al. 2018). Compared to other high-performance materials, basalt fiber is a healthy and environmentally friendly material, which is widely used in military and civilian fields (Thorhallsson et al. 2013; Zhu and Tian 2013; Wlodarczyk and Jedrzejewski 2016; Ouyang et al. 2017; Raleaonkar et al. 2018; Xiaomin et al. 2019). In comparison with steel, the fibers from basalt are lighter in weight and lower in cost (Pareek et al. 2019). Composites made with basalt fibers are of higher high-tensile strength than steel or E-glass, and competitive in many applications with carbon-fiber composites. For example, basalt-fiber composites are in use as replacement for carbon-fiber composites in high-performance venues, including lightweight applications in transport and high-strength sports equipment (Pareek et al. 2019). The recorded history of basalt fiber dates back to 1923 (US Patent 1923), additional development occurred during and after World War II. Much of the activity during the Cold War period occurred in the Soviet Union, with fibers pulled from basalt melts being investigated for aerospace and military purposes, including insulation and textile applications (Acar et al. 2017). After the dissolution of the Soviet Union, basalt fibers began to be produced and used on a commercial scale as the research was declassified, with the primary locus of fiber production being in Ukraine.

Basalt fiber applications and scientific research have been ramped up particularly since the turn of the century, and applications have broadened to include many different composite applications (potential substitute for glass and carbon fibers for strength and stiffness) and as ballistic

materials. Due to its resistance to high temperature, basalt fiber is often used for high-temperature applications such as flame-retardant materials, disk brakes, and thermal insulation applications (Li et al. 2018). Moreover, basalt fibers have excellent chemical resistance to alkaline attack (Acar et al. 2017) and due to their good electric insulating properties, basalt fibers have been used in printed circuit boards. Overall, basalt fibers exhibit better physical and mechanical properties than glass fiber, and the cost of basalt fiber is less than carbon fiber and comparable to glass fiber (Pareek et al. 2019). Other applications include basalt fiber composite rebars that have the potential to replace steel in reinforced concrete structures, in particular wherever a corrosion problem exists because of the noncorrosive behavior of basalt rebars (Fan and Zhang 2016, Lapko and Urbanski 2015, Hassan et al. 2016, Elgabbas et al. 2016). In addition, chopped basalt fibers have been used as a strengthening material for existing conventional building materials, such as concrete and mortar (Zych and Wojciech 2012, Jiang et al. 2014), and basalt fiber-based panels and laminates have been used as thermal and acoustic insulation in buildings.

The general composition of basalt rocks is given in Fig. 1 and the percentages are shown in Table 1. The dominant chemical compounds are SiO2, Al2O3, Fe2O3, and CaO (Dhand et al. 2015.

Table 1 Basalt Composition

Oxide	Percent
SiO2	52.5
Al2O3	17.5
Fe2O3	10.2
CaO	8.5
MgO	4.62
Na2O	3.34
K2O	1.46
TiO2	1.38
PsO5	0.28
MnO	0.16
Cr2O3	0.06

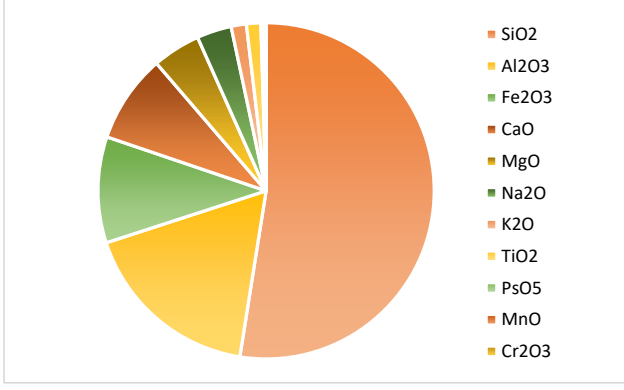

Figure 1 Oxide Components of Basalt

We propose the use of earth resource waste (i.e., mine and process (mill) tailings) as the source material for the melt, an application that will have the environmental and economic benefit of reducing mine waste and supporting sustainable mining operations. Moreover, future planetary surface missions to the Moon or Mars, for example, could be augmented by the use of melted local materials in order to reduce launch mass and expand mission capability (Fateri and Gebhardt 2015; Schleppi et al. 2019).

2 BASALT FIBER MANUFACTURE

Basalt fiber manufacturing technology is remarkably simple, and the production of continuous basalt fibers has many similarities to glass fibers. Such fibers are produced by spinning melted basalt from a spinneret after heating to the general range of 1,500°C. Fibers are pulled or dropped through a bushing at rates between 2000 and 5000 m/min and then spooled. The general procedures for continuous basalt fiber production are shown in Fig. 2 (after Acar et al. 2017, Dea´k and Cziga´ny 2009, and Leed 2015).

After spinning, the fibers are generally woven or pultruded to form composite materials and structures. Woven fabrics of basalt (A) and carbon (B) fibers and also strands of carbon (C) and basalt (D) fibers are all shown in Fig. 3.

Various thermoset and thermoplastic resins are used in composites manufacture with basalt fibers. For durable composite bonding, the surfaces of the fibers are modified with "sizing" materials. Since the discovery of glass fiber in 1937, there have been many important studies on the surface modification of glass and more recently for carbon fibers for use in various polymer

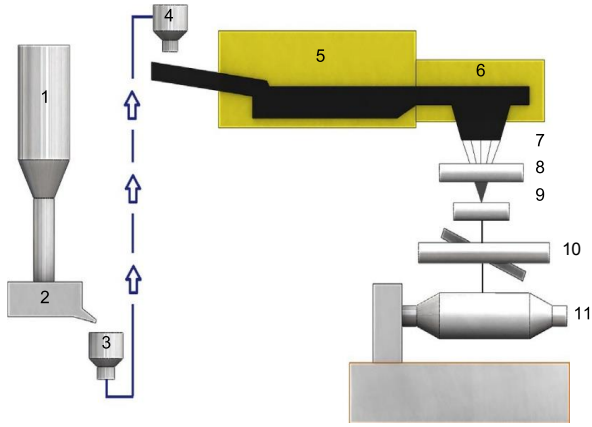

2a.

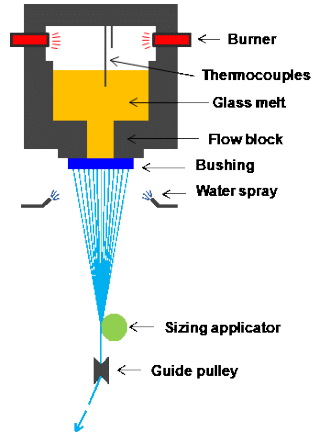

2b.

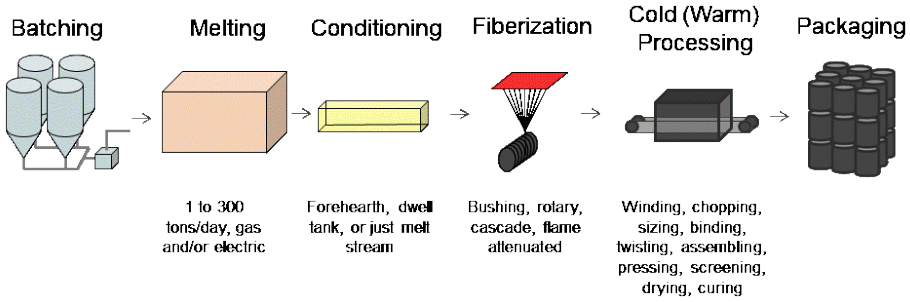

2c.

Figure 2a. Basalt fiber manufacturing procedure: (1) raw material silo, (2) loading station, (3) transport system, (4) batch charging station, (5) initial melt zone, (6) secondary heat zone with precise temperature control, (7) filament-forming bushings, (8) sizing applicator, (9) strand formation station, (10) fiber tensioning station, and (11) automated winding station (from Acar et al. 2017 and Dea´k and Cziga´ny 2009).

Figure 2b. Schematic of fiber-pulling apparatus (from Leed 2015).

Figure 2c. Schematic of generalized process flow (from Leed 2015).

matrices. Often a polymeric emulsion sizing has been used, with the fibers passed through a water-based emulsion tank. Then the emulsion is dried in a furnace to enable the vaporization of the water on the surface (reference). Sizing formulations have been closely protected trade secrets, and the details of these emulsions are difficult to find in academic literature. Besides sizing, various surface modification techniques such as silane coupling agents, titanate coupling agents, and urethane coatings have been studied (reference). However, basalt fibers have been

commercially available only since 1995, so that study of the surface modification of basalt fibers is young, and the studies are very limited.

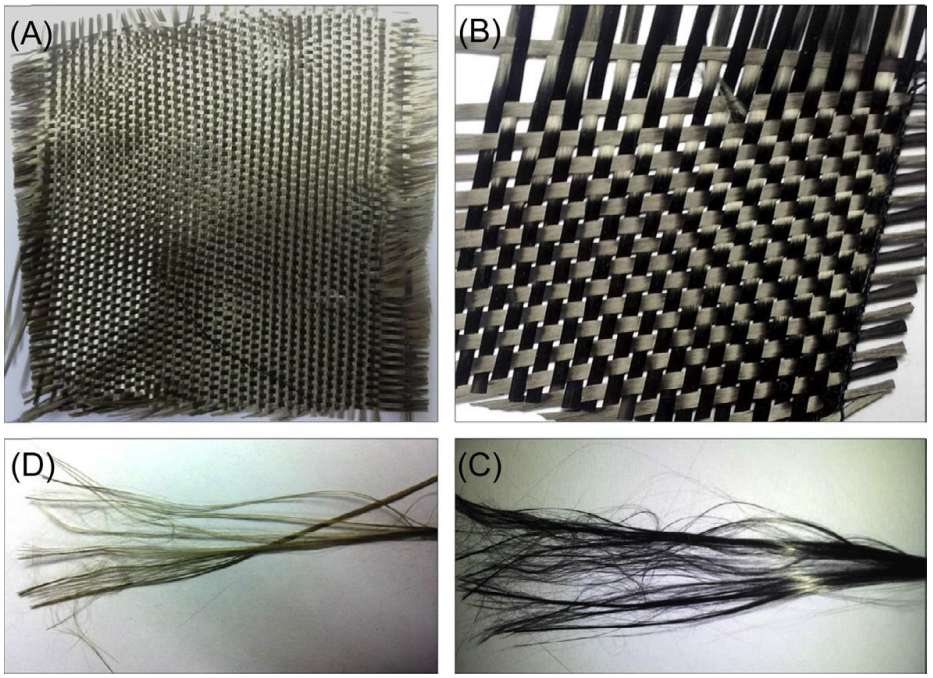

Figure 3. Woven fabrics, (A) basalt fiber fabric, (B) carbon fiber fabric, (C) strands of carbon fiber, and (D) strands of basalt fiber (Dhand et al. 2019).

3 PREVIOUS WORK ON MELTING TAILINGS

In one of the earliest studies, Chinnam et al. (2013) report on recycling of industrial wastes, with glasses and glass–ceramics attracting particular interest. They focused on iron rich waste materials and demonstrated the possibility to turn these silicate-based wastes into functional glass-based products. By properly selecting iron oxide containing residues and processing parameters, functional glass-based products with suitable catalytic activity, magnetic, optical and electrical properties could be obtained.

Alfonso et al. (2016) report on a project aimed at environmental remediation of tungsten mining areas through vitrification, a process that offers an alternative for stabilization of hazardous wastes. The chemical composition of the tailings to be used as raw materials was determined by X-ray fluorescence and their mineralogy by X-ray diffraction. At this site, wastes were of granitic composition enriched in minerals with potentially toxic elements (scheelite, wolframite, pyrite, abundant arsenopyrite and minor amounts of chalcopyrite, molybdenite and cassiterite). The investigators performed systematic sampling in order to obtain 11 samples, which were considered representative of the different areas of the tailings disposal.

For this study, they used a representative sample of mining wastes of sandy grain size to make the glass. On the basis of its composition, glass was formulated by adding 29.28 mass% $CaCO_3$ and 14.03 mass% Na_2CO_3. Crystallization temperatures, obtained by DTA, were 875 and 1022°C and the melting temperature was 1175°C. The transition temperature of glass was 644°C. The temperatures for the fixed viscosity points, and the working temperatures were obtained. Leaching tests of the obtained glass confirmed its capacity to retain potentially toxic elements.

Alfonso et al. (2018) later broadened the study to include tailings of granitic composition, calc-silicate wastes, and of schists and quartz tails. They again found that addition of $CaCO_3$ and

$NaCO_3$ was necessary for the manufacture of the glass. Samples were characterized by XRF, XRD, HSM and DTA-TG. The results show that granitic and schist tailings used were suitable for the manufacture of commercial glass, with the addition of calcium and soda. The calc-silicate tailings needed less additives to produce a glass, and they present lower workability temperatures and higher durability. Glasses obtained from all the tested tailings retain the potentially toxic elements in their structure preventing environmental pollution.

Kazmina et al. (2016) investigated the processing of mine refuse non-ferrous metal ore in the production of foamed glass. The subject of this research is a low-temperature frit synthesis (<900 °C), allowing for the high-temperature glass melting process to be avoided. The technology for the production of frit without complete melting of the batch and without using glass-making units represented a considerable reduction in energy consumption.

Kim et al. (2018) studied the utilization of gold tailings, waste limestone, red mud, and ferronickel slag for producing continuous glass fibers. To verify the applicability of the down-drawing process, the viscosity of the present mixture was measured in the molten state at a high temperature. The viscosity in the low temperature range was estimated using the Mauro-Yue-Ellison-Gupta-Allan equation. Compared to other commercially used basalt fiber systems, they found a similar fiber-forming temperature with viscosities ranging from log 2.5 to log 3.0 dPa/s observed, which indicates the applicability of the down-drawing process. Measurements of the tensile strength and the Young's modulus of a single filament were carried out following standard test methods. In spite of the thick diameter of the present filament, the fiber produced in the present study exhibited a Young's modulus of 60 to 80 GPa, which was found similar to those of other commercial fibers. They anticipate that a higher tensile strength can be achieved by reducing the diameter of the filament below 10 mm by increasing the drawing speed. They concluded that their mixture of mining wastes and smelting byproducts, was feasible for producing continuous glass fibers.

Heo et al. (2019) investigated the impact of the CaO/SiO_2 (C/S) ratio on the crystallization behavior of the CaO-SiO_2-Fe_tO-Al_2O_3 system, which modelled the mixed mineral wastes of red mud, mine tailings, and waste limestone, using a differential scanning calorimetry (DSC) technique. Melts in this system exhibited strong vitrification characteristics. They found that control of melt viscosity was important to the production of commercial grade glass.

Okereafor et al. (2020) utilized a vitrification process to manufacture glass from gold mine tailings. X-ray fluorescence was used to determine the chemical composition of the tailings while X-ray diffraction was adopted for the mineralogy. The tailings were of granitic composition enriched in potentially toxic elements such as copper, cadmium, zinc, lead, arsenic, and chromium. They separated the sand grain sized material, added $CaCO_3$ and Na_2CO_3 which resulted in the production of usable glass. At odds with this literature review, they also claimed that "For the first time, this study investigated mine tailings as a source of silica in glassmaking to mitigate the negative environmental burden that these tailings possess."

Tailings have not only been the focus of scientific studies, but in several countries, patent applications have been made for tailings processing and glass production:

- Chinese patent CN104261677B presents a method for preparing microcrystalline glass from lithium beryllium tailings, to which limestone and cupronickel slag are added The microcrystalline glass prepared by a melting process has the advantages of favorable mechanical properties, favorable thermal shock performance and favorable chemical stability.
- Chinese patent CN103396002A provides a process to prepare metal tailing glass fibers from a specified mix of raw materials including metal tailings, silica sand, limestone, magnesium and sodium carbonate, NaNO3, Sb2O3, 1 Na2SO4 and CaF2. The metal tailings were obtained from a gold mine, and the glass fiber produced is expected to exhibit high strength (higher than that of the glass fiber prepared by an ordinary industrial method).
- South Korea patent KR101848730B1 presents a method for producing glass fiber, and more particularly, a method for producing glass fiber utilizing mine waste and smelting by-products. The patent indicates success in providing glass fibers having properties equal to or higher than that of the basalt fibers using natural basalt as a raw material.

4 TARGET TAILINGS PRODUCTS

Why make fibers? Generally, fibers can be produced as continuous filaments (that may be woven or chopped) or as discontinuous fibers that may be used as rock wool. Fibers are produced for several reasons (Leed 2015), including:

a) Developing a material with a large surface area, typically on the order of 0.05 to 15 square meters per gram. A large fiber or rock wool manufacturing line can produce $2000m^2/s$ or $170km^2$ per day. The large surface area maximizes the interface available for activity or interaction, fiber coupling, and the potential for filtration.
b) Developing a material that exhibits tortured flow paths for filtration (air, liquid), acoustic wave transmission, thermal flow (e.g., conduction, convection, radiation) and fracture propagation.
c) Developing a material that can be made very thin, stiff, and strong, and excellent feed for composites manufacture.

A description and illustration of the characteristics of continuous filaments and discontinuous fibers is presented in Table 2. The project beginning at the Colorado School of Mines will consider both options as end products.

Table 2 Fiber Production Types (Leed 2015)

	Continuous Filament	**Wool (Discontinuous)**
Processing	Pulled in a continuous filament parallel with other strands (often chopped downstream)	Process inherently creates discontinuous sections of fiber that have somewhat random orientation
Typical Fiber Diameters	4-30 micron	0.2 to 10 micron
Glass Types	E-glass, C-glass, R-glass, S-glass, AR-glass, A-glass, D-glass, basalt, others	Soft alkali borosilicates, mineral wool, modified slag & basalt, RCF, others
Uses	Reinforcement (chopped fiber, rovings, wovens, non-wovens) filtration, separation, facers, thermal insulation, fireblocking	Thermal insulation (blanket, board, pipe, paper), acoustic insulation, filtration, separation

5 THE TAILINGS TO GLASS PROJECT AT THE COLORADO SCHOOL OF MINES

The "Glass from Tailings" team at the Colorado School of Mines is investigating the melting of earth resources (including waste rock and mill tailings) to produce a silicate melt that can be pulled into fibers which in turn can be fabricated into fabric, building materials, rebar, ballistic cloth, and other chemically inert products that have advantageous properties. Materials development of melted basalt rock, a mafic (rich in magnesium and iron minerals) material consisting principally of plagioclase and pyroxene minerals, was carried out in the Soviet Union in the last century. Since then, this class of materials has been commercially produced from basalt due to its favorable

fireproof, ballistic and strength characteristics, and resistance to corrosion and chemical attack (Thorhallsson et al. 2013, Zhu and Tian 2012, Wlodarczyk and Jedrzejewski 2016, Ouyang et al. 2017, Raleaonkar et al. 2018, Xiaomin et al. 2019).

The Glass from Tailings project at Mines addresses the grand challenge nexus of energy/water/food and minerals. Ore grades have been decreasing in past decades, and this means that the amount of waste materials has been increasing exponentially. Traditional mining disposes of waste rock and tailings from mineral processing operations at or near the mine site, which often cause environmental problems. The least expensive approach to process tailings disposal is the use of tailings dams, and both legacy dams from past operations and those in use currently have inherent stability concerns (e.g., the numerous dam failures with loss of life, damage to the environment, and economic impact).

We propose the use of earth resource waste (e.g., mine and process tailings) as the source material for glass. Parenthetically, we also note that future planetary surface missions to the Moon or Mars, for example, could be augmented by the use of melted local materials, in order to reduce launch mass and expand mission capability (Fateri and Gebhardt 2015, Schleppi et al. 2019).

Glass fibers pulled from melts are commonly used in composites, and the combination of fiber and substrates (e.g., resins) can enhance the composite properties, resulting in a stiff but ductile material with high strength that is lightweight and cost effective. For example, 1 kilogram of basalt reinforcement provides the strength equivalent of 9.6 kilogram of steel (Pareek et al. 2019) in reinforced concrete applications. Regarding other applications, the basalt fiber production cost is approximately US$5/kg, whereas production costs are US$15/kg for glass fiber and US$30/kg for carbon fiber (Pareek et al. 2019).

Process tailings principally consist of a mixture of rock fragments and minerals that remain after the valuable minerals have been recovered by mineral processing. In most cases of metals mining, the minerals that make up tailings are predominantly silicates - plagioclase, biotite, amphibole and pyroxene – similar to the mineralogy of basalt (but with higher iron and magnesium content), which has a melt temperature of about 1500°C). Table 3 displays a representative ideal basalt composition to be used at a basalt fiber production site in North Carolina operated by MAFIC USA (pers. communication). It is possible that certain process tailings can be re-processed to form a lower-temperature melt that is easily drawn into fiber.

Table 3: Representative compositional range of raw material (basalt) used by MAFIC USA at Shelby, North Carolina basalt fiber production site.

Components	Weight%
SiO_2	50 – 60
Al_2O_3	14 - 19
CaO	5 - 10
MgO	3 - 5
$Na_2O + K_2O$	3 - 5
TiO_2	0.5 - 3.0
$Fe_2O_3 + FeO$	9 - 14
Others	0.05-1.0

For evaluating whether tailings may constitute a viable raw-material source, the feedstock has to be characterized in terms of chemical constituents to evaluate whether it is suitable for processing and product quality, either as is or with an economic amount of reprocessing. To some extent, deviating mineralogy and chemistry may be adjusted through fluxing.

The objective the "Tailings to Glass" team is to investigate and better understand the chemical and mineralogical characteristics of mine and process tailings. Our approach is to determine the chemical and mineralogical characteristics of mine and mineral processing tailings, which will allow determination of melt composition and variability possible to achieve desired melt temperatures and other process-pertinent properties. The silicate mineralogy of basalt and mine tailings, as well as molten oxide slags, is characterized largely by polymeric networks of Si-4O tetrahedrons joined at corners. The networks may be modified by metal (Me) oxides:

$$\boldsymbol{Si_{x+1}O_{3x+3}^{2(x+2)-} + O^{2-} + Me^{2+} = SiO_4^{4-} + Si_xO_{3x+1}^{2(x+1)-} + Me^{2+}} \quad (1)$$

In multicomponent earth-resource mixes, the relationships between chemistry and physical properties (viscosity, interfacial/surface tension, crystallization temperature) and thermodynamic properties (T_L, T_G, and chemical activities) constitute a complex network of chemistry-temperature-structure-property relationships. Traditionally, these would need to be quantified with extensive experimentation in traditional, mechanistic models.

We plan to investigate: (a) the development of a tailings characterization protocol; (b) the development of a data base of tailings mineralogy and geochemistry for bulk rock/tailings, as a function of particle size, assessment of chemical and mineralogical variability, and physical properties including density; (c) thermodynamic considerations to predict melting temperatures and glass formation temperatures and thermos-physical considerations for viscosity, surface tension etc.; and, (d) a preliminary economic and life cycle assessment model for selected applications.

We will determine what protocols need to be put in place for adequate characterization of tailings, and this will allow determination of melt varieties possible to achieve desired melt temperatures, glass-formation temperatures and viscosities. We are developing the industry and university network needed to achieve our purpose, and we plan to complete the following steps on the road to our success:

(a) A mineralogy and geochemistry characterization protocol, following best practices from the basalt fiber industry, will be established. This will include quantitative automated mineralogy and X-ray diffraction (XRD) for a better understanding of the mineralogy and X-ray fluorescence (XRF) analyses for concomitant chemistry data. Representative samples will be sent to an external lab for chemical analyses for quality control.
    - The samples will be dried, crushed and homogenized. Once homogenized, representative samples will be taken and split into four aliquots for further quantitative automated mineralogy, XRD and XRF analysis in the Department of Geology and Geological Engineering (Mineral and Materials Characterization (MMC) Facility) and sent for commercial chemical analysis for comparison and quality control.
    - We will conduct a literature survey to gather published data on the mineralogy and chemistry of tailing materials. Our data will be added to this, and a user-friendly data base of tailings and their properties will be developed.

(b) Best practices for bulk mineralogy and geochemistry based on the outcomes from step (a) will be established. Application of established analytical protocol will be applied to particle size splits, spatially diverse samples to understand the variability of the mineralogy and geochemistry across a tailings impoundment. Moreover, simple mineral separation methods such as gravity separation may be used to better understand the mineralogy and geochemistry of the material.

(c) Thermodynamic modelling will be conducted using CALPHAD-based simulations (Bales, et al. 2002). If the mineralogy and geochemistry of a material are known, it is possible to predict its melting point, glass formation temperature and viscosity through thermodynamic and thermos-physical property modelling (VDEh 1995). This is an important analysis to better understand which of the tailings samples are most suitable for fiber production. We will determine those samples with the most favorable bulk rock compositions based on modelled melting temperatures and glass transition temperatures and we will compare our outcomes with results from the basalt fiber industry through our partner, MAFIC USA.

(d) A preliminary technical economic assessment (TEA) model will be developed, and research into potential applications of tailings fiber will be conducted. For example, we anticipate that reinforcing materials made from basalt and tailings fibers will disrupt the construction market and offer a cheap, durable, and versatile alternative to steel. The model will be compared to current costs for glass fiber manufacturing with conventional feedstock and with basalt.

6 CONCLUSIONS

The "Tailings to Glass" team at the Colorado School of Mines embarks upon a project to use earth resource wastes (e.g., mine and process tailings) as the source material for high valued fiber, glass and sintered products that will have the environmental and economic benefit of reducing mine waste and supporting sustainable mining operations.

REFERENCES

Acar, V., et al. 2017. "Basalt fibers." in Fiber Technology for Fiber-Reinforced Composites, Elsevier. http://dx.doi.org/10.1016/B978-0-08-101871-2.00008-4

Alfonso, P., et al., 2016. "Recycling of tailings from the Barruecopardo tungsten deposit for the production of glass." Minerals & Metallurgical Processing, 2016, Vol. 33, No. 1, pp. 23-30. http://dx.doi.org/10.19150/mmp.6464

Alfonso, P., et al., 2018. "Potential of tungsten tailings as glass raw materials." Materials Letters, 228, 456-458.

Bale, C. W., et al, 2002. "FactSage Thermochemical Software and Databases," Calphad Journal 62: 189–228.

Chinnam, A. A., et al., 2013. "Functional glasses and glass-ceramics derived from iron rich waste and combination of industrial residues." Journal of Non-Crystalline Solids 365 (2013) 63-74. http://dx.doi.org/10.1016/j.jnoncrysol.2012.12.006

Czigany, T., 2005. "Discontinuous basalt fiber-reinforced hybrid composites." In: Friedrich K,

Dhand, V., et al., 2015. "A short review on basalt fiber reinforced polymer composites." Compos Part B 2015;73:166–80. http://dx.doi.org/10.1016/j.compositesb.2014.12.011

Dea´k, T. and T. Cziga´ny, 2009. "Chemical composition and mechanical properties of basalt and glass fibers: a comparison." Text Res J 2009;79(7):645–51. http://dx.doi.org/10.1177/0040517508095597

Deng, L., et al., 2019. "Structure and properties of in situ synthesized FeSi2-diopside glass ceramic composites from Bayan Obo tailings, blast furnace slag, and flyash." Journal of Alloys and Compounds, 785, 932-943. Elgabbas, F. et al., 2016. "Experimental testing of basalt-fiber reinforced polymer bars in concrete beams." Compos Part B 2016;91:205–18. http://dx.doi.org/10.1016/j.compositesb.2016.01.045

Fakirov S. and Z. Zhang, eds., 2005. "Polymer composites: from nano- to macro-scale." London: Springer Science+Business Media; 2005. p. 309–28. http://dx.doi.org/10.1007/0-387-26213-X_17. ISBN: 978-0-387-24176-0 (Print) 978-0-387-26213-0.

Fan, X. and M. Zhang, 2016. "Experimental study on flexural behaviour of inorganic polymer concrete beams reinforced with basalt rebar." Compos Part B 2016;93:174–83. http://dx.doi.org/10.1016/j.compositesb.2016.03.021.

Farsani, R., et al., 2014. "Influence of thermal conditions on the tensile properties of basalt fiber reinforced polypropylene-clay nanocomposites." Materials and Design, 53, 540-549.

Fateri, M. and A. Gebhardt, 2015. "Process parameters development of selective laser melting of lunar regolith for on-site manufacturing applications." Int. J. Appl. Ceram. Technol., 12, 46-52.

Fiore, V., et al., 2015. "A review on basalt fibre and its composites." Compos Part B;74:74–94. http://dx.doi.org/10.1016/j.compositesb.2014.12.034

Gao, W.-Y., et al., 2018. "Repair of fire-damaged RC slabs with basalt fabric-reinforced shotcrete." Construction and Building Materials, 185, 79-92.

Hassan, M., et al., 2016. "Bond durability of basalt-fibe rreinforced-polymer (BFRP) bars embedded in concrete in aggressive environments." Compos Part B 2016;106:262–72. http://dx.doi.org/10.1061/(ASCE)CC.1943-5614.0000270

Heo, J. H., et al., 2019. "Crystallization and vitrification behavior of CaO-SiO2-FetO-Al2O3 slag: Fundamentals to use mineral wastes in production of glass ball." Journal of Cleaner Production 225 (2019) 743-754. https://doi.org/10.1016/j.jclepro.2019.04.035

Jiang, C., et al., 2014. "Experimental study on the mechanical properties and microstructure of chopped basalt fibre reinforced concrete." Mater Des 2014;58:187–93. http://dx.doi.org/10.1016/j.matdes.2014.01.056

Karhu, M., et al., 2019. "Mining tailings as raw materials for reaction-sintered aluminosilicate ceramics: Effect of mineralogical composition on microstructure and properties." Ceramics International, 45, 4840-4848.

Kazmina, O. V., et al., 2016. "Using quartzofeldspathic waste to obtain foamed glass material." Resource-Efficient Technologies 2 (2016) 23–29. http://dx.doi.org/10.1016/j.reffit.2016.05.001

Kim, Y., et al., 2018. "Applicability of gold tailings, waste limestone, red mud, and ferronickel slag for producing glass fibers." Journal of Cleaner Production, 203, 957-965.

Lapko A. and M. Urbanski, 2015. "Experimental and theoretical analysis of deflections of concrete beams reinforced with basalt rebar." Arch Civ Mech Eng 2015;15(1):223–30. http://dx.doi.org/10.1016/j.acme.2014.03.008

Leed, E., 2015. "Lecture 14. Fiberglass Processing." Spring Class on Glass Processing at Lehigh University, www.lehigh.edu/imi

Li, Z., et al., 2018. "Properties and applications of basalt fiber and its composites." GBEM IOP. Conf. Series: Earth and Environmental Science, 186, 012052.

Okereafor, U., et al. 2020. "Mine Tailings: A Potential Source of Silica Sand for Glass Making." Minerals:10(5), 448; https://doi.org/10.3390/min10050448

Ouyang, L.-J., et al., 2017. "Seismic retrofit of square reinforced concrete columns using basalt and carbon fiber-reinforced polymer sheets: A comparative study." Composite Structures, 162, 294-307.

Pareek, S., 2019. "Basalt fiber and its composites: An overview." Proceedings of National Conference on Advances in Structural Technologies (CoAST-2019), 1-3 Feb, 2019.

Ralegaonkar, R., et al., 2018. "Application of chopped basalt fibers in reinforced mortar: A review." Construction and Building Materials, 164, 589-602.

Schleppi, J., et al., 2019. "Manufacture of glass and mirrors from lunar regolith simulant." Journal of Materials Science, 54, 3726-3747.

Thorhallsson, E., et al., 2013. "Basalt fiber introduction." Conference Paper. https://www.researchgate.net/publication/265694778

Tirillo, J., et al., 2017. "High velocity impact behavior of hybrid basalt-carbon/epoxy composites." Composite Structures, 168, 305-312.

U.S. Patent, 1923. "Tipping crucible for basalt furnaces." U.S. Patent Number, US1462446A.

Vasil'eva, A. A., et al., 2014. "Investigation into the properties of basalt of the Vasil'evskoe deposit in Yakutia as the raw material for obtaining continuous fibers." Theoretical Foundations of Chemical Engineering, 48, 667-670.

Verein Deutscher Eisenhuttenleute (VDEh), (ed.). 1995 *Slag Atlas* Dusseldorf: Verlag Stahleisen GmbH.

Wei, B,. et al., 2011. "Degradation of basalt fibre and glass fibre/exposy resin composites in seawater." Corrosion Science, 53, 426-431.

Wlodarczyk, M. and I. Jedrzejewski, 2016. "Concrete slabs strengthened with basalt fibres – experimental tests results." Procedia Engineering, 153, 866-873.

Xiaomin, M., et al., 2019. "Blast response of gradient honeycomb sandwich panels with basalt fiber metal laminates as skins." International Journal of Impact Engineering, 123, 126-139.

Zhu, J. and Y. Tian, 2012. "Applications of advanced composite materials in bullet-proof fields and their study." Advanced Materials Research, 391-392, 242-245.

Zych T. and K. Wojciech, 2012. "Brittle matrix composites: study on the properties of cement mortars with basalt fibres." Cambridge: Woodhead Publishing Ltd.

Integrated Storage Facility – A New Concept for Mine Waste Storage

David Saiang
New Mexico Institute of Mining and Technology, Socorro, NM, USA

Martin Torovi
East Sepik Mining Desk, Wewak, East Sepik Province, Papua New Guinea

Robert D.Y. Warigen
East Sepik Mining Desk, Wewak, East Sepik Province, Papua New Guinea

Edward Wiruk
East Sepik Mining Desk, Wewak, East Sepik Province, Papua New Guinea

ABSTRACT: A new concept for mine waste storage called Integrated Storage Facility has been touted in places where managing mine waste is extremely challenging. Such a concept has been conceived to be pioneered for a massive copper-gold project in Papua New Guinea, where rugged tropical terrains, tough climatic and geological conditions make building of conventional mine waste storage facility one of the biggest challenges in the country. The developer of Frieda River Copper-Gold project in Papua New Guinea, PanAust, plans to create a huge man-made lake, occupying an area of 12,700 hectares and perched between several valleys at an elevation of 400 to 800 m above sea level. This Integrated Storage Facility will serve two functions: (i) submarine environment for underwater storage of mine tailings and waste rock and (ii) hydro-electric facility to power the mine and excess power for export. The facility is planned to hold 2.13 billion cubic meters of tailings and waste rock over the life of the mine, and 0.04 billion cubic meters of water. Since this infrastructure is neither a classical hydro-power dam, nor a tailings dam, the design of the infrastructure was difficult to benchmark against existing hydro-power dams and tailings dams. In view of the nature of the infrastructure the government of East Sepik Province, a stake holder in the project, engaged a team of engineers to carry out high level review of the design cncept of the infrastructure considering the risks and consequences. This paper is the result of this review and highlights some of the challenges facing such a concept.

INTRODUCTION

Storing mine waste in areas of high rainfall, rugged terrain and high seismicity can be a taunting task. This is very much the case for Frieda River copper-gold project in Papua New Guinea (PNG). Since its discovery in 1966, it remains one of the largest known copper-gold deposits that is yet to be developed. The Frieda River deposit lies along the famous New Guinea Mobile Belt, home to some of the world's largest copper and gold deposits including Ertsberg, Grasberg, Ok Tedi, Porgera, Wafi-Golpu, Lihir and Panguna to name a few.

The New Guinea Mobile Belt is a tectonic belt that stretches through the middle of the island of New Guinea and it is part of the greater Pacific Ring of Fire. It is a seismically active zone that comprises 5 to 10% of the world's total earthquakes (Brooks, 1963). The region is also known for very steep rugged terrains with razor sharp ridges and vertical rock cliffs, thick tropical jungles and swamps, high rainfall (3,000 to 10,000 mm per year), fast flowing rivers, pristine wildlife and native inhabitants with diverse culture and heritage. The ambitious construction of Ertsburg and Ok Tedi in the 1970s and 1980s, respectively, by Bechtel Engineering highlights the enormous engineering undertaking to access the valuable resources of New Guinea at costs of billions of dollars. The estimated price tag for construction of Frieda River copper-gold deposit stands at 8 billion USD today.

The increase in awareness of the risk of mining activities has resulted in all stakeholders (local populations, local and national governments, and resource developers) to actively participate in new mineral resource development projects. For the last 10 years the Frieda River copper-gold project and its current owner, PanAust, has been actively engaged in detailed feasibility studies that involved inputs from all stakeholders. One of the major projects in these feasibility studies concerned mine waste and tailings management system.

An innovative concept known as 'Integrated Storage Facility (ISF)' was first coined by Xstrata plc, one of the past owners of the Frieda River Au-Cu project preceding PanAust. The proposal was to build a massive water storage infrastructure or dam to serve two functions: (i) as submarine environment for subaqueous storage of mine wastes and tailings and (ii) to generate hydro-electric power for the mine and the region. This facility, with total areal occupation of 12,700 hectares, is planned to hold over 2 billion cubic meters of mine waste and tailings that will be produced over the life of the mine, and 0.04 billion cubic meters of water as cover for mine waste and for power generation. The facility will be the core asset that will determine whether the resource will be developed or remain further undeveloped.

Although the concept is inovative, it is seen as an ambitious undertaking by some observers, with significant risks to be addressed. The uncertainty in the concept is very significant since it is a first of its kind. There exist no such facility of this magnitude neither in Papua New Guinea nor the Southern Hemisphere. The inherent climatic, topographical, seismological, environmental, and socio-economic risks are to be carefully evaluated. Various stakeholders and independent experts are presently engaged in these evaluation processes. The East Provincial Government, a major stakeholder in the project, has engaged a group of independent experts to assist in the independent evaluation of the ISF. The results from this evaluation is published in this paper. The review focused on the safety aspect of the ISF.

1 BACKGROUND

1.1 *Frieda River Copper-Gold Project*

Frieda River Copper-Gold is one of the largest known world class deposits that is yet to be developed. It is located along the New Guinea Mobile belt, the region which hosts some of the world's largest copper and gold deposits including; Grasberg, Ok Tedi, Porgera, Wafi-Golpu, etc (Figure 1). Frieda River deposit has a current estimated resource of 2.6 billion tonnes containing 13 million tonnes of copper and 20 million ounces of gold. It has potential to develop into a Grasberg size deposit. With current resources, it can sustain a mine life of up to 40 years with estimated yearly production of 40 million tonnes, excluding wastes.

Developing a mine waste management plan for this potential mine has always been very difficult. Hostile terrain, high rainfall (averaging 8000 mm/yr), high seismicity, pristine biodiversity and concentration of native populations along the vast river ways has discouraged many potential developers to abandon the project since its discovery in 1966. However, the current project owner, PanAust, intends to follow on with an ambitious mine waste management plan, originally proposed by Xstrata, to integrate mine waste storage with civil infrastructure. The concept is known as the Integrated Storage Facility (ISF). This concept has not been tested elsewhere and is a first of its kind. The concept of storing mine waste under marine environment though is a known practice. PanAust presently manages a large dam at its Phu Kham mine in Laos where it stores mine waste under the man-made lake. This facility does not generate hydro-power as a secondary purpose. PanAust intends to use the Phu Kham experience on the Frieda River copper-gold project. However, the sites of these two projects are drastically different, with Frieda River being a mammoth compared to Phu Kham.

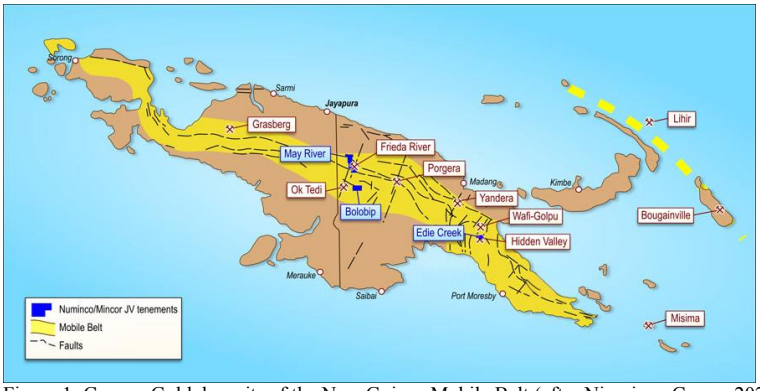

Figure 1: Copper-Gold deposits of the New Guinea Mobile Belt (after Niuminco Group, 2020).

1.2 *Conflicts with marine disposal of mine wastes in Papua New Guinea*

It is worthwhile to give some historical background to the issue of marine and riverine disposal of mine waste in PNG to set the context for the new concept for mine waste management – the Integrated Storage Facility (ISF).

Riverine and marine disposal of mine waste was approved by the PNG government as early as the 1960s because it was difficult to build mine waste and tailings dams given the country's geo-environmentally hostile environment. Furthermore, with the already inflated costs of building the mine in difficult conditions, the costs of building and managing mine wastes would make mine development practically impossible. It was also argued that the consequences of a dam failure would be far more devasting than managing the waste through a marine disposal system. Hence, mines were allowed to dispose mine wastes directly into riverine and marine systems. Riverine disposal led to serious destruction of riverine and marine environments and is a major source of discontent and animosity between the local population, the government and resource developers.

After nearly 30 years of operation the once famous Panguna mine owned by Rio Tinto, on the island of Bougainville was forced to shut down after disgruntled local population formed a militia to fight the company and the government because of the destruction to the environment and the riverine systems. The civil war lasted 10 years and the Panguna mine has not recovered to this day. The Ok Tedi mine and BHP-Billiton (past owner) has been battling a series of court cases for years for riverine destruction of the Fly River system that channels through to the coral reefs of Australia. Porgera mine has recently suspended operations as the local and national governments demand more in stake holding from Barrick and its partners to compensate for the environmental damages. Lihir mine has been placing its mine waste undersea off the coast of the Island of Lihir.

Meanwhile, the Frieda River copper-gold deposit lies at the headwaters of the Sepik River (Figure 2), which is one of the largest rivers in Papua New Guinea with vast catchment area of over 100,000 km^2. The Sepik River system is possibly one of the largest uncontaminated fresh-water wetland in the Asia-Pacific region. A vast majority of the population of the East Sepik province is concentrated along the Sepik River system and depend on its waterways for their daily livelihood and nourishment. The native population have deep spiritual connections with the river system and pay greater homage to it as a living being. Hence, any disposal of mine waste into the Sepik River system and its catchment areas will be considered a major disaster. This lead to the concept of ISF to manage mine waste from the Frieda River Project.

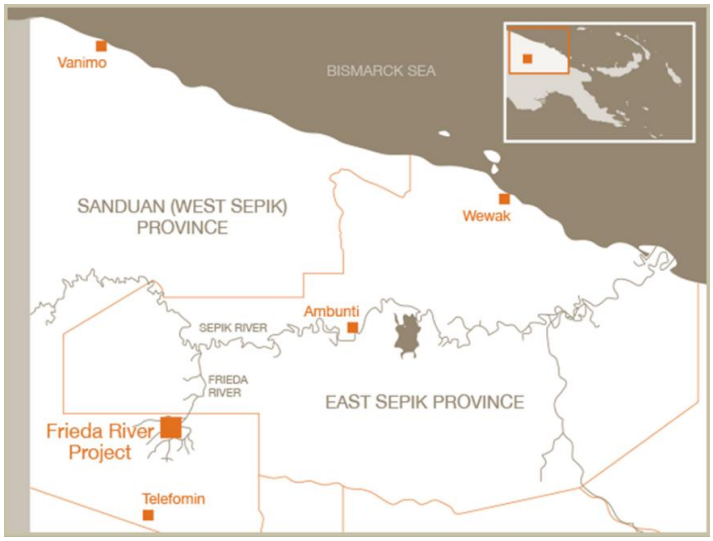

Figure 2: Frieda River Project lies in the catchment area of the Sepik River system, one of the largest uncontaminated freshwater wetland in the Asia-Pacific region.

1.3 *Integrated Storage Facility (ISF)*

The Frieda River ISF is simply a large man-made lake that will serve primarily as a marine environment for subaqueous storage of mine wastes (tailings and waste rocks) and secondarily the excess water will be used to generate hydro-electricity to power the mine (Figure 3).
The key components of the ISF will thus consist of the large reservoir occupying an area of 12,700 hectares, dam embankment, hydro-power infrastructure, and mine waste and tailings handling systems. The ISF will comprise approximately 75% of the Frieda River Project footprint. Management of the submerged waste rocks and tailings, and the reliability or safety of the embankment will be critical to the ISF.

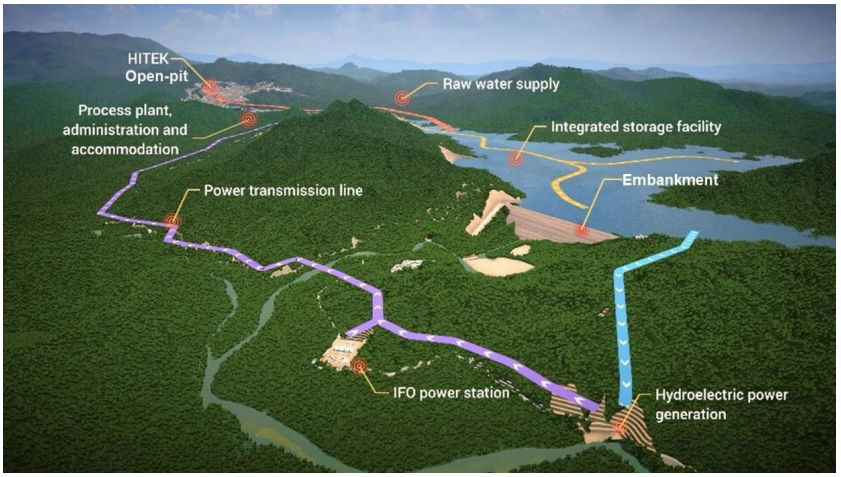

Figure 3: The ISF consist principally of the reservoir under which tailings and waste rocks will be stored and access cover water for power generation and their related infrastructures.

1.4 *ISF site investigation*

The site for the ISF was investigated by several reputable international consulting companies. These investigations included characterization of sites for specific engineering infrastructures, such as the dam embankment and hydropower infrastructure. The execution of each task followed standard industrial and scientific best practices and procedures.

Even though the site investigations around Frieda River project area has been on-going for several decades, the focus on the ISF area has intensified within the last 10 years since the concept of integrated infrastructure for mine waste storage was conceived. Geological, geotechnical, hydrological and seismological studies were conducted within the ISF area. However, the footprint of the ISF is very large, 12,700 hectares, making it overwhelming for detailed investigation over rugged terrains. Therefore, detailed site investigations were conducted using the so-called 'target approach'. Areas of specific interest were targeted for instance with drill-holes and high resolution LiDAR survey. Even though this is a normal industry practice it still left significant gaps in the data for the whole area. Such data gaps can raise the level of uncertainty on the safety of the ISF. For example, the soil cover on which the mine waste will be bedded is composed of tens of meters of deeply weathered soils and colluviums that exhibit highly liquefiable characteristics. This poses significant safety risk to the infrastructure. Existence of major faults, with history of being the epicenters of earthquakes in this area, one as recent as 2016, lie within the ISF footprint. Detailed site investigation of these parameters and others will require a research level undertaking and thus delay the commercial ambitions.

1.5 *Design criteria for the ISF embankment*

A key component of the ISF is the dam embankment. The embankment is designed as zoned rockfill dam with an impermeable asphalt core in the center of the embankment. The final height of the embankment is 191 m, making it one of the tallest in the world. There are no

specific criteria or guidelines for designing an embankment for such as a facility as the Frieda River ISF that serves a dual purpose, for mine waste storage and hydro-power generation.

The challenging task of designing the embankment was handed to SRK Consulting Australasia. Considering the significant risk the embankment would carry, SRK Consulting resorted to risk-consequence based design approach. This meant back engineering the design to reduce the consequences in the event of a failure. Hence, SRK used the criteria established by International Committee on Large Dams (ICOLD) and Australian National Committee on Large Dams (ANCOLD) to undertake a dam break analysis for an informed design based on the consequence categories of different break scenarios. The result of this analysis is shown in Table 1, which shows the severity being divided into 4 categories: Minor, Medium, Major and Catastrophic. The Frieda River ISF embankment falls under the category of "Extreme Consequence" or "High Catastrophic" in the event of failure. Even though the risk of dam failure is low, as per the design, the consequence is still on the catastrophic level.

Table 1. Consequence category. Frieda River ISF embankment category is highlighted (SRK Consulting, 2018).

Population at Risk	Severity of Damage and Loss			
	Minor	Medium	Major	Catastrophic
<1	Very Low	Low	Significant	High C
≥1 to <10	Significant	Significant	High C	High B
≥10 to <100	High C	High C	High B	High A
≥100 to <1,000	-	High B	High A	Extreme
≥1,000	-	-	Extreme	Extreme

Source: ANCOLD, 2012. Guidelines on the Consequence Categories for Dams.

1.6 *Consultations with local population*

The government and resource developers are well aware of the risks of excluding local population in resource development negotiations. In Papua New Guinea these negotiations can take 4 to 5 years or even more before an agreement can be reached. The challenge has always been to provide balanced and factual views. Those that directly benefit from resource development are usually elevated to believe that the benefits are too great compared to the negative impacts. On the contrary are those that will be affected by the negative consequences of the project, but are not direct beneficiaries from it. This group is always negative about the project. They are usually seen as the bad ones trying to stop economic developments. Often they are supported by NGOs while the former is supported by the wealthy resource developers to voice their respective stands. Over the last 20 years the potential developers of the Frieda River copper-gold deposit, along with the national government, have engaged themselves on roadshows to publically engage every stakeholder population with both views, for and against (Figure 4). The public engagement is in line with IFC Performance Standard on Social and Environmental Assessment and Management Systems (IFC, 2012).

The ISF concept alone is quite controversial among the local population. Being an infrastructure with low probability to fail is a good news for the "for group". However, for the "against group" the probability of a "catastrophic consequence" overrides any economic benefits and they do not want to see the project go ahead. It is a dilemma that requires honest and transparent engagements guided by scientific and engineering facts.

Figure 3: A roadshow for public awareness and engagement concerning the Frieda River Project and importantly the ISF (source of the photo: https://www.pngreport.com/mining/news/frieda-river).

2 ISF SAFETY

To ensure the safety of the ISF, its overall life cycle would ideally serve as control points. Four key life cycle stages will be: (i) Design Stage (ii) Construction Stage (iii) Operational Stage and (iv) Closure Stage. Flaws in each of these stages would significantly impair the full functionality of the infrastructure and thus jeopardize its safety.

2.1 *Design Stage*

A high level review panel was established by PanAust under its stewardship program for mine waste management to review the design of the ISF. The panel made several recommendations for further improvement to the ISF design and its individual components. Recommendation were also made for the steps to be observed during construction, operation and closure of the ISF, including monitoring and quality assurance procedures.

The ISF designers have consulted various international standards, among them the respectable ones such as International Committee on Large Dams (ICOLD), Australian National Committee on Large Dams (ANCOLD), Canadian Dam Association (CDA) and US Army Corps of Engineers (USACE). The designers however, admitted that the ISF is not a classical hydro-power dam and therefore some design elements from the mentioned standards are limited.

The design depends on several factors such as inputs, method of analysis and design methodology. Coupled with uncertainty in the input data, designing a massive infrastructure which is a first of its kind poses a significant risk of the unknown. Hence, detailed scientific study is required to give confidence to the design. As noted earlier, data gathering over 12, 700 hectares is an overwhelming task. Selective use of inputs based on targeted survey is insufficient to boost the safety of a highly sensitive infrastructure. Some analyses, for example the underwater landslip potential, were not fully realized for the fact that such analyses would incorporate the entire footprint of the ISF (requiring reliable inputs) and overwhelming computational efforts. Selective modelling was done to support the design efforts, which when considering the sensitivity of the ISF, it does not improve it's safety.

2.2 *Construction Stage*

The construction of the ISF will take 6 to 8 years under very difficult construction conditions. These include severe weather conditions (high precipitation, constant flooding and erosion), steep tropical terrains, deep tropical weathered soils and limited access to the construction site. Access to the construction will be mostly by helicopters and ferries along rivers. An airstrip is also planned to ferry in workers to the site by light fixed-wing aircrafts.

The design consultants emphasized the need for 'stewardship' and quality assurance during construction. This means the tendency to take shortcuts to accelerate construction under difficult conditions to avoid delays should be avoided at all costs. The catastrophic failure of Samarco Tailings Dam in Brazil in 2015, had the original source of the problem traced to construction flaws (do Carmo et al, 2017). Hence stewardship during the construction stage will be a critical factor in the construction of the Frieda River ISF.

2.3 *Operational Stage*

The Frieda ISF is designed to have a minimum operational life of 35 years. This is also the expected life of the Frieda River copper-gold mine. The ISF will principally have the capacity to hold waste rocks and tailings produced over the 35 years, but with capacity to take more in case of mine life extension. The infrastructure will be operated both as a mine waste storage facility and as a hydro-power facility. Meaning, the operational procedures and safety protocols will follow the respective demands of each component of the infrastructure.

At the downstream the dam is designed as a 'flow-through' facility. Which means that the discharge water must meet 'end-of-pipe' discharge standards. This requires that the oxidation of the tailings and waste rock must be limited prior to subaqueous disposal. Contaminated water inflows must be controlled or treated before being discharged. Once inundated, the water cover will provide an oxidation barrier to inhibit further oxidation. The waste rock will be crushed to allow proper sitting and distribution on the lake floor. The tailings will be pretreated to remove toxic mineral extraction agents. The likely condition in the reservoir will be as illustrated in Figure 4.

Keeping the toxic sediments stable and settled on the floor of the dam and not suspended in the water during discharge is critical. This is a delicate process and will need to be thoroughly controlled to prevent the suspended fines from entering the "flow-through" path. Methods to assist in rapid settlement of tailings will be required. Furthermore, the ISF will be highly prone to turbulent underwater floods during wet seasons as a result of inrush from the feeder streams. The agitation caused by flooding will cause the tailings to suspend and easily get transported to the discharge facility. This factor is absolutely critical as the dam is designed for continuous discharge during wet seasons to maintain its capacity.

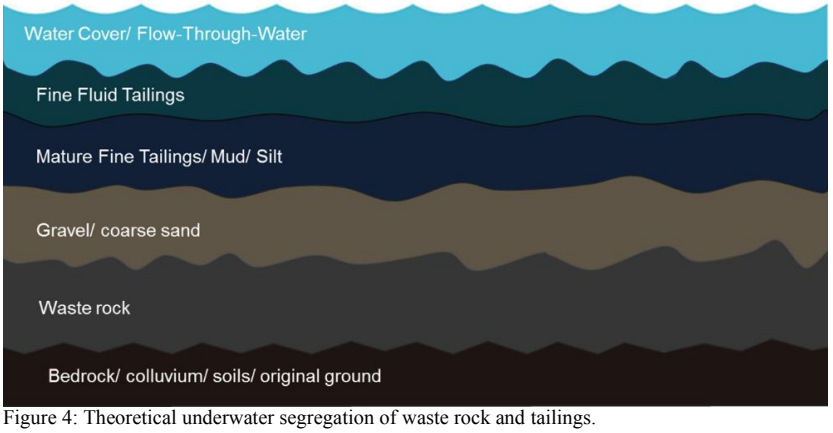

Figure 4: Theoretical underwater segregation of waste rock and tailings.

2.4 *Closure Stage*

The Frieda River ISF is designed for 200 years. The project developer has put together a comprehensive plan and implementation strategy from operation to closure. It is anticipated that this plan will be followed through and implemented with various milestones leading up to the closure stage. However, it is not clear who will be responsible during and after the closure stage of the ISF. The mine operator will be responsible until end of operational phase. That is, after 35 years when the mining activity ceases the mine operator will consider facility closed, and will seek to hand over the facility to a nominated entity to manage it as a civil infrastructure for continued hydro-power generation. This is partly a legal matter and is required to be sorted out between the government and the mine operator.

Maintaining the infrastructure during its closure life is as critical as its operational life. Monitoring, care and maintenance will be on-going. Although PanAust has put together a closure plan, it remains uncertain how this will be executed and by whom. The closure stage has not been properly researched to determine when the mine wastes will reach some form of neutralized state to safely accommodate marine life.

2.5 *Monitoring*

Monitoring is a key element of all engineering infrastructure and the Frieda ISF will be no exception. Even though a full monitoring program is yet to be developed the expert panel put together by PanAust has highlighted the importance of instrumentation and monitoring of such a sensitive infrastructure. It is anticipated that, the nature of the infrastructure will demand some of the best monitoring techniques available to ensure facility safety .

Monitoring has been recommended to start immediately during the construction stage and reservoir filling to keep track of landslips (SRK Consulting Australasia, 2018). Other monitoring, such as for rainfall and flood measurements, are in place.

3 SAFETY RISKS

There are two key factors regarding the safety of the ISF. The first is whether the site is safe enough to host the ISF and the second is whether the ISF and its components is safely designed

and operated, including its closure life. Some common safety risks related to site and the ISF's structural safety are highlighted in the following sections.

3.1 *Site Risks*

3.1.1 *Geological hazard*

The site on which the ISF will be located is an area of substantial geological hazards, both local and regional. Local geo-hazards include tens of meters of highly weathered bed rock, soils and colluvium, dominated by landslip scarps. Figure 5 shows an example the typical soil profile, in this case through the Frieda River channel, upstream from the proposed site for the embankment. Figure 6 shows the regional geology within the footprint of the ISF. Consultants (Douglas and Partners, 2009) note that, 60-80% of the area covered by the ISF consists of these liquefiable soils and colluviums. If buried under water these materials will dramatically lose their cohesive strength and the risk of sudden liquefaction becomes too high. The risk is exacerbated if the mine wastes are bedded on these materials.

Another major risk is the existence of major faults in the area (Figure 6). The ISF will sit on top of a series of thrust faults, one of which was the epicenter of the most recent Magnitude 4.2 earthquake that occurred in 2015 at a depth of 43 km within the fault (indicated by red asterisk in Figure 6). These faults are seismically alive.

It is known that hydro-power reservoirs can also induce earthquakes. The most powerful earthquake thought to have been induced by a reservoir is a Magnitude 6.3 tremor within the Koyna hydro-power dam in India in 1967, it devastated one village, killed several hundreds of people, injured thousands and rendered thousands homeless (Chobra and Chakrabarti, 1973). Hence, one of the biggest risks for Frieda River ISF is that, the reservoir itself could trigger an earthquake within the thrust faults. With the facility already classed as "Extreme Catastrophic" in the consequence category the site may render itself unsafe for the ISF.

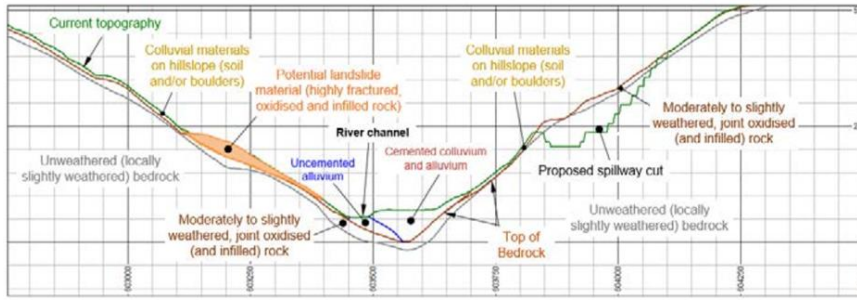

Figure 5: A typical cross-section of the soil profile across the Frieda River valley – considered typical within the ISF footprint (SRK Consulting Australasia, 2019).

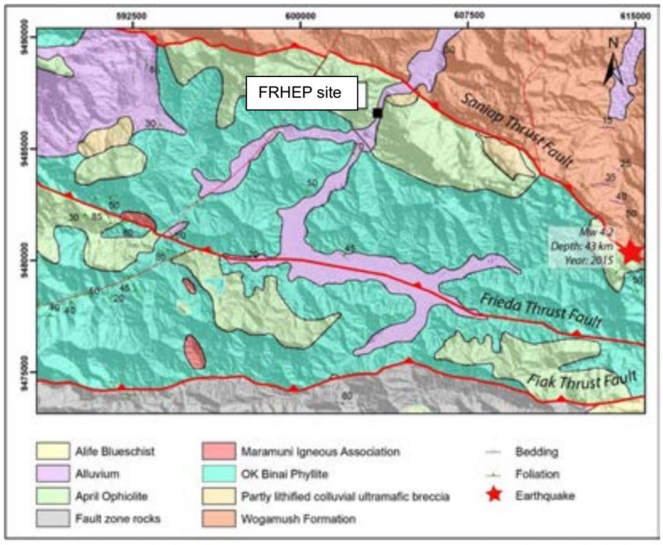

Figure 6: Main geology within the ISF, 60-80% of the base formation comprises liquefiable soils and alluviums/colluviums up to tens of meters thick (Coffey, 2019).

3.1.2 *Seismic hazard*

The Global Seismic Hazard Assessment Program (GSHAP) identifies the area of the Frieda River ISF as a Moderate hazard with peak ground accelerations (PGAs) between 1.6 m/s^2 and 2.4 m/s^2. Figure 7 shows seismic hazard grading for the Southwest Pacific region, with the Frieda River project location and ISF shown. Some of the largest tailings dams in areas classed as High hazard are located in South America in arid environments. The Frieda River ISF embankment is designed for PGA of up to 10.69 m/s^2 with an operational PGA of 3.8 m/s^2. Analyses of a series of dam break scenarios were conducted to arrive at these PGAs.

However, in February 2018 a Magnitude 7.5 earthquake with ground acceleration of 3.2 g or 31.39 m/s^2 was registered (USGS, 2018) with the epicentre located roughly 200 km southeast of the Frieda River project site. Ground failures resulting from the tremor were reported at the Ok Tedi mine, located about 210 km from the epicentre. In May 2016 a Magnitude 7.9 earthquake, with epicentre located only tens of kilometres from Lihir mine (USGS 2016), sent tsunami waves into Lihir Island causing the mine to temporarily halt operation as a precautionary measure. In 2010 a Magnitude 7.1 earthquake within the proximity of the Hidden Valley mine (USGS, 2010) caused the mine to suspend mining for a day to stocktake for damages. Mines in PNG are prone to earthquakes with Magnitudes greater than 7.0 with PGAs potentially greater than the operating PGA of a mine infrastructure. All mines generally take precautionary measures when large earthquakes occur within their proximity.

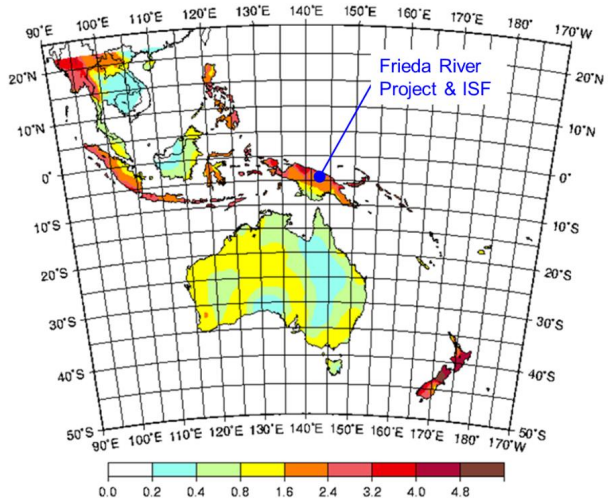

Figure 7: Global Seismic Hazard of the Southwest Pacific region (http://static.seismo.ethz.ch/gshap/swpacific).

3.1.3 *Rainfall*

The Frieda River ISF will be located in one of the wettest places on earth. It will experience an average rainfall of 8,000 mm annually. In terms of wettest tailings dams worldwide the current record is 4,000 mm in Hidden Valley mine, also in Papua New Guinea. If the Frieda ISF comes into operation then it will hold the record of being the wettest mine waste and tailings dam infrastructure in the world.

The risk culminating from rainfall cannot be underestimated. Flooding, erosion and sedimentation resulting from heavy rainfalls will undermine the safety of the ISF. The recent changes in global weather patterns has seen frequent occurrence of prolonged wet and dry seasons in PNG. Historical weather patterns of the last 50 to 100 years are no longer reliable. The impact of which need to be studied thoroughly. The year-long drought experienced in PNG between 2015 and 2016 led to the suspension of the massive Ok Tedi mine, when the reliable Fly River turned into dry sandy banks, grounding barges from transporting ore and supplies to and from the mine. A drought is a likely scenario and is obviously a significant risk to the ISF. Lowering of the water level at the ISF will risk exposing the toxic mine waste to oxidization. Hydro-power generation would also be interrupted.

3.2 *Structural risks*

3.2.1 *Design standard for the embankment*

The embankment is the key component of the ISF. The designers of the 191 m high and 550 m wide embankment consulted a number of respected standards for dam embankment design including ICOLD, ANCOLD, CDA and USACE. There are no specific Standards for Dams in Papua New Guinea. The design consultants only consulted the relevant environmental regulations concerning such a facility. Although these reputable standards are applicable for water dams, combing with toxic mine waste storage is difficult.

The facility is one of the first of its kind. It will also be one of the largest in the southern hemisphere and located in harsh environment. Benchmarking the Frieda River ISF was made very difficult because there exists no similar infrastructure. The consultants benchmarked the infrastructure separately against tailings and against water dams. At 191 m it will be the 6th tallest tailings dam in the world. In comparison to asphalt core rockfill water dams the Frieda River ISF dam will be the tallest. It's capability to serve dual purpose remains indeterminate.

3.2.2 *Design factor of safety*
The design factor of safety (FOS) for the ISF embankment was based on ANCOLD (2012) minimum FOS guidelines, where FOS of 1.5 is used for long-term drained conditions and 1.2 for post-seismic conditions. The FOS however, does not necessarily correlate to risk and consequences. Therefore, it cannot be assumed that the probability of failure is low with higher FOS or vice versa. It is a factor that is dependent on the uncertainty in the inputs. The designers and investigators of the Frieda River ISF have highlighted the need for further "ground-truthing" to improve the reliability of the inputs (SRK Consulting Australasia, 2018).

The consequence or severity class assigned to the Frieda River ISF based on ANCOLD (2012) classification is based on the consequence of a failure. Reducing the severity of consequences will require schemes to counter, control and limit the impact.

3.2.3 *Seismic tolerance*
Seismicity is a major risk to the ISF. The ISF is designed to withstand ground accelerations of up to 1.09 g or 10.69 m/s^2, assuming that an earthquake is initiated by one of the thrust faults located within the footprint of the ISF resulting in maximum ground acceleration. The operating basis earthquake (OBE) peak ground acceleration for the ISF is pegged at 3.8 m/s^2. However, the recent 2018 Magnitude 7.5 earthquake with epicenter located 200 km southeast from the Frieda River project site registered a peak ground acceleration of 3.2 g or 31.39 m/s^2. Thus, this serves as a warning that, an earthquake with Magnitude 7.0 or greater, generating PGAs greater 1.0 g, with the risk of exceeding design PGA range of the ISF can be expected.

Furthermore, it appears that the designers of the ISF missed to consider the risk of reservoir-induced seismicity. The potential for the reservoir to induce slip along the thrust faults located within the footprint of the ISF is realistically a genuine risk.

3.2.4 *Tolerance to underwater landslip*
Underwater landslip is noted as highly likely scenario by the design consultants. The ISF footprint is covered with evidences of local and regional landslips, both fresh and old. Analyses and simulations of landslips during and after reservoir filling has been limited. The consultants alluded to the limited evaluations to lack of sufficient data from the entire ISF footprint. They have recommended "ground-truthing' investigations, using for example high resolution LiDAR (e.g. 1 m resolution). The current landslip studies intended to support the design of the embankment were principally conceptual based on the limited data. The tolerance of the infrastructure in the event of an underwater landslip requires further study.

3.2.5 *Uncertainty of the unknown*
Uncertainty of the unknown remains a source of great fear among the stakeholders. No one knows exactly what the real magnitude of the consequence will be in the event of ISF failure, except the fact that it will be catastrophic. This scenario has left many observers to doubt the feasibility of the concept. It will require scientifically based studies to prove its viability or development of a comprehensive crises management plan and possibly auxiliary facilities to reduce the impact in the event of failure.

4 DISCUSSIONS

PanAust, the current owner of the Frieda River copper-gold project, is quite keen to get the project rolling and has therefore submitted the Environmental Impact Assessment (EIS) reports and other supporting documents to Papua New Guinea's environmental and mining authorities for review and approval. However, the participating stakeholders are quite adamant and are pursuing their own independent assessments of the design concept of the ISF and the environment consequences of such an infrastructure. Their assessments will be submitted to the Conservation and Environmental Protection Authority (CEPA) which will be taken into consideration during the review of the company's (PanAust) application for the development of the infrastructure.

Meanwhile, the review team engaged by the East Provincial Government, a stakeholder who will be greatly affected by the negative consequences of the ISF, observed that, even though the risk of a dam failure is probably low, the severity of the consequences is too great. Efforts need to be made to reduce the severity or the impact in case of failure.

Papua New Guineans are very knowledgeable about the impacts of mine waste and tailings on their environments. Many who live within mining areas have been directly exposed to mine

waste contaminated riverine and marine systems. In the last decade or so the government has attempted to find ways to encourage miners to better manage their mine wastes. Emphasis is now on tailings dam being a pre-requisite for mine development, unless specific circumstances forbid. This led to the first official tailings dam in the country that was built at the Hidden Valley mine in Morobe Province. Current mineral developers are encouraged to follow suit as is the Frieda River copper-gold project

However, the increasing frequency of tailings dam disasters world-wide is not an encouraging scenario for Papua New Guinea. Nevertheless, it is bringing about major discussions among government authorities and mineral resource developers on the subject. Some discussions center on whether or not mine wastes should be classed in the same manner as radio-active nuclear wastes. After-all, mine waste can also be highly toxic with potentially devastating consequences. The Chairman of BHP-Billiton, Mr. Andrew Mackenzie, recently made a brave statement that, "*it is about time the tailings classification be raised to the same standards as radio-active nuclear waste*" (Financial Times, Feb. 2020). This could be a start to very important step towards the safety of tailings dams.

5 CONCLUSIONS

The Frieda ISF is an interesting concept for managing waste management in very difficult environment. It may have a future in Papua New Guinea if it is advanced with sound engineering and scientifically researched basis.

The safety of the site that will host an infrastructure such as the Frieda River ISF is very important. The question in this regard is, whether the site is safe enough to host such an infrastructure. The review reveals that, there are significant representative data gaps within the ISF footprint, which requires detailed site investigation to prove its reliability to host the infrastructure.

The next item related to the safety of the ISF is its structural integrity. This depends on the design and analyses methodologies, and guiding standards used in the design. The design of ISF was based on international standards such as the ICOLD. However, the most obvious observation is the uncertainty in the design inputs. The designers of the ISF have admitted the lack of sufficient and quality data for the entire footprint of the ISF. This poses a significant risk to the structural integrity of the infrastructure.

Despite the above scenarios, the designers of the ISF believe they have produced a design that has a low probability of failure, after performing a series of back engineering analyses based on extreme conditions of dam break. However, the consequences in the event of a failure is still the highest. The ISF is categorized as 'Extreme Catastrophic' according to ICOLD classification. Which means thorough efforts are needed to investigate options to minimize the severity of the consequence.

The Frieda River ISF and any similar infrastructure in PNG will have to overcome some of the most difficult and challenging climatic and topographic conditions. Further still they must be able to overcome the hazardous seismic conditions. If the Frieda River ISF ever gets built it will be ranked as one of the largest tailings and water dam in one of the most difficult and geo-environmentally hostile places on earth. Since there exists no such infrastructure as the Frieda River ISF presently anywhere in the world benchmarking it is difficult. However, it is the only way forward if PNG ever wants to manage mine waste in a responsible way rather than allowing them to be disposed directly into natural marine and riverine systems.

6 ACKNOWELDGEMENT

The authors wish to acknowledge the East Sepik Provincial Government for sponsoring the review of the Frieda River Project Environment Impact Assessment, which includes the Integrated Storage Facility (ISF). Specific mention to Hon. Governor Mr. Alan Bird who advocated for the independent reviews, and his provincial administrators; Dr. Clement Malau (Provincial Administrator) and Mr. Godfried Rahuasem (Executive Director Technical Services) who facilitated the review work. Frieda River Limited (subsidiary of PanAust) provided site logistics during field visit.

7 REFERENCES

Australian National Committee On Large Dams (ANCOLD). 2012. Guidelines on the Consequence Categories for Dams.

Brooks, J.A. 1963. Earthquake activity and seismic risks in Papua & New Guinea. Commonwealth of Australia. Bureau of Mineral Resources, Geology and Geophysics, Record no. 1963/162.

Coffey. 2019. Frieda River Sepik Development Project Environmental Impact Assessment- Appendix 2A.

Chopra A.K and Chakrabarti P. 1973. *The Koyna Earthquake and the Damage to Koyna Dam*. Bulletin of Seismological Society of America. Vol. 63, No.2, pp. 381-397.

Douglas and Partners. 2009. Frieda River Extended Scoping Study.

Global Seismic Hazard Assessment Program. 2020. (http://static.seismo.ethz.ch/gshap/swpacific). Citation June 2020.

do Carmo F.F., Kamino L.H.Y., Tobias Jr. R., de Campos I.C., do Carmo F.F., Silvino G., de Castro, do.S.X., Mauro, M.L, Rodrigues N.U.A., Miranda M.P. de S and Pinto C.E.F. 2017. *Fundão tailings dam failures: the environment tragedy of the largest technological disaster of Brazilian mining in global context.* Perspectives in Ecology and Conservation 15 (2017) 145-151

Financial Times. 2020. https://www.ft.com/content/aa236fbe-33ea-11e9-bd3a-8b2a211d90d5. Citation February 2020.

IFC. 2012. Guidance notes: performance standards on social and environmental sustainability. International Finance Corporation, Washington, USA.

Niuminco Group. 2020. http://www.niuminco.com.au/. Citation June 2020.

PNG Report. 2020. https://www.pngreport.com/mining/news/1388845/permitting-goes-on-at-frieda-river. Citation June 2020.

SRK Consulting Australasia. 2019. Frieda River Hydroelectric Project Selection Phase Study. Environmental Impact Assessment Appendix 2b.

SRK Consulting Australasia. 2018. Frieda River Hydroelectric Project Dam Break Analysis. Frieda River Limited.

USGS. 2020. https://earthquake.usgs.gov/earthquakes/eventpage/us7000aq3e/executive. Citation June 2020.

Nano Meso Inorganic Technology: Bind & Contain RCRA 8 Metals & Stabilize Mine Tailings

Authors:
T.J. Brammer, Pro-SealCorp, Phoenix, AZ, USA
M.A. Stone, PSP Labs, Kirkland, WA, USA

Contributors:
Dr. J. Lee University of Arizona, Tucson, Arizona, USA
USACE Tests and Criteria, USA, Dr. West, National Labs

ABSTRACT: Nano meso inorganic polymers technology versus Portland cement and geopolymers tailings stabilization and toxic leachate containment. Goal: stop failures that create serious environmental impact, safety, and stakeholder concerns. Determine containment of RCRA 8 metals. Comparing polymer's structural values for earthen berms and ponds. Comparing absorptive properties relating to stability and toxic leachate binding containment of earthen structures.

Testing performed to determine what currently available technology binds leachates, increase hydrophobic and structural integrity. Tests performed using Portland cement, geo-polymer's, and nano technology as tailings additives. Tests undertaken; Atterberg, ASTM and TCLP test criterion. Some tests modified to accurately fit field environments.

Tests determine liquid limits, flow limits, plasticity, water absorption, compressive strengths, liquefaction, and leachate restriction.

Tests results differed: Portland cement; low compressive strengths and hydrophilic properties. Geopolymer's; higher compressive strengths and increased leaching. Nano meso inorganic polymers; higher compressive strengths, strong hydrophobic properties and substantial leachate binding properties, binding below EPA TCLP limits for seven of the RCRA 8 metals. Eighth RCRA 8 metal was not determined to be present in the tailings tested.

1.0 INTRODUCTION

Presenting nano technology accomplishing significant stabilization of tailings soils while substantially prohibiting leaching RCRA 8 metals and toxic leachates. Comparing nano technology to existing stabilization/containment technologies. Different materials have been used to stabilize mine fines, clay, toxic and natural tailings. Studies have been performed of geopolymers, including Portland cement to condense and tighten tailings soil masses to stable condition (Tchadjie, Ranjbar, et al 2015). Such materials have limited success as marked by increasing numbers of berm failures seen today (Chambers 2015 Mount Polley 2014, Sanmarco 2015). Berm and dam failures more than doubled in the last 15 years (Chambers 2015). Nano meso inorganic polymers Novel properties, peculiar to nano and sub nano scale, are directly compared to more common Vander Waal properties of Portland cement and other geopolymer's results recorded herein (Asta et al 2007). This technology addresses safety, environmental preservation, property loss, and economic loss issues in mining.

2.0 ATTERBERG TESTING

2.1 *Objective, Preparation and Method*

Objective: Tests were performed to determine liquid limit, plastic limit, and shrinkage of soils.
Tests were performed under the Atterberg testing criteria, using New York Department of Transportation method tables (modified).
Specimens prepared as follows: Dry Specimens ten each of 5 pairs, in groups: natural dry soil, Portland cement and nano meso inorganic polymers with ≤16% moisture content and ten each wet specimen's, in paired groups, with >16% minimum plus 4% moisture content. Save control natural tailings soils, dry specimens receive 5% additive and wet specimens receive 6% additives. Specimens include equal numbers of paired CH soils and CL Soils.
Methods: Using a mechanical Liquid Limit device specimen are placed per test requirements on device. Soil in the cup was divided equally by a firm stroke so that a clean, sharp groove of the proper dimensions was formed. We lift and drop the cup turning the crank at the rate of 2 revolutions per second, until two halves of the sample flowed together and came in contact at the bottom groove along a-distance-of ½ in. The blow range was ≥15 - 35 to pass. Plastic Limit determined , 6 each 1.3 g masses rolled to 3 mm threads, crushed, rerolled to reform threads of 3mm or failure.

2.2 *Results, control soils – Atterberg tables averaged results NY DOT (modified), Table 1, following page*

Table 1. Atterberg Limits soils test results recorded.

Tailings Soil Type	Moisture Content	Additive	Additive %	Paired Sets	Average Blows Acceptable Minimium	< > % Change	Avgerage Liquid Limit %	Avgerage Plastic Limit %	Average Plastic index %
CH	16%	Control	0	5	21	<40%	39	31	8
CL	16%	Control	0	5	23	<34%	40	32	8
CH	16%	Portland cement	5	5	77	>55%	18	17	1
CL	16%	Portland cement	5	5	78	>55%	18	17	1
CH	16%	Nanocrete	5	5	100	>65%	17	18	-1
CL	16%	Nanocrete	5	5	100	>65%	17	18	-1
CH	> 16%	Portland cement	6	5	67	>48%	16	15	1
CL	> 16%	Portland cement	6	5	67	>48%	17	16	1
CH	> 16%	XWCrete	6	5	100	>65%	15	16	-1
CL	> 16%	XWCrete	6	5	100	>65%	16	17	-1

Table 1, above, demonstrates treated samples, all mediums, are non-plastic (NP). This test measurement is modified to determine the percent variance of the plasticity between the additives. A complete set of these documents is available in a white paper (Brammer, Stone 2019).

2.3 *Results and Discussion*

This test section determined differences between soil tailings types CH and CL and same soils mixed under dry and wet conditions with Portland cement additive and Nano meso inorganic polymer additives for stabilization purposes.
CL and CH soil specimens with Portland cement additives or Nano meso inorganic polymer additives met or exceeded liquid limit ranges. The plastic limit for both additives met the criteria. Determinations: CH and CL soils with Portland cement, while stiffening, have slight positive Plastic Index, indicating mix has hydrophilic properties, this is consistent with Portland cement properties. CH and CL soils dry and wet, with Nano meso inorganic polymer additives, have slightly negative Plastic Index numbers, indicating structural rigidity and non-shrink properties.
Natural soil's Types CH and CL performed as depicted in Table 1, as controls. Performance observed clear contrasting qualities of additives, under given criteria. Portland cement additives and Nano meso inorganic polymer additives achieved positive congealing while densifying mass. Portland cement performed as would be expected according to the many studies of that material.
Nano meso inorganic polymers perform differently than the Portland cement stabilization process. This is due to its rapidity of cure and nano particle size differential compared to Portland

cements slower exothermic cure. Nano meso inorganic polymers contain particles of ≤ one nano. Decreased particle size allows the polymer access to greater surface area affording more reactive bonding surface area and far more tightly packed and bonded masses (Bhagyaraj 2018).

3.0 COMPRESSIVE STRENGTH TESTS (modified) – ASTM C39

3.1 *Objective, Preparation and Method*

Objective: Compressive strength tests, as modified, were performed to determine value variances between standards.

Specimens are prepared as follows: CH and CL soils moisture contents both at ≤16% moisture content nominal and >16% moisture content (minimum increase is plus 4% moisture). Nano meso inorganic polymer and Portland cement additives added to soils separately. They are added at 5% for dry soils and 6% for wet soils, sample cylinders prepared per ASTM C39 (American Standard Test Methods, Army Corps of Engineers) at 50 psi compression (Brammer, Stone 2019 white paper). Dry specimens twenty-one each in groups: natural dry soil, Portland cement and nano meso inorganic polymers with ≤16% moisture content and twenty-one each wet specimen's, by group, with >16% minimum plus 4% moisture content. Except for control natural tailings soils, dry specimens receive 5% additive and wet specimens receive 6% additives, ASTM C39.

Methods: Samples are placed in a Forney FX-250T compression Testing machine, compresses per ASTM C39 guidelines and the results were averaged by group.

3.2 *Results CH soils (CL soils, not shown, demonstrated the same result ratios)*

Compressive Strength Tests type CH tailings soil, tests observed ASTM C39 Tables 2 and 3, below. For more details see (Brammer, Stone 2019 white paper).

Table 2. Compressive Strength test Portland cement vs Nano meso inorganic polymer, dry soil.

Condition	Tailings Type Soil	Moisture Content	Additive	Topical Spray Post Mix	Dry Additive%	Additive Volume /ml	PSI Day 3	PSI Day 7	PSI Day 28
	CH 1	≤16%	Portland cement		5		231	290	416
			Water			To plasticity			
	CH 2	≤16%	Portland cement		5		231	319	450
			Water			To plasticity			
			Bed ROC			177			
Dry Soils ≤ 16% Moisture Content	CH 3	≤16%	Portland Cement		5		243	330	495
			Water			To plasticity			
			Bed ROC			177	279	270	1302
				TopROC		15			
			NanoCrete		5		276	631	1281
			BedROC			177			
			NanoCrete		5				
			BedROC			177			
				TopROC		15			

Rate of Loading calculations, Tables 2, above, Table 3, following page, apply to all compressive strength tailings test. Nominal Sample Diameter Stress Rate Load Rates: 35± 7 psi/sec 3 in., 250 ± 50 lbs./sec 4 in., 440 ± 90 lbs./sec 6 in., 900 ± 200 lbs./sec 8 in. Load is applied continuously until the sample fails and displays a well-defined fracture pattern. As calculated, Nano meso technology, in dry soil condition, averaged 62 % greater compressive strength over Portland cement and 58 % greater compressive strength in wet soils conditions.

Table 3. Compressive Strength test Portland cement vs Nano meso inorganic polymer, wet soil.

Condition	Tailings Soil Type	Moisture Content	Additive	Topical Spray Post Mix	Dry Additive %	Additive Volume / ml	PSI Day 3	PSI Day 7	PSI Day 28
	CH 1	>16%	Portland cement		6		229	270	399
			Water			to plasticity			
	CH 2	>16%	Portland cement		6		231	282	412
			BedROC			177			
			Water			to plasticity			
Wet Soils 16% + Minimum 4% Moisture content	CH 3	>16%	Portland cement		6		232	226	479
			BedROC			177			
			Water			to plasticity			
				TopROC		15			
		>16%	XWCrete		6		269	589	1098
			BedROC			177			
		>16%	XWCrete		6		278	599	1133
			BedROC o			177			
			Water			to plasticity			
				TopROC		15			

3.3 *Results and Discussions*

Nano meso inorganic polymer additives soil achieved greater compressive strengths than Portland cement additive soils under both dry and wet soil conditions.

Nano meso inorganic polymers demonstrated more than two times greater compressive strength than Portland cement, Tables 2 and 3, above. Portland cement granules are far larger disallowing the compaction density and the number of stereoisomers coordinated connections afforded by the nano sized particles in the Nano meso inorganic materials. Portland cement bond strength is less due to large particle size and less available reactive surface area afford by typical Van der Waal attractions compared to the Novel properties reactive surface area due to nano and sub nano particles sizes.

3.4 *Section Conclusion*

Compressive strength testing compares additive strengths of treated soils for earthen structures such as berms and roads. Nano meso inorganic polymers demonstrate increased strengthening in earthen applications when compared to Portland cement, Tables 2 and 3, previous page. Nano meso inorganic polymer technology influenced masses are significantly denser due to particle screen line gradient, nano and sub-nano sizes. Nano particles, $\leq$1bn m^3, allow access to greatly increased reactive surface area, facilitating inorganic structured stereoisomers the opportunity of ligand bonding reactions via ionization, coordination, and linkage (Pilkington PhD 2002).

4.0 ABSOPRTION TEST, ANIONIC, HYDROPHOBIC, OR HYDROPHILIC; NANO MESO INORGANIC POLYMERS COMPARED TO PORTLAND CEMENT AND GEOPOLYMER

4.1 *Objective, Preparation and Method*

Objective: Determine rate of absorption of water by mine tailings mixed with stabilizing additives.

Specimens prepared as follows: Nano meso inorganic polymers or Portland cement additives, mixed with soils, Table 4, below, then compression cast and applied in unconfined application, Figure 1, below. Test specimens prepared per ASTM 2C31/6 31m and C42/6 42m making and curing specimens (American Standard Test Methods, Army Corps of Engineers), Figure 1, below.

Method: Measures increase in mass of specimens resulting from absorption of water as a function of time. Only one surface of a specimen is exposed to water. Exposed surface of specimen is immersed in water. Water ingress, of unsaturated specimens, is dominated by capillary suction during initial contact with water per C642 Absorption and Density, C1005 Determining Mass (American Standard Test Methods, Army Corps of Engineers), Figure 1, Following page.

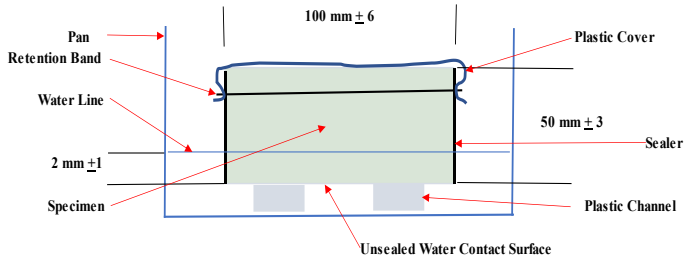

Figure 1. Water Absorption mechanism for ASTM 642 Water Absorption tests.

Table 4. Absorption specimens defined.

	Description	Condition	Soil Type	Moisture Content %	Additives	% Added	Number of specimens
ASTM C 642	Natural soil Dry	Dry	CH	16	Portland cement	5	3
	Natural soil Dry	Dry	CL	16	Portland cement	5	3
	Natural soil Dry	Dry	CH	16	NanoCrete	5	3
	Natural soil Dry	Dry	CL	16	NanoCrete	5	3
	Natural soil Dry	wet	CH	> 16 + 4% minimum	Portland cement	6	3
	Natural soil Dry	wet	CL	> 16 + 4% minimum	Portland cement	6	3
	Natural soil Dry	wet	CH	> 16 + 4% minimum	NanoCrete	6	3
	Natural soil Dry	wet	CL	> 16 + 4% minimum	NanoCrete	6	3

4.2 *Results Recorded*

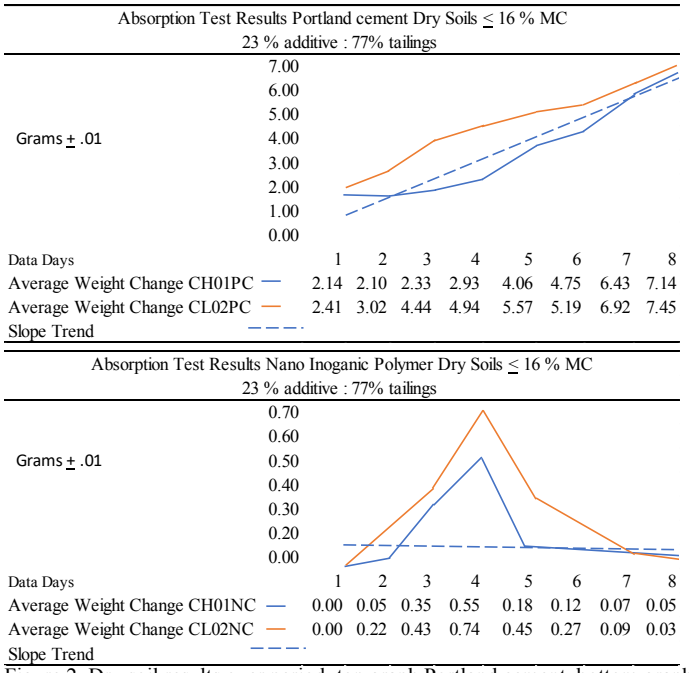

Figure 2. Dry soil results over period, top graph Portland cement, bottom graph Meso inorganic polymer.

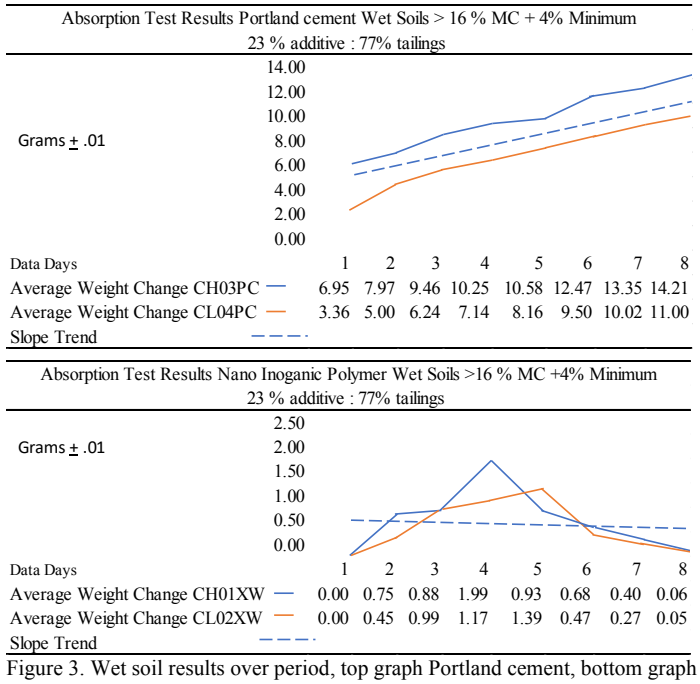

Figure 3. Wet soil results over period, top graph Portland cement, bottom graph Meso inorganic polymer.

Figure 2, previous page, Portland cement additive specimen's CH01PC, CL02PC soils, averaged water uptake results recorded. Nano meso inorganic polymer additive specimen's CH01NC and CL02NC soils, water uptake results recorded.

Portland cement specimens are dry soil ≤16% moisture content. Dry specimen's CH01PC and CL02PC contain 5% Portland cement additive. These Portland cement specimens averaged a gain of 14 grams of water over the test period on rising slope trend.

Nano meso inorganic polymer (NanoCrete) specimens are dry soil ≤16% moisture content. Specimens CH01NC and CL02NC contain 5% Nano meso inorganic polymer additive. Nano meso inorganic polymer specimens averaged a gain of .74 grams of water through day 4 of the test period, then rejected water, at end of test water is reduced to .05 grams on a declining slope trend.

Figure 3, above, Portland cement additive specimen's CH03PC and CL04PC soils, averaged water uptake results recorded. Nano meso inorganic polymer additive specimen's CH 01XW and CL02XW soils, averaged water uptake results recorded.

Portland cement specimens are wet soil >16% plus 4% minimum moisture content. Specimens CH03PC and CL04PC contain 6% Portland cement additive. Portland cement specimens gained an average of 14 grams of water over the test period on a rising slope.

Nano meso inorganic polymer (XWCrete) specimens, wet soil, >16% plus 4% minimum moisture content. Specimens CH01XW, CL02XW contain 6% Nano meso inorganic X polymer additive. Nano meso inorganic polymer specimens gained an average of 1.99 grams of water through CH01XW day 4, CL02XW day 5, then rejected water, at test end water is reduced to .06 grams on a declining slope.

4.3 *Submersion Test Custom, Long Term 72 Months*

4.31 Objective, *Preparation and Method*

Objective: Determine the failure point over time of soils mixed with additives exposed to long term submersion in water.

Specimens prepared as follows: Two each nano meso inorganic polymer, Portland cement and Geopolymer are mixed and compresses into spheres weighing 113 grams, at a ratio of 23% additive to 80% tailings soil and then placed in water in sealed vessels numbered 1 through 6.

Method: Specimens are fully submerged in pH 7.3 tap water to failure or a maximum of 72 months in a sealed vessel. Specimen were drawn from the sealed vessels once every 120 days and visually observed. Once every 12 months ± 15 days specimens were removed from vessel, weighed observations and average results by type are recorded in Table 5, below.

Table 5. Results recorded.

	All Specimens 23% Additive Submersion Test Customised 72 Months						
					Water /Specimen Sphere Condition		
Specime type	Nano meso inorganic polymer	Portland cement	Geopolymer	All Medium pH 7.3	Nano meso inorganic polymer	Portland cement	Geopolymer
Avg Wt g 2 specimens each	113	113	113				
Longest fail date 2 specimens		1.06.2018	01.12.2016				
Start Date	01.06.2014	01.06.2014	01.06.2014				
12 Month Average Weight g	113	126	197	Water	Clear	Minor Debris	Milky
24 Month Average Weight g	113	158	0.0-failed	same water	Minor Debris	Heavy Debris	Heavy Debris
36 Month Average Weight g	114	189		same water	No Change	Leachate on Sphere/ Muddy	Mud Final Sphere Failed
48 Month Average Weight g	114	0.0 - failed		same water	No Change	Sphere Soft Water Muddy	
60 Month Average Weight g	114			same water	No Change	Mud Final Sphere Desolved / Failed	
72 Month Average Weight g	114			same water	No change		

Geopolymer gained significant weight in first 24 months, failed on or before 24 months. Portland cement steadily gained water weight year on year for 48 months, failed at or before 48 months. Nano meso inorganic polymer gained 1 gram in month 36, no change and no failure experienced by month 72, Table 5, previous page.

Figure 4. Nano meso inorganic polymer treated soil as observed after 72-month submersion test: no softening of surface, no cracking, no material debris in water, no material breakdown of mass of paired samples 5 and 6, pictured above.

4.4 *Results and Discussion*

Absorption tests measures and graphs water absorption or desorption rate and ascending or descending slope trends over an eight-day period. Tests demonstrate differences in water absorption or desorption rates when comparing Portland cement and Geopolymers to Nano meso inorganic technology additives in tailings. Soil with Nano meso inorganic polymer additives clearly demonstrate hydrophobic properties of the structured negative ion field created by the coordinated stereoisomer formations. The Nano meso inorganic polymer additive soils take on water during the cure and as the mass tightens water is expelled, as the last water is expelled anionic/hydrophobic properties of the mass are completed. The mass once cured is then essentially waterproof. Nano meso inorganic polymers exhibited descending slope trends or desorption.

Portland cement is absorptive, making it susceptible to shrinkage, freeze-thaw, and carbonation, breaking it down, these Portland cement properties are commonly known. Portland cement additive expressed rising slope water gains/absorption trends.

Submersion test: two each specimen spheres of Nano meso inorganic polymer, Portland cement and geopolymer were fully submerged for 72 months. Water weight gain was averaged for each test group and results recorded in table 5, above. Geopolymer specimens failed on or before month 24, Portland cement specimens failed on or before month 48, Nano meso inorganic polymer specimens demonstrated no material change over the 72 months of the full submersion test. Anionic/hydrophobic behavior is due to the peculiar Novel properties created by the nano and sub nano size particle in the gradient of the masses screen line.

4.5 *Section Conclusions*

Portland cement, known to be absorptive, specimens failed in submersion at ≤48 months due to water egress. Indicating unknown wetting climate impacts may create sudden unquantifiable wetting, allowing chemical reactions, and weight gain of structure by incident and/or over time. Suggesting Portland cement stabilization format, initially appearing to have positive properties, has a limited period of positive outcome.

Geopolymers, known to be absorptive, specimens failed in submersion due to water egress in a short ≤24 months.

Nano meso inorganic polymers demonstrate hydrophobic/anionic behavior, reject water from mass no material change in 72 months. Previous test results herein, Nano meso inorganic polymers demonstrate significant increased strength. Submersion test of Nano meso inorganic polymer treated soils indicate stabilizing with Nano meso inorganic polymers stop water egress. The hydrophobic/anionic properties created are due to nano and sub-nano scale peculiar to Novel properties. Hydrophobic properties allow near to no water into mass. Basic chemistry principle: No water gained in mass, no creation of corrosives in mass. If no corrosives are created, mass will not breakdown from chemical reactions. If no water is gained; no liquefaction is possible. This characteristic is due to the minute particle sizes in the matrix of Nano meso inorganic polymers, the increased available reactive surface area allows for far more stereoisomer ligands, connectors and links within a given mass (Lian 2020).

5.0 TOXIC LEACHATE BINDING CONTAINMENT PROPERTIES COMPARED

5.1 *Objective, Preparation and Method*

Objective: Demonstrate overall containment binding and leaching properties of Nano meso inorganic polymerizing containment technology compared to Portland cement and Geopolymers. Determine if Nano meso inorganic polymers are a viable toxic soils containment technology. If so, to demonstrate binding containment in measurable results. Special attention is paid to the RCRA 8 (Resource Conservation and Recovery Act, 8 metals).

Specimens prepared as follows: Bricks of control soils and soils each with separate additive are fabricated; bricks are approximately 8 cm X 16 cm X 8 cm, using 50% natural soils, Geopolymer, Portland cement, and 22% Nano meso inorganic polymer as a stabilizing medium. All specimens are cured to full cure.

Method: Control tailings soils were leach tested, (TCLP protocols US Environmental Protection Agency), in plain tap water, pH7, tumbled for 18 hours and samples were drawn, then subjected to Inductive Coupled Plasma (ICP) analysis.

Geopolymer (modified TCLP) specimens were placed in plain tap water, pH 7, specimens were tumbled for 18 hours, specimens were tested and then the results measured over seven days, every 24 hours. Samples were drawn, then subjected to Inductive Coupled Plasma (ICP) analysis.

Portland cement (standard TCLP) tailings from an iron ore mine and one tailing material from a copper mine were used to fabricate small Bricks were cured to full cure. Specimens were tested for pH and then placed in acetic acid ratio 100g soil:2000ml acetic acid, pH 3.4. Samples were then tumbled for 18 hours to simulate in ground saturation. Test period 72 hours. Samples were drawn, then subjected to Inductive Coupled Plasma (ICP) analysis.

Nano meso inorganic polymer bricks were tumbled for 18 hours. Test period was thirty days, treated specimens were placed in a solution of DI water and sulfuric acid, solution pH3. Samples were drawn and results measured, every 24 hours for 30 days. Samples subjected to Inductive Coupled Plasma (ICP) analysis.

Nano meso inorganic polymer binder was tested by a modified TCLP process created by Dr. J Lee of the University of Arizona. His test methodology is extremely aggressive, reflecting actual harsh mine site conditions. Tailings from an iron ore mine and one tailing material from a copper mine were used. hours. This extreme measure was performed to replicate field environment conditions, in comparison to the standard TCLP test of 72 hours.

5.2 *Results recorded*

Geopolymer treated iron and copper tailings leachate results in parts per million (ppm). Two tailings materials bricks were submerged in plain tap water, pH7, for seven days, solution filtered to separate matter from solution, solution was then subjected to Inductive Coupled Plasma (ICP) analysis, tested for content. Results in Table 4, below.

Table 4. Geopolymers treated tailings tested for content in parts per million.

Tailings	ICP-EOS Analysis Leach Results From Geopolymerized Mine Tailings, Tumbled and Submerged in Plain Tap Water, pH 7												
Type	In ppm	Na	Mg	Al	K	Ca	V	Cr	Mn	Fe	Ni	Cu	Zn	As
FE A	LW1	1,625.45	6.812	1.12	5.84	25.1	0.036	0.055	0.005	0.194	0.002	0.036	0.03	0.37
CU B	LW 2	2,793.95	1.698	1.16	6.81	20.9	0.81	0.029	0.011	0.075	0.001	0.038	0.03	0.546

Mix Ratio: Estimated; > 50% geopolymer by volume: < 50% mine tailings. Table 4, above, displays the results indicating: 1.65 -2.79 g/l of sodium concentration derived of NAOH (sodium hydroxide), 1.66 g a higher copper and 1.67 g higher arsenic concentration. While geopolymer material significantly stabilized mass, leaching rate was increased over natural leachate patterns of soils, in plain tap water with pH7.

Portland cement two tailings material bricks, 1 Fe and 1 Cu created, samples solution are drawn, filtered separating matter from solution, subjected to Inductive Coupled Plasma (ICP) analysis. Results in Table 5, below.

Table 5. Portland cement treated tailings tested for content in parts per million.

Tailings	ICP-EOS Analysis Leach Results From Portland cement polymerizd Mine Tailings Tumbled and Submerged Acidic Acid Solution, pH 3.4												
Type	In ppm	Na	Mg	Al	K	Ca	V	Cr	Mn	Fe	Ni	Cu	Zn	As
FE A	LW1	1650.98	7.39	1.598	6.234	26.89	0.0415	0.02	0.02	0.711	1.27	0.035	6.42	0.265
CU B	LW 2	2791.21	2.21	1.792	7.186	22.07	0.902	0.043	0.025	0.093	1.09	0.073	5.47	0.499

Mix ratio 50% Portland cement by volume: 50% mine tailings. Table 5, above, displays results:1.65 -2.79 g/l of sodium NAOH (sodium hydroxide), increased calcium from additives content, increased leaching due to absorptive, hydrophilic properties.

Nano meso inorganic polymers two tailings material bricks created, 1 Fe and 1 Cu. Samples were drawn, solution filtered separating matter from solution, subjected to Inductive Coupled Plasma (ICP) analysis. Procedure repeated every 24 hours for 30 days. results in Table 6, below.

Table 6, following page, mix ratio: 22% Nano meso inorganic polymers by volume to 78% mine tailings by volume. 1.65 -2.79 g/l of sodium concentration from NAOH (sodium hydroxide), increased calcium due to additives calcium content, decreased over all leaching due to desorption/hydrophobic properties. More particle surface area is accessible due to nano and sub nano particles affording greater stereoisomeric ligands formations of material.

Table 6. Nano meso inorganic treated tailings tested for content in parts per million.

Tailings	ICP-EOS Analysis Leach Results From Nanocrete, Nano technology polymerized Mine Tailings Submerged in DI Water sufuric Acid Solution, pH												
Type	In ppm	Na	Mg	Al	K	Ca	V	Cr	Mn	Fe	Ni	Cu	Zn	As
FE	A LW1	616.11	<.1	<.1	43.5	0.03	<.1	<.5	<.2	<.1	<.1	<.1	<.1	<.05
CU	B LW 2	514.4	<.1	<.1	47.1	0.03	<.1	<.5	<.1	<.1	<.1	<.1	<.1	<.05

6.0 EPA ALLOWABLE LIMITS AND CONTROL SOILS BASE LINE

This section represent known published Environmental Protection Agency (EPA) allowable limits of metals named in tables (Secondary Drinking Water Standards Tables) (EPA Water Maximum Contaminant Level's, MCL's) (Hazardous Waste Screening Criteria for ground water, waste soils and TCLP limits). RCRA 8 metals Table 7, below, expresses allowable limits (Research Conservation and Recovery Act 2020, Environmental Protection Agency.

Table 7. EPA allowable standards.

		EPA Tailings Leachates Allowable Standards							
RCRA 8 metals	Units	AG	AS	Ba	Cd	Cr	Hg	Pb	Se
Common Range Natural Soils	mg/kg	0.6	50;1-40[10]	100-3,000[10]	.01-70,000	5-3,000	.01-30	2.0-200	.10-20
Hazardous Waste Screening Criteria (TCLP)	mg/kg	100.00	100.00	2,000.00	20.00	100.00	4.00	100.00	20.00
TCLP Hazardous Waste Limits Water	mg/L	5.00	500.00	100.00	1.00	5.00	0.20	5.00	1.00

Ag (silver), As (arsenic), Ba (barium), Cd (cadmium), Cr (chromium), Hg (mercury), Pb (lead), and Se (selenium)

In this test section we measure and record RCRA8 metal results. The control tailing soils, partial record, in ppm and recorded in Tables 8 and 9, below. Tailings types from iron (Fe) and copper (Cu) mines are tested under standard TCLP protocols. Soils are tested for pH and mixed with acetic acid ratio 100g soil:2000ml acetic acid. Samples are tumbled for 18 hours to simulate in-ground-saturation. Samples are drawn from tumbler, filtered separating matter from solution, then subjected to Inductive Coupled Plasma (ICP) analysis, tested for content.

6.1 *Recorded Results*

Tailings bricks were removed from tumblers,1 Fe and 1 Cu, solution filtered to separate matter from solution, samples were drawn, subjected to Inductive Coupled Plasma (ICP) analysis. Results in Table 8 and 9, following.

Table 8. Fe tailings and treated tailing tested for RCRA 8 metals content in parts per million, results.

Tailings Type		ICP-EOS Analysis Leach Results From Nanocrete, Nano technology polymerized Fe Tailings							
	In ppm	Ag	As	Ba	Cd	Cr	Hg	Pb	Se
Fe	Raw Tailings	1.00	1.32	100.10	0.11	2.10	0.00	2.30	1.20
Fe	w/ Nano meso inorganic polymerization	<.10	<.50	<.10	<.10	0.50	0.00	<.10	<.10
% Change		90%	62%	100%	9%	76%	N/A	96%	92%
Change +/-		+	+	+	+	+	N/A	+	+

Ag (silver), As(arsenic), Ba (barium), Cd (cadmium), Cr (chromium), Hg (mercury), Pb (lead), and Se (selenium)

Table 9. Cu tailings and treated tailing tested for RCRA 8 metals content in parts per million, results.

Tailings Type		ICP-EOS Analysis Leach Results From Nanocrete, Nano technology polymerized Cu Tailings							
	In ppm	Ag	As	Ba	Cd	Cr	Hg	Pb	Se
Cu	Raw Tailings	1.28	1.24	89.23	0.18	1.78	0.00	1.97	1.10
Cu	w/ Nano meso inorganic polymerization	<.10	<.50	<.10	<.10	0.50	0.00	<.10	<.10
% Change		92%	60%	100%	44%	72%	N/A	95%	91%
Change +/-		+	+	+	+	+	N/A	+	+

Ag (silver), As(arsenic), Ba (barium), Cd (cadmium), Cr (chromium), Hg (mercury), Pb (lead), and Se (selenium)

6.2 *Nano meso inorganic polymer results, in parts per million*

Tailings bricks were removed from tumblers; 1 each Fe and 1 each Cu, solution filtered to separate matter from solution, samples were drawn, subjected to Inductive Coupled Plasma (ICP) analysis. Results in Table 10, next page.

Table 10. Fe tailings results tested for RCRA 8 metals contents in parts per billion.

Tailings Type		ICP-EOS Analysis Leach Results From Nanocrete, Nano technology polymerized Fe Tailings							
	In ppb	Ag	As	Ba	Cd	Cr	Hg	Pb	Se
Fe	Raw Tailings	1.00	1.32	100.10	0.11	2.10	0.00	2.30	1.20
Fe	w/ Nano meso inorganic polymerization	0.0140	0.0500	0.0330	0.0100	0.0068	0.0000	0.0150	0.0020
% Change		99%	96%	100%	91%	100%	N/A	99%	100%
Change +/-		+	+	+	+	+	N/A	+	+

Ag (silver), As(arsenic), Ba (barium), Cd (cadmium), Cr (chromium), Hg (mercury), Pb (lead), and Se (selenium)

Mix ratio: 22% Nano meso inorganic polymers with Nano-polymers by volume: 78% mine iron (Fe) tailings by volume, for both Tables 18 and 19, previous page.

6.3 *Results and Discussion*

Nano meso inorganic binding, stabilizing, polymer treated tailings recorded a significant reduction of leachate over original raw tailings leachate volumes. Tests demonstrate Nano meso inorganic polymers, at two times less additive in the mix, allowed thousands-of-times less leachate than Portland cement or Geopolymers. All leachate containment results for Nano meso inorganic polymer treated tailings soils are equal to or are far below TCLP leachate containment limits. The increased leaching result in geopolymers, fly ash, lime and Portland cement are due to the corrosives created in wet soils breaking down the polymerization. Nano and sub nano particle size creates tighter compaction, greater surface area for bonds is accessed creating more bonding sites. Nano polymers hydrophobic properties disallow water hydration of mass. Once the mass is cured the restriction of available water disallows basic chemical exchanges occurring in the presence of water, that create corrosive properties from certain minerals or bio-mass decomposition in the soil, that break down polymer bonds.

6.4 *Section Conclusion*

Nano meso inorganic polymers create a dense, stable mass, desorption properties, stop osmotic flow and corrosive agent development. Nano meso inorganic polymers significantly halt leaching and enhanced binding properties due to increased accessible surface area, multiplying stereoisomeric reactions available due to nano and sub nano particle sizes. Increased bonding surface from Novel properties, demonstrate probable structured coordinated linking relationships to metals, as all seven tested RCRA 8 metals, are leached at or below EPA allowable levels.

7.0 PAPER RESULTS AND DISCUSSION

Comparative Atterberg tests demonstrate Nano meso inorganic polymers and Portland cement have similar Liquid Limit characteristics. Testing indicates Nano meso inorganic polymer in both dry and wet soils are more ridged than Portland cement. Both materials passed test criteria.

Nano meso inorganic technology under ASTM C39 compressive strength criteria develops 58% to 64% greater compressive strength than Portland cement. Results determine Nano meso inorganic polymer is more structural in earthen environments than Portland cement.

Under ASTM C 64 absorption criteria, Nano meso inorganic polymers gained no material grams of water revealing a negative declining graphed slope, under both dry soil and wet soil criteria, indicating hydrophobic properties. Portland cement gained significant grams of water in both dry soils and wet soils. Portland cements ascending positive graphed slopes indicates it is hydrophilic.

Long-term full water submersion test demonstrates Geopolymers fail rapidly $\leq$ 24 months with a mild alternating exposure to water and atmosphere. Portland cement failed in $\leq$ 48 months under this same criterion. Nano meso inorganic polymers demonstrated no material change over the 72-month same test criterion. It can be determined by these results Nano meso inorganic polymer technology rejects water while Portland cement and geopolymers absorb water gaining water weight.

Under stated standard TCLP (acidic acid pH 3.4, 72 hours) criteria Portland cement allowed significant leaching and slightly promoted leaching over control soils. Under modified TCLP criterion (leached in tap water, pH 7.3) Geopolymers promoted leaching greater than control soils results. Nano meso inorganic polymers under modified TCLP (sulfuric acid pH 3.0, 30 days) significantly contained all leachates. Results demonstrate differences in leaching properties of each technology. Nano meso inorganic polymers under more extreme testing criterion reduced or contained leachates; Portland cement and geopolymer under far less harsh criterion promoted leaching. Nano meso inorganic polymers contained seven of tested RCRA 8 metals. Differences in performance is explained by Nano meso inorganic polymers use of Novel properties versus Portland cement and Geopolymer use of less robust Ver der Waal forces. The peculiar Novel properties are due to nano and sub nano particle sizes. Nano and sub nano scale have access to far greater reactive surface area in earthen mass. They incorporate three inorganic isomer properties: ionization, coordination, and linkage enhancing the potential for more stereoisomer reactions, stacking negative ions, coordinating greater numbers of ligands, developing more linkages. Figure 4, below, illustrates Van der Waal forces known to be the attraction properties of Portland cement and geopolymer technology compared to Novel properties of Nano meso inorganic polymers.

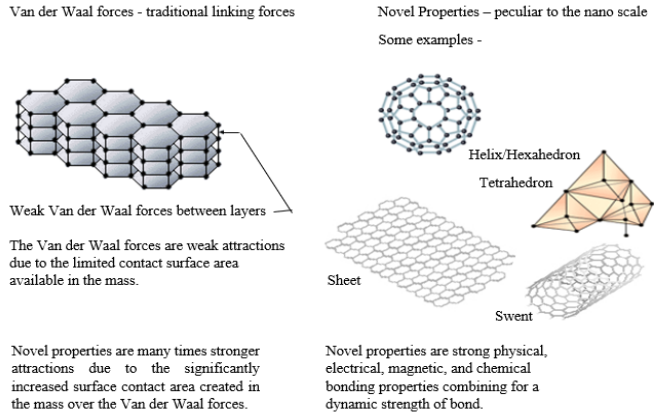

Figure 4. The attraction properties defined.

Novel properties strengthen attraction forces via structuring ability of isomers and greatly increased surface area access afforded from nano and sub nano particle sizes. Increased surface area access offers many more isomer potential ionized, coordinated, and linked ligand sites. Offering a myriad of isomer configuration possibilities, see figures 5 and 6, below.

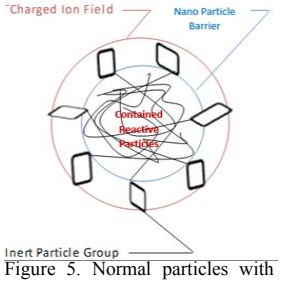

Figure 5. Normal particles with naturalized ion fields.

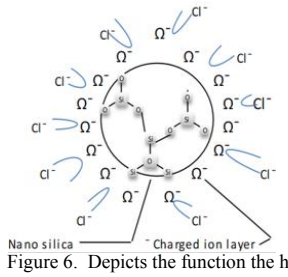

Figure 6. Depicts the function the hydrophobic/anionic barrier.

Particles are freely able to exchange ions with other normalized particles ions, such as high or low pH materials effecting the leching properties, Figure 5. Hydrophobic/anionic barrier's repel aggressive reactive ions, creating a strong anionic barrier between normalized particles to prevent ion exchange, Figure 6.

8.0 REPORT CONCLUSION

New Nano meso inorganic polymer technologies stabilization/toxic leachate binding materials substantially increase stability of tailings mass. Portland cement and geopolymer treated tailings absorb water, gain weight, create greater potential for reactive destabilization and liquefaction as commonly occurs in tailings.

Demonstrated leaching of toxics in Nano meso inorganic technology treated tailings soils is suppressed to far greater levels than Portland cement, Geopolymers or other known current technology. Seven of the eight RCRA 8 metals tested have been determined to be contained by Nano meso inorganic polymerization at or below EPA acceptable levels. The eighth metal (Mercury) has not yet been tested. Portland cement and Geopolymers increased the promotion of leaching. Nano meso inorganic technology substantially contains the other soil leachates to acceptable levels.

As with all technology, there is potential for greater improvements. Nano meso inorganic polymers, testing demonstrates, are currently developed to important viable, performance levels. Nano meso inorganic polymers stabilize tailings soils to a greater degree than that of known current technology. Significant reduction of berm failures is achievable. Conclusion: Nano meso inorganic polymers significantly contain leachates, resulting in protection of ground water, greater bio-habitat, creating an environment positive impact, reducing environmental damage to benefit humanity.

REFERENCES

Abdoulaye A. & et al 2018. Stability of a new geopolymer grout: Rheological and mechanical performances of metakaolin-fly ash binary mixtures *Construction and Building Materials* Volume 18: 420-436.

Abdullah M.M.A.B. & et al. 2014. Characterization of Soils as Potential Raw Materials for Soil Stabilization Application Using Geopolymerization Method *Department of Interior:* 135-143.

Asta M et al 2020. Inorganic Nano Particles – Unique properties and Novel Applications *Millipore Sigma, Material Matters* Volume 2 Issue 1.

ASTM 2C31/6 31m and ASTM C42/6 42m. *Making and Curing Specimens American Standard Test Methods* Manual.

ASTM C39 .Compressive Strength, *American Standard Test Methods* Manual.
ASTM C642. Absorption and Density, *Strength American Standard Test Methods* Manual.
ASTM C1005. Determining Mass, *American Standard Test Methods* Manual.
Atterberg A 1911. Atterberg Limits, *Geotechniqe* Volume 3 Issue 1.
Bhagyaraj SN 2018. *Synthesis of Inorganic Nano Material, Nano Technology*; Science of the Invisible. Cambridge: Woodhead Publishing. Chapter 1:1-18.
Brammer T & Stone J 2019. Mine Tailing, Soils Stabilization and Toxic Tailings Leachate Containment Properties Nano Tech Additives Versus Portland Cement and Geopolymer Additives *White Paper*.
Chambers D 2015. Long Term Risk of Tailings Dam Failures, *National Park Service Series Alaska Park Science* Volume 13 Issue 2, Mineral and Energy Development.
EPA Water maximum Containment levels, *Environmental Protection Agency*.
EPA RCRA 8, , Research Conservation and Recovery Act, *Environmental Protection Agency*.
EPA TCLP, Toxicity Characteristic Leaching Procedure, *Environmental Protection Agency*
Kumar D et al 2018. *Synthesis of Inorganic Nano Material;* Quantum Nanostructures. Cambridge: Woodhead Publishing. Chapter 3: 59 - 88.
Pilkington M 2002. Principals of Inorganic Chemistry *Lecture.*
Shiding *M*. Ph.D. & et al. 2017. Stabilization of Highly Expansive Black Cotton Soils by Means of Geopolymerization *Journal of materials and Civil engineering* Volume 29 Issue 10.
Tchadjié L.N. & et al. 2015. Potential of using granite waste as raw material for geopolymer synthesis, *Ceramics International* Volume 42 Issue 2.
Thankachan RM 2018. *Synthesis of Inorganic Nano Material*; Synthesis strategies of Single-Phase and Composite MultiFerroic Nanostructures. Cambridge: Woodhead Publishing. Chapter 8: 185 – 211.
Yan-Jun D. & et al. 2017. Physical, Hydraulic, and Mechanical Properties of Clayey Soil Stabilized by Lightweight Alkali Activated Slag Geopolymer *Journal of Materials and Civil Engineering* Volume 29, Issue 10.
Lien X, PhD 2020. Novel Properties of Chiral Inorganic Nanostructures *Nano Today* Volume 3.

Geochemical and Hydrological Lags and Impact on Covers on PAG Mine Wastes

David J. Williams
The University of Queensland, Brisbane, Queensland, Australia

ABSTRACT: Sulfidic waste rock and tailings have, with the passage of time, the potential to generate acid and metalliferous drainage (AMD). This occurs on oxidation when the wastes are exposed to the atmosphere, any acid neutralizing capacity present in the wastes or process water has been exhausted, and the transport of the oxidation products by rainfall runoff and/or infiltration, or by groundwater. Waste rock typically emerges from an open pit relatively dry and when conventionally end-dumped in a surface waste rock dump has ready access to atmospheric oxygen, allowing the oxidation of any sulfidic minerals. The transport of any oxidation products occurs once the dump has wet-up sufficiently to produce seepage. Tailings are typically in slurry form, and if the surface of the tailings is allowed to desiccate, exposed sulfidic tailings can undergo oxidation. The oxidation products can then be mobilized by the deposition of fresh tailings, or by rainfall runoff and/or infiltration, or by seepage to the foundation or through the containment. The purpose of covers over potentially acid generating (PAG) mine wastes is to minimize the ingress of oxygen into the wastes and/or minimize transport of any AMD via the net percolation of rainfall into the wastes. The appropriate choice and effectiveness of covers is a function of the climatic settings, the mine wastes, and the management of the wastes.

1 INTRODUCTION

All too often, the observance of AMD takes sites by surprise. Initially, it is absent, while some years after the start of mining and processing it appears, both from surface waste rock dumps and from tailings storage facilities. There is a number of reasons for this.

For conventional surface waste rock dumps, formed by end-dumping, there will likely be a period of time before contaminated interstitial water forms within the dump – the "geochemical lag". During this period, any neutralizing capacity will ameliorate any acidity production, although neutral drainage may still form. Further, the acidity reaction will tend to continue during the dry season, while the alkalinity reaction will be subdued during this season. Hence, once the dump is producing seepage, the "first flush" at the start of the wet season will be most acidic and contaminated with dissolved metals, and the quality of any seepage will tend to improve as the wet season progresses. The same pattern is followed in subsequent seasonal wetting and drying cycles. The initially relatively dry waste rock must first wet up sufficiently to release water – the "hydrological lag". The initiation of seepage from the dump will initially require a substantial rainfall event, while lesser rainfall events are required to generate seepage once the dump has wet-up.

For conventional surface tailings storage facilities, involving slurry tailings deposition, there will also likely be a period of time before contaminated interstitial water forms, since the near-saturated tailings must first desaturate to allow any oxidation – the "hydrological lag", which

comes first. Desaturation of the tailings will commence from the surface once it becomes exposed, and the extent and depth of oxidation will be a function of the climate and season, the water and air permeability of the tailings, and the duration of exposure before fresh tailings slurry is placed or re-wetting due to rainfall occurs. There will also likely be a period of time before contaminated interstitial water forms within the tailings – the "geochemical lag". During this period, any neutralizing capacity will ameliorate any acidity production, although neutral drainage may still form.

The geochemical and hydrological processes of surface waste rock dumps and surface tailings storage facilities are discussed in the following sections. This is followed by discussion covers over potentially contaminating mine wastes to minimize the ingress of oxygen and/or the net percolation of rainfall. Then follows a discussion of the effectiveness of covers over mine wastes in addressing the AMD geochemical and hydrological lags.

2 SURFACE WASTE ROCK DUMPS

Surface waste rock dumps are typically constructed by end-dumping from a tip-head, which results in the characteristic structure shown schematically in Figure 1 (after Herasymuik et al. 1995). The structure comprises a base rubble zone formed by the raveling of boulders to the base of the dump, and discontinuous, alternating coarse- and fine-grained layers of waste rock at the angle of repose of the material of typically 35° for weathered rock to 40° for fresh rock. The top layer of the dump becomes broken down and compacted by haul truck traffic. The base rubble zone allows unhindered ingress of air and readily drains if wet-up. The coarse-grained angle of repose layers serve mainly as oxygen pathways, and the fine-grained layers store both air and water. If the top of the dump is compacted by loaded haul trucks this will inhibit both air flow and rainfall infiltration.

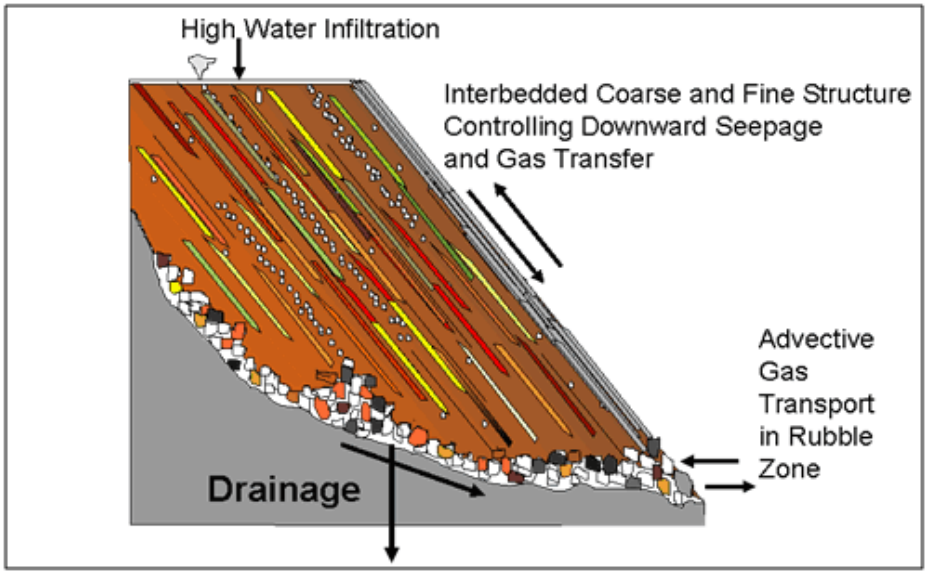

Figure 1. Schematic of end-dumped waste rock (after Herasymuik et al. 1995).

2.1 *Oxidation process*

The oxidation of an end-dumped waste rock dump comprising sulfidic materials is promoted by the ready supply of oxygen via advection into the base rubble zone shown in Figure 1. Oxygen then readily flows up the coarse-grained angle of repose layers by convection and is available to

the adjacent fine-grained angle of repose layers via slower diffusion. Oxygen diffusion can also occur through the traffic-compacted top layer and the face of the dump. The fine-grained waste rock presents the highest surface area per unit volume and hence is responsible for the greatest generation of any acidity. Being an exothermic reaction, oxidation generates heat, and the fine-grained angle of repose layers become the hottest. Excessive heat generation can lead to spontaneous combustion.

2.2 *Wetting-up of dump*

Williams (2006) described the physical characteristics of typical weathered and fresh waste rock in a dump, and the evolution of their moisture state as they are wet-up by rainfall infiltration over time. Weathered waste rock is typically dominated by about 50% gravel-sized particles (2 to 60 mm in size), with a smaller proportion of sand-sized particles (0.06 to 2 mm in size), cobble-sized particles (60 to 200 mm in size) and boulders (larger than 200 mm in size), and minor fines (silt and clay-sized particles finer than 0.06 mm). A typical median particle size for weathered waste would be less than 5 mm. As the material weathers further, the gradation becomes finer. Fresh waste rock has perhaps 40% cobble and boulder-sized particles, perhaps 40% gravel-sized particles, and the remainder mainly sand-sized. A typical median particle size for fresh waste rock would be about 50 mm.

Incident rainfall readily infiltrates a waste rock dump. A proportion of the rainfall infiltration will go into storage within the voids in the dump, with any excess infiltrating further into the dump, ultimately causing seepage into the foundation and/or emerging at the toe. Due to its very low hydraulic conductivity, the initially dry waste rock will store infiltration from light rainfall events, and a high waste rock dump of relatively dry material may be capable of storing considerable infiltration without significant breakthrough. The wetting front will progress through the dump as the ability of the waste rock pores to store water is exceeded, this occurring well below the fully saturated state, since the waste rock will have achieved a sufficiently high hydraulic conductivity to pass further rainfall infiltration.

Williams (2006) applied unsaturated soil mechanics principles to estimate the wetting-up due to rainfall infiltration of a waste rock dump, leading to seepage reaching the base of the dump. Williams estimated, for a weathered waste rock dump, that once the degree of saturation of the pore space within the dump reached about 60% the rate of seepage would approach the rate of rainfall infiltration. For a fresh waste rock dump, only 25% saturation was required. The time taken to achieve this "continuum breakthrough" of seepage is a function of the height of the dump, the degree of weathering of the waste rock, and the climate.

Williams (2008) produced a chart to estimate the time for the start and fully-developed continuum breakthrough of seepage as a function of dump height and average annual rainfall for a weathered waste rock dump, which is reproduced as Figure 2. For a fresh waste rock dump, continuum breakthrough would occur in about 40% of the time it takes for a weathered waste rock dump.

Rohde et al. (2011) monitored the seepage reporting to the base of a 15 m high trial waste rock dump at Cadia Mine, which demonstrated that continuum breakthrough peaked after about 4 years at only 5% of cumulative rainfall (totalling about 3,000 mm) beneath the traffic-compacted top of the dump and at only 10% beneath the angle of repose side slopes of the dump. This implies that the proportion of rainfall that infiltrated into the dump was relatively low at about 22%, with the majority going to storage within the dump. The waste rock wet-up to an estimated 43% saturation beneath the top of the dump and 56% saturation beneath the side slopes over the 4-year monitoring period. The average hydraulic conductivities beneath the top and sides of the dump were calculated to be 3×10^{-6} m/s and 6×10^{-6} m/s, respectively.

Depending on the hydraulic conductivity of the foundation beneath a dump, only a small proportion of the seepage (perhaps as low as 0.1% of rainfall) would emerge at topographic low points around the toe of the dump. If an effective low net percolation cover is achieved over a dump at closure, water stored within the dump would draw down within a similar amount of time to that required to reach full continuum breakthrough. A less effective cover would delay this, and the dump would be subject to re-wetting by extreme rainfall events. The progressive encapsulation of sulfidic waste rock during the mine life could accommodate both the geochemical and hydrological lags.

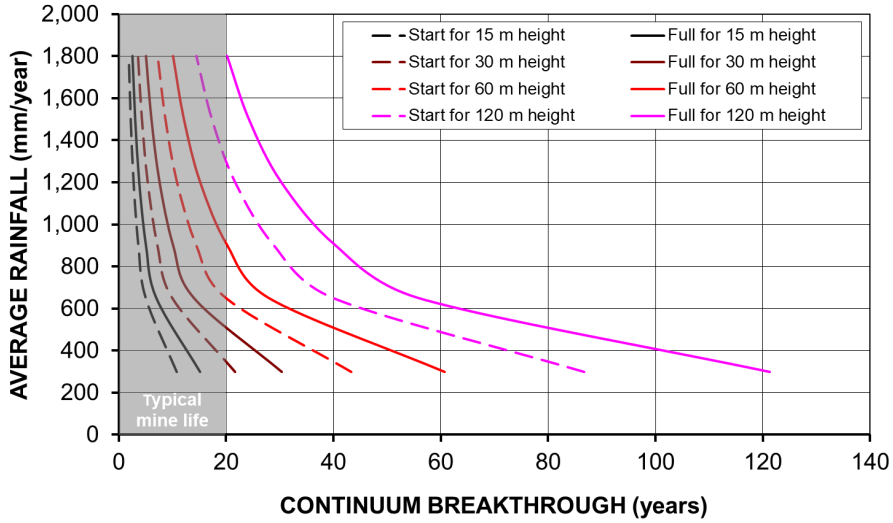

Figure 2. Estimated time for start of and fully-developed continuum breakthrough of seepage as a function of dump height and average annual rainfall for a weathered waste rock dump (after Williams, 2008).

3 SURFACE TAILINGS STORAGE FACILITIES

Tailings are typically deposited in a surface storage facility as a slurry, forming a shallow beach (with a typical average slope of the order of 1%) and a decant pond at the end of the beach, from which process water can be recovered if it is suitable for re-use. On beaching, the tailings will sort hydraulically according to their particle size and specific gravity, with coarser-grained and heavier particles settling on the upper part of the beach and finer-grained and lighter particles flowing towards the pond. Suspended tailings will settle and consolidate under their self-weight, reducing the hydraulic conductivity.

The majority of the water (perhaps 75%) that does not remain entrained within the tailings will drain to the surface as the tailings settle and consolidate. Tailings will also likely generate seepage to the foundation and through the tailings dam, limited by their saturated hydraulic conductivity, which will diminish as the tailings consolidate. Evaporation takes place from the decant pond, and from wet tailings on exposure of the tailings beach to sun and wind, accompanied by desaturation.

3.1 *Desaturation of exposed tailings*

Williams (2007) described the physical characteristics of typical tailings, and the evolution of their moisture state as they may be subjected to periodic desiccation and are wet-up by fresh tailings and rainfall. Tailings are typically dominated by about 50% silt-sized particles, with the remainder sand and clay-sized (finer than 0.002 mm). A typical median particle size for tailings would be less than 0.06 mm.

Williams (2007) applied unsaturated soil mechanics principles to estimate the desiccation of exposed tailings. The formation of a desiccated crust will dramatically reduce the hydraulic conductivity of the tailings and dramatically reduce the continuation of desaturation at depth. The desaturation profile will diminish exponentially with depth and typically be limited to a depth of less than about 600 mm. As the tailings desaturate, seepage rates will reduce, as will evaporation rates from the surface. The deposition of fresh tailings or rainfall will inundate the drying tailings and re-saturate them, commencing from any desiccation cracks that form. Re-wetting will recharge downward seepage and evaporation from the surface.

3.2 *Oxidation process*

As exposed tailings desaturate, they will become exposed to atmospheric oxygen via slow diffusion, and sulfidic tailings will start to oxidize. However, since the depth and extent of desiccation is limited by the reducing hydraulic conductivity of the drying tailings, the extent of oxygen ingress and hence oxidation is also limited. If the degree of saturation remains above 80 to 85%, oxidation will be limited. Any oxidation products can be delivered to the foundation and toe of the tailings dam by ongoing seepage, while oxidation products and sediments at the surface may be transported by fresh tailings and rainfall runoff, potentially overtopping a spillway if one is provided.

3.3 *Hardpan development*

Agnew (1998) investigated the natural formation of tailings hardpans as possible inhibitors of AMD, contaminant release and dusting. Agnew found that the effectiveness of hardpans in inhibiting acid generation is dependent on their reducing oxygen diffusion and rainfall infiltration into the tailings, while maintaining long-term erosional stability. A reduction in rainfall infiltration will diminish the potential seepage of contaminants. The low permeability of the hardpan will also inhibit upward flow and hence the uptake of salts into an overlying growth medium. The mineralogy, morphology, lateral extent, depth (typically less than 100 mm, but diminishing with depth) and rate of formation (typically 6 to 12 months, but at a diminishing rate with time) of hardpans is dictated by the sulfide mineralogy and content of the tailings, their particle size distribution, the method of deposition of the tailings, and the climate. Hardpans can have a hydraulic conductivity 10 to 100 times lower than that of uncemented tailings causing them to maintain high saturation, and an oxygen diffusion rate up to 1,000 times lower.

Liu et al. (2018 and 2019) found that iron-rich cemented hardpans over sulfidic copper-lead-zinc tailings were critical in immobilizing zinc and lead via mineral passivation and encapsulation, and supporting native vegetation under semi-arid conditions.

4 COVERS ON POTENTIALLY CONTAMINATING MINE WASTES

The choice of cover on potentially contaminating mine wastes is largely a function of the climate; in particular, wet, net positive water balance or humid, and net negative water balance or evaporative. Guidance on the choice of cover and cover design are given in the following two sections based on the GARD Guide (2009), with consideration of covers with capillary barrier effects discussed in the following section.

4.1 *Choice of cover based on climate*

Guidance on the choice of cover type for PAG mine wastes for different climatic settings is provided by the GARD Guide (2009), as reproduced in Figure 3. The role of covers on PAG mine wastes is to: (i) limit oxygen ingress, and/or (ii) limit net percolation of rainfall. As soil covers are difficult to construct and remain effective on dump slopes, the recommended cover types only apply to the tops or benches of waste rock dumps, implying that no PAG waste rock should be placed beneath the side slopes unless a horizontal seal can be constructed over the PAG waste rock. Tailings beaches, being relatively flat, can readily be covered.

In a wet climate, a water cover could be effective in limiting exposure to oxygen, although it should be maintained to limit any oxidation of the mine wastes. For waste rock, this would only be possible by disposal in-pit or in tailings slurry, maintained permanently under water. For tailings, sub-aqueous slurry disposal would be required. A water cover depth of 2 m is recommended, to avoid exposure of the tailings by wind-induced wave-action. Further, there must be sufficient recharge to maintain the water cover and a spillway to discharge excess water and maintain the stability of the dam, which would be required in perpetuity. Even the gentle slope of a tailings beach would likely require a series of terraced ponds, with separating dams. These would be difficult to construct retrospectively on deposited tailings and their stability may not be assured in perpetuity, resulting in water covers over tailings going out of favor, even at sites where the topography and rainfall support them.

In a humid or seasonally wet climate a water-shedding cover is recommended, to limit rainfall infiltration and hence the generation of acidic seepage. In a dry climate, a store and release cover is recommended, to limit net percolation of rainfall and hence the generation of acidic seepage.

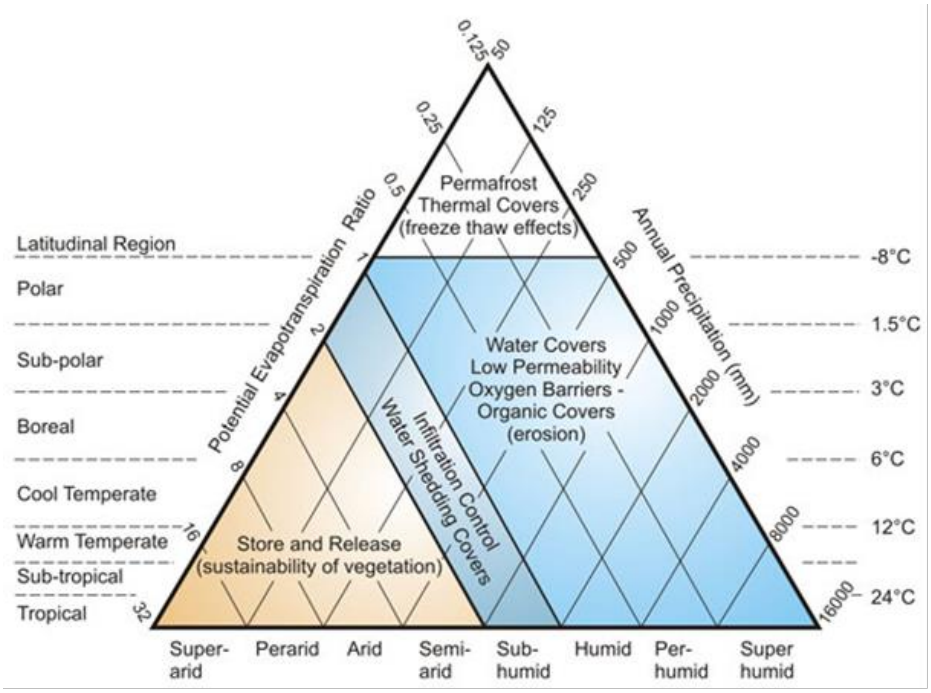

Figure 3. Covers and climate types (after GARD Guide, 2009).

4.2 *Schematics of soil cover designs*

The GARD Guide (2009) also provides schematics of soil cover designs, reproduced in Figure 4, which increase in complexity, construction difficulties, potential performance and cost from left to right. These schematics have generated much confusion, particularly in Australia. Cover I, indicating a thicker single-layer of growth medium than the Base Case, is inferred to be "better" than the base case. However, thicker is not necessarily better. A thick "native material or barren waste or oxidized waste" layer intended to serve as a growth medium can lead to the infiltration of rainfall to a depth that makes it inaccessible to revegetation. This can also lead to increased net percolation into the underlying waste rock or tailings, and hence the generation of acidic seepage. The net result may be worse than having no cover at all, since the cover would constitute a "sponge" that would increase rainfall infiltration compared with a traffic-compacted waste rock dump top or a desiccated tailings surface.

Cover II adds a capillary barrier (or break) beneath the growth medium, which may be desirable to limit the uptake of salts from the underlying waste rock or tailings into the growth medium. A capillary barrier must be carefully selected and sized to ensure that it is effective and will remain so. Suitable capillary barriers may include clean gravel and clean sand. Run-of-mine waste rock would likely not be suitable for use as a capillary barrier, without crushing of coarse-grained particles and screening to remove fines.

Capillary rise dictates that clean gravel would require a thickness of greater than 300 mm to remain effective as a barrier, while a clean sand would require a thickness in excess of 1 m. The capillary barrier must allow for the possible infiltration of fines from the overlying growth medium, which would render it ineffective over time. The particle size of the capillary barrier

must be matched to that of the overlying growth medium, using filter criteria to ensure that the infiltration of fines into the capillary barrier is limited.

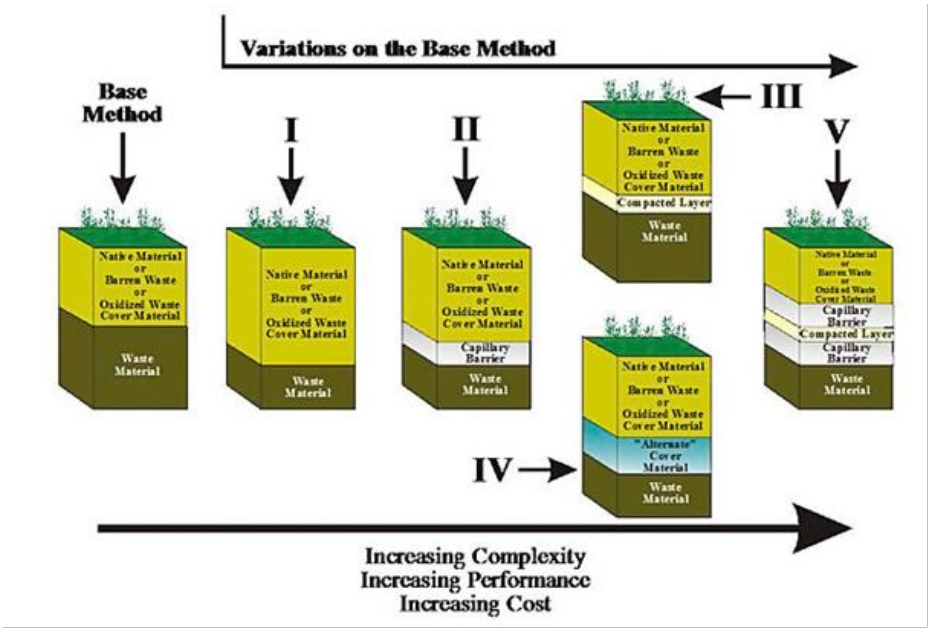

Figure 4. Sample soil cover designs (after GARD Guide, 2009).

Cover III adds a compacted (clayey) layer beneath the growth medium, which is desirable, particularly for a store and release cover to "hold-up" rainfall infiltration within the overlying "rocky soil mulch" layer. Cover IV is a variation on Cover III, in which the compacted layer is replaced by an "alternative" sealing layer, such as a geomembrane, bituminous geomembrane, or geosynthetic clay liner (GCL). A seal could also potentially be achieved by heavily compacting the top of a waste rock dump by loaded haul trucks, or due the development of a hardpan on sulfidic tailings, or by compaction of the tailings surface.

Cover V incorporates three layers separating the growth medium from the waste rock or tailings, comprising a compacted layer sandwiched between two capillary barriers. The intent of such a "double capillary barrier" is difficult to understand. If it were to provide greater surety that a capillary barrier would limit the uptake of salts into the overlying growth medium due to evapotranspiration, a single, thicker capillary barrier would likely be more effective. If a sealing layer is required, this would best be placed between the capillary barrier and the waste rock or tailings, or possibly above the capillary barrier. Cover type V is very uncommon.

The two most common cover types applied to potentially contaminating mine wastes are: (i) rainfall-shedding or barrier covers and, (ii) store and release covers (Williams et al. 1997 and 2006), as shown schematically in Figure 5. Rainfall-shedding covers were developed for landfills, partly to limit the net percolation of rainfall into the potentially contaminating landfill, but also to accommodate the inevitable large total and differential settlements of the landfill. The key element of a rainfall-shedding cover is a sealing layer, comprising compacted clayey soil, a geomembrane or GCL, or a composite, which is overlain by a growth medium. Rainfall-shedding covers are applied in wet or humid climates, in which a substantial vegetative cover can be established and sustained to limit erosion. The growth medium has a store and release function, supplied by the wet or humid climate, supporting revegetation.

The key elements of a store and release cover, developed for seasonal, dry climates are: (i) a thick loose "rocky soil mulch" layer with an undulating surface to store the wet season rainfall without inducing runoff, (ii) an effective sealing layer at the base of the cover to "hold-up" rainfall

infiltration, and (iii) the appropriate choice of sustainable revegetation to release the stored rainfall during the wet season, through evapotranspiration. The required thickness of rocky soil mulch will depend on the wet season rainfall pattern and the rooting depth of the vegetative cover, and is typically 1 to 2 m. Too thick a growth medium could lead to rainfall infiltration beyond the reach of the revegetation. In a dry climate, store and release covers are more robust than rainfall-shedding covers.

The sealing layer should achieve a saturated hydraulic conductivity of less than 10^{-8} m/s (equivalent to a potential percolation rate of less than 300 mm/year, when water is available), so that in its usual unsaturated state in a dry climate its hydraulic conductivity will be less than perhaps 10^{-10} m/s (a potential percolation rate of less than 3 mm/year). In Australia's typically dry climate, rainfall occurs about 30 days/year, so that water may be available on top of the sealing layer for perhaps 10% of the time, reducing the potential percolation rate to less than 30 mm/year, or less than 5% of the typical average annual rainfall, similar to the typical natural percolation rate. High net percolation will be associated mainly with extreme rainfall events. The cover should cycle annually between wet and dry states without a net wetting up (which would lead to net percolation) or drying out (which would cause revegetation die-back and subsequent rainfall-induced erosion). An extreme rainfall event may wet-up the cover, potentially leading to breakthrough into the underlying mine wastes.

In Australia's generally arid to semi-arid climate, a eucalypt tree cover represents the only means of achieving the required evapotranspiration rates from a store and release cover to handle extreme rainfall events, and be sustainable in the long-term. Since the rocky soil mulch is loose and granular, the trees are unlikely to promote cracking and the development of preferred seepage pathways. The height of trees will be limited by the thickness and water-holding capacity of the rocky soil mulch, while their root patterns will not penetrate the sealing layer. The limited tree height will limit the possibility of wind blowdown and possible threat to the integrity of the cover.

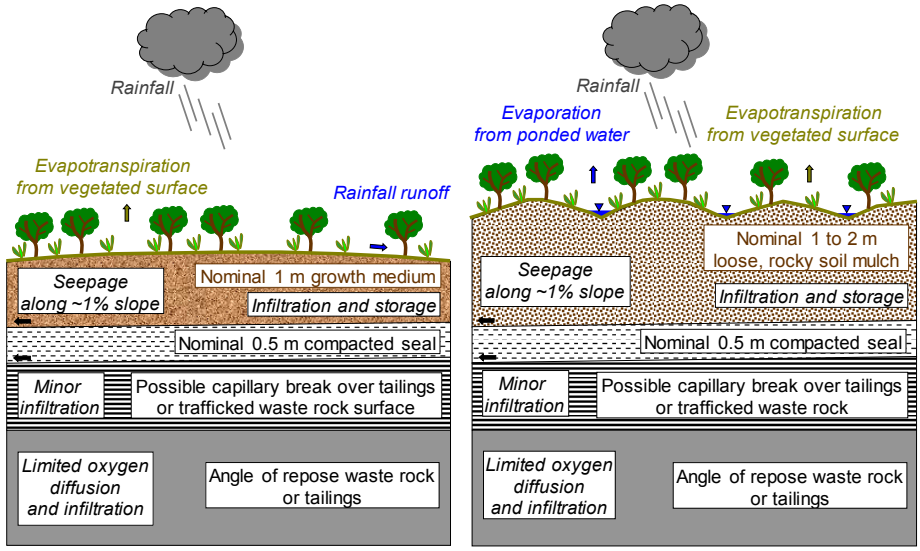

(a) (b)

Figure 5. Most common cover types applied to mine wastes: (a) rainfall-shedding and, (b) store and release (after Williams, 2012).

4.3 *Covers with capillary break effects*

Capillary barriers have been considered for limiting the net percolation of rainfall into underlying mine wastes. However, this relies on the capillary barrier remaining unsaturated to limit its hydraulic conductivity. If extreme rainfall events are possible, they could saturate the capillary

barrier, rendering it quite permeable and able to pass rainfall infiltration into the underlying mine wastes.

Covers with capillary barrier effects (CCBE) bear the closest resemblance to the GARD Guide's (2009) Cover V. Bussière et al. (2006) described a CCBE first employed at the Les Terrains Aurifères (LTA, Figure 6) mine site tailings impoundment, approximately 8 km south-east of Malartic, Abitibi, in Québec, Canada, in a net positive precipitation climate. The LTA tailings impoundment is approximately 60 ha in area and has a height of 12 m. It comprises 7 m of sulfidic (acid-generating) tailings placed over 5 m of non-acid-generating oxide tailings.

Figure 6. LTA site, Quebec Canada and proposed CCBE (after Bussière et al. 2006).

The CCBE, purpose-designed for and constructed on the LTA tailings impoundment in 1998, comprises 500 mm of sand (a capillary barrier) placed on the sulfidic tailings, overlain by 800 mm of fine-grained, non-acid-generating tailings (a moisture-retaining layer), in turn overlain by more than 300 mm of sand and gravel (protection and drainage layer). The design objective was to maintain a minimum degree of saturation of 85% in the moisture-retaining layer to effectively reduce the oxygen flux from the atmosphere to the acid-generating tailings. Near-saturation of the moisture-retaining layer was to be maintained by a combination of rainfall infiltration and the suction in the underlying capillary barrier. The intention of the sand and gravel surface layer was to limit revegetation, so as not to reduce rainfall infiltration. The same cover was applied to the side slopes of the tailings impoundment (also comprising sulfidic tailings). The cover initially functioned as intended on the top of the impoundment, which initially remained un-vegetated, but not so well on the side slopes, due to gravity drainage.

Smirnova *et al.* (2011) investigated volunteer revegetation on the LTA CCBE, which commenced the year after construction. Eight functional groups of plants were identified, with herbaceous plants being the most abundant. Of the 11 tree species identified, the four most abundant were poplar, paper birch, black spruce and willow. Root excavation showed that tree roots penetrated the moisture-retaining layer, with an average root depth of 400 mm and a maximum root depth of 1.7 m.

Bussière et al. (2015) reported that after 10 years, the LTA CCBE was effective in reducing the oxygen flux from the atmosphere to the acid-generating tailings. However, the quality of the seepage from the tailings impoundment still did not meet Québec water quality standards, and

dolomitic drains were constructed as passive treatment. Views of the LTA tailings impoundment before CCBE construction in 1998, after CCBE construction in 1998, and 10 years later in 2007 are shown in Figure 7.

Figure 7. LTA tailings impoundment before CCBE construction in 1998, after CCBE construction in 1998, and 10 years later in 2007 (after Bussière *et al.* 2015).

Double capillary barrier (or break) covers have been promoted by some Regulators in Australia, notably in Queensland. This is perplexing, since the majority of mine sites in Queensland, and elsewhere in Australia, are in semi-arid to arid climates, for which the GARD Guide (2009; Figure 3 herein) recommends a store and release cover. The reason for this may relate more to deficiencies in the design, materials selection and construction of store and release covers over potentially contaminating mine wastes in Australia, and elsewhere. The preferred approach would be to improve the design, materials selection and construction of the appropriate cover type for the potentially contaminating wastes and climatic setting of the mine.

5 EFFECTIVENESS OF COVERS IN ADDRESSING AMD LAGS

Apparent deficiencies in the design, materials selection and construction of the appropriate cover type for potentially contaminating mine wastes in a particular climatic setting is compounded by a lack of appreciation of the need to address geochemical and hydrological AMD lags. Surface waste rock dumps and tailings storage facilities experience different geochemical and hydrological AMD lags, which are closely related to the climatic setting.

5.1 *Influence of climate*

Climate is the key determinant for the cover types recommended by the GARD Guide (2009, Figure 3 herein). Recommended cover types range from water covers for wet climates (although these have gone somewhat out of favor due to the need for water dams to persist in perpetuity), through rainfall-shedding covers for humid climates, to store and release overs for dry climates.

5.2 *Covers on sulfidic waste rock*

The conventional end-dumping of waste rock from a tip-head in a surface dump promotes the oxidation of the initially relatively dry sulfidic waste rock due to the ready supply of oxygen via advection into the base rubble zone, convection up the coarse-grained angle of repose layers, and diffusion into the adjacent fine-grained angle of repose layers. Oxygen diffusion can also occur through the traffic-compacted top layer.

The dump is wet-up by rainfall infiltration, initially going into storage within the dump, until seepage eventually emerges from the base of the dump. The time taken to reach breakthrough is a function of the site rainfall, the degree of weathering and hence particle size distribution of the waste rock, and the height of the dump. For a fresh waste rock dump, breakthrough would occur in about 40% of the time it takes for a weathered waste rock dump, since a lower degree of saturation is required to create continuous water flow paths through the dump. Continuum

breakthrough may peak at only about 5% of cumulative rainfall beneath the traffic-compacted top of the dump and at only about 10% beneath the angle of repose side slopes of the dump, implying average hydraulic conductivities beneath the top and sides of the dump of the order of 3 x 10^{-6} m/s and 6 x 10^{-6} m/s, respectively. Depending on the hydraulic conductivity of the foundation beneath a dump, only a small proportion of the seepage (perhaps as low as 0.1% of rainfall) would emerge at topographic low points around the toe of the dump. Extreme rainfall events will generate high seepage rates, with a time lag.

For a typical mine life of say 20 years, it is likely that a conventional end-dumped waste rock dump containing sulfidic waste rock will oxidize and generate AMD well within the mine life. Indeed, this is often the case, and yet it continues to surprise operators. The generation of AMD some years after the start of construction of the dump occurs due to both the geochemical and hydrological lags having been exceeded, and in the absence of progressive mitigation. If an appropriate and effective cover is placed after the end of the mine life, the best that can be achieved is that the dump will continue to drain down, generating AMD, for about as long a period as it remained uncovered, say another 20 years.

The solution to this is fairly obvious, sulfidic waste rock should be identified and placed in cells well encapsulated by non-acid generating (NAG) waste rock or, preferably waste rock with ANC, if this is available, as shown in Figure 8 (after Williams, 2019). The cells should be periodically covered with traffic-compacted NAG or ANC waste rock as soon as practicable, and particularly prior to a defined wet season, in much the same way as landfills are encapsulated and regularly covered. By this means the geochemical and/or hydrological lags could be accommodated. A sustainable dump cover at closure should include an appropriate and effective cover on the dump top, and a textured cover on the side slopes of the dump for erosion protection, with no sulfidic waste rock placed beneath slopes unless protected by an appropriate and effective cover on a flat bench above.

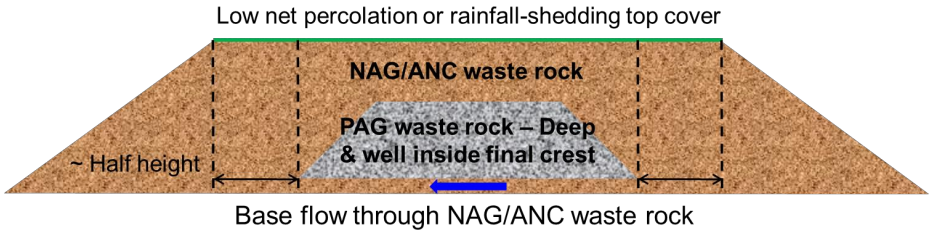

Figure 8. Encapsulation of PAG waste rock (after Williams, 2019).

5.3 *Covers on sulfidic tailings*

The conventional deposition of tailings as a slurry in a surface tailings storage facility results in desaturation of any exposed tailings, particularly in a dry climate. The formation of a desiccated crust will dramatically reduce the hydraulic conductivity of the tailings and cause the desaturation profile to diminish exponentially with depth and typically be limited to a depth of less than about 600 mm. As tailings desaturate, seepage rates will reduce, as will evaporation rates from the surface. The deposition of fresh tailings or rainfall will inundate the drying tailings and re-saturate them, commencing from any desiccation cracks that form. Re-wetting will recharge downward seepage and evaporation from the surface.

Oxygen will slowly diffuse into sulfidic tailings with degrees of saturation of less than 80 to 85%, promoting oxidation. Any oxidation products can be delivered to the foundation and toe of the tailings dam by ongoing seepage, while surface oxidation products and sediments may be transported by fresh tailings and rainfall runoff, potentially overtopping a spillway if one is provided.

Tailings that hardpan on desiccation, which is reasonably common for sulfidic tailings, can inhibit AMD, contaminant release and dusting, due to reduced oxygen diffusion and rainfall infiltration into the tailings, while maintaining long-term erosional stability. This can also be

achieved by compacting the tailings surface. A tailings hardpan or compacted tailings surface will act as a sealing layer for a cover, and will likely inhibit the uptake of salts into the cover. A reduction in rainfall infiltration will diminish the potential seepage of contaminants. The low permeability of the tailings will also inhibit upward flow and hence the uptake of salts into an overlying growth medium cover.

Relatively few covers have been placed on tailings compared with waste rock dumps. This is likely due to the soft and wet nature of many tailings deposits, compared with readily trafficable waste rock dump tops and benches. The progressive covering of tailings is even more rare, since this is incompatible with their ongoing operation. Hence, covering tailings deposits must await their closure, by which time the geochemical and hydrological lags will have been exceeded for any sulfidic tailings that become desiccated. The generation of AMD could potentially be avoided by careful management of tailings deposition. This could include maintaining sulfide tailings underwater in a wet climate, or managing tailings deposition cycles to maintain sulfidic tailings above the saturation threshold for oxidation. A balance is required between maximizing the dry density and physical stability of the tailings, while maximizing their chemical stability.

A sustainable tailings storage facility cover at closure should include an appropriate and effective cover on the relatively flat tailings beach, and a textured cover on the side slopes of the tailings dam for erosion protection. A tailings hardpan or compacted tailings surface will act as a sealing layer for a cover, and will likely inhibit the uptake of salts into the cover. Tailings that have achieved a high dry density and high strength will likely be trafficable by appropriately-sized earthmoving equipment for the purposes of placing a cover. Soft and wet tailings can be covered by pushing fill in thin lifts using a low bearing pressure dozer, by displacement of the tailings by end-dumped coarse-grained cover materials, or by placing coarse-grained cover materials hydraulically.

6 CONCLUSIONS

Sulfidic waste rock and tailings have the potential to generate AMD over time. Waste rock typically emerges from an open pit relatively dry and is conventionally end-dumped in a surface waste rock dump, giving it ready access to atmospheric oxygen and allowing the oxidation of any sulfidic minerals. The geochemical lag before the generation of net acidity is a function of the ANC present in the waste rock and the relative rates of production of acidity and alkalinity.

The hydrological lag before the emergence of AMD from the dump is a function of the extent and rate of wetting-up due to rainfall infiltration. This is in turn governed by the climatic setting and the physical and chemical nature of the waste rock. Initially, rainfall infiltration is largely taken up as storage in the void spaces within the dump. Cumulative rainfall infiltration, particularly intense rainfall events, result in seepage eventually reaching the base and perimeter of the dump, potentially carrying with it any net acidity.

Tailings are typically pumped to a surface storage as a slurry. If the surface of the tailings is allowed to desiccate, exposed sulfidic tailings can undergo oxidation. The oxidation products can then be mobilized by the deposition of fresh tailings, or by rainfall runoff and/or infiltration. If the runoff is discharged via a spillway, any acidity can be released to the environment via a spill. Seepage laden with oxidation products can eventually reach the foundation and/or toe of the tailings storage facility.

The purpose of covers over PAG mine wastes is to minimize the ingress of oxygen into the wastes and/or minimize transport of any AMD via the net percolation of rainfall into the wastes. The appropriate choice and effectiveness of covers is a function of the climatic setting, the mine wastes, and the management of the wastes.

Sulfidic waste rock should be identified and placed in cells well encapsulated by NAG waste rock or, preferably waste rock with ANC, if available. The cells should be periodically covered with NAG or ANC waste rock as soon as practicable, and particularly prior to a defined wet season, in much the same way as landfills are encapsulated and regularly covered. By this means the geochemical and/or hydrological lags could be accommodated. A sustainable dump cover at closure should include an appropriate and effective cover on the dump top, and a textured cover on the side slopes of the dump for erosion protection, with no sulfidic waste rock placed beneath slopes unless protected by an appropriate and effective cover on a flat bench above.

Covering tailings deposits must await their closure, by which time the geochemical and hydrological lags will have been exceeded for any sulfidic tailings that become desiccated. The generation of AMD could potentially be avoided by careful management of tailings deposition. This could include maintaining sulfide tailings underwater in a wet climate, or managing tailings deposition cycles to maintain sulfidic tailings above the saturation threshold for oxidation. A balance is required between maximizing the dry density and physical stability of the tailings, while maximizing their chemical stability.

A sustainable tailings storage facility cover at closure should include an appropriate and effective cover on the relatively flat tailings beach, and a textured cover on the side slopes of the tailings dam for erosion protection. A tailings hardpan or compacted tailings surface will act as a sealing layer for a cover, and will likely inhibit the uptake of salts into the cover. Tailings that have achieved a high dry density and high strength can be trafficked using appropriately-sized earthmoving equipment. Soft and wet tailings can be covered by pushing fill in thin lifts using a low bearing pressure dozer, by displacement of the tailings by end-dumped coarse-grained cover materials, or by placing coarse-grained cover materials hydraulically.

7 REFERENCES

Agnew, M.K. 1998. *The formation of hardpans within tailings as possible inhibitors of acid mine drainage, contaminant release and dusting*. PhD Thesis, The University of Adelaide.

Bussière, B., Maqsoud, A., Aubertin, M., Martschuk, J., McMullen, J. and Julien, M. 2006. Performance of the oxygen limiting cover at the LTA site, Malartic, Québec. *CIM Magazine*, Vol 1, Paper 20.

Bussière, B., Potvin, R., Dagenais, A.-M., Aubertin, M., Maqsoud, A. et Cyr, J. 2015. Restauration du site minier Lorraine, Latulipe, Québec : Résultats de 10 ans de suivi. *Sciences & Techniques*, 54, 49-64.

GARD Guide. 2009. www.gardguide.com.

Herasymuik, G.M., Wilson, G.W., Barbour, S.L. and Smith, T. 1995. The characterization of hydrologic properties and moisture migration pathways of a waste rock dump. *Proceedings of Nineteenth Annual British Columbia Mine Reclamation Symposium, Dawson Creek, British Columbia, Canada, 19-23 June 1995*, 234-244.

Liu, Y., Wu, S., Nguyen, T.A.H., Southam, G., Chan, T.-S., Lu, Y.-R. and Huang, L. 2018. Microstructural characteristics of naturally formed hardpan capping sulfidic copper-lead-zinc tailings. *Environmental Pollution*, 242, 1500-1509.

Liu, Y., Wu, S., Southam, G., Nguyen, T.A.H., Kopittke, P.M., Paterson, D.J. and Huang, L. 2019. Zinc and lead encapsulated in amorphous ferric cements within hardpans in situ formed from sulfidic Cu-Pb-Zn tailings. *Environmental Pollution*, 252, 1106-1116.

Rohde, T.K., Williams, D.J. and Burton, J. 2011. Waste Rock Dump Rainfall Infiltration and Base Seepage. *Proceedings of Fourteenth Australian Workshop on Acid and Metalliferous Drainage, Darwin, Australia, 21-24 June 2011*, 13 pp.

Smirnova, E., Bussière, B., Tremblay, F. and Bergeron, Y. 2011. Vegetation succession and impacts of bio-intrusion on covers used to limit acid mine drainage. *Journal of Environmental Quality*, 40(1),133-143.

Williams, D.J., Wilson, G.W. and Currey, N.A. 1997. A cover system for a potentially acid forming waste rock dump in a dry climate. *Proceedings of Tailings and Mine Waste 1997, Fort Collins, Colorado, 13-17 January 1997*, 231-235.

Williams, D.J. 2006. Mine closure as a driver for waste rock dump construction. *Proceedings of Mine Closure Seminar, Perth, Australia, 13-15 September 2006*, 697-706.

Williams, D.J. 2007. Strategies for reducing seepage from surface tailings storage facilities during operation and post-closure. *Proceedings of Mine Closure Seminar, Santiago, Chile, 16-19 October 2007*, 533-542.

Williams, D.J. 2008. The influence of climate on seepage from mine waste storages during deposition and post-closure. *Proceedings of Mine Closure Seminar, Johannesburg, South Africa, 14-17 October 2008*, 461-473.

Williams, D.J. 2012. In closing a surface waste rock dump it is not simply a matter of constructing a cover retrospectively. *Proceedings of Mine Closure 2012, Brisbane, Australia, 25-27 September 2012*, 379-392.

Williams, D.J. 2019. Obstacles to effective mine closure, rehabilitation and relinquishment. *Proceedings of Tailings and Mine Waste 2019, Vancouver, Canada, 17-20 November 2019*, 16 pp.

Influence of Residual Sulfide Content and Mineralogical Composition of Desulfurized Tailings on Performance as Reclamation Cover

Isabelle Demers, Hamza Berrouch, Benoît Plante
Research Institute on Mines and Environment, University of Quebec in Abitibi-Témiscamingue, Rouyn-Noranda, Quebec, Canada

Thomas Pabst
Polytechnique Montréal, Montreal, Quebec, Canada

ABSTRACT: Environmental desulfurization is a process that produces sulfide-lean tailings from acid-generating tailings. A laboratory study was performed to assess the geochemical behavior of four desulfurized tailings (0.12 to 0.26 % S) from gold mines in Abitibi, Quebec, Canada, used as cover material for the reclamation of acid-generating tailings. The neutralizing (buffering) minerals were composed of various proportions of silicate and carbonate minerals. Column tests were performed for over a year; testing desulfurized tailings separately and as single-layer cover with elevated water table over acid-generating tailings. The four desulfurized tailings maintained neutral leachates throughout the testing period, with low concentrations of dissolved metals. However, when the desulfurized tailings were used as covers under similar non-optimized hydrogeological conditions, they were not all successful in maintaining neutral leachates. The difference in geochemical behavior of desulfurized tailings used as cover is related to the type of neutralizing minerals and residual sulfides.

1 INTRODUCTION

Sulfidic mine tailings represent significant environmental challenges related to their potential to generation acid mine drainage (AMD) and metalliferous leaching (ML) (e.g Ritcey 1989). When exposed to atmospheric conditions (oxygen and humidity), several gangue sulfide minerals, such as pyrite and pyrrhotite, oxidize and release acid that favors metal solubility. Since the oxidation process is difficult to stop once begun, prevention is the favored approach to reduce the environmental risks of sulfidic mine tailings. Reclamation of tailings storage facilities aim to impede oxidation reactions by removing at least one component of the reaction: oxygen, water, or sulfide minerals. Engineered covers can reduce the oxygen flux reaching the sulfidic tailings. Monolayer covers made of fine-grained materials is one of these covers, which consists of a single layer of a material that can retain a high degree of saturation and limit oxygen diffusion (Dagenais 2005, Ouangrawa et al. 2006, Demers et al. 2008, Pabst et al. 2017). The monolayer cover is used when the water table is sufficiently high to ensure that the sulfidic tailings remain saturated at all times (elevated water table concept).

Environmental desulfurization is a process by which sulfide minerals are removed from tailings by flotation, to reduce liabilities related to the management of sulfidic mine tailings. Froth flotation is generally used to separate sulfides from non sulfides in the tailings stream, thus producing a sulfide concentrate and a desulfurized (or sulfide-lean) tailings (Benzaazoua et al. 2000, McLaughlin and Stuparyk 1994; Humber 1997). The desulfurized tailings have been shown in several studies to have adequate hydrogeological properties to be used as cover material in tailings storage facility reclamation (Benzaazoua et al. 2008; Bussière et al. 1997; Demers et al. 2009). Their suitability in terms of geochemical properties is usually verified by typical acid-base

accounting (ABA) criteria, such as %S and NP/AP ratio (Miller et al. 1991). Desulfurized tailings can also reduce the oxygen diffusion toward acid-generating tailings by consuming oxygen by the residual sulfide content (Demers et al. 2009; Bussière et al. 2004; Dobchuk et al. 2013). However, ABA criteria may not be sufficient to ensure performance of desulfurized tailings as cover material over the long term. Indeed, recent work by Rey et al. (2020) showed that even with a desulfurized tailings cover that maintain the target degree of saturation, some oxidation can still occur. While it is not enough to produce AMD, it may be sufficient for metal leaching (in this case zinc). So beyond sulfide content, how does the mineralogical composition of desulfurized tailings influence their hydrogeochemical behavior as cover material? How can characterization be used to hint on evolution of desulfurized tailings cover performance?

The experimental work presented in this paper studied four different desulfurized tailings as cover material to prevent AMD generation from sulfidic tailings. Their geochemical behavior was evaluated in kinetic column tests individually and when used as cover material over sulfidic tailings.

2 MATERIALS AND METHODS

2.1 *Sampling and characterization*

The materials tailings used in this study were sampled from mine sites in the Abitibi-Témiscamingue region, Quebec (Canada). Reactive tailings T were sampled from a tailings impoundment storage facility (at approximately 40 cm depth) at Laronde mine site. Three desulfurized tailings (<0.3% S) from Abitibi mine sites were used as a cover material: Laronde, Westwood, and Canadian Malartic; these are identified respectively as L, W, and CM. The fourth cover material G is a low sulfur tailings (< 0.15%), sampled from the Goldex mine site. In the laboratory, tailing samples were homogenized prior to their use and were stored submerged in containers to avoid sulfide oxidation.

The five tailings T, L, W, G, and CM were characterized in the laboratory. The particle-size distribution was obtained using Malvern Mastersizer laser particle size analyzer for diameters from 0.05 to 900 µm. Specific gravity (Gs) was measured with a Micromeritics AccuPyc 1330 helium pycnometer (ASTM 2014). Specific surface area was obtained using a Micrometrics Surface Area Analyser by the BET method (Brunauer et al.,1938). Saturated hydraulic conductivity (k_{sat}) of tailings was determined using a rigid-wall permeameter (ASTM D5084). Water retention curves (WRC) were determined using Tempe cell (ASTM 2016). Experimental data were fitted using the van Genuchten (1980) model.

The bulk chemical composition of tailings was determined by inductively coupled plasma-atomic emission spectrometry (ICP-AES) after 4 acids digestion ($HNO_3/H_2SO_4/HF/HClO_4$). The total sulfur (S_{total}) and carbon (C_{total}) were analyzed using Eltra CS-2000 induction furnace. The whole rock analysis was performed using X-ray fluorescence (XRF, Bruker Tiger series) to determine the major elements (Ca, Mg, Mn, Na, Si) contents within samples. The mineralogical analysis was performed with a Bruker A.X.S. D8 Advance X-Ray diffraction (XRD) instrument (detection limit ~ 1 wt. %). The mineralogical identification was performed with EVA software, while the mineralogical quantification was performed with the Rietveld (1993) method and fitted with the TOPAS software. All XRD data were reconciled in order to determine the mineralogical modal composition with more accuracy using ICP, XRF, and S/C results. The acid-base accounting (ABA) parameters were calculated using S_{total} and C_{total} contents (Miller et al. 1991) and the net neutralization potential (NNP=NP−AP) and the neutralization potential ratio (NPR=NP/AP) were calculated from static tests.

2.2 *Kinetic column tests*

The laboratory study included nine cylindrical experimental columns with different tailings, placed at a porosity of 0.43 (Rey et al. 2020, Demers et al. 2009) (Fig. 1). Nine plexiglas columns (inner diameter of 0.14 m), including five control columns, and four covered tailings columns, were filled with 0.3 m of reactive tailings T and covered by 0.5 m of cover materials.

Control columns were set up for each material. Instruments were installed in each column (same instruments for the nine columns) (Fig. 1). Volumetric water content was monitored every 6 hours using Decagon probe (EC-5) with a precision of 0.03 m^3/m^3, using the frequency domain method. Suctions were measured with Watermark sensors from Irrometer Company, Inc. Column T was setup with 0.3 m reactive tailings (T) and equipped with volumetric water content and suction sensors at 15 cm below the material interface. Columns LT, WT, GT, and CMT were filled with 0.5 m of desulphurized tailings. Two volumetric water content and suction sensors were placed at 15 cm below the material surface and the other at 15 cm from the bottom. Sampling ports for oxygen, identified as "septum O_2" on Figure 1, were located at each 5 cm intervals along the column. A saturated ceramic plate was placed at the base of all the columns, and negative pressure (suction) was applied to simulate a water table 1.0 m below the base of the columns. Column T had free drainage at the base (no ceramic).

Four columns representing a monolayer cover system were set up using 0.5 m of desulfurized tailings over 0.3 m of sulfidic T tailings. These columns were named LC, WC, CMC, and GC, according to the type of tailings cover. The instrumentation for LC, WC, GC, and CMC was the same as control columns. Water table was set 1 m below the base of the column, which represents conservative hydrogeological conditions.

Columns were subjected to thirteen wetting-drainage cycles. Approximately once a month, two liters (i.e. 13 cm) of deionized water was added to the top of the columns to simulate precipitation. The volume of water added to the top of the columns corresponds to approximately one month of precipitation (according to the climate of Abitibi), and it is generally used in similar tests (Kabambi et al. 2020a, 2020b, Rey et al. 2020). The leachates issued from column tests were analyzed for elemental concentrations (Al, Ba, Ca, Cd, Co, Cr, Cu, Fe, K, Mg, Mn, Mo, Ni, Pb, S, Sn, Ti, Zn) by ICP-AES. The pH was obtained with a Thermo Scientific Orion Green pH electrode (± 0.02). The electrical conductivity was determined using an Oakton SS rings PP and Ultem-body electrode (± 0.5%) and the redox potential (Eh) was measured by using a Cole Parmer Oakton Epoxy probe (symphony meter ± 0.05%). Acidity and alkalinity were measured using a Metrohm 848 Titrino plus automatic titrator.

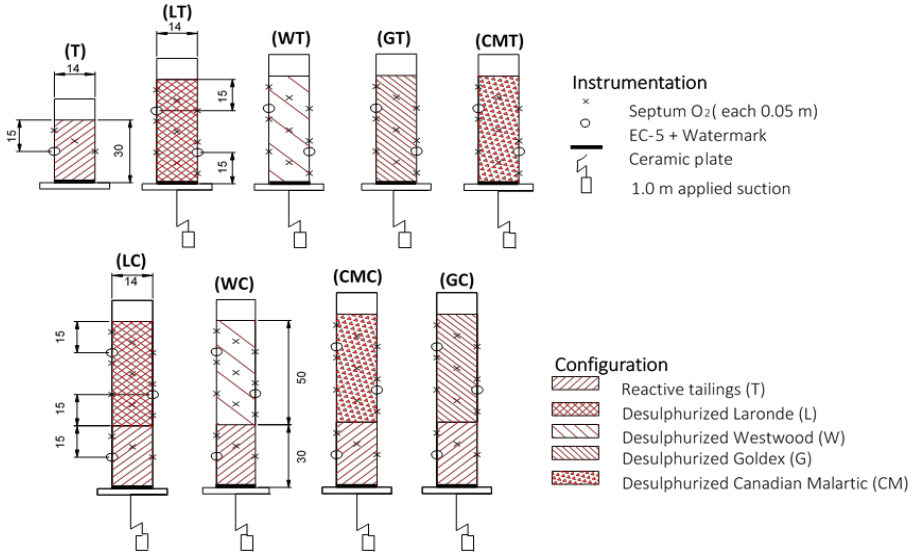

Figure 1: Configuration of columns and instrumentation

3 RESULTS

3.1 *Materials characterization results*

The particle size distributions of the five tailings samples were variable (Fig. 2), with a particle passing 80 µm (P80) of 85% for reactive tailings T, 43%, 83% and 76% for desulphurized tailings L, W and CM respectively, and 33% for low sulfur content tailings G. Tailings T and desulfurized tailings L and tailings G were coarser than desulphurized tailings CM and W. Results from specific gravity, saturated hydraulic conductivity and WRC are presented in Table 1. The values of saturated hydraulic conductivity k_{sat} were determined experimentally and predicted using the Mbonimpa et al. (2002) model, and were between 10^{-5} cm/s and 10^{-3} cm/s for the same testing porosity (n=0.43). Saturated hydraulic conductivity k_{sat} is higher for desulphurized tailings CM, W and tailings T than for tailings G and desulfurized tailings L. Based on the results obtained from the water retention curves, the air entry values (ψa) were approximately 2.2 m (~ 21.5 kPa) for T, 1.0 m (~9.8 kPa) for L, 2.2 m (~21.5 kPa) for W, 0.8 m (~7.8 kPa) for G. and 2.0 m (~19.6 kPa) for CM.

Table 1. Summary of selected tailings hydrogeotechnical properties

Parameter	Units	T	L	W	G	CM
G_s	_	3.25	2.82	2.78	2.74	2.75
k_{sat}	cm/s	1.56E-4	3.37E-4	1.32E-5	3.13E-4	_
$k_{sat\ (predicted)}$	cm/s	9,01E-05	1,33E-03	9,43E-05	6,69E-04	3,96E-05
ψ_a	m of water	2.2	1.0	2.2	0.8	2.0
n	_	0.43	0.43	0.43	0.43	0.43
α_v	m^{-1}	0.13	0.14	0.19	0.59	0.24
m_v	_	1.99	2.43	2.03	2.10	2.19

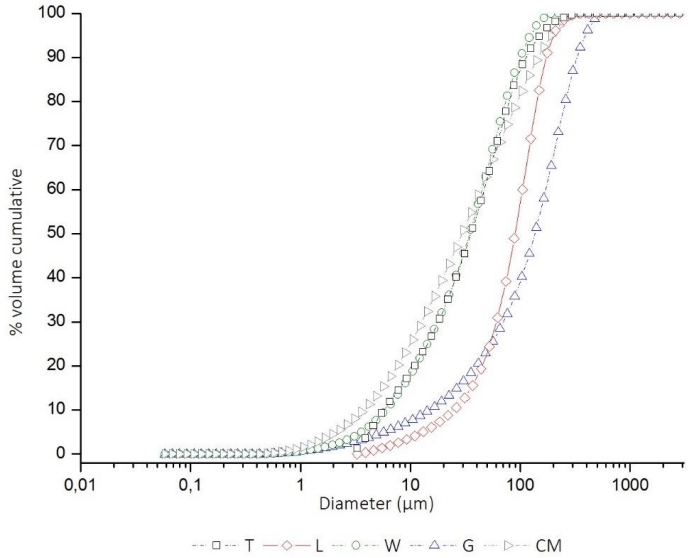

Figure 2: Particle size distribution of tailings samples

The results obtained with the XRD analysis show that: (i) the sulfide minerals were mainly represented by pyrite (0.34 – 23.86 wt. %; Table 2), (ii) five types of silicate minerals (i.e. quartz, chlorite, micas, plagioclase, and pyroxene) were identified with variable content within samples (∑silicate minerals ~ 64 – 93 wt. %), (iii) the carbonates which contribute to the neutralization reactions were mainly represented by calcite, dolomite, and siderite. Calcite was the most abundant in all samples, with a maximum content observed in tailings CM at 6.01 wt. %, and a minimum content in tailings L at 0.28 wt. %, and (iv) the oxide (rutile) and sulfate (anhydrite and gypsum) minerals were present in low amounts except in tailings G where gypsum reached 7.12 wt. %. Based on the mineralogical results, it is expected that the tailings (T) will be more reactive and acid generating than other tailings.

Table 2: Mineralogical composition estimated by XRD and chemical content

	T	L	W	G	CM
Pyrite (FeS_2)	23.9	0.5	0.34	0.34	0.34
Quartz (SiO_2)	53.2	77.8	46.0	25.6	26.8
Chlorite ($(Fe,Mg,Al)_6(Si,Al)_4O_{10}(OH)_8$)	3.85	2.36	5.34	4.6	3.18
Muscovite ($KAl_2[(OH,F)_2\|AlSi_3O_{10}]$)	7.21	5.03	25.3	9.85	3.01
Albite ($NaAlSi_3O_8$)	_	3.34	10.7	45.0	45.3
Diopside ($CaMgSi_2O_6$)	_	_	6.05		
Biotite ($K(Mg,Fe^{2+})_3[AlSi_3O_{10}(OH,F)_2)$	_	_	_	7.12	10.4
Calcite ($CaCO_3$)	0.75	0.28	1.23	5.61	6.01
Dolomite ($CaMg(CO_3)_2$)	_	_	_	_	2.82
Siderite ($Fe^{2+}CO_3$)	_	_	1.2	0.76	1.67
Rutile (TiO_2)	_	0.38	0.58	0.35	0.86
Anhydrite ($CaSO_4$)	_	_	0.04	_	
Gypsum ($CaSO_4 \cdot 2H_2O$)	_	_	_	7.12	

Table 3 shows acid-base accounting (ABA) results. The net neutralization potential (NNP = AP-NP) for tailings T was -362 kg $CaCO_3$/t and the AP/NP ratio was 0.02, signifying that T is acid generating. NNP for the tailings G and CM were 59 kg $CaCO_3$/t and 45 kg $CaCO_3$/t respectively, and AP/NP ratios were significantly higher than 4, indicating that G and CM are non-acid generating. Tailings L and W were in the zone of uncertainty with an NNP of -5.4 kg $CaCO_3$/t and 17.8 kg $CaCO_3$/t respectively (between − 20 and 20 kg $CaCO_3$/t), and AP/NP ratio was below 1 for tailings L.

Table 3: Acid-base accounting results

Parameter	Units	T	L	W	G	CM
C_{total}	%	0.09	0.03	0.27	0.75	0.59
S_{total}	%	11.84	0.26	0.15	0.12	0.14
AP	kg $CaCO_3$/t	369.87	8.24	4.73	3.6	4.48
NP	kg $CaCO_3$/t	7.53	2.79	22.62	62.7	49.34
NNP	kg $CaCO_3$/t	-362.34	-5.45	17.89	59.1	44.86
AP/NP	_	0.02	0.34	4.79	17.43	11.02

3.2 *Water quality evolution*

3.2.1 *pH, acidity, alkalinity and electrical conductivity*

The leachate water quality evolution of the column experiments is shown in Figures 3 and 4. The pH of all low sulfide and desulfurized tailings control columns leachates (LT, WT, GT, and CMT) remained near-neutral to slightly alkaline (6.9–8.2) over the entire experiment period. Reactive tailings T had an acidic pH starting from the second cycle as expected based on its high pyrite content (23.7 %) and lower calcite content (0.75%). These geochemical results of the leachates are consistent with the ABA classification, where tailings G and CM were identified as non-acid generating, while tailings L and W were within the uncertainty zone.

In general, cover systems contributed to reduce AMD generation, and delay the onset of pH drop. After the 11th cycle, pH values of covered columns dropped from 8 to 4, except column WC where the pH remained neutral. The alkalinity of the leachate of the control column T decreased from the 2nd cycle to until the end of the test. The sudden decrease in alkalinity could be explained by the probable depletion of the neutralizing minerals in response to sulfide oxidation, and corresponds to the decrease in pH. After the 13th cycle, the alkalinity of the control columns (LT, WT, GT, and CMT) varied between 60 and 180 mg $CaCO_3$/L. Columns LC and GC had low alkalinity (~ 20 mg $CaCO_3$/L), while CMC and WC had higher alkalinity (116 and 98 mg $CaCO_3$/L) from the first cycle.

The acidity of the control column T remained above 10,000 mg $CaCO_3$/L from cycle 5 onwards. Control columns LT, WT, GT, and CMT had relatively stable acidity throughout the test period, staying below 40 mg $CaCO_3$/L. For the cover scenario columns, an increase in acidity during the experiment was observed for columns LC and GC up to 300 mg CaCO3/L, and up to 10,000 mg $CaCO_3$/L for CMC, as shown by their acidic pH. WC maintained acidity below 65 mg $CaCO_3$/L by the end of the test. The electrical conductivity of the leachates (not shown graphically) varied between 0.5 and 26 mS/cm. The lowest conductivity throughout the experiment (<5 mS/cm) was observed for all the control columns and the highest for tailings T (26 mS/cm). Columns LC, WC, GC, and CMC showed a gradual decrease (down to 3-4 mS/cm) through time, except for column CMC which exhibited an increase after the 9th cycle, corresponding to lower pH values and more ions in solution.

All cover systems were able to reduce AMD indicators (pH, acidity, conductivity) compared to the uncovered reactive tailings.

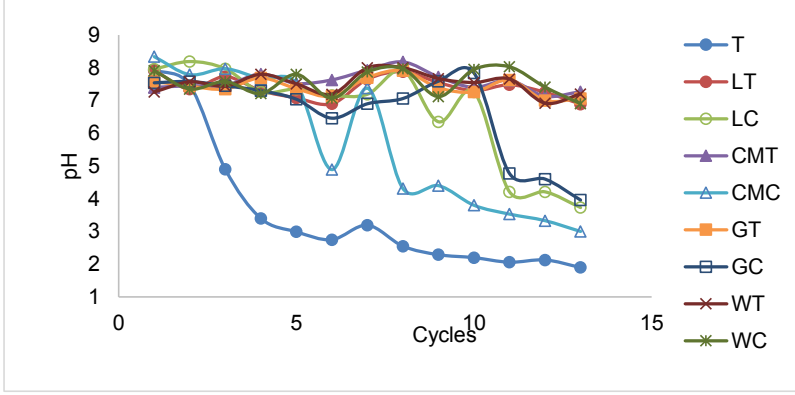

(a)

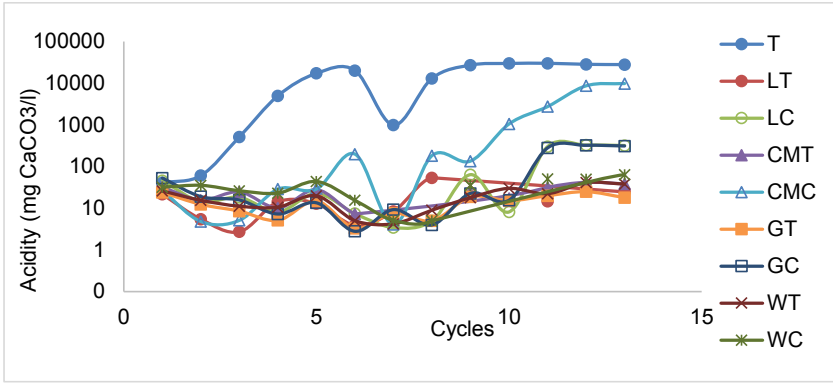

(b)

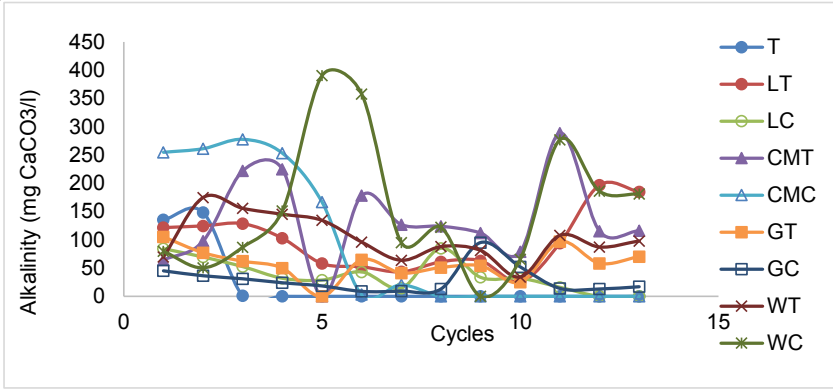

(c)

Figure 3: Leachate quality evolution during column tests: a) pH, b) acidity, and c) alkalinity results

3.2.2 *Elemental concentrations*

Elemental concentrations of selected species (Ca, Mg, Fe, S, Zn) in the nine column leachates are shown in Figure 4. It was assumed that all S was present in the form of sulfate. This assumption was verified and validated through ion chromatography analyses from the 3rd to the 13th cycle. A slight dip in concentrations can be observed in cycle 8 results and was caused by a large volume of water added to perform a resaturation of the column materials.

The concentration of Ca, Mg, Fe, S, and Zn in the leachates of the reactive tailings T were high and typical of AMD. Ca concentrations remained low because of its low calcite content (0.75 wt. %). Strong leaching of Mg, Fe, sulfate, and Zn was observed from the 3rd cycle onwards because of the pH decrease. After the 8th cycle, the concentrations of Fe and S reached 13,000 mg/L and 12,000 mg/L respectively, indicating a strong oxidation of metal sulfides. High concentrations of Zn (up to 1000 mg/L) were observed in all the cycles, exceeding the environmental regulation in Quebec Province (0.5 mg/L).

The control columns LT, WT, GT, and CMT showed slightly different geochemical results depending on the material. LT had decreasing concentrations of Ca, Mg and sulfate, while Fe and Zn were relatively stable at concentrations of approximately 0.3 mg/L. Ca concentrations were stable in CMT, GT and WT; whereas Mg decreased in GT and WT, and S decreased in CMT and WT. Fe was relatively stable in all columns, with concentrations around 0.2 and 0.3 mg/L. Zn was also stable at different concentrations depending on the column; 0.1 mg/L for GT, 0.3 mg/L for

WT, and 1 mg/L for CMT. At the end of the 13th cycle, Zn concentrations had increased for all control columns above the effluent quality criterion in Quebec (0.5 mg/L).

For columns LC, WC, GC, and CMC, starting from the 1st cycle, the S concentrations decreased from ~2500 mg/L at the beginning of the experiment to reach 500 mg/L at the end of the experiment for LC and GC columns. The WC column had a low concentration in the beginning and reached a concentration of ~400 mg/L towards the end of the experiment. The S concentrations in the CMC column also showed a large increase (up to 5900 mg/L). These S concentrations are significantly lower than in the uncovered reactive tailings (12,000 mg/L), indicating that the covers slowed down oxidation.

Fe concentrations in the leachates varied according to the tailings used as the monolayer cover. Once the pH dropped, Fe concentrations tended to increase. After the 13th cycle, Fe concentrations were approximately 190 mg/L for column LC, 140 mg/L for GC, 1000 mg/L for column WC, and 4700 mg/L for CMC. Zinc concentration in covered column effluents were also lower than in the uncovered reactive column, therefore the covers were efficient to reduce Zn leaching, at least for most of the testing period.

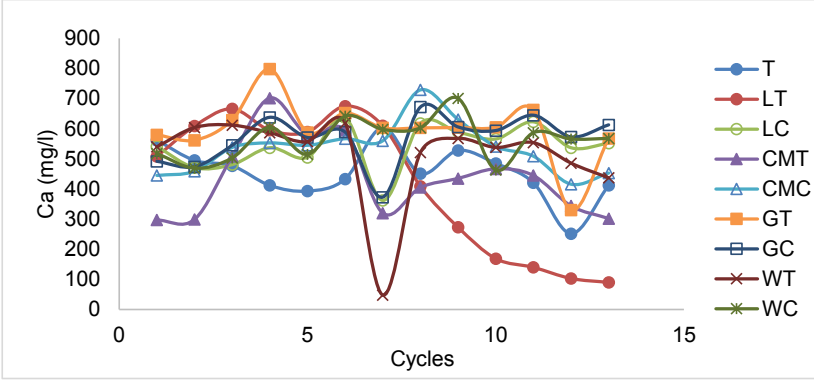

(a)

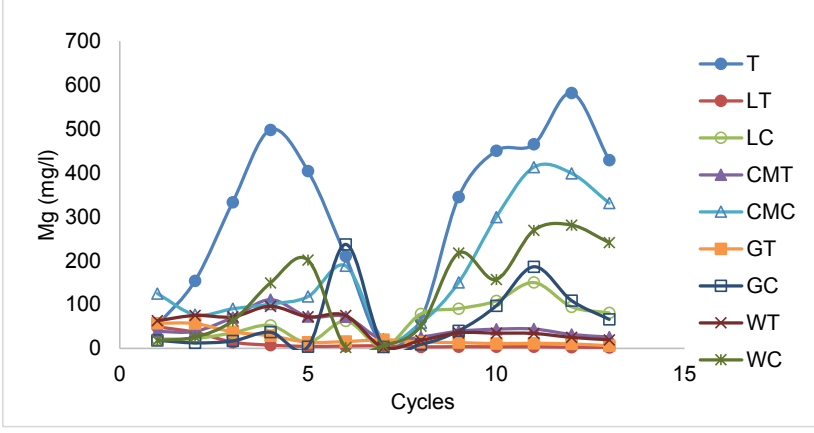

(b)

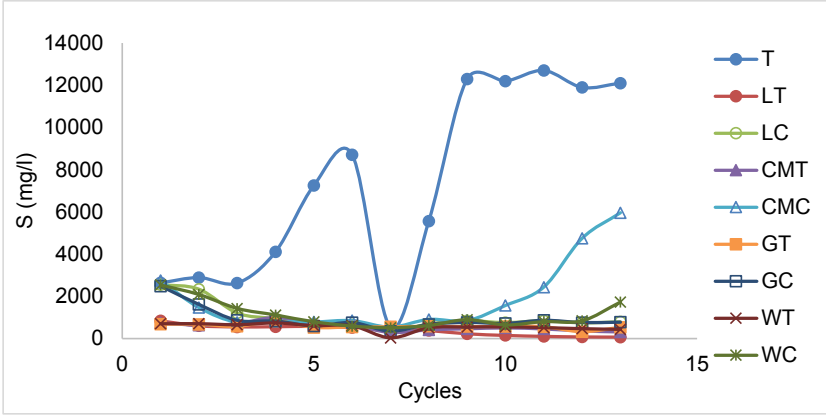

(c)

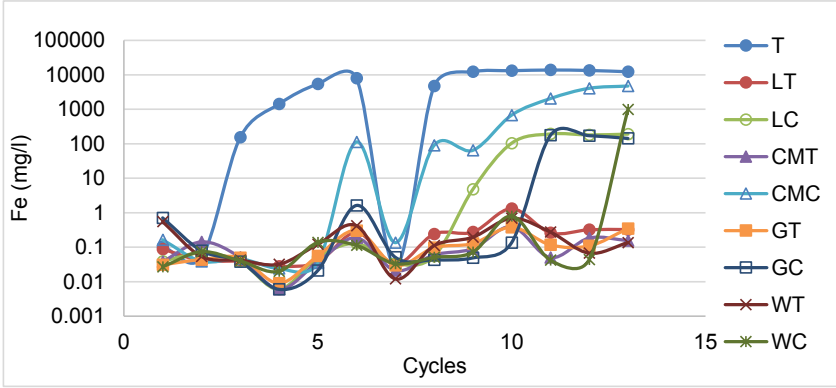

(d)

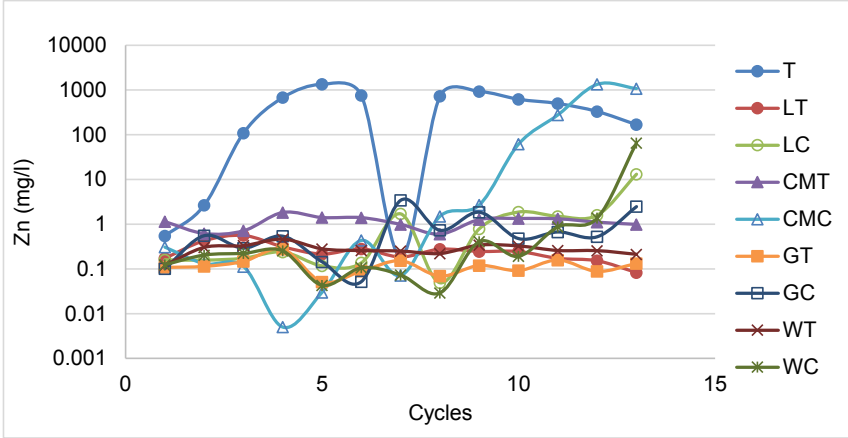

(e)

Figure 4: Leachate quality evolution during column tests: a) Ca, b) Mg, c)S, d) Fe, and e) Zn results

4 DISCUSSION

The elemental concentration evolutions in columns without cover were consistent with pH, acidity and alkalinity, and the tailings ABA test results. The desulfurized and low sulfide tailings, when tested alone, maintained neutral conditions. When used as single-layer covers, they were able to maintain a neutral effluent for at least a portion of the testing period, and reduced the metal concentrations in the effluents. However, their performance was not ideal. More specifically, results showed that CMC column was the first one to experience a drop in pH and increased element solubility, starting at cycle 6. Then, LC and GC dropped in pH at cycle 11. WC maintained a neutral pH for the 13 cycles, but Fe and Zn concentrations spiked at cycle 13, indicating the beginning of oxidation. Further cycles would probably have shown a decrease in pH as observed in the other columns.

Several aspects may explain this different behavior when these materials are used as cover. The first is related to the hydrogeological conditions within the cover. The hydrogeological conditions were not optimized in this project in order to force geochemical reactions and observe the differences between materials. The suction applied to all column tests was the same, however the suction measured in the desulfurized tailings covers was not identical. Table 4 presents the typical results for all columns at the topmost sensor (15 cm from the top) compared to the air entry value of the materials. According to the hydrostatic equilibrium, and assuming no evaporation, suction should read approximately 20 kPa for covered columns, and 15 kPa for control columns. For most materials, suction measurements are above their air entry value, indicating a possible desaturation and facilitated oxygen diffusion through the cover. Indeed, volumetric water content measurements indicated that degree of saturation was between 60% and 70% for all columns, therefore all columns had a relatively similar hydrogeological behavior.

Table 4: Typical suction mesurements obtained during column tests compared to air entry values

Column	Measured suction (kPa)	Air entry value (kPa)
T	14	22
LT	20	10
WT	28	22
GT	14	8
CMT	29	20
LC	18	10
WC	20	22
GC	18	8
CMC	28	20

A second aspect to consider is the presence of residual sulfides in the cover materials. When hydrogeological conditions are not optimal, the presence of residual sulfides in the desulfurized (or low sulfide) tailings can consume oxygen that diffuses through the cover. The low S content ensures that the reaction products (acidity) is readily buffered or is not enough to produce AMD. The four tailings tested as covers had S content between 0.12 and 0.26% S, which may have been enough to reduce temporarily the oxygen flux reaching the reactive tailings, but not enough to sustain an oxygen consumption at the oxygen diffusion rates experienced for the degree of saturation in the column tests.

A third aspect that can explain the difference in geochemical behavior is the mineralogical composition of the desulfurized and low sulfide tailings. Since most desulfurized and low sulfide tailings have similar pyrite content (0.3 to 0.5 %), neutralizing minerals can be considered. The presence of neutralizing minerals can buffer the products of residual sulfide oxidation within the cover, and their soluble components can be transported with water flow in the reactive tailings. CMC was the first column to experience AMD generation, although it was classified as non acid generating. CM desulfurized tailings had the highest amount of carbonates, and approximately

88% silicates (similar to L and G). W desulfurized tailings were able to maintain a neutral effluent in the column tests for the longest duration, even if they were classified in the uncertainty zone of acid generation potential. W had the highest amount of silicates with approximately 93%. It is therefore possible that neutralizing minerals with a lower reaction rates, such as silicates, can still provide some buffering from residual sulfide oxidation products, especially when the degree of saturation is low.

A final aspect that was not yet investigated is mineralogical texture of sulfide and neutralizing minerals. Mineral associations, liberation, and solid solutions can affect the reaction rates and can influence the geochemical behavior. Future work will look into detailed mineralogical characterization of the materials and reactive transport modeling to investigate reaction rates and provide long-term prediction of the cover behavior.

5 CONCLUSION

Desulfurized tailings and low sulfide tailings were proposed as alternative cover material for the reclamation of AMD generating tailings disposal facilities. Requirements to ensure proper cover performance generally include appropriate hydrogeological properties, and non-acid generating tailings as cover material. Kinetic column tests were performed using four desulfurized tailings and low sulfide tailings as single layer cover associated with a control of the water table level. The same cover materials were also tested individually to confirm the ABA classification.

While the four desulfurized and low sulfide tailings were not acid generating when submitted to the column kinetic test, they did not perform equally when used as a cover. They were all successful in reducing the acidity and metal concentrations in the column effluents. CMC column was the first one to experience a drop in pH and increased element solubility, starting at cycle 6. Then, LC and GC dropped in pH at cycle 11. WC maintained a neutral pH for the 13 cycles, but Fe and Zn concentrations spiked at cycle 13, indicating the beginning of oxidation.

Results have shown that ABA and presence of neutralizing minerals are not sufficient to ensure that desulfurized tailings or low-sulfide tailings provide an efficient cover. For similar hydrogeological conditions, geochemical behavior is also influenced by chemical and mineralogical composition, beyond the typical acid generating or non-acid generating classification. Residual sulfide in the cover material can reduce the oxygen flux reaching the reactive tailings, especially when the degree of saturation is lower than 85%. Results from this experiment showed that in the four cases studied, residual sulfides were not sufficient to prevent AMD for a very long period of time. Further work will include detailed mineralogical assessment and reactive transport modeling.

6 ACKNOWLEDGEMENTS

The authors would like to acknowledge the financial support obtained through a FRQNT Développement durable du secteur minier grant, in partnership with Iamgold Corp. The authors thank UQAT technical personnel for assistance in tailings desulfurization and laboratory assistance, and RIME partners for access to tailings samples.

REFERENCES

Benzaazoua, M., Bussière, B., Kongolo, M., McLaughlin, J., and Marion, P. 2000. Environmental desulphurization of four canadian mine tailings using froth flotation. *International Journal of Mineral Processing* 60:57-74.

Benzaazoua, M., Bussiere, B., Demers, I., Aubertin, M., Fried, E., & Blier, A. 2008. Integrated mine tailings management by combining environmental desulphurization and cemented paste backfill: Application to mine Doyon, Quebec, Canada. *Minerals Engineering* 21 (4):330-340.

Bussière, B., Nicholson, R.V., Aubertin, M., & Benzaazoua, M. 1997. Evaluation of the effectiveness of covers built with desulfurized tailings for preventing Acid Mine Drainage. *50th Canadian Geotechnical Conference*, Ottawa, Canada.

Bussière, B., Benzaazoua, M., Aubertin, M., & Mbonimpa, M. 2004. A laboratory study of covers made of low sulphide tailings to prevent acid mine drainage. *Environmental Geology* 45:609-622.

Dagenais, A-M. 2005. *Techniques de contrôle du drainage minier acide basées sur les effets capillaires.* Ph.D thesis, Mineral Engineering, Ecole Polytechnique de Montréal.

Demers, I., Bussière, B., Benzaazoua, M., Mbonimpa, M., & Blier, A. 2008. Optimisation of single-layer cover made of desulphurized tailings: application to the Doyon mine tailings impoundment. *SME annual meeting 2008*, 24 - 27 February, Salt Lake City.

Demers, I., Bussière, B., Mbonimpa, M., Aubertin, M., & Benzaazoua, M. 2009. Oxygen diffusion and consumption in low sulphide tailings covers. *Canadian Geotechnical Journal* (46):454-469.

Dobchuk, B., Nichol, C., Wilson, G.W., & Aubertin, M. 2013. Evaluation of a single-layer desulphurized tailings cover. *Canadian Geotechnical Journal* 50 (7):777-792.

Humber, A.J. 1997. Separation of sulphide minerals from mill tailings. *Land Contamination and Reclamation* 5 (2):109-116

Kalonji-Kabambi, A., Bussiere, B., Demers, I. 2020a. Hydrogeochemical behavior of reclaimed highly reactive tailings, Part 1: characterization of reclamation materials. *Minerals* 2020, 10, 596.

Kalonji-Kabambi, A., Bussiere, B., Demers, I. 2020b. Hydrogeochemical behavior of reclaimed highly reactive tailings, Part 2: laboratory and field results of covers made with mine waste materials. *Minerals* 2020, 10, 589.

Mbonimpa, M., Aubertin, M., Chapuis, R., & Bussière, B. 2002. Pratical pedotransfer functions for estimating the saturated hydraulic conductivity. *Geotechnical and Geological Engineering* 20(3):235-259.

McLaughlin, J., & Stuparyk, R. 1994. Evaluation of low sulphur rock tailings production at Inco's Clarabelle mill. *Innovation in Mineral Processing*, Sudbury, Ontario.

Miller, S.D, Jeffery, J.J., & Wong, J.W.C. 1991. Use and misuse of the acid-base account for "AMD" prediction. *2nd International Conference on the Abatement of Acidic Drainage*, Montreal, QC.

Ouangrawa, M, Molson, J.W., Aubertin, M., Zagury, G., & Bussière, B. 2006. The effect of water table elevation on acid mine drainage from reactive tailings: a laboratory and numerical modelling study. *7th ICARD*, March 26-30, 2006, St.Louis, MO.

Pabst, T, M Aubertin, B Bussière, and J. Molson. 2017. "Experimental and numerical evaluation of single-layer covers placed on acid-generating tailings." Geotechnical and Geological Engineering 35 (4):1421-1438.

Rey, N., Demers, I., Bussière, B., Mbonimpa, M., & Gagnon, M. 2020. A geochemical evaluation of a monolayer cover with elevated water table for the reclamation of Doyon-Westwood tailings ponds, Canada. *Environmental Earth Sciences* 79:58.

Ritcey GM (1989) *Tailings management, problems and solutions in the mining industries*. Elsevier.

Hydrologic Predictions of Water Content and Oxygen Concentration in a Geowaste Test Pile

Mohammad H. Gorakhki
Barr Engineering, Minneapolis, Minnesota, USA

Christopher A. Bareither
Colorado State University, Fort Collins, Colorado, USA

Joseph Scalia
Colorado State University, Fort Collins, Colorado, USA

Greg Butters
Colorado State University, Fort Collins, Colorado, USA

ABSTRACT: The objective of this study was to predict volumetric water content and oxygen concentration within a field-scale GeoWaste test pile. GeoWaste is a mixture of fast-filtered tailings and waste rock blended to create a tailings-dominated mixture. In situ water content and oxygen concentration were monitored in the test pile for a period of 26 months. Hydrologic predictions in HYDRUS 1D and HYDRUS 2D were conducted for the entire duration of the experiment using the initial water content distribution within the pile, field and laboratory measured soil hydraulic parameters, metrological data, and vegetation information. Close comparison between saturation predictions in HYDRUS 1D and 2D indicated that HYDRUS 1D could predict water movement in the field-scale test piles with similar accuracy as HYDRUS 2D. The comparison supported the use of HYDRUS 1D to predict oxygen concentration based on a solute flux module. A transient change from laboratory-measured to in situ measured hydraulic parameters yielded the best prediction of saturation in the test pile. Predictions of oxygen concentration for the GW pile were in close agreement with measured values throughout the entire 26-month experiment.

1 INTRODUCTION

Standard mine waste management involves storing tailings and waste rock separately. Waste rock piles can be susceptible to acid rock drainage (ARD) and tailings storage facilities (TSFs) can be susceptible to failure (Blight 2009). The typically high permeability of waste rock allows ingress of atmospheric oxygen and precipitation, which may lead to ARD when sulfide-rich minerals are present. The blending of filtered tailings and waste rock in a tailings-dominated mixture, referred to as GeoWaste, is a co-disposal approach to create impoundments that do not require dams or embankments. The addition of waste rock to filtered tailings improves shear strength of the tailings that can enhance geotechnical stability (e.g., Burden et al. 2018; Borja and Bareither 2020). The tailings-dominated mixture of GeoWaste is envisioned to encapsulate potentially acid-generating waste rock in tailings to inhibit the ingress of oxygen and mitigate ARD potential, which enhances geochemical stability. Moreover, GeoWaste has a lower hydraulic conductivity and higher water retention relative to waste rock alone, which can enable the use of mixed mine waste rock and tailings in a water balance cover (Gorakhki and Bareither 2017). A water balance cover can decrease leachate generation by storing water during the wet part of a year and releasing the stored water back to atmosphere via evapotranspiration during the dry part of a year. Evaluating the water-phase balance (e.g., water content distribution, water percolation) and gas-phase balance (e.g., oxygen concentration distribution) are important factors to consider when comparing the hydrologic and environmental behavior of GeoWaste.

A GeoWaste test pile was constructed and monitored for 26 months at a mine in Central America. The purpose of this study was to evaluate the ability of a commercially-available hydrologic model (via HYDRUS) to predict water and gas flow in GeoWaste test pile. The test pile

was monitored for water content and oxygen concentration for a period of 26 months. HYDRUS 2D and 1D models were conducted for the entire 26-month period using local meteorological data and soil hydraulic properties obtained via field- and laboratory-scale testing. Modeled and measured volumetric water content and oxygen concentration within the piles were compared to assess validity of the numerical models to describe the behavior of GW.

2 UNSATURATED MODELING OF GEOWASTE

2.1 *Water Balance*

The volume of generated leachate from a mine waste impoundment depends on climate, vegetation, and hydrologic parameters. The water balance of a mine waste deposit was computed as

$$P_r = P - R - ET - L - \Delta S \tag{1}$$

where P_r is leachate percolation at the base of the deposit, P is precipitation, R is surface runoff, ET is evapotranspiration, L is lateral drainage, and ΔS is the change in soil water storage.

2.2 *Oxygen Diffusion and Consumption*

Consumption of oxygen (O_2) in the pore space of mine waste via ARD reactions lowers the O_2 concentration, which promotes oxygen diffusion into the mine waste due to an O_2 gradient with the atmosphere. The diffusion flux (F) of O_2 can be calculated in 1D using Fick's first law:

$$F = -D_e \frac{\partial C}{\partial_z} \tag{2}$$

where D_e is the effective diffusion coefficient, C is oxygen concentration, and z is vertical distance. A lower O_2 diffusive flux will decrease the rate of O_2 replenishment, which lowers O_2 concentrations in mine waste and reduce the magnitude of ARD reactions. The main parameters controlling O_2 diffusion into mine waste are D_e and the concentration gradient.

The effective diffusion coefficient is composed of two components (Collin 1987):

$$D_e = D_a + H \cdot D_w \tag{3}$$

where D_a is the effective diffusion coefficient in the gas phase, D_w is the effective diffusion coefficient in the liquid phase, and H is Henry's constant (i.e., approximately 0.03 at 25 °C). Oxygen diffusion through water contributes much less than diffusion through air. The expression in Eq. 3 can be expanded as

$$D_e = \theta_a \cdot T_a \cdot D_a^{\,0} + 0.03(\theta_w \cdot T_w \cdot D_w^{\,0}) \tag{4}$$

where θ_a and θ_w are the volumetric air and water content ($\theta_a + \theta_w$ = porosity), T_a and T_w are the air and water phase tortuosity, and D_{a0} and D_{w0} are the free diffusion coefficient in air and water ($D_{a0} = 1.8\times10^{-5}$ and $D_{w0} = 2.2\times10^{-9}$ m^2/s). The parameters T_a and T_w can be estimated as a function of saturation (e.g., Millington-Quirk 1961). In general, D_e reduces approximately two to three orders of magnitude by increasing saturation from 50% to 90% (Millington and Quirk 1961; Elberling et al. 1994). A reduction in D_e produces a corresponding reduction in the diffusive flux of O_2 (Eq. 2), and consequently, reduces O_2 within the pore space of mine waste that reduces ARD potential.

The rate change of O_2 concentration ($\partial C/\partial t$) with O_2 consumption can be computed using a modified version of Fick's second law:

$$\frac{\partial C}{\partial_t} = \frac{D_e}{\theta_{eq}} g \frac{\partial^2 C}{\partial_z^{\,2}} - \frac{K_r}{\theta_{eq}} g C \tag{5}$$

where K_r is a consumption rate coefficient and θ_{eq} is the equivalent porosity. The equivalent porosity can be calculated as

$$\theta_{eq} = \theta_a + H \cdot \theta_w \tag{6}$$

where Henry's constant is typically assumed as H ≈ 0.03. The K_r parameter in Eq. 5 depends on soil mineralogy, bacterial activity, mine waste pyrite content (i.e., mineralogy), and particle-size distribution (i.e., surface area) (Demers et al. 2009). The K_r parameter can be measured by monitoring the O_2 concentration in a closed chamber over time.
Empirical relationships can also be used to estimate K_r when O_2 consumption rate experiments are not available. The most commonly used empirical relationship for O_2 consumption rate in mine waste is presented by Collin (1987):

$$K_r = k \frac{6}{D_H} (1 - n) C_{py} \tag{7}$$

where k is reactivity of pyrite with oxygen [1.58×10^{-2} m^3-O_2/m^2-pyrite/yr], C_{py} is pyrite content (by mass), n is porosity, and D_H is equivalent particle-size diameter. The D_H can be calculated as

$$D_H = [1 + 1.17 \log(C_u)] D_{10} \tag{8}$$

where C_u is the coefficient of uniformity and D_{10} is the particle size at 10% passing on a PSD. Larger particle sizes typically have lower surface area and lower reactivity, which leads to larger D_H and lower K_r.

3 METHODS AND MATERIALS

3.1 *GeoWaste Test Pile*

The GeoWaste pile was constructed at a mine in Central America. Plan view and cross-section schematics of the test pile are shown in Gorakhki et al. (2019). The pile was designed as a truncated 5 m tall pyramid with 25 m base sides and a flat 5 m × 5 m top surface. GeoWaste was prepared to a target mixture ratio of 0.43 (R = dry mass of WR / dry mass of tailings), which was approximately 2/3 fast-filtered tailings and 1/3 waste rock. All materials were mixed on site using an excavator prior to placement. GeoWaste for the side slopes of the test pile was prepared with non-potentially acid generating (non-PAG) waste rock that was placed using an excavator to support the 5 m × 5 m central core. GeoWaste for the central core was prepared with PAG WR and was placed via dropping the mixture from a height of 2 to 3 m using an excavator. This deposition process for the central core simulated anticipated full-scale GeoWaste placement via disposal at the end of a conveyor system.

The pile was instrumented with four layers of sensors. Each layer contained five sets of sensors, one set in the center and four sets positioned approximately 2-m radially from the center on each side of the pile. Each sensor set contained (i) a TDR-315L Acclima sensor to measure volumetric water content, and (ii) a SO-110 Apogee sensor to measure oxygen concentration. All sensors were connected to a CR-1000 Campbell Scientific datalogger interfaced with an AM 16/32B Campbell Scientific multiplexer.

3.2 *Mine Waste Parameters*

Hydraulic parameters required for numerical modelling include parameters describing the soil water characteristic curve (SWCC) and saturated hydraulic conductivity (k_{sat}). The SWCC was approximated the van Genuchten equation (van Genuchten 1980), which includes the following parameters: saturated volumetric water content (θ_s), residual volumetric water content (θ_r), and fitting parameters α and *n*. The θ_s of the GeoWaste test pile was obtained from in situ density tests and the θ_r for was obtained from laboratory tests on tailings.

A summary of the numerical models completed for this study is in Table 1. Multiple scenarios were considered for SWCC parameters α and *n*, and k_{sat}, which led to six unique models. Models GW1, GW2, and GW3 were developed for the GeoWaste pile and included hydraulic parameters obtained via a sealed double-ring infiltration test conducted at the end of the 26-month pile experiment (Gorakhki et al. 2019). Model GW4 included estimates of α, *n*, and k_{sat} from laboratory experiments (Gorakhki et al. 2018). The laboratory experiments were conducted on the same mine waste materials, but did not include soil structure within the pile that developed during the duration of experiment. Models GW5 and GW6 were developed to incorporate a transient change in soil hydraulic parameters from the laboratory-measured condition to the in situ condition. The transient change was assumed to occur during the first year of the pile experiment as a linear, monthly change, from laboratory to in situ hydraulic parameters at the start of Year 2. In situ parameters for Model GW5 were determined for the upper 2.0 m of the pile (i.e., Model GW1), whereas in situ parameters for Model GW6 were determined for the entire pile (i.e., Model GW3). The transient change in hydraulic parameters in Models GW5 and GW6 is supported by Benson et al. (2007), who report that α, *n*, and k_{sat} of surficial soils used in earthen cover systems for waste containment changed during operation due to pedeogenesis.

Table 1. Summary of parameters used for variable models in GeoWaste and waste rock piles.

Model	Parameter Consideration			Parameters		
	Moisture Retention	Hydraulic conductivity	Wetting front	α (1/m)	*n*	k_{sat} (m/s)
GW1	Inverse solution in infiltration experiment	Inverse solution in infiltration experiment	Upper 2.0 m	3.47	1.75	2.9×10^{-6}
GW2	Inverse solution in infiltration experiment	Sealed double ring infiltrometer	Upper 2.0 m	0.41	1.75	1.8×10^{-6}
GW3	Inverse solution in infiltration experiment	Inverse solution in infiltration experiment	Lower 2.7 m	0.38	1.74	7.2×10^{-7}
GW4	Laboratory measured	Laboratory measured	NA	0.68	1.25	1.4×10^{-8}
GW5	Year 1: GW4 to GW1 in 12 steps (monthly)	Year 1: GW4 to GW1 in 12 steps (monthly)	NA	0.68 → 3.47	1.25 → 1.75	1.4×10^{-8} → 2.9×10^{-6}
	Year 2 and 3: GW1	Year 2 and 3: GW1	NA	3.47	1.75	2.9×10^{-6}
GW6	Year 1: GW4 to GW2 in 12 steps (monthly)	Year 1: GW4 to GW2 in 12 steps (monthly)	NA	0.68 → 0.41	1.25 → 1.75	1.4×10^{-8} → 1.8×10^{-6}
	Year 2 and 3: GW2	Year 2 and 3: GW2	NA	0.41	1.75	1.8×10^{-6}

3.3 *Model Setup*

HYDRUS 1D and 2D models were used to simulate the air and water phase of the GeoWaste pile. In the 2D analysis, an atmospheric boundary condition was set for the 5-m-wide pile surface. Although side slopes of the pile were subjected to atmospheric interaction, they were simulated as no flux boundaries because they did not receive irrigation, and separation of irrigation and precipitation was not possible. The base boundary condition was set as a seepage face because a gravel layer within a lysimeter underlined the pile. In HYDRUS 1D, the top surface was set as an atmospheric boundary and the bottom as a seepage face. The initial condition in the 1D and 2D models was based on initial water content readings at the start of the pile experiments, which was an average of 12%.

A preliminary comparison between 1D and 2D simulations for the GW6 model was performed to assess differences between water content profiles. Temporal changes in water content for the 26-month simulation were evaluated at four locations representative of each layer of sensor measurements corresponding to depths of 0.5 m, 2.0 m, 3.5 m, and 4.8 m from the pile surface. Furthermore, two observation points were identified in each layer in the 2D simulation: at the center of each layer and 2-m radially outward from the center (i.e., representative of where sensors were located in each layer). A single, average, observation node was identified for each layer in the 1D simulation. Water contents in the 1D simulation were within the range of water contents predicted for the two observation nodes in the 2D simulation, which implied similarity of hydrologic predictions between 1D and 2D simulations and that 1D and 2D water flow was similar in the GeoWaste pile.

Similarity of 1D and 2D hydrologic predictions for the GW pile supported the use of gas-phase modeling in HYDRUS 1D. Although HYDRUS does not have direct capabilities to predict gas flow, the solute transport module in HYDRUS was parameterized to simulate gas flow because solute and gas transport in porous media follow Fick's first and second laws. Consumption of oxygen in the pore voids lowers the oxygen concentration within the pile. The difference between oxygen concentration in the pile and in the atmosphere results in oxygen flow from the atmosphere into the piles. Oxygen concentrations at the upper boundary and oxygen concentrations for initial conditions in the pore voids were set at atmospheric conditions. Pyrite content was approximately 0.3% in the GeoWaste, which were converted to a $K_r = 0.1\ d^{-1}$ (Eq. 8).

4 RESULTS

4.1 *Prediction of Volumetric Water Content*

A comparison of predicted and measured volumetric water content (VWC) in the four layers of the GW pile is shown in Fig. 1. The measured VWCs plotted in Fig. 1 are averages of the five sensors in each layer. In general, all models predicted similar temporal fluctuations in VWC that were observed in VWCs measured during the experiment. Models GW1, GW2, and GW3 all considered hydraulic parameters that were representative of conditions at the end of the 26-month experiment. These hydraulic parameters led to under predictions of VWC relative to the other three models. Model GW4 included hydraulic parameters from laboratory specimens, and yielded consistent overpredictions of VWC relative to field measurements, which were also the highest VWCs among all models. Finally, Models GW5 and GW6 considered temporally changing hydraulic parameters from laboratory-based parameters at the onset of the model to in situ parameters at the start of Year 2. Volumetric water content predictions from GW5 and GW6 transition from predicted VWCs similar to GW4 in the first 150 d to VWC predictions more comparable to models that included in situ parameters (GW1, GW2, and GW3) until the end of the 26-month experiment duration.

During the first 120 d in Layer 1 (Fig. 1a), all models overpredicted peak VWC relative to the average measured VWC. The differences between predicted and measured VWC were attributed to (i) physical differences between the model and experiment and (ii) averaging the VWC measurements. Runoff and infiltration were not measured during the period of irrigation; however, ponded water was observed on top of the GeoWaste pile. The presence of ponded water could lead to evaporation prior to infiltration, which would correspond to lower measured VWC compared to predicted VWCs. Furthermore, HYDRUS does not simulate ponded water, and considering runoff was set to zero in all models, all precipitation and irrigation water input in the model was simulated to infiltrate into the pile. This is because HYDRUS applied irrigation water uniformly during the day instead of applying irrigation in 30 minutes. The additional inflow simulated in the models explains the trend for higher predicted versus measured VWCs during the period of irrigation. Secondly, although measured VWC peaked on Day 90 at approximately 18%, this was the average of five measurements, whereas the maximum VWC measured during the first 120 d was 30% (central sensor). This higher measured VWC in the first 120 d agrees with the higher predicted VWC and suggests more appropriate comparisons between predicted and measured VWCs should include the range of measured VWCs within each layer.

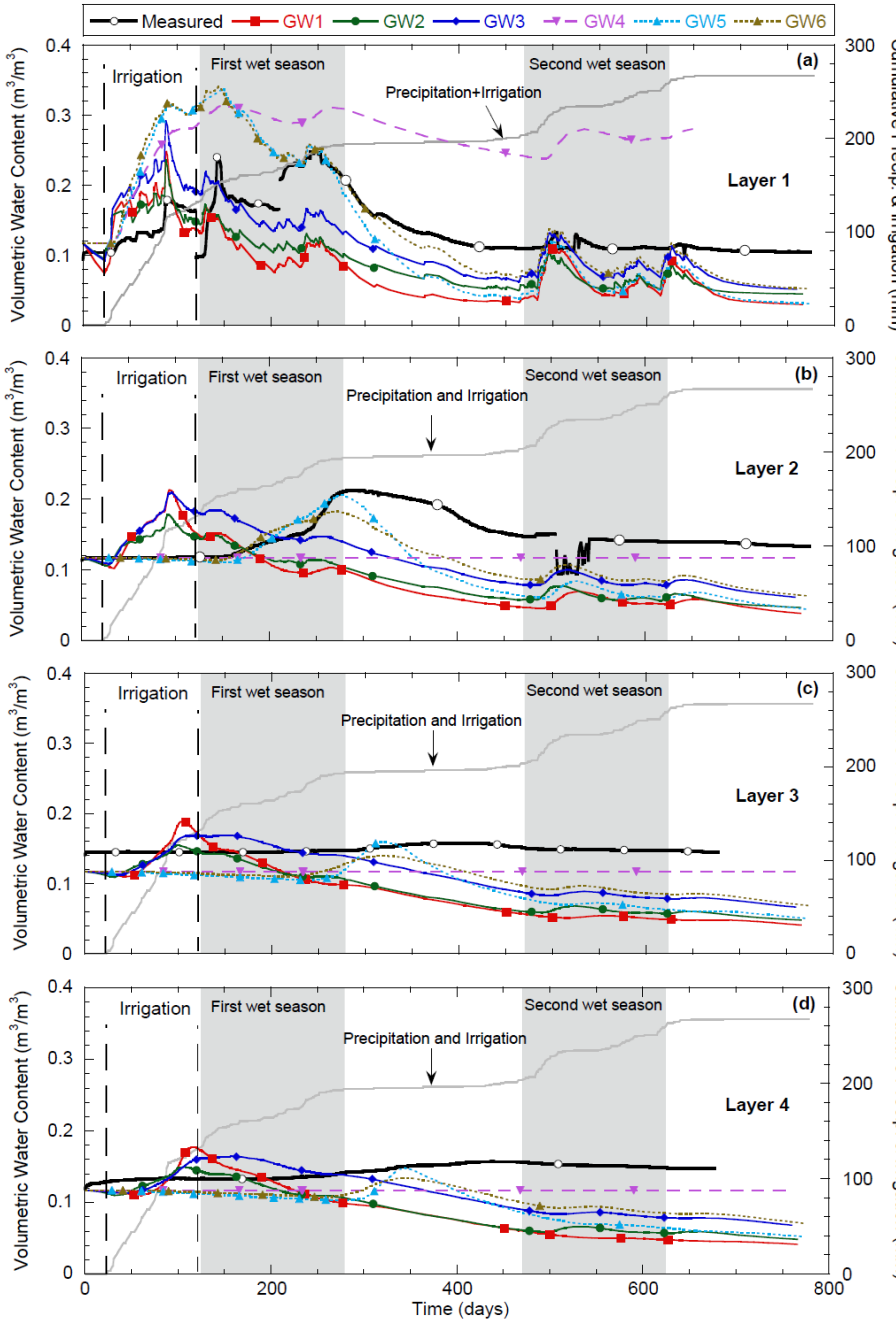

Fig. 1. Comparison between temporal volumetric water content of Models GW1-GW6 and measured values in GeoWaste pile in (a) Layer 1, and (b) Layer 2 (c) Layer 3, and (d) Layer 4.

The difference in hydraulic parameters used in the six GW models can be observed via the VWCs predicated for Layer 1 at the end of the irrigation period to the end of the experiment. Models GW1, GW2, and GW3 yielded VWC predictions that compared favorably with the average measured VWC at the end of irrigation (Fig. 1a). Subsequently from the start of the first wet season until the end of the experiment, these models generally underpredicted VWC. The use of hydraulic parameters based only on in situ conditions in Models GW1, GW2, and GW3 appears to limit higher moisture retention and slower seepage that would be simulated with laboratory parameters to lead to higher VWCs. For example, GW4 only incorporated laboratory-based hydraulic parameters, which included lower hydraulic conductivity and higher moisture retention characteristics. Thus, the VWC in Layer 1 for GW4 is overpredicted at the start of the first wet season and for the remainder of the experiment. Finally, although VWC was overpredicted in Layer 1 at the end of irrigation for GW5 and GW6, the measured VWCs are accurately predicted for these two models towards the end of the first wet season.

Measured VWCs between Days 120 and 210 in Layer 1 only were based on one sensor, southwest of the pile center, because the other four sensors were not functional during this time. This sensor consistently recorded lower VWCs relative to the other four sensors during the entire experiment. Thus, measured VWCs in Layer 1 from Day 120 to Day 210 may not have represent the true average VWC for the GeoWaste pile.

The increasing and subsequently decreasing trends in measured VWC in Layer 1 from Day 210 to Day 425 were captured by all models. Models GW5 and GW6 predicted the magnitude and decreasing trend in VWC more effectively compared to the other four models. The more rapid reduction in VWC predicted with GW5 relative to GW6 was attributed to the modestly higher hydraulic conductivity used for Years 2 and 3 of the simulation. Although Models GW1 through GW4 captured the temporal fluctuations in VWC in Layer 1 between 210 and 425 d, GW1, GW2, and GW3 consistently underpredicted VWC, whereas GW4 consistently overpredicted VWC (Fig. 1-a). The measured VWC in Layer 1 increased with onset of the second wet season beginning on Day 500. All models predicted an increase in VWC at approximately the same time and all models except GW4 predicted VWCs that were comparable, but typically lower than the measured VWCs.

Comparison between measured and predicted VWC in Layer 2 of the GW pile is shown in Fig. 1b. Measured VWC in Layer 2 increased due to irrigation and precipitation approximately on Day 160 and reached a maximum of 21% on Day 300. Subsequently, measured VWC decreased and then remained approximately constant between Day 500 and the end of the experiment. The wetting front was predicted to reach Layer 2 between 41 and 43 d for models GW1, GW2, and GW3, which was more than 100 d early relative to the measured increase in VWC. In contrast, the wetting front was predicted to reach Layer 2 on Day 178 for Model GW5 and on Day 160 for Model GW6. The predictions of arrival of the wetting front for GW5 and GW6, as well the subsequent increase in VWC measured in Layer 2 until the end of the first wet season, compared favorably with VWC measurements. However, the subsequent decrease in predicted VWC for GW5 and GW6 during the first dry season underpredicted the measured VWC. Finally, the wetting front was not predicted to arrive in Layer 2 in Model GW4, which implies that the use of only laboratory-based model parameters for the entire GW test pile throughout the entire experiment duration did not yield appropriate predictions of VWC.

Comparisons between measured and predicted VWC in Layers 3 and 4 of the GW test pile are shown in Figs. 1c and 1d, respectively. The measured response in VWC, temporal behavior of the predictions, and comparison between measured and predicted are similar for Layers 3 and 4. The measured VWC increased slightly from the start of the experiment to approximately the start of the second wet season, and then transitioned to a slow decreasing trend. The small fluctuations in measured VWC suggest that a wetting front similar to that observed via the increase in VWC in Layers 1 and 2 (Figs. 1a and 1b) did not reach Layers 3 and 4. The predicted increase in VWC that occurs around 40 to 50 d in Layers 3 and 4 based on Models GW1, GW2, and GW3 corresponds to arrival of wetting front that never developed. This predicted response suggests the hydraulic parameters used in models GW1, GW2, and GW3 include a hydraulic conductivity that was too high and/or moisture retention parameters do not promote enough retention to restrict downward water migration. Thus, the use of hydraulic parameters based on in situ measurements representative of conditions after 26 months do not yield accurate predictions of moisture movement in Layers 3 and 4 during the first 200 d of the pile experiment.

The arrival of a wetting front to Layers 3 and 4 was also predicted via Models GW5 and GW6; however, arrival occurred after 300 d and did not yield as high of a predicted peak VWC. Finally, Model GW4 predicted that the VWC in Layers 3 and 4 would not fluctuate during the entire experiment. Comparing measured VWC in Layers 3 and 4 to the more reasonable predictions observed in Models GW4, GW5, and GW6, the actual hydraulic response of the deeper layers of the GeoWaste pile (i.e., Layers 3 and 4) would appear to fall somewhere within the range of hydraulic parameters measured in the laboratory and in situ.

Differences between measured and predicted VWC in Layers 3 and 4 could be due a number of factors. First, during pile decommissioning roots were observed up to 3 m deep in the pile, whereas roots were not simulated to this depth in any of the models. The presence of roots between 0.5 m (max extent assumed in model) and 3 m can remove water from within the pile, which can decrease hydraulic conductivity and limit a wetting front from developing and ultimately reaching Layers 3 and 4. Secondly, GeoWaste in the vicinity of Layers 3 and 4 would have less influence from pedeogenesis compared to the top half of the pile based on observations during SDRI experiment. The limited development or absence of pedogenesis at depth would lead to a lower hydraulic conductivity and higher water retention in Layers 3 and 4, whereas the pile was simulated as a homogeneous material in the models.

4.2 *Prediction of Oxygen Concentration*

The O_2 concentration in the GeoWaste pile was computed considering $K_r = 0.1\ d^{-1}$ based on mineralogy and Eq. 8. Predictions of O_2 concentration from HYDRUS 1D are considered representative of 2D conditions considering that similar predictions in VWC were obtained from HYDRUS 1D and HYDRUS 2D. Oxygen concentration only was predicted based on VWC prediction in Model GW6 because this model yielded the best overall prediction of hydrological behavior of the GeoWaste pile.

A comparison between predicted and measured O_2 concentrations in Layer 1 of the GeoWaste pile is shown in Fig. 2a. The predicted O_2 was in good agreement with measured O_2 during the entire duration of the pile experiment. The rate of reduction in O_2 was predicted faster than observed in the measurements. Oxygen concentration of 0% in Layer 1 was predicted on Day 90, whereas the measured O_2 reached 0% on Day 130. This difference was attributed to higher VWC predictions compared to measured VWCs immediately following the onset of irrigation (Fig. 1a). The measured O_2 fluctuated with VWC changes in Layer 1 between 130 and 300 d, and the model predicted the change in O_2 accurately during this period (Fig. 2a). Measured O_2 was approximately in the range of 16% to 18% from the first dry season until the end of the experiment. The two small decreases in measured O_2 (approximately Days 500 and 630) corresponded with predicted (and measured) increases in VWC (Fig. 1a). The predicted O_2 during this same time was approximately 18%, and both localized decreases in measured O_2 were captured by the model.

A comparison between predicted and measured O_2 in Layer 2 of the GW pile is in Fig. 2b. The overall prediction of O_2 showed close agreement to temporal changes and magnitude of the measurements. Similar to Layer 1, predicted O_2 decreased at a faster rate relative to the measured O_2, and a concentration of 0% was predicted on Day 85, whereas an O_2 of 0% was measured on Day 125. Subsequent to this day, predicted and measured O_2 were in close agreement for the remainder of the experiment. Predicted and measured O_2 increased at the same rate between Day 250 and 440, and predictions typically were 2% higher than measured. The reduction in measured O_2 that coincided with the second wet season (Day ~ 500) and increase in VWC in Layer 1 (Fig. 1a), was effectively predicted by the model. After the second wet season, predicted O_2 was approximately 2% lower than measured O_2 until the end of the experiment.

Predicted and measured O_2 in Layers 3 and 4 are shown in Figs. 2c and 2d. Similar to Layers 1 and 2, the rate of reduction in O_2 in the model was faster than observed in the measurements for Layers 3 and 4. Predictions of O_2 in both layers agreed well with measured O_2 up to Day 500. However, predicted O_2 in Layers 3 and 4 were consistently smaller than measured values from Day 500 to the end of the experiment. The higher O_2 measurements were attributed, in part, to a small air leak detected within the pipe network and cistern that were connected to the base lysimeter of the pile. Thus, higher measured O_2 may be attributed to atmospheric air entering the base lysimeter that increased O_2 measured in Layers 3 and 4.

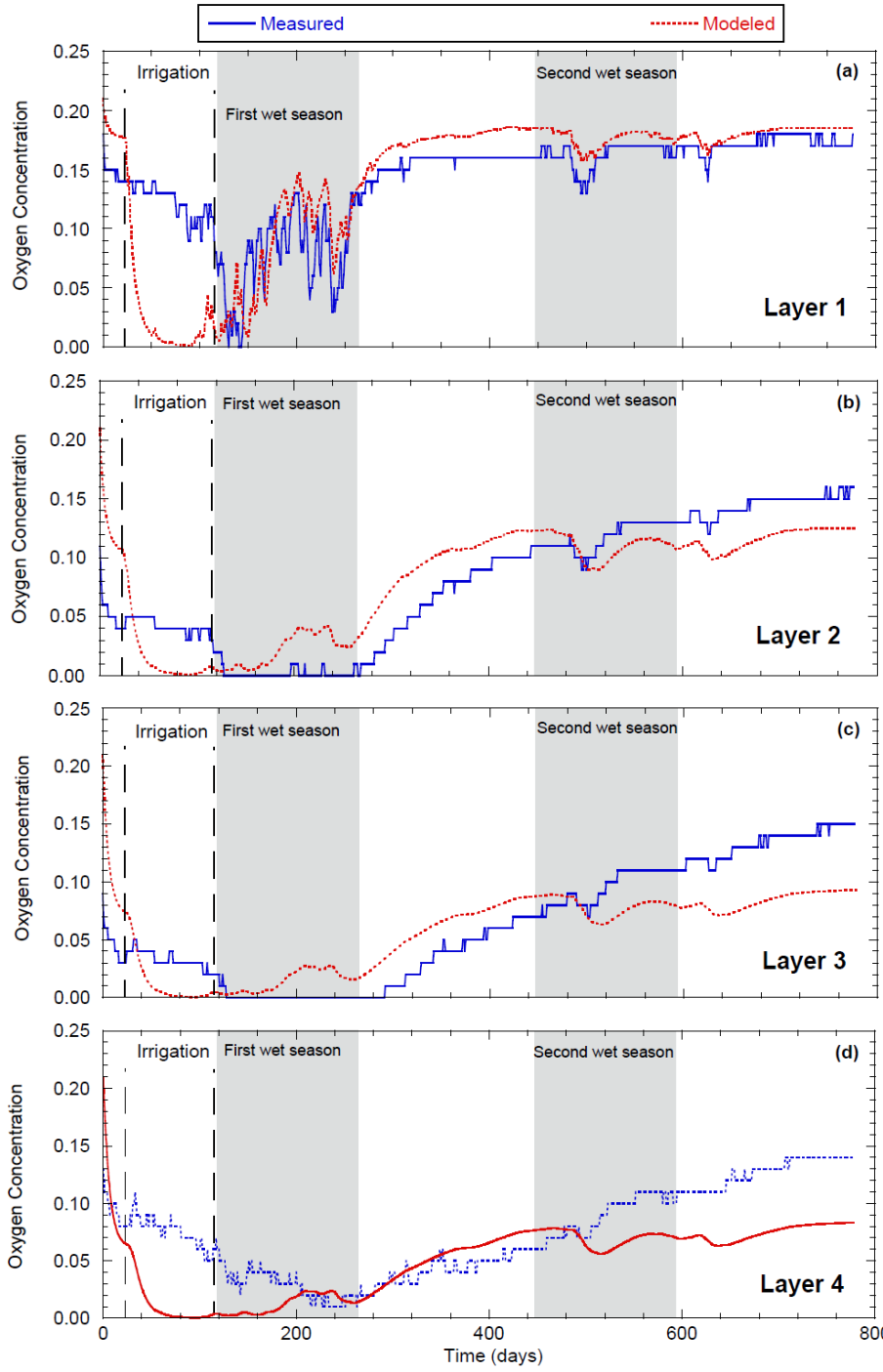

Fig. 2. Comparison between temporal oxygen concentration of Model GW6 and measured values in GeoWaste pile in (a) Layer 1, and (b) Layer 2 (c) Layer 3, and (d) Layer 4.

5 CONCLUSIONS

Volumetric water content (VWC) and oxygen concentration (O_2) profiles of a GeoWaste test pile were predicted in HYDRUS-1D and HYDRUS-2D and compared to 26-months of in situ monitoring data. Predictions included hydraulic parameters measured in field- and laboratory-scale experiments and incorporated site-specific climate and vegetation data. Comparisons were made between predicted and modeled VWC and O_2 at depths of 0.5 m, 2.0 m, 3.5 m, and 4.8 m.

Volumetric water content in the GeoWaste pile was overpredicted in all four layers of the pile when using laboratory-measured hydraulic parameters. In contrast, VWC predominantly was underpredicted via in situ hydraulic parameters measured at the end of monitoring (i.e., after 26 months of pile operation). The two models that incorporated a transient change from laboratory-measured to in situ measured hydraulic parameters yielded the best predictions of VWC in the GW pile. Predictions of O_2 for the GeoWaste pile were in close agreement with measured values throughout the entire 26-month experiment.

HYDRUS was used effectively to predict the water content and O_2 concentration profile of a GeoWaste test pile. Validating HYDRUS can help to understand the volume of leachate and/or acid rock generation potential in the long-term or in extreme conditions.

6 ACKNOWLEDGMENTS

Financial support for this study was provided by Newmont Inc. and the National Science Foundation (CMMI #1538344). The opinions, findings, and conclusions expressed herein are those of the authors and do not necessarily represent the views of the Newmont Goldcorp or the National Science Foundation.

7 REFERENCES

Benson, C. H., Sawangsuriya, A., Trzebiatowski, B., Albright, W. H. (2007). Postconstruction changes in the hydraulic properties of water balance cover soils. *Journal of Geotechnical and Geoenvironmental engineering*, *133*(4), 349-359.

Blight, G. (2009). Geotechnical engineering for mine waste storage facilities, Taylor & Francis, London, UK.

Borja, R.N. and Bareither, C.A. (2020). Shear behavior of waste rock and filtered tailings mixtures, *GeoCongress 2020 GCP 318*, ASCE, 872-880.

Burden, R.N., Wilson, G.W., Williams, D., Jacobs, M. (2018). The shear strength of filtered tailings and waste rock blends, *Proc. Tailings and Mine Waste 2018*, UBC Studios, University of British Columbia, Vancouver, BC, 347-355.

Collin, M. 1987. Mathematical modeling of water and oxygen transport in layered soil covers for deposits of pyritic mine tailings. Licenciate Treatise. *Royal Institute of Technology. Department of Chemical Engineering. S-10044 Stockholm, Sweden*.

Demers, I., Bussiere, B., Mbonimpa, M., Benzaazoua, M. (2009). Oxygen diffusion and consumption in low-sulphide tailings covers. *Canadian Geotechnical Journal*, *46*(4), 454-469.

Elberling, B., Nicholson, R. V., Reardon, E. J., Tibble, R. (1994). Evaluation of sulphide oxidation rates: a laboratory study comparing oxygen fluxes and rates of oxidation product release. *Canadian Geotechnical Journal*, *31*(3), 375-383.

Gorakhki, M. H., Bareither, C. A. (2017). Sustainable reuse of mine tailings and waste rock as water-balance covers. *Minerals*, *7*(7), 128.

Gorakhki, M.R.H., Bareither, C.A., Scalia, J., Aparicio, M., Jacobs, M. (2019). In situ hydraulic conductivity testing of a GeoWaste test pile, *Proc. Tailings and Mine Waste 2019*, UBC Studios, University of British Columbia, Vancouver, BC.

Millington, R. J., and Quirk, J. P. (1961). Permeability of porous solids. *Transactions of the Faraday Society*, *57*, 1200-1207.

Van Genuchten, M. T. (1980). A closed-form equation for predicting the hydraulic conductivity of unsaturated soils. *Soil Science Society of America Journal*, *44*(5), 892-898.

Gas Transport Inside Co-disposal of Desulfurized Tailings and Sulfidic Waste Rocks

Cheng Huang, Liang Ma, Zhong-Sheng (Simon) Liu, Eben Dy, Kidus Tufa, Elizabeth Fisher, Jianqin (James) Zhou, and Mireille Goulet
Energy, Mining and Environment Research Centre, the National Research Council Canada,

4250 Wesbrook Mall, Vancouver, BC V6T 1W5 Canada

Kevin Morin
Minesite Drainage Assessment Group, Surrey, BC, Canada

Martine Paradis
Nouveau Monde Graphite, Saint-Michel-des-Saints, Québec, Canada

ABSTRACT: The mining industry is trending towards the co-disposal of desulfurized tailings with sulfidic waste rocks for acid rock drainage (ARD) mitigation. Fine-grained, desulfurized tailings can be used as a cover on sulfidic waste rocks. ARD mitigation is advanced by reducing air permeability and diffusivity of the co-disposal layers. Oxygen, the primary oxidant, is transported into the co-disposal layers by means of air convection and diffusion, and oxidizes sulfidic tailings and waste rock. Oxygen depletion inside the waste rocks induces oxygen concentration gradient from outside to inside, which drives oxygen diffusion into the layers. Furthermore, air convection happens due to the partial pressure change by both oxygen depletion and heat expansion caused by the exothermic oxidation reactions. In this study, the fully coupled gas transport mechanisms across one layer of a co-disposal design are modeled. Environmental temperatures including monthly ambient air temperature and ground temperature are applied as boundary conditions. Evolutions of temperature and oxygen consumption rates across the layers are simulated from the initial deposition up to five years. These are to study the efficacy of different configurations of the desulfurized tailings as the overlying cover to minimize air transport pathways into waste rocks. The effects of water saturation inside the layers and of the thickness of the tailings layer on the oxidation reaction rate into waste rocks were evaluated. This study provides important insights into how to improve the mitigating efficiency of the co-disposal strategies.

1 INTRODUCTION

Tailing ponds are often massive structures up to square kilometers in size and impounded by earth-filled dams, which can reach as high as several hundred meters. Tailings impoundments often generate the largest concern and environmental cost at a mine site. Most of the tailings dams require perpetual monitoring and management, and the risks and costs are the largest concern for the mining industry and local communities. In recent years, there have been increasing concerns due to catastrophic tailings dam failures occurring worldwide. The most recent in Canada occurred at Mt. Polley in 2014 (Shandro et al., 2017) and in Brazil the Brumadinho dam disaster occurred on 25 January 2019 at the Córrego do Feijão iron ore mine (Silva et al., 2019). Mining companies and governments are looking for safer alternatives to store mine tailings. Dry-stacking of tailings provides opportunities for no-dam solutions for managing mine tailings.

Acid rock drainage (ARD) from sulfidic waste rock is also a large environmental problem at mine sites. Inside waste rock piles, there typically are partially water-saturated coarser pores, allowing fresh air to enter the pile, providing oxygen as the prime oxidant to sulfide oxidation reactions (Morin et al., 1991 and Ma et al., 2019). The co-disposal of tailings and waste rock uses layers of compacted fine-grain tailings during the construction of a waste rock pile. The partially

saturated tailings can reduce gas permeability and diffusivity greatly, which limit the transport of oxygen into the waste rock. The co-disposal aims to minimize the production of ARD in the waste rock pile and at the same time safely dispose the dewatered mine tailings (Lamontagne et al, 1999). The final goal is to facilitate the final closure of the mine site.

Understanding the physical controls on each of the mechanisms is a key in the co-disposal design. This paper provides gas transport and heat transfer models, which consider the environment temperature including ambient air temperature and ground temperature. The models were demonstrated with parametric studies of some theoretical configurations and conditions of one part of the co-disposal designs of Matawinie Project, an open mine project in Canada owned by Nouveau Monde Graphite (NMG),. The modeling tools can be used for evaluating the effectiveness of different configurations and operating conditions of the co-disposal in reducing ARD generation in waste rock.

2 CO-DISPOSAL OF TAILINGS AND WASTE ROCK

ARD generation inside sulfidic waste rock involves a variety of coupled physical, geochemical and microbial processes including transport of air, water and heat, acidification/neutralization reactions, and microbial activities. When the surface of sulfides is exposed to oxygen in air and water, oxidation reactions occur consuming oxygen. Heat production also occurs since sulfide oxidation could be strongly exothermic. The release of heat drives temperature up, as high as 70 ºC, has been observed in some local spots (Gélinas et al., 1992). The temperature rise is important since it changes the mechanisms of oxygen transport to oxidation sites. Air transport to the reaction sites can involve both convection and diffusion fluxes.

Water reaches the reaction sites through infiltration of rain or snow melt. Additionally, the gas phase in the pores contains water moisture that can condense and/or evaporate on the rock surface. As a result, moisture can reach waste rock through water vapor transport, to the sites not influenced directly by the flow of liquid water.

Oxygen ingress control is the key to manage production of ARD in waste rock. Management of gas flux requires control of diffusion and convection gas fluxes.

Co-disposal is a method whereby waste rock is co-disposed with dewatered tailings, so that the modified waste materials has a lower bulk permeability and effective gas diffusivity. The dewatering is a prerequisite for compacting the tailings layer, which is necessary to obtain the capillary barrier effect. Control of gas flux resulting from diffusion can be done through managing the effective diffusion coefficient of waste rock, tailings, and cover materials. Effective diffusion coefficients can be reduced through the use of finer grained material, or by decreasing the air filled porosity of the material by increasing water contents. Maintaining high water content in the tailings layer is critical for a lower air permeability and effective gas diffusivity. Diffusive flux can also be controlled by decreasing the diffusion gradient through varying path length, i.e. thickness of the tailings layers.

2.1 *Desulfurized tailings*

Tailings are desulfurized to obtain around 78 wt. % desulfurized tailings and around 22 wt. % sulfurized tailings. In the case of co-disposal desulfurized tailings, comprising less than 0.2 wt. % sulfur is used in the study with the particle size distribution as shown in Figure 1.

The relative permeability is the ratio of the permeability under partial saturation to the one under full saturation conditions. Relative water permeability and relative air permeability the tailings are represented by van Genuchten (1980) relationship and Mualem capillary model (1976).

$$\frac{\theta(h)-\theta_r}{\theta_s-\theta_r}=\left[1+(\alpha\,|\,h\,|)^n\right]^{-m} \tag{1}$$

$$\frac{K_w}{K_S} = \left(\frac{\theta(h)-\theta_r}{\theta_s-\theta_r}\right)^{0.5}\left[1-\left\{1-\left(\frac{\theta(h)-\theta_r}{\theta_s-\theta_r}\right)^{1/m}\right\}^{m}\right]^{2} \tag{2}$$

$$\frac{K_a}{K_S} = \left(1-\frac{\theta(h)-\theta_r}{\theta_s-\theta_r}\right)^{0.5}\left[1-\left(\frac{\theta(h)-\theta_r}{\theta_s-\theta_r}\right)^{1/m}\right]^{2m} \tag{3}$$

where θ_r and θ_s = residual and saturated volumetric water content, respectively; α = scale parameter for capillary pressure head; h = capillary pressure head; n and m = shape parameters; K_s = saturated hydraulic conductivity; K_w = unsaturated hydraulic conductivity; K_a = unsaturated air conductivity.

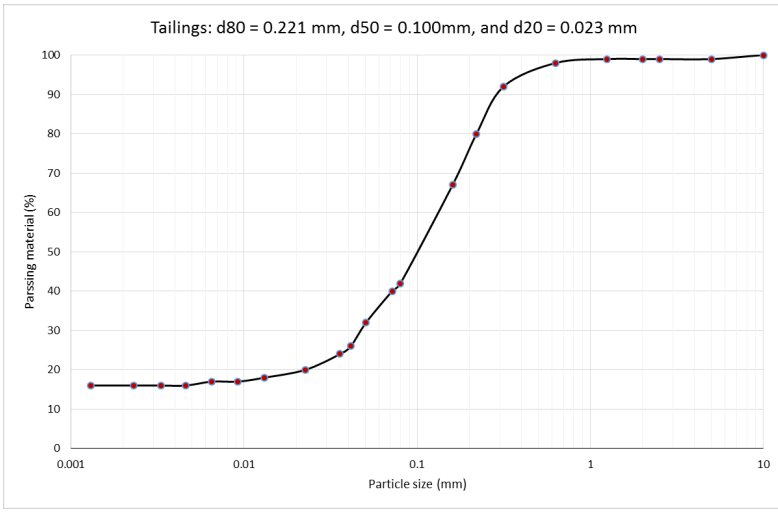

Figure 1. Particle size distribution of desulfurized tailings.

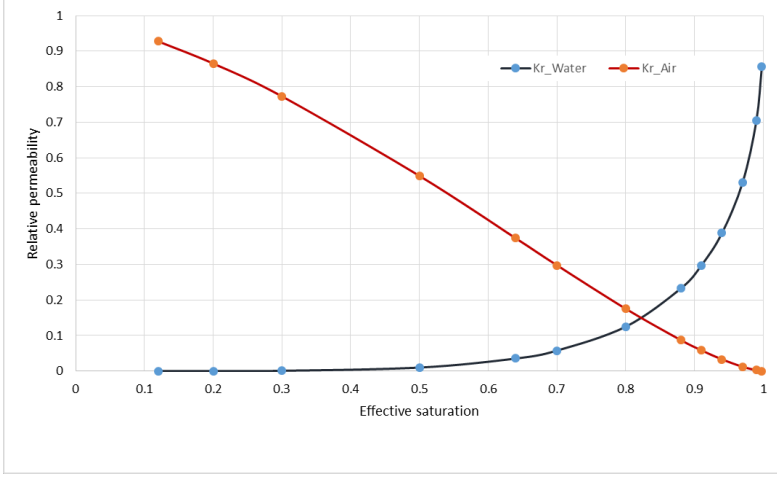

Figure 2. Relative air (Kr_Air) and water (Kr_Water) permeability for the tailings.

Figure 2 shows the relative air permeability, Kr_Air and the relative water permeability, Kr_Water, which are calculated from Equations (2) and (3). It shows that water relative permeability decreases very rapidly when water saturation decreases. The properties and characteristics of the tailings are shown in Section 3.3 and Table 1.

Waste rock

The waste rock with an average of about 1.58 wt. % sulfur is co-disposed in layered configuration to minimize oxygen ingress to the sulfide minerals exposed on the rock surface. The objective of the modelling is to better understand the gas transport processes involved in ARD production in a waste rocks covered by desulfurized tailings in a co-disposal design. The oxygen consumption rate, as shown in later Section 3.3, was extracted from kinetic testing of the waste rock. Due to much higher permeability, water saturation inside the waste rock is kept constant at 36% in the parametric study.

2.2 *Foundation soils and rock*

The temperature variation at the surface is normally equal to that of the ambient air. The variation can decrease exponentially with the distance from the surface, as shown in Figure 3. For depths below 5 to 6 m, ground temperatures are almost constant throughout the year. The average annual ground temperature is not changing with the variation of air temperature, increasing about 1 ºC per 50 m due to geothermal heat flow from the center of the earth to the surface (Williams et al., 1976).

In this study, the heat transfer from the bottom of the co-disposal to the ground depth of 6 m is included in the model and a constant temperature of 8 ºC is set at the depth of 6 m below the surface.

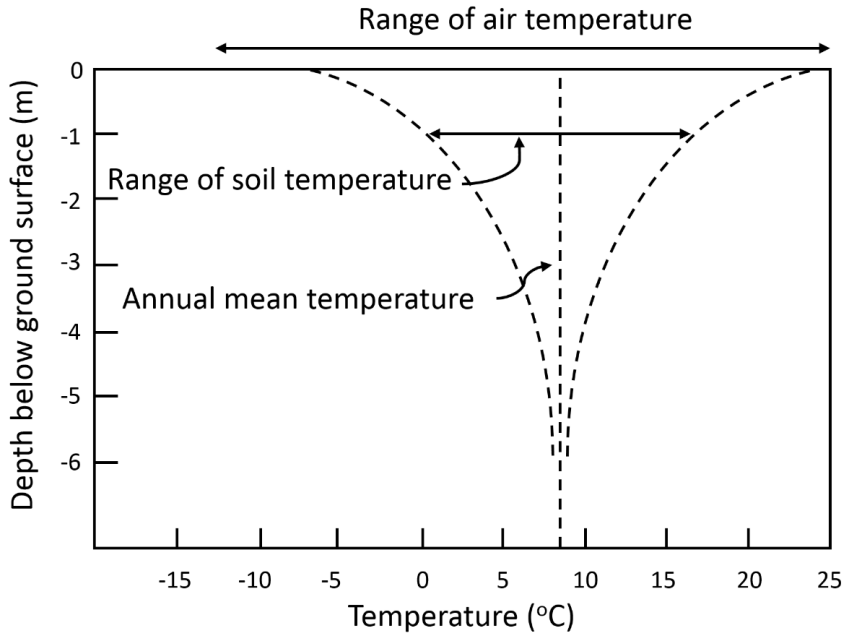

Figure 3. An example of the depth dependence of the annual range of ground temperature.

2.3 *Environmental temperature*

Temperature distribution in the co-disposal pile is an important factor affecting gas transport into the layers. It is important to know how much oxidation reactions affect the temperature rise inside the layers in the field environment. In this study, the seasonal air temperature variation is considered at the top surface of the co-disposal. Figure 4 shows a five-year monthly mean temperature data from a nearby weather station. The monthly mean temperature profile is applied as temperature boundary condition at the top surface of the co-disposal.

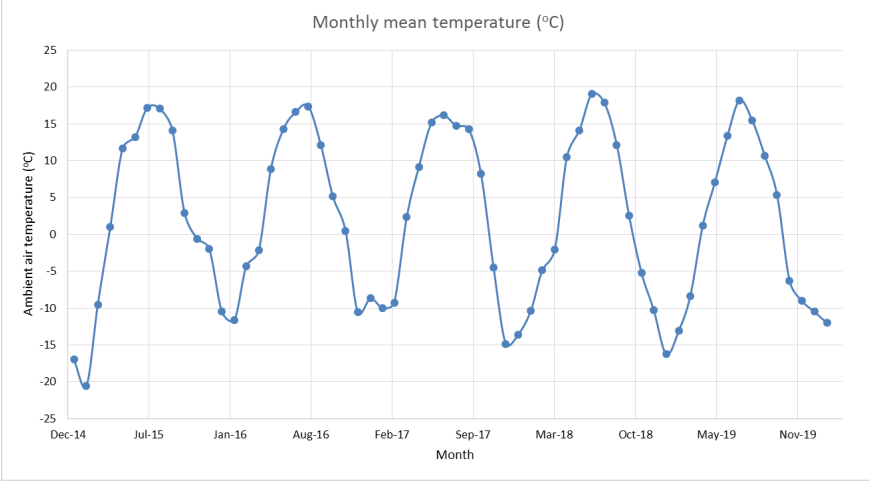

Figure 4. Monthly mean temperature profile over the past five years.

3 MODELS

3.1 *Gases transport*

Sulfide oxidation reactions in the tailings and waste rock consume oxygen. When oxygen is consumed, lower concentration inside the co-disposal drives oxygen diffusion into the layers. And the depletion of oxygen reduces oxygen partial pressure, which drives convection flow of gases in the air. In addition, the exothermic oxidation reactions increase local temperature, which promotes air convection flow and volume expansion of pore gases. The fully coupled gas transport mechanisms are modeled in the following equations.

O_2 transport is described by the equation:

$$\varepsilon \frac{\partial C_{O2}}{\partial t} = D_{ij}^{eff} \frac{\partial^2 C_{O2}}{\partial x^2} + \left[\frac{K}{\mu} \frac{\partial p}{\partial x} \frac{\partial C_{O2}}{\partial x} + \frac{K}{\mu} \frac{\partial^2 p}{\partial x^2} C_{O2} \right] - \lambda k C_{O2} \tag{4}$$

with boundary conditions:

$$C_{O2}(0,t) = 21.0\%; \ \frac{\partial C_{O2}(L,t)}{\partial x} = 0 \tag{5}$$

where ε =porosity; C_{O2} = oxygen concentration; D_{ij}^{eff} = effective gas diffusivities; K = permeability; μ = air viscosity; p = gas pressure; λ = specific surface area; k = kinetic constant of sulfide oxidation (Mbonimpa et al., 2003). Oxygen concentration at the top surface is 21% by volume in the ambient air; no flux at the bottom of the co-disposal (L).

N_2 transport is described by the equation:

$$\varepsilon \frac{\partial C_{N2}}{\partial t} = D_{ij}^{eff} \frac{\partial^2 C_{N2}}{\partial x^2} + \left[\frac{K}{\mu} \frac{\partial p}{\partial x} \frac{\partial C_{N2}}{\partial x} + \frac{K}{\mu} \frac{\partial^2 p}{\partial x^2} C_{N2} \right] \tag{6}$$

with boundary conditions:

$$C_{N2}(0,t) \approx 78.96\% \,;\; \frac{\partial C_{N2}(L,t)}{\partial x} = 0 \tag{7}$$

where C_{N2} = nitrogen concentration. Nitrogen concentration at the top surface is about 78.9% in the ambient air; no flux at the bottom of the co-disposal.

In case there is neutralization reaction, CO_2 transport is described by the equation:

$$\varepsilon \frac{\partial C_{CO2}}{\partial t} = D_{ij}^{eff} \frac{\partial^2 C_{CO2}}{\partial x^2} + \left[\frac{K}{\mu} \frac{\partial p}{\partial x} \frac{\partial C_{CO2}}{\partial x} + \frac{K}{\mu} \frac{\partial^2 p}{\partial x^2} C_{CO2} \right] + a(\lambda k) C_{CO2} \tag{8}$$

with boundary conditions:

$$C_{CO2}(0,t) = 0.04\% \,;\; \frac{\partial C_{CO2}(L,t)}{\partial x} = 0 \tag{9}$$

where C_{CO2} = CO_2 concentration; a = coefficient of neutralization. CO_2 concentration at the top surface is about 0.04% in the ambient air; no flux at the bottom of the co-disposal. In this study, neutralization reactions are ignored.

3.2 *Heat generation and transfer*

The heat equations to model heat transfer in tailings and waste rock as porous media filled with gases are:

$$(\rho C_P)_{eff} \frac{\partial T}{\partial t} + \rho C_p \vec{u} \cdot \nabla T + \nabla \cdot \vec{q} = H_P \lambda k C_{O2} \tag{10}$$

$$\vec{q} = -k_{eff} \nabla T \tag{11}$$

with boundary conditions:

$$T(0,t) = \text{ambient temperature};\; T(L+6,t) = \text{stable ground temperature} \tag{12}$$

where ρ = air density; C_P = heat capacity; $\vec{u}$ = Darcy velocity; k_{eff} = effective thermal conductivity; H_P = heat production by sulfide oxidation (Harries et al., 1981). Temperature at the top surface is the ambient air temperature; temperature at the depth of 6 m below the bottom surface of the co-disposal is set at a constant ground temperature.

The pressure, temperature and gases concentration also follow the idea gas law, $P = RT \sum C_i$.

All modules are built and integrated together on the platform of the commercial software COMSOL Multiphysics, with all connecting parameters fully coupled.

3.3 *Properties of tailings and waste rock*

The case studies are modelled for the first 5 years. We assume that the physical properties are constant, even though the materials evolve with the sulfide oxidation reactions and the formation of secondary minerals change the physical properties. Table 1 summarizes the physical parameters used in the model.

Table 1. Properties of tailings and waste rock

Property	Desulfurized Tailings	Waste rock
Porosity	0.40	0.38
Kinetic constant of sulfide oxidation	8.0×10^{-8} s^{-1}	7.5×10^{-7} s^{-1}

Sulfur content	~0.2 wt. %	1.58 wt. %t
Saturated hydraulic conductivity	1.7 x 10^{-6} m/s	2.5 x 10^{-3} m/s
Heat production by sulfide oxidation	1.71x10^{7} J/m^3	1.71x10^{7} J/m^3
Density	1900 kg/m^3	2100 kg/m^3
Dry thermal conductivity	0.9 W/mK	0.9 W/mK
Heat capacity of solids	840 J/kgK	837 J/kgK
Bulk diffusion coefficient	1.75 x 10^{-5} m^2/s	1.76 x 10^{-5} m^2/s
van Genuchten "m" parameter	0.476	m = 0.510
van Genuchten "α" parameter	0.8	2.8
Residual water saturation	S_{wr} = 0.17	S_{wr} = 0.10
Density of the foundation	2008.6 kg/m^3	
Thermal conductivity of the foundation	1 W/mK	
Heat capacity of the foundation	900 J/kgK	

3.4 *Parametric studies of co-disposal*

In the parametric studies of the co-disposal, thickness of the desulfurized tailings layers was varied from 1 m to 4 m. For each thickness of the tailings, water saturation 80%, 70%, and 50% in the tailings layer were studied. The waste rock layer was 5 m and water saturation was kept 36%, as shown in Table 2.

Table 2. Parametric studies of the co-disposal.

Tailings layer thickness (m)	1.0	1.5	2.0	2.5	3.0	3.5	4.0
Saturation	80%						
	70%						
	50%						
Waste rock (m)	5	5	5	5	5	5	5
Saturation	36%	36%	36%	36%	36%	36%	36%

4 RESULTS

Figure 5 shows oxygen model fraction profile evolution in 4 m tailings (50% saturation) and 5 m waste rock over five years. The initial oxygen concentration was 21% in fresh air; after 14 days, initial oxygen trapped in the pore space was consumed and oxygen transport mechanisms control the oxygen concentration profile. As we can see in the figure, the oxygen concentration profiles in the tailings are close to straight lines, which mean the oxidation reaction rates are very small. And the oxygen concentration profiles in the waste rock are much curved, meaning the oxidation reaction rates are much higher; but close to the bottom the waste rock layer, due to the very low level of oxygen concentration, the oxidation reactions almost stopped.

Figure 6 shows weekly temperature profiles of the co-disposal over five years, red arrow shows the direction of temperature change over the time. The figure shows the thinnest layer case of one meter tailings (50% saturation) covering the waste rock, in which the initial temperature was 8 ºC and gradually increased to the maximum temperature, 26 ºC, inside the waste rock layer. The temperature at the top surface is the ambient air temperature.

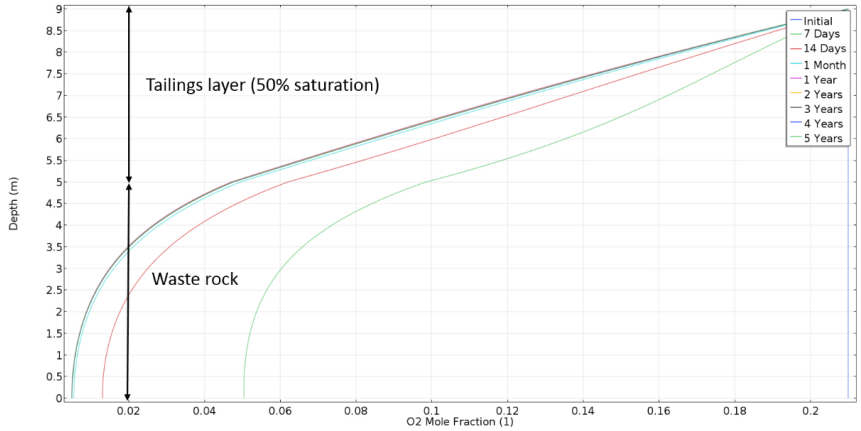

Figure 5. Oxygen mole fraction profile inside the co-disposal layers (4 m tailings and 5 m waste rock) over five years.

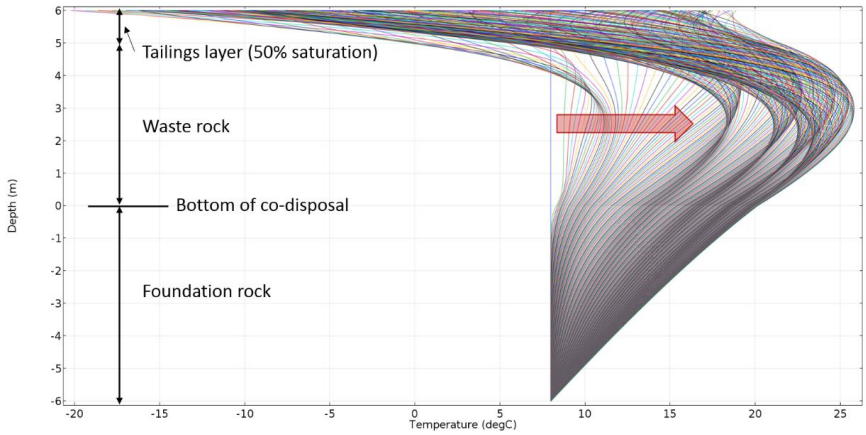

Figure 6. Weekly temperature profile inside the co-disposal layers (1 m tailings and 5 m waste rock) over five years; arrow shows the overall trend of increasing temperature in the waste rock.

Figure 7 shows the frozen depth from the top surface of the co-disposal during winter months. We can see that the smallest reaction rates with least heat production result in the deepest frozen depth. Among all the cases, the cases with 80% saturation in the tailings have the deepest frozen depths from the top surface of the co-disposal, which are from 1.83 m to 1.97 m; in the cases with 70% and 50% saturation, the frozen depths are 1.18 m - 1.33 m and 1.03 m – 1.28 m, respectively. With the expansion of frozen water, the pore space for gas phase will be decreased, which can further block gas transport into the co-disposal. But the impact of freeze-thaw cycle on the integrity of the tailings layer need to be investigated to avoid cracks formation in the tailings layer.

As shown in Figure 8, saturation inside the tailings plays a significant role of controlling the oxidation rate inside the co-disposal layers. When the saturation is over 80%, the oxidation is greatly reduced and most oxidation is in the overlying desulfurized tailings. In contrast, lower saturations (70% and 50%) result in higher oxidation rates in the waste rock increasing as tailings saturation decreases. Thickness of the tailings also plays a role of controlling the oxidation rate.

Thicker layer of the tailings can reduce the total oxidation rate of the co-disposal and reduce the oxidation rate inside the waste rock, with increased oxidation rate inside the desulfurized tailings layer.

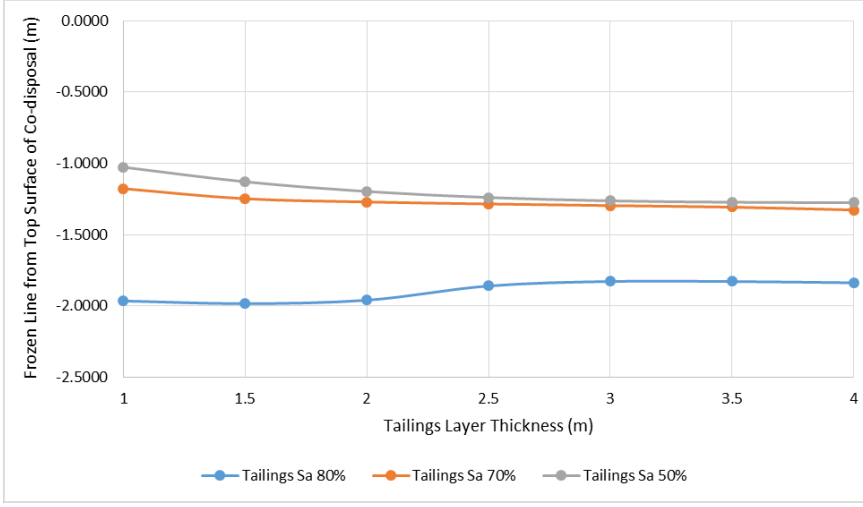

Figure 7. Frozen line from the top surface of co-disposal based on tailings water saturation of 80%, 70%, and 50%.

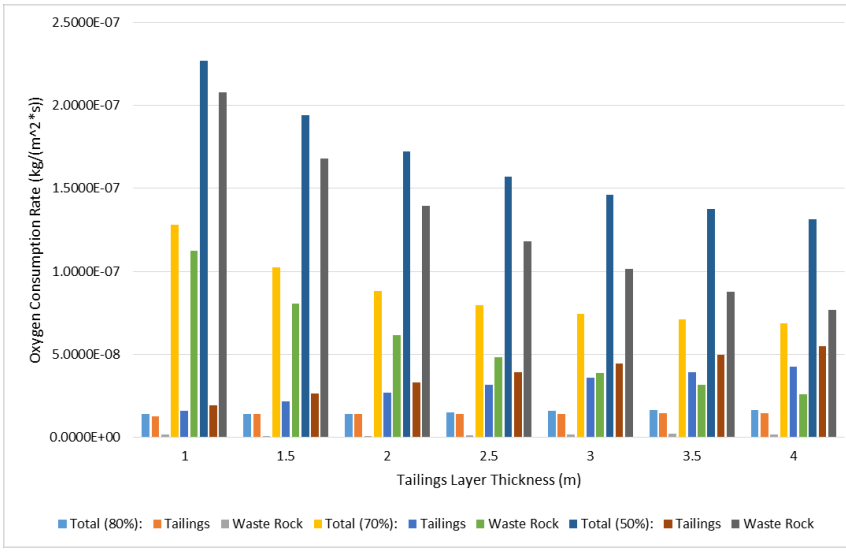

Figure 8. Comparison of oxygen consumption rates for various thicknesses of overlying tailings and for various levels of saturation (Total = Tailings at that saturation + Waste Rock).

5 CONCLUSION

The COMSOL gas transport models include air convection and oxygen diffusion in the co-disposal of tailings and waste rock. The air convection is promoted by thermal convection due to the heat generated from exothermic oxidation reactions and partial pressure change due to oxygen depletion by the oxidation reactions. The models considered environmental temperatures as boundary conditions including monthly ambient air temperature changes and ground temperature.

Temperature profiles over 5 years show the frozen depth of the co-disposal and indicate that part of the tailings layer was frozen during winter. Freezing of water can reduce the air-filled pore space, which can further reduce air permeability and diffusivity during winter.

The results of oxygen consumption rate of the parametric studies reflect the sulfide oxidation reaction rate in some theoretical configuration and conditions of one part of the co-disposal design at NMG. Saturation of the tailings has the biggest influence on the co-disposal design, thickness of the tailings has bigger influence when tailings has lower saturation. When water saturation in the tailings layer is kept above 80%, the tailings layers can greatly reduce oxidation reactions inside the waste rock; close to the bottom the waste rock layer, due to the very low level of oxygen concentration, the oxidation reactions almost stopped. When water saturation in the tailings layer is below 80%, oxidation reaction rate increases with lowering water saturation. Increasing the thickness of the tailings layer can reduce overall oxidation reaction rate, but with increased oxidation rate inside the desulfurized tailings layer. The acidity from the tailings layer is controlled with low sulfur content and the neutralization and acid potentials content. In addition, the NMG co-disposal includes other considerations not discussed in the paper, such as the final cover and/or adding impervious or thicker layer at the toe of the co-disposal pile to avoid oxygen entrance at specific place.

The models provide a tool for optimizing the design of co-disposal. It could be used to study different options with respect to cost, geotechnical and field operation constraints.

6 REFERENCES

Gélinas, P., Lefebvre, R., Choquette, M. 1992. Characterization of acid mine drainage production from waste rock dumps at La Mine Doyon, Quebec. *Second Int. Conf. on Environm. Issues and Manage of Waste in Energy and Mineral Prod.*, Calgary, Sept. 92.

Lamontagne, A., Lefebvre, R., Poulin, R., Leroueil, S. 1999. Modeling of acid mine drainage physical processes in a waste rock pile with layered co-mingling, 52nd Canadian Geotechnical Conference, oct. 25 to 27, Saskatchewan.

Ma, L.; Huang, C.; Liu, Z.S.; Morin, K.; Aziz, M.; Meints, C. 2019. Prediction of acid rock drainage in waste rock piles Part 1: Water film model for geochemical reactions and application to a full-scale case study. *Journal of Contaminant Hydrology* 220, 98-107.

Mbonimpa, M.; Aubertin, M.; Aachib, M.; and Bussière, B. 2003. Diffusion and consumption of oxygen in unsaturated cover materials. *Can. Geotech. J.* 40: 916–932.

Harries, J. R. & Ritchie, A. I. M. 1981. The use of temperature profiles to estimate the pyritic oxidation rate in a waste rock dump from an opencut mine. *Water, Air, and Soil Pollution* 15 405-423.

Morin, K. A.; Gerencher, E.; Jones, C. E.; Konasewich, D. E. 1991. Critical Literature Review of Acid Drainage from Waste Rock. MEND Project 1.11.1.

Mualem, Y. 1976. A new model for predicting the hydraulic conductivity of unsaturated porous media. *Water Resour. Res*. 12: 513–522.

Shandro, J.; Jokinen, L.; Stockwell, A.; Mazzei, F.; Winkler, M.S. 2017. Risks and Impacts to First Nation Health and the Mount Polley Mine Tailings Dam Failure. *International Journal of Indigenous Health*; Victoria Vol. 12, Iss. 2: 84-102.

Silva, A.A.; Lunas, D.A.L.; Bicalho, P.S.S. 2019. The impact of the Brumadinho dam failure in Naô Xohâ village. *Sustentabilidade em Debate*, 12, Volume 10, Issue 3.

van Genuchten, M.Th. 1980. A closed form equation for predicting the hydraulic conductivity of unsaturated soils. *Soil Sci. Soc. Am. J.* 44: 892–898.

Williams, G. P.; Gold, L. W. 1976. Ground temperatures. *Canadian Building Digest*, 1976-07.

All Hands on Deck! - A Semi-Quantitative Attempt to Characterize the Impending Qualified Tailings Professional Resource Shortage

Christopher N. Hatton
Haley and Aldrich, Inc., Greenwood Village, Colorado, USA

D. Louise Spencer
Colorado State University, Fort Collins, Colorado, USA

Christopher A. Bareither
Colorado State University, Fort Collins, Colorado, USA

Kelly J. Ward
Marsh, Denver, Colorado, USA

ABSTRACT: The mining industry is experiencing a radical change in the governance of tailings storage facilities. Guidance and regulations crossing many jurisdictions continue to contribute to this amorphous change. The Canadian Dam Association, Mining Association of Canada, Australian National Committee on Large Dams, and the Global Tailings Standard being produced by the International Council on Mining and Metals, among others, are establishing guidelines for more rigorous industry governance. This new and evolving guidance regarding tailings storage facilities (TSFs) is developing concurrently with a historic shortage of experienced tailings engineers, which adversely affects the resource base available to deploy and support the new governance. An inventory was made to quantify the number and size of TSFs worldwide, and to estimate labor required by qualified professionals and associated costs to meet ongoing tailings stewardship initiatives. The evaluation was initiated using available data documenting active and inactive jurisdictional TSFs. Several jurisdictions queried produced searchable inventories synthesized based on dam height and hazard classification. The research presented herein represents a discrete moment in time as contributions to the available information and inventories accessed continues and, today, is incomplete; however, the data used provides essential insight into the resource deficiencies that currently exist within our profession.

1 INTRODUCTION

The recent Mount Polley (Morgenstern, Vick, & Van Zyl 2015), Fundão (Morgenstern et al. 2016), and Feijão (Robertson et al. 2019) TSF failures have had profound and pivotal impacts on the mining industry and tailings stewardship. The Mount Polley failure in British Columbia, Canada, raised awareness of the distribution of responsibility, the importance of governance, and the role of the Engineer of Record (EoR). The immediate outcome from Mount Polley was a renewed focus on tailings governance documents such as those developed by the Canadian Dam Association (CDA), the Mining Association of Canada (MAC), and others, with anticipated contributions from jurisdictions in Australia via Australian National Committee on Large Dams (ANCOLD). Further, EoR guidance was established by the Geoprofessional Business Association (GBA) post-Mount Polley.

The Fundão failure in Mariana, Brazil, reinforced the importance of governance, highlighted the importance of monitoring systems, and provided further understanding of collapse mechanisms that occur in extrusive TSF failures. The failure also put the industry on notice that further attention to TSFs was required beyond that which is partially implemented by major mining companies.

The Feijão Dam failure in Brumadinho, Brazil, sparked a shift to action. The International Council on Mining and Metals (ICMM) convened tailings professionals from mining companies worldwide to provide input for a new guidance document, recently released for industry-wide

comment and known as the Global Tailings Standard (GTS). The Church of England, supported by 100 investors with over $13 trillion USD in assets under management, made a call to action to request dam-by-dam disclosure of TSFs. This initiative is named the Investor Mining and Tailings Safety Initiative and is co-chaired by the Church of England Pensions Board and Swedish National Pension Funds' Council on Ethics, with additional support from the UN Environment Programme.

These recent tailings dam failures have reaffirmed the need for enhanced tailings governance, which is evident in the anticipated updates to monitoring and regulatory requirements of TSFs from the CDA, MAC, ANCOLD, and ICMM. The promulgated guidance establishes requirements for EoR experience, development requirements for conducting dam safety reviews, and inspections for the ever-changing state-of-practice and associated standard of care. We are beginning to see developments of prescriptive requirements for engaging the EoR and established frameworks for owner-defined responsibilities and expectations thereof. Continued concerns of TSF failures, demands for tailings governance, and new monitoring and regulatory requirements justify the question: ***Do we have enough professional labor resources to serve the mining industry?*** The lack of labor resources was first brought to the industry's attention by Hatton and Morrison (2016). Our profession needs justifiable estimates of the number and characteristics of TSFs worldwide to make relevant predictions for the labor force needed to serve the mining industry in our collective mission to make tailings management safer for human health and the environment.

Our preliminary literature review revealed that most studies that compile TSF data focus on the 356 documented tailings dam failures that have occurred since 1915 (Bowker and Chambers 2019). Limited studies have been conducted to compile active and inactive TSFs throughout the world. Thus, commonly referenced estimates of the number of worldwide TSFs vary between 3,500 (Davies et al. 2000) and 18,400 (Herza et al. 2019).

The Investor Mining and Tailings Safety Initiative sent disclosure request letters regarding TSF data disclosures in April 2019 to 727 publicly listed companies. Disclosed data is currently being compiled by GRID-Arendal in collaboration with the Investor Mining and Tailings Safety Initiative to create the Global Tailings Portal (2020). The most recent release of information from the Global Tailings Portal identified only 1,939 TSFs and suggests, based on the research presented in this paper, there remains a large information gap with regards to the number of TSFs worldwide (Global Tailings Portal 2020).

This paper presents an initial estimate of the number of TSFs that is then used to estimate the labor resources necessary to service these structures in our global economy. The information available is generally sparse with limited documentation concerning the existence of TSFs, let alone the additional information related to physical geometry, downstream consequences, and risks of failure. The initial presentation of these data was in a keynote lecture at the 2019 Tailings and Mine Waste Conference in Vancouver, Canada (Hatton 2019). Since that time, the team has refined the database and will continue to pursue opportunities to improve the efficacy of these data further.

2 METHODS

2.1 *Worldwide TSF Inventory*

2.1.1 *Compilation of Publicly Available Information*

An initial literature review was performed to compile data on TSFs for select regions, including North America, South America, and Australia. Focus regions were selected based on anticipated publicly available information. The search was performed using online platforms, including Google Scholar, Colorado State University Library, and OneMine. Literature was queried for the regions as mentioned above with terms such as "tailings," "tailing," and "tails."

Preliminary search efforts for a global inventory of TSFs yielded two potential sources. The International Committee on Large Dams (ICOLD) maintains a World Register of Dams (WRD) with data furnished by the ICOLD National Committees. However, the Secretary-General of ICOLD indicated that 'only very recently' the WRD has included TSFs (LeDelliou 2019, personal communication). On 5 April 2019, the Investor Mining and Safety Initiative issued a request for disclosure of TSFs from 727 publicly listed extractive companies, which includes companies in mining, oil, and gas industries. As of 20 December 2019, 46% of the companies contacted responded with disclosures of TSFs.

2.1.2 *Direct Contact with Regulatory Agencies*

Screening for a global TSF inventory was supplemented with efforts to locate publicly available TSF inventories at the national level with a continued focus on North America, South America, and Australia. Direct contact was initiated with regulators via email at the state and/or province-level within Australia, Canada, and the United States (Table 1) to identify the quantity and characteristics of TSFs within each regulatory jurisdiction. The specific agencies contacted for each jurisdictional region are summarized in Table 1. Agencies that responded with TSF information are bolded in the table below.

Table 1. Summary of regulatory agencies contacted.

Country	**Regulator** (Jurisdictional Region Contacted)
United States	**Mine Safety and Health Administration** (United States), Bureau of Land Management (Alaska, Arizona, California, Colorado, Idaho, Nevada, Oregon/Washington, **Utah**, Wyoming), **Department of Natural Resources** (Colorado), **Department of Water Resources** (Idaho), **Division of Environmental Protection** (Nevada).
Canada	Enterprise and Trade Resource Development Division (Manitoba), **Department of Natural Resources and Energy Development** (New Brunswick), Dam Safety Program (Newfoundland and Labrador) **Mackenzie Valley Land and Water Board** (Northwest Territories**), Environment, Inspection Compliance and Enforcement** (Nova Scotia**), Ministry of Energy, Northern Development and Mines** (Ontario), Ministry of Natural Resources and Forestry (Ontario), **Ministry of Environment, Environmental Protection Division** (Saskatchewan), Minerals Resources Branch (Yukon Territory), Yukon Water Board (Yukon Territory), **Energy, Mines and Resources, Mineral Resources** (Yukon)
Australia	Department of National Resources, Mines and Energy (Queensland), Department of Environment and Science (Queensland), **Department for Energy and Mining** (South Australia), Environment Protection Authority, Licensing and Community Responses (South Australia), **Department of Primary Industries, Parks, Water and Environment** (Tasmania), Department of Environment, Land, Water, and Planning (Victoria), **Department of Jobs, Precincts and Regions** (Victoria), **Department of Mines, Industry Regulation and Safety, Resource and Environmental Compliance Division** (Western Australia)

Note: Regulatory Agencies that responded with TSF information are noted in **bold** font

2.2 *TSF Classification Types*

Acquired TSF inventories were screened for available information pertaining to dam geometry and/or risk criteria and subsequently divided into classification types. Criteria used to separate TSFs into classification types were selected for convenience in our work with the recognition that there are multiple permutations and screening levels that could be applied. These screening criteria were tailored to the available resource databases.

The TSF classification types were developed to proportionally estimate labor resources with an inherent understanding that the level of effort required to service a smaller, lower production

TSF (for example) is less compared to a sizeable, world-class facility. In this example, the smaller facility would require a much smaller amount of time to provide appropriate EoR support (e.g. eight hours of senior engineer time per month), whereas a large, world-class facility would require a dedicated team of professionals working daily throughout the structure's operational life. A similar proportional distribution of labor resource time could be applied when TSFs are viewed in terms of risk classification as assigned by their given jurisdictions, with high-risk TSFs requiring more time.

In recognition that every TSF is unique, (i) dam height and (ii) hazard or risk rating categories were used to assign three TSF classifications for each: Type A, Type B, and Type C (described subsequently). The TSF classification types helped address variability across the inventoried TSFs and served to simplify the albeit rough estimate of labor resource needs.

An initial comparison was made between the number and percentages of TSFs falling within the Types A, B, and C classifications for jurisdictions with available information. The proportion range for Types A, B, and C defined from this exercise were subsequently extrapolated to our estimate of TSFs worldwide to assign classification types for labor force calculations.

2.2.1 *Screening Criteria by Height*

Dam geometry was initially selected as a screening criterion with the intent to use available TSF characteristics, such as embankment height, surface area, storage volume, or other attributes in the compiled information. Embankment (crest) height was the most ubiquitous TSF characteristic within the inventories available, while other data was often limited. Therefore, height was selected as the preferred screening criterion.

TSFs were grouped into the following three classification types based on crest height (thresholds arbitrarily selected) provided in the available inventories:

- Type A - small structures with crest height < 12 m (40 ft);
- Type B - intermediate structures with crest height > 12 m (40 ft) but < 30 m (100 ft); and
- Type C - large structures with crest height > 30 m (100 ft).

Within a given classification type, other TSF characteristics, such as retained tailings or pond surface area, vary due to different elevation and topography characteristics between structures. For example, in mountainous regions, TSFs with high crest heights built across narrow valleys may contain small volumes of tailings compared to TSFs built on flatter topography where low crest heights can retain large volumes of tailings. Thus, using only crest height as a screening tool does not capture the substantial differences between any two TSFs and is not a reliable indicator of risk when compared to other geometric characteristics.

2.2.2 *Screening Criteria by Hazard*

Hazard or risk rating was the second criterion used for assigning TSF classification type. Different guidelines were used to assign risk/hazard ratings in TSF inventories for the U.S., Canada, and Brazil. For example, the United States hazard potential is defined by the Mine Safety Health Administration (MSHA) as "low," "significant", or "high" following the Federal Emergency Management Act (FEMA 1998). In Canada, consequence potentials are defined as "low," "significant," "high," "very high," or "extreme," as outlined by the Canadian Dam Association (CDA 2013). Finally, in Brazil, the Agência Nacional de Mineração (2019) assigns each TSF a potential associated damage rating of "low," "medium," or "high."

TSFs from the U.S., Canada, and Brazil were separated into the following classification types:

- Type A – low hazard potential (United States), low consequence potential (Canada), and low potential associated damage (Brazil);
- Type B – significant hazard potential (United States), significant consequence potential (Canada), high consequence potential (Canada), and medium potential associated damage (Brazil); and
- Type C – high hazard potential (United States), very high consequence potential (Canada), extreme consequence potential (Canada), and high potential associated damage (Brazil).

The selected hazard potential classification types were not meant to represent an established risk or hazard classification, but only to serve as a constructive grouping for comparison and to support labor force calculations presented below.

2.3 *Personnel and Labor Resource Calculations*

The exercise for calculating labor resources needs was conservatively approached with simplified assumptions using broad generalizations with the intent of obtaining an order of magnitude estimate. This estimate, in this context, has been made to illustrate the more significant point regarding available tailings professional resources within the industry.

Calculations for personnel and labor resources were estimated with consideration of requirements for TSF governance and informed by our experience in the execution of EoR duties. Limits for resource demands were further refined and focused on a tangible, measurable task such as the requirements for servicing the facility as the EoR. The service needs of an EoR for a given type of TSF (e.g. Type A, B, C) were assumed to be generally consistent based on anticipated needs and represent activities that can be estimated and roughly quantified. Assumptions used for quantification of EoR duties as described within this paper was associated with day-to-day TSF operations based on established or forthcoming governance. These responsibilities cover the interaction with operations and the continuous engineering support required.

The resource demand calculations included operational support for day-to-day safe dam operation and intentionally excluded the engineering demand outside of EoR, such as the design of capital expenditure projects (CAPEX), sustaining capital projects, and specific aspects of operational expenditures (OPEX). The exercise also focused on the use of external resources with an outside party serving as the EoR, which is a common approach in the industry. Associated overhead costs, supporting labor such as word processing, and other administrative support services such as drafting and communications were not included.

A summary of the personnel, billing rates, and resource demands used for the labor resource calculations is presented in Table 2 below. The EoR is assumed to be a Senior Engineer that fulfills the following expectations:

- Subject matter expert in tailings dam design, construction, and operation;
- 10 years (minimum) of qualifying experience;
- Liaise with responsible tailings facility engineer(s);
- Regular and proactive engagement with operations;
- Conduct regular dam safety inspections (e.g. monthly, quarterly, annually);
- Develop and/or update operational documents (e.g. Emergency Action Plans, Operation, and Maintenance Manuals, Tracking Action Response Plans [TARPs], Emergency Preparedness Response Plan [EPRP]);
- Oversee environmental and regulatory compliance;
- Prepare for third-party reviews; and
- Support tailings stewardship boards.

Table 2. Personnel, rates, and resource demands used for labor resource calculations

Personnel	**Experience**	**Billing**	**Resource Demand as Billable Hours per Month**		
			Type A TSF	**Type B TSF**	**Type C TSF**
EoR	10-25 years	$200 USD/hour	8	48	64
Junior Eng.	5-10 years	$140 USD/hour	16	48	120

3 RESULTS

3.1 *Worldwide TSF Inventory*

3.1.1 *Literature Review*

A summary of country-specific TSF quantities based on numbers reported in the literature is presented in Table 3. The literature review revealed two sources widely referenced regarding the estimated number of global TSFs. Davies et al. (2000) provide an estimate of "more than 3500 tailings storage facilities worldwide," which included TSFs quantified in Western Australia, Quebec, British Columbia, South Africa, and Zimbabwe. Azam and Li (2010) directly reference "a world inventory of 18,401 mine sites". Other papers found in the literature (e.g. Herza et al. 2019) reference Azam and Li (2010) as approximately 18,400 tailings storage facilities, which appears to assume that each mine site, on average, has one TSF.

Table 3. Tailings storage facility quantities reported in literature

Region	TSFs Reported	Literature Source
Peru	183	H.R. Wallingford 2019
China	8869	Li, Agioutantis, & Zou 2017
South Africa	400	Davies, Martin, & Lighthall 2000
Zimbabwe	500	Davies, Martin, & Lighthall 2000
Alberta	48	Alberta Energy Regulator 2018
British Columbia	98	Chernoloz 2017; Government of British Columbia 2015
British Columbia	118	Casino Mining Corp
British Columbia	130	Davies, Martin, & Lighthall 2000
Quebec	65	Davies, Martin, & Lighthall 2000
Western Australia	350	Davies, Martin, & Lighthall 2000
Western Australia	800	ASMJ 2019
Brazil	633	Oliveira & Kerbauy 2016
Chile	449	Villavicencio 2013
Chile	740	Honrubia 2019
Chile	660	Ghorbani & Kuan 2016

3.1.2 *Internet Resources*

3.1.2.1 Global

The current version of ICOLD's WRD, updated in September 2019, includes 74 dams with a listed purpose of "tailings." After manual inspection of the inventory, an additional 65 TSFs were identified by the words "tails" or "tailings" contained in the name. These additional 65 TSFs were classified with the purpose of "Other" and not "Tailings." Including these facilities identified by name, the current WRD contains 139 TSFs.

As of 30 January 2020, the total number of individual TSFs submitted to and compiled by the Investor Mining and Safety Initiative was 1,939, which pertain to 305 mining operators at 764 mine sites within 60 countries (Figure 1). The currently disclosed volume of tailings in storage totals 45 billion m3 (Global Tailings Portal 2020). Information disclosed through the Investor Mining and Tailings Safety Initiative is publicly available on both the Church of England website and the Global Tailings Portal website hosted by GRID-Arsenal.

3.1.2.2 National Inventories

Publicly available national inventories were found for the U.S., Chile, and Brazil. Three TSF inventories were obtained for the U.S.: (i) MSHA, (ii) National Performance of Dams Program (NPDP), and (iii) National Inventory of Dams (NID), facilitated by the United States Army

Corps of Engineers (USACE). The Mine Safety and Health Impoundment inventory (MSHA 2019) contains active dams associated with MSHA regulated sites that are classified by purpose. In the MSHA database, there currently are 470 dams that classify as "tailings" or contain "tails" or "tailings" within the name of the impoundment.

The NPDP (NPDP 2015) is an inventory compiled by Stanford University that includes active and inactive dams, of which 848 dams identify with the purpose "tailings." Finally, the NID (NID 2018) is an inventory maintained by the USACE that also contains active and inactive dams classified by purpose. As of 2018, the NID reports 1,363 dams in the U.S. with purpose listed as "tailings." The NID is believed to be the most complete database as MSHA provides its list of active dams to the NID each year.

A national compilation for Chile is published by the Servicio Nacional de Geología y Minería of Chile (2019). The published inventory in 2019 includes 742 tailings storage facilities, which are classified as "depositos relaves" in the Chilean compilation. Similarly, the Agência Nacional de Mineração of Brazil (2019) published an inventory of "barragens de mineração" on 31 January 2019, through which 717 tailings storage facilities were identified.

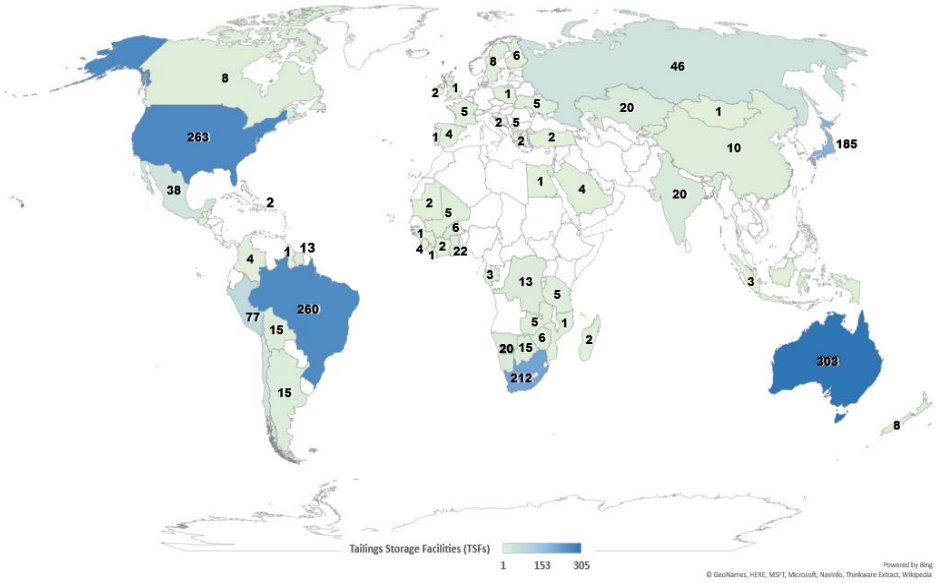

Figure 1. TSFs disclosed as of 30/1/2020 from the Investor Mining & Tailings Safety Initiative request for disclosure.

3.1.3 *Direct Contact with Regulatory Agencies*

Direct contact with regulatory agencies in the U.S., Canada, and Australia provided additional TSF data. The number of TSFs reported from regulatory jurisdictions are summarized in Table 4. The coverage of any single country was not complete. However, reported TSFs by regional jurisdiction provided valuable data to compare with the national inventories.

3.1.4 *National TSF Compilation and Global Estimate*

National estimates of the number of TSFs throughout the world are shown in Figure 2. Publicly available information on TSF quantities was combined with state/provincial regulatory data to create national estimates. Each national TSF estimate was rounded to the nearest ten to reflect data uncertainty for each country as well as variability in the number of TSFs for a given country when referencing different databases. Also included in Figure 2 are reported TSFs in the Church of England database for countries not yet compiled in this study.

Table 4. Tailings storage facilities reported from direct contact with regulators.

Country	Jurisdictional Region	Regulator Reported Tailings Storage Facilities
United States	Idaho	39
	Nevada	150
Canada	New Brunswick	19
	Newfoundland and Labrador	60
	Northwest Territories	10
	Nova Scotia	15
	Ontario	30
	Saskatchewan	18
	Yukon Territory	10
Australia	New South Wales	59
	South Australia	33
	Tasmania	16
	Victoria	10

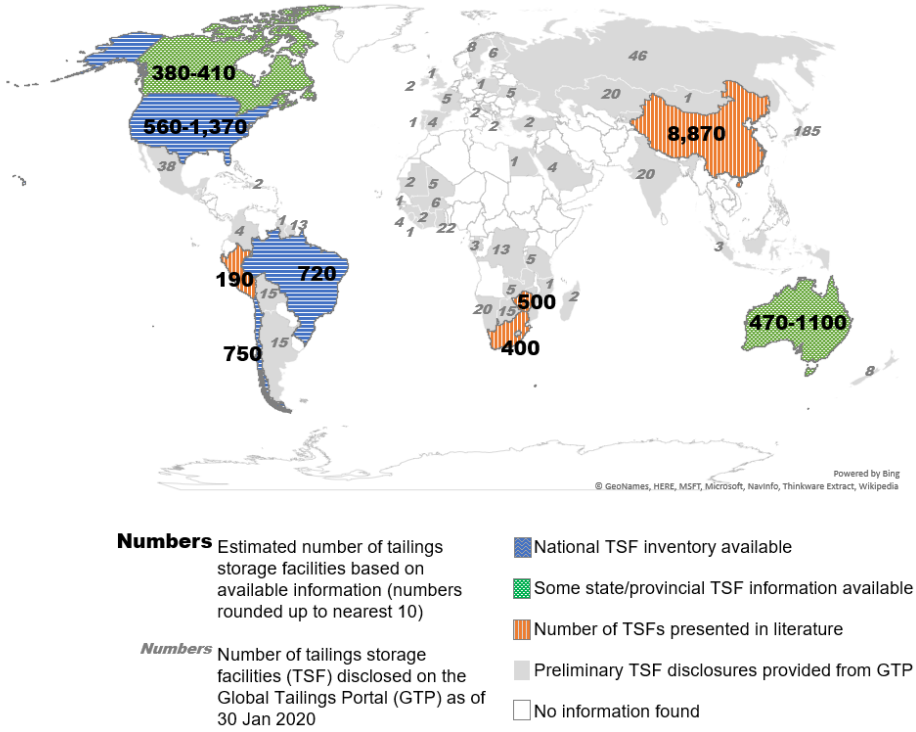

Figure 2. Available information on tailings storage facilities by country.

3.1.4.1 United States

Comparisons between the number of TSFs reported in three available inventories for the U.S. and reported directly from the regulator are in Table 5. The MSHA database provided the lowest quantity of reported TSFs. The regulator provided the highest number of TSFs for the two states

evaluated (Nevada and Idaho). The MSHA impoundment inventory only reported active TSFs, of which they report 560 active TSFs in the U.S. Data from the MSHA inventory are provided to the NID data, who report a total of 1,370 active and inactive TSFs. In this study, the NID estimate was used for labor resource calculations under the presumption that inactive dams still require engineering oversight. The NID also maintains the most substantial, current, and comprehensive data set on tailings storage facilities within each state.

Table 5. Comparison of tailings storage facilities reported by public inventories and regulators.

	Idaho	Nevada	Arizona	Texas
MSHA 2019 Inventory	6	18	24	1
NPDP 2015 Stanford Inventory	36	74	12	46
NID 2018 Inventory	22	74	11	50
Regulator Reported	39	150	---	---

3.1.4.2 Canada

Publicly available data in literature were combined with regulator-provided estimates to generate an estimate of 370-410 TSFs in Canada. The range, for example, represents varying estimates in literature for the number of TSFs in British Columbia. No references or responses from regulators were obtained for Manitoba, Prince Edward Island, or the Nunavut Territory.

3.1.4.3 Australia

Publicly available data in literature were combined with regulator-provided estimates to generate an estimate of 610 – 1,090 TSFs in Australia. The large range in TSFs reflects discrepancies between several literature sources, and the regulator provided information for Western Australia. For example, Davies and Martin (2000) refer to 350 tailings dams within the state, while the Australian Safety and Mine Journal (2019) reports more than 800 TSFs. The mine infrastructure database available through the Department of Mines, Industry, Regulation and Safety (2019) indicates there are 976 entries classified as TSFs. However, multiple entries could be associated with a single TSF (for example, one TSF can have several cells, with each cell having an entry in the infrastructure database). No references or responses from regulators were obtained for Queensland or the Northern Territory.

3.1.4.4 South America

National estimates of TSF in South America were used directly from the reporting organization. The Agência Nacional de Mineração in Brazil reports 720 TSFs and the Servicio Nacional de Geología y Minería in Chile reports 750 TSFs. An estimate of 190 TSFs in Peru was taken from the Wallingford (2019), which references the Organismo Supervisor de la Inversión en Energía y Minería website inventory on TSFs. The remaining countries in South America are still being researched to obtain estimates of the number of TSFs.

3.1.4.5 Other

National estimates of TSFs for the remaining countries throughout the world are also in progress. Estimates in Figure 2 developed in this study include 8,870 TSFs in China (Agioutantis and Zou 2017), as well as 400 TSFs in South Africa and 500 TSFs in Zimbabwe obtained from Davies et al. (2000). All remaining estimates in Figure 2 shown as grey text with grey-highlighted countries were derived from the Global Tailings Portal's current disclosure.

3.1.4.6 Global Estimate

Our study found 12,970 – 14,300 active and inactive tailings storage facilities in the following countries: Canada, United States, Brazil, Peru, Chile, China, Zimbabwe, South Africa, and Australia. Including the additional 550 TSFs disclosed on the Global Tailings Portal in countries outside of the ones listed above suggests more than 13,520 – 14,850 active and inactive TSFs worldwide. The lowest estimated quantity of TSFs worldwide, for this paper, totals 15,000 in-

corporating the number of countries with partial disclosure of information from the Investor Mining and Tailings Safety Initiative and countries lacking any information on TSF quantities.

3.2 *TSF Classifications*

Inventories acquired that included information on TSF geometry and/or hazard/risk classification included the following: United States, Brazil, New South Wales (Australia), Tasmania (Australia), New Brunswick (Canada), and Alberta (Canada). Estimates of the number of TSFs and proportion of Type A, B, or C TSF classification are summarized below in Table 5 for embankment crest height and in Table 6 for hazard potential.

TSF classification by crest height (Table 6) yielded a wide range of type distributions by country. Type A classifications ranged from 8% - 63%, Type B from 17% - 50%, and Type C from 13% - 75%. Data from Australia and Canada are only available for two jurisdictional regions representing less than 100 TSFs in each country. These data are therefore judged to be not representative of the distribution of dam geometry country-wide. Data from the U.S. and Brazil appear to reasonably cover active and inactive TSFs within the country and have detailed information on geometry.

Table 6. Tailings storage facility screening by height

	United States		Brazil		Australia				Canada			
Tailings Storage Facilities	1362		717		New South Wales 58		Tasmania 16		New Brunswick 19		Alberta 48	
Type A Height < 40ft	593	44%	361	50%	12	21%	10	63%	4	21%	4	8%
Type B 40ft ≤ Height ≤100ft	542	40%	231	32%	29	50%	4	25%	12	63%	8	17%
Type C Height > 100ft	227	17%	125	17%	17	29%	2	13%	3	16%	36	75%

TSF classification by hazard (Table 7) resulted in a heavier classification of Type C dams. Type A classifications ranged from 0% - 32%, Type B from 17% - 37%, and Type C from 30% - 63%. The dam inventory available for Alberta, Canada, contains only "high consequence" dams and therefore does not include any Type A TSFs, skewing the classification distribution towards the Type C category. TSF data for New Brunswick only includes hazard classifications for 10 of the 19 TSFs within the inventory. Data from the U.S. and Brazil appear to comprehensively cover active and inactive TSFs within the country and have detailed information on geometry.

The highest country-wide coverage and level of detail in disclosed information is available for the inventories of active TSFs within the United States (MSHA 2019) and within Brazil (Agência Nacional de Mineração 2019). Note: of the 717 TSFs listed in Brazil, 292 do not have an associated potential damage rating. Percentages calculated for this study are percentages of the categorized 425 TSFs. A comparison was made between the U.S. and Brazil to assess similarities and differences in the percent distribution of TSFs in the three classification types. Figure 3 shows the distribution of Type A, Type B, and Type C TSFs within Brazil and the U.S. based on height and hazard classification.

Classification by crest height is biased towards small dams, as shown in Figure 3. This is likely attributed to not accounting for other factors (e.g. the volume of tailings impounded, distance from towns/cities, etc.) that can influence the hazard rating. In contrast, the hazard rating is biased toward high hazard facilities. Thus, using both estimates for labor resources led to what is believed a lower-bound estimate based on crest height and upper bound estimate based on hazard potential.

Table 7. Tailings storage facility screening by hazard classification.

	United States		Brazil		Canada			
Tailings Storage Facilities	559		425		New Brunswick 10		Alberta 48	
Type A "Low" Hazard	180	32%	50	12%	4	40%	0	0%
Type B "Medium" Hazard	94	17%	157	37%	3	30%	18	38%
Type C "High" Hazard	285	51%	218	51%	3	30%	30	63%
Not classified	0	---	292	---	9	---	0	---

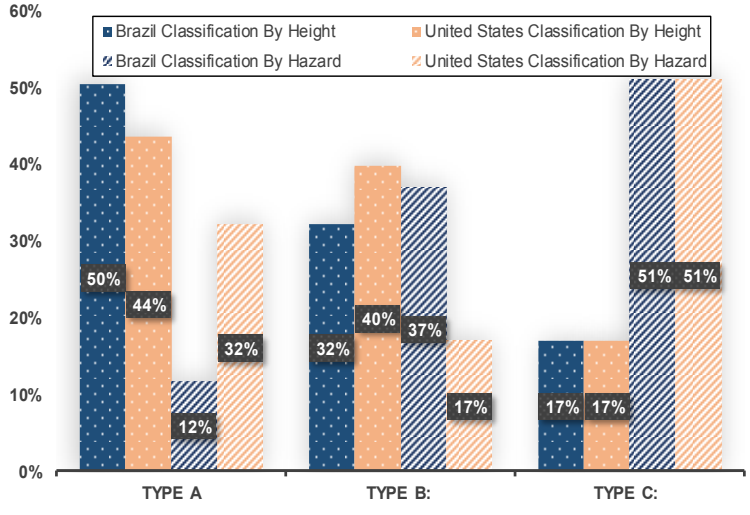

Figure 3. Tailings storage facility classification by type.

3.3 *Personnel and Labor Resource Calculation*

Estimates of annual personnel and labor resources required to service the current estimate of 15,000 global TSFs are shown in Table 8. The ranges of percent contribution of TSFs for each type classification were chosen from the data available for the United States and Brazil due to the high quality of information available on tailings dam quantities and characteristics for these two countries. For each range of type distribution, the monthly hours for junior engineers and EoRs were calculated using the labor distribution by type described above in Table 2. The number of monthly hours was then multiplied by the billing rate shown in Table 2 to calculate a total annual cost in USD. Finally, using a 52-week average year and an average of 40 hours per week, the number of full-time equivalents (FTEs) were calculated by dividing the total number of hours for each engineer type by the 2080 average work hours per FTE per year.

The calculations from this study indicate that the annual cost for EoR duties totals between $2.2 – $3.9 billion USD. The estimate shows, based on our assumptions and inputs, that roughly 6,500 to 11,500 FTEs will be required to provide EoR services annually.

Table 8. Estimates of TSF type classification and labor resource demands.

TSF Screening Criteria	Percent Contribution of TSFs			Annual Cost (USD)	Full Time Equivalents (FTEs) - Junior Engineer	FTEs - Engineer of Record (EoR)
	Type A	Type B	Type C			
Crest Height	44 – 51	32 – 40	17	$2.2 - 2.4 billion	3800 - 4030	2630 - 2900
Hazard Potential	12 – 32	17 – 37	51	$3.4 - 3.9 billion	6450 - 7000	3760 - 4450

4 CALL TO ACTION

The shrinking numbers of talent within the industry – through retirement and lack of "fresh" tailings personnel entering in the past 20 years – is significant, and the time required to develop sustainable personnel resources that comply with the existing and known forthcoming guidance must be thoroughly developed within the next decade. This is a call to action directed at the Owners and Operators, Tailings Consultants, and Universities and Colleges. This triumvirate of resources must provide the training ground for individuals that would eventually serve the role of the Engineer of Record (EoR).

These groups are interlinked regarding mutual financial and resource support needs, and each should serve as an asset to TSF stewardship. Competition between these groups and a lack of collaboration will continue to dilute the resource base negatively. We need to change the way we do business.

This is a call to action for mining industry Owners and Operators. The greater community is asking Owners and Operators to:

- Commit to TSF planning and operation with a "no failures" mindset,
- Raise awareness of the necessity of mining in the global supply chain and that waste management including TSFs are a fundamental necessity to almost every operation,
- Develop comprehensive and well-structured stewardship programs that include comprehensive training programs,
- Deliberate and evaluate the long-term effects of every decision made or not made, and temper quarterly reporting that lacks alignment with long-term vision and stewardship needs. In other words, quit kicking the can down the road,
- Engage and share resources through training, secondment, and apprenticeships,
- Establish favorable contract conditions that allow consultants and universities to function as partners and extensions of the operations. These resources should be used to provide a knowledge transfer, not a liability transfer,
- Commit to extending the State of the Practice through research and embracing innovations;
- Allow and encourage service providers to share project experiences to advance the State of the Practice. The amount of experience and information that has been prevented from dissemination by intervention from corporate attorneys and other company representatives over the last 20 years is immense and to the detriment of the industry, and
- Share lessons learned and best practices with peers, even externally.

This is a call to action for Tailings Consultants. The greater community is asking Tailings Consultants to:

- Pledge to protect communities and the environment through safe and robust TSF design,
- Commit to developing and sustaining the EoR role through comprehensive training programs, focused mentorship from senior practitioners, and practicable attrition programs,
- Cultivate a "dirty boots" mindset through site visits and engaging with site operations personnel. Sitting behind a desk for 10 years will not create a high-caliber, proactive EoR,
- Engage with local universities or alma matters to help attract new talent,

- Provide and support continued education opportunities, industry initiatives, and thereby advance the State of the Practice. This initiative should include shared resources through training, secondment and apprenticeships,
- Commit to developing soft skills and raising the emotional IQ of engineers and scientists, and
- Encourage and even demand practitioners publish journal articles, conference papers, and white papers.

This is a call to action for Universities and Colleges worldwide. The greater community is asking Universities and Colleges worldwide to:

- Bridge the gap between mining and civil engineering programs to develop tailings-centric curriculum and elevate tailings engineering as a viable area of focus,
- Invest in research and laboratory support to evaluate tailings with an understanding of the industry values practicality and applicability,
- Develop certification programs related to tailings engineering and tailings/deposition management techniques, and
- Engage undergraduate leadership in the training of individuals at the university level.

These groups provide the resources available in the tailings labor pool, but there are, however, two additional groups that have a profound effect on the industry. It is now time to demand a call to action from the nongovernmental organizations (NGOs) and regulatory agencies. These groups provide a significant backdrop to the enforcement of established guidelines as well as represent a link beyond our industry to the greater public at large. The greater community is asking NGOs and regulatory agencies worldwide to:

- Invest in universities and colleges for training,
- Develop core practitioners with a comprehensive technical and practical understanding of TSF design and operation including engineering principles and operating constraints from both a professional and a nontechnical standpoint,
- Acknowledge the contribution to consumer goods and technological/digital innovation mining provides – remember, "if it can't be grown, it must be mined,"
- Acknowledge the government's role and responsibility in sustainable mining and enforcing their designated legal frameworks,
- Learn to interact with a high emotional IQ and establish these expectations within peer groups,
- Understand and respect the difference between transparency and entitlement
- Avoid the development, support, and deployment of pseudoscience,
- Communicate with the general public in a way that is educational and fair, and
- Avoid public shaming when the standard of care is met, and negligence is unproven (see BC regulatory agencies).

Finally, there is a call to each of us as individuals. The greater community is asking each of us for our contributions beyond the work environment including:

- Mentoring and actively cultivating young professionals and "who's next",
- Exercising personal accountability for professional growth, from both technical and emotional IQ/"soft skill" perspectives,
- Engaging in and supporting Science Technology Engineering and Math (STEM) -based educational initiatives beginning at the elementary school level, drawing attention to the earth sciences and not just technology, and
- Advocating for OUR mining industry.

We need to change the philosophy and alignment of the industry. As an industry, we need to raise our emotional IQ. We need to understand the spirit of transparency and the need to share information. Together we will get farther faster. We need to share lessons learned from best practices and negative experiences and focus on making positive contributions. We also need to understand that openness contributes to the State of the Practice; it does not provide access to business strategies and other proprietary information, so there is nothing to "protect."

We need to maintain a vigilant awareness that our professional decisions create wider repercussions to surrounding communities, the environment, and even investors; as such, we must strive for excellence. However, when bad things happen – and they will – we need to thoughtfully evaluate the causes, present solutions and implement improvements moving forward, thus capitalizing on a learning opportunity in a mature fashion. Collectively and collaboratively, we can improve the industry "black eye" tailings disasters have created. The future does not exist without mining, and safer TSFs do not exist without all of us working together.

ACKNOWLEDGMENTS

Financial support for this study was provided by Haley and Aldrich, Inc. and Colorado State University via the Tailings and Mine Waste Conference. The findings presented in this paper are solely those of the authors, and do not reflect the opinions of Haley and Aldrich or Colorado State University.

REFERENCES

Agência Nacional de Mineração, 2019. CLASSIFICAÇÃO DAS BARRAGENS DE MINERAÇÃO BRASILEIRAS - DATA BASE JANEIRO/2019. Accessed at http://www.anm.gov.br/assuntos /barragens/pasta-cadastro-nacional-de-barragens-de-mineracao/extracao-sigbm-para-classificacao-site-atualizada-31jan2019.

Alberta Energy Regulator, 2018. Alberta Dams by Consequence. https://extmapviewer.aer.ca/DamSafety/index.html.

Army Corps of Engineers, 2019. National Inventory of Dams. Accessed at http://nid.usace.army.mil.

Australasian Mine Safety Journal (AMSJ), 2019. Accessed at https://www.amsj.com.au/western-australias-tailings-dams-are-well-managed/.

Azam, S, Li, Q, 2010. Tailings Dam Failures: A Review of the Last One Hundred Years, in Geotechnical News.

Casino Mining Corporation (-). Accessed at http://casinomining.com/_resources/Casino_Tailings_Dam_Q&A.pdf.

Chernoloz, O, 2017. Cataloging Tailings Dams in Arizona, in A Thesis Submitted to the Faculty of the Department of Mining and Geological Engineering.

Church of England, 2019. "Investors, banks, and insurers review global progress in addressing tailings dam safety". 31 October 2019. Accessed at https://www.churchofengland.org/more/media-centre/news/finance-news/investors-banks-and-insurers-review-global-progress-addressing.

Davies, M, Martin, T and Lighthall, P, 2000. Mine Tailings Dams: When Things Go Wrong in AGRA Earth & Environmental Limited, Burnaby, BC.

Department of Mines, Industry Regulation and Safety, 2019. MINDEX Database. Accessed at https://minedex.dmirs.wa.gov.au/Web/home.

Oliveira, MGS and Kerbauy, MTM, 2016. Environmental Vulnerability and Technological Risks in Collapse and Break of Dams in Brazil: Lessons from Mariana (Mg) Disaster, Faculty of Science and Letters, UNESP / Araraquara-SP, Brazil.

Ghorbani, Y and Kuan, S H, 2016. A Review of Sustainable Development in the Chilean Mining Sector: Past, Present and Future, in International Journal of Mining, Reclamation and Environment, ISSN: 1748-0930 (Print) 1748-0949.

Global Tailings Portal, 2019. Beta Version 2.0. Accessed at http://tailing.grida.no/#header.

Government of British Columbia, 2015. Accessed at https://www2.gov.bc.ca/assets/gov/farming-natural-resources-and-industry/mineral-exploration-mining/faq_tailingsdam_jan_30_2015_final.pdf.

Hatton, C, and Morrison, K, 2016. "Engineer(s) of Record, Changing the Dam Paradigm". Tailings and Mine Waste, Keystone Colorado.

Hatton, C, 2019. Keynote: Affecting Change Through Investment, Tailings and Mine Waste, Vancouver Canada, delivered 19 November.

Herza, J, Ashley, M, Thorp, J, Small, A, 2019. A Consequence-Based Tailings Dam Safety Framework in Conference Paper.

Li, ZX, Agioutantis, Z. and Zou, DH, 2017. Tailings Pond Life Cycle Safety Management System in Proceedings of the 8th International Conference on Sustainable Development in the Minerals Industry.

Morgenstern, N.R., Vick, S.G. and Van Zyl, D., 2015. Report on Mount Polley tailings storage facility breach. Report of independent expert engineering investigation and review panel. Prepared on behalf of the Government of British Columbia and the Williams Lake and Soda Creek Indian Bands.

Morgenstern, N.R., Vick, S.G., Viotti, C.B. and Watts, B.D., 2016. Fundão Tailings Dam Review Panel. Retrieved December, 13, p.2016.

Organismo Supervisor de la Inversión en Energía y Minería (OSINERGMIN) (-). Accessed at https://gisem.osinergmin.gob.pe/.

Robertson, P.K., Melo, L.d., Williams, D.J., Wilson, G.W., 2019. Report of the Expert Panel on the Technical Causes of the Failure of Feijão Dam I.

Servicio Nacional de Geología y Minería (Sernageomin), 2019. Catastro de Depósitos de Relaves en Chile. Accessed at https://www.sernageomin.cl/wpcontent/uploads/2019/04/CDR_CHILE_23_04_2019.xls.

Stanford University, Department of Civil and Environmental Engineering. National Performance of Dams Program Dams Directory (NPDP), 2015. Accessed at http://npdp.stanford.edu/dams _database.

U.S. Mine Safety and Health Administration (MSHA), 2019. MSHA Impoundment Inventory. October.

U.S. Department of Homeland Security Federal Emergency Management Agency (FEMA), 1998. Federal Guidelines For Dam Safety: Hazard Potential Classification System For Dams in U.S. Prepared by the Interagency Committee On Dam Safety. Reprinted January 2004.

Villavicencio, G, Espinace, R, Palma, J, Fourie, A, and Valenzuela, P, 2013. Failures of Sand Tailings Dams in a Highly Seismic Country J. 51: 449–464, Can. Geotech.

Wallingford, HR, Roca, M, Murphy, A, Walker, L, Vallesi, S, 2019. A Review of the Risk Posed by the Failure of Tailings Dams in HR Wallingford Ltd.

Developing Trigger Action Response Plans (TARPS) in a Changing Regulatory Environment

Michael G. Davis
Stantec Consulting Services Inc., Salt Lake City, UT, USA

ABSTRACT: As part of the risk management process employed by mining companies, Trigger Action Response Plans (TARPs) serve as guidance to owners and operators of tailings facilities of actions to be taken when abnormal or upset conditions are reached (as measured against structure specific design parameters). However, external factors unrelated to engineering parameters are causing a shift in how engineers and designers evaluate geotechnical surveillance results, which in turn influences how TARPs are developed, standardized, and implemented within an organization. In response to the public, Government, and regulatory agencies losing faith in the ability of mining companies to prevent tailings facility failures, the social license that engineers, designers, and operators maintain over those facilities is being replaced with regulation. Currently, the loss of social license and increasing regulatory pressure is nowhere more apparent than in Brazil. Since the Fundão failure in 2015 and the Brumadinho failure in 2019, the Government of Brazil has continually increased regulation regarding how tailings facilities are built, operated, and managed. This paper references work that was completed in 2019 to explain how TARPs for two tailings retainment structures at the Samarco Mine, located in Minas Gerais, Brazil were evolved. The work at the Samarco Mine illustrates that merely meeting the demands of regulation is not enough to keep people and the environment safe from catastrophic dam failures. The development and management of TARPs needs to be dynamic and uniquely tailored to each tailings retainment structure and environment, and not fixed by standing regulatory impositions.

1 THE PURPOSE OF A TRIGGER ACTION RESPONSE PLAN

A Trigger Action Response Plan (TARP) forms one part of the Quantitative Performance Objectives (QPOs) which are established for operation and maintenance activities on tailings dams. The overarching goal of a TARP is to determine meaningful predictors – trigger thresholds – of failure mechanisms based upon readings from geotechnical instruments (measuring pore water pressures and water levels, settlement, and displacement) installed within the tailings deposit, dam, and underlying foundation materials. TARPs describe the actions to be taken when the trigger thresholds are exceeded. The trigger thresholds aim to be precautionary in nature and are intended to identify conditions of unexpected performance while it is still possible to react to prevent failure or minimize the consequences thereof.

TARPs are synonymous with critical controls and this concept is further described in many international tailings management standards, including:

- Developing an Operation, Maintenance, and Surveillance Manual for Tailings and Water Management Facilities (MAC, 2019)
- Global Industry Standard on Tailings Management (ICMM et al., 2020)
- Proposed Best Practices for the Engineer of Record (EOR) for Tailings Dams (GBA, 2018)
- Dam Surveillance Guide (ICOLD, 2018)

Every tailings dam, reservoir, and surrounding natural environment is unique, and the warning signs associated with a potential dam failure scenario will also be unique. Therefore, the TARP levels chosen must consider the potential dam failure scenarios, the current structural and environmental conditions, the geotechnical measurements available, operational practices, the regulatory environment in which the dam is operated, and the design and performance criteria.

In the context of dam safety management, performance is a comparison of actual versus predicted behavior. Geotechnical instruments provide a means to accurately measure behavior,

most typically in terms of deformations and pore water pressures and water levels, settlement, and displacement. Data derived from a well-designed geotechnical monitoring program is fundamental to dam safety. Regular measurements and analysis of those measurements are required to track trends and ensure conformance within targeted levels. Measurements that fall outside of targeted levels require appropriate action; this is the purpose of a TARP.

As conditions on and around the dam change over time, the TARP must be revisited and analyzed to test the relevancy of the plan in relation to the critical failure modes at that point in the dam's life cycle.

2 DEVELOPING A TARP

To be effective, a TARP should be developed by the design team, the engineer of record, and the operations staff. This provides the TARP with aspects of technical importance as well as aspects of operational importance, and promotes buy-in, understanding, and accountability from everyone involved. An understanding of the following characteristics of the tailings management structure is important to the development of a relevant TARP:

- Site layout, foundation conditions, geomorphology, hydrologic conditions, and the results of geotechnical investigations.
- Dam characteristics, structural material properties, tailings properties and depositional practices, construction specifications, engineering guidance, and mine planning.
- As-built information, construction activities and sequences, structural performance, geotechnical instrumentation results, visual observations made by qualified and trained personnel, and changes to downstream land uses and downstream infrastructure.
- Relevant historical, current, and proposed future operational practices
- Regulatory constraints and global best practices.

Consideration of the following practices will increase the effectiveness of a TARP to identify critical conditions within a tailings retainment structure:

- The geotechnical instruments should be considered holistically as a system of measurement points rather than a set of discrete measurement points.
- Critical conditions must be understood. A Potential Failure Mode Analysis (PFMA, or other risk assessment tools), design constraints, and best practices must be considered in determining the critical conditions.
- A straightforward TARP will be easier to implement and administer in practice. Administration of the TARP should not detract from other critical tasks of the dam safety management system.
- The time taken from when an instrument is read in the field until the data is processed, analyzed, and reviewed should be minimized and automated when possible.

Regulatory constraints and global best practices are becoming increasingly important factors in the development of TARPs for tailings dams. In Brazil, where the regulatory constraints are changing rapidly, TARPs need to be revisited frequently to assess whether new regulatory constraints impact the design, implementation, and relevancy of a TARP as part of the dam safety management system.

3 DEVELOPING TARPS FOR TAILINGS DAMS IN BRAZIL

In response to the Brumadinho dam failure on January 25, 2019, the Agência Nacional de Mineração (ANM), an extension of the Brazilian Government which oversees the mining industry, released Resolution 13 on August 8, 2019. Resolution 13 amended the federal law regarding the regulation of tailings dams within Brazil (ANM, 2019). Within this resolution, new federal mandates were established for the consideration of TARPs for geotechnical instrumentation installed on tailings dams.

Resolution 13 requires that a tailings dam in Brazil must have a minimum Factor of Safety (FOS) of 1.3 against instability using total stress (undrained strength) parameters for operational tailings retainment structures containing potentially liquefiable tailings. Undrained strength parameters are used to represent the generation of excess pore water pressure which occur after

an external load is applied to the dam structure (static or dynamic). The imposed conditions for failing to meet a FOS equal to or greater than 1.3 using undrained strength parameters involves immediate suspension of tailings deposition within the facility, reporting the condition to the ANM, implementing mitigation measures to re-establish the minimum FOS, public notification of the condition, and assessment of the need for downstream evacuation.

Samarco's existing TARPs had not specifically considered the undrained strength case. Work to update the existing TARPs for two of Samarco's dams (the Germano Dam and the Germano Pit Dam) was undertaken to satisfy the requirements of Resolution 13.

3.1 *Issues with Samarco's Existing TARPs*

At the time Resolution 13 was released, Samarco's TARPs for the Germano Dam and Germano Pit Dam were already struggling to maintain relevancy under the scrutiny of government officials and teams of third-party experts hired by the State of Minas Gerais to oversee Samarco's dam safety management systems.

The TARPs were complex; each geotechnical instrument had three individually assigned threshold phreatic surfaces and action levels (Attention, Alert, and Emergency). Each geotechnical instrument was treated as an isolated measurement point; meaning that the trigger thresholds were dependent on localized conditions immediately around the measurement point.

In practice, the TARPs resulted in the exceedance of numerous low level (Attention and Alert) trigger thresholds monthly. Each exceedance required investigation and assessment by Samarco's internal engineering team with the help of Samarco's third-party consultants. The measurements exceeding the TARP parameters were then resolved in a monthly presentation to a panel of reviewers. This process was taxing Samarco's engineering teams with an unnecessary administrative burden. The exceedances were often the result of localized conditions or anomalies caused by the installation and completion methods of the geotechnical instruments themselves and did not represent conditions which indicated instability of the structure.

It was clear that the existing TARPs were not identifying the critical controls for Samarco's tailings retainment structures. Moreover, the constant exceedance of the TARP criterion was creating a potentially dangerous operating environment – when the alarm bells are always ringing, our response to them is diminished and often dismissive. This condition was also creating an administrative burden which took attention away from other critical aspects of Samarco's dam safety management system.

3.2 *Developing the TARPs*

Updating the TARPs for Germano Dam and Germano Pit Dam began with a review of the potential failure modes for each structure. The design cross-sections (used for the slope stability evaluation) were used to model various failure scenarios based on the critical design parameters and minimum FOS to select the critical conditions. The methods followed in the assessment of the critical water levels consisted of the following three steps (Figure 1 shows a flow chart of the process):

1. Defining the base-case phreatic surface for each structure, based on the current water levels measured by the geotechnical instrumentation. This analysis generated the initial FOS for each structure.
2. The phreatic surface was then increased in small increments (resulting in small incremental decreases in the FOS) until the minimum (critical) FOS criterion was achieved for each failure mode scenario and conditions evaluated (e.g. failure through a contractive tailings sand, or through a normally consolidated soil unit in the foundation). The overall shape of the phreatic surface was maintained as it was increased to limit the modeling scenarios. However, hydraulic conveyance structures within the dam were always considered to convey the total flow through the structure. Seepage analyses were also run to confirm the overall shape of the phreatic surface.
3. The lowest overall phreatic surface was selected from among the cases analyzed and was used to generate a three-dimensional phreatic surface within the structure. The phreatic surface was interpolated (where necessary) to each geotechnical monitoring point on the dam.

The stability analyses were focused on deep-seated failure mechanisms that would result in failure of the dam (loss of containment).

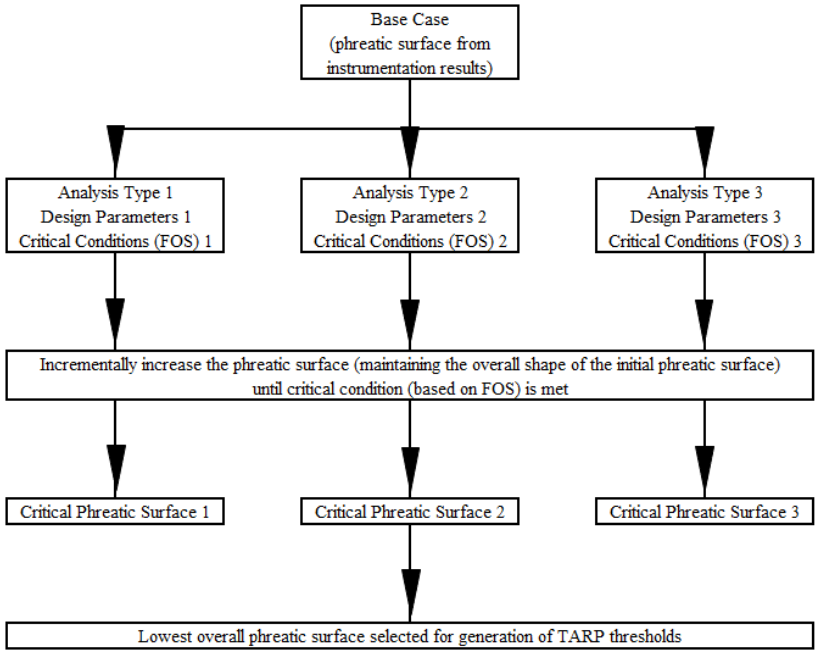

Figure 1. Flow chart for assessment of the lowest overall phreatic surface.

3.3 *Developing a Binary TARP*

The TARPs were simplified with a binary value associated with each pore water pressure and water level monitoring instrument. The lowest overall phreatic surface elevation (generated from the critical analysis condition) for each geotechnical instrument would become the only value used in setting action responses for the TARP.

This singular value would be used to generate two sets of actions, based on whether the trigger thresholds were reached locally (in one instrument or within a localized cluster of instruments) or globally (over a widespread area/zone of the dam). Localized exceedances of the trigger thresholds would lead to internal checks of the instrumentation and surveillance systems (Warning Level) as these exceedances would not decrease the overall FOS to critical levels. Widespread exceedances of the trigger thresholds, at multiple instruments, would lead to more critical actions being taken.

- Warning Level trigger threshold actions were assigned for localized increases in the phreatic surface above the critical phreatic surface (as well as several other anomalous conditions). A localized exceedance of the trigger thresholds results in further investigation and visual observation of the area.
- Emergency Level trigger threshold actions were assigned for global increases in the phreatic surface above the critical phreatic surface. A global exceedance of the trigger thresholds results in the implementation of the Emergency Action Plan (EAP), suspending construction activities, and reviewing and implementing mitigation scenarios.

Engineering judgement must be applied during the decision-making process regarding whether the Emergency level is triggered. Reviewing and updating the TARP was a valuable step in outlining the action protocols to be taken in the event of trigger threshold exceedance.

3.4 *Results of the TARP Update*

Geotechnical analyses performed to update the TARP for Samarco's tailings retainment structures found that the regulation imposed by ANM (Resolution 13) was not the critical condition for the structures analyzed. The TARP update was initially focused on meeting the requirements of Resolution 13, however, the geotechnical conditions and parameters imposed by Resolution 13 represented only one of the many failure modes of the dam. Engineers and designers must remain focused on all possible failure modes to determine the critical controls of a tailings retainment structure.

The process of updating the TARPs for Samarco's tailings retainment structures generated several important enhancements to the TARPs and the overall dam safety management system, including:

- The water level and pore water pressure monitoring instruments as a system instead of as discrete measurement points.
- Trigger thresholds were based on the critical conditions.
- TARP trigger thresholds and action sets were simplified.

The updated TARPs for Germano Dam and Germano Pit Dam were implemented in February 2020; the TARPs are working as designed and no revisions have been required. Warning levels have been triggered at localized areas of the dam and these occurrences have been investigated, explained, and closed out without need for unnecessary scrutiny. However, the warning levels have brought attention to minor issues where maintenance to the dams has been required. The frustrating and burdensome reporting of minor issues has been alleviated, and thoughtful discussion of maintenance activities and operating procedures have occurred. Overall, the updated TARPs have facilitated greater value in the information shared between Samarco's operations staff, Samarco's engineering staff, and the design engineering team.

Collaboration between the teams and stakeholders throughout the process of updating the TARPs helped all involved understand the basis of the action plan (critical conditions) and identified opportunities to enhance how the TARPs were designed and put into practice. The result of this project has been a greater appreciation for how a TARP can be an effective part of the dam safety management system. Instrument results have a greater meaning when important results and trends can be identified efficiently, understood, and acted upon.

4 CONCLUSION

Using TARPs to assess and quantify geotechnical performance is one gauge of structure specific performance, addressing critical controls, and understanding risk. In addition, a comprehensive and evolving understanding of site specific design criteria, geology, hydrology, construction activity and specifications, mine planning, tailings deposition, structural performance, geotechnical instrumentation results, visual observations, regulatory constraints, and downstream land uses and infrastructure should be used to assess the accuracy, relevancy, and value of a TARP in terms of making timely informed risk management decisions for tailings retainment facilities.

The lessons learned from developing a TARP for tailings retainment structures at the Samarco Mine in Brazil can be adapted for tailings retainment structures industry wide. TARPs must be easily understood in practice and need to address the specific failure modes which are relevant to each individual tailings retainment structure. Trigger thresholds are effective at identifying critical conditions when the supporting geotechnical instrumentation results are used holistically as a system of measurement points. An effective TARP will also promote greater value in the communications between operations staff and engineering teams and will increase the overall effectiveness of the dam safety management systems which they serve.

Regulatory pressure can be a catalyst for evolving engineering practice, even though the regulatory constraints may not govern the critical controls for the tailings structure. Engineers, designers, tailings planners, and operations staff should understand that merely satisfying regulatory requirements is insufficient for managing dam safety requirements. Despite attempts by regulatory bodies to minimize the need for engineering judgement, which is subject to all manner of unconscious bias, sound engineering judgement remains fundamental in developing, implementing, and administering TARPs for tailings retainment structures.

REFERENCES

Geoprofessional Business Association (GBA) 2018. *Proposed Best Practices for the Engineer of Record (EOR) for Tailings Dams.*

International Commission on Large Dams (ICOLD) 2018. *Dam Surveillance Guide – Bulletin 158*

International Council on Mining & Metals (ICMM), Principles for Responsible Investment (PRI), and United Nations Environment Programme (UNEP) 2020. *Global Industry Standard on Tailings Management.*

Mining Association of Canada (MAC) 2019. *Developing an Operation, Maintenance, and Surveillance Manual for Tailings and Water Management Facilities – Second Edition.*

Preparation of an ISO Standard for Mine Closure and Reclamation Planning

Dirk Van Zyl, PhD., P.Eng.
University of British Columbia, Vancouver, BC., Canada

Michael Nahir, P.Eng.
Parsons Corporation, Ottawa, ON., Canada

Ian Hutchison, PhD., P.Eng.,
Hutchison Engineering, Laguna Nigel, CA., USA

ABSTRACT: This presentation and accompanying article provide an overview and an update on an ISO standard (ISO 21795 - Mine Closure and Reclamation Planning) that is currently being finalized. This Standard contains two separate Parts: Part 1 provides key requirements and recommendations while Part 2 provides guidance and supporting information. The two overarching objectives of the standard are to provide a key international resource that encapsulates best practices and related guidance across the many areas of specialty involved with planning for mine closure and reclamation and to make this available to a wide range of stakeholders, and especially countries with minimal access to best practices and guidance on the topic area. The intended audience for the Standard includes those with responsibility for, or an interest in, planning for mine closure and reclamation. This includes mine planners and designers, mine operators, regulators, environmental assessors, communities, Indigenous Peoples, and financial stakeholders, amongst others. The Working Group developing the Mine Closure and Reclamation Planning Standard is made up of over 60 experts representing 13 countries, including a number of developing countries that we hope will benefit from both the involvement in the standards development process as well as the best practices and guidance encapsulated by these two documents once published. The two Parts of ISO 21795 have been prepared to cover the lifecycle of requirements, recommendations, and supporting information that apply to mine closure and reclamation planning, including consideration of mine closure and reclamation objectives, technical procedures, consideration and mitigation of socio-economic impacts, financial planning and assurance, unplanned and post-closure activities, as well as data and knowledge management, amongst others. This paper describes these requirements, recommendations, and supporting information.

1 INTRODUCTION

1.1 Background

In 2016 a new project was launched through the International Organization for Standardization (ISO), led by Canada, to develop an international standard on the topic of mine closure and reclamation planning. The overarching objective of the project and ensuing international standard was to promote consistency and quality in planning for mine closure and reclamation internationally.

The Standard, formally titled 'ISO 21795', is being developed for use by those with a responsibility for, or an interest in, planning for mine closure and reclamation. This could include, for example, mine planners and designers, mine operators, regulators, environmental assessors, communities, Indigenous Peoples, and financial stake holders, amongst others.

The Working Group developing the standard has representatives from 13 different countries. Dirk van Zyl is the International Convenor while Michael Nahir is the International Project Leader. CSA Group supports both the Project Leadership and International Working Group by providing the International Secretary for the project. CSA Group also manages a Canadian Harmonized Mirror Committee to the parent ISO committee through which ISO 21795 is being developed (i.e. ISO TC 82/SC7), thereby allowing Canada the possibility to adopt this Standard once published.

Currently, the international working group is in the 'Draft International Standard' stage of development for ISO 21795 (ISO 21795 contains two separate Parts: Part 1 provides key requirements and recommendations while Part 2 provides Guidance). The target is to publish both Parts in late 2021.

1.2 The need for an international standard on mine closure and reclamation planning

The development of a mine site can have significant environmental impacts and leave behind a sizable environmental legacy upon closure if adequate controls are not put in place at both the start of the mine and during its operations. Similarly, closing a large mine will have far reaching social impacts with the loss of employment and a local revenue generator, but likewise with opportunities throughout the life of the mine to maximize the potential social benefits of mining and to minimize the impacts once the mining activity ceases.

Although adequate mine closure and reclamation planning is of paramount importance globally, this is especially true when considering the role of mines in lesser developed and developing economies. Often, the effects of such large industrial projects in such regions are exacerbated compared to more developed economies since they have such a more pronounced local impact. In addition, often these countries rely on the best practices employed by the respective mine company in terms of both limiting the environmental impact of the mine site and also maximizing the socio-economic benefits of the mining activity.

Advancing best practices with respect to early and continuous planning for mine closure and reclamation and making these widely available, such as through an international standard, therefore is essential to helping minimize the global environmental impacts of mining and maximizing the social and economic benefits. Early as well as continuous mine closure and reclamation planning can:

- Lead to greater protection of the environment, usually at a lower cost than if mine closure and reclamation planning is not done from the beginning of the mining project
- Reduce risks and liabilities throughout the mine's operational life
- Foster stakeholder involvement
- Help build trust with governments, stakeholders and international communities
- Allows companies to better integrate closure and reclamation activities with operations
- Provide time to identify, research and develop new technologies for mine closure strategies and mine closure treatments that increase robustness and resilience of mine closure and reclamation
- Bolster the provision for and schedule of closure and reclamation funding by companies
- Help manage the socio-economic impacts as the mining operation ceases

It is also recognized that there are other guidance documents related to mine closure and reclamation planning available in various jurisdictions and used by some mining companies and stakeholders. As such, within this particular exercise to develop an international standard on the topic of mine closure and reclamation planning, it was also the intent that the international standard would help encapsulate the knowledge of such guidance documents so that this information could be applied globally.

1.3 Objectives of Working Group and Standard

From the outset of this project, two broad-based objectives have underlain the work and efforts of the Working Group, including:

1. To provide a key international resource that encapsulates best practices and related guidance across the many areas of specialty involved with planning for mine closure and reclamation
2. To make this available to a wide range of stakeholders, but especially countries with minimal access to best practices and guidance on the topic area

As per the first point above, it must also be recognized that planning for the closure and reclamation of a mine site is very interdisciplinary and subsequently involves a wide range of areas of expertise and knowledge. For example, this includes the domains of soil science, biology, ecology, hydrology, hydrogeology, water management and treatment, civil, geotechnical and environmental engineering, stakeholder engagement, amongst others. As such, the topic areas covered by this standard are broad and diverse – as detailed in section 3 of this article.

1.4 Working Group membership

The International Working Group developing ISO 21795 has a broad membership in terms of number of countries (13 represented in total) and regions of the world represented, including a number of countries with developing economies that we hope will benefit from both the involvement in the standards development process as well as the best practices and guidance encapsulated by these two documents once published.

The countries involved as well as the number of experts appointed by each country is provided in Table 1.

Table 1. Country membership and appointed experts

Country	Number of appointed experts
Canada	8
Australia	7
Burkina Faso	4
Chile	2
China	3
Côte d'Ivoire	3
France	2
Iran, Islamic Republic of	1
Korea, Republic of	8
Mali	1
Morocco	1
Senegal	4
United States	2

1.5 Organization of article

The rest of this article is organized as follows. To explain the 'ISO context', the article first reviews the general process for developing international standards through ISO, including how the widest breadth of stakeholders are consulted and how consensus is sought. Section 3 then provides an overview of the content of ISO 21795 – including providing more context and explanation of its organization as well as providing an overview of the specific topic areas covered by each part of the standard. Section 4 concludes.

2 ISO STANDARDS DEVELOPMENT PROCESS

The development of international standards through ISO follows a systematic process through six separate stages which allow for the progressive development of the document. This includes a distinct series of activities involving the working group (WG) developing the content of the standard, a review and ballot of the parent committee to which the working group reports (optional), and one to two reviews and ballots at the international level. The overall process, including stage and state of the document, is shown in Figure 1.

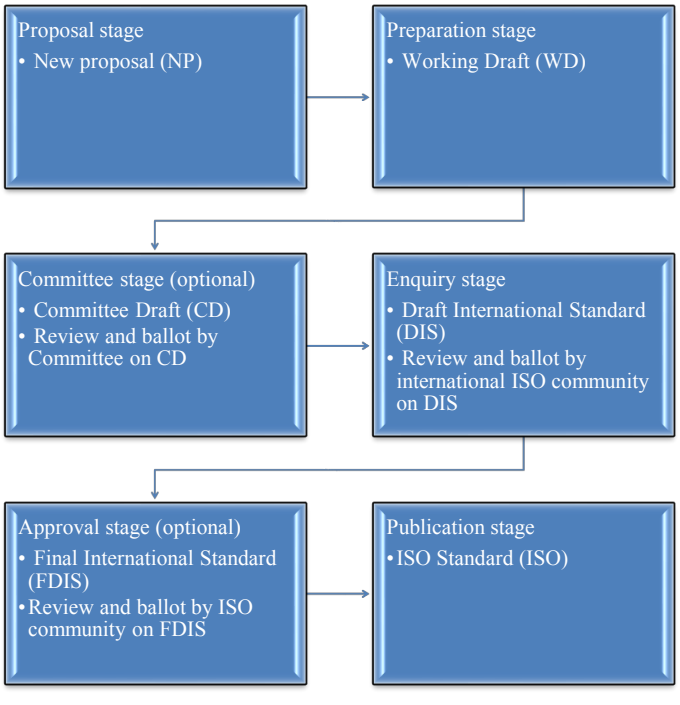

Figure 1. Schematic of ISO process

The first stage is initiated by a proposal for a new work item (NP), which involves either a new piece of work based on as little as a table of contents or the adoption of an existing document that can be used to seed the international standard. New international standards are proposed through a specific parent committee with a scope that includes the topic area of the standard. These parent technical committees are made up of members from individual countries that can either have voting privileges (termed participating or P-members) or act as observing countries to the process (O-members). Countries who have voting privileges on a committee can propose new work items; in doing so, they are also responsible for appointing an international convenor who will act to lead the working group responsible for developing the technical content of the standard. New work items are voted upon in terms of their market demand and the relevance of the standard on a global scale.

Another important element of this phase is the creation of a working group (WG), composed of international experts who develop the actual content of the standard. Depending on the size of the parent committee, the WG will be made up of experts from a minimum of four or five different countries.

The preparatory stage involves the preparation of a working draft (WD) of the international standard. This work is done largely within the relevant ISO working group.

After the WG is satisfied on the technical merits of the working draft, this document is put forward to the working group's parent committee for comment and vote. Although technically this stage is optional, most new standards go through this stage. This stage, which is termed the committee stage of the development process, is where each participating member country registers its official comments and votes on the WD: a yes vote means that the working draft meets the requirements to move on to the next phase. Successive committee drafts may be considered until consensus, which is reached when at least two-thirds of the P-members register a yes vote. Once agreed upon, the text is finalised for submission as a draft international standard (DIS).

The fourth stage, or the enquiry stage, involves the DIS being circulated by ISO to all of the member countries of ISO for voting and comment over a three-month period. This is the second voting stage. The member countries, in turn, are encouraged to make the DIS text available to the widest range of national stakeholders possible in order to obtain the national vote of each member body. The text is approved if two-thirds of the P-members of the committee under which the work item falls vote in favour and if not more than one-quarter of the total votes cast are negative.

The fifth stage of development is the approval stage. This involves the final draft international standard being circulated to all ISO member bodies for a final two-month yes or no vote. The text is approved for the final stage, the publication stage, using the same criteria as for the enquiry stage. The final document is published by ISO as an official ISO international standard.

2.2 A consultation approach to standards development

The ISO standards development process has been structured in such a way so to allow for, and ultimately encourage, the widest possible participation and consultation of experts and stakeholders involved with the subject at hand. From the starting point, an international working group is comprised of individuals with expertise on the subject, who each represent their own expertise. This is meant to encourage unfettered input of technical content as a starting point for the standard.

The successive review and commenting stages are also structured to encourage a progressively widening consultation process. The broadest of these stages is at the enquiry stage, when the ISO document under development is made available to all member bodies of ISO. ISO is made up of 121 member countries that have the ability to vote on ISO standards. This means that 121 countries will ultimately be given access to the standard and encouraged to seek the input of stakeholders in these countries to inform their national position.

2.3 A consensus-based approach to standards development

International standards developed through ISO are developed following a consensus-based approach, whereby consensus amongst member countries is sought at multiple stages. This process of consensus building helps ensure unbiased content and technical integrity of the standard being developed.

Consensus building starts at the very beginning of the ISO standards development process, where new work items being proposed will only pass if a majority of the voting countries of the particular committee approves the work item. At the working group level, consensus building is focused on developing the technical content of the work item and does not involve voting; during the committee stages of review, consensus is sought through reviewing, commenting, and voting on the document. This occurs at three distinct stages, namely, at the committee, enquiry, and approval stages, as discussed above.

2.4 Use of international standards in the mining sector

There are a number of broad uses of standards in the mining sector. Beyond the general objectives of helping to mainstream best practices that help improve the safety and performance of operations, promote the safe use of equipment, or improve the sustainability of mining itself, standards can be referenced in regulations or can help mining companies demonstrate that they have met certain performance and operational criteria.

Although regulations usually stipulate what is required from a mine, they do not necessarily provide guidance on how these requirements can be achieved. The development and implementation of international standards therefore can assist companies to meet the requirements of such regulations as they provide key guidance on the actions that should be undertaken. Regulations may also directly reference standards to help establish performance requirements (i.e., regulation by reference).

Another key use of international standards in the mining sector and by industry generally, is that these can allow companies and practitioners to demonstrate conformance to the requirements set forth in international standards. Prime examples include the use of the ISO 9000 family of standards, which sets forth requirements for various aspects of quality management. This in turn can benefit companies through marketing and improved public credibility.

There are two ISO technical committees (TC) focused specifically on mining - ISO/TC 82 (Mining) and ISO/TC 127 (Earth-moving machinery) - while there are many others developing complementary standards often used within the mining sector. This latter group includes committees focused on topics such as water quality (ISO/TC 147), environmental management (ISO/TC 207), and water re-use (ISO/TC 282); other TCs are involved with developing standards for mining-related operations such as risk management (ISO/TC 262) or occupational health and safety (ISO/PC 283).

Any ISO technical committee can have one or a series of subcommittees that focus on a specific scope area. ISO TC 82 has two subcommittees (SCs): SC7 on 'Mine Closure and Reclamation Planning', and SC8 on 'Advanced Automated Mining Systems'.

3 ISO 21795: A TWO-PART STANDARD ON MINE CLOSURE AND RECLAMATION PLANNING

3.1 General

Through the development process of ISO 21795, it became evident that there are both key requirements for mine closure and reclamation planning, and also related guidance and information spanning the multiple aspects involved with planning for the closure and reclamation of a mining site.

As such, ISO 21795 has been organized into two distinct Parts. Part 1 provides key requirements (i.e. 'shalls') for effective mine closure and reclamation planning, while Part 2 contains no requirements but guidance (i.e. 'should', 'can', 'may') as well as supporting information.

Each Part can be used on its own and adopted individually by member countries and also used for different purposes. Also notable, since Part 1 contains requirements, it can be used for the purpose of conformity assessment. Since Part 2 contains only recommendations, it cannot.

The two Parts therefore have distinctly different intentions in terms of the ultimate potential use. It is intended that Part 1 be used by both industry and other stakeholders to help foster consistency in the use of key best practices in planning the closure and reclamation of a mine site. Further, it is hoped the standard can be used to support proactive mine closure and reclamation planning that can be assessed for the purposes of conformity. Meanwhile, Part 2 is meant to be a resource that provides detail on some of the complexities involved with mine closure and reclamation planning. In part, the intent is that countries as well as other stakeholders that do not necessarily have access to best practices spanning the very interdisciplinary and diverse practice of mine closure and reclamation planning will benefit from this support.

In general, neither Part of ISO 21795 is meant to provide detailed survey, testing or monitoring methods, detailed engineering procedures, detailed product requirements, or detailed construction and operational procedures. Occupational health and safety management related to closure and reclamation, construction and exploration activities are also excluded.

Finally, a decision was also explicitly made that the standard is not intended to be applied to closure and reclamation of abandoned mines. A separate standard is under development through ISO TC 82/SC7 on the topic of abandoned mine management.

3.2 Part 1

As highlighted earlier, Part 1 of ISO 21795 provides key requirements for mine closure and reclamation planning. It does so by first providing a framework meant to help lay out the major 'building blocks' of mine closure and reclamation planning, as shown in Figure 2:

Figure 2. Mine Closure and Reclamation Planning Framework

Each framework element is further explaining below.

Responsibility: inherent to the entire mine closure and reclamation planning process is company responsibility (a specific clause provides key requirements), including stakeholder engagement (a specific clause provides key requirements) and that local jurisdictional requirements can exist (a specific clause provides key requirements). Critical to responsibility is financial management and provisioning for closure (a specific clause provides key requirements).

Integration: mine closure and reclamation planning is an integral part of the mining life cycle, including with respect to physical and chemical controls for sustainable land and water use (a specific clause provides key requirements), that mine closure and reclamation treatments are required to be resilient, and socio-economic considerations in the transition to closure are considered, Engagement with stakeholders on mine closure and reclamation is also a critical element.

Design: developed in the context of meeting closure and rehabilitation objectives which in turn are developed in consultation with stakeholders. Robust lifecycle design and management need to reflect this to facilitate successful mine closure and reclamation.

Risk and opportunity assessment and management: the process to assess and manage mine closure and reclamation risks, and to identify and act on opportunities throughout the life of mine.

Evaluation and improvement: quality assurance provides the maintenance of the mine closure and reclamation planning standard at the corporate and operational level, while the process of adaptive management facilitates continuous improvement through the life of mine.

Knowledge: identifying uncertainty through knowledge gaps, building knowledge, managing, disseminating and retaining knowledge and data that support mine closure and reclamation planning throughout the life of mine and beyond (a specific clause provides key requirements).

Requirements and recommendations are also provided on:

- Mine closure and reclamation plan objectives and commitments
- Technical procedures and techniques, including
    - Mine site characterization
    - Physical and chemical stability
    - Contaminated media
    - Infrastructure decommissioning and disposal
    - Post-closure land use plan
    - Alternatives and opportunities analyses
    - Reclamation
    - Progressive mine closure and reclamation
    - Mine closure and reclamation schedule
    - Mine closure and reclamation cost estimate
    - Management of risks and opportunities
- Mitigating socio-economic impacts
- Financial assurance and associated planning
- Mine closure and reclamation planning for unplanned closure
- Post-closure management plan
- Mine closure and reclamation plan documentation

3.3 Part 2

Part 2 of ISO 21795 is much more detailed in terms of the material presented. This was intentional as the hope is that these details will be useful for those without access to this information.

Recommendations are provided on:

- Closure and reclamation of mine site, including:
    - Tailings storage facilities
    - Water storage facilities
    - Waste rock management facilities
    - Heap leach facilities
    - Open pits
    - Underground workings
    - Mine infrastructure
    - Temporary closure
- Land reclamation and water management, including:
    - Landforms
    - Surface preparation
    - Vegetation establishment
    - Water management
    - Covers
    - Climate change effects
- Stakeholder engagement, including:
    - Objectives
    - Approach
- Decision and analysis tools, including:
    - Design levels
    - Alternatives identification and analysis
    - Designing and operating for closure and reclamation
    - Risk assessment and management
    - Cost estimating
    - Performance monitoring and reporting
    - Adaptive management
    - Application to the long-term care phase

4 CONCLUSIONS

In this article we have provided the background, ISO context, and content overview of a new international standard on mine closure and reclamation planning (ISO 21795 'Mine Closure and Reclamation Planning'). The target date for publication is late 2021. Once published, our hope is that it will help support mine closure and reclamation planning activities globally, thereby bolstering sustainability, environmental protection, and the local economies and communities that depend on mining.

Mineral Industry in Armenia: Management Issues and Perspectives for Tailings Retreatment

Vicken Aprahamian
Royal Canadian Mint, Canada

Harutyun Movsisyan
Yerevan State University, Armenia

Alexander Arakelyan
Center for Responsible Mining, American University of Armenia/Institute of Geological Sciences of NAS, Armenia

Alen Amirkhanian
Center for Responsible Mining, American University of Armenia

ABSTRACT: Armenia is a small, land-locked country located in the southern part of the Caucasus at the geological convergence between Eurasia and Africa. The Lesser Caucasus mountain range extends through its northern zone and runs southeast to the border with Iran. These geological formations are highly mineralized.
Modern metal mining activity in Armenia began with copper extraction and dates back to the 18th century. There are currently seven active metal mines and 23 tailings dams in the country.
Environmental management programs mainly are not up to international standards and companies struggle with frequent effluent releases contaminating the environment. In addition, widespread seepage from existing waste areas occurs as acid mine drainage. Due to high seismic activity, dam failure risk mitigation is a top priority. To begin addressing the most pressing issues related to active and legacy sites, multi-stakeholder discussions began in 2016, involving government, mining companies, communities and civil society.

A HISTORICAL PERSPECTIVE

Armenia is a country which lies along the northern section of the Lesser Caucasus mountain range which runs into Iran to the south east and geological formations in the region are highly mineralized.

Due to its complex physico-geographic conditions, almost all climate types can be observed in the country - from dry subtropical to cold mountainous. The average annual air temperature ranges from -8°C in high mountainous areas (2500m and above) to 12-14°C in low valley regions. The average annual precipitation in the country is 592 mm. The highest precipitation is observed in high mountainous regions - 800-1,000 mm annually. The most arid regions are Ararat Valley and Meghri region. Annual precipitation in the most arid regions (Ararat Valley and Meghri region) amounts to 200-250 mm (4th National Communication, 2020). In the central and southern regions of Armenia, the largest portion of precipitation falls in spring and autumn period. In the northern part of the country, most of the precipitation falls in summer due to the water vapor transported from the Black Sea. Winter precipitation falls mainly in the form of snow.

During the operation of the gold mines and the many archeological studies have shown that the extraction of gold and other metals in Armenia has been carried out since time immemorial, several millennia ago.

Modern Armenian metal ore exploitation developed during the 19th century revolving for the most part around copper extraction in the regions of Alaverdi, Akhtala, and Shamlugh, in the very north of present-day Armenia (US Commerce Report 1919). Similar activity took place in Kapan in the southeastern region but was not developed further due to difficult road access. Primitive smelters were set up to recover the metal close to the mines. In the 1860s all the Trans-Caucasus copper was from these localities. Around the turn of the 20th century a French

company, Société industrielle et métallurgique du Caucase, acquired the concessions and further developed the deposits around Akhtala where the ore was relatively high-grade chalcopyrite after manual sorting. By 1900, Armenia produced 20% of the copper of the Russian Empire.

By the end of the First World War, the French withdrew from the copper mines, leaving behind a smelter in Alaverdi, another mining town in the northern sector. The smelter had a capacity of 160 metric tons of ore per day and was accepting copper ore with grades of 10 to 36% by weight and was also producing small amounts of fine copper by electrorefining (Melkonyan 1955). A second smaller smelter also remained in the Zangezur area. By 1926 the smelter at Alaverdi was re-started to process ore (Strishkov 1984). As lesser grades became prominent and flotation technology became available, concentrators were installed at the Alaverdi and Kapan sites during the years 1928-1933 (Bond et al 1997). In 1948 an electro-refining complex was installed followed by a second in 1961 to fully refine copper but also produce by-product copper sulphate crystal. After the end of the Second World War, the Soviet Union encouraged the recovery of molybdenum concentrate from the copper ores in the Zangezur zone due to demand for special alloy steels. Lead and zinc concentrate were also recovered from a few locations but were of lesser economic importance. Precious metal values were exclusively recovered from copper electrolytic anode slimes.

The gold mining industry emerged in 1953 with the discovery of important reserves of a gold-quartz deposit at Sotk (Zod) by Armzoloto, east of lake Sevan. It took several years to develop the mine with the first gold poured in 1966 in a pilot facility. The Sotk tailings dam was reportedly constructed around 1955-1957 (MNP Report 2019) suggesting that before the main extraction/production in Sotk, gold was mined. At first, annual production was limited to less than one metric ton per year. Due to the proximity of lake Sevan and risk of cyanide polluting the waterways, it was decided to transport the crushed ore by rail 270 km to a new facility in an industrial town called Ararat, south of Yerevan. A resin-in-pulp cyanide circuit was adopted and by 1978, throughput increased yielding 10 metric tons of gold in doré per year (Jensen et al 1983).

In 1988 a devastating earthquake with its epicenter on the western side of the country resulted in major loss of life and made half a million homeless. It also destroyed over 150 major industrial facilities. In particular, it caused the shutdown of the only nuclear power plant, Metsamor, which provided 30% of the country's electricity. The interruption included Alaverdi copper smelter which was producing 55,000 mt of blister copper per annum. Furthermore, efforts to rebuild were hindered by the disintegration of the USSR and Armenia's involvement in armed conflict in Nagorno-Karabakh.

PRESENT DAY MINING AND METAL EXTRACTION IN ARMENIA

There are currently seven main active mines which produce mineral concentrate. The products (concentrate, alloy, doré, etc.) are sold both domestically and for export. Copper, zinc concentrates are all transported by road to the Georgian ports on the Black Sea for shipment to foreign smelters. Any gold and silver recovered in Armenian copper bearing mines are collected in copper concentrate. Molybdenum concentrates are partially or entirely processed at two roasting operations on the outskirts of Yerevan which also recover rhenium and minor amounts of copper. A third molybdenum roasting facility was started up in 2019 in the city of Armavir by repurposing an old glass factory. The molybdenum is transformed into ferromolybdenum alloy as a final product. The Ararat gold recovery plant is the only facility which produces mine doré and it has been able to continue to do so after depletion of the gold-quartz reserves in 2012, thanks to the successful installation and start-up of Albion fine grinding technology. The new technology has been efficiently liberating gold from refractory sulfide ore mined at the Sotk site since 2014 (Voigt et al 2018). Smaller tonnages of precious metals concentrate with gold content are also recovered by other companies (mainly Meghradzor Gold and Vayk Gold, sometimes also Kapan MPC) in Armenia.

The Alaverdi smelter was shut down in late 2018 due to its poor operating record and safety issues. The vision for all Armenian copper concentrates is for their processing to blister copper at a suitable central location once a new smelter is built and commissioned. However, the sale or disposal of by-product sulphuric acid is considered problematic and currently negatively

impacts project economics (Aprahamian 2019). Alternative hydrometallurgical processing routes for chalcopyrite ores, which do not generate by-product acid, represent higher risk for an operating company as they are still not fully proven and widely adopted.

The active mines and operating details as of June 2020 are listed in the Table 1.

Table 1. Main Extracted Products of Metal Mining Sector in 2018 (according to EITI Armenia Report 2018, draft)

N	Company	Ore type	Volume, tonnes
1	"Lichkvaz" CJSC	gold, silver and copper ores	40,031
2	"Meghradzor Gold" Ltd.	precious metals ores	72,025
3	"GeoProMining Gold" Ltd.	gold	1,141,600
4	"Akhtala Mining and Processing Enterprise" CJSC	copper	560,397
5	"Teghout" CJSC	copper-molybdenum	243,730
6	"Zangezur Copper-Molybdenum Combine" CJSC	copper-molybdenum	21,286,100
7	"Agarak Copper-Molybdenum Combine" CJSC	copper-molybdenum	3,213,951
8	"Kapan Mining and Processing Company" CJSC	polymetallic	637,441

ISSUES AND ENVIRONMENTAL LEGACY

The soviet years left many polluted sites and countless abandoned mines. In particular, numerous tailings dams with upstream raise wall construction of questionable stability and resistance to seismic activity remain. Waste rock heaps prone to landslides and exposed pits, tunnels, quarries, abandoned equipment are also present. Other wastes such as slag from copper smelting and molybdenum roasting also contribute to this list of legacy issues. In effect, large areas of unusable land for a country the size of Belgium.

Re-adjustment of the industry after the 1988 earthquake, independence from the Soviet Union and a war that lasted from 1990 to 2004, all affected the recovery of the mining industry. During that period, the mining industry was gradually privatized and operating laws and permits were loosened to attract foreign investment, resulting in industry growth. Following years of hardship, the environment as well as the health and safety of workers took a back seat to the focus on resurrecting industry. Lack of governance and transparency resulted in a flow of funds to foreign banks. Ultimately the legacy of the Soviet years and ongoing poorly regulated exploitation, led to further catastrophic impact on communities living close to mining operations. Proximity to a mining or metallurgical operation often meant heavy exposure to contaminants from releases to the air and waterways. To this day the outcome has been a marked increase in illnesses, birth defects, sickened cattle and wildlife as well as significant change to biodiversity (AUA Center for Responsible Mining 2016).

Active Tailings and Waste Sites

In recent years, foreign-owned mines in Armenia have begun to address shortcomings in environmental management, through adoption of corporate sustainability programs but these remain at a very embryonic stage with regards to managing mine wastes. Generated flotation tailings continue to be non-thickened suspensions pumped to conventional dams. The challenges remain, particularly for active sites. The risks are elevated as Armenia lies in a zone of high seismicity. The following situations exist in the industry:

1) Embankments with upstream raise designs featuring poor stability.
2) Dams are often raised and filled further with uncontrolled flow rates of effluent.
3) Lack of regulation or specific design criteria.

4) Dam stability requires continuous monitoring and any issues are addressed by reactive actions rather than preventive approaches.

Thus, the issues are similar to the reality in most other mining areas of the world (Rico et al 2007). Therefore, in addition to more detailed regulation for the management of existing sites as well as maintaining their enforcement, there is an urgent need to carry out planning of new tailings and waste rock depositories through an integrated approach with transparency, creating a platform for accountability and involvement of all stakeholders.

In the beginning of the 2020, 23 tailing storage facilities (TSFs) associated with metal mining operations were recorded. Nine of those are currently operational, the rest are closed or non-operational (Movsisyan et al 2020). Closed TSFs were operated mainly during the Soviet years, and according to the preliminary estimates, tailings accumulated in some of these TSFs (Akhtala 2/Nazik, Alaverdi, Sotk, Tukhmanuk, Lickvaz-Tey, Pukhrut, and Voghji) have a relatively high content of metals and may be of interest for further processing and as a secondary source of mineral raw materials (Movsesyan et al 2014).

The existing issues in storage and management of mining waste, as well as the impact of mining activities on the environment, have an overall negative impact on the reputation of the mining sector in Armenia (The World Bank 2016, Amirkhanian 2019). Taking into account the importance of mining for the Armenian economy, the gaps in the transparency and accountability of the sector, and a number of problems arising from it, the Armenian Government decided to join the Extractive Industries Transparency Initiative (also known as EITI). Armenia's EITI candidature application was approved on 9 March 2017 at the EITI Board Meeting in Bogota, Colombia.

One important step being taken is the amendments to the Republic of Armenia Mining Code: the new changes planned for 2020 are related to the organization of mining activities and waste (also TSF) management. In particular, it is planned to establish clear requirements in the process of issuing mine permits with regard to preferred processing technologies, dry or wet tailings production and for the construction of new TSFs - approaches favoring dry tailing technology, circulating water systems, and downstream raise methods/design of TSFs.

Another project focused on addressing the risks posed by active tailings dams called the Alliance for Disaster Risk Reduction also known as ALTER was conducted in 2018-2020.

ALTER was implemented by a multi-national team representing universities and organizations from Armenia, Greece, Cyprus, and Bulgaria.

For project implementation, the project focused on three pilot sites in the Republic of Armenia:

1. The Debed River Area of Lori Marz, the community of Akhtala and the tailing management facilities located in the area.
2. The Vorotan Cascade series of dams and hydroelectric infrastructure centered around the city of Sisian in Syunik Marz.
3. The Voghji River and water and mine tailing dams that affect the Kapan area of Syunik Marz.

Key accomplishments of the ALTER project include the following:

1. Table-top and field exercises were conducted in all three pilot sites of the project aimed to understand the risks, enhance preparedness of communities to mine and water dam breaks resulting from strong earthquakes and establish cooperation between local governments, mining companies, and the Ministry of Emergency Situations (MES) of Armenia for addressing those risks. The exercises were coordinated directly with MES. Representatives from key stakeholders in each pilot site also participated in the exercises.

Key goals of the tabletop exercises were to help all parties understand the current situation and plans in place, gather input from stakeholders on improving current emergency plans, and to prepare key scenarios for field exercises. Prior to the tabletop exercise, the results of dam break models developed by the ALTER project were presented to participants to help them better understand the temporal and geographic scale of the exercise.

The tabletop exercises provided valuable data and input for field exercises which were held in October and November of 2019. An important component of these exercises was the willingness of MES to hold concurrent exercises and fully integrate their annual trainings with ALTER's field exercises. Thus, the initial project goal of small-scale exercises was improved upon by the ability to create larger scale exercises that included first responder training as well.

The field exercises tested and simulated scenarios on urgent evacuation after a collapse of the mine tailing and water dams, engaging all local stakeholders.

Overall, the small-scale exercises were considered to be an outstanding success and created significant synergy and goodwill for stakeholders to work towards formalizing future collaboration.

2. A key goal for the ALTER project was the signing of MOUs between stakeholders in ALTER's pilot communities. The MOUs were signed at the project's final conference in December of 2019. The MOUs, signed under the framework of the ALTER project will form the basis for coordination of civil protection activities between public and private sector stakeholders.

3. A series of three sensors were installed on the Geghi dam located near the city of Kapan in Armenia's Syunik province. Three Apatite seismic sensors were installed at three locations around the dam along with one Guralp seismometer. Together, these sensors monitor movement around the dam or of the dam itself. The sensors are also connected to the existing warning system monitored in the city of Kapan. Moving forward, any issue detected at the dam will immediately be transmitted to the city and to national authorities and in certain cases can trigger evacuations. In addition, in the Sisian community, alerting sensors were installed in six locations.

4. In the scope of the ALTER project, along with the measures aimed at enhancing the communities resilience, dam-break flood modeling was performed using modern hydrological models and GIS spatial analysis and visualization tools.

5. Another important result of the project is the development of a web-based GIS tool through which layers collected and developed within the project are presented online (http://alter-flood-crm.aua.am/). The web-GIS system is hosted on a project purchased server at the American University of Armenia ensuring that it will be available for use as a platform which can be used by future projects. The files themselves are also hosted for download at vgse.geology.am.

THOUGHTS ON HOW TO REDUCE WET TAILINGS GENERATION IN ARMENIA

Mining is a very intensive process of digging out large tonnages of earth from the ground and returning 99% of it back to nature. Like in the rest of the world, the adoption of flotation in the early 1930s in Armenia led to major capacity increases with little thought on whether large conventional slurry deposited, upstream TSFs would be a suitable long term solution for wet rejected tailings. The practice of walking away from sites, disastrous impact on the environment, poor management practices, climate change and social acceptance are now putting added pressure on companies to think again about responsible waste management practices.

It is generally accepted that volume reduction can be achieved by selective mining of higher-grade ore or reducing the volume of water sent to the tailings area. In Armenia, it is hoped that some operations will begin to consider and trial technologies which reduce water in tailings. The better-known methods include dry-stacking following the dewatering of tailings or thickening and paste filling. The obvious benefits are minimization of waste site footprint, water recovery for re-use and less costly and complex mine closure steps. If these technologies can be technically demonstrated, filtered or decanted tailings and dry-stacking represent the most attractive method. For a complete evaluation, the economics of implementation need to include the cost and benefits to the company and society for conventional closure of a tailings site and possible re-use of this land for other purposes..

Further value extraction from waste material is an approach which has been proposed for the recovery of magnetite and alumina from oxide ores (Harris 2016). The possibility of recovering further values from flotation circuits to significantly reduce volumes to tailings is limited in the Armenian situation as all active mines process sulfide ore and minerals held within tails such as pyrite and some clays have no commercial value. Pyrite represents a source of sulfur for the manufacture of sulfuric acid, for which there is little or no demand in Armenia or bordering countries. However, the separation of pyrite and other sulfides from a reject wet tailings stream can be an option at the end of a flotation circuit to split the material into nonacid-generating and acid generating streams. Isolated nonacid-generating material is far easier to dispose and rehabilitate, whereas the acid-generating would require a different strategy for disposal, possibly

as paste fill (Yilmaz 2011). Another option may be to make use of dry ore-sorting systems with sensors upstream of flotation.

RECENT INITIATIVES ON RE-TREATMENT OF LEGACY TAILINGS AND WASTES

Legacy tailings dams and waste rock sites represent potential resources for mineral recovering through reprocessing. This potential has gained the attention of the government, some mining companies, and potential private investors. These waste facilities have no owner and were orphaned during the Soviet era.

The oldest sites holding wet tailings, waste rock and even smelter slags are likely to hold the highest concentrations of metal values, as mineral separations were not as efficient in the past. These sites may feature favorable economics, subject to further evaluation.

A single bio-leaching laboratory study is reported which evaluated gold, copper and zinc recovery from Shahumyan mine sulfidic tailings (Vardanyan et al 2018) yet the findings were inconclusive and no further work was carried out. Testwork carried out on Armenian copper smelter and molybdenum roaster slags to generate value added iron and silica by-products (Martirosyan et al 2019) is the only other recent published Armenian study on waste retreatment.

With regards to mine wastes, the approach is to tackle each site as a unique scenario. Once an earmarked site has been properly sampled and resources estimated, the most appropriate process can be selected after thorough mineralogical analysis. An experienced technical team will have to include the afterthought of containing and stabilizing the reject material. In an ideal situation, the barren material would be filtered and dry-stacked. The lack of laboratory facilities and expertise in Armenia means that collaborations with established international institutions and specialized firms are the way forward.

The American University of Armenia, Acopian Center for Responsible Mining will continue to participate in initiatives which bring best practices to the Armenian mining industry and this will include exploring ways to reprocess old wastes, minimize risks posed by existing mine sites and evaluate novel routes of returning sites back to nature.

CONCLUSIONS

Armenia has important mineral reserves of copper-molybdenum and gold. The mining industry was developed during the Soviet years and went through adjustments following years of turmoil and independence from the Soviet Union.

Past and recent containment strategies for wet and dry tailings are visible as areas suffering from seepage and extensive acid mine and rock drainage. Concentrators discharge into waterways on a regular basis. There is also reliance on upstream wet tailings dam wall design and overfilling which is not recommended, particularly in a very active seismic region.

In order to address the many issues and improve governance over mine activities, the country adhered to the Extractive Industries Transparency Initiative (EITI) in 2017. Amendments to the Republic of Armenia Mining Code are currently in the making and will address better oversight of mining activities, technologies and mine waste management. In addition, and because of imminent dangers from active wet tailings dams, an emergency preparedness project related to protecting downstream areas was initiated in 2018 called the Alliance for Disaster Risk Reduction (ALTER).

Lastly, there has been strong interest by government and mining firms to focus on re-treatment of metal-rich wet sulfidic tailings and dry waste rock from some of the older waste sites. Such projects will need to include careful thought on the safe disposal of the barren material. It is hoped that metallurgical test work through collaborations with foreign and well-established laboratories and institutions will pave the way to future successful re-treatment projects.

REFERENCES

Amirkhanian, A. 2019. On Mining - Which Way Armenia? *Amcham, fall/winter:* 28-29.
Aprahamian, V. 2019. Personal Communication.
AUA Center for Responsible Mining. 2016. Results of Soil and Drinking-Water Testing in Kindergartens and Schools of Kajaran City and Artsvanik Tailing Site, Syunik Marz, Republic of Armenia. Yerevan.
Bond, A. & Levine, R.M. 1997. Development of the Copper and Molybdenum Industries and the Armenian Economy. *Geography and Economics* No. 2: 105-120
Dobrinkova, N., Arakelyan, A., Harutyunyan, A., & Reynolds, S. 2019. Project for an Open Source GIS Tool for Visualization of Flood Risk Analysis after Mining Dam Failures. *Large-Scale Scientific Computing, Springer Nature Switzerland AG*: 295-303.
Dobrinkova, N., Arakelyan, A., Harutyunyan, A., & Zlatkova, A. 2019. GIS Flood Decision Support Tool after Dam Break (Armenian Test Case). *Proceedings of 19th International Multidisciplinary Scientific GeoConference SGEM 2019, 30 June – 6 July*: 911-918.
Dobrinkova, N., Stefanov, S., Hadjitodorov, S., Arakelyan, A., Amirkhanian, A., Barseghyan, A., Mnatsakanian, S., Drakatos, G., Evangelidis, Ch, Katsaros E., & Boustras G. 2019. Emergency planning and optimizations based on dam break flood risk maps visualized with open source web-GIS tool. *Position Papers of the 2019 Federated Conference on Computer Science and Information Systems, M. Ganzha, L. Maciaszek, M. Paprzycki (eds)*. ACSIS, Vol. 19: 3–7.
Fourth National Communication on Climate Change. Yerevan. UNDP Armenia, 2020.- 213p.
Harris, B. 2016. Innovation, Sustainability and the Future of Metals Extraction. *ALTA Conference Proceedings.*
Jensen, R.G., Shabad, T. & Wright, A.W. 1983, Soviet Natural Resources in the World Economy. *University of Chicago Press*: 583.
Martirosyan, V.A. & Sasuntsyan, M.E. 2019. Investigating the Slags of the Metallurgical Plants of Armenia at Fine Grinding. *Steel in Translation* 49(1): 1-6.
Melkonyan, V.A. 1955. Metallurgy of Copper in Armenia. *Metallurgizdat* (in Russian).
MNP Report. 2019. RA Ministry of Environment. Information database (report) on abandoned/production dumps without owner and closed facilities generated as a result of metallic mineral mining. http://mnp.am/uploads/1/1561026142HASHVETVUTYUN_Geraka_kayq.pdf
Movsesyan, R.S., Mkrtchyan, H.H. & Movsisyan, H.I. 2014. Prospects for Industrial Developing of Technogeneous Mineral Resources of the Republic of Armenia. *Yerevan: Proceedings of NAS RA, Earth Sciences* 67 (1): 30-39 (in Russian).
Movsisyan, H., Karapetyan, K., Hovhannisyan, H., - authors; Matevosyan, H., Arakelyan, A., - eds. 2020. Mine Waste and Tailing Storage Facilities in Armenia: Disaster Risk Management. Yerevan: Alliance for Disaster Risk Reduction (ALTER). AUA Center for Responsible Mining: 161 (in Armenian) https://crm.aua.am/files/2020/02/ALTER-Handbook.pdf
Rico, M., Benito, G., Salguiero, R., Diez-Herrero A. 2007. Reported Tailings Dam Failures - A Review of the European Incidents in the Worldwide Context. *Journal of Hazardous Materials* 152(2): 852.
Strishkov, V.V. 1984 The Copper Industry of the USSR, Problems, Issues, Outlook. *US Bureau of Mines*: 52
The World Bank. 2016. Armenia: Strategic Mineral Sector Sustainability Assessment (English). Washington, D.C.: World Bank Group. http://documents.worldbank.org/curated/en/289051468186845846/Armenia-Strategic-mineral-sector-sustainability-assessment
US Commerce Report. 1919. Annual Series, Russia. November 3.
Vardanyan, N.S., Sevoyan, G., Navasardyan, T. & Vardanyan, A. 2018. Recovery of Valuable Metals from Polymetallic Mine Tailings by Natural Microbial Consortium. *Environmental Technology* 40(26): 1-23.
Voigt, P. & Walker, D.. 2018. The Albion Process at the GPM Gold Project - The Success of a sTechnology. *CIM Convention presentation*, Vancouver, Canada.
Yilmaz, E. 2001. Advances in Reducing Large Volumes of Environmentally Harmful Mine Waste Rocks and Tailings. *Gospodarka Surowcami Mineralnimy* (27).

Risks of Dormancy: Reducing Tailings Risk after Operations, before Closure

Jeremy E.S. Boswell, John C. Sobkowicz & Amy K. Rentz
Thurber Engineering Ltd., Calgary, AB, Canada

ABSTRACT: Recent catastrophic tailings dam failures (Mount Polley, Samarco, Brumadinho) have substantially altered mining industry thinking in regard to risk. What is perhaps less well known, is that some failures have taken place while the facility is non-operational, or dormant (Merriespruit, 1994, Brumadinho, 2019). This paper asks a few questions:

- In moving beyond the operational phase, could a tailings dam be exposed to elevated risks?
- What might these risks be?
- What measures would be needed to avoid or control such risks?
- What guiding principles should be uppermost in closure thinking?

The purpose of this paper is to raise awareness of heightened risk associated with cessation of operations, dormancy or poorly managed closure, and to provide interventions, tools and remedies to reduce risk. The paper lists twelve precautionary guiding principles which may be applied to dormant tailings facilities to prepare for the period after operations cease, and before closure is achieved.

1 INTRODUCTION

Many tailings facilities are well operated, to very high standards, employing leading practice engineering. Morgenstern (2010) highlighted in his keynote address to a previous Colorado conference that "*It is the view of the Writer that the dam safety system applied to the Alberta oil sands industry is the best in the world*".

So why is it that catastrophic failures continue to occur on an annual basis? In pursuing (like many of us in the industry) answers to this vexing question, Morgenstern (2019) addressed a more recent keynote to the Canadian Dam Association annual conference in Calgary. He considered 22 significant failures over the past 55 years and found good reason why failures continue to occur: weakness in engineering: a failure to apply already well-known geotechnical engineering principles to tailings dam safety.

This paper delves further into the causes of tailings failures and finds a disturbing trend: Many failures have occurred when a tailings dam is dormant (alternatively moth-balled or non-operational), and before closure has been achieved.

This paper is not intended as a step-by-step guide as to how to engineer a tailings facility, nor even how to proceed with closure. It also does not seek to replace the many excellent postgraduate level courses now available at universities such as the University of Alberta, University of British Columbia, and many others.

Instead, the paper seeks to highlight awareness of the risks of dormancy: suggesting twelve guiding principles which are required after operations cease, and before closure can be embarked upon.

2 A SNAPSHOT OF THE ROLE OF DORMANCY IN HISTORIC TAILINGS FAILURES

2.1 *A view on the statistics*

Accurate statistics on the total number of tailings dams worldwide are unpublished and unavailable. Broad estimates range from as low as 5000 to over 30,000 facilities. While several countries have very accurate records, many others do not.

The recent questionnaire distributed by the Church of England yielded responses for under 2000 facilities. Grid-Arendal (2020) lists 1938 facilities on the online global tailings portal and categorizes them into status. Just over 40% were listed as active. Many fascinating analyses will no doubt be produced from this list, but this list includes less than 10% of all tailings facilities worldwide.

Wei et al. (2013) record that at time of writing there were over 12,000 tailings dams in China alone.

Very few tailings dams have been comprehensively closed. Significantly less than 10% of the facilities listed on the global tailings portal may be comprehensively closed.

Most tailings dams are neither actively operating nor closed. Multiple thousands of dams are simply dormant.

2.2 *Brief reference to the role of dormancy in tailings failures*

2.2.1 *El Cobre, Chile, 1965*

According to Dobry & Alvares (1967), Dams 1 and 2 were dormant and not in use. Dam 3, upstream of Dams 1 and 2, failed spectacularly, causing substantial cascading damage, especially to Dam 2 as a result of an earthquake. Many lessons were learned from this failure, including an immediate and subsequent ban on upstream construction of tailings dams in Chile.

Dam 2 was not protected because it was simply dormant and not fully closed and therefore vulnerable.

An additional lesson relevant to this paper is that dormant dams need to be protected from risks such as the cascading failure of adjacent dams.

2.2.2 *Stava, Italy, 1985*

The Stava facility had recently been dormant and had been recommissioned.

According to Simeoni et al. (2017), referencing Lucchi (2005), "In 1969, in order to deal with increased mining production, it was necessary to construct a second basin just upstream of the first one. The dam of this second basin was raised without any provision either for anchoring it to the ground or for draining. As the dam grew higher, the base of its embankment grew wider until eventually it rested partly on the silt of the lower basin. The decant pipes were placed inside the basins and discharged outside by passing through the dams. For a period (1978 to 1982), the basins were not in use. Activity resumed in 1983 and continued until the collapse of the structures in July 1985".

In disturbing agreement with the causes of the El Cobre failure twenty years earlier, the damage to dormant dams and tragic loss of life from the errors of adjacent site location causing cascading failure, were repeated.

2.2.3 *Merriespruit, South Africa, 1994*

The Merriespruit No. 4 dam was in a dormant phase at the time of failure. Deposition of tailings was taking place on an emergency basis, as a result of slurry pumping underperformance in delivering tailings to the actively operated alternative location.

Fourie et al. (2001) noted "In March 1993 the decision was taken to suspend tailings deposition on the northern compartment of the dam (i.e. the compartment that breached on February 22, 1994). For reasons that were attributed to poor communication, unauthorized deposition of tailings still took place on this compartment from time to time after March 1993".

In other words, Merriespruit No. 4 stood dormant for almost a full year before the failure occurred.

2.2.4 *Mount Polley, Canada, 2014*

In common with many other mining operations, and in similar fashion to the economics of the Stava facility, Mount Polley had been returned from a state of dormancy, and returned to service, prior to the failure.

As noted in the Mount Polley Breach Report (Morgenstern et al. 2015), "As a result of low copper prices, the Mine suspended operations from October 2001 to February 2005. A small staff was maintained at the Mine and they managed the TSF water balance carefully, making sure that sufficient freeboard was maintained. Towards the end of the Care and Maintenance period, mine development in preparation for start-up was underway and surface water accumulated in the TSF. It was recognized at this time that plans would have to be developed to discharge water to the environment".

When one rereads the Mount Polley report years later, it is apparent that a multitude of actions were taking place all at the same time just before the failure occurred. Unless a strategic view is taken for a tailings facility, similar risks may arise.

As observed in the report: "Something had to give, and the result was oversteepened dam slopes, deferred buttressing, and the seemingly ad hoc nature of dam expansion that so often ended up constructing something different from what had originally been designed. Ultimately, the tortuous, incremental nature of this process, and the constraints under which it was conducted, caused it to lose sight of basic precedent."

The care of a dormant tailings facility cannot be ad hoc. Neither can its return to active deposition be.

2.2.5 *Brumadinho, Brazil, 2019*

The Brumadinho facility was dormant at the time of failure. Deposition had not occurred on the dam for two and a half years.

Robertson et al. (2019) observed that "Dam I was developed to store tailings that were produced during mining operations at the Córrego do Feijão Mine…. Dam I was constructed over a 37-year period from 1976 to 2013 in 15 stages…. No new raisings were constructed after 2013, and the placement of tailings ceased in July 2016."

Troubling signs of rising risk associated with dormancy are included in the report, such as "Water management within the tailings impoundment that at times allowed ponded water to get close to the crest of the dam".

3 SOME RELEVANT DEFINITIONS

In order to more fully explore some of the risks faced once a tailings facility ceases operation, it is perhaps useful to define a few terms used in this paper:

- Dormancy: The (unacceptable) condition of a tailings facility in the time period between the cessation of operations and the start of reclamation and closure activities. This can vary from months to years. No assumption is made about activities in the mine or in other tailings facilities – mining may be active or suspended or ended. As implied by the term, insufficient attention is paid to a tailings facility which is allowed to remain in a state of dormancy, instead of being decommissioned.
- Latency: The condition of existing but not being very noticeable or well developed. In the context of dormant tailings facilities, may apply to conditions or processes that are evolving slowly, not necessarily noticed, and that might threaten the safety of the structure.
- Time bomb: A situation that is likely to cause serious problems at some future time. It may at present be only latent.
- Black Swan event: A Black Swan is a rare, unexpected event. That is, it is truly rare (hardly ever happens) and it is far outside of the collective experience of a group of people, so that they would not consider it to be possible. It can have positive or negative consequences, but those consequences are usually extreme.
- Fragility: The condition of being weak, easily damaged or easily broken.
- Robust: The condition of being strong, able to survive being used a lot and not likely to become weak or break.

- Resilient: Able to quickly return to original shape or serviceability after being subject to stress and/or shock.
- Anti-fragility: The opposite of fragility. In its fullness, a condition beyond robustness or resilience; an ability to not only survive stress and/or shock, but to improve as a result of that stress and/or shock.

4 RISKS TO MANAGE IN MOVING FROM OPERATION TO CLOSURE

Mining commodities are cyclical in nature, and as such, the operational status of tailings facilities can change very quickly, as mine owners adapt to market changes. Tailings facilities may cease operations very unexpectedly, temporarily, or permanently.

Unless this eventuality is planned for, a state of dormancy may result, in which closure is neither anticipated nor implemented, and the facility may face unexpected risks, with few resources to manage the risks. What are some of these risks?

4.1 *Planning risks*

Dormancy at worst, or a decommissioning phase, at best, should be contemplated, as a risk. What happens if the tailings facility must curtail or cease operations unexpectedly? This must be planned for.

4.1.1 *No plan at all*

Despite all that has happened in the tailings industry in the past six years, there are still active tailings operations around the world today which do not have a closure plan in place. Some closure plans have not included a risk assessment. A Failure Modes and Effects Analysis (FMEA) is now a requirement for each phase of a tailings facility in British Columbia, Canada (BC Government 2016).

One of the risks that should be considered in an FMEA, is the possibility that a facility could cease operations suddenly. This is the risk of dormancy. A phase of decommissioning should be entered immediately, to address risk. Risks do not go away by themselves: when left to themselves, risks tend to increase rather than diminish.

4.1.2 *Starting too late*

Planning for closure cannot start too early. A sound life cycle plan for a tailings facility commences with planning for closure during the design phase.

The profitability of a mine declines over time, as reserves are depleted, ore grades deteriorate, equipment becomes inefficient and outdated, and staff and community morale wanes. This is often the backdrop against which tailings facility closure must take place. Early planning for closure and dormancy can provide a defense against these limitations.

4.1.3 *Short sighted mine planning*

Tailings plans typically do not look far enough. A true life of mine plan looks way beyond ten years. A trend in recent Geotechnical Review Board (GRB) advice is to look at both life of mine as well as closure time frames.

4.1.4 *A lack of integrated planning*

If a mine should suddenly cease tailings deposition, planning and preparedness for closure might find itself out of sync with operational realities.

More than one tailings plan the authors worked on over the years, relied on a different technology for operations to that required for closure. Unless plans for the facility are integrated, the risk of dormancy remains a real threat.

There is a need for mid-range planners, who can match the short-term requirements of operations while not losing focus on the longer term demands of closure.

4.1.5 *Inflexibility of plans*

Closure plans (and plans to deal with dormancy) need to be adaptable and able to evolve to account for changes in:

- commodity price,
- mine ownership and management,
- regulation,
- materials,
- operations,
- performance of structures and
- weather.

4.2 *Risks arising from decision making based solely on financial information*

Some risks imposed upon tailings facilities derive from the nature of the decision-making process. Most mining companies are privately owned and are measured within annual and quarterly financial windows. This is a substantial influence on operational decisions, including those impacting on tailings. This introduces many potential risks, for tailings operations and closure planning:

4.2.1 *Ignorance of mining commodity cycles*

Saving for closure costs early and during the life of mine to avoid the vagaries of uncertain commodity fluctuations is prudent.

An approach to mine planning and closure which ignores commodity cycles is naïve at best, and a target for prosecution, at worst. Overly optimistic reserve and mine valuations make matters worse.

4.2.2 *Ill fated, continued reliance on NPV instead of Life Cycle Costing*

So much has been written by Van Zyl (2009) and many others. Ongoing reliance on Net Present Value (NPV) instead of the ethical alternative of Life Cycle Costing to guide closure decisions can no longer be excused and will lead to a loss of social license to operate. Even within NPV analysis, discounting is used to justify deferring almost any decision with long term implications, especially in high inflation economies.

4.2.3 *Shortage of funds and materials (such as crushed rock)*

Apart from the shortage of funds, other resources may be missing:

- Equipment
- Materials, such as crushed rock
- Emergency supplies
- Power supply

As noted in Mount Polley Report (Morgenstern et al. 2015), "The design was caught between the rising water and the Mine plan, between the imperative of raising the dam and the scarcity of materials for building it."

A sound decommissioning and closure plan considers the restrictions of reduced access and limited resources and provides accordingly.

4.2.4 *Avoiding expensive Sustaining CAPEX*

Certain designs are predicated on the regular expenditure of Sustaining CAPEX. This might include adding an extra stage of slurry pumps or implementing a berm step back to control erosion and stability or relocating a decant point to move the pond away from a vulnerable slope.

Such designs are inherently fragile, since it is all too easy to defer such expenditure, and to continue to rationalize such deferrals for many years: "Nothing fell down; Let's not fix what's not broken; it was an overdesign anyway; we'll use the observation method." We have all heard the rationalizations.

4.2.5 *"Mothballing" to avoid decommissioning and closure*
Mothballing or the temporary cessation of operations, without the necessary precautions of decommissioning and closure, may be simply lighting the fuse for the time bomb of catastrophic failure for hydraulic fill structures. Mothballing continues to happen.

4.2.6 *Mine bankruptcy or foreclosure*
At least two tailings facilities known to the authors have recently failed or narrowly avoided failure while the company owning the mine was undergoing bankruptcy procedures. Are tailings risks even considered in mining foreclosure?

4.3 *Regulatory risks*

The regulation of mining and mine waste disposal requires interaction between mine owner and regulator in many areas, including permitting and approval of mine operating and closure plans. As further reported in section 5.5 of this paper, Alberta, Canada is an example of a jurisdiction in which regulatory and mining teamwork is relatively effective. Unless the regulatory interaction occurs efficiently, several risks may arise during the dormancy, decommissioning and closure phases:

4.3.1 *Poorly defined closure acceptance process*
Historically, the process for regulatory approval of waste or tailings facility closure plans in many jurisdictions has been uncertain, iterative, even tortuous, and very time- and resource- consuming (Morgenstern 2012, Boswell 1996). Usually, the applicant engages the regulator, while neither has a complete picture of what is required. Prevailing law and regulations usually stop short of defining the detail. Stakeholder and environmental issues tend to confuse matters further, and the requirements for closure often take a great deal of time to be defined and agreed to.

Most mining jurisdictions have not yet sufficiently defined a practical closure acceptance process, nor achieved maturity in implementing tailings closure. End use planning, stakeholder engagement, release of water to the environment and administrative delays are some of the challenges that have been encountered.

Morgenstern (2012) reports on the early struggles in Alberta with achieving true closure for an overburden waste dump at Syncrude, known as Gateway Hill. Eventually true closure was successfully achieved, but only after a closure acceptance process had been developed, agreed and implemented, between the mine and the regulator, over a ten-year period. These early lessons paved the way for a better collaboration in Alberta between regulators and mining, including publication of guidelines (Kupper et al. 2014, subsequently in the process of substantial revision), development of metrics and practical implementation of administrative measures.

4.3.2 *Non-holistic regulation*
A chain is only as strong as its weakest link. The many components of mining and closure regulation require holistic thinking and implementation.

4.3.3 *New risks arising from imposed regulations/interventions*
For a mining economy to thrive, investors require a measure of certainty. Ever-changing rules and requirements erode investor confidence.

Morrison (2018, 2019) reports on some of the difficulties encountered in Brazil with the introduction of substantial, new tailings regulations over the past five years. A ban on upstream construction has required the immediate cessation of tailings deposition for many facilities.

4.3.4 *Disallowed discharge of water*
In the absence of release water guidelines and criteria, even in case of emergency only, the storage of excess water on tailings facilities remains one of the single largest risks for hydraulic fill structures.

4.3.5 *Jurisdictional conflicts and/or gaps in addressing closure*
The regulation of mine and tailings closure requires significant collaboration between different levels of government, and between different departments within each regulator. Unless

regulations and administration are implemented collaboratively, a fragmented approach will usually result in prolonged delays and high cost to the mine and to the environment.

4.4 *Technical risks*

Neither time nor space affords opportunity within this paper to fully describe many of the technical risks faced during dormancy, decommissioning and closure, many of which are well reported in conferences, an excellent example of which is this Tailings and Mine Waste series within the USA and Canada. Previous papers by many leading practitioners have provided insight into the technical risks of tailings dams, for many decades.

Instead, a few salient technical risks are simply listed below, for reasons of currency:

- Settlement, and the absence of geotechnical readiness for reclamation (Sawatsky et al. 2018).
- Absence of water treatment.
- Ponded water.
- Impact of climate change on reclamation strategies.
- Co-disposal with other wastes.
- Long-term reliance on external tailings facilities.
- Absence of comprehensive closure plans for deep in-pit deposits.

5 GUIDING PRINCIPLES FOR MANAGING RISKS AFTER OPERATIONS CEASE, AND BEFORE CLOSURE IS IMPLEMENTED

Once a facility ceases operation, new risks are introduced. In addition, some risks previously considered to be under control, may reappear at heightened levels. Faced with this scenario, what remedies and interventions could be available to the dam owner or person responsible for dam integrity?

5.1 *Recognize the risk of dormancy, and the critical role of decommissioning in reducing risk*

Recognition of the risk of dormancy is an important first step. Whether active closure is immediately being considered, or whether the facility is non-operational, dormant or "moth-balled", growing new risks as outlined in the section above, require dedicated attention.

Two phases in the life cycle of tailings facility development are often overlooked:

- Commissioning – the transition between construction, and operation: preparing, equipping, and making the facility ready for operation.
- Decommissioning – the transition between operations and closure: taking out of service and making safe.

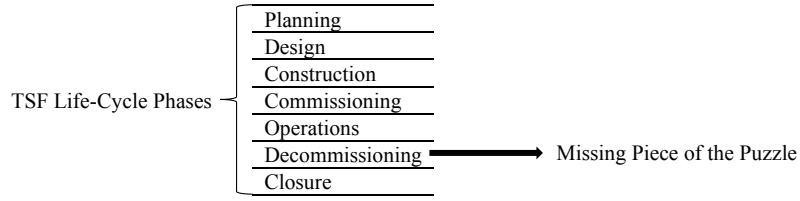

Figure 1. Decommissioning, the missing piece in the puzzle.

Preparing a facility for closure is not a trivial task. The facility may not be ready for closure. It needs to be decommissioned in an orderly manner, in order to control risk. This decommissioning phase needs to fill the gap between operations and closure.

In other words, recognize that a phase of dormancy may follow operations and needs to be properly managed. If it is, then decommissioning will provide protection to the facility until closure is implemented.

5.2 *Target reclamation readiness*

Leading mining sectors evaluate this condition in considering "reclamation readiness", by identifying and tracking key geotechnical performance criteria, such as:

- degree of consolidation,
- vulnerability to liquefaction, and
- settlement.

The process of advancing a facility to reclamation readiness may take many years. Careful planning should commence years before operations cease, to avoid rising risks and expensive emergency interventions.

Most tailings facilities are operated as hydraulic fill structures, and for good reason. The lower daily operating costs of slurry hydrotransport and beached deposition for separating solids from liquids is attractive and has been employed for many decades.

However, this technology may not immediately lend itself to ready closure, nor to managing and reducing long term risk. A transitional or decommissioning phase can be used to strengthen the defensive measures of the facility, by altering the operation of the facility as it nears the end of useful life, through:

- Reducing supernatant pond volumes, also leveraging the benefits of reducing the area occupied by the pond. (Rourke & Luppnow 2018, Boswell & Sobkowicz 2018).
- Reducing the mine process water inventory, including water treatment and release.
- Removing and treating fluid tailings.
- Reducing catchment areas to decrease risks associated with extreme precipitation and flooding.
- Compartmentalizing.
- Changing or reversing beach angles.
- Controlling the impacts of desiccation, especially dust generation and windblown erosion.
- Mulching of top surfaces, using rock or by providing a growing medium for vegetation.
- Improving drainage.

5.3 *Pursue antifragility*

Nassim Nicholas Taleb (2014) provides an excellent insight into the concept of antifragility.

While an awkward term, "antifragility" is the opposite of fragility, a condition beyond resilience and robustness (see definitions in Section 3). What is the difference between robustness, resilience and antifragility? Something that is robust or resilient resists shocks and stays the same or returns to the same serviceability. However, something that is antifragile, when exposed to shocks, gets better.

Some things benefit from shocks: they thrive and grow when exposed to volatility, randomness, disorder, risk, and uncertainty.

Not all systems can be made fully anti-fragile, but if that is the goal, then measures can be taken to move in that direction.

- The first step is to become less fragile and more robust. For example, in a personal or business sense, debt results in fragility, so avoid debt.
- Introduce redundancies into systems and processes to make them more robust.
- Contrary to much advice in the financial and engineering fields, optimization is not possible in a Black Swan world. Avoid efforts to optimize tailings facility systems but instead work on making them more robust, resilient and ultimately anti-fragile.
- Build reclamation surfaces and closure landscapes that have the potential to improve over time, even when subject to at least known stressors. Lessons from natural landscapes that have survived and thrived over time can be instructive, in this regard. Blight & Amponsah-Da Costa (2004) describe such a condition in the chapter contributing to a book on the subject: "Towards the 1000-year erosion-free tailings dam slope" based on Blight's visit to China where naturally occurring slopes were observed.

5.4 *Characterize Risk by considering True Decommissioning (not dormancy or latency)*

Section 4 of this paper has listed some of the key risks which are often overlooked after operations cease. In characterizing these decommissioning phase risks, there are key elements to bear in mind in the risk characterization process:

5.4.1 *Identify and characterize decommissioning risks well in advance*

Time is an important resource in planning for decommissioning. Environmental and natural processes may be harnessed in reducing human intervention. Well planned decommissioning can leverage many cost savings by using mine-based human and material resources during the operational phase, to prepare for decommissioning.

5.4.2 *In assessing likelihood consider a longer window than a simple annual period*

Conventional risk management usually considers annual probability in assessing likelihood and risk. This approach has limitations for closure thinking. It behoves the dam owner to consider medium- and longer-term risks for more special attention.

5.4.3 *Engage the full breadth of multidisciplinary knowledge and expertise*

Decommissioning (like closure) thinking and planning requires a broader range of disciplines than those tasked with day-to-day tailings operation.

5.4.4 *For longer term risk management, a focus on reducing consequence is preferred over reducing likelihood*

Robertson (2011) observed that unlikelihood is no defense at all, in the face of perpetuity. At a previous Colorado TMW conference, Boswell & Sobkowicz (2016) discouraged unlikelihood as a defense against extreme and imponderable consequences.

While addressing post-operating and closure risk, make use of the opportunity to reduce consequences, looking for "low hanging fruit", while isolating and avoiding the hidden costs of long-term active care.

5.4.5 *Review and reevaluate risks regularly and address rising risks promptly*

Dormancy risks tend to grow and accelerate. Consider risks such as flooding, inundation, surface and internal erosion, freeze-thaw, etc. The adage is never truer: "a stitch in time saves nine".

The province of British Columbia now requires a formal Failure Modes and Effects Analysis (FMEA) to be conducted, updated and submitted regularly, for regulatory scrutiny.

5.4.6 *Continued reliance on the observational method requires continued observation*

The above statement seems redundant but does reflect the implied risks of employing the observational method once active deposition and attention ceases. The observational method must either be continued, or adequately replaced.

5.4.7 *Recognize that Black Swans will occur*

Caldwell & Charlebois (2010) provide valuable insight into taking account of the influence of Black Swans (completely unforeseeable events) on tailings management.

5.4.8 *Recognize if you cannot mitigate a risk, you have to monitor*

It goes without saying that if a risk cannot be eliminated, reduced or transferred, then the long-term impact of the risk on the facility must be closely watched.

5.5 *Develop metrics for decommissioning and closure through effective collaboration between regulator and industry*

In section 4.3.1 of this paper, some of the significant risks faced during the regulatory process of tailings closure are described. How may these risks be addressed?

In Alberta, the following process has evolved in discussions over the past four years or so, with the regulator:

- One mine or dam owner raises an issue with the regulator. It could be closure parameters, implementation schedules and dispensations for new regulations, requirements for as yet undefined activities (such as release of water to the environment), etc.
- The regulator (typically more frequently AER on Energy dams, but also sometimes AEP on other dams) has then approached the Alberta Dam Integrity Advisory Committee (DIAC) to say: "We would like industry to help us define what parameters and standards we should use, and provide practical, measurable and existing leading practice direction, so that we can implement something fair and reasonable across the board that is also workable and practical, and supported by public and external stakeholders."
- DIAC would then consider the task in one of their subcommittees, and then forward material to the regulator, usually accompanied with a series of workshops, presentations, and discussion. There is often a lot of back-and-forth as the best approach is developed, discussed and confirmed.
- In other words, industry is invited to assist the regulator to define the process, parameters, and implementation. Of course, the regulator will always make their own decisions on the right balance to be achieved.
- This process is now working reasonably well. All parties are in support of this process.

Early experience supports the promise of prescribing and implementing practical, reasonable and equitable metrics for decommissioning and closure. As an alternative model, this presents avenues for more efficient collaboration between regulator and industry.

5.6 *Prepare a comprehensive plan to address post-operative risks*

Evaluation of risk and development of appropriate mitigation plans is a critical but also a standard exercise in the design, construction and operation of tailings facilities. This is normally carried out through various risk assessment methods (or a combination thereof), such as Failure Modes and Effects Analyses, Bow Tie Analyses, and for more complex issues, Multiple Accounts Analyses. These can be carried out at various stages during the design, construction and operation, which may overlap somewhat with one another.

It is essential to carry this risk assessment/mitigation approach through into the dormant period of a tailings facility, and then further into the reclamation and closure period. What is important from the perspective of this paper is that the same careful evaluation is required during dormancy as is required for all other stages of a tailings facility's life.

5.7 *Actively maintain mitigation measures*

In regard to the point in the previous section, mitigation measures need to be defined and carried out with the same level of care and attention to detail as during earlier stages of the life of the tailings facility. This could include a continued application of the observational approach, which requires ongoing monitoring and response to adverse performance, or in the event of inability to mitigate over time, the implementation of pre-emptive mitigation measures.

5.8 *Maintenance during Tailings Facility dormancy*

In some cases, the ability to respond quickly (or at all) to observed inadequate performance (of any kind) raises the stakes in terms of facility maintenance. Maintenance items that under normal operations might have a low priority, under the conditions of a dormant facility take on a higher priority. This seems counter-intuitive to many, who tend to ignore low priority maintenance during periods of dormancy. However, a heightened attention to maintenance is the main defense against the development of adverse, latent conditions and in some cases, hidden time bombs.

5.9 *Continue with vigilance to inspect and report on the condition of the structure*

The longer a tailings facility continues in a dormant state, with little visually observable change, the greater the temptation to become complacent with both its condition and its performance. This is particularly true when there is a lack of the normal types of "stressors" (such as increased

loading on a dam or its foundation from construction or from operations [e.g. beaching, pond level increases]) that result in continued, observable performance changes.

This vigilance could have been of life-saving value in the cases quoted in Section 2 above.

During dormancy, the changes in the condition of the structure may be much more subtle (e.g. slow internal erosion, gradually rising pore pressures that could trigger instability, etc.). Detecting these changes can require more diligence in assessing and monitoring for failure mechanisms that can develop slowly over time. A good example of this type of condition is the "sudden" appearance of sinkholes on the Bennett Dam in northern BC, 30 years after construction and initial reservoir impoundment (Stewart et. al. 1997).

5.10 *Ensure instrumentation is appropriate for inoperative phase*

Defining the requirements for instrumentation during the dormant stage of a tailings facility is related to previous sections (5.6 to 5.9). As during other stages of a tailings facility's life, the instrumentation must be selected, located and monitored in a fashion that is at least consistent with the anticipated failure modes and ongoing processes. These requirements may be significantly different than those established for the construction and operations stages, but no less important. Thought should be given to meeting changing regulatory requirements and maintaining long-term access to instruments (for readings and/or for maintenance). In addition, consideration should also be given to making the instrumentation system itself anti-fragile, which is particularly important for longer periods of dormancy

5.11 *Plan Effectively for True Closure*

Many unsuccessful attempts at true closure may be traced back to a lack of foresight and planning. Conversely, the benefits of timely and effective use of resources in introducing closure actions early, during the operational phase, cannot be overstated.

5.11.1 *Engage the closure approach*

Recently updated tailings guidelines as referenced in Section 6 and the References Section below, suggest a significant and early focus on closure, and closure planning. Closure is considered as a critical action which should start well before operations cease – in fact, as early as during the design phase.

A platinum tailings facility which was designed by one of the authors nearly four decades ago, commenced closure actions, including top-soiling and revegetation of the sideslopes of the upstream facility early in the operational life, long before closure was even considered. The advantages of this early initiative included the availability in an arid region, of (operational supernatant-fed) moisture for root growth and penetration and significant cost savings. The contractor even offered the service without additional charge, as enough personnel were already on site with ongoing surveillance and other routine responsibilities.

5.11.2 *Recognize the high costs of real closure*

Traditional mining economics has often relied on the NPV approach to decision-making. Van Zyl (2009) and others have pointed out the severe limitations of the approach, advocating instead, a life cycle approach to costing, economics and decision-making, which is less likely to allow postponement of closure activities for reasons of short-term financial benefit only.

The benefit of starting the planning for closure early, is that financial and other provision can be made slowly, over time, without placing extreme and unaffordable demands on the mine once its most profitable years have passed.

5.11.3 *Establish objectives and solutions*

A useful approach for closure planning is to pursue a risk management approach, targeting and prioritizing those risks which are highest, for closest attention.

As an example: many operations rely on a significant inventory of process water. However, large volumes of supernatant contained on a tailings facility have been shown to be a leading indicator of tailings failure (Boswell & Sobkowicz, 2018), and usually one of the highest risks. In

developing strategies to reduce water inventory, closure planning will be addressing one of the highest risk items.

5.11.4 *Plan for both life of mine and closure*
Current review practice in the Oil Sands of Alberta, is to consider implications for both life of mine, as well as the closure phase. An important consideration is the selection of design life of the structure. Clearly, the risk profile and design life of the operating phase are substantially different from those in the closure phase.

5.11.5 *Engage early with regulators and stakeholders, to unlock innovative closure options*
Section 5.5 above has described the obvious benefits of regulatory engagement, which may be extended to conversations with other stakeholders.

5.11.6 *Deal with closure risks early enough to avoid legacy challenges*
In 2008, the erstwhile Energy Resources Conservation Board of Alberta (ERCB, now known as the Alberta Energy Regulator, or AER), having become concerned about the steady accumulation of mature fine tailings (MFT) in the Oil Sands, issued Mining Directive 074, which introduced the first of a number of initiatives to measure, limit and curtail the generation of legacy MFT tailings. They obliged operators to set thresholds which would limit the long-term growth of legacy tailings. More recent lease owners have been set strict limits, to avoid the accumulation of legacy tailings.

5.11.7 *Facilitate sound decision making by accounting for the true value of closure solutions*
By embracing the full ethos of the principle of sustainable development, in recognizing the triple bottom line of economics, environment and society, the quality of decision-making may be improved.

5.11.8 *Schedule closure plan actions recognizing that mine decisions are guided by when money is spent*
Recognition of mining economics, and adapting closure interventions and expenditure to match mine financial planning and cash flow demands, is likely to deliver mining decisions that are more sustainable and suitable for tailings closure. Provision accounting for emergency dormancy would also appear to be prudent.

5.12 *Manage Water with Intentionality*

It may be argued that this point is in fact the most important: in the absence of water, none of the catastrophic tailings failures in history would have occurred.

5.12.1 *Remove the pond contents*
This may be not nearly as easy as it sounds, but it is an obvious fix for many structures, substantially reducing both the risk and the consequences of failure.

5.12.2 *The use of water covers to control emissions is outdated, and risky*
The control of fugitive emissions from mine tailings has traditionally been achieved through submerging the tailings below a water cap. The risks associated with the storage of water in above original ground facilities have now been found to significantly outweigh the benefits. Different technology options are readily available, and must be employed, including the engineering of final covers.

5.12.3 *Secure the deposit*
Ensure that the dam contents do not escape and damage the environment. It is important to look beyond mere management of water, supernatant and water inventory. It is just as important to recognize the risks associated with fluid tailings and liquefiable tailings, and to address the risk.

6 LITERATURE REVIEW

There are several published documents which provide guidelines and standards that relate to planning, closure and post-closure activities of tailings dams and impoundments, many of which are currently under revision as a result of changes in industry due to the recent tailings failures (e.g. Brumadinho).

One example of these guidelines is the 2019 Mining Association of Canada (MAC) Guide to the Management of Tailings Facilities, which outlines a tailings management framework which applies to all phases of the mine life cycle including temporary closure, permanent closure, post-closure and even reopening of closed facilities. The 2019 MAC guidelines not only provide a tailings management framework but also highlight the long-term risks of tailings facilities and the need to prioritize closure planning, which states "Designing and operating for closure requires a long-term view" and "It is important to ensure that short-term financial or operational priorities do not prevail over better design and operational practices that would have lower long-term impacts, complexity or risks" (MAC 2019).

It is not the intent of this paper to present a literature review of existing regulations, guidelines and standards, as they relate to dormancy, closure and post-closure activities. Several organizations have published relevant material, and most are in the process of updating their publications. The reader would do well to track the publications of:

- Canadian Dam Association (CDA)
- International Commission on Large Dams (ICOLD)
- The United States Society on Dams (USSD)
- The Association of State Dam Safety Officials (ASDSO)
- Federal Energy Management Agency (FEMA)
- Federal Energy Regulatory Commission (FERC)
- Alberta Dam and Canal Safety Directive (promulgated by AB AEP, supported by AER)
- BC Dam Safety Regulations (a broad array of publications)
- Australian National Committee on Large Dams (ANCOLD)
- International Council on Mining and Metals (ICMM)
- Global Tailings Standard (GTS)

7 CONCLUSION

If the mining industry is to protect its social license to operate, then thinking and action regarding tailings dam dormancy needs to change. The notion that a tailings facility or a mine may simply be "mothballed" until commodity prices improve, or closure can be afforded, or nature can remedy all ills, is fatally flawed.

Dormant tailings dams pose real, sometimes extreme risks. The risks require strategic intervention and ongoing vigilance from owners, managers, regulators, and consulting engineers.

Recent tailings failures have focused worldwide attention on active tailings dam operations. However, many thousands of dormant tailings dams worldwide continue to pose real risks to human beings and the environment. They cannot simply be studied or reviewed. They must be actively managed during their dormant state, as discussed herein, with the objective of achieving real closure in a short period of time.

The technology and engineering knowledge are readily available. They need merely to be harnessed, as described in the twelve precautionary guiding principles above.

The challenge for the mining industry is to move tailings from dormancy, through ordered decommissioning, to full closure.

8 ACKNOWLEDGMENTS

The authors wish to acknowledge the support of our colleagues at Thurber, including Colin Schmidt and Hiva Jalilzadeh, for their inputs into the paper.

REFERENCES

Blight, G.E. & Amponsah-Da Cost, F. 2004. Towards the 1000-year erosion-free tailings dam slope- a study in South Africa. *D.H. Barker, A.J. Watson, S. Sombatpanit, B. Northcutt, A.R. Maglinao, (eds) Ground and Water Bioengineering for Erosion Control and Slope Stabilization*. NH, Science Publishers, 2004: 365–376.

Boswell, J.E.S. 1996. Practical experiences in the application of the minimum requirements. *Proc. of Wastecon, int. cong. of inst. of waste mgmt. of South Africa, Durban, SA, September 1996*.

Boswell, J.E.S., Cavanagh, P. & Staples, L. 2018. Stewarding dam safety in Alberta: the dam integrity advisory committee. *Proc. int. oil sands tailings conf, Edmonton, AB, 9-12 December 2018.*

Boswell, J.E.S. & Sobkowicz, J.C. 2018. Leading versus lagging indicators of tailings dam integrity. *Proc. tailings & mine waste, Keystone, CO, 30 September-2 October 2018.*

Boswell, J.E.S. & Sobkowicz, J.C. 2016. Avoidance of imponderable consequences in tailings. *Proc. tailings & mine waste, Keystone, CO, 2-5 October 2016.*

Caldwell, J., & Charlebois, L., 2010. Tailings impoundment failures, black swans, incident avoidance and checklists. *Proc. tailings & mine waste, Vail, CO, 17-20 October 2010.*

Dobry, R. & Alvares, L. 1967. Seismic failures in Chilean tailings dams. *J. soil mechs. & fdn. engng., div., ASCE* 93, SM6: 237-260.

Fourie, A., Blight, G.E. & Papageorgiou, G. 2001. Static liquefaction as a possible explanation for the Merriespruit tailings dam failure. *CA geotech. j.* (38): 707-719.

Grid-Arendal. 2020. Global tailings portal. https://tailing.grida.no/. Accessed on 14 July 2020.

Kupper, A.G., Hurndall, B., Morgenstern, N.R., Sobkowicz, J.C., Abeda, W., Baldwin, G., Cameron, R., Eenkooren, N., Grapel, C., Martens, S., McKenna, G., Mihiretu, Y., Mimura, W., Parson, K., Paz, S., Petersen, T., Small, A., Tan, S., Wog, K., & Yazdanpanah, S. 2014. De-licensing oil sands tailings dams – technical guidance document. *Oil sands tailings dam committee.* March 2014.

Lucchi, G. 2005. Stava Perché. *3rd Edition, Curcu & Genovese, Trento.* 245 p.

Morgenstern, N.R. 2019. Geotechnical risk, regulation, and public policy: an update. *Keynote address, CA dam assoc. conf., Calgary, AB, 6-10 October 2019*.

Morgenstern, N.R. 2012. Oil sands mine closure – the end game: an update. *Keynote address int. oil sands tailings conf., Edmonton, AB, 2-5 December 2012*.

Morgenstern, N.R. 2010. Improving the safety of mine waste impoundments. *Keynote address tailings & mine waste, Vail, CO, 17-20 October 2010*.

Morgenstern, N.R., Vick, S.G. & Van Zyl, D. 2015. *Independent expert engineering investigation and review panel: report on Mount Polley tailings storage facility breach*. 30 January 2015.

Morrison, K.F., Pedrosa, H.G., Santos, G.J.I., Gomide, P. & Ferreira, A.M. 2018. Changes to Tailings Dam Regulation in Brazil in the Aftermath of Failures. *Proc. tailings & mine waste, Keystone, CO, 30 September-2 October 2018.*

Morrison, K.F. & Gomide, P. 2019. Post-Corrego do Feijao: continued evolution of tailings dam regulations in Brazil. *Proc. tailings & mine waste, Vancouver, BC, 17-20 November 2019.*

Robertson, A.M. 2011. Mine waste management in the 21st century challenges & solutions beyond incremental changes. *Keynote address tailings & mine waste, Vancouver, BC, 6-9 November 2011.*

Robertson, P., de Melo, L., Williams, D., & Wilson, W. 2019. *Report of the Expert Panel on the Technical Causes of the Failure of Feijão Dam I.* 12 December 2019.

Rourke, H. & Luppnow, D. 2018. The risks of excess water on tailings facilities and its application to dam-break studies. *Proc. tailings & mine waste mgmt., Sydney, NSW, 27-28 July 2015.*

Sawatsky, L., Hyndman, A., McKenna, G. & Vandenberg, J. 2018. Fluid fine tailings processes: disposal, capping, and closure alternatives. *Proc. int. oil sands tailings conf. Edmonton, AB, 9-12 December 2018.*

Simeoni, L., Tosatti, G., Lucchi, G. & Longo, M. 2017. The Stava catastrophic failure of 19th July 1985 (Italy): technical-scientific data and socioeconomic aspects. *CSE j.* (1): 17-30.

Stewart, R.A., Watts, B.C., Sobkowicz, J.C. & Kupper, A.G. 1997. Bennett dam sinkhole investigation. *Geotech. news* 15(1): 32-40.

Taleb, N.N. 2014. *Antifragile: Things that gain from disorder.* Random House Trade Paperbacks.

Van Zyl, D. 2009. Mining company corporate life cycle closure cost (CL3C). *Proc. tailings & mine waste, 1-4 November 2009.*

Wei, Z., Yin, G., Wang, J.G., Wan, L. & Li, G. 2013. Design, construction and management of tailings storage facilities for surface disposal in China: Case studies of failures. *Waste mgmt. res.* 2013, 31(1):106-112.

Reducing Long Term Risk at the Candelaria Tailings Storage Facility

Antonio Sotil, M.A.Sc., P.Eng.
Knight Piésold Consultores S.A., Lima, Peru

Victor Soto
Compañía Contractual Minera Candelaria – Lundin Mining, Santiago, Chile

Ken Brouwer, P.Eng.
Knight Piésold Ltd., Vancouver, Canada

ABSTRACT: The Candelaria Mine is an active open pit copper mine operated by Compañía Contractual Minera Candelaria located in the Atacama region of Chile, 20 km south of Copiapó. The Candelaria Tailings Storage Facility (TSF) was deactivated in 2018 and a surface cap is planned for closure of the impoundment. Mining activities will generate approximately 800 Mt of waste rock during ongoing open pit mining operations, and the decommissioned TSF provides an opportunity for TSF closure capping activities to be integrated with long term waste rock disposal. Capping the Candelaria TSF will provide significant storage capacity for waste rock within a reasonable hauling distance from the open pit, reduce additional site disturbance during ongoing mine operations, and minimize post-closure water management by providing a naturally-appearing convex, free-draining, stable post-closure landform. As an added benefit, the waste rock load will promote consolidation, densification, and dewatering of the underlying tailings, further reducing the potential for the impounded tailings to fluidize and flow in the event of a hypothetical dam breach. The closure cap will be developed on the Candelaria TSF by progressive placement of a thick (20 m to 60 m) waste rock cap with flat 20H:1V overall slopes. Engineering work to support permitting applications includes detailed field studies to characterize the current and future tailings behaviour, and design studies to optimize the final geometry, supported by geotechnical analyses. The field component incorporates two site investigation programs to evaluate tailings properties before and after construction of two 30 m high surcharge loads simulating the future loading during the staged development of the closure cap. The closure cap will provide economic benefits for secure waste rock storage, while enhancing impoundment stability as the tailings mass is stabilized through stress densification. These improvements will lead to a reduction in the risks associated with the project, both during ongoing mine operations and after closure of the facilities.

1 INTRODUCTION

Tailings from hard rock copper mining operations typically comprise fine-grained sand, silt, and clay sized rock fragments mixed with water to facilitate slurry transport and deposition into the tailings impoundment. The characteristics of the tailings deposit can vary significantly between different mine sites and depend on material characteristics, impoundment filling rates and the extent that free water is recovered and/or removed from the facility. Loose saturated tailings can be present within certain areas of tailings impoundments, and these soft, saturated tailings can represent a potential hazard, particularly if the materials are sufficiently wet such that a mudflood or mudflow could develop from a hypothetical dam breach scenario (Martin et al, 2019). This risk must be managed throughout the life cycle of a mine, and necessary objectives are to provide for long-term public safety and protection of valued components of the ecosystem such as air, surface water, and groundwater resources.

It can be challenging to demonstrate long-term stability after closure given the complexity and uncertainty associated with future performance predictions. During the post-closure period, there is the potential for changes in the local environment, land use, meteoric conditions, topography, geology, and state of practice. Increasing the density and reducing the flowability of the tailings within a tailings impoundment can reduce the consequence of a hypothetical dam breach and de-risk the tailings impoundment following closure (Adams et al, 2018).

Modern tailings impoundments are commonly closed in phases (CDA, 2014). The active closure phase begins once the impoundment reaches the ultimate capacity or the mine ceases production, and typically involves the construction of a closure cap to form a stable landform and minimize dusting. The impoundment is closely monitored for a number of years during the active closure phase and will transition to passive closure once the long term physical and chemical stability of the impoundment has been demonstrated. The surfaces of many tailings impoundments have been reclaimed by shaping, capping, and revegetation, but there are fewer examples where the tailings pile can be shown to be suitably stabilized to a landform condition, with no potentially flowable materials impounded (Adams et al, 2017c).

This paper presents a case history for the closure design and proposed closure enhancement for the Candelaria Tailings Storage Facility (TSF) at the Candelaria Mine. Additional waste rock disposal capacity is required for ongoing operations. This provides an opportunity to integrate the waste rock dump arrangements with closure capping at the TSF, and to promote the development of a stable post closure landform at the Candelaria TSF. The integrated waste rock closure capping strategy has been named the El Buitre Closure Cap (EBCC). There are also opportunities to simplify the storm water management systems during operations and particularly for the post closure site arrangement by incorporating suitable drainage and diversions along the upslope portion of the proposed EBCC.

Placement and storage of waste rock on the decommissioned tailings impoundment will result in increased consolidation, dewatering, and densification of the underlying tailings. This will further stabilize and de-risk the closed tailings impoundment by reducing the potential for the impounded tailings to flow in a hypothetical dam failure scenario. Additionally, use of areas already affected by the mine operations for waste rock storage will reduce the need for new site disturbance and minimize the overall environmental impact of the ongoing mining operations. These improvements will lead to a reduction in the risks associated with waste management at the project, during the operations, closure, and post-closure phases (Adams et al, 2019).

2 PROJECT OVERVIEW

The Candelaria Mine has been in operation since 1993 and is currently operated by Compañía Contractual Minera Candelaria (CCMC). The key waste and water management facilities include the Candelaria TSF, the more recently commissioned Los Diques TSF, and several waste rock disposal sites including the North Waste Dump, and the proposed EBCC. A general arrangement of the mine site illustrating key facility locations and future expansion areas is shown on Figure 1. Tailings deposition transitioned from the Candelaria TSF to the Los Diques TSF during 2018 and 2019. Tailings deposition into the Candelaria TSF ceased completely by the end of 2019.

The Candelaria TSF includes a Main Embankment and two saddle embankments (North and South) and a seepage collection system (SCS). The SCS collects drainage via an underdrain system excavated into the underlying alluvium at the Starter Embankment and is conveyed towards the cut-off trench downstream of the Main Embankment. Seepage water is recovered by pumping wells (named Pique Mina) located upstream of the cut-off trench and transferred to the plant for use as process water. During past operations, a reclaim barge and pump were located at the southeast corner of the TSF, where reclaim water was pumped from the slimes pond to the concentrator for use in processing. Figures 2 and 3 show an overview of the Candelaria TSF and the location of the SCS. Hydrogeology studies concluded that all seepage water to the SCS was coming from the tailings pond. Phreatic conditions within the Candelaria TSF are significantly less than hydrostatic with actual measured equilibrium pore pressures (from Cone Penetration Testing (CPT) pore pressure dissipation tests) plotting well below the hydrostatic line in all cases. All pore pressure dissipation tests conducted between 2014 and 2020 yielded pore pressure profiles with total head decreasing with depth, indicating that the tailings are draining downwards.

Figure 1. General Mine Site Arrangement

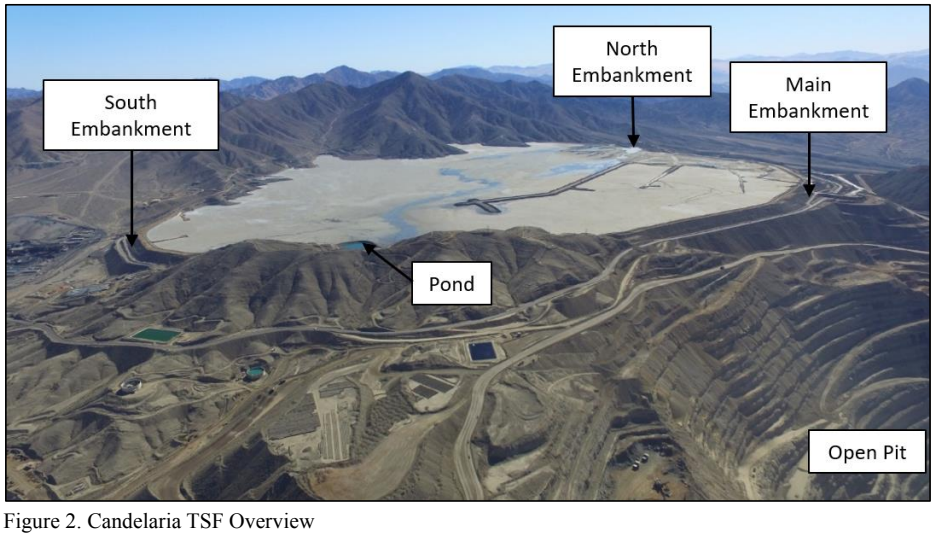

Figure 2. Candelaria TSF Overview

Foundation materials within the Candelaria TSF are generally comprised of alluvium deposits, which are typically dense sandy gravel with an average thickness of 20 m. The alluvium materials are underlain by fractured bedrock to a depth of approximately 30 m, with less fracturing below this depth. Tailings draindown indicates that the alluvial foundation material is significantly more permeable than the tailings and provides a drainage zone at the base of the impoundment.

Seepage flows captured at the Pique Mina consistently decrease with time after decommissioning of the Candelaria TSF. Measured annual pumping flows collected at the SCS were around 300 l/sec in 2018 when tailings deposition ceased at the Candelaria TSF and were less than 220 l/sec at the end of Q2 2020. Some ongoing seepage relating to draindown in the tailings mass is anticipated, as well as from seepage caused by consolidation-induced pore water expulsion during future EBCC loading on the Candelaria TSF.

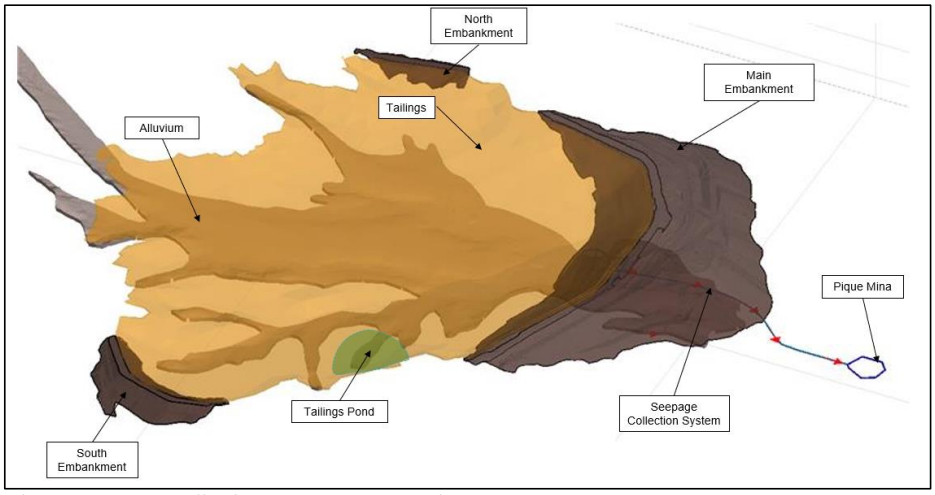

Figure 3. Seepage Collection System – 3D Overview

3 EL BUITRE CLOSURE CAP OVERVIEW

3.1 *Design Objectives*

The proposed EBCC will provide permanent and secure storage of waste rock from mining operations and will be progressively developed in stages. Staged construction of the EBCC has the following objectives:

- Enhance the overall stability and minimize the long-term risks of the Candelaria TSF by further consolidating, densifying, and dewatering the tailings contained within the closed impoundment, thus, increasing the density and reducing the fluidity or flowability of the impounded tailings. A higher density and lower flowability has the potential to reduce the consequences associated with a tailings dam breach and improve tailings behavior during seismic loading (less susceptible to liquefaction).
- Provide additional waste storage capacity to support ongoing mine operations without requiring significant additional site disturbance for a new or expanded dump footprint.
- Provide a waste rock storage area located within a reasonable haul distance from the open pit.

The EBCC final configuration and cross section are illustrated on Figures 4 and 5, respectively. The total mass and placement geometry of waste rock that could potentially be stored over the Candelaria TSF is dependent on the strength, deformability, and drainage characteristics of the underlying tailings, the rate of waste rock placement, and the geotechnical stability of the impoundment embankments. Waste rock will be selectively placed to buttress the accessible northern embankments, and runout from a hypothetical dam breach would be contained within the open pit. The waste rock placement schedule for the cap will allow time for water pore pressures that develop in the underlying tailings to dissipate. The tailings response to surcharge loading is being assessed in the test pad program (see Section 4), in order to demonstrate that foundation stability will be maintained. The EBCC configuration will ensure that runout from a hypothetical failure of the embankment would report to the open pit and thus preclude impact to the public.

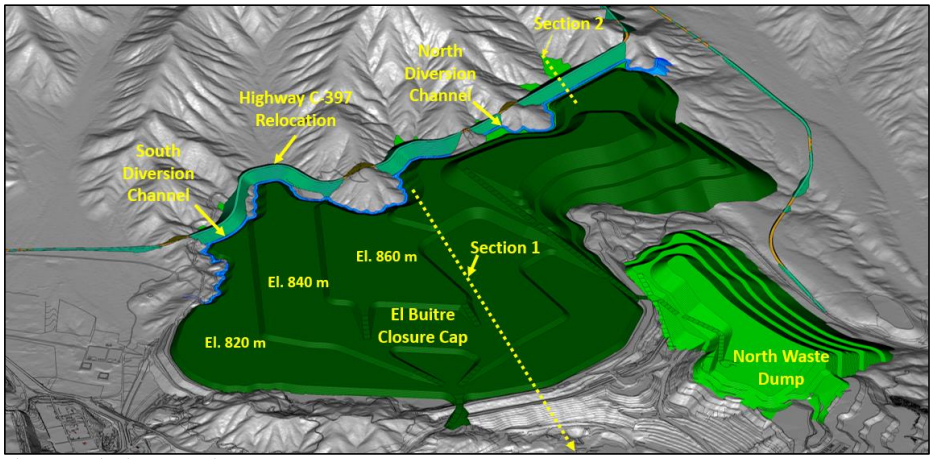

Figure 4. Final Proposed EBCC Arrangement

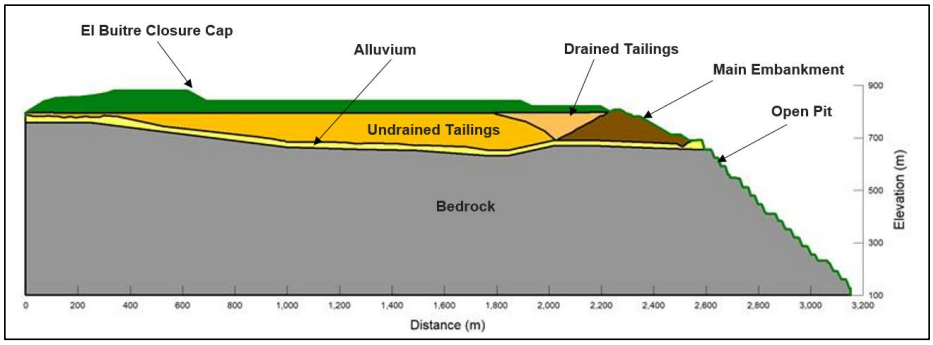

Figure 5. Final Proposed EBCC Cross Section

Pore pressure response in the saturated tailings is expected, and the potential for excess pore pressure development, leading to undrained failure or bearing capacity instability were carefully considered in the trial program. The Pinto Valley tailings impoundment failure provides an example of instability induced by waste dump loading onto a decommissioned tailings impoundment. This incident occurred in 1997 (Hansen and LaFronz, 2000, Adams et al, 2018), during placement of 50 ft. (17 m) thick lifts of waste rock on the tailings surface. The sand dam, which had been developed using the upstream construction method, had a relatively thin zone of drained sandy materials along the face, with saturated fine tailings within the impoundment. Bulging was observed during placement of the second waste rock lift, and the failure resulted when the face of the dam ruptured as the liquefied fine tailings broke through the sandy embankment crust. This failure resulted in the release of tailings and waste rock which flowed viscously downgradient to Pinto Creek located approximately 2,000 ft (610 m) downstream of the impoundment. The failure was directly related to rapid, undrained loading caused by the placement of waste rock over the saturated tailings (Adams et al, 2018).

The overall stability of the EBCC closure cap will be maintained by staged loading of waste rock layers. It is anticipated that pore pressures will increase in the underlying saturated fine-grained tailings, and then dissipate adequately prior to placement of subsequent waste rock layers. Instrumentation systems will include several piezometers installed within the tailings mass, and these will be used to monitor pore pressure development and dissipation throughout the waste rock loading cycles. The pore pressure monitoring will be utilized to control the waste rock loading sequence and is anticipated to be most useful for establishing the layer thicknesses and loading sequence during the first layers of waste rock placement. It is anticipated that the pore

pressure response in the tailings will become muted as the waste rock stack gets higher and the underlying tailings become more drained and compressed.

3.2 *Configuration Requirements*

The proposed EBCC will be constructed over the Candelaria TSF, and also within the area directly to the north of the TSF. The EBCC will initially be developed using shallow terraced geometry to facilitate the loading sequence, in order to maintain the trafficability and stability of the capping layers. Permitted tailings surface and embankment crest elevations are 798.5 m and are 800 m, respectively. The EBCC will be constructed to El. 860 m in three stages, with additional waste rock placed to El. 940 m along the north side of the North Embankment (adjacent to the Candelaria TSF footprint). The tailings surface will initially be capped with 4 m of waste rock followed by placement of subsequent layers ranging in thickness from 5 to 15 m. The EBCC will be constructed at a flat overall benched slope of 20H:1V up to El. 860 m.
The toe of the final benches will encroach on the adjacent Highway C-397, which will be relocated prior to and during the initial capping stage of the EBCC and will extend along the west side of the facility. A haul truck access ramp will be constructed on the northern edge of the Candelaria TSF near the North Embankment.

The main components of the Candelaria TSF include a free draining Main Embankment and two saddle dams (North and South). The Main Embankment is located along the east side of the facility and separates the TSF from the Open Pit and the North Waste Dump. The South and North Embankments are located in topographical low points along the south and north sides of the TSF. The North embankment will be buttressed by the EBCC waste rock storage areas, whereas the Main and South embankments will be largely unaffected during development of the EBCC.

Stability analyses indicate that the Main and South embankments will remain stable following construction of the proposed EBCC and exceeds local and international factor of safety requirements for static, seismic (pseudo-static) and post-earthquake conditions. Preliminary tailings consolidation analyses have been conducted to estimate the expected tailings consolidation seepage volumes generated by the waste rock loading.

3.3 *Water Management*

The configuration of the proposed EBCC will create a mounded landform with drainage towards the perimeter of the TSF. Stormwater runoff from the western catchment area will be directed by culverts under Highway C-397, and then routed around the perimeter of the EBCC via diversion channels. The channels will include North and South Diversion Channels, which drain to the north and south respectively, and discharge to existing drainage features beyond the extent of the EBCC. Waste rock fill will be placed on the west side of the relocated highway to avoid pooling and to allow the upper catchments to drain into the diversion channels.

4 SITE WORK

4.1 *Site Investigations*

Numerous site investigations have been conducted at the Candelaria TSF over the years. Historical SI programs (in 2009, 2011 and 2014) have mostly consisted of cone penetration testing (CPT), Seismic CPT (SCPT), sonic drilling, and Vibrating Wire Piezometer (VWP) installations. Historical SCPT data collected in 2009 and 2014 have been compared to the 2018 and 2019 SCPT data to analyze the impact of subsequent tailings deposition on the stiffness and state of the tailings.

The detailed design of the EBCC will rely on information collected during construction of two waste rock test pads and a two-phase site investigation (SI) program. To date the 2019 Phase 1 SI program has defined the baseline geotechnical and hydrogeological conditions for the tailings contained within the deactivated Candelaria TSF. The 2020 Phase 2 SI program (in progress) will evaluate the densification and foundation improvements that result after loading at each of the two test pad sites.

The interlayered tailings at the Candelaria TSF can be separated into two general material types: (1) sandy tailings and (2) fine-grained tailings. Sandy tailings have been deposited adjacent to the embankments and along the impoundment perimeter where tailings spigots have been situated. Fine-grained tailings slimes tended to accumulate near the supernatant pond area, farther from the discharge spigots. Tailings adjacent to the embankments are generally coarser than tailings at Test Pad 1, and tailings below the supernatant pond would be expected to be somewhat finer than tailings at Test Pad 2. The approximate extent of fine-grained tailings, with respect to the test pad areas and embankments, is shown on Figure 6.

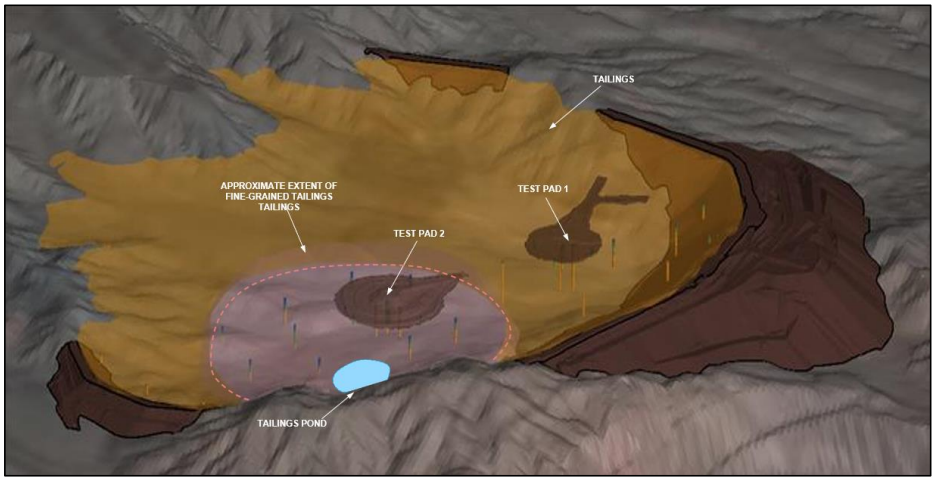

Figure 6. Tailings Distribution Overview

The 2019 Phase 1 SI program investigated the Test Pads 1 and 2 areas, and the tailings located at the upstream side of the Main Embankment and South Embankment. The SI program included 12 sonic geotechnical drillholes with Lexan/Shelby tube sampling, 11 SCPT, tailings sampling for geotechnical and rheological testing, electronic vane shear testing (VST) and installation of 60 VWPs. The SCPT soundings included pore pressure dissipation (PPD) tests at selected depth intervals, as well as compression wave (P-wave) and shear wave (S-wave) measurements.

Laboratory testing (rheology and index testing) of the tailings was conducted during Q1 2020. Supplementary laboratory testing to determine the Critical State Line (CSL) and deformation/strength characteristics of the tailings is currently in-progress. The tailings state and strength parameters interpretation will be refined to include the laboratory testing results.

4.2 *Data Interpretation*

4.2.1 *Tailings Characterization*

Tailings samples collected at the two test pad areas were found to contain silt and sand mixtures (fines contents varying from 36% to 94%) with an average specific gravity of approximately 3.0. Particle size distribution (PSD) results indicate interlayering of fine-grained with coarse-grained tailings at both test pad locations. The range of values obtained for Atterberg Limits was consistent between both test pad locations. Samples tested were found to be non-plastic to slightly plastic (PI < 4) and with measured Liquid Limits in the range of 16 to 20. Moisture contents relative to the estimated Liquid Limits indicate the tailings become less flowable with rheological characteristics that can be described as paste-like to soil-like.

The SCPT probes indicate that the tailings are generally contractive and saturated at depth. The data indicate that sandy tailings near the embankments have lower state parameters (less contractive) than those located at the test pad locations. Tailings upstream of the Main Embankment become slightly dilative below depths of approximately 50 m.

The comparison with historical SCPT (2009 and 2014 with 2019, and recently with 2020) data suggests an increase in stiffness and reduction in brittleness, as the tailings become denser (less

contractive) due to the additional loading from tailings deposition and/or the fill loadings at the trial pads. CPT data obtainedfor the foundation tailings, both before and after Test Pad 2 loading, confirmed a general reduction in the state parameter and an increase in the normalized cone resistance (Q_{tn}), as shown on Figure 7. The undrained strength of the in-situ tailings increased significantly due to consolidation from test pad construction.

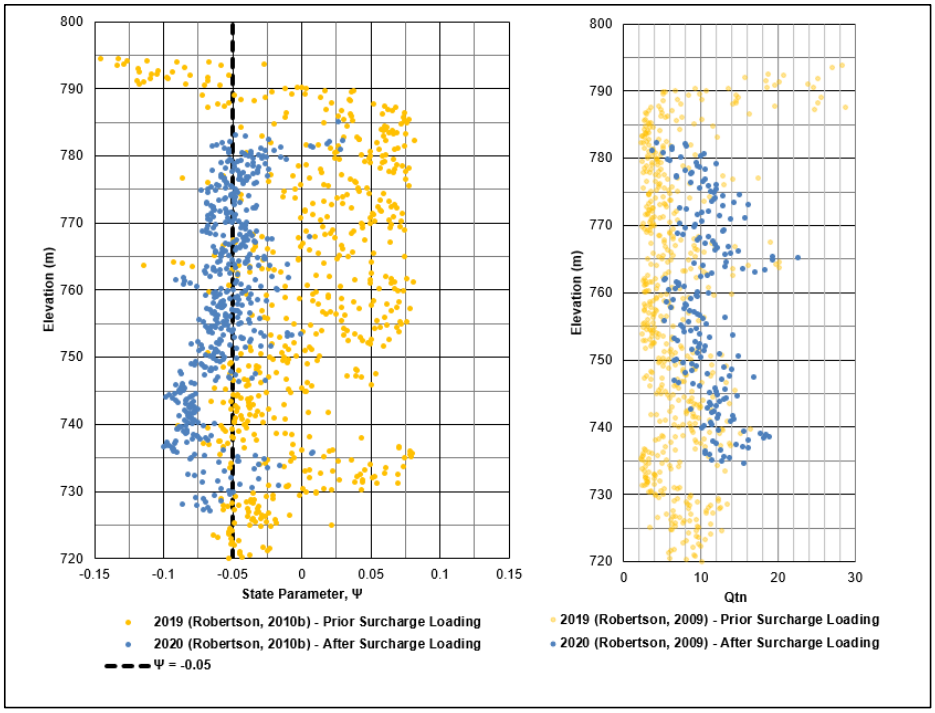

Figure 7. CPT Data Interpretation Before (2019) and After (2020) Test Pad 2 Construction

4.2.2 *Pore Pressure Conditions*

The PPD data recorded in the tailings deposit shows that pore pressure conditions are below hydrostatic, which indicates that the underlying alluvium contributes to an effective underdrainage system. VWP measurements at the embankments and test pad areas indicate that the tailings are continuing to drain. Piezometers adjacent to the Test Pad 1 area indicate that the phreatic surface is steadily dropping at a rate of about 0.5 m per month. The pore pressure data near the embankments indicate drained, partially saturated conditions within the upper 20 to 30 m of tailings, where drainage is further enhanced by the coarser tailings sands, and the adjacent free draining rockfill materials in the embankment.

4.3 *Trial Program*

4.3.1 *General*

Information collected during the development of the test pad program allows for tailings parameters and geotechnical analyses to be updated and calibrated and facilitates the determination of appropriate waste rock loading rates. The overall construction sequence/configuration and water management plan for the EBCC will also be refined on the basis of this updated information. Test Pad 2 has been constructed on more compressible finer grained slimes tailings (Pond Tailings), and Test Pad 1 on more sandy beach tailings (Beach Tailings). Field monitoring results will also facilitate updating estimates of tailings settlements and consolidation seepage during development of the proposed EBCC. Figure 8 shows an overview of the trial program as of August 2020.

4.3.2 *Test Pad 2 (Pond Tailings)*

Construction of Test Pad 2 started on September 2019 and was completed by mid-January 2020. It was constructed by placing 2 to 3 m thick lifts to its final height of 30 m. A total of approximately 3.1 million tonnes of waste rock material was placed on Test Pad 2, at an average rate of approximately 26,000 tonnes per day. The original test pad configuration allowed for 5H:1V slopes along with a 45 m diameter crest. During construction, the test pad geometry was revised to incorporate a broader 70 m diameter crest to allow the continued use of CAT 793 haul trucks for the upper lifts. Steeper test pad side slopes of 2H:1V were also incorporated into the design to accelerate the schedule and reduce waste rock quantities.

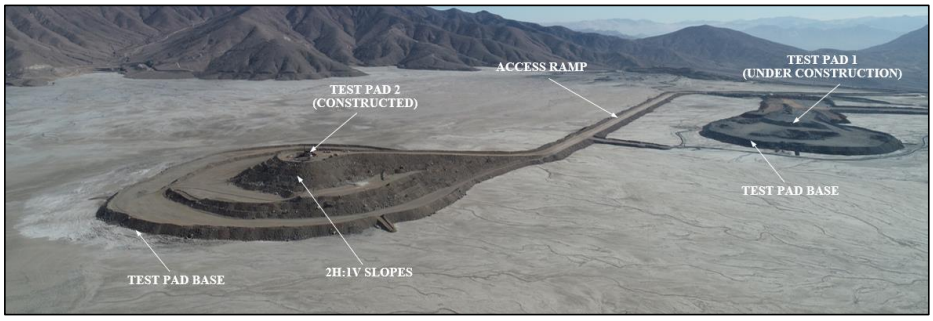

Figure 8. Trial Program Overview (As of August 2020)

The tailings response to the surcharge loading was carefully monitored during construction with detailed visual monitoring, settlement measurements plus pore pressure response at various locations and depths within the foundation tailings. Monitoring instrumentation at Test Pad 2 included 26 VWPs, four (4) settlement plates and four (4) survey monuments. The central piezometers were lost during construction of the upper lifts, due to large consolidation settlements. Ongoing pore pressure monitoring continued using the VWPs installed at the base of the 2H:1V conical load.

Pore pressures increased during loading as expected, with relatively rapid incremental responses observed for each construction lift. Excess pore pressures have continuously dissipated, since construction was completed in January 2020, at an average dissipation rate of about 5 kPa/day. Excess pore water pressures fully disipated two months later after construction ended.

Settlement plates show the greatest settlements below the center of the pad, which is consistent with the higher loading conditions. Foundation settlements of up to 6.0 m have been recorded to date. The rate of settlement has slowly decreased with time, as the excess pore pressure continues to dissipate. An average initial settlement of about 2 m occurred before detailed settlement plate readings commenced. Some of this vertical displacement was associated with lateral displacement of saturated near-surface tailings, as indicated by the development of bulging or 'waves' in the tailings during placement of the initial waste rock layer. The estimated settlement prior to the installation varies within the test pad footprint, with larger settlements observed in finer tailings at the south side of the pad near the supernatant pond area.

The latest monitoring data, from the remaining VWPs at Test Pad 2, indicate that excess pore pressures generated during pad construction have completely dissipated. The phreatic level at these locations has continued to drop below pre-loading levels. Tailings pore pressure profiles for Test Pad 2 are shown on Figure 9.

4.3.3 *Test Pad 1 (Beach Tailings)*

Construction of Test Pad 1 started in May 2020. It will include a 70 m diameter crest, slopes at 2.0H:1.0V and will be raised to a height of 30 m above the tailings surface. A 6 m thick test pad base platform is currently under construction to develop a suitable buttress. CAT 793 haul trucks will continue to be used for the construction. Test Pad 1 is constructed on sandy beach tailings and was observed to experience less foundation response during surcharge loading in comparison with Test Pad 2. Figure 10 shows the construction of the test pad base.

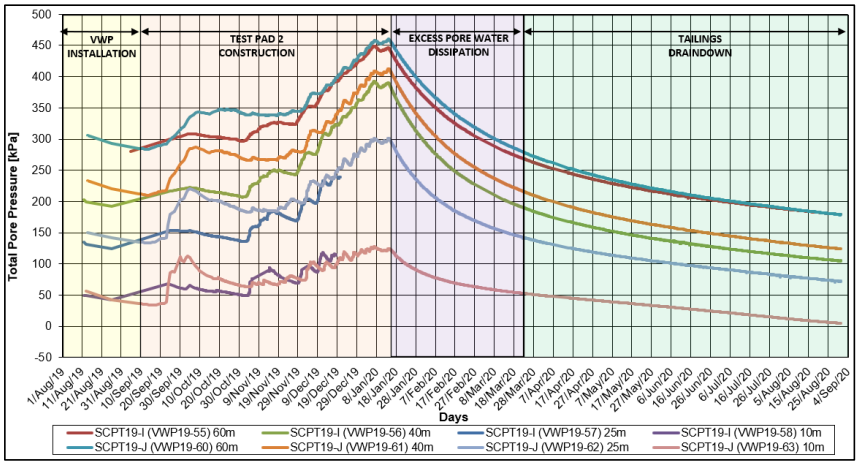

Figure 9. VWP Measurements near the Center of Test Pad 2

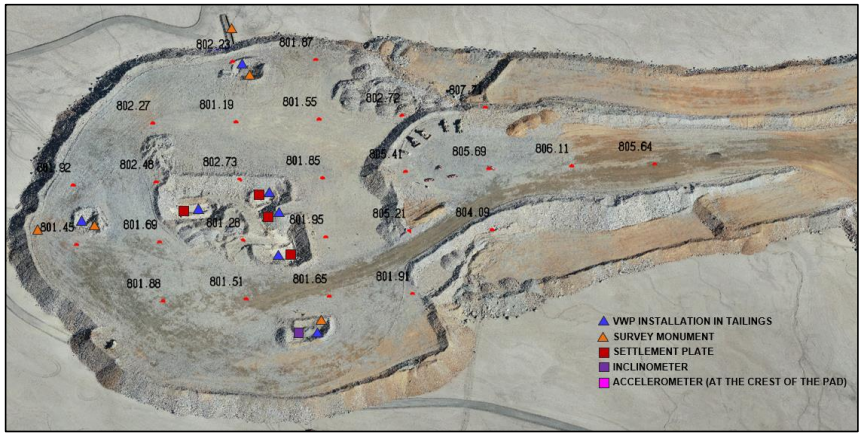

Figure 10. Test Pad 1 Construction (As of August 2020)

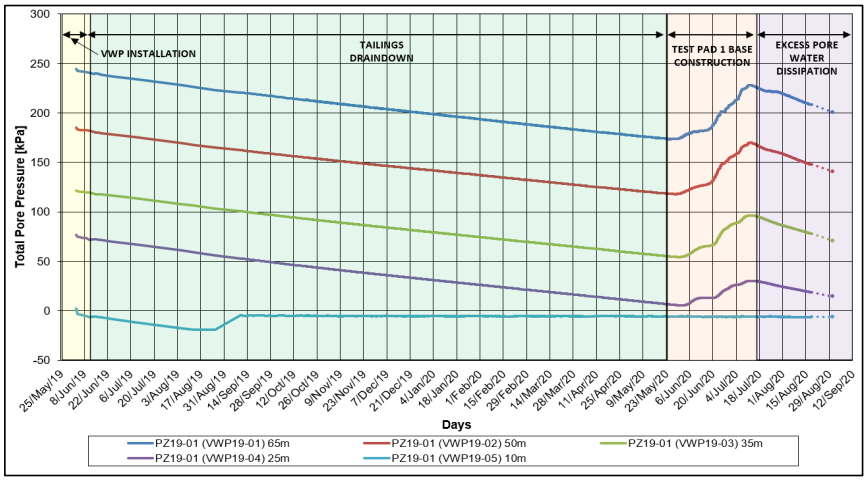

Figure 11. VWP Measurements at the Center of Test Pad 1

The sandy beach tailings located within the Test Pad 1 footprint are relatively coarser grained, and a significant drained and unsaturated zone has already been established within the upper 10 m. Very little response was observed in these materials during construction of the access roads or the test pad base (Lift 1). Monitoring data also indicates that desaturation of the upper tailings is ongoing.

Pore pressure measurements at Test Pad 1 show that the phreatic surface has dropped approximately 5 m since monitoring was started in June 2019. The data indicates unsaturated conditions are generally present in approximately the upper 10 m of tailings. Pore pressure profiles at the center of the Test Pad 1 are shown on Figure 11. Test Pad 1 is expected to be fully constructed during Q3 2020.

5 SUMMARY

There are significant opportunities to integrate the waste rock disposal sites with the development of a thicker closure cap on top of the decommissioned Candelaria TSF. This integrated waste management strategy, which is named the EBCC, will result in the development of a stable post closure landform that, in combination with contingency containment in the open pit, virtually eliminates risk to the public and downstream communities.

The proposed EBCC also provides an opportunity to simplify the storm water management systems during operations and particularly for the post closure site arrangement, by incorporating suitable drainage and diversions along the upslope portion of the EBCC. Storm water drainage to be routed around the facility, thus removing the potential for stormwater pooling on the capped impoundment and the need for an overflow spillway after closure. The EBCC will be integrated with the realignment of Highway C-397 to provide appropriate storm water management, as the upslope catchment areas will be diverted around the facility through drainage swales.

The development of the proposed EBCC will enhance the physical stability of the tailings impoundment and will provide permanent and secure storage of waste rock derived from ongoing mine operations. The EBCC will be constructed both on the Candelaria TSF, and within the area directly to the north of the TSF.

The EBCC will initially be developed using shallow terraced geometry to facilitate the loading sequence, in order to maintain the trafficability and stability of the capping layers. It will be developed in stages to allow enough time for consolidation and stabilization of the underlying tailings. It is anticipated that pore pressures will be generated in the saturated fine-grained tailings materials, but these excess pore pressures will dissipate adequately prior to placement of subsequent waste rock layers. As the tailings are progressively compressed and drained with the development of the EBCC, the overall stability of the Candelaria TSF will be enhanced. The overall slope of the waste rock pile will be maintained at approximately 20H:1V during operations to provide a stable and robust arrangement.

Consolidation of the tailings mass will also result in a reduced void ratio with a corresponding reduction in the moisture content of the densified tailings. The potential fluidity of remoulded tailings (due to liquefaction) will be reduced significantly as the moisture content is reduced below the Liquid Limit. The dense and more plastic nature of the densified tailings will reduce the potential consequences of a hypothetical tailings release from an assumed post-closure breach.

Detailed design of the EBCC will rely on information collected during construction of Test Pads 1 and 2, in conjunction with a two-phase SI program. Test Pad 2 was completed by mid-January 2020 and incorporated 2 to 3 m thick lifts to its final height of 30 m. Foundation tailings pore pressures increased during loading as expected, with relatively rapid incremental responses observed for each construction lift. The sandy beach tailings located within the Test Pad 1 footprint are coarser and a significant drained and unsaturated zone had developed within the upper 10 m prior to commencing pad loading. Very little response was observed in these materials during construction of the access roads or the test pad base (Lift 1). Monitoring data also indicates that desaturation of the upper tailings is ongoing. Test Pad 1 is expected to be fully constructed by Q3 2020.

The Phase 2 SI program will evaluate the densification and tailings foundation improvements that result after loading at each of the two test pad sites. In-situ testing and laboratory testing of the tailings will be performed to estimate the changes in density and moisture content within the

tailings. The results of the Phase 2 SI, laboratory testing and monitoring programs will be used to update the tailings characterization and geotechnical analysis conducted to date, as well as to conduct dam breach modelling, seismic response and deformation analyses of the Candelaria TSF and EBCC and review the interaction of the open pit with the Candelaria TSF Main Embankment.

Construction of the EBCC will provide storage for waste rock generated from ongoing mining operations. The placement of waste rock is expected to densify and further dewater the tailings, increasing the solids content and reducing the potential fluidity (flowability) of the tailings. This will reduce the overall risk of the facility by reducing the potential consequences of a post-closure dam failure event, as the tailings will be significantly less flowable. This integrated waste management strategy for the Candelaria Mine will provide operational benefits for ongoing waste rock management while concurrently stabilizing the impounded tailings to reduce the long term risks, and to enhance the reclamation objectives for the mine site.

6 REFERENCES

Adams, A., Friedman, D., Brouwer, K., and Davidson, S. 2017a. Tailings Impoundment Stabilization to Mitigate Mudrush Risk. Proceedings of the 85th Annual Meeting of the International Commission on Large Dams (ICOLD). July 5. Prague, Czech Republic.

Adams, A., Friedman, D., Brouwer, K., and Davidson, S., 2017b. Novel Application of Proven Best Available Technologies to Stabilize a Historical Tailings Impoundment. Canadian Dam Association Annual Conference, Kelowna, British Columbia. October 16 to 18.

Adams, A., Friedman, D., Davidson, S. 2017c. Characterizing and Stabilizing a Historical Tailings Facility: The Rheology to Soil Mechanics Continuum. Proceedings of the 2017 Tailings and Mine Waste Conference. November 5 to 8. Banff, Alberta, Canada.

Adams, A., Brouwer, K., Davidson, S. 2017d. Best Available Technologies to Stabilize a Historical Tailings Impoundment. Proceedings of the 2017 Tailings and Mine Waste Conference. November 5 to 8. Banff, Alberta, Canada.

Adams, A., Hall, C., and Brouwer, K., 2018. Tailings Impoundment Closure Enhancement. Proceedings of the 2018 Canadian Dam Association (CDA). October 13-18. Quebec City, Quebec.

Adams, A., Hall, C., and Brouwer, K., 2019. Reducing the Long Term Risk and Enhancing the Closure of Tailings Impoundments. June 9-14. 87th Annual Meeting of the International Commission on Large Dams. Ottawa. Canada.

Canadian Dam Association (CDA), 2014. Technical Bulletin - Application of Dam Safety Guidelines to Mining Dams.

Fontaine D.D. and V. Martin. 2015. Tailings Mobilization Estimates for Dam Breach Studies. Proceedings of the 2015 Tailings and Mine Waste Conference. Vancouver, BC, October 26-28, 2015.

Hansen, L.A. and LaFronz, N.J., 2000. Stabilization of the Pinto Valley Tailings Impoundment Slide. Tailings and Mine Waste 2000.

Martin, V., Fontaine, D.D., and J.G. Cathcart. 2015. Practical Tools for Conducting Tailings Dam Breach Studies. Proceedings of Canadian Dam Association 2015 Annual Conference, Mississauga, ON. Oct. 5-8, 2015.

Martin V., Al-Mamun M., Small A., 2019. CDA Technical Bulletin on Tailings Dam Breach Analyses. June 9-14, 2019. 87th Annual Meeting of the International Commission on Large Dam. Ottawa. Canada.

Robertson, P.K. 2009. Interpretation of Cone Penetration Tests - A Unified Approach. Canadian Geotechnical Journal, 46 (11): 1337-1355.

Robertson, P.K., 2010. Evaluation of Flow Liquefaction and Liquefied strength using the Cone Penetration Test. Journal of Geotechnical and Geoenvironmental Engineering, ASCE, 136(6): 842-853.

Robertson, P.K., 2010b. Estimating In-situ Parameter and Friction Angle in Sandy Soils from the CPT. 2nd International Symposium on Cone Penetration Testing, CPT´10, Huntington Beach, CA, USA.

Risk-Based Prioritization of Improvement Plans for Critical Infrastructure

Karen M. Chovan
Enviro Integration Strategies, Saskatoon, Saskatchewan, Canada

Michel R. Julien, Édouard Masengo, Édouardine-Pascale Ingabire, Michael James, Thomas Lépine & Pascal Lavoie
Agnico Eagle Mines Limited, Toronto, Ontario, Canada

ABSTRACT: The occurrence of several highly consequential failures of critical infrastructure, particularly tailings management facilities, have streamlined industry's focus on improving their management, design and performance. Best practice guidance recommends strong governance, multi-tiered management systems, including external third-party review and oversight, and applying a risk-based approach to all designs, decisions, operations and management activities. This work presents a rational approach to assess the levels of risk associated with an organization's critical infrastructure, consolidating relevant information into a visual assessment tool. The approach is applicable to tailings storage, heap leach, and rockfill storage facilities, as well as water management infrastructure. The outcomes of the assessment process provide the means of communicating relative risks, and to prioritize corrective actions across the portfolio. It also facilitates the implementation of risk-based management practices, while allowing consideration of the unique organizational structure and internal practices of any company, and the varied characteristics of assessed infrastructure.

1 INTRODUCTION

In 2019, the Mining Association of Canada (MAC) updated its Guide to the Management of Tailings Facilities (MAC 2019), maintaining a strong emphasis on risk-based management systems and use of critical controls as performance monitoring indicators, and clarity of roles and responsibilities including focus on strong governance. The mining industry is increasingly incorporating risk assessment to better understand the complexity of risks related to evaluating the stability of its critical infrastructure. However, the calculation of risk, a product of the probability of failure and the consequences of failure, is not a trivial exercise.

Within most larger mining organizations, diverse and complex critical infrastructure exist, including not only tailings storage facilities (TSF), but also heap leach facilities (HLF), rockfill storage facilities (RSF), and water management infrastructure (WMI). The diversity can stem from differing ore bodies and mineralogy, ore processing, climate, environment, operating conditions, and regulations. Materials are stored in infrastructure of many different types and design, as well as age - some designed only a few years ago, while others have been evolving over several decades.

This paper presents a holistic risk evaluation process developed for critical infrastructure, and a tool allowing for comparison of multiple infrastructure owned by one company. The process includes a semi-empirical method to estimate the annual probability of failure that is then combined with a quantitative evaluation of the consequences of failure to produce an objective and detailed assessment of the risk. It was developed to improve internal communication and documentation of critical infrastructure, making the compiled information readily understood by

technical and non-technical mining professionals, to facilitate transparent risk-based decision-making. Such an approach integrates MAC's Tailings Guide (2019) intent and requirements into complex operating realities, and allows an organization to treat all of their critical infrastructure in an analogous manner. While the following discussion focuses on TSF, it should be assumed it applies as well to the other critical infrastructure listed.

2 FACTOR OF SAFETY VERSUS THE ANNUAL PROBABLITY OF FAILURE

The factor of safety (FS) is the most common metric used to evaluate the stability of containment infrastructure during operations and closure. However, as discussed in Duncan (2000) and Herzal et al. (2017), the FS has an inherent notion of uncertainty traditionally built into it. The reliability of the FS as a metric of stability is dependent on the quality of, and degree of uncertainty associated with, all aspects of an infrastructure's engineering and lifecycle (i.e. investigation, design, construction, operation).

The proposed method is based upon original work published by Silva et al. (2008). Hereafter referred to as the Silva Method, and illustrated in Figure 1, it is described as follows. Using case histories of failure of earth structures that included tailings dikes, empirical relationships were developed between static factor of safety (FS), Level of Engineering (LOE) and annual probability of failure (APF). The LOE is a quantification of the quality and the degree of uncertainty associated with specific categories of the engineering of a structure. In the Silva Method, there are 5 categories with a total of 17 objective criteria that are rated for a total score, where each category holds equivalent ponderation of 20% each. The evaluation categories include Design, Construction and Operation & Monitoring (collectively, DCO). The Design category is composed of Investigation, Laboratory Testing and Analysis & Documentation subcategories. Final DCO scores vary from 1 to 4, which is then used to determine the LOE with values of 1, 2, 3 and 4 respectively equivalent to LOE Levels of I (High), II (Above Average), III (Average) and IV (Poor).

Note that the APF increases with increasing FS as well as LOE, with a much as two orders of magnitude difference in APF for the same FS between two LOE, and approximately 5 orders of magnitude difference between the LOE I to IV at FS 1.5 and higher. This clearly shows the deficiency of over-reliance on the FS as a metric of stability.

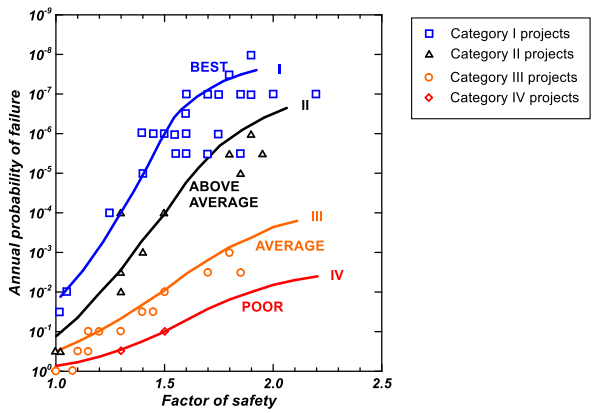

Figure 1. Relationship of Annual Probability of Failure with Factor of Safety for Level of Engineering (adapted from Silva et al., 2008).

The Silva Method was selected as a basis of evaluation for several reasons. It was developed from case histories for soil embankments that have similar construction methods and failure

mechanisms as TSF dikes. It includes the LOE which recognizes that the quality and degree of uncertainty in design, construction, operation and monitoring can directly influence the probability of failure for a given FS. Though the state of practice, regulations and guidelines are strongly driven by a deterministic view of the FS, using APF is seen as a much more palatable concept to non-experts. This holistic strategy of determining APF ultimately helps the Owner understand the risks and to exercise control, it also serves as a means to prioritize mitigation work. In our opinion, the Silva Method relationships are powerful tools to communicate actual risks in a language that non-experts can understand.

3 PROPOSED METHODOLOGY

The APF-FS-LOE relationships and list of criteria of Silva et al. (2008) were modified to adapt it for the unique conditions of mining critical infrastructure, and to introduce the importance of risk management and monitoring systems, while respecting its original intent.

An expanded list of 45 relevant criteria are considered, including further aspects regarding the complexities of the phased design and construction and continuous operation of critical infrastructure over many years, the evolution of engineering practice, which includes increased emphasis on management systems, internal and external review (e.g. Engineers of Record [EoR], and Independent Review Boards [IRB]) as well as consideration of changing in situ conditions and observations of performance (e.g. displacement). Consequently, the LOE expands beyond "just the dam", and is now referred to as the Level of Practice (LOP). Each criterion is equally weighted, with an overall ponderation of the DCO categories equating to 51% for Design (20%, 13% and 18% respectively for Investigation, Laboratory Testing and Analysis & Documentation), 18% for Construction, and 31% for Operation & Monitoring (which includes performance aspects). The final list of criteria for TSF are included in Table 1.

In addition, intermediate LOP were added, and minimum APFs established for each LOP following review of published works on risk tolerance. Reviewed resources included the Federal Guidelines for Dam Safety Risk Management (Federal Emergency Management Association [FEMA], 2015), the Risk-Informed Decision-Making Guideline (Federal Energy Regulatory Commission [FERC], 2016) and the Safety of Dams Policy and Procedures (United States Army Core of Engineers [USACE], 2014).

For Level I infrastructure, the lowest APF was set at $1x10^{-8}$, as this is the lowest APF plotted on most risk tolerance charts for dams. For Level IIb infrastructure, the lowest APF was set at $1x10^{-6}$, as this is generally considered tolerable for estimated loss of life over 1000 persons in each of the reviewed references. For Level IIIb infrastructure, the lowest APF was set at $1x10^{-4}$, as this is considered tolerable provided mitigation measures can be taken in accordance with "*As Low As Reasonably Practical*" (ALARP). The use of minimum APF values assumes any critical infrastructure can fail and that there is always a certain degree of uncertainty, which decreases with increasing LOE and FS but is never null.

The modifications were first developed for tailings storage facilities (TSF) and then a few of the criteria were further modified for water management infrastructure, heap leach facilities and rockfill storage facilities. Due to limitations on the length of this paper, some information is not included herein. Further details on the proposed methodology and TSF LOP definitions for each criterion are provided in Chovan et al. (2020). The proposed APF-FS-LOP relationships are shown on Figure 2 with the original relationships in grey.

Table 1. Modified evaluation criteria list.

Design - investigation
1.1 Baseline and background information collected about infrastructure-specific siting
1.2 Investigation program development, and adjustments to fill gaps, in relation to design, construction and operation phases
1.3 Investigation quality assurance / quality control (QA/QC) program
1.4 Current understanding of soil profile, stratigraphy, and geology for infrastructure-specific foundations and embankment conditions
1.5 Current understanding of foundational strength characteristics, particularly for weak and soft zones, and level of reliance on in situ information
1.6 Current understanding of tailings or other contained materials' mechanical behaviour, based on in situ characteristics and strength
1.7 Current understanding of groundwater conditions and piezometry, and basis on field data through time
1.8 Robustness of hydrology assessments, including catchment area and site water balance, and basis on relevant field data
1.9 Assessment of borrow resources (quantities and qualities) of construction materials over lifecycle
Design - laboratory testing
2.1 Laboratory test program development, level of collaboration to date
2.2 Testing and verification between lab results and field investigations
2.3 Lab / sampling QA/QC program
2.4 Current understanding of geochemistry and physical properties of tailings (or other contained material)
2.5 Current understanding of geochemistry and physical properties of materials used for construction
2.6 Reporting, completeness, accessibility, and security of information
Design - analysis & documentation
3.1 Site selection study (historical)
3.2 Design basis memorandum (DBM) development, collaborative review through the project life to date & alignment with current state of practice
3.3 Stability analysis, based on current understanding from investigations, and failure modes
3.4 Flood routing (capacity and discharge, design storm events)
3.5 Hydrogeological analysis, based on current understanding from investigations and projections
3.6 Risk analysis, based on current understanding from investigations, and failure modes
3.7 Review process through every design phase, including raises
3.8 Reporting, completeness, accessibility, and security of information
Construction management and quality assurance / quality control
4.1 Project management program
4.2 Supervision program through life of construction
4.3 Construction QA/QC program through life of construction
4.4 Monitoring of infrastructure and foundation performance through life of construction
4.5 Construction reports through life of construction
4.6 Construction meetings between owner and contractor, involvement of Designer and Engineer of Record (as applicable) for critical aspects, through life of construction
4.7 Review process through life of construction
4.8 Management of change through life of construction
Operation, monitoring and performance
5.1 Governance
5.2 Management system (e.g. MAC Towards Sustainable Mining)
5.3 Operation, maintenance and surveillance (OMS) manual
5.4 Monitoring program and system
5.5 Disclosure & external consultation
5.6 Containment infilling / development planning (in consideration and respective of DBM)
5.7 Emergency preparedness program
5.8 Formal review process (internal and external)
5.9 Follow-up on all improvement recommendations and concerns
5.10 Management of operational risks
5.11 Geotechnical performance of infrastructure (movement, settlement, tension cracks, etc.)
5.12 Hydrogeological performance of infrastructure (seepage, piezometric levels, internal erosion, impact to groundwater)
5.13 Hydrological performance of infrastructure (inclusive of freeboard, beach and spillway management and operations)
5.14 Performance of foundation (movement &/or settlement)

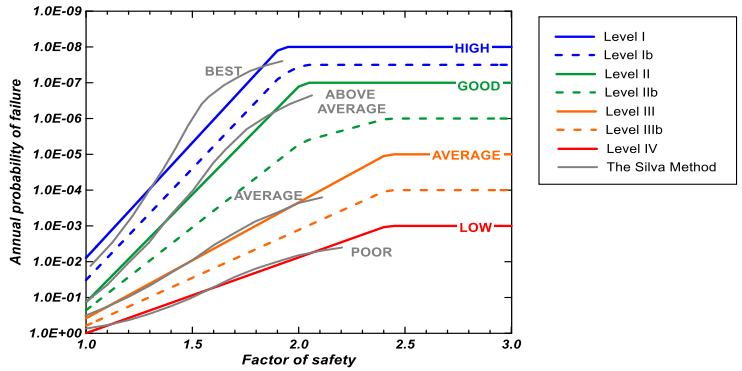

Figure 2. Comparison of relationships of Annual Probability of Failure with Factor of Safety for Level of Engineering (grey) (adapted from Silva et al., 2008) and proposed modified relationships for Level of Practice (Chovan et al, 2020).

4 EVALUATION PROCESS AND IMPLEMENTATION

4.1 *Process of Evaluation*

The risk assessment for a structure is conducted as follows:

1. Evaluation of the LOP;
2. Selection of the appropriate FS;
3. Determination of the APF;
4. Evaluation of the consequences of failure; and
5. Evaluation of the risk.

The semi-quantitative assessment is conducted for the section of the structure where the failure could result in the consequences considered in the risk assessment. If failure of different sections of a structure could have different consequences, then an assessment is conducted for each section.

The evaluation of the LOP is conducted by a technical professional with access to all of the available DCO information, and the relevant knowledge and experience to interpret the documented information, e.g. the EoR. The DCO criteria are each evaluated individually and documents supporting the evaluation are referenced. Table 2 provides two examples as to how each criterion is evaluated.

Table 2. Example DCO criteria (Design: investigation; Operations & monitoring)

Criterion	Level of practice descriptions
1.5 Current understanding of foundational strength characteristics, particularly for weak and soft zones, and level of reliance on in situ information	I - High level of certainty, heavy reliance on in situ information II - Good level of certainty, reliance on in situ information, some gaps III - Average to good level of certainty, limited in situ information IV - Low level of certainty, particularly for weak zones
5.4 Monitoring Program and System	I - In place, comprehensive coverage, with data acquisition system, proper real-time analysis and follow-up II - In place, comprehensive coverage, with follow-up on regular basis III - In place, partial coverage, and occasional follow-up IV - Limited monitoring and/or lack of follow-up

The factored scores for the individual DCO criterion are tallied to determine the overall LOP score. The static factor of safety in drained or undrained conditions, whichever is appropriate, is selected from the stability analyses for the structure, and the source referenced. The APF of the structure is determined using the LOP score, FS and Figure 2 relationships.

The consequences associated with the assumed failure are determined using dam breach analysis, slope failure run-out analysis or other appropriate method. The consequences are based on the potential for loss of life, environmental damage, economic losses to other parties and damage to infrastructure (e.g. Canadian Dam Association [CDA], 2013). Many mining companies also include the effects on local communities and direct costs. The consequences are then classified from Negligible to Extreme based on the worst potential consequences of any potential for impact.

The traditional risk classification or Risk Rating (RR) is a product of the Probability Rating (PR) and the Consequence Rating (CR). To determine an appropriate PR, the range of APFs are cross-referenced to traditional probability ratings (1 to 5, where 1 is very low probability and 5 is very high probability). For the risk evaluation process, the PR was assigned according to the ranges of APF in Table 3 below.

Table 3. Conversion from annual probability of failure to probability rating

Annual Probability of Failure (APF)	Probability Rating descriptor	Probability Rating (PR)
$<= 1x10^{-6}$	Negligible	0
$>1x10^{-6}$ to $1x10^{-5}$	Very Low	1
$>1x10^{-5}$ to $1x10^{-4}$	Low	2
$>1x10^{-4}$ to $1x10^{-3}$	Moderate	3
$>1x10^{-3}$ to $1x10^{-2}$	High	4
$>1x10^{-2}$	Very High	5

Based on this table, APF values less than $1x10^{-6}$ (an occurrence of 1 in 1,000,000 years) are considered Negligible and values greater than $1x10^{-2}$ (1 in 100 years) are considered Very High. Similarly, CR were based on a classification chart typical of that used in the mining industry, and include ratings of Negligible (1), Low (2), Medium (3), Major (4) and Extreme/Critical (5).

The resulting risk rating can then be calculated (PR x CR) to provide an equivalent RR score to compare to other enterprise risks. Otherwise, the risk results can be plotted on a graph to easily compare each infrastructure's risk to others within the portfolio, as demonstrated with the case studies described in Section 6.

4.2 *Validation and implementation*

The criteria list and descriptions, LOP definitions for each criterion, and the process of evaluation and reporting mechanisms were developed through several improvement iterations. Revisiting the process in this way helped to create consistency in scoring between end users, and to ensure agreement with performance expectations at each of the four Levels of Practice.

Careful attention was paid in both the development of the LOP definitions and the evaluation process to align with the expectations of performance in accordance to best practices and standards expected at this time – and not to consider what might have been best practice at the time of design and construction of the infrastructure being assessed. This means that a High LOP (Level I) requires that throughout the whole life cycle of an infrastructure, the same high level of practice would have been applied on all aspects, as would be applied today. A Good LOP (Level II) requires that throughout most of the life cycle of an infrastructure, a high level of practice has been applied but not necessarily at all times, or, its level of practice was not of the highest level on all aspects at all times. Similarly, an Average LOP (Level III) suggests that an infrastructure may have undergone a variable level of practice over the years or would show some clear gaps in terms of the practice as it is today. Finally, a Low LOP (Level IV) is characterized by clear gaps in terms of the practice as it is today.

Criteria and definitions initially developed were tested with several EoRs on several unique infrastructure, and variable cross sections of the infrastructure. Interpretations and results of

different EoRs were collaboratively reviewed and compared with the team of EoRs and the Accountable Executive Officer (AEO). Both criteria descriptions and respective LOP definitions, as well as scoring of similarly designed, constructed and performing infrastructure, were iteratively adjusted until alignment and consistency in appropriate ratings was achieved by all.

In addition, several visual reporting strategies were tested to help clarify the results of the risk assessment for non-technical reviewers, a step involving management individuals without detailed TSF design or management experience and/or background knowledge.

After finalizing the evaluation tools and methodology, the remainder of the validation and implementation sequence commenced, as follows:

1. Preliminary assessments finalized by EoR and external auditor;
2. Consolidation of individual assessments into site and corporate-based reporting tools;
3. Review of consolidated preliminary results with corporate management team;
4. Review of consolidated preliminary results with operations' critical infrastructure management teams;
5. Updates of preliminary assessments with any new information gained from the sites;
6. Final reporting of consolidated risk results.

There were several benefits of each stage of iteration in development and having multiple stages of implementation. First, by working on alignment with multiple EoRs focused on separate infrastructure, but familiar with each assessed, bias of personal perspective was largely reduced. This combined with a requirement that all scoring be backed by supporting documentation ensures verifiable results and not subject to beliefs or opinions. These aspects combined allow greater consistency in rating.

Second, by ensuring review stages with both management and site representatives allowed for the incorporation of additional information that might have been missing or unknown to the EoR during the preliminary assessment. In fact, on several occasions, site-based archives or files stored with engineering firms were brought to light, allowing for preliminary scores to be improved – more on this in the results section.

Thirdly, with the reliance on documentation to perform the evaluation, the compilation of important and relevant documents is facilitated. Review of "new" information, and follow-up review of updated risk results helps all personnel involved to gain a better understanding of the infrastructure being managed, both in terms of site conditions, historical performance, as well as current potential issues.

Lastly, consolidating all of the results into one reporting tool allows for a clear understanding of the level of risks associated with the portfolio of critical infrastructure, and also enables comparison of risks, and prioritization of needs for addressing risks from one site to another.

4.3 *Integration with Management Systems*

The evaluation tool supports existing enterprise risk management and critical infrastructure management system elements, such as the Operations, Maintenance and Surveillance (OMS) Manuals and Trigger Action Response Plans (TARP).

Aligned with the cycle of Plan, Do, Check, Act (PDCA), the evaluation process facilitates:

- a cross-portfolio review of the companies' levels of risk associated with critical infrastructure (Check),
- risk-informed decisions (Act),
- development of plans to make improvements (Plan), and
- the execution of plans to reduce the level of risk associated with specific infrastructure needing attention (Act).

Evaluations are reviewed and updated iteratively, including as a defined response to specific triggers of changing conditions in the field, as should be described in a TARP for a particular facility. Updates to the evaluation can also be done when uncertainty is introduced, such as when something problematic (i.e. a previously unidentified weak plane) is discovered in the field, but the pervasiveness of the challenge is yet unknown, as well as following actions to better understand the situation, and after taking any necessary actions to reduce the risks again. It is meant to be a living process fully integrated with the management systems already in place.

5 PRIORITIZATION AND IMPROVEMENT PLANNING

Traditional risk assessment processes often place most critical infrastructure into the same categories: high to extreme potential consequences of failure, combined with very low to low to medium probabilities of failure, resulting in overall risk classification of low to medium risk. Without drilling down into specific design and performance aspects, it becomes difficult to gain a quick understanding of where efforts should be made to make improvements.

As was indicated in Section 2, referral only to infrastructure design FS also creates challenges with understanding whether one infrastructure has a higher probability of failure than another. For example, an infrastructure rated as LOP III and FS 1.8 has a higher APF ($1x10^{-3}$) than an infrastructure rated as LOP II and FS 1.5 (APF = $1x10^{-4}$).

For this reason, it is recommended that the implementation of a risk-based approach within any organization requires that the Owner look beyond the FS alone, and go through a risk tolerance exercise, to identify what is considered tolerable with respect to probability of failure and overall risk, and the operating limits or boundaries in which it will accept for standard operations.

5.1 *Risk tolerance and prioritization*

Application of risk assessment is facilitated by the identification of the tolerable level of risk of an organization. This can be expressed as a probability of failure, on an annual basis or on an expected lifespan, as a recurrence interval, or as a Risk Rating. Note that this exercise is independent of the selection of design criteria. When a probability of failure or recurrence interval is used, the consequences of failure are not considered, as they are with the Risk Rating.

For the prioritization stage, an APF of $1x10^{-4}$, corresponding to a recurrence interval of 1:10 000 years, was selected as a tolerable occurrence rate for a failure event. As mentioned, this level is considered tolerable at the individual level for loss of life, and is the societal tolerable risk limit provided risk mitigation measures are taken in accordance with "*As Low As Reasonably Practical*" principles (FEMA, 2015; FERC, 2016; USACE, 2014). Alternatively, it could have been decided to set a maximum Risk Rating of 3 (Medium Risk), for example, as the objective.

By setting a maximum APF (i.e. APF should be lower), instead of a minimum FS, it becomes easier to prioritize improvement efforts on infrastructure; we simply look at which infrastructures' APF is higher than the target. Combining this with the consequence rating of each highlighted infrastructure then allows further prioritization, where those having the highest potential consequences can be addressed first.

Finally, we can then look to the LOP scores to see whether there are infrastructure with lower scores that would reveal some obvious, quick, and easy to implement improvement actions.

5.2 *Improvement planning*

To improve the LOP performance scores, and hence lower the APF, several strategies can be applied, including:

- Discovery and review of archived documentation for improved understanding of site and foundation conditions, material characteristics, and construction quality, for various phases of the infrastructure lifecycle;
- Updating stability and failure analyses using newly discovered information, ongoing operational and performance data, updated geometry and piezometric profiles, altered climate assumptions, and more;
- Improvements to governance, management and reporting systems, monitoring and maintenance programs, and communications and general understanding of the tailings management system and performance for all involved;
- Additional field investigations and/or installation of additional instrumentation to obtain missing or unknown information, followed by updates to analyses as above; and
- Physical buttressing, ground stabilization, densification of contained materials, or other strengthening mechanisms that would improve the design, the FS and the resilience of the infrastructure.

- Reduction of the consequences of failure, including addition of downstream catchment or flow diversion systems (e.g. into a pit), or relocation of downstream people, housing and infrastructure.

There may be opportunities for relatively quick implementation of improvements depending on the shift in APF required to meet the targeted performance level and the respective level of effort to do so.

6 ILLUSTRATIVE EXAMPLES

A preliminary risk evaluation of a TSF portfolio of a large mining company was conducted using this tool and is presented in Chovan et al. (2020). For illustrative purposes, examples are presented to show potential changes in LOP scores, APF determination and risk levels, before and after, the implementation of different strategies to remove uncertainties, improve understanding of infrastructure conditions, and to reduce identified risks.

6.1 *Example 1: Discovery & Detailed Review of Archived Records (TSF1)*

TSF1 is an older, stable infrastructure where, at the time the risk evaluation process commenced, many historical documents regarding site investigation, testing, and construction were not readily available. As such, many criteria in these categories were rated as LOP III or IV. As a result, the infrastructure was rated overall as DCO score of 2.63 (LOP IIb), and an APF of 1.9×10^{-3} or 526-year recurrence interval.

After reviewing the initial evaluation results with the operating site, there was a clear discomfort from the site that the evaluation results were impacted by missing information. This motivated them to track the missing reports. Many historic records were located and provided, both from site archives, as well as from the design consulting firm, allowing an improvement in DCO score to 2.22 (LOP II), and an APF of 3.4×10^{-4} or 2,941-year recurrence interval.

Detailed review of the information within the archived reports allowed the individuals performing the risk evaluation to demonstrate that their understanding was supported by factual information of the site conditions and materials used for construction, the design and the construction quality. Many uncertainties were then removed, allowing for further adjustment of additional criterion scores. The current DCO score is now 1.82 (LOP II), and an APF of 7.3×10^{-5} or 13,699-year recurrence interval.

With a consequence rating of 4, the risk rating was shifted from high (close to very high) down to medium risk, and below but close to the objective APF of 10^{-4}. Further work was commissioned to further review and update the design basis memorandum and stability analyses to bring these up to date with current standards and to ensure the FS remains valid.

6.2 *Example 2: Discovery & Review of Archived Records & New Instrumentation (TSF2)*

TSF2 is a site where there were uncertainties with respect to the geotechnical performance of the infrastructure due to a lack of instrumentation. As such, site investigations, planning for the installation of additional instrumentation, and review of the infrastructure details, had already commenced at the time of the risk evaluation.

Along with the review process, it was determined that this was another scenario where some of the historic information for TSF2 was not readily available, and in particular regarding the borrow reports and construction records. As such, the initial evaluation resulted in a DCO score of 2.13 (LOP II), and an APF of 8.5×10^{-4} or 1,176-year recurrence interval.

After the operating site provided historic construction records, and instruments were installed, the EoR was able to validate the quality of construction was in accordance with design, as well as better understand the performance of the infrastructure (no movement was detected, nor were there any excess pore pressure). This allowed an improvement in DCO score to 1.76 (LOP II), and an APF of 2.4×10^{-4} or 4,166-year recurrence interval.

With only these additional insights and monitoring capabilities, and a consistent consequence rating of 5, the risk rating shifted from almost very high down to high risk, and the infrastructure

remained above the objective APF of 10^{-4}. Further work was commissioned to review and update the stability analyses, based on the new site investigation information, for the critical sections of the infrastructure.

For one of the most critical sections of the infrastructure, the stability analyses indicated a need for additional buttressing. The buttress along the toe of this section improved the FS of the infrastructure.

With these modifications, the score improved alongside the FS, to make a much larger shift in evaluation results. The DCO score is now 1.73 (LOP Ib), and the FS is 1.5 (improved from 1.4). This results in an APF of 5.4×10^{-5} or 18,518-year recurrence interval.

With a consequence rating of 5, the risk rating has now shifted from the almost very high down to medium risk, and now resides below the objective APF of 10^{-4}.

6.3 *Example 3: Changing Conditions, Field Investigations & Update of Stability Analyses, & Projected Impact of Corrective Actions (TSF3)*

TSF3 was chosen to demonstrate the need for adaption as new information becomes available and for utilizing the risk evaluation process on an ongoing basis. As a result of the site's risk management process, additional instrumentation was installed at this site to improve the TSF monitoring program. One of the new inclinometers indicated movement at depth below the upstream raises.

With this new information, additional site investigations were requested, and it was discovered that a frozen layer existed at depth within the tailings. Using the new information, an update of the stability analysis resulted in a decrease in the factor of safety from 1.6 to 1.3. A few of the criterion scores had also to be adjusted, for example those related the understanding of the tailings and materials used for the raise. With those changes, an update to the risk evaluation resulted in a DCO score of 1.91 (LOP II), and the APF increased to 1.1×10^{-3} or a 909-year recurrence interval, overall indicating a high-risk rating.

This case study exemplifies the criticality of having the ability to detect, measure and communicate changes in performance of infrastructure during its operation and construction. It also supports the proposed method's emphasis on integration and evaluation of management processes in all categories of the risk evaluation. Having an appropriate management system in place is what ensured appropriate monitoring was put in place, it ensured that triggers were set for communicating and acting on unexpected changes, and ensured that reviews were made to stability analyses and also operational practices as a result of changing conditions in the field.

Had there not been a proper risk management system in place, the monitoring system may not have been flagged for improvements. Had additional instrumentation not been installed, this situation would not have come to light as quickly as it did, nor would the level of risk have been as well understood. As a result of the updated stability analyses and risk evaluation, the design was adjusted and a stabilization berm was recommended to provide more buttressing and to further stabilize the infrastructure.

A review of the stability incorporating the berm resulted in a FS of 1.6 which, along with a few more adjustments to the evaluation of the LOP scores, resulted in this infrastructure having an APF of 1.2×10^{-5}, or 81,300-yr recurrence interval. The additional stabilization work allowed the risk rating to be lowered to medium risk, and below the targeted APF. This example showed the importance of ongoing adaption of the risk assessment to changing conditions as information becomes available.

6.4 *Summary of Evaluation Changes*

The changes in the LOP scores for the illustrative examples above are shown graphically in Figure 3, where the labels of A, B, C represent the sequence of change for each example provided. The black and white segments of each bar represent the contribution of the Design categories while the green and blue hashed segments respectively represent the contributions of the Construction, and Operation & Monitoring. Shorter segments indicate greater certainty and higher quality (lower scores are more favourable).

The changes in FS, APF and risk rating are plotted on Figure 4, where the solid symbols represent the initial evaluation, the open symbols are the second, and the x symbols indicate the

final updates (or projections). The sequence of changes are also shown by a dashed arrow for the first shift, and the second shift by the solid arrow.

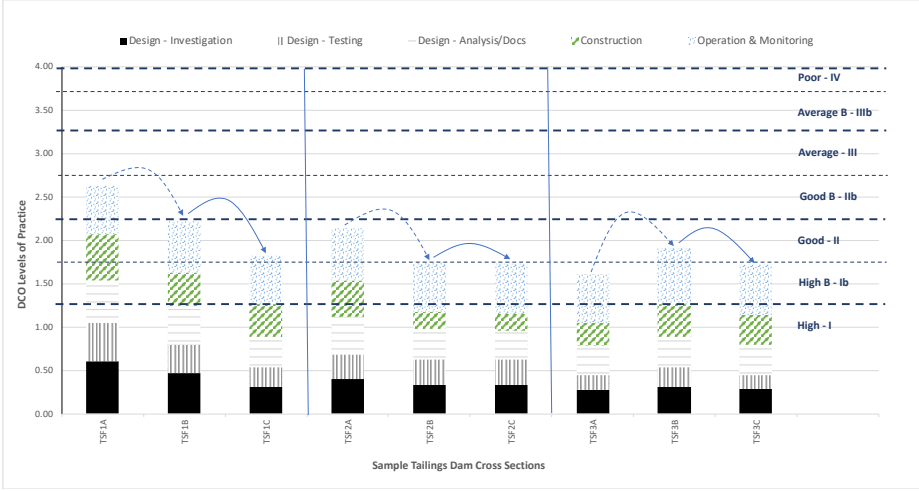

Figure 3. DCO LOP Scores before and after applying improvement strategies for example TSF.

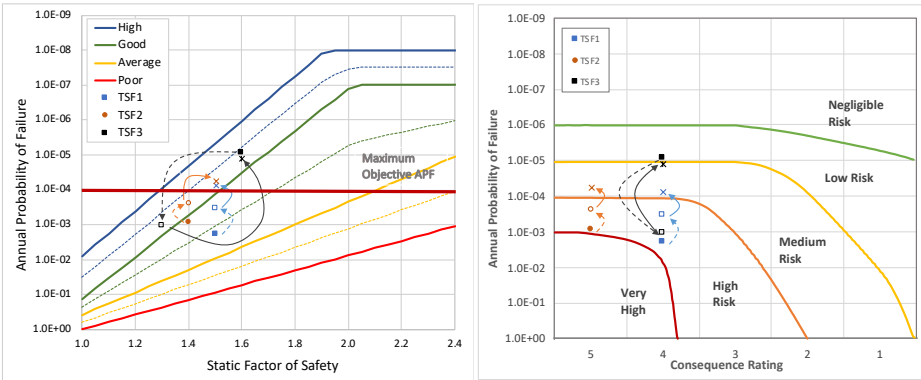

Figure 4. a) Changes in Annual Probabilities of Failure of the example TSF, b) Changes in Risk Rating of the example TSF.

The results of risk assessment, updated in an iterative cycle and aligned with other management systems, such as that demonstrated here, can be used to better manage critical infrastructure during operations and for closure. As shown above, the detailed information can be used to target aspects of specific facilities to improve the APF and lower the overall risk of the infrastructure.

7 CONCLUSION

This paper presents a risk assessment process derived from the original work of Silva et al. (2008) that more explicitly integrates management systems and performance of critical infrastructure. As a first phase of implementation, the evaluation tool has proven to be powerful in clearly

highlighting risks associated with complex critical infrastructure, supporting best practice for risk-informed decision making as recommended in MAC's Guide (2019).

Decisions can be more easily made when it is apparent which infrastructure have higher risks associated with them, and this is not solely dependent on the FS. Although one infrastructure might have a lower FS than another (i.e. less than the current dam design standard of 1.5), it should not automatically be designated the priority for immediate improvements. Targeted efforts should instead be made on the infrastructure having the highest APF and highest risk.

While any risk-based approach includes a part that may be considered subjective or dependent on the persons applying it, the proposed approach was found to provide quite realistic assessment in the context of built-in redundancy with the review and collaborative process such a management system promotes. A primary benefit of carrying out the evaluation process first with the EoR, and then reviewing with operations, was the facilitation of a rapid implementation of the process because operators typically dislike low scores – where information was lacking and scores were low, sites were quick to provide any additional documentation they could, install additional instrumentation or perform additional investigations to further remove uncertainties, thus improving the scores. The site operators also appreciated having a full checklist of criteria upon which their performance is evaluated, enhancing their ability to support better management systems.

The evaluation process presented here can provide detailed and actionable results that can readily be understood by technical and nontechnical mining professionals as well as owners and stakeholders.

8 REFERENCES

Canadian Dam Association (2013) *Dam Safety Guidelines 2007*, (2013 Edition), Canadian Dam Association, Toronto.

Chovan. K. M., Julien, M. R., Ingabire, E-P., Masengo, E., Lépine, T. James, M. and Lavoie, P. (2020) 'A Risk-Based Portfolio Evaluation Approach for Mine Waste Infrastructures' manuscript submitted to the *Canadian Institute of Mining, Metallurgy & Petroleum Technical Library* on May 26, 2020.

Julien, M., E. Masengo, P. Lavoie, T. Lepine (2019a) 'A risk-based approach to support the implementation of the new guidelines related to tailings management', 6th International Seminar on Tailings Management, July 10-12, 2019. GECAMIN, Santiago.

Julien, M., E. Masengo, P. Lavoie, T. Lepine (2019b) 'An operational perspective on the implementation of the new guidelines related to tailings management'. Sustainable and Safe Dams Around the World / Proceedings of the ICOLD 2019 Symposium, June 9-14, 2019. ICOLD, Ottawa.

Silva, F., Lambe, W.T. and Marr, W.A. (2008) 'Probability and risk of slope failure'. *Journal of Geotechnical and Geoenvironmental Engineering*, American Society of Civil Engineering 134 (12), p. 1691-1699.

Improved Tailings Dam Design and Management through Smarter Modeling

Josh Moncrieff
Capstone Mining Corp., Vancouver, BC, Canada,

ABSTRACT: Tailings dam stability is typically dependent in part on pore pressure conditions in the dam and its foundation. Dam stability analyses are often supported by seepage models that utilize the conventional 'crystal ball' approach. The use of such models is predicated on the assumption that they can be good predictors of the future. This paper discusses why this is not necessarily the case and proposes an alternative 'decision support' modelling approach, which aims not to precisely predict the future, but to assess the likelihood of an adverse outcome occurring in the future. A case study is presented illustrating how this approach can support tailings design and management decisions, with less potential for overly precise and inaccurate predictions that often result from 'crystal ball' approach. This paper focuses on seepage and stability models, but the proposed modeling approach can be applied to many other types of models used in tailings design and management.

1 INTRODUCTION

Tailings stakeholders typically rely on an assortment of geotechnical, hydrological, geochemical and other models to understand tailings risks and to support tailings design and management. As computing power has increased, these types of mathematical models have tended to become increasingly complex, striving to simulate the real world as closely as possible. With this increasing complexity has come a tendency to believe that these models are effective predictors of the future. As highlighted by NCGRT (2019), Doherty (2010), Doherty & Moore (2019), White (2017) and many others, this belief will never be true. The real world is infinitely complex, meaning that model predictions can either be precisely wrong, or imprecisely right; no model of a tailings storage facility (TSF) can make predictions that we can be confident are both accurate and precise. This is the case even for a model that has been well calibrated (Lotti & Doherty 2016). As a result, assessment of a model's uncertainty, and consideration of this uncertainty in decision making, is essential. Relying only on the precise predictions of a model, without consideration of uncertainty, can be misleading, but is also widespread.

The stability of a TSF is typically dependent in part on pore pressure conditions in the dam and its foundation. There exist many examples of tailings dam failures related to pore pressures exceeding design assumptions. Dam stability analyses are usually supported by numerical seepage models that aim to predict future pore pressure distributions. The use of such models is predicated on the assumption that a numerical model is capable of precisely simulating these future pore pressures. As discussed above, this assumption is not realistic.

To better utilize the potential of mathematical models, it is necessary to move away for this 'crystal ball' approach of model predictions (Lotti & Doherty 2016), which tries in vain to precisely predict the future. This paper, along with other publications (Freeze et al. 1990); (NCGRT 2020); (Doherty & Moore 2019), proposes an alternative 'decision support' approach to modeling. Rather than attempting to precisely predict the future, this alternative approach assesses the range of outcomes that are unlikely to occur in the future, a task that mathematical models are well suited for. This approach enables prediction of whether a particular adverse outcome, or 'bad thing' (BT), is likely to occur. This knowledge can then support decisions around how to design or manage a TSF in a way that limits the likelihood of that BT occurring.

For the purposes of this paper, the BT is pore pressures in a TSF exceeding the critical level at which minimum required factors of safety (FOS) for slope stability are not met. This paper details and contrasts the conventional 'crystal ball' approach to seepage modeling with the proposed 'decision support' approach. It then presents a case study illustrating how this approach can, with

relatively little effort, improve understanding of geotechnical risk and support risk-informed decisions around tailings design and management.

While this paper focuses on seepage and stability models of tailings storage facilities, the principles that it discusses, and the approach to modeling that is proposes, can be applied to most types of geotechnical, hydrological, geochemical and other models used in tailings design and management.

2 CONVENTIONAL 'CRYSTAL BALL' MODELING APPROACH

The conventional 'crystal ball' approach to groundwater modelling is based on the assumption that once a model has been calibrated, it can be a good predictor of the future. As discussed above, this expectation of a model is not realistic, even in cases where a good calibration is possible. This is particularly true for numerical models of tailings seepage. During dam design or early operations, there are little or no data upon which to define, calibrate or verify a seepage model. At mature operations, there can be an extensive record of observed data, but models calibrated to historic conditions may not be appropriate for predicting future conditions, when TSF geometries, material properties and boundary conditions will have changed.

Despite its shortcomings, this conventional approach to predicting pore pressures is used in the design of most tailings dams. As a result, dams may be constructed that are not adequately conservative, giving stakeholders a false sense of security in a relatively high-risk design. Alternatively, dams may be constructed that are overly conservative and unnecessarily costly. Many guidance documents have been commissioned that espouse this approach to modeling, including in British Columbia (Wels et al. 2012), California (Joseph et al. 2016), Nevada (Newman 2018) and Australia (Barnett et al. 2012), among others. These guidelines all advocate this 'crystal ball' approach, generally entailing: i) proposing and refining a conceptual model; ii) building a numerical model based on this conceptual model; iii) calibrating the numerical model; iv) using the calibrated model to make predictions; and v) quantifying the uncertainty associated with those predictions (Doherty & Moore 2019).

This conventional approach can be very useful, if emphasis is placed on quantifying the uncertainty associated with model predictions, and if the results of this uncertainty analysis are used in subsequent decision making. In many applications, including tailings seepage and stability modeling, most effort is spent on model calibration and predictions, and little emphasis is placed on uncertainty analysis and its application. This is not entirely a fault of the consulting firms typically engaged to develop these models. Mine owners, regulators, the public and other stakeholders are often unaware of the importance of uncertainty analysis, or may want to feel that models provide the 'correct' answer. Many stakeholders would be uncomfortable with the reality that the best answer possible from a numerical model is actually a range of answers falling within a relatively broad uncertainty spectrum. This sentiment is not a reason to forego the use of mathematical models. It is, however, a reason to support smarter modelling that aims not to precisely predict the future, but to assess whether it's likely that a particular BT will occur in the future. In most cases, this information is exactly what stakeholders want to know.

3 PROPOSED 'DECISION SUPPORT' MODELING APPROACH

Components of this proposed 'decision support' approach are shown and are contrasted with the 'crystal ball' approach in Figure 1, and include: A) identifying the BT that the model will consider; B) proposing and refining a conceptual model; C) identifying system properties that contribute most to uncertainty in the likelihood of the BT occurring (i.e. a sensitivity analysis); D) constructing a numerical model based on the conceptual model; and E) using the numerical model to run numerous simulations to assess the likelihood of the BT occurring. As in the 'crystal ball' approach, earlier steps can be revisited throughout the process as needed to yield acceptable results.

Some key aspects of this 'decision support' process should be highlighted. Firstly, a good conceptual model is a fundamental step, as it is in the 'crystal ball' approach. In both approaches, the conceptual model should include details of parameter uncertainty, instead of only what is considered the most likely value for each parameter. Secondly, the model should be only as

complex as is justified by the available data, as is the case in the 'crystal ball' approach. Thirdly, there is no model calibration. Calibration is unnecessary and potentially misleading in the 'decision support' modeling approach, and the limited value that it may add generally does not justify the significant effort that it requires. Finally, model simulations can be performed in many ways. They may be run manually, completing as many runs as needed to understand the predicted range of solutions possible given the range of plausible model parameter values. They may also be run automatically, using software dedicated to stochastic modelling, such as PEST or GoldSim.

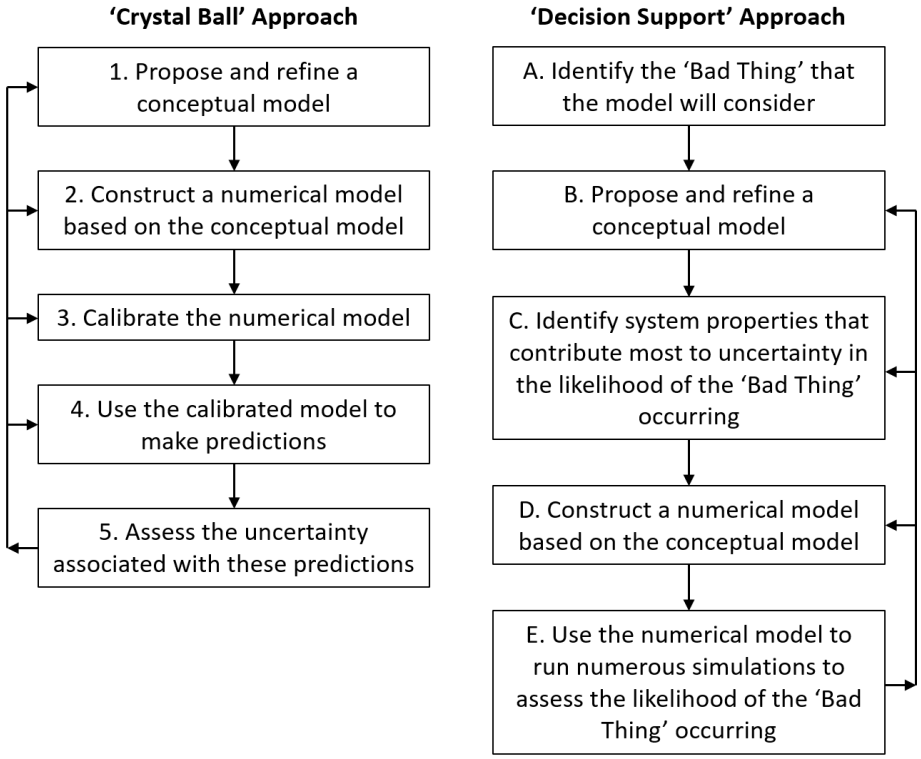

Figure 1. Typical workflow for 'crystal ball' and 'decision support' modelling approaches (revised from Doherty & Moore 2019).

Many publications (e.g. (Freeze et al. 1990); (Doherty et al. 2010); (Doherty 2019); (Doherty & Moore 2019); (NCGRT 2020)), provide a thorough review of the conceptual and mathematical framework for this type of 'decision support' approach. This paper provides limited details of this framework, focusing instead on the approach's value. It does this by presenting a problem that is very common in design and management of tailings facilities: assessing whether dam stability FOS will meet minimum criteria given future pore pressure conditions.

4 CASE STUDY

4.1 *Concept*

This case study assesses future pore pressures in a theoretical upstream-raised cyclone sand TSF, to support dam stability analyses. It could be either a proposed facility that has not yet been built, or an existing facility that is being considered for a significant expansion. It is not based on any actual TSF, though is similar in concept to many facilities currently in operation around the world.

The conventional 'crystal ball' approach to this problem would follow the workflow summarized in Figure 1. In essence, this approach asks a seepage model what future pore pressures

will be, then uses those predicted pore pressures to ask a stability model whether the dam will be stable or not. For the reasons discussed above, this approach could only make accurate predictions if a comprehensive uncertainty analysis were completed, which is often not the case.

The 'decision support' approach to this problem would follow the workflow summarized in Figure 1 and detailed below. This approach first asks the stability model what maximum pore pressures are acceptable for the dam to be stable, then asks the seepage model whether it's likely that those pore pressures will be exceeded. Numerical models are well suited to answer this question with relatively little effort.

4.2 *Modelling Workflow*

This case study considers three scenarios to illustrate how different results from the 'decision support' modeling approach can be used to make design and management decisions. These scenarios are referred to as the 'No Case', the 'Yes Case', and the 'Maybe Case'.

4.2.1 *Step A – Define the 'Bad Thing'*

In this case study, the BT is pore pressures in the TSF exceeding the critical level at which minimum required FOS for slope stability are not met. This level is determined using slope stability analyses. For simplicity in this case study, it is assumed that the critical pore pressure distribution is hydrostatic, so can be defined by a phreatic surface.

4.2.2 *Step B - Propose and Refine a Conceptual Model*

The development of conceptual seepage models has been discussed at length in many publications and a detailed treatment is beyond the scope of this paper. For this case study, key aspects of the conceptual model include:

- Sources of water to the system include inflows from upgradient of the TSF, infiltration from the pond, and infiltration of rainfall on the tailings beach and embankment. Infiltration rates for the beach and embankment for the three scenarios or listed in Table 1.
- Hydrostratigraphic units include tailings slimes, the cyclone sand embankment, and the foundation, and hydraulic properties of each unit are listed in Table 1.
- Losses of water from the system include outflow through the foundation downgradient of the TSF, and exfiltration from the foundation and embankment face.

Table 1. Model parameter value ranges.

Scenario	Hydraulic Conductivity Embankment (m/s)	Hydraulic Conductivity Fines (m/s)	Hydraulic Conductivity Foundation (m/s)	Beach Infiltration (m/yr)	Embankment Infiltration (m/yr)
Yes Case	1×10^{-5} to 1×10^{-4}	1×10^{-8} to 1×10^{-7}	1×10^{-6} to 1×10^{-5}	0.05 to 0.1	0.15 to 0.3
No Case	1×10^{-7} to 1×10^{-6}	1×10^{-9} to 1×10^{-8}	1×10^{-12} to 1×10^{-8}	0.25 to 0.5	0.2 to 0.5
Maybe Case	7×10^{-7} to 2×10^{-6}	1×10^{-7} to 2×10^{-8}	3×10^{-6} to 1×10^{-5}	0.25 to 0.5	0.5 to 3.0

4.2.3 *Step C - Identify System Properties that Contribute most to Uncertainty in the Likelihood of the BT Occurring*

Sensitivity analysis has been discussed at length in many publications and a detailed treatment is beyond the scope of this paper. For this case study, the system properties to which model predictions are highly sensitive include hydraulic conductivity of the embankment, tailings fines, and foundation, and infiltration to the beach and embankment. Model predictions are minimally sensitive to other system properties.

4.2.4 *Step D – Construct a Numerical Model Based on the Conceptual Model*

As discussed above, a model should only be as complex as is justified by the available data. Given the paucity of data available in this case study, it was determined that a steady-state 2D model with only three hydrostratigraphic units was justified. Infiltration from the pond, beach and embankment are the only internal boundary conditions. Constant head boundaries are applied at the upstream and downstream ends of the model domain.

4.2.5 *Step E – Use the Numerical Model to Run Numerous Simulations to Assess the Likelihood of the BT Occurring*

As discussed above, this step can be performed manually or automatically, depending upon the number and complexity of models to be run, available resources, and other factors. As the model in this case study is very simple, simulations were run manually. Only the three parameters to which the model was found to be sensitive in Step C were varied in each simulation. It is expected that variation of other parameters would not materially impact model predictions.

For each scenario, three simulations were run, including: i) a low pore pressure simulation with the highest plausible hydraulic conductivity values, and the lowest infiltration rates plausible for those hydraulic conductivity values; ii) a medium pore pressure simulation with hydraulic conductivity values and infiltration rates in the middle of the plausible ranges; and, iii) a high pore pressure simulation with the lowest plausible hydraulic conductivity values, and the highest infiltration rates plausible for those hydraulic conductivity values. This range of models is expected to delineate the plausible range of phreatic surface levels for each scenario. Predicted phreatic surfaces are shown alongside the critical phreatic surface for each scenario in Figure 2 through Figure 4.

4.3 *Modelling Workflow*

4.3.1 *No Case*

As shown in Figure 2, the predicted phreatic surface in this case is well below the critical phreatic surface for all plausible parameter values. This indicates that the FOS for slope stability for the current design will exceed minimum FOS targets. Depending upon the owner's risk appetite, economic considerations and other factors, this result could be used to support one or more of the following actions:

- Collect additional data, if possible, to refine the conceptual model and numerical model predictions. Data collection efforts can be guided by model sensitivity analysis results to ensure that new data significantly improves predictions.
- Construct the TSF as designed, expecting a relatively high FOS and low risk of dam instability.
- Develop a less conservative and less costly design that will have a lower FOS.

4.3.2 *Yes Case*

As shown in Figure 3, the predicted phreatic surface in this case is well above the critical phreatic surface for all plausible parameter values. This indicates that the FOS for slope stability for the current design will not meet minimum FOS targets. This result could be used to support one or more of the following decisions:

- Collect additional data, if possible, to refine the conceptual model and numerical model predictions.
- Develop a more conservative design that is more likely to meet minimum FOS targets.

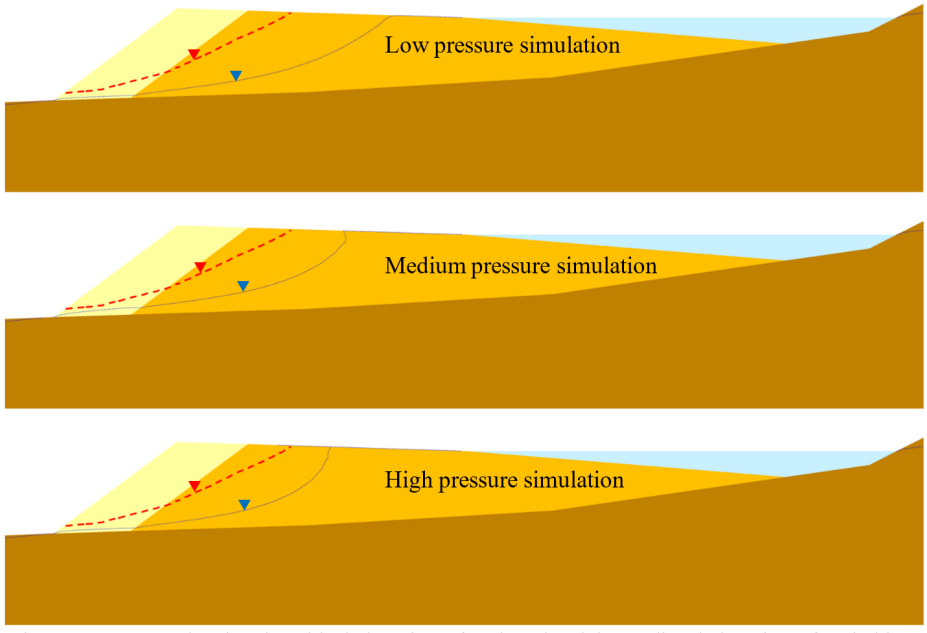

Figure 2. No Case, showing the critical phreatic surface in red and the predicted phreatic surface in blue.

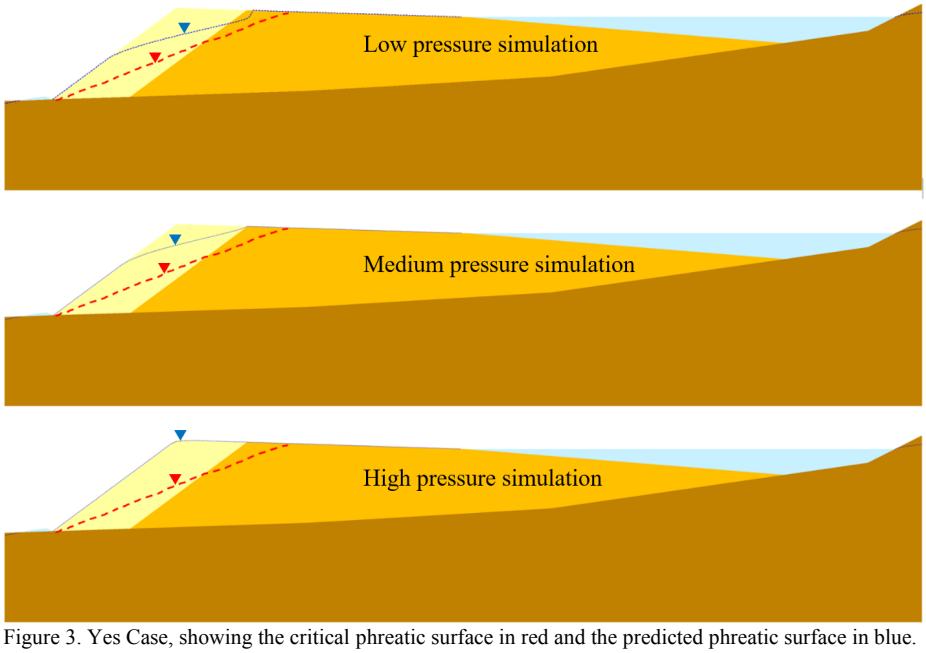

Figure 3. Yes Case, showing the critical phreatic surface in red and the predicted phreatic surface in blue.

4.3.3 *Maybe Case*

As shown in Figure 4, the predicted phreatic surface in this case can be above or below the critical phreatic surface given the range of plausible parameter values. This indicates that the FOS for slope stability of the current design may or may not meet minimum FOS targets. This result could be used to support one or more of the following decisions:

- Collect additional data, if possible, to refine the conceptual model and numerical model predictions.
- Construct the TSF as designed, expecting marginal FOS and with plans in place to employ adaptive management to monitor the TSF closely and mitigate higher pore pressures where needed.
- Develop a more conservative design that is more likely to meet minimum FOS targets.

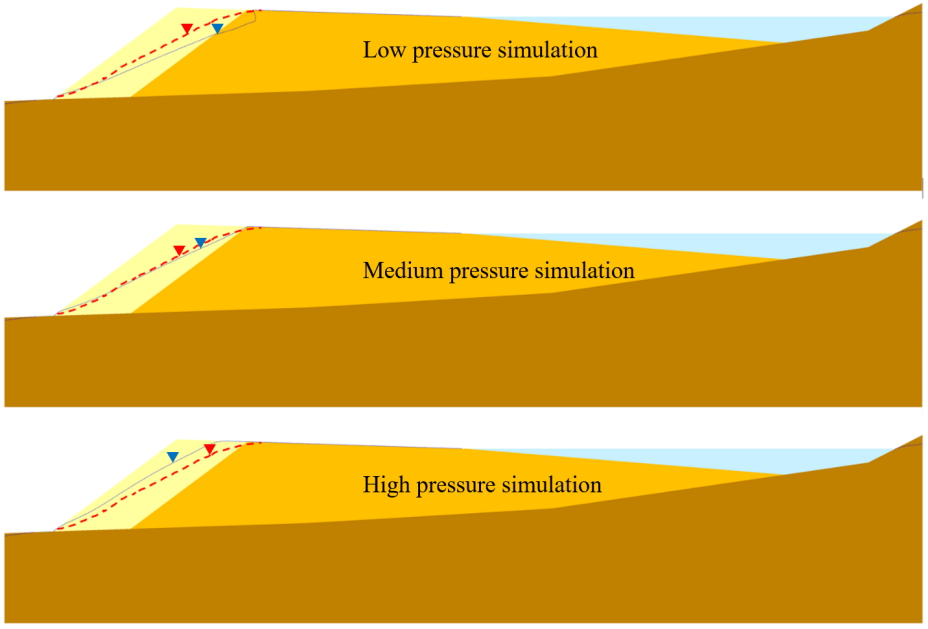

Figure 4. Maybe Case, showing the critical phreatic surface in red and the predicted phreatic surface in blue.

5 SUMMARY AND CONCLUSIONS

This simple case study has illustrated how the 'decision support' approach to seepage modelling can be an effective and efficient alternative to the conventional 'crystal ball' approach. With relatively little effort, it can provide realistic answers in support of tailings design and management decisions, without the potential for overly precise and inaccurate predictions that often result from the 'crystal ball' approach.

In most cases, stakeholders are interested in whether a particular BT is likely to occur, rather than in a detailed prediction of the future. The BT considered in this paper is pore pressures in a tailings dam that exceed the critical level at which minimum required FOS for slope stability are not met. However, this approach to modelling can be applied to most types of geotechnical, hydrological, geochemical and other models, and is particularly useful for models supported by a paucity of data. Some examples of other BTs that could be assessed using this approach include:

- A water quality parameter exceeding regulated limits.
- Pond evaporation leading to a water shortage and curtailment of mill production.
- Peak pond discharge exceeding spillway capacity.
- Seepage through a dam leading to internal erosion.
- Pumping from seepage interception wells leading to a decrease in surface water flow.

REFERENCES

Barnett, B., Townley, L.R., Post, V., Evans, R.E., Hunt, R.J., Peeters, L., Richardson, S., Wenner, A.D., Kanapton, A. & Boronsky, A. 2012. *Australian Groundwater Modelling Guidelines*. National Water Commission, Canberra.

Doherty, J.E., Hunt, R.J., & Tonkin, M.J. 2010. *Approaches to highly parameterized inversion: A guide to using PEST for model-parameter and predictive-uncertainty analysis*. U.S. Geological Survey Scientific Investigations Report 2010–5211.

Doherty, J. 2010. *Model-Based Environmental Decision Making*. Watermark Numerical Computing.

Doherty, J. 2019. *Starting from the Problem and Working Backwards.* 2019 Darcy Lecture.

Doherty, J. & Moore, C. 2020. Decision Support Modeling: Data Assimilation, Uncertainty Quantification, and Strategic Abstraction. *Groundwater* 58: 327-337.

Freeze, R.A., Massmann, J., Smith, L., Sperling, T. & James, B. 1990. Hydrogeological decision analysis I: A framework. *Groundwater* 28(5) 738– 766.

Joseph, T., Godwin, T., McManus, D., Nordberg, M., Shannon, H. & Springhorn, S. 2016. *Best Management Practices for the Sustainable Management of Groundwater; Modeling BMP*. California Department of Water Resources Sustainable Groundwater Management Program.

Lotti, F. & Doherty, J. 2016. The role of numerical models in environmental decision-making. *Acque Sotterranee – Italian Journal of Groundwater* AS18-231: 73-75.

National Centre for Groundwater Research and Training (NCGRT) 2019. *Webinar 1 – Groundwater Modelling for Decision Support: Concepts and Fundamentals*. Retrieved from http://www.groundwater.com.au/research_projects/groundwater-modelling-decision-support-initiative-gmdsi.

Newman, C.P. 2018. *Guidance for Hydrogeologic Groundwater Flow Modeling at Mine Sites*. Nevada Division of Environmental Protection, Bureau of Mining Regulation and Reclamation.

Wels, C., Mackie, D. & Scibek, J. 2012. *Guidelines for Groundwater Modelling to Assess Impacts of Proposed Natural Resource Development Activities*. British Columbia Ministry of Environment, Water Protection & Sustainability Branch.

White, J.T. 2017. Forecast first: an argument for groundwater modeling in reverse. *Groundwater* 55(5) 660–664.

The Factor of Safety and Probability of Failure relationship

Franco Oboni
Oboni Riskope Associates Inc., Vancouver, British Columbia, Canada

Cesar Oboni
Oboni Riskope Associates Inc., Vancouver, British Columbia, Canada

ABSTRACT: The Factor of Safety (FoS) measures the ability of a structure to withstand its loadings. It is the ratio between resisting forces R_f and driving forces D_f acting on or within a structure. Both R_f and D_f are stochastic variables influenced by the intrinsic variability of geomechanical parameters, water table position, external loadings etc. Common practice engineering implicitly considers those variabilities by reducing resistance and increasing loadings to "prudent" values leading to a single FoS. The reliability $R_s=R_f-D_f$ also expresses the ability of a structure to withstand its loadings. The probability of failure (p_f) is the probability $R_s \leq 0$. Oftentimes p_f appears as the probability of $p(FoS \leq 1)$. In recent years various authors have expressed p_f as a combination of Key Performance Indicators (KPIs), including human factors, etc.

This paper builds a FoS-p_f relationship using a simple slope example. The paper shows how such a relationship compares with empirical solutions from literature. This is paramount for the formulation of risk informed design and to foster engineer's confidence in probabilistic solutions.

1 INTRODUCTION

This paper discusses the Factor of Safety (FoS) and the probability of failure p_f of geostructures.

The information contained in this paper is applicable to dams as well as dumps and pits slopes provided the analyst pay attention to the specific details pertaining each type of structure. FoS is generally used to measure the ability of a structure to withstand its loadings. Common practice engineering implicitly considers uncertainties by reducing resistance and increasing loadings to "prudent" values. It then expresses FoS as a single number.

The probability of failure p_f expresses how likely a failure (say slope instability) is to occur. Uncertainties (e.g. soil geomechanical parameters) are explicitly considered. Many techniques, including direct mathematical formulation, point estimates methods (Rosenblueth, 1975) and Monte Carlo simulation can be used to evaluate p_f using geomechanical models.

In recent years, various authors have expressed the probability of failure as a combination of Key Performance Indicators (KPIs), including human factors and quality of studies, design, monitoring, maintenance. These expressions have generally been empirical or semi-empirical. In some cases, these formulations have found fierce opposition: their detractors consider them as doubtful and unverifiable, however, without delivering a counter-proof. This paper shows how a FoS-p_f relationship can be rigorously built, based on geomechanical probabilistic considerations, using a simple slope as an example. The paper then shows how such a geomechanically derived relationship compares with empirical solutions from literature finally shedding some light on possible verification and solving lingering doubts.

The ability to generate and compare such a relationship is paramount for the formulation of risk informed design and to foster engineer's confidence in probabilistic solutions.

2 FOS, RELIABILITY, P_F AND SOME PERPLEXING UNANSWERED QUESTIONS

The Factor of Safety (FoS) is generally used to measure the ability of a structure to withstand its loadings. FoS is defined as the ratio between resisting forces R_f and driving forces D_f: $FoS=R_f/D_f$ acting on or within a structure. Due to various uncertainties both R_f and D_f are stochastic variables. Indeed, their behavior and spread are influenced by the intrinsic variability of cohesion, friction, water table position, external loadings, etc. Common practice engineering implicitly considers those variabilities by reducing resistance and increasing loadings to "prudent" values. It then expresses FoS as a single number.

The reliability of a structure R_s is the difference between R_f, D_f: $R_s=R_f-D_f$. Therefore, R_s also expresses the ability of a structure to withstand its loadings. Reliability analyses generally consider the variability of R_f and D_f. For simplification, their possible dependence is oftentimes neglected.

Probabilistic methods allow these uncertainties to be considered. These approaches can be classified into two families:

1. hybrid or semi-probabilistic methods (Baecher, 1984, Kanjanakul, Chub-Uppakarn, 2018, Kavvadas et al., 2009, Oboni, Martinenghi, 1983, Peterson, 1999),
2. purely probabilistic methods (Oboni, Bourdeau 1984, Oboni, Bourdeau, Bonnard, 1984).

The first belongs to the classical methods of soil mechanics, rendered probabilistic (Alonso 1976). These methods, after introducing the soil parameters of mechanical resistance as random variables, seek to define (Figure 1, 2) the probability of failure (p_f) as the probability $p_f = p(R_f/D_f \leq 1)$ or simply $p_f = p(FoS \leq 1)$ (Harr, 1977) (Figure 1).

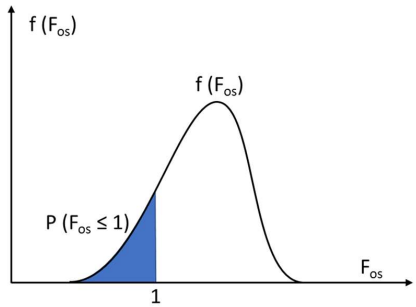

Fig. 1 Probability of failure can be evaluated as $p_f = p(FoS \leq 1)$

An alternative solution, mathematically more rigorous, consists in defining p_f as the probability that the forces or stresses D_f exceed the resistances R_f. That is equivalent to stating that $p_f=p(R_f-D_f. \leq 0)$ or simply $p_f=p(R_s \leq 0)$ (Figure 2).

$$pf = \int_{-\infty}^{\infty} F_c(C) f_D(D) dD \quad (1)$$

Oftentimes however, p_f is simply expressed as the probability of $FoS \leq 1$ (Figure 1), as this formulation is "conceptually nearer" to common practice approaches. The second family of "purely probabilistic" approaches groups together the methods involving probabilistic concept at mechanical level.

In the following paragraphs we will deal with examples relating to the first family which, from a practical point of view, has the advantage of allowing the use of traditional engineering methods.

To avoid unnecessarily complicated calculations, it is interesting to select the parameters presenting the greatest uncertainties. It is usual, for this purpose, to neglect the variability of the forces transmitted by buildings and other loadings to the slope. We therefore only consider geotechnical parameters as:

- cohesion c,
- friction φ,
- bulk density γ and finally
- position of the water table.

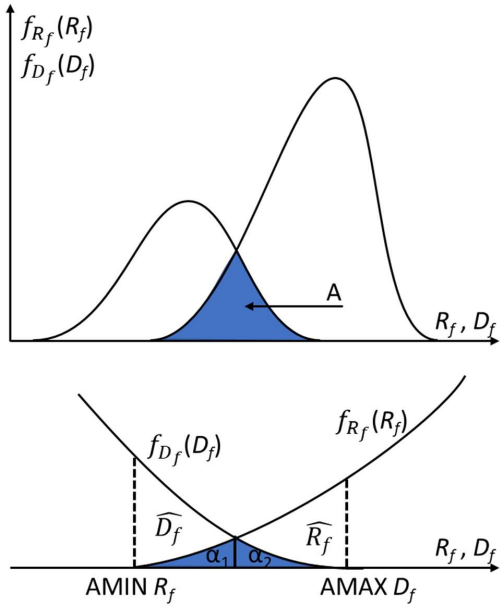

Fig. 2 Probability of failure can be evaluated as that p_f=p(R_f-D_f ≤0) or simply p_f=p(R_s≤0) provided the distributions are known: α1*α2 ≤ p_f ≤α1+α2 and for R_f and D_f independent, (Freudenthal et al., 1966).

Statistical studies carried out on "homogeneous" soils make it possible to eliminate γ, given its generally low variability (Recordon, Despond, 1977).

Numerous studies (Shultze, 1972, Hammit, 1966, Lumb, Holt, 1968) showed that the variability of the other soil parameters is relatively constant per soil types, e.g. various densities of sands, gravel and even clays. Variability is generally expressed with the coefficient of variation called V in this paper, i.e. the ratio of standard deviation and average value expressed in percentage. Thus, based on literature, it is oftentimes assumed, as a first approximation, V_φ= 10% -15% and V_c = 50% (careful with cohesion variability!) to evaluate a structure performance at the preliminary stages. Probabilistic evaluations can therefore be applied even if a statistical analysis of the characteristics of each soil layer is not economically possible. The unfortunate reality is that values obtained following this geomechanical correct procedure are indeed quite different from those obtained by observation of real-life structures.

A paper (Christian, Baecher, 2011) discusses ten unresolved problems in geotechnical engineering. The first one is: why are failures less frequent than our reliability studies predict?

The authors note that reliability studies carried out over the past few decades generally give probabilities of failure on the order of several percent or more for the usual range of uncertainties in soil properties and analytical tools. Then they state: "we do not observe this frequency of failures (in the field)." Thus, they ask: "why not?"

If we consider the typical V reported from soil engineering property testing are in the range discussed above, presuming a mean FoS=1.5, the corresponding p_f is evaluated in the vicinity of 0.1 for a Normal distribution of FoS. This value -0.1- is at least an order of magnitude larger than the observed frequency of adverse field performance! It is also at least two orders of magnitude larger than the frequency of all-modes failures of earth dams, as we showed in a 2013 paper

(Oboni, Oboni, 2013). Obviously, there are some underlying issues that make the purely geomechanical considerations insufficient. Below are four potential reasons for the systematic overestimation of p_f when using geomechanical models: Uncertainty in soil properties is being overestimated. If the V in the field is smaller than the value used to estimate the p_f, it will be overestimated.

1. We do not apply FoS to mean property values but to some conservative fraction of the mean. US Army Corps of Engineers practice, as an example, is to use a 1/3-rule in choosing engineering properties: the design property is taken at that value which is larger than 1/3 of the observations and smaller than 2/3 (USACE 2003). For Normally distributed data, that is approximately the mean less 0.4 standard deviations. This implies a p_f in the vicinity of 0.05. This last value is more in keeping with observed rates, but still too high.
2. The variation we observe in test data includes both actual variations of in situ properties and measurement error (i.e., noise). That measurement error can be large. Care must be exercised in assigning V to soil engineering properties, and we may over-estimate the uncertainties in soil properties by a great deal.
3. Many analytical models used to calculate FoS and p_f are not accurate. Most analytical models used in geotechnical engineering are conservatively biased.

It is however important to note a few other elements:

- the actual rate of unsatisfactory performance, leading to benchmark thresholds may be under-reported. Indeed, unless the failure is spectacular, it is unlikely that every case of failure, excessive settlement, slope distress, and so on is included in the data repositories for geotechnical facilities. That is why we stress the need for constant updates, calibration and re-evaluation.
- FoS are deterministic and do not consider the occurrence of extreme events along the life of the structure.
- FoS do not include the "history" of the structure, its management, and human factors.

3 CHARACTERIZING THE HAZARD OF A SLOPE

FoS and p_f are commonly used to characterize the hazard of a slope as, in this case, they describe the state of equilibrium of a potential volume (on a slope cross section) limited by the topography and a potential sliding surface with respect to sliding. Common methods to evaluate FoS and p_f are based on Limit Equilibrium Method (LEM) and do not support the type of risk-based decision making currently required in the mining industry (Adams, 2015).

As stated earlier, p_f can be determined by various means. Significant parameters are considered as stochastic variables defined either by their first and second moment (average and variance), possibly their bounds and in some cases their third statistical moment (skewness). If data quality and quantity is high, the Probability Density Function (PDF, aka distribution) of each parameter can be estimated by the analyst. Once all the significant selected parameters have been described as above, the calculation of p_f can proceed (Figures 1,2).

Based on the definitions above, FoS and p_f express the proneness of a potential volume (on a slope cross section) limited by the topography and a potential sliding surface to fail as a "monolith", thus they constitute a rough hazard quantification. However, while the first is deterministic and the second is probabilistic, both approaches are geomechanical, meaning they are based on forces and strength parameters. Thus, they deliver values that are not annualized, as they are precisely, geomechanical only.

Adams (2015) noted that a major problem of p_f evaluated using LEM is indeed the *lack of time dependency*: in the absence of time-dependent input variables, the computed p_f does not have a timescale. In order to calculate the annual p_f, the reference time is often assumed to be related to the design life of the slope. But in reality, the p_f of a slope is likely to be related to the rate of stress redistribution, the rate of material strength degradation (e.g. via weathering, etc.), and the temporal probabilities of triggering (extreme) events such as rainfall or earthquakes.

Furthermore, these classic geomechanical approaches have no provision for evaluating the impact of a multitude of important parameters such as human factors, monitoring maintenance and care of the slope under consideration, potential for exceptional meteorological conditions, etc.. In recent years more sophisticated approaches offering a blend between the geomechanical approaches and semi-empirical evaluations of the quality of the slope have been published, used and proven (Silva et al., 2008, referred to in this report as SLM). They allow to fill the gap of the "annualization of probabilities" and the lack of consideration for "human factors", maintenance, etc.. Thus, these allow to bridge over to estimating the number of potential accidents over a certain time, e.g. next five years, life of the structure. Of course, these approaches require regular updates as conditions and parameters change over time.

4 EARLY ATTEMPTS TO LINK FoS AND P_f

In this section we show how a geomechancal FoS-p_f relationship can be built, based on geomechanical probabilistic considerations. A simple slope is used as an example, varying the main geomechanical parameters and their uncertainties and possible correlations among them.

This deliberately simple example of application (Figure 3), lends itself well to showing the influence of uncertainties on the various parameters of LEM stability.

Geometric data:

- H[m], α, β [°]

Geotechnical data:

- c [kN x m^{-2}], V_c [%]
- φ [°], V_φ [%]
- γ [kN*m^{-3}].

Hydraulic data: no water table in this simple example

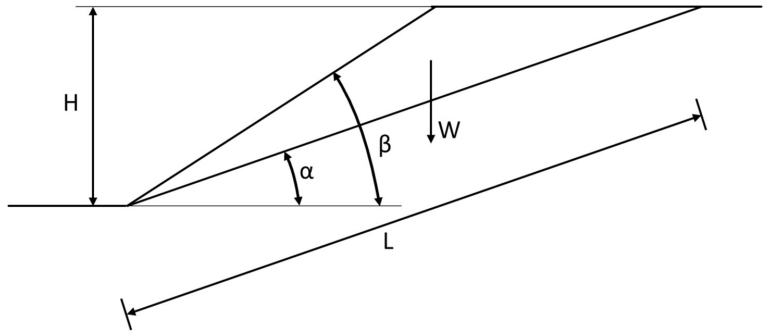

Fig. 3 A simple triangular slope used as an example in this paper.

Deterministic calculation:

$$FoS = \frac{cL}{W \sin\alpha} + \frac{\tan\varphi}{\tan\alpha} \tag{2}$$

With:

$$W = \frac{\gamma - H^2}{2}\left(\frac{1}{\tan\alpha} - \frac{1}{\tan\beta}\right) \tag{3}$$

$$L = \frac{H}{\sin\alpha} \tag{4}$$

By putting:

$$a = \frac{L}{W \sin \alpha} \tag{5}$$

$$b = \frac{1}{\tan \alpha} \tag{6}$$

$$p = \tan \varphi \tag{7}$$

We find the following linear expression where c and p are stochastic, while a and b are constants:

$$FoS = ac + bp \tag{8}$$

In case of a relation of the type:

$$y = \alpha_1 x_1 + \alpha_2 x_2 \tag{9}$$

which is exactly what we have here, we can evaluate the average $\bar{y}$, variance S_y^2 and then standard deviation S_y using respectively simple formulae as follows:

$$\bar{y} = \alpha_1 \overline{x_1} + \alpha_2 \overline{x_2} \tag{10}$$

$$S_y^2 = \alpha_1^2 S_{x_1}^2 + \alpha_2^2 S_{x_2}^2 + 2\alpha_1 \alpha_2 \rho_{x_1 x_2} S_{x_1} S_{x_2} \tag{11}$$

Where $\rho_{x_1 x_2}$ is the correlation coefficient between $x_1,\ x_2$.
By using the formulae above we find:

$$\overline{FoS} = a\bar{c} + b\bar{p} \tag{12}$$

$$S_{FoS}^2 = \mathrm{a}^2 \mathrm{S}_c^2 + \mathrm{b}^2 \mathrm{S}_p^2 + 2\mathrm{ab}\rho_{cp}\, S_c S_p \tag{13}$$

$$S_{FoS} = \sqrt{S_{FoS}^2} \tag{14}$$

In more complex cases (geometry, layers, water table, etc.) one can use point estimates methods (Rosenblueth, 1975) applied to LEM to define the variability of the FoS. With the evaluated mean and standard deviation of the FoS, and assuming that it follows a normal (or Gaussian) distribution, we can calculate $p_f = p$ [FoS <1] (Harr, 1977). The assumption regarding the Normal distribution of FoS is only acceptable if:

$$\overline{FoS} - 3S_{FoS} > 0 \tag{15}$$

In all other cases the use of an empirical distribution (e.g. Beta distribution) is recommended.
Numerical example data:

- H = 5 m
- α = 21.8° (2v/5h)
- β = 33.7° (2v/3h)
- γ = 20.0 kNm^{-3}
- $\bar{\varphi}$ = 15°, V_φ = 10%
- $\bar{p} = \tan \varphi = 0.268$
- $\bar{c} = 5$ kNm^{-2}
- V_c= 50%
- $\rho_{c\varphi}$=0%.

Calculation:

- L = 13.46 m
- W = 250 kN
- a = 0.144
- b = 2.5.

Thus

$$\overline{Fs} = 0.144 * 5 + 2.5 * 0.268 = 1.39$$

$$S_{Fs}^2 = 0.128$$

$$S_{Fs} = 0.358$$

And assuming FoS is following a Gaussian distribution have $p_f = 0.138 = 13.8\%$.

Using the data from the previous example, it is possible to study the variation of p_f as a function of the correlation $\rho_{c\varphi}$ (Figure 4 top left) and the differences in cohesion (Figure 4 right) and friction (Figure 4 bottom left). The influence of each parameter is studied while keeping the other two constants, as follows:

- $\rho_{c\varphi}$ = varies V_c= 50% $V\varphi$= 10%
- $\rho_{c\varphi}$ = 0 V_c= varies $V\varphi$= 10%
- $\rho_{c\varphi}$ = 0 V_c= 50% $V\varphi$= varies.

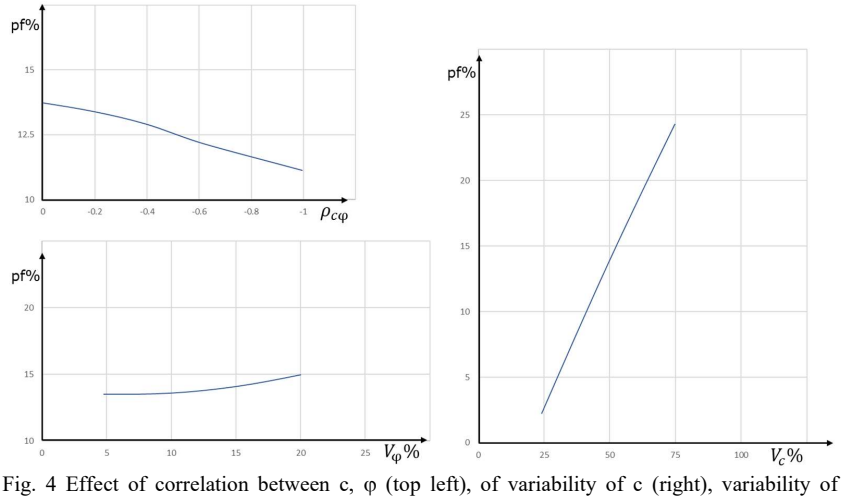

Fig. 4 Effect of correlation between c, φ (top left), of variability of c (right), variability of φ on the probability of failure p_f of the example slope. It can immediately be seen that the variability of the cohesion has by far the most significant impact on p_f.

For simple cases like the one presented in the previous paragraphs, it is possible to compile a chart useful for design (Figure 5). The interest of this type of chart also lies in allowing an easy comparison between a classic safety indicator, FoS, and a much more sensitive one, the probability of failure p_f.

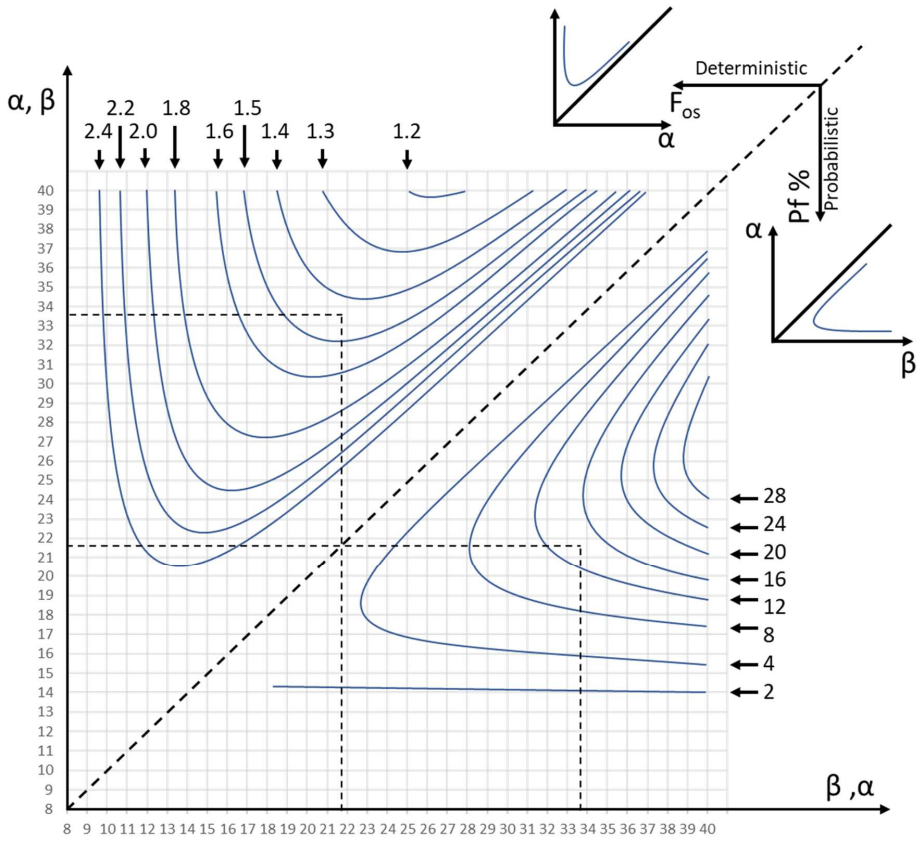

Fig. 5 Chart of the comparison between FoS and p_f for the case studied $\rho_{c\varphi}$= 0. Dotted lines: solution for the case α = 21.8° (2v/5h), β = 33.7° (2v/3h). FoS = 1.42; p_f = 14%

5 MODERN ATTEMPTS TO LINK FOS AND POF

As stated earlier, in recent years various authors (Silva et al., 2008, Altarejos-García et al, 2015) have expressed the annual probability of failure as a combination of Key Performance Indicators (KPIs), including human factors and quality of studies, design, monitoring, maintenance. These expressions have generally been empirical or semi-empirical. In some cases, these formulations have found fierce opposition: their detractors consider them as doubtful and unverifiable, however, without delivering a counterproof.

In order to work within the effort limits normally consented for this type of risk assessment, especially if swift prioritization of slopes' portfolios is the goal, we will now examine if the set of SLM empirical relations between FoS and p_f could be used.

As with all empirical and simplified approaches caution must be exerted before using these slopes' relations for tailings dams, in particular because those publications makes neither explicit mention of construction mode (downstream, centre-line, upstream) nor provide a specific discussion of seismic loading, static and/or dynamic liquefaction. In our practice, we have modified and re-calibrated these approaches specifically for tailings dams and other structures (Oboni, Oboni 2019).

SLM links the FoS (stability) defined by the geotechnical engineers in charge of a project, using classical stability methods, to the annual p_f for slopes.

In order to link FoS to p_f, the first step is to define the "category" of the structure under examination. This is done by examining sequentially the aspects of the design (D1, investigation; D2, testing; D3, analyses and documentation) and construction (CO) as well as operations and monitoring (OM).

The methodology considers four categories ranging from I (best) to IV (poor, i.e., non-engineered). Experience has shown (over a rather large array of cases studied by the authors) that structures with high failure consequences are generally designed, built and operated in such a way that they fall into category I or between I and II. Of course, if a structure has received little or no engineering it will fall in category III and even IV.

The approach lends itself to define the causality of the potential failure. Figure 6 shows a pie diagram for two slopes (names X1 -right-, X2 -left-) in a same project where the different KPIs lead to different causalities distributions.

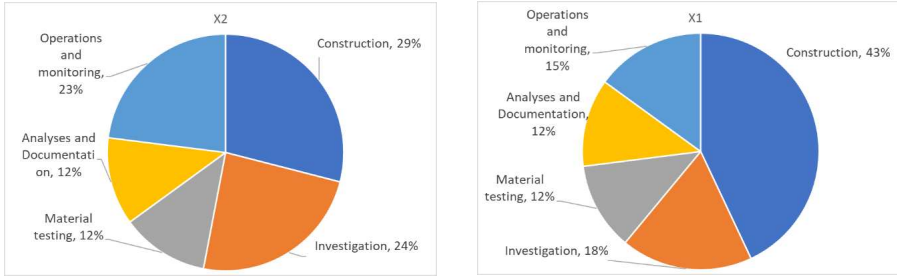

Fig. 6 Causality pie diagrams for two slopes in the same project

Figure 7 shows the semi-empirical FoS vs. p_f for sections X1,X2 vs. world-wide performance benchmark for tailings dams over the last hundred years (Oboni, Oboni, 2013, Oboni, Oboni, 2016). We can see from Figure 7 that if the engineer evaluated a FoS slightly above 1.3, both slopes X1 and X2 would "intersect" the historic benchmark of tailings dams (10^{-3} to $1.2*10^{-4}$ respectively for the decades around 1979 and 1999).

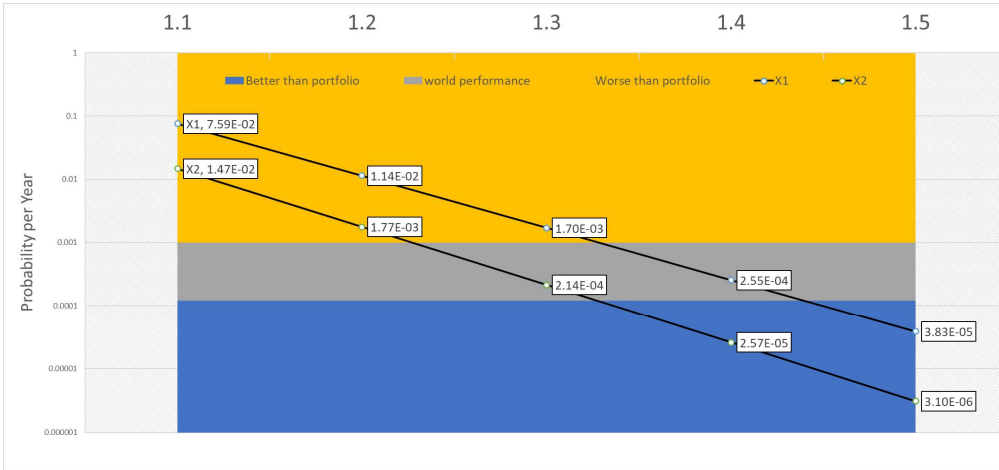

Fig. 7 FoS vs. annual p_f for slopes X1, X2 vs. world-wide benchmark for tailings dams. NB: the lowest annual probability shown on the vertical axis is 10^{-6} which corresponds to the credibility threshold in hazardous industries. The horizontal axis displays the FoS.

This result makes sense: as the two slopes are "common practice" slopes with an "average level" of investigation, design, construction, management, maintenance and monitoring it is logical that they would have a forecasted behavior similar to their peers around the world.

Now, from the prior section we remember that the simple slope example, with a geomechanical FoS appx. 1.4, had a p_f of 14%. That result does not make any sense! How is it possible that such a slope, that any engineer would consider as "safe" has such a high evaluation of the p_f, that does not match at all world-wide real-life experience? In the next section we endeavor to bring an answer to this question.

6 COMPARING THE APPROACHES

As described earlier (Christian, Baecher, 2011) the gap between geomechanical models and reality is a known fact. In the case cited above, it is in the order of two orders of magnitude.

We know out of experience that the gap between geomechanically derived p_f and semi-empirical approaches is reduced if better models are used. In a recent real-life risk assessment we noticed, for example, that using sophisticated 3-D slope stability analyses led the engineers to p_f within the same order of magnitude, still with the geomechanical values higher (and mostly out of range) with respect to the semi-empirical ones and the historic benchmarks (Table 1). Within the same study it also appeared that minor changes in numerical interpolation techniques necessary with the 3D slope stability method would have brought the geomechanical p_f within reach of the semi-empirical p_f, the difference being of course the effect of many KPIs that the geomechanical p_f does not consider and the lack of systemic view of geomechanical approaches, as discussed below. Remember that geomechanical p_f are not annualized, thus comparisons must be cautious.

Table 1. Probability of failure of a slope

Slope	3D slope analysis p_f	Reduction applied due to interpolation p_f	Empirical p_f annualized
1	$6.9*10^{-2}$	$3.5*10^{-2}$	$1.2*10^{-2}$
2	$9.6*10^{-2}$	$4.8*10^{-2}$	$3.0*10^{-2}$
3	$13.6*10^{-2}$	$6.8*10^{-2}$	$2.9*10^{-2}$

Now, let's push the analysis a bit further. We carried out a number of trials using a probabilistic geomechanical approach and compared the results to a semi-empirical empirical methodology (Oboni, Oboni, 2020). These trials considered cohesive and granular slopes of non-engineered materials (natural soils).

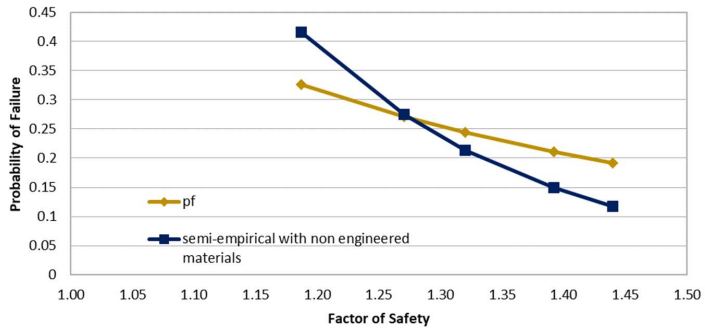

Fig. 8 Comparison of the direct geomechanical probabilistic approach (yellow) and the semi-empirical method results for cohesive soils (blue). These results are not directly comparable as only one is annualized.

In each case we found comparable results (that is, within the same order of magnitude) of the p_f, as depicted in Figures 8 and 9 for non-engineered structures and the purely geomechanical evaluation respectively for cohesive and granular soils.

As the probability of failure of real-life dams lies in a range of six orders of magnitude and world-wide historic tailings dams performance lies within one order of magnitude, finding a correspondence between a theoretical and empirical p_f within one order of magnitude is sufficient for the purposes, for example, of portfolio prioritization, given all the other present uncertainties. Thus, it can be assumed that the direct geomechanical probabilistic approach and the empirical method deliver comparable results for non-engineered (natural) materials.

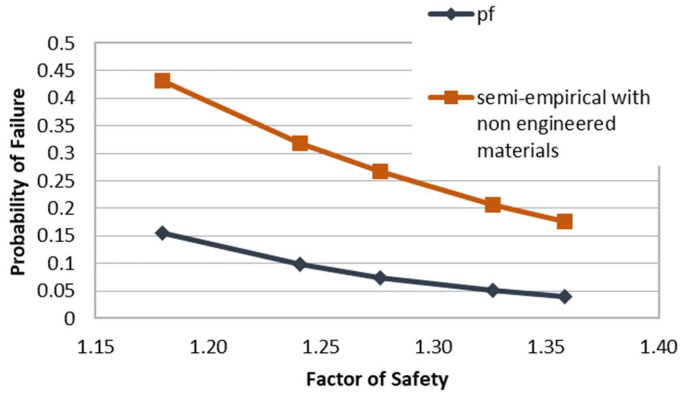

Fig. 9 Comparison of the direct geomechanical probabilistic approach (orange) and the semi-empirical method results for granular soils. These results are not directly comparable as only one is annualized.

Now, engineered materials have fewer uncertainties than natural non engineered ones, as they are selected and carefully compacted under controlled water content. This reduces their variability. Proper management, monitoring, etc., further reduce uncertainties and thus enhance reliability of structures using them.

As a result, engineered slopes necessarily have way better (lower) p_f than non-engineered slopes and the empirical methods reflect the reduction of uncertainties leading to lower annualized probabilities for each value of FoS. We think that this reasoning "solves" the question raised by Christian and Baecher (2011).

7 CONCLUSIONS

The ability to generate and compare FoS-p_f relationship is paramount for the formulation of risk informed design and to foster engineer's confidence in probabilistic solutions.

Our advice is to « forget » the FoS as a decision tool and only perform probabilistic analyses. Our preference is to rely on semi-empirical systemic approaches, provided they are coupled with benchmarking, to ensure anchoring to reality. Geomechanical p_f can be used for comparing design alternatives among themselves, but not to perform risk assessments, in particular at portfolio level. Indeed, geomechanical p_f are too high and correspond to non-engineered geotechnical structures. However, one big merit of the purely geomechanical approaches is to show, for example, that FoS should be different for slopes built with different materials and that, in particular, clayey slopes should have a larger FoS than granular slopes, because the variability of cohesion is way larger than the variability of friction.

REFERENCES

Adams, B.M., 2015, Slope stability acceptance criteria for opencast mine design. In Proceedings of the 12th Australia—New Zealand conference on geomechanics, Wellington, New Zealand, Paper (No. 120).

Alonso, E.E., 1976, Risk analysis of slopes and its application to slopes in Canadian sensitive clays. Geotechnique, 26(3), pp.453-472.

Altarejos-García, L., Escuder-Bueno, I. and Morales-Torres, A., 2015, Advances on the failure analysis of the Dam—Foundation interface of concrete dams. Materials, 8(12), pp.8255-8278.

Baecher, G., Geostatistics, 1984, Reliability and Risk Assessment in Geotechnical Engineering, Geostatistics for natural resources characterization, Part II, pp 731-744.

Christian, J. T., Baecher, G.B., 2011, Unresolved Problems in Geotechnical Risk and Reliability, Geotechnical Special Publication.

Freudenthal, A.M., Garrelts, J.M. and Shinozuka, M., 1966, The Analysis of Structural Safety, ASCE, Vol. 92, No. ST, 1, pp.267-325.

Hammitt, G.M., 1966, Statistical analysis of data from a comparative laboratory test program sponsored by ACIL.

Harr, M.E., 1977. Mechanics of particulate media (ISBN 0-07-26698-6). McGraw-Hill.

Lumb, P., Holt, J.K., 1968, The undrained shear strength of a soft marine clay from Hong Kong. Géotechnique, 18 (1), pp. 25–36.

Kanjanakul, C., Chub-Uppakarn, T., 2018, Method to estimate the system probability of failure for slope stability analysis. International Journal, 14(45), pp.162-169.

Kavvadas, M., Karlaftis, M., Fortsakis, P. and Stylianidi, E., 2009, Probabilistic analysis in slope stability. In Proceedings from the 17th International Conference on Soil Mechanics and Geotechnical Engineering (pp. 1650-1653).

Oboni, C., Oboni F., 2013, Factual and Foreseeable Reliability of Tailings Dams and Nuclear Reactors -a Societal Acceptability Perspective, Tailings and Mine Waste 2013, Banff, AB.

Oboni, F., Bourdeau, P.L. and Russo, F., 1984, Utilisation des processus markoviens dans les analyses de stabilité des pentes. 2ème Séminaire sur l'Utilisation des Méthodes Probabilistes en Géotechnique, LMS, EPFL, Lausanne.

Oboni, F. Bourdeau, P.L., 1983. Determination of the critical slip surface in stability problems. In International conference on applications of statistics and probability in soil and structural engineering. 4 (pp. 1413-1424).

Oboni, F., Bourdeau, P.L. and Bonnard, C., 1984. Probabilistic analysis of Swiss landslides. In Proceedings of IVth International Symposium on Landslides–ISL (Toronto) (Vol. 2, pp. 473-478).

Oboni, F., Martinenghi, T., 1984, Quelques aspects pratiques du calcul probabiliste en geotechnique, Ingenieurs et Architectes Suisses, No 3.

Oboni, F., Oboni, C., 2016, A systemic look at tailings dams failure process, Tailings and Mine Waste 2016, Keystone, Colorado, USA, October 2-5.

Oboni, F. and Oboni, C., 2020. Tailings Dam Management for the Twenty-First Century. Springer International Publishing.

Oboni F., Oboni C., 2019, Tailings dams quantitative risk prioritization, Tailings and Mine Waste 2019, Vancouver, BC.

Peterson, J. L., 1999, Probability analysis of slope stability, Graduate Theses, Dissertations, and Problem Reports. 990, College of Engineering and Mineral Resources At West Virginia University.

Recordon, E., Despond, J. M., 1977, Dispersion des caractéristiques des sols considérés comme homogènes. IX ICSMFE, Session spéciale n° 6, Tokyo.

Rosenblueth, E., 1975. Point estimates for probability moments. Proceedings of the National Academy of Sciences, 72(10), pp.3812-3814.

Shultze, E., 1972, Frequency distributions and correlation of soil properties. Proc. ICASP I, Hong-Kong University Press, Hong-Kong.

Silva, F., Lambe, T.W. and Marr, W.A., 2008. Probability and risk of slope failure. Journal of geotechnical and geoenvironmental engineering, 134(12), pp.1691-1699.

USACE, 2003, Slope Stability. U. S. Army Corps of Engineers. Washington, USACE.

Boosting a more efficient Tailings Dam risk management service through an innovative IoT ecosystem

Andrea Bartoli
Worldsensing S.L, Barcelona, Spain

Denis Guilhot
Worldsensing S.L, Barcelona, Spain

Xavier Vilajosana
Worldsensing S.L, Barcelona, Spain

ABSTRACT: Today, implementing measures to ensure that risks are properly managed is mandatory for tailings dam monitoring operators, but traditional operations and processes are not cost-effective. While the collapse of some tailing dams show that physical/structural, operational, and environmental aspects are serious issues to be monitored, efforts to reduce and ultimately avoid risks are often taken on a reactive basis. To avoid these failures and run safe operations, mining operators and engineers should create and follow a proactive and more affordable prevention and monitoring framework for tailings dam. The aim of this paper is to present an evolutive Internet of Things (IOT)-based monitoring and operational risk management framework based on the ISO 31000 Standard adapted for securing tailings dams that will: a) vastly improve the monitoring and maintenance processes of mines infrastructure and b) prevent, detect, respond and mitigate physical threats that mine infrastructure operators are facing today in the management of tailings dams.

1 INTRODUCTION

Securing mine sites is a challenging task due to the complexity of the infrastructure, the variety of physical and digital components, the distribution of assets and machineries, and the large number of workers and stakeholders involved. In the last years, mine operator companies have been adopting digital components (innovative Information and Communications Technologies - ICT) but still use archaic/manual processes, thus making the protection of the critical assets a costly and highly complex problem. Furthermore, existing mines' assets are deployed across large and harsh environments, where they are vulnerable to a long list of human errors and natural disasters, including climate change issues.

The aim of this paper is to present an evolutive monitoring and operational risk management framework by connecting the PHYSICAL and DIGITAL worlds in order to take advantage of the recent ICT innovations: IoT, drones, earth observation algorithms, etc., at the same time as exploiting novel mathematical models and simulation tools to deal with the continuously increasing sophistication issues originating from the coexistence of multiple technology and to comply with a stricter legal framework to guarantee sustainability and safety for tailings dams.

The proposed Internet of Things (IoT) end-to-end tailings dam monitoring system connects several data collection and management systems and processes the information that is relevant for the stability analysis, such as pore pressure from piezometers, horizontal displacements from inclinometers or stresses from pressure cells, etc. Once new data is available, the proposed model automatically incorporates this information to the stability analysis calculation and performs a safety factor calculation in real-time using the available computing infrastructure. This new paradigm of risk management provides stability assessment in terms of safety factors in a continuous manner (from daily to weekly) connecting the analysis tools and the monitoring data.

The IoT is about extending the power of the internet beyond computers and smartphones to a whole range of other things, processes, and environments. Those "connected" things are used to gather information, send information back, or both. IoT provides to mining actors and decision-makers better insight into and control over the 99 percent of objects and environments that are deployed in mining infrastructure and assets (even in remote location). And by doing so, IoT allows mining stakeholders to be more connected to the world around them and to do more meaningful, higher-level work and to take smarter decision driven by reliable data. IoT is mainly build up from the coexistence of three main technology aspects (see Figure 1):

- data collection smart objects in "**Mining**".
- data transmission for **"Connectivity"**.
- data management, especially exploiting data processing available in **"Internet"**.

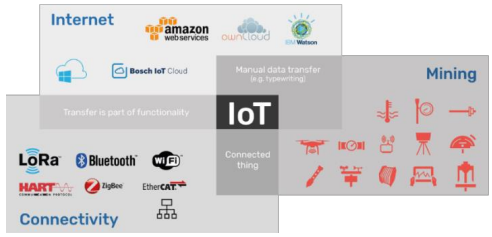

Figure 1- Mining equipment, connectivity, and internet enabled applications convergence.

This paper is structured as follow: in Section 2, we will present the current safety risks for tailings dam, in Section 3, we will analyze the state of art regarding products in the market and main research and innovation opportunities for tailings dam monitoring, in Section 4, we will introduce the proposed risk management framework based on ISO 31000, in Section 5, we present the complete end-to-end architecture while in Section 6 and 7 we will analyze a specific Use Case in Brazil and we will provide simulation results of the economic impact of the proposed ecosystem mainly stressing the benefits of IoT wireless technology. Section 8 concludes the document.

2 MINING ISSUES AND SAFETY RISK

One of the most critical within a mine are the tailings dams. Tailings dams are embankments constructed to store the tailings generated in a mineral processing plant. Tailings often contain hazardous substances that can significantly contaminate the environment. The failure of a tailing dam causes irreversible damage to ecosystems leading to large economic losses and even compromising human lives (Song, et. al 2011). The major causes for tailing dam failures can be attributed to different events that traditionally are classified in three wide categories including physical/structural, environmental, and operational (Zhang, et. al 2011).

2.1 *Tailings dam issues and failure causes*

As described from past studies (Villavicencio, et. al 2014), the major structural problems of tailings dam involve deficiencies in the construction method, poor compaction, internal erosion, high fine contents in the tailings and an elevated degree of saturation. These physical/structural issues may be the focus of critical failures including structural or foundation collapsing, mine subsidence and seepage. Poor designs and modifications over time may also cause the dam to overtop or even overflow, causing different events such as floods or landslides.

External conditions also have a significant importance in the safety of tailings dams. Certain areas are for example subject to external hazards, such as extreme weather conditions or subject to geological events including earthquakes, seismic activity, or seasonal landslides. The major causes for tailing dam failure due to these external events are the liquefaction (due to earthquakes), slope instability (with seismic induced deformations) and overtopping. Table 1. summarizes the main tailings dam failure causes.

Table 1. Main causes of critical failures in tailing dams.

Physical /Structural	Environmental	Operational
• Slope instability	• Rain	• Design
• Seepage	• Noise	• Construction
• Internal erosion	• Vibration	• Monitoring
• Overtopping	• Groundwater	• Maintenance
• Structural failure	• Surface water	• Etc.
• Foundation failure	• Dust	
• Subsidence	• Etc.	
• Etc.		

2.2 *Risks*

The safety risks associated with the failure of tailings dams impose a severe threat to the environment due to the presence of hazardous and toxic elements in the tailings, including heavy metals, arsenic and cyanide. Any release of these substances into fluvial systems has a long-standing impact in the ecosystem, including acidification of the river, as the concentration of those pollutants lasts for decades (Hatje, et. al 2017). Biosphere impact happens during the early stages of a failure, being drowning and suffocation the main causes for loss of life. In a longer term, toxic elements may be transported or deposited in agricultural fields entering the food chain or polluting water.

2.3 *Safety risk sources*

In engineering, a factor of safety (FoS), also known as safety factor (SF), expresses how much stronger a system is than it needs to be for an intended load. Safety factors are often calculated using detailed analysis because comprehensive testing is impractical on many projects, such as bridges and buildings, but the structure's ability to carry a load must be determined to a reasonable accuracy.

Many systems are intentionally built much stronger than needed for normal usage to allow for emergency situations, unexpected loads, misuse, or degradation. With respect to slope stability (potential failure for tailings dam), SF is the ratio of shear resistance to driving force along a potential failure plane:

$$Safety\ Factor\ (SF) = \frac{Shear\ Strength}{Shear\ Stress}$$

A SF greater than 1.0 implies that the available shear strength to resist failure is greater than the driving force to initiate failure. There is no means of quantitatively measuring the "real" SF of a slope at a given time. Therefore, the SF of a slope is estimated based on industry standard analytical methods with assumed material parameters inferred from various data sources.

In the context of tailings dam, one big challenge is that the variables used to calculate the SF can change over time, so a dam that is deemed stable upon construction may become unstable later. These changes can affect not only the SF itself but also the probability of failure. The only way to detect changes in the SF and the probability of failure has traditionally been for dam design professionals to re-run geotechnical and soil models using up-to-date monitoring data. The need to do this on a regular or ongoing basis is increasingly being incorporated into safety risk management system in-line with ISO 31000 guidelines.

3 TECHNOLOGICAL STATE OF THE ART

The monitoring and control of parts of critical infrastructures has been addressed by numerous academic and industrial developments which materialized a rich ecosystem of solutions. Those solutions are mostly verticalized and aim to address specific problems in the mining infrastructure being designed from different perspectives and goals. A holistic approach is not entirely addressed and critical infrastructures such as tailings dam end up integrating isolated and fragmented subsystems to address specific problems.

3.1 *Data Collection*

The smart sensor and remote monitoring paradigm have promoted the development of low cost, low power, mostly unattended monitoring systems that can be deployed in vast geographic areas to provide specific monitoring points of a magnitude. The research in the technological and application areas of smart devices is vast and addresses many challenges such as network coverage, low power sensing and smart data processing algorithms (Sganzerla, et. al 2016). We can find in the market numerous geotechnical development companies providing sensing solutions for specific applications, but the holistic end-to-end approach is mostly not addressed.

The observation of a vast terrain is commonly addressed through image processing technologies, mainly observing the geological evolution of the area. Advanced technologies rely on satellite remote sensing, referred to as Interferometric synthetic aperture radar (InSAR) in which terrain deformation is analyzed (Iannacone, et. al 2018). The images can also be obtained from dual synthetic aperture radar (SAR) systems and video cameras installed in drones. InSAR Stability Monitoring is used as an offline tool to provide early warning of ground movement across the entire mine site. This warning system triggers operators when to mobilize for visual inspection or assign other available site resources like ground-based radar (GB-SAR) or drone-based systems for an emergency survey of the site (Hui, et. al 2018, Draeyer, et al 2014).

GNSS solutions aim to provide accurate positioning or fix reference points within the mine infrastructure to enable multiple applications such as machine guidance, grading, dozing, drilling, collision avoidance, surveying, and fleet management, among others. Most GNSS systems designed for the mining industry exploit concepts such as Differential GNSS (DGNSS) or Real Time Kinematics (RTK). The system requires reference stations with a very accurately defined position allowing the deviations between measured position and the actual position be determined. These corrections can thereby be used for the correction of the measured positions of other GNSS user receivers (Li, et. al 2011).

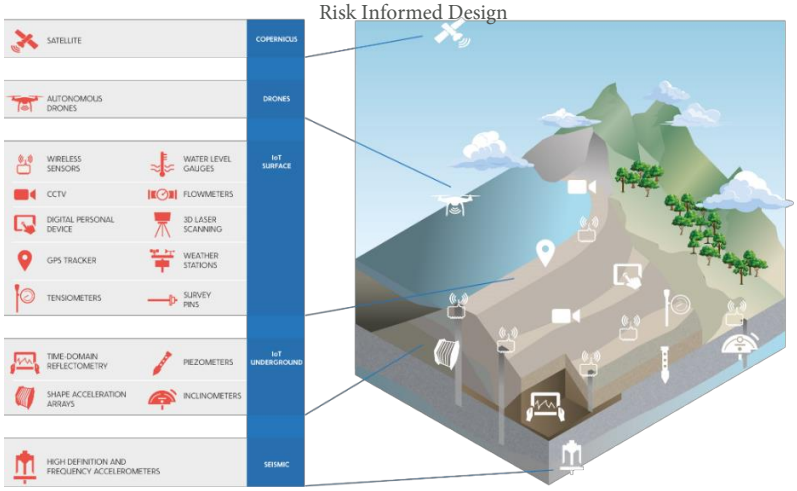

Figure 2 Types of IoT/monitoring solutions in the mining sector

3.2 *Data Transmission*

A major and disruptive change in the last years has been promoted by the emergence of wireless communication technologies with special application in battery operated, isolated, remote sensing and monitoring systems. This has enabled the geotechnical sector to develop automated solutions leveraging wireless communication capabilities. However, as the communications market is very fragmented, we observe a wide range of technologies being used in existing products and solutions. Yet, as the communication technologies trade off bandwidth to data rate, data rate to energy consumption, and energy consumption to transmission power, application requirements limit the number of options available.

Short range wireless technologies are mainly used for low data rate, ultra-low power applications in which battery operation is critical. Those encompass different protocol stacks built on top of the IEEE802.15 standard suite, including IEEE802.15.1 (Bluetooth) and IEEE802.15.4 technologies. Short range wireless provides a coverage in the order of 10s of meters in indoor industrial deployments while, in outdoor scenarios, few hundred meters can be reached. Coverage extension is provided by mesh network topologies, although they still require dense and well-connected structures to deliver the reliability required in such scenarios (Palattella et. al 2013). High data rate, short range wireless is also present in the field, mainly with IEEE802.11 (WiFi) based communication. While high data rate is supported, they are limited in terms of reliability and range, being an option mostly limited for indoor non-dense deployments.

Low Power Wide Area networks (Raza et, al. 2017) emerged as an alternative to the short-range, low power technologies, LPWAN trade off data rate to range but maintain the ultra-low power operation. This technology, despite its bandwidth and data rate limitations (sometimes limited to few messages per hour), is quickly entering the critical infrastructure monitoring market as a large set of use cases can be supported even with those limitations. Seeing the success of LPWAN technologies, the 3GPP consortium has also focused on providing broadband connectivity to support IoT and industrial use cases (Martinez, et. al 2019). The so-called 5G technology is evolving to support LPWAN scenarios but providing higher levels of guarantees given the spectrum in use is proprietary. In addition, the upcoming 3GPP releases are already defining radio technologies to support ultra-reliable low latency (Froytlog, et. al 2019) use cases, aiming for real time control. This technology may revolutionize the infrastructure control and monitoring industry given that proper use cases are clearly identified.

3.3 *Data Management*

In most of the mining sites, data from specific sensors is still manually collected and post-processed offline through specialized tools for the sector. Most of the decisions are based on the results of this offline analysis. As most of the tools are designed to address one issue, data fusion

and correlations are generally done by experts in the matter and relying on their expertise to identify critical situations by studying those different information sources.

In the ICT world, automation and data fusion are widely adopted methodologies applied in sectors such as health, finance, energy, and commerce among many others (Lau, et. al 2019). These techniques rely on Cloud and Edge computing infrastructures and data mining, and knowledge management methods that enable knowledge extraction, and derive assessment and recommendations to the operators. In the mining industry, this holistic approach is still not fully developed, nor the advantages it brings fully assessed. We therefore present the integral *IoT end-to-end tailings dam monitoring system* as a holistic system in which several data collection and management sub-systems are interconnected, and data fused to derive tailing dam stability analysis prospects, etc.

4 INNOVATIVE RISK MANAGEMENT FRAMEWORK IN-LINE WITH ISO 31000

Risk management needs to be addressed from a holistic perspective, embracing all the technical, operational, and human resources in the mining field as well as defining action plans including preventive and reactive strategies to address and respond to risks. The ISO 31000 Risk Management (ISO31000, 2020) introduces the concept of continuous monitoring for typical business and organization as a tool to minimize operational risks as well as define the procedures for proper planning, monitoring, and addressing risk situations.

To fully materialize the framework proposed by the ISO 31000, innovative technologies become essential as automation enables widespread monitoring of processes and human activities to control and assess the risk level in an efficient, safe, and cost-effective manner. In this section, we map the ISO principles and methodology to technological requirements procedures and existing technologies that can be used to facilitate the risk assessment and design of mitigation strategies. In Table 2. we present a mapping between the principles defined by the ISO31000 to the requirements of an ICT integrated solution.

Table 2. Mapping between the IS31000 principles and requirements to any ICT based solution.

ISO Principles	ICT requirements
Continual improvement	● Virtualization of software and hardware components to be updatable and adaptable to continuous improvement, ● Support for over the air updates, ● Standards compliance to support multi-vendor technologies.
Integrated	● Systems to provide holistic vision exploiting APIs and connectors, ● Data fusion, ● Cross technology information.
Structured and comprehensive	● Functionalities should be structured organized at different levels, having a complete view of the processes, ● Inter departmental communication, ● Knowledge extraction from semantics of the metadata.
Customized	● Configurable, ● Multitenant, multivendor, ● Technology needs to be compliant to regulations and Standards.
Inclusive	● Favour open source for extensibility, ● Open APIs and extensible, ● Secure.
Dynamic	● Scalable and upgradable, ● Support integration to other systems, ● Interoperable to different standards.
Best available information	● Derives information from raw data, ● Extends the information through predictive and forecasting techniques, ● Enables filtering and segmentation of the information.
Human and cultural factors	● Adapted to human factors including: Safety, human operations, ● Support for training, ● Dynamization of teams through engagement (e.g. gamification).

The implementation of risk management policies goes beyond applying the principles to the technology requirements, it also requires following a methodology to properly deploy the risk management infrastructure. This is a continuous and iterative process in which technology and proper assessment and evaluation are interrelated. Following the methodology defined by the ISO31000. Table 3. describes the required steps and how they map to specific processes in the deployment of an ICT technology.

Table 3. Mapping between the ISO31000 framework and methodology to the design and operation of ICT technology in the mine site.

ISO31000 Framework	Mapping to an ICT development and integration process
Design	The design phase involves the proper selection of ICT technologies based on the use case requirements. This may involve selecting different solutions from different vendors and defining the procedures for their integration. It may involve the definition of pilots in localized and safe areas before committing for a global deployment. It also involves the design of the human processes to operate the technology, identifying possible training needs.
Implementation	The technology needs to be deployed in the infrastructure, probably in early pilots in a first round and culminating in a full deployment in subsequent iterations. During the process integration needs are requalified according to the functionalities and specific needs for the target deployment. Moreover, clear procedures must be defined to deploy the selected technology accordingly to specification. In this case, the coexistence of several technology in a holistic solution will be a key factor to evaluate.
Evaluation	Assess the performance of the solution through well-defined KPIs. In a first stage in the pilot areas. In this step both the technology and operational aspects are evaluated and corrected according to the identified results. The evaluation of integrated systems needs to involve different departments and verticals within the infrastructure to assess the value of cross-department information.
Improvement	After an evaluation, for each of the iterations there is a need to re-plan and improve the solution based on the lessons learnt. The complete system must be re-configured with new parameters where such configuration will depend on two main drivers: external factor and result evaluation.
Integration	After the consolidation of one or several iterations, the systems need to be integrated to operational subsystems of the infrastructure. Such new solution will become an innovative process in the typical industrial operation and will guarantee added value at several level.

At this point, with a clear requirements list and a well-defined integration methodology there is a need to map the specific requirements in terms of risk mitigation to specific ICT technologies. For that purposes, Table 4. presents the mapping between innovative IoT and ICT technology versus the already defined tailings dam main threats (Section 2).

5 INNOVATIVE END-TO-END ARCHITECTURE

In this Section, we introduce the proposed holistic risk management solution for tailings dam. Such solution is subdivided in four concepts:

- **Concept_1 – Digital physical assets:** The operational control center of a mine infrastructure has to receive appropriate information regarding tailings dam stability (the technical staff needs to have real-time access to reliable information) to detect anomalous situations, plan actions and take necessary corrective measures. Such information originates from various distributed diverse sources, which could be structured in 5-layer: 1) deep underground, 2) underground, 3) surface, 4) aerial and 5) space. It will be orchestrated and exploited to gather distributed and accurate data regarding mines infrastructure and asset state (including staff position and updated working processes). As an example, the following source of data must

Table 4. Mapping of risks and technologies to mitigate them.

Monitoring & Review - Identification / Analysis / Evolution			
Risks			**Technology as solution**
Physical	Slope instability	IoT tiltmeter	**Tiltmeter:** It is a sensitive inclinometer designed to measure very small changes from the vertical or horizontal level, either on the ground or in structures.
		InSAR	**Interferometric synthetic aperture radar:** this geodetic method uses two or more synthetic aperture radar images to generate maps of surface deformation or digital elevation, using differences in the phase of the waves returning to the satellite
		GBSAR	**Ground-based synthetic aperture radar:** GBSAR s an efficient tool to monitor the potential land deformation area; it is used to continuous monitor the high-risk area which prone to landslide.
	Seepage	IoT piezometer	**Piezometer:** Electric piezometers consist of a deflecting diaphragm and a porous filter separated by a small reservoir of water. Deflections of the diaphragm are detected using a vibrating wire or a strain gauge and are converted to an equivalent pressure using a suitable calibration.
	Internal erosion	IoT in-place inclinometer	**In-place Inclinometers (IPI)** are used primarily for monitoring the downstream concrete face of rock filled dams or other inclined applications. They consist of a series of wheeled sensors placed at various depths within a casing which are interconnected with extension rods.
	Overtopping	IoT level sensor	**Level sensors** are used to detect the level of substances in specific area. Such substances include liquids, slurries, etc. Level measurements can be done inside containers or it can be the level of a "lake" surface. Pressure, radar, and ultrasonic sensors could be used in this specific application.
	Structural and foundation failure	IoT load cell	**Load cell sensor:** it is a transducer which converts force into a measurable electrical output. Strain gauge load cells are the most used type.
		IoT extensometer	**Extensometer:** It is a device that is used to measure changes in the length of an object. It is developed to monitor lateral and longitudinal displacement from a fixed point of reference.
		IoT crack meter	**Crack meter:** It is used to measure movement across surface cracks and joints in concrete, rock, soil, and structures. They consist of a sensor outer body tube and an inner free-sliding rod which is connected at the internal end to a vibrating wire sensor by a spring
	Subsidence	GNSS	**GNSS**: It provides general-purpose, real-time, high-accuracy, absolute positioning applications, with additionally accurate heading measurements and relative positioning. It is used to detect specific movement in a surface.
		IoT extensometer	See above extensometer
		IoT laser	**Laser:** It measures the relative distance between pairs of reference points. One of the two points can be a natural surface or target foils while the node can be placed at the other end point. It can be used to measure changes in distance for slope movements and for fracture and faults surveillance
Environmental	Rain	IoT pluviometer sensor	**Pluviometer:** It is an instrument used to gather and measure the amount of liquid precipitation over an area in a predefined period
	Noise	IoT acoustic sensor	**Acoustic sensor:** It is an electronic device that measure sound levels. This sensor can detection a variation/modulation of the sound waves to sense a phenomenon.
	Vibration	IoT accelerometer	**Accelerometer:** Vibration is most measured using a ceramic piezoelectric sensor or accelerometer. An accelerometer is a sensor that measures the dynamic acceleration of a physical device as a voltage. Accelerometers are full-contact transducers typically mounted directly on the physical elements.
	Groundwater	IoT piezometer	See above piezometer
	Surface	IoT level sensor	See above level sensor
	Dust	IoT dust sensor	**Dust sensor** detects the dust particle concentration in air by using several techniques, such as optical sensing method.
	Wind	IoT anemometer	**Anemometer:** it is a device for measuring the speed of airflow in the atmosphere, in wind tunnels, and in other gas-flow applications
Operational	Design, Construction, Monitoring, Maintenance	Risk management system (ISO 31000)	An integrated solution, where the geodetic, geospatial and geotechnical sensors are plugged to IoT devices (to provide the interconnected capability) together with GBSAR and inSAR source of information, with continuous monitoring features could provide the basis for an efficient and secure Tailings Dam monitoring and maintenance system able to validate the daily operations as well as detect potential issues at design and construction level.

be integrated: seismic, IoT, trackers, cameras, drones, InSAR, GBSAR, etc.

- **Concept_2 and Concept_3 – Data Hub and Analytics:** Basic and advanced SW-tools will be interconnected to process heterogenous data and to guarantee basic requirements such as security, scalability, reliability, delay, etc. With the use of innovative mathematical models and Business Intelligence, agnostic and advanced services will be produced such as: anomaly detection, expected impact, event forecast, action recommendation functionalities, etc.; and
- **Concept_4 – Output:** Advanced applications for monitoring and maintenance will be implemented exploiting the collected data and the advanced mathematical model toolkit through a common interface. The proposed application for an advanced risk management system that comply with the ISO 31000 are: Advanced Monitoring and Event Forecasts (AMEFs), Trigger Action Response Plans (TARPs) and Emergency Response Plans (ERPs).

The proposed framework connects several data collection and management systems and processes the data that is relevant for the stability analysis, such as pore pressure from piezometers, horizontal displacements from inclinometers or stresses from pressure cells (see Figure 3). Once new data is available, the proposed stability analysis model automatically incorporates this information to the calculation and performs a safety factor calculation in real-time using the cloud-based infrastructure.

This new paradigm of risk management provides stability assessment in terms of safety factor in a continuous manner (from daily to weekly) connecting the analysis tools and the monitoring data. Moreover, this updated stability calculation model provides more accurate predictions regarding the stability of future tailings dam geometries. Finally, a scheduling and planification tool will allow to manage staff based on risks and cost, whilst eventually management alerts, triggering emergency response plans when the proposed system detects a dangerous situation.

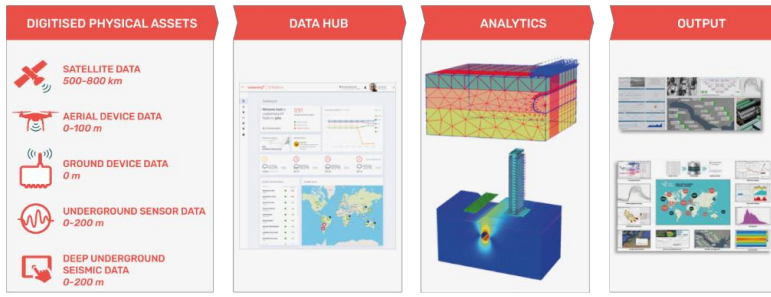

Figure 3. Architecture for an integrated mine risk management framework

6 USE CASE IN BRAZIL

Challenge: A Brazilian mine has a complex tailings dam monitoring system that covers 22 dams (Figure 4). The mine consultant and partners in charge of dam monitoring need to gather real-time data from various sensors (piezometers, water level sensors and inclinometers) installed across different tailings dams and send the data to a database server and workstation. One site includes seven dams within a 7 km radio range. Moreover, the collected data should be connected to a data hub platform to provide a stability calculation on a real-time basis. To comply with the ISO 3100, a scheduling and planification tool will be used to manage staff to eventually activate emergency response plans when the proposed system detects a dangerous situation. Finally, a reporting tool of the collected LOGs will be used to facilitate audit processes with reliable information.

Solution: A network of 467 vibrating wire, analog and digital data nodes sends real-time data to 10 wireless gateways connected to the mine's private network. Two gateways at one of the sites receive data from 158 data nodes including vibrating wire 1-channel nodes connected to piezometers, analog nodes connected to ultrasonic water level meters and digital data nodes

connected to chains of in-place inclinometers. For connectivity, the selected solution uses LPWAN communication system: a long-range, low-power wireless technology used by IoT networks operators worldwide. Features of the system include:

- Range: The monitoring system uses a star network topology that can cover a range of up to nine miles/15 km without any repeaters.
- Radio: the data nodes have a radio sensitivity of up to -137 dBm, which makes the signal up to 32 times stronger than other wireless monitoring systems with typical radio sensitivity of only -101dBm.
- Casing: The nodes are IP-67 rated and have been tested in temperatures ranging from -40ºC to +80ºC, so they are able to withstand the harshest environments.
- Certification: The data nodes have been tested and certified by the telecommunications regulation agency in Brazil, making it apt for deployment across the country.

Benefits: The wireless configuration of the data acquisition system eliminates the need for expensive cabling and manual monitoring. Laying cables in a tailings dam requires trenches and cable protection against issues such as settlements in the embankment. At each regrowth, new sensors must be added, again requiring expensive cable installation. A wireless system provides data from sensors in near-real time, versus manually collected readings with a more sporadic periodicity and vulnerability to human errors. With the provided solution, mines may realize savings of up to 30% on the acquisition of materials and infrastructure (cabling, network material and equipment, specific equipment for manual measurement, etc.) and up to 40% on installation (since cabled technology will not be needed, specific costs for operations and human resources for installation will be reduced). Reliable data related to the behavior of the dam also helps minimize risks and to ensure the safety not only of mine employees but also of residents.

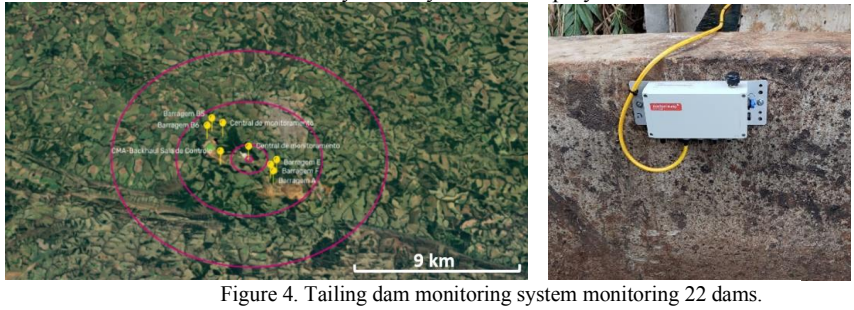

Figure 4. Tailing dam monitoring system monitoring 22 dams.

7 SIMULATION OF ECONOMIC IMPACT

A digitization solution such as the one presented in this use case reduces the need for site visits and expensive cabling, wireless monitoring offers a significantly better return on investment (ROI) than cabled networks or regular manual inspections and represents the first step towers an ISO 31000 risk management framework to guarantee tailings dam safety in cost-effective manner. The improvement in ROI is particularly clear when compared to manual inspections, and all cases improve with the number of years that monitoring will be required (Table 5 and Figure 5).

Table 5. Estimated savings comparing wireless, cabled and manual inspection systems.

Years	Estimated Savings % from using Wireless Monitoring vs.	
	Cable	Manual
20	68.26%	86.64%
10	48.96%	76.09%
5	19.77%	55.00%
3	-8.76%	26.88%

Table 5 presents a sample ROI savings of wireless monitoring versus cable networks or manual inspections. Note the numbers presented here are based on estimates and are only indicative of the potential savings. Actual figures may change depending on the variables mentioned above.

A cost comparison exercise for two mines in Brazil shows that for long-term projects such as mining operations, which can last for around 15 years, wireless monitoring can generate savings from 20% (over five years) to 70% (over 20 years), considering the following variables:

- Manpower: number of people deployed and estimated daily rate of field geotechnical engineers, including insurance.
- Number and cost of wireless monitoring equipment deployed: based on a LPWAN wireless monitoring system.
- Number of days allocated for monitoring and maintenance per month or year.
- Vehicle deployment: including daily cost of fuel and maintenance.
- Cable: estimated length per sensor and cost per meter.
- Project duration: from three to 20 years.
- Number of mining sensors deployed.

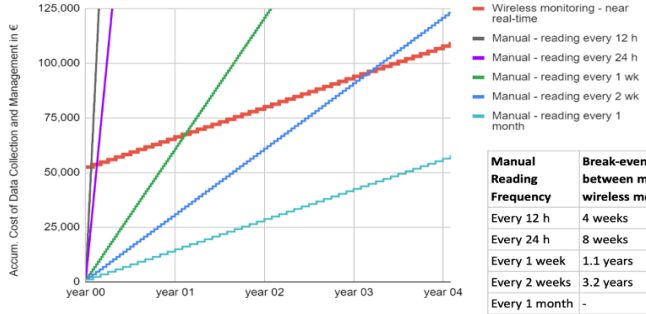

Manual Reading Frequency	Break-even point between manual and wireless monitoring
Every 12 h	4 weeks
Every 24 h	8 weeks
Every 1 week	1.1 years
Every 2 weeks	3.2 years
Every 1 month	-

Figure 5 When to switch from manual to wireless monitoring, based on a European tailings dam with 20 single and 15 multiple piezometers

The exact point at which it can become more cost-effective to implement integrated solutions based on wireless monitoring systems depends on a number of factors, including the project duration, vehicle fuel and maintenance, number of sensors, and cabling and/or geotechnical engineering team costs. For manual monitoring, the frequency of sensor readings is a key consideration. Figure 5 presents a break-even analysis for a mine in Europe. This analysis can be considered a reference for other mine sites. As can be observed, with monthly readings, manual monitoring may be competitive to wireless systems.

But if readings are required every two weeks, then it becomes more cost effective to switch to wireless monitoring within three and a half years. And for daily readings, the wireless option would make sense within weeks. If there is a clear business case for implementing wireless monitoring, then it is important to select systems that use the most appropriate technology. There are several potential wireless technologies that can be used, each with advantages and disadvantages.

8 CONCLUSION

In this study, we reviewed the application of the ISO31000 to the risk assessment and mitigation in a mining infrastructure. To efficiently fulfil the risk mitigation requirements imposed by the regulation, we define a cost-effective ICT architecture and demonstrate its effectiveness through a cost-benefit analysis based on a real tailings dam monitoring use case in a large deployment in Brazil. The presented use case demonstrates cost savings up to 20% in the first 5 years and forecasts 80% savings in the long term (20 years). The proper adoption and combination of

heterogeneous IoT and digital services is a key asset to the reduction of operational and risk mitigation costs in critical infrastructures. A holistic and cross-departmental monitoring and operation system needs to be integrated in the mine risk assessment and mitigation plans, investing in infrastructure digitization and automation to safe human costs in low value tasks. This article aimed to introduce the reader to the ISO31000 methodologies and mapped it to digitization technologies, aiming to put some order in the fragmented critical infrastructure management technology ecosystem.

ACKNOWLEDGEMENTS

This activity has received funding from European Institute of Innovation and Technology (EIT), a body of the European Union, under the H2020, the EU Framework Programme for Research and Innovation. This publication is funded by the EIT RAW MATERIAL project "AMICOS: Autonomous Monitoring and Control System for Mining Plants" – Project Number 19018.

9 REFERENCES

C. Song, G. Yu and B. Xue, "A huge source of pollution hazard — Disaster and cure of tailings pond," 2011 International Conference on Electronics, Communications and Control (ICECC), Ningbo, 2011, pp. 3486-3489, doi: 10.1109/ICECC.2011.6068057.

Q. Zhang, G. Yin, Y. Chen, W. Geng and W. Wang, "Experimental study on the affecting factors of the shear strength of unsaturated tailings," 2011 International Symposium on Water Resource and Environmental Protection, Xi'an, 2011, pp. 89-93, doi: 10.1109/ISWREP.2011.5892951.

Villavicencio, G., Espinace, R., Palma, J, Fourie, A, Valenzuela, P. (2014) Failures of sand tailings dams in a highly seismic country. Canadian Geotechnical Journal, 51 (4) 449-464

Hatje V, Pedreira RMA, de Rezende CE, et al. The environmental impacts of one of the largest tailing dam failures worldwide. Sci Rep. 2017;7(1):10706. Published 2017 Sep 6. doi:10.1038/s41598-017-11143-x

Clau Sganzerla, Constantino Seixas, Alexander Conti, Disruptive Innovation in Digital Mining, Procedia Engineering, Volume 138, 2016, Pages 64-71, ISSN 1877-7058, https://doi.org/10.1016/j.proeng.2016.02.057.

Iannacone, Jean Pascal & Lato, Matthew & Troncoso, Jorge & Perissin, D., (2018). InSAR Monitoring of Active, Inactive and Abandoned Tailing Facilities.

Hui, Shiqiang Rob & Charlebois, Lawrence & Sun, Colin. (2017). Real-time monitoring for structural health, public safety, and risk management of mine tailings dams. Canadian Journal of Earth Sciences. 55. 10.1139/cjes-2017-0186.

B. Draeyer, C. Strecha, (2014) "How accurate are UAV surveying methods," Pix4D White paper, February 2014, pp.1-8.

Li, Wei & Wang, Chang. (2011). GPS in the Tailings Dam Deformation Monitoring. Procedia Engineering. 26. 1648-1657. 10.1016/j.proeng.2011.11.2350.

Palattella, Maria & Accettura, Nicola & Vilajosana, Xavier & Watteyne, Thomas & Grieco, Luigi & Boggia, Gennaro & Dohler, Mischa. (2013). Standardized Protocol Stack For The Internet Of (Important) Things. IEEE Communications Surveys and Tutorials. 15. 10.1109/SURV.2012.111412.00158.

U. Raza, P. Kulkarni and M. Sooriyabandara, "Low Power Wide Area Networks: An Overview," in IEEE Communications Surveys & Tutorials, vol. 19, no. 2, pp. 855-873, 2017, doi: 10.1109/COMST.2017.2652320.

B. Martinez, F. Adelantado, A. Bartoli and X. Vilajosana, "Exploring the Performance Boundaries of NB-IoT," in IEEE Internet of Things Journal, vol. 6, no. 3, pp. 5702-5712, June 2019, doi: 10.1109/JIOT.2019.2904799.

A. Froytlog et al., "Ultra-Low Power Wake-up Radio for 5G IoT," in IEEE Communications Magazine, vol. 57, no. 3, pp. 111-117, March 2019, doi: 10.1109/MCOM.2019.1701288.

Lau, Billy Pik Lik et al. "A Survey of Data Fusion in Smart City Applications." Information Fusion 52 (2019): 357–374. Crossref. Web.

Automated Hazard Mapping of Tailings Storage Facility Failures

Sally Innis
The University of British Columbia, Vancouver, Canada

Negar Ghahramani
The University of British Columbia, Vancouver, Canada

Nahyan M. Rana
University of Waterloo, Waterloo, Canada

Dr. Scott McDougall
The University of British Columbia, Vancouver, Canada

Dr. Steven G. Evans
University of Waterloo, Waterloo, Canada

Dr. W. Andy Take
Queen's University, Kingston, Canada

Dr. Nadja Kunz
The University of British Columbia, Vancouver, Canada

ABSTRACT: Tailings-flows resulting from tailings storage facility (TSF) failures can pose great risks to downstream people, property and ecosystems. Recent devastating TSF failures, such as the 2019 Córrego do Feijão dam failure in Brazil, have inundated large areas and resulted in significant life loss, environmental damage and economic costs. Establishing inundation-area relationships for tailings-flows is a crucial step in risk reduction, enabling the delineation of hazard zones that could potentially be inundated by future TSF failures. This research develops a first-order methodology to assess areas with the potential of being affected by downstream runout of tailings-flows by recalibrating Laharz, a Geographic Information System (GIS)-based computer program originally developed for lahar inundation zone mapping. Laharz uses empirical equations to predict inundated valley cross-sectional and planimetric areas as a function of the flow volume. The recalibrated Laharz model offers a convenient method for high-level risk profiling of potential TSF failures. However, further research is required to understand the limitations and uncertainties of Laharz for this application.

1 INTRODUCTION

Mine tailings storage facilities (TSF) are among some of the world's largest engineered structures (Owen et al. 2019). The failure of TSFs can produce tailings-flows that travel substantial distances and result in long-lasting environmental, social and economic impacts (Ghahramani et al. 2019; Rico et al. 2008). Over the last thirty years, there has been an upward trend in high-consequence TSF failures (Bowker & Chambers 2015; WISE 2015), leading to growing concerns from communities and investors alike about the risks that TSF failures may pose to people and ecosystems (BC First Nations Energy & Mining Council 2015). The creation of tools to predict the inundation paths of potential tailings-flows is critical to inform risk-based decision making and mitigate future losses from TSF failures (Armstrong et al. 2019; Concha Larrauri & Lall 2017; MAC 2017).

The continuous and increasing need for minerals and metals has resulted in gradual declines in the average ore grade of many mineral commodities (Prior et al. 2012). Technological improvements have allowed for previously uneconomic low-grade, complex deposits to become

economically feasible. However, the improved accessibility of large, low-grade deposits often accompanies social-environmental trade-offs (Mudd 2007; Schulz et al. 2018). From a tailings perspective, elevated throughput resulting in increased tailings production per tonne of mined product will likely lead to larger TSFs (Mudd 2007; Prior et al. 2012) and, potentially, higher associated downstream risks in the event of a failure. These risks are increasingly acknowledged by groups external to the mining sector, including investors, who have a desire for relatively simple tools that can provide a high-level picture of regional risk exposure (Innis & Kunz 2019).

Research surrounding tailings failures has predominantly focused on the mechanisms of failures and facility monitoring (Lyu et al. 2019). However, since the recent high-profile failures at Mount Polley Mine (Canada), Samarco (Brazil) and Córrego do Feijão (Brazil), there has been an increase in research on failure consequence and risk reduction (Armstrong et al. 2019; Schoenberger 2016). Improving modelling of the runout of potential future TSF failures is an important step in this direction. The research presented in this paper contributes to the growing field of tailings-flow runout modelling and presents preliminary results from the development of an empirical inundation model considering both the total planimetric and maximum cross-sectional extents of tailings-flows. Empirical models (Iverson et al. 1998; Rico et al. 2008) are particularly important for creating first-order estimates of potential inundation areas to support risk-based decision making, especially when detailed facility information is unavailable and the use of complex numerical models is not justified (Iverson et al. 1998; Rico et al. 2008).

To this end, the objective of this research is to adapt the existing empirical model Laharz, which was originally developed for lahar inundation zone mapping, to tailings-flows (Schilling 2014). This paper describes the original foundations of the Laharz model and introduces an updated dataset of historical tailings-flow data that were used for its recalibration, which builds upon previous work by Ghahramani et al. (2019). The recent Córrego do Feijão TSF failure is modelled to demonstrate the applicability of the recalibrated Laharz model. The objective of recalibrating Laharz for tailings-flows is to create an efficient, low cost tool to understand overall regional risk profiles associated with TSFs, to inform policy, community risk response, and enable stakeholder participation in improved TSF management.

2 REVIEW OF PREVIOUS WORK

2.1 *Tailings-flow Empirical Models*

Potential tailings-flow runout distances and inundation areas are challenging to predict. The diversity of TSF construction, tailings rheology and downstream geomorphology, as well as limited case study information, are some reasons why researchers have struggled to create predictive tailings-flow models (Rico et al. 2008; Wang et al. 2018). Early empirical models required detailed geotechnical and downstream geomorphology data (e.g. Costa 1985). Rico et al. (2008) developed a set of empirical relationships that related tailings-flow runout distance to other variables such as outflow volume, dam height and a parameter called "dam factor" (dam height times tailings outflow volume), which was later built on by other authors (Concha Larrauri & Lall 2018; Small et al. 2017). In the case of Concha Laurrari & Lall (2018), Rico et al.'s (2008) original TSF failure dataset was expanded to include cases of TSFs with larger volumes and dam heights. Their runout distance model was also updated to include a new predictor variable, H_f, the product of the dam factor and the ratio of tailings outflow volume to tailings storage volume.

Comparatively little work has been carried out to develop similar empirical relationships for tailings-flow inundation area prediction. However, the following general relationship between flow volume and inundation or deposit area is well-established for natural flow-like landslides, including lahars (volcanic debris flows), debris flows and rock avalanches (Davies 1982; Hungr 1981; Hungr & Evans 1993; Li 1983):

$$A \text{ or } B = c_{A \text{ or } B} V^{2/3} \tag{1}$$

Where A and B are the total planimetric and maximum cross-sectional inundation areas, respectively, V is the total flow volume and c is an empirical coefficient related to flow mobility (Iverson et al. 1998; Schilling 2014).

Ghahramani et al. (2019) introduced a runout zone classification method for tailings-flows and investigated the applicability of Equation 1 to what they called "Zone 1" (the primary impact zone). Based on Zone 1 planimetric inundation area data collected for 27 historical TSF failures, they found that, for a given volume, tailings-flows are, on average, less mobile than lahars (c_A = 200) but more mobile than debris flows (c_A = 17-20) and rock avalanches (c_A = 12-20).

2.2 *Laharz*

Laharz is an ArcGIS plug-in program based on the empirical relationship shown in Equation 1. Laharz uses calibrated mobility coefficients to delineate potential areas inundated by a flow as it descends a given drainage (Schilling 2014). The program was originally created to delineate areas of potential lahar inundation based on one or more user-specified volumes (Iverson et al. 1998) and has since been updated to model debris flows and rock avalanches (Griswold & Iverson 2008). The input data required by Laharz includes digital elevation models (DEMs), flow path data derived from the topography, identification of source areas where failures may originate and a range of potential flow volumes (Schilling 2014).

3 METHODOLOGY

In this study, the same methodology used by Ghahramani et al. (2019) to investigate planimetric inundation area correlations was used to investigate the adaptability of the Equation 1 scaling relationship for the cross-sectional inundation area, as both relationships are needed to run Laharz. The analysis relates the estimated Zone 1 maximum cross-sectional area to the reported total released volume. Zone 1 is defined as the extent of the main solid tailings deposit, which is characterized by remotely visible or field-confirmed sedimentation, above typical bankfull elevations if extending into downstream water channels (Ghahramani et al. 2019). An example demonstrating the cross-sectional estimation method, detailed below, is shown in Figure 1.

We estimated the Zone 1 maximum cross-sectional area for 26 cases using the updated tailings dam breach database presented in Ghahramani et al. (2020). The cases are global, well documented failures from 1965 to 2019 and range in commodity, downstream topography and final release volume. The estimated runout distances for these failures are in the range of 0.5 to 100 km. The methodology used to calibrate Laharz for tailings-flows is analogous to the approach used by Iverson et al. (1998) and Grisworld & Iverson (2008) to calibrate the model for lahars, debris flows and rock avalanches. Depending on runout distance, between 3 and 20 cross-sectional lines were defined perpendicular to the Zone 1 travel path. For each case, the cross-sectional area at each reference location was measured using the Shuttle Radar Topography Mission (USGS EROS 2000), 30 m resolution, digital elevation model. The maximum cross-sectional area value was then selected.

The results of the maximum cross-sectional areas of the 26 cases were used to fit a regression model and examine the adaptability of Equation 1 ($B= c_B V^{2/3}$) for tailings-flows. The data were transformed into a logarithmic scale and the standard least-squares linear regression method was then applied. A linear regression model was fit to the data using a specified 2/3 slope.

Ghahramani et al.'s (2019) results for the tailings-flow specific planimetric mobility coefficient and the above calculated cross-sectional mobility coefficient were then embedded within the Laharz program. To demonstrate the applicability of the recalibrated Laharz program, the model was applied to the 2019 Brazil Córrego do Feijão TSF failure.

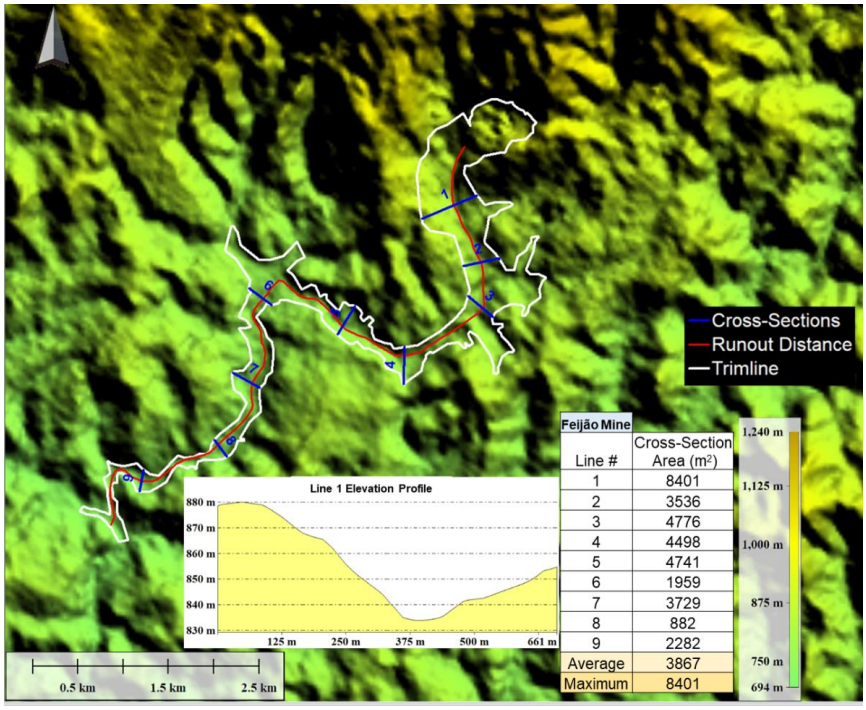

Feijão Mine	
Line #	Cross-Section Area (m²)
1	8401
2	3536
3	4776
4	4498
5	4741
6	1959
7	3729
8	882
9	2282
Average	3867
Maximum	8401

Figure 1. Demonstration of the methodology used to estimate Zone 1 maximum cross-sectional area in this study. The solid white polygon shows the trimline (including source and inundation area) for the 2019 Feijão tailings-flow. The red line is the Zone 1 runout distance and the blue lines are the cross-sectional lines perpendicular to the flow path. The inset (a) shows the elevation profile for the maximum cross-sectional value.

4 RESULTS

4.1 *Calibration*

Figure 2 shows the log-linear regression line for Zone 1 cross-sectional area as a function of total released volume. The regression with a specified 2/3 slope (consistent with the relationship presented earlier in Equation 1) plots within the 95% confidence interval of the best-fit regression, supporting the hypothesis that this same scaling relationship holds in the case of tailings breach data. The following regression equation was obtained in power-law form for the specified 2/3 slope regression model:

$$B = 0.1V^{2/3} \tag{2}$$

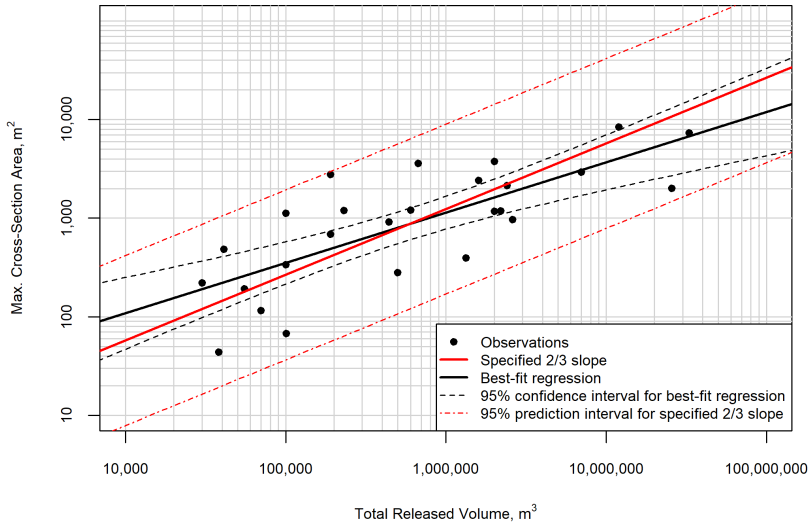

Figure 2 . Log-log scatter plot of Zone 1 cross-sectional area versus total released volume for 26 tailings-flows. The specified 2/3 slope regression line (in red) is fitted to the data and the 95% prediction intervals associated with this trend are shown . The best-fit regression line (in black) and the 95% confidence intervals (red dashed lines) of the best-fit regression are plotted for comparison.

The 95% prediction interval for the specified 2/3 slope regression is also plotted in Figure 2. The lower and upper 95% prediction intervals indicate the level of uncertainty associated with the prediction of inundation areas using this empirical approach.

Table 1 compares mobility coefficients for various types of flow-like mass movements. The results of the present study support the preliminary conclusion of Ghahramani et al. (2019) that the mobility of tailings-flows is, on average, intermediate between lahars and non-volcanic debris flows.

Table 1. Comparison of the cross-sectional and planimetric coefficients for different flow types embedded within the Laharz program, illustrating the difference in the relative mobility of tailings flows.

Flow Type	Planimetric *c* coefficient, c_A	Cross-Sectional *c* coefficient, c_B	Source
Tailings-flows	80	0.1*	(Ghahramani et al. 2020; *this paper.)
Lahars	200	0.05	(Iverson et al 1998)
Debris Flows	20	0.1	(Griswold and Iverson 2008)
Rock Avalanches	20	0.2	(Griswold and Iverson 2008)

4.2 *: Laharz Demonstration: Córrego do Feijão Failure*

On January 25th 2019, a TSF at the Córrego do Feijão (Feijão) mine collapsed and released approximately 9.65 M m^3 of tailings waste (Robertson et al. 2020).The failure resulted in at least 259 deaths and extensive environmental, social and economic consequences (WISE 2019). The tailings-flow travelled approximately 9 km before reaching the Paraopeba River and covered an area of 3 M m^2 (Rotta et al. 2020).

Following the recalibration of Laharz to obtain the tailings-flow coefficients (c_A and c_B in Table 1), we applied the Laharz model to the 2019 Feijão tailings dam breach. Since the Feijão case was included in the model calibration dataset, this step is only intended to demonstrate (not strictly validate/test) the method at this stage of the research.

The results of the demonstration are shown in Figure 3. The 30-m DEM used within the Laharz model is sourced from the Alaska Satellite Facility Hi-Resolution Terrain ALOS PALSAR dataset (JAXA/METI 2007). The recalibrated Laharz model simulated a primary impact zone runout of 7 km compared to the observed runout of 9 km (Ghahramani et al. 2020) and, as a result, did not simulate the flow entering the Paraopeba River. Aside from this key difference, the model generally simulated the observed deviances from the primary flow path, where the tailings-flow travelled short distances laterally. These results suggest that the updated Laharz model generally captures the influence of downstream topography and shows some promise as a first-order tailings-flow mapping tool.

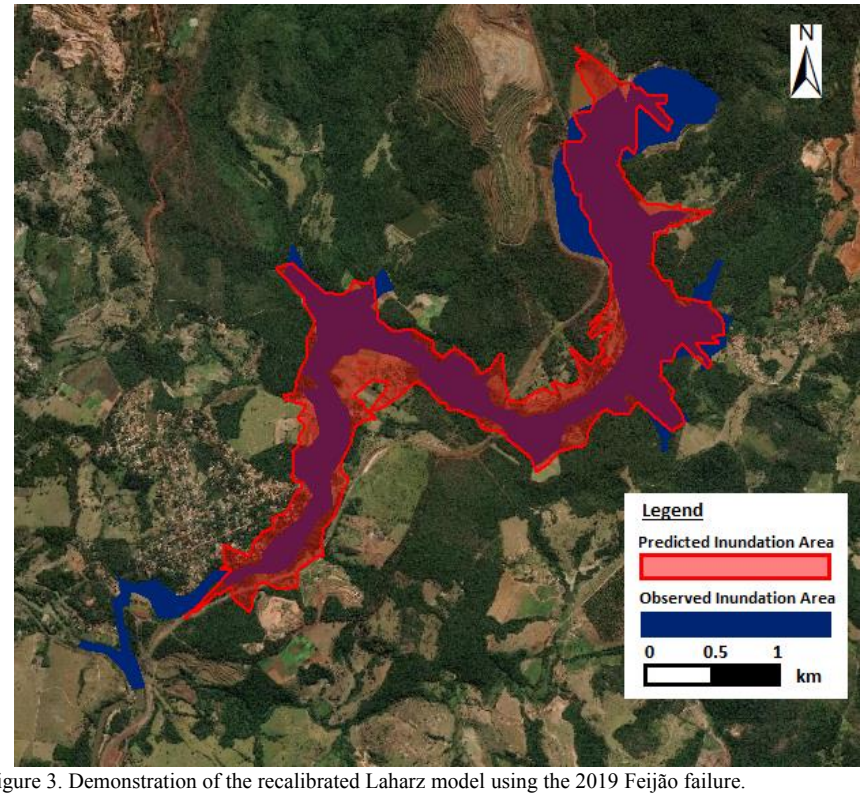

Figure 3. Demonstration of the recalibrated Laharz model using the 2019 Feijão failure.

5 DISCUSSION

5.1 *General*

The application of the scaling equation (Equation 1) within Laharz provides a first step to improve empirical modelling for tailings-flow runout analysis. Applying Laharz to the Feijão tailings dam breach demonstrates that Laharz may provide a relatively simple way to characterize areas that may be impacted by tailings dam breaches, particularly in the context of regional-scale risk profiling work, when a number of different sites must be analyzed and limited site-specific information may be available.

However, these analyses must also be completed with caution and an adequate appreciation of the inherent uncertainties. Studies have focused on improving estimates of release volume (Quelopana 2019), however, tailings release volume is still a source of uncertainty (Concha Larrauri & Lall 2018; Rico et al. 2008). Recent numerical models rely on the assumption that the entirety of the TSF will be released at the time of failure, which is not always the case (Wang et al. 2018). Therefore, Laharz's ability to model several potential tailings release volumes efficiently and within a probabilistic framework provides a methodology to form a more robust understanding of potential hazard zones.

The characterization of tailings-flows cannot be fully constrained by empirical equations. Many factors that influence the runout and inundation of tailings-flows are not explicitly included in the recalibrated Laharz model. These factors include tailings rheology, percentage of free water, and failure mechanism. These conditions and other sources of potential error are site and event specific and challenging to consider using empirical equations (Rico et al. 2008).

5.2 *Areas for Future Research*

Despite the above limitations, the recalibrated Laharz model provides a step-off point for high-level risk mapping of potential TSF failures. Such models are important for responding to community and investor demand to improve understanding of the risks that TSF failures may pose to people and ecosystems, and for informing policy to mitigate against potential associated losses.

However, research is required to further validate the model presented in this paper and to add probabilistic elements to account for some of the uncertainties described earlier. One such opportunity is to validate the recalibrated Laharz model through back-analyses of additional historical TSF failures that were not used in the calibration dataset. These back-analyses may provide more insight on the model's potential limitations, such as whether Laharz is able to successfully predict tailings flows in unconfined topographies. Additionally, research is ongoing to incorporate uncertainty distributions for tailings-flows within Laharz. Prediction uncertainty maps are available in Laharz for lahars but are not yet available for debris flows and rock avalanches. The incorporation of prediction intervals within Laharz will allow for probabilistic risk evaluation and a more robust understanding of the model output uncertainty.

The objective of recalibrating Laharz was to create an efficient, low-cost empirical inundation model. At this stage, Laharz allows for order-of-magnitude estimates of potential inundation zones for the purposes of regional-scale risk profiling. Laharz-based regional risk profiling results may eventually be used to map and communicate consequences of potential TSF failures to regulators, policy makers and mining stakeholders.

6 CONCLUSIONS

Serious TSF failures have been increasingly coming to light in recent years. Global tailings standards, improved regulations and failure mitigation measures have been attracting more attention from government, owners, and stakeholders. Empirical modelling of inundation areas, having the advantage of low costs, accessibility, and high efficiency, could play a role in TSF risk management. The objective of this research was to adapt the well-established Laharz model to tailings-flows, thereby providing researchers and practitioners with a relatively simple risk mapping tool.

The results presented in this paper support the hypothesis that tailings breaches follow the same general relationships between flow volume and inundation area as those for natural flow-like landslides, including lahars, debris flows and rock avalanches. Through a recalibration of the Laharz program using 26 historical tailings dam breach cases, correlations between release volume and Zone 1 cross sectional area were calculated. The results were subsequently embedded within the Laharz program. The study of the Feijão TSF failure using the recalibrated Laharz model demonstrates the potential utility of the proposed method.

This paper highlights the complexity of tailings-flows and the need for improved empirical and numerical models to better understand the risks of TSF failures. The diversity of tailings structures, rheologies and externalities affecting TSF inundation zones cannot be perfectly modelled within a single program, if at all. However, the recalibrated Laharz model offers promise

for high-level risk profiling. Further work is ongoing to validate the model, understand its limitations and incorporate probabilistic mapping.

ACKNOWLEDGEMENTS

This work was partially funded by the British Columbia Graduate Scholarship, fellowships from the University of British Columbia (NG) and University of Waterloo (NR), as well as a Collaborative Research and Development grant from the Natural Sciences and Engineering Research Council of Canada, in partnership with Imperial Oil Resources Inc., Suncor Energy Inc., BGC Engineering Inc., Golder Associates Ltd., and Klohn Crippen Berger.

REFERENCES

Armstrong, M,, Langrené N., Petter R., Chen W. & Petter C.. 2019. Accounting for Tailings Dam Failures in the Valuation of Mining Projects. *Resources Policy* 63.

BC First Nations Energy & Mining Council. 2015. *Uncertainty Upstream: Potential Threats from Tailings Facility Failures in Northern British Columbia*.

Bowker, L., & Chambers D. 2015. *The Risk, Public Liability and Economics of Tailings Storage Facility Failures*.

Concha Larrauri, P. & Lall U. 2017. *Assessing Risks of Mine Tailing Dam Failures*.

Concha Larrauri, P. & Lall U. 2018. Tailings Dams Failures: Updated Statistical Model for Discharge Volume and Runout. *Environments* 5(2):28.

Costa, J.E. 1985. *Floods from Dam Failures*.

Davies, T.R.H. 1982. *Spreading of Rock Avalanche Debris by Mechanical Fluidization*.

Ghahramani N., Mitchell A., Rana, S. McDougall, Evans S.G. & Take A.. 2020. Tailings-Flow Runout Analysis: Examining the Applicability of a Semi-Physical Area-Volume Relationship Using a Novel Database. Submitted to - *Natural Hazards and Earth System Sciences*.

Ghahramani, N., McDougall S., Mitchell A., Evans S.G., and Take W.A. 2019. Introducing a Runout Zone Classification for the Analysis of Tailings Flows. *Proceedings Tailings and Mine Waste 2019*. Vancouver. 555-568.

Hungr, O. 1981. *Dynamics of Rock Avalanches and Other Types of Slope Movements*. Edmonton.

Hungr, O., & Evans S.G. 1993. *The Failure Behaviour of Large Rockslides in Mountainous Regions*.

Innis, S., & Kunz N.. 2019. The Role of Institutional Mining Investors in Driving Responsible Tailings Management. *Proceedings of Tailings and Mine Waste 2019*. Vancouver. 361-370

Iverson, R.M., Schilling S.P., & Vallance J.W. 1998. Objective Delineation of Lahar-Inundation Hazard Zones. *Geological Society of America Bulletin* 110(8):972–84.

JAXA/METI. 2007. "ALOS PALSAR L 1.0."

Li, T. 1983. A Mathematical Model for Predicting the Extend of a Major Rockfall. *Zeitschrift Für Geomorphologie* 27(7):473–82.

Lyu, Z., Junrui C., Zengguang X., Qin Y. & Cao J. 2019. A Comprehensive Review on Reasons for Tailings Dam Failures Based on Case History. *Advances in Civil Engineering.*

Mining Association of Canada (MAC). 2017. *A Guide to the Management of Tailings Facilities*.

Mudd, G.M. 2007. An Analysis of Historic Production Trends in Australian Base Metal Mining. *Ore Geology Reviews* 32(1–2):227–61.

Owen, J. R., Kemp D., Lèbre E., Svobodova K., & Murillo G.P. 2019. Catastrophic Tailings Dam Failures and Disaster Risk Disclosure. *International Journal of Disaster Risk Reduction*.

Prior, T., Giurco D., Mudd G., Mason L., & Behrisch J. 2012. Resource Depletion, Peak Minerals and the Implications for Sustainable Resource Management. *Global Environmental Change* 22(3):577–87.

Rico, M., Benito, G. & Díez-Herrero A. 2008. Floods from Tailings Dam Failures. *Journal of Hazardous Materials* 154(1–3):79–87.

Robertson, P.K., Melo L., Williams D.J. & Wilson G.W. 2020. *Report of the Expert Panel on the Technical Causes of the Failure of Feijão Dam I*.

Schilling, S.P. 2014. *Laharz_py: GIS Tools for Automated Mapping of Lahar Inundation Hazard Zones*.

Schoenberger, E. 2016. Environmentally Sustainable Mining: The Case of Tailings Storage Facilities. *Resources Policy* 49:119–28.

Schulz, K.J., DeYoung J.H., Seal R.R, & Bradley D.C. 2018. *Critical Mineral Resources of the United States: Economic and Environmental Geology and Prospects for Future Supply*.

Rotta S., Henrique L., Alcântara E.,Park E., Negri R.G., Lin Y.N., Bernardo N., Mendes T.S.G., & Filho C.R.S. 2020. The 2019 Brumadinho Tailings Dam Collapse: Possible Cause and Impacts of the Worst Human and Environmental Disaster in Brazil. *International Journal of Applied Earth Observation and Geoinformation* 90:102119.

Small, A., James M., & Al-mamun M. 2017. Advancing the State of Practice for Tailings Dam Breach Assessment Using Empirical Correlations. in *Canadian Dam Association Annual Conference*. Kelowna.

USGS EROS. 2000. "EROS Archive - Digital Elevation - Shuttle Radar Topography Mission (SRTM) 1 Arc-Second Global."

Wang, K., Yang P., Hudson-Edwards K., Lyu W., Yang C., & Jing X.. 2018. Integration of DSM and SPH to Model Tailings Dam Failure Run-Out Slurry Routing Across 3D Real Terrain. *Water* 10(8):1087.

WISE. 2019. "Chronology of Major Tailings Dam Failures."

The Effect of Assumed Residual Strength on Remediation Cost of a Typical Tailings Dam

E. Sarantonis
BGC Engineering, Vancouver, British Columbia, Canada

M. Etezad
Golder, Mississauga, Ontario, Canada

M. Ghafghazi
University of Toronto, Ontario, Canada

ABSTRACT: Liquefaction is a major design concern for tailing dams, as it can result in a catastrophic failure with little warning. When there is potential for liquefaction of tailings, the dam design is typically carried out using the post-liquefied residual strength. However, assigning a reliable post-liquefied strength is currently challenging due to the limitations and inaccuracies associated with the available methods. This paper provides a parametric study on the effect of assumed residual strength on remediation cost of a typical upstream raise tailing dam. Toe berm and stone columns were the ground improvement methods that were considered in a stability model and analyzed separately to determine the required upgrades to the dam. A considerable cost difference was observed by assigning different post-liquefied strengths in the model. Design for the most conservative residual strength may result in significant additional and unnecessary cost. This manuscript reiterates the urgent need to develop a reliable method to determine the post liquefied strength of tailings.

1 *INTRODUCTION*

The design of tailings storage structures has been a challenge for many years as numerous minor or catastrophic failures have been documented. One reason for such failures for the upstream and centerline raise of tailings dam is the high liquefaction potential of tailings, often underestimated in the design of these structures. Soil liquefaction is a phenomenon in which soil shifts towards behaving like a liquid. This occurs as a result of the soil losing strength from pore water pressure buildup (Jefferies & Been, 2015). Liquefaction failure of tailing dams, is currently an important design concern in geotechnical engineering, as seen from the recent Brumadinho dam collapse in early 2019.

Jefferies & Been (2015) mention a few of the many facets of tailings engineering; quantifying the susceptibility of tailings to liquefaction. Slurry tailings are generally deposited in a loose, saturated state, which results in contractive condition prone to liquefaction. The integrity of a tailings dam raised upstream and prone to liquefaction is evaluated through the tailings' residual strength. Because of the high level of uncertainty regarding laboratory experiments, engineers are faced with the challenge to estimate in-situ residual strength based on empirical field-based methods and select an appropriate strength parameter in numerical modelling (Idriss & Boulanger, 2008).

1.1 *Background*

Tailings storage facilities (TSFs) impose many challenges for engineers mainly due to the behaviour of tailings. Upstream tailings dam construction method is known as a cost-efficient method for the tailings dam construction. However, as each embankment lift imposes its load on the loose tailings that are acting as foundation, this method is prone to seismic and flow liquefaction. Many of the existing upstream raise dams have been constructed, without

considering the effect of flow liquefaction. These dams present many risks, including the potential for significant loss of life, environmental damage and financial loss. Therefore, it is of utmost importance to address their liquefaction potential, and to have access to effective ground improvements with manageable financial burden to mining companies.

1.2 *Post-liquefaction residual strength*

Post-liquefaction residual strength of tailings, s_r, is an important parameter that needs to be determined as it quantifies the shear strength left over in liquefied soil (Olson & Stark, 2002). However, s_r is not a parameter that can be directly measured in a laboratory, as opposed to peak shear strength or critical state strength. The peak shear strength can be defined as the maximum shear stress experienced by a soil sample in a triaxial test, whereas the critical state strength can be defined as the shear stress at which a soil experiences no more volume or stress change. Unlike these, the residual strength is a product of many factors within a system including loading mode, drainage conditions, soil profile, and potential for formations of cracks, boils, etc.

Many empirical methods exist in estimating s_r, such as Seed (1987) incorporating SPT resistance. Researchers such as Stark and Mesri (1992), Olson and Stark (2002), and Kramer and Wang (2015) express the residual shear strength as the strength ratio i.e. s_r/σ'_v (where σ'_v is the vertical effective stress). Some proposed methods such as Olson and Stark (2002) and Kramer and Wang (2015) recommend not to apply the influence of fines content, whereas some other methods recommend applying the fines content effect.

1.3 *Challenges in quantifying for a geomaterial*

Applying various methods to a site, or even one method with a range of possible input scenarios often results in a wide range of possible s_r/σ'_v values. Having a range of s_r/σ'_v values for a given geomaterial results in significant uncertainty in designing liquefaction remediation. Failure to quantify the liquefaction potential effectively can lead to under-reinforcing tailings dams, at the potential cost of lives, financial resources, and environmental damage. On the other hand, with over-reinforcing there is unnecessary overspending of monetary and human and natural resources. Methods to upgrade tailings dams include installing toe berms and vibro-replacement stone columns among other somewhat less popular methods. Toe berms act as a structural element of reinforcement providing additional shear resistance at the downstream face of tailings dike. Stone columns play a role in reinforcing the soil and enhancing its density and stiffness (Adalier et al., 2003). Both of these reinforcing strategies provide resistance to liquefaction consequences; however, the construction cost is an important design consideration. This provides motivation to analyze both methods to optimize cost. To tackle this issue, a numerical slope stability model can be generated to evaluate how these two ground improvement methods perform towards reinforcing tailings whose strength is defined by a range of s_r/σ'_v, and how this range affects costs.

2 MODEL CHARACTERISTICS

The geometry, soil type and parameters of the numerical model were chosen based on typical dam sections and in-situ conditions.

2.1 *Geomaterials*

The TSF model resembles an upstream tailings construction that is underlain by a 20 m thick silty sand foundation and then impenetrable bedrock. The tailings pumped into the facility are of mostly silt-size particle composition. The initial dike is composed of an outer shell consisting of rockfill, and an inner clay core. The main components within the model are labelled in Figure 1, and the main geomaterial elements are listed in Table 1.

Unit weight, strength type, strength parameters and hydraulic conductivity parameters that were assigned to each soil type are also listed in the table. Several assumptions made in defining and assigning parameters include the following:

- The silty sand foundation is dense and not prone to liquefaction;

- Bedrock is assumed to be impenetrable in strength, i.e. possesses infinite strength and is impermeable;
- All the soils except the bedrock and tailings above the phreatic surface were subjected to hydrostatic conditions;
- Clay core was compacted during the construction and it is in dilative condition;
- Saturated, unsaturated hydraulic conductivity function was used for all materials except the silty sand foundation and bedrock;
- The dry, unsaturated and saturated unit weight of each soil is the same.

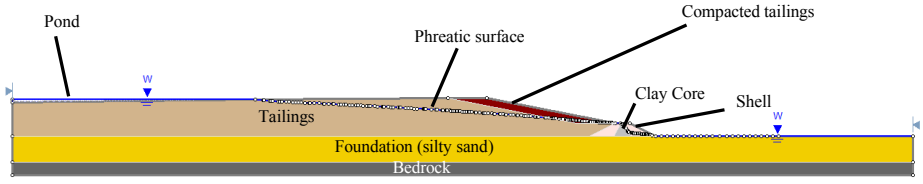

Figure 1. Geomaterial Composition of the TSF Model.

Table 1. Geomaterial components and parameters used in the TSF model.

Geomaterial	Unit weight γ (kN/m^3)	Strength Type and Parameters	Saturated hydraulic conductivity
Silty sand foundation	19	Mohr-Coulomb c' = 0kPa φ' = 30°	k_s = 1 x 10^{-5}m/s
Clay core	19	Mohr-Coulomb c' = 0kPa φ' = 28°	k_s = 1 x 10^{-8}m/s
Shell rockfill	20	Mohr-Coulomb c' = 0kPa φ' = 40°	k_s = 1 x 10^{-3}m/s
Bedrock	26	Impenetrable	k_s = n/a
Compacted tailings (mainly sand-size particles)	19	Mohr-Coulomb c' = 0kPa φ' = 35°	k_s = 2 x 10^{-4}m/s
Tailings above phreatic surface (sand and silt-size particles)	18.5	Mohr-Coulomb c' = 0kPa φ' = 28°	k_s = 2 x 10^{-4}m/s
Tailings below phreatic surface (sand and silt-size particles)	18.5	Vertical Stress Ratio s_u/σ_v' = 0.05 s_u/σ_v' = 0.08 s_u/σ_v' = 0.10 s_u/σ_v' = 0.12 s_u/σ_v' = 0.15 s_u/σ_v' = 0.20	k_s = 2x10^{-4}m/s

2.2 *Geometry*

The geometry of the model is that of a standard upstream tailings dam with an initial upstream slope of 2H:1V and subsequent upstream constructed slope of 5H:1V. The tailings beach is inclined at 1%. A pond exists 150 m away from the beach creating a freeboard of 1.5 m. The fully detailed model with dimensions in meters is presented as follows.

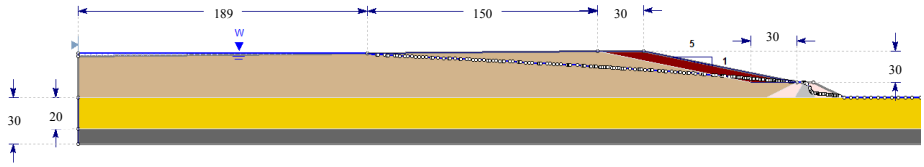

Figure 2. TSF model dimensions.

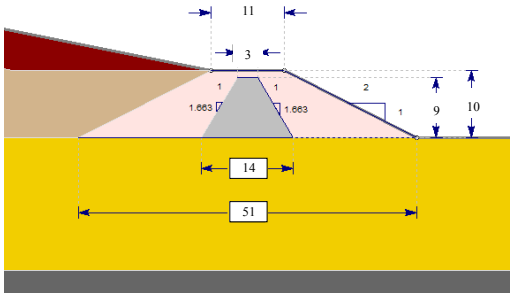

Figure 3. Starter dike dimensions.

3 COMPUTATION METHODOLOGY

Evaluating the effect of reduced strength of liquefied tailings on slope stability first involved computing the location of the phreatic surface generated by the pond and the accumulated precipitation and water from slurry transportation within the centre of the facility. The phreatic surface obtained from the seepage analysis was then used in the stability analysis, where post-liquefied parameters were assigned to the tailings below the phreatic surface and drained parameters were assigned above the phreatic surface.

Limit equilibrium method was used to carry out the stability analyses. Circular and non-circular failure surfaces were evaluated using grid and block searches respectively with optimized surfaces using the Morgenstern-Price method.

The approach taken to evaluate post-liquefaction residual strength of tailings was to compute separate models with identical parameters except for the residual strength s_u/σ_v' ratio of liquefied tailings. A total of six models were generated each representing tailings assigned to a post-liquefaction residual strength of 0.05, 0.08, 0.10, 0.12, 0.15 and 0.20. Following the Canadian Dam Association (2014), the minimum required post-earthquake Factor of safety (FoS) of 1.2 was used in the analyses, implying that analysis results with FoS of less than 1.2 requires remedial measures. Based on this, all six models required remediation. Figure 4 shows the analysis results for tailings with strength parameter s_u/σ_v' of 0.12.

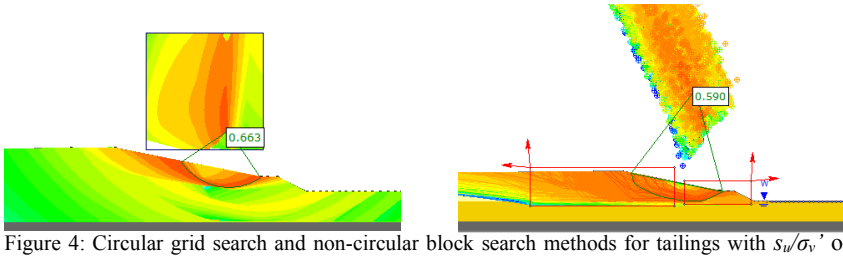

Figure 4: Circular grid search and non-circular block search methods for tailings with s_u/σ_v' of 0.12, at grid-searched circular failure (left) and block-searched non-circular failure (right).

3.1 *Toe berm construction option*

A toe berm construction was added as reinforcement on the downstream side of the starter dike in order to enhance the shear resistance of the slope model. The toe berm properties used were the same as the shell, with c' and φ' of 0kPa and 40°, respectively. The toe berm has the downstream slope of 2H:1V. The dimensions of toe berm were determined to achieve the minimum required FoS of 1.2. Figure 5 presents the results of toe berm remedial design for tailings $s_u/\sigma_v' = 0.12$.

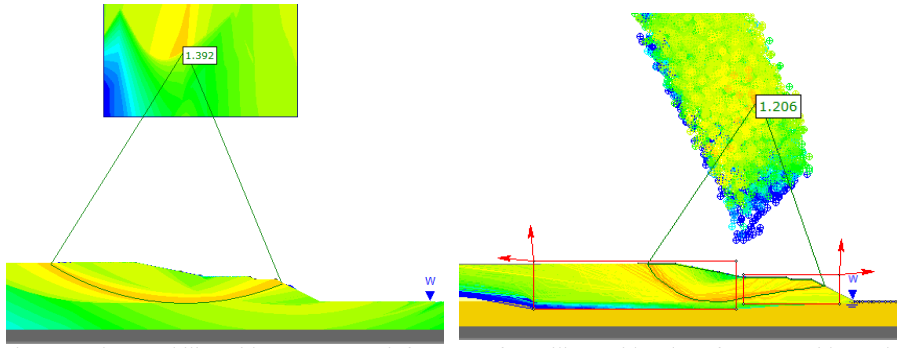

Figure 5: Slope Stability with Toe Berm Reinforcement for Tailings with s_u/σ_v' of 0.12, at grid-searched circular failure (left) and block-searched non-circular failure (right).

3.2 *Stone column option*

There are three factors to consider in implementing stone columns: the configuration of stone columns in a grid, the type of installation, and their design.

The two typical stone column grid configurations are square and triangular. The effective diameter and spacing between two consecutive stone columns from centre-to-centre are represented by parameters d_e and s respectively (Figure 6).

The vibro-replacement method of stone columns comprises of lowering a vibrating apparatus in the soil with a crane to a target depth, and then pulling it out while releasing stone aggregate through the tip of the apparatus by air or water pressure. The methodology proposed by Priebe (1995) was used for the liquefaction remediation design. Priebe (1995) establishes an improvement factor n, which defines the ratio between the amount of settlement without stone column reinforcement to the amount of settlement with it.

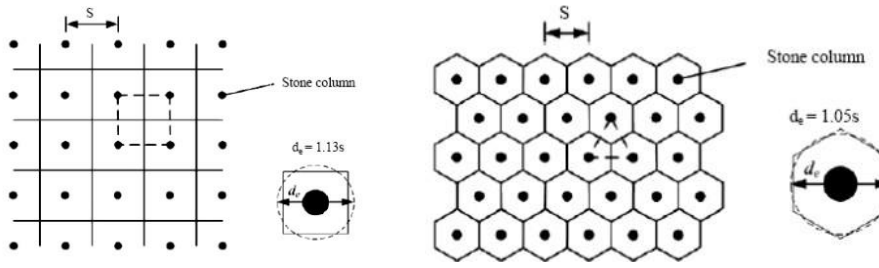

Figure 6: Square (left) and Triangular (right) Stone Column Configurations (Balaam and Booker 1981).

The design was carried out for reduction factor α of 0.4, stone columns friction angle φ' of 45°, unit weight γ of 19kN/m^3, column diameter d_c of 1m and a Poisson's ratio of 1/3. Using the reduction factor diagram provided by Priebe (1995) correlating the friction angle, stress ratio and area ratio, the 2.15 m spacing for the triangular stone column grid was determined.

The method explained by Etezad et al. (2014) was used to determine the equivalent properties of the reinforced ground. The equivalent cohesion c_{eq}, unit weight γ_{eq} and friction angle φ_{eq} of 0, 18.6 kN/m3 and 35º was determined, respectively.

The soil-stone column grid properties calculated are summarized in Table 2. Figure 7 shows the results of the stability analysis for the stone columns remedial design. The stone columns reinforced area is shown as hatched brown zone. The width of the stone column grid was increased upstream and/or downstream depending on where the failure surface lied. An initial column grid was added at a location where the target FoS downstream will be achieved. Following this, the width of the column grid would be extended to a point where it can be ensured that the upstream slip surface FoS and the overall FoS are satisfied.

Table 2. Stone column zone equivalent parameters.

Parameter	Value calculated
Equivalent cohesion, c_{eq}	0 kPa
Equivalent unit weight, γ_{eq}	18.6 kN/m^3
Equivalent friction angle, φ_{eq}	35°

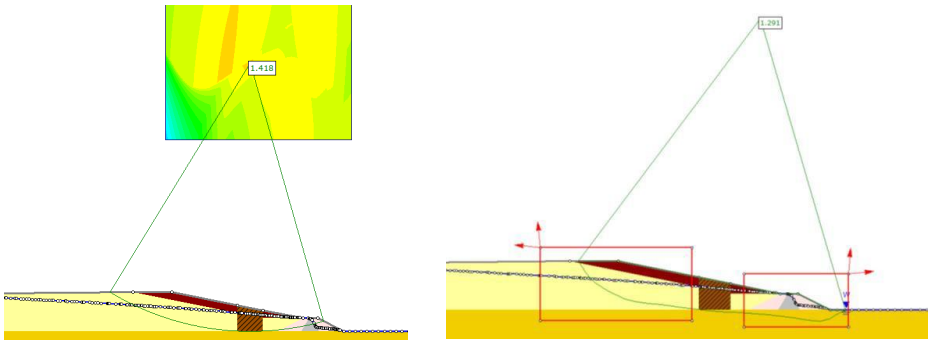

Figure 7: Slope stability with stone column reinforcement for tailings with s_u/σ_v' of 0.12, at grid-searched circular failure (left) and block-searched non-circular failure (right).

4 COST IMPLICATIONS

To carry out the cost estimation, the amount of construction volume required to obtain a Factor of Safety of at least 1.2 was determined. The optimal construction volumes for toe berms and stone columns required to satisfy the target FoS for different residual strengths, and associated costs are presented in Table 3 and Figure 8. Toe berm costs were considered at US$19 per cubic metre and stone column costs were considered at US$104 per linear metre, as typical prices encountered in industry (e.g. Schaefer et al., 2016).

The higher stone column costs are associated with the higher construction cost and the high transportation/crushing costs of the aggregate material used for them due to potential scarcity of the specific aggregate in the near vicinity of the construction site. On the other hand, toe berm rockfill is usually readily available on mine sites. However, the availability of the large volumes of these materials needed, potential environmental problems (e.g. Acid rock drainage) that they may cause, and availability of real estate to accommodate the footprint of the berm are factors that may justify opting for stone columns.

Another factor that should be considered is the construction sequencing of these two options. Constructing toe berms does not usually disrupt the operations of a TSF. On the other hand, stone columns may affect the operations and require access berms to install them. There is eventually a trade-off to be considered between the cost of construction, additional operations costs and

footprint restrictions among other factors. For all intents and purposes, the results below only reflect a rough estimate on the cost of remediation.

Table 3. Summary of the effect of assumed residual strength on remediation cost of a typical tailings dam for toe berm and stone column remediation options.

s_r/σ_v'	Toe berm volume (m3 for 100m of dam length)	Toe berm cost (thousands of US$ for 100m of dam length)	Stone column length (linear meters for 100m of dam length)	Stone column cost (thousands of US$ for 100m of dam length)
0.05	80,000	1500	23,000	2400
0.08	63,750	1200	20,600	2100
0.10	49,000	900	15,700	1600
0.12	39,750	800	12,600	1300
0.15	31,400	600	9700	1000
0.20	24,250	500	5000	500

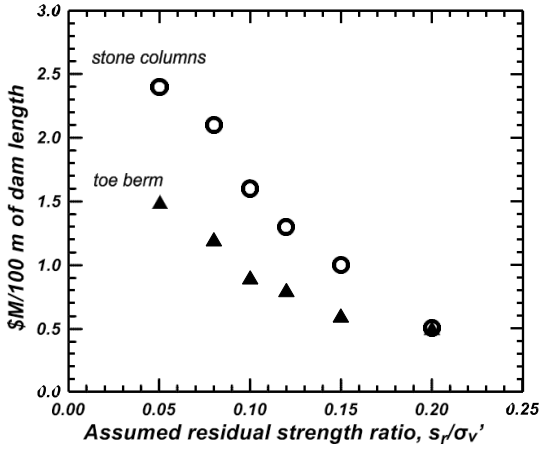

Figure 8: The effect of assumed residual strength on remediation cost of a typical tailings dam for toe berm and stone column remediation options.

5 CONCLUSION

Stone columns were shown to be the more expensive option by a wide margin even though its construction volume requirement is lower than that of the toe berm as seen in Figure 8. It can be noticed that costs become comparable between both options for increasing s_u/σ_v', seen more notably at s_u/σ_v' of 0.20, where there is potential cost convergence, and consequently, a flexibility in choosing either reinforcement option at that point.

The results of analysis indicated that as the residual strength ratio varied between 0.05 and 0.20, the cost of a toe berm changed by a factor of three, and the cost of stone columns by a factor of five. The cost of remediation is especially sensitive to the choice of residual strength in the often-contested range of 0.05 and 0.10 where both methods roughly double in cost.

The higher construction cost and material haul distance are factors that result in stone column costs being greater than toe berm costs in this study. However, opting for stone columns may be justified by the availability of the materials required for berms, their potential to cause environmental problems (e.g. Acid rock drainage), and spatial restrictions for construction.

REFERENCES

Adalier, K., Elgamal, A., Meneses, J., & Baez, J. I. (2003). Stone columns as liquefaction countermeasure in non-plastic silty soils. Soil Dynamics and Earthquake Engineering, 23(7), 571-584.

Canadian Dam Association (CDA). (2014). Technical Bulletin: Application of Dam Safety Guidelines to Mining Dams

Balaam, N. P., and Booker, J. R. (1981). Analysis of rigid rafts sup-ported by granular piles. Int. J. Numer. Analyt. Meth. Geomech.,5 (4): 379–403.

Etezad, M., Hanna, A. M., & Ayadat, T. (2014). Bearing capacity of a group of stone columns in soft soil. International Journal of Geomechanics ASCE15(2), 04014043.

Jefferies, M., & Been, K. (2015). Soil liquefaction: a critical state approach. CRC press.

Kramer, S. L. (1996). Geotechnical earthquake engineering. Upper Saddle River, N.J: Prentice Hall.

Kramer, S.L, and C. Wang. (2015). Empirical model for estimation of the residual strength of liquefied soil. Journal of Geotechnical and Geoenvironmental Engineering ASCE 141(9):04015038.

Olson, S. M., & Stark, T. D. (2002). Liquefied strength ratio from liquefaction flow failure case histories. Canadian Geotechnical Journal, 39(3), 629-647.

Priebe, H. J. (1995). The design of vibro replacement. Ground engineering, 28(10), 31.

Seed, H. B. (1987). Design problems in soil liquefaction. Journal of Geotechnical Engineering ASCE, 113(8), 827-845.

Schaefer, V. R., Berg, R. R., Collin, J. G., Christopher, B. R., DiMaggio, J. A., Filz, G. M., ... & Berg, R. R. (2016). Geotechnical Engineering Circular No. 12 Ground Modification Methods-Reference Manual Volume I (No. FHWA-NHI-16-027). National Highway Institute (US).

Stark, T.D., and G. Mesri. (1992). Undrained shear strength of liquefied sands for stability analysis. Journal of Geotechnical Engineering ASCE 118(11):1727–1747.

Variable Penetration Rate CPT Testing for Mine Tailings Characterization

J.T. DeJong & K.C. Green
University of California, Davis, United States

Characterization of the strength and volume change behavior upon shearing of tailings materials is critical for accurate assessment of facility stability and design. The index properties (i.e. the particle size, gradation, state), in-situ state (e.g. loose, lightly cemented), and low strength and plasticity of tailings make the process of sampling, testing and characterization particularly difficult relative to that typically required for clean sands or moderate plasticity clays. The permeability and coefficient of consolidation can produce partially drained conditions when cone penetration testing (CPT) is performed at a standard penetration rate of 2 cm/s, rendering interpretation and estimation of engineering properties difficult. This paper reviews the variable rate cone penetration test (VRCPT) method and how it can be used to control drainage conditions, from drained to undrained, in order to obtain CPT measurements under known conditions to aid in evaluation and characterization of tailings.

INTRODUCTION

Characterizing the geotechnical properties and behavior of tailings dams poses a formidable challenge to geotechnical engineers due to the processes that create and deposit tailings materials. Still, characterizing these materials is critical due to the economic and safety consequences of tailings dam failures. In the past 5 years alone, there have been over 20 incidences of tailings dam failures around the world, including a 12 million cubic meter volume failure at the Brumadinho dam in Brazil that resulted in major economic damage and 232 human deaths (Santamarina et al 2019). Reliable and repeatable characterization and understanding of the materials that comprise tailings dam structures is therefore paramount for the performance of such structures and facilities. The application of conventional in-situ and laboratory testing can be problematic in execution and/or in results interpretation due to the unique properties of tailings materials. One variant of the cone penetration test (CPT), the variable rate cone penetration test (VRCPT), wherein the penetration velocity is systematically varied to control and modify the drainage conditions during penetration, may be an effective method to evaluate how the penetration resistance in tailings will change from drained to undrained conditions.

This paper reviews previous work performed on tailings samples to broadly summarize tailings properties and loading behavior under the normalized velocity framework. Non-tailings materials such as clays, silts and sands are also reviewed to compare behavior of tailings to those of more common materials. This paper will introduce tailings and some of their general characteristics, outline the normalized velocity framework, discuss existing data regarding tailings tested within the normalized velocity framework, and recommend practices for the using the VRCPT method for tailings characterization.

GENERALIZED PROPERTIES OF TAILINGS

Tailings materials are unlike most soils encountered in the geotechnical engineering profession in that they are not natural materials. Tailings materials are a waste byproduct of the mining process that are deposited hydraulically behind a dam in a loose, saturated state. During the deposition process, the tailings flow from a discharge area to fill the storage space retained on the upstream side of the tailings dam. In high flow regions, e.g. closest to the dam, the larger particles are deposited first, with smaller and smaller particles being deposited as flow velocity reduces further behind the dam. The dam itself that retains the tailings may be constructed from tailings materials, and it may be supported by tailings materials if the upstream construction method is used.

Tailings materials generally consist of clay to sand sized particles (less than 0.002 mm to 2 mm) with typical grain-size distributions about 5 to 20 percent clay, 35 to 50 percent silt and 20 to 60 percent sand for gold, copper, molybdenum and fine coal tailings (Sarsby 2000), although variations within the tailings regions exist due to flow velocity segregation. Permeabilities are in the range of typical silt values; work by Bjelkevik & Knutsson (2005) found typical values of permeability for Swedish tailings to be 10^{-6} m/s with the ratio of horizontal to vertical permeability being 2 to 10 (Vick 1990). Volpe (1979) found that for copper tailings sands the specific gravity was 2.6, void ratios ranged from 0.6 to 0.8 and dry densities ranged from 1,490 to 1,750 kg/m^3. Tests on copper slimes had a specific grav ity of 2.8, void ratios ranging from 0.9 to 1.4, and dry densities from 1,120 to 1,440 kg/m^3. Oliveria et al. (2011) tested reconstituted samples of iron ore silt tailings from the Samarco Mineracao in Brazil and found a grain size distribution of 7 percent clay, 71 percent silt and 22 percent sand, e_{min} to e_{max} of 0.49 to 1.36, permeability of 5 to 8 x 10^{-6} m/s, and specific gravity of 3.22. Schnaid et al. (2014) tested bauxite tailings and found a grain size distribution of 80 percent silt, 15 percent clay, and 5 percent sand, permeability of 2 x 10^{-8} m/s, specific gravity from 2.7 to 3.0, and unit weight of 16 kN/m^3. The relative density of tailings ranges from 30 to 50 percent (Vick 1990).

The depositional energy and subsequent consolidation and/or thixotropic changes to tailings can significantly influence their state and stress-strain behavior. Tests by Zhang et al. (2015) showed that tailings from an iron mine in Sichuan, China, exhibit positive pore pressure generation (contractive behavior) under monotonic loading in an undrained triaxial test under confining pressures of 50 kPa to 300 kPa, reaching critical state conditions at axial strains of 2 to 15%. Schnaid et al. (2014) found similar results for bauxite tailings: samples tested from 40 kPa to 360 kPa confining pressure in undrained triaxial compression tests exhibited similar contractive behavior and gradual strain softening to a critical state condition at about 15% axial strain. Davies et al. (2002) noted that tailings can experience brittle strain softening, characterized by a sharp post-peak decrease in shear strength with increasing monotonic or cyclic loading, down to a residual shear strength state. Triaxial testing on silts performed by Schnaid et al. (2013) showed that the critical state line of tailings materials becomes flatter at low mean stresses (less than 50 kPa), which can lead to a decrease in shear strength with increased strain (strain softening) and ultimately static flow liquefaction for a loose sample that experiences a reduction in mean effective stress. As the mean stress increases, samples can develop strain-hardening and/or constant deviatoric critical state conditions. Schnaid showed that undrained samples with confining pressures of about 0 to 50 kPa experienced strain softening behavior down to 0 kPa mean effective stress (liquefaction), 50 to 200 kPa experienced strain softening but did not decrease to 0 kPa mean effective stress, and above 200 kPa experienced strain hardening. Furthermore, at high mean stresses, the critical state line is curved downward due to particle breakage. Tailings can also exhibit chemical bonding of particles that influences the stress strain behavior of the material. Notably, the Brumadinho dam failure was in part attributed to brittle strength loss due to iron oxide bonding (Robertson et al. 2019). In this case, insignificant deformations were observed in the dam up until failure, at which point large deformations and failure occurred.

CONE PENETRATION TESTING AND DRAINAGE CONDITIONS

The behavior and properties of tailings clearly can vary significantly among material types and even within a single impoundment facility, as a function of distance from pumping works and with depth. These variations mandate substantial, accurate testing and analysis to determine site/location-specific tailings properties and behavior. However, tailings are difficult to sample. Undisturbed samples are difficult to obtain unless using expensive sampling methods such as frozen or block samplers, which are economically unfeasible for most projects. Laboratories can create reconstituted samples using dry or wet pluviation, slurry or vibration processes, but these methods do not replicate in-situ fabric nor do they produce representative stress-strain behavior (Ladd et al. 1997, Vaid et al. 1995) and therefore are only desirable when critical state conditions are needed. Therefore, in-situ testing is an attractive alternative as it allows testing of mine tailings materials in their in situ state.

The most common method to test tailings materials in situ is the cone penetration test (CPT) (Lunne et al. 1997). During a cone penetration test, a cone is advanced at a standard rate of 2 cm/s and the penetration resistance, q_c, is measured. The corrected cone penetration resistance (q_t), obtained by correcting the measured penetration resistance (q_c) for pore pressure (u_2), can be normalized by the overburden stress (σ_v) and normalized by the effective overburden stress (σ'_v) at the test depth to yield

$$Q = \frac{q_t - \sigma_v}{\sigma'_v} \tag{1}$$

which is referred to as the normalized penetration resistance and is used as a metric for estimating soil shear strength.

Testing soils at the same drainage condition as the expected large-scale failure mechanism (e.g. flow liquefaction of a dam) is necessary for reliable evaluation of facility stability and failure prediction. Shear and volumetric response of soil, and therefore strength, during loading will depend on the drainage condition, which can range from fully drained, to partially drained/undrained, to fully undrained. During drained loading, where the loading rate is sufficiently slow such that pore water can simultaneously flow to prevent pore pressure buildup, the soil skeleton is directly loaded and the effective stress changes. In contrast, during undrained loading, where the loading rate is sufficiently fast that there is no water flow, the pore pressure increases above hydrostatic and the soil skeleton does not experience an immediate change in load. Between these two limiting conditions exists partially drained conditions, where some excess pore pressure is generated and some increase in effective stress occurs. Established frameworks for estimating soil shear and volumetric response during loading are based on the assumption that the soil is either in a drained or undrained state during loading; therefore, it is important to know what drainage condition governs the soil response during testing. If a structure is expected to fail in an undrained loading state (e.g. flow liquefaction), then testing should be performed in undrained conditions.

The drainage condition during loading will depend on its horizontal coefficient of consolidation (c_h), which is directly related to the soil's permeability (k), volumetric compressibility (m_v) and weight of water (γ_w), expressed by the following equation:

$$c_h = \frac{k}{m_v \gamma_w} \tag{2}$$

High permeability soils such as sands ($k = 10^{-2}$ to 10^{-5} m/s) often experience drained conditions during loading because the pore water can dissipate faster than the loading rate. Low permeability materials such as clays ($k = 1 \times 10^{-8}$ to 8×10^{-11} m/s) often experience undrained conditions because the pore water cannot dissipate during loading. However, if a load is applied fast enough even a high permeability material will experience undrained loading, and the converse is true for a low permeability soil.

Materials such as tailings have permeabilities (and therefore coefficients of consolidation) in between those of sands and clays ($k = 10^{-5}$ to 10^{-8} m/s), and therefore can have different drainage conditions during loading. During the advancement of a CPT in sands and clays at the standard

rate of 2 cm/s, the drainage condition is likely to be drained and undrained, respectively (Randolph & Hope 2004). However, during advancement in silty materials such as tailings, penetration may produce partially drained conditions. In this drainage condition, the shear and volumetric response of the soil will be different than that during an undrained failure, and the results cannot be used to directly predict the soil response at failure. Instead, drained and/or undrained conditions need to be established so the responses during those conditions can be evaluated.

An increasingly common method to estimate the state and strength of soils which have partially drained conditions during conventional 2 cm/s CPT testing is to vary the speed at which the cone is advanced, known as variable rate cone penetration testing (VRCPT). By increasing or decreasing penetration rates the soil response will tend towards undrained or drained, respectively. At and beyond some sufficiently high and low advancement rate, the soil will behave undrained or drained and will have a constant value of Q (ignoring viscous rate effects sometimes exhibited by finer grained soils), with advancement rates in between responding in a partially drained manner. To compare advancement rates against soils with different coefficients of consolidation, Randolph & Hope (2004) defined a normalized velocity parameter

$$V = \frac{vd}{c_h} \tag{3}$$

where v is velocity, d is probe diameter and c_h is the horizontal coefficient of consolidation. Plotting Q versus V is a useful way to map the regions of drained, partially drained and undrained conditions based on penetration rate. After a series of penetration tests at variable rates (or a single test in a layer at variable rates, known as a twitch test (House et al. 2001)), results can be plotted in V-Q/Q_{ref} space to map changes in Q from drained to undrained (DeJong & Randolph 2012).

The coefficient of consolidation must be estimated to compute V in equation (3). The coefficient of consolidation should be determined based on dissipation tests when possible as it provides the most accurate evaluation of the dissipation conditions around the cone penetrometer. Due to permeability anisotropy this value primarily represents the horizontal coefficient of consolidation, c_h (DeJong & Randolph 2012). When other methods, such as laboratory consolidation tests, are used, the vertical coefficient of consolidation, c_v, is determined. This can produce a value 2 to >10 times less than c_h, depending on the fabric and stratigraphic anisotropy, resulting in the computed V value to >10 times larger. Hence, the coefficient of consolidation value, as well as the method used to measure it, should be noted and documented.

Sample dissipation test results from bauxite tailings are shown in Figure 1, where t_{50} is estimated as 35 seconds. Interpretations of dissipation data to estimate c_h historically have been based on the method presented by Teh & Houlsby (1991). However, when using this method, the interpreted c_h will be underestimated (and consequently t_{50} will be overestimated) when conditions are partially drained because the method was developed for the undrained case of cone penetration. DeJong & Randolph (2012) introduced the following equation to estimate c_h from dissipation test data obtained with a 10 cm^2 CPT:

$$t_{50} = \frac{\sqrt{I_r}}{c_h}[78 + 0.25{c_h}^{1.2}] \tag{4}$$

where I_r is the ratio of shear modulus, G, to undrained shear strength, s_u, referred to as the rigidity index. For 15 cm^2 cones, the coefficients in equation (4) should be multiplied by 1.5.

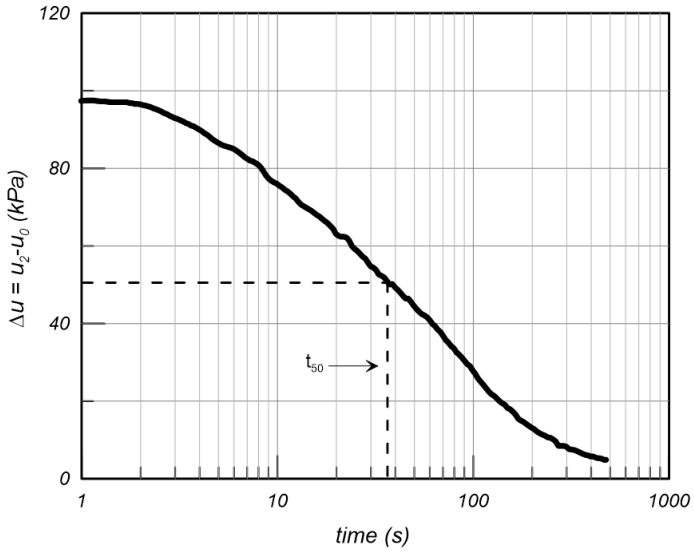

Figure 1 – Dissipation Test in Gold Tailings (after Dienstmann et al. 2019).

Partial drainage conditions can exist in any material, depending on rate of loading. At the standard rate of CPT advancement of 2 cm/s, partial drainage conditions will exist when t_{50} measured from a dissipation test is between 0 and 100 seconds (DeJong & Randolph 2012). More practically, nearly drained conditions exist if t_{50} is less than 10 seconds and nearly undrained conditions exist if t_{50} is greater than 75 seconds. Based on testing using the normalized velocity framework, this region of partial drainage generally corresponds to a normalized penetration rate range of 0.3 to 30, although it can vary from this typical range based on the selection of c_h (e.g. Figure 2b).

TRENDS IN VRCPT PENETRATION RESISTANCE FOR DIFFERENT SOILS

VRCPT data obtained and analyzed within the normalized velocity framework for natural soils and tailings materials is presented and analyzed in this section. Previous research includes data from natural soils, pure kaolin, kaolin/silt mixtures, silts, and tailings samples at various overconsolidation ratios (OCR) and states. The ratio of drained ($Q_{drained}$) to undrained ($Q_{undrained}$) penetration resistance, or Q_d/Q_u, is typically governed by soil type (and therefore plasticity index and coefficient of consolidation) and OCR for clayey soils and state for silty soils.

Each set of reviewed data has been curve fitted using equation (5), introduced by DeJong & Randolph (2012), to predict the change of Q/Q_{ref} across a range of V:

$$\frac{Q}{Q_{ref}} = 1 + \frac{\frac{Q_{drained}}{Q_{ref}} - 1}{1 + (\frac{V}{V_{50}})^c} \quad (5)$$

In equation (5), Q_{ref} is a reference Q value, V_{50} is the normalized velocity V at which the corresponding Q is midway between $Q_{drained}$ and Q_{ref}, and c is a curve fitting parameter. Q_{ref} is typically taken as $Q_{undrained}$ for soils such as silts and clays where undrained conditions during penetration testing are readily achievable. It is noted that equation (5) does not account for rate effects that are present in some soils, whereby the soil experiences an increase in undrained shear strength as the rate of shearing increases. Prior researchers (e.g. Lehane et al. 2009) have presented equations that do account for rate effects in the normalized velocity space. Test result values and

other soil properties reported in the original research are summarized in Table 1 (located at the end of the document).

Clay-like Soils

VRCPT testing was originally developed for the characterization of clays, and as a result a majority of data exists for these materials. Studies consisting of soils that exhibit clay-like behavior include pure kaolin and kaolin/silt samples. Randolph & Hope (2004) explored changes in drained to undrained penetration resistance in pure kaolin samples (c_h = 1 to 10 m^2/yr) based on pore pressure generation using twitch tests (where a single cone is slowed down during penetration) and multiple VRCPTs, finding Q_d/Q_u to be about 3 (Figure 2a). Schneider et al. (2007) tested similar soils as Randolph & Hope (2004) at various OCRs to evaluate the effect of OCR on Q_d/Q_u, finding that higher OCR soils experienced larger Q_d/Q_u values. Lehane et al. (2009) tested similar soils to Schneider et al. (2007) and Randolph & Hope (2004) and presented an equation to predict the change from drained to undrained strength in kaolin with normalized velocity, which included viscous effects in the undrained region. The tests performed in this study had opposite results of Schneider (2007), indicating that higher OCR kaolin soils had a smaller change from drained to undrained strengths, potentially due to smaller overall pore pressure generation because of the soil state being close to the critical state line in e (void ratio) – ln(p') (mean effective stress) space. Average values for Q_d/Q_u for the three pure kaolin tests were 2 to 4. Other tests in similar materials performed by Silva (2005), Schneider et al. (2008), and Yi et al. (2012), not presented here, showed similar results for ranges of Q_d/Q_u and the region of normalized velocity corresponding to partial drainage (10^{-1} to 10^{1}). Kim et al. (2008) and Kim et al. (2010) tested in-situ soils comprising of silty clay and clayey silt and laboratory tests of sand/clay mixtures, which had c_h values 1 to 3 orders of magnitude greater than those of the kaolin samples, and the region of partial drainage for normalized velocity was about an order of magnitude less (10^{-2} - 10^{0}), which may have been due to selection of the c_h value (Figure 2b). Q_d/Q_u was slightly higher than those of the pure Kaolin, with values ranging from about 3 to 6.

Silt-like Silica-based Soils

More recently VRCPT testing has been performed on intermediate soils, such as silty silica-based soils, as they often produce partially drained conditions during conventional CPT testing at 2 cm/s. Krage & DeJong (2016) and Holmsgaard et al. (2016) performed in-situ CPTs on low-plasticity silt/clay/sand with coefficients of consolidation two to three orders of magnitude greater than the kaolin samples described above. The trends showed on average smaller ratios of Q_d/Q_u at about 1 to 2.5, potentially due to small state parameter values of the silts and sands, which corresponds to smaller volume changes during loading (Figure 3a). Price et al. (2019) tested normally consolidated/lightly overconsolidated low- to non-plastic mixtures of clay and silt (Figure 3b). Trends were, on average, similar to those described by Krage & DeJong (2016), where greater percentages of silt and smaller plasticity indices compared to kaolin resulted in smaller Q_d/Q_u ratios. A sample with 100% silt (PI = 0) resulted in net negative pore pressure generation during shearing, which resulted in a Q_d/Q_u ratio less than 1 (i.e. dilative behavior, compared to contractive for all other soils tested). Results of the test with 20% clay and 80% silt (PI = 6) resulted in a Q_d/Q_u ratio of about 9. All samples tested by Price et al. (2019) were at OCRs of 1 to 2, indicating that the sample behavior was virtually independent of OCR. Schneider et al. (2007) also tested lightly and heavily overconsolidated mixtures of 95% silica flour and 5% bentonite (PI = 12 to 14) (Figure 3c). Similar to tests on clays from Lehane et al. (2009), the normally consolidated soil had a greater Q_d/Q_u at about 5.5, compared to the heavily overconsolidated soil at about 3.

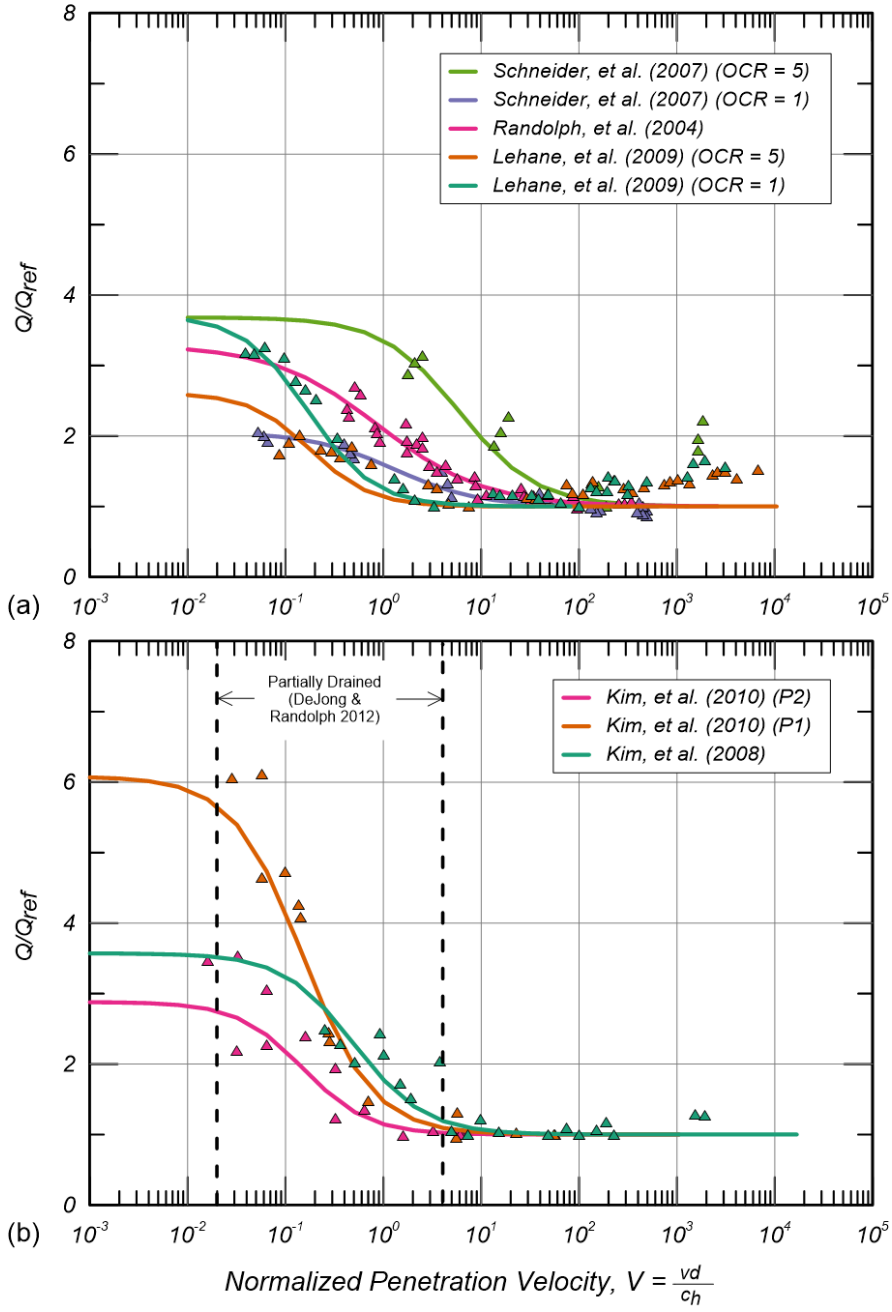

Figure 2 – Summary of VRCPT data on clayey soils.

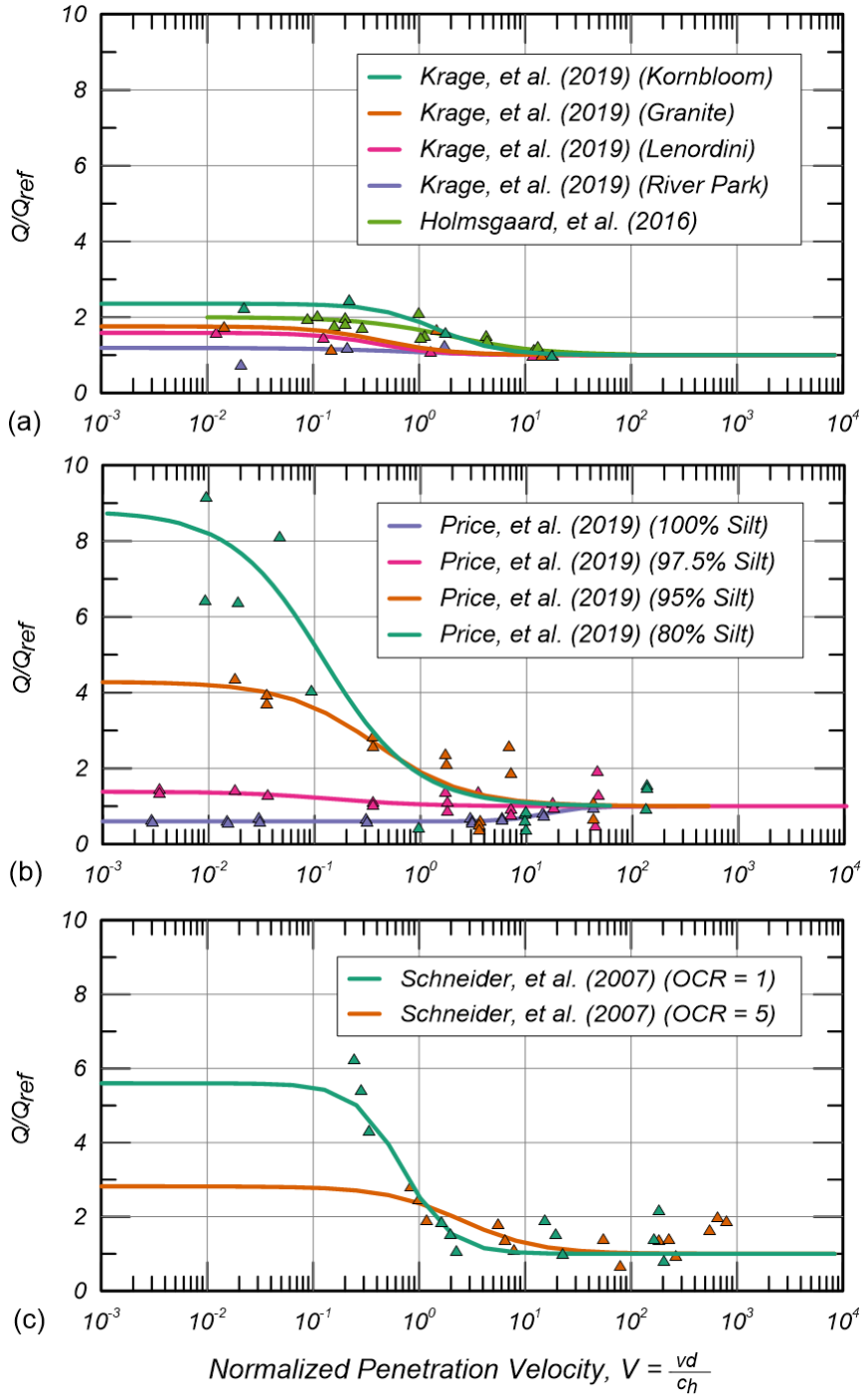

Figure 3 – Summary of VRCPT data on silty soils.

Tailings

Limited studies have been performed on tailings materials. Tailings studies performed by Dienstmann et al. (2018) and Oliveira et al. (2011) show materials that generally have larger Q_d/Q_u ratios than those of natural deposits (Figure 4). Tests in gold tailings by Dienstmann et al. (2018) exhibited a Q_d/Q_u ratio of about 12 over two orders of magnitude of V. Tests in iron ore tailings (Oliveira et al. 2011) exhibited a Q_d/Q_u of about 4 over a single order of magnitude. Although not shown here, tests by Schnaid et al. (2020) resulted in Q_d/Q_u of about 20, substantially higher than any test on a natural soil. Large values of Q_d/Q_u can potentially be explained by the in-situ state being highly contractive (well above the critical state line), which leads to significant strength loss during undrained penetration due to fabric collapse and a strong tendency for volumetric contraction.

Summary of Trends

The following general observations can be made:

- The range from drained to undrained conditions spans roughly two orders of magnitude consistently among samples of all soil types, with some data sets exhibiting smaller ranges (e.g. Schneider et al. (2007) and Oliveira et al. (2011)). The range of V from drained to undrained is roughly 0.3 to 30, however, variations in estimations for c_h, or in some cases, use of c_v instead, affect the absolute range over which partially drained conditions prevail.
- Q_d/Q_u can be an effective indicator of the tendency of a soil to contract or dilate. A drained resistance significantly higher than the undrained resistance is indicative of contractive behavior. Conversely, in the case of the 100% silt sample (Price et al. 2019), Q_d less than Q_u indicates dilative behavior, where negative excess pore pressures are generated during shearing.
- Q_d/Q_u provides insight into the amount of strength loss a soil might experience from drained to undrained conditions. Q_d/Q_u tends to be more consistent for clays on the order of 2 to 6; more varied for silts and can be dependent on plasticity index, percentage of silt, and state; and can be much higher (up to 20) for tailings.
- Scatter of Q_d/Q_u in the data sets appears to correlate with soil type. It can be seen in Figures 1 to 3 that the variability in recorded Q_d/Q_u from the curve fit appears to be relatively small for clay-like samples, with increasing variability for silt-like and tailings samples. This is attributed to the greater variability in the depositional process.

METHOD FOR TESTING

Determination of the Q_d/Q_u ratio, and mapping of the entire V - Q_d/Q_u trend, requires testing across a range of penetration rates which is dependent on the soil drainage properties. As detailed by DeJong et al. (2012), this can be accomplished through the following steps:

1) Perform CPT testing at the standard rate of 2 cm/s, pausing penetration at select depths to run pore pressure dissipation tests.

2) Interpret pore pressure dissipation tests to estimate t_{50}. If t_{50} is greater than 75 seconds, then undrained conditions prevail. Conversely, drained conditions prevail when pore pressures generated during penetration are equivalent to hydrostatic ($t_{50} < 10$ seconds).

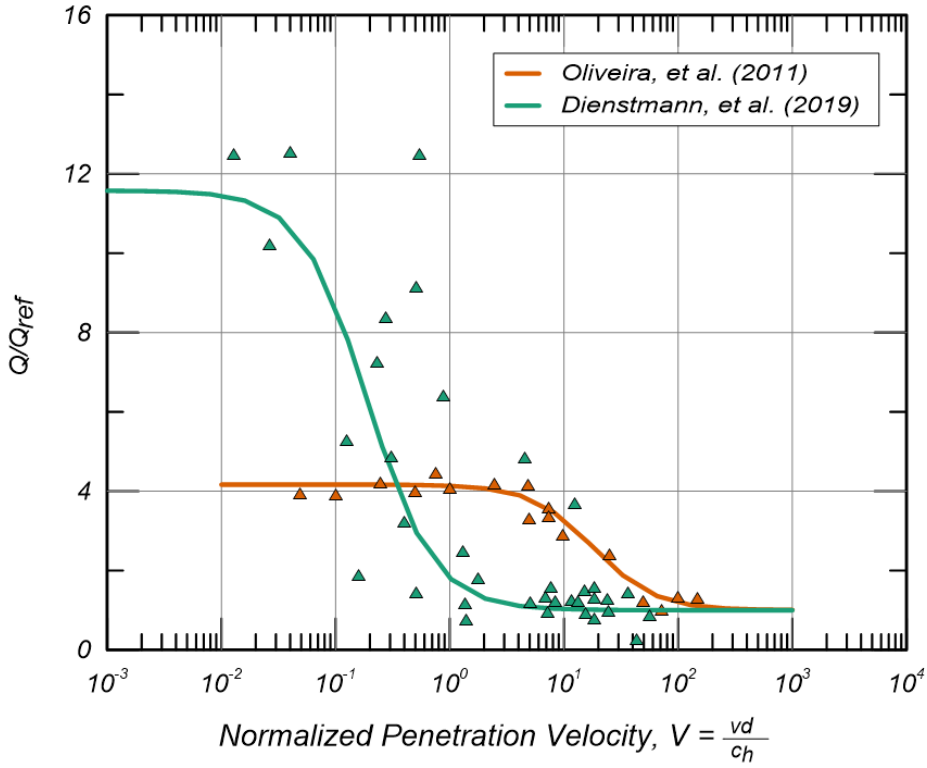

Figure 4 – Summary of VRCPT data on mine tailings.

3) Estimate c_h from the pore pressure dissipation tests using equation (4). I_r can be determined by measuring G with shear wave velocity tests or by estimation (see Schnaid, et al. 2004) using equation (6)

$$G_{max} = 320\sqrt[3]{q_c \sigma'_v p_a} \tag{6}$$

where p_a is the atmospheric pressure, and then by using equation (7) proposed by Krage et al. (2014).

$$I_r = 0.26\left(\frac{G_{max}}{\sigma'_{vo}}\right)\left(\frac{1}{0.33\left[\frac{0.33(q_t-\sigma_{vo})}{\sigma'_{vo}}\right]^{0.75}}\right) \tag{7}$$

Alternatively, I_r can be estimated using chart solutions proposed by Keavany (1985) and updated by Mayne (2007), or by assuming a value. However, typical values of I_r for tailings can vary significantly, as shown by Dienstmann (2018), where values of I_r for gold tailings ranged from approximately 100 to 900. Robertson (2016) found for young, uncemented silica based soils, I_r could be predicted by the relationship:

$$I_r = \frac{215}{\left[\left(\frac{p_a - \sigma_{vo}}{\sigma'_{vo}}\right)\left(\frac{p_a}{\sigma'_{vo}}\right)^n\right]^{0.75}} \quad (8)$$

where n ranges from 0.75 for clean sands to 1.0 for clays.

4) Determine the normalized velocity for the standard penetration rate conditions. Using Figure 5 determine existing drainage conditions, as well as how much slower and/or faster the penetration rate must be changed to achieve drained and undrained conditions, respectively.

5) Perform additional CPT soundings, either with separate soundings for each additional penetration rate or by twitch testing.

VRCPT can be implemented in the field with relative ease, however, some practical factors should be considered, including proper equipment modification, soil properties, and time management. Commercially available CPT rigs can be modified to perform variable rate testing from about 20 cm/s to 0.002 cm/s (DeJong et al. 2012). Speeds above 50 cm/s are generally not feasible to due safety concerns and hydraulic demands, and speeds lower than 0.02 cm/s are possible but generally considered impractical due to costs associated with lengthy penetration times. Therefore, site-specific soil conditions (c_h) will dictate the range of practical obtainable data with VRCPT; for example, drained data in soils with c_h greater than 10 cm^2/s is not available with current VRCPT methods, and soil with c_h = 0.2 cm/s will require a penetration rate of 0.02 cm/s to achieve drained conditions, or 0.72 meters per hour. Project specific needs, such as the time available for field exploration, must be evaluated against the practical and financial feasibility of generating sufficient data for a given soil condition.

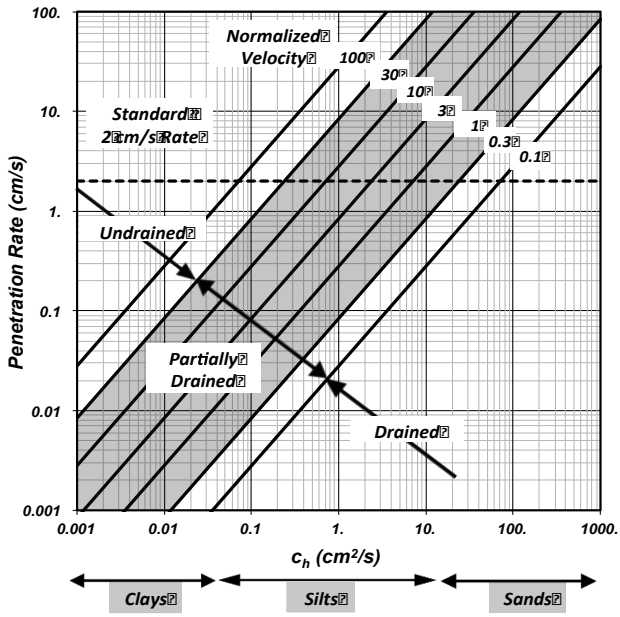

(Divide Penetration Rate by 1.22 for 15 cm^2 cone.)

Figure 5 – Chart to evaluate drainage conditions during standard CPT testing at 2 cm/sec and to selected rates required to achieve drained and undrained penetration conditions.

When performing field tests, multiple CPTs should be advanced close together at different rates to evaluate the effect of penetration rate on cone tip resistance. To do this rigorously, spatial variability should also be assessed and additional CPTs will be required for sites with higher spatial variability. Figure 6 (Krage & DeJong 2016) presents a test layout designed to systematically evaluate local spatial variability results and determine its influence on trends in VRCPT data. This layout required 3 outside CPTs performed at the conventional penetration rate and 3 (or more) internal VRCPT profiles. Additionally, discrete disturbed samples were obtained from the center of the array to verify soil conditions. Speeds shown in the inner triangular array in Figure 6 are site-specific; each site will require different penetration speeds based on Figure 5.

Occasionally it is not possible to perform such an extensive plan due to site access or time, in which case twitch tests can be performed (see House et al. 2001, Chung et al. 2006, and Jaeger et al. 2010). Twitch tests should be pushed for 4 cone diameters before changing speeds to allow for steady state conditions and sufficient data acquisition at each testing rate (i.e. 4 to 5 twitch intervals per 1 meter of testing for a 15 cm^2 cone).

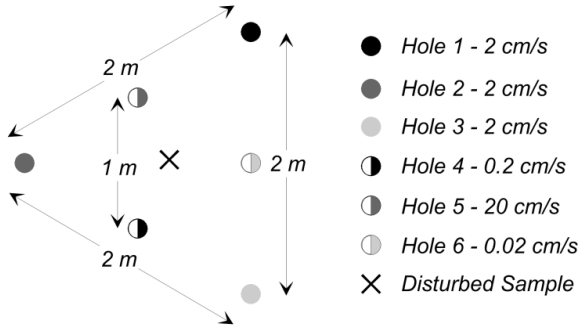

Figure 6 – Example layout of field test program to evaluate spatial variability and the effect penetration rate on cone penetration resistance.

CONCLUSIONS

This paper presented a summary of the variable rate cone penetration test method (VRCPT) and reviewed results obtained in a range of different soils including mine tailings. The following observations have been made:

- The VRCPT method provides the ability to obtain the Q_d/Q_u ratio and mapping of the entire V - Q_d/Q_u trend in order to determine what conditions exist during conventional CPT testing at 2 cm/s and what the penetration resistance is for drained and undrained conditions.
- The Q_d/Q_u ratio can provide insight into the soil state, and whether or not the soil will tend to contract or dilate upon loading. A high Q_d/Q_u ratio indicates that the soil is strongly contractive and may exhibit significant strength loss upon shearing.
- The implementation of a VRCPT field program, which properly quantifies and manages depositional spatial variability, is relatively straightforward and can be completed with relative ease at project sites.

Additional work is needed in mine tailing deposits to clarify how the trends observed in natural soils translate to manufactured mine tailings and to further develop the analysis framework using a combination of field, centrifuge, and numerical and analytical methods.

ACKNOWLEDGEMENTS

The financial support provided to Mr. Green by the ConeTec Educational Foundation and the Woeller Family Foundation is appreciated.

REFERENCES

Bjelkevik, A., & Knutsson, S. (2005). Swedish tailings: comparison of mechanical properties between tailings and natural geological materials. In *International Conference on Mining and the Environment, Metals and Energy Recovery: 27/06/2005-01/07/2005* (pp. 117-129). SveMin.

Chronology of Major Tailings Dam Failures 2020. Retrieved from Wise Uranium Project: https://www.wise-uranium.org/mdaf.html

Chung, S. F., Randolph, M. F., & Schneider, J. A. (2006). Effect of penetration rate on penetrometer resistance in clay. *Journal of geotechnical and geoenvironmental engineering*, *132*(9), 1188-1196.

Davies, M., & Martin, T. (2002). Static liquefaction of tailings–fundamentals and case histories.

DeJong, J. T., Jaeger, R. A., Boulanger, R. W., Randolph, M. F., & Wahl, D. A. J. (2012). Variable penetration rate cone testing for characterization of intermediate soils. *Geotechnical and geophysical site characterization*, *4*(1), 25-42. DeJong, J. T., & Randolph, M. 2012. "Influence of partial consolidation during cone penetration on estimated soil behavior type and pore pressure dissipation measurements." Journal of Geotechnical and Geoenvironmental Engineering 138.7: 777-788.

DeJong, J. T., & Randolph, M. (2012). Influence of partial consolidation during cone penetration on estimated soil behavior type and pore pressure dissipation measurements. *Journal of Geotechnical and Geoenvironmental Engineering*, *138*(7), 777-788.

Dienstmann, G., Schnaid, F., Maghous, S., & DeJong, J. (2018). Piezocone penetration rate effects in transient gold tailings. *Journal of Geotechnical and Geoenvironmental Engineering*, *144*(2), 04017116.

Holmsgaard, R., Nielsen, B. N., & Ibsen, L. B. (2016). Interpretation of cone penetration testing in silty soils conducted under partially drained conditions. *Journal of Geotechnical and Geoenvironmental Engineering*, 142(1), 04015064.

House, A. R., Oliveira, J. R. M. S., & Randolph, M. F. (2001). Evaluating the coefficient of consolidation using penetration tests. *International Journal of Physical Modelling in Geotechnics*, *1*(3), 17-26.

Jaeger, R. A., DeJong, J. T., Boulanger, R. W., Low, H. E., & Randolph, M. F. (2010, May). Variable penetration rate CPT in an intermediate soil. In *Proceedings of the International Symposium on Cone Penetration Testing, Huntington Beach, Calif*.

Keaveny, J. (1985). In-Situ Determination of Drained and Undrained Soil Strength Using the Cone Penetration Test. PhD dissertation, University of California, Berkeley.

Kim, K., Prezzi, M., Salgado, R., & Lee, W. (2008). Effect of penetration rate on cone penetration resistance in saturated clayey soils. *Journal of geotechnical and geoenvironmental engineering*, *134*(8), 1142-1153.

Kim, K., Prezzi, M., Salgado, R., & Lee, W. (2010). Penetration rate effects on cone resistance measured in a calibration chamber. In *2nd International Symposium on Cone Penetration Testing* (Vol. 2, pp. 2-03).

Krage, C. P., Broussard, N. S., & DeJong, J. T. (2014). Estimating rigidity index (IR) based on CPT measurements. In *Proceedings of the 3rd International Symposium on Cone Penetration Testing, Las Vegas, Nev* (pp. 727-735).

Krage, C. P., & DeJong, J. T. (2016). Influence of drainage conditions during cone penetration on the estimation of engineering properties and liquefaction potential of silty and sandy soils. *Journal of Geotechnical and Geoenvironmental Engineering*, *142*(11), 04016059.

Ladd, C. C., Foott, R., Ishihara, K., Schlosser, F., Poulos, H.G. (1977). Stress-deformation and strength characteristics.

Lehane, B. M., O'loughlin, C. D., Gaudin, C., & Randolph, M. F. (2009). Rate effects on penetrometer resistance in kaolin. *Géotechnique*, *59*(1), 41-52.

Lunne, T., Powell, J. J., & Robertson, P. K. (1997). *Cone penetration testing in geotechnical practice*. CRC Press.Oliveira, J. R., Almeida, M. S., Motta, H. P., & Almeida, M. C. (2011). Influence of

penetration rate on penetrometer resistance. *Journal of Geotechnical and Geoenvironmental Engineering*, *137*(7), 695-703.

Mayne, P.W. (2007). Cone Penetration Testing state of practice. NCHRP Project 20-05.

Price, A. B., Boulanger, R. W., & DeJong, J. T. (2019). Centrifuge Modeling of Variable-Rate Cone Penetration in Low-Plasticity Silts. *Journal of Geotechnical and Geoenvironmental Engineering*, *145*(11), 04019098.

Randolph, M., & Hope, S. (2004). Effect of cone velocity on cone resistance and excess pore pressures. In *Effect of cone velocity on cone resistance and excess pore pressures* (pp. 147-152). Yodogawa Kogisha Co. Ltd.

Robertson, P.K. (2016). Cone penetration test (CPT)-based soil behaviour type (SBT) classification system – an update. *Canadian Geotechnical Journal*.

Robertson, P. K., Melo, L., Williams, D.J., & Wilson, G.W. (2019). Report of the Expert Panel on the Technical Causes of the Failure of Feijão Dam I.

Santamarina, J. Carlos, Luis A. Torres-Cruz, and Robert C. Bachus. "Why coal ash and tailings dam disasters occur." *Science* 364.6440 (2019): 526-528.

Sarsby, R. W. (2000). *Environmental geotechnics*. Thomas Telford.

Schnaid, F., Lehane, B. M., & Fahey, M. (2004). In situ test characterisation of unusual soils. Keynote lecture. In *Proceedings of the 2nd International Conference on Geotechnical and Geophysical Site Characterization, Porto* (Vol. 1, pp. 49-74).

Schnaid, F., Bedin, J., Viana da Fonseca, A. J. P., & de Moura Costa Filho, L. (2013). Stiffness and strength governing the static liquefaction of tailings. *Journal of Geotechnical and Geoenvironmental Engineering*, *139*(12), 2136-2144.

Schnaid, F., Nierwinski, H. P., Bedin, J., & Odebrecht, E. (2014). On the characterization and classification of bauxite tailings. *Soils and Rocks*, *37*(3), 277-284.

Schnaid, F., Dienstmann, G., Odebrecht, E., & Maghous, S. (2020). A simplified approach to normalisation of piezocone penetration rate effects. *Géotechnique*, *70*(7), 630-635.

Schneider, J. A., Lehane, B. M., & Schnaid, F. (2007). Velocity effects on piezocone measurements in normally and over consolidated clays. *International Journal of Physical Modelling in Geotechnics*, *7*(2), 23-34.

Schneider, J. A., Randolph, M. F., Mayne, P. W., & Ramsey, N. R. (2008). Analysis of factors influencing soil classification using normalized piezocone tip resistance and pore pressure parameters. *Journal of geotechnical and geoenvironmental engineering*, *134*(11), 1569-1586.

Silva, M. F. (2005). Numerical and physical models of rate effects in soil penetration. PhD Dissertation, University of Cambridge.

Teh, C. I., & Houlsby, G. T. (1991). An analytical study of the cone penetration test in clay. *Geotechnique*, *41*(1), 17-34.

Wahl, D. A. J. (2012). Implementation of variable rate cone penetration testing: an experimental field study. University of California, Davis.

Vaid, Y.P. & Thomas, J. (1995). Liquefaction and post liquefaction behavior of sand. *ASCE Journal of Geotechnical Engineering*, 121(2), 163-173.

Vick, S. G. (1990). Planning, design, and analysis of tailings dams.

Volpe, R. (1979). Physical and engineering properties of copper tailings. *Current Geotechnical Practice in Mine Waste Disposal, ASCE, New York, NY*.

Yi, J. T., Goh, S. H., Lee, F. H., & Randolph, M. F. (2012). A numerical study of cone penetration in fine-grained soils allowing for consolidation effects. *Géotechnique*, *62*(8), 707-719.

Zhang, Q., Yin, G., Wei, Z., Fan, X., Wang, W., & Nie, W. (2015). An experimental study of the mechanical features of layered structures in dam tailings from macroscopic and microscopic points of view. *Engineering geology*, *195*, 142-154.

Table 1a. Reference Sample Summary

	Reference	*Soil Description*	*Test Environment*	*% Clay*	*% Silt*	*% Sand*	*PI*
Clay	Randolph et al. (2004)	Kaolin	CPT and T-Bar test in 1.8 meter radius centrifuge	100*	0	0	34
	Lehane, et al. (2009)	Kaolin	T-bar and Ball Penetration tests in a Drum or Beam Centrifuge	70	30	0	34
	Schneider et al. (2007)	Kaolin	CPT in 1.8 meter radius centrifuge	100*	0	0	34
	Kim et al. (2008)	Silty clay and clayey silt	In-situ CPTs spaced 1 meter apart (from 2 separate sites)	10 - 25	25 - 35	--	--
	Kim et al. (2010)	Kaolin Clay and Jumunjin Sand	CPT (conical and flat tip) in Calibration Chamber Tests	25 18	0 0	75 82	--
Silt	Krage et al. (2016)	Deltaic and lacustrine deposits (ML) SP/SM SM ML	In-situ CPTs, 6 per site in double traingular array - Kornbloom Granite Lenordini River Park	62 - 95 18 36 80		-- -- -- --	0 - 5 --
	Holmsgaard et al. (2016)	Silty clay to sandy silt	In-Situ CPTs	11 - 23	45 - 54	23 - 51	0 - 12
	Price et al. (2019)	Mixture of US Silica SIL-CO-SIL 250 and Old Hickory No. 1 Glaze	CPT and T-Bar test in 1 meter radius centrifuge	20 5 2.5 0	80 95 97.5 100	0 0 0 0	6 0
	Schneider et al. (2007)	Heavily overconsolidated silica flour and bentonite Lightly overconsolidated silica flour and bentonite	CPT in 1.8 meter radius centrifuge	5	95	0	12 - 14
Tailings	Dienstmann, et al. (2018)	Sandy Silt Gold Tailings	In-situ CPTs at the Fazenda Brasilerio Mine	7 - 15	57 - 65	--	0
	Oliveira, et al. (2011)	Sandy Silt Iron Ore and Silica Tailings	CPTs in 1 meter radius centrifuge	7	71	--	--

* assumed

-- information not provided in paper

Table 1b. Reference Sample Summary

	Reference	*OCR*	*Unit Weight* (kN/m^3)	C_v/C_h (m^2/yr)	*Range of Normalized Velocity*	Q_u	Q_d	V_{50}	c
Clay	Randolph et al. (2004)	1	16.5	2.6 (c_v)	0.3 - 400	0.93	3.1	0.9	0.8
	Lehane, et al. (2009)	1	--	7.8 (c_h)	0.03 - 10,000	1.6	5.9	0.17	1.3
		5				6.6	17	0.18	1.4
	Schneider et al. (2007)	1	--	1.9 - 2.1 (c_v)	0.6 - 1000	3.6	7.4	1.3	1.0
		5 - 6.5		0.5 - 0.7 (c_v)		9.5	35	6.0	1.1
	Kim et al. (2008)	--	--	11 - 184 (c_v)	0.2 - 2000	7	25	0.5	1.2
	Kim et al. (2010)	--	--	109 (c_v)	0.01 - 60	2	12	0.15	1.2
				2175 (c_v)		6.3	18	0.15	1.3
Silt	Krage et al. (2016)	10 - 15	--	15,768 (c_h)	0.01 - 200	28	66	1.5	1.5
		--	--	--		24	42	0.45	1.3
						30	48	0.41	1.5
						17	20	0.7	1.0
	Holmsgaard et al. (2016)	--	20	5045 (c_h)	0.1 - 15	55	110	2.0	1.0
	Price et al. (2019)	1 - 2	--	94.6 (c_h)	0.01 - 100	0.9	7.9	0.12	1.0
				268 (c_h)		7	30	0.38	1.0
						26	36	0.15	1.0
				315 (c_h)		400	240	15	2.4
	Schneider et al. (2007)	5 - 6.5	--	1.2 - 1.6 (c_v)	0.2 - 900	10	28	2.5	1.2
		1.5 - 2		4.6 - 5.3 (c_v)		10	56	0.7	1.9
Tailings	Dienstmann, et al. (2018)	--	--	504 - 14,506 (c_h)	0.01 - 60	1.9	22	0.19	1.5
	Oliveira, et al. (2011)	1	21	44 (c_v)	0.05 - 300	4.8	20	18	1.6

* assumed

-- information not provided in paper

Tailings Characterization using Cone Penetration Testing and Machine Learning

Iman Entezari, Dallas McGowan & James Sharp
ConeTec Investigations Ltd., Richmond, British Columbia, Canada
ConeTec Inc., USA

ABSTRACT: This paper presents the development of empirical relationships to estimate tailings constituents from in-situ Gamma Cone Penetration Test (GCPTu) measurements. A dataset of paired GCPTs and laboratory results is compiled and neural networks are employed to calibrate models to estimate tailings solids and fines content from in-situ GCPTu data. We call these relationships Tailings Behaviour Type (TBT) models. The development dataset is comprised of paired GCPTu-laboratory results collected over the past ten years from a mining area with predominately clay mineral and quartz sand tailings. Results show that TBT models predict the solids and fines content of the studied deposits within 4 and 4.9 wt% errors, respectively. Employing TBT can increase the utility of required in-situ measurements and add more meaning to the in-situ test profile. In-situ testing of tailings is more rapid, cost-effective, and repeatable than sampling and laboratory testing, and may accurately estimate tailings constituents continuously rather than at discrete depths.

1 INTRODUCTION

Mining companies frequently need to characterize their tailings to assess tailings dewatering and consolidation performance, to meet regulatory reporting requirements, to monitor deposition and volume, and to determine geotechnical stability.

Water cap, fluid tailings (slimes), and soil-like tailings are the components of a typical tailings profile. The solids content of the water cap, also called recycle water, is very low. The boundary between the water cap and fluid tailings is called the mudline and is the point at which the solids content increases sharply. Fluid tailings are characterized by high fines, very low effective stress, and an undrained shear strength less than 5kPa. Over time, and depending on the mineralogy and particle size, fluid tailings densify and form a soil-skeleton that develops effective stress. The boundary between fluid tailings and soil-like tailings is termed the hard bottom. The geotechnical behaviour of soil-like tailings depends largely on the effective stress. For geotechnical assessment, tailings management, and reclamation efforts, it is of importance to characterize the entire tailings profile, from the water cap down to the original ground. In-situ tests are routinely required to measure and monitor the tailings profile, including measure their strength. Accurate and expedient characterization of tailings requires a combination of in-situ testing and sampling. Cone Penetration Testing (CPTu) and laboratory analysis of tailings samples are two of the common testing methods used to characterize tailings.

CPTu is performed by advancing an instrumented probe with various sensors into the tailings. The CPTu probe includes sensors to measure the tip resistance, sleeve friction, dynamic pore pressure, inclination, and temperature; recorded continuously with depth. For some applications, measuring the in-situ concentrations of natural radioactivity may be simultaneously measured using a passive-gamma module behind the cone. In tailings with clay minerals, the gamma

measurements have been shown to be proportional to the clay content. Gamma Cone Penetration Test (GCPTu) profiles in tailings can readily identify and differentiate recycle water, mudline, fluid tailings, hard bottom, soil-like tailings, and natural ground (Styler et al. 2018). Laboratory testing normally provides tailings properties including the particle size distribution, water content, and residual commodity content. However, it is a time consuming and costly process involving drilling, sampling, collection, and shipment of thousands of tailings samples to laboratories each year. The sample collection, sub-sampling, handling, and homogenization, along with variable laboratory procedures, may influence the results, resulting in poor repeatability of the tests for some tailings types.

This paper presents the development of empirical relationships to estimate the laboratory characterizations from the in-situ GCPTu measurements in a specific mining region. Leveraging more than 3 decades of experience carrying out in-situ testing in this region, we are able to build a large geospatial dataset of paired GCPTs and laboratory results. Considering the large size of this dataset and complexity of the problem, a machine learning approach is used to perform the regression task. Neural Networks are employed to analyze the paired datasets and calibrate models to estimate tailings solids and fines content from in-situ GCPTu measurements. We call these relationships Tailings Behaviour Type (TBT) models. With more accurate in-situ predictions of tailings properties, geotechnical analysis using CPTu may be improved. For example, liquefaction analysis using the CPT data could be considerably improved with a more accurate fines estimate, without the need for sampling and laboratory testing.

Section 2 covers in-situ testing using GCPTu, sampling, and laboratory procedures. The characteristics of this example dataset that is used to calibrate the empirical relationships are described in section 3. The structure and training of the neural networks are covered in section 4. The developed empirical relationships, the accuracy of the models, and a discussion on the results is presented in section 5.

2 BACKGROUND

2.1 *Gamma cone penetration testing*

The CPTu is a highly-instrumented direct push probe used as an efficient, accurate, and repeatable means to collect subsurface geotechnical data in soils and have a wide variety of applications throughout geotechnical practice. The CPTu can be directly pushed into a variety of soil types including dyke, beach, slimes, and fluid tailings. To enhance CPTu data, the cone can be outfitted with additional modules to collect a variety of other in-situ data. One such module useful for characterizing tailings with clay mineralogy is the passive gamma module. This module houses a scintillating crystal that responds to naturally occurring radioisotopes, namely radioisotopes of Potassium (^{40}K), Thorium (^{232}Th), and Uranium (^{238}U). The received gamma ray incidents are counted and reported as counts per second (cps) during GCPTu advancement. In tailings where the fines are dominated by illite clays, we have observed that the gamma counts are proportional to the total fines content. Figure 1 shows various components of a GCPTu probe.

The GCPTu is typically advanced at a standard rate of 2 cm/s through the soil and all measurements are made near continuously with depth. The CPTu measures tip resistance (q_c), sleeve friction (f_s), dynamic pore pressure (u_2), inclination, and temperature. Systematic corrections are required to calculate corrected tip resistance (q_t).

$$q_t = q_c + u_2(1 - a) \tag{1}$$

In this equation, a is net area ratio for the piezocone. During undrained penetration, the scaled net tip resistance is approximately equal to the undrained shear strength (S_u). The net tip resistance for CPTu (q_{net}) is calculated using equation below:

$$q_{net} = q_t - \sigma_{v0} \tag{2}$$

where σ_{v0} is the total vertical stress which depends on the unit weight of the material. The undrained shear strength is finally calculated using the following equation:

$$S_u = \frac{q_{net}}{N_{kt}} \tag{3}$$

The N_{kt} in Equation 3 is a bearing factor that depends on theory or numerical simulation methods (Konrad & Law 1987, Yu & Mitchell 1998).

The piezometer included in the CPTu is used to measure the dynamic pore pressure in-situ during penetration, the decay or rise of pore pressure after pausing penetration, and the static equilibrium pore pressure during a sufficiently long pause in penetration. In fluid tailings where the fine solids are suspended, the effective stress is zero and the dynamic pore pressure equals the equilibrium pore pressure which equals the total stress. In soil-like tailings where tailings particles are touching and their behaviour is frictional, the pore pressure measurement is affected by transient pore pressures generated from both cavity-expansion and shear of the tailings during the insertion of the probe. A pore pressure dissipation (PPD) test can be performed to measure the rise or decay or dynamic pore pressure, and to determine the in-situ equilibrium pressure.

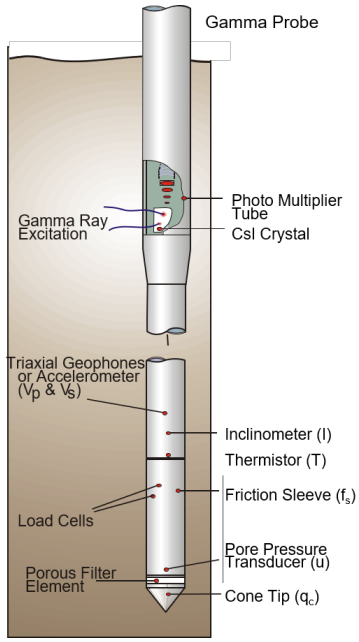

Figure 1. Components of a GCPTu probe (note: diameter change is for illustration only).

2.2 *Sampling and laboratory analysis*

Several different types of sampling equipment may be employed to collect samples from tailings. The type of the sampling equipment depends on the type of material to be collected. Sonic and fluid samplers are two common disturbed sampling tools for general sampling purposes in tailings. Sonic sampling can be used in a variety of material from dense beach sand tailings to slimes. It collects a continuous core sample with certain diameter and length (e.g. 50 mm x 2 m). The fluid sampler on the other hand is an effective tool for sampling in fluid or slurry tailings, collecting a point sample (normally ~3 liters) at a specific depth.

Typically, a laboratory program is carried out to measure tailings characteristics including the solids and total fines content of interest in this paper. Methods such as oven-drying are used to measure the solid or water content of tailings, while the total fines content is normally measured through a sieve analysis or laser diffraction. The type of sampler used, subsampling methods, sample transport and handling, as well as the repeatability of laboratory testing may all impact the consistency, repeatability, and accuracy of the results.

3 DEVELOPMENT DATASET

To create the dataset of paired GCPTu profiles with adjacent sample holes and laboratory results, our geospatial database was queried to find GCPTu and sample results collected over a ten-year period within a single geological mining region. The GCPTu soundings were paired with sample results collected within a 5-meter radius, at the same elevation, and within 1 month of the GCPTu sounding being completed (x, y, z, t pairs of data). For point fluid samples, the median GCPTu measurements over a 0.5 m depth window centered at the fluid sample elevation was paired with the laboratory results. For core samples (sonic), the window size was equal to the length of the sample. The geographical location of the query was restricted to a specific mining and geological area of approximately 2500 square kilometers. This mining region is dominated by upstream constructed sand tailings dams, with tailings composition ranging from medium quartz sand to clay. The fines are dominated by clay minerals, resulting in large volumes of fluid clay slurry tailings. The result of the database query led to a dataset of more than 20,000 data points.

Calibrating the TBT model requires a representative dataset. A representative dataset includes pairs of in-situ measurements and sample results that are well correlated. Non-representative data is possible when samples and in-situ measurements are paired in non-homogenous layered deposits, native ground, or in some specific treated tailings areas. As such, these pairs are excluded from the representative dataset for model calibration.

To compile a representative dataset, the paired data points were inspected. The data points in recycle water, natural ground, treated tailings areas, or near layer boundaries are screened out. The screening process resulted in a working dataset of approximately 13,000 data points for this study. Figure 2 shows a ternary diagram of the paired dataset. The dataset shows a crescent-shaped property distribution of the study tailings. This figure shows that the tailings range from sandy soil-like tailings with high solids and low water content in the lower left corner to tailings with high fines, low sand, and high water content along the top-right edge.

This is an ideal dataset for modelling as it contains variety of materials paired with in-situ measurements collected from multiple tailings facilities operated by different mining companies over a significant period of time. Therefore, the models developed using this dataset are robust against equipment, procedural, and temporal variations, and should work to predict the properties of most tailings types within the geological region of the original data.

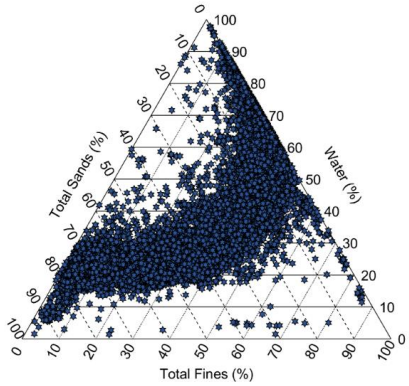

Figure 2. The ternary diagram of the development dataset.

4 MACHINE LEARNING MODELLING

Machine Learning is a subfield of Artificial Intelligence, dealing with developing algorithms and models that enable computers to perform a specific task, without the need of developing a set of explicit rules. A machine learning model learns from existing data that is often labeled and allows the computers to discover the patterns and predictive rules.

Machine Learning has become popular in almost all industries and disciplines to provide valuable data-driven insights and make better decisions. Geotechnical engineering is a discipline that frequently uses empirical relationships to estimate soil properties and thus can greatly benefit from machine learning (e.g. Goh 2002, Kim & Kim 2006, Hanna et al. 2007). The data-driven approaches have gained substantial interest over traditional modelling because not only do they deal better with uncertainties and complexities in geotechnical engineering problems, they also do not require prior assumptions about the fundamental and physical relationships between parameters (Shahin et al. 2008, Puri et al. 2018). The machine learning algorithms can therefore lead to more robust predictive models compared to traditional modelling.

Neural Networks have recently shown great promise in modelling problems including classification and regression tasks. The architecture of neural networks allows us to combine multiple layers and neurons so that the entire network can make complex and accurate decisions. They are particularly powerful in modelling nonlinear relationships between input and output variables. We thus examined the potential of neural networks in modelling the relationship between the in-situ and laboratory measurements of tailings.

4.1 *Neural networks and learning algorithm*

Neural Networks were employed to develop the TBT models and calibrate the GCPTu data to the laboratory results. For this study, a feed-forward backpropagation neural network structure with one hidden layer consisting of 10 neurons was used. An ensemble-based learning approach using bootstrap aggregation technique (Bagging) was employed to train the neural networks (Sollich & Krogh 1996, Breiman 1996). In the Bagging method, several uniformly distributed training sets are randomly selected from the original training set and neural networks are trained using each of these training sets. The outputs of these trained networks are then combined to generate the final prediction results.

To ensure the neural networks and thus the TBT models were not over-fitted to the data, the development dataset was split to training and test datasets so that the performance of the final models could be examined on the test set (i.e. the test dataset is not seen by the neural networks during the training phase). Approximately 10% of the development dataset was put aside as the test set. The remaining 90% of the development dataset was used as the training set. To train the neural networks, 20 bootstrapped training sets were generated from the original training set. The size of each bootstrapped training set is equal to the size of the original training set (due to replacement in bootstrap sampling, in each training set some of the samples are missing and some occur several times). The final neural network model was thus an ensemble (average) of 20 neural networks trained using each of the bootstrapped training sets.

4.2 *Input parameters*

The input variables used in neural networks included the undrained shear strength, the slope of the dynamic pore water pressure versus depth, the passive gamma rate, as well as the latitude, longitude, and the mining property name where the data was collected. Because the dataset consisted of data from multiple sites operated by multiple mining companies, including the geographical location and the operator name as input variables potentially added information about unquantified mineralogy variances between different deposits as well as known variations in laboratory procedures. Including geographical and owner information significantly improved the performance of the models, allowing them to seamlessly predict tailings properties as they would normally be reported at that particular mine.

Although Ball Penetration Testing is not discussed in this paper, it is frequently used to measure shear strength of fine tailings. The undrained shear strength was used as an input parameter in this model because this allows the TBT model to work for both GCPTu and Gamma-Ball profiles. To

calculate the net tip resistance for CPTu measurements (Eq.2), an estimate of total vertical stress is required which depends on the unit weight of the tailings. In fluid tailings, the inverse slope of the dynamic pore water pressure is used as the total unit weight. The slope of the dynamic pore water pressure is calculated over a moving depth window of 0.5 m. Within the window, the data points with an effective tip resistance (q_t-u_2) greater than 100 kPa are excluded from the calculation of the slope. The calculated slope is constrained between 9.8 and 18 kN/m^3. In non-fluid tailings (soil-like tailings with effective stress), an average uniform unit weight of 18.21 kN/m^3 is assumed for this study. This corresponds to a solids content of 75% when a specific gravity (G_s) of 2.6 is used in Equation 4. Small variations in the actual effective stress of these tailings do not have a material impact on the calculated undrained shear strength of solid tailings. However, a potential improvement in the method may be the addition of an iteration cycle to predict the actual unit weight from the percent solids.

$$Solids = \left(\frac{G_s}{G_s-1}\right) - \frac{9.8(\frac{kN}{m^3})}{\gamma_t}\left(\frac{G_s}{G_s-1}\right) \tag{4}$$

4.3 *Error assessment*

The performance of the models was evaluated by quantifying properties of the cumulative distribution function (CDF) of errors on the test set. The error was defined as the discrepancy between the lab results and model predicted results (Equation 5). The error for each paired data point in the test dataset was calculated and sorted in ascending order to form the CDF. The 50$_{th}$ percentile in the CDF is taken as the bias of the TBT prediction. We assumed that the TBT error follows a normal distribution, such that the CDF values at 15.9% and 84.1% correspond to ±1 standard deviation. The TBT error is the dispersion around the median to the 15.9 and 84.1 percentiles.

$$Lab\ Results = TBT\ Estimate + TBT\ Error \tag{5}$$

5 RESULTS AND DISCUSSIONS

The relationship between the laboratory measured and TBT predicted solids content is shown in Figure 3a. Both training set (blue dots) and test set (red dots) are displayed in this figure. As can be seen a strong correlation is observed between the measured and predicted results (R^2 of 0.87 on the test set). The bias and error of the model is observed to be 0.39% and 4%, respectively. This positive bias value means the model slightly underestimates the laboratory solids content measurements by 0.39%. The error of 4% means that 68.2% of the predicted solids content results fall within ±4% of the laboratory measured solids content.

Figure 4a shows the relationship between the total fines content measured in the laboratory vs the total fines content predicted by neural networks-based modelling. The R^2 on the test set is calculated to be 0.75. The CDF of errors in Figure 4b shows a bias of -0.35% and error of 4.9%. The model slightly over-predicts the total fines content.

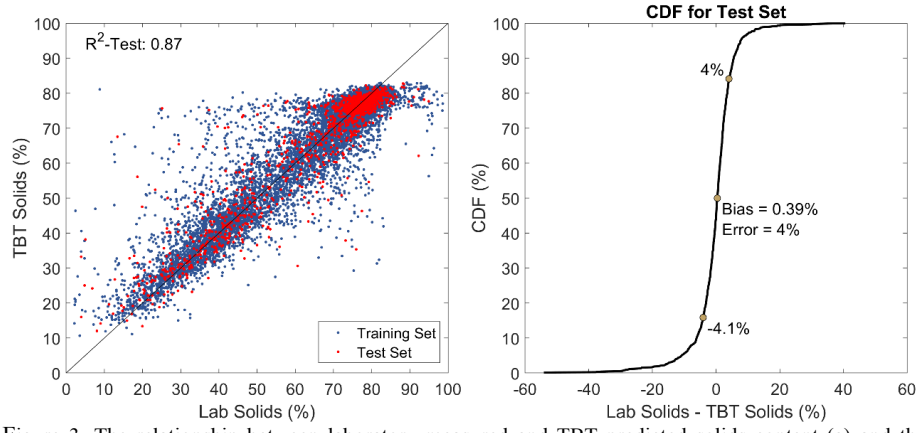

Figure 3. The relationship between laboratory measured and TBT predicted solids content (a) and the cumulative distribution function (CDF) of errors on the test set.

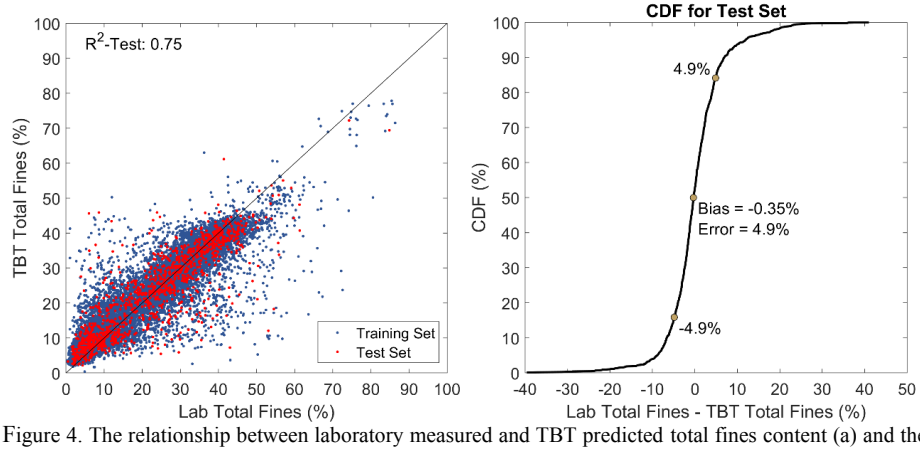

Figure 4. The relationship between laboratory measured and TBT predicted total fines content (a) and the cumulative distribution function (CDF) of errors on the test set.

5.1 *TBT profiles*

Example tailings constituent profiles estimated using the developed TBT model are shown in Figures 5 and 6. The laboratory results are over-plotted in these figures to visually assess the performance of the TBT model.

In Figure 5, the mudline is at 3 m based on the low cone tip resistance and rising gamma counts. The higher gamma counts and low cone tip resistance between 3 and 10.5 m is indicative of fluid tailings. The solids content and total fines content are nearly equal in the fluid tailings which indicates a low sand content. The low gamma counts and relatively high cone tip resistance from 10.5 to 16 m is indicative of soil-like tailings. As seen in this figure, the TBT estimated constituents successfully follow the laboratory results over the entire tailings profile.

An example TBT profile in soil-like tailings is shown in Figure 6. The high solid content, low total fines content and low gamma counts between 0 m to 30 m is characteristic of soil-like deposits. The TBT estimated constituents agree with the laboratory results.

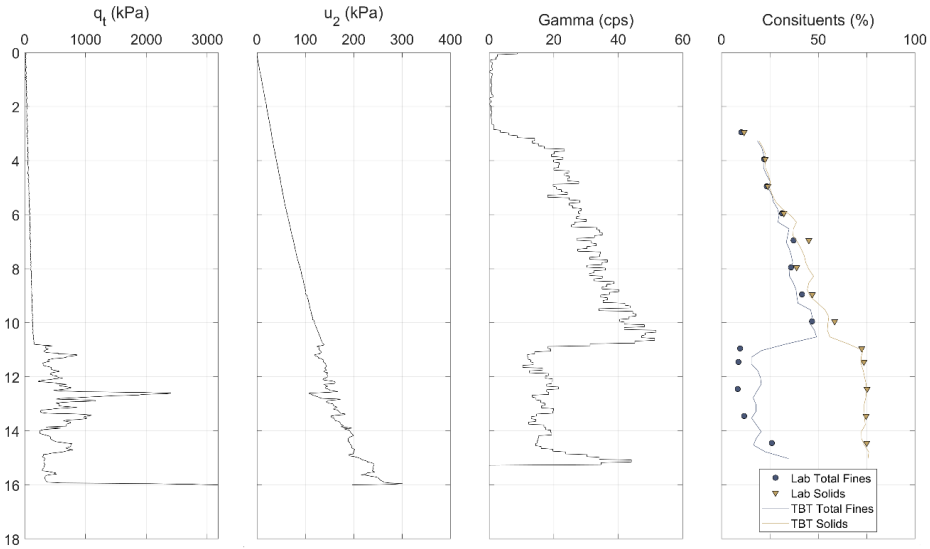

Figure 5. Example TBT profile in fluid and soil-like tailings.

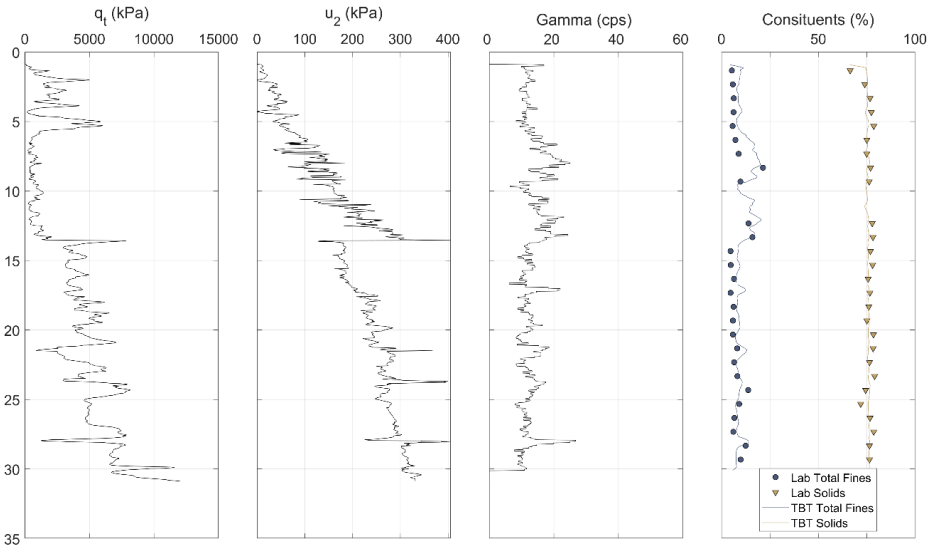

Figure 6. Example TBT profile in soil-like (beach) tailings.

5.2 *Outliers and sources of error*

In both Figures 3a and 4a, there are datapoints with high errors. These outliers could generally be attributed to three factors. First, these samples may not be representative of the typical tailings. Although when compiling the dataset, efforts were made to screen non-representative samples, it was not possible to check all 20,000 points manually. Therefore, some of these outliers are tailings contaminated with natural soil, or completely natural soils, or non-homogenous tailings at stratigraphic layer boundaries, or treated tailings with different and non-modelled properties. The layer boundaries are particularly problematic when sampled by coring using sonic or direct push

piston samplers. A core sample is typically homogenized before being analyzed in the laboratory, and if the core is across a layer boundary and not subdivided, then the materials will be mixed in analysis. Due to the heterogeneity of a boundary sample, the laboratory result may not be comparable with the adjacent in-situ GCPTu predicted result, from up to 5m away. Second, while compiling the paired dataset, the query was restricted such that only sample results falling withing a 5-meter and 1-month buffer from the GCPTu soundings are paired with the in-situ soundings. Given the moderate rate of change in tailings facilities, this restriction criterion is considered sufficient to minimize the temporal and spatial variation between the in-situ and laboratory results. However, there might be activities (e.g. deposition of new material and dredging) within a tailings pond causing localized inconsistencies between the laboratory results and in-situ measurements. Third, the laboratory analysis may be prone to poor repeatability between different labs, as well as sample preparation and human errors. The QA/QC procedures in place significantly reduce errors but cannot eliminate all of them. For the purposes of quantifying error, the lab data is assumed to be perfect and the model predictions are measured against the lab data. Ultimately, investigating outliers and eliminating them from the dataset (with justification), and then recalibrating the models may further improve the performance of the TBT.

5.3 *Generalization and robustness of the models*

The performance of the models was assessed using a test set. This is considered a class-A error assessment or a blind test to evaluate the generalization and robustness of the models when applied on data other than the data used for the training and calibration of the models. However, since the geographical locations of the in-situ soundings are included in the input variables fed into the neural networks, the models are only valid for the region of study. Furthermore, even within this region, the models may not perform well when in-situ tests are carried out outside the current boundaries of the region. This implies that if a new mining facility is developed, these models may need to be revisited and recalibrated with new data. Similarly, the use of the operator names (proxy for tailings processing and laboratory methods) as an input variable means that the model currently only works on the data acquired from the operators used in the current study. Further investigation is required to assess the impact of the geographical location and operators name on the performance of the models when applied on new data in the future.

6 CONCLUSIONS

This paper presented a novel method to estimate mine tailings characteristics from in-situ GCPTu measurements. The potential of machine learning was evaluated to develop empirical correlations, called tailings behaviour types (TBT), between the solids and total fines contents of tailings measured in the laboratory and the in-situ GCPTu measurements. A development dataset was compiled with over 13,000 samples results paired with adjacent GCPTu measurements collected over the past ten years in a large geological and mining region. Neural Networks were used to calibrate models capable of predicting the laboratory results for a given sounding. The input variables used in modelling included variables calculated from in-situ measurements as well as geographical location and the name of the mine operator. The latter set of variables were used to provide descriptive information about the variation in the mineralogy and treatment of tailings as well as the variability existing between the laboratory procedures. The results showed that the developed models can predict the solids content and total fines content of the deposits under study with 4% and 4.9% error, respectively, and with a negligible bias.

In-situ testing of tailings is more rapid, cost effective, and repeatable than sampling and laboratory testing. Using the GCPTu data, tailings constituents can be estimated with adequate accuracy and continuously with depth rather than at discrete depths. This results in detailed tailings constituent profiles, and thus improves information on tailings deposits compared to conventional discrete sampling and laboratory analysis. Furthermore, engineering analysis of CPTu data may be improved with better insight into the tailings constituents, such as assessing compressibility from an accurate prediction of fines content. Through utilization of TBT models,

mine operators may be able to increase the spatial density of tailings data, and ultimately improve modelling and management at a reduced cost and greater efficiency.

In future research, we aim to investigate the use of new emerging machine learning methods, evaluate the addition of other in-situ derived data (e.g. shear wave velocity), develop correlations for other tailings constituents (e.g. clay content), and explore the applicability of such models on natural soils and tailings deposits outside the region investigated in this study.

REFERENCES

Breiman, L. 1996. Bagging predictors. *Machine Learning* 24 (2): 123-140.

Goh, A.T. 2002. Probabilistic neural network for evaluating seismic liquefaction potential. *Canadian Geotechnical Journal* 39(1): 219-232.

Hanna, A.M., Ural, D., & Saygili, G. 2007. Neural network model for liquefaction potential in soil deposits using Turkey and Taiwan earthquake data. *Soil Dynamics and Earthquake Engineering* 27(6): 521-540.

Kim, Y. & Kim, B. 2006. Use of artificial neural networks in the prediction of liquefaction resistance of sands. *Journal of Geotechnical and Geoenvironmental Engineering* 132(11): 1502-1504.

Konrad, J.M. & Law, K.T. 1987. Undrained shear strength from piezocone tests. *Canadian Geotechnical Journal* 24 (3): 392-405.

Puri N., Prasad H.D. & Jain A. 2018. Prediction of geotechnical parameters using machine learning techniques. *Procedia Computer Science* 125: 509-517.

Shahin, M., Jaksa, M. & Maier, H. 2008. State of the art of artificial neural networks in geotechnical engineering. *The Electronic Journal of Geotechnical Engineering*. Bouquest08: 1-26.

Sollich, P. & Krogh. A. 1996. Learning with ensembles: how over-fitting can be useful. In D.S. Touretzky, MozerM.C. Touretzky and M.E. Hasselmo (eds), *Advances in Neural Information Processing Systems*, MIT Press, Cambridge, MA: 8: 190–196.

Styler, M.A., McGowan, D., & Sharp J. 2018. Characterizing soft oil sand tailings by gamma cone penetration testing. *Proceedings of the 6th International Oil Sands Tailings Conference*. 9-12 December 2018, Edmonton, Alberta, pp. 112-120.

Yu, H.S. & Mitchell, J.K. 1998. Analysis of cone resistance: review of methods. *Journal of Geotechnical & Geoenvironmental Engineering* 124 (2): 140-149.

CPT Dynamic Pore Water Pressure and Liquefaction Potential in Tailings Sand at Suncor

Ayman H. Abusaid, Ying Zhang & Gordon W. Pollock
Wood Environment & Infrastructure, Edmonton, Alberta, Canada

Ryan Moore & Jason Rhee
Suncor Energy Inc., Calgary, Alberta, Canada

ABSTRACT: Pore pressure response during Cone Penetration Testing (CPT) in tailings sand is governed by the degree of saturation, density and state of the sand, fines content, cone apparatus, and cone penetration speed. This paper presents the pore pressure response in tailings sand of different degree of saturation, density, and fines content. Conventionally, it has been assumed that CPT penetration generates positive excess pore pressure in contractive material and negative excess pore pressure in dilative material. However, this is not always the case. This paper presents data showing the opposite trend and provides discussion regarding the phenomenon.

1 INTRODUCTION

Liquefaction is associated with large positive excess pore pressure generated in an undrained manner in saturated or nearly saturated loose (contractive) sand/ silt/ sensitive clay. The trigger event can be large or small. It can be static load, cyclic load, or rise of the water table. Silvis & de Groot (1995) and Robertson (2010) suggested that triggering should always be assumed for potentially liquefiable soils.

CPT with pore pressure measurement (CPTu) is widely used in liquefaction susceptibility analyses. Criteria has been developed using corrected tip resistance ($Q_{tn,cs}$) by Robertson (2010) and using state parameter (ψ) under the framework of critical state soil mechanics by Jefferies & Been (2016). Winckler et al. (2014) discussed using the measured pore pressure as part of the CPT assessment in determining the liquefaction susceptibility of saturated non-plastic tailings. The reasonable premise of the assessment is that potentially contractive soils would generate positive excess pore pressure during the CPT penetration and dilative tailings would generate negative excess pore pressures. Excess pore pressure (U_e) is defined as the difference between the dynamic pore pressure and pore pressure at equilibrium.

The focus of this paper is to highlight potential challenges with using pore pressure measurements from CPTu testing. Data from a large hydraulically placed sand structure at Suncor oilsands mine is used for the basis of this assessment. Data is available for both compacted and uncompacted regions.

2 SAND DUMP 8

Sand Dump 8 is an upstream constructed tailings structure at Suncor. It is located at the Suncor Millennium mine site north of Fort McMurray, as shown in Figure 1. Whole tailings are hydraulically transported from the extraction plants through pipelines to the perimeter of Sand Dump 8. Upon deposition, the sand particles settle down near the discharge points to form

the sand beach. Some fines are trapped in the sand beach while the rest flows to the center fluid pond. Continuous dozer track packing has been implemented during tailings placement to form a non-liquefiable shell as part of the upstream tailings dam. Figure 2 presents a recent satellite image showing the compacted sand zone and uncompacted sand beach at Sand Dump 8.

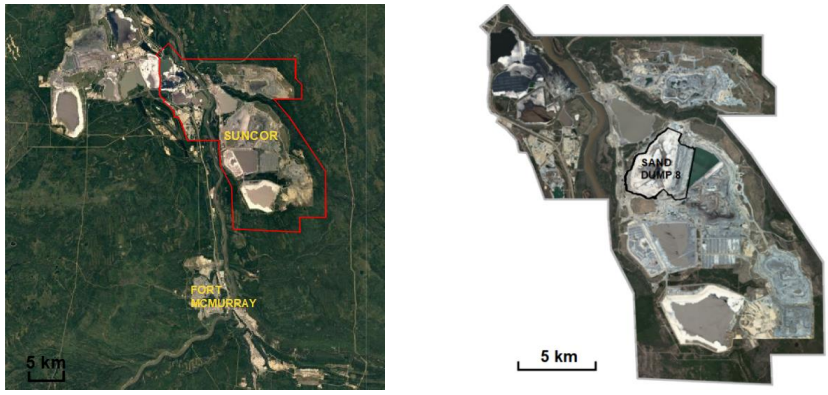

Figure 1 Location and plan view of Suncor Sand Dump 8

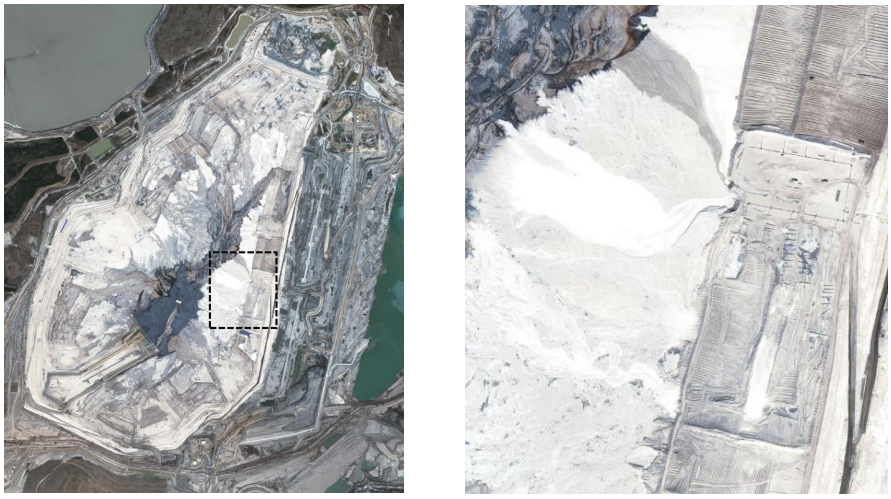

a) Overall site plan of Sand Dump 8 b) Tailing beach at Sand Dump 8

Figure 2 Satellite image of Sand Dump 8 as of May 2020

CPTu has been regularly conducted in the compacted tailings sand at Sand Dump 8 to assess its susceptibility to liquefaction. The method(s) used for evaluating susceptibility to liquefaction and the results of the CPTu in the compacted zones are presented and discussed in detail in a companion paper by Zhang et al (2020). CPTu has also been conducted in the uncompacted zone to study the behavior of uncompacted beach sand. This paper presents and evaluates the pore pressure response in tailings sand in both the compacted and uncompacted zones at Sand Dump 8. It should be noted that “pore pressure” is used interchangeably with “pore water pressure” in this paper.

3 TAILINGS SAND PROPERTIES AND CPT EQUIPMENT USED AT SAND DUMP 8

Tailings sand at Sand Dump 8 is fine-grained sand with a trace (< 5%) of medium-grained sand and a trace of silt and clay. The fines content (particle size < 45 µm) is typically in the range of 3% to 5% in the compacted zone and 3% to 7% in the uncompacted sand zone.

Figure 3 shows the CPT track rig, ramset with CPT probe, CPT probe (without the filter), and filter element used at Sand Dump 8. Standard cone penetrometer has been used, which has a tip base area of 15 cm^2, an apex angle of 60°, and porous filter element at the cone shoulder (u_2 location). The porous filter element is made of polyethylene with pore sizes in the range of 90 µm to 160 µm. The saturation fluid for the filter element is silicone oil. The penetration speed is 2 cm/second. Penetration is paused at specified depths for pore pressure dissipation (PPD) tests.

Figure 3 CPT equipment used at Sand Dump 8

4 DYNAMIC PORE PRESSURE RESULTS

In this study, CPT data from 30 tests located in the compacted zone and from 20 tests located in the uncompacted zone were used. The 30 tests were conducted in October 2019 in the compacted zone at Sand Dump 8. The 20 test locations in the uncompacted zone were from CPT programs conducted between 2015 and 2017. The test locations used in this study are shown in Figure 4.

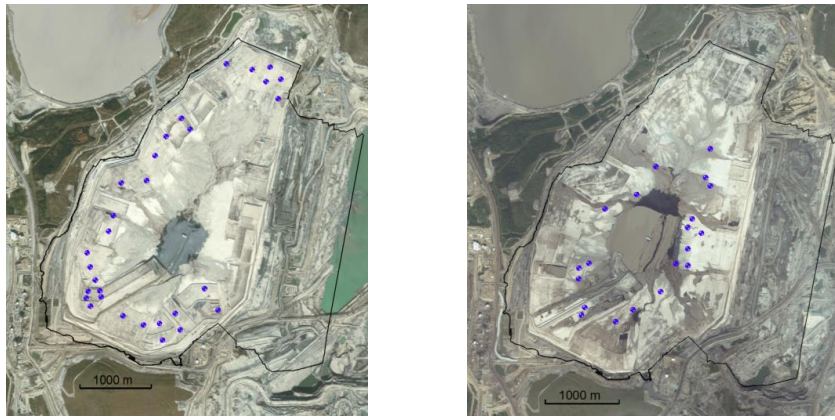

a) CPT Locations in Compacted Zone (Satellite Photo 2019)

b) CPT Locations in Uncompacted Zone (Satellite Photo 2016)

Figure 4 Site plan with CPT locations

4.1 *Compacted Tailings Sand*

Figure 5 shows four representative dynamic pore pressure profiles along with PPD and $Q_{tn,cs}$ data in compacted tailings sand at Sand Dump 8. Tailings sand in the compacted zone receives constant track-packing during tailings placement. The majority of the tailings sand has a high $Q_{tn,cs}$ value (i.e. greater than 70) and is considered dilative (Robertson 2010). However, there are isolated zones with low $Q_{tn,cs}$ values which are typically thin and surrounded with sand with high $Q_{tn,cs}$ values. The variability of $Q_{tn,cs}$ is due to the challenges associated with compaction during active tailings placement.

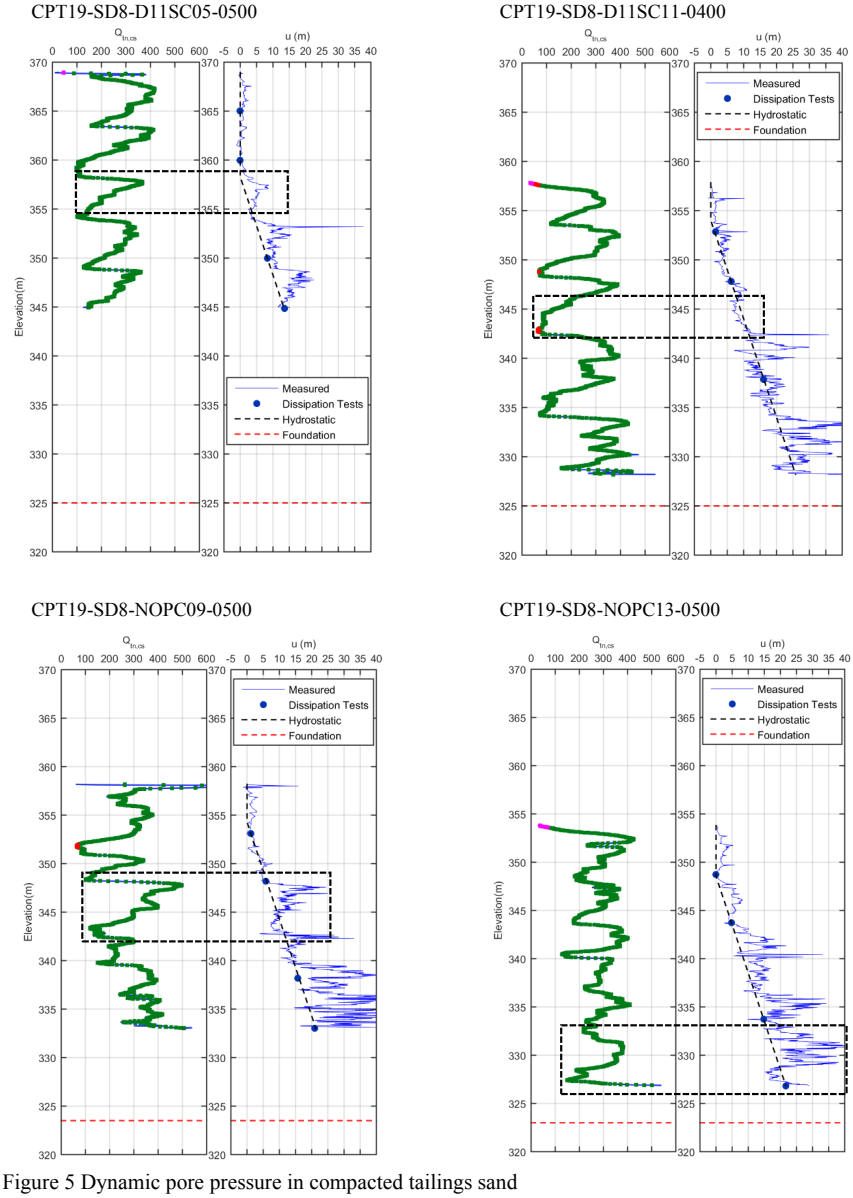

Figure 5 Dynamic pore pressure in compacted tailings sand

As shown in Figure 5, dynamic pore pressure increases with increasing $Q_{tn,cs}$ and decreases with decreasing $Q_{tn,cs}$. Consequently, positive excess pore pressure was measured in zones with high $Q_{tn,cs}$ values and negative excess pore pressure was measured in zones with low $Q_{tn,cs}$ values which is the opposite of what would be expected. The same trend was also observed in the other CPT tests in the compacted zone.

Figure 6 shows all the CPT data below the water table at the 30 test locations on the updated soil behavior type (SBT) classification system by Robertson (2016). Robertson (2016) divided soils into seven categories per their behavior. A modified soil behavior index, I_B, was used to distinguish clay-like, sand-like, and transitional zone soils. Based on the SBT chart, the majority (98.5%) of the tailings sand in the compacted zone is classified as sand-like ($I_B > 32$). Data points with $I_B \leq 32$ appear to be from thin layers (1.5% of the total data points). The sand-like soil behavior is consistent with the tailings sand properties in Section 3.

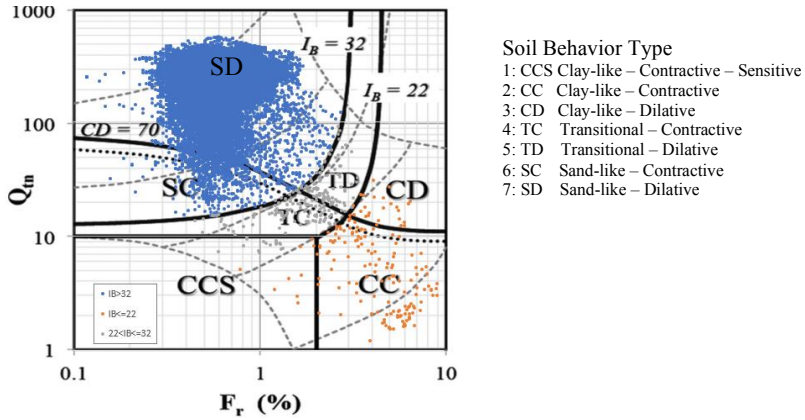

Figure 6 Updated soil behavior type chart (modified after Robertson 2016)

Robertson (2010) found that $Q_{tn,cs}$ contours are nearly parallel to the state parameter contours in the SBT chart. $Q_{tn,cs}$ is therefore considered an indication of the relative density to the critical state. Figure 7 presents the distribution of $Q_{tn,cs}$ values for the same CPT data shown in Figure 6. The wide distribution of $Q_{tn,cs}$ indicates the variability in the tailings sand with respect to density or state, while over 95% of the $Q_{tn,cs}$ is higher than 70 and is considered dilative (Robertson 2010).

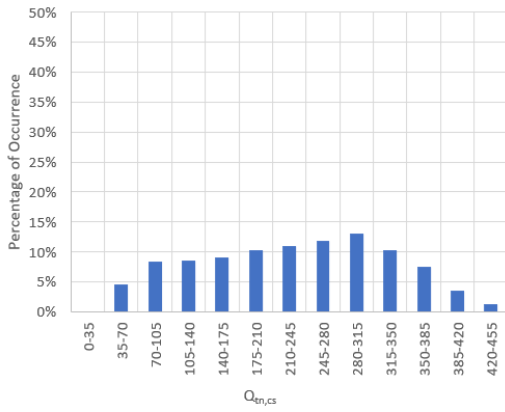

Figure 7 Distribution of $Q_{tn,cs}$ in compacted tailings sand

Figure 8 presents the $Q_{tn,cs}$ – U_e chart for data points with I_B > 32 (sand-like). As shown in Figure 8, both positive and negative excess pore pressures were observed for all $Q_{tn,cs}$ < 500. The 10th percentile, 20th percentile, and average of U_e show that excess pore pressure slightly increases with increasing $Q_{tn,cs}$ as opposed to the expected trend of decrease in excess pore pressure with increase in $Q_{tn,cs}$.

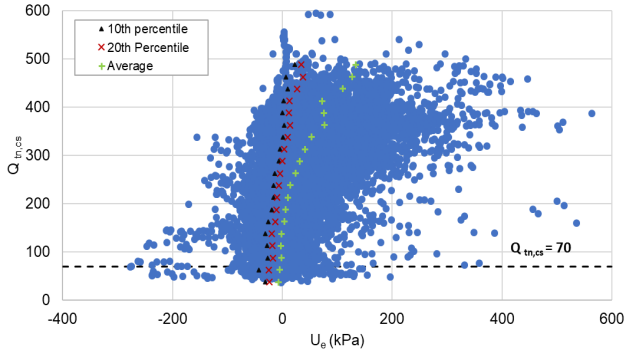

Figure 8 $Q_{tn,cs}$ – U_e Chart with I_B > 32

The measured pore pressure was also evaluated in terms of normalized pore pressure. CPT dynamic pore pressure is typically normalized with the overburden stress and tip resistance, such as the normalized pore pressure parameter $B_q = \Delta u_2/(q_t - \sigma_{v0})$ proposed by Robertson (1990). Schneider et al. (2008) showed that a new normalized pore pressure parameter ($U_2 = \Delta u_2/\sigma_{v0}'$) is superior to B_q in the soil classification of North Sea clay.

Figure 9 shows the CPTu data from the 30 test locations on a quadrant plot as presented by Winckler et al (2014) which plots the normalized pore pressure parameter (U_2) against the state parameter difference (ψ+0.05). As discussed in their paper, if the data plots in Quadrant 1, there is confidence in classifying the material as contractive (positive excess pore pressure and state parameter indicative of loose soil). Conversely if the data plots in Quadrant 3, there is confidence in classifying the material as dilative (negative excess pore pressure and state parameter indicative of dense soil). As shown on Figure 9, the data for Sand Dump 8 lies predominantly within Quadrant 2 indicating less confidence of a liquefaction classification. This is in spite of the vast majority of data having a $Q_{tn,cs}$ of greater than 100 which would put the material as being clearly dilative by any method of interpreting the data. It is proposed that this contradiction does not imply an error with the concept of correlating positive U_2 to contraction and negative U_2 to dilation, but rather to the actual measurement of the dynamic pore pressure as discussed in Section 5.

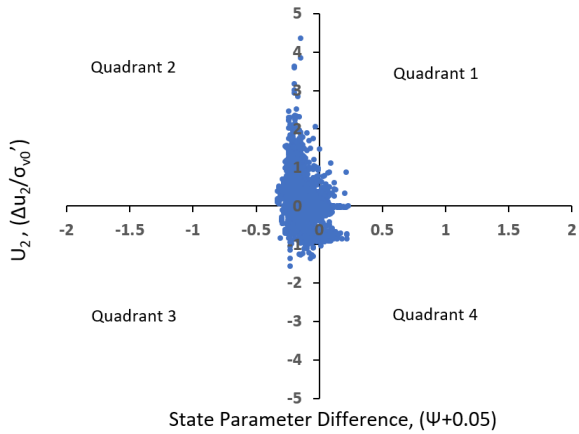

Figure 9 U_2 – State Parameter Difference Chart (modified after Winckler et al. 2014)

In addition, the CPT data from the 30 test locations in the compacted zone is also shown on the modified Q_{tn} – U_2 chart by Robertson (2016) in Figure 10. Approximately 96% of the data points are in the sand-like dilative (SD) zone. The SD zone is labelled as the "essentially drained zone" in Schneider et al (2008), which implies that the tailings sand in the compacted zone at Sand Dump 8 is fully drained or nearly drained during cone penetration. Pore pressure in drained soils dissipate and stays at hydrostatic pore pressure. Therefore, the positive and negative excess pore pressure could be muted because of the nearly drained behavior during CPT penetration. In other words, the dynamic pore pressure in fully drained or nearly drained soils relative to CPT penetration may not measure the excess pore pressure expected in undrained soils.

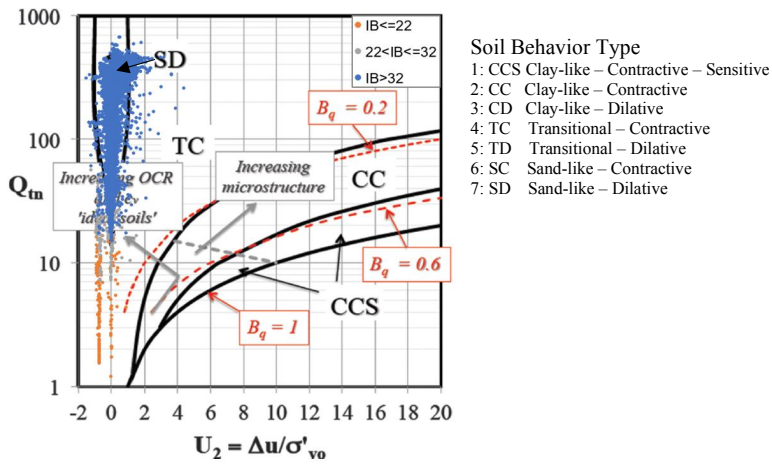

Figure 10 Q_{tn} – U_2 Chart (modified after Robertson 2016)

4.2 *Uncompacted Tailings Sand*

Figure 11 shows four representative dynamic pore pressure profiles along with PPD and $Q_{tn,cs}$ data in uncompacted tailings sand at Sand Dump 8. Tailings sand in the uncompacted zone does

not receive dozer compaction during tailings placement. Therefore, uncompacted tailings sand is expected to be more uniform (with respect to density and state) and looser ($Q_{tn,cs}$) compared to the compacted tailings sand. As shown in Figure 11, the dynamic pore pressure is generally near hydrostatic and fluctuates around the hydrostatic pore pressure line, which indicates the uncompacted tailings sand could be drained or nearly drained during CPT penetration. The same trend was also observed in the other CPT tests in the uncompacted zone. The measured pore pressure response is further discussed in Section 5.

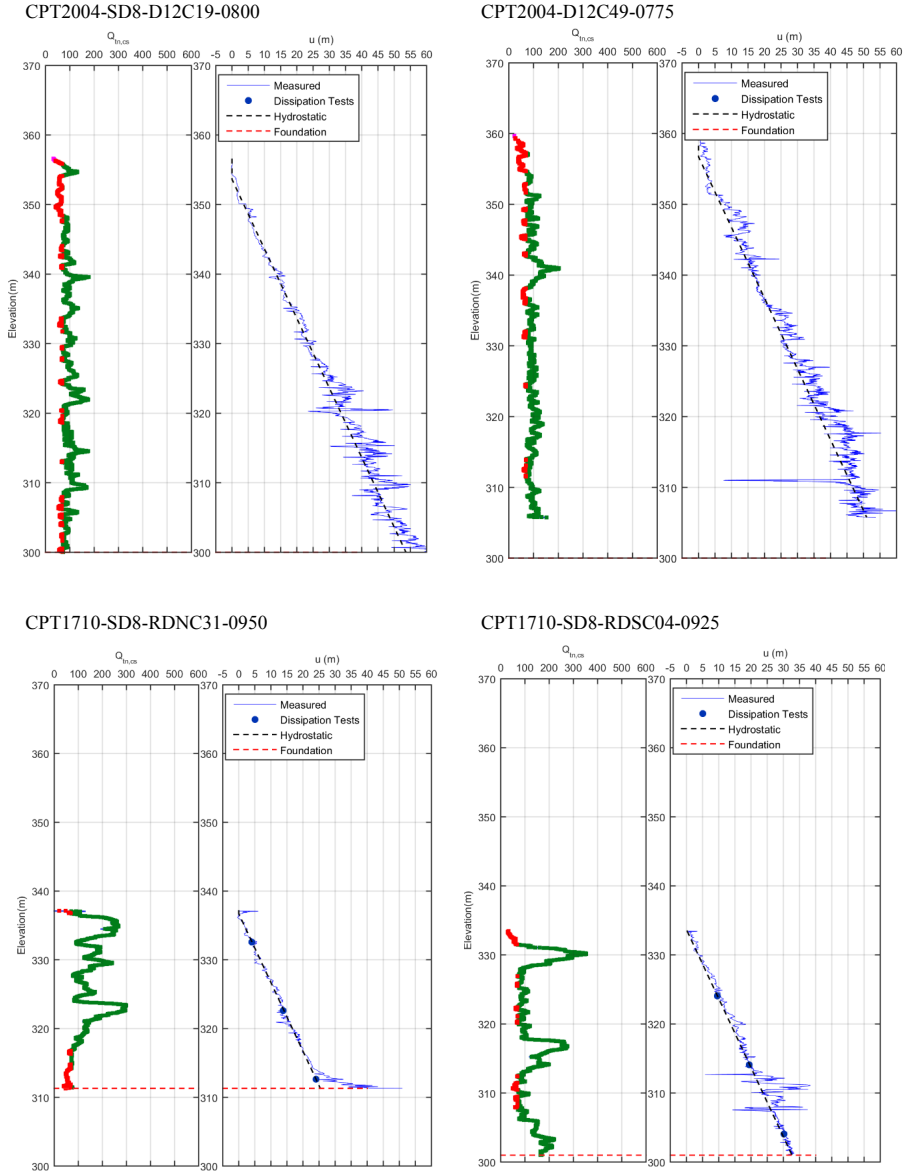

Figure 11 Dynamic pore pressure in uncompacted tailings sand

Figure 12 shows the distribution of $Q_{tn,cs}$ below the water table from the 20 CPT test locations. The distribution of $Q_{tn,cs}$ confirms that the uncompacted tailings is less dense and more uniform in terms of density and state compared to the compacted tailings sand. About 45% of the $Q_{tn,cs}$ is in the range of 70 to 105, which are slightly dilative (Robertson, 2010).

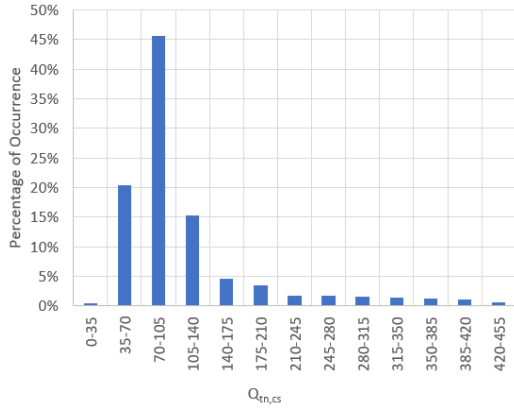

Figure 12 Distribution of $Q_{tn,cs}$ in uncompacted tailings sand

5 POSSIBLE IMPACTS OF CPTU METHOD AND EQUIPMENT ON MEASURED PORE PRESSURE

Standard CPT probe and penetration speed have been used at Sand Dump 8. The CPT probe displaces soils and measures the response of soils in the influence zone. Robertson & Cabal (2015) stated that the influence zone can be as small as one cone diameter in soft soils and as large as 15 cone diameters in very stiff soils. Pore pressure response depends on whether the soil in the influence zone is drained, undrained, or partially drained during cone penetration. Figures 10 and 11 indicate the tailings sand at Sand Dump 8 is drained (or nearly drained) during cone penetration, in other words, the pore pressure in sand stays close to hydrostatic condition during cone penetration. The effect of drained conditions during the push will mute the dynamic pore pressure response thereby limiting the ability to discern the state of the sand.

As discussed above, noticeably high excess pore pressures are observed in sand that is in a dense state as interpreted from $Q_{tn,cs}$. It is likely that the measurement is being affected by the pore pressure apparatus in the CPTu probe. Dense sand dilates at large shear strain and the sand could compress the polyethylene filter element. Silicone oil is viscous and is expected to take some time to dissipate. An abrupt increase in density and state of sand ($Q_{tn,cs}$) could result in sudden increase in the compression on the filters. This can lead to a spike in pore pressure detected by the sensor which is immersed in the silicone oil, as shown in Figure 5. Conversely, a drop in pore pressure could be measured along with an abrupt decrease in density and state of sand ($Q_{tn,cs}$) due to rebound of filter element. Negative excess pore pressure could occur if the reduction in $Q_{tn,cs}$ is large, which is also shown in Figure 5.

On the other hand, uncompacted sand is less dense and generally more uniform in density and state ($Q_{tn,cs}$). The filter element is relatively stiff compared to the density of the sand. The volume change of the filter element could be negligible due to compression of slightly dilative sand and contractive sand. Silicone oil also has more time to respond and dissipate during the cone penetration in uncompacted tailings sand which has low variability in density and state ($Q_{tn,cs}$). The impact of the filter element and the silicone oil is expected to be much less in uncompacted sand than that of compacted sand. Therefore, the measured dynamic pore pressure could be near hydrostatic pore pressure for a drained or nearly drained tailings sand relative to CPT penetration, as shown in Figure 11.

6 CONCLUSIONS

Dynamic pore pressure in CPT testing can be impacted by soil properties, cone penetrometers, and testing procedures. Positive excess pore pressures were observed for sand with high $Q_{tn,cs}$ (i.e. dilative sand) and negative excess pore pressures were measured in relatively loose sand in compacted tailings sand at Sand Dump 8. This is contrary to the expected pore pressure response. It is being proposed that this behavior is caused by the impact of the filter element and the saturation fluid (silicone oil) used in the CPT apparatus. In addition, the tailings sand at Sand Dump 8 was found to be drained or nearly drained during CPT penetration, which may mute the positive and negative excess pore pressure response typically encountered in undrained soils, and reduce the reliability of referencing the excess pore pressure behavior when assessing liquefaction susceptibility.

The reliability of using the dynamic pore pressure in engineering practice to evaluate flow liquefaction susceptibility of tailings sand should be examined prior to its application. Further work is being proposed to confirm these assertions relating to the influence of the composition of the filter element and/or the silicone oil in the filter element.

7 ACKNOWLEDGEMENTS

The authors would like to recognize Tanys MacGowan of Suncor for her stewardship of the Sand Dump 8 structure. The authors would like to acknowledge Jamie Sharp of ConeTec for providing detailed information about the cone penetrometer equipment used in the testing at Sand Dump 8. The authors would also like to recognize Yirao (Yvonne) Qiu of Wood for her contributions to the data analyses.

REFERENCE

Jefferies, M.G., & Been, K. 2016. *Soil liquefaction: a critical state approach, 2nd edition*. CRC Press.

Randolph, M. F., & Hope, S. 2004. Effect of cone velocity on cone resistance and excess pore pressures. *Proc., Int. Symp. on Engineering Practice and Performance of Soft Deposits*, Yodagawa Kogisha Co., Ltd., Japan, 147–152.

Robertson, P. K. 1990. Soil classification using the cone penetration test. *Canadian Geotechnical Journal*, 27(1), 151–158.

Robertson, P.K. 2010. Evaluation of flow liquefaction and liquefied strength using the cone penetration test. *Journal of Geotechnical and Geoenvironmental Engineering*, ASCE, 136(6): 842–853.

Robertson, P.K. & Cabal, K. L. 2015 Guide to cone penetration testing for geotechnical engineering, 6th edition.

Robertson, P.K. 2016. Cone penetration test (CPT)-based soil behaviour type (SBT) classification system — an update. *Canadian Geotechnical Journal*, 53(12): 1910–1927.

Schneider, J.A., Randolph, M.F., Mayne, P.W., & Ramsey, N.R. 2008. Analysis of factors influencing soil classification using normalized piezocone tip resistance and pore pressure parameters. *Journal of Geotechnical and Geoenvironmental Engineering*, ASCE, 134(11): 1569–1586.

Silvis, F. & de Groot, D. 1995. Flow slides in the Netherlands: Experience and engineering practice. *Canadian Geotechnical Journal*, 32, 1086–1092.

Winckler, C, Davidson, R., Yenne, L, & Pilz, J. 2014. CPTu-based state characterization of tailings liquefaction susceptibility. *Proceedings Tailings and Mine Waste 2014,* Keystone, CO, USA, October, 247-256.

Zhang, Y., Abusaid, A.H., Pollock, G.W., Moore, R. & Rhee, J. 2020. Managing the liquefaction potential of compacted tailings sand at Suncor, *Tailings and Mine Waste 2020*.

Evaluation of Shear Wave Velocity and Void Ratio in Mine Tailings using the Field Velocity Resistivity Probe

Iván A. Contreras, Ph.D., Jason W. Harvey, P.E., Mathew D. Walker, P.E., Jacob D. Sharpe & Aaron T. Grosser, P.E.
Barr Engineering Co., Minneapolis, MN, USA

ABSTRACT: The seismic cone penetration test (sCPT) is the most common in-situ testing technique utilized for determination of the shear wave velocity in soils. This technique yields results that are adequate in natural soils. However, sCPT has important limitations when used in mine tailing deposits because mine tailings can exhibit significant differences between the intact shear wave velocity and that measured by the sCPT. This paper describes the field velocity resistivity probe (FVRP) which is a recently developed tool that allows for improved accuracy in the determination of in-situ shear wave velocity when compared to sCPT. The paper presents the results of shear wave velocity measurements on two soundings side by side which illustrate the difference between the sCPT and the FVRP in the determination of shear wave velocities in mine tailings deposits.

1 INTRODUCTION

Measurement of the shear wave velocity in soils has become common practice in geotechnical engineering. The determination of the shear wave velocity in soils is important because it is directly related to small-strain mechanical behavior of soil. For example, the shear wave velocity can be converted to small-strain shear modulus using elasticity principles ($G_{max} = \rho V_s^2$). The shear modulus is an important parameter in advanced numerical modeling of soil behavior and engineered structures. Robertson (2016) also indicated that shear wave velocity can potentially identify micro-structure in soils. Shear wave velocity can also be used to identify liquefaction susceptibility in soil and determine the in-situ state parameter (Fear and Robertson, 1995; Schnaid et al., 2020).

In the laboratory, wave propagation and shear wave velocity of undisturbed specimens is measured using bender elements mounted at the platens of a triaxial cell. In the field, the most common in-situ testing technique is the seismic cone penetration test (sCPT). However, for materials that are recently deposited and very soft or loose, such as mine tailings, collection of undisturbed specimens for laboratory testing and determination of the shear wave velocity using the sCPT presents some important limitations, as described below. The field velocity resistivity probe (FVRP) is an in-situ testing tool that uses bender elements to more accurately measure the shear wave velocity of the intact material (Lee et al., 2010). The FVRP may overcome many of the limitations of the sCPT in mine tailings deposits by reducing the impact of soil disturbance around the probe and eliminating the errors due to aggregation. This paper presents a discussion of the limitations and over prediction of the shear wave velocity measured by the sCPT. A comparison of the measured shear wave velocity profiles from SCPT and FVRP soundings performed side-by-side through mine tailings deposit is also presented and discussed.

2 SCPT

The sCPT was introduced in the early 1980s when significant advances were made with the cone penetration test (CPT) and new sensors were experimentally added to the CPT. sCPT is a simple, reliable, and relatively inexpensive tool to determine the seismic wave profile of a soil deposit. The seismic wave velocity measurements are typically made at 1-meter intervals and can be combined with other CPT measurements to obtain a comprehensive soil profile characterization to use in design. Both compression waves (P-waves) and shear waves (S-waves) can be measured with sCPT.

The basic sCPT configuration consists of a wave source, trigger circuit, geophone in the penetrometer, and digital storage oscilloscope in addition to the standard CPT acquisition system. The wave source typically consists of a steel beam set on the ground surface parallel to the geophone axis that is acted upon by a normal force at the time of the test. The sCPT is pushed into the ground and penetration is stopped at the desired depth for measurements. The steel beam is hit by the hammer with a contact trigger, generating a front of waves that travel through the ground; the signal is picked up by the geophone and recorded in the digital storage device. Two hits of the steel beam are performed at each test depth to generate polarized wave traces, facilitating the interpretation of wave arrival times. Modern CPT trucks include built-in seismic beams utilized for shear and compression wave velocity determinations.

Engineers utilize the time of wave arrival and the distance from the shear beam to the geophone to compute the wave velocity. It is assumed that the travel path of the waves from the beam to the geophone is a straight line. Early sCPT versions used dual arrays with two receivers (geophones) separated by a set distance on the rods allowing for determination of the "true time" of wave arrival, defined as the time difference between both locations, as shown by Butcher, et al. (2005). Other sCPT units used a single receiver for determination of the "pseudo-time" of wave arrival, defined as the time difference of two readings at two test depths. However, Robertson, et al. (1986) found that the difference of the "true time" and the "pseudo-time" were very small with an error generally less than 2 percent.

Other automatic seismic sources, such as "auto-seis" (Mayne & McGillivray, 2005), which use a single hammer have been developed. Similarly, the "auto-seis" allows for wave recording at 10-centimeter intervals (Mayne, 2014). However, these devices are not extensively used in practice at the present time.

Measurement of shear wave velocity has evolved from a research technique into routine engineering practice due to the simplicity and repeatability of the measurements. In fact, sCPT is the most used tool for this determination. This is because it allows for different uses as follows: (1) direct measurement of soil stiffness for use in settlement calculation and numerical modelling, (2) estimate of soil parameters correlated to shear wave velocity, (3) evaluation of soil liquefaction susceptibility based on shear wave velocity, (4) determination of soil saturation based on compression wave velocity, and (5) identification of soils with micro-structure. These attributes make the sCPT a very powerful tool in geotechnical engineering. As a result, its use has been extended extensively in the characterization of natural soils.

2.1 *Limitations of sCPT*

In spite of the benefits of the sCPT to characterize soils, it presents some important limitations. Most notably, the measured arrival time and total travel distance of the signal represent the aggregated time and material travelled by the wave from the ground surface to the downhole receiver (geophone). To better illustrate this aspect, Figure 1 shows the geometry associated with the sCPT.

Figure 1 shows the typical arrangement of the sCPT which includes the axis of the sCPT, shear beam, and receiver (geophone). It can be seen in Figure 1 that the shear beam is located at a horizontal distance, X, from the axis of the sCPT. The receiver (geophone) is located in the axis line of the sCPT at depth, D, from the ground surface. Finally, the travel path of the seismic waves from the shear beam to the receiver (geophone) is a straight line, L. Figure 1 includes two positions at depths, D_1 and D_2, and their associated travel paths, L_1 and L_2.

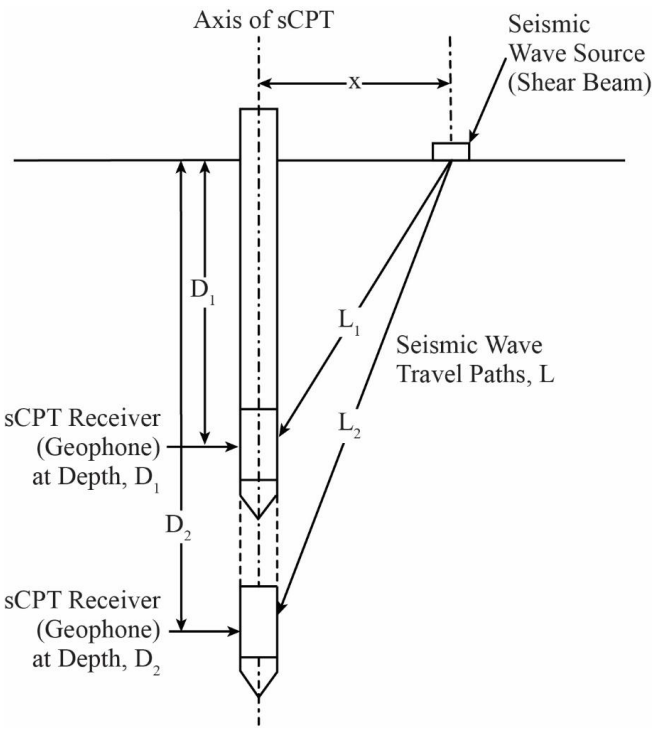

Figure 1. Typical Arrangement for sCPT Measurements (adapted from Butcher, et al., 2005)

In Figure 1, the arrival or travel time of the seismic waves associated with positions 1 and 2 are t_1 and t_2, respectively. The interval velocity in the segment between positions 1 and 2, typically one (1) meter, is computed using Equation (1) as follows:

$$V_s = \frac{(L_2 - L_1)}{(t_2 - t_1)} \tag{1}$$

It is clear from Figure 1 and Equation 1 that a significant limitation of the sCPT is the fact that the measured arrival time and total travel distance of the signal represent the aggregated time and material travelled by the wave from the ground surface to the downhole receiver (geophone). The numerator in Equation 1 represents the difference between two hypotenuses of two right triangles. The denominator represents the incremental arrival time, Δt, between positions 1 and 2. As a result, there is not a direct measurement of the arrival time at the interval distance. Therefore, the wave velocity calculated by Equation 1 represents an aggregate value, which works relatively well in most soils because of their relatively higher seismic velocity . However, in very soft or loose soils, such as mine tailings, this aggregation may not provide an accurate measurement of the actual seismic wave velocity of the in-situ material because with their much lower seismic wave velocities the errors may be more impactful.

3 FVRP

The FVRP is an in-situ tool that uses bender elements to more accurately measure the seismic wave velocity profiles of the intact soil and was initially introduced by Lee, et al. (2008) and Yoon, et al. (2008) with subsequent improvements by the same team of researchers (Lee, et al.,

2010; Yoon, et al., 2010). FVRP provides a direct measurement of seismic wave velocities of nearly undisturbed soil at discrete locations without the distortion from aggregation. It generally consists of two tines with bender elements and other sensors connected to a stem and an adapter to drill rods as shown in Figure 2. The distance between the tines is approximately 88 mm, and the distance between the source and receiver bender elements mounted on the inside of the tines is approximately 68 mm. As such, the material between the tines is nearly undisturbed. One set of bender elements is used for measuring the shear wave, and another set of bender elements is used for measuring the compression wave. A triangular fin is welded at the end of the tines to minimize soil abrasion and protect the bender elements during penetration. Additional sensors, such as electrical resistivity and temperature, are installed within the leading edge of the polymer blade at the base of the tines.

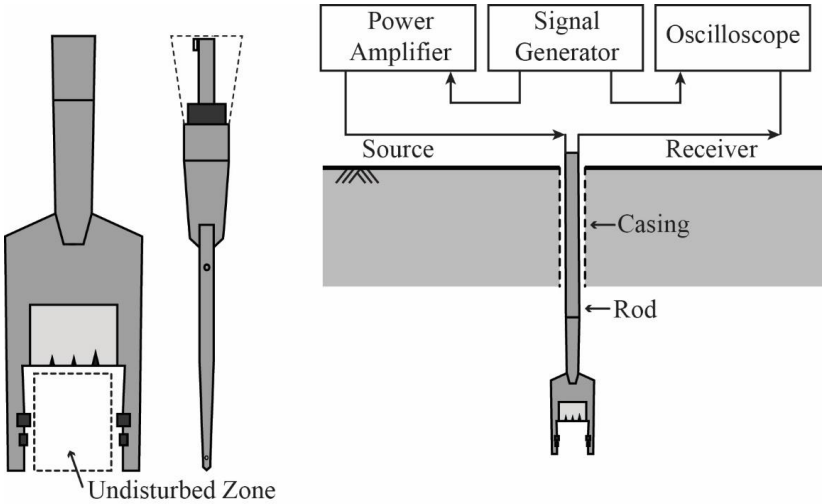

Figure 2. Schematic and Arrangement of FVRP Apparatus (adapted from Jung, et al., 2008)

The source and receiver bender elements are mounted facing each other so that the signal travels through the nearly undisturbed soil. The signals are generated at the surface using a waveform generator with power amplifier and are applied to the source bender element. Subsequently, the signal is read by the receiver bender element, which transmits the signal to an oscilloscope at the surface as shown in Figure 2. The signals generated by the waveform generator are also sent directly to the oscilloscope for comparison of the signal arrival time. The automatically generated signals are stacked to increase the signal-to-noise ratio producing higher quality signals. Because of the configuration of the FVRP and the location of the source and receiver bender elements, the measurements of seismic waves are essentially oriented in the horizontal direction. In addition to the seismic wave velocities, the FVRP is also equipped with electrodes to determine the electrical resistivity of the in-situ material.

In practice, the FVRP is advanced in the borehole to the desired test depth using direct-push methods. At the desired test depth, the signals are generated and the arrival times are measured. By knowing the distance between bender elements and the arrival times, the seismic wave velocities are calculated. Electrical resistivity and temperature measurements are also made at each test depth. Then, the FVRP is advanced to the next desired depth for each subsequent test and the procedure is repeated. For practical purposes, there is no minimum depth interval between subsequent tests, although depth intervals less than 10 cm may become overly time-consuming.

The main benefits of the FVRP are: (1) the measurement of seismic wave velocity is representative of the nearly undisturbed soil, (2) the measurements can be performed as often with depth as desired which can be used to develop a more dense data profile through the soil column, and (3) automatic signal generation reduces manual labor and allows for increased stacking that

results in higher quality signals. Further, Jung, et al. (2008) demonstrated in a laboratory chamber that the FVRP provides accurate measurements of nearly undisturbed soil. This validation was performed by setting two instrumented rods with source and receiving bender elements, similar to an in-situ cross-hole seismic test, to measure the seismic wave velocity in the soil column. The FVRP was then inserted between the two instrumented rods to measure the seismic wave velocity profile once again. Comparison of the seismic wave velocity profiles were nearly identical demonstrating that the FVRP causes minimal disturbance and measures seismic waves of intact material. Robertson (2016) highlighted the challenge of using sCPT for seismic wave velocity in the determination of the parameter K_G^* to identify soils with microstructure. This is due to the fact CPT generates nearly continuous profiles of tip resistance, sleeve resistance, and dynamic pore-water pressure with measurement at 10- to 50-mm intervals, whereas the sCPT provides seismic wave velocity profiles with 1-m intervals, as typically implemented.

4 IMPORTANCE IN MINE TAILINGS DEPOSITS

Obtaining accurate measurements of seismic wave velocities is very important in mine tailings deposits because of the following unique characteristics of these materials: (1) mine tailings are very soft or loose materials due to their recent deposition history and high water content during deposition, and thus low shear wave velocity as compared to natural soils, (2) mine tailings are frequently layered with combinations of materials having different gradations which can be missed by the sCPT due to its aggregated seismic wave values at relatively large intervals, and (3) aggregation of the seismic wave velocities by the sCPT tend to skew the actual seismic wave velocity of the undisturbed material. As a result, the FVRP has many advantages in tailings characterization with seismic wave velocities when compared to sCPT.

5 COMPARISON OF SEISMIC WAVE VELOCITIES FROM SCPT AND FVRP

The authors were involved in a field campaign that utilized the FVRP in a tailings basin. As part of this field campaign, two soundings (sCPT and FVRP) were performed side-by-side with the purpose of evaluating the accuracy of the seismic wave velocity measurements from both systems. Figure 3 shows the results of the sCPT and FVRP. The upper 9 m were pre-drilled due to the presence of an overlying dense tailings layer. Layered tailings are present in the depth interval between 9 and 17.5 m. In the depth interval between 17.5 and 24.3 m, the deposit consists of uniform tailings. Native soils exist below a depth of 24.3 m. The profile described above is interpreted from the sCPT sounding profiles of tip and sleeve resistance in Figure 3.

The shear wave velocity from the sCPT is plotted in Figure 3 as segments in approximately 1-m intervals, whereas the shear wave velocity from the FVRP is plotted as markers in approximately 0.3-m intervals. It can be seen from Figure 3 that the shear wave velocity from the sCPT is usually larger than the shear wave velocity from the FVRP. In many instances the difference is 50 percent or more. This difference is attributed to the fact that the FVRP makes a direct measurement of the nearly undisturbed material at discrete depths, whereas the sCPT makes an aggregate measurement as previously described. While the difference in shear wave velocity by the sCPT and FVRP may not be relevant or significantly important in natural soils, this significant difference is very important and relevant in mine tailings due to their soft or loose nature and significant impact on interpreted properties.

Figure 3 shows how the FVRP measurements better capture the layered nature of the mine tailings deposit, as compared to the sCPT which obscures the layering due to aggregation. The FVRP also provides a profile of the compression wave velocity, electrical resistivity, and temperature as shown in Figure 3. The compression wave velocity is associated with the water compression and can be used to identify the saturated nature of the deposit. The electrical resistivity can be used in the estimation of void ratio.

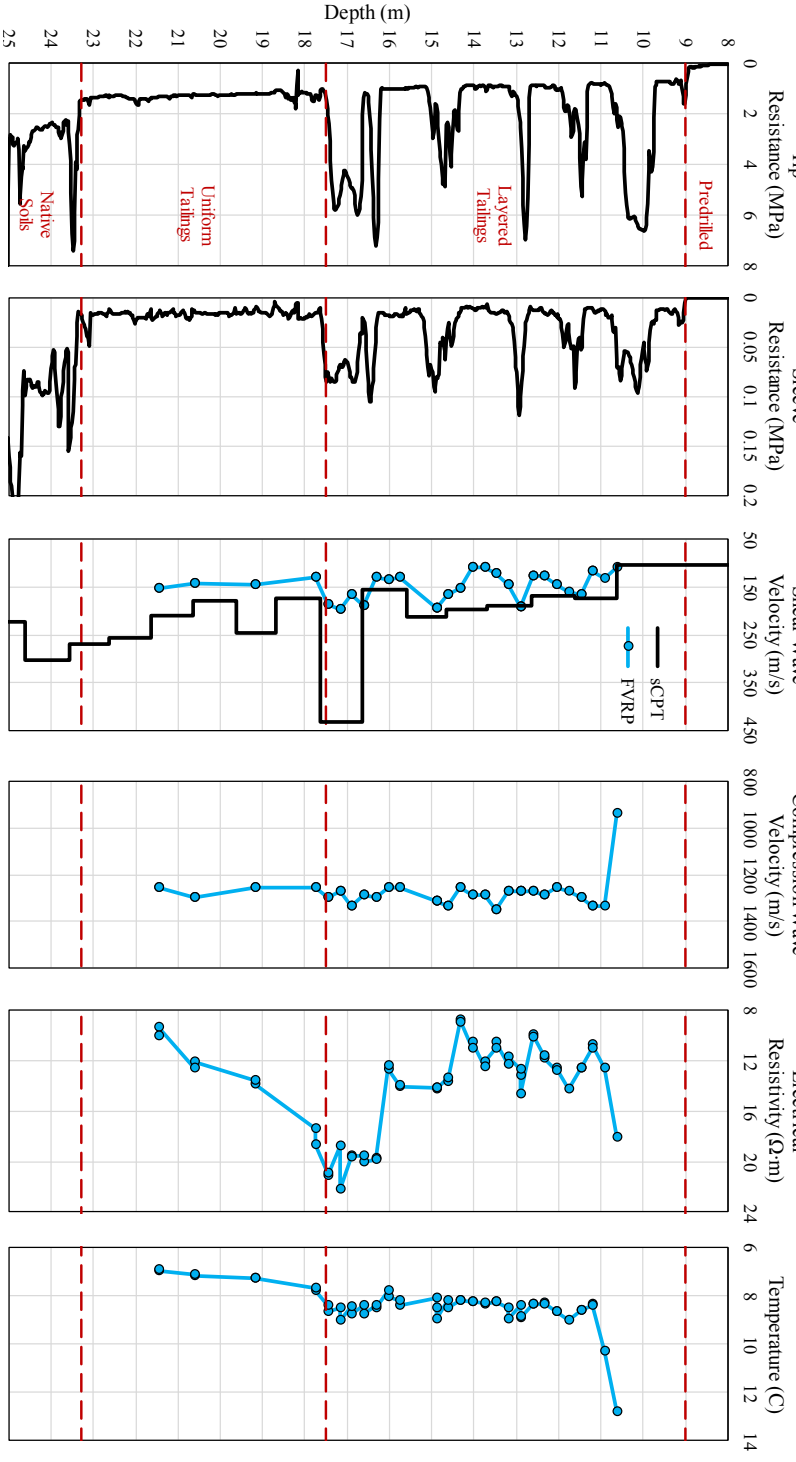

Figure 3. Comparison of Data from Seismic Cone Penetration Testing (sCPT) and Field Velocity Resistivity Probe (FVRP)

The importance of accurate and closely spaced shear wave velocity, in conjunction with electrical resistivity measurements, can be seen when performing calculations to estimate the void ratio profile of the tailings deposit. The in-situ void ratio is an important element in evaluating the liquefaction susceptibility and the post-liquefaction shear strength of the tailings deposit when assessing within the critical state soil mechanics (CSSM) framework. Numerous correlations are available to estimate the in-situ void ratio or state parameter (ψ) based on in-situ moisture content, standard penetration test (SPT), and CPT among others. The benefit of the FVRP is that the void ratio can be measured in-situ with greater accuracy and at relatively close intervals throughout the tailings profile. Figure 4 shows the application of the FVRP to estimate the in-situ void ratio and state parameter (ψ) for use in comparison of the laboratory measured critical state line (CSL) for three representative tailings types encountered at the CPT and FVRP sounding location shown in Figure 3. Further development of this approach is in progress and will be presented in subsequent publications.

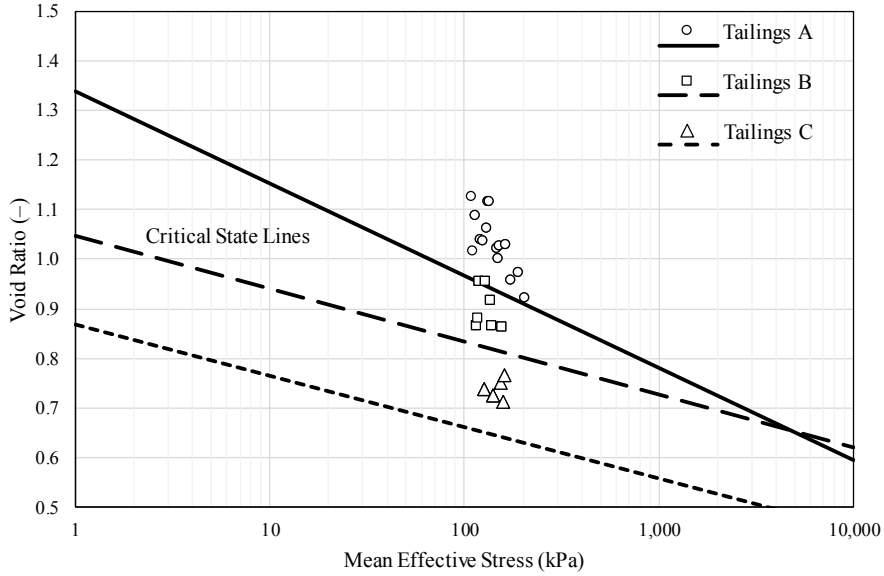

Figure 4. Application of FVRP to Critical State Soil Mechanics Approach to Liquefaction Assessment

6 SUMMARY AND CONCLUSIONS

The most common in-situ testing technique in geotechnical engineering to determine the seismic wave velocities is the sCPT. While this technique generally provides acceptable results in natural soils, it may have some limitations in its application to mine tailing deposits. This is because mine tailings are high water content materials that were recently deposited and thus very soft or loose. As a result, the aggregation of the seismic wave velocities from the sCPT can fail to characterize the low seismic wave velocity nature of the in-situ material and its layering. Therefore, the FVRP may provide an improvement in the accuracy and definition of seismic wave velocity measurements.

Data from a mine tailings deposit where side-by-side soundings of sCPT and FVRP were performed are presented. It is shown that the shear wave velocity from the FVRP is consistently lower than the aggregated value obtained from the sCPT. Additionally, the aggregation produced by the sCPT does not allow for identification of the variations in seismic wave velocity profile of the in-situ material generated by the layered nature of the tailings deposit, as compared to the FVRP.

These important differences and limitations of the sCPT suggest that the FVRP is a better specialty tool to determine the shear wave velocity in mine tailings deposits. The difference in shear wave velocity from the sCPT and FVRP may be up to 50 percent or more. This significant difference is very important when using the shear wave velocity results to compute geotechnical parameters. As a result, the authors support the further use of the FVRP over the sCPT in mine tailings deposits because FVRP provides a more accurate direct measurement of the in-situ shear wave velocity of the tailings material. FVRP also captures the layered nature of mine tailings deposits better than the sCPT, and thus can be used for more accurate determination of geotechnical parameters. In this regard, the authors are currently assessing the use of the FVRP to estimate the in-situ void ratio with the purpose of determining the state parameter (ψ) for use in liquefaction assessment and slope stability analysis within the CSSM framework. This aspect of the seismic wave interpretation from FVRP will be the subject of a separate future publication.

ACKNOWLEDGEMENTS

The authors would like to acknowledge the support of Professor Jong-Sub Lee, Dr. Sang-Yeob Kim, and Mr. Namsun Kim of Korea University. Without their technical and hands-on support, this work would not have been possible. Dr. Jeong-Yun Won, formerly of Barr Engineering Co., was also instrumental to planning and facilitating the work.

REFERENCES

Butcher, A.P., Campanella, R.G., Kaynia, A.M., Massarch, K.R. 2005. "Seismic cone downhole procedure to measure shear wave velocity- a guide." *International Society of Soil Mechanics and Geotechnical Engineering*. Technical Committee No. 10.

Fear, C.E. and Robertson, P.K. 1995. Estimating the undrained strength of sand: a theoretical framework. *Canadian Geotechnical Journal*, *32*(5), pp.859-870.

Jung, J.W., Kim, H.S., Kim, B.C., Park, I.B., and Mok, Y.J. 2008. "In-situ Stiffness Evaluation of Soft Ground Using Bender Elements." The 14th World Conference on Earthquake Engineering. October, Beijing, China.

Lee, J.S., Lee, C., Yoon, H.K., and Lee, W. 2010. "Penetration Type Field Vane Velocity Probe for Soft Soils." *Journal of Geotechnical and Geoenvironmental Engineering*, ASCE 136 (1), 199-206.

Lee, J.S., Yoon, H.K., Truong, Q.H., Lee, C., Choi, H., and Cho, G.C. 2008. "Shear wave measurements using blade-type field velocity probe in soft ground." Proceeding of the third international conference on site characterization (ISC). Taipei, Taiwan. 713-718.

Mayne, P.W. & McGillivray, A. 2005. "Seismic Piezocone and Seismic Flat Dilatometer Tests at Treporti." Proceedings of the Second International Conference on Site Characterization ISC'2, Porto Portugal.

Mayne, P. 2014. "Interpretation of geotechnical parameters from seismic piezocone tests." Third international symposium on CPT.

Robertson, P.K. 2016 "Cone Penetration Test (CPT)-based Soil Behaviour Type (SBT) Classification System - an Update." *Canadian Geotechnical Journal*, 53: 1910-1927.

Robertson, P.K., Campanella, R.G., Gillespie, D., and Rice, A. 1986. "Seismic CPT to measure in-situ shear wave velocity."

Schnaid, F., Nierwinski, H.P. and Odebrecht, E. 2020. Classification and State-Parameter Assessment of Granular Soils Using the Seismic Cone. *Journal of Geotechnical and Geoenvironmental Engineering*, *146*(8), p.06020009.

Yoon, H.K., and Lee, J.S. 2010. "Field velocity resistivity probe for estimating stiffness and void ratio." *Soil Dynamics and Earthquake Engineering*, Elsevier 30 (12), 1540-1549.

Yoon, H.K., Lee, J.S., Kim, Y.U., and Yoon, S. 2008. "Fork bladed-type field shear wave velocity probe for measuring shear wave." *Modern Physics Letter B 22 (11)*, 965-969.

Tailings Dam Monitoring: Time for an Integrated System Approach

Luciano Oliveira
Stratalis Consulting, Phoenix, AZ, USA

ABSTRACT: With recent accidents of unprecedented scale, the Mining industry is seeking better ways to manage the risk associated with tailings dams. Numerous work groups have been created around the world to discuss updates to guidelines and standards, while in some jurisdictions authorities are already demanding increased levels of transparency and preparedness. Despite CEO level attention and increased investments in monitoring technology, accidents continue to happen in dams deemed as safe by audit experts. In fact, a report on the Brumadinho accident revealed the use of multiple state-of-the-art sensor devices at the site that were still unable to predict the dam failure. That report also points out that a computer model used in the forensic analysis of the accident was able to simulate the conditions of the failure. While the current monitoring approach is not producing the desired results, accidents can be prevented with computer models capable of real time multi-variate simulation. These computer models will evolve over time, and will become connected, intelligent, and predictive. At its evolved stage, models will seamlessly integrate multiple data inputs, combining detailed structure characterization, weather APIs, connected sensors and access to external databases. These systems will feed all data into both physical and statistical models, leveraging AI for advanced simulation and predictive features, and providing real time alerts to centralized monitoring centers staffed 24/7. As a result, this models will be able to update risk trees on real time, reliably detect anomalies, trigger internal and external alerts, automate compliance and reporting, trigger emergency preparedness plans, as well as constantly update themselves through a continuous data assimilation feedback loop.

1 INTRODUCTION

The objective of this paper is to propose a conceptual framework for the monitoring of tailings dams with the potential to overcome many of the current shortcomings, through better integration of multiple sensor and survey data into a real time, continuously updated monitoring model.

Tailings dams failures of unprecedented scale have plagued the Mining industry[1], challenging its license to operate, increasing insurance and monitoring costs, and rebalancing the assessment of risk associated with operating these facilities. As a result, industry level work groups[2] have been created to review tailings guidelines and standards. There are over 30 work groups across with either a global or regional scope across all Mining jurisdictions, as tailings relevance is at an all time high.

One of the most prominent of such groups is the Global Tailings Review[3], that is working on guidelines likely to influence guidelines groups in all regions. Despite this globally coordinated efforts, guidelines and standards are likely to remain regional. While reviews are likely to influence all regions, the contents published for public consultation do not indicate a major

disruption to how the industry is operated and regulated. Guidelines are not evolving to strict technical specifications.

That doesn't mean that standards are not becoming stricter, though. More frequent audits, emergency plans and reporting requirements all are featured recommendations. The state of Minas Gerais in Brazil is an early adopter of stricter regulations[4], as a result of recent tragedies; and Chile a leader in adopting transparency[5].

2 LIMITATIONS OF THE CURRENT MONITORING APPROACH

The forensic analysis on the Brumadinho[6] accident provides valuable insight into the limitations of current monitoring approach. It is fair to say that the site had best in class instrumentation and imaging data capture devices, including drones and ground-based radars that provide real time displacement information. Additionally, there was detailed characterization information on the site, including drilling sampling, CPTu, FVT, and shear wave surveys. As the accident happened, even more inclinometers were being installed. Therefore, the failure was not a result of lack of information, but a flawed data processing methodology. The monitoring strategy was based on comparing measurements with thresholds established in the risk analysis calculation of the safety margin. This safety margin was not accurate at the time of the failure, though. The expert panel concluded that the failure was a result of 5 factors combined: (i) steep slope design; (ii) poor water management that led to accumulation of coarse material in certain areas and weakened the structure; (iii) poor drainage systems; (iv) build-up of stress (creeping) due to high iron content and oxidation; and (iv) high seasonal rainfall leading to loss of suction. These factors combined led to a condition of static liquefaction, very difficult to be detected by direct measurements. The report points out, though, that there was acceleration of the displacement prior to the failure, a typical early warning signal:

"*Post-failure satellite image analyses indicated slow and essentially continuous small downward deformations of less than 36 millimeters per year (mm/year) were occurring on the dam face in the year prior to the failure, with some acceleration of deformation during the wet season.*"

The report is also clear to indicate that a computer system capable of multi-variate simulation, including weather information, was able to simulate the conditions of the failure:

"*The simulations further showed that internal creep, when combined with the loss of suction discussed above, would be sufficient to trigger the observed global failure of the dam on January 25, 2019.*"

Could a system like this be up and running before the accident, and helped prevent it, rather than explain it after the tragic fact?

3 POTENTIAL SOLUTIONS

A study conducted by Stratalis Consulting analyzed thousands of technology solutions in Mining, as well as in related industries such as Defense, Oil & Gas, and Civil Construction, Food Processing, and Weather Forecasting, with similar problem statements. Systems and Modeling solutions analyzed included packages from companies such as Dassault Systemes, Emerson, Hexagon, Maptek, Seequent, Sensemetrics, Intelltech, Descartes Labs, GroundProbe, Aspentech, Canary Systems, Rocscience, Isometrix, Vista Data Vision, DHI, GoldSim, Inmarsat, Decipher, GE Digital, Microsoft, ESRI, L3 Harris, SAS, Oracle, and others. The features analyzed comprised 3 performance areas:

- Risk Assessment: FMEA and root cause analysis, probability vs. consequence matrix, risk trees, compliance & guidelines, risk reviews.

- Advanced Modeling & Simulation Systems: IoT, real time connectivity, cloud/ server solutions, GIS systems, visualization, dashboards, analytics, collaboration, scenario analysis.
- Predictive Models: physical models, stochastic models, ensemble models, artificial intelligence, data fusion, data assimilation.

While different solutions proved to be capable in many of the performance areas listed above, we could not find evidence of a deployment that successfully combined most of these elements. The study showed significant potential for integrated computer model systems to complement expert judgement and be a valuable tool in risk mitigation.

In fact, there are several industry level initiatives already moving in this direction. Key examples of work groups developing integrated solutions include DAMSAT, STINGS, Programa Tranque, and a project jointly conducted by AMIRA International and the University of Western Canada. These initiatives share a few common characteristics:

- Ability to acquire real time data from multiple types of sensors, including advanced imaging techniques involving drones and satellites;
- Automated data validation and harmonization protocols, that allow the data to be seamlessly overlaid and combined;
- Centralized data storage and collaborative access controls ("one source of truth");
- Analytics capability to perform stability analysis, trend analysis, velocity/ acceleration analysis and other parameters of risk and vulnerability;
- Data integration and modeling capabilities, so control thresholds can be defined for metrics combining more than one raw input;
- Advanced visualization and communication tools that enable different teams to see consolidated information and collaborate effectively;
- Reporting and friendly user interfaces that can be configured for multiple classes of stakeholders.

Stratalis study concluded that he future of Monitoring is Connected, Intelligent, and Predictive (see Exhibit 1).

Many sites today still operate at Stage 1, "Semi Automated Monitoring". It means that they may run some automated sensors (e.g. piezometers, inclinometers), and may even have real time data collection (e.g. dataloggers, IoT devices), but this data is not integrated, leaving different teams with partial information only. Control thresholds are set by individual direct measurement, and overlay of information is a difficult task, since each hardware manufacturer has different standards and protocols. Sites at Stage 1 typically rely on visual inspection to monitor many hazards such as animal presence, vegetation outgrowth, and health of drainage systems.

Some mining companies have active initiatives to upgrade their tailings storage facilities to Stage 2, " Connected Monitoring", with corporate level efforts to install advanced sensors and imaging devices (e.g. satellite-based InSAR, ground based radars), harmonize and integrate data into unified database systems, and even run advanced analytics, including 3D visualization tools. At this stage, data retrieval and analysis are facilitated by faster connectivity systems, and modern database architectures. Engineers and other technical experts are able to share information, discuss potential interpretations and make decisions much faster, and based on more accurate and reliable information. A few companies at this stage already go as far as establishing centralized monitoring centers capable of receiving information from multiple sites, and providing 24/7 real time monitoring services such as anomaly detection, alert and notification according to pre-defined workflows.

Some of the most cutting-edge teams are currently considering Stage 3 systems, "Digital Twin Advanced Monitoring", that leverage detailed digital twin physical models, for a level of accuracy that is one step ahead of what is currently available today. At this stage, solutions make extensive use of imaging techniques, and simulation capabilities enable the study of the structure behavior under hypothetical stress conditions, such as heavy rain or a seismic event, or both combined. A

key enabler for digital twin models are advanced characterization techniques, including non-invasive tomography-like survey techniques such as resistivity and seismic, that combined with CPTu calibration datapoints and proper understanding of the tailings geochemistry, enable accurate prediction of the structure behavior under multiple conditions. The structure model is constantly updated with real time data, and continuously recalculates critical parameters. This approach reduces uncertainties and allows a much better understanding of the structural stability of the dam, in an evergreen way.

The Stratalis study also points out that a Stage 4, "AI Driven Predictive Monitoring", can be envisioned. At this stage, both physical and statistical models are combined. Stochastic models fill in the gaps for missing information, providing alternatives to better understand uncertainties. External databases (e.g. weather, seismicity, other benchmarking data) inform the model algorithms, and the model learns from the real time data collected, continuously updating itself for improved accuracy at every moment. At this stage, anomaly detection is much more reliable, since it leverages historical data sets. Hazard monitoring is mostly automated, with software automatically recognizing patterns and structuring the information for quantitative use and fusion with other structured datasets. The frequency of data collection is much increased with the automation, making it easier to detect issues and trends before they reach critical stages. This type of model is already a reality in advanced applications such Weather Forecasting[7], Disease Control and National Security monitoring.

A few critical challenges have kept most of the companies in stages 3 and 4. Among them, it is worth noting:

- Many critical enabling technologies such as IoT devices, cloud servers, 5G connectivity, drones with high power density batteries, constellations of nano satellites, GIS software, digital twin modeling software, non-invasive characterization surveys, AI pattern recognition software, and others, are relatively new. These technologies have found early adopters in other industries and are still being disseminated in the Mining industry;
- Tailings monitoring is a critical safety activity that requires the highest levels of reliability. In that sense, it is difficult for technical decision makers to propose new solutions that, while bringing performance advantages vs. more established solutions, also bring risks;
- New technologies come at a cost, and sometimes it is difficult to articulate a clear business case, since the benefits are mostly a reduction in operational risk that is not easy to quantify;
- Many of the new technologies require new professional skills that are not easily found within traditional settings and suppliers.

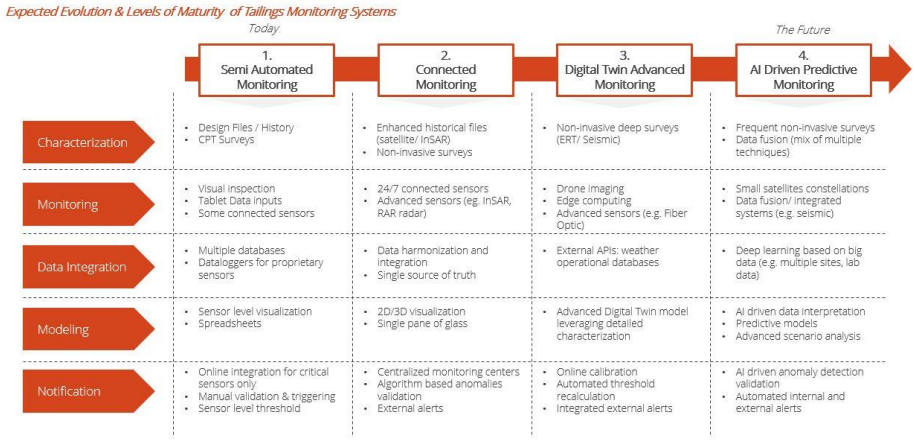

Exhibit 1 – Expected Evolution and Levels of Maturity of Tailings Dam Monitoring Systems

4 THE PATH FORWARD: THE FUTURE OF TAILINGS MONITORING SYSTEMS

At its evolved stage (Exhibit 2), models will seamlessly integrate multiple data inputs, combining detailed structure characterization, weather APIs, connected sensors and access to external databases. These systems will feed all data into both physical and statistical models, leveraging AI for advanced simulation and predictive features, and providing real time alerts to centralized monitoring centers staffed 24/7. As a result, this models will be able to update risk trees on real time, reliably detect anomalies, trigger internal and external alerts, automate compliance and reporting, trigger emergency preparedness plans, as well as constantly update themselves through a continuous data assimilation feedback loop.

Improving tailings dam risk profile through Integrated Systems requires a change in mindset and immediate action. Updated risk assessments must be followed by a technology roadmap to continuously deliver state of the art monitoring capabilities. In the short term, these roadmaps should focus on quick wins such as InSAR imaging and upgrades in data logging and connectivity, as well as enablers such as data integration technologies. For the mid-long term, focus should shift to transformational changes that may require deeper coordination and longer lead times, such as pilots with new characterization technologies, implementation of integrated systems, and modeling projects. In parallel to internal projects with immediate impact on existing assets, companies should also plan to continuously interact with academic research projects, develop industry-level partnerships, and make selective investments in the ecosystem.

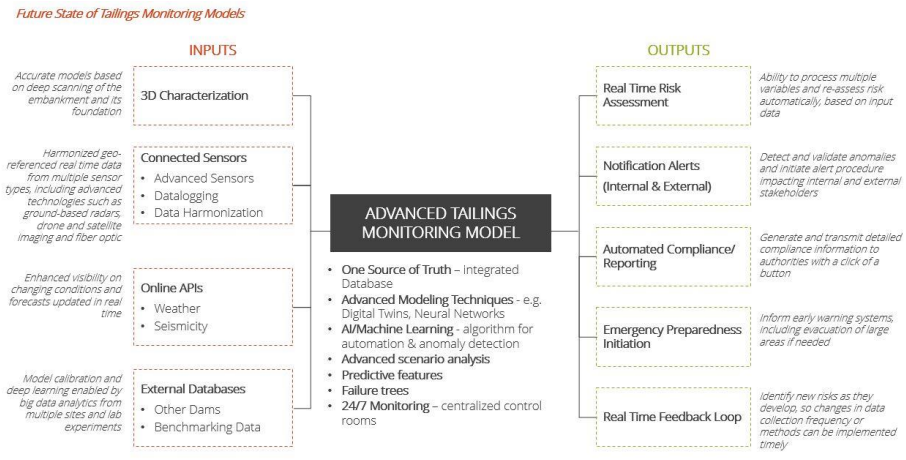

Exhibit 2 – Vision of the Future for an Integrated Tailings Dam Monitoring System

5 REFERENCES

1 https://worldminetailingsfailures.org/
2 https://gmggroup.org/tailings/
3 https://globaltailingsreview.org/
4 https://www.almg.gov.br/consulte/legislacao/completa/completa.html?ano=2019&num=23291&tipo=LEI
5 https://fch.cl/iniciativa/tranque/
6 http://www.b1technicalinvestigation.com/
7 https://www.ncdc.noaa.gov/data-access/model-data/model-datasets/global-data-assimilation-system-gdas

Permanent Geoelectrical Monitoring of Tailings Dams using the Autonomous G.RE.T.A. System

G Tresoldi
LSI Lastem, Settala (MI), Italy

A Hojat
Shahid Bahonar University of Kerman, Kerman, Iran – Politecnico di Milano, Milan, Italy

Leopoldo Cordova
Geosinergia Ingeniería Y Medio Ambiente Ltda., Santiago, Chile

Luigi Zanzi
Politecnico di Milano, Milan, Italy

ABSTRACT: The capability of a new geo-electrical monitoring system to be used for permanent monitoring of tailings dams is presented. G.RE.T.A. (Geo REsistivimeter for Time-lapse Analysis), is an autonomous programmable system including a remotely controlled low-power resistivity meter with two cables that can be permanently buried in shallow trenches. Time-lapse data analysis algorithms to visualize resistivity differences for any desired measurements are available on a cloud to monitor the subsoil in real-time. An automatic control algorithm can detect whether changes have approached predefined thresholds to send alarms about anomalous changes to the customer. The efficiency of the system has been demonstrated in pilot sites for monitoring the internal conditions of river levees and through laboratory tests for shallow landslides. The system is being used in several projects regarding tailings dams monitoring.

1 INTRODUCTION

During 1915-2019, 344 failures of tailings dams have occurred (Center for science in public participation, 2020), from which, 9 very serious incidents occurred during 2010-2019. The risk connected to tailings dams failure gained recognition after the Second World War due to the increased mining activity in that period; nowadays it is still an open issue without a standardised solution to avoid the disruptive impact on the environment, human activities, and human lives. The importance of tailings dam safety has been enhanced worldwide due to the recent failures that have occurred and the increased consciousness among the society.

Today, the issue is far from resolved, as the necessity for tailings dams and addressed volumes grows and consequently the related risk. Since the extracted metal represents only a small percentage of the entire ore mass, most of the extracted material is stored as tailings. Due to the small concentration of quality metals in the mined material, the dimensions of the storage basin and the dam become imposing.

After the recent dam breaches and failures, many projects, organizations, and research topics are addressing the issue of sustainable management of mine tailings, as, for example, the one run by NGI (Norwegian Geotechnical Institute, 2020), the creation of the Global Tailing Portal, where all the disclosures available about tailings dams are listed (GRID-Arendal, 2019) or the work developed by ICMM (International Council on Mining & Metals), dedicated to obtain a safer, fairer, and more sustainable mining and metals industry (ICMM, 2020).

The most frequent causes of tailings dam failure are related to the action of water resulting in overtopping, slope instability, seepage, and foundation failure. The tailings dam is subjected to different loads deriving not only from water but also from the load of the structure itself. The failure rate of tailings dams is estimated to be 10 to 100 times higher than the failure rate of other earthen dams, also because the construction procedure is carried out using locally available

unselected materials resulting from mining activities and raising the dam in different stages to increment the size and storage capacity of the basin along with the ongoing mine production of tailings. Another issue regarding tailings disposal is that, even if the majority of the quality minerals have been extracted through metallurgic processes, a fraction of sulphides, such as pyrite, chalcopyrite and arsenopyrite, remains in the disposal and originates acid mine drainage (AMD), with a high risk of contamination of the subsoil and the groundwater.

The problem of how to improve security level and lower the hydrogeological and environmental risk in tailings dams is a primary issue that must be faced by the whole society. The integrity and safety of tailings dams is a function of many aspects, but one of the most important is the continuous (high frequency) monitoring of the relevant parameters connected to the dam instability. The most important parameters to be monitored are: the phreatic surface or water level, the seepage flow, the pore water pressure, the superficial or internal movements.

The trend is moving forward standards and norms to homogenise the management and monitoring strategies in tailings dams (ICMM et al., 2020) but a unique and definitive solution to this topic has not been found so far. Monitored parameters are normally acquired as punctual measurements, for example with piezometers, elevation gauges, flow meters, extensometers, inclinometers, shear stripes. These technologies provide accurate values, but only in the point of the measurements, and they cannot be used to cover large parts of the structure due to technical and economic issues, related most of all to the coring process.

In last decades, different and new monitoring strategies have emerged, trying to fill the gap of punctual measurements with volumetric or 2D measurements. Topographic measurements, such as InSAR, terrestrial Lidar, total stations and GPS, monitor the surface of the dam, in order to detect movements comparing current images or point clouds to the previous situation (Alba et al., 2006; Alba et al., 2008; Lusi et al., 2010; Li and Wang, 2011; Sousa et al., 2016). Each method has its own resolution, acquisition rate and level of automatization, with advantages and some limitations. Terrestrial Lidar can give false alarms with open tailings dams, but can work efficiently in closed sites, even if it does not provide an insight about the ongoing inner processes. InSAR is very useful to take under control the topography of the dam, but it has a low rate of acquisition (8-12 days), unsuitable for sudden changes.

Geophysical measurements have been also used in monitoring of tailings dams to map the inner composition of the structure, for example using Ground Penetrating Radar (GPR) and Electrical Resistivity Tomography (ERT), or to detect vibrations originating by movements of the dam, using seismic sensors. Geophysical measurements have the great advantage of being non-invasive and of exploring large parts of the subsoils with volumetric prospections, exploiting the physical properties of the means. Nevertheless, some disadvantages are present: GPR for example, works well with regular surfaces, but has a low penetration depth and is operator dependant. Seismic sensors are not suitable for active mines where false alarms can be triggered.

Soil resistivity depends on soil composition, porosity, water content and resistivity of the circulating fluids, thanks to this characteristic, geoelectrical measurements can underline inhomogeneities in the subsoil originated by accumulation of water, presence of acid drainage, formation of cavities. For this reason ERT method is well known in the mining industry, especially for mineral exploration, groundwater studies, monitoring the mine wastes (Karimi Nasab et al. 2011; Camarero et al. 2019; Dimech et al. 2019; Martín-Crespo et al. 2019) and acid mine drainage (Rucker et al. 2009; Moradipour et al. 2016; Hudson et al. 2018).

In this paper, we present the capability of a new geo-electrical monitoring system to be used for permanent monitoring of tailings dams. This geo-electrical system, G.RE.T.A. (Geo REsistivimeter for Time-lapse Analysis), is an autonomous system including a remotely controlled low-power resistivity meter with two cables connected to maximum 48 stainless steel plate electrodes. The protected cables can be permanently buried in shallow trenches in the study sites. The monitoring system can be powered by solar panels or by power grid. All parameters are set according to the requirements of each specific site. Datasets of resistivity sections, measurement parameters and the status of the device are available on a cloud system. Time-lapse data analysis algorithms and tools to visualize resistivity differences for any desired measurements are available online in order to monitor the subsoil in real-time. An automatic control algorithm can detect whether changes have approached predefined thresholds to send alarms about anomalous changes to the customer.

The efficiency of the system has been demonstrated in pilot sites for monitoring the internal conditions of river levees (saturation condition, seepage presence, etc.) in northern Italy in last 6 years in projects of national importance (Tresoldi et al. 2018; Hojat et al. 2019a; Tresoldi et al. 2019; Hojat et al. 2020). The technology has been also applied through laboratory tests for shallow landslides (Hojat et al., 2019b; Ivanov et al., 2020) to detect non homogenous water accumulation zones and formation of fractures.

The newly designed version of the system, that is to be permanently installed to monitor tailings dams, is presented, along with recent tests done to assess the performances of the instrument in the mining environment. This recent version has been installed in a test site in Chile, in 2019. In the last months, a project has been carried out with the aim of monitoring a tailings dam of a copper mine located north of Santiago. The target is to detect underseepage below the dam's base, to avoid the contamination of the surrounding area and groundwater and to prevent the dam failure.

2 THE G.RE.T.A. SYSTEM DEVELOPMENT

During last year, a research and development process has been carried out to yield many improvements to refine the G.RE.T.A. and make it more robust, reliable and suitable for mining applications. The development was oriented 360 degrees, also through the introduction of new features, both on the instrument (mechanical, electrical, firmware), and on the cloud software platform. In the following sections, some of the instrument improvements are detailed.

2.1 *Mechanics*

The mechanics has been completely redesigned and rationalized to obtain a single box that contains both the measuring modules as well as the power modules, previously contained in two separate boxes (Fig. 1). This solution substantially offers the advantage of a simpler structure that is preassembled and much easier to install and maintain in the field. Moreover, an optional meteorological datalogging module has been foreseen in case the customer wishes to integrate meteorological sensors in the same installation.

The improvement is beneficial in remote places, where the weight and dimension of the device may be a constrain for transport and management. The possibility of integrating meteorological sensors with the geo-resistivity meter has been carried out with a view to the key point of integration of systems in the monitoring of tailings dams.

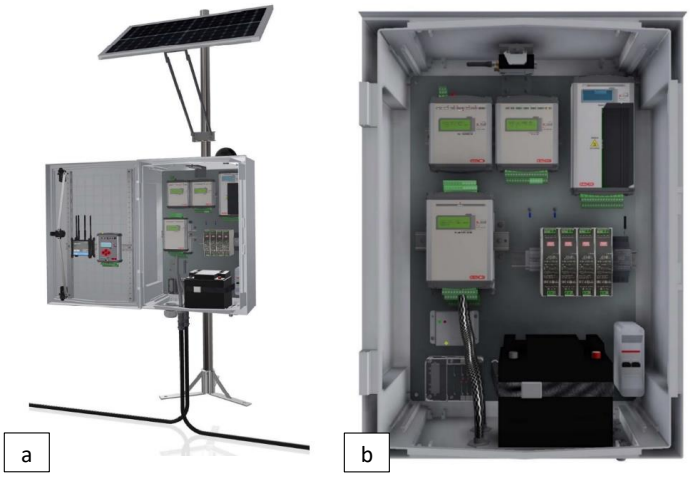

Figure 1. Improved mechanics of G.Re.T.A.: a) Box, solar panel and cables; b) Internal view of the box

2.2 *Line of electrodes*

2.2.1 *Cables*

The cables to which the electrodes are connected have been re-engineered to avoid the disconnection of the electric wires from the electrodes during cable traction on the ground. The cable has also been revised in terms of general robustness, increasing and better protecting the points of contact between the cable sheath and the electrodes. Arduous mining sites need robust equipment that can withstand traction, mobilization and repositioning.

2.2.2 *Electrodes*

Mining sites are often in arid zones, with dry soils of high resistivity. After the field tests were realized in Chile, tests to improve the contact resistance, also on new designed electrodes, were carried out.

Obtaining good ground contact is an issue in ERT. Geo-resistivity meters can supply certain maximum potential difference to inject the current and the electrode contact resistance may be the limiting factor of good quality measurements. In order to lower the contact resistance between soil and electrodes, some precautions can be adopted, such as enlarging the contact surface (Telford et al., 1990; Zonge et al., 2005) or adding conductive fluids in the surrounding soil, such as saline water or gel (Athanasiou et al., 2007) or coupling the electrode with clay or bentonite during installation (Reynolds, 1997; Zonge et al., 2005).

During the designing phase, plate electrodes were selected to guarantee a better coupling with soil compared to rod electrodes, but sometimes further measures are needed. During the field tests in Chile, bentonite was added during installation to improve current injection.

A mesh variant of electrodes was developed and tested, based on a research work by Tomaskovicova et al. (2016). They discovered that, as the plate and mesh electrodes are similarly shaped, the main difference is in the effective surface area of the electrodes, which is five times larger for the mesh electrodes (in their study four overlapping metallic meshes were used). The increased effective surface area seems to be an advantage when the electrodes are inserted or buried in fine-grained mineral or organic soils with some cohesive properties, in which the soil grains may fill the mesh network.

In order to understand the effective contribution of the mesh electrode and of exposed surface on lowering the contact resistance, an experiment was performed using 11 plate electrodes buried at 20 cm depth. The mesh electrodes were made of two overlapping layers of stainless-steel mesh

and the dimension was the same of the normally used plate electrodes. Contact resistances were measured along time with the focus-one method (Ingeman-Nielsen et al. (2016))(see *2.3.4*) using five (N.1-5) 15x20cm and six (N.6-11) 15x4,8cm stainless steel plate electrodes. After the first measurement, the electrodes 2 and 3 were changed with mesh electrodes and then contact resistances were measured once every hour for six hours. Electrode 3 was placed in a more humid zone compared to the location of electrode 2.

The results show that, as expected, contact surface and contact resistance are inversely proportional (Fig. 2a): larger plate electrodes (dotted lines) maintain lower resistance than smaller ones (solid lines) along time excepting for electrodes 5 and 8 that have a similar behavior.

The substitution of electrode 2 and 3 with mesh electrodes did not affect dramatically the resistance values (Fig. 2b), with two opposite responses: contact resistance of electrode 2, positioned in a dryer zone, was increased about 10 Ω, while it was decreased for electrode 3. Both electrodes, in the subsequent measurements had a decreasing trend of contact resistance, but not significantly. Other electrodes had different behaviors: electrode 4 had a constant trend, contact resistances were decreased for electrodes 2, 7, 8, 11 and increased for electrodes 5, 6, 9, 10 with time.

Using mesh electrodes instead of plate electrodes did not largely affect contact resistance of electrodes, the explanation can be related to the soil type, since, as explained in Tomaskovicova et al. (2016), mesh electrodes are convenient with fine grained soils, which fill the mesh apertures enhancing current flow.

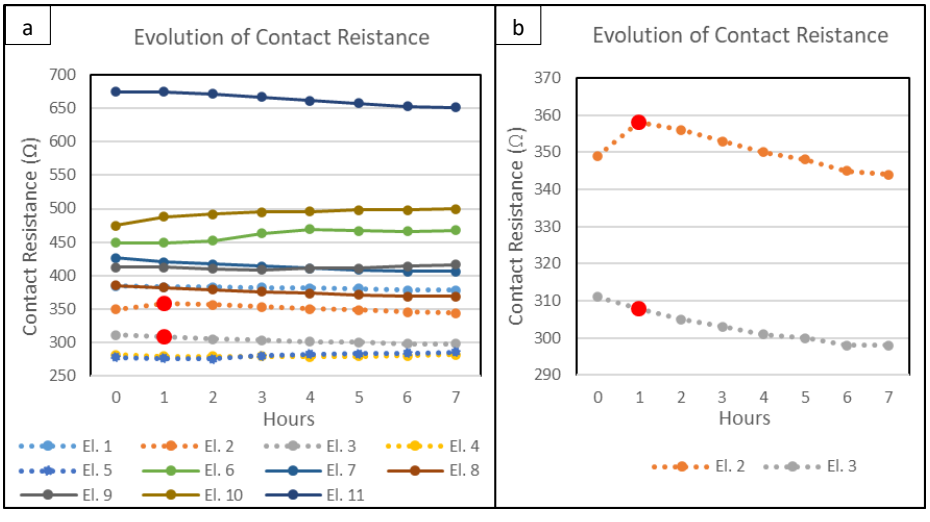

Figure 2. Test on contact resistance of mesh electrodes: a) Entire electrode line along time b) Electrode 2 and 3, before (hour 0) and after (from hour 1 to 7) the substitution with mesh electrodes. Red point is the first measured contact resistance of mesh electrodes after substitution

2.3 *Firmware*

2.3.1 *Low level measurements*

A new injection and signal sampling algorithm has been introduced to improve the measurement of the apparent resistivity on the single point when the ground manifests linear variations in its spontaneous electric potentials. The new algorithm adopts the plus-2minus-plus method described in research works produced by Madden and Cantwell (1967) and Dahlin (2000). In order to suppress low-frequency variations in back-ground spontaneous potentials, the current injection

may consist in a positive injection, a double negative one and finally another positive pulse. The filter with coefficients (0.25, -0.50, 0.25) suppresses linear terms.

2.3.2 *Measurement sequence*

The measurement sequence used in electric resistivity campaign should be carefully designed to minimize the effects of electrode charge-up, that can be significant also for several minutes (Dahlin, 2000). Making potential measurements with an electrode that has just been used to inject current should be avoided, as the decay curve after current switch-off is non-linear. The injection sequence for the Wenner array used by G.RE.T.A. has been improved in order to avoid using current electrodes that will be immediately used as measurement electrodes in the next cycle. This leads to an improvement in the stability of the measurements, therefore, lower standard deviation values on measurements.

2.3.3 *Electrode depth compensation*

Standard geometrical factors of geoelectrical measurements are calculated with the hypothesis of electrodes fixed on the ground surface, so with the complete reflection of electric field at the surface. The geometric factor for Wenner configuration is $2\pi a$ (a being the electrode spacing).

In most applications where G.Re.T.A. is used, electrode line is buried a few tens of centimetres, so a different geometrical factor must be considered for the apparent resistivity calculations, function of electrode burial depth. The image sources method has been used for the calculation, considering the reflections from the interface soil-air (Equation 1).

$$C_{buried} = \frac{2\pi a}{\left[\frac{1}{2} + \frac{1}{\sqrt{1+\left(\frac{2h_1}{a}\right)^2}} - \frac{1}{\sqrt{4+\left(\frac{2h_1}{a}\right)^2}}\right]} \quad (1)$$

Where: a is the electrode spacing and h_1 is the burial depth of electrodes. It should be noted that, when h_1 is equal to 0 (surface electrodes), the geometrical factor is again $2\pi a$, while in the limit case of h_1 equal to infinite, the geometrical factor is $4\pi a$ (homogenous space).

If the correct geometrical factor is not used, de-amplification of the apparent resistivity values happens. The effect decreases with the depth and mainly the first two/three levels of measurements are affected.

2.3.4 *Contact resistance measurement*

A new measurement and calculation protocol for the contact resistances of the electrodes has been adopted, using the "focus one" protocol derived from the research of Ingeman-Nielsen et al. (2016). To estimate the contact resistance of a single electrode, the resistance between the electrode in the array and all the other electrodes connected in parallel is measured. The contact resistance measurement is now more precise and provides a better indication of the installation conditions of each electrode.

3 THE MINING EXPERIENCE

The upgraded G.Re.T.A. system with 3 m spacing between plate electrodes was sent to Chile to be installed on a tailings dam of a copper mine located north of Santiago. Before the installation, some field tests were done to assess the functionality of the system in the dry soil of the zone and to evaluate the improvements of the device.

3.1 *Well test*

In February 2020, a field test was done in Talca city, near Santiago, in order to test the device against piezometer data (Fig. 3). The system was moved to acquire three profiles in a 3D configuration around the well position. The hard and dry soil made current penetration difficult resulting in high contact resistances. Therefore, ideas of pouring salt water and using bentonite to

maintain the humidity around the buried electrodes were followed. Profile 1 was acquired in the vicinity of the well, Profile 2 was parallel to Profile 1 while Profile 3 crossed both profiles (Fig. 4).

The inversions were carried on using the cloud software and Res2dInv (Loke, 2018), to make a comparison of the results. Looking at Profile 1 inversion result (Fig. 5), a heterogeneous subsoil (smooth changes of resistivity through the profile) can be observed. There is a low resistivity zone between 50 m and 70 m along the profile and from 12,9 m depth. A second focus of low resistivity centered at 90 m along the profile and between 8 m to 12 m of depth can be seen. Crossing the information of the existing well with the profile, we found that the phreatic level of the well matches at 12,9 m depth as indicated by the ERT result. Also, observing the results of the three profiles (Fig. 6) and the location of saturated zone only near the well, it appeared that the well could correspond to an artesian one, since the surrounding zones investigated by Profile 2 and Profile 3 do not underline the presence of a free aquifer.

Figure 3. G.Re.T.A. system installed for the well test, the blue arrow points to the 148m-deep water well

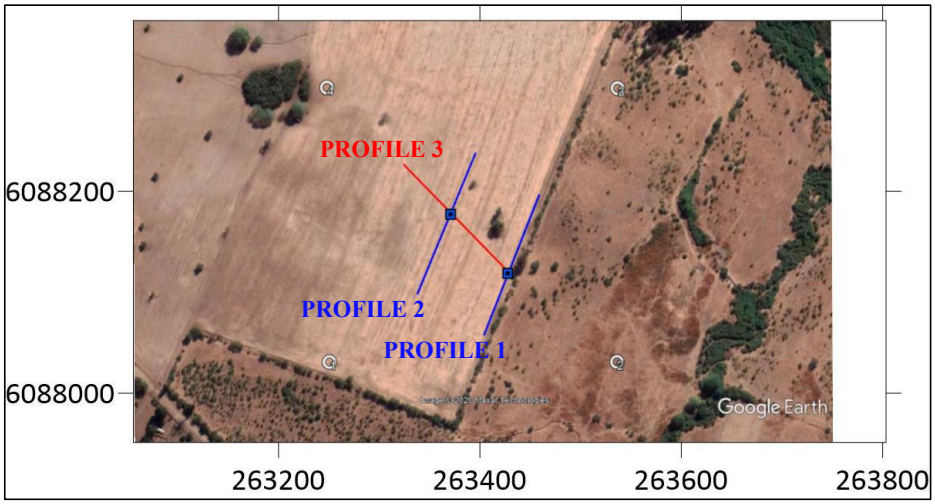

Figure 4. Disposition of Profile 1, Profile 2 and Profile 3 in the test site with UTM coordinates

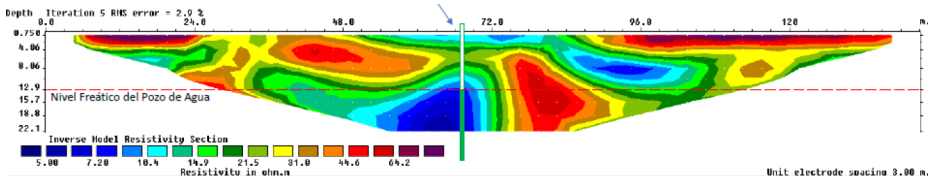

Figure 5. Resistivity section of Profile 1, the blue arrow points to the well position and the red dashed line shows the measured piezometric level

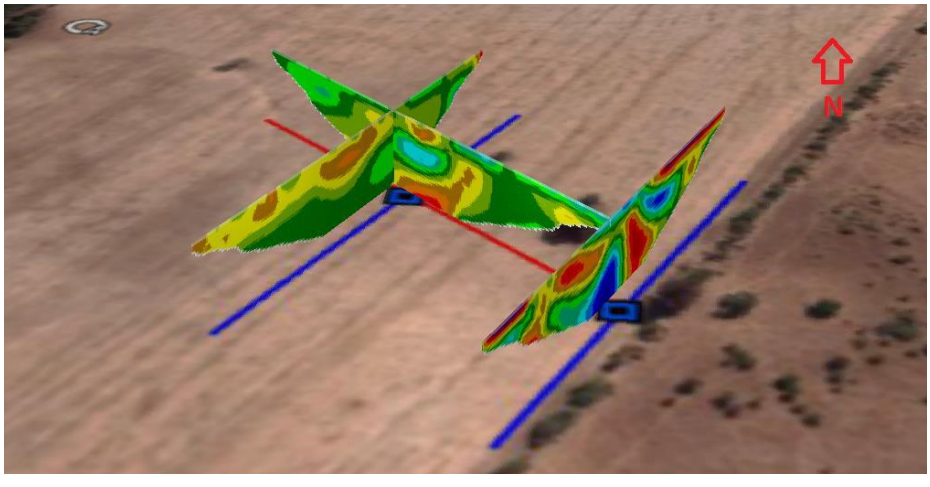

Figure 6. Resistivity sections of Profile 1, Profile 2 and Profile 3 in 3D configuration

3.2 *Installation on a tailings dam of a copper mine*

The mine is a sulfide deposit north-east of Santiago. The production is focused on copper concentrate, that contains gold and silver, and molybdenum concentrate, obtained through a milling and flotation process.

With the objective of ensuring the community of the surroundings on the safety of the tailings dam, a G.Re.T.A. system was installed in the site in August 2020 after a survey period (Fig. 7).

The monitored profile was placed at the base of the tailings dam, in order to detect possible under-seepages that can pollute the groundwater and the surrounding exposed area, with the presence of a city.

Figure 7. Site of the G.Re.T.A. installation: tailings dam in Chile

4 CONCLUSIONS

The G.Re.T.A. system, an autonomous geo-resistivimeter for time lapse analysis, can fill the gap for monitoring the tailings dams. Geoelectrical measurements vary with soil composition, water content, presence of voids, the resulting measurements can thus indicate variations in the dam structure related to seepages, fracture formations or different water contents.

During the last year, many improvements have been carried out in order to adapt the system for mining environment, where robust and reliable devices are needed. Mechanics, electrode cables and firmware were improved and tested to achieve the best results also in extreme conditions. The system was then designed with only one box, the cables were improved with more resistant connections, the mesh electrodes were tested but no significant results were obtained in organic soil, further tests will be carried out with different kind of soils, since the mesh shape works well with fine grained soils. Injection algorithm was upgraded with the plus-2 minus-plus method and the measurement sequence was modified to reduce polarization effects. Depth compensation for electrode burial was introduced in the apparent resistivity calculation and focus-one method was added to measure contact resistance.

The updated system was tested on a hard and dry soil during a well test, comparing geoelectrical measurements with piezometric data and good results were obtained, because the groundwater depth was perfectly identified, as long as contact resistances were maintained low.

In August 2020 an investigation campaign with a view to G.Re.T.A. installation was performed at a tailings dam in Chile. The aim of this monitoring project is the detection of possible under-seepages below the dam's base.

5 AKNOWLEDGMENTS

The research of Politecnico di Milano was partially funded by Ministero dell'Ambiente e della Tutela del Territorio e del Mare, Italy, project DILEMMA – Imaging, Modeling, Monitoring and Design of Earthen Levees.

Authors are grateful to LSI-Lastem for the permission to publish this contribution about the use of the G.Re.T.A. monitoring system.

We would like to thank Geosinergia for contributing with photos, tests and results on site, their undergoing projects and operations in Chile helped to improve the capabilities of the tomography equipment and served as an example for scientific exploration.

REFERENCES

Alba, M., Fregonese, L., Prandi, F., Scaioni, M. & Valgoi, P. 2006. Structural Monitoring of a Large Dam by Terrestrial Laser Scanning. In Maas, H.-G. and Schneider, D. (ed.), *Int. Arch. Photogramm. Remote Sens., ISPRS Commission V Symposium on Image Engineering and Vision Metrology*; *Proc. symp., 25-27 September 2006*. Dresden, Germany. XXXVI, Part 5: 6 pp.

Alba, M., Bernardini, G., Giussani, A., Ricci, P.P., Roncoronia, F., Scaioni, M., Valgoic, P. & Zhangd, K. 2008. Measurement of dam deformations by terrestrial interferometric techniques. *Int. Arch. Photogramm. Remote Sens. Spatial Inf. Sci*. 37 (part b1): 133-139.

Athanasiou, E.N., Tsourlos, P.I., Vargemezis, G.N., Papazachos, C.B. & Tsokas, G.N. 2007. Non-destructive DC resistivity surveying using flatbase electrodes. *Near Surface Geophysics* 5: 263–272, doi: 10.3997/1873-0604.2007008.

Camarero, P.L., Moreira, C.A. & Pereira, H.G. 2019. Analysis of the physical integrity of earth dams from electrical resistivity tomography (ERT) in Brazil. *Pure of Applied Geophysics*: 1–13. https://doi.org/10.1007/s00024-019-02271-8

Center for science in public participation (2020). Tsf failures from 1915, *csp2*. Retrieved from http://www.csp2.org/tsf-failures-from-1915

Dahlin T. 2000. Short note on electrode charge-up effects in DC resistivity data acquisition using multi-electrode arrays. *Geophysical Prospecting* 48: 181-187.

Dimech, A., Chouteau, M., Aubertin, M., Bussière, B., Martin, V. & Plante B. 2019. Three-dimensional time-lapse geoelectrical monitoring of water infiltration in an experimental mine waste rock pile. *Vadose Zone Journal* 18(1). https://doi.org/10.2136/vzj2018.05.0098

GRID-Arendal (2019). *Global Tailings Portal*. Retrieved from https://tailing.grida.no/

Hojat, A., Arosio, D., Longoni, L., Papini, M., Tresoldi, G. & Zanzi, L, 2019a. Installation and validation of a customized resistivity system for permanent monitoring of a river embankment. *EAGE-GSM 2nd Asia Pacific Meeting on near Surface Geoscience & Engineering*; *Proc. symp.,* European Association of Geoscientists & Engineers, Houten. https://doi.org/10.3997/2214-4609.201900421

Hojat, A., Arosio, D., Ivanov, V.I., Longoni, L., Papini, M., Scaioni, M., Tresoldi, G. & Zanzi, L. 2019b. Geoelectrical characterization and monitoring of slopes on a rainfall-triggered landslide simulator, *Journal of Applied Geophysics* 107, 103844. https://doi.org/10.1016/j.jappgeo.2019.103844

Hojat, A., Arosio, D., Ivanov, V.I., Loke, M.H., Longoni, L., Papini, M., Tresoldi, G. & Zanzi, L. 2020. Quantifying seasonal 3D effects for a permanent electrical resistivity tomography monitoring system along the embankment of an irrigation canal. *Near Surface Geophysics*. doi:10.1002/nsg.12110

Hudson, E., Kulessa, B., Edwards, P., William, T. & Walsh, R. 2018. Integrated hydrological and geophysical characterisation of surface and subsurface water contamination at abandoned metal mines. *Water Air Soil* Pollution 229: 256. https://doi.org/10.1007/s11270-018-3880-4

ICMM (2020). *International Council on Mining and Metals.* Retrieved from https://www.icmm.com/

ICMM, United Nations Environment Programme & Principles for Responsible Investment (2020). *Global Tailings Review*. Retrieved from https://globaltailingsreview.org/

Ingeman-Nielsen, T., Tomaskovicova, S., & Dahlin, T. 2016. Effect of electrode shape on grounding resistances - Part 1: The focus-one protocol. *Geophysics* 81(1): WA159-WA167. https://doi.org/10.1190/geo2015-0484.1

Ivanov, V., Arosio, D., Tresoldi, G., Hojat, A., Zanzi, L., Papini, M. & Longoni, L. 2020. Investigation on the Role of Water for the Stability of Shallow Landslides—Insights from Experimental Tests. *Water* 12(1203). https://doi.org/10.3390/w12041203

Karimi Nasab, S., Hojat, A., Kamkar-Rouhani, A., Akbari Javar, H. & Maknooni, S. 2011. Successful use of geoelectrical surveys in Area 3 of the Gol-e-Gohar iron ore mine, Iran. *Mine Water and the Environment* 30(208). https://doi.org/10.1007/s10230-011-0135-7

Li, W. & Wang, C. 2011. GPS in the Tailings Dam Deformation Monitoring. *Procedia Engineering* 26: 1648-1657. ISSN 1877-7058. https://doi.org/10.1016/j.proeng.2011.11.2350.

Loke, M.H. 2018. Rapid 2-D resistivity and IP inversion using the least-squares method. www.geotomosoft.com.

Luzi, G., Crosetto, M. & Monserrat, O. 2010. Advanced techniques for dam monitoring. *II International Congress on Dam Maintenance and Rehabilitation*; *Proc. symp.:* 23–25, Zaragoza, Spain, November 2010.

Madden, T.R. & Cantwell T. 1967. Induced polarization, a review. In Society of Exploration Geophysicists (ed.)*, Mining Geophysics*, Vol. 2, Theory: 373-400.

Martín-Crespo, T., Gómez-Ortiz, D., Martín-Velázquez, S., Lillo, J. & Faz, A. 2019. Geoenvironmental characterization of sulfide mine tailings. In Intechopen (eds.), *Geochemistry*. https://doi.org/10.5772/intechopen.84795

Moradipour, M., Ranjbar, H., Hojat, A., Karimi Nasab, S. & Daneshpajouh, S. 2016. Laboratory and field measurements of electrical resistivity to study heap leaching pad no. 3 at Sarcheshmeh copper mine. *Near Surface Geoscience 2016; Proc. symp.,* European Association of Geoscientists & Engineers, Houten https://doi.org/10.3997/2214-4609.201602140

Norwegian Geotechnical Institute (2020). Towards sustainable mine tailings. Retrieved from https://spark.adobe.com/page/plAIOgPCgfKvI/

Reynolds, J.M. 1997. In Wiley-Blackwell (ed.), *An introduction to applied and environmental geophysics*.

Rucker, D.F., Schindler, A., Levitt, M.T. & Glaser, D.R. 2009. Three-dimensional electrical resistivity imaging of a gold heap. *Hydrometallurgy* 98: 267–275. https://doi.org/10.1016/j.hydromet.2009.05.011

Sousa, J.J., Ruiz, A.M., Bakoň, M., Lazecky, M., Hlaváčová I., Patrício, G., Delgado, J.M.& Perissin, D. 2016. Potential of C-Band SAR Interferometry for Dam Monitoring. *Procedia Computer Science* 100: 1103-1114. ISSN 1877-0509. https://doi.org/10.1016/j.procs.2016.09.258.

Telford, W.M., Geldart, L.P. & Sheriff, R.E. 1990. In Cambridge University Press (ed.), Applied geophysics..

Tomaskovicova, S., Ingeman-Nielsen, T., Christiansen, A.V., Brandt, I., Dahlin, T., & Elberling, B. 2016. Effect of electrode shape on grounding resistances - Part 2: Experimental results and cryospheric monitoring. *Geophysics*, 81(1), WA159-WA172. DOI: 10.1190/GEO2015-0148.1

Tresoldi, G., Arosio, D., Hojat, A., Longoni, L., Papini, M. & Zanzi, L. 2018. Tech-Levee-Watch: experimenting an integrated geophysical system for stability assessment of levees. *Rendiconti Online Societa Geologica Italiana* 46: 38–43. https://doi.org/10.3301/ROL.2018.49

Tresoldi, G., Arosio, D., Hojat, A., Longoni, L., Papini, M. & Zanzi, L. 2019. Long-term hydrogeophysical monitoring of the internal conditions of river levees. *Engineering Geol*ogy 259(105139). https://doi.org/10.1016/j.enggeo.2019.05.016

Tresoldi, G., Hojat, A., Zanzi, L. & Certo, A. 2020. Introducing G.RE.T.A. – an innovative geo-resistivimeter for long-term monitoring of earthen dams and unstable slopes. In PM Dight (ed.), *2020 International Symposium on Slope Stability in Open Pit Mining and Civil Engineering*; *Proc. Intern. symp*, Australian Centre for Geomechanics, Perth: 487-498. https://doi.org/10.36487/ACG_repo/2025_28

Zonge, K., Wynn, J. & Urquhart, S. 2005. Resistivity, induced polarization and complex resistivity. In D. K. Butler (ed.), *Near-surface geophysics: SEG*: 265–300.

Mine Tailings Surveying after the Brumadinho Dam Failure

Gerry Mitchell, Jim Turner, & Sam Rivett
PhotoSat, Vancouver, BC, Canada

ABSTRACT: The investigation committee report into the causes of the Brumadinho Dam failure has re-emphasized on-going shortcomings in surveying methods and practices for tailings facilities. These shortcomings were also highlighted in the causes of failure report for Fundao dam which was published in 2016. The authors see some of these same shortcomings at many mines around the world.

These reports highlight the fact that many mines do not maintain complete, verifiable, as-built surveys of their facilities which can be used to show that the TSF was constructed and operated in accordance with the dam's design.

The authors have extensive experience in producing surveys of TSF and mine sites at a globally diverse range of locations. Based on this experience we will show examples and explanations of the shortcomings of commonly used survey methods that are highlighted in the dam failure investigation reports, with a real-world example of best practices.

1 INTRODUCTION

There have been several recent tailings dam failures with significant human and environmental impacts, notably the Feijão Dam I, Brazil (Brumadinho) and the Fundão Dam, Brazil (Samarco). Investigation reports have emphasized the critical nature of maintaining complete, verifiable, as-built surveys.

PhotoSat has completed over 1,200 mine tailings surveys around the world. This includes producing over 600 time-stamped surveys of mine tailings facilities since 2012, and three technical reviews of major mine tailings failures.

2 FUNDÃO AND FEIJÃO DAM FAILURES

Both the Fundão and Feijão tailings dams were designed to be upstream tailings dams composed of unsaturated sands. Some areas of the sands in both dams was water saturated, making the dams only marginally stable.

Fundão Dam I failed at the left abutment most probably due in part to the presence of tailings slimes beneath this portion of the raised dam.

Feijão Dam 1 failed most probably due to strains from internal creep combined with the influx of surface water from heavy rainfall in Q4 2018.

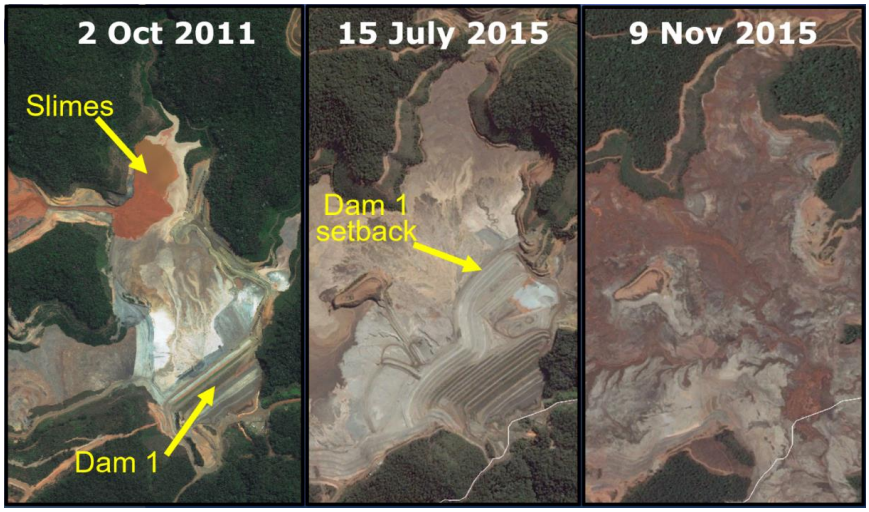

Figure 1. WorldView satellite photos of the Fundão dam. October 2011 showing the introduction of tailings slimes to Dam 1. July 2015 showing the Dam 1 setback over the tailings slimes. November 2015, four days after the failure of Dam 1.

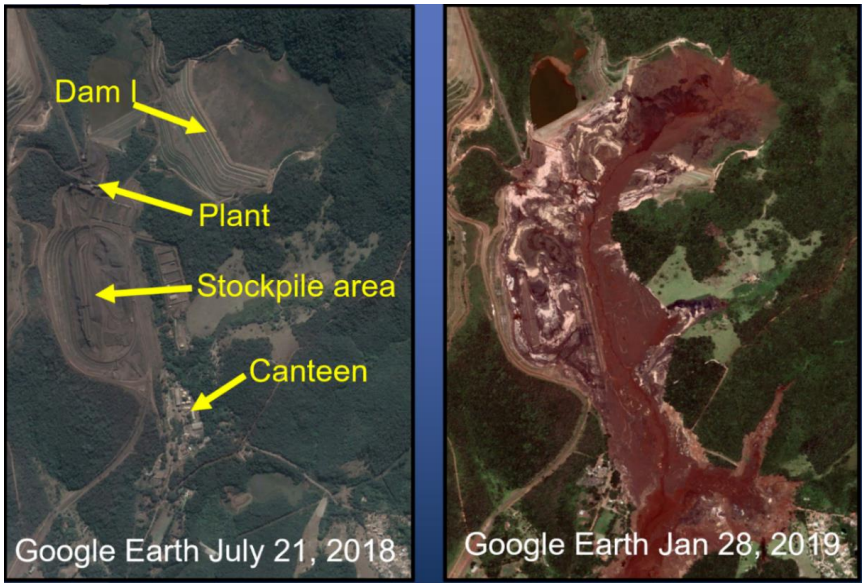

Figure 2. WorldView satellite photos of the Feijão dam I. July 21, 2019, six months prior to the failure. January 28, 2019, three days after the failure.

2.1 *Surveying issues at the Fundão Dam*

The Report on the Immediate Causes of the Failure of the Fundão Dam noted surveying issues "…typical for a large tailings dam…", including data inconsistencies, sporadic surveys that only covered a small area and did not appear to have been done for the purposes of monitoring tailings deposits, and the utilization of drone data patched over several survey periods and which did not follow accepted contouring standards.

2.2 *Surveying issues at the Feijão Dam*

The Report of the Expert Panel on the Technical Causes of the Failure of the Feijão Dam commented on the limited number of topographic surveys available for the investigation, and noted, "Because as-built drawings were either not prepared or not available for review, many of the design features and specifications described below are based on the Panel's understanding of the plan for dam construction, rather than confirmation of what was constructed."

3 GLOBAL TAILINGS STANDARD DRAFT REPORT

Global Tailings Standard Draft provides recommendations for officials and experts responsible for tailings facility safety oversight including a Responsible Tailings Facility Engineer (RTFE), Independent Tailings Review Board (ITRB), Senior Technical Reviewer, Engineer of Record (EOR), an Independent Tailings Review Board, and regularly conducted risk assessments with a qualified multidisciplinary team.

3.1 *Tailings facility surveying requirements*

Tailings surveying must meet daily, weekly and monthly operational needs, provide a long-term overview of the tailings facility development (i.e. monthly survey snapshots), meet external perceptions that the best technology and practices are being used to keep the tailings facility safe, and must fit within any budget constraints.

4 PHOTOSAT'S MINE TAILINGS SURVEYING EXPERIENCE

PhotoSat has carried out over 600 surveys of mine tailings facilities since 2012. Over 100 of these surveys have covered the tailings facility for the Steepbank and Millennium oil sands mines in Northern Alberta, Canada. PhotoSat surveyed this facility monthly during the winter and twice monthly the rest of the year since January 2013. This is one of the largest tailings facilities in the world, handling over 40 million m3 of mine tailings per year.

PhotoSat regularly surveys tailings facilities at operating mines in most of the major mining regions of the world. Depending on the volume of tailings at these mines, surveys may be completed monthly, quarterly, or twice annually. The watersheds upstream from the mine sites and the potential inundation areas downstream tend to be photographed annually and surveyed every three years at larger mines.

Currently, many mine owners and tailings engineers rely on various survey reports from ground GPS, terrestrial scanners, and drones to build a comprehensive view of their tailings facility. They believe this process provides them with enough information to maximize the long-term safety and stability of their tailings facility. They often underestimate the extent to which their current survey data limits their long-term overview of the facility.

A few mine owners and tailings engineers continue to manage tailings facilities using only pumping volumes, on-foot dam inspections and boat bathymetry. They may unaware that their tailings facility surveys may be inconsistent or error-prone, or that more reliable surveying is practically possible. It is also possible that the potential impact of those errors on the long-term management of the tailings facility is not well understood.

4.1 *Understanding common mine site surveying errors and deficiencies*

When surveying a mine site for the first time, PhotoSat always tries to compare our first survey to the existing mine site survey data. This existing survey data is usually a combination of ground GPS and drone surveys. This experience has given PhotoSat insights into common exceptions and errors in mine sites surveying, particularly mine tailings facility surveying.

In reviewing survey data from many mine sites over the past several years, the most-frequently observed survey problem is that mines attempt to produce monthly site wide survey overviews by patching survey data from multiple sources. Each of the individual surveys are usually

collected for specific operational needs and are not designed nor intended to be part of a regular site wide survey overview.

PhotoSat's experience working with tailings engineers has determined that elevation surveying accuracy better than 20 cm RMSE in elevation is required to accurately monitor tailings dam heights, tailings beach lift thicknesses and deposition locations.

5 MINE SITE SURVEY CONTROL

Mine site topographic surfaces are continually changing. Some mine site-wide surveys are composed of mosaics of several smaller surveys completed on different days. When check surveys and other survey data sets are compared to these mine site wide survey mosaics, it is often difficult to determine the actual date of the relevant portion of the overall mine site survey. Survey difference and discontinuities are then often dismissed as being due to topographic changes between the survey dates.

Individual, separate, mine site survey data sets may be compared to the time-stamped, mine site wide survey. Mismatches between the individual topographic surfaces and/or the photos of each of the individual surveys and the mine site wide survey often reveal survey errors. Once these survey errors are identified most mine site operators usually move quickly to rectify them.

Consistent, routine surveys and photographic snapshots of entire mine sites enable mine owners, tailings engineers, and independent reviewers to better understand and demonstrate the safety and stability of the tailings facilities. With consistent, routine surveys and photographic snapshots they are better able to monitor the tailings facility's conformity to, or departure from, the design criteria and evolving national and international tailings facility safety standards.

A monthly or quarterly series of consistent, uniform time-stamped surveys that cover the entire mine site and surrounding areas, with each survey completed in a single day, provide a long-term auditable record of the state of the mine site including the tailings facility. Surveying of an entire mine area in a single day can currently be accomplished with air photo, airborne LiDAR and satellite surveying. Only satellite surveying can survey an entire mine site in a single minute.

6 EXAMPLE OF GOOD TAILINGS FACILITY SURVEYING PRACTICES

The Suncor Millennium Mine is PhotoSat's best example of good mine site surveying practices. The oil sands mines of northern Alberta Canada have the world's largest volume mine tailings facilities. In PhotoSat's view, these are among the most meticulously engineered and carefully managed tailings facilities on the globe.

Suncor Millennium Mine does monthly surveys which provide photos and topography that cover the entire site plus a large area surrounding it (no patching), are consistent to 15 cm vertical accuracy in all areas of the site, ensure consistent accuracy month-to-month, are tested and validated monthly, are used as operational data by many groups daily. Site-wide surveys have been conducted at least monthly since 2013.

6.1 *PhotoSat survey specifications for the Millennium Mine*

PhotoSat provides the Millennium Mine with:

Elevation Grids: (1 m or 50 cm grids of elevation values, vertical accuracy of 15 cm RMSE, thinned versions for engineering software, mine grid and UTM projections, and tiled to match application areas)

Toes and Crests: (breaklines of the toes and crests of all step changes in elevation on the mine site)

Waterbody Polygons: (boundaries or all ponds and water bodies over 400 m^2)

Orthophoto: (50 cm or 30 cm resolution satellite photo, precision orthorectified)

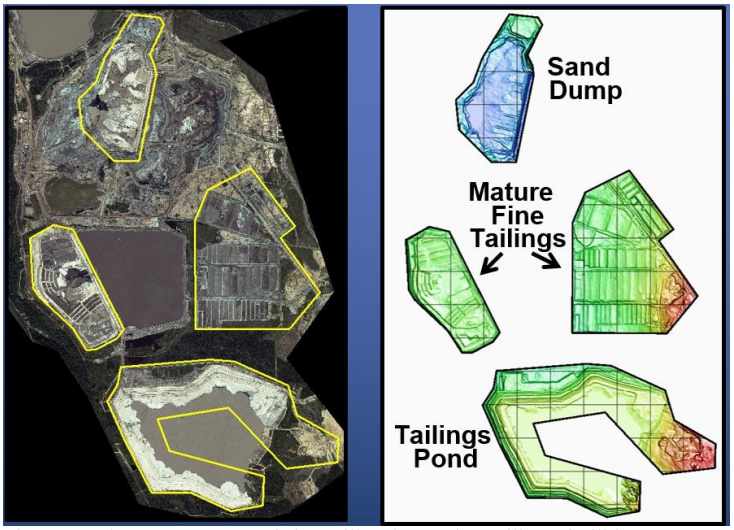

Figure 3. PhotoSat surveys of the Millennium Mine tailings facilities. Surveys accurate to 15 cm in elevation. Figure from a published Suncor presentation.

7 IMPROVING MINE SITE SAFETY THROUGH BETTER SURVEYING

Highly accurate and reliable survey data leads to a better-informed decision making process, with the potential to improve safety and management practices. PhotoSat recommends the following mine site survey standards for mines with large tailings facilities: monthly, time-stamped, surveys of the mine site; annual photographic surveys of the watershed upstream of the tailings facility; topographic surveys of the watershed upstream of the tailings facility every three years; annual photographic surveys of the potential inundation area downstream of the tailings facility; and topographic surveys of the potential inundation area downstream of the tailings facility every three years.

8 CONCLUSION

Both the Fundão and Feijão tailings dams investigations documented poor or incomplete surveying practices which are common in many mines with large tailings dams.

A long-term, auditable record of the state of the tailings facilities can be achieved with a monthly or quarterly series of consistent, uniform time-stamped surveys that cover the entire mine site and surrounding areas.

Surveying of an entire mine area in a single day can currently be accomplished with air photo, airborne LiDAR and satellite surveying. Only satellite surveying can survey an entire mine site in a single minute.

In our experience the above recommendations will improve the surveying deficiencies that are the result of the piecemeal surveying currently employed in many mine tailings facilities in various places in the world.

REFERENCES

Lomond, P. & Turner, J. Trimble Dimensions Conference, 2014. Mapping and Monitoring for Suncor's Oil Sands Tailings Reduction Operation process using GPS surveying and PhotoSat satellite topography. Available At: https://www.photosat.ca/pdf/photosat-suncor-trimble-presentation-nov2014.pdf.

Robertson, P. K., de Melo, L., Williams D. J, & Wilson, G. December 12, 2019. Report of the Expert Panel on the Technical Causes of the Failure of Feijão Dam I. Available at: https://bdrb1investigationstacc.z15.web.core.windows.net/assets/Feijao-Dam-I-Expert-Panel-Report-ENG.pdf

Oberle, B. November 15, 2019. TAILINGS STANDARD Draft for Public. Available at: https://globaltailingsreview.org/wp-content/uploads/2019/11/EN-Global-Tailings-Standard_CONSULTATION-DRAFT.pdf

Jefferies, M., Morgenstern, N. R., Van Zyl, D., & Wates, J. April 17, 2019. Report on NTSF Embankment Failure Cadia Valley Operations for Ashurst Australia By Independent Technical Review Board. Available at:https://www.newcrest.com/sites/default/files/2019-10/190430_NTSF%20Embankment%20Slump%20Report%20-%20Market%20Release.pdf

Recent Geotechnical Monitoring Results Reflect Operational Improvements at the Newmont Peñasquito

E. J. García Romero & V. V. Sosa Dávila
Newmont Peñasquito, Mazapil, Zacatecas, México

Geotechnical parameters assessed between 2015 and 2019 through Cone Penetration Tests (CPT), show step change improvements implemented at Newmont's Peñasquito Mine Tailings Facility in Mazapil, Zacatecas, México. Step change improvements include optimization of tailings cycloning and implementation of a beach management and tailings deposition plan. Improvements are reflected in the TSF resulting in longer tailings beaches, improved reclaim pond management, and tailings densities. Comparing cone penetration test results collected between 2015 and 2019, demonstrates the improvements that operational practices have had on the segregation and quality of the tailings beach. Additionally, the CPT program allowed installation of additional piezometers to monitor pore pressures and phreatic surface levels within the tailings beach. This paper presents an overview of the Peñasquito Tailings Storage Facility, and how the improvements in operation of the facility have resulted in improved geotechnical performance and monitoring.

1 PEÑASQUITO TAILINGS STORAGE FACILITY

1.1 *General*

Minera Peñasquito (MP), located in Zacatecas state in México, is a polymetallic open pit mine that has been operational for 13 years. The Tailings Storage Facility (TSF) is a four-sided structure with an 11 kilometer (km) perimeter and a maximum height of approximately 93 meters (m), as shown on Photo 1. The TSF receives 100,000 tons of tailings per day and has been in operation since 2009. Future plans for the TSF include a staged centerline raised to a maximum height of 120 m, with an ultimate storage capacity of 808 million tons. Table 1 presents the planned centerline raise project construction and status.

The construction history for the Penasquito TSF included a 20 m high starter dam constructed of borrowed alluvial fill with 2H:1V outer slopes (Golder 2008). A rockfill buttress was constructed in 2011, and the dam has been raised continuously using rockfill as the outer shell and cyclone sand as a compacted core separating the deposited tailings from the rockfill. Tailings are conveyed by gravity from two cyclone stations located along the north and south dams. Cyclone underflow sand is separated from the whole tailings and used for dam construction, and cyclone overflow slimes are deposited uniformly from the perimeter of the north, west, and south dams.

The construction of the TSF has been dynamic; responding to changes in availability of materials, operational experience and variations in quality sand production.

Construction of the TSF is separated into three activities defined as buttress fills, sliver fills and crown fills, the first two are compounded by rock only, meanwhile crownfill is a combined rock and sand section. Buttress fills are required to enhance stability of the TSF dams as the facility is raised. Sliver fills are constructed overtop of the buttress fills on the downstream side of the dam

to allow for widening of the dam crest, which facilitates the centerline raise. Crown fills are constructed on the sliver fills to raise the elevation of the dams.

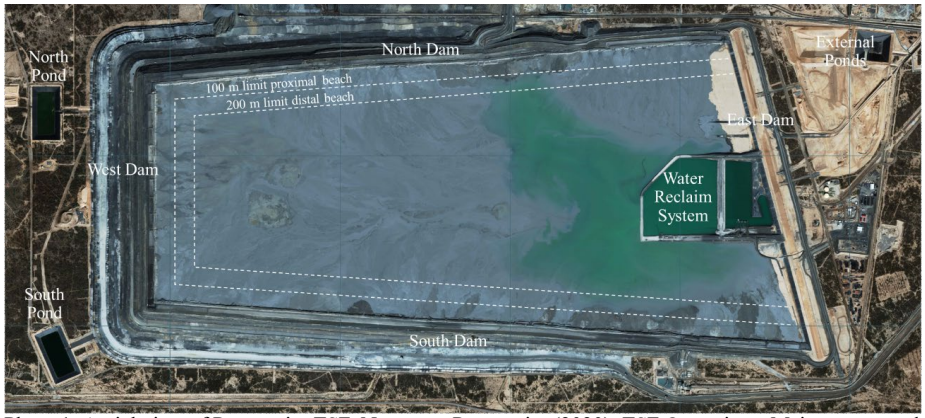

Photo 1. Aerial view of Peñasquito TSF. Newmont Peñasquito (2020). TSF Operations, Maintenance and Surveillance Manual (OMS).

Table 1. TSF Centerline Raise Project Stage Definition

Stage	Maximum Crest Elevation (masl) (WGS 84)	Notes
0	1862.70	Completed
1	1875.70	Under construction
2	1888.70	Under construction
3	1900.70	Future construction stage at feasibility level of design
4	1912.70	Future construction stage conceptual level of design

Golder Associates (2019), Minera Peñasquito Tailings Storage Facility Centerline Raise Project Feasibility Study Report Stage 2 Project Execution Update.

Peñasquito is also upgrading the water reclaim system to include external reclaim ponds that will facilitate removal of water from the TSF to reduce operational risk. These external ponds include sedimentation and polishing cells to improve water clarity (reduced solids) for return water back to the mill. The external pond system also includes an emergency tailings discharge pond to mitigate risks associated with loss of available gravity discharge as the TSF is raised.

2 CONSTRUCTION AND OPERATIONAL ASPECTS

2.1 *Tailings transport, classification and distribution*

Tailings management initiates with flows coming from the Tailings Box, which are discharged into the cyclone feed sumps. The cyclone feed pumps pump whole tailings from the Sulphides plant or Pyrite Leach Plant (PLP) that are pumped to cyclone stations for classification into underflow and underflow tailings. The nominal design for the incoming slurry from the process mill is 110,000 tpd.

The tailings distribution system comprises the cyclone underflow and overflow distribution pipelines. The objective of the underflow distribution pipelines is to transport all underflow from the cyclone stations to the TSF for dam construction. The objective of the cyclone overflow distribution pipelines is to transport overflow when the cyclones are operating or whole tailings when the cyclone towers are bypassed, from the cyclone stations to the TSF for reclaim pond water management.

The objective of the cyclone stations is to separate (i.e. classify) underflow sand from the whole

tailings for use as a dam construction material. The underflow sand is required to have a fines content of less than 25% passing the #200 mesh (75 micron). The remaining fines fraction or overflow is deposited along the perimeter of the dam and used to develop the beach. When underflow sand is not needed for dam construction, the cyclones are bypassed and whole tailings is directly deposited into the impoundment to develop the beach and feed the reclaim pond

Tailings deposition is carefully managed for successful operation of the TSF. Tailings must be deposited so that the beach rises relatively evenly around the facility. Even deposition is required for successful management of the reclaim pond location and its water quality and maintaining a minimum 200 m exposed beach length (north, west and south embankments only), according to the Trigger Action and Response Plan (TARP) standard (Golder 2018). Additionally, continuous construction of the TSF is necessary to maintain the minimum freeboard of two meters as required in the TARP.

To achieve relatively even beaches, deposition points must be rotated frequently according to the tailings deposition plan produced by the MP Technical Services Department (no more than 4-5 days per spigot). Special attention is needed on the eastern portion of the dam to prevent solids from entering the reclaim system. Changes in spigotting may be required based on actual production rates and the beach formation behavior of deposited tailings. As part of a series of good operational practices, the successful management of tailings deposition goes hand in hand with diligent monitoring and execution of a daily deposition plan. Monitoring of the evolution of the beaches is done visually on a daily basis and through topographic surveys twice per week.

A weekly topographical survey of the outer portions of the beach is performed to facilitate deposition planning. The survey is performed by a drone. The drone also provides an opportunity for visual inspection of the beach conditions. The topographical survey aids in verifying minimum beach lengths, which is used as input into overall deposition planning. Operators and planners work together to proactively identify non-uniform beach development so that changes in deposition can be made.

2.2 *Construction aspects*

2.2.1 *General*

The north, west, and south segments of the TSF dam currently provide containment for the deposited tailings. As the impoundment continues to be filled and the tailings deposit continues to rise, the crest of the TSF dam will be raised so that the cycloned underflow sand portion maintains 2 m freeboard above the reclaim pond The north, west, and south segments are considered centerline construction, as shown on Figure 1. The east dam is constructed from rock using downstream construction methods, it is a lined, water retaining structure that supports the reclaim pond as the TSF is raised. The east embankment includes rockfill, filter zone and geosynthetic lining system. The east embankment is designed to allow water to be within or adjacent to the embankment. However, the north, south and west embankments must maintain 200 m of exposed beach length with no standing water.

2.2.2 *Underflow sand*

Underflow sand is used for TSF dam construction, being hydraulically placed in paddocks or stockpiled and placed mechanically on the north, west and south sides. The width of the sand fill zone of the dam vary based on the constructed width of rockfill portion at this section of the dam (crown fill) and its elevation.

Before placement of underflow sand, survey control and grade stakes are set as required by the specifications. Hydraulically placed underflow sand is placed in paddocks that are constructed to be less than 2.5 m deep with a base at least 1 m above the elevation of the reclaim pond. Paddocks are typically 100 m long and vary in width based upon the construction stage. Paddocks are also constructed to promote drainage of water towards the interior of the TSF. Tailings transport piping is operated to deposit underflow sand into the paddock and must be controlled to prevent overtopping of the paddock berms.

As the paddock is filled, water is allowed to drain from the sand into the TSF via drain pipes before being used for subsequent paddock construction or mechanical underflow sand fill

placement, as shown in Photo 2. During filling and hydraulic underflow sand placement, berms are monitored for signs of seepage.

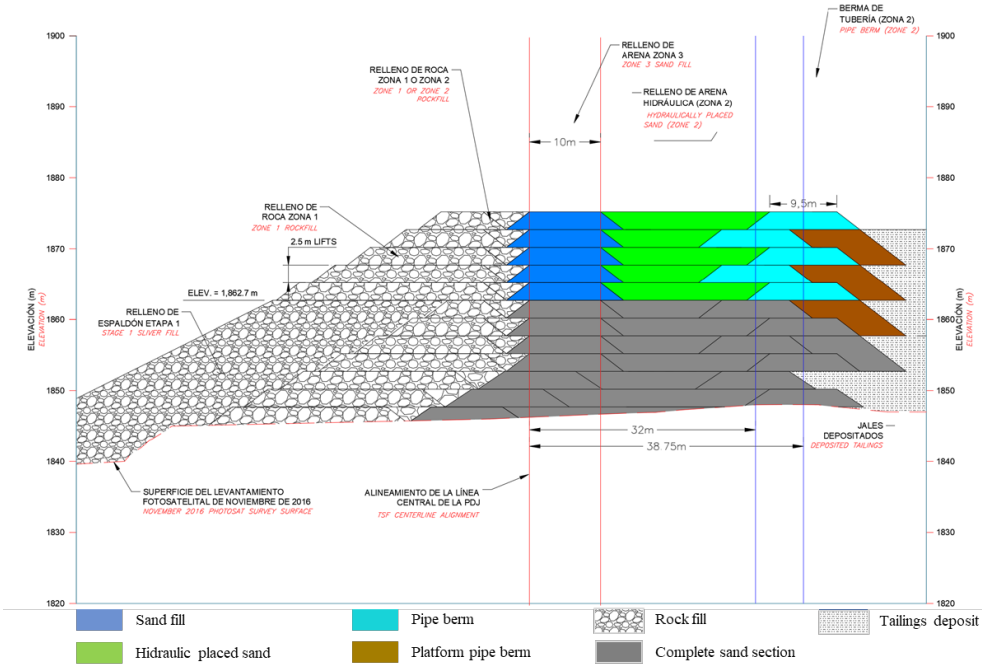

Figure 1. Peñasquito TSF Typical Section. Newmont Peñasquito TSF Technical Services Department (2019).

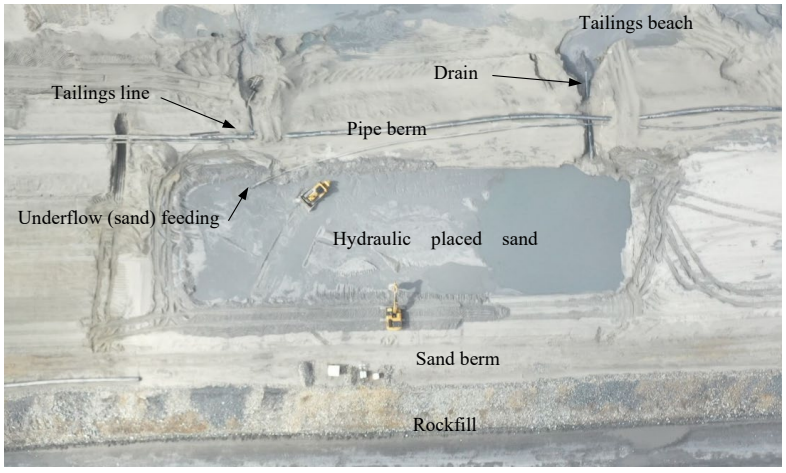

Photo 2. Aerial view of a underflow sand paddock under construction at Newmont Peñasquito TSF. Newmont Peñasquito TSF Technical Services Department (2019).

In accordance with the technical specifications and Construction Quality Control (QC) and Quality Assurance (QA) Plan, the following testing is performed as the underflow sand is placed:

- Lift thickness – measured continuously.
- Elevation of compacted lift – measured continuously.
- Number of passes of compactor – continuous visual inspection.
- Particle size analysis (ASTM D422) – minimum of 1 test per 2,000 cubie meters (m^3) of material placed and minimum of 1 test per 5000 m^3 of material produced at the cyclone stations.
- Water content and compacted density (ASTM D698) tested at a minimum frequency of one test per 10,000 m^3 of mechanically-placed or hydraulically-placed fill.

2.2.3 *Pipe berms*

Pipe berms are included in the design to facilitate the construction of TSF dam raises. The 12 m wide pipe berms are constructed within the TSF impoundment on the tailings beach, upstream of the TSF centerline. The pipe berms are constructed of cycloned underflow sand. The purpose of the pipe berms is to allow for vertical raising of the tailings distribution pipelines to facilitate maintenance and operational access, while keeping the piping outside of the dam construction zone.

Before 2019, pipe berms were formed from borrowing materials from the beach and further filling with whole tailings and tailings slimes into the pipe berms paddocks. This practice did not allow for the natural deposition-induced segregation process to occur, and instead fine tailings particles were trapped against the cyclone sand portion of the dam (Golder 2020). Improvements in construction brought back the natural segregation process to the beach, influencing the grain transition and further depletion of the phreatic surface.

2.2.4 *Rockfill*

The downstream portion of the dam is constructed with rockfill from approved borrow sources, which are typically sized rock and Run-of-Mine (ROM) waste. Rockfill shall conform to have 100% of particles smaller than 24” (600 mm), satisfy International Society of Rock Mechanics (ISRM) hardness of R1 or higher, and be durable so as to not break down during construction.

Rockfill is loaded into trucks and transported to the active filling area of the dam. Trucks end-dump rockfill over or near to the leading edge of the fill in maximum 5 m thick loose lifts for the buttress and 2.5 m thick loose lifts for the sliver and crown fill construction. The dumped rockfill is spread and leveled with tractor-crawler bulldozers. Subsequent haul truck traffic is used to provide compaction. Construction traffic travel parallel to the axis of the TSF dam and is routed so that the wheel paths of the loaded trucks are staggered and distributed evenly across the surface of the lift. The active filling area of the dam progress in a manner to promote haul traffic over recently placed rockfill material.

2.2.5 *Reclaim water management system*

Reclaim water generated from tailings deposition is collected in an internal water reclaim pond that is separated from the tailings by an open graded rockfill berm, as shown in Figure 1.

Water from the internal reclaim pond is pumped by a series of barge pumps back to the mill at a rate of approximately 245,000 m^3 per day. Additionally, in excess of freshwater production from the Peñasquito pit dewatering system, it is directed to the internal cell of the TSF. MP water requirements are currently in the order of 2.61 m^3 of water per processed ton at the plant.

3 GEOTECHNICAL ASPECTS

3.1 *Overview*

Geotechnical characterizations of the ground and foundation area of the TSF started during early design stages. The foundation of the TSF consists of several alluvial and colluvial deposits overlying bedrock at a thickness that varies between 20 and 40 m. Geotechnical investigations and observations are used to guide the construction process. Throughout the process several drilling and CPT campaigns have been conducted with accompanied field testing and instrumentation installation.

3.2 *Geotechnical monitoring*

As with all TSFs, geotechnical instrumentation and monitoring is vital to assessing the behavior and performance of the facility. The Peñasquito TSF monitoring system includes 170 vibrating wire piezometers (VWPs), 3 digital inclinometers and 4 mechanical inclinometers. Sixty seven of the existing VWPs were installed in the tailings during a 2019 CPT program. Data from piezometers and digital inclinometers is obtained through a wireless network that provides real time information to MP staff, Newmont Corporate and the Engineer of Record.

The geotechnical instrumentation installed within the TSF and in the foundation provide information related to responses to construction loading and operation, as well as fluctuations in the phreatic surface within the impoundment.

The analysis of historical monitoring data collected since 2015 has demonstrated that improvements in construction processes and best practices in tailings management and planning, have brought noticeable results in the TSF performance, as discussed later in this paper.

4 2019 CONE PENETRATION TESTS CAMPAIGN

4.1 *General*

A 2019 Cone Penetration Test (CPT) campaign was executed by Conetec Inc.(Conetec) and Golder in partnership with Newmont Peñasquito, with the objectives of investigating tailings geotechnical properties and changes in tailings characteristics over time. This campaign also included the installation of VWPs. The 2019 program performed 22 non-seismic and 38 seismic soundings as well as the installation of 67 VWPs at several locations in the tailings beach.

CPT soundings were located inside the TSF on the tailings beach, with the furthest locations at approximately 250 m from the centerline of the dam. The soundings were located along 12 alignments that were oriented perpendicular to the dam crest. The CPTs were performed at approximately 50 m spacing along the alignments, with generally five soundings at each alignment.

The field program was executed by using an amphibious rig equipped with a hydraulic platform able to push the cone into the ground, as shown on Photo 3. The Conetec used a 15 cm^2 seismic piezocone able to measure tip resistance, sleeve friction, pore pressure, inclination and temperature, by following ASTM D5778 Standard Test Method for Electronic Friction Cone and Piezocone Penetration Testing of Soils.

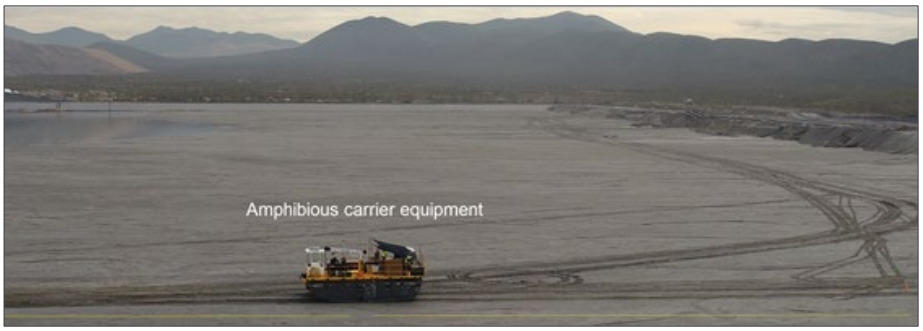

Photo 3. Amphibious rig in the interior of the tailings beach for CPT soundings. Newmont Minera Peñasquito TSF Technical Services Department (2019).

4.2 *Results*

Data analysis was carried out by Golder Associates that evaluated a variety of ways to segregate and summarize the CPT data into zones proximal (<100 m) and distal (>100 m) from the dam centerline.

Figure 2 contains interpreted data of two aligned soundings; CPTs 3+0-16 and 3+0-20 which were carried out at distances of 30 m and 170 m from the center line into the tailings beach, respectively.

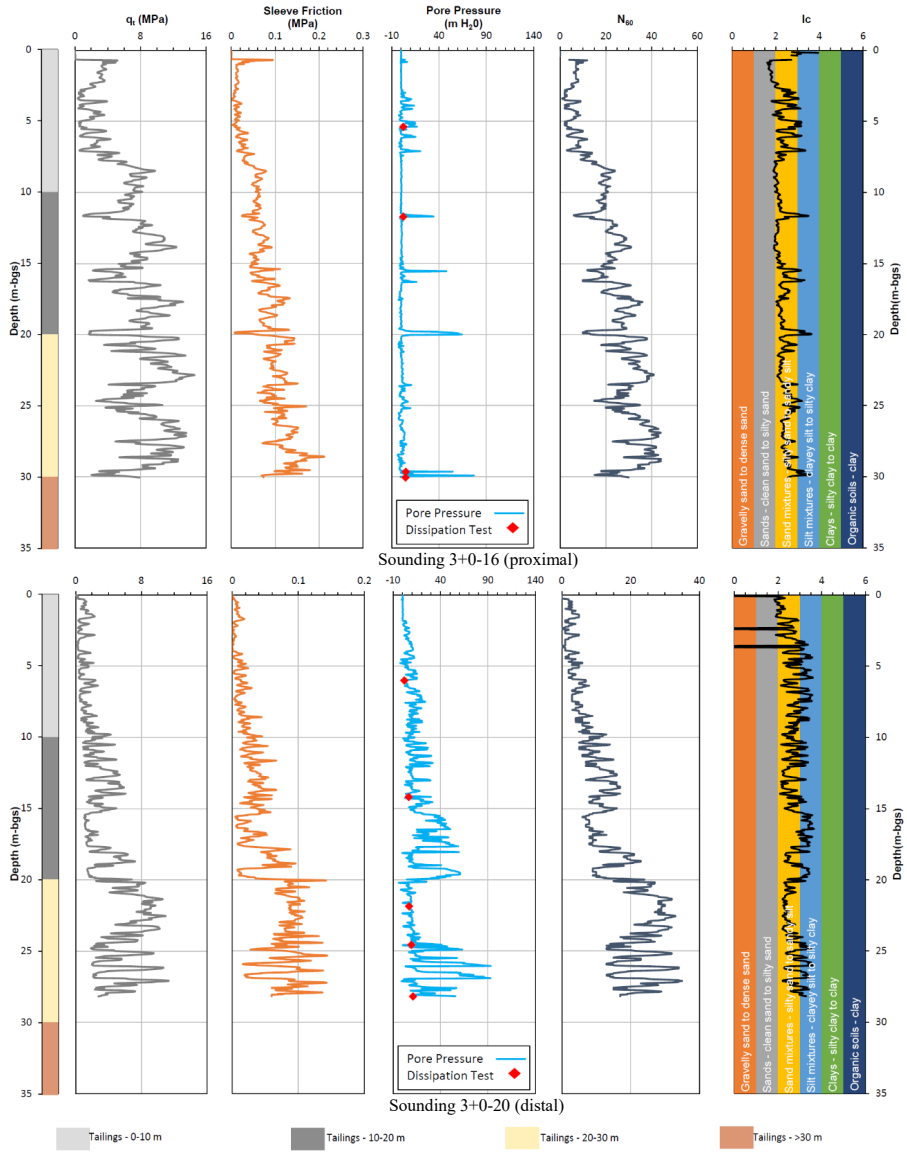

Figure 2. Analyzed CPT parameters for an aligned set of proximal and distal soundings. Golder Associates (2020). 2019 CPT Tailings Geotechnical Factual Report.

Tip resistance and sleeve friction data from the shallower intervals in the proximal sounding represent an interbedded sand to sandy silt sequence in thick lithological intervals. The distal results showed sand and silt mixtures intercalate into thin to very thin patterns as correlated to the Soil Behavior Type index classification (Ic) or soil behavior type by Robertson (2015) in Golder (2020).

Golder (2020) also states that comparison of the 2015 to the 2019 CPT grain index classification, allow for the evaluation of the effectiveness of the ongoing operational tailings management procedures.

As well as for grain index classification and its correlation with position in the impoundment and distance from the tailings spigots, hydrogeological conditions are represented by having lower pore pressures on soundings closer to the dams centerlines, as seen in Figure 2.

Figure 3 presents three different normalized and non-normalized Soil Behavior Type (SBT) classification charts for CPT soundings 3+0-16 and 3+0-20, proximal and distal, respectively. Qtn is the normalized tip resistance using a variable stress ratio exponent based on the Soil Behavior Type Index (Ic) and friction ratio is the percentage difference between the sleeve friction and the tip resistance.

The correlation of natural segregation in distance into the impoundment is clearly observed, especially in the Qtn and non-normalized SBT charts, where intervals from surface up to 15 m trend to be clustered and closer to sand and sand mixtures bands. The Modified SBTn chart indicates that proximal materials from surface up to depths of 22.5 m trend to be closer to a coarser and more dilative classification, meanwhile distal soundings suggest that the tailings are remarkable clayey with clear contractive properties, that as mentioned by Mayne (2019) are materials with tendencies to flow by liquefaction.

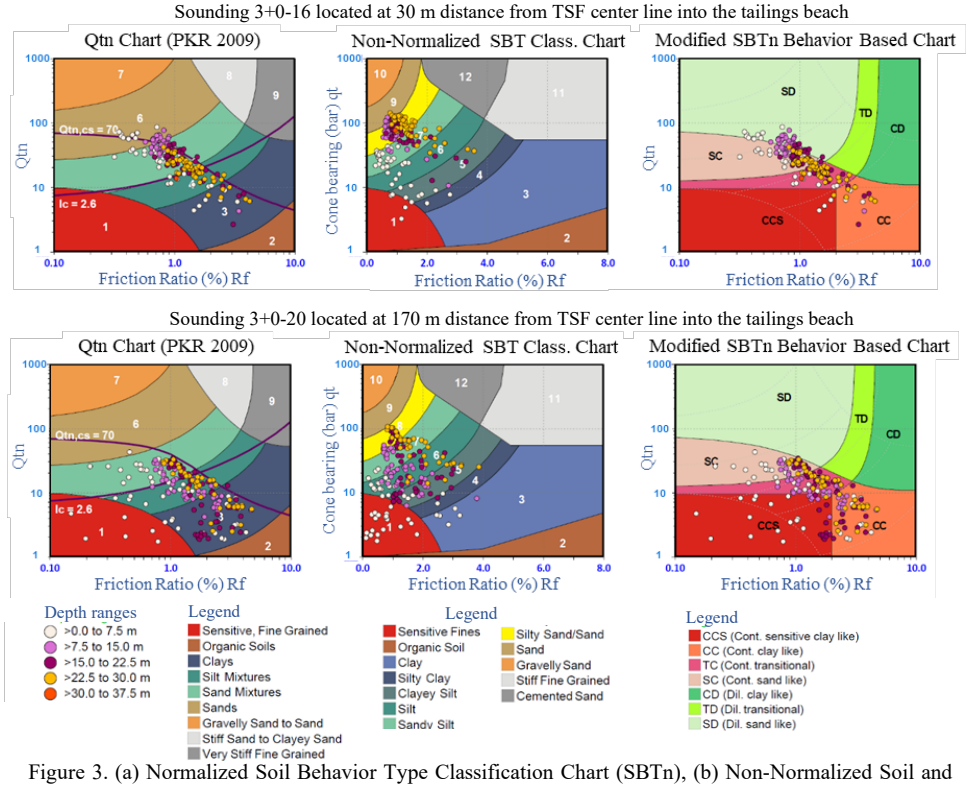

Figure 3. (a) Normalized Soil Behavior Type Classification Chart (SBTn), (b) Non-Normalized Soil and (c) Modified SBTn Behavior Based Chart for Proximal (3+0-16) and distal (3+0-20) tests. Conetec (2019). Presentation of CPT site investigation results for Minera Peñasquito.

There were 43 CPT distal data points in 2019 and 17 in 2015, the distal soundings in 2019 were further into the impoundment due to the robustness and versatility of the amphibious rig used. It was observed that the 2019 results have an overall improvement in density and strength with respect to the 2015 assessment.

According to Golder (2020), measured densities in 2019 were within an average of 17 to 21.5 kN/m^3 increasing progressively in the tailings column. Meanwhile, the 2015 tests were erratically between 16.5 and 19.5 kN/m^3. The trend of decreasing density with distance into the impoundment was observed in 2019 tests, as shown on Figure 4.

As determined by Golder (2020), the phreatic surface determined in the 2019 CPT campaign is deeper downstream of the dam as compared to the surface obtained in 2015. The distance at which the tailings are fully saturated is also further from the dam crest, as detailed in Figure 5.

In 2015, tailings were fully saturated to the surface approximately 100 m upstream from the center line of the dam, while in 2019 they do not reach saturation until more than 250 m into the impoundment, with minor exceptions in the northwest corner of the dam.

In 2015, the phreatic surface was located within the cyclone sand at an elevation above the starter dam. In 2019, the same VWPs that previously showed water within the dam centerline are now dry. The phreatic surface presently exits below the starter dam within the foundation soils.

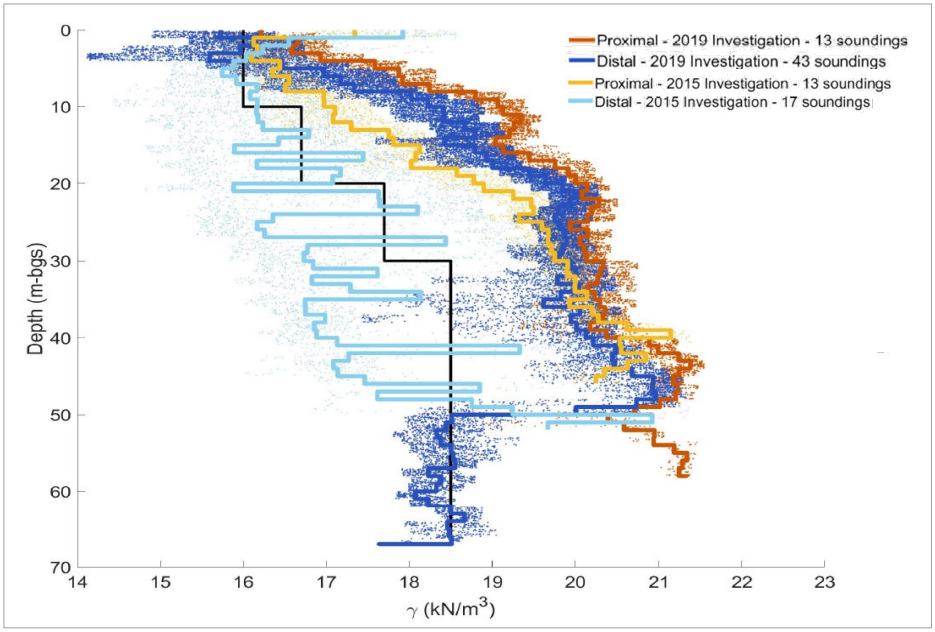

Figure 4. Comparison of 2015 to 2019 results in density profiles with respect to depth below tailings surface. Golder Associates (2020). 2019 CPT Tailings Geotechnical Factual Report.

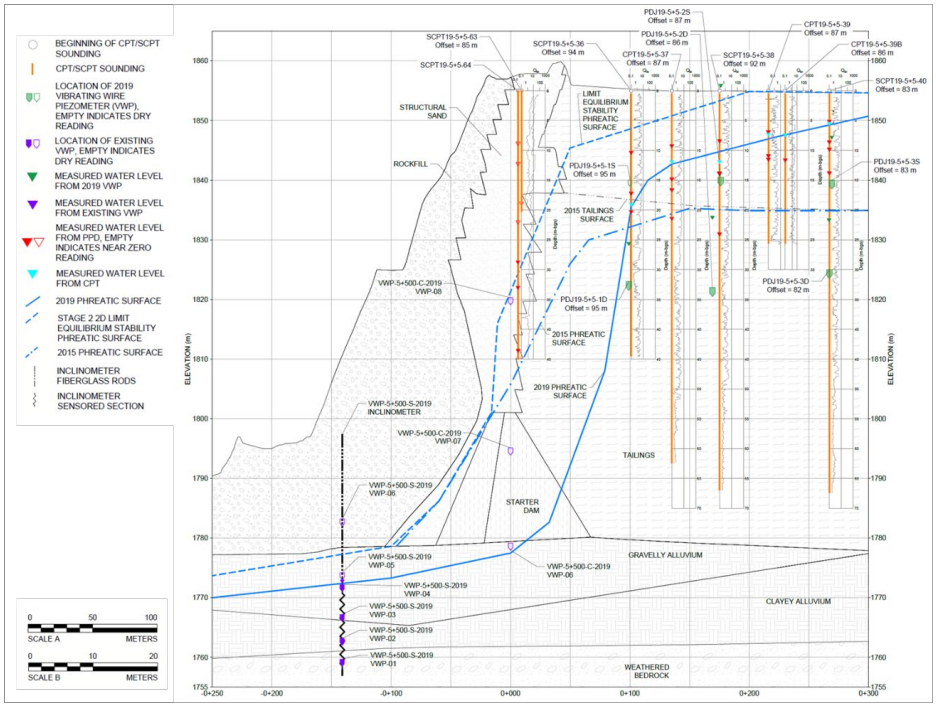

Figure 5. Results of 2019 CPT campaign, detail of geotechnical instrumentation and comparison of phreatic surfaces obtained in 2015 and 2019. Golder Associates (2020). 2019 CPT Tailings Geotechnical Factual Report.

5 CONCLUSIONS

The CPTs geotechnical campaigns carried out in the Peñasquito TSF in 2015 and 2019 have provided valuable information on characteristics of the tailings over time. Both campaigns resulted in significant additional data that has been incorporated in several stability models and will served as tools for optimization of design, management and performance of this TSF.

The correlation of results from the 2019 CPT geotechnical campaign with the optimization of procedures and the continuous improvement on operational processes is noticeable. Tailings CPT data indicates a coarse to fine segregation that somewhat uniformly results in a lower phreatic surface downstream the dams; measured densities in 2019 were within an average of 17 to 21.5 kN/m^3 increasing progressively in the tailings column, meanwhile in the 2015 tests were erratically between 16.5 and 19.5 kN/m^3.

After four years from the 2015 CPT campaign, geotechnical and hydrogeological characteristics of the tailings are in accordance to design and performance expectations.

Tailings management processes improve constantly and have incorporated better practices that are in support of a more efficient and well managed facility (e.g. the use of underflow for the construction of berm paddocks and a planned pouring program analyzed and produced by Technical Services Department), which incorporates state-of-the-art survey data acquisition together with tailings plan optimization and analysis.

Beach management as a daily team integrated activity that provides a link to planners, surveyors and operators together with Quality Assurance Site Engineer. The latter being a crucial aspect in the management and performance of the TSF, as stated in reference procedures like the TARP. TARP indicates that exposed beaches between the upstream boundary of the dam ridge and the water level at the reclaim pond must be larger than 200 m.

Good operational practices are also reflected in the performance of the reclaim water system, which takes advantage of having a more segregated and less permeable bottom level, as well as an efficient concentration of water in the center of the impoundment against the filter dyke thanks to the beach management plan.

Operational and construction areas have optimized practices that are framed by an accurate, dedicated and reliable process of QC and QA. MP staff are committed to follow processes attached to a very well-structured workflow, which follows high level technical directrices and promotes the intertwined work among all technical areas.

6 REFERENCES

Conetec Inc. 2017. Calculated CPT Geotechnical Parameters. Revision SZW- Rev 12.
Conetec Inc. 2019. Presentation of site investigation results, 2019 CPT geotechnical campaign.
Golder Associates. 2018. Trigger Action Response Plan.
Golder Associates. 2019. Geotechnical Analysis Report, Center Line Raise Project Stage 2 Update.
Golder Associates. 2020. 2019 CPT Tailings Geotechnical Factual Report.
Mayne, P.W. et al. 2017. Identifying contractive soils by CPT material index for flow liquefaction concerns. Geo Ottawa 2017.
Newmont Peñasquito. 2020. TSF Operations, Maintenance and Surveillance Manual (OMS). Document MP-MN-PJ-OM-01.

Tailings Dewatering – Analysis of Cases to Understand Trends in Capex and Opex

Mark Wallgren
MetsoOutotec, Burlington, Ontario, Canada

Jason Palmer
MetsoOutotec, Brisbane, Queensland, Australia

Elio Tomini
MetsoOutotec, Sudbury, Ontario, Canada

ABSTRACT: This paper will look at case studies of thickening and filtering plants and providing some comparisons of examples of capital and operating costs for processing tailings at different sites. The design parameters for the case studies will be based on years of dewatering tests performed at Outotec covering a wide variety of ores. The plant cost estimates will be analyzed to illustrate the amount of these step changes in cost for three different plant throughputs. Based on this analysis, the author will provide examples which will allow the reader to develop an understanding of plant costs and allow these examples to provide a baseline cost which can be applied to other specific sites. The data provided and an understanding how it relates to a specific project can be useful to a mine owner when initially exploring the possibility of modifying an existing tailings system or developing a new project.

1 INTRODUCTION

Recent trends in tailings storage facilities are moving towards more dewatering prior to storage to reduce risk in tailings storage facilities. There are several options for dewatering and most of the technology being used has been around and in use in the mining industry for a long time. Although the technologies are mature, the application for tailings has so far been limited to a small portion of the mine sites around the world, particularly where water costs and geotechnical reasons have driven the justification. The tailings applications are much higher throughput than for example concentrate filtering and hence the capital and operating costs of the dewatering plants can have a significant effect in the economics of a mine site. In many cases, the investment in dewatering is offset by reduced cost in the tailings deposition due to higher placed density, a more geotechnically stable, or a hydrogeologically preferred material. Ultimately the dewatering technology selected has an impact on the complete system. This paper will look at several case studies of thickening and filtering plants and providing some comparisons of examples of capital and operating costs for processing tailings at different sites. The case studies reviewed will include sites covering a wide variety of climates – hot to cold and wet to dry.

Dewatering plants for tailings from hard rock mines are typically using thickening or filtration technologies. The trend in the industry is to consider dewatering of tailings to reduce the risk of tailings impoundment failures as well as reduce the impact of such failures. Thickeners and filters have been used in the industry for a long time, but the application for tailings dewatering has been limited. The majority of ore processed turns into tailings and as such any additional processing of this large material stream adds significant cost to the overall system. This paper looks at three cases where the cost of the dewatering system has been estimated using different technologies.

The intent is to provide the reader with a reference frame for the cost of dewatering systems which can be expected for different tailings throughput rates and characteristics.

2 TYPES OF DEWATERING PLANTS

2.1 *Thickening plants*

Tailings thickeners are typically classified into 4 groups:

- Conventional thickeners- An old industry standard which is not included in the analysis in this paper.
- High rate thickeners (HRT) – These thickeners are a relatively inexpensive way for dewatering the material to a low-density slurry (LDS). The underflow is still very much like a liquid and can be pumped using regular slurry pumps. Unsheared yield strength in the range 20-80Pa, and the largest installed thickeners of this style are ~120 m diameter.
- High compression thickeners – These thickeners generate a slightly higher compression by increasing the height of the thickener wall which results in an increased bed depth. The thickened slurry is a more viscous high-density slurry (HDS). Due to the increased viscosity, the angle of the bottom cone is typically a bit steeper to promote material flow into the underflow and the raking mechanism is more robust to handle the higher torques required to move through the thickened material. Typically, the underflow is still a segregating slurry and can be pumped using heavy duty slurry pumps. Unsheared yield strength in the range 80 – 150 Pa and the upper limit of size is 65m diameter.
- Paste thickeners – These thickeners have a much deeper design with a bottom cone at 45 degrees to the horizontal. The raking mechanism is very robust with high drive torques and pickets may be required to provide effective thickening. The underflow material is much more viscous. If there is enough fines (> 15% less than 20µm) the material can sometimes exhibit a paste like quality as a non-segregating slurry. The underflow material mostly requires positive displacement pumps for transportation. Currently paste thickeners are offered up to ~45 m diameter with 150 – 300 Pa of unsheared yield strength.

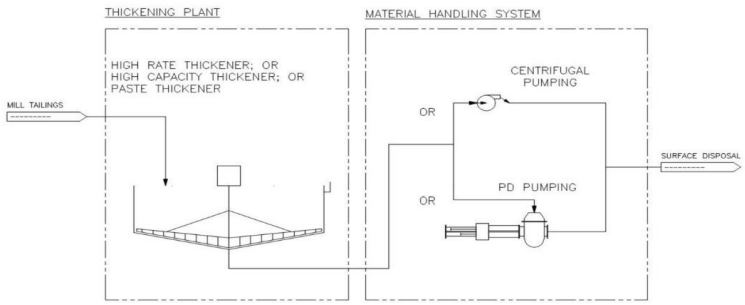

Figure 1. Process Flow Diagram - Thickening Plant

The process flow diagrams for the 3 types of thickening plants are generally the same, a simplified process flow diagram is depicted in Figure 1. As the solids content increases, the rake torque and pumping duty increases driving up the cost of the plant. Another large increase in cost occurs where the centrifugal pumps are replaced by positive displacement pumps. It is important to remember that the higher operating pressures do not only affect the cost of the pumps but also all the downstream piping system specifications which is typically a significant part of the system cost depending of the length of piping.

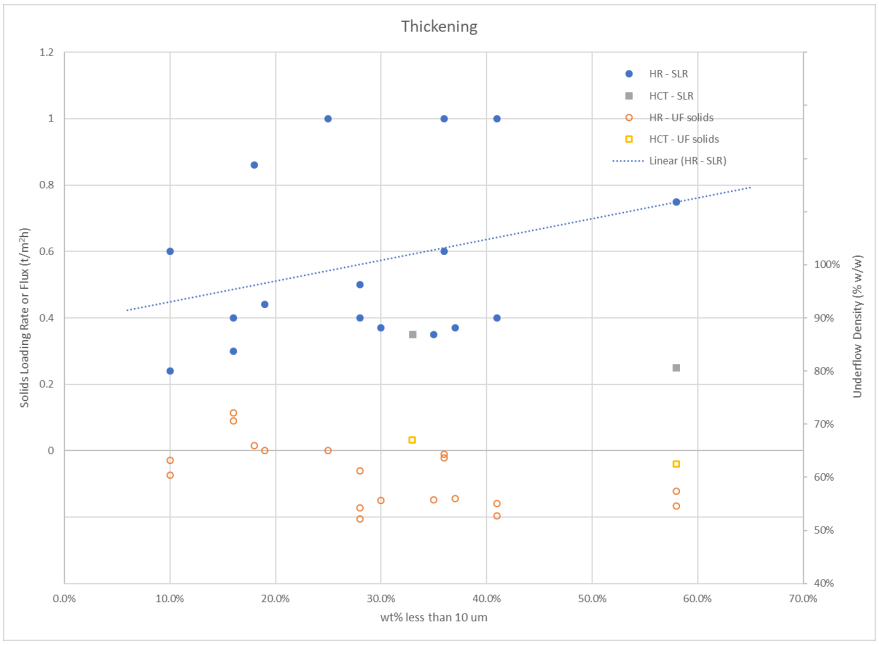

Figure 2. Thickening test results

The graph in figure 2 illustrates a wide variety of results based on the tailings test work which has been done at Outotec over the years. It is well known that smaller particles tend to settle at a slower rate within a thickener. As such we expect that tailings samples with more fines would result in selecting a lower Solid Load Rating (SLR or flux). However, it is interesting to note that the SLR selected for design seems to stay between 0.25 t/m^{2}h and 1.00 t/m^{2}h for most of the tests performed, and there is not a strong correlation between the solids load rating and the amount of fines in the samples we tested. This does not mean that there is no correlation between particle size and settling rate, but rather that the selection of SLR is more multidimensional.

- Use of flocculant agents allows particles to bond together and generate agglomerated particles, effectively producing a modified particle size during the thickening process.
- Mineralogy has arguably a greater effect on the underflow densities and unlike particle size, can not be temporarily modified.

There is another effect which needs to be considered. The SLR selected for plant designs, determines the size of the thickener and hence greatly affects the cost of the thickening plant. The optimal system will not thicken the material beyond the needs of the application, in this case the tailings deposition.

- When it comes to thickened tailings slurry, as long as the material is saturated and acting as a slurry, the geotechnical design of the tailings facility is similar. Hence there is no specific design parameter that provides a specific threshold which must be met. The selection of the SLR becomes a continuum and may be adjusted based on budget and other non-technical factors (ie. social license to operate).
- If the rheological (flow) properties of the thickened tailings exceed the ability to pump using centrifugal pumps, positive displacement pumps must be used. This becomes a significant increase in capex and opex and hence provides a significant step in the cost curve and a technical threshold in the plant design. The paste like properties of this type of tailings can sometimes be used to generate beach angles and provide properties which can significantly alter the design of the tailings deposit. In this case there would

be some geotechnical parameters which sets the required underflow density and hence the SLR must be selected to provide the required material properties.

We conclude that the SLR selected by the plant designers is based on the needs of the application. The applications in tailings often does not push the envelope for thickening technology but rather is determined by other factors. Outotec's testing program seem to indicate that plant designers tend to stay within the same band of SLRs for a wide variety of applications. For the exercise of pricing plants in this case, SLR's of 0.25 t/m^{2}h and 0.9 t/m^{2}h were selected.

It is also important to note that the unsheared yield strength at the bottom of the thickeners, used in the design of the thickener includes the effects of the flocculant. Significant agitation in the subsequent pumping and pipelines produces a material with a sheared yield strength. Shearing of the material (typically by mixing it at high energy) breaks up the flocculant. The sheared yield strength can be much lower than the unsheared and allows for easier pumping of the material.

Often, thickener designs are specified for a target solids density in the underflow. In terms of pumping and geotechnical design the sheared rheology (viscosity, yield strength, settling characteristics) is a better indication of the performance of the material. However rheology requires special equipment for measuring in the field and so solids density is more practical to work with for operations.

2.2 *Filtration plants*

There are typically three types of filters being used in tailings filtration

- Vacuum filters (disk and belt filters) – These filters are commonly used in tailings based mine backfill plants. The filter cake is higher moisture and as such is not as cohesive as the pressure filter cake. This makes re-pulping the cake easy for the mixing plant. However, for tailings disposal on surface, based on our testing, it appears the vacuum filter cakes typically do not approach the optimum moisture content as determined by Proctor testing. In order to reach the moistures stipulated by the geotechnical testing typically these filter cakes are exposed to desiccation by ambient evaporation. It is a technique which works well in dry climates and lower production but can become very limiting in wet and cold climates. In some installations, sheds are used to protect the filter cake from rain and snow to allow it to dry up enough before placement. Currently vacuum filters are offered with up to 250 – 300 m^2 filtration area.
- Ceramic filters – These filters have been used successfully in some installations. It is a filter design using capillary forces to pull the water out of the tailing's slurry. The capillary tubes have a distinct size and in many cases the tailings material contains too many fines to achieve the required moisture and availability. Depending on the water chemistry there can also be a risk of blinding (precipitation, pegging or modification of the surface properties) and derogation by chemical attack (fluoride corrosion). In those operations where the tailings are compatible with this filter, it is a good solution. But pilot testing on site is usually recommended to ensure compatibility. Ceramic filters are currently available up to 250 – 300 m^2 filtration area.
- Pressure filters – Vertical plate pressure filters have become the default in tailings filtration plants which the other options are evaluated against. The pressure filters are less sensitive to variability in the tailings, ambient temperatures and pressures, and provide a reliable means for filtration. Very large pressure filters have been developed specifically for tailings applications with unit areas up to ~ 2000 m^2.

The simplified process flow diagram for a filtration plant, shown in Figure 3, is similar for all three technologies. Some minor variations exist, but these are within the filter package itself. All filtration technologies typically benefit from thickening the slurry to higher density prior to filtration and high compression or high rate thickeners are suitable for the application. In some cases, particularly with lower throughput, it may make sense to eliminate the thickener and feed the tailings slurry direct to the filter. Typically, this is justified more by simplification of the flow sheet rather than on a cost basis.

All the filter units require a continuous maintenance program (replacement of filter cloths for pressure and vacuum filters and backflushing/acid washing of ceramic filters). Filter availability for tailings can be in the 50 to 90% range depending on the technology and the material being filtered, and at the lower end this availability is significantly lower than typical minerals

processing equipment. The plant design must provide redundancy and/or surge tanks to allow for filter maintenance on a regular basis.

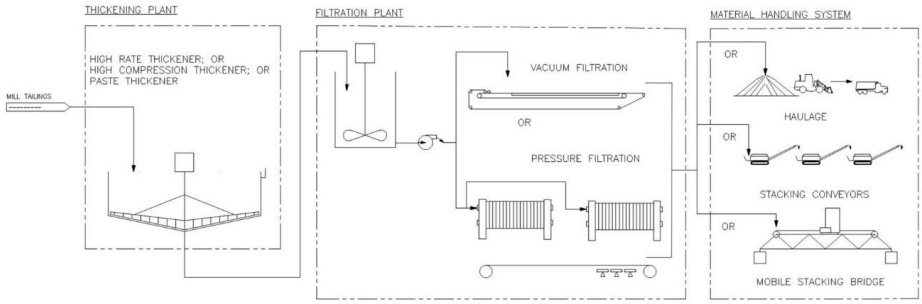

Figure 3. Process Flow Diagram - Filtration Plant

Filters are sized based on the filtration rates determined by testing. Figure 4 illustrates an excerpt of tailings filtration test work completed at Outotec over the years. Just as with thickeners, it tends to be more difficult to dewater tailings with a higher portion of fines. In the graph, there is a stronger relation between the filtration rate and portion of particles less than 10 µm than for thickener testing. Typically, pressure filtration rates for tailings falls into the range of 50 – 350 k/m^{2}h.

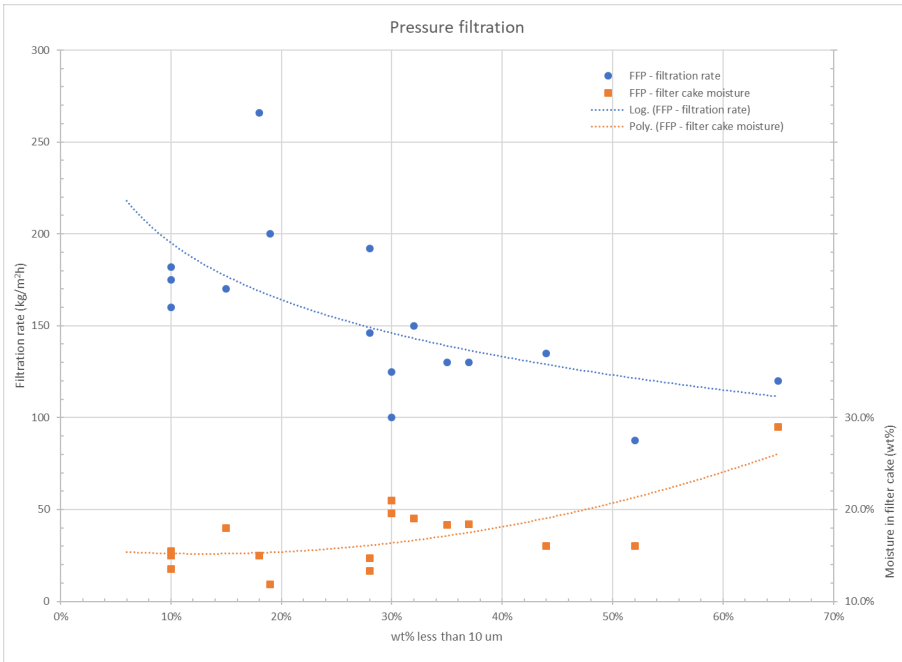

Figure 4. Pressure filtration test results

It is important to note that several other factors affect the filtration rate and in this case we have selected only to look at the amount of fines (in this case defined as <10µm) in the tailings sample.

Dewatering of tailings is also strongly dependent on mineral constituents, water chemistry, and particle shapes among other things. In the interest of simplification, we have selected only to look at the amount of fines in order to present the test results. Investigating the relationship between tailings characteristics and filtration rates is outside the scope of this paper.

Filtered tailings are typically used for producing mine backfill (for use underground) or deposited for storage in a dry-stack facility. The applications are very different.

- Filtered tailings for use in backfill are normally mixed with tailings slurry and binder to produce a paste or non-segregating slurry which will be transported to the backfill locations in a piping system. Ideally the filter cake should have a higher moisture content and vacuum filtration is typically selected.
- Filtered tailings produced for dry stack deposition needs to have geotechnical properties which meet the requirements for stacking. Typically proctor compaction tests give a good indication of the moisture required for stacking. Once the stacking parameters and site conditions are defined, geotechnical testing is required to define the *in situ* density required to maintain a stable tailings deposit. Stability is typically characterized by the material remaining in a dilative state when placed under the worst case stress condition (during and after life of mine) for each specific application. Testing of tailings at Outotec show that in some cases it is difficult to reach this moisture content through filtration alone. In order to minimize the cost of the filtration capex and opex, testing of target moistures is usually cut off at the upper end of the acceptable moisture range (and with limited blowing time) as opposed to the absolute limit of the technology. Pressure filtration provides lower cake moistures than vacuum filtration and is typically favored. Sometimes vacuum or ceramic filtration can also be used if the tailings are suitable, but usually further desiccation (drying) of the filter cake is required to meet specifications.

2.3 *Dewatering performance*

The test work, which has been done on tailings over the years at Outotec, illustrates that the tailings dewatering is a complex process which can be difficult to theoretically predict with any accuracy. One of the first steps to take when considering tailings dewatering should always be to test the dewatering properties. It is a good idea to provide several tailings samples to reflect the range of mineralogy expected from day to day and over the life of mine. Composite samples can understate the range in filtration rates. Nothing is as important as understanding the filtration and settling rates of the material in sizing the equipment in order to understand the cost of the overall system.

However, sometimes tailings samples are not available and estimated tailings dewatering rates must be used to provide some ideas of cost. The graphs in the previous sections show a cross section of test results for a group of varying mining applications. With some additional information on the mineralogy and the PSD of the tailings, this range in dewatering rates can usually be narrowed down.

It should be noted that, due to availability, the test results in figure 2 and figure 4 contain more data points from precious metal mines than other types of ore.

3 CAPITAL COST ESTIMATES

For the purpose of generating capital cost estimates of dewatering plants we used the design criteria in Table 1 for three different throughput rates. In order to provide a range of costs for thickening and filtration plants a high and a low value for solids load ratings and pressure filtration rates were selected. Each was evaluated for a case representing difficult to dewater tailings (high cost) and easier to dewater tailings (low cost). All costs are provided in USD.

Table 1. Design Criteria

Parameter	Unit	Values	
Tailings throughput	kt/d	3 cases - 2.5 kt/d, 25 kt/d and 100 kt/d	
Dewatering properties		Difficult	Easier
Ore type examples		Clay, gold tails	Sulphide ore tailings
Thickening rates	t/m^2h	0.35	0.9
Filtration rates	kg/m^2h	100	180
Solids S.G.		2.4 to 2.6	2.6 to 3.0

Each case was evaluated for providing 4 different tailings products:

- Low density tailings slurry (LDT) using high rate thickening and centrifugal pumps (CP)
- High density tailings slurry (HDT) using high compression thickening and centrifugal pumps (CP)
- Paste like tailings (PT) using paste thickening and positive displacement pumps (PD)
- Filtered tailings (FT) for dry stacking using pressure filtration

The scope of the cost estimates includes the following items:

- Process equipment (filters, thickeners, tanks, pumps, compressors, and flocculant dosing system).
- Electrical, instrumentation and automation equipment (MCC's, Control system hardware and software, field instruments, and control valves).
- Piping internal to the plant is included in the plant pricing.
- Pipelines from the dewatering plant to the tailings facility are included in the material handling system cost (slurry and paste).
- Conveyors from the dewatering plant to the tailings facility are included in the material handling system cost (filter cake).
- Cost of trucks, dozers, and loaders are included as leased equipment in the opex.
- Structural steel, platforms, buildings, etc.
- Engineering, project management, procurement, expediting and shipping costs.
- Installation costs are factored and will vary from site to site. This cost includes construction management, earthworks, concrete, structural erection, mechanical and electrical installation.

The following is a list of some of the excluded items:

- Civil infrastructure to the plant (roads, grading, excavation of rock)
- Services to the plant site (electrical, internet, potable water, process water, seal water)
- Any water treatment of the thickener overflow.
- Costs associated with tailings facility construction and management – dams, dam lifts, liners, drains, closure, etc.

Assumptions:

- The tailings dewatering plant is located next to the concentrator plant.
- The distance from the concentrator to the tailings facility for the 2.5 kt/d plant is 1km.
- The distance from the concentrator to the tailings facility for the 25 and 100 kt/d plants is 5km.
- The cost of the piping systems and the conveyor system for transporting the tailings will not be affected by the variability in the dewatering properties.

3.1 *Plant cost estimates (All costs in USD)*

Some observations from cost Table 2 for the 2.5kt/d case:

- The high cost (difficult to dewater material) is only 10 – 20% higher than the low cost (easier to dewater material).
- The capex for the filtration plant (PFT) is lower than for the paste plant (PT) because lease cost of the trucks, and other mobile equipment is allocated to the opex.
- The capex cost per throughput varies from $ 2 – 7 million USD / (kt/d).
- The overall cost of the filtration option is difficult to compare to the other options since a significant part of the equipment is leased and reports to the opex.

Table 2. Cost estimates for 2.5kt/d case (in USD)

Description	LDT		HDT		PT		FT	
Cost estimate	Low	High	Low	High	Low	High	Low	High
Design								
Thickener	12m HRT	20m HRT	12m HCT	20m HCT	12m PT	20m PT	12m HRT	20m HRT
Filter							2 x FFP2512	3 x FFP2512
Material handling	CP	CP	CP	CP	PD	PD	trucked	trucked
Capex cost (M$)								
Thickener plant (EPS)	2.0	2.4	2.9	3.4	3.2	4.0	2.0	2.4
Filter plant (EPS)	0.0	0.0	0.0	0.0	0.0	0.0	4.1	5.6
Material handling (EPS)	1.4	1.4	1.8	1.8	9.3	9.3	0.7	0.7
Subtotal EPS (Engineer, Procure, Supply)	3.4	3.7	4.7	5.2	12.4	13.2	6.9	8.7
Construction	1.7	1.9	2.4	2.7	4.4	5.0	4.9	5.5
Total Capex (M$)	5.1	5.6	7.1	7.9	16.9	18.2	11.8	14.2
Capex M$/(kt/d)	2.0	2.3	2.8	3.2	6.7	7.3	4.7	5.7
Opex cost ($/t)								
Dewatering plant opex	0.13	0.14	0.15	0.17	0.16	0.19	2.22	3.23
Material handling opex	0.08	0.08	0.08	0.08	0.40	0.40	4.13	4.13
Total opex ($/t)	0.20	0.21	0.23	0.25	0.56	0.59	6.35	7.36

The estimated capital costs can be compared with those estimated by Carniero (2019). The graph illustrates overall cost of a tailings system (at the time of writing 1 AUD = 0.7 USD) including the dewatering plants and the tailings facility. The costs in Table 2 are only for the dewatering portion.

- Option A High rate thickener, centrifugal pumps, upstream dam construction.
- Option B High rate thickener, centrifugal pumps, downstream dam construction.
- Option C High compression thickener, PD pumps, central point slope deposition.
- Option D Pressure filter, trucked tailings, placed by dozer.

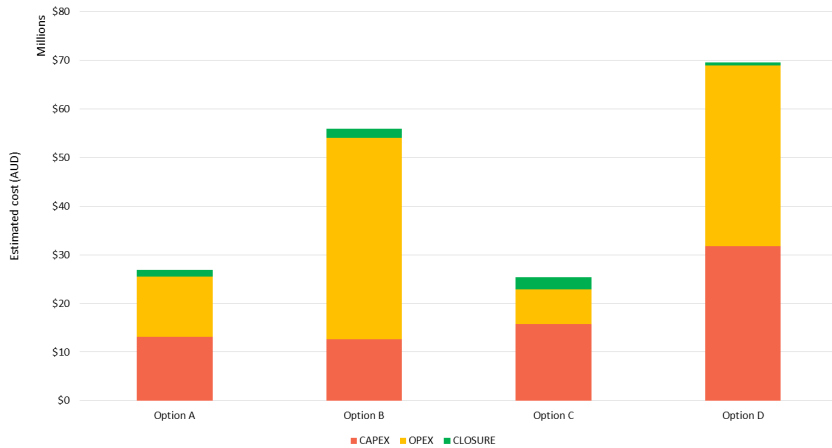

Figure 5. Overall tailings facility cost estimate for a 5.5 kt/d gold operation in Australia

Table 3. Cost Estimates for 25kt/d case (in USD)

Description	LDT		HDT		PT		FT	
Cost estimate	Low	High	Low	High	Low	High	Low	High
Design								
Thickener	38m HRT	2 x 43m HRT	38m HCT	2 x 43m HCT	38m PT	2 x 43m HRT	38m HRT	2 x 43m HRT
Filter							5 x FFP3512 stacker	8 x FFP3512 stacker
Material handling	CP	CP	CP	CP	PD	PD		
Capex cost (M$)								
Thickener plant (EPS)	4.3	8.5	6.3	12.5	8.3	17.7	4.3	8.5
Filter plant (EPS)	0.0	0.0	0.0	0.0	0.0	0.0	32.8	46.4
Material handling (EPS)	4.9	4.9	5.2	5.2	30.9	30.9	24.5	24.5
Subtotal EPS (Engineer, Procure, Supply)	9.1	13.3	11.5	17.7	39.2	48.6	61.6	79.3
Construction	4.1	6.9	5.5	9.6	13.3	19.5	33.1	48.0
Total Capex (M$)	13.2	20.2	16.9	27.3	52.5	68.2	94.6	127.3
Capex M$/(kt/d)	0.5	0.8	0.7	1.1	2.1	2.7	3.8	5.1
Opex cost ($/t)								
Dewatering plant opex	0.07	0.09	0.08	0.10	0.09	0.12	0.77	1.00
Material handling opex	0.05	0.05	0.05	0.05	0.26	0.26	0.75	0.76
Total opex ($/t)	0.12	0.14	0.13	0.15	0.35	0.38	1.52	1.76

Some observations from cost table 3 for the 25 kt/d case:

- The high cost (difficult to dewater material) is 30 - 60% higher than the low cost (easier to dewater material).
- The trucking system for the tailings in the 2.5 kt/d system has now been replaced by a conveying system.
- The capex cost per throughput varies from $ 0.5 - 5 million USD / (kt/d).

Table 4. Cost Estimates for 100kt/d case (in USD)

Description	LDT		HDT		PT		FT	
Cost estimate	Low	High	Low	High	Low	High	Low	High
Design								
Thickener	2 x 54m HRT	5 x 55m HRT	2 x 54m HCT	5 x 55m HCT			2 x 54m HRT	5 x 55m HRT
Filter							18 x FFP3512 track mount	30 x FFP3512 track mount
Material handling	CP	CP	CP	CP	PD	PD		
Capex cost (M$)								
Thickener plant (EPS)	8.2	18.7	12.0	27.7	16.3	38.4	8.2	18.7
Filter plant (EPS)	0.0	0.0	0.0	0.0	0.0	0.0	50.7	123.3
Material handling (EPS)	11.5	11.5	11.8	11.8	64.6	64.6	59.2	59.2
Subtotal EPS (Engineer, Procure, Supply)	19.7	30.2	23.8	39.6	80.9	103.0	118.1	201.3
Construction	8.3	15.3	10.9	21.5	27.0	41.7	60.4	135.1
Total Capex (M$)	28.1	45.6	34.8	61.0	107.9	144.7	178.4	336.4
Capex M$/(kt/d)	0.3	0.5	0.3	0.6	1.1	1.4	1.8	3.4
Opex cost ($/t)								
Dewatering plant opex	0.07	0.08	0.07	0.08	0.07	0.09	0.61	1.23
Material handling opex	0.05	0.05	0.05	0.05	0.24	0.24	0.61	0.65
Total opex ($/t)	0.11	0.12	0.12	0.13	0.31	0.33	1.22	1.88

Some observations from this cost Table 4 for the 100 kt/d case:

- The high cost (difficult to dewater material) is 30 - 90% higher than the low cost (easier to dewater material) for any option.
- The capex cost per throughput varies from $ 0.3 – 3.5 million USD / (kt/d).

3.2 *Comparing the cost of dewatering technologies and cost per throughput*

The average capital cost for each technology option, can be compared to the other average costs. In table 5 the average between the high and the low cost for each option is divided by the cost of the LDT (low density tailings option). This allows us to anticipate that for example a paste plant would cost ~3.5 times that of a low density tailings plant. A filtered tailings plant (PFT) will be about 2 x the cost of a paste plant.

Table 5. Comparison of Capex for technology options

Throughput	LDT	HDT	PT	FT
2.5 kt/d	1	1.4	3.3	2.4
25 kt/d	1	1.3	3.6	6.6
100 kt/d	1	1.3	3.4	7.0

A similar table can be made averaging the high and the low opex costs for each option and comparing them to the low density case.

Table 6. Comparison of Opex for technology options

Throughput	LDT	HDT	PT	FT
2.5 kt/d	1	1.1	2.8	32.8
25 kt/d	1	1.1	2.8	12.5
100 kt/d	1	1.0	2.7	13.3

There is a large reduction in the cost per ton as the throughput increases from 2.5 kt/d to 100 kt/d as expected both on the opex and on the capex. Again, we can average costs and compare the capex costs per ton of the lower throughput cases with the high throughput case, see Table 7. As in the previous tables, there is an interesting trend to consider.

Table 7.Comparison of capex per throughput

Throughput	LDT	HDT	PT	FT
2.5 kt/d	5.8	6.3	5.6	2.0
25 kt/d	1.8	1.8	1.9	1.7
100 kt/d	1	1	1	1

Finally, the same table is generated for the opex, with costs at the lower throughput options normalized to the high throughput case, see Table 8.

Table 8. Comparison of opex per ton of ore

Throughput	LDT	HDT	PT	FT
2.5 kt/d	1.8	2.0	1.8	4.4
25 kt/d	1.1	1.2	1.1	1.1
100 kt/d	1	1	1	1

3.3 *Accuracy of the estimates*

It is critical to understand that these plant estimates are based on many assumptions and design considerations that may be unique to a given site. Furthermore, the prices have an estimated accuracy of +/- 30%. The costing should only be used to provide an order of magnitude idea on capital and operating costs and need to be adjusted for the local conditions of a specific site such as labour rates, freight, duties, installation location, tailings characteristics, etc.

4 CONCLUSIONS

The test work completed at Outotec for tailings can be used to illustrate the range of dewatering properties encountered. When the solid load ratings for thickening used for design are plotted against the amount of fines in the samples, there is not a strong relationship. However plotting the filtration rates used for design against the amount of fines in the tailings samples, there is a stronger relation. The result is not surprising given that mineralogy of the samples were not accounted for and highlights the need for laboratory testing to determine dewatering properties of a material. However, the range in test results provides an idea of the range in filtration rates and thickening fluxes or solid load rating used in design. This information was used to establish typical dewatering properties for a difficult to dewater sample and easier to dewater sample to be used for equipment selection and sizing in the cost estimates.

Cost estimates were generated based on the selected dewatering properties for a 2.5kt/d, 25kt/d and a 100kt/d throughput plant for a difficult to dewater and easier to dewater case (6 cases). For each case 4 options were evaluated (low density slurry, high density slurry, paste, and filtered tailings). The 24 cost estimates generated provided a basis to compare some of the trends in the capex and opex.

- The difficult to dewater tailings were up to ~20% higher capital cost at the 2.5 kt/d throughput, but the discrepancy increased to ~90% in the extreme case for the 100 kt/d operation.
- The cost per ton ratios between dewatering technology showed a strong trend. Costs can be normalized to the cost of the low density slurry system and ratios are presented in table 9 below.
- The cost per ton ratios between throughput also showed a strong trend. Note that for the filtration option, we are comparing trucking vs. conveying in the 2.5 kt/d case which is perhaps not that useful.

Table 9. Ratio of capex and opex costs for dewatering technology

	LDT	HDT	PT	PFT
Capex	1x	1.3 – 1.4x	3 – 4x	~ 2.5x for trucking of tailings ~ 6-7x for conveying
Opex	1x	1.1x	3x	~30-35x for trucking of tailings ~10-15x for conveying

Table 10. Ratio of capex and opex for different throughput

	100 kt/d	25 kt/d	2.5 kt/d
Capex	1x	1.5 – 2x	5.5 – 6.5x for thickening 2x for filtration w/ trucking
Opex	1x	1.0 – 1.3x	1.5 – 2.0x for thickening 4x for filtration w/ trucking

Through this comparison exercise we can conclude that factoring of costs based on ratios of throughputs and comparison of technology can be a useful tool to estimate what a dewatering system may cost for a specific site. However, limitations exist in the accuracy of this factoring approach as all sites have very specific needs and variability of tailings also plays a factor on the cost. It is easy to fall into a trap and put too much faith into these comparisons. The costs generated with this method should only be used as order of magnitude estimates. Proper testing of tailings materials followed by the appropriate level of engineering should always be used for establishing budgets for the project.

REFERENCES

Carniero, A. & Fourie, A.B. 2019. An integrated approach to cost comparisons of different tailings management options. In AJC Paterson, AB Fourie and D Reid (eds), *Proceedings of the 22nd*

International Seminar on Paste and Thickened tailings, Australian Centre for Geomechanics, Perth: pg 115 126.

Klohn Crippen Berger on behalf of Mine Environment Neutral Drainage Program (2017). 2017. Study of Tailings Management Technologies, MEND Report 2.50.1.

Crawford, J. & Bessett, N. 2019. Development of centrifugal slurry pumps in tailings disposal and comparison with positive displacement pumps. In AJC Paterson, AB Fourie and D Reid (eds), *Proceedings of the 22nd International Seminar on Paste and Thickened tailings*, Australian Centre for Geomechanics, Perth: pg 517-530.

Palmer, J. 2015. Advances in testing and simulation of filtration performance with tailings. *Proceedings of the 3rd International Seminar on Tailings Management,*

Jewell, R.J. & Fourie, A.B. 2006. Paste and Thickened tailings – A guide, 2nd Edition, Australian Centre for Geomechanics, Perth Australia, 242 pg.

Reid, D. & Fourie, A.B. 2015. The influence of slurry density on in situ density. In RJ Jewel and AB Fourie (eds), *Proceedings of the 19th International Seminar on Paste and Thickened tailings*, Australian Centre for Geomechanics, Perth: pg 95-106

Davies, M. 2011. Filtered dry stacked tailings – the fundamentals. In Tailings and mine waste '11: *Proceedings of the 15th International Conference on Tailings and Mine Waste*, Vancouver BC, Canada, November 6 – 9, 2011.

Amoah, N. 2019. Large-Scale Tailings Filtration and Dry Stacking at Karara Magnetite Iron Ore Operation. In Tailings and Mine Waste 2019: *Proceedings of Tailings and Mine Waste 2019*, November 17 – 20, 2019, Vancouver, Canada. Pg 15 – 32.

Consideration of Polymers to Create a More Cost-Effective and Sustainable Approach to Contaminated River Sediment Remediation

Raymond Guang
Golder Associates, Sudbury, Ontario, Canada

Doug Reid-Green
BASF, US

ABSTRACT: The use of polyacrylamide (PAM) high-molecular-weight polymers at the tailings storage facility (TSF) discharge location is a well-known practice in the mining industry. The technique is called in-line polymer treatment of tailings and involves adding polymer to the tailings stream upstream of the discharge spigot with the goal of generating a tailings slurry release water with lower turbidity and create a steepened tailings beach due to increase in yield stress.

This paper presents preliminary evaluations of re-purposing the in-line polymer treatment process now used on mining projects, for use on sediment remediation projects. A common bottle-neck on those remediation projects that involve dredging, resulting in both increased costs and schedule, is the effort needed to prepare the dredged material for offsite disposal. The objectives of this study were to assess and evaluate the ability of two BASF polymers to dewater dredged river sediments collected from a remediation site in New York state to a point where they are complaint with offsite disposal parameters.

During the laboratory testing phase, tests were performed to determine the best polymer, dosage and strength gain over time in terms of yield stress, supernatant water solids content and final solids content. The results indicated that both polymers were effective in dewatering the dredged material. This paper presented an improved understanding of how polymer could be used in remediation project.

1 INTRODUCTION

Sediments in general are major problems in aquatic ecosystem management. Globally, several hundred million cubic meters of sediments must be disposed of (Forged et al, 2007). One of the sediment treatment options is dredging. However, disposal of dredged sediments can also cause numerous issues, some of which are political, economic, legal and difficult to control (Murphy et al, 1999). Land management of dredged sediment is expensive since the cost of the disposal is calculated in terms of volume. Lesser disposal volume would lead to a reduced disposal cost. Therefore, dewatering of sediment before disposal becomes an important step for cost reduction. Furthermore, dewatering dredged sediment, an end of product with good soil mechanical characteristics can be produced.

The use of polyacrylamide-based high molecular weight polymer addition at the tailings storage facility (TSF) discharge location has become an increasingly common technology for dewatering tailings. The method of applying polymer to treat tailings is known as in-line flocculation or in-line polymer addition (Bembrick, 2008., Wells et al, 2011, Guang et al, 2014., Guang et al, 2017., Costine et al, 2018).

Polymers were also used in wastewater treatment industry since 1950. Most polymer used in dredging takes place around the solids dewatering operations in which enhanced solids/liquid separation and/or consolidation is desired (Hunter et al, 2006). In this study, polymers were added

to the sediment without further mechanical dewatering step. The objective of this paper is to showcase the authors' experience with in-line polymer treatment on a typical river sediment.

2 FACATORS INFLUENCING FLOCCULATION

The effect of polymers on the flocculation of tailings has been well studied and understood since 1950s (Henderson & Wheatley 1987). Flocculation occurs when individual particles in suspension form aggregates by the action of polymeric chains attaching and bridging the particles, overcoming the repulsive forces between particles. The effectiveness of a polymer in flocculating a tailings sample has been demonstrated to be a function of:

- The polymer chemistry
- The presence coagulants that destabilize colloidal dispersion and their order of addition (Sabah & Cengiz, 2004)
- Mineral surface charge and chemistry
- Particle size, shape and surface texture (Stocks, 2006)
- Slurry density (or solids content), which affects the ability for the polymer to disperse and mix through the sample
- Polymer dilution, which will also affect its ability to disperse and mix through the sample (Pillai 1997)
- pH (Atesok et al, 1988, Pillai 1997)
- Water chemistry (Stocks 2006)

In terms of treating sediment, majority of the abovementioned points can still apply. Particle size, solids content, polymer dilution concentration, pH, and water chemistry are extremely important for polymer selection on a sediment treatment project.

3 SAMPLE INFORMATION

3.1 *Sediment sampling*

The representative sediment sample for the testing was collected from Rensselaer, New York facility, which included: six 3-gallon buckets of sediment materials and four 3-gallon buckets containing river water.

Generally, dredged material contains a large portion of water and small amount of dry material. For this project, it was confirmed that the samples were dredged mechanically, and the solids content was found to vary between 66.3% and 68.3%.

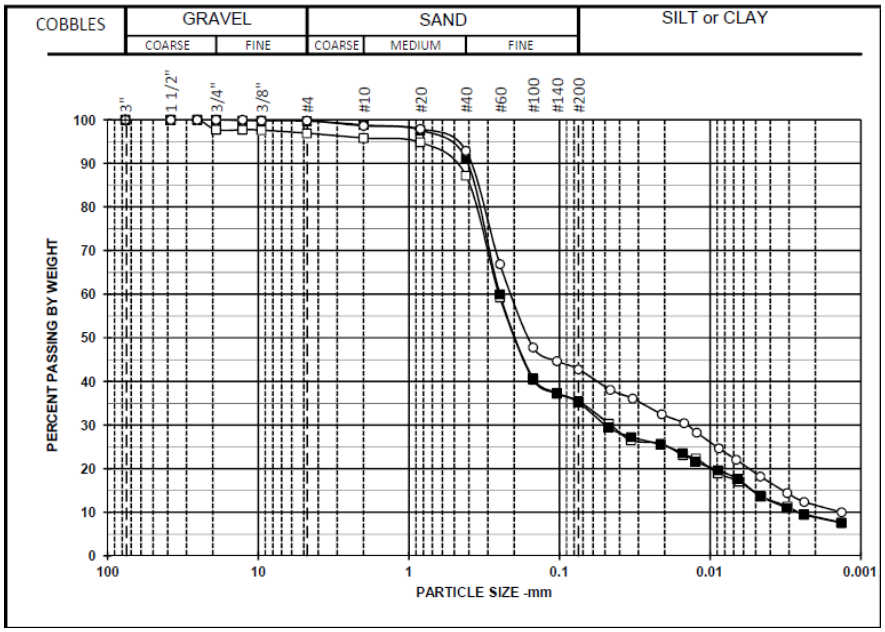

Figure 1. Particle size distribution for the received sediment sample

3.2 *Polymer preparation*

For each tested polymer (in dry powder form), diluted polymers were prepared, by mixing dry polymer power with tap water, to produce both 0.25% and 0.05% polymer solutions. Polymer preparation was carried out using tap water and not river water because the use of river water could potentially impact the polymer performance.

3.3 *Yield stress measurements*

Yield stress measurement were performed about 5 minutes after the addition of polymer. In particular, yield stress measurements were collected using a Brookfield DV-III rheometer using a V71-73 vane spindle within a 600 ml beaker at rotation speeds of about 0.2 rpm.

Figure 2. Typical V71 vane spindle

3.4 *Water release measurements*

Following polymer addition, the free water released from the sediment was decanted and the net water recovery (release) was computed at varying time intervals, following polymer addition. Net water release represents the quantity of free water decanted from the treated sample compared to the quantity of water contained in the sample, and can be calculated using the following expression:

$$Net\ water\ recovery\ \% = \frac{water\ recovered - water\ added\ in\ polymer\ solution}{water\ in\ slurry} \times 100$$

When the quantity of water released is less than the quantity of water added in the polymer solution, the net water recovery value is negative.

4 LABORATORY TESTS

4.1 *Phase 1: Polymer Screening Results*

Overall, twenty-two commercially available polymers were screened to identify those polymers that may be effective in achieving the objective. The polymer process involved:

- Sediment sample, at known initial solids content, were placed within separate centrifuge tubes.
- Sediment samples were diluted using river water, to achieve uniform solids content of about 30%.
- Each screened polymer was introduced, at dosage varying between 178-186 g/t, into centrifuge tubes of prepared sediment samples.
- Sediment samples were mixed.
- After mixing, degrees of floc formation were qualitatively observed with each centrifuge tube.

Based on observation of screened results, the following four polymers were found to have relatively fast settling rates and clearer supernatant water quality, and were selected for further phase 2 testing.

- Rheomax® 9030
- Magnafloc® 10 (MF10)
- Magnafloc® 155 (MF155)
- Magnafloc® 345 (MF345)

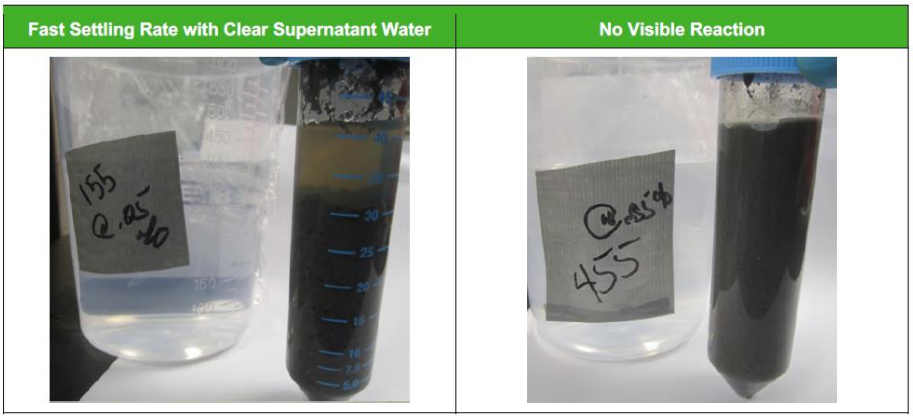

Figure 3. Typical polymer screening observations

4.2 *Phase 2: Polymer selection*

4.2.1 *Part 1 testing*

4.2.1.1 0.25% Polymer solution results

During Part 1 testing, the four selected polymers were tested for net water release, yield stress, supernatant solids content, and final solids content at 24 hours. Additionally, sediment samples were tested at three different polymer dosage (ie. 286, 345, 406 g/t) and two different polymer solution (0.25 and 0.05% solutions)

Based on results, Magnafloc® 155 achieved the highest net water release (after 24 hours). However, the results for MF155 was found to be inconsistent over varying polymer dosage. Magnafloc® 155 achieved higher values for 346 g/t, but lower values at 286 and 406 g/t.

The net water release value for Rheomax®9030 and Magnafloc® 345 were consistently higher than the other two polymers tested.

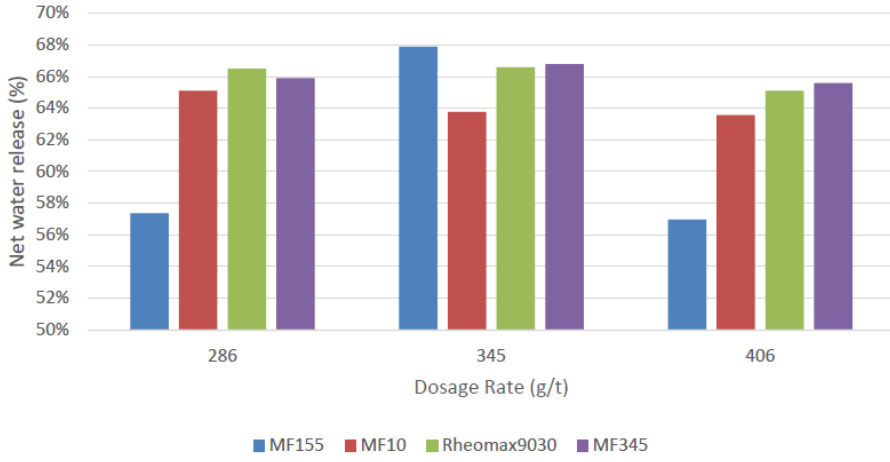

Figure 4. Net water release (after 24 hours)

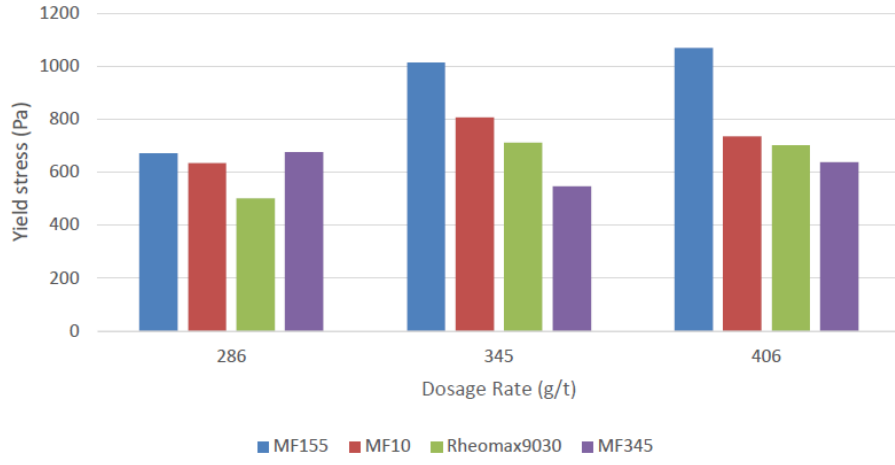

Figure 5. Yield stress after 24 hours

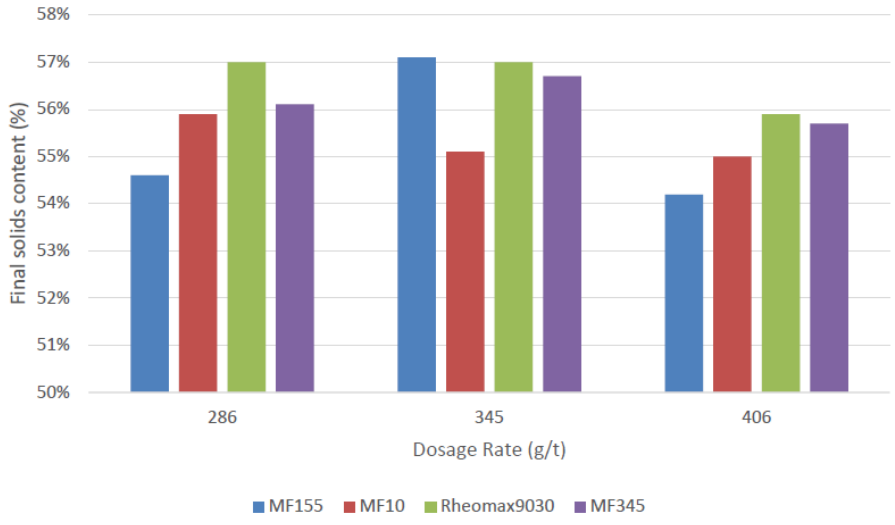

Figure 6. Final solids content after 24 hours

In general, yield stress increased from unmeasurable to between 500 and 1000 Pa at 24 hours, and Magnafloc® 155 yielded the highest yield stress for all tested dosage.

Final solids content for Rheomax®9030 and Magnafloc® 345 were found to be consistently higher than the other tested polymers. Additionally, the Magnafloc® 155 results at a dosage of 345 g/t were found to be inconsistent with its other two tested polymer dosage, as noted with its net water release properties.

4.2.1.2 0.05% Polymer solution results

Rheomax®9030 and Magnafloc® 10 achieved the higher net water release (after 24 hours) at different dosage. Yield stress increased from unmeasurable to between 460 and 750 Pa at 24 hours, and no particular polymer stood out from the others. Magnafloc® 10, Magnafloc® 345, and Rheomax® 9030 yielded high yield stress (after 24 hours) for different dosage.

Final solids content for Rheomax® 9030 and Magnafloc® 345, and Magnafloc® 10 were found to be consistently higher than Magnafloc® 155.

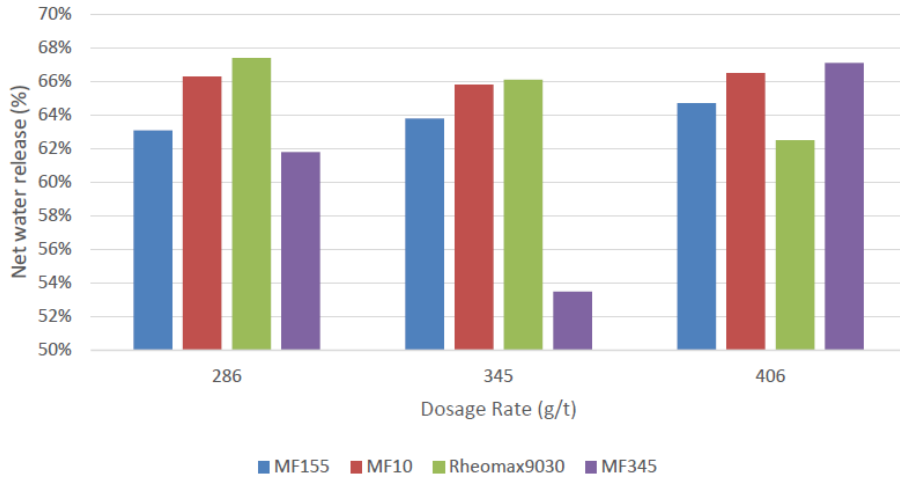

Figure 7. Net water release (after 24 hours)

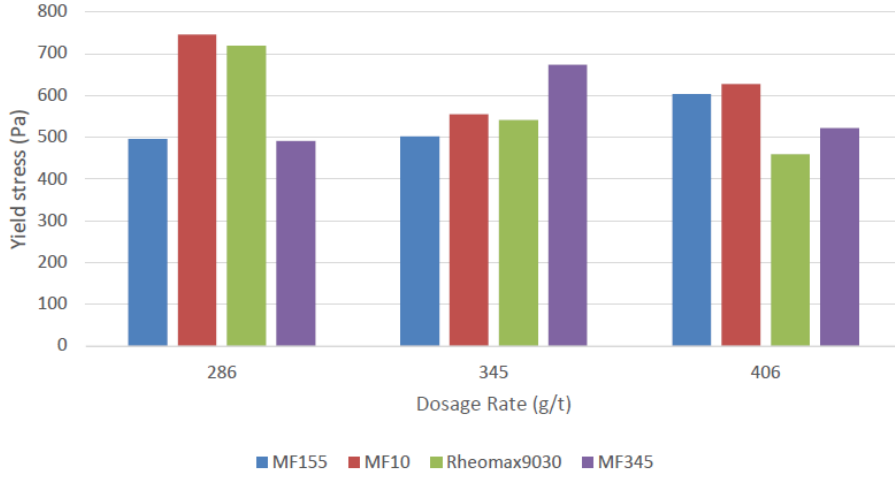

Figure 8. Yield stress after 24 hours

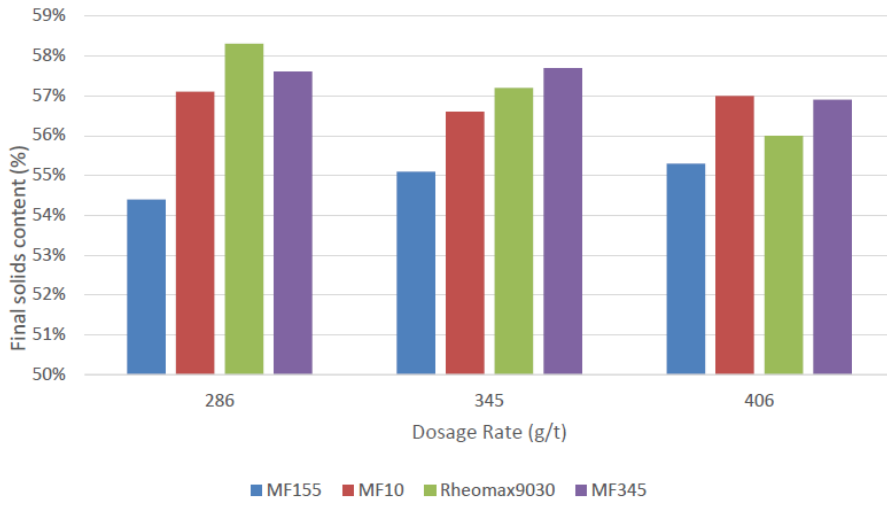

Figure 9. Final solids content after 24 hours

Based on above-noted testing results, it appears both Rheomax® 9030 and Magnafloc® 10 polymers would be capable of achieving better key indicator (i.e., net water release, yield stress, and final solids content) performance. Therefore, both Rheomax® 9030 and Magnafloc® 10 were selected for advancement into Part 2 testing.

4.2.2 *Part 2 testing*

4.2.2.1 Rheomax® 9030 results

See below figures for final solids content and yield stress results, respectively, for 50% and 30% solids content samples with 0.25% polymer solution.

The highest final solids content values were achieved at dosage of 180g/t for 30% solids content samples and 270 g/t for 50% solids content samples. However, the supernatant water solids content (0.8%) for the 30% initial solids content samples at a dosage of 180g/t was higher than usual (0.08-0.19%), which is an indicator of under-dosing.

For 30% solids content samples, dosage between 207 and 285 g/t achieved consistent results in terms of solids content, and the sample yield stress values tended to increase with increasing polymer dosage rates. Additionally, a polymer dosage rate of 337g/t produced very high yield stress, which would be an indicator of over-dosage.

For 50% solids content samples, dosage between 270 and 446 g/t achieved fairly consistent results in terms of solid content. At lower dosage rates (e.g., 270 g/t), there were more solids present in the supernatant water. At higher dosage rates, the yield stress increased substantially, which would be an indicator of over-dosage.

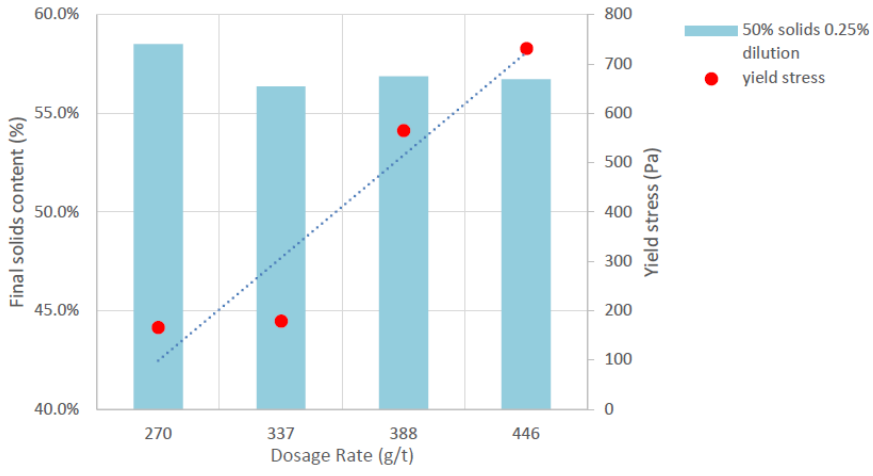

Figure 10. Final solids content and yield stress results for Rheomax® 9030 with 0.25% polymer solution for 50% initial solids content samples

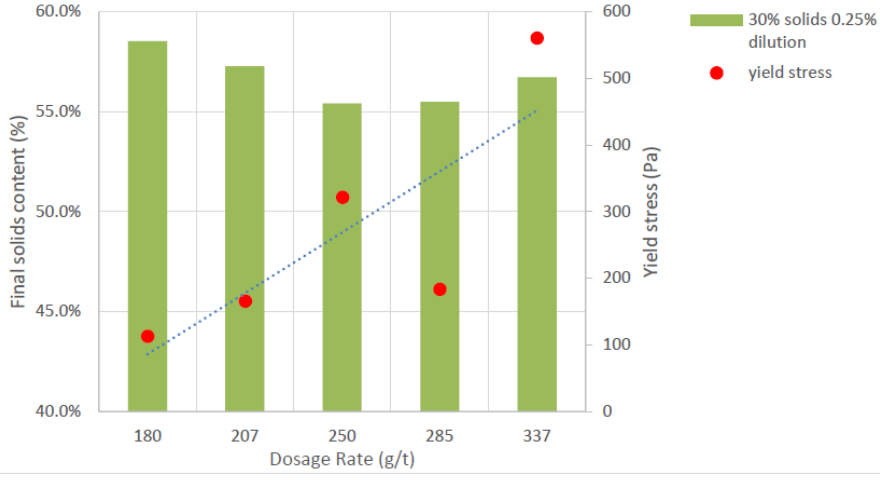

Figure 11. Final solids content and yield stress results for Rheomax® 9030 with 0.25% polymer solution for 30% initial solids content samples

4.2.2.2 Magnafloc® 10 results

During testing, some of the 30% initial solids content samples with 0.25% polymer solution produced inconsistent result. To further explore said inconsistent results, testing these samples were repeated three times, resulting in similar inconsistent results. The reasons for noted inconsistent results are not known with certainty but may be associated with the variability of the raw sediment material. Based on the trend lines shown in Figure 12, it appears that final solids content values tend to decrease with increasing polymer dosage, which is typical where the difference between underdose and optimal dosage is minimal.

Based on the trendline shown in Figure 13, it appears that yield stress tends to increase (with exception of the 30% intimal solids content with 0.05% polymer solution) with increasing polymer dosage.

The 30% and 50% initial solids content sample with 0.05% polymer solution yielded higher, increasing yield stress results with increased polymer dosage. However, the 40% initial solid content sample with 0.05% polymer solution yielded decreasing yield stress results with increasing polymer dosage, which appears counter-intuitive and could not be explained with certainty.

Overall, the 0.25% Magnafloc® 10 polymer solution testing results appear inconsistent, given both the 30% and 40% initial solids content samples yielded relatively high supernatant water solids content (up to 1.71%). However, the 0.25% Magnafloc® 10 polymer solution samples with 50% initial solids content yielded satisfactory (i.e., lower) supernatant water solids content results (up to 0.58%).

For the 0.05% Magnafloc® 10 polymer solution samples, the testing results yielded more consistent, reasonable yield stress and supernatant water solids content results, but lower final solids content, as compared to comparable 0.25% polymer solution testing results.

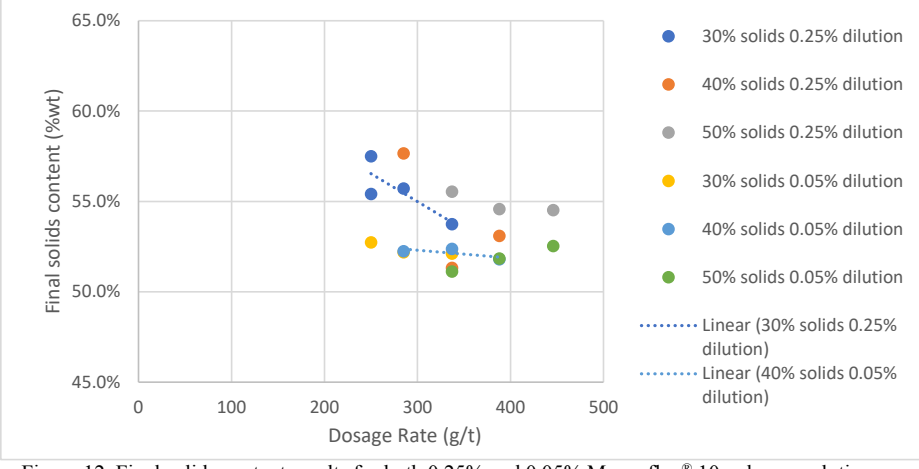

Figure 12. Final solids content results for both 0.25% and 0.05% Magnafloc® 10 polymer solutions

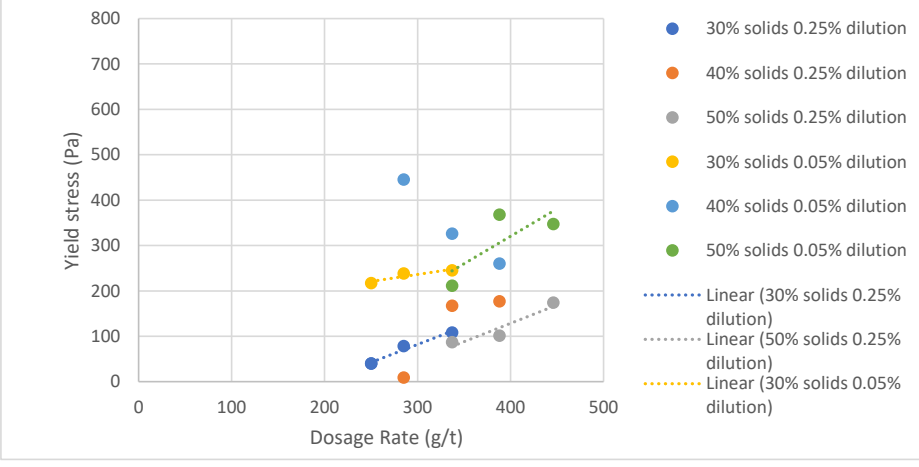

Figure 13. Yield stress results for both 0.25% and 0.05% Magnafloc® 10 polymer solutions

5 DISCUSSION

Currently, the dredged sediment in this study is treated with cement. In general, cement and lime are used as solidificants, but the treated sediments have high pH values (Renholds, 1998). The goal of adding cementitious material to sediment prior to landfilling is to achieve good physical properties and immobilize harmful components.

By using polymer as a treatment option for sediment, supernatant water will be released from the sediment immediately. This will lead to a reduction of final disposal weight of the sediment for landfill. Further, with in-line polymer addition method, the overall footprint and capital cost will be relatively lower than the traditional mechanical methods. Using polymer to treat contaminated sediment can provide significant economic benefits compare to tradition solids/liquid separation mechanical equipment.

In terms of polymer selection, it is important to understand that the type of polymer selected will depend on the application and properties of the sediment samples to be treated. Different functional group are attached to the backbone of the polymer to adjust its properties for specific application or minerals.

The polymer dosage required to create desired effects may also vary significant between different sediment sample types and application. Polymer dosage is an important factor in deciding whether this technology is suitable for a project.

6 CONCLUSION

The study shown in the paper provided a preliminary evaluation of polymer treatment on dredged river sediment. Based on current result, it is concluded that polymers allow a rapid dewatering of river sediment that provide immediately available clarified water. The final solids content achieved in this study achieve to approximately 57-58%. Obviously, for mining projects, treated tailings can be disposed via pipelines and allowed to consolidate over time. With remediation, treated sediment needs to be transported to landfill which will lead to a higher final solids content requirement (ie pass the paint filter test).

Polymer treatment is a fast-moving area in both mining and remediation industry. With testing and experience, a knowledge base is growing to gain the maximum benefit from polymer technology.

7 REFERENCES

Atesok, G., Somasundran, P., Morgan, L., 1988, Charge effects in the adsorption of polyacrylamides on sodium kaolinite and its flocculation, *Powder Technology*, vol.54, pp77-83.

Bembrick, D., 2008, The impact of flocculant addition on a tailings storage facility, *Metallurgical plant design and operating strategies,* Perth, pp541-549.

Costine, A., Benn, F., Fawell, P., Edraki, M., Baumgartl, T., Bellwood, J., 2018, Understanding factors affecting the stability of inline polymer – amended tailings, in Proceeding of the 21st International Seminar on Paste and Thickened Tailings, RJ Jewell, AB Fourie (eds), Australian Centre for Geomechanics, Perth, pp 103-116.

Englis, M., Hunter, D., 2007, A description of sediment dewatering methods, In proceedings eighteenth World Dredging Congress, R.E. Randall (eds), Florida, USA, Newman Printing Company, pp1451-1466.

Forged, S., Duerinckx, L., Vandekeybus, J., 2007, An innovative and sustainable solution for sediment disposal problems, In proceedings eighteenth World Dredging Congress, R.E. Randall (eds), Florida, USA, Newman Printing Company, pp1513-1528.

Guang, R., Tshibang, M., Loayza, C., 2014, Application of in-line polymer addition for tailings disposal in Australia – learning and challenges, In proceedings seventeenth International Seminar on Paste and Thickened Tailings (Paste14), R.J. Jewell, A.B. Fourie, P.S. Wells., D. van Zyl (eds), Vancouver,

Canada, InfoMine Inc, pp87-99.

Guang, R., Longo, S., 2017, Application of in-line polymer addition for tailings disposal- learning and challenges part II, in A Wu, RJ Jewell (eds), in *Proceeding of the 20th International Seminar on Paste and Thickened Tailings,* Australian Centre for Geomechanics, Perth, pp 371-379.

Henderson, J., Wheatley, A., 1987, Factors affecting the efficient flocculation of tailings by polyacrylamides, *Coal Preparation*, vol.4, pp1-49.

Hunter, D.W., Heard, M., Baron, K., 2006, The positive impact of polymers on sediment treatment and handling, In proceedings twenty sixth Western Dredging Association Technical Conference, San Diego, USA, pp131-146.

Murphy, T.P., Lawson, A., Kumagai, M., Babin, J., 1999, Review of emerging issues in sediment treatment, *Aquatic ecosystem health and management 2,* p419-434.

Pillai, J., 1997, Flocculant and coagulants: the keys to water and waste management in aggregate production, Internal Document, Nalco Company.

Renholds, Jon., 1998, *In site treatment of contaminated sediments*, U.S. Environmental Protection Agency, Washington, D.C.

Revington, A., Sanchez, A., Wells, P., 2012, Principles of TRO high density flocculation using a pipe reactor, in *Proceeding of the 15th International Seminar on Paste and Thickened Tailings,* Australian Centre for Geomechanics.

Sabah, E., Cengiz, I., 2004, An evaluation procedure for flocculation of coal preparation plant tailings, *Water Research*, vol.38, pp1542-1549.

Stocks, P., 2006, Chapter 6 Reagents, *Paste and Thickened Tailings – A Guide*, Third Edition, ed. Jewel R.J., Fourie, A.B., Australian Centre for Geomechanics.

Wells, P.S., Revington, A., Omotoso, O., 2011, Mature fine tailings drying – technology update, In proceedings fourteenth International Seminar on Paste and Thickened Tailings (Paste11), R.J. Jewell, A.B. Fourie, (eds), Perth, Australia, Australian centre for geomechanics, pp155-166.

Incorporating Lime Treatment as Part of Innovative Mine Water Treatment Strategies

Kristina Minchow, Bridgette Hendricks & Ryan Schipper
Golder Associates Inc., CO, USA

ABSTRACT: Precipitation of metal hydroxides using lime has traditionally been one of the most common mine water treatment technologies. While lime treatment continues to have a place in the water treatment arsenal for mining applications, usage of other technologies is on the rise. New mine water treatment processes include new technologies and technologies that are proven in other applications but are "innovative" to mining. This paper compares lime treatment to alternative proven and emerging technologies for mine water treatment and presents a summary of indicator factors that can be used when considering alternatives. More stringent effluent regulations and waste management challenges drive the consideration of technologies that have not typically been used for mining impacted waters. This paper reviews lime treatment applicability for mining-waters versus alternate technologies and considers methods for integrating lime treatment into an innovative treatment strategy.

1 INTRODUCTION

Sources of mining impacted water (MIW) that may require treatment typically include non-contact dewatering water, contact water, excess tailings water, seeps, and other similar sources present at active, inactive, and legacy mine sites. Lime treatment for metals removal has been one of the more commonly implemented water treatment technologies and continues to be an important component of MIW treatment. The selection of technologies required to produce a compliant effluent is dependent on the specifics of the site, the water quality, flowrate, and the discharge limits. This paper targets general conditions when lime treatment is typically the most cost effective technology, when additional treatment steps are required, and some innovative technologies that are being evaluated and/or installed to replace or complement lime treatment.

Key components of a typical lime treatment system include the following:

- Reaction tank is a well-mixed aerated tank with typical reaction time from ten minutes to two hours. Lime is added to increase the pH with most metals precipitating in the range of 8.5 to 10.5.
- Solids separation process such as a conventional clarifier, settling pond, inclined plate clarifier, tube settler, ballasted clarifier, and similar. Polymers are typically added to promote settling.
- Polishing filtration may or may not be included.

- Effluent pH adjustment to neutralize pH to required range for discharge.
- Sludge management systems.
- Chemical feed systems.

Dissolved metals precipitate in the reaction tank when the hydroxide ions in the hydrated (slaked) lime combine with metal ions. Then solids separation steps remove the precipitated metals from the treated water. Calcium concentrations increase as a result of the lime addition. Calcium sulfate and/or calcium carbonate will also precipitate if present above their solubility limits.

The components above are part of a typical low-density sludge (LDS) system; high density sludge (HDS) systems are discussed in later sections but generally make use of the same equipment as well as additional reaction and mixing tanks.

2 BENEFITS OF LIME TREATMENT IN MINING APPLICATIONS

Lime treatment has a long history of application at mining sites for treatment of metal and sulfate impacted water. The primary benefits of metal hydroxide precipitation over other treatment processes and the use of lime over other chemical agents for treatment of MIW include the following:

- Availability – lime is readily available in several areas where mining occurs and is typically transported in bulk to operating mines for other purposes.
- Cost - lime is a fairly low-cost water treatment chemical relative to other alternatives. The water treatment usage requirements for lime on an annual or daily basis are typically much less than required for other purposes at the mine, such as in froth flotation in copper, nickel and zinc production and for maintaining pH in a cyanide leach circuit for gold/silver recovery. As a result of its wide use, mining companies can typically negotiate favorable pricing.
- Effectiveness – hydroxide precipitation is effective for the precipitation of many metals, sulfate, and carbonate in MIW. Strict surface water metal discharge limits can often be achieved with just chemical reaction and solids removal (clarification). Polishing filtration may be required. Oxidation and iron (naturally occurring or supplemental) can improve the removal of target metals.
- Flexibility – lime treatment systems can handle changes in flow and concentration, and be operated intermittently unlike many other treatment processes (membranes, biological processes, IX, etc).
- Secondary waste form – the sludge produced from precipitation is often easier to manage at active mine sites than liquid waste (brine). Lime sludge generally dewaters more effectively than sludge from caustic treatment, producing less dewatered sludge for disposal.
- Equipment – the equipment required for a lime treatment system is similar to other equipment used at operating mine sites (pumps, tanks, mixers, and clarifiers).
- Safety – lime slurry requires less special handling, storage and safety protocols than concentrated sodium hydroxide.
- Proven and effective with a long track record of operating and meeting surface water discharge limits at mine sites throughout the world.
- Treatability testing can be accomplished effectively through jar testing and settling testing. Scale up from bench test data is not uncommon.

While the situation at non-operating mine sites (historic, undergoing reclamation, closed, and similar) may not present as many advantages as operating mine sites for implementing lime treatment, the technology is often still cost effective for many of the reasons listed above.

In particular, when the MIW has a high metals load, high dissolved iron content and high dissolved sulfate with a requirement for sulfate removal, lime treatment provides cost effective bulk contaminant removal. See Table 1 for the results of lime addition to various pH set points in acid mine drainage water with high sulfate and metals concentrations. The concentrations presented in the table are representative of residual parameter concentrations following lime addition and solids removal. In this common example, lime treatment provides reductions in the concentrations of metals as well as TDS and sulfate.

Table 1: Lime Treatment of Acid Mine Drainage

Parameter	Raw Water mg/L	pH 8 mg/L	pH 9 mg/L	pH 10 mg/L	pH 11 mg/L
TDS	27,687	7,570	2,766	2,454	2,426
Fluoride	52	6	4	7	<1
Sulfate	18,500	5,390	1,840	1,610	1,610
Aluminum	1,100	0.10	1.4	16	1.04
Cobalt	13	0.023	0.009	0.0084	0.038
Copper	878	0.13	0.10	0.11	0.13
Iron	1100	<0.07	<0.07	<0.07	<0.07
Lead	0.34	<0.073	<0.073	<0.073	<0.073
Magnesium	1,300	890	56	0.91	0.55
Manganese	210	17	0.21	<0.005	0.0066
Nickel	3.6	0.037	<0.03	<0.03	<0.03
Silica	140	0.91	0.35	0.12	0.89
Strontium	1.5	0.66	0.68	0.64	1.0
Zinc	69	0.11	<0.03	<0.03	<0.03

3 ALTERNATIVE TECHNOLOGIES TO LIME TREATMENT

In many cases, MIW lime treatment still represents the most cost-effective treatment process for mine water; however, alternative technologies may be a more appropriate option depending on the site conditions and mine-life stage, water chemistry, discharge limits, and options for sludge or secondary waste disposal. In general alternative technologies can be more favorable than lime treatment at sites where:

- The site is in reclamation, lime is not available and the sites may be remote with no or poorly maintained roads. Often power is not available at these sites either.
- The cost for lime sludge disposal is high and/or trucking offsite is required.
- A relatively low flow (less than 10 to 20 m3/hr) requires treatment which increases the unit operational cost for a lime system. The operational labor may be similar to a much larger system.
- Where constituents are present and regulated that are not effectively treated by lime addition including selenium, boron, nitrogen species (ammonia, nitrate, nitrite), chloride, sodium, potassium, TDS, and sulfate (to levels lower than approximately 1,800 mg/L)

Lime treatment may be used in combination with alternative technologies to provide pretreatment or residuals (brine) treatment for bulk metals removal and then a more specialized process is used to reduce contaminants not well treated by lime. Technologies often evaluated and increasingly implemented at mine sites are summarized below. Lime treatment is included in the Precipitation Technologies section below for completeness and contrast to other precipitation technologies. The technologies discussed below include processes that are considered a replacement to lime treatment and also in addition to lime treatment.

3.1 *Precipitation Technologies*

Precipitation technologies, including lime treatment, provide removal of dissolved species from MIW through a change in pH. The precipitation step changes the form of the target species from soluble to particulate and is followed by a solid liquid separation step. Typical solids removal steps include clarification, dissolved air flotation, ballasted clarification, microfiltration or ultrafiltration, and other types of conventional filtration.

In hydroxide precipitation the alkali chemical provides hydroxide ions that combine with the metal cations in the water to form insoluble metal hydroxides. Hydrated lime, Ca(OH)2, also adds calcium that may precipitate sulfate and/or carbonate present in the water to form additional precipitated solids (either calcium sulfate or calcium carbonate). Most metals in MIW precipitate at elevated pH values, commonly in the range of 8.5 to 10.5. Other typical alkali chemicals include limestone, sodium hydroxide, and magnesium hydroxide. Most are more expensive than lime and are not as commonly used at mine sites. These other alkali chemicals may be used to minimize sludge if sulfate or carbonate are present above saturation limits and do not require removal, if the alternative chemicals have a price advantage, or if they have a treatment advantage. For instance, boron has been shown to precipitate/co-precipitate with magnesium at pH values near 10.5. Hydroxide precipitation efficiency is improved by co-precipitation with iron (either naturally occurring or added to the reaction tank) and by oxidation.

Sulfide precipitation differs from hydroxide precipitation in that it is more specific for precipitation of cationic heavy metals, does not affect pH, is not as dependent upon pH for effective metals treatment, and generates a smaller volume of sludge (metal-sulfide solids) relative to hydroxide precipitation. Constituents such as sulfate, manganese, and alkalinity will not be removed by sulfide precipitation. Metals may be economically recovered from the sulfide precipitate in some cases, defraying the treatment costs. Reagents include iron sulfide, sodium hydrosulfide, sodium sulfide, calcium sulfide, organo-sulfide (trade name TMT®), and biologically produced sulfide. Sulfide precipitation can often achieve lower residual metals levels than hydroxide precipitation; however, the reagents are more expensive and there is the potential for sulfide gas formation and release if the pH is not monitored and maintained at target levels. Sulfide precipitation was selected over lime precipitation and installed at the Wellington-Oro mine site near the ski town of Breckenridge, Colorado in 2008 for the selective removal of cadmium and zinc. The plant is located near tourist destinations and operated by the town's municipal operators. The system operates between 12 and 34 m3/hr (spring runoff flow) and removes cadmium from 0.059 mg/L to less than the discharge limit of 0.004 mg/L and zinc from 123 mg/L to less than 0.225 mg/L.

3.2 *Electrocoagulation*

The electrocoagulation (EC) process involves passing an electrical current through water disrupting the ionic charges of dissolved species. Precipitation and co-precipitation of dissolved species result due to several mechanisms. One of the primary mechanisms is coagulation by iron or aluminum (depending on the electrode metal type) cations released from the corrosion of the electrode blades at the anode. Since chemicals are not added, there are no supplemental ions added to the water due to treatment chemicals. The EC unit replaces the reaction tank and chemical feed systems used in conventional precipitation, however, downstream solids separation is still required. EC has been used extensively in the treatment of metal finishing wastewater, shipyard runoff water and food processing wastewater.

Typically the capital equipment cost for EC is higher than chemical precipitation for most MIW treatment cases, however, standard models and designs are becoming more common. EC operating costs may be lower than chemical precipitation for labor, sludge disposal, and chemicals. Electrode blades require replacement and cost can be a factor in operating cost depending on local availability of metal material for electrode replacement Electrical power demand is likely higher and varies inversely with the ionic strength of the water being treated.

EC can generally remove most metals encountered at mine sites, although limited success with antimony and boron has been reported, and it is not effective at low pH so EC is not a candidate for acid mine drainage. Selenium removal to less than 0.005 mg/L has been achieved in bench

tests, however, the sludge production is very high and longer reaction times required increasing the EC equipment cost.

3.3 *Biological Treatment*

For treatment of MIW, biological systems may be effective for cyanide, ammonia, nitrate, some metals, and phosphorus. Various configurations of biological systems are commercially developed and have been used on MIW treatment. Biological systems can operate aerobically, anaerobically or anoxically depending on the target contaminants, space available, water matrix and other factors. At mine sites, biological treatment has been used for removal of metals, nitrogen species and cyanide. The Homestake Mine in Lead South Dakota used a rotating biological contactor (RBC) fixed film biosystem to treat cyanide, ammonia and metals in MIW sources. Biological treatment of selenium is one of the commercially proven methods to treat selenium in water. Challenges associated with implementing biological treatment at mine sites include: the often cold water temperatures; the requirement for supplementation of nutrients (often carbon is required and phosphorus); polishing treatment; the negative impact of higher TDS (above 15,000 mg/L) and bio-toxic metals such as copper; the space required; and the limited flexibility with regard to flow and contaminant load.

3.4 *Passive Treatment*

Passive treatment has a proven track record in the treatment of mining wastewater. Passive configurations that are considered proven include wetlands, anaerobic biochemical reactors (BCRs), and aeration channels with settling basins. Passive configurations that are emerging include alternatives to limestone for alkalinity addition (kiln dust, steel slag, ViroMine™, Ecotite™) specialty media for adsorption or ion exchange (peat, Ecotite™) and variations of the proven passive configurations. The appropriate selection of a passive process or processes is driven primarily by water quality and flow rate, against the site-specific availability of open area. Treatability testing is required for implementation of passive treatment with both bench-scale and pilot scale testing recommended. The testing can take several weeks to several months.

While passive treatment has been proven effective in treatment of MIW with systems in operation more than twenty years, innovations and improvements are constantly being made. Winter operations on cold water can reduce treatment efficiency and spring runoff or other high flows can be difficult to manage and so implementation should be considered on a case-by-case basis but the technology has a place in mining water treatment, particularly at closed mine sites.

One of the more commonly implemented passive treatment systems for acid mine drainage is the BCR. The BCR is often followed by an aeration channel, aeration pond, or wetland to polish and oxygenate the water prior to discharge. The BCR is also one of the few established technologies for selenium treatment at mine sites.

3.5 *Reverse Osmosis*

RO treatment is a high-pressure filtration process that utilizes a series of semipermeable membranes to reject most dissolved ions in a concentrated brine stream producing a high quality effluent (permeate) stream. The brine is typically in the range of 25 to 50 percent of the influent, but can be lower depending on influent water chemistry and level of pretreatment. Pretreatment may be required to remove organic compounds, fouling compounds, scaling compounds, or suspended solids. Antiscalant addition and pH adjustment are typically included with an RO system. MIW sources may require pretreatment to reduce aluminum, iron, manganese, and silica concentrations. A typical RO system will be skid mounted and include the membranes, high pressure feed pump, a pretreatment cartridge filter, and membrane cleaning skid.

Regulation of TDS, sulfate, chloride, sodium, and other difficult to treat, highly soluble parameters makes RO one of the few process equipment choices. Brine management is key to the successful implementation of an RO system. In cases where the TDS load is predominately sulfate, an RO system can be used to concentrate sulfate in the brine stream. Lime treatment of the brine reduces the sulfate and allows blending of all, or a portion of the treated brine with the permeate prior to discharge, thus minimizing or eliminating the brine.

Nanofiltration (NF) is also used in some innovative MIW treatment applications. The NF concentrates primarily divalent species (metals and sulfate) while allowing most of the monovalent ions to pass through the membrane to the NF permeate. The NF brine can be recycled, as the divalent species are concentrated, and managed by a lime precipitation process which eliminates the brine stream.

3.6 *Selective Media – Ion exchange, adsorptive media, titanium media, iron based media, activated alumina, etc.*

Ion exchange/adsorptive media has been used in a variety of applications for removal of trace levels of metals and other contaminants and, in some applications, removal of higher concentrations of target species. The equipment consists of simple column systems loaded with the resin or media. MIW is pumped through the columns at a rate that provides the appropriate contact time. When the resin or media is loaded with contaminants, it is either replaced or regenerated. The volume of secondary waste generated by these column systems are typically less than 10% of the forward flow and less than RO brine. At mine sites, these types of systems are used as a polishing process after a bulk metals removal step or used when the MIW is a fairly low TDS and fairly clean water. Several products have been deployed as innovative solutions for metals removal from MIW, or are in development, for treatment of key parameters such as mercury, selenium, boron, and arsenic.

3.7 *Evaporation*

Evaporation technologies concentrate the soluble constituents in wastewater by removing the water as a vapor, where it may or may not be condensed. Both passive and active types of evaporation could be used to manage MIW and, in particular, high TDS MIW or concentrated liquid residuals from other treatment processes. Equipment such as a mechanical vapor recompression (MVR) evaporator can be used as part of an active treatment train or more passive systems such as pond evaporation could be used. The MVR evaporator produces a high quality liquid condensate that is virtually contaminant free but must be discharged or managed, while MVR brine will contain virtually the entire contaminant load in a volume of 1 to 10 percent relative to influent flow. Thermal evaporator systems without steam condensers are typically less capital cost than MVR systems, however, have much higher energy costs and do not produce a liquid distillate stream. Passive or semi-passive evaporation include solar evaporation ponds, and enhancements such as sprayers. Water is not recovered from the passive and semi-passive processes and the residue must be removed in intermittent campaigns. Evaporation can serve as the primary treatment system for contaminated water or more commonly for management of secondary waste streams from other water treatment processes such as RO brine.

4 INNOVATIONS IN LIME TREATMENT

One of the upgrades to the LDS process that is being implemented more often is the HDS process that reduces the volume of sludge for disposal. The HDS process promotes densification of the sludge so the volume of sludge requiring management and disposal is much less than conventional LDS treatment.

Figure 1: Lime HDS system

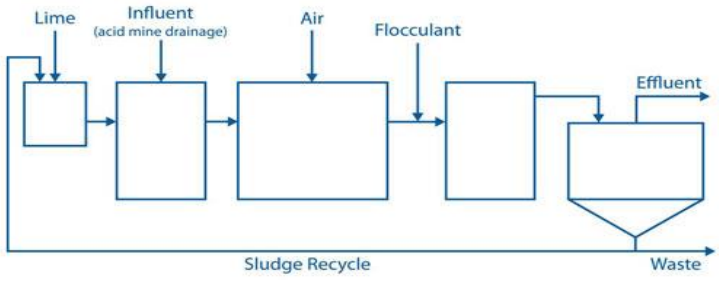

Other variations or enhancements to traditional lime treatment include sludge recycle back to the reaction tank rather than the lime mix tank, ettringite precipitation, combination of lime and caustic to minimize sludge, addition of barium for sulfate precipitation, and use of a microfilter or ultrafilter for solid liquid separation. Typical drivers for implementing these strategies and limitations include:

- Sludge recycle – provides surface area for precipitate formation and enhances the settleability of precipitate in cases where the solids generated are low. Also useful when high levels of calcium sulfate precipitation are expected to reduce scaling on equipment.
- Ettringite precipitation – achieves low residual sulfate concentrations; however, this requires careful metering of chemical feeds and tight pH control. The effectiveness is impacted by the overall ionic strength of the water. Limited full-scale implementation.
- Lime and sodium hydroxide combination – adding a target dose of lime and then polishing to a target pH value with sodium hydroxide can be used to get the benefits of both chemicals. Less sludge is produced than with a fully lime system, but with improved dewatering performance. Barium – barium precipitates sulfate very effectively and to very low residual levels. The downside of the process is the high cost of the barium. Could be effective for short term treatment projects, low flows or targeted removal requirements.
- Microfiltration – microfiltration is replacing conventional clarification in some applications and being used to polish clarifier overflow in other applications where high quality effluent is required for discharge or as a feed to another process such as an RO.

5 MINE WATER TREATMENT APPLICATIONS - COLORADO

To illustrate how widely lime treatment is used, Table 2 presents a snapshot of treatment plant for AMD in an area of Colorado, called the mineral belt, characterized by extensive mining activity. Along and near the heavily travelled interstate corridor are the remnants of historic mines and several operating (or soon to be in closure) mines. Many of these sites have active MIW treatment facilities that are based around lime treatment. The table also shows the cases where lime treatment has evolved to the currently implemented technology and two cases where an alternate to lime is currently in use. All information presented in Table 2 was obtained from public documents presented in references 1-6.

Table 2: Overview of installed Treatment Systems in Colorado's mineral belt region

Plant Name	Mine Status	Treatment System	Installed
Argo Tunnel	Historic mine drainage – State of Colorado	NaOH	1998
		Lime	2005
		Lime HDS	2013
North Clear Creek	Historic mine drainage – State of Colorado	Lime HDS	2017
Climax Molybdenum	In operation	Lime Ponds	1983

		Lime Treatment Plant	2014
Henderson Urad	Closure announced	Lime Treatment Plant	1997
Eagle Mine	Closed	Lime	1990
LMDT	Historic mine under Bureau of Reclamation	NaOH	1992
Wellington ORO	Closed – Town of Breckenridge and Summit County	Sulfide Precipitation	2008
Summitville	Closed - EPA	Lime emergency action	mid 1990's
	Closed – State of Colorado	Lime HDS	2011
Keystone	Care/Maintenance	Lime with DAF	
Confidential Mine	Closed	Passive BCR and Wetlands	2016
Gold King Emergency Response	Closed	Lime	2016

As demonstrated above, lime treatment remains a viable and competitive treatment approach. The most recently constructed lime treatment plants (North Clear Creek, Climax, and Summitville) are all treating higher flows (115 to 350 m3/hr) and higher metals loads.

6 CASE STUDIES:

6.1 *Case Study: Closed Mine Site (Colorado)*

Alternative and innovative treatment technologies were evaluated for treatment of MIW as part of a historic mine clean-up project. Water in the underground workings of the mine causes seeps from several adits and impacts ground water in the surrounding area. These sources of MIW are collected with seepage from a former tailing disposal area and are treated in a common active treatment plant. This plant, which has been operating for 20+ years, uses oxidation and lime addition to precipitate metals and settle them in a conventional clarifier. Treated water is discharged to surface water. Waste sludge is currently disposed of on-site, however the capacity for disposal is limited and expected to run-out. The blended influent water can be characterized as a typical acid mine drainage water with low pH, high iron, sulfate and other metals.

Evaluation of a new water treatment process was completed with a key objective of decreasing the waste for disposal that may need to be hauled off-site in the future. Minimize the overall operational costs of a new plant was also part of the evaluation criteria. Technologies included in the treatment evaluation were: lime HDS, sulfide precipitation, passive treatment (several configurations), in-mine treatment, and electrocoagulation.

In-mine treatment and electrocoagulation were determined to be not well suited to the site constraints and water quality. Passive treatment, with options including aerobic wetlands, manganese removal beds, and biochemical reactors were ruled out based on the total land area required, which exceeded 8 hectares for treatment of less than 70 m3/hr.

Sulfide and lime precipitation were tested to determine sludge production and chemical dosing for development of a life cycle cost comparison. The final cost evaluation matrix is presented below:

Table 3: Cost Comparison for Sulfide Precipitation and Lime HDS Treatment

Alternative	CAPEX/Year(s) Incurred ($millions)	WTP Chemical plus Sludge Disposal Cost ($/year)	OPEX/Year(s) Incurred ($/year)	Life Cycle Cost ($millions)

Alternative 1: Sulfide Precipitation	$5.43/ 0	$217,000	$560,000/ 1–25	$16.44
Alternative 2: Lime HDS	$8.06/ 0	$200,000	$590,000/ 1–25	$19.66

Two important drivers to the operational cost were the chemical consumption and sludge disposal. Sulfide precipitation required considerable chemical input in order to precipitate the high levels of influent manganese. Despite the increased chemical usage, the volume of sludge produced from the sulfide precipitation treatment was less than 0.9 tonnes per day, compared to almost 3.5 tonnes from lime treatment.

6.2 *Case Study: Closed Mine Site (Western US)*

A low volume acid mine drainage seep from historic mine workings had historically been captured and pumped back to the mine workings. As levels rose in the workings, one treatment campaign was undertaken to reduce the volume of MIW in the mine pool. The campaign was a several week operation of a mobile RO system that discharged the permeate water and returned the brine to the mine pool. As the levels in the mine pool again rose to critical levels, alternatives were evaluated including bench-scale passive treatment testing and active treatment that would include RO treatment with discharge of permeate and brine returned to the mine pool after lime treatment. Bench testing of active treatment included both RO testing and lime testing. The results of the treatability studies were used to develop economics for active, passive and semi passive treatment options. The economics showed that the active treatment could be accomplished in three months at a cost of approximately $2,200,000 while the passive treatment would require 23 months and cost approximately $800,000. Once the mine pool was drained down, the passive option could then be used long-term to treat the seep rather than continue to return water to the mine pool and treat in a campaign style. The passive treatment system has been operational since 2009.

Since the start of operations, the passive treatment system has successfully drained down the mine pool and continues to successfully treat the seep water. The seep water is a typical AMD water with pH as low as 2.1 and many dissolved metals concentrations in the 100+ mg/L range. During the first 9 years of operation, the passive treatment system has removed approximately 95% of the combined iron, zinc, aluminum, copper, and cadmium. After bulk metal removal, a constructed wetland downstream provides complete evapotranspiration of the treated water.

This system has been successful and was preferable to a lime treatment system due to a number of site specific factors including:

- The unattended historic site is in a remote area that is not easily accessible for ongoing treatment operations and lime deliveries (ample area was also available for passive treatment at the site);
- The site does not have line power and generators would be required to operate active treatment components;
- The climate of the site allows for year round operation of the wetland that provides complete evapotranspiration;
- The seep flow is less than 3 m3/hr, which is more amenable to passive treatment technologies.

The site factors for this project were key to the selection and favorable economics of the passive treatment system. Every site is different and it is important to evaluate those differences and how they impact the various treatment technologies.

6.3 *Case Study: Active Mine Site (South America)*

A gold mine in South America was evaluated for upgrades to their water treatment facility which manages excess tailings water. The treatment process currently includes pH adjustment with caustic and an added ferric coagulant but does not achieve proposed treatment objectives for

several metals, including copper. Since this is an operating mine, lime is used in large quantities in the mill and solids are managed via recirculation to the tailing storage facility.

Bench testing was performed on-site to compare the use of caustic to lime for precipitation of metals. All bench testing was carried out with set points reflective of the existing infrastructure including reaction times, chemical additions, and aeration capacity. The results of the tests are shown in Table 4.

Table 4: Bench Scale Treatability Testing Results

Parameter	Raw Water	Caustic Addition (pH 10)	Lime Addition (pH 10)
	mg/L	mg/L	mg/L
Aluminum	0.129	0.045	0.047
Cobalt	0.11	0.10	0.11
Copper	0.0396	0.0129	<0.0005
Iron	0.057	0.019	0.017
Lead	0.0121	0.0035	0.0023

Overall, the use of lime was advantageous for removal of metals to low levels and enhanced the solids settling. The lime treatment tests produced larger volumes of sludge, but this does not have a negative impact since the sludge is disposed of on-site. In addition to greater metals removal, the cost of lime is significantly cheaper than that of caustic and will reduce the operating cost of the treatment facility while using the existing equipment. The key driver was achieving a residual copper of less than 0.005 mg/L and this level was achieved with the lime.

6.4 *Case Study: Active Mine (Europe)*

As part of the pre-feasibility evaluation for a developing mine site in southern Europe, an alternative assessment was performed to look at treatment of the projected MIW. The water was different than typical acid mine drainage water with near neutral pH, but elevated metals concentrations. The treatment limits were very stringent and required removal of many different constituents to very low levels. Several constituents including lead, aluminum and zinc were evaluated for treatment using lime precipitation, while other metals such as molybdenum and arsenic required precipitation with iron addition at a low pH. Alternative technologies were also evaluated in addition to these chemical precipitation processes for the removal of selenium.

In this case, the stringent treatment limits drove a need for multiple processes in addition to lime treatment. Since the selenium treatment process was a significant driver to cost, it was recommended that a more complete water quality characterization be performed to confirm the need for alternative treatment technologies.

7 CONCLUSION

Precipitation of metal hydroxides using lime will continue to be an important tool in treatment of MIW. While evaluation and implementation of other technologies is on the rise, the benefits of lime treatment continues to have a place in the water treatment arsenal for mining applications. The drivers for implementation of alternatives to lime treatment or supplemental processes include regulatory changes to meet lower limits, limits on constituents not previously regulated, cost and operational factors, and technology improvements. These drivers may impact the placement of lime in the water treatment system as a pretreatment process to a membrane system, a biological selenium treatment system, or other targeted treatment processes. In addition, lime treatment may play a role as a residuals management process such as a brine treatment process rather than as the main treatment step at an MIW treatment plant. It is apparent that in most cases for treatment of MIW, implementation of emerging technologies will be in addition to lime treatment rather than

as a replacement. The implementation of alternative technologies to lime treatment is very site dependent but can provide great benefits should the opportunity arise.

8 REFERENCES

"Eagle Mine site summary." Eagle Mine site summary | Department of Public Health and Environment. Accessed January 2018. https://www.colorado.gov/pacific/cdphe/eagle-mine-site-summary.

Martinek, Marcia. "Climax water treatment plant is open for business - Leadville Herald." August 14, 2014. Accessed January 2018. http://www.leadvilleherald.com/news/article_2aa322b2-232c-11e4-b610-001a4bcf6878.html.

Mining Waste Treatment Technology Selection-Case Study-Argo Tunnel Site–Clear Creek, Colorado. August 2010. Accessed January 2018. https://www.itrcweb.org/miningwaste-guidance/cs41_argo_tunnel.htm.

Mining Waste Treatment Technology Selection-Case Study-Wellington-Oro Water Treatment Plant–Summit County, Colorado. August 2010. Accessed January 2018. https://www.itrcweb.org/miningwaste-guidance/cs67_wellington_oro.htm.

"Summitville Mine." Summitville Mine | Department of Public Health and Environment. Accessed January 2018. https://www.colorado.gov/pacific/cdphe/summitville-mine.

U.S. Bureau of Reclamation (BOR). U.S. Bureau of Reclamation Leadville Mine Drainage Tunnel Treatment Plant (LMDT) -Fact Sheet. Responsible Official Signe Snortland, ECAO Area Manager. Loveland, CO: U.S. BOR, 2016. https://19january2017snapshot.epa.gov/sites/production/files/2016-12/documents/co-0021717-leadville-mdt-final-sob-2016.pdf.

Author Index

This is the twenty-fourth annual Tailings and Mine Waste Conference which is being hosted by Colorado State University of Fort Collins, Colorado and now alternating odd years with the University of Alberta and the University of British Columbia. The purpose of these conferences is to provide a forum for discussion and establishment of dialogue among all people in the mining industry and environmental community regarding tailings and mine waste.

This year's conference includes papers which present state-of-the-art on mine and mill tailings and mine waste, as well as current and future issues facing the mining and environmental communities. Matters dealing with technical capabilities and developments, design and operations of tailings, and environmental concerns are discussed.